frontiers | Research Topics

Protection and healing in the digestive system and other tissues: Novel factors, mechanisms, and pharmaceutical targets

Edited by
Predrag Sikiric, Thomas Brzozowski, Duan Chen, Ki Baik Hahm and Sven Seiwerth

Published in
Frontiers in Pharmacology

ISSN 1664-8714
ISBN 978-2-83251-596-9
DOI 10.3389/978-2-83251-596-9

About Frontiers

Frontiers is more than just an open access publisher of scholarly articles: it is a pioneering approach to the world of academia, radically improving the way scholarly research is managed. The grand vision of Frontiers is a world where all people have an equal opportunity to seek, share and generate knowledge. Frontiers provides immediate and permanent online open access to all its publications, but this alone is not enough to realize our grand goals.

Frontiers journal series

The Frontiers journal series is a multi-tier and interdisciplinary set of open-access, online journals, promising a paradigm shift from the current review, selection and dissemination processes in academic publishing. All Frontiers journals are driven by researchers for researchers; therefore, they constitute a service to the scholarly community. At the same time, the *Frontiers journal series* operates on a revolutionary invention, the tiered publishing system, initially addressing specific communities of scholars, and gradually climbing up to broader public understanding, thus serving the interests of the lay society, too.

Dedication to quality

Each Frontiers article is a landmark of the highest quality, thanks to genuinely collaborative interactions between authors and review editors, who include some of the world's best academicians. Research must be certified by peers before entering a stream of knowledge that may eventually reach the public - and shape society; therefore, Frontiers only applies the most rigorous and unbiased reviews. Frontiers revolutionizes research publishing by freely delivering the most outstanding research, evaluated with no bias from both the academic and social point of view. By applying the most advanced information technologies, Frontiers is catapulting scholarly publishing into a new generation.

What are Frontiers Research Topics?

Frontiers Research Topics are very popular trademarks of the *Frontiers journals series*: they are collections of at least ten articles, all centered on a particular subject. With their unique mix of varied contributions from Original Research to Review Articles, Frontiers Research Topics unify the most influential researchers, the latest key findings and historical advances in a hot research area.

Find out more on how to host your own Frontiers Research Topic or contribute to one as an author by contacting the Frontiers editorial office: frontiersin.org/about/contact

Protection and healing in the digestive system and other tissues: Novel factors, mechanisms, and pharmaceutical targets

Topic editors

Predrag Sikiric — University of Zagreb, Croatia
Thomas Brzozowski — Jagiellonian University Medical College, Poland
Duan Chen — Norwegian University of Science and Technology, Norway
Ki Baik Hahm — CHA University School of Medicine
Sven Seiwerth — University of Zagreb, Croatia

Citation

Sikiric, P., Brzozowski, T., Chen, D., Hahm, K. B., Seiwerth, S., eds. (2023). *Protection and healing in the digestive system and other tissues: Novel factors, mechanisms, and pharmaceutical targets*. Lausanne: Frontiers Media SA.
doi: 10.3389/978-2-83251-596-9

Table of contents

frontiers | Frontiers in Pharmacology

TYPE Editorial
PUBLISHED 20 December 2022
DOI 10.3389/fphar.2022.1116643

OPEN ACCESS

EDITED AND REVIEWED BY
Angelo A. Izzo,
University of Naples Federico II, Italy

*CORRESPONDENCE
Thomas Brzozowski,
mpbrzozo@cyf-kr.edu.pl

SPECIALTY SECTION
This article was submitted to Gastrointestinal and Hepatic Pharmacology, a section of the journal Frontiers in Pharmacology

RECEIVED 05 December 2022
ACCEPTED 07 December 2022
PUBLISHED 20 December 2022

CITATION
Brzozowski T, Sikiric P, Chen D, Hahm K-B and Seiwerth S (2022), Editorial: Protection and healing in the digestive system and other tissues: Novel factors, mechanisms, and pharmaceutical targets.
Front. Pharmacol. 13:1116643.
doi: 10.3389/fphar.2022.1116643

Editorial: Protection and healing in the digestive system and other tissues: Novel factors, mechanisms, and pharmaceutical targets

Thomas Brzozowski[1]*, Predrag Sikiric[2], Duan Chen[3], Ki-Baik Hahm[4] and Sven Seiwerth[2]

[1]Jagiellonian University Medical College, Faculty of Medicine, Cracow, Poland, [2]School of Medicine, University of Zagreb, Zagreb, Croatia, [3]Norwegian University of Science and Technology, Trondheim, Norway, [4]Digestive Disease Center, CHA Bundang Medical Center, CHA University, Seongnam, South Korea

KEYWORDS

gastrointestinal injury, protection, ulcer healing, pharmacotherapy, cancer, drug repurposing, non-digestive tissues

Editorial on the Research Topic
Protection and healing in the digestive system and other tissues: Novel factors, mechanisms, and pharmaceutical targets

Damage to the surface layer of the gastrointestinal tract, caused by strong irritants, necrotizing agents or drugs such as non-steroidal anti-inflammatory drugs, is a serious clinical entity that can ultimately lead to the development of a chronic stage, including peptic ulcer disease and, consequently, neoplastic changes, which requires greater effort from the side of pharmacotherapy and even surgery. The original term "cytoprotection" was pioneered by Andre Robert who discovered the protection of the gastric mucosa by endogenous prostaglandins (PGs) stimulated by intragastric administration of "mild irritants" or by exogenous PGs used at doses that induced this protective effect when administered in non-antisecretory doses. Later, most researchers focused on the mechanism and pharmacotherapy of gastrointestinal injuries and chronic gastroduodenal ulcers, more relevant to clinical gastroenterology. Both protection and healing are universal and can affect other then digestive tissues and even body organs nowadays defined as "organoprotection." Therefore, our current Research Topic was dedicated to the latest developments in the field of injuries, protection and healing not only of gastrointestinal organs but also non-digestive cells and tissues. We have encouraged world-recognized experts working in that field to address this Research Topic focusing on understanding of mechanism of action of central and peripheral molecular regulators and pharmacological agents that provide new insights into the concept of injury, protection, and healing.

The articles received by the journal were carefully reviewed, thus offering a high-quality Research Topic. As editors of this Research Topic, we have thoroughly enjoyed serving as Guest Editors and reviewing a wide variety of interesting manuscripts related to new targets and therapies to protect and heal gastrointestinal and non-gastrointestinal cells, tissues, and organs, including the utility of new drugs, drugs repurposing, pharmacological tools, and an introduction of original approaches. Below we summarize the main findings and perspectives detailed in each of the twenty-seven accepted articles.

An important report by Zhou et al. revealed that NAFLD is exacerbated by insulin in T2DM and treatment with liraglutide, a GLP-1 agonist, ameliorated hepatic steatosis and liver damage by directly activating hepatic GLP-1R to stimulate PPARα expression by activating the PKA-AMPK signaling pathway and reducing ROS-related apoptosis. These results support the notion that liraglutide may be useful in the treatment of T2DM. Rabben et al. studied the chemopreventive effect of isocyanates administered before tumor initiation in mouse models of gastric cancer, including INS-GAS mice, against potentiating the efficacy of cytotoxic drugs such as cisplatin, prompting the interest of clinicians to use a combination strategy in gastric cancer. Given the side effects such as drug resistance and failure of conventional 5-ASA drug therapy for inflammatory bowel disease, He et al. demonstrated a synergistic effect of 5-ASA and vorinostat (SAHA), a histone deacetylase (HDAC) inhibitor, in the treatment of experimental dextran sulfate colitis *in vivo*, associated with lower toxicity and p65 mRNA expression in Caco-2 and HCT-116 human colonic epithelial cell lines *in vitro*. These findings highlight the efficacy of SAHA acting synergistically with 5-ASA in the treatment of human UC, primarily by inhibiting the nuclear factor kappa B (NF-κB) signaling pathway. Rabben et al. used computational predictions based on the gene expression profiles of the human and mouse gastric cancer (GC) model to reposition ivermectin in the treatment of GC, validated by *in silico*, *in vitro* and *in vivo* methods. Ivermectin reduced the tumor size which was associated with inactivation of WNT/β-catenin signaling and cell proliferation pathways and activation of cell death signaling pathways. In their review, Seiwerth et al. have demonstrated the summary of practical applicability the pleiotropic drug BPC 157 capable of curing the cutaneous and other tissue wounds in rodent models by preventing vessel constriction, the formation of fibrin mesh which may stabilize the platelet plug, thus promoting resolution of the clot. Thereby, BPC 157 deserves to be used in clinical scenario of wound healing external (skin) and/or internal (i.e., abdominal) associated with bleeding disorders. The turmeric agent curcumin has a protective effect on the stomach, but its effectiveness in the lower digestive tract is less known. Zhong et al. found that curcumin is effective in regulating naïve, cell differentiation, TCM and TEM in peripheral blood to ameliorate experimental DSS-induced colitis, and the beneficial effects of this turmeric may depend on inhibition of JAK1/STAT5 signaling activity. Sun et al. studied the role of intestinal glial cells in the mechanism of intestinal barrier disruption in mice with intestinal injury exposed to acute ischemia-reperfusion (I/R). They discovered for the first time that glial cells can modulate intestinal barrier function through A2A adenosine receptors (A2ARs), as a marked exacerbation of I/R damage was observed in A2AR knockout (KO) mice. Moreover, they shed further insight into the mechanism of this protection, demonstrating that A2AR agonists increased barrier proteins ZO-1 and occludin expression in glial cells co-cultured in Caco-2 monolayers, and that the PKCα-dependent signaling pathway in response to hypoxia *in vitro* may be due to a synergistic effect A2AR and metabotropic glutamate receptor 5. It is known that the gaseous mediator's nitric oxide (NO), hydrogen sulfide (H_2S) and carbon monoxide (CO) play a key role in the regulation of many physiological functions, including the mechanism of gastrointestinal protection and ulcer healing. Danielak et al. presented an update on the therapeutic properties of a new class of synthesized NSAIDs equipped with NO, H_2S or CO molecules and releasing one or more of these gaseous messengers. These physiological mediators have attracted widespread attention as agents capable of reducing the side effects of non-steroidal anti-inflammatory drugs (NSAIDs), which are known to be among the most used drugs in the treatment of numerous inflammatory diseases. In their review, the authors cite preclinical and clinical evidence demonstrating the promising anti-inflammatory power and gastrointestinal safety of these new NSAIDs and their mechanisms of action, confirming the real contribution of "gaseous" NSAIDs to the defense mechanism of the gastrointestinal mucosa by reducing the side effects of these parent drugs in the intestine. Honjo et al. provided new insight into the potential target of IBD therapeutic intervention, including receptor-interacting serine/threonine kinase 2 (RIPK2), now also recognized as receptor-interacting protein 2 (RIP2). This small molecule acts as a downstream signaling molecule for nucleotide-binding oligomerization domain 1 (NOD1), NOD2, and Toll-like receptors (TLRs). The biologically active molecule, RIPK2, is expressed in antigen-presenting cells such as dendritic cells and macrophages, triggering the expression and release of pro-inflammatory cytokines such as TNF-α, IL-6 and IL-12/23p40 by activating NFκB and mitogen activated protein kinases, thus playing an important role in infection by microorganisms inducing host defense. This review elucidated the recent advances in RIP2-induced IBD immune-pathogenesis and presented the prospect of therapy for autoimmune disorders such as IBD. Kim and Kim reviewed the physiology and pharmacology of the pluripotent peptide hormone leptin, which is produced by adipocytes but also in the gastric mucosa. Leptin affects the hypothalamus by suppressing appetite and is involved in the regulation of energy homeostasis and neuroendocrine functions. The authors referred

to leptin downstream signaling in the digestive tract and accessory digestive organs. The diverse roles of leptin in the digestive system, including immune regulation, cell proliferation, tissue healing and glucose metabolism, are discussed, as well as current therapeutic applications of recombinant leptin. Nicotinamide riboside (NR), vitamin B_3 and sirtuins play a key role in the aging process, neurodegenerative processes, and myopathy. Hutka et al. provided evidence that ingestion of NR-containing pellets attenuated tumor cachexia and accompanying sarcopenia in a C26 mouse model of adenocarcinoma. In addition, NR administration significantly increased the levels of key enzymes involved in the biosynthesis of NAD^+ and nicotinamide phosphoribosyl transferase, and significantly inhibited NAD^+-sensitive sirtuin deacetylase 1 (SIRT1), indicating that NR treatment may be useful in the treatment of human cancer cachexia. Park et al. discussed whether NSAID-induced dysbiosis and associated intestinal disorders are manifested by direct antibacterial effects or delayed peristalsis induced by these drugs. They reported that ketorolac, an NSAID, has a significant effect on the gut microbiota and bile acids in the absence of *mucositis*, and that ketorolac has no effect on gastrointestinal transit delay. Gravina et al. selected a patient population with areas of clarithromycin (CLA) resistance to investigate the efficacy and safety of bismuth quadruple therapy (BQT) or bismuth-free quadruple therapy against *Helicobacter pylori* (Hp) infection. They found that in an area with a high prevalence of CLA-resistant or CLA + metronidazole-resistant Hp strains, the BQT containing Pylera is an effective therapeutic strategy against Hp-infection associated with good adherence and low incidence of adverse events. Park et al. theorized that human placenta-derived mesenchymal stem cells (PD-MSCs) could repair Hp-associated precancerous chronic atrophic gastritis (CAG) in mice, thereby preventing gastric carcinogenicity. The PD-MSC treatment groups showed significantly reduced inflammation, gastric atrophy, erosions/ulcerations, and dysplastic changes and associated with normalization of microbial communities after treatment comparing to pathogenic microbiota in the CAG mice. Nam et al. identified triptolide as a novel NRF2 inhibitor that significantly attenuates ARE-luciferase activity at nanomolar concentrations and reduces NRF2 accumulation in the nucleus, promoting nuclear export of this factor. Moreover, oral administration of triptolide inhibited the growth of A549 xenografts in athymic mice by promoting oxidative damage through nuclear export of NRF2, indicating that inhibition of NRF2 by increasing the cytoplasmic localization of this factor may be the main mechanism of triptolide anti-tumor effect. In a review by Dahlgren et al. the toxicity of chemotherapeutic agents in the gut, leading to chemotherapeutics-induced intestinal mucositis affecting the normal gut microbiota, was described. The authors proposed a combination therapy of chemotherapeutics with prophylactic drugs, such as antibiotics or probiotics, antioxidants, apoptosis inhibitors, anti-inflammatory agents or agents that promote cell proliferation and adaptation. The claudin family, which are transmembrane proteins, are believed to act as the potential targets in patients with IBD, and therefore, Ćužić et al. studied claudin expression in human diseases and two different animal models of IBD: sodium dextran sulfate (DSS)-induced colitis and an adoptive model of transmission of colitis. They found that claudins are not exclusively expressed in epithelial cells, but in some cell types of mesodermal origin, and concluded that these proteins could be considered as a therapeutic target for pharmacotherapy against intestinal inflammation in preclinical animal models and human IBD. Filaretova et al. considered the role of glucocorticoids in the mechanism of distant preconditioning, a therapeutic intervention of short ischemia known to protect organs such as the heart, brain, lungs, and kidneys from various tissue damage because of severe ischemia-reperfusion (I/R). They found that the glucocorticoid synthesis inhibitor metyrapone, which caused a considerable decrease in plasma corticosterone levels, reduced the protective effect of preconditioning in the stomach exposed to I/R, while the corticosterone replacement in rats with adrenalectomy, restored gastric protection exhibited by preconditioning against I/R-induced damage. This is first evidence that glucocorticoids may be involved in the gastroprotective mechanism of ischemic preconditioning against I/R-induced gastric damage. Földes et al. attempted to optimize culture conditions for three-dimensional growth of ameloblast-derived HAT-7 cells useful for assessing the effect of fluoride exposure on HAT-7 spheroid formation. They concluded that such a new 3D model would be suitable for studying the mechanism of amelogenesis, which is evidently affected by exposure to fluoride. Sang-Ngoen et al. conducted a meta-analysis to summarize the effects of probiotics on periodontal disease microbiota and oral health. They described the beneficial effect of probiotics on the reduction of some pathogenic bacterial strains, with little or no effect on others, supporting the notion that, due to the complexity of periodontal disease, there is a need for well-designed randomized clinical trials to evaluate the real effectiveness of probiotics. Nakamura et al. studied the effect of elevated pH induced by acid suppressants, including vonoprazan, lansoprazole and famotidine, on the viability of non-*Helicobacter pylori* helicobacters (NHPH) in mice. They observed that NHPH urease activity as assessed by urea breath tests and the number of these pathogenic bacteria decreased after the use of acid suppressors, i.e., vonoprazan, indicating that NHPH damage may be dependent on changes in pH. Revenko et al. studied the effects of sodium hydrosulfide (NaHS), an H_2S donor, on stress-induced gastric injury and associated changes in essential H_2S enzymes, mesenteric vessels, and connective and adipose tissues of aged rats fed a high-fructose diet. They reported that in stressed elderly rats, treatment with NaHS protected mesenteric cell mitochondria and microvascular endothelial and subendothelial structures,

including fibroblasts, and restored the activity of H_2S-related enzymes. They concluded that the H_2S donor improves both H_2S signaling and mitochondrial redox balance, which are crucial, especially in advanced age-related high-fructose diet injury. Wang et al. determined the role of metastasis-associated lung adenocarcinoma transcript 1 (MALAT1) in diabetic gastroparesis (DGP). They showed that MALAT1 expression was upregulated in gastric tissues of DGP mice, in adjacent healthy tissues from diabetic gastric cancer patients with symptoms of DGP, and in glucose-fed cultures of human gastric smooth muscle cells. Their study points to a new regulatory signaling pathway in the human diabetic gastroparesis, including MALAT1, miR-449a and delta-like ligand 1. Tepes et al. determined whether the stable gastric pentadecapeptide BPC 157, which has been shown to prevent large vessel occlusion syndromes, may also be effective in a model of multiple occlusion syndrome in rats. By improving the function of the venous system with BPC 157, these authors convincingly demonstrated the counteraction of the chain of arterial-vascular harmful events, the preservation of collateral circulation and the reversal of symptoms not only in gastrointestinal organs such as stomach, but also the cerebral edema and venous and arterial thrombosis, indicating that BPC 157 has cured primary abdominal compartment syndrome. Dong et al. studied the efficacy of naringin in two experimental murine models of colitis *in vivo* and *in vitro* using RAW264.7 cells stimulated with lipopolysaccharide (LPS). They found that this polyphenolic compound alleviated symptoms of colitis and suppressed the LPS-induced high expression of NF-κB-p65, which was further inhibited by small interfering RNAs targeting PPAR-γ, revealing a new therapeutic role for polyphenolic naringin and its usefulness in the treatment of colitis and, perhaps human IBD in the future clinical trials. Skroza et al. presented an analysis of a retrospective single-centre study of the efficacy and safety of isotretinoin in the treatment of moderate to severe acne in real clinical practice. Indeed, early systemic treatment with isotretinoin in patients suffering from moderate acne has shown health benefits, however, the authors recommend an appropriate dose adjustment to minimize side effects. Hou et al. studied the hepatoprotective properties of a natural plant mixture of *Panax notoginseng* (PNM) against mouse liver damage caused by hepatic ischemia/reperfusion (HIR). They documented that PNM exerted a protective effect against HIR-induced hepatic damage and investigated further the plant-pharmacology of the network by evaluating the target genes responsible for this protection by searching various databases that were later validated by immunohistochemical analysis of the mice liver tissues. As a result, they concluded that PNM may exhibit hepatoprotection by reducing the gene expression of nuclear receptor subfamily3 group C member 2 (NR3C2), SRC and GAPDH.

Author contributions

TB wrote the first draft of the manuscript. PS, DC, K-BH, and SS authors contributed to manuscript revision, read, and approved the submitted version.

Conflict of interest

The authors declare that the research was conducted in the absence of any commercial or financial relationships that could be construed as a potential conflict of interest.

Publisher's note

frontiers in Pharmacology

ORIGINAL RESEARCH
published: 01 February 2021
doi: 10.3389/fphar.2020.630244

Curcumin Regulated the Homeostasis of Memory T Cell and Ameliorated Dextran Sulfate Sodium-Induced Experimental Colitis

You-Bao Zhong[1,2,3], Zeng-Ping Kang[1], Bu-Gao Zhou[4], Hai-Yan Wang[4], Jian Long[1], Wen Zhou[5], Hai-Mei Zhao[2] and Duan-Yong Liu[4,5]**

[1]Department of Postgraduate, Jiangxi University of Traditional Chinese Medicine, Nanchang, China, [2]College of Traditional Chinese Medicine, Jiangxi University of Traditional Chinese Medicine, Nanchang, China, [3]Laboratory Animal Research Center for Science and Technology, Jiangxi University of Traditional Chinese Medicine, Nanchang, China, [4]Formula-Pattern Research Center of Jiangxi University of Traditional Chinese Medicine, Nanchang, China, [5]Science and Technology College, Jiangxi University of Traditional Chinese Medicine, Nanchang, China

Immune memory is protective against reinvasion by pathogens in the homeostatic state, while immune memory disorders can cause autoimmune disease, including inflammatory bowel disease. Curcumin is a natural compound shown to be effective against human inflammatory bowel disease and experimental colitis, but the underlying mechanism is unclear. Here, experimental colitis was induced by dextran sulfate sodium (DSS) in this study. Significant changes in the percentages of naïve, central memory T (TCM), and effector memory (TEM) cells and their $CD4^+$ and $CD8^+$ subsets were found in the peripheral blood of mice with colitis using flow cytometry. After 7 days of continuous curcumin (100 mg/kg/day) administration, the DSS-induced experimental colitis was effectively relieved, with significant decreases in the ratio of day weight to initial body weight, colonic weight, pathological injury score, levels of proinflammatory cytokines IL-7, IL-15, and IL-21, colonic mucosal ulceration, and amount of inflammatory infiltrate. Importantly, curcumin significantly restored the percentages of naïve, TCM, and TEM cells and their $CD4^+$ and $CD8^+$ subpopulations. In addition, curcumin significantly inhibited the activation of the JAK1/STAT5 signaling pathway, downregulation of JAK1, STAT5, and p-STAT5 proteins in colon tissue, and upregulation of PIAS1 proteins. These results suggested that curcumin effectively regulated the differentiation of naïve, TCM, and TEM cells in the peripheral blood to alleviate DSS-induced experimental colitis, which might be related to the inhibition of JAK1/STAT5 signaling activity.

Keywords: curcumin, experimental colitis, JAK1/STAT5 signaling pathway, memory T cells, mechanism of action

OPEN ACCESS

Edited by:
Duan Chen,
Norwegian University of Science and Technology, Norway

Reviewed by:
Yoku Hayakawa,
The University of Tokyo, Japan
Martin Diener,
University of Giessen, Germany

****Correspondence:***
Hai-Mei Zhao
haimei79@163.com
Duan-Yong Liu
liuduanyong@163.com

Specialty section:
This article was submitted to Gastrointestinal and Hepatic Pharmacology, a section of the journal Frontiers in Pharmacology

Received: *17 November 2020*
Accepted: *29 December 2020*
Published: *01 February 2021*

Citation:
Zhong Y-B, Kang Z-P, Zhou B-G, Wang H-Y, Long J, Zhou W, Zhao H-M and Liu D-Y (2021) Curcumin Regulated the Homeostasis of Memory T Cell and Ameliorated Dextran Sulfate Sodium-Induced Experimental Colitis. Front. Pharmacol. 11:630244. doi: 10.3389/fphar.2020.630244

INTRODUCTION

Inflammatory bowel disease (IBD) refers to chronic autoimmune diseases of the gastrointestinal tract, including Crohn's disease (CD) and ulcerative colitis (UC) (Hodson, 2016). IBD is a global disease with a high prevalence in developed countries (prevalence >0.3%) (Ungaro et al., 2017) and an accelerating prevalence in newly industrialized countries, especially in Asia (Ng et al., 2018). In addition, IBD has a high recurrence rate and is so difficult to cure to the extent that the World Health

Organization has classified it as one of the modern intractable diseases (Jackson and De Cruz, 2019). The advent of IBD has created a serious medical burden on national healthcare finance and has influenced the quality of life of patients. The etiology and pathogenesis of IBD are not fully understood. However, growing evidence indicates that these disorders are the result of the interplay between genetic, environmental, intestinal microflora and immune factors (Xavier and Podolsky, 2007). In particular, T-cell-mediated inflammation is important in experimental colitis and human IBD (Strober et al., 2007; Zundler and Neurath, 2017).

Immune memory dysfunction is a typical feature of IBD onset (Gattinoni et al., 2011). Immune memory is the phenomenon in which the immune system, after initial contact with an antigen that produces a specific immune response, usually responds again when it encounters that antigen. The re-response produced by immune memory is often characterized by rapid, strong, specific elevation and persistence. It can prevent the recurrence of the same disease and play a protective role for the organism, while immune memory disorders can result in the dysregulation of the inflammatory response and local tissue injury (Natoli and Ostuni, 2019). Some studies have shown that memory cells, including central memory T cells ($CD45RA^{-}CD62L^{+}CCR7^{+}$, TCM) and effector memory T cells ($CD45RA^{-}CD62L^{-}CCR7^{-}$, TEM), are involved in the onset and course of autoimmune diseases including rheumatoid arthritis and IBD (Belarif et al., 2018; Pardieck et al., 2018). IBD recurrence may be caused by the long-term colonization of colitogenic memory T cells (Kanai et al., 2009; Gattinoni et al., 2011). Excessive colitogenic $CD4^{+}$ central memory T cells ($CD4^{+}$ TCM) are preferentially retained in the bone marrow of mice with colitis, and they circulate between the bone marrow and the lamina propria (Whiteoak et al., 2018). The aforementioned studies suggested that restoring memory T-cell homeostasis is one of the effective measures of IBD therapy.

Importantly, a natural anti-inflammatory compound, curcumin, can effectively relieve chronic IBD by regulating T-cell proliferation and differentiation (Gao et al., 2004; Pang et al., 2018). Curcumin has antioxidant properties; it inhibits the activity of ribonucleotide reductase and DNA polymerases in the cell cycle (Shakeri and Boskabady, 2017), thereby effectively inhibiting lymphocyte proliferation. In addition, curcumin inhibits nuclear factor κB (NF-κB) signal activation and the production of proinflammatory cytokines activated by T cells, including Th1-type cytokines interleukin (IL)-2 and interferon (IFN)-γ, further inhibiting lymphocyte proliferation (Ukil et al., 2003). In CD, Th1 cells are the major drivers of acquired immune-related inflammation (Brand, 2009). Curcumin can block Th1 subpopulation differentiation by inhibiting IL-12 production by macrophages and can promote Th2 subpopulation proliferation and secretion of anti-inflammatory cytokines IL-4 and IL-10 (Zhang et al., 2006). For example, 30 mg/kg curcumin treatment promoted Th2 differentiation and inhibited Th1 proliferation in a rat model of TNBS-induced colitis (Zhang et al., 2006). Curcumin also inhibited the development of Th17, thereby reducing the production of the proinflammatory cytokines IL-6, IL-21, and IL-17 (Bakir et al., 2016). However, whether curcumin has an effect on memory T-cell differentiation and subpopulation homeostasis has not been reported at home or abroad.

In addition, the JAK/STAT signaling pathway has been shown to play an important role in memory T-cell differentiation (Ashrafizadeh et al., 2020). IL-7 promotes the survival of human $CD4^{+}$ effector/memory T cells by activating the JAK/STAT signaling pathway (Chetoui et al., 2010). However, evidence showing that drugs can modulate the differentiation of memory T cells or activate JAK-STAT signaling to treat IBD is scarce. Based on the aforementioned findings, it was hypothesized that curcumin might regulate the differentiation balance of memory T cells to treat IBD. The present study investigated the mechanism underlying curcumin treatment of IBD by observing the number of naïve, TEM, and TCM cells and the expression levels of related proteins in the JAK1/STAT5 signaling pathway in mice with colitis. The data from this study might contribute to a better understanding of the mechanism underlying curcumin treatment of IBD and provide experimental evidence for curcumin as a possible treatment for UC.

MATERIALS AND METHODS

Mice

Male specific pathogen-free (SPF) BALB/c (aged 8–9 weeks, weighing 20–22 g) were purchased from the Hunan Slack Landscape Laboratory Animal Co. Ltd. (Changsha, China) (Animal Certificate Number SCXK (Xiang) 2016-0002). The mice were bred and maintained under SPF conditions, and experiments were conducted following the Institutional Animal Care and Use Committee at the animal facility of Traditional Chinese Medicine (Nanchang, China). The experimental protocols were approved by the Animal Care and Use Committee of Jiangxi University of Traditional Chinese Medicine (identification code: JZLLSC2018-024; date of approval: September 22, 2018).

All mice were acclimatized for 3 days prior to starting the study. Forty mice were randomly and equally divided into 4 groups with 10 mice in each group: normal group (Nor), DSS group (DSS), DSS + Cur group (DSS + Cur), and DSS + mesalazine group (DSS + 5-ASA).

Induction and Treatment of Experimental Colitis

To induce colitis in mice, male BALB/c mice in the DSS, DSS + Cur group and DSS + 5-ASA group were administered with 3.0% (*w*/*v*) dextran sulfate sodium (batch number: 160110; DSS, 36–50KDs; MP Biomedicals, CA, United States) in drinking water for 7 days. The mice in the normal group received normal drinking water.

Before administration, curcumin (batch number: GR-133-140421; Gangrun Biotechnology, Nanjing, China) was dissolved in 1.5% carboxymethyl cellulose solution at a dose of 100 mg/kg (purity >95% by high performance liquid chromatography (HPLC)). On day 8, the mice in the DSS + Cur and DSS + 5-ASA groups were administered, respectively, curcumin (100 mg/kg) and mesalazine (300 mg/kg; batch number: 130407; Sunflower Pharma, Jiamusi, China) by oral

gavage for 7 days; the mice in the normal and DSS groups were treated with equal volume of saline. Throughout the study, all mice were weighed once daily (09:00) and monitored daily for diarrhea, hematochezia, hunched posture, and hair loss.

Pathological Histology Analysis

The colons were dissected, washed with phosphate-buffered saline (PBS, pH = 7.3), fixed with precooled 4.0% paraformaldehyde (PFA) overnight at 4°C, dehydrated using an alcohol gradient (from 50% to 100%), rendered transparent in xylol, and embedded in paraffin. Then, these samples were cut into 4 μm thickness sections. After deparaffinization and rehydration, the slices were stained with hematoxylin-eosin (H and E) (Solarbio, Beijing, China). Subsequently, the slices were imaged with a biomicroscope (Lecia, Wetzlar, Germany).

The microscopic scores were obtained by two different pathologists blinded to evaluation. Histopathological injury scores included inflammatory infiltrate and tissue damage (Schmidt et al., 2010). Points for infiltration were given as follows: 0, no infiltration; 1, increased number of inflammatory cells in the lamina propria; 2, inflammatory cells extending into the submucosa; and 3, transmural inflammatory infiltrates; and, for tissue damage: 0, no mucosal damage; 1, discrete epithelial lesions; 2, erosions or focal ulcerations; and 3, severe mucosal damage with extensive ulceration extending into the bowel wall.

Enzyme-linked Immunosorbent Assay

The colon tissue of the mice was collected, and RIPA (Radio Immunoprecipitation Assay) buffer was used to lyse tissue at a ratio of 1:10, homogenized with an electric homogenizer in ice water, incubated at 4°C for 30 min, and centrifugated at 12,000 rpm for 10 min, and the tissue supernatant was obtained and analyzed. The total protein in each mouse was quantified with a total protein detection kit (Aidlab Biotechnologies Co., Ltd., Beijing, China). Where indicated, the samples were normalized to 5000 ng/mL in colon tissue supernatants of the respective experiment. The levels of cytokines, IL-7, IL-15, and IL-21, were measured using commercial enzyme-linked immunosorbent assay (ELISA) kits (BD Biosciences, NJ, United States) following the manufacturer's protocol, and optical density values of cytokines in each sample were detected on a microplate reader (Thermo, Varioskan, MA, United States). Then, each cytokine was quantified basally based on a standard curve established using an ELISA kit.

Flow Cytometry

The numbers of $CD45RA^+CD62L^+CCR7^+$ (naïve T) cells, $CD45RA^-CD62L^+CCR7^+$ (TCM) cells, and $CD45RA^-CD62L^-CCR7^+$ (TEM) cells in peripheral blood were detected by flow cytometry, and their $CD4^+$ and $CD8^+$ subsets were assessed too. The obtained lymphocytes were incubated with fluorescence-conjugated monoclonal antibodies in a staining buffer. Eight-color flow cytometry analysis (n = 8) was performed on a FACSCalibur device (Becton-Dickinson, CA, USA). A lymphocyte suspension was prepared as follows: 100 μL of anticoagulant, 100 μL of RPMI 1640 medium, and 1 mL of hemolysin were added to fresh blood and incubated for 15 min. The mixture was centrifuged at 300 g for 5 min, and the supernatant was removed. Then, 1 mL of stain buffer was added, and the cells were rinsed twice and centrifuged at 350 g for 5 min. The supernatant was discarded, and the cells were resuspended in 100 μL stain buffer. Further, 1 μg FcR blocking sealant was added and incubated at 4°C for 8 min. Primary antibodies were added and incubated for 15 min at room temperature. The cells were washed twice with 1 mL of stain buffer, the supernatant was discarded, and 500 μL of stain buffer was added to resuspend cells. The samples were detected using a FACSCanto II flow cytometer (BD Biosciences, NJ, United States). The following mAbs were used: PE rat anti-mouse CD4 (1:200), Alexa Fluor 647 rat anti-mouse CCR7 (1:100), BV510 rat anti-mouse CD45RA (1:100), BV421 rat anti-mouse CD62L (1:100), and FITC rat anti-mouse CD8 (1:100) (BD Biosciences). The limits for the quadrant markers were set based on negative populations and isotype controls. The analysis of acquired data was performed with the FlowJo software (Tree Star, OR, United States).

Western Blotting

The normalized supernatants (5 μg/μL) of colonic tissues were prepared as described in *Enzyme-linked Immunosorbent Assay*. An equivalent amount of protein in each sample was fractionated onto sodium dodecyl sulfate–polyacrylamide gel electrophoresis and transferred to a polyvinylidene fluoride membrane (PVDF) with a Bio-Rad Western blot apparatus. The PVDF membranes were blocked with 5% fat-free milk or 5% bovine serum albumin and then incubated overnight with the following primary antibodies at 4°C. The primary antibodies were JAK1 (1: 2000), STAT5 (1:1000), p-STAT5 (1:800), PIAS1 (1:1000), and GAPDH (1:5000) (Abcam, MA, USA). These membranes were treated with the corresponding secondary antibody [HRP-conjugated AffiniPure Goat Anti-Rabbit IgG or HRP-conjugated AffiniPure Goat Anti-Mouse IgG (1:5000–1:10000) (Proteintech, IL, United States] for 1-2 h at room temperature. Subsequently, these membranes were visualized with ECL western blot substrate. The specific protein bands were scanned with a UVP Chen Studio (Analytik Jena, Germany) and quantified using Image-Pro Plus 6.0 software (Media Cybernetic, MD, United States).

Statistical Analysis

Data were expressed as the mean ± standard error of mean (SEM). Statistical analyses were carried out using GraphPad Prism 8.0 software (CA, United States). Student t test or one-way analysis of variance (ANOVA), followed by the Tukey test for multiple comparisons, was performed to determine significance. All P values less than 0.05 indicated a statistically significant difference.

RESULTS

Curcumin Relieved DSS-Induced Colitis

DSS-induced experimental colitis is a classic model for studying the pathogenesis of IBD and the techniques and drug development for IBD treatment. In the present study, hematochezia, diarrhea, and rough and lusterless hair of BALB/c mice were visible with naked eyes after 4–5 days of

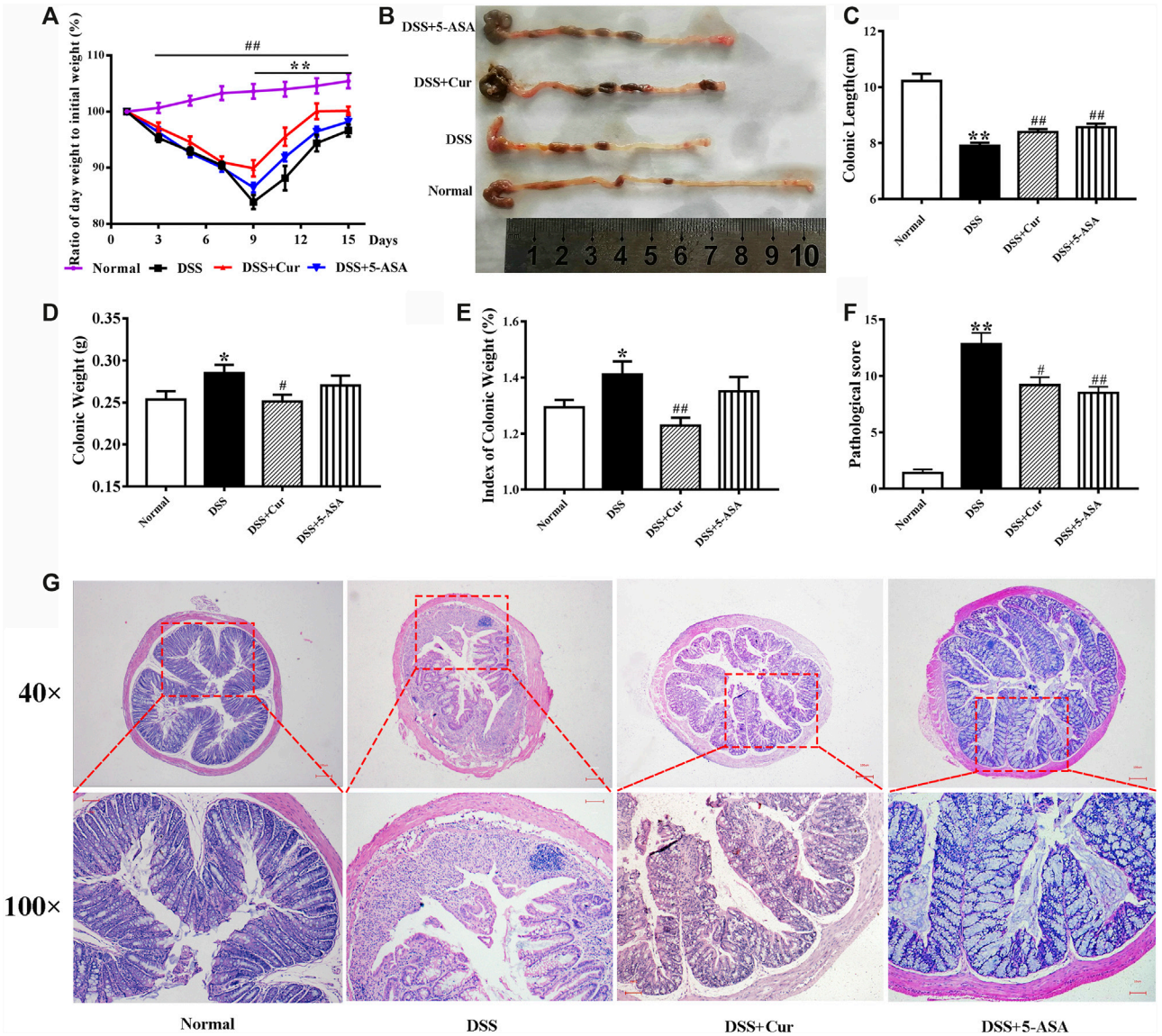

FIGURE 1 | Therapeutic evaluation of curcumin on DSS-induced colitis in mice. **(A)** Ratio of day weight to initial body weight. **(B)** Changes in colonic length by naked eye. **(C)** Colonic length. **(D)** Colonic weight. **(E)** Index of colonic weight. **(F)** Histopathological score. **(G)** Histological appearance of the colons from individual groups of mice; the colonic sections were stained with hematoxylin and eosin. Data are representative images or as the mean ± SEM (n = 10 mice per group). $^{*}P < 0.05$ and $^{**}P < 0.01$ versus the DSS group, $^{\#}P < 0.05$ and $^{\#\#}P < 0.01$ versus the normal group, analyzed by ANOVA or Student t test.

DSS induction. The mice in the DSS group had significantly shorter colonic length (**Figure 1B,C**), higher colonic weight (**Figure 1D**) and colonic weight index (**Figure 1E**), and lower body weight change rate (**Figure 1A**), compared with the mice in the normal group. Pathological observations found disorganized mucosal structure, thickened colonic wall, ulcer formation, severe congestion, and edema, as well as inflammatory cell infiltration, in mice with colitis in the DSS group (**Figure 1G**). In addition, colonic histopathological damage scores were higher in the DSS group than in the normal group (**Figure 1F**). This was consistent with previous reports (Ge et al., 2020), suggesting that the DSS-induced experimental colitis was successfully replicated.

After curcumin treatment, the mice in the DSS + Cur group had significantly higher colonic length (**Figure 1B,C**) and significantly lower colonic weight (**Figure 1D**) and colonic weight index (**Figure 1E**) compared with mice in the DSS group. The ratio of daily body weight to initial body weight of mice was significantly higher in the DSS + Cur group than in the DSS group from day 9 (two doses) to the end of the experiment (**Figure 1A**). The mice in the DSS + Cur and DSS + 5-ASA groups showed a significant improvement in pathological injury, suppression of ulceration and epithelial proliferation, less inflammatory cell infiltration (**Figure 1G**), and significantly lower pathological injury scores compared with mice in the

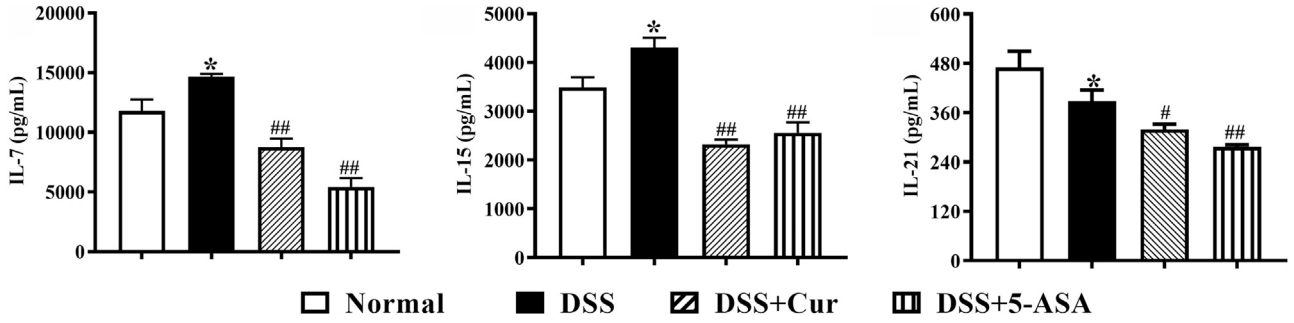

FIGURE 2 | Curcumin regulated the expression levels of inflammatory cytokines IL-7, IL-15, and IL-21 in mice with colitis. The levels of cytokines, **(A)** IL-7, **(B)** IL-15, and **(C)** IL-21, were measured by ELISA. Data are presented as mean ± SEM ($n = 8$). $^{\#}P < 0.05$ and $^{\#\#}P < 0.01$ versus the normal group, $^{*}P < 0.05$ and $^{**}P < 0.01$ versus the DSS group, analyzed by ANOVA or Student *t* test.

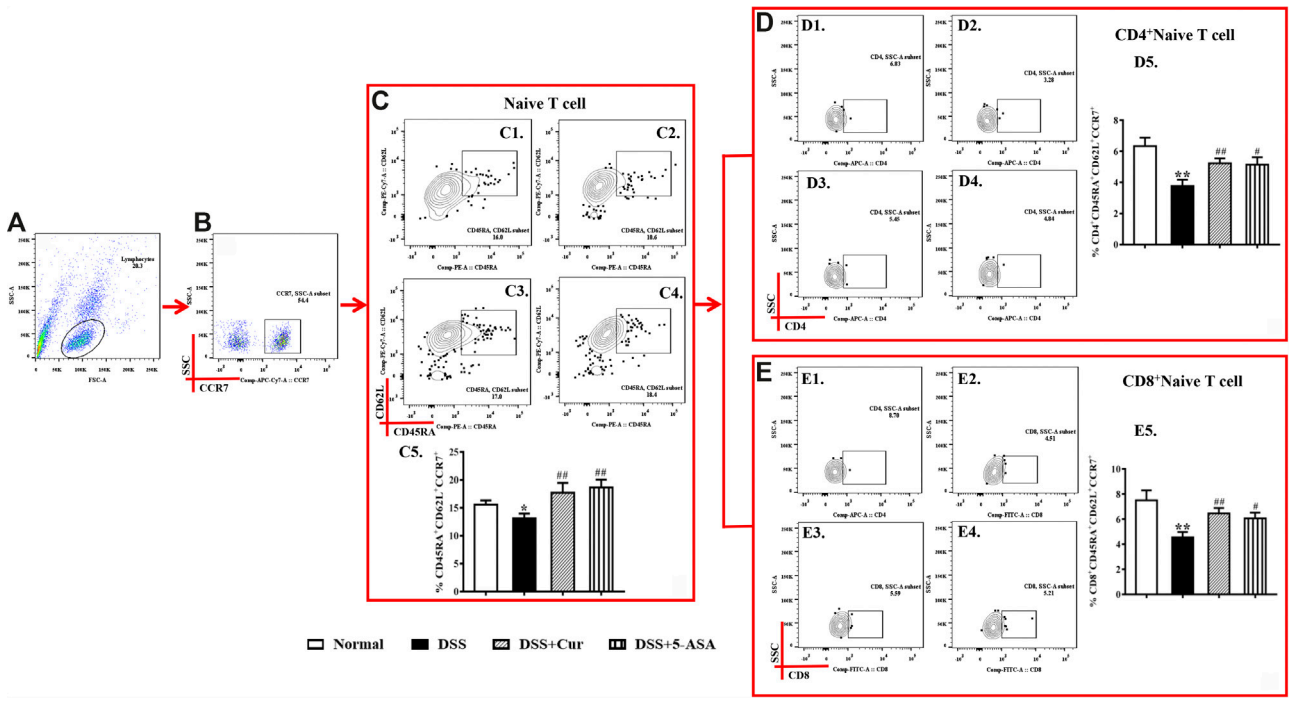

FIGURE 3 | Curcumin regulated the number of naïve T cells in colitis mice. **(A)** Total lymphocytes in peripheral blood. **(B)** CCR7+ lymphocytes measured by flow cytometry. **(C)** Double-positive CD45R and CD62L lymphocytes; the cells in the upper left corner are naïve cells; C1–C4 represent naïve T cells in the normal, DSS, DSS + Cur, and DSS + 5-ASA group in order; C5: statistical analysis of naïve T cell frequencies in these four groups. **(D)** Flow cytometry analysis of $CD4^+$ naïve T cell frequencies; D1–D4 represent naïve T cells in the normal, DSS, DSS + Cur, and DSS + 5-ASA groups in order; D5: statistical analysis of $CD4^+$ naïve T cells frequencies in these 4 groups. **(E)** Frequency of $CD8^+$ naïve T cells analyzed by flow cytometry. E1–E4 represent naïve T cells in the normal, DSS, DSS + Cur, and DSS + 5-ASA groups in order; E5: statistical analysis of $CD4^+$ naïve T cells frequencies in these four groups. Data are presented as mean ± SEM ($n = 10$). $^{\#}P < 0.05$, $^{\#\#}P < 0.01$ versus the normal group; $^{*}P < 0.05$ and $^{**}P < 0.01$ versus the DSS group.

DSS group (**Figure 1F**). These results suggested that curcumin effectively relieved UC in mice.

Curcumin Regulated the Expression of Cytokines in Colon Tissue

Cytokines play an important role in intestinal homeostasis and inflammation-related pathological processes (Friedrich et al., 2019), and their abnormal expression is typical for UC, such as IL-7, IL-15, and IL-21. The levels of IL-7 (**Figure 2A**) and IL-15 (**Figure 2B**) in the colon tissue were significantly increased, while the levels of IL-21 (Figure 2C) significantly decreased in the DSS group compared with the normal group. After 7 days of treatment with curcumin and melaxazine, the levels of IL-7 (**Figure 2A**), IL-15 (**Figure 2B**), and IL-21 (**Figure 2C**) in the colon tissues were significantly lower in the DSS + Cur and DSS + 5-ASA groups

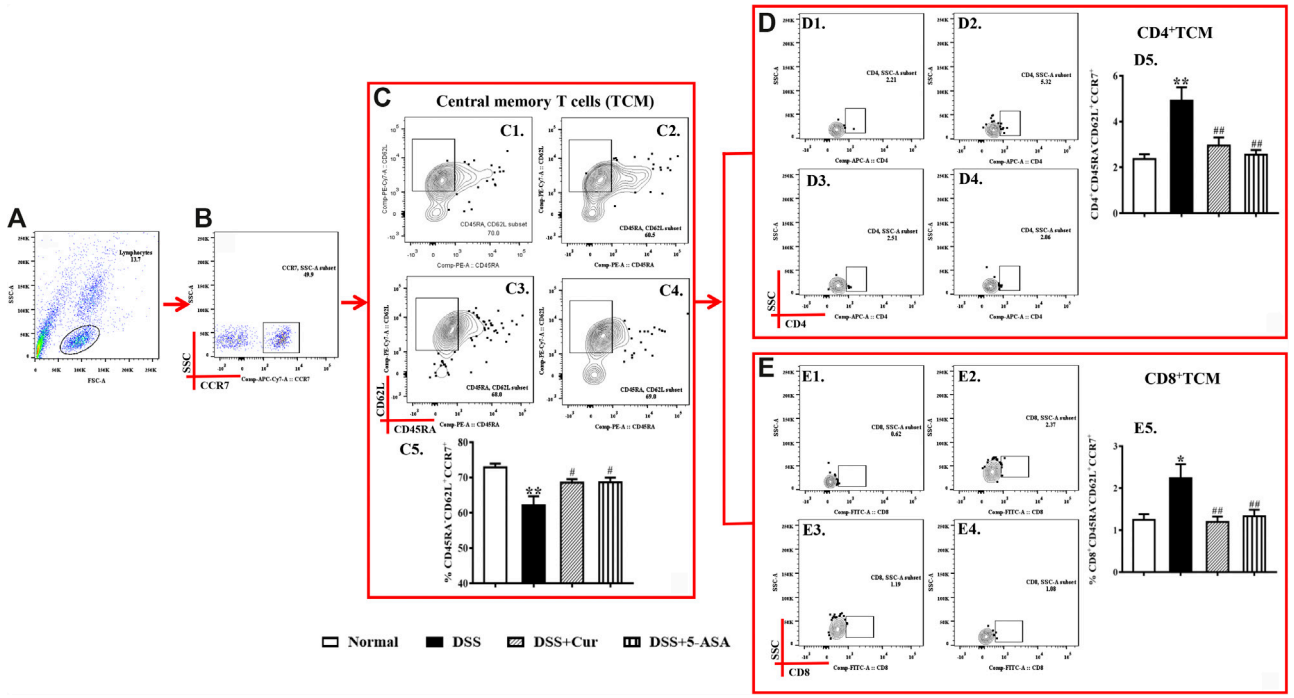

FIGURE 4 | Curcumin regulated TCM cells in mice with colitis. (A) Total lymphocytes in peripheral blood. **(B)** CCR7+ lymphocytes measured by flow cytometry. **(C)** The CD45RA–CD62L+ labelled cells are TCM cells, located in the upper right corner; C1–C4 represent naïve T cells in the normal, DSS, DSS + Cur, and DSS + 5-ASA groups in order; C5: statistical analysis of TCM cells frequencies in these four groups. **(D)** Flow cytometry analysis of $CD4^+$ TCM cell frequencies; D1–D4 represent $CD4^+$ TCM cells in the normal, DSS, DSS + Cur, and DSS + 5-ASA groups in order; D5: statistical analysis of $CD4^+$ TCM cell frequencies in these 4 groups. **(E)** The frequency of $CD8^+$ TCM cells distribution analyzed by flow cytometry; E1–E4 represented $CD8^+$ TCM cells in the normal, DSS, DSS + Cur, and DSS + 5-ASA groups in order; E5: statistical analysis of $CD8^+$ TCM cells frequencies in these four groups. Data are presented as mean ± SEM ($n = 10$). $^{\#}P < 0.05$ and $^{\#\#}P < 0.01$ versus the normal group; $^{*}P < 0.05$ and $^{**}P < 0.01$ versus the DSS group.

than in the DSS group. These results suggested that curcumin effectively inhibited the secretion of proinflammatory cytokine in mice with colitis.

Curcumin Regulated Memory T-Cell Differentiation

When T cells are not stimulated with antigens, naïve T cells are in a quiescent state and biologically marked by triple positivity for lymph node homing receptor CD62L, chemokine receptor 7 CCR7, and leukocyte common antigen CD45RA (**Figure 3A–C**). In this study, $CD45RA^+CD62L^+CCR7^+$ cells were naïve T cells (**Figures 3C1–4**). The frequency of $CD45RA^+CD62L^+CCR7^+$cells was significantly lower in the DSS group than in the normal group (**Figures 3C1–5**). This finding indicated that DSS antigen activated naïve T cells to differentiate into effector T cells. The frequency of $CD45RA^+CD62L^+CCR7^+$ cells significantly increased in the DSS + Cur and DSS + 5-ASA groups compared with the DSS group (**Figures 3C1–5**). The frequency of two subsets of naïve T cells, $CD4^+$ naïve T cells (**Figures 3D1–5**) and $CD8^+$ naïve T cells (**Figures 3E1–5**) was significantly lower in the DSS group than in the normal, DSS + Cur, and DSS + 5-ASA groups. These results suggested that curcumin could effectively promote the number of naïve T cells and their subsets in mice with colitis.

Upon antigen activation, naïve T cells give rise to long-term memory T cells, which are T cells that could proliferate clonally through the lymphatic circulation back to secondary lymphoid organs and differentiate into TEM cells upon restimulation with homologous antigens. In this study, $CD45RA^-CD62L^+CCR7^+$ cells were TCM cells (**Figure 4C1–4**). The number of $CD45RA^-CD62L^+CCR7^+$ cells significantly reduced in mice with colitis in the DSS group compared with the normal group (**Figures 4C1–5**), but the numbers of two main subsets of TCM cells, $CD4^+$ TCM (**Figures 4D1–5**) and $CD8^+$ TCM (**Figures 4E1–5**), were significantly higher in the DSS group than in the normal group. After the mice with colitis were treated with curcumin and mesalazine, the number of TEM cells (**Figures 4C1–5**) was significantly higher than that in mice with untreated colitis, while the number of $CD4^+$ TEM (**Figures 4D1–5**) and $CD8^+$ TEM cells (**Figures 4E1–5**) decreased significantly. This study showed that curcumin could regulate the differentiation of TCM cells and their subpopulations.

TEM cells can migrate to peripheral inflammation sites and exert an immune function; they do not express CCR7, CD45RA, and CD62L on their surface. In this study, $CD45RA^-CD62L^-CCR7^-$ cells were TEM cells. The number of TEM cells (**Figure 5C1–5**) in the peripheral blood of mice in the DSS group was significantly higher than that in the normal group, the number of their subsets $CD4^+$ TEM (**Figure 5D1–5**)

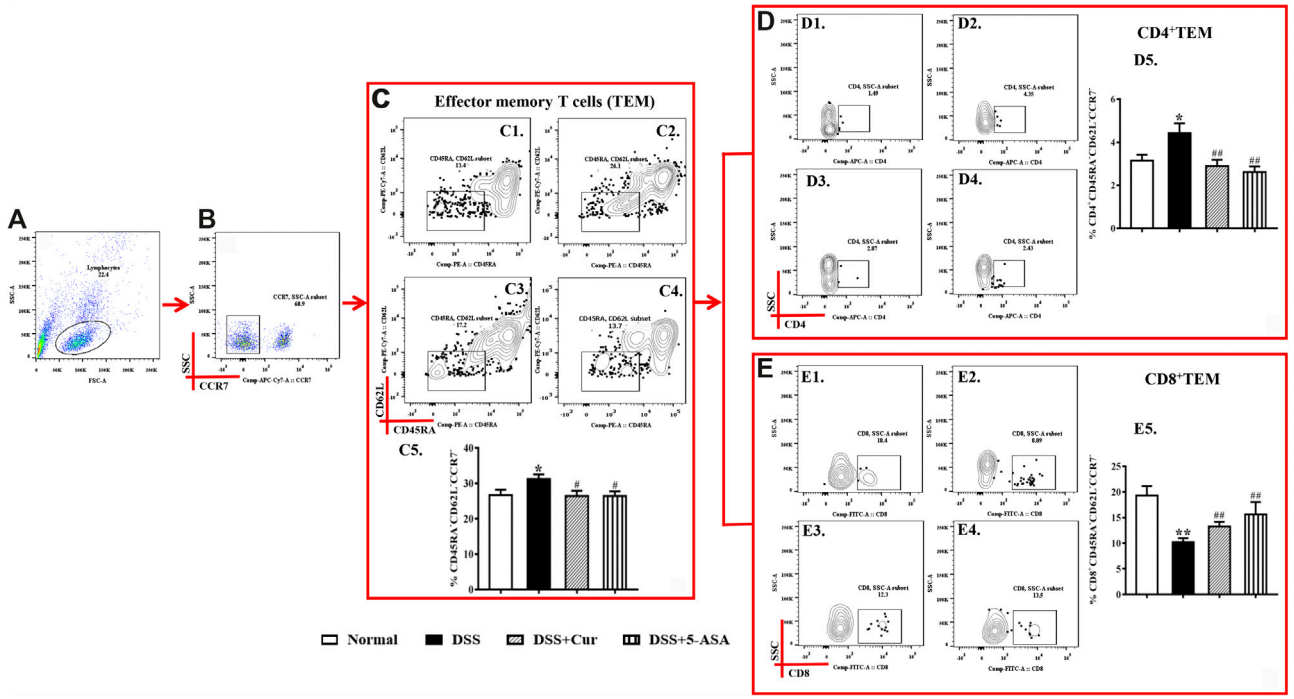

FIGURE 5 | Curcumin regulated TEM cells in mice with colitis. **(A)** Total lymphocytes in peripheral blood. **(B)** CCR7-lymphocytes measured by flow cytometry. **(C)** The CD45RA–CD62L– labelled cells are TCM cells, located in the lower right corner; C1–C4 represent TEM cells of the normal, DSS, DSS + Cur, and DSS + 5-ASA groups in order; C5: statistical analysis of TEM cells frequencies in these four groups. **(D)** Flow cytometry analysis of CD4+ TEM cells frequencies; D1–D4 represent CD4+ TEM cells in the normal, DSS, DSS + Cur, and DSS + 5-ASA groups in order; D5: statistical analysis of CD4+ TEM cells frequencies in these 4 groups. **(E)** The frequency of CD8+ TEM cells distribution analyzed by flow cytometry; E1–E4 represented CD8+ TEM cells in the normal, DSS, DSS + Cur, and DSS + 5-ASA groups in order; E5: statistical analysis of CD8+ TEM cells frequencies in these four groups. Data are presented as mean ± SEM (n = 10). $^{\#}P < 0.05$ and $^{\#\#}P < 0.01$ versus the normal group; $^{*}P < 0.05$ and $^{**}P < 0.01$ versus the DSS group.

significantly increased, and $CD8^+$ TEM (**Figure 5E1–5**) remarkably reduced. The numbers of TEM cells (**Figure 5C1–5**) and their subsets $CD4^+$ TEM (**Figure 5D1–5**) significantly reduced in the peripheral blood after 7 days of treatment with curcumin and 5-ASA compared with DSS treatment, and $CD8^+$ TEM cells remarkably upregulated (**Figure 5E1–5**). The results showed that curcumin could effectively regulate the differentiation balance of TEM cells in DSS-induced experimental colitis.

Curcumin Regulated JAK1/STAT5 Signal Activation

JAK1/STAT5 signaling is activated with the involvement of γc family receptors to regulate memory T-cell differentiation (Rochman et al., 2009). Therefore, the western blotting technique was further used to measure the protein levels of JAK1, STAT5, p-STAT5, and JAK1/STAT5 signal negative regulator PIAS1 (protein inhibitor of activated signal transducer and activators of transcription 1) in colon tissue (**Figure 6A**). The levels of JAK1 (**Figure 6B**) and STAT5 (**Figure 6C**) proteins in the colon tissues of mice significantly increased, the changes in the levels of p-STAT5 (**Figure 6D**) were not statistically significant, and the protein level of PIAS1 (**Figure 6E**) significantly decreased in the DSS group compared with the normal group. The colonic protein levels of JAK1 (**Figure 6B**), STAT5 (**Figure 6C**), and p-STAT5 (**Figure 6D**) were significantly decreased, and the protein level of PIAS1 (**Figure 6E**) was significantly increased in the DSS + Cur and DSS + 5-ASA groups compared with the DSS group. The results indicated that curcumin could effectively inhibit the activation of the JAK1/STAT5 signaling pathway in DSS-induced experimental colitis.

DISCUSSION

In the present study, the onset of IBD in humans was simulated using an experimental DSS-induced UC. After DSS induction, the mice with colitis showed significant weight loss, hematochezia, and an increase in disease activity index score; colonic shortening, epithelial erosion of the colonic mucosa on microscopic examination, formation of ulcers and granulation tissue, disorganized crypt structure, and inflammatory cell infiltration; and a significant increase in the levels of proinflammatory cytokines IL-7, IL-15, and IL-21 in colonic tissues. These results suggested that DSS successfully recapitulated colitis. The number of naïve T cells $CD4^+$, naïve T and $CD8^+$ naïve T cells decreased significantly; the number of TCM cells decreased significantly, while the number of $CD4^+$ TCM and

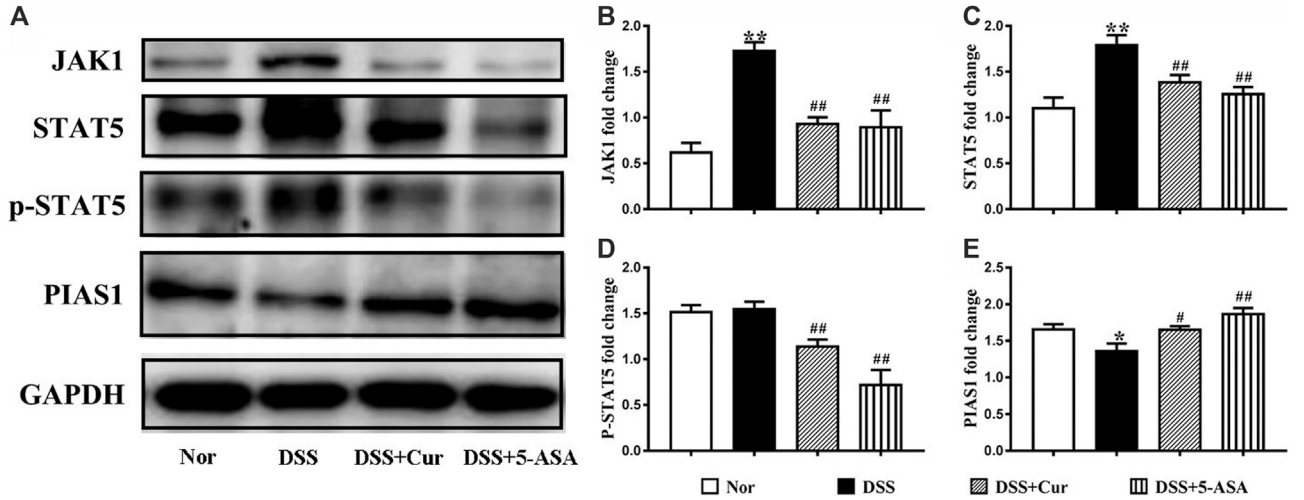

FIGURE 6 | Curcumin regulated JAK1/STAT5 signaling activation in mice with colitis. **(A)** The protein expression in the JAK/STAT5 signaling pathway, such as JAK1, STAT5, p-STAT5 and PIAS, was analyzed by western blotting analysis. **(B)** Quantitative analysis of the expression of JAK1 protein. **(C)** Quantitative analysis of the expression of STAT5 protein. **(D)** Quantitative analysis of the expression of p-STAT5 protein. **(E)** Quantitative analysis of the expression of PIAS1 protein. Data are presented as mean ± SEM (n = 8). $^{\#}P < 0.05$ and $^{\#\#}P < 0.01$ versus the normal group, $^{*}P < 0.05$ and $^{**}P < 0.01$ versus the DSS group, analyzed by ANOVA or Student t-test.

$CD8^+$ TCM cells increased significantly; and the number of TEM and $CD4^+$ TEM increased significantly, while $CD8^+$ TEM cells decreased significantly. These results indicated that the numbers of memory T cells and their subsets significantly changed in DSS-induced colitis, suggesting that immune memory cell differentiation disorders might be closely related to the onset and development of IBD.

In terms of acquired immunity, "memory" is now generally considered to be the ability to respond once to an antigen and a stronger response the next time the same antigen is stimulated (Netea et al., 2016). The main antigens in IBD are intestinal commensal and autoantigens, which are not completely eliminated resulting in recurrent episodes of IBD (Franzosa et al., 2019). Given the aging and atrophy of the human thymus, naïve T cells, which are not readily available in the thymus, continue to differentiate into colon effector T cells (Kondo et al., 2019). Naïve T cells differentiate rapidly into effector T cells under the stimulation by TCRs and costimulatory molecules (Jenkins et al., 2001). When antigen elimination is cleared, apoptosis of most effector T cells occurs and the remaining effector T cells are converted into long-lived memory T cells (Pepper and Jenkins, 2011). Thus, when the physical barrier of the intestinal mucosa is compromised, symbiotic bacteria enter the lamina propria through the leaky gut to induce an inflammatory response (Friedrich et al., 2019). TCM cells, which express CCR7 and CD62L, migrate through the bone marrow and bloodstream to secondary lymphoid organs (Reinhardt et al., 2001), proliferate, and differentiate into TEM cells, which then exert their effects at the site of lost inflammation. When the intestinal tract is in direct contact with the outside world and the intestinal mucosal epithelium is inevitably damaged, intestinal commensal bacteria and auto-reactive antigens enter the mucosal tissues and repeatedly stimulate them, leading to abnormal activation of memory T cells. Therefore, the dynamic equilibrium of pathogenic memory T cells plays an important role in the pathogenesis of autoimmune diseases.

The immune memory dysfunction is the key characteristic of IBD. Growing evidence shows that IBD is caused by innate and adaptive immune system responses to intestinal symbionts, which frequently recur and persist despite going into remission after treatment (Weingarden and Vaughn, 2017; Nishida et al., 2018). In mice with UC, excessive inflammatory $CD4^+$ TEM cells infiltrated into the epithelium and lamina propria of colon mucosa (Wirtz et al., 2017). $CD4^+$ Tm ($CD4^+$ $CD45RB^{high}$) cells isolated from the lamina propria of mice with colitis were cultured *in vitro* for 8 weeks and transplanted into SCID mice to cause acute colitis, and $CD4^+CD44^+CD62L^-$ memory T cells were found to overaggregate in the lamina propria of the colon (Takahara et al., 2013). The differentiation status of $CD4^+$ Tm in the gut determines the relapse-remitting process of chronic UC (Jameson and Masopust, 2018). These studies suggested that targeting colon-causing inflammatory memory T cells would be one of the targets of IBD therapy. Japanese scholars, Fujii et al. (2006), effectively alleviated IBD by interfering with memory T-cell differentiation homeostasis. $CD4^+CD45RB^{high}$ T cells were injected into SCID mice to induce immune memory dysfunction in colitis mice. A 2 week intervention treatment with the immunosuppressant fingolimod (FTY20) resulted in significant remission of colitis. The levels of effector memory T cells, such as $CD4^+CD62L^-$ ($CD4^+$TEM) T cells, and the expression of the homing cell adhesion molecule CD44 in the peripheral blood, spleen, lamina propria of the small intestine, and mesenteric lymph nodes of mice with colitis were found to be decreased.

Curcumin is a natural hydrophobic polyphenol extracted from turmeric rhizome, which has been widely used as an herbal medicine in China and Southeast Asia for hundreds of years

(Lestari and Indrayanto, 2014; He et al., 2015). It has many pharmacological activities, such as anti-inflammatory, antioxidant, and antitumor (Sharma et al., 2005). Curcumin is widely used in the clinical treatment of human UC patients and the evaluation of animal therapeutic effect of colitis (Epstein et al., 2010; Sareen et al., 2013). In this study, colonic injury was alleviated or disappeared, including a decrease in colonic weight index, downregulation of histopathological scores, and restoration of colonic length, and the numbers of naïve, TEM, and TCM cells and their respective subpopulations were restored to normal after 14 days of continuous treatment with curcumin in mice with DSS-induced colitis. Strong evidence showed that curcumin might treat IBD by modulating memory T-cell differentiation.

In our study, DSS-induced mice treated with curcumin showed significant decreases in the levels of proinflammatory cytokines IL-7, IL-15, and IL-21 in colonic tissues. Cytokines IL-7, IL-15, and IL-21 mediate transmission signals following binding of the common γ-chain (Kohn et al., 2014) (JAK1 and γc) of type I receptors with JAK1 and JAK3 (Rochman et al., 2009; Salas et al., 2020), resulting in phosphorylation and nuclear translocation of STAT5A and/or STAT5B (in response to IL-2). Molecular interactions between JAKs and STATs mediate cellular responses that play a fundamental role in both intestinal homeostasis and inflammation (Coskun et al., 2013). Molecules that interfere with these interactions, especially those targeting JAK1 and JAK3, such as TNF antagonists (Jones-Hall and Nakatsu, 2016), have shown promising efficacy and safety in IBD treatment. The protein levels of JAK1, JAK3, and STAT5 were downregulated in mice with colitis after curcumin treatment, indicating that curcumin inhibited JAK-STAT signal activation. This finding suggested that curcumin might interfere with JAK-STAT signaling to modulate the differentiation of memory T cells for UC, which requires further exploration with a separate JAK-STAT intervention group or specific gene knockout mice.

In addition, cytokines IL-7, IL-15, and IL-21 play key roles in the differentiation of memory T cells. L-7 receptors are highly expressed in memory T cells (Tm), naïve T cells (Tn) receptors. IL-7 activates IL-7 receptor α and induces proliferation and long-term survival of effector memory $CD4^+$ T cells (Takahara et al., 2013), leading to chronic colitis. IL-15 regulates memory $CD8^+$ T cell lifespan and effector function (Yoshihara et al., 2006). Under steady-state or lymphopenic conditions, IL-21 acts directly on $CD8^+$ T cells, favoring the accumulation of TE/TEM populations (Tian et al., 2016). It is implied that regulation of memory T cell differentiation through intervention with IL-7, IL-15, and IL-21 is an effective measure for the treatment of ulcerative colitis. In the present study, the decreasing trend of IL-7 concentration in colitis mice after curcumin intervention was consistent with $CD4^+$ TEM; however, the trend of IL-15 and IL-21 change was not consistent with $CD8^+$ TEM cells, probably due to the fact that IL-15 and IL-21 were detected in colonic tissue while $CD8^+$ TEM was in blood. Therefore, our next step is to further test the levels of cytokines IL-7, IL-15, and IL-21 by isolating $CD4^+$ TEM, $CD8^+$ TEM, and coculturing them with curcumin *in vitro*. Surprisingly, the levels of the proinflammatory cytokine IL-21 were lower in the colitis mice than in the normal group of mice. This may be due to the fact that the source of IL-21 is not only produced by activated $CD4^+$ T cells (Harada et al., 2006), but also derived from other cells such as natural killer cells. We will explore the role played by IL-21 in DSS-induced colitis by knocking out the IL-21 gene.

DATA AVAILABILITY STATEMENT

The original contributions presented in the study are included in the article/Supplementary Material; further inquiries can be directed to the corresponding authors.

ETHICS STATEMENT

The animal study was reviewed and approved by the Animal Care and Use Committee of Jiangxi University of Traditional Chinese Medicine.

AUTHOR CONTRIBUTIONS

D-YL and H-MZ conceived and designed the experiments. Y-BZ, Z-PK, B-GZ, JL, WZ, and H-YW performed the experiments. D-YL and H-MZ contributed reagents/materials/analytical tools. D-YL and Y-BZ analyzed the data. Y-BZ and D-YL wrote the manuscript.

FUNDING

This study was supported in part by the National Natural Science Foundation of China (Nos. 82060799, 8180792, 81760838, and 81760808), Natural Science Foundation of Jiangxi Province (Nos. 20192ACB20015, 20192BAB215050, and 20181BAB205082), Education Department of Jiangxi Province (Nos. GJJ181582, GJJ196047, and 20181969), and 1050 Young talents project (No. 1141900603) and first-class subjects starting funds (Nos. JXSYLXK-ZHYI022, JXSYLXK-ZHYAO132, and JXSYLXK-ZHYAO108) of Jiangxi University of Traditional Chinese Medicine.

REFERENCES

Ashrafizadeh, M., Rafiei, H., Mohammadinejad, R., Afshar, E. G., Farkhondeh, T., and Samarghandian, S. (2020). Potential therapeutic effects of curcumin mediated by JAK/STAT signaling pathway: a review. *Phytother Res.* 34, 1745–1760. doi:10.1002/ptr.6642

Bakir, B., Yetkin, A. Z., Buyukbayram, H. I., Kumbul, D. D., Bayram, D., Candan, I. A., et al. (2016). Effect of curcumin on systemic T helper 17 cell response; gingival expressions of interleukin-17 and retinoic acid receptor-related orphan

receptor gammat; and alveolar bone loss in experimental periodontitis. *J. Periodontol.* 87, e183–e191. doi:10.1902/jop.2016.150722

Belarif, L., Mary, C., Jacquemont, L., Mai, H. L., Danger, R., Hervouet, J., et al. (2018). IL-7 receptor blockade blunts antigen-specific memory T cell responses and chronic inflammation in primates. *Nat. Commun.* 9, 4483. doi:10.1038/s41467-018-06804-y

Brand, S. (2009). Crohn's disease: Th1, Th17 or both? The change of a paradigm: new immunological and genetic insights implicate Th17 cells in the pathogenesis of Crohn's disease. *Gut* 58, 1152–1167. doi:10.1136/gut.2008.163667

Chetoui, N., Boisvert, M., Gendron, S., and Aoudjit, F. (2010). Interleukin-7 promotes the survival of human $CD4^+$ effector/memory T cells by up-regulating Bcl-2 proteins and activating the JAK/STAT signalling pathway. *Immunology* 130, 418–426. doi:10.1111/j.1365-2567.2009.03244.x

Coskun, M., Salem, M., Pedersen, J., and Nielsen, O. H. (2013). Involvement of JAK/STAT signaling in the pathogenesis of inflammatory bowel disease. *Pharmacol. Res.* 76, 1–8. doi:10.1016/j.phrs.2013.06.007

Epstein, J., Docena, G., MacDonald, T. T., and Sanderson, I. R. (2010). Curcumin suppresses p38 mitogen-activated protein kinase activation, reduces IL-1beta and matrix metalloproteinase-3 and enhances IL-10 in the mucosa of children and adults with inflammatory bowel disease. *Br. J. Nutr.* 103, 824–832. doi:10.1017/S0007114509992510

Franzosa, E. A., Sirota-Madi, A., Avila-Pacheco, J., Fornelos, N., Haiser, H. J., Reinker, S., et al. (2019). Gut microbiome structure and metabolic activity in inflammatory bowel disease. *Nat Microbiol* 4, 293–305. doi:10.1038/s41564-018-0306-4

Friedrich, M., Pohin, M., and Powrie, F. (2019). Cytokine networks in the pathophysiology of inflammatory bowel disease. *Immunity* 50, 992–1006. doi:10.1016/j.immuni.2019.03.017

Fujii, R., Kanai, T., Nemoto, Y., Makita, S., Oshima, S., Okamoto, R., et al. (2006). FTY720 suppresses $CD4^+CD44^+CD62L^-$ effector memory T cell-mediated colitis. *Am. J. Physiol. Gastrointest. Liver Physiol.* 291, G267–G274. doi:10.1152/ajpgi.00496.2005

Gao, X., Kuo, J., Jiang, H., Deeb, D., Liu, Y., Divine, G., et al. (2004). Immunomodulatory activity of curcumin: suppression of lymphocyte proliferation, development of cell-mediated cytotoxicity, and cytokine production *in vitro*. *Biochem. Pharmacol.* 68, 51–61. doi:10.1016/j.bcp.2004.03.015

Gattinoni, L., Lugli, E., Ji, Y., Pos, Z., Paulos, C. M., Quigley, M. F., et al. (2011). A human memory T cell subset with stem cell-like properties. *Nat. Med.* 17, 1290–1297. doi:10.1038/nm.2446

Ge, W., Wang, H. Y., Zhao, H. M., Liu, X. K., Zhong, Y. B., Long, J., et al. (2020). Effect of sishen pill on memory T cells from experimental colitis induced by dextran sulfate sodium. *Front. Pharmacol.* 11, 908. doi:10.3389/fphar.2020.00908

Harada, M., Magara-Koyanagi, K., Watarai, H., Nagata, Y., Ishii, Y., Kojo, S., et al. (2006). IL-21-induced Bepsilon cell apoptosis mediated by natural killer T cells suppresses IgE responses. *J. Exp. Med.* 203, 2929–2937. doi:10.1084/jem.20062206

He, Y., Yue, Y., Zheng, X., Zhang, K., Chen, S., and Du, Z. (2015). Curcumin, inflammation, and chronic diseases: how are they linked? *Molecules* 20, 9183–9213. doi:10.3390/molecules20059183

Hodson, R. (2016). Inflammatory bowel disease. *Nature* 540, S97. doi:10.1038/540S97a

Jackson, B. D., and De Cruz, P. (2019). Quality of Care in patients with inflammatory bowel disease. *Inflamm. Bowel Dis.* 25, 479–489. doi:10.1093/ibd/izy276

Jameson, S. C., and Masopust, D. (2018). Understanding subset diversity in T cell memory. *Immunity* 48, 214–226. doi:10.1016/j.immuni.2018.02.010

Jenkins, M. K., Khoruts, A., Ingulli, E., Mueller, D. L., McSorley, S. J., Reinhardt, R. L., et al. (2001). *In vivo* activation of antigen-specific CD4 T cells. *Annu. Rev. Immunol.* 19, 23–45. doi:10.1146/annurev.immunol.19.1.23

Jones-Hall, Y. L., and Nakatsu, C. H. (2016). The intersection of TNF, IBD and the microbiome. *Gut Microb.* 7 (1), 58–62. doi:10.1080/19490976.2015.1121364

Kanai, T., Nemoto, Y., Tomita, T., Totsuka, T., Watanabe, M., and Hibi, T. (2009). Persistent retention of colitogenic $CD4^+$ memory T cells causes inflammatory bowel diseases to become intractable. *Inflamm. Bowel Dis.* 15, 926–934. doi:10.1002/ibd.20738

Kohn, L. A., Seet, C. S., Scholes, J., Codrea, F., Chan, R., Zaidi-Merchant, S., et al. (2014). Human lymphoid development in the absence of common γ-chain receptor signaling. *J. Immunol.* 192, 5050–5058. doi:10.4049/jimmunol.1303496

Kondo, K., Ohigashi, I., and Takahama, Y. (2019). Thymus machinery for T-cell selection. *Int. Immunol.* 31, 119–125. doi:10.1093/intimm/dxy081

Lestari, M. L., and Indrayanto, G. (2014). Curcumin. *Profiles Drug Subst. Excipients Relat. Methodol.* 39, 113–204. doi:10.1016/B978-0-12-800173-8.00003-9

Natoli, G., and Ostuni, R. (2019). Adaptation and memory in immune responses. *Nat. Immunol.* 20, 783–792. doi:10.1038/s41590-019-0399-9

Netea, M. G., Joosten, L. A., Latz, E., Mills, K. H., Natoli, G., Stunnenberg, H. G., et al. (2016). Trained immunity: a program of innate immune memory in health and disease. *Science* 352, aaf1098. doi:10.1126/science.aaf1098

Ng, S. C., Shi, H. Y., Hamidi, N., Underwood, F. E., Tang, W., Benchimol, E. I., et al. (2018). Worldwide incidence and prevalence of inflammatory bowel disease in the 21st century: a systematic review of population-based studies. *Lancet* 390, 2769–2778. doi:10.1016/S0140-6736(17)32448-0

Nishida, A., Inoue, R., Inatomi, O., Bamba, S., Naito, Y., and Andoh, A. (2018). Gut microbiota in the pathogenesis of inflammatory bowel disease. *Clin J Gastroenterol* 11, 1–10. doi:10.1007/s12328-017-0813-5

Pang, Y., Du, X., Xu, X., Wang, M., and Li, Z. (2018). Monocyte activation and inflammation can exacerbate Treg/Th17 imbalance in infants with neonatal necrotizing enterocolitis. *Int. Immunopharm.* 59, 354–360. doi:10.1016/j.intimp.2018.04.026

Pardieck, I. N., Beyrend, G., Redeker, A., and Arens, R. (2018). Cytomegalovirus infection and progressive differentiation of effector-memory T cells. *F1000Res* 7, 1554. doi:10.12688/f1000research.15753.1

Pepper, M., and Jenkins, M. K. (2011). Origins of CD4(+) effector and central memory T cells. *Nat. Immunol.* 12, 467–471. doi:10.1038/ni.2038

Reinhardt, R. L., Khoruts, A., Merica, R., Zell, T., and Jenkins, M. K. (2001). Visualizing the generation of memory CD4 T cells in the whole body. *Nature* 410, 101–105. doi:10.1038/35065111

Rochman, Y., Spolski, R., and Leonard, W. J. (2009). New insights into the regulation of T cells by gamma(c) family cytokines. *Nat. Rev. Immunol.* 9, 480–490. doi:10.1038/nri2580

Salas, A., Hernandez-Rocha, C., Duijvestein, M., Faubion, W., McGovern, D., Vermeire, S., et al. (2020). JAK-STAT pathway targeting for the treatment of inflammatory bowel disease. *Nat. Rev. Gastroenterol. Hepatol.* 17, 323–337. doi:10.1038/s41575-020-0273-0

Sareen, R., Jain, N., and Pandit, V. (2013). Curcumin: a boon to colonic diseases. *Curr. Drug Targets* 14, 1210–1218. doi:10.2174/13894501113149990168

Schmidt, N., Gonzalez, E., Visekruna, A., Kühl, A. A., Loddenkemper, C., Mollenkopf, H., et al. (2010). Targeting the proteasome: partial inhibition of the proteasome by bortezomib or deletion of the immunosubunit LMP7 attenuates experimental colitis. *Gut* 59, 896–906. doi:10.1136/gut.2009.203554

Shakeri, F., and Boskabady, M. H. (2017). Anti-inflammatory, antioxidant, and immunomodulatory effects of curcumin in ovalbumin-sensitized rat. *Biofactors* 43, 567–576. doi:10.1002/biof.1364

Sharma, R. A., Gescher, A. J., and Steward, W. P. (2005). Curcumin: the story so far. *Eur. J. Canc.* 41, 1955–1968. doi:10.1016/j.ejca.2005.05.009

Strober, W., Fuss, I., and Mannon, P. (2007). The fundamental basis of inflammatory bowel disease. *J. Clin. Invest.* 117, 514–521. doi:10.1172/JCI30587

Takahara, M., Nemoto, Y., Oshima, S., Matsuzawa, Y., Kanai, T., Okamoto, R., et al. (2013). IL-7 promotes long-term *in vitro* survival of unique long-lived memory subset generated from mucosal effector memory $CD4^+$ T cells in chronic colitis mice. *Immunol. Lett.* 156, 82–93. doi:10.1016/j.imlet.2013.09.001

Tian, Y., Cox, M. A., Kahan, S. M., Ingram, J. T., Bakshi, R. K., and Zajac, A. J. (2016). A context-dependent role for IL-21 in modulating the differentiation, distribution, and abundance of effector and memory CD8 T cell subsets. *J. Immunol.* 196, 2153–2166. doi:10.4049/jimmunol.1401236

Ukil, A., Maity, S., Karmakar, S., Datta, N., Vedasiromoni, J. R., and Das, P. K. (2003). Curcumin, the major component of food flavour turmeric, reduces mucosal injury in trinitrobenzene sulphonic acid-induced colitis. *Br. J. Pharmacol.* 139, 209–218. doi:10.1038/sj.bjp.0705241

Ungaro, R., Mehandru, S., Allen, P. B., Peyrin-Biroulet, L., and Colombel, J. F. (2017). Ulcerative colitis. *Lancet* 389, 1756–1770. doi:10.1016/S0140-6736(16)32126-2

Weingarden, A. R., and Vaughn, B. P. (2017). Intestinal microbiota, fecal microbiota transplantation, and inflammatory bowel disease. *Gut Microb.* 8, 238–252. doi:10.1080/19490976.2017.1290757

Whiteoak, S. R., Claridge, A., Balendran, C. A., Harris, R. J., Gwiggner, M., Bondanese, V. P., et al. (2018). MicroRNA-31 targets thymic stromal lymphopoietin in mucosal infiltrated $CD4^+$ T cells: a role in achieving mucosal healing in ulcerative colitis? *Inflamm. Bowel Dis.* 24, 2377–2385. doi:10.1093/ibd/izy213

Wirtz, S., Popp, V., Kindermann, M., Gerlach, K., Weigmann, B., Fichtner-Feigl, S., et al. (2017). Chemically induced mouse models of acute and chronic intestinal inflammation. *Nat. Protoc.* 12, 1295–1309. doi:10.1038/nprot.2017.044

Xavier, R. J., and Podolsky, D. K. (2007). Unravelling the pathogenesis of inflammatory bowel disease. *Nature* 448, 427–434. doi:10.1038/nature06005

Yoshihara, K., Yajima, T., Kubo, C., and Yoshikai, Y. (2006). Role of interleukin 15 in colitis induced by dextran sulphate sodium in mice. *Gut* 55, 334–341. doi:10.1136/gut.2005.076000

Zhang, M., Deng, C. S., Zheng, J. J., and Xia, J. (2006). Curcumin regulated shift from Th1 to Th2 in trinitrobenzene sulphonic acid-induced chronic colitis. *Acta Pharmacol. Sin.* 27, 1071–1077. doi:10.1111/j.1745-7254.2006.00322.x

Zundler, S., and Neurath, M. F. (2017). Pathogenic T cell subsets in allergic and chronic inflammatory bowel disorders. *Immunol. Rev.* 278, 263–276. doi:10.1111/imr.12544

Conflict of Interest: The authors declare that the research was conducted in the absence of any commercial or financial relationships that could be construed as a potential conflict of interest.

frontiers in Pharmacology

ORIGINAL RESEARCH
published: 04 March 2021
doi: 10.3389/fphar.2020.600175

Liraglutide Alleviates Hepatic Steatosis and Liver Injury in T2MD Rats via a GLP-1R Dependent AMPK Pathway

Rui Zhou[1,3,4†], *Chuman Lin*[1,2†], *Yanzhen Cheng*[2], *Xiaoyun Zhuo*[1,2], *Qinghua Li*[1,2], *Wen Xu*[5], *Liang Zhao*[3,4*] *and Li Yang*[1,2*]

[1]Department of Nutrition, Zhujiang Hospital, Southern Medical University, Guangzhou, China, [2]Department of Endocrinology, Zhujiang Hospital, Southern Medical University, Guangzhou, China, [3]Department of Pathology, Nanfang Hospital, Southern Medical University, Guangzhou, China, [4]Department of Pathology, School of Basic Medical Sciences, Southern Medical University, Guangzhou, China, [5] Department of Endocrinology and Metabolism, Guangdong Provincial Key Laboratory of Diabetology, Third Affiliated Hospital of Sun Yat-sen University, Guangzhou, China

OPEN ACCESS

Edited by:
Predrag Sikiric,
University of Zagreb, Croatia

Reviewed by:
Na Li,
Shanghai Jiao Tong University, China
Gabor Varga,
Semmelweis University, Hungary

***Correspondence:**
Liang Zhao
liangsmu@foxmail.com
Li Yang
yangli19762009@163.com

[†]These authors have contributed equally to this work

Specialty section:
This article was submitted to Gastrointestinal and Hepatic Pharmacology, a section of the journal Frontiers in Pharmacology

Received: 29 August 2020
Accepted: 18 December 2020
Published: 04 March 2021

Citation:
Zhou R, Lin C, Cheng Y, Zhuo X, Li Q, Xu W, Zhao L and Yang L (2021) Liraglutide Alleviates Hepatic Steatosis and Liver Injury in T2MD Rats via a GLP-1R Dependent AMPK Pathway. Front. Pharmacol. 11:600175. doi: 10.3389/fphar.2020.600175

Non-alcoholic fatty liver disease (NAFLD), ranging from non-alcoholic fatty liver to non-alcoholic steatohepatitis, can be prevalent in patients with type 2 diabetes mellitus (T2DM). However, no antidiabetic drug has been approved for the treatment of NAFLD in T2DM patients. Multiple daily injections of basal-bolus insulin are often the final therapeutic option for T2DM. We found that insulin treatment aggravated hepatic steatosis and oxidative stress in Zucker diabetic fatty (ZDF) rats. In addition to glycaemic control, we demonstrated the stimulatory role of liraglutide in relieving hepatic steatosis and liver injury in ZDF rats. Interestingly, liraglutide could also alleviate insulin-aggravated hepatic fatty accumulation. The glucagon-like peptide-1 (GLP-1) agonists liraglutide and Ex-4 activated the expression of peroxisome proliferator-activated receptor alpha (PPARα) via a GLP-1 receptor-dependent 5′ AMP-activated protein kinase pathway. As a nuclear transcription factor, PPARα could mediate the effect of GLP-1 in alleviating hepatic steatosis by differentially regulating the expression of its target genes, including acetyl CoA carboxylase and carnitine palmitoyl transferase Ia both *in vitro* and *in vivo*. Moreover, GLP-1 could relieve liver injury by decreasing oxidative stress stimulated by hepatic steatosis. Insulin might aggravate hepatic steatosis and liver injury by inhibiting GLP-1R expression. The findings indicate the feasibility of liraglutide treatment combined with basal insulin in attenuating hepatic steatosis and liver injury in ZDF rats. This knowledge, and the evidence for the underlying mechanism, provide a theoretical basis for the combination treatment recommended by the latest clinical practice guidelines for T2DM.

Keywords: liraglutide, hepatic steatosis, liver injury, T2DM, PPARα

INTRODUCTION

Diabetes mellitus (DM) is a common non-communicable disease that affects the global population, including an estimated 11.6% of the Chinese adult population (Wang et al., 2017). Approximately 50–70% of diabetics in China have type 2 DM (T2DM). They are more likely to develop non-alcoholic fatty liver disease (NAFLD) (Fruci et al., 2013). NAFLD is strongly related to metabolic risk

factors such as DM, obesity and dyslipidaemia (Cazzo et al., 2018). Diabetes increases the mortality rate of hepatic diseases by accelerating the progression of NAFLD from excessive hepatic fat deposition into non-alcoholic steatohepatitis (NASH), hepatic fibrosis and even hepatic carcinoma (Diehl and Day, 2017).

T2DM is characterized by insulin resistance and lesions of pancreatic beta cells, resulting in a worsening glycaemic control and an increasing use of antidiabetic drugs including insulin (Kahn et al., 2009). If synthetic antidiabetic drugs or basal insulin is unable to achieve glycaemic control, the final therapeutic step is often multiple daily injections of basal-bolus insulin (American Diabetes Association, 2018). However, in most cases, it is still difficult to achieve excellent clinical glycaemic control due to the high risks of hypoglycaemia and weight gain caused by inappropriate insulin dosage. Relief of NAFLD in patients with T2DM is also difficult (Horie et al., 2018). A combination treatment has been suggested by the latest American Association of Clinical Endocrinology/American College of Endocrinology (AACE/ACE) clinical practice guidelines (American Diabetes Association, 2019; Garber et al., 2019).

Glucagon-like peptide-1 (GLP-1) is an incretin hormone that is secreted from intestinal L-cells and circulates through the ingestion of nutrients (Baggio and Drucker, 2007). The pleiotropic functions of GLP-1 in mammals include promoting insulin secretion, suppressing glucagon release, slowing gastric emptying, and minimizing insulin-mediated glucose uptake (Guo et al., 2017). As a new class of antidiabetic drugs, GLP-1 agonists like exenatide and liraglutide are already in use for the clinical treatment of T2DM. In addition to improved glycaemic control, GLP-1 also effectively reduces lipid load and free fatty acid (FFA)-induced liver steatosis (Gupta et al., 2010; Wajcberg and Amarah, 2010; Cuthbertson et al., 2012). The combination treatment with GLP-1 agonists and basal insulin synergistically lowers the level of glucose and reduces postprandial glycaemic excursion (Balena et al., 2013; Campbell and Drucker, 2013; Holst and Vilsboll, 2013). This combination also allows a reduced insulin dosage, lessens the risk of insulin-induced hypoglycaemia, and reduces weight gain. The combination treatment with liraglutide and metformin also was reported to dramatically reduce the body weight and intrahepatic lipid of T2DM patients with NAFLD (Yan et al., 2018). Unfortunately, most of the conclusions came from clinical trials, and the underlying mechanisms remain elusive.

Peroxisome proliferator-activated receptor alpha (PPARα) is a ligand-activated transcription factor of the NR1C nuclear receptor subfamily (Pawlak et al., 2015). In rodents, high PPARα expression has been detected in tissues characterized by a high rate of fatty acid oxidation, including brown adipose tissue, liver, kidney and heart (Escher et al., 2001; Bookout et al., 2006). Hepatic PPARα deletion in mouse models results in impaired fatty acid catabolism and hepatic lipid deposition (Montagner et al., 2016). Several studies have indicated that PPARα is a crucial regulator of lipid metabolism in the liver through the activation of target genes (Kersten et al., 1999; Leone et al., 1999; Hashimoto et al., 2000; Pawlak et al., 2015). In patients with atherogenic dyslipidaemia, synthetic PPARα agonists (fibrates) can lower the levels of plasma triglycerides (TGs) and low-density lipoprotein (LDL) while raising the levels of high-density lipoprotein cholesterol (HDL-C) (Staels et al., 2008).

GLP-1 receptor (GLP-1R) is present on human hepatocytes (Gupta et al., 2010). Thus, GLP-1 might reduce NAFLD in T2DM patients by directly acting on hepatic GLP-1Rs. As well, since PPARα is also highly expressed in human hepatocytes (Kersten and Stienstra, 2017), it is reasonable to hypothesize that PPARα is involved in GLP-1 mediated lipid metabolism in the liver.

In this study, Zucker diabetic fatty (ZDF) mice were treated with the combination of liraglutide and insulin. The effects on hepatic steatosis and liver injury were studied. The involvement of PPARα in GLP-1 mediated amelioration of hepatic steatosis, oxidative stress and liver injury was investigated *in vivo* and *in vitro*. The study explored the feasibility of the liraglutide–insulin combination treatment to alleviating T2DM-induced or insulin aggravated NAFLD and provide the first details of the mechanism of these effects. The findings will inform improvements to clinical practice guidelines for T2DM.

MATERIALS AND METHODS

Animal Studies

Male ZDF rats (Fa/Fa, $n = 30$) and control lean rats (+/Fa, $n = 7$) were obtained from the Laboratory Animal Center of Vital River (Beijing, China; license number, SYXK (Yue) 2011-0074). The average weight of ZDF and lean rats at 8 weeks of age was 286 and 233 g, respectively. Rats were housed in an identical room with free access to a high-fat diet and purified water throughout the experiment. A high-fat diet (Purina 5008, PA) was provided from 8 weeks of age to the end of the study. After four weeks of induction, the glucose levels of the rats ranged between 19.3.3 and 33.3 mmol/L (average 26.53 ± 0.69 mmol/L). At of 12 weeks age, the ZDF rats were randomly divided into four groups: 1) diabetic control group (PC, $n = 7$); 2) diabetic group treated with insulin glargine (INS, $n = 7$); 3) diabetic group treated with the saxagliptin inhibitor dipeptidyl peptidase 4 (DPP-4) (Saxag, $n = 7$); and 4) diabetic group treated with the GLP-1 analogue liraglutide (Lirag, $n = 9$). The normal control group (NC, $n = 7$) and PC group were treated with 0.9% normal saline. Insulin glargine was intravenously injected into the INS group once a day and the dosage was set according to the changes in glucose levels of the Lirag group throughout the experiment. The Saxag group received saxagliptin (AstraZeneca, London, England) by intragastric gavage at a dosage of 5 mg/kg/24 h. The Lirag group was administered liraglutide (Novo Nordisk, Copenhagen, Denmark) at a dose of 200 μg/kg/12 h for 8 weeks, as previously described (Hayes et al., 2011). Glucose levels, body weight and food intake were measured every week. At the age of 20 weeks, the rats were anesthetized with 2.5% pentobarbital sodium and the left ventricular was punctured for blood sampling. The livers of rats were fixed in 4% paraformaldehyde or frozen in liquid nitrogen. All animal experiments were approved by the Institutional Animal Care

and Use Committee of the Southern Medical University (Guangzhou, China).

Cell Culture and Treatment

Normal hepatocytes LO2 and hepatoma HepG2 cells were obtained from the Cell Bank of the Chinese Academy of Sciences (Shanghai, China). Exendin-4 was purchased from MedChemExpress (United States). Exendin Fragment 9-39 (Exendin-9) was obtained from Sigma-Aldrich (United States). All the cells were cultured in DMEM (Invitrogen; Invitrogen; Paisley, United Kingdom) with 10% fetal bovine serum (FBS; Gibco-BRL, Invitrogen; Paisley, United Kingdom) in a 5% CO2 incubator at 37°C. ShPPARα (targeting 5′-GACTCAAGCTGG TGTATGA-3′) was purchased from Sangon Biotech (Shanghai, China). Exponential growth phase cells were transfected with 2.5 μg shPPARα in reduced serum medium (OPTI-MEM-I) according to the manufacturer's protocol at 50–70% confluence. To build the hepatocyte steatosis model, the cells were exposed to sodium palmitate (PA) at a final concentration of 0.3 μM. The cells were divided into the following groups: 1) normal control group (NC): the cells were cultured in DMEM for 24 h; 2) PA group: the cells were exposed to PA (0.3 μM) in DMEM for 24 h; 3) PA + Exendin-4 group (PA + Ex-4): the cells were co-treated with PA (0.3 μM) and Exendin-4 (100 nM) in DMEM for 24 h; 4) PA + Exendin-4+Exendin-9 group (PA + Ex-4+Ex-9): the cells were cultured in PA (0.3 μM) and Exendin-9 (100 nM) for 1 h and were then co-administered with Exendin-4 (100 nM) for 24 h. 5) Insulin group (Insulin): the cells were exposed to Insulin (100 nM) in DMEM for 24 h; 6) PA + Insulin group (PA + Insulin): the cells were co-treated with PA (0.3 μM) and Insulin (100 nM) in DMEM for 24 h; 7) PA + Exendin-4+Insulin group (PA + Ex-4+Insulin): the cells were co-treated with PA (0.3 μM), Exendin-4 (100 nM) and Insulin (100 nM) in DMEM for 24 h; 8) sh PPARα group: the cells transfected with shRNA duplexes targeting PPARα were cultured in DMEM for 48 h; 9) PA + Exendin-4+shPPARα group (PA + Ex-4+shPPARα): the cells transfected with shRNA duplexes targeting PPARα were cultured in DMEM for 48 h and were then co-administered with PA (0.3 μM) and Exendin-4 (100 nM) for 24 h.

Blood Biochemical Analysis

After overnight fasting, blood samples were collected from left ventricular puncturing and subsequently centrifuged at 3,000 rpm for 10 min after standing at room temperature for 3 h. Total cholesterol (mM), triglycerides (mM), HDL cholesterol (mM), LDL cholesterol (mM), AST (IU/L) and ALT (IU/L) were determined by an automated biochemistry analyzer (Cobas Integra 400 Plus; Roche Diagnostics, Basel, Switzerland).

Oral Glucose Tolerance Test

Oral glucose tolerance test was conducted on rats at the age of 20 weeks after an overnight fasting. After testing fasting blood glucose (FBG), rats were intragastrically given glucose solution at 2 g/kg body weight. The blood samples were collected from the rats' tail vein and the plasma glucose was measured by a glucose meter 0, 30, 60, and 120 min after glucose administration. The area under the curve of glucose was calculated using the trapezoidal method (AUC = 1/4 fasting glucose +1/2 30 min glucose +3/4 60 min glucose +1/2 120 min glucose).

Histological and Immunohistochemistry Analysis

Liver tissues were fixed in 4% paraformaldehyde for 24 h and maintained in 70% alcohol for subsequent paraffin embedding. Paraffin sections were cut at a thickness of 3 μm and hematoxylin-eosin (HE) staining was performed after removal of paraffin. The hepatic steatosis of each section was observed by optical microscope using a model BX53 instrument (Olympus, Tokyo, Japan). IHC was performed to investigate the expression of proteins in human hepatic tissues. The sections were incubated overnight with 1:100 dilutions of primary antibodies against PPARα (bs-3614R; Bioss Antibodies, Boston, MA, United States) and GLP-1R (bs-1559R; Bioss) overnight at 4°C. This was followed by incubation with goat anti-rabbit secondary antibody conjugated with 3,3′-diaminobenzidine (DAB) chromogen. Samples were examined by optical microscopy. The slides were reviewed concerning low or high expression in a blinded manner by two pathologists.

Oil Red O Staining

LO2 cells were stained with Oil red O (ORO, Solarbio, Beijing, China) solution to visualize the accumulation of intracellular lipids. In brief, LO2 cells were washed with PBS for three times before fixing with 10% formalin for 20 min. After washing with 60% isopropanol for 5 min, the cells were stained with ORO solution for 20 min at room temperature. Then, the cells were washed by distilled water to remove the excess dyestuff and counterstained with hematoxylin. The red-stained lipid droplets were observed and photographed using a light microscope.

RNA Isolation, Reverse Transcription and Real-Time Quantitative PCR

Total RNA was extracted using Trizol reagent (Invitrogen Life Technologies, Carlsbad, CA, United States) according to the manufacturer's instructions. The total RNA was transcribed into cDNA using PrimeScript RT reagent Kit with gDNA Eraser (DRR047A, TaKaRa). Real-time quantitative PCR (qPCR) was carried out using SYBR Green PCR master mix (Applied Biosystems; Foster City, CA) on ABI 7500HT system. GAPDH was chosen as endogenous control. All the primers shown in **Table 1** were synthesized from Sangon Biotech (Shanghai, China). The expression level of each targeted gene was normalized as fold change compared to control or reference group. Fold changes were calculated through relative quantification ($2^{-\Delta\Delta CT}$).

Western-Blot Analysis

Western blot analysis was conducted to investigate the expression of proteins and their phosphorylation level in hepatic tissues and cells. Hepatic tissues were ground into powders with liquid

TABLE 1 | The primers sequences used for real-time quantitive PCR.

Genes	Forward primer	Reverse primer
$PPAR\alpha^{H}$	ATGGTGGACACGGAAAGCC	CGATGGATTGCGAAATCTCTTGG
$PPAR\alpha^{M}$	AAGGGCTTCTTTCGGCGAAC	TGACCTTGTTCATGTTGAAGTTCTTCA
$CPT1a^{H}$	CCTCCAGTTGGCTTATCGTG	TTCTTCGTCTGGCTGGACAT
$CPT1a^{M}$	TTGGGCCGGTTGCTGAT	GTCTCAGGGCTAGAGAACTTGGAA
$ACC^{H\ and\ m}$	ATGTCTGGCTTGCACCTAGTA	CCCCAAAGCGAGTAACAAATTCT
$GAPDH^{H}$	AAGGTCGGAGTCAACGGATTTG	CCATGGGTGGAATCATATTGGAA
$GAPDH^{M}$	GAACATCATCCCTGCATCCA	CCAGTGAGCTTCCCGTTCA

[H], Human; [M], Mouse.

nitrogen and hepatic cells were homogenized in RIPA lysis buffer (1% leagene PMSF, 1% protease and Phosphatase Inhibitor Cocktail). Proteins extracted from each group were separated by SDS-PAGE and transferred to PVDF membranes. Nonspecific binding was blocked using a blocking reagent (0.1% Tween 20 and 5% Bovine Serum Albumin in TBS) and the membranes were then incubated with specific primary antibodies overnight at 4°C. Primary antibodies (1:1000) used in this manuscript are: anti-AMPK alpha 1 and anti-p-AMPK alpha 2 (S345) obtained from Biohua (Hangzhou, China); anti-GAPDH purchased from Santa Cruz (Biotechnology, Santa Cruz, CA, United States); anti-PPARα obtained from Proteintech (Chicago, CA, United States), anti-ACC was obtained from Abcam (Cambridge, England); anti-GLP-1R (Beijing, China, Bioss), and anti-p-ACC purchased from Affinity Biosciences (OH, United States). After incubating the membrane with the appropriate secondary antibodies for 1 h at room temperature, Perkinelmer western lightning Plus-ECL was used to detect the specific bands. The immunoblots were quantified by densitometric analysis using Quantity One software (Bio-Rad, Hercules, United States).

Reactive Oxygen Species Assessment

Intracellular accumulation of ROS was measured using a Reactive Oxygen Species assay kit (Beyotime Institute of Biotechnology) containing fluorescent probe, 2′,7′-dichloro-dihydro-fluorescein diacetate (DCFH-DA). In brief, cells were seeded in serum-free medium containing 10 μM DCFH-DA (v/v, 1:1,000) and incubated at 37°C for 30 min. The residual DCFH-DA solution was removed and cells were washed with serum-free medium three times for 5 min, and then washing with PBS. Cells were observed under a fluorescence microscope (Olympus Corporation). Moreover, intracellular fluorescence intensity were analyzed by flow cytometry (FACSCalibur, Becton–Dickinson, United States) in PBS dissolved 10,000 cells of each sample. The total intracellular ROS level is calculated as the percentage of control cells and is directly proportional to the fluorescence intensity.

Immunofluorescence

Immunofluorescence staining was performed according to the standard protocol described previously (Liao et al., 2017). Polyclonal rabbit primary antibody to GLP-1R (Bioss, bs-1559R; 1:100), HRP-conjugated secondary antibody and DAB staining kit (CWBIO, Beijing, China) were used in the experiment. Images were captured with a laser confocal microscope (FV10-ASW, Olympus, Tokyo, Japan).

Apoptosis Assay and TUNEL Assay

Propidium iodide (PI) and Annexin V-FITC-flow cytometry assay (BD Pharmingen, CA) was used to detect the apoptosis in the cells. Cells were stained with FITC-conjugated annexin V and PI (KeyGEN BioTECH, China, KGA107) according to the manufacturer's instructions. After staining, the cells were analyzed by flow cytometry (FACS Calibar; Becton-Dickinson) using Cell Quest software.

TUNEL assay was processed using the *in situ* cell death detection kit (KeyGEN BioTECH, China, KGA7071). Hepatic tissues were stained according to the manufacturer's instructions. The apoptosis index was captured using a fluorescence microscope (Olympus IX73, Japan).

Statistical Analyses

Data were analyzed using SPSS version19.0 (SPSS, Chicago, IL, United States). The Student's t-test and one-way ANOVA test were carried out for RT-PCR. Statistical significance was set at $p < 0.05$.

RESULTS

Liraglutide Improves Glycaemic Control of Zucker Diabetic Fatty Rats

To confirm the effects of GLP-1 on glycaemic control, both liraglutide and saxagliptin (dipeptidyl peptidase 4 inhibitor, which can increase the secretion of endogenous GLP-1), were used to treat ZDF rats. The food intake of both compounds resulted in decreased food intake at most time points, especially 4 weeks after antidiabetic drug treatment (**Figure 1A**, first panel). At the end of the treatment, the cumulative food intake of ZDF rats treated with liraglutide and saxagliptin had increased to a level similar to that of the positive control group. However, the food intake of the liraglutide group remained lower than that of the other groups.

The body weights of ZDF rats were higher than those of lean rats at all time points. Insulin significantly and continuously produced an increased weight gain of the ZDF rats. Notably, liraglutide decreased the weight of ZDF rats, especially after

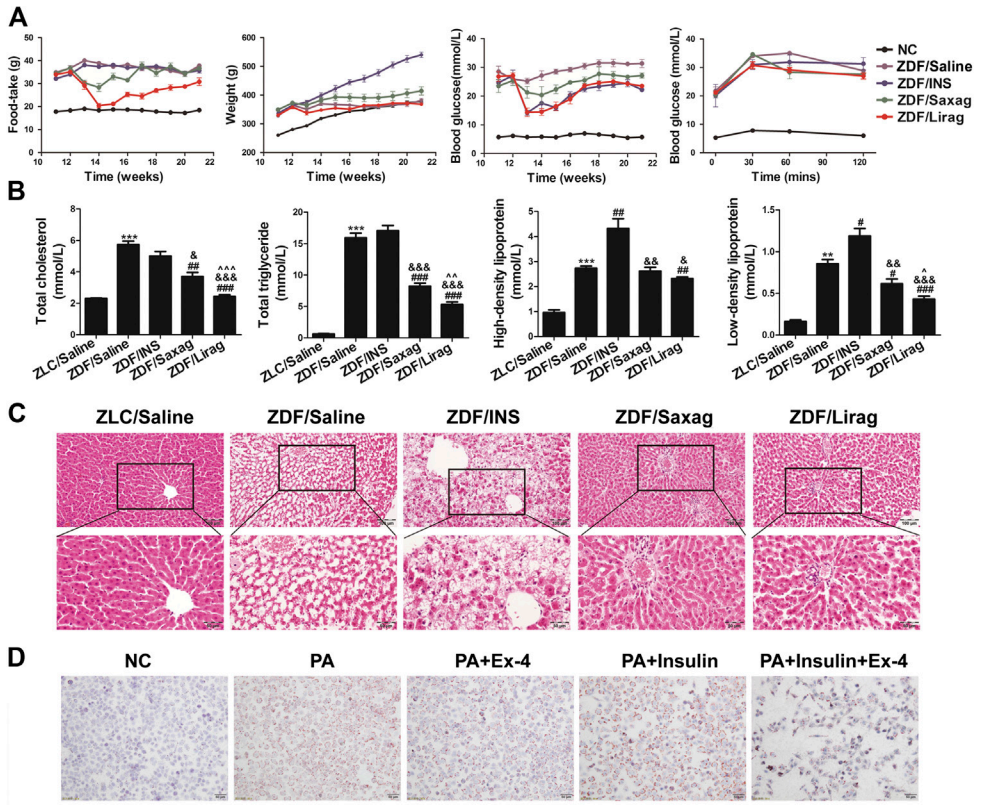

FIGURE 1 | Liraglutide improves the glycemic control and alleviates hepatic steatosis of ZDF rats. **(A)** Foodtake, body weight, blood glucose and glucose tolerate of lean and indicated ZDF rats. **(B)** Serum lipid profiles of lean and indicated ZDF rats ($^{*}p < 0.05$, $^{**}p < 0.01$, $^{***}p < 0.001$ vs. ZLC group; $^{\#}p < 0.05$, $^{\#\#}p < 0.01$, $^{\#\#\#}p < 0.001$ vs. ZDF/saline group; $^{\&}p < 0.05$, $^{\&\&}p < 0.01$, $^{\&\&\&}p < 0.001$ vs. ZDF/INS group; $\hat{}p < 0.05$, $\hat{}p < 0.01$, $\hat{}p < 0.001$ vs. ZDF/Lirag group). **(C)** HE staining of hepatic tissues of lean and indicated ZDF rats. **(D)** Oil O staining indicates the lipid accumulation in indicated hepatic cells.

9 weeks of treatment (**Figure 1A**, second panel). However, a similar decrease in body weight was not detected in ZDF rats treated with saxagliptin.

As expected, blood glucose levels increased significantly in ZDF rats compared with lean rats. Insulin, liraglutide and saxagliptin dramatically alleviated the blood glucose level in ZDF rats (**Figure 1A**, third panel). The oral glucose tolerance test analysis showed that lean rats were tolerant to glucose, whereas ZDF rats had an impaired tolerance to glucose (**Figure 1D**). Although the fasting glucose levels in all ZDF rats subjected to different treatments were the same, liraglutide-treated rats showed a significant decrease the glucose level at each time point after oral glucose intake (**Figure 1A**, fourth panel). Saxagliptin also improved glucose tolerance in ZDF rats.

Liraglutide Alleviates Hepatic Steatosis *in vivo* and *in vitro*

We also examined serum lipid profiles that included total cholesterol (TC), TG, LDL-cholesterol (LDL-C), and HDL-C in ZDF and lean rats, including. Administration of liraglutide and saxagliptin decreased the levels of TC, TG, and LDL-C in ZDF rats. The effects of liraglutide were more dramatic than those of saxagliptin (**Figure 1B**). Both liraglutide and saxagliptin slightly decreased HDL-C levels (**Figure 1B**, third panel). Conversely, insulin dramatically increased the levels of LDL-C and HDL-C in ZDF rats. The livers of ZDF and lean rats were dissected and observed by optical microscopy after HE staining. Compared with lean rats, ZDF rats exhibited severe hepatic steatosis. To our surprise, big and confluent regions of lipid were detected in the liver of insulin treated ZDF mice. In these mice, hepatic steatosis was more severe compared to control ZDF rats. Administration of liraglutide and saxagliptin completely prevented the establishment of hepatic steatosis (**Figure 1C**). The GLP-agonist Ex-4 significantly alleviated PA induced lipid accumulation in LO2 cells (**Figure 1D**). Similar to *in vivo* experiments, insulin aggravated PA induced lipid accumulation, while Ex-4 dramatically relieved the insulin aggravated lipid accumulation.

Liraglutide Alleviates Hepatic Injury by Reducing Oxidative Stress

The levels of aspartate aminotransferase (AST) and alanine aminotransferase (ALT) levels were detected in the blood serum of ZDF and lean rats to study liver injury. Liraglutide treatment produced decreased levels of AST and ALT levels in

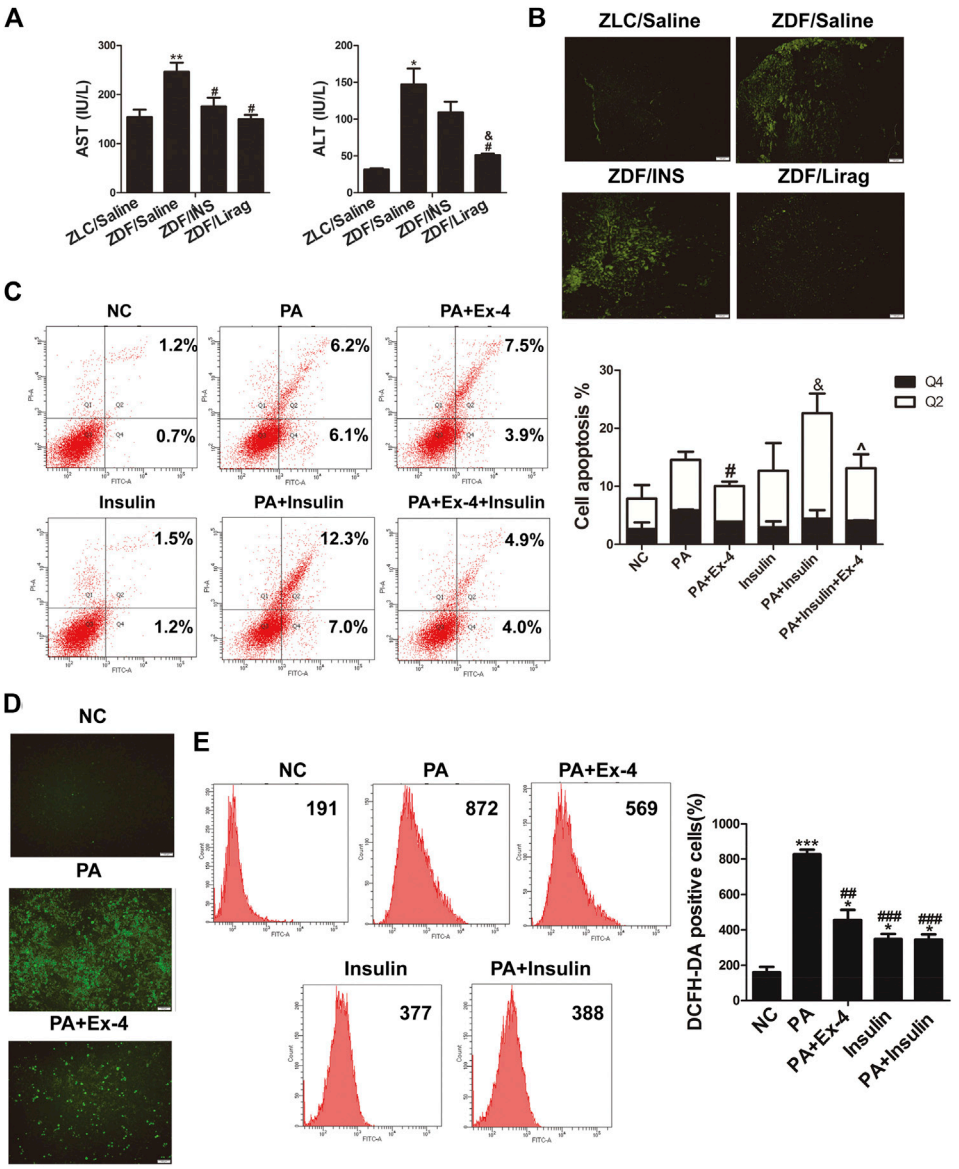

FIGURE 2 | Liraglutide alleviates hepatic steatosis through increasing oxidative stress. **(A)** AST and ALT levels in the serum of lean and indicated ZDF rats ($^{*}p < 0.05$, $^{**}p < 0.01$, $^{***}p < 0.001$ vs. ZLC group; $^{\#}p < 0.05$, $^{\#\#}p < 0.01$, $^{\#\#\#}p < 0.001$ vs. ZDF/saline group; $^{\&}p < 0.05$, $^{\&\&}p < 0.01$, $^{\&\&\&}p < 0.001$ vs. ZDF/INS group; $\hat{p} < 0.05$, $\hat{p} < 0.01$, $\hat{p} < 0.001$ vs. ZDF/Lirag group). **(B)** TUNEL assay shows the liver injury of lean and indicated ZDF rats. **(C)** Annexin V-FITC/PI flow cytometry assay shows the effects of Ex-4 on PA induced apoptosis. Bars on the right panel represent percentage of cells in Q2+Q4 ($^{*}p < 0.05$, $^{**}p < 0.01$, $^{***}p < 0.001$ vs. NC group; $^{\#}p < 0.05$, $^{\#\#}p < 0.01$, $^{\#\#\#}p < 0.001$ vs. PA group; $^{\&}p < 0.05$, $^{\&\&}p < 0.01$, $^{\&\&\&}p < 0.001$ vs. PA + Ex-4 group; $\hat{p} < 0.05$, $\hat{p} < 0.01$, $\hat{p} < 0.001$ vs. shPPARα group). **(D)** DCFH-DA signals indicate the ROS level in indicated hepatic cells. **(E)** Flow cytometry shows DCFH-DA positive cells in indicated PA treated hepatic cells. Bars on the right panel represent DCFH-DA positive cells ($^{*}p < 0.05$, $^{**}p < 0.01$, $^{***}p < 0.001$ vs. NC group; $^{\#}p < 0.05$, $^{\#\#}p < 0.01$, $^{\#\#\#}p < 0.001$ vs. PA group).

ZDF rats, while only AST levels were significantly downregulated in the insulin treated group (**Figure 2A**). The terminal deoxynucleotidyl transferase dUTP nick end labeling (TUNEL) assay was also performed on hepatic tissues of ZDF and lean rats. Compared with lean rats, the apoptosis of liver cells was dramatically increased in ZDF rats. Administration of liraglutide completely abolished the apoptosis of liver cells in ZDF rats (**Figure 2B**). Flow cytometry assays indicated that incubation in the presence of PA dramatically increased the apoptosis of LO2 cells, while Ex-4 significantly alleviated PA induced apoptosis (**Figure 2C**). Although insulin did not influence the apoptosis of liver cells, it aggravated PA induced hepatic cell apoptosis.

Increased oxidative stress has been identified as a major cause of liver injury (Lirussi et al., 2007). A reactive oxygen species (ROS) assay kit was used to detect the ROS level in LO2 cells with different treatments. PA treated hepatic cells displayed more intense DCFH-DA signals compared with the control group

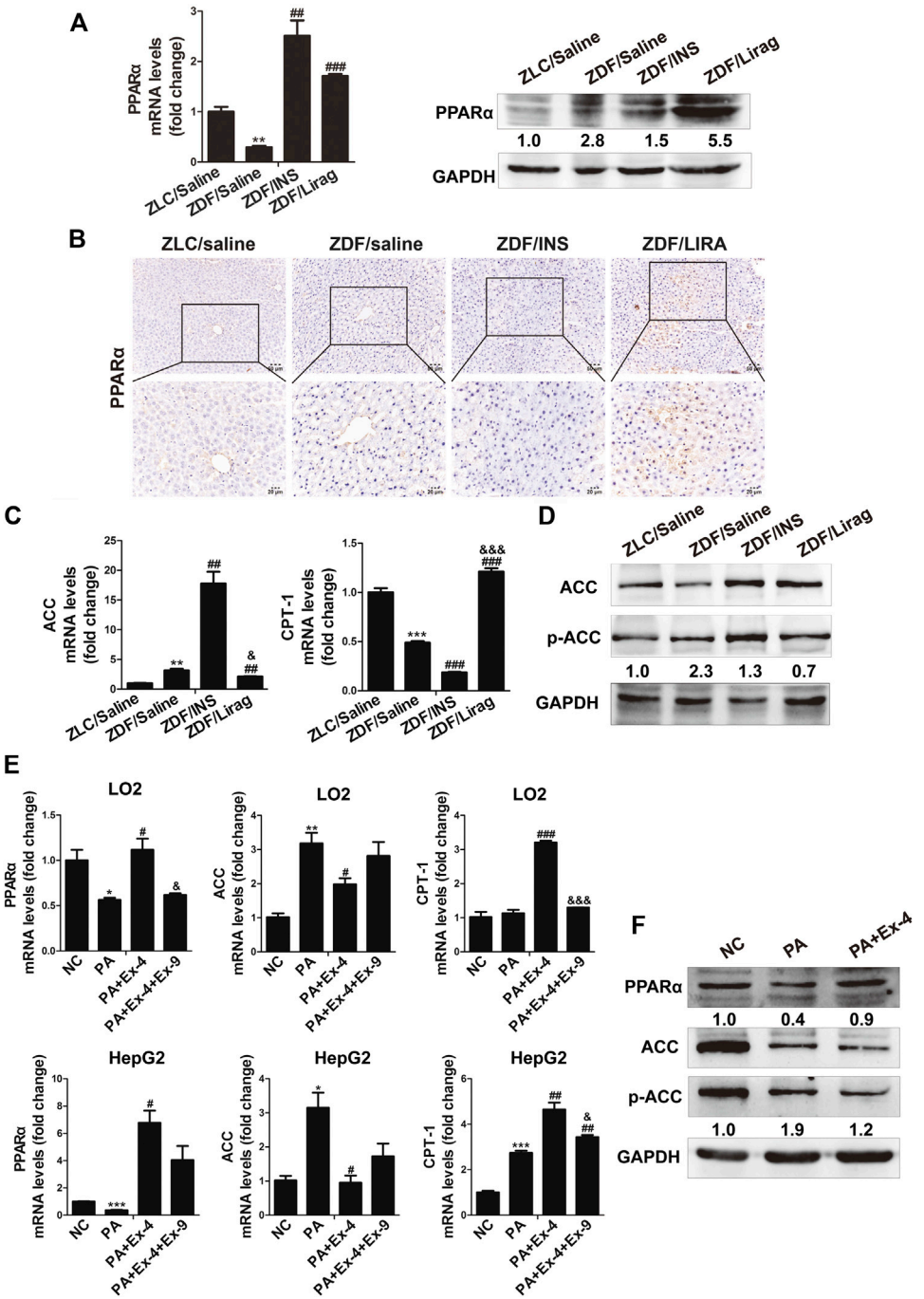

FIGURE 3 | PPARα mediates GLP-1 induced lipid metabolism both *in vivo* and *in vitro*. **(A)** Real-time PCR and western blot detects the expression of PPARα in the hepatic tissues of lean and indicated ZDF rats (*$p < 0.05$, **$p < 0.01$, ***$p < 0.001$ vs. ZLC group; #$p < 0.05$, ##$p < 0.01$, ###$p < 0.001$ vs. ZDF/saline group). **(B)** IHC staining shows the expression of PPARα in the hepatic tissues of lean and indicated ZDF rats. **(C)** Real-time PCR shows the expression of ACC and CPT-1 in the hepatic tissues of lean and indicated ZDF rats (*$p < 0.05$, **$p < 0.01$, ***$p < 0.001$ vs. ZLC group; #$p < 0.05$, ##$p < 0.01$, ###$p < 0.001$ vs. ZDF/saline group; &$p < 0.05$, &&$p < 0.01$, &&&$p < 0.001$ vs. ZDF/INS). **(D)** Western blot shows the expression of ACC and p-ACC in the hepatic tissues of lean and indicated ZDF rats. **(E)** Real-time PCR and western blot shows the expression of ACC and CPT-1 in LO2 and HepG2 cells (*$p < 0.05$, **$p < 0.01$, ***$p < 0.001$ vs. NC group; #$p < 0.05$, ##$p < 0.01$, ###$p < 0.001$ vs. PA group; &$p < 0.05$, &&$p < 0.01$, &&&$p < 0.001$ vs. PA + Ex-4 group).

when examined by fluorescence microscopy. Liraglutide dramatically reduced the DCFH-DA signals in the PA treated hepatic cells (**Figure 2D**). Flow cytometry indicated that Ex-4 remarkably reduced the number of DCFH-DA-positive cells in PA treated hepatic cells. Insulin dramatically increased oxidative stress (**Figure 2E**).

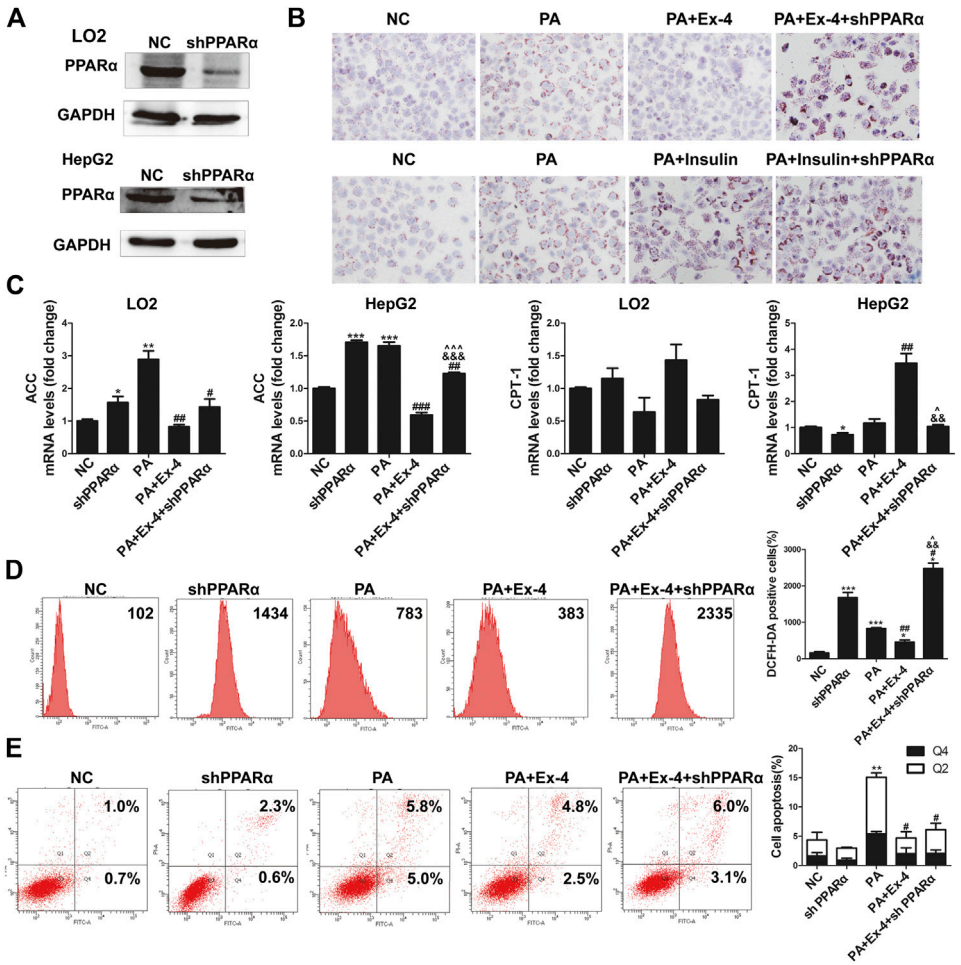

FIGURE 4 | Silencing PPARα aggravates PA increased of oxidative stress and hepatic cell apoptosis. **(A)** Western blot indicates that shPPARα reduced the expression of PPARα in hepatic cells. **(B)** Oil Red O staining shows that shPPARα reversed the Ex-4 alleviated lipid accumulation in hepatic cells. **(C)** Real-time PCR shows that shPPARα reversed the effects of Ex-4 on the expression of ACC and CPT-1 ($^{*}p < 0.05$, $^{**}p < 0.01$, $^{***}p < 0.001$ vs. NC group; $^{\#}p < 0.05$, $^{\#\#}p < 0.01$, $^{\#\#\#}p < 0.001$ vs. PA group; $^{\&}p < 0.05$, $^{\&\&}p < 0.01$, $^{\&\&\&}p < 0.001$ vs. PA + Ex-4 group; $\hat{p} < 0.05$, $\hat{p} < 0.01$, $\hat{p} < 0.001$ vs. shPPARα group). **(D)** Flow cytometry shows DCFH-DA positive cells indicate that shPPARα reversed the Ex-4 suppressed ROS level in indicated hepatic cells. Bars on the right panel represent the DCFH-DA positive cells ($^{*}p < 0.05$, $^{**}p < 0.01$, $^{***}p < 0.001$ vs. NC group; $^{\#}p < 0.05$, $^{\#\#}p < 0.01$, $^{\#\#\#}p < 0.001$ vs. PA group; $^{\&}p < 0.05$, $^{\&\&}p < 0.01$, $^{\&\&\&}p < 0.001$ vs. PA + Ex-4 group; $\hat{p} < 0.05$, $\hat{p} < 0.01$, $\hat{p} < 0.001$ vs. shPPARα group). **(E)** Annexin V-FITC/PI flow cytometry assay showed the effects of shPPARα on Ex-4 suppressed apoptosis. Bars on the right panel represent percentage of cells in Q2+Q4 ($^{*}p < 0.05$, $^{**}p < 0.01$, $^{***}p < 0.001$ vs. NC group; $^{\#}p < 0.05$, $^{\#\#}p < 0.01$, $^{\#\#\#}p < 0.001$ vs. PA group).

PPARα Mediates GLP-1 Induced Lipid Metabolism *In Vivo* and *In Vitro*

PPARα is a nuclear transcription factor that can activate the expression of enzymes related to fat metabolism (Pawlak et al., 2015). To confirm the involvement of PPARα in GLP-1 induced metabolism, the expression of PPARα and its target genes were detected in ZDF and lean rats. The RNA expression of PPARα was dramatically decreased in the liver of ZDF rats compared with that in lean rats. Although the expression of PPARα was increased in the liver of insulin- and liraglutide-treated ZDF rats at the transcriptional level, PPARα protein was only overexpressed in the liraglutide group (**Figure 3A**). This was confirmed by IHC data. Compared with lean rats, stronger PPARα staining was detected in liver sections of liraglutide-treated ZDF rats (**Figure 3B**). The expression of acetyl CoA carboxylase (ACC) and carnitine palmitoyl transferase la (CPT1a), two PPARα targeting genes related to fat metabolism, were studied in both hepatic tissues and cell lines. The liraglutide group showed decreased hepatic expression of ACC and p-ACC, but increased expression of CPT1a. In contrast, insulin stimulated the hepatic expression of ACC and p-ACC, but inhibited that of CPT1a (**Figure 3C,D**). In PA treated LO2 and HepG2 cells, administration of Ex-4 dramatically stimulated the expression of PPARα and its target gene CPT1a, and inhibited the expression of ACC (**Figure 3E,F**). The GLP-1 antagonist Ex-9 reversed the effects of Ex-4 on the expression of ACC and CPT1a.

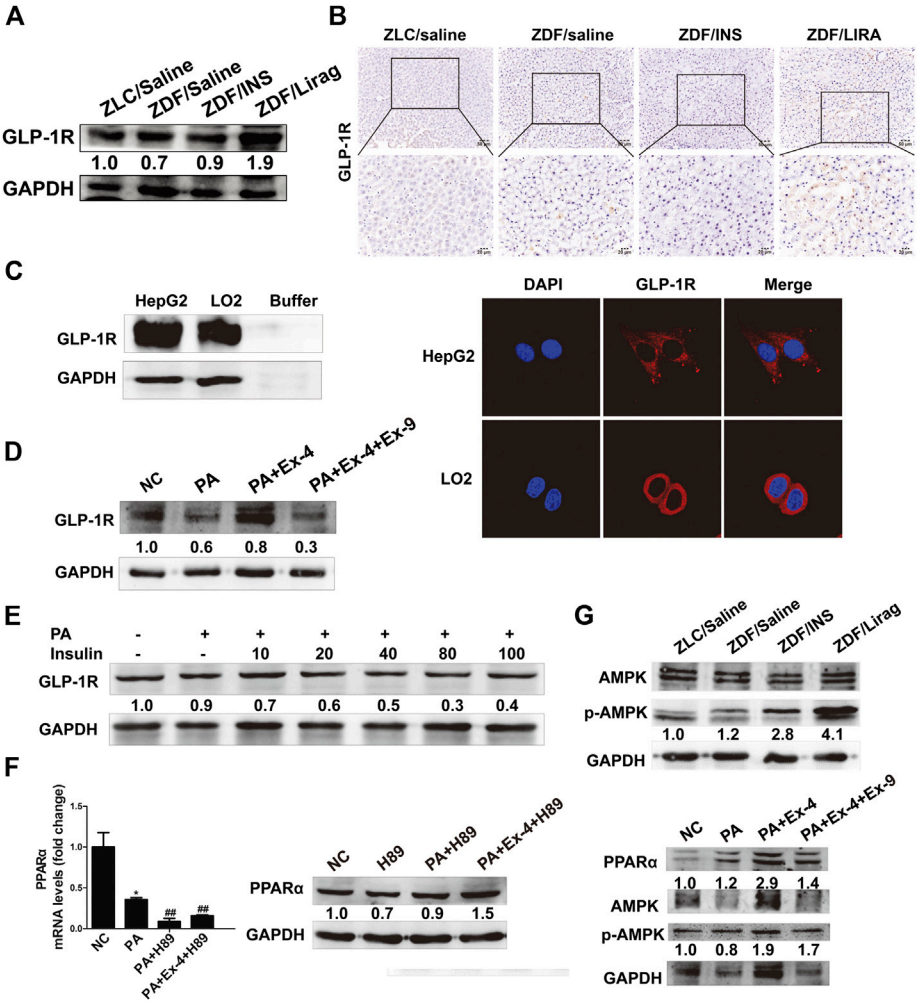

FIGURE 5 | GLP-1 regulates lipid metabolism and liver injury via a GLP-1R-dependent AMPK signaling pathway. **(A)** Western blot shows the expression of GLP-1R in the hepatic tissues of lean and indicated ZDF rats. **(B)** IHC staining shows the expression of GLP-1R in the hepatic tissues of lean and indicated ZDF rats. **(C)** Western blot and immunofluorescence staining shows the expression of GLP-1R in hepatic cell lines. **(D)** The expression of GLP-1 in Ex-4 and Ex-9 treated hepatic cells. **(E)** The expression of GLP-1R after insulin treatment. **(F)** Real-time PCR and western blot assay shows the expression of PPARα after the treatment of H89 ($^{*}p < 0.05$, $^{**}p < 0.01$, $^{***}p < 0.001$ vs. NC group; $^{\#}p < 0.05$, $^{\#\#}p < 0.01$, $^{\#\#\#}p < 0.001$ vs. PA group). **(G)** Western blot assay shows the activation of AMPK signaling in lean rats, indicated ZDF rats and hepatic cells.

PPARα Silencing Inhibits the Effects of GLP-1 on Lipid Metabolism, Oxidative Stress and Hepatic Cell Apoptosis *In Vitro*

To further confirm the mediating role of PPARα in GLP-1 stimulated hepatic lipid metabolism, we silenced PPARα using short hairpin (sh)PPARα in LO2 and HepG2 cells. Administration of shPPARα dramatically inhibited the expression of PPARα protein in both cell lines (**Figure 4A**). Silencing of PPARα removed the inhibitory effect of GLP-1 on lipid accumulation in hepatic cells (**Figure 4B**, upper panel). Silencing of PPARα also aggravated insulin stimulated lipid accumulation in hepatic cells (**Figure 4B**, lower panel). Moreover, the basal expression of ACC was increased and CPT1a was decreased in the two hepatic cell lines when PPARα was silenced. Knockdown of PPARα suppressed the Ex-4 stimulated expression of CPT1a, while stimulation of Ex-4 inhibited the expression of ACC in hepatic cells (**Figure 4C**).

As detected by the ROS assay, silencing of PPARα reversed the Ex-4 suppressed oxidative stress, and the number of DCFH-DA-positive cells in the shPPARα group was even larger than that in the PA group (**Figure 4D**). Flow cytometry revealed that silencing of PPARα reversed the Ex-4 rescued apoptosis of hepatic cells (**Figure 4E**).

GLP-1R-Dependent AMPK Signaling Pathway Is Involved in GLP-1 Regulated Lipid Metabolism and Liver Injury

GLP-1 receptor expression was confirmed in both hepatic tissues and cells. Among the ZDF rats, the liraglutide group showed the highest expression of GLP-1R (**Figure 5A**). IHC staining of GLP-

1R showed the same trends of expression in lean rats and ZDF rats with different treatments (**Figure 5B**). High GLP-1R expression was also detected in LO2 and HepG2 cells detected by western blot and immunofluorescence staining (**Figure 5C**). Ex-4 dramatically stimulated the expression of GLP-1R in hepatic cells, while Ex-9 totally abolished the Ex-4 induced GLP-1R increase (**Figure 5D**). The PA diet suppressed the expression of GLP-1R. Interestingly, insulin significantly inhibited the expression of GLP-1R in a dose-dependent manner (**Figure 5E**). H89, an inhibitor of protein kinase A, blocked the basal and Ex-4 stimulated expression of PPARα (**Figure 5F**). The AMPK pathway is involved in GLP-1R mediated downstream signaling both *in vivo* and *in vitro*. AMPK signaling was active in the hepatic tissues of liraglutide-treated ZDF rats compared with lean rats and other antidiabetic drug treated ZDF rats (**Figure 5G**, upper panel). Consistent with this, Ex-9 completely blocked the Ex-4 activated AMPK signaling (**Figure 5G**, lower panel).

DISCUSSION

NAFLD is a common liver disease worldwide, ranging from NAFL to NASH. Fatty liver may not severely disturb liver functions. However, steatohepatitis combined with inflammation and fibrosis can progress to liver damage with many complications (Friedman et al., 2018). Accumulating evidence indicates that T2DM is closely associated with NAFLD. T2DM has been identified in 23 and 47% of patients with NAFL and NASH, respectively (Younossi et al., 2016). No effective pharmacotherapy has been approved for NAFLD, let alone T2DM with NAFLD. The use of GLP-1 agonist as a novel antidiabetic drug can alleviate lipid accumulation and inflammation in hepatocytes (Cuthbertson et al., 2012; Wang et al., 2014; Xu et al., 2014). However, the underlying mechanisms are not fully understood.

Directly modified from native GLP-1, liraglutide shares 97% homology with native GLP-1, and could successfully protract the GLP-1 activity, resist DPP4 activity and limit renal clearance (Aroda, 2018). In our previous study, besides reducing blood glucose, the protective role of liraglutide in different organs, including the bone, heart, kidney and liver were studied (Yang et al., 2020). Besides glycaemic control, histological studies indicated that liraglutide could also dramatically alleviate fatty liver in ZDF rats. To our surprise, ZDF rats in the insulin group, which acted as a control to remove the influence of blood glucose, displayed severe hepatic steatosis without significantly influencing food intake compared with the control ZDF rats. As the combination treatment tends to be the most promising solution suggested by the latest AACE/ACE clinical practice guidelines, we proposed that the combined liraglutide and insulin treatment might alleviate insulin aggravated hepatic steatosis. As expected, our results indicated that liraglutide could dramatically alleviate the insulin aggravated fatty liver *in vitro*. Although the role of liraglutide in alleviating hepatic fatty accumulation has been controversial, the idea is consistent with a recent reports that described that liraglutide combined with metformin significantly reduced body weight and intrahepatic lipid and visceral adipose tissue in patients with T2DM and NAFLD (Tang et al., 2015; Yan et al., 2018). Despite the fact that insulin reduces total liver fat in a previous clinical trial, it is still reasonable to believe that insulin, as a recognized anabolism stimulator, is associated with weight gain and could increase hepatic fatty synthesis by activating lipogenic and glycolytic enzymes (Tilg and Moschen, 2008; Tang et al., 2015; Smits et al., 2016).

Clinically, liraglutide could reduce body weight and hepatic fatty accumulation (Kelly et al., 2020). However, researches on the underlying mechanisms are still limited. Liraglutide treatment could improve insulin sensitivity, accompanied with the reduced expression of the phosphorylated Acetyl-CoA carboxylase-2 and upregulation of long chain acyl CoA dehydrogenase (LCAD) (Zhou et al., 2019). The administration of liraglutide could activate the expression and downstream signaling of GLP-1R (Kushima et al., 2017; Cheng et al., 2019). GLP-1 receptor belongs to a class B G-protein-coupled receptor family that signals primarily through the stimulatory G protein Gs, and activates the protein kinase A (PKA), extracellular signal-regulated kinase (ERK)1/2 and phosphoinositol 3 kinase (PI3K)/protein kinase B (PKB) (Thorens, 1992; Arnette et al., 2003; Briaud et al., 2003; Zhang et al., 2017). The expression of GLP-1R have been demonstrated in many tissues and organs, such as adipocyte, hepatocyte and endothelial cells (Kushima et al., 2017). Consistently, we confirmed the expression of GLP-1R and the GLP-1 (liraglutide or Ex-4) upregulated expression of GLP-1R in hepatic tissues and cells. Meanwhile, PKA signaling directly downstream of GLP-1R is also activated, indicating a direct involvement of hepatic GLP-1R in GLP-1 mediated alleviation of fatty liver and liver injury. In this study, we also demonstrated the inhibition of hepatic GLP-1R by insulin for the first time. Thus, insulin might stimulate hepatic fatty deposition and liver injury by blocking GLP-1R mediated hepatic lipolysis. The heterotrimeric protein AMPK, consisting of a catalytic α and regulatory β and γ subunits, is ubiquitously expressed and plays a pivotal role as a regulator of energy homeostasis, such as mitochondrial biogenesis, fatty acid synthesis and glucose uptake (Hardie et al., 2012). Liraglutide could activate the AMPK during glucose transportation (Andreozzi et al., 2016). AMPK signaling is also involved in liraglutide stimulated fatty degradation in both hepatic and adipose tissues (He et al., 2016; He et al., 2020). DPP4 inhibitor, which could inhibit the degradation of endogenous GLP-1, can stimulate the activation of AMPK and fatty degeneration in adipocyte (Cheng et al., 2019). In our current study, we confirmed the involvement of AMPK signaling in liraglutide stimulated fatty degradation.

The balance between fatty synthesis and lipolysis, which is catalyzed by related enzymes, determines fatty accumulation in the liver. PPARα is a ligand-activated transcription factor that along with PPARδ and PPARγ belongs to the NRIC nuclear receptor subfamily (Pawlak et al., 2015). PPARα can activate lipid metabolism by stimulating the metabolism of fat by peroxisomal and mitochondrial fatty acid β-oxidation and microsomal ω-oxidation (Misra and Reddy, 2014; Kersten and Stienstra, 2017). PPARs can also activate the metabolism of carbohydrates and lipids by regulating its target genes, including UCP2, HSL, CPT1 and ACC (Li et al., 2019). Presently, PPARα was overexpressed in the liver of liraglutide- and saxagliptin-treated ZDF rats. Oil Red O staining

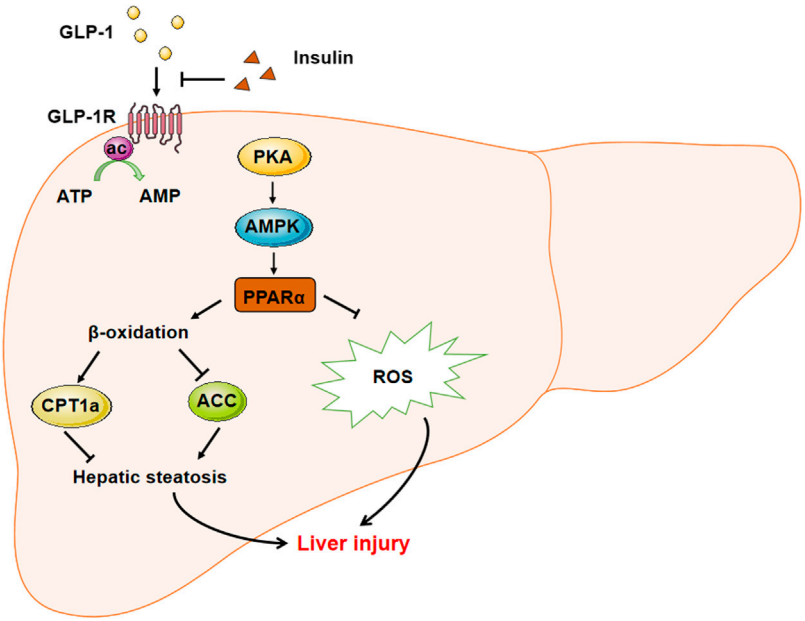

FIGURE 6 | The sketch map demonstrated the mechanism involved in liraglutide alleviated hepatic steatosis and liver injury. GLP-1 agonist liraglutide could directly act on hepatic GLP-1R to stimulate the expression of PPARα through activating the PKA-AMPK signaling pathway. PPARα could stimulate the β-oxidation to relieve hepatic steatosis through stimulating the expression of CPT1a and decreasing that of ACC. Meanwhile, PPARα could also decrease the intracellular ROS level to alleviate the liver injury. On the other hand, insulin could suppress the expression of GLP-1R to inhibit its downstream signaling, while the administration of GLP-1 could recover the insulin aggravated hepatic steatosis.

demonstrated that shPPARα could relieve the PA induced hepatic fatty deposition, indicating a role in mediating GLP-1 mediated remission of fatty liver. Moreover, Ex-4 stimulated the expression of PPARα and its downstream CPT1a, while inhibiting the expression of its downstream ACC. Administration of the GLP-1 antagonist Ex-9 abolished the effects of Ex-4 on PPARα, CPT1a and ACC. Consistent with previous studies (Ip et al., 2003; Gervois et al., 2004), our findings strengthened the mediatory role of PPARα in liraglutide ameliorated fatty accumulation, and confirm the potential of PPARα as a drug target in the management of NAFLD.

Liver injury manifested by hepatic cell apoptosis was also observed in ZDF rats and PA treated liver cells. Liraglutide remarkably reduced apoptosis in hepatic tissues of ZDF rats. Oxidative stress contributes to liver injury. The GLP-1 agonist Ex-4 dramatically reduced the ROS level in PA treated hepatic cells, whereas insulin increased the basal ROS level. This is because insulin increased hepatic steatosis could also elevate the ROS level. TUNEL and flow cytometry analyses demonstrated an inhibitory role of liraglutide in liver apoptosis *in vivo* and *in vitro*. Although insulin did not stimulate basal hepatic cell apoptosis, it aggravated PA induced liver injury. Blockage of GLP-1R by Ex-9 dramatically restored the Ex-4 reduced ROS levels and liver cell apoptosis, indicating that GLP-1 reduced liver cell apoptosis by decreasing ROS levels. Moreover, we also revealed the mediatory role of PPARα in alleviating liver injury.

In summary, this study is the first exploration of the liraglutide and insulin combination treatment to alleviate the basal insulin aggravated NAFLD in T2DM. The underlying mechanism was also clarified (**Figure 6**). PPARα mediated the GLP-1-regulated fatty metabolism as a transcription factor, and alleviated liver injury by reducing ROS-related apoptosis. Our findings also provide the first evidence of the inhibitory role of insulin on the basal expression of GLP-1R, which might explain why liraglutide could alleviate the insulin aggravated hepatic steatosis. The data provide a theoretical basis for the clinical use of liraglutide combination to treat T2DM.

DATA AVAILABILITY STATEMENT

The original contribution presented in the study are included in the article/Supplementary Material, further inquries can be directed to the corresponding authors.

ETHICS STATEMENT

The animal study was reviewed and approved by the Institutional Animal Care and Use Committee of Southern Medical University (Guangzhou, China).

AUTHOR CONTRIBUTIONS

All authors listed have made a substantial, direct, and intellectual contribution to the work and approved it for publication.

FUNDING

This work was supported by grants from the National Natural Science Foundation of China (Grant Nos. 81270966, 81500679, 81702903, 81770821), the Natural Science Foundation of Guangdong Province, China (Grant Nos. 2014A030310036, 2014A030310472, 2017A030310038, 2017A030313519, and 2018A030313609), Science and Technology Plan of Guangdong Province (Grant No. 2016A020215097, 2017A020215045).

REFERENCES

American Diabetes Association (2018). 8. Pharmacologic approaches to glycemic treatment: standards of medical care in diabetes-2018. *Diabetes Care* 41 (Suppl. 1), S73–S85. doi:10.2337/dc18-S008

American Diabetes Association (2019). Professional practice committee: standards of medical care in diabetes-2019. *Diabetes Care* 42 (Suppl. 1), S3. doi:10.2337/dc19-SppC01

Andreozzi, F., Raciti, G. A., Nigro, C., Mannino, G. C., Procopio, T., Davalli, A. M., et al. (2016). The GLP-1 receptor agonists exenatide and liraglutide activate Glucose transport by an AMPK-dependent mechanism. *J. Transl. Med.* 14 (1), 229. doi:10.1186/s12967-016-0985-7

Arnette, D., Gibson, T. B., Lawrence, M. C., January, B., Khoo, S., McGlynn, K., et al. (2003). Regulation of ERK1 and ERK2 by glucose and peptide hormones in pancreatic beta cells. *J. Biol. Chem.* 278 (35), 32517–32525. doi:10.1074/jbc.M301174200

Aroda, V. R. (2018). A review of GLP-1 receptor agonists: evolution and advancement, through the lens of randomised controlled trials. *Diabetes Obes. Metab.* 20 (Suppl. 1), 22–33. doi:10.1111/dom.13162

Baggio, L. L., and Drucker, D. J. (2007). Biology of incretins: GLP-1 and GIP. *Gastroenterology* 132 (6), 2131–2157. doi:10.1053/j.gastro.2007.03.054

Balena, R., Hensley, I. E., Miller, S., and Barnett, A. H. (2013). Combination therapy with GLP-1 receptor agonists and basal insulin: a systematic review of the literature. *Diabetes Obes. Metab.* 15 (6), 485–502. doi:10.1111/dom.12025

Bookout, A. L., Jeong, Y., Downes, M., Yu, R. T., Evans, R. M., and Mangelsdorf, D. J. (2006). Anatomical profiling of nuclear receptor expression reveals a hierarchical transcriptional network. *Cell* 126 (4), 789–799. doi:10.1016/j.cell.2006.06.049

Briaud, I., Lingohr, M. K., Dickson, L. M., Wrede, C. E., and Rhodes, C. J. (2003). Differential activation mechanisms of Erk-1/2 and p70(S6K) by glucose in pancreatic beta-cells. *Diabetes* 52 (4), 974–983. doi:10.2337/diabetes.52.4.974

Campbell, J. E., and Drucker, D. J. (2013). Pharmacology, physiology, and mechanisms of incretin hormone action. *Cell Metab.* 17 (6), 819–837. doi:10.1016/j.cmet.2013.04.008

Cazzo, E., Jimenez, L. S., Gestic, M. A., Utrini, M. P., Chaim, F. H. M., Chaim, F. D. M., et al. (2018). Type 2 diabetes mellitus and simple glucose metabolism parameters may reliably predict nonalcoholic fatty liver disease features. *Obes. Surg.* 28 (1), 187–194. doi:10.1007/s11695-017-2829-9

Cheng, F., Yuan, G., He, J., Shao, Y., Zhang, J., and Guo, X. (2019). Dysregulation of DPP4 is associated with the AMPK/JAK2/STAT3 pathway in adipocytes under insulin resistance status and liraglutide intervention. *Diabetes Metab. Syndr. Obes.* 12, 2635–2644. doi:10.2147/dmso.s229838

Cuthbertson, D. J., Irwin, A., Gardner, C. J., Daousi, C., Purewal, T., Furlong, N., et al. (2012). Improved glycaemia correlates with liver fat reduction in obese, type 2 diabetes, patients given glucagon-like peptide-1 (GLP-1) receptor agonists. *PLoS One* 7 (12), e50117. doi:10.1371/journal.pone.0050117

Diehl, A. M., and Day, C. (2017). Cause, pathogenesis, and treatment of nonalcoholic steatohepatitis. *N. Engl. J. Med.* 377 (21), 2063–2072. doi:10.1056/NEJMra1503519

Escher, P., Braissant, O., Basu-Modak, S., Michalik, L., Wahli, W., and Desvergne, B. (2001). Rat PPARs: quantitative analysis in adult rat tissues and regulation in fasting and refeeding. *Endocrinology* 142 (10), 4195–4202. doi:10.1210/endo.142.10.8458

Friedman, S. L., Neuschwander-Tetri, B. A., Rinella, M., and Sanyal, A. J. (2018). Mechanisms of NAFLD development and therapeutic strategies. *Nat. Med.* 24 (7), 908–922. doi:10.1038/s41591-018-0104-9

Fruci, B., Giuliano, S., Mazza, A., Malaguarnera, R., and Belfiore, A. (2013). Nonalcoholic Fatty liver: a possible new target for type 2 diabetes prevention and treatment. *Int. J. Mol. Sci.* 14 (11), 22933–22966. doi:10.3390/ijms141122933

Garber, A. J., Abrahamson, M. J., Barzilay, J. I., Blonde, L., Bloomgarden, Z. T., Bush, M. A., et al. (2019). Consensus statement by the American association of clinical endocrinologists and American College of endocrinology on the comprehensive type 2 diabetes management algorithm–2019 executive summary. *Endocr. Pract.* 25 (1), 69–100. doi:10.4158/cs-2018-0535

Gervois, P., Kleemann, R., Pilon, A., Percevault, F., Koenig, W., Staels, B., et al. (2004). Global suppression of IL-6-induced acute phase response gene expression after chronic *in vivo* treatment with the peroxisome proliferator-activated receptor-alpha activator fenofibrate. *J. Biol. Chem.* 279 (16), 16154–16160. doi:10.1074/jbc.M400346200

Guo, H., Li, H., Wang, B., Ding, W., Ling, L., Yang, M., et al. (2017). Protective effects of glucagon-like peptide-1 analog on renal tubular injury in mice on high-fat diet. *Cell Physiol. Biochem.* 41 (3), 1113–1124. doi:10.1159/000464118

Gupta, N. A., Mells, J., Dunham, R. M., Grakoui, A., Handy, J., Saxena, N. K., et al. (2010). Glucagon-like peptide-1 receptor is present on human hepatocytes and has a direct role in decreasing hepatic steatosis *in vitro* by modulating elements of the insulin signaling pathway. *Hepatology* 51 (5), 1584–1592. doi:10.1002/hep.23569

Hardie, D. G., Ross, F. A., and Hawley, S. A. (2012). AMPK: a nutrient and energy sensor that maintains energy homeostasis. *Nat. Rev. Mol. Cell Biol.* 13 (4), 251–262. doi:10.1038/nrm3311

Hashimoto, T., Cook, W. S., Qi, C., Yeldandi, A. V., Reddy, J. K., and Rao, M. S. (2000). Defect in peroxisome proliferator-activated receptor alpha-inducible fatty acid oxidation determines the severity of hepatic steatosis in response to fasting. *J. Biol. Chem.* 275 (37), 28918–28928. doi:10.1074/jbc.M910350199

Hayes, M. R., Kanoski, S. E., Alhadeff, A. L., and Grill, H. J. (2011). Comparative effects of the long-acting GLP-1 receptor ligands, liraglutide and exendin-4, on food intake and body weight suppression in rats. *Obesity* 19 (7), 1342–1349. doi:10.1038/oby.2011.50

He, Q., Sha, S., Sun, L., Zhang, J., and Dong, M. (2016). GLP-1 analogue improves hepatic lipid accumulation by inducing autophagy via AMPK/mTOR pathway. *Biochem. Biophys. Res. Commun.* 476 (4), 196–203. doi:10.1016/j.bbrc.2016.05.086

He, Y., Ao, N., Yang, J., Wang, X., Jin, S., and Du, J. (2020). The preventive effect of liraglutide on the lipotoxic liver injury via increasing autophagy. *Ann. Hepatol.* 19 (1), 44–52. doi:10.1016/j.aohep.2019.06.023

Holst, J. J., and Vilsboll, T. (2013). Combining GLP-1 receptor agonists with insulin: therapeutic rationales and clinical findings. *Diabetes Obes. Metab.* 15 (1), 3–14. doi:10.1111/j.1463-1326.2012.01628.x

Horie, I., Haraguchi, A., Sako, A., Akeshima, J., Niri, T., Shigeno, R., et al. (2018). Predictive factors of efficacy of combination therapy with basal insulin and liraglutide in type 2 diabetes when switched from longstanding basal-bolus insulin: Association between the responses of beta- and alpha-cells to GLP-1 stimulation and the glycaemic control at 6months after switching therapy. *Diabetes Res. Clin. Pract.* 144, 161–170. doi:10.1016/j.diabres.2018.08.015

Ip, E., Farrell, G. C., Robertson, G., Hall, P., Kirsch, R., and Leclercq, I. (2003). Central role of PPARalpha-dependent hepatic lipid turnover in dietary steatohepatitis in mice. *Hepatology* 38 (1), 123–132. doi:10.1053/jhep.2003.50307

Kahn, S. E., Zraika, S., Utzschneider, K. M., and Hull, R. L. (2009). The beta cell lesion in type 2 diabetes: there has to be a primary functional abnormality. *Diabetologia* 52 (6), 1003–1012. doi:10.1007/s00125-009-1321-z

Kelly, A. S., Auerbach, P., Barrientos-Perez, M., Gies, I., Hale, P. M., Marcus, C., et al. (2020). A randomized, controlled trial of liraglutide for adolescents with obesity. *N. Engl. J. Med.* 382 (22), 2117–2128. doi:10.1056/nejmoa1916038

Kersten, S., Seydoux, J., Peters, J. M., Gonzalez, F. J., Desvergne, B., and Wahli, W. (1999). Peroxisome proliferator-activated receptor alpha mediates the adaptive response to fasting. *J. Clin. Invest.* 103 (11), 1489–1498. doi:10.1056/nejmoa1916038

Kersten, S., and Stienstra, R. (2017). The role and regulation of the peroxisome proliferator activated receptor alpha in human liver. *Biochimie* 136, 75–84. doi:10.1016/j.biochi.2016.12.019

Kushima, H., Mori, Y., Koshibu, M., Hiromura, M., Kohashi, K., Terasaki, M., et al. (2017). The role of endothelial nitric oxide in the anti-restenotic effects of liraglutide in a mouse model of restenosis. *Cardiovasc. Diabetol.* 16 (1), 122. doi:10.1186/s12933-017-0603-x

Leone, T. C., Weinheimer, C. J., and Kelly, D. P. (1999). A critical role for the peroxisome proliferator-activated receptor alpha (PPARalpha) in the cellular fasting response: the PPARalpha-null mouse as a model of fatty acid oxidation disorders. *Proc. Natl. Acad. Sci. U.S.A.* 96 (13), 7473–7478. doi:10.1073/pnas.96.13.7473

Li, D., Wu, H., and Dou, H. (2019). Weight loss effect of sweet orange essential oil microcapsules on obese SD rats induced by high-fat diet. *Biosci. Biotechnol. Biochem.* 85, 1–10. doi:10.1080/09168451.2019.1578640

Liao, Q., Li, R., Zhou, R., Pan, Z., Xu, L., Ding, Y., et al. (2017). LIM kinase 1 interacts with myosin-9 and alpha-actinin-4 and promotes colorectal cancer progression. *Br. J. Cancer* 117 (4), 563–571. doi:10.1038/bjc.2017.193

Lirussi, F., Azzalini, L., Orando, S., Orlando, R., and Angelico, F. (2007). Antioxidant supplements for non-alcoholic fatty liver disease and/or steatohepatitis. *Cochrane Database Syst. Rev.* 1, CD004996. doi:10.1002/14651858.CD004996.pub3

Misra, P., and Reddy, J. K. (2014). Peroxisome proliferator-activated receptor-alpha activation and excess energy burning in hepatocarcinogenesis. *Biochimie* 98, 63–74. doi:10.1016/j.biochi.2013.11.011

Montagner, A., Polizzi, A., Fouche, E., Ducheix, S., Lippi, Y., Lasserre, F., et al. (2016). Liver PPARalpha is crucial for whole-body fatty acid homeostasis and is protective against NAFLD. *Gut* 65 (7), 1202–1214. doi:10.1136/gutjnl-2015-310798

Pawlak, M., Lefebvre, P., and Staels, B. (2015). Molecular mechanism of PPARalpha action and its impact on lipid metabolism, inflammation and fibrosis in non-alcoholic fatty liver disease. *J. Hepatol.* 62 (3), 720–733. doi:10.1016/j.jhep.2014.10.039

Smits, M. M., Tonneijck, L., Muskiet, M. H., Kramer, M. H., Pouwels, P. J., Pieters-van den Bos, I. C., et al. (2016). Twelve week liraglutide or sitagliptin does not affect hepatic fat in type 2 diabetes: a randomised placebo-controlled trial. *Diabetologia* 59 (12), 2588–2593. doi:10.1007/s00125-016-4100-7

Staels, B., Maes, M., and Zambon, A. (2008). Fibrates and future PPARalpha agonists in the treatment of cardiovascular disease. *Nat. Clin. Pract. Cardiovasc. Med.* 5 (9), 542–553. doi:10.1038/ncpcardio1278

Tang, A., Rabasa-Lhoret, R., Castel, H., Wartelle-Bladou, C., Gilbert, G., Massicotte-Tisluck, K., et al. (2015). Effects of insulin glargine and liraglutide therapy on liver fat as measured by magnetic resonance in patients with type 2 diabetes: a randomized trial. *Diabetes Care* 38 (7), 1339–1346. doi:10.1038/ncpcardio1278

Thorens, B. (1992). Expression cloning of the pancreatic beta cell receptor for the gluco-incretin hormone glucagon-like peptide 1. *Proc. Natl. Acad. Sci. U.S.A.* 89 (18), 8641–8645. doi:10.1073/pnas.89.18.8641

Tilg, H., and Moschen, A. R. (2008). Insulin resistance, inflammation, and non-alcoholic fatty liver disease. *Trends Endocrinol. Metab.* 19 (10), 371–379. doi:10.1016/j.tem.2008.08.005

Wajcberg, E., and Amarah, A. (2010). Liraglutide in the management of type 2 diabetes. *Drug Des. Devel. Ther.* 4, 279–290. doi:10.2147/DDDT.S10180

Wang, L., Gao, P., Zhang, M., Huang, Z., Zhang, D., Deng, Q., et al. (2017). Prevalence and ethnic pattern of diabetes and prediabetes in China in 2013. *JAMA* 317 (24), 2515–2523. doi:10.1001/jama.2017.7596

Wang, Y., Parlevliet, E. T., Geerling, J. J., van der Tuin, S. J., Zhang, H., Bieghs, V., et al. (2014). Exendin-4 decreases liver inflammation and atherosclerosis development simultaneously by reducing macrophage infiltration. *Br. J. Pharmacol.* 171 (3), 723–734. doi:10.1111/bph.12490

Xu, F., Li, Z., Zheng, X., Liu, H., Liang, H., Xu, H., et al. (2014). SIRT1 mediates the effect of GLP-1 receptor agonist exenatide on ameliorating hepatic steatosis. *Diabetes* 63 (11), 3637–3646. doi:10.2337/db14-0263

Yan, J., Yao, B., Kuang, H., Yang, X., Huang, Q., Hong, T., et al. (2018). Liraglutide, sitagliptin and insulin glargine added to metformin: the effect on body weight and intrahepatic lipid in patients with type 2 diabetes mellitus and NAFLD. *Hepatology* 69 (6), 2414–2426. doi:10.1002/hep.30320

Yang, S., Lin, C., Zhuo, X., Wang, J., Rao, S., Xu, W., et al. (2020). Glucagon-like peptide-1 alleviates diabetic kidney disease through activation of autophagy by regulating AMP-activated protein kinase-mammalian target of rapamycin pathway. *Am. J. Physiol. Endocrinol. Metab.* 319 (6), E1019–E1030. doi:10.1152/ajpendo.00195.2019

Younossi, Z. M., Koenig, A. B., Abdelatif, D., Fazel, Y., Henry, L., and Wymer, M. (2016). Global epidemiology of nonalcoholic fatty liver disease-Meta-analytic assessment of prevalence, incidence, and outcomes. *Hepatology* 64 (1), 73–84. doi:10.1002/hep.28431

Zhang, Y., Sun, B., Feng, D., Hu, H., Chu, M., Qu, Q., et al. (2017). Cryo-EM structure of the activated GLP-1 receptor in complex with a G protein. *Nature* 546 (7657), 248–253. doi:10.1038/nature22394

Zhou, J. Y., Poudel, A., Welchko, R., Mekala, N., Chandramani-Shivalingappa, P., Rosca, M. G., et al. (2019). Liraglutide improves insulin sensitivity in high fat diet induced diabetic mice through multiple pathways. *Eur. J. Pharmacol.* 861, 172594. doi:10.1016/j.ejphar.2019.172594

Conflict of Interest: The authors declare that the research was conducted in the absence of any commercial or financial relationships that could be construed as a potential conflict of interest.

frontiers in Pharmacology

ORIGINAL RESEARCH
published: 31 March 2021
doi: 10.3389/fphar.2021.625991

Computational Drug Repositioning and Experimental Validation of Ivermectin in Treatment of Gastric Cancer

*Hanne-Line Rabben[1,2], Gøran Troseth Andersen[1], Aleksandr Ianevski[1], Magnus Kringstad Olsen[1], Denis Kainov[1], Jon Erik Grønbech[3], Timothy Cragin Wang[4], Duan Chen[1] and Chun-Mei Zhao[1,2]**

[1]Department of Clinical and Molecular Medicine, Norwegian University of Science and Technology (NTNU), Trondheim, Norway, [2]The Central Norway Regional Health Authority (RHA), Stjørdal, Norway, [3]Surgical Clinic, St. Olavs Hospital, Trondheim University Hospital, Trondheim, Norway, [4]Division of Digestive and Liver Diseases, Columbia University College of Physicians and Surgeons, New York, NY, United States

OPEN ACCESS

Edited by:
Klara Gyires, Semmelweis University, Hungary

Reviewed by:
Cedric Coulouarn, INSERM U1242 Laboratoire COSS, France
Pedro Miguel Rodrigues, Biodonostia Health Research Institute (IIS Biodonostia), Spain

***Correspondence:**
Chun-Mei Zhao
chun-mei.zhao@ntnu.no

Specialty section:
This article was submitted to Gastrointestinal and Hepatic Pharmacology, a section of the journal Frontiers in Pharmacology

Received: *04 November 2020*
Accepted: *10 February 2021*
Published: *31 March 2021*

Citation:
Rabben H-L, Andersen GT, Ianevski A, Olsen MK, Kainov D, Grønbech JE, Wang TC, Chen D and Zhao C-M (2021) Computational Drug Repositioning and Experimental Validation of Ivermectin in Treatment of Gastric Cancer. Front. Pharmacol. 12:625991. doi: 10.3389/fphar.2021.625991

Objective: The aim of the present study was repositioning of ivermectin in treatment of gastric cancer (GC) by computational prediction based on gene expression profiles of human and mouse model of GC and validations with *in silico*, *in vitro* and *in vivo* approaches.

Methods: Computational drug repositioning was performed using connectivity map (cMap) and data/pathway mining with the Ingenuity Knowledge Base. Tissue samples of GC were collected from 16 patients and 57 mice for gene expression profiling. Additional seven independent datasets of gene expression of human GC from the TCGA database were used for validation. *In silico* testing was performed by constructing interaction networks of ivermectin and the downstream effects in targeted signaling pathways. *In vitro* testing was carried out in human GC cell lines (MKN74 and KATO-III). *In vivo* testing was performed in a transgenic mouse model of GC (INS-GAS mice).

Results: GC gene expression "signature" and data/pathway mining but not cMAP revealed nine molecular targets of ivermectin in both human and mouse GC associated with WNT/β-catenin signaling as well as cell proliferation pathways. *In silico* inhibition of the targets of ivermectin and concomitant activation of ivermectin led to the inhibition of WNT/β-catenin signaling pathway in "dose-depended" manner. *In vitro*, ivermectin inhibited cell proliferation in time- and concentration-depended manners, and cells were arrested in the G_1 phase at IC_{50} and shifted to S phase arrest at $>IC_{50}$. *In vivo*, ivermectin reduced the tumor size which was associated with inactivation of WNT/β-catenin signaling and cell proliferation pathways and activation of cell death signaling pathways.

Conclusion: Ivermectin could be recognized as a repositioning candidate in treatment of gastric cancer.

Keywords: gastric cancer, ivermectin, drug repositioning, ingenuity pathway analysis, *in silico*

INTRODUCTION

Drug repositioning (also called drug repurposing) is a strategy for identifying new uses for approved or investigational drugs that are outside the scope of the original medical indications. Repositioned drugs may reveal new targets and pathways that can be further exploited (Ashburn and Thor, 2004; Pushpakom et al., 2019). Advantages of drug repositioning are related to the drugs that have known mechanisms of action, pharmacological properties, such as pharmacokinetics, pharmacodynamics, posology (the appropriate doses of drugs) and toxicity (Verbaanderd et al., 2017). Of note is that both the pre-clinical and clinical safety data are available (Verbaanderd et al., 2017; Antoszczak et al., 2020). Thus, compared to traditional methods of drug development, drug repositioning requires drastically shortened development time and reduced costs while providing similar therapeutic benefits. Approaches of drug repositioning include computational methods, such as connectivity map (cMap), data mining, pathway mining, ontology modeling, *in silico* and biological experimental validations (e.g., *in vitro* and *in vivo*). The computational drug repositioning can be conducted as repurposing with a defined purpose, repurposing with a strategy, and repurposing with confidence by utilizing reference datasets which are disease-based, drug-based, or knowledge-based (Liu et al., 2013; Subramanian et al., 2017; Xue et al., 2018).

Ivermectin was identified in late 1960s, first approved as veterinary medicine and then human medicine in 1980s for the control of parasitic infection. The discovery and development of ivermectin by William C. Campbell and Satoshi Ōmura were recognized by Nobel Prize in Physiology or Medicine in 2015 (Callaway and Cyranoski, 2015). Ivermectin acts on γ-aminobutyric acid (GABA)-gated chloride channels in the interneuronic synapses of a parasite, whereas in humans, the nerves that are sensitive to GABA, are protected by the blood/brain barrier (Sutherland and Campbell, 1990; Davis et al., 1999; Ikeda, 2003; Chen and Kubo, 2018). However, ivermectin has been repositioned as a broad-spectrum antiviral and antimicrobial agent (Andersen et al., 2020). Interestingly, it is also known that ivermectin can be widely distributed in humans because of its high lipophilicity and thus might exhibit anti-tumor activity in colorectal cancer, breast cancer, glioma, head and neck cancer, leukemia, melanoma, pancreatic cancer, and prostate cancer (Chiou et al., 1987; Juarez et al., 2018).

Gastric cancer (GC) is the fifth most common malignant disease worldwide with the third highest incidence and mortality rate among all cancers (Rawla and Barsouk, 2019). The 5 years overall survival rate is 10–30% except for Japan (50–70%) (Parkin et al., 2002; Matsuda and Saika, 2013). Gastrectomy combined with platinum-based chemotherapy is the most beneficial approach in patient care, and novel targeted therapy, including PD-1 inhibitor in first and second-line setting for advanced GC, are under development (Sitarz et al., 2018; Selim et al., 2019; GBD 2017 Stomach Cancer Collaborators, 2020). However, new drugs and drug repositioning are needed particularly in consideration of the global burden of this deadly disease.

Previously, we have showed repositioning of botulinum toxin type A (also known as botox), everolimus (RAD001) and devimistat (CPI-613) in treatment of GC (Zhao et al., 2014; Rabben et al., 2016; Rabben et al., 2021). The aim of the present study was to reposition ivermectin in treatment of GC. To this end, we have developed and/or utilized the approaches from computational drug repositioning to *in silico*, *in vitro* and *in vivo* validations (**Figure 1**).

MATERIALS AND METHODS

Patients and Animals

Surgical biopsies were collected from 16 patients who underwent total/subtotal or distal gastrectomy because of GC since 2012 at St. Olav's Hospital, Trondheim, Norway (**Table 1**). Four biopsies per patients were taken from tumor and normal tissue and used for clinical pathological evolution and gene expression profiling. The study was approved by the Regional Committees for Medical and Health Research Ethics Central Norway (REK 2012-1029). Furthermore, seven independent datasets of human GC from the TCGA database were used (**Table 2**).

The mouse model of GC, i.e., the transgenic INS-GAS mice which spontaneously develop gastric cancer, was used (Zhao et al., 2014). Stomachs were collected from 26 mice, i.e., six

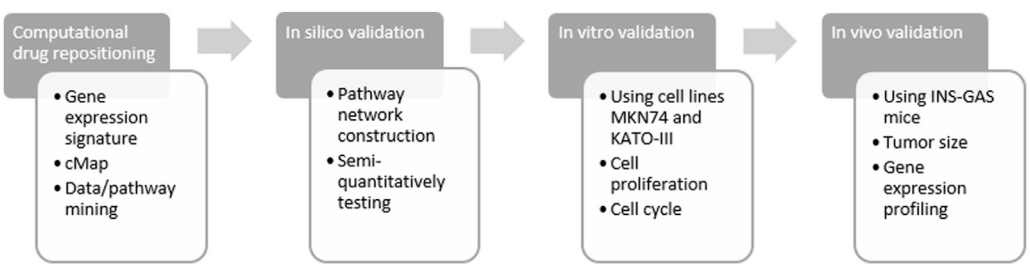

FIGURE 1 | Flow chart of study design. Computational drug repositioning was carried out by using gene expression signatures representing gastric cancer of both patients and mouse model and connectivity map (cMap) and data/pathway mining with the Ingenuity Knowledge Base. Validation included *in silico*, *in vitro* and *in vivo* methods of ivermectin treatment. The rationale of using human samples of GC (without ivermectin treatment) was *i*) to perform computational prediction and data mining and *ii*) to make a comparison with the animal model in order to demonstrate that the animal study could be relevant in the design of clinical trial of ivermectin in the future.

TABLE 1 | Demographic and clinical parameters of gastric cancer patients.

Number of patients		
Age group	49–53	1
	54–58	1
	59–63	2
	64–68	1
	69–73	2
	74–78	5
	79–83	3
	84+	1
Sex	Male	11
	Female	5
Pathologic characteristics		
Lauren classification	Intestinal	3
	Diffuse	4
	Mixed	2
	Not classified	7
Type of gastric resection	Total gastrectomy	7
	Subtotal gastrectomy	5
	Distal gastrectomy	4

females and four males INS-GAS mice at age of 15 months and eight females and eight males wild-type (WT) mice at age of 12 months, for gene expression profiling. In addition, 31 INS-GAS mice, i.e., 12 females and nine males at age of 10 months, and 10 WT mice, i.e., 6 females and four males at age of 10 months, were used for *in vivo* testing.

Animals were housed as four to five mice per cage on wood chip bedding with a 12 h light/dark cycle in a specific pathogen free environment with room temperature of 22°C and 40–60% relative humidity. Animals were inspected daily by investigators and authorized veterinarian using a scoring sheet. Animals should be euthanized at score of 10 if they are emaciated, underconditioned in five consecutive days, or show poor clinical signs (e.g., body weight, appearance, and behavior) before end of the study. This was done according to the Directive 2010/63/EU in which human primary endpoint are defined as "the earliest indicator in an animal experiment of (potential) pain and/or distress that, within the context of moral justification and scientific endpoints to be met, can be used to avoid or limit pain and/or distress by taking actions such as humane killing or terminating or alleviating the pain and distress (Hendriksen and Morton, 1999)" (https://www.humane-endpoints.info/en/council-directive-2010-63-eu). The study was approved by The Norwegian Food Safety Authority (Mattilsynet).

Transcriptomics

Total RNA was extracted from the surgical biopsies of patients and harvested stomachs of mice. RNA quality and quantity were obtained using NanoDrop One (Thermo Scientific, Norway) and Agilent Bioanalyser. For human samples, RNA microarray of GC samples, including 24 tumors of intestinal, diffuse and mixed types from seven patients and 37 normal tissue from six patients, was performed using Illumina platform as described earlier (Zhao et al., 2014). Illumina microarray data was analyzed using Lumi on the $\log_2$ scale and analyzed using the empirical Bayesian method implemented in Limma. The data is accessible via Mendeley Data repository with DOI link at http://dx.doi.org/10.17632/hzmfshy7hp.1. Illumina identifiers (ILMN) were uploaded to Ingenuity Pathway Analysis (IPA, QIAGEN, Hilden, Germany) together with $\log_2$-fold change, p-values and q-values (false discovery rates). For mouse samples, RNA sequencing was performed using Illumina HiSeqNS500 instrument (NextSeq 500) at 75 bp with paired end (PE) reads using NS500H flow cells with 25M reads/sample. Paired end forward read length (R1): 81, reverse read length (R2): 81. Downstream processing and analysis of the data was performed in the Bioconductor environment in R. For humans, a total of 47,323 transcripts was assigned to analysis in which 37,489 transcripts were mapped and 9,834 transcripts unmapped by Ingenuity Pathway Analysis (IPA) (QIAGEN, Hilden, Germany). For mice, a total of 54,460 transcripts was loaded in which 54,162 were mapped/298 transcripts were unmapped in IPA. For mouse GC after ivermectin treatment, 54,416 transcripts were loaded in which all were mapped in IPA. Filtering of datasets included species (mouse or human) and p-value cut-off ($p < 0.05$). Gene expression was analyzed using a t-test between tumor and normal tissue in patients, between INS-GAS and WT mice and between INS-GAS mice with and without ivermectin. Genes with a p-value of less than 0.05 were considered to be differentially expressed. Transcriptomics datasets were analyzed using IPA. Molecular networks and canonical pathways were algorithmically constructed based on known connectivity and relationships among genes/proteins/metabolites using Ingenuity Knowledge Base. Local and

TABLE 2 | WNT/β-catenin signaling in human gastric cancer (one in the present study and 7 STAD datasets deposited in the TCGA database).

TCGA/Ingenuity Knowledge Base	WNT/β-catenin signaling		N (tumor samples)	N (control samples)
	Z-score	$-\log_{10}(p)$		
Human gastric cancer (the present study)	1.604	1.86E00	24	37
GSE48433; 354-stomach cancer [stomach] NA 3485 (PMID: 24885658) Hollingshead et al. (2014)	0.728	N/A	5	5
GSE48433; 171-stomach cancer [stomach] NA 3282 (PMID: 24885658) Hollingshead et al. (2014)	1.155	1.64E00	5	5
GSE118897; 1- stomach cancer [stomach] NA 628 (PMID: 30404039) Yang et al. (2019)	2.121	1.45E00	10	10
1-gastric adenocarcinoma (STAD) [stomach] NA 4052 Ingenuity Knowledge Base	2.138	2.29E00	70	36
10-gastric adenocarcinoma (STAD) [stomach] NA 4053 Ingenuity Knowledge Base	1.342	0	16	71
102-gastric adenocarcinoma (STAD) [stomach] NA 4056 Ingenuity Knowledge Base	1.134	0	20	71
111-gastric adenocarcinoma (STAD) [stomach] NA 4066 Ingenuity Knowledge Base	0.447	0	21	71

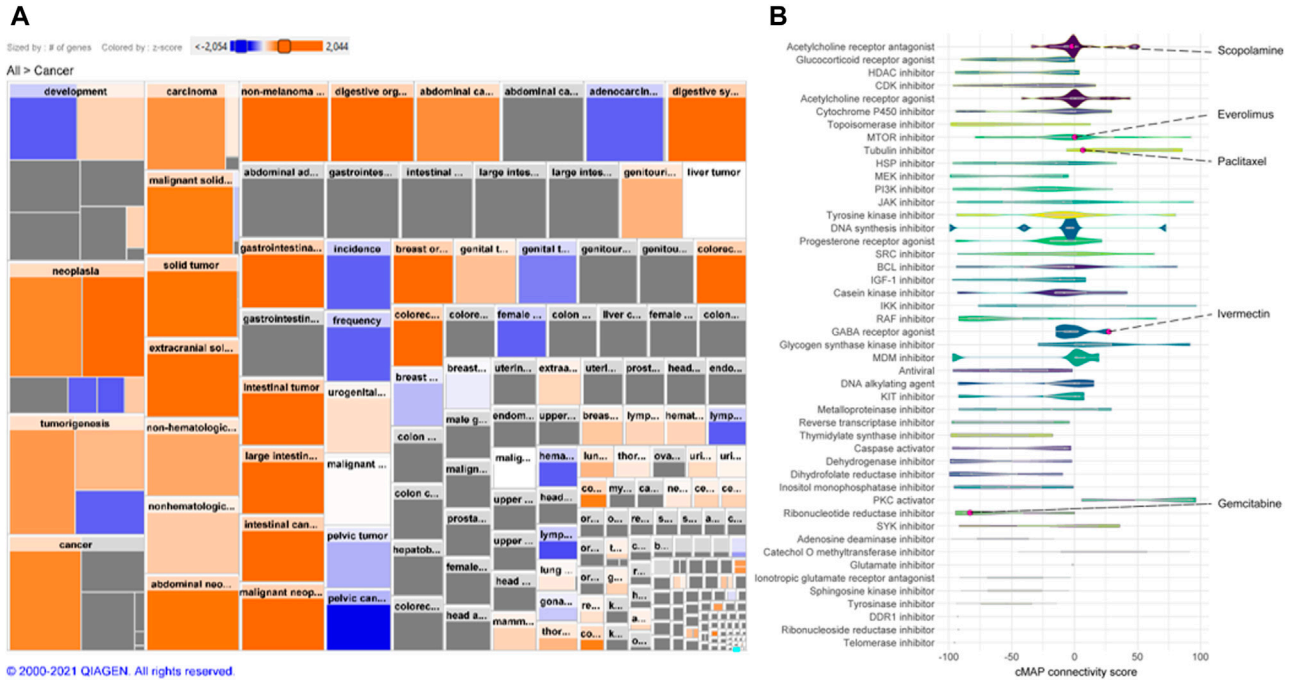

FIGURE 2 | Gene expression signature and connectivity map (cMAP). **(A)** Heatmap of human GC gene expression signature that constitutes an activation of cancer disease based on differential expression of >22,000 genes. Size of square is proportional to the number of genes contained in the specific function and color represent activity state (z-score; orange: activated, blue: decreased). **(B)** Connectivity map (cMap) showing associations between a large-scale compendium of functional perturbations in cancer cell lines coupled to the human GC gene expression signature based on the L1000 assay (Subramanian et al., 2017). Note: Ivermectin and other known drugs are visualized.

regulatory *z*-scores for canonical pathways and diseases and biofunctions that overlapped with the experimental data of the present study were calculated using the formula described previously (Sitarz et al., 2018). IPA has sophisticated algorithms to calculate predicted functional activation/inhibition of canonical pathways, diseases and functions, transcription regulators and regulators based on their downstream molecule expressions (QIAGEN Inc., https://www.qiagenbioinformatics.com/products/ingenuitypathway-analysis). Fischer's exact test was used to calculate a *p*-value determining the probability that the association between the genes in the datasets from human GC and mouse GC and the canonical pathway or disease/function by chance alone.

Connectivity Map and Data/Pathway Mining

The concept of a Connectivity Map (cMap) was recently developed, whereby genes, drugs, and disease states are connected by virtue of common gene expression signatures (Qu and Rajpal, 2012; Subramanian et al., 2017; Musa et al., 2018). To identify candidate drugs, the gene expression signature of GC was generated based on the gene expression profile of human GC. A positive cMap score indicates there is a positive similarity between a given perturbagen's signature, i.e., genes that are increased by treatment (in reference datasets) are also upregulated in the human GC dataset, while a negative score indicates that the two signatures are opposing. cMap was performed using the gene expression signature of human GC (n = 7 GC vs. n = 6 normal tissue).

Data mining was performed using the gene expression profile data of 61 samples from 16 patients, 26 samples from 26 mice, and 324 samples from seven independent datasets from the TCGA database. Furthermore, knowledge-based pathway mining was used based on previous studies that showed WNT/β-catenin signaling pathway as one of the important pathways in gastric tumorigenesis (Zhao et al., 2014; Rabben et al., 2021). Custom-made molecular networks were generated using the Ingenuity Knowledge Base. Networks were then algorithmically generated based on their interrelationships. WNT/β-catenin signaling pathway was constructed based on the transcriptomic data of INS-GAS mice and were then entered into the "Pathway" module of the IPA to obtain the nodes in every corresponding signaling pathway. Nodes from pathways were added as entries into the "My list"-function and all entries in the list were added to the "My pathway" in IPA. My pathway was used to produce a network of nodes/genes from the WNT/β-catenin signaling pathway that matched with our experimental data from INS-GAS vs. WT mice. The build-tool was used to connect nodes using edges, i.e., relationships including both direct and indirect interactions like chemical-protein interactions, ubiquitination, molecular cleavage, translocation, localization, phosphorylation, expression, protein-protein interactions, activation, regulation of binding, inhibition, membership, reaction, protein-DNA interactions,

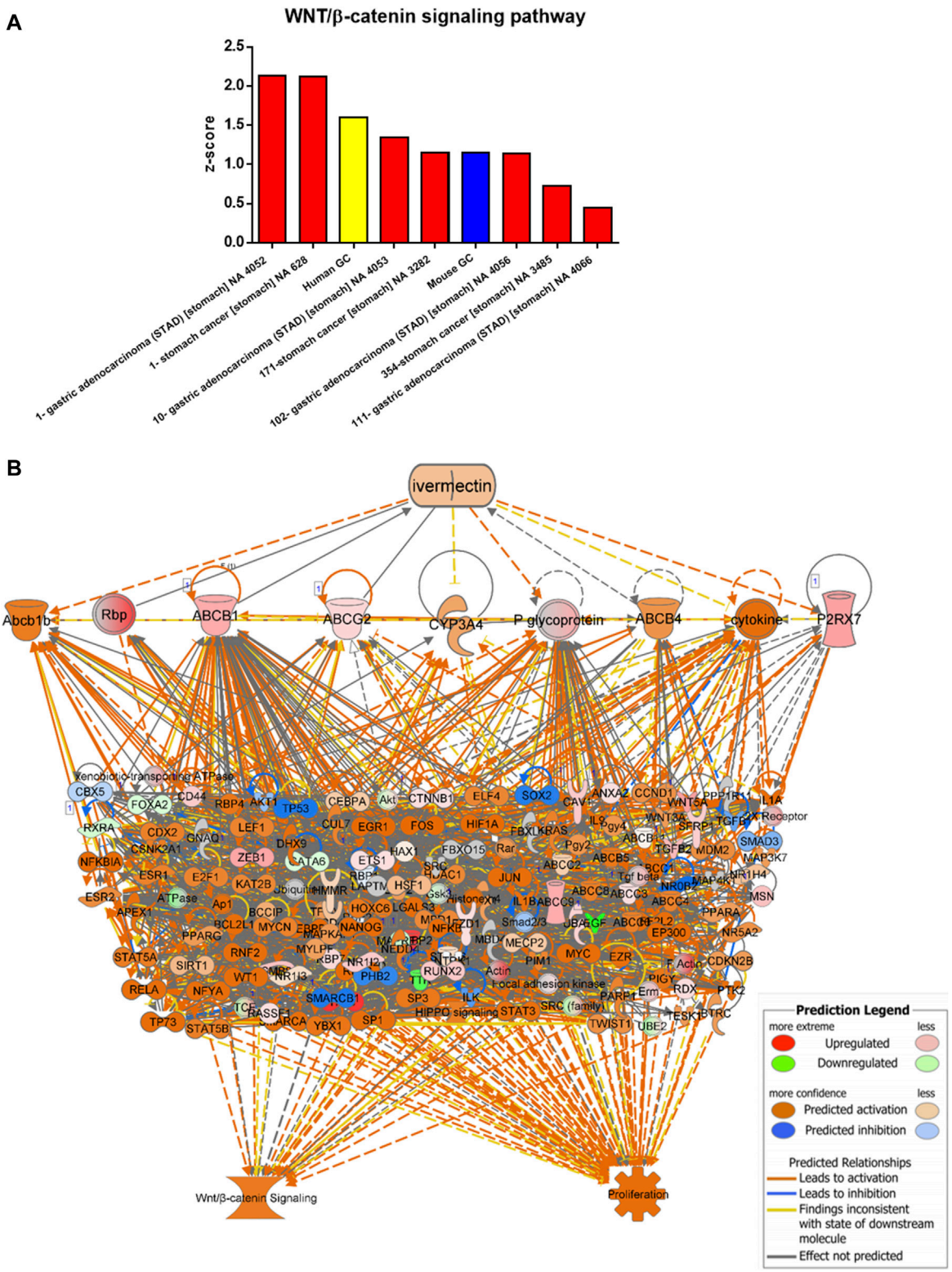

FIGURE 3 | Data/pathway mining of WNT/β-catenin signaling pathway. **(A)** Activation of WNT/β-catenin signaling pathway in eight datasets of human GC (including one used in the present study as indicated in yellow) and one dataset of mouse GC (in blue). **(B)** Hierarchical network representation showing ivermectin and drug targets with downstream signaling pathways of WNT/β-catenin and proliferation. The schema was created in IPA using the grow-tool and the Ingenuity Knowledge Base. The molecular entities (genes and proteins) as well as molecular functions and interactive networks were connected based on interrelationships identified by the Ingenuity Knowledge Base. Expression levels from mouse GC vs. WT. $p < 0.05$. See also **Table 3** *In silico* testing shows ivermectin inhibits WNT/β-catenin signaling.

transcription and modification. The Canonical Pathway overlay-tool was used to arrange the entries into clusters based on pathway. Local *z*-scores were calculated in IPA based on the dataset's correlation with the activated state. Negative *z*-scores indicate a decrease in activity, positive *z*-scores indicate an increase in activity. Canonical pathways were identified using statistical cut-offs at $p < 0.05$.

In Silico Testing

The expression data from mouse GC was compared to all genes in the pathway. The molecule activity predictor (MAP)-function was used to predict activation/inhibition between the nodes in the network. The *in silico* tool integrated with the MAP-function was employed to predict effects on the network after gene inhibition and/or stimulation in the ivermectin cluster. Connections between genes were then algorithmically generated based on their interrelationships including both direct and indirect interactions like chemical-protein interactions, ubiquitination, molecular cleavage, translocation, localization, phosphorylation, expression, protein-protein interactions, activation, regulation of binding, inhibition, membership, reaction, protein-DNA interactions, transcription and modification. Network clusters of WNT/β-catenin pathway was constructed based on the transcriptomic data of INS-GAS mice (i.e., limited to and built on genes from the dataset). The build-tool was used to connect nodes using edges, i.e., relationships. Categorical values were set to each gene/node using a semi-quantitative method to quantify the color-change resulting from *in silico* inhibition. Local *z*-scores were calculated in IPA based on the dataset's correlation with the activated state. Negative *z*-scores indicate a decrease in activity, positive *z*-scores indicate an increase in activity. Canonical pathways were identified using statistical cut-offs at $p < 0.05$.

In Vitro Testing

GC cell lines included human gastric cancer cells MKN74 (intestinal type) and KATO-III (diffuse type) (for detailed information on molecular characteristic, see Yokozaki, 2000). It should be noticed that both cell lines overexpress β-catenin (Asciutti et al., 2011). Cells were maintained in RPMI-1640 medium (Sigma Aldrich, Oslo, Norway) supplemented with fetal bovine serum (10%, FBS), Sodium pyruvate and penicillin streptomycin solution (1%) (Sigma Aldrich, Oslo, Norway) in a humidified incubator holding 5% CO_2 and 37°C. For proliferation assay, MKN74 and KATO-III were seeded in 96-well plates (2,500 cells/well and 3,000 cells/well, respectively) and incubated overnight. Ivermectin (MW: 875.09 g/mol) was dissolved in DMSO (100%) to 50 mM stock solution. Cells were treated with ivermectin (0–50 μM) or vehicle control (0.45% v/v DMSO) for 24, 48, and 72 h. Proliferation was measured using a commercial CCK-8 Kit (Sigma Aldrich, Oslo, Norway) with absorbance read at 450 nm. For cell cycle analysis, KATO-III cells were seeded as 3.0×10^5 cells/well in 6-well plates and incubated for 72 h with medium change after 48 h. Ivermectin was added to the wells as final concentrations of 12, 15 or 18 μM for 24 h. Cells were harvested by trypsin, washed twice in room tempered PBS, resuspended in ice cold ethanol (70%) and kept at −20°C for minimum 15 min. Cells were washed twice in cold PBS and centrifuged (1,500 rpm, 5 min, 4°C), and resuspended in freshly prepared PI staining solution (0.25% Triton- X-100, 50 μg/ml propidium iodide (PI) and 200 μg/ml RNAase) for minimum 30 min. Cell cycle distribution was analyzed using FACS. Single cells were gated to exclude doublets and clustered cells. 2.0×10^4 cells were counted per sample, and percentage cell distribution was derived from obtained histograms in the FACSDiva software. Results are presented as means of $n = 3$ replicates/treatments. Data was analyzed using Microsoft Excel 2010.

In Vivo Testing

Thirty-one INS-GAS mice were randomly divided into two groups: ivermectin treatment (12 females and nine males at age of 10 months) and controls (no treatment, six females and four males at age of 10 months). Ivermectin was reconstituted from lyophilized powder in DMSO to 50 mM solution and then diluted in saline before use. The treatment regimen was designed to let the mice tolerate the procedure easily, i.e., intraperitoneal injection at a dose of 10 mg/kg in a volume of about 0.5 ml/mouse with 27G needle once per day for 5 days, followed by no treatment for 5 days and then injection once per day for 10 days. This regimen was repeated 10 days later. The total duration of treatment was 2 months (2 × 30 days). Vehicle treatment was not performed because neither vehicle *per se* nor procedure would lead to any significant stress response. The mice were euthanized under isoflurane inhalation anesthesia (2–3%), and stomachs were collected as described previously (Zhao et al., 2014). Tumor volume density (% of glandular area of the stomach occupied by tumor) was measured using a point count method (Zhao et al., 2014). The tissue samples were collected for transcriptomics as aforementioned.

Statistical Analysis

Values are expressed as means ± SEM or SD (stated in individual figure legend). For comparison of two independent groups, student independent *t*-test was used. For comparison of multiple groups, one-way ANOVA with Tukey's or Dunnett's post-hoc tests were used (stated in individual figure legend). SPSS version 26.0 for Windows (SPSS Inc., Chicago, IL, United States) was used and a *p*-value < 0.05 was considered to be statistically significant. Other methods are stated in corresponding figure legends.

RESULTS

Computational Drug Repositioning Suggests the WNT/β-Catenin Signaling as Potential Target of Ivermectin

A cMap was created according to the gene expression signature (**Figures 2A,B**). A total of 2,428 drugs were categorized into 47 groups of inhibitors for, e.g., DNA synthesis, murine double minute (MDM) and lactate dehydrogenase, including ivermectin. Additionally, drugs we have demonstrated previously, including

TABLE 3 | Gene expression in networks comprised of ivermectin interactions and WNT/β-catenin signaling pathways in mouse gastric cancer (as presented in **Figure 4A**).

Gene	Ensembl ID	Log_2 FC	*p*-value	Entrez gene ID for patients	Entrez gene ID for mice
ABCB1	ENSMUSG00000040584	1.877	2.04E-04	5243	18671
ABCC3	ENSMUSG00000020865	0.525	1.16E-02	8714	76408
ABCC9	ENSMUSG00000030249	1.835	2.74E-11	10060	20928
ABCG2	ENSMUSG00000029802	0.921	3.97E-03	9429	26357
ANXA2	ENSMUSG00000032231	0.679	3.38E-04	302	12306
CAV1	ENSMUSG00000007655	1.181	8.61E-04	857	12389
CD44	ENSMUSG00000005087	1.156	1.42E-05	960	12505
CRABP2	ENSMUSG00000004885	4.298	2.97E-02	1382	12904
CTNNB1	ENSMUSG00000006932	0.208	4.75E-02	1499	12387
EGF	ENSMUSG00000028017	−1.946	3.86E-03	1950	13645
ETS1	ENSMUSG00000032035	0.621	2.69E-02	2113	23871
FBXL13	ENSMUSG00000048520	3.359	3.15E-02	222235	320118
FOXA2	ENSMUSG00000037025	−0.351	1.45E-02	3170	15376
FZD1	ENSMUSG00000044674	0.670	1.76E-03	8321	14362
GATA6	ENSMUSG00000005836	−0.331	1.95E-02	2627	14465
IL1A	ENSMUSG00000027399	3.560	1.60E-02	3552	16175
MAPRE1	ENSMUSG00000027479	−0.456	5.95E-03	22919	13589
MECP2	ENSMUSG00000031393	−0.374	5.89E-02	4204	17257
MSN	ENSMUSG00000031207	1.383	1.79E-17	4478	17698
NR1I2	ENSMUSG00000022809	1.174	2.29E-08	8856	18171
P2RX7	ENSMUSG00000029468	2.097	3.93E-07	5027	18439
PSMB8	ENSMUSG00000024338	1.376	8.55E-03	5696	16913
RASSF1	ENSMUSG00000010067	0.291	4.88E-02	11186	56289
RBP7	ENSMUSG00000028996	0.851	4.24E-02	116362	63954
RDX	ENSMUSG00000032050	0.749	1.53E-03	5962	19684
RUNX2	ENSMUSG00000039153	1.241	2.32E-04	860	12393
RXRA	ENSMUSG00000015846	−0.404	2.74E-03	6256	20181
SFRP1	ENSMUSG00000031548	1.093	2.91E-03	6422	20377
TGFB2	ENSMUSG00000039239	1.573	3.53E-05	7042	21808
TP63	ENSMUSG00000022510	5.030	2.28E-02	8626	22061
TTR	ENSMUSG00000061808	−1.516	1.78E-04	7276	22139
UBA7	ENSMUSG00000032596	1.008	2.12E-03	7318	74153
WNT5A	ENSMUSG00000021994	2.170	1.90E-14	7474	22418
ZEB1	ENSMUSG00000024238	2.031	8.00E-12	6935	21417

gemcitabine, paclitaxel, everolimus, and scopolamine, were also found (Zhao et al., 2014; Rabben et al., 2021).

Data/pathway mining revealed activation of the WNT/β-catenin signaling in human as well as mouse GC (**Table 2**). In addition to our own human GC and mouse GC data, seven independent datasets of human stomach adenocarcinoma (STAD) were found to have activation of the WNT/β-catenin (**Figure 3A** and **Table 2**). Using the knowledge-based repositioning strategy, nine targets were identified in connection with WNT/β-catenin signaling pathway and proliferation in both human and mouse GC (**Figure 3B**), i.e., ATP-dependent translocase (Abcb1b), retinol-binding proteins (Rbp), ATP binding cassette subfamily B member 1 (ABCB1), ATP Binding cassette subfamily G member 2 (ABCG2), cytochrome P450 family 3 subfamily A member 4 (CYP3A4), P-glycoprotein (also known as multi-drug resistant protein, MDRP), ATP binding cassette subfamily B member 4 (ABCB4), cytokine, and P2X purinoceptor 7 (P2RX7). Each gene/protein connected to a subset of algorithmically chosen genes based on the Ingenuity Knowledge Base. These genes were collectively activating both WNT/β-catenin signaling and proliferation, resulting in locally activated *z*-scores (shown in orange) (**Table 3**).

An *in silico* interaction network of ivermectin with WNT/β-catenin signaling pathway was constructed (**Figure 4A**). Inhibition of the targets of ivermectin led to the inhibition of downstream nodes in a "dose-dependent manner" (**Figure 4B**). It should be noticed that the inhibition of single molecules was not enough to have inhibitory or stimulatory effects on the signaling pathway.

Ivermectin Inhibits Cell Proliferation and Induces Cell Cycle Arrest

Testing of ivermectin in MKN74 and KATO-III cells showed that there were time- and concentration-depended inhibitions of proliferation by the drug with similar IC_{50} values for the periods of 24, 48 and 72 h (**Figures 5A,B**). Furthermore, ivermectin induced cell cycle arrest in a concentration-depended manner (**Figure 5C**). It should be noticed that ivermectin at IC_{50} did not affect the cells in S-phase but increased percentage of cells in G_1 while reducing percentage of cells in G_2/M phases. By contrast, higher concentration of ivermectin increased percentage of cells in S phase while reducing the percentage of cells in G_1 and G_2/M phases, suggesting that

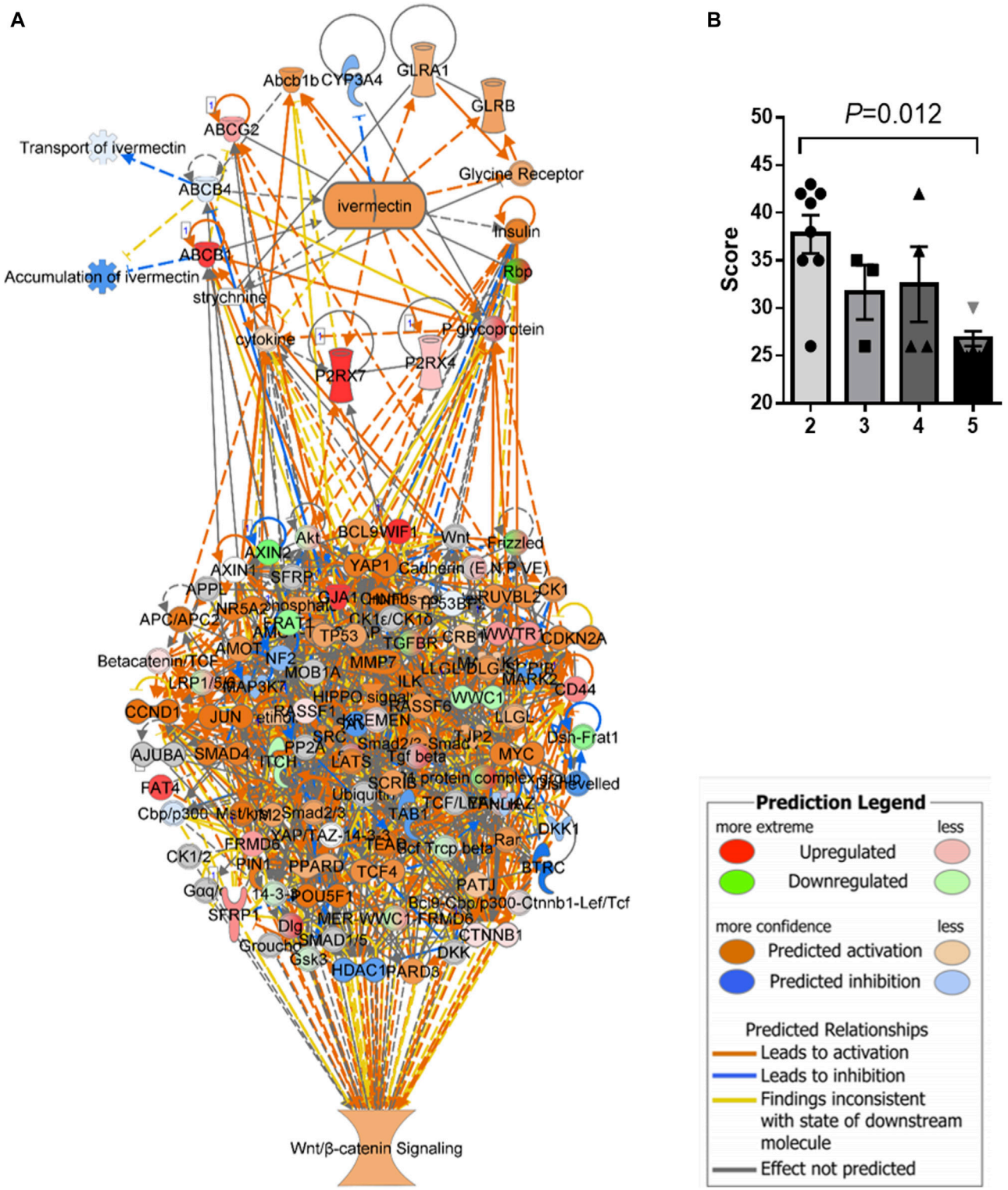

FIGURE 4 | *In silico* interaction network of ivermectin with WNT/β-catenin signaling pathway. **(A)** An interaction network of ivermectin with WNT/β-catenin signaling pathway was made using the Ingenuity Knowledge Base. **(B)** Two-/three-/four-/five combinations of inhibition/stimulation of nodes in the ivermectin cluster (**A**, upper cluster) had "dose-dependent" effect of the sum network scores of WNT/β-catenin (including HIPPO) pathway (**A**, lower cluster). Categorical values were set to each gene/node using a semi-quantitative method to quantify the color-change resulting from *in silico* inhibition. Dark blue colored nodes were represented by – 2, light blue as – 1, white as 0, light orange as +1 and dark orange as +2. Values are represented of means of $n = 3–8$ experiments per node/gene. Multiple comparison using one-way ANOVA with Tukey post hoc test was used. Created in IPA (QIAGEN).

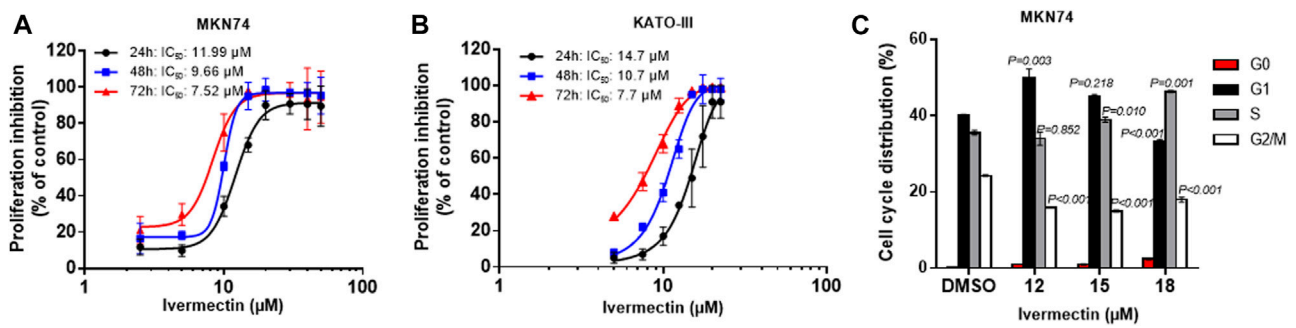

FIGURE 5 | Time- and concentration-dependent effects of ivermectin on proliferation and cell cycle. **(A,B)** Concentration-response curves upon 24–72 h ivermectin-treatment in MKN74 and KATO-III cells. Proliferation was assessed using CCK-8 Kit at 450 nm. IC_{50} values were calculated from sigmoidal regression curve fitting using variable slope on normalized response from log_{10}-transformed x-values (GraphPad Prism v.6). **(C)** Cell cycle analysis of KATO-III cells. Means of $n = 3$ replicates/treatment with SD. One-way ANOVA with Dunnett's post hoc test (2-sided) compared to respective control groups.

ivermectin arrested cells at the G_1 phase at IC_{50} and higher dose of the drug shifted cells to S phase.

Ivermectin Reduces Tumor Size Which Was Associated With Inactivation of WNT/β-Catenin Signaling, Down Regulation of Cell Proliferation and Upregulation of Cell Death Signaling Networks

A treatment regimen using ivermectin at 10 mg/kg for 2 months was established based on the *in silico* and pilot experiments. Mice tolerated the treatment well, although some mice had weight loss during treatment (<15%, $p > 0.05$, two-tailed). The mice had no serious side effects of ivermectin and no mice that were treated with ivermectin were killed according to the human primary endpoints which include stressful behavior, abdominal pain and impaired physical activity. The tumor size was reduced by ivermectin treatment (**Figure 6A**). Comparison analysis between mouse GC with and without ivermectin treatment revealed 4,112 differentially expressed genes (**Figure 6B**). The genes involved in WNT/β-catenin signaling pathway were particularly inhibited by ivermectin treatment, as shown by a change in *z*-scores from 1.151 (mouse GC without treatment) down to −1.789 (mouse GC after ivermectin treatment) (**Figure 6C** and **Table 2**) and log_2 fold-changes (**Figure 6D vs. 6E**).

Expression analysis in IPA revealed that cell proliferation was activated in mouse GC without treatment and inactivated in mouse GC with treatment. On the other hand, cell death including apoptosis was inactivated in mouse GC without treatment but activated in mouse GC with treatment (**Figures 7A–D**).

DISCUSSION

The next generation connectivity map (cMap) has been recently developed and should be acknowledged that the cMap methods and data are available without restriction to the research community (Subramanian et al., 2017). As pointed out in the original paper, a future comprehensive cMap might expand in multiple dimensions, e.g., new cell types, patient-derived induced pluripotent stem cells and genome-edited isogenic cell lines (Subramanian et al., 2017). Using this method, we found that the scores of the known drugs in treatment of GC (including ivermectin) were too low to indicate strong associations between these drugs and human GC gene expression signature, which was most likely due to the fact that the reference profile catalogue of cMap has been built to date on 12,328 genes of various cancer cell lines (including AGS which is a moderately differentiated human gastric adenocarcinoma hyperdiploid cell line) but not tumor tissues (https://clue.io/connectopedia/l1000_gene_space and https://clue.io/connectopedia/core_cmap_cell_panel).

In addition to the hypothesis generation approach by cMap, we further utilized data mining and pathway mining of knowledge-based datasets to identify the potential drugs in connection with a broad concept ranging from molecular entities (such as genes and proteins) to biological phenomena (such as molecular functions, pathways and phenotypes). Based on a better understanding of GC biology and signaling pathways, in the present study we focused on the WNT/β-catenin pathway by utilizing the algorithms of IPA which is built on a comprehensive, manually curated content of the QIAGEN Knowledge Base (over 57,000 publicly available datasets and continuously updated).

The results of the present study showed that the potential molecular targets and the mechanisms of action of ivermectin in GC differed from those in parasites in which ivermectin causes an influx of Cl-ions through the cell membrane of invertebrates by activation of specific ivermectin-sensitive ion channels (Laing et al., 2017; Chen and Kubo, 2018). In the present study, we identified ivermectin in connection with cell proliferation, particularly towards the genes (e.g., members of the adenosine triphosphate (ATP)-binding cassette (ABC) transporters). ABC are a superfamily of membrane proteins which play significant roles in transporting various exogenous and endogenous

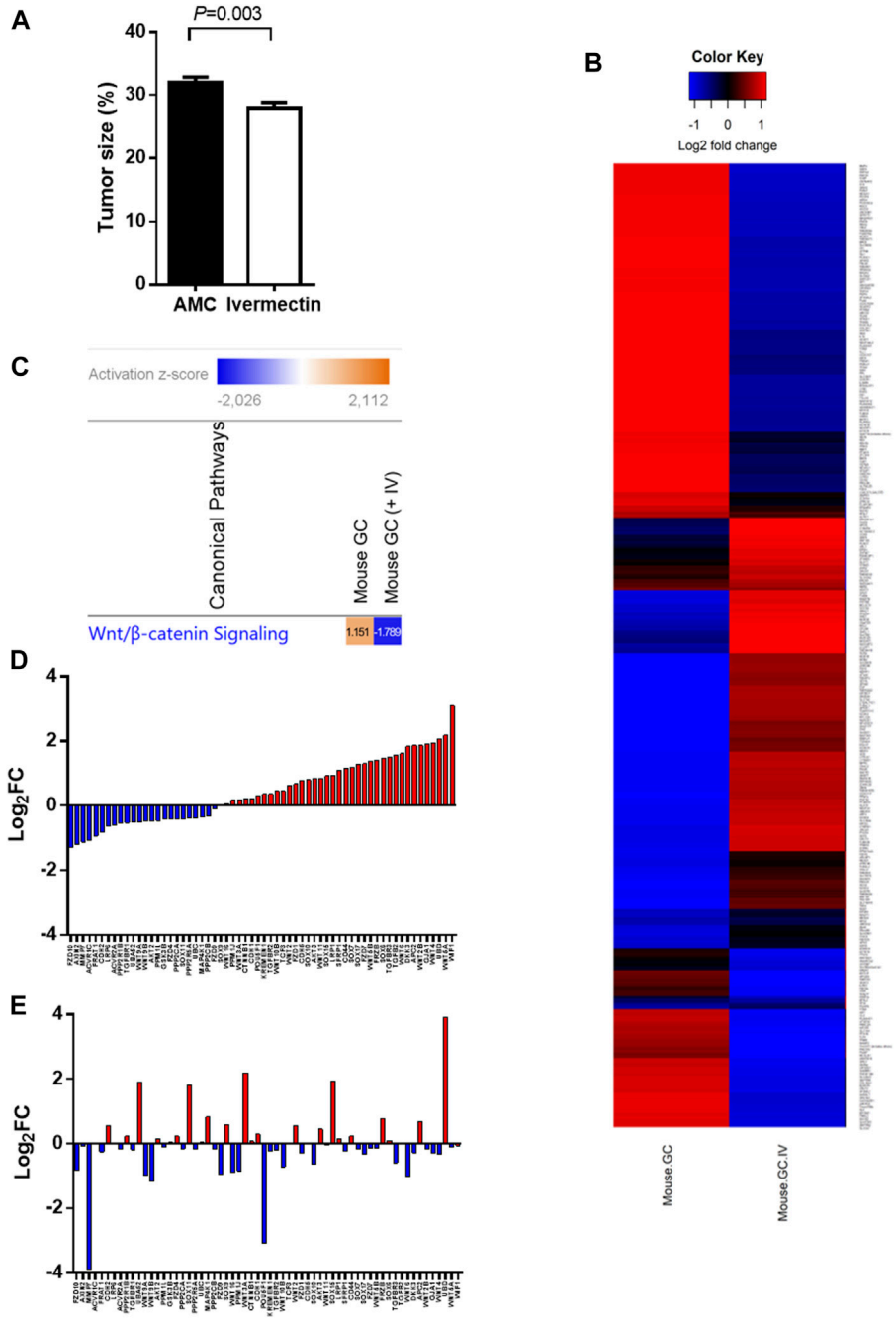

FIGURE 6 | Tumor size and gene expression profiles in response to ivermectin. **(A)** Tumor size (% of glandular area of stomach occupied by tumor) in age-matched controls (AMC, n = 14) and ivermectin-treated mice (n = 17) (Ivermectin). Independent t-test (2-sided) between group means (normality assumption met). Error bars represent SEM. **(B)** Global gene expression profile of mouse GC with and without ivermectin treatment (created in RStudio using heatmap.2 function). Only differentially expressed genes with $p < 0.05$ are included (4,112 genes). **(C)** WNT/β-catenin pathway was activated (z-score = 1.151) in mouse GC without treatment but inhibited in mouse GC with ivermectin treatment (z-score = −1.789). **(D,E)** WNT/β-catenin gene expressions in mouse GC mice without treatment **(D)** and with ivermectin treatment **(E)**. Note: same orders of individual genes in **(D)** and **(E)**.

substances across membranes against concentration gradients through ATP hydrolysis, and many of these transporters are known as multidrug resistance proteins (MRPs) (Mao et al., 2019). As showed in the present study, ivermectin also acted on the ABC and the signaling pathways, leading to inhibition of cell proliferation by deactivating LXR/RXR signaling (Beltowski, 2011; Saito-Hakoda et al., 2015).

It has been shown that activation of the WNT/β-catenin signaling pathway plays a pivotal role in many types of cancer (Clevers, 2006; Zhan et al., 2017). Previously, we and other

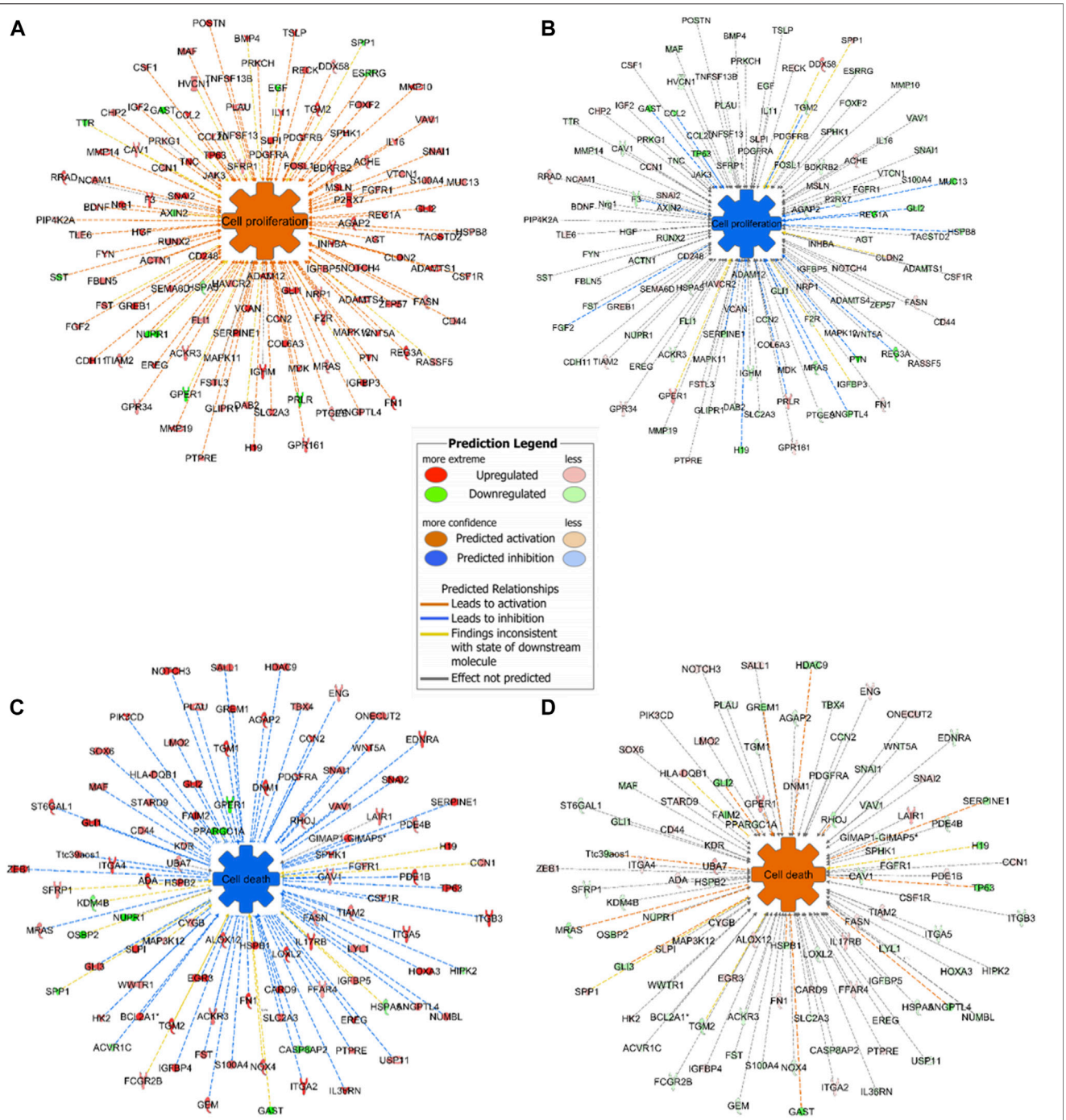

FIGURE 7 | Representative networks of cell proliferation and cell death in mice with or without ivermectin treatment. **(A)** Mouse GC cell proliferation network was created using BioProfiler in IPA. Only genes differentially expressed ($p < 0.05$, $Log_2FC \pm 1.0$) between mouse GC vs. WT were included. Overexpression of genes in the network results in activation of cell proliferation (orange; *z*-score > 0). **(B)** Genes in the cell proliferation network was downregulated in GC mice with ivermectin treatment (blue; *z*-score < 0). **(C)** Mouse GC cell death network including apoptotic markers was created using BioProfiler in IPA. Only genes differentially expressed ($p < 0.05$, $Log_2FC \pm 1.0$) between mouse GC vs. WT were included. Overexpression of genes in the network results in inhibition of cell death (blue; *z*-score < 0). **(D)** Cell death network was aberrantly expressed in GC mice with ivermectin treatment (orange; *z*-score > 0).

research groups have demonstrated that the tumorigenesis of gastric cancer involves the WNT/β-catenin signaling pathway and the inhibition of the signaling pathways by means of denervation can suppress the tumorigenesis (Zhao et al., 2014; Chiurillo, 2015; Koushyar et al., 2020; Rabben et al., 2021). In the present study, we applied *in silico* modelling to

show that ivermectin could inhibit the WNT/β-catenin signaling pathway including HIPPO signaling pathway, which is known to interact each other (Hayakawa et al., 2017; Li et al., 2019). We then employed *in vitro* and *in vivo* approaches to show that ivermectin could inhibit cell proliferation and reduce tumor size, which was associated with the inhibition of the WNT/β-catenin signaling pathway. Thus, we may suggest that ivermectin could target the WNT/β-catenin singling pathway, leading to a reduced tumorigenesis. This was also in line with possible antitumor actions of ivermectin in other types of cancer cells, such as breast, colon, lung, prostate and bladder (Melotti et al., 2014; Diao et al., 2019; Nappi et al., 2020).

Control of cell proliferation generally occurs during the G_1 phase and multiple signals, ranging from growth factors to DNA damage to developmental cues, influence the decision to enter S phase, when DNA is replicated (Duronio and Xiong, 2013). The results of the present study showed that ivermectin altered cell cycle in a concentration-dependent manner, which is consistent with a previous report showing accumulation of cells in the G_1/S phases (Zhang et al., 2019). In the present study, IC_{50}-dose of ivermectin caused cell cycle arrest at G_1 phase, whereas at higher doses, it caused S phase arrest. It has been suggested that WNT/β-catenin activation triggered cells in S phase, and HIPPO signaling might involve in G_1 phase (Benham-Pyle et al., 2016; Kim et al., 2019). The evidence of possible link between the cell cycle arrest and inhibition of WNT/β-catenin and/or HIPPO singling pathways is needed to be further investigated, particularly in the context of ivermectin for GC.

There were several limitations of the present study. The cell proliferation and apoptosis in the *in vitro* experiment were not evaluated further by flow cytometry nor specific assays, e.g., annexin V staining or caspase activity. However, the gene expression profiling confirmed the association between the activities of networks of cell proliferation and cell death in mice, namely increased in cell proliferation and decrease in cell death in GC mice without treatment, and reversed activities in GC mice treated with ivermectin. It should be noticed that the decrease in tumor size 2 months after ivermectin treatment was modest. As a matter of fact, in a separate experiment, we found that chemotherapy with 5-FU and oxaliplatin at the maximal dosage given to GC mice at the same age as ones in this study was without inhibition on the tumor size during 2 months of treatment (as same as in this study) (data not shown). However, the impacts of ivermectin treatment after a longer period of treatment alone and/or in combination with chemotherapy on resistance, migration and invasion could be worthwhile for future investigation. The results of the present study showed evidence of possible involvement of WNT/β-catenin signaling pathway in connection with the anti-cancer effect of ivermectin. For instance, prediction of ivermectin was successfully made by the WNT/β-catenin signaling pathway mining but not cMap. Validation of ivermectin was significant *in silico* model of the WNT/β-catenin signaling pathway. Up-regulation of WNT/β-catenin signaling pathway took place in patients, human cell lines and mouse model of GC. Ivermectin treatment induced downregulation of the WNT/β-catenin signaling pathway in the mouse GC. However, additional evidence is needed to demonstrate that the effect of ivermectin is dependent on WNT/β-catenin signaling pathway. For instance, it would be worthwhile to further investigate how modulation of the WNT/β- catenin signaling pathway with specific inhibitors and activators will affect the response to ivermectin treatment *in vitro* and *in vivo*.

CONCLUSIONS

The results of the present study show that ivermectin is a promising drug candidate for treatment of GC. The results may indicate an alternative mechanism of action of ivermectin, i.e., inhibition of the WNT/β-catenin signaling pathway in mammals rather than it acts on glutamate-gated chloride channels, which are common in nematodes, insects and ticks, thereby paralysing pharyngeal and somatic muscles. As ivermectin is exceptionally safe for mammals because of the blood/brain barrier, further pre-clinical and clinical studies of repositioning ivermectin for GC are warranted.

DATA AVAILABILITY STATEMENT

The original contributions presented in the study are publicly available. This data can be found here: The mouse RNA seq/microarray data have been deposited in the NCBI Bioproject database under the accession number PRJNA690520 which can be accessed using the following link: http://www.ncbi.nlm.nih.gov/bioproject/690520. The human microarray data is available online via Mendeley Data repository with DOI link at http://dx.doi.org/10.17632/hzmfshy7hp.1. The RNAseq data in mouse GC after ivermectin treatment is available from the authors upon request.

ETHICS STATEMENT

The studies involving human participants were reviewed and approved by Regional Committees for Medical and Health Research Ethics Central Norway (REK 2012-1029). The patients/participants provided their written informed consent to participate in this study. The animal study was reviewed and approved by Mattilsynet. Written informed consent was obtained from the individual(s) for the publication of any potentially identifiable images or data included in this article.

AUTHOR CONTRIBUTIONS

H-LR: *In vitro* and *in vivo* experiments, data analysis, manuscript writing; GTA: Patient samples, *in vivo* experiment and manuscript writing; AI and DK: cMap and manuscript writing; MKO: *In vivo* experiments and manuscript writing;

JEG: Patient samples and manuscript writing; TCW: *In vivo* model, manuscript writing; DC: Study idea and design, manuscript writing; C-MZ: Study idea and design, *in vivo* experiment and patient samples; manuscript writing.

FUNDING

We thank the research grants and PhD fellowships supported by the Liaison Committee between the Central Norway Regional Health Authority (Helse-Midt Norge RHF) and Norwegian University of Science and Technology (NTNU) (grant numbers 46056636/46056928/90061700/90061701), Joint Program of the Medical Faculty of NTNU and St. Olavs University Hospital, the Cancer Foundation of St. Olavs Hospital (Kreftfondet ved St. Olavs hospital), and the technical support by Genomics Core Facility (GCF) which is funded by the Faculty of Medicine and Health Sciences at NTNU and RHF.

REFERENCES

Andersen, P. I., Ianevski, A., Lysvand, H., Vitkauskiene, A., Oksenych, V., Bjørås, M., et al. (2020). Discovery and development of safe-in-man broad-spectrum antiviral agents. *Int. J. Infect. Dis.* 93, 268–276. doi:10.1016/j.ijid.2020.02.018

Antoszczak, M., Markowska, A., Markowska, J., and Huczyński, A. (2020). Old wine in new bottles: drug repurposing in oncology. *Eur. J. Pharmacol.* 866, 172784. doi:10.1016/j.ejphar.2019.172784

Asciutti, S., Akiri, G., Grumolato, L., Vijayakumar, S., and Aaronson, S. A. (2011). Diverse mechanisms of Wnt activation and effects of pathway inhibition on proliferation of human gastric carcinoma cells. *Oncogene* 30, 956–966. doi:10.1038/onc.2010.475

Ashburn, T. T., and Thor, K. B. (2004). Drug repositioning: identifying and developing new uses for existing drugs. *Nat. Rev. Drug Discov.* 3, 673–683. doi:10.1038/nrd1468

Beltowski, J. (2011). Inhibition of cell proliferation: a new role of liver X receptors. *Clin. Lipidol.* 6, 137–141. doi:10.2217/clp.11.3

Benham-Pyle, B. W., Sim, J. Y., Hart, K. C., Pruitt, B. L., and Nelson, W. J. (2016). Increasing β-catenin/Wnt3A activity levels drive mechanical strain-induced cell cycle progression through mitosis. *Elife* 5, e19799. doi:10.7554/eLife.19799

Callaway, E., and Cyranoski, D. (2015). Anti-parasite drugs sweep Nobel prize in medicine 2015. *Nature* 526, 174–175. doi:10.1038/nature.2015.18507

Chen, I. S., and Kubo, Y. (2018). Ivermectin and its target molecules: shared and unique modulation mechanisms of ion channels and receptors by ivermectin. *J. Physiol.* 596, 1833–1845. doi:10.1113/JP275236

Chiou, R., Stubbs, R. J., and Bayne, W. F. (1987). Determination of ivermectin in human plasma and milk by high-performance liquid chromatography with fluorescence detection. *J. Chromatogr.* 416, 196–202. doi:10.1016/0378-4347(87)80502-9

Chiurillo, M. A. (2015). Role of the Wnt/β-catenin pathway in gastric cancer: an in-depth literature review. *World J. Exp. Med.* 5, 84–102. doi:10.5493/wjem.v5.i2.84

Clevers, H. (2006). Wnt/beta-catenin signaling in development and disease. *Cell* 127, 469–480. doi:10.1016/j.cell.2006.10.018

GBD 2017 Stomach Cancer Collaborators (2020). The global, regional, and national burden of stomach cancer in 195 countries, 1990-2017: a systematic analysis for the global burden of disease study 2017. *Lancet Gastroenterol. Hepatol.* 5, 42–54. doi:10.1016/S2468-1253(19)30328-0

Davis, J. A., Paylor, R., McDonald, M. P., Libbey, M., Ligler, A., Bryant, K., et al. (1999). Behavioral effects of ivermectin in mice. *Lab. Anim. Sci.* 49, 288–296.

Diao, H., Cheng, N., Zhao, Y., Xu, H., Dong, H., Thamm, D. H., et al. (2019). Ivermectin inhibits canine mammary tumor growth by regulating cell cycle progression and WNT signaling. *BMC Vet. Res.* 15, 276. doi:10.1186/s12917-019-2026-2

Duronio, R. J., and Xiong, Y. (2013). Signaling pathways that control cell proliferation. *Cold Spring Harb. Perspect. Biol.* 5, a008904. doi:10.1101/cshperspect.a008904

Hayakawa, Y., Sakitani, K., Konishi, M., Asfaha, S., Niikura, R., Tomita, H., et al. (2017). Nerve growth factor promotes gastric tumorigenesis through aberrant cholinergic signaling. *Cancer Cell* 31, 21–34. doi:10.1016/j.ccell.2016.11.005

Hendriksen, C. F. M., and Morton, D. B.(Editors) (1999). "Humane endpoints in animal experiments for biomedical research," in Proceedings of the International Conference, Zeist, The Netherlands, November 22–25 (1998), (London: Royal Society of Medicine Press Limited, Laboratory Animals Supplement).

Hollingshead, M. G., Stockwin, L. H., Alcoser, S. Y., Newton, D. L., Orsburn, B. C., Bonomi, C. A., et al. (2014). Gene expression profiling of 49 human tumor xenografts from *in vitro* culture through multiple *in vivo* passages--strategies for data mining in support of therapeutic studies. *BMC Genomics* 15, 393. doi:10.1186/1471-2164-15-393

Ikeda, T. (2003). Pharmacological effects of ivermectin, an antiparasitic agent for intestinal strongyloidiasis: its mode of action and clinical efficacy. *Nippon Yakurigaku Zasshi* 122, 527–(538.) [in Japanese, with English summary]. doi:10.1254/fpj.122.527

Juarez, M., Schcolnik-Cabrera, A., and Dueñas-Gonzalez, A. (2018). The multitargeted drug ivermectin: from an antiparasitic agent to a repositioned cancer drug. *Am. J. Cancer Res.* 8, 317–331.

Kim, W., Cho, Y. S., Wang, X., Park, O., Ma, X., Kim, H., et al. (2019). Hippo signaling is intrinsically regulated during cell cycle progression by APC/CCdh1. *Proc. Natl. Acad. Sci. U.S.A.* 116, 9423–9432. doi:10.1073/pnas.1821370116

Koushyar, S., Powell, A. G., Vincan, E., and Phesse, T. J. (2020). Targeting wnt signaling for the treatment of gastric cancer. *Int. J. Mol. Sci.* 21, 3927. doi:10.3390/ijms21113927

Laing, R., Gillan, V., and Devaney, E. (2017). Ivermectin–old drug, new tricks?. *Trends Parasitol.* 33, 463–472. doi:10.1016/j.pt.2017.02.004

Li, N., Lu, N., and Xie, C. (2019). The Hippo and Wnt signalling pathways: crosstalk during neoplastic progression in gastrointestinal tissue. *FEBS J.* 286, 3745–3756. doi:10.1111/febs.15017

Liu, Z., Fang, H., Reagan, K., Xu, X., Mendrick, D. L., Slikker, W., Jr, et al. (2013). *In silico* drug repositioning: what we need to know. *Drug Discov. Today* 18, 110–115. doi:10.1016/j.drudis.2012.08.005

Mao, X., He, Z., Zhou, F., Huang, Y., and Zhu, G. (2019). Prognostic significance and molecular mechanisms of adenosine triphosphate-binding cassette subfamily C members in gastric cancer. *Medicine* 98, e18347. doi:10.1097/md.0000000000018347

Matsuda, T., and Saika, K. (2013). The 5-year relative survival rate of stomach cancer in the USA, Europe and Japan. *Jpn. J. Clin. Oncol.* 43, 1157–1158. doi:10.1093/jjco/hyt166

Melotti, A., Mas, C., Kuciak, M., Lorente-Trigos, A., Borges, I., and Ruiz i Altaba, A. (2014). The river blindness drug Ivermectin and related macrocyclic lactones inhibit WNT-TCF pathway responses in human cancer. *EMBO Mol. Med.* 6, 1263–1278. doi:10.15252/emmm.201404084

Musa, A., Ghoraie, L. S., Zhang, S. D., Glazko, G., Yli-Harja, O., Dehmer, M., et al. (2018). A review of connectivity map and computational approaches in pharmacogenomics. *Brief. Bioinform.* 19, 506–523. doi:10.1093/bib/bbw112

Nappi, L., Aguda, A. H., Nakouzi, N. A., Lelj-Garolla, B., Beraldi, E., Lallous, N., et al. (2020). Ivermectin inhibits HSP27 and potentiates efficacy of oncogene targeting in tumor models. *J. Clin. Invest.* 130, 699–714. doi:10.1172/JCI130819

Parkin, D. M., Bray, F., Ferlay, J., and Pisani, P. (2002). Global cancer statistics, 2002. *CA Cancer J. Clin.* 55, 74–108. doi:10.3322/canjclin.55.2.74

Pushpakom, S., Iorio, F., Eyers, P. A., Escott, K. J., Hopper, S., Wells, A., et al. (2019). Drug repurposing: progress, challenges and recommendations. *Nat. Rev. Drug Discov.* 18, 41–58. doi:10.1038/nrd.2018.168

Qu, X. A., and Rajpal, D. K. (2012). Applications of connectivity map in drug discovery and development. *Drug Discov. Today* 17, 1289–1298. doi:10.1016/j.drudis.2012.07.017

Rabben, H. L., Zhao, C. M., Hayakawa, Y., Wang, T. C., and Chen, D. (2016). Vagotomy and gastric tumorigenesis. *Curr. Neuropharmacol.* 14, 967–972. doi:10.2174/1570159x14666160121114854

Rabben, H. L., Andersen, G. T., Olsen, M. K., Øverby, A., Ianevski, A., Kainov, A., et al. (2021). Neural signaling modulates metabolism of gastric cancer. *iScience* 24, 102091. doi:10.1016/j.isci.2021.102091

Rawla, P., and Barsouk, A. (2019). Epidemiology of gastric cancer: global trends, risk factors and prevention. *Prz. Gastroenterol.* 14, 26–38. doi:10.5114/pg.2018.80001

Saito-Hakoda, A., Uruno, A., Yokoyama, A., Shimizu, K., Parvin, R., Kudo, M., et al. (2015). Effects of RXR agonists on cell proliferation/apoptosis and ACTH secretion/pomc expression. *PLoS One* 10, e0141960. doi:10.1371/journal.pone.0141960

Selim, J. H., Shaheen, S., Sheu, W. C., and Hsueh, C. T. (2019). Targeted and novel therapy in advanced gastric cancer. *Exp. Hematol. Oncol.* 8, 25. doi:10.1186/s40164-019-0149-6

Sitarz, R., Skierucha, M., Mielko, J., Offerhaus, J., Maciejewski, R., and Polkowski, W. (2018). Gastric cancer: epidemiology, prevention, classification, and treatment. *Cancer Manag. Res.* 10, 239–248. doi:10.2147/cmar.s149619

Subramanian, A., Narayan, R., Corsello, S. M., Peck, D. D., Natoli, T. E., Lu, X., et al. (2017). A next generation connectivity map: L1000 platform and the first 1,000,000 profiles. *Cell* 171, 1437–1452.e17. doi:10.1016/j.cell.2017.10.049

Sutherland, I. H., and Campbell, W. C. (1990). Development, pharmacokinetics and mode of action of ivermectin. *Acta Leiden* 59, 161–168.

Verbaanderd, C., Maes, H., Schaaf, M. B., Sukhatme, V. P., Pantziarka, P., Sukhatme, V., et al. (2017). Repurposing drugs in oncology (ReDO)-chloroquine and hydroxychloroquine as anti-cancer agents. *Ecancermedicalscience* 11, 781. doi:10.3332/ecancer.2017.781

Verbaanderd, C., Meheus, L., Huys, I., and Pantziarka, P. (2017). Repurposing drugs in oncology: next steps. *Trends Cancer* 3, 543–546. doi:10.1016/j.trecan.2017.06.007

Xue, H., Li, J., Xie, H., and Wang, Y. (2018). Review of drug repositioning approaches and resources. *Int. J. Biol. Sci.* 14, 1232–1244. doi:10.7150/ijbs.24612

Yang, Z., Li, C., Yan, C., Li, J., Yan, M., Liu, B., et al. (2019). KIF14 promotes tumor progression and metastasis and is an independent predictor of poor prognosis in human gastric cancer. *Biochim. Biophys. Acta Mol. Basis Dis.* 1865, 181–192. doi:10.1016/j.bbadis.2018.10.039

Yokozaki, H. (2000). Molecular characteristics of eight gastric cancer cell lines established in Japan. *Pathol. Int.* 50, 767–777. doi:10.1046/j.1440-1827.2000.01117.x

Zhan, T., Rindtorff, N., and Boutros, M. (2017). Wnt signaling in cancer. *Oncogene* 36, 1461–1473. doi:10.1038/onc.2016.304

Zhang, P., Zhang, Y., Liu, K., Liu, B., Xu, W., Gao, J., et al. (2019). Ivermectin induces cell cycle arrest and apoptosis of HeLa cells via mitochondrial pathway. *Cell Prolif.* 52, e12543. doi:10.1111/cpr.12543

Zhao, C. M., Hayakawa, Y., Kodama, Y., Muthupalani, S., Westphalen, C. B., Andersen, G. T., et al. (2014). Denervation suppresses gastric tumorigenesis. *Sci. Transl. Med.* 6, 250ra115. doi:10.1126/scitranslmed.3009569

Conflict of Interest: The authors declare that the research was conducted in the absence of any commercial or financial relationships that could be construed as a potential conflict of interest.

frontiers in Pharmacology

ORIGINAL RESEARCH
published: 08 April 2021
doi: 10.3389/fphar.2021.613458

Chemopreventive Effects of Dietary Isothiocyanates in Animal Models of Gastric Cancer and Synergistic Anticancer Effects With Cisplatin in Human Gastric Cancer Cells

Hanne-Line Rabben[1,2], Yosuke Kodama[1], Masahiko Nakamura[3], Atle Magnar Bones[4], Timothy Cragin Wang[1,5], Duan Chen[1], Chun-Mei Zhao[1,2] and Anders Øverby[1,3]*

[1]Department of Clinical and Molecular Medicine, Norwegian University of Science and Technology (NTNU), Trondheim, Norway, [2]The Central Norway Regional Health Authority, Stjørdal, Norway, [3]Center for Clinical Pharmacy and Clinical Sciences, School of Pharmacy, Kitasato University, Tokyo, Japan, [4]Cell, Molecular Biology and Genomics Group, Department of Biology, Norwegian University of Science and Technology (NTNU), Trondheim, Norway, [5]Division of Digestive and Liver Diseases, Columbia University College of Physicians and Surgeons, New York, NY, United States

OPEN ACCESS

Edited by:
Ramin Massoumi, Lund University, Sweden

Reviewed by:
Thomas Brzozowski, Jagiellonian University Medical College, Poland
Jianwei Zhou, Nanjing Medical University, China

***Correspondence:**
Hanne-Line Rabben
hanne.l.rabben@ntnu.no

Specialty section:
This article was submitted to Gastrointestinal and Hepatic Pharmacology, a section of the journal Frontiers in Pharmacology

Received: *02 October 2020*
Accepted: *09 February 2021*
Published: *08 April 2021*

Citation:
Rabben H-L, Kodama Y, Nakamura M, Bones AM, Wang TC, Chen D, Zhao C-M and Øverby A (2021) Chemopreventive Effects of Dietary Isothiocyanates in Animal Models of Gastric Cancer and Synergistic Anticancer Effects With Cisplatin in Human Gastric Cancer Cells. Front. Pharmacol. 12:613458. doi: 10.3389/fphar.2021.613458

Naturally occurring isothiocyanates (ITCs) from edible vegetables have shown potential as chemopreventive agents against several types of cancer. The aims of the present study were to study the potential of ITCs in chemoprevention and in potentiating the efficacy of cytotoxic drugs in gastric cancer treatment. The chemoprevention was studied in chemically induced mouse model of gastric cancer, namely N-methyl-N-nitrosourea (MNU) in drinking water, and in a genetically engineered mouse model of gastric cancer (the so-called INS-GAS mice). The pharmacological effects of ITCs with or without cisplatin were studied in human gastric cell lines MKN45, AGS, MKN74 and KATO-III, which were derived from either intestinal or diffused types of gastric carcinoma. The results showed that dietary phenethyl isothiocyanate (PEITC) reduced the tumor size when PEITC was given simultaneously with MNU, but neither when administrated after MNU nor in INS-GAS mice. Treatments of gastric cancer cells with ITCs resulted in a time- and concentration-dependent inhibition on cell proliferation. Pretreatment of gastric cancer cells with ITCs enhanced the inhibitory effects of cisplatin (but not 5-fluorouracil) in time- and concentration-dependent manners. Treatments of gastric cancer cells with PEITC plus cisplatin simultaneously at different concentrations of either PEITC or cisplatin exhibited neither additive nor synergetic inhibitory effect. Furthermore, PEITC depleted glutathione and induced G_2/M cell cycle arrest in gastric cancer cells. In conclusion, the results of the present study showed that PEITC displayed anti-cancer effects, particularly when given before the tumor initiation, suggesting a chemopreventive effect in gastric cancer, and that pretreatment of PEITC potentiated the anti-cancer effects of cisplatin, possibly by reducing the intracellular pool of glutathione, suggesting a possible combination strategy of chemotherapy with pretreatment with PEITC.

Keywords: dietary (or plant) isothiocyanates, gastric cancer, glutathione, glutamine, cisplatin, mice

INTRODUCTION

Gastric cancer is one of the leading causes of cancer in the world with over one million new cases reported in 2018 (GLOBOCAN) (Ferlay et al., 2013; Bray et al., 2018). Despite dramatic decline in gastric cancer incidences in later years, gastric cancer is the fifth most common cancer with a 5-year survival rate below 25%, making gastric cancer the third leading cause of cancer mortality worldwide (Ferlay et al., 2010; Ferlay et al., 2013). Chemoprevention of gastric cancer is to chemically prevent or delay the occurrence of malignancy. Although *Helicobacter pylori (H. pylori)* eradication can be an effective preventive method due to the putative pathogenic mechanisms, the chemoprevention using natural, synthetic or biological agents has enormous potential, given the high incidence together with the healthcare costs of treatment (Steward and Brown, 2013; Tan and Wong, 2013; Dunn et al., 2016). The treatments of gastric cancer include surgery, and chemotherapy regimens with either mono-chemotherapy (using single drug) or combination-chemotherapy (e.g., fluoropyrimidines and platinum-based therapies) for inoperable or metastatic gastric cancer (Van Cutsem et al., 2006; Cunningham et al., 2008; Koizumi et al., 2008; Kang et al., 2009; Orditura et al., 2014). However, patients with unresectable advanced gastric cancer usually have poor outcomes with median survivals of 10–18 months. Nearly half of patients with resectable gastric cancer have a recurrence and median survival is about 6 months (Leiting and Grotz, 2019). Thus, a challenge for improving patient care of gastric cancer in terms of survival and quality of life appears to be ineffective cytotoxic chemotherapy. These facts indicate that there are still great needs for improvement in the prevention and treatment of gastric cancer. Previously, we have showed that denervation (surgically, pharmacologically or genetically) suppressed the tumorigenesis of gastric cancer, which was associated with a decrease in WNT/β-catenin signaling, the suppression of stem cell expansion through M3 receptor-mediated cholinergic signaling and the reversion of metabolic reprogramming, and that the combination of denervation and mono-chemotherapy led to an enhanced effect on tumor growth and survival in an animal model of gastric cancer (Zhao et al., 2014; Rabben et al., 2016). Recently, we have further shown that neural signaling modulated metabolism of gastric cancer, reflected by metabolic switch from glutaminolysis to OXPHOS/glycolysis and normalization of the energy metabolism after denervation (Rabben et al., 2021). In the present study, we wanted to explore the potential of a class of anti-cancer agents, isothiocyanates (ITCs) for chemoprevention and enhancement of chemotherapy as they are also shown to interfere with tumor metabolism (Conaway et al., 2002; Lv et al., 2020).

Naturally occurring isothiocyanates (ITCs) are electrophilic plant phytochemicals derived from glucosinolates of edible vegetables such as broccoli, cauliflower, brussels sprouts, and cabbage. Phenethyl isothiocyanate (PEITC) has been tested in *in vitro*, *in vivo* and in clinical trials to study about the potential effects of prevention and treatment of different types of cancer (Hu and Morris, 2004; Keum et al., 2004; Keum et al., 2005; Clarke et al., 2008; Chu et al., 2009; Wu et al., 2009; Li et al., 2010; Tomczyk and Olejnik, 2010; Zhang, 2010; Chung et al., 2013; Li and Zhang, 2013). The aims of the present study were to study whether ITCs could prevent gastric tumorigenesis and whether ITCs could enhance the inhibitory effect of mono-chemotherapy on gastric cancer; and if so, to investigate the possible underlying mechanisms. To these ends, we utilized chemically induced mouse model of gastric cancer, i.e., N-methyl-N-nitrosourea (MNU) in drinking water, and genetically engineered mouse model of gastric cancer (the so-called INS-GAS mice) for studying chemoprevention, and used human gastric cancer cell lines, i.e., MKN45, AGS, MKN74 and KATO-III derived from either intestinal or diffused types of gastric carcinoma for studying the pharmacological effects of ITCs with or without cisplatin *in vitro*.

The possible mechanisms underlying the anti-cancer effects of ITCs have been suggested to involve inhibition of cytochrome P450 enzymes, induction of phase II detoxification enzymes, such as glutathione S-transferase (GST) and apoptosis, and cell cycle arrest, inhibition of migration, disruption of microtubules, and dysregulation of signaling pathways including major regulators such as WNT/β-catenin signaling pathway, NRF2, ERK, Jun and Akt signaling pathways (Yang et al., 2010; Gupta et al., 2014; Øverby et al., 2014; Lawson et al., 2015; Chen et al., 2018). In addition, glutathione (GSH) is a powerful regulatory tripeptide with antioxidant function that protects cells from oxidative stress by removing free radicals and peroxides. We and others have shown that ITCs conjugate with GSH, leading to depletion of GSH, elevation of oxidative stress and expression of GST-encoding genes, and that there are close relationship between glutathione and the levels of glutamine and glutamate in the cell-pool important for redox homeostasis (Øverby et al., 2015). Thus, we hypothesized that ITCs would enhance the cytotoxicity of cisplatin by depleting cells of GSH, and thus measured the levels of GSH and the ratio between glutamine and glutamate in connection with cell growth inhibition after treatment of ITCs.

MATERIALS AND METHODS

Animals and Experimental Groups

All mice at ages between 1–12 months were housed three to four mice per cage on wood chip bedding with a 12 h light/dark cycle, room temperature of 22°C and 40–60% relative humidity at the standard housing conditions in a specific pathogen-free environment. Ninety mice including 54 wild-type (FVB) mice and 26 INS-GAS mice were divided into the following experimental groups: FVB mice (n = 16, eight male, eight female), FVB mice + MNU (n = 11, five female, six male), FVB mice + MNU + prePEITC (n = 16, eight female, eight male), FVB mice + MNU + postPEITC (n = 11, five female, six male), INS-GAS mice (n = 24, 10 female, 14 male), and INS-GAS mice + PEITC (n = 12, six female, six male). In each experiment, mice were randomly divided into different subgroups with gender-balance.

Treatment of Phenethyl Isothiocyanate in a Chemically Induced Mouse Model of Gastric Cancer

The chemically induced gastric cancer model (FVB + MNU) was established according to our previous report (Zhao et al., 2014). In brief, mice were exposed to N-Methyl-N-nitrosourea (MNU, Sigma Chemicals), which was dissolved in distilled water at a concentration of 240 ppm and freshly prepared twice per week for administration in drinking water in light-shielded bottles ad libitum. MNU was administered in the drinking water starting at 4 weeks of age and continued from the next 10 weeks followed by euthanization at age 12 months. PEITC was administered through an AIN-76A diet (3–5 μmol PEITC/g diet) either during or following administration of MNU. Mice were euthanized at age of 12 months.

Treatment of Phenethyl Isothiocyanate in Genetically Engineered Mouse Model of Gastric Cancer

The transgenic insulin-gastrin mice (INS-GAS mice) that over-express gastrin develop spontaneously gastric cancer were generated as previously described (Zhao et al., 2014). Mice received PEITC through an AIN-76A diet (3–5 μmol PEITC/g diet) for 10 weeks or standard pellet food (RM1801002, Scanbur BK AS). Mice were euthanized at the age of 12 months.

Tissue Sampling

The stomachs were removed, opened along the greater curvature, washed in 0.9% (w/v) NaCl, and pinned flat on a petri-dish-silicone board. Each stomach was photographed digitally; the tumor profiles in both anterior and posterior sides of the stomach were drawn separately and subjected to morphometric analysis of the volume density (expressed as the percentage of glandular volume occupied by the tumor) using point-counting technique with a test grid comprised of a 1.0 cm square lattice. This grid was placed over each photograph (40 cm^2 × 30 cm^2), and the numbers of test points overlying the tumor and gastric glandular area were determined.

Chemicals and Reagents

Phenethyl isothiocyanate (PEITC, Sigma Aldrich, United States, cat. no. 253731-5G), Benzyl isothiocyanate (BITC, Sigma Aldrich, Poland, cat. no. 252492-5G) and Allyl isothiocyanate (AITC, Sigma Aldrich, Germany, cat. no. 377430-100G) were dissolved in 100% dimethylsulfoxide (DMSO) to working concentrations. Cisplatin (Wako Pure Chemical Industries Ltd., Osaka, Japan, cat. no. 033-20091, Lot. SAQ1693 or TOCRIS Bioscience, Abingdon, United Kingdom, cat. no. 2251) was dissolved in PBS (Nacalai Tescue, Japan, cat. no. 14249-24) under gentle warming, and 5-fluorouracil (Sigma Aldrich, China) was dissolved in 100% DMSO. The following cell culture supplements were used: DMEM (Nacalai tesque, Japan, cat. no 08456-65); Fetal Bovine Serum (FBS; ThermoFisher Scientific, United States), antibiotic-antimycotic solution containing penicillin, streptomycin and amphotericin B (Nacalai tesque, Japan, cat. no. 02892-54), Penicillin-streptomycin solution (Sigma Aldrich, Oslo, Norway, cat. no. P4333-100ML), RPMI-1640 medium (Sigma Aldrich, Norway, cat. no. R8758-500ML with 0.3 g/L (2 mM) glutamine), DMEM (Gibco, ThermoFisher Scientific, Oslo, Norway, cat. no. A14430-01 without L-glutamine, D-glucose, phenol red and sodium pyruvate); dialyzed FBS (Life technologies, United States, Cat. no 26400-036); L-glutamine (Sigma Aldrich, Oslo, Norway, cat. no G7513); Sodium pyruvate (Sigma Aldrich, Oslo, Norway, cat. no. S8636). For cell cycle analysis: Propidium iodide (P1, Sigma Aldrich, Oslo, Norway, cat. no P4170-10MG); Triton-X (Sigma Aldrich, Oslo, Norway, cat. no. T9284), RNase A (Sigma Aldrich, Oslo, Norway, cat. no R4875-100MG). For GSH determination: 5-Sulfosalicylic acid (SSA) solution (5.0%); For Western Blot: RIPA cell lysis buffer (Pierce) containing 0.1% MG132 Proteasome Inhibitor (Cayman Chemical), 1.0% Protease inhibitor cocktail (Sigma Aldrich) and 10% PhosStop Phosphatase Inhibitor Cocktail (Roche). Antibodies: Primary antibody mouse monoclonal anti human p53 clone DO-1 (Santa Cruz: sc-126); Mouse monoclonal anti-β-actin clone; Anti-mouse IgG HRP-linked whole Ab sheep (GE Healthcare: NA931)/Anti-Rabbit IgG, HRP-linked whole Ab donkey (GE Healthcare: NA934).

Cell Culture

Human gastric carcinoma cancer cell lines AGS and MKN45 were maintained in Dulbecco's Modified Eagle's Medium (DMEM; Nacalai tesque, Japan) supplemented with 10% fetal bovine serum and 1% antibiotic-antimycotic solution containing penicillin, streptomycin and amphotericin B in a humidified incubator holding 5% CO_2 and 37°C. Human gastric carcinoma cancer cell lines MKN74 and KATO-III were maintained in RPMI-1640 medium supplemented with 10% FBS and 1% penicillin-streptomycin solution. Passages were performed when cultures reached 70–80% confluency. For the studies investigating glutamate and glutamine contents, DMEM containing 4.5 g/L glucose, 2 mM glutamine or 0.2 mM glutamine and 1 mM sodium pyruvate supplemented with dialyzed FBS was used.

Proliferation Assay

For proliferation assay, 1,500 cells of AGS, 2,500 of MKN45 or MKN74 or 3,000 cells of KATO-III were seeded in 96-well plates before incubated overnight allowing cells to confluate. Treatments were always accompanied by vehicle controls (n = 12) on each plate (0.05% DMSO). Cells were treated with AITC (Sigma Aldrich, Germany), BITC (Sigma Aldrich, Poland), PEITC (Sigma Aldrich, United States), cisplatin (Wako Pure Chemical Industries Ltd., Japan) or (Tocris, Norway) and 5-fluorouracil (Sigma Aldrich, China) as indicated in the text. Following treatment, Cell Count Reagent SF (Nacalai tesque, Japan) was added according to providers' instructions to each well before mixing and incubating for 1.0–1.5 h. Proliferation was determined by measuring absorbance at 450 nm using a well plate reader. Defined DMEM was used to perform experiments with controlled levels of glutamine and glucose.

Cell Cycle Analysis

Human gastric cancer cells KATO-III were seeded as 2.5 × 10^5 cells in 6-well plates and incubated over two nights before treated with 0, 5 or 10 μM PEITC for 12 and 24 h or PEITC (0, 5, 10 μM)

together with cisplatin (25 or 50 μM) for 24 h. Cells were harvested, resuspended in PBS and fixated in chilled ethanol (−20°C, 70%, Kemetyl Norway) for minimum 15 min. Cells were then pelleted and resuspended in freshly prepared propidium iodide (PI) staining solution (0.25% Triton- X-100, 50 μg/ml PI and 200 μg/ml RNase A) for 30 min. Cell cycle distribution was analyzed using a FACS Canto flow cytometer counting 2×10^4 cells per sample in triplicates. Cell cycle distribution was acquired from the obtained histograms using FACS Diva software.

Morphology

To study the effect of PEITC on cells, AGS and MKN74 cells were seeded in T_{25} flasks (1.5×10^5 cells per flask) and left for overnight incubation before treating with 5–20 μM PEITC or vehicle control (0.1% DMSO) for 24 h. The cultures were then observed and pictures captured through an inverted microscope in phase contrast mode.

Total GSH Determination

Total cellular glutathione level was determined in PEITC, AITC or BSO-treated AGS cells. Cells were seeded in T_{25} flasks (1.5×10^5 cells per flask) and incubated overnight prior to treatment. The cultures were treated with either 10–20 μM PEITC, 50–100 μM AITC, or 0–100 μM BSO or vehicle control (0.1% DMSO) for 3 or 6 h. The doses were based on IC_{50}-range and previous literature. Each treatment was performed in quadruples. Cells were harvested and centrifuged (1,500 rpm, 5 min) before determination of total cellular glutathione using a commercial glutathione assay kit (Sigma, United States) according to manufacturers' instructions. Briefly, cell pellets were deproteinized in 5-sulfosalicylic acid (SSA) solution (5%), vortexed and snap-freezed (3 times in total) before centrifugation (1,500 rpm, 5 min). Supernatants were transferred to clean tubes and stored on ice until analysis. 10 μl from each sample was applied to a 96—well plate in separate wells in duplicates and mixed together with 150 μl reaction mixture containing 95 mM potassium phosphate buffer (pH 7), 0.95 mM EDTA, 0.031 mg/ml DTNB, 0.115 units/ml glutathione reductase and 0.24% 5-sulfosalicylic acid. Finally, 50 μl of NADPH solution (0.16 mg/ml, resulting in final concentration of 0.038 mg/ml (48 μM) NADPH) was added to each well and mixed. Immediately after mixing, a kinetic read was performed in 1 min intervals for 5 min at 412 nm using a spectrophotometric plate reader in order to detect the formation of the yellow product 5-thio-2-nitrobenzoic acid (TNB).

Glutamate/Glutamine Determination

For glutamate/glutamine detection, AGS cells were seeded in 24-well plates (1.0×10^4 cells per well) and incubated over night to attain confluency. The cultures were then treated with PEITC (10–30 μM) and AITC (50–200 μM) for 2–24 h in defined DMEM containing dialyzed FBS before samples were collected and analyzed for glutamate and glutamine content. Determination of glutamate/glutamine was performed using a detection kit (Sigma, United States) following the manufacturers' instructions. Briefly, from each sample to be analyzed, one sample was prepared for estimating endogenous glutamate, and one sample was prepared for estimating glutamate converted from glutamine based on an initial deamination reaction catalyzed by glutaminase of the samples. All samples were then mixed with glutamic dehydrogenase which generates α-ketoglutarate and converts NAD^+ to NADH which was detected spectrophotometrically at 340 nm. Glutamate content was then calculated using a standard curve, whereas glutamine content was calculated by subtracting the endogenous glutamate concentration from the total concentration of endogenous glutamate and glutamine-derived glutamate.

Spheroid 3D Culture

AGS cells were seeded in 96-well plates (1,500 cells per well) with U-shaped bottoms with surface that prevents cells from attaching to the surface (Sumitomo Bakelite Co. Ltd., Japan). The cells were then incubated for 1 day to allow the cells to generate a spheroid-like structure before these spheroids were treated with PEITC (0–50 μM) for 48 h. After treatment, proliferation was assayed as described above.

Western Blot

Western Blot from whole cell extract was performed in order to investigate the presence of protein p53. Cell extracts were prepared using ice-cold RIPA cell lysis buffer (Pierce) containing 0.1% MG132 Proteasome inhibitor (Cayman Chemical), 1% Protease inhibitor cocktail (Sigma Aldrich) and 10% PhosStop phosphatase inhibitor Cocktail (Roche). Bicinchoninate protein quantification (BCA) assay (Nacalai Tesque) was performed in order to determine protein concentrations in the cell lysates prior to SDS PAGE. Samples were denatured in sample buffer (4x) (NuPAGE LDS, Novex, Life Technologies, pH 8.4) with 5% 2-mercaptoethanol at 100°C for 10 min. Five microgram of protein or molecular weights marker were loaded into the lanes on the SDS PAGE gel and run in MOPS running buffer (NuPAGE, Life Technologies, pH 7.7) for 5 min at 150 V followed by 40 min at 200 V. After electrophoresis, gels were blotted onto polyvinylidene difluoride (PVDF) membranes in NuPAGE transfer buffer (Life Technologies). Block ACE solution (DS Pharma Biomedical) was used to block the membrane for 1 h at room temperature. Primary antibody mouse monoclonal anti human p53 clone DO-1 (1:200, Santacruz: sc-126) was added to the membrane and incubated overnight at 4°C. Mouse monoclonal anti-β-actin clone, which recognize β-actin, was used as internal standard. The membrane was washed in tris-buffered saline with 0.5% Tween 20 (TBST) followed by incubation with secondary antibody anti-mouse IgG HRP-linked whole Ab sheep (1:500) (GE Healthcare: NA931)/Anti-Rabbit IgG, HRP-linked whole Ab donkey (1:500) (GE Healthcare: NA934) for 1 h at room temperature. Finally, chemiluminescence capturing using Clarity Western ECL substrate (Bio-RAD) was applied, and images were acquired using a ImageQuant LAS 500 system (GE Healthcare). Quantification of p53 band area was performed in Image studio Lite (LI-COR Biosciences).

Statistical Analysis

Values are expressed as means ± SEM in *in vivo* experiments. Pairwise comparisons between experimental groups were done using one-way ANOVA with Dunnett's test (1-sided) or student's

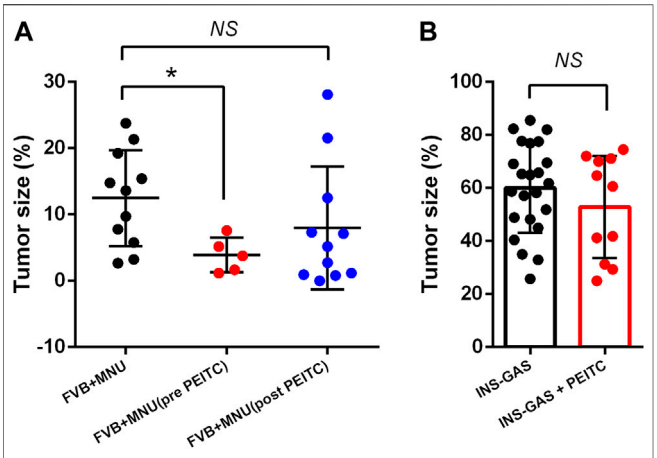

FIGURE 1 | Tumor size of gastric cancer in mice that completed the study period of 45–50 weeks. FVB mice received MNU for 10 weeks (n = 11) or MNU together with PEITC (3–5 μmol PEITC/g diet) for 10 weeks (n = 5) or post MNU treatment (n = 11) **(A)** and in INS-GAS mice with or without PEITC (3–5 μmol PEITC/g diet) for 10 weeks **(B)**. Mean ± SEM. Tumor size expressed as volume density (% of glandular area occupied by tumor). ANOVA + Dunnett's test (1-tailed) in **(A)**, student t-test in **(B)**. *$p < 0.05$; NS, not significant; PEITC, phenethyl isothiocyanate; MNU, N-methyl-N-nitrosourea.

t-test between INS-GAS mouse GC tumors with *vs.* without PEITC. In *in vitro* experiments, cell proliferation is represented by means of n = 3-6 replicates/treatment ± SD. IC_{50} values were calculated from sigmoidal regression curve fitting using variable slope on normalized response from log (10)-transformed x-values (GraphPad Prism v.6). Standard deviation (SD) values (%) were omitted from cultures with 98% or higher inhibited growth as these yielded non-representatively high SD values. Cell cycle distribution was analyzed using one-way ANOVA on normally distributed data with Dunnett's 2-sided post hoc test *vs.* control groups. All tests were with a significance cutoff of $p < 0.05$.

RESULTS

Two mouse models of gastric cancer were used, i.e., MNU-induced gastric cancer (MNU mice) and genetically engineered spontaneously gastric cancer (INS-GAS mice). Body weight of mice with or without PEITC increased due to aging of the mice but was not affected by PEITC treatment during the period of experiment (10 weeks). Tumour size of gastric cancer was significantly reduced by PEITC when given during MNU but neither after MNU, nor in INS-GAS mice (**Figures 1A,B**).

To demonstrate the cytotoxicity of ITCs in gastric cancer, four human gastric carcinoma cell lines were used; MKN45, AGS, MKN74 and KATO-III. Aromatic PEITC, BITC or aliphatic AITC resulted in a time and dose-dependent inhibition of cell proliferation (**Figures 2A–E**). The aromatic ITCs displayed a higher potential in inhibiting cell proliferation in both MKN45 and AGS compared to AITC. The MKN74, MKN45 and KATO-III cells proved to be more tolerant to ITC-treatment than the AGS cells in terms of IC_{50}-values. All cell lines showed alterations in cell morphology by ITC-treatments with a gradual increase in non-confluent cells with increasing ITC-doses as demonstrated by PEITC-treated AGS cells (**Figure 2F**). A spheroid 3D culture of AGS cells treated with PEITC for 24 and 48 h showed decreased growth upon increasing doses (**Figure 2G**).

Due to the electrophilic central C-atom in the reactive –N=C=S group, ITCs are able to antagonize multiple targets including glutathione. We therefore next examined the GSH concentration upon PEITC and AITC treatment. GSH depletion was both time- and dose-dependent in AGS cells (**Figures 3A,B**). Additionally, the synthetic amino acid Buthionine sulfoximine (BSO) depleted GSH in time- and dose-dependent manner (**Figure 3C**).

Reflected by the glutathione cycle, there are close relationships between glutathione and the levels of glutamine and glutamate in the cell-pool important for redox homeostasis. We next investigated the ratio between glutamine and glutamate after PEITC. PEITC increased the ratio of glutamine/glutamate in a dose-dependent manner, and furthermore inhibited cell proliferation in glutamine-reduced medium in a concentration-depended manner (**Figures 4A,B**).

The GSH-pool is an important factor for the cancer cells to maintain redox homeostasis. By depleting cells of glutathione, we hypothesized that ITCs would enhance the *in vitro* cytotoxicity of cisplatin. To investigate the potential effects of ITCs, AGS and MKN45 cells were pretreated with PEITC, BITC or AITC for 1, 3 or 24 h followed by cisplatin or 5-FU treatment for 48 h (**Figures 5A–E**). Pretreatment with 20 μM PEITC in MKN45 cells for 1 h lowered the IC_{50} of cisplatin by 2.7-fold, while pretreatment for 3 h lowered the IC_{50} of cisplatin 7-fold. After 24 h, the reduction in IC_{50} was 8.5-fold (**Figure 5A**, third panel). Pre-treatment with 20 μM PEITC in AGS cells showed 10-fold reduction after 1 h (**Figure 5B**). A similar observation was made for the BITC compound, where 20 μM BITC showed 4.6 and 5.7-folds reductions in IC_{50} after 1 and 24 h, respectively (**Figure 5C**). The aliphatic AITC failed to induce the synergistic effects with cisplatin, only lowering the IC_{50} by 1.3-fold after 3 h or even showing increased IC_{50} upon pretreatment (1 and 24 h, **Figure 5D**). Substituting cisplatin by 5-FU did not achieve the same inhibition using PEITC (**Figure 5E**).

Simultaneous treatments with PEITC (2.5 μM) and cisplatin at increasing doses showed no additional inhibitory effect or even had antagonistic effect as reflected in increased IC_{50} values when PEITC was added (**Figures 6A,B**).

Cell cycle distribution of KATO-III cells upon 12 and 24 h treatments with PEITC resulted in G_2/M phase arrest (**Figure 7A**). However, when treated with 0, 5 or 10 μM PEITC together with 0, 25 or 50 μM cisplatin, a decrease in G_1 phase was accompanied by increase in G_2/M phase and slight increase in apoptotic cells (reflected by sub G_1/G_0 phase increase) (**Figure 7B**). Treatment of AGS cells with 0 or 5 μM PEITC for 24 h showed increased level of protein p53 as determined by Western Blot (**Figures 7C,D**).

DISCUSSION

Long-term exposure to *H. pylori* is associated with progression of precancerous lesions in the stomach and infected individuals may

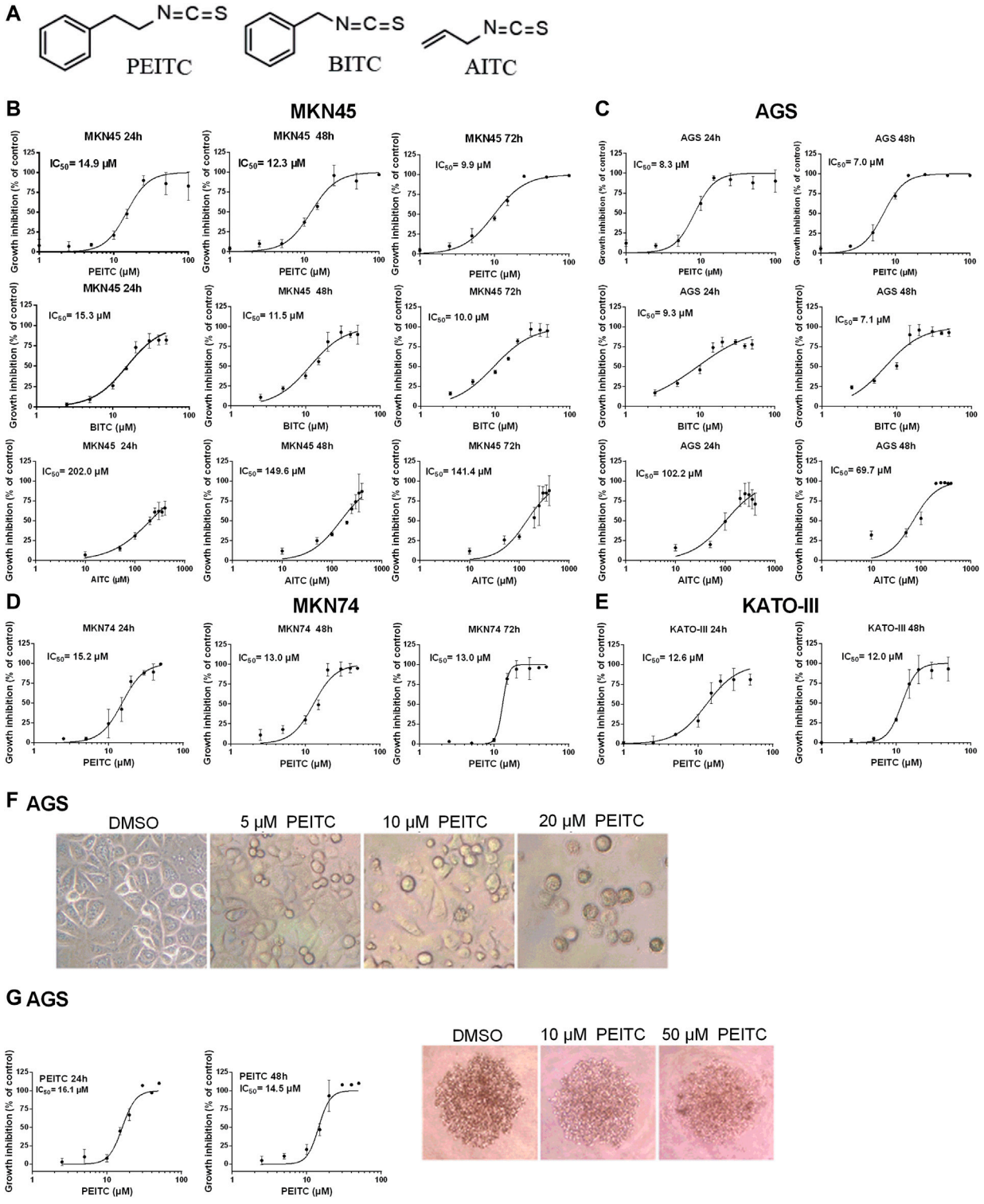

FIGURE 2 | Chemical structures of ITCs **(A)** and proliferation dose-response curves of gastric cancer cell lines MKN45 **(B)** and AGS **(C)** when treated with PEITC (1–100 μM), BITC (2.5–50 μM) and AITC (10–400 μM) for 24, 48 and 72 h in medium containing 1.0 g/L (5.6 mM) glucose and 0.584 g/L (4 mM) glutamine. Values represent means of n = 3–6 replicates relative to vehicle control (0.1% DMSO), and IC_{50} values were calculated from the logistic sigmoidal regression curves shown. Standard deviation (SD) values were omitted from cultures with 98% or higher inhibited growth as these yielded non-representatively high SD values. Proliferation dose-response curves of gastric cancer cell lines MKN74 and KATO-III when treated with PEITC (1–50 μM) **(D, E)**. Morphology of AGS cells affected by ITC-treatments **(F)**. Proliferation and morphology of spheroid 3D cultures of AGS cells treated with PEITC for 24–48 h **(G)**. PEITC, phenethyl isothiocyanate; BITC, benzyl isothiocyanate; AITC, allyl isothiocyanate; DMSO, dimethylsulfoxide.

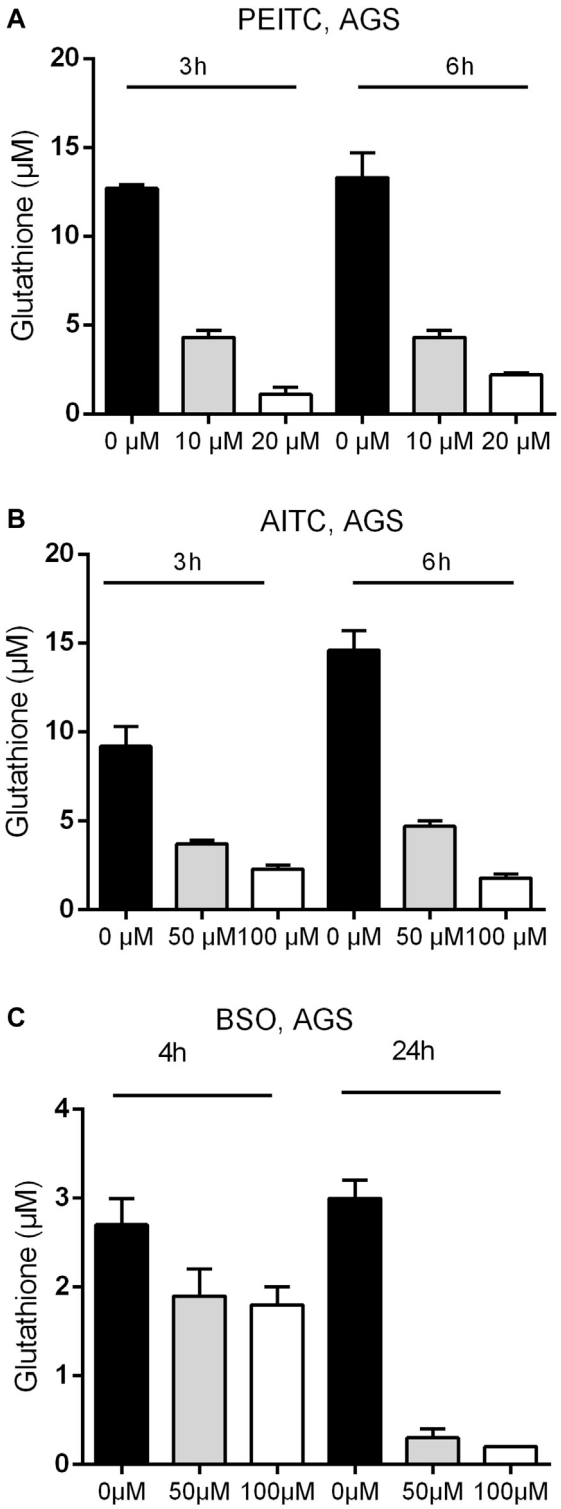

FIGURE 3 | Glutathione concentration upon 3 and 6 h treatments with PEITC **(A)** or AITC **(B)** on AGS cells and upon 4 and 24 h of treatment with BSO **(C)** on AGS cells. Mean + SD of $n = 4$ replicates/treatment. PEITC, phenethyl isothiocyanate; AITC, allyl isothiocyanate; BSO, Buthionine sulfoximine.

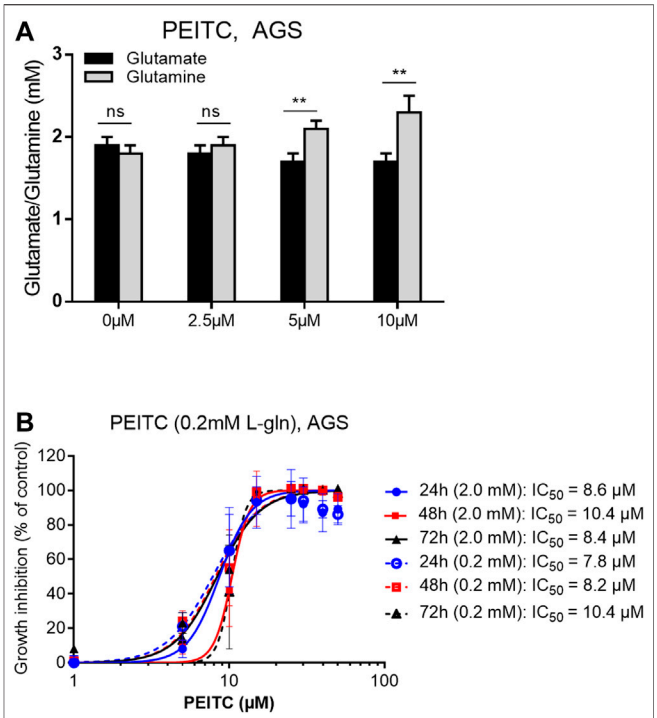

FIGURE 4 | Glutamate/glutamine determination upon 6 h treatments with 0, 2.5, 5 or 10 μM PEITC on AGS cells **(A)**. PEITC treatment in L-glutamine-reduced (×10) DMEM medium **(B)**. Mean ± SD. Paired *t*-test in **(A)**. $^{**}p < 0.01$; ns, not significant; PEITC, phenethyl isothiocyanate; L-gln, L-glutamine.

benefit from successful *H. pylori* eradication, and population-based chemopreventive strategy of *H. pylori* eradication is still under the development (Tan and Wong, 2013; Mera et al., 2018). Other strategies using drugs, such as non-steroidal anti-inflammatory drugs and statins, have also been suggested (Ford, 2011). In the present study, we found the chemopreventive effects by PEITC in chemically induced (MNU) animal model of gastric cancer. Interestingly, the chemopreventive effects were neither seen when PEITC was given after the tumor initiation by MNU nor in genetically induced (INS-GAS) gastric cancer. Thus, it is unlikely that PEITC interacts directly with MNU on one hand, but on the other hand, PEITC may act on gastric epithelial cells to prevent the initiation of tumorigenesis as it has been suggested that PEITC induce apoptosis, inhibits cell cycle progression and inhibits angiogenesis (Mitsiogianni et al., 2019). It is known that the regulation of apoptosis by ITC is achieved primarily through mitochondrial cytochrome c release, regulation of the Bcl-2 family, MAPK signaling and subsequent activation of caspases, responsible for the initiation and execution of apoptosis. Specifically, AITC and phenyl-ITC (PITC) inhibit TNF (extrinsic apoptosis), generating a mycelial inhibition for several months, while BITC and PEITC induce a cytochrome c release-dependent type of apoptosis from mitochondria (intrinsic apoptosis) that generates a mycelial inhibition that lasts only for a

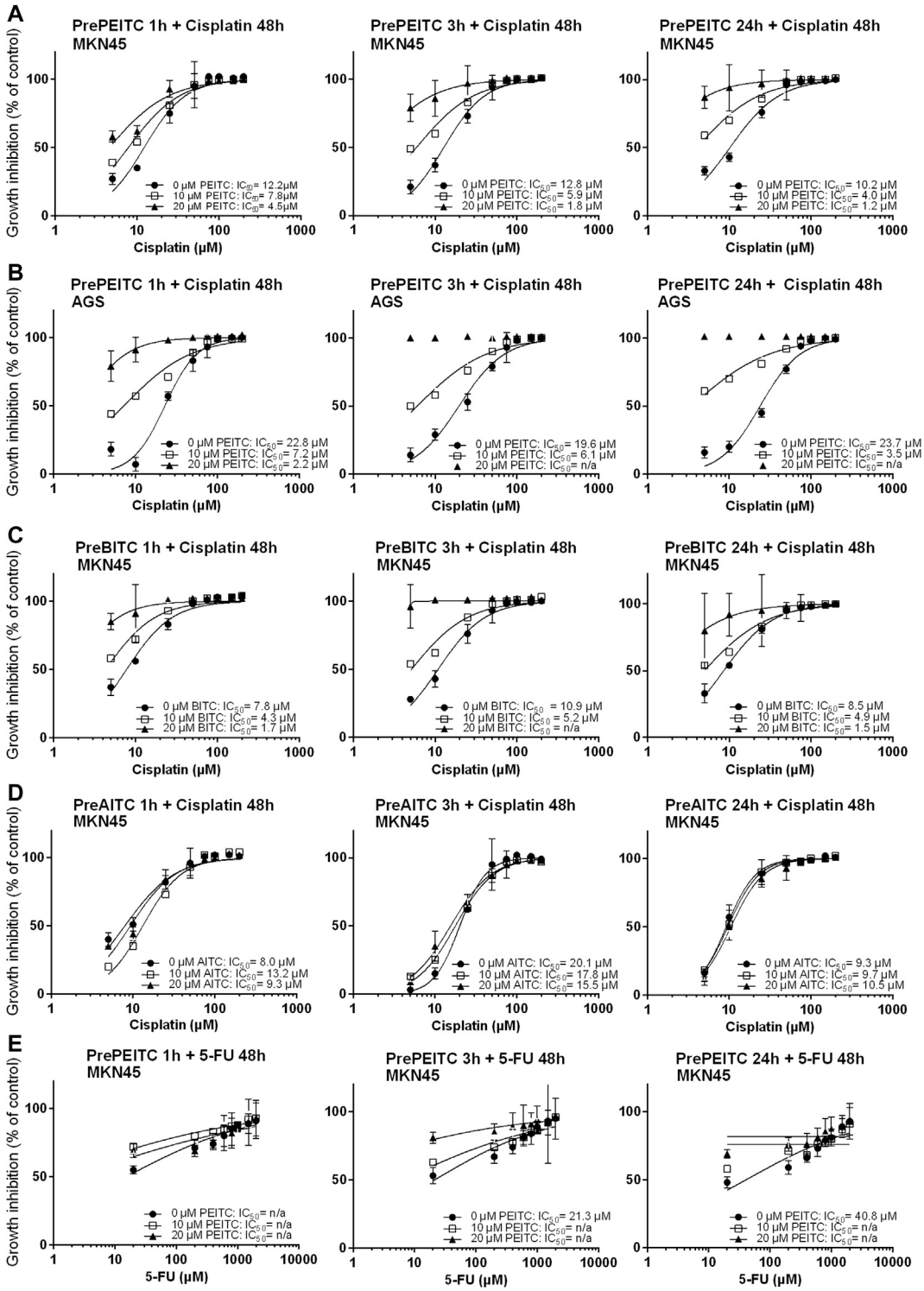

FIGURE 5 | Inhibition of proliferation (relative to vehicle control, 3% PBS) in cell cultures of MKN45 pre-treated with 10 and 20 μM PEITC for 1, 3 and 24 h before treated with 5–200 μM Cisplatin for 48 h **(A–E)**. (**B, C)** same as **(A)** but with pre-treatment with BITC or AITC instead of PEITC, respectively. **(D)** same as in **(A)** using AGS cells instead of MKN45. **(E)** same as in **(A)** but treating cells with 5-fluorouracil for 48 h instead of cisplatin following pre-treatment with PEITC. Values represent mean of n = 3–6 replicates. SD values were omitted from cultures with 98% or higher inhibited growth as these yielded non-representatively high SD values. PEITC: phenethyl isothiocyanate; BITC, benzyl isothiocyanate; AITC, allyl isothiocyanate.

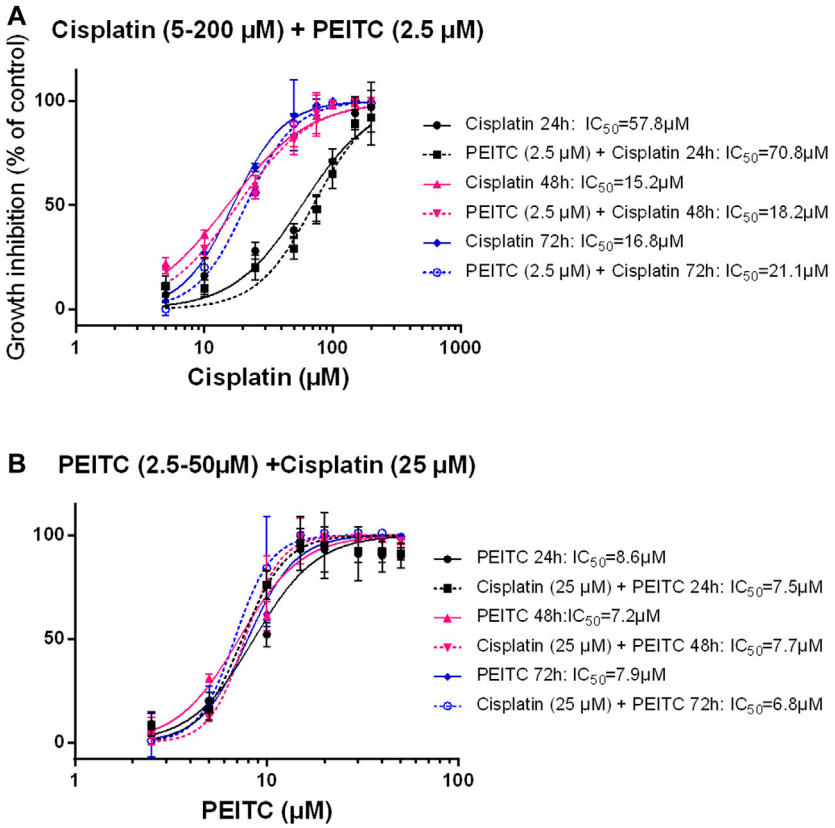

FIGURE 6 | Simultaneous treatment with PEITC and Cisplatin as different concentrations of cisplatin **(A)** and different concentrations of PEITC **(B)**. Mean ± SD. PEITC, phenethyl isothiocyanate.

few days. The differences in the fungistatic effect of ITC are possibly due to the type of apoptosis induced. It appears that significant portion of the chemopreventive effects of ITCs might be associated with the inhibition of the metabolic activation of carcinogens by cytochrome P450s (Phase I), coupled with strong induction of Phase II detoxifying and cellular defensive enzymes. Inductions of Phase II cellular enzymes are largely mediated by the antioxidant responsive element (ARE), which is regulated by the transcriptional factor (Nrf2). Additional potent regulatory mechanisms of Nrf2 include the different signaling kinase pathways (MAPK, PI3K, PKC and PERK) as well as other non-kinase dependent mechanisms. Moreover, apoptosis and cell cycle perturbations appear to be yet another potential chemopreventive mechanisms elicited by ITCs, especially with respect to the effects on pre-initiated or initiated tumor cells. Finally, modulation of other critical signaling mediators, including the NF-κB and AP-1 by a wide array of chemopreventive agents including ITCs might also contribute to the overall chemopreventive mechanisms (Keum et al., 2004).

Although surgery-related outcomes for treatment of gastric cancer, e.g., minimally invasive surgery techniques, continue to improve, the best regimen of either mono- or combination chemotherapy treatments still needs to be improved (Leiting and Grotz, 2019). In fact, the survival benefit of combinations of 5-fluorouracil (5-FU) with leucovorin, etoposide, methotrexate, doxorubicin, epidoxorubicin, cisplatin or oxaliplatin has been demonstrated (Sjoquist and Zalcberg, 2015). The results of the present study showed that there were time- and dose-dependent proliferative inhibitions by PEITC, BITC or AITC *in vitro* using the human cancer cell lines MKN45, AGS, MKN74 and KATO-III which were derived from intestinal and diffuse types of gastric carcinoma. Furthermore, the results of the present study showed that PEITC depleted intracellular levels of GSH and induced G_2/M arrest. It is well established that ITCs conjugate with GSH which is a linear tripeptide of L-glutamine, L-cysteine, and glycine. GSH is the main antioxidant metabolite in the cell and provides electrons for enzymes such as glutathione peroxidase, which reduce H_2O_2 to H_2O. GSH is crucial for cell proliferation, cell cycle progression and apoptosis and to protect cells from toxic insult by detoxifying toxic metabolites of drugs and ROS (Aquilano et al., 2014; Diaz-Vivancos et al., 2015). The results of the present study showed that intracellular GSH depletion upon PEITC and AITC treatment was both time- and dose-dependent, suggesting gastric cancer are susceptible to glutathione depletion. In fact, it was also reported that combined targeting of the epidermal growth factor receptor effector AKT and the glutathione antioxidant pathway mimicked Nrf2 ablation to potently inhibit pancreatic cancer, representing a promising synthetic lethal strategy for treating pancreatic cancer (Chio et al., 2016). This was in line with the

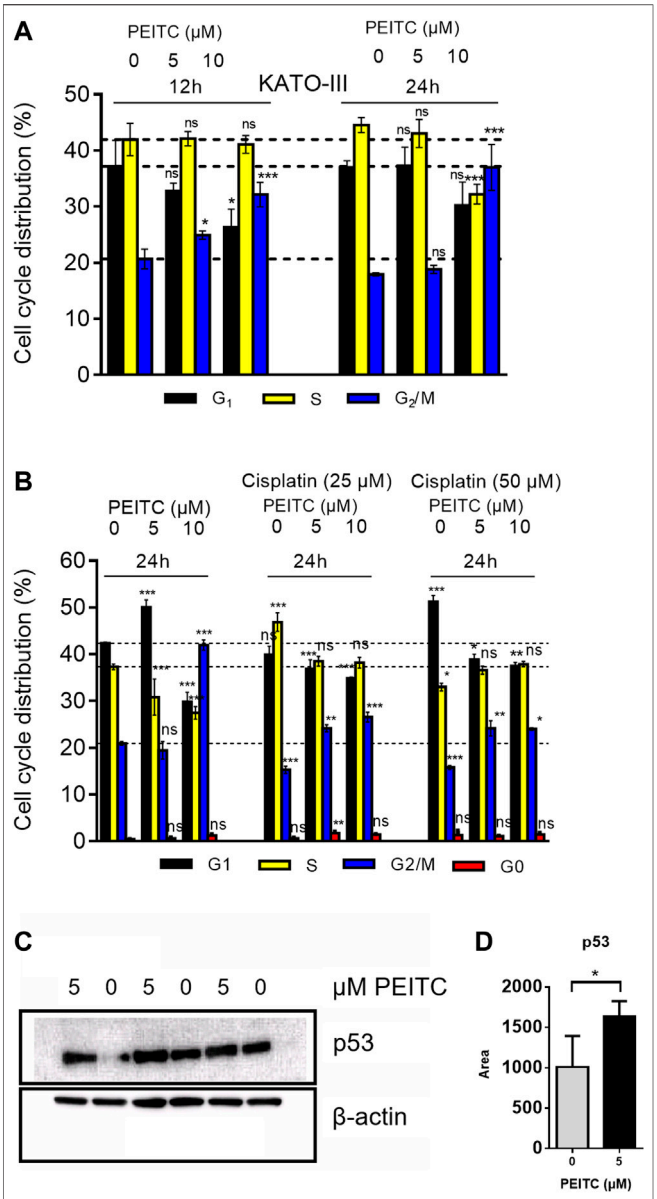

FIGURE 7 | Cell cycle analysis of PEITC **(A)** and PEITC + cisplatin **(B)** in KATO-III cells. Analyzed using FACS Canto cell cycle sorter with 20,000 cell reads/sample. Distribution is derived from histograms in FACS Diva software. Mean ± SD of $n = 3$ replicates/treatment. ANOVA with Dunnett's test (2-sided) vs. control groups was used. Western blot assessment of proteins p53 and β-actin (control) in response to PEITC were included in triplicates **(C)**. p53 band area were quantified in Image Studio Lite **(D)**. Bars represent means ± SD. Independent samples *t*-test (one-tailed) between 0 and 5 μM *: $p < 0.05$.

results of the present study showing that the synergistic effect of PEITC took place when it was given prior to cisplatin but not simultaneously with cisplatin, as it needs to deplete the intracellular pool of glutathione in order to achieve cell cycle arrest in response to cisplatin. Of note, the results of the present study also showed that pretreatment with PEITC could enhance the cytotoxicity of cisplatin but not of 5-FU. This effect should be explained by the different mechanisms of action between cisplatin (forming DNA crosslinks) and 5-FU (inhibiting thymidylate synthase) (Larionova et al., 2019). It would be of interest to investigate further the effects of PEITC in combination with different chemotherapeutic agents (including cisplatin, 5-FU, paclitaxel, gemcitabine, and trabectedin) that have different mechanisms of action in order to explore the mechanism of PEITC and to find the best combination therapy.

Interference of ITC with microtubules have also been established as a contributor to cells stagnating in the G_2/M-phase (Mi et al., 2009; Øverby et al., 2014). Buthionine sulfoximine (BSO), a synthetic amino acid, is an inhibitor of GSH synthesis on intracellular GSH levels (Griffith and Meister, 1979; Aldini et al., 2018). The results of the present study showed that BSO depleted GSH in a time- and dose-dependent manner and that PEITC-treatment altered the intracellular glutamine/glutamate ratio, providing a possible link between ITCs and amino acid metabolism. We suggested that the increase in glutamine but not glutamate levels shown in the present study could be attributed to compensatory mechanisms towards GSH replenishment in the cell when GSH level decreases. Indeed, a previous report has found that glutamine consumption correlated with glutathione excretion (Sappington et al., 2016).

It is known that elevated GSH levels are associated with tumor cell resistance to alkylating agents and platinum compounds (Estrela et al., 2006; Ortega et al., 2011; Bansal and Simon, 2018). Elevated GSH levels are observed in various types of tumors (Calvert et al., 1998). It has been suggested that high intracellular GSH level increases the antioxidant capacity and is thus conferring therapeutic resistance to cancer cells through the ability to resist oxidative stress which is a critical component of cisplatin cytotoxicity (Yu et al., 2018). We hypothesized that ITCs would enhance the cytotoxicity of cisplatin by depleting cells of glutathione, and indeed we found that PEITC and BITC but not AITC sensitized the gastric cancer cells to cisplatin. Conceivably, when the cell is depleted of GSH and oxidative stress is introduced using cytotoxic agents, a collapse in the antioxidant system eventually leads to cell death. Although reduction in GSH is proposed as a possible mechanism in the present study, it should be noticed that ITCs at sufficiently low doses might actually increase GSH levels as a consequence of ROS induction. Di Pasqua and colleagues described reduction of GSH as a less likely explanation to potentiating lung cancer cells by ITC but accredited the binding to tubulin as a more plausible explanation (Di Pasqua et al., 2010). In fact, PEITC and cisplatin have been co-administered using liposomal nanoparticles for treatment of non-small cell lung cancer (Sun et al., 2019). The efficacy potentiating of ITCs on existing chemotherapy has also been studied in cancers such as Barrett esophageal adenocarcinoma (Qazi et al., 2010), ovarian carcinoma (Stehlik et al., 2010), non-small cell lung carcinoma (Di Pasqua et al., 2010), prostate cancer (Xiao and Singh, 2010) and cervical cancer cells (Wang et al., 2011) in combination with drugs such as paclitaxel, MST-312, GRN163L, cisplatin and docetaxel. Thus, the results of the present study provide additional evidence in gastric cancer. The results of the present study also showed that PEITC induced cell cycle arrest in G_2/M phase which was associated with increased p53 protein

levels. p53 is one of the classical tumor suppressor genes that interferes with cell transformation events and plays a critical role in cell cycle control and induction of apoptosis (Ozaki and Nakagawara, 2011; Bykov et al., 2016; Bykov et al., 2018). It can be elevated in response to genotoxic agents, such as ionizing radiation, UV light, or chemicals. It has been shown that p53 elevation was required for PEITC-induced apoptosis (Huang et al., 1998).

However, some limitations of the present study should be noticed. First, we did not include additional animal groups, e.g., normal mice, MNU and INS-GAS mice that should be treated with PEITC or cisplatin alone and combination of PEITC plus cisplatin to explore the possibilities that PEITC may have differential effects on gastric cancer cells compared to normal gastric epithelial cells and that there is likely a synergistic anticancer effect *in vivo*. In fact, it has been showed that combining AITC with cisplatin reduced tumor volume in a mouse model of human lung cancer (Ling et al., 2015), thus this could also be a promising strategy in gastric cancer. Secondly, we did not investigate the molecular mechanism of action including signaling pathways of ITCs in combination with cisplatin, in gastric cancer cells. Third, we did not perform the combination of denervation and PEITC with or without chemotherapy, as initially planned. Forth, we did not further investigate the possible mechanism by which the only pretreatment with PEITC was effective against NMU-induced gastric cancer, and neither concomitant treatment nor administration of this agent after cancer development (either in NMU or INS-GAS mice) was successful. In addition to pre-initiated or initiated tumor cells as a possible target of PEITC (aforementioned), there are other possible hypotheses/explanations. It has been known that there are different windows for chemoprevention and therapeutic effects during the tumorigenesis from initiation, promotion and progression (Hanahan and Weinberg, 2011; Liu et al., 2015). It is also possible that the anti-cancer agents (e.g., ITCs) exhibit the effect on the initiation phase when given at a low dose and on the progression phase at a high dose. In the present study, PEITC (MW 163.24 g/mol) was given at 3–5 μmol/g diet in mice. Based on the pharmacokinetics of PEITC, the oral administration of PEITC at this dose level would reach a circulation level that is in a similar order of magnitude of IC_{50} (15 μM) *in vitro* but be a lower order of magnitude in gastric tissue (pmol/mg) (Reimer, 1972; Conaway et al., 1999). Fifth, it is still unclear why the synergistic effect was not obtained when PEITC and cisplatin were given simultaneously in the cell culture model. In fact, we failed to measure GSH levels because of heavily fluctuating potentiating effect. Fluctuating levels of GSH was found across our experiments measuring GSH concentration, where the intracellular GSH levels ranged between 3 and 10 μM GSH between experiments, adding to the complexity of GSH's role in the observations. Finally, it should also be noticed that this study was carried out in the mouse models of gastric cancer and in the cell lines derived from human gastric cancer. It would be of interest to study the possible cytotoxic effects of ITCs in normal tissue and/or cell lines derived from normal healthy human stomach, e.g., cell line of HGaEpC, in the future. Taken together, it is still a challenge for future development of food products that contains high levels of edible ITCs for chemoprevention and for being used during chemotherapy in patients with gastric cancer.

It would also be of interest to explore the possible efficacy's potentiating role of ITCs on other therapies, such as targeted therapy and immunotherapy. In fact, combination of ERBB2 antagonist or RARA agonist was reported to be effective synergistic regimens for ERBB2 positive gastric cancer (Xiang et al., 2018). In clinical setting, the treatment options for advanced-stage gastric cancer are limited, despite an approval of two targeted agents, trastuzumab and ramucirumab. Consequently, the overall clinical outcomes for patients with advanced-stage gastric cancer remain poor. Numerous agents that are active against novel targets have been evaluated in the course of randomized trials; however, most have produced disappointing results because of the heterogeneity of gastric cancer (Kumar et al., 2018). Immunotherapy, e.g., immune checkpoint inhibitors (ICIs), has been tested in gastric cancer. Despite having good efficacy and safety profile, ICIs are clinically active only in small subset of patients and therefore, there is a huge unmet need to enhance their efficacy. Indeed, there are several ongoing clinical trials that are exploring the role of ICIs in various gastrointestinal cancers either as single agent or in combination with chemotherapy, radiation therapy, targeted agents or other immunotherapeutic agents, but not yet ITC (Mazloom et al., 2020).

CONCLUSION

PEITC displayed anti-cancer effects, particularly when given before the tumor initiation, suggesting a chemopreventive effect in gastric cancer, and that aromatic ITCs potentiated the anti-cancer effects of cisplatin, particularly when given before cisplatin, suggesting a possible combination strategy in treatment of gastric cancer.

DATA AVAILABILITY STATEMENT

The raw data supporting the conclusions of this article will be made available by the authors, without undue reservation.

ETHICS STATEMENT

The animal study was reviewed and approved by The Norwegian Food Safety Authority (Mattilsynet).

AUTHOR CONTRIBUTIONS

H-LR: *in vitro* experiments, all sample/data collection and preparation, data analysis and interpretation, writing manuscript. YK: *in vivo* Experiments, sample/data collection and preparation, writing manuscript. MN, AMB, and TCW: Project discussion, data interpretation, writing manuscript. DC: Project concept, study idea

and design, data analysis and interpretation, writing manuscript. C-MZ: Project concept, study idea and design, *in vivo* experiments, sample collection and preparation, data interpretation, writing manuscript. AØ: project design, *in vivo* and *in vitro* experiments, sample/data collection and preparation, data analysis and interpretation, writing manuscript.

FUNDING

The research was supported by the Liaison Committee between the Central Norway Regional Health Authority (Helse-Midt Norge RHF), Norwegian University of Science and Technology (NTNU grant no. 46056636/46056928/90061700/90061701), Joint Program of the Medical Faculty of NTNU, the Research Council of Norway, and the Cancer Foundation of St. Olavs Hospital (Kreftfondet ved St. Olavs hospital), the Japan Society for the Promotion of Science (JSPS grant no. 15F14741) and the Scandinavia-Japan Sasakawa Foundation (SJSF).

ACKNOWLEDGMENTS

We thank Dr. Signe E. Åsberg and Ragni A. Stokland (NTNU) for participating in animal experiments and Dr. Tetsufumi Takahashi (Kitasato University) for assisting on *in vitro* experiments.

REFERENCES

Aldini, G., Altomare, A., Baron, G., Vistoli, G., Carini, M., Borsani, L., et al. (2018). N-Acetylcysteine as an antioxidant and disulphide breaking agent: the reasons why. *Free Radic. Res.* 52, 751–762. doi:10.1080/10715762.2018.1468564

Aquilano, K., Baldelli, S., and Ciriolo, M. R. (2014). Glutathione: new roles in redox signaling for an old antioxidant. *Front. Pharmacol.* 5, 196. doi:10.3389/fphar.2014.00196

Bansal, A., and Simon, M. C. (2018). Glutathione metabolism in cancer progression and treatment resistance. *J. Cell Biol.* 217, 2291–2298. doi:10.1083/jcb.201804161

Bray, F., Ferlay, J., Soerjomataram, I., Siegel, R. L., Torre, L. A., and Jemal, A. (2018). Global cancer statistics 2018: GLOBOCAN estimates of incidence and mortality worldwide for 36 cancers in 185 countries. *CA Cancer J. Clin.* 68, 394–424. doi:10.3322/caac.21492

Bykov, V. J., Zhang, Q., Zhang, M., Ceder, S., Abrahmsen, L., and Wiman, K. G. (2016). Targeting of mutant p53 and the cellular redox balance by APR-246 as a strategy for efficient cancer therapy. *Front. Oncol.* 6, 21. doi:10.3389/fonc.2016.00021

Bykov, V. J. N., Eriksson, S. E., Bianchi, J., and Wiman, K. G. (2018). Targeting mutant p53 for efficient cancer therapy. *Nat. Rev. Cancer* 18, 89–102. doi:10.1038/nrc.2017.109

Calvert, P., Yao, K. S., Hamilton, T. C., and O'Dwyer, P. J. (1998). Clinical studies of reversal of drug resistance based on glutathione. *Chem. Biol. Interact.* 111–112, 213–224. doi:10.1016/s0009-2797(98)00008-8

Chen, Y., Li, Y., Wang, X. Q., Meng, Y., Zhang, Q., Zhu, J. Y., et al. (2018). Phenethyl isothiocyanate inhibits colorectal cancer stem cells by suppressing Wnt/β-catenin pathway. *Phytother. Res.* 32, 2447–2455. doi:10.1002/ptr.6183

Chio, I. I. C., Jafarnejad, S. M., Ponz-Sarvise, M., Park, Y., Rivera, K., Palm, W., et al. (2016). NRF2 promotes tumor maintenance by modulating mRNA translation in pancreatic cancer. *Cell* 166, 963–976. doi:10.1016/j.cell.2016.06.056

Chu, W. F., Wu, D. M., Liu, W., Wu, L. J., Li, D. Z., Xu, D. Y., et al. (2009). Sulforaphane induces G2-M arrest and apoptosis in high metastasis cell line of salivary gland adenoid cystic carcinoma. *Oral Oncol.* 45, 998–1004. doi:10.1016/j.oraloncology.2009.05.641

Chung, M. Y., Lim, T. G., and Lee, K. W. (2013). Molecular mechanisms of chemopreventive phytochemicals against gastroenterological cancer development. *World J. Gastroenterol.* 19, 984–993. doi:10.3748/wjg.v19.i7.984

Clarke, J. D., Dashwood, R. H., and Ho, E. (2008). Multi-targeted prevention of cancer by sulforaphane. *Cancer Lett.* 269, 291–304. doi:10.1016/j.canlet.2008.04.018

Conaway, C. C., Jiao, D., Kohri, T., Liebes, L., and Chung, F. L. (1999). Disposition and pharmacokinetics of phenethyl isothiocyanate and 6-phenylhexyl isothiocyanate in F344 rats. *Drug Metab. Dispos.* 27, 13–20.

Conaway, C. C., Yang, Y. M., and Chung, F. L. (2002). Isothiocyanates as cancer chemopreventive agents: their biological activities and metabolism in rodents and humans. *Curr. Drug Metab.* 3, 233–255. doi:10.2174/1389200023337496

Cunningham, D., Starling, N., Rao, S., Iveson, T., Nicolson, M., Coxon, F., et al. (2008). Capecitabine and oxaliplatin for advanced esophagogastric cancer. *N. Engl. J. Med.* 358, 36–46. doi:10.1056/NEJMoa073149

Di Pasqua, A. J., Hong, C., Wu, M. Y., McCracken, E., Wang, X., Mi, L., et al. (2010). Sensitization of non-small cell lung cancer cells to cisplatin by naturally occurring isothiocyanates. *Chem. Res. Toxicol.* 23, 1307–1309. doi:10.1021/tx100187f

Diaz-Vivancos, P., de Simone, A., Kiddle, G., and Foyer, C. H. (2015). Glutathione--linking cell proliferation to oxidative stress. *Free Radic. Biol. Med.* 89, 1154–1164. doi:10.1016/j.freeradbiomed.2015.09.023

Dunn, B. K., Umar, A., and Richmond, E. (2016). Introduction: cancer chemoprevention and its context. *Semin. Oncol.* 43, 19–21. doi:10.1053/j.seminoncol.2015.11.002

Estrela, J. M., Ortega, A., and Obrador, E. (2006). Glutathione in cancer biology and therapy. *Crit. Rev. Clin. Lab Sci.* 43, 143–181. doi:10.1080/10408360500523878

Ferlay, J., Shin, H. R., Bray, F., Forman, D., Mathers, C., and Parkin, D. M. (2010). Estimates of worldwide burden of cancer in 2008: GLOBOCAN 2008. *Int. J. Cancer* 127, 2893–2917. doi:10.1002/ijc.25516

Ferlay, J. S. I., Ervik, M., Dikshit, R., Eser, S., Mathers, C., et al. (2013). *GLOBOCAN 2012 v1.0, cancer incidence and mortality worldwide: IARC CancerBase No. 11*. Lyon, France: International Agency for Research on Cancer.

Ford, A. C. (2011). Chemoprevention for gastric cancer. *Best Pract. Res. Clin. Gastroenterol.* 25, 581–592. doi:10.1016/j.bpg.2011.09.002

Griffith, O. W., and Meister, A. (1979). Potent and specific inhibition of glutathione synthesis by buthionine sulfoximine (S-n-butyl homocysteine sulfoximine). *J. Biol. Chem.* 254, 7558–7560. doi:10.1016/s0021-9258(18)35980-5

Gupta, P., Wright, S. E., Kim, S. H., and Srivastava, S. K. (2014). Phenethyl isothiocyanate: a comprehensive review of anti-cancer mechanisms. *Biochim. Biophys. Acta* 1846, 405–424. doi:10.1016/j.bbcan.2014.08.003

Hanahan, D., and Weinberg, R. A. (2011). Hallmarks of cancer: the next generation. *Cell* 144, 646–674. doi:10.1016/j.cell.2011.02.013

Hu, K., and Morris, M. E. (2004). Effects of benzyl-, phenethyl-, and alpha-naphthyl isothiocyanates on P-glycoprotein- and MRP1-mediated transport. *J. Pharm. Sci.* 93, 1901–1911. doi:10.1002/jps.20101

Huang, C., Ma, W. Y., Li, J., Hecht, S. S., and Dong, Z. (1998). Essential role of p53 in phenethyl isothiocyanate-induced apoptosis. *Cancer Res.* 58, 4102–4106.

Kang, Y. K., Kang, W. K., Shin, D. B., Chen, J., Xiong, J., Wang, J., et al. (2009). Capecitabine/cisplatin versus 5-fluorouracil/cisplatin as first-line therapy in patients with advanced gastric cancer: a randomised phase III noninferiority trial. *Ann. Oncol.* 20, 666–673. doi:10.1093/annonc/mdn717

Keum, Y. S., Jeong, W. S., and Kong, A. N. (2004). Chemoprevention by isothiocyanates and their underlying molecular signaling mechanisms. *Mutat. Res.* 555, 191–202. doi:10.1016/j.mrfmmm.2004.05.024

Keum, Y. S., Jeong, W. S., and Kong, A. N. (2005). Chemopreventive functions of isothiocyanates. *Drug News Perspect.* 18, 445–451. doi:10.1358/dnp.2005.18.7.939350

Koizumi, W., Narahara, H., Hara, T., Takagane, A., Akiya, T., Takagi, M., et al. (2008). S-1 plus cisplatin versus S-1 alone for first-line treatment of advanced gastric cancer (SPIRITS trial): a phase III trial. *Lancet Oncol.* 9, 215–221. doi:10.1016/S1470-2045(08)70035-4

Kumar, V., Soni, P., Garg, M., Kamholz, S., and Chandra, A. B. (2018). Emerging therapies in the management of advanced-stage gastric cancer. *Front. Pharmacol.* 9, 404. doi:10.3389/fphar.2018.00404

Larionova, I., Cherdyntseva, N., Liu, T., Patysheva, M., Rakina, M., and Kzhyshkowska, J. (2019). Interaction of tumor-associated macrophages and cancer chemotherapy. *Oncoimmunology* 8, e1596004. doi:10.1080/2162402X.2019.1596004

Lawson, A. P., Long, M. J. C., Coffey, R. T., Qian, Y., Weerapana, E., El Oualid, F., et al. (2015). Naturally occurring isothiocyanates exert anticancer effects by inhibiting deubiquitinating enzymes. *Cancer Res.* 75, 5130–5142. doi:10.1158/0008-5472.CAN-15-1544

Leiting, J. L., and Grotz, T. E. (2019). Advancements and challenges in treating advanced gastric cancer in the West. *World J. Gastrointest. Oncol.* 11, 652–664. doi:10.4251/wjgo.v11.i9.652

Li, Y., Zhang, T., Korkaya, H., Liu, S., Lee, H. F., Newman, B., et al. (2010). Sulforaphane, a dietary component of broccoli/broccoli sprouts, inhibits breast cancer stem cells. *Clin. Cancer Res.* 16, 2580–2590. doi:10.1158/1078-0432.CCR-09-2937

Li, Y., and Zhang, T. (2013). Targeting cancer stem cells with sulforaphane, a dietary component from broccoli and broccoli sprouts. *Future Oncol.* 9, 1097–1103. doi:10.2217/fon.13.108

Ling, X., Westover, D., Cao, F., Cao, S., He, X., Kim, H. R., et al. (2015). Synergistic effect of allyl isothiocyanate (AITC) on cisplatin efficacy *in vitro* and *in vivo*. *Am. J. Cancer Res.* 5, 2516–2530.

Liu, Y., Yin, T., Feng, Y., Cona, M. M., Huang, G., Liu, J., et al. (2015). Mammalian models of chemically induced primary malignancies exploitable for imaging-based preclinical theragnostic research. *Quant Imaging Med. Surg.* 5, 708–729. doi:10.3978/j.issn.2223-4292.2015.06.01

Lv, H., Zhen, C., Liu, J., and Shang, P. (2020). β-Phenethyl isothiocyanate induces cell death in human osteosarcoma through altering iron metabolism, disturbing the redox balance, and activating the MAPK signaling pathway. *Oxid Med. Cell Longev.* 2020, 5021983. doi:10.1155/2020/5021983

Mazloom, A., Ghalehsari, N., Gazivoda, V., Nimkar, N., Paul, S., Gregos, P., et al. (2020). Role of immune checkpoint inhibitors in gastrointestinal malignancies. *J. Clin. Med.* 9, 2533. doi:10.3390/jcm9082533

Mera, R. M., Bravo, L. E., Camargo, M. C., Bravo, J. C., Delgado, A. G., Romero-Gallo, J., et al. (2018). Dynamics of *Helicobacter pylori* infection as a determinant of progression of gastric precancerous lesions: 16-year follow-up of an eradication trial. *Gut* 67, 1239–1246. doi:10.1136/gutjnl-2016-311685

Mi, L., Gan, N., and Chung, F. L. (2009). Aggresome-like structure induced by isothiocyanates is novel proteasome-dependent degradation machinery. *Biochem. Biophys. Res. Commun.* 388, 456–462. doi:10.1016/j.bbrc.2009.08.047

Mitsiogianni, M., Koutsidis, G., Mavroudis, N., Trafalis, D. T., Botaitis, S., Franco, R., et al. (2019). The role of isothiocyanates as cancer chemo-preventive, chemo-therapeutic and anti-melanoma agents. *Antioxidants (Basel)* 8, 106. doi:10.3390/antiox8040106

Orditura, M., Galizia, G., Sforza, V., Gambardella, V., Fabozzi, A., Laterza, M. M., et al. (2014). Treatment of gastric cancer. *World J. Gastroenterol.* 20, 1635–1649. doi:10.3748/wjg.v20.i7.1635

Ortega, A. L., Mena, S., and Estrela, J. M. (2011). Glutathione in cancer cell death. *Cancers (Basel)* 3, 1285–1310. doi:10.3390/cancers3011285

Øverby, A., Stokland, R. A., Åsberg, S. E., Sporsheim, B., and Bones, A. M. (2015). Allyl isothiocyanate depletes glutathione and upregulates expression of glutathione S-transferases in *Arabidopsis thaliana*. *Front. Plant Sci.* 6, 277. doi:10.3389/fpls.2015.00277

Øverby, A., Zhao, C. M., Bones, A. M., and Chen, D. (2014). Naturally occurring phenethyl isothiocyanate-induced inhibition of gastric cancer cell growth by disruption of microtubules. *J. Gastroenterol. Hepatol.* 29 (Suppl. 4), 99–106. doi:10.1111/jgh.12732

Ozaki, T., and Nakagawara, A. (2011). Role of p53 in cell death and human cancers. *Cancers (Basel)* 3, 994–1013. doi:10.3390/cancers3010994

Qazi, A., Pal, J., Maitah, M., Fulciniti, M., Pelluru, D., Nanjappa, P., et al. (2010). Anticancer activity of a broccoli derivative, sulforaphane, in barrett adenocarcinoma: potential use in chemoprevention and as adjuvant in chemotherapy. *Transl. Oncol.* 3, 389–399. doi:10.1593/tlo.10235

Rabben, H.-L., Andersen, G. T., Olsen, M. K., Øverby, A., Ianevski, A., et al. (2021). Neural signaling modulates metabolism of gastric cancer. *iScience* 24, 102091. doi:10.1016/j.isci.2021.102091

Rabben, H. L., Zhao, C. M., Hayakawa, Y., Wang, T. C., and Chen, D. (2016). Vagotomy and gastric tumorigenesis. *Curr. Neuropharmacol.* 14, 967–972. doi:10.2174/1570159x14666160121114854

Reimer, F. (1972). Developmental trends in psychiatric hospitals. *Offentl. Gesundheitswes.* 34 (Suppl. 1), 26–33.

Sappington, D. R., Siegel, E. R., Hiatt, G., Desai, A., Penney, R. B., Jamshidi-Parsian, A., et al. (2016). Glutamine drives glutathione synthesis and contributes to radiation sensitivity of A549 and H460 lung cancer cell lines. *Biochim. Biophys. Acta* 1860, 836–843. doi:10.1016/j.bbagen.2016.01.021

Sjoquist, K. M., and Zalcberg, J. R. (2015). Gastric cancer: past progress and present challenges. *Gastric Cancer* 18, 205–209. doi:10.1007/s10120-014-0437-0

Stehlik, P., Paulikova, H., and Hunakova, L. (2010). Synthetic isothiocyanate indole-3-ethyl isothiocyanate (homoITC) enhances sensitivity of human ovarian carcinoma cell lines A2780 and A2780/CP to cisplatin. *Neoplasma* 57, 473–481. doi:10.4149/neo_2010_05_473

Steward, W. P., and Brown, K. (2013). Cancer chemoprevention: a rapidly evolving field. *Br. J. Cancer* 109, 1–7. doi:10.1038/bjc.2013.280

Sun, M., Shi, Y., Dang, U. J., and Di Pasqua, A. J. (2019). Phenethyl isothiocyanate and cisplatin Co-encapsulated in a liposomal nanoparticle for treatment of non-small cell lung cancer. *Molecules* 24, 801. doi:10.3390/molecules24040801

Tan, V. P., and Wong, B. C. (2013). Gastric cancer chemoprevention: the current evidence. *Gastroenterol. Clin. N. Am.* 42, 299–316. doi:10.1016/j.gtc.2013.02.001

Tomczyk, J., and Olejnik, A. (2010). Sulforaphane–a possible agent in prevention and therapy of cancer. *Postepy Hig Med Dosw (Online)* 64, 590–603.

Van Cutsem, E., Moiseyenko, V. M., Tjulandin, S., Majlis, A., Constenla, M., Boni, C., et al. (2006). Phase III study of docetaxel and cisplatin plus fluorouracil compared with cisplatin and fluorouracil as first-line therapy for advanced gastric cancer: a report of the V325 Study Group. *J. Clin. Oncol.* 24, 4991–4997. doi:10.1200/JCO.2006.06.8429

Wang, X., Govind, S., Sajankila, S. P., Mi, L., Roy, R., and Chung, F. L. (2011). Phenethyl isothiocyanate sensitizes human cervical cancer cells to apoptosis induced by cisplatin. *Mol. Nutr. Food Res.* 55, 1572–1581. doi:10.1002/mnfr.201000560

Wu, X., Zhou, Q. H., and Xu, K. (2009). Are isothiocyanates potential anti-cancer drugs?. *Acta Pharmacol. Sin* 30, 501–512. doi:10.1038/aps.2009.50

Xiang, Z., Huang, X., Wang, J., Zhang, J., Ji, J., Yan, R., et al. (2018). Cross-database analysis reveals sensitive biomarkers for combined therapy for ERBB2+ gastric cancer. *Front. Pharmacol.* 9, 861. doi:10.3389/fphar.2018.00861

Xiao, D., and Singh, S. V. (2010). Phenethyl isothiocyanate sensitizes androgen-independent human prostate cancer cells to docetaxel-induced apoptosis *in vitro* and *in vivo*. *Pharm. Res.* 27, 722–731. doi:10.1007/s11095-010-0079-9

Yang, M. D., Lai, K. C., Lai, T. Y., Hsu, S. C., Kuo, C. L., Yu, C. S., et al. (2010). Phenethyl isothiocyanate inhibits migration and invasion of human gastric cancer AGS cells through suppressing MAPK and NF-kappaB signal pathways. *Anticancer Res.* 30, 2135–2143.

Yu, W., Chen, Y., Dubrulle, J., Stossi, F., Putluri, V., Sreekumar, A., et al. (2018). Cisplatin generates oxidative stress which is accompanied by rapid shifts in central carbon metabolism. *Sci. Rep.* 8, 4306. doi:10.1038/s41598-018-22640-y

Zhang, Y. (2010). Allyl isothiocyanate as a cancer chemopreventive phytochemical. *Mol. Nutr. Food Res.* 54, 127–135. doi:10.1002/mnfr.200900323

Zhao, C. M., Hayakawa, Y., Kodama, Y., Muthupalani, S., Westphalen, C. B., Andersen, G. T., et al. (2014). Denervation suppresses gastric tumorigenesis. *Sci. Transl. Med.* 6, 250ra115. doi:10.1126/scitranslmed.3009569

Conflict of Interest: The authors declare that the research was conducted in the absence of any commercial or financial relationships that could be construed as a potential conflict of interest.

frontiers in Pharmacology

REVIEW
published: 14 April 2021
doi: 10.3389/fphar.2021.650403

RIPK2 as a New Therapeutic Target in Inflammatory Bowel Diseases

Hajime Honjo, Tomohiro Watanabe, Ken Kamata, Kosuke Minaga and Masatoshi Kudo*

Department of Gastroenterology and Hepatology, Kindai University Faculty of Medicine, Osaka-Sayama, Japan

Inflammatory bowel diseases (IBDs) are becoming more frequent worldwide. A significant fraction of patients with IBD are refractory to various types of therapeutic biologics and small molecules. Therefore, identification of novel therapeutic targets in IBD is required. Receptor-interacting serine/threonine kinase 2 (RIPK2), also known as receptor-interacting protein 2 (RIP2), is a downstream signaling molecule for nucleotide-binding oligomerization domain 1 (NOD1), NOD2, and Toll-like receptors (TLRs). RIPK2 is expressed in antigen-presenting cells, such as dendritic cells and macrophages. Recognition of microbe-associated molecular patterns by NOD1, NOD2, and TLRs leads to the interaction between RIPK2 and these innate immune receptors, followed by the release of pro-inflammatory cytokines such as TNF-α, IL-6, and IL-12/23p40 through the activation of nuclear factor kappa B and mitogen-activated protein kinases. Thus, activation of RIPK2 plays a critical role in host defense against microbial infections. Recent experimental and clinical studies have provided evidence that activation of RIPK2 is involved in the development of autoimmune diseases, especially IBDs. In addition, the colonic mucosa of patients with IBD exhibits enhanced expression of RIPK2 and associated signaling molecules. Furthermore, the blockage of RIPK2 activation ameliorates the development of experimental murine colitis. Thus, activation of RIPK2 underlies IBD immunopathogenesis. In this review, we attempt to clarify the roles played by RIPK2 in the development of IBD by focusing on its associated signaling pathways. We also discuss the possibility of using RIPK2 as a new therapeutic target in IBD.

Keywords: inflammatory bowel diseases, pro-inflammatory cytokines, toll-like receptors, nuclear factor-kappa B, RIPK2

OPEN ACCESS

Edited by:
Thomas Brzozowski, Jagiellonian University Medical College, Poland

Reviewed by:
Mads Gyrd-Hansen, University of Oxford, United Kingdom
Claudio Bernardazzi, University of Arizona, United States
Jong-Hwan Park, Chonnam National University, South Korea
Atle Van Beelen Granlund, Norwegian University of Science and Technology, Norway

****Correspondence:***
Tomohiro Watanabe
tomohiro@med.kindai.ac.jp

Specialty section:
This article was submitted to Gastrointestinal and Hepatic Pharmacology, a section of the journal Frontiers in Pharmacology

Received: *07 January 2021*
Accepted: *26 February 2021*
Published: *14 April 2021*

Citation:
Honjo H, Watanabe T, Kamata K, Minaga K and Kudo M (2021) RIPK2 as a New Therapeutic Target in Inflammatory Bowel Diseases. Front. Pharmacol. 12:650403. doi: 10.3389/fphar.2021.650403

INTRODUCTION

Inflammatory bowel diseases (IBDs) include Crohn's disease (CD) and ulcerative colitis (UC), chronic inflammatory and relapsing disorders of the gastrointestinal tract that are becoming more frequent worldwide (Baumgart and Sandborn, 2012; Ungaro et al., 2017). Genetic susceptibility and intestinal dysbiosis together mediate dysregulated immune responses against the intestinal microbiota, in patients with IBD (Strober et al., 2007; Strober and Fuss, 2011; Caruso et al., 2020). It is now generally accepted that excessive release of pro-inflammatory cytokines such as TNF-α, IL-12/23p40, and IL-6 underlies the immunopathogenesis of IBDs (Strober et al., 2007; Strober and Fuss, 2011; Caruso et al., 2020). This notion has been fully supported by the fact that biologics and small molecules targeting pro-inflammatory cytokine signaling pathways have been used with remarkable success in the treatment of IBD patients (Neurath, 2014; Verstockt et al., 2018; Shivaji et al., 2020). However, a significant fraction of patients with IBD are refractory to various types of biologics and small molecules. Therefore, identification of novel therapeutic targets in IBD is required.

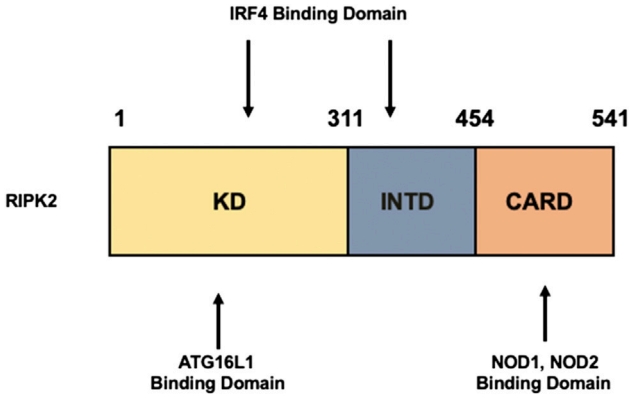

FIGURE 1 | Structure of RIPK2. Receptor-interacting serine/threonine kinase 2 (RIPK2) is composed of a kinase domain (KD), an intermediate domain (INTD), and a caspase activation and recruitment domain (CARD). Interferon regulatory factor 4 (IRF4) binds to the KD and INTD. Autophagy related 16 like 1 (ATG16L1) binds to the KD, whereas nucleotide-binding oligomerization domain 1 (NOD1) and NOD2 interact with RIPK2 via CARDs.

Genome-wide association studies have identified susceptibility loci for the development of CD. The loss-of-function mutations in the caspase activation and recruitment domain 15 (*CARD15*) gene encoding nucleotide-binding oligomerization domain 2 (NOD2) and in the autophagy related 16 like 1 (*ATG16L1*) gene are the strongest genetic risk factors for CD (Inohara et al., 2005; Cho, 2008; Chen et al., 2009; Strober and Watanabe, 2011; Jostins et al., 2012; Philpott et al., 2014). NOD2 is an intracellular receptor for muramyl dipeptide (MDP), a small molecule derived from gut bacterial wall components (Inohara et al., 2005; Cho, 2008; Chen et al., 2009; Strober and Watanabe, 2011; Philpott et al., 2014). On the other hand, ATG16L1 functions as a critical molecule for autophagy, which is an indispensable process for the digestion and degradation of invading gut pathogens (Mizushima et al., 2008; Virgin and Levine, 2009; Salem et al., 2015). Receptor-interacting serine/threonine kinase 2 (RIPK2), also known as receptor-interacting protein 2 (RIP2), is a signaling molecule downstream of NOD2 and ATG16L1 (Inohara et al., 2005; Chen et al., 2009; Cooney et al., 2010; Strober and Watanabe, 2011; Philpott et al., 2014; Honjo et al., 2021). Recent studies have provided evidence that excessive activation of RIPK2 is involved in the development of experimental and human IBD (Jun et al., 2013; Hofmann et al., 2020). Moreover, small molecules inhibiting the activation of RIPK2 both *in vitro* and *in vivo* have been identified. In this review article, we summarize RIPK2-mediated signaling pathways with a focus on pro-inflammatory cytokine responses and discuss the colitogenic roles played by RIPK2.

EXPRESSION AND STRUCTURE OF RECEPTOR-INTERACTING SERINE/THREONINE KINASE 2

RIPK2 is expressed in the cytoplasm of antigen-presenting cells (APCs), such as dendritic cells (DCs) and macrophages (Chen et al., 2009; Strober and Watanabe, 2011; Philpott et al., 2014; Strober et al., 2014), and is also expressed in T cells (Shimada et al., 2018). In addition to hematopoietic cells, epithelial cells also express functional RIPK2 (Inohara et al., 2005; Kobayashi et al., 2005; Chen et al., 2009; Philpott et al., 2014). Thus, innate immune cells, including APCs, and epithelial cells express functional RIPK2.

RIPK2 is an obligate signaling molecule downstream of NOD1 and NOD2 (Chen et al., 2009; Strober and Watanabe, 2011; Philpott et al., 2014; Strober et al., 2014) (Park et al., 2007; Hall et al., 2008). It is composed of a kinase domain (KD), an intermediate domain (INTD), and a caspase activation and recruitment domain (CARD) (**Figure 1**). NOD1 and NOD2 bind to the CARD of RIPK2 through a CARD–CARD interaction (Strober et al., 2006; Chen et al., 2009; Strober and Watanabe, 2011; Philpott et al., 2014; Strober et al., 2014). A serine residue at position 176 in the KD is necessary for the activation of RIPK2 because a S176A RIPK2 mutant exhibited defective autophosphorylation and catalytic activity (Dorsch et al., 2006). Further, the interaction between ATG16L1 and RIPK2 is mediated by the KD (Honjo et al., 2021) whereas interferon regulatory factor 4 (IRF4) binds to the KD and INTD of RIPK2 (Watanabe et al., 2008; Watanabe et al., 2014). Thus, each domain of RIPK2 plays an indispensable role in protein–protein interactions.

ACTIVATION OF RECEPTOR-INTERACTING SERINE/THREONINE KINASE 2 BY PATTERN RECOGNITION RECEPTORS

Sensing of microbe-associated molecular patterns (MAMPs) activates cell surface TLRs as well as cytosolic NOD1 and NOD2 (Takeda and Akira, 2005; Strober et al., 2006; Strober and Fuss, 2011). Recognition of TLR and NOD1/NOD2 ligands by these pattern recognition receptors leads to a subsequent activation and ubiquitination of RIPK2 followed by the nuclear translocation of nuclear factor κB (NF-κB) subunits and activation of mitogen-activated protein kinases (Takeda and Akira, 2005; Strober et al., 2006; Strober et al., 2007; Strober and Fuss, 2011) (**Figure 2**). TGF-β–activated kinase 1 (TAK1) is a critical downstream signaling molecule for RIPK2-mediated production of pro-inflammatory cytokines such as IL-6, TNF-α, and IL-12/23p40 (Takeda and Akira, 2005; Strober et al., 2006; Strober et al., 2007; Strober and Fuss, 2011). Signaling pathways mediated by RIPK2 have been well studied in terms of NOD1 and NOD2 activation. Macrophages isolated from RIPK2-deficient mice exhibited defective pro-inflammatory cytokine responses upon stimulation with NOD1 and NOD2 ligands, but not with TLR ligands (Park et al., 2007; Hall et al., 2008), suggesting that cytokine responses mediated by NOD1 and NOD2 are dependent on RIPK2. Therefore, it is established that RIPK2 functions as a critical signaling molecule in the production of pro-inflammatory cytokines mediated by NOD1 and NOD2.

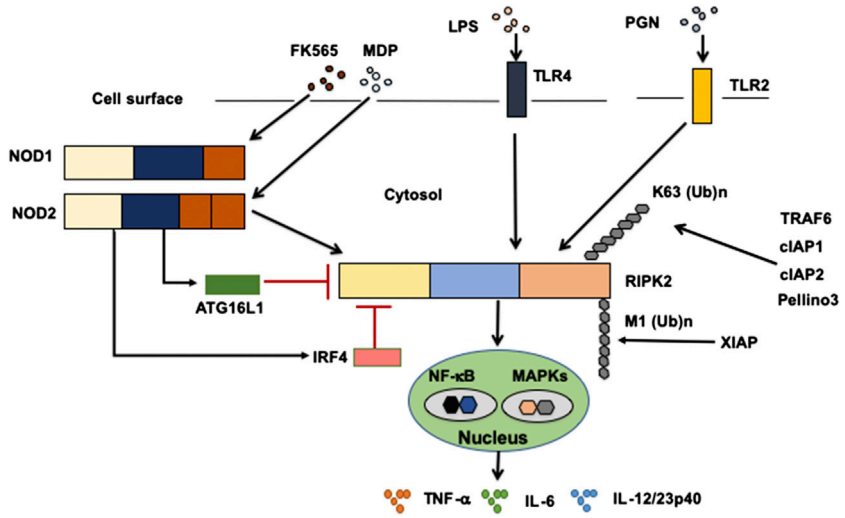

FIGURE 2 | Signaling pathways mediated by RIPK2. Receptor-interacting serine/threonine kinase 2 (RIPK2) is a signaling molecule downstream of nucleotide-binding oligomerization domain 1 (NOD1), NOD2, and Toll-like receptors (TLRs). Activation of RIPK2 by TLRs results in a robust production of pro-inflammatory cytokines, including TNF-α, IL-6, and IL-12/23p40, through the nuclear translocation of nuclear factor-κB (NF-κB) subunits. Cellular inhibitor of apoptosis protein 1 (cIAP1), cIAP2, TNF receptor-associated factor 6 (TRAF6), Pellino 3 and X-linked inhibitor of apoptosis protein (XIAP) ubiquitinate RIPK2. RIPK2 is subjected to lysine 63 (K63)-linked polyubiquitination by TRAF6, cIAP1, cIAP2, and Pellino3. RIPK2 is also subjected to N-terminal methionine (M1)-linked polyubiquitination by XIAP. Interferon regulatory factor 4 (IRF4) and autophagy related 16 like 1 (ATG16L1) negatively regulate RIPK2-mediated pro-inflammatory cytokine responses. LPS, lipopolysaccharide; PGN, peptidoglycan, MDP, muramyl dipeptide.

However, others have demonstrated RIPK2-dependent TLRs-induced pro-inflammatory cytokine production (Kobayashi et al., 2002; Lu et al., 2005; Dorsch et al., 2006; Usluoglu et al., 2007). In fact, the molecular interaction between TLRs and RIPK2 was observed after the stimulation with TLR ligands (Kobayashi et al., 2002; Lu et al., 2005). Moreover, macrophages isolated from RIPK2-deficient mice exhibited markedly reduced production of IL-6 and TNF-α upon the stimulation with TLR2 and TLR4 ligands compared with that observed in stimulated macrophages from RIPK2-intact mice (Kobayashi et al., 2002). Another report showed that activation of RIPK2 was involved in the production of IL-12/23p40 in human DCs stimulated with TLR4 ligands (Usluoglu et al., 2007). Therefore, these studies suggest that RIPK2 functions as a critical signaling molecule for the production of IL-6, TNF-α, and IL-12/23p40 mediated by TLRs and NOD1/NOD2. It should be emphasized that the magnitude of pro-inflammatory cytokine responses mediated by the TLRs–RIPK2 pathway is much greater than that of the responses mediated by the NOD2–RIPK2 pathway (Watanabe et al., 2004). Such strong pro-inflammatory responses mediated by the TLRs–RIPK2 pathway are negatively regulated by IRF4 and ATG16L1 (see below). Involvement of RIPK2 in TLRs-mediated signaling requires evaluation in future studies, because the current reports fail to clarify the role of RIPK2 in TLRs-mediated signaling pathways (Park et al., 2007; Hall et al., 2008).

In addition to the activation of NF-κB, RIPK2 is involved in type I IFN signaling pathways. Sensing of MAMPs by NOD1 leads to robust production of IFN-β by gastric epithelial cells in a RIPK2-dependent manner (Watanabe et al., 2010). Upon its activation, RIPK2 binds to TNF receptor-associated factor 3 (TRAF3), followed by the activation of TANK-binding kinase 1 and IκB kinase ε, as well as the subsequent nuclear translocation of IRF7. These processes subsequently trigger robust production of IFN-β. Furthermore, type I IFN responses mediated by the NOD1–RIPK2–TRAF3–IRF7 axis play critical roles in mucosal host defense against *Helicobacter pylori* infection of the stomach (Watanabe et al., 2010).

UBIQUITINATION OF RECEPTOR-INTERACTING SERINE/THREONINE KINASE 2

Activation of RIPK2 is tightly regulated by polyubiquitination (Yang et al., 2007; Hasegawa et al., 2008; Bertrand et al., 2009; Tao et al., 2009; Bertrand et al., 2011; Damgaard et al., 2012; Damgaard et al., 2013; Yang et al., 2013; Hrdinka et al., 2016), a post-translational modification that determines the activation or degradation of a target protein (Wullaert et al., 2006). It is well established that lysine 48 (K48)- and K63-linked polyubiquitination reactions induce degradation and activation of ubiquitinated proteins, respectively (Wullaert et al., 2006). RIPK2-mediated activation of NF-κB depends on RIPK2 K63–linked polyubiquitination by various E3 ligases, including cellular inhibitor of apoptosis protein 1 (cIAP1), cIAP2, X-linked inhibitor of apoptosis protein (XIAP), Pellino 3, and TRAF6 (Yang et al., 2007; Hasegawa et al., 2008; Bertrand et al., 2009; Tao et al., 2009; Bertrand et al., 2011; Damgaard et al., 2012; Damgaard et al., 2013; Yang et al., 2013; Hrdinka et al., 2016) (**Figure 2**). However, the role of cIAPs in polyubiquitination of RIPK2 upon exposure to NOD1 and NOD2 ligands is

controversial, because other studies failed to reproduce the ubiquitination of RIPK2 by cIAPs (Damgaard et al., 2013; Stafford et al., 2018). In addition to K63-linked polyubiquitination, XIAP recruits the linear ubiquitin chain assembly complex (LUBAC) to induce NF-κB activation (Damgaard et al., 2012). RIPK2 is subjected to N-terminal methionine (Met1)-linked polyubiquitination by LUBAC after the interaction between RIPK2 and XIAP (Damgaard et al., 2012; Fiil et al., 2013). Thus, K63-linked polyubiquitination and recruitment of LUBAC are indispensable steps for NF-κB activation by RIPK2.

Various negative regulators of RIPK2 inhibit its polyubiquitination. For example, IRF4 and ATG16L1 physically interact with RIPK2 inhibiting its K63-linked polyubiquitination, thereby reducing pro-inflammatory cytokine production (Sorbara et al., 2013; Watanabe et al., 2014; Honjo et al., 2021). These studies support the concept that pro-inflammatory cytokine responses mediated by RIPK2 depend upon polyubiquitination and subsequent NF-κB activation.

AUTOPHAGY AND RECEPTOR-INTERACTING SERINE/THREONINE KINASE 2

Autophagy is a process of regulated degradation of cytoplasmic constituents and intracellular pathogens (Mizushima et al., 2008; Virgin and Levine, 2009). It has been linked to mucosal host defense against invading pathogens in the gastrointestinal tract: mice deficient in ATG16L1, a critical regulator of the autophagic machinery, displayed impaired gut pathogen clearance (Kuballa et al., 2008; Travassos et al., 2010). Sensing of MDP or gut bacteria by intracellular NOD2 efficiently induces autophagy (Cooney et al., 2010; Travassos et al., 2010). Cooney et al. showed that the intact NOD2–RIPK2 pathway mediates autophagy in an ATG16L1-dependent manner in human DCs. However, Travassos et al. provided evidence that ATG16L1-mediated autophagy does not require the activation of RIPK2 in mouse embryonic fibroblasts (MEFs) (Travassos et al., 2010). This discrepancy can be partially explained by the type of cell studied, i.e., DCs vs. MEFs. Thus, RIPK2 is also involved in mucosal host defense mechanisms through the induction of ATG16L1-dependent autophagy in human DCs.

NOD2–RIPK2 AND TLRS–RIPK2 AXES IN INFLAMMATORY BOWEL DISEASE

Given that loss-of-function mutations in *NOD2* or *ATG16L1* are associated with the development of CD (Cho, 2008; Chen et al., 2009; Philpott et al., 2014; Caruso et al., 2020), it is plausible that signaling pathways mediated by intact NOD2 and ATG16L1 prevent chronic inflammation of the gastrointestinal tract. In fact, MDP activation of NOD2 reduced pro-inflammatory cytokine responses, such as the release of IL-6, TNF-α, and IL-12/23p40, by colonic lamina propria APCs upon subsequent exposure to TLR and NOD1/NOD2 ligands, thereby inhibiting the development of colitis induced by dextran sulfate sodium (DSS) and trinitrobenzene sulfonic acid (TNBS) (Watanabe et al., 2008; Watanabe et al., 2014; Udden et al., 2017). The inhibition of DSS-induced colitis by NOD2 activation required a molecular interaction between NOD2 and RIPK2, because administration of MDP failed to prevent colonic inflammation in mice deficient in RIPK2 (Bertrand et al., 2009). Moreover, mice deficient in NOD2 or RIPK2 displayed enhanced susceptibility to DSS-induced colitis due to intestinal dysbiosis (Couturier-Maillard et al., 2013). Thus, MDP activation of NOD2 and RIPK2 plays a protective role in the development of experimental IBD.

Regarding the molecular mechanisms accounting for the inhibition of colitogenic cytokine responses by the intact NOD2–RIPK2 pathway, we and others have identified IRF4 to be a critical negative regulator (Watanabe et al., 2008; Watanabe et al., 2014; Udden et al., 2017). MDP activation of NOD2 induced IRF4 expression in DCs through the interaction of NOD2 with RIPK2, and then IRF4 suppressed the production of pro-inflammatory cytokines by DCs upon subsequent exposure to TLR ligands (Watanabe et al., 2008; Watanabe et al., 2014; Cavallari et al., 2017; Udden et al., 2017). IRF4 induced by the MDP-mediated activation of NOD2 inhibited activation of NF-κB through a physical interaction with myeloid differentiation factor 88, TRAF6, and RIPK2, which are all key signaling molecules in TLR pathways (Watanabe et al., 2008; Strober et al., 2014; Udden et al., 2017) (**Figure 2**). Likewise, K63-linked polyubiquitination of RIPK2 and TRAF6 was efficiently prevented by IRF4 induced by the MDP-mediated activation of NOD2 (Watanabe et al., 2008; Watanabe et al., 2014) (**Figure 2**). IRF4 binds to the KD and INTD of RIPK2 and inhibits polyubiquitination (**Figure 1**). Considering that MDP and TLR ligands are derived from intestinal bacteria, the intact NOD2–RIPK2 pathway activated by gut microbiota likely maintains intestinal homeostasis through the negative regulation of pro-inflammatory cytokine responses mediated by TLRs. CD-associated *NOD2* mutations decrease the ability of NOD2 to induce IRF4 expression due to defective recognition of MDP. In turn, the attenuated IRF4 expression leads to the excessive pro-inflammatory cytokine responses mediated by TLRs, which cause chronic colonic inflammation (Strober et al., 2006; Strober et al., 2007; Strober and Watanabe, 2011). This idea is fully supported by our data obtained in a unique model of experimental IBD induced by colonization with *Escherichia coli* and subsequent adoptive transfer of $CD4^+$ T cells specific for *E. coli* (Watanabe et al., 2006). NOD2-deficient mice were susceptible to this unique type of colitis due to the excessive production of pro-inflammatory cytokines via TLR2 activation, because the mice deficient in both NOD2 and TLR2 were protected from colitis (Watanabe et al., 2006). Therefore, these studies suggest that the intact NOD2–RIPK2 pathway activated by the gut microbiota protects mice from experimental IBD through the IRF4-mediated suppression of pro-inflammatory TLR pathways. Protection by the intact NOD2–RIPK2 pathway against experimental IBD required polyubiquitination of RIPK2 as MDP activation of NOD2 did not ameliorate DSS-induced colitis in mice deficient in cIAP2 or

Pollino3, the E3 ligases for K63-linked polyubiquitination of RIPK2 (Bertrand et al., 2009; Yang et al., 2013).

MDP activation of NOD2 acts synergistically with TLR ligands to induce pro-inflammatory cytokine responses (Fritz et al., 2005; Kim et al., 2008; Pashenkov et al., 2019). APCs produce a large amount of pro-inflammatory cytokines upon concomitant stimulation with MDP and TLR ligands. This is different from the prior exposure to MDP, because simultaneous exposures to MDP and TLR ligands lead to the enhanced generation of pro-inflammatory cytokine responses (Fritz et al., 2005; Kim et al., 2008; Pashenkov et al., 2019). Such synergistic effects of NOD2 on TLRs-mediated pro-inflammatory responses may play important roles in host defense against microbial infections (Fritz et al., 2005; Kim et al., 2008; Pashenkov et al., 2019). In addition, lack of these synergistic effects in the presence of CD-associated NOD2 mutations may lead to the development of chronic inflammation, because of gut bacterial overgrowth.

NOD2 is constitutively expressed in Paneth cells, which are specialized epithelial cells located in the crypts of the ileal mucosa (Inohara et al., 2005; Chen et al., 2009). Recognition of MDP by NOD2 induces robust production of α-defensin, a prototypical anti-microbial peptide, through RIPK2 activation followed by the nuclear translocation of NF-κB subunits in Paneth cells (Inohara et al., 2005; Chen et al., 2009). Indeed, NOD2-deficient mice displayed impaired protection against oral infection with *Listeria monocytogenes* (Kobayashi et al., 2005). Consistent with these data, ileal mucosa of CD patients with *NOD2* mutations, have a reduced expression of α-defensin in Paneth cells (Wehkamp et al., 2004; Wehkamp et al., 2005). In addition, mice deficient in NOD2 or RIPK2 develop granulomatous inflammation in the ileum when inoculated with *Helicobacter hepaticus*, and the effects are accompanied by a diminished expression of α-defensin (Biswas et al., 2010). These data suggest that the intact NOD2–RIPK2 pathway functions as a critical regulator of mucosal host defense mechanisms against gut microbiota through the production of α-defensin, and that impaired activation of RIPK2 in the presence of CD-associated *NOD2* mutations predisposes hosts to chronic inflammation due to bacterial overgrowth (Inohara et al., 2005; Kobayashi et al., 2005; Chen et al., 2009; Philpott et al., 2014). However, others reported conflicting results. Ileal mucosa from NOD2-intact and NOD2-defcient mice express comparable levels of α-defensin (Shanahan et al., 2014). In addition, reduced expression of ileal α-defensin is not associated with the *NOD2* mutations in patients with CD (Simms et al., 2008).

As mentioned above, RIPK2 activation by NOD2 and TLRs plays protective and pathogenic roles in the development of experimental IBD, respectively. Therefore, it is logical to ask whether RIPK2 could be a therapeutic target in IBD. In this regard, we recently provided evidence that NOD1-and/or NOD2-independent activation of RIPK2 caused experimental IBD through TLRs-induced pro-inflammatory cytokine responses (Watanabe et al., 2019). The blockade of RIPK2 activation by an intrarectal administration of a plasmid harboring RIPK2-specific siRNA encapsulated in the hemagglutinating virus of Japan envelope efficiently prevented the development of DSS- and TNBS-induced colitis in mice with intact NOD1 and NOD2, whereas colitis was manifested in animals that received intrarectal administration of the plasmid carrying control siRNA (Watanabe et al., 2019). Intrarectal administration of the plasmid encoding RIPK2-specific siRNA markedly reduced the production of the pro-inflammatory cytokines IL-6, TNF-α, and IL-12/23p40 by colonic lamina propria APCs upon the subsequent exposure to TLR ligands *in vitro* (Watanabe et al., 2019). Interestingly, siRNA-mediated knockdown of RIPK2 expression inhibited the development of both DSS- and TNBS-induced colitis in a NOD1/NOD2-independent manner because mice deficient in both NOD1 and NOD2 or in NOD2 only displayed significantly attenuated levels of DSS- and TNBS-induced colitis following the intrarectal administration of the plasmid carrying RIPK2-specific siRNA (Watanabe et al., 2019). Thus, TLRs-dependent and NOD2-independent activation of RIPK2 mediated the development of experimental IBD. Consistent with this idea, Hollenbach et al. showed that inhibition of RIPK2 by intraperitoneal administration of SB203580 improved clinical and histological scores in DSS- and TNBS-induced colitis, which was accompanied by the downregulation of pro-inflammatory cytokine responses and NF-κB activation (Hollenbach et al., 2004; Hollenbach et al., 2005). Another study tested gefitinib as a RIPK2 inhibitor and found that spontaneous development of ileitis seen in SAMP1/YitFc mice was ameliorated by oral administration of the drug (Tigno-Aranjuez et al., 2014). WEHI-345, which was identified as a RIPK2 inhibitor by screening a proprietary library of 120 kinase inhibitors, delayed NF-κB activation by inhibiting polyubiquitination of RIPK2 and ameliorated experimental autoimmune encephalomyelitis (Nachbur et al., 2015). Salla et al. (2018) identified and characterized two novel RIPK2 inhibitors by using molecular modeling and chemoinformatics analysis (Salla et al., 2018). The degree of suppression in DSS-induced colitis was significantly greater in mice treated with these RIPK2 inhibitors than in those treated with gefitinib (Salla et al., 2018). Although these studies utilizing RIPK2 inhibitors have not clearly shown whether such small molecules suppressed the activity of the NOD2–RIPK2 and TLRs–RIPK2 pathways to improve inflammation, their therapeutic and preventive effects seen in experimental IBD allow considering RIPK2 as a new therapeutic target in human IBD.

The clinical relevance of RIPK2 activation was examined by using colonic biopsy samples obtained from CD and UC patients during colonoscopy (Watanabe et al., 2019). Expression of RIPK2 as determined by qPCR was much higher in colonic lesions of patients with CD and UC than in normal colonic mucosa (Watanabe et al., 2019). Expression levels of RIPK2-related signaling molecules such as cIAP1, cIAP2, TRAF6, and TAK1 were significantly higher in patients with CD and UC than those in normal colonic mucosa (Watanabe et al., 2019). Although RIPK2 expression positively correlated with that of pro-inflammatory cytokines in the colonic mucosa of patients with CD and UC, enhanced expression of NOD1 and NOD2 was not observed in IBD patients (Watanabe et al., 2019). Consistent with qPCR data, immunofluorescence studies showed that colonic DCs expressing RIPK2 and cIAP2 produce TNF-α. Moreover, the intensity of the molecular interaction between cIAP2 and

RIPK2 and between RIPK2 and TAK1 is positively correlated with expression levels of IL-6 and TNF-α in the inflamed colonic mucosa of patients with CD and UC (Watanabe et al., 2019). Thus, our study highlighted the importance of RIPK2 activation in the generation of colitogenic cytokine responses in human IBD. Excessive activation of RIPK2 has also been observed in the inflamed mucosa of pediatric CD patients (Negroni et al., 2009). In line with these data, GSK583, a highly potent and selective inhibitor of RIPK2, efficiently suppressed the spontaneous release of pro-inflammatory cytokines in colonic biopsy samples obtained from CD patients (Haile et al., 2016.). Taken together, these studies utilizing human IBD samples fully support the view that activation of RIPK2 plays a pathogenic role in the development of both murine and human IBD by promoting the production of pro-inflammatory cytokines. Therefore, RIPK2 can be a novel therapeutic target in human IBD.

ATG16L1–RIPK2 AXIS IN INFLAMMATORY BOWEL DISEASE

APCs or epithelial cells expressing CD-associated *ATG16L1* mutations displayed diminished autophagic responses to invading the gut microbiota (Kuballa et al., 2008; Cooney et al., 2010; Travassos et al., 2010). NOD2 activation induced by MDP or intestinal bacteria is a potent trigger of autophagy (Cooney et al., 2010; Travassos et al., 2010). DCs isolated from CD patients bearing CD-associated *NOD2* mutations showed defective autophagy upon the exposure to MDP or *Salmonella enterica* (Cooney et al., 2010). Thus, impaired autophagy in response to invasion of the gut microbiota, underlies the immunopathogenesis of CD in the presence of *NOD2* or *ATG16L1* mutations (Cho, 2008; Kaser and Blumberg, 2011; Salem et al., 2015).

Diminished autophagy caused by CD-associated *ATG16L1* mutations or a complete lack of the *ATG16L1* gene results in enhanced pro-inflammatory cytokine responses, including excessive release of IL-1β, IL-6, and TNF-α, triggered by TLR2 and TLR4 ligands (Saitoh et al., 2008; Lassen et al., 2014; Murthy et al., 2014). Thus, enhanced pro-inflammatory cytokine responses to TLR ligands caused by defective autophagy drive chronic inflammation in CD patients with *ATG16L1* mutations. In other words, intact ATG16L1 pathways maintain intestinal homeostasis through the negative regulation of TLRs-mediated pro-inflammatory responses. However, the molecular mechanisms by which such cytokine responses are negatively regulated by intact ATG16L1 pathways are poorly understood.

Given that RIPK2 functions as a signaling molecule downstream of not only NOD1 and NOD2 but also of TLRs, it is possible that ATG16L1 negatively regulates pro-inflammatory cytokine responses mediated by the TLRs–RIPK2 pathway. We have demonstrated previously that ATG16L1 binds to the KD of RIPK2 (Honjo et al., 2021) (**Figure 1**). The TLR2-mediated NF-κB activation was significantly suppressed by the overexpression of intact *ATG16L1*, but not by the overexpression of *ATG16L1* harboring CD-associated mutations, in reporter gene assays. In human monocyte–derived DCs, MDP activation of NOD2 induced physical interaction between ATG16L1 and RIPK2 and negatively regulated TLR2-mediated NF-κB activation and pro-inflammatory cytokine responses by inhibiting the interaction between TLRs and RIPK2 (Honjo et al., 2021). Consistent with the data from a previous report (Sorbara et al., 2013), ATG16L1 binding to RIPK2 suppressed NF-κB activation by downregulating polyubiquitination of RIPK2 (Honjo et al., 2021) (**Figure 2**). Importantly, ATG16L1 acts synergistically with IRF4 to inhibit RIPK2 polyubiquitination. These data suggest that ATG16L1 functions as a negative regulator of the TLR2–RIPK2 pathway.

The clinical relevance of these findings was examined in samples obtained from patients with CD and UC. The percentages of colonic DCs expressing ATG16L1 were inversely correlated with the expression levels of IL-6 in the colon of both CD and UC patients and with TNF-α expression level in the colon of CD patients only (Honjo et al., 2021). Induction of remission was associated with the accumulation of colonic DCs expressing ATG16L1 in CD patients (Honjo et al., 2021), which was consistent with aggregated DSS-induced colitis in mice with DC-specific *Atg16l1* deletion (Zhang et al., 2017; Honjo et al., 2021). Together, these data suggest that the interaction between ATG16L1 and RIPK2 induced by NOD2 activation prevents colitogenic cytokine responses mediated by TLRs. It should be noted, however, that confirmation of this idea awaits future studies that should utilize samples from CD patients with *ATG16L1* mutations. Plantinga et al. (2011) showed comparable levels of pro-inflammatory cytokine production by peripheral blood mononuclear cells isolated from CD patients with and without *ATG16L1* mutations upon the stimulation with TLR2 and TLR4 ligands (Plantinga et al., 2011).

Epithelial cells express functional NOD2, RIPK2, and ATG16L1. MDP activation of NOD2 induces autophagy and mediates the anti-bacterial response (Homer et al., 2010). Epithelial cells expressing CD-associated *NOD2* or *ATG16L1* mutations, exhibit impaired autophagy when exposed to MDP (Homer et al., 2010). Induction of autophagy mediated by NOD2 and ATG16L1 requires intact RIPK2, because epithelial cells with defective expression of RIPK2 also exhibit a reduced induction of autophagy (Homer et al., 2010). Collectively, the NOD2-RIPK2-ATG16L1 axis operating in epithelial cells contributes to the maintenance of intestinal homeostasis through induction of autophagy.

RECENT PROGRESS IN RECEPTOR-INTERACTING SERINE/THREONINE KINASE 2 INHIBITORS

Several RIPK2 inhibitors have been used for the treatment of experimental colitis. These RIPK2 inhibitors are believed to inhibit kinase activity of RIPK2 (Hollenbach et al., 2005; Tigno-Aranjuez et al., 2014; Nachbur et al., 2015; Salla et al., 2018). However, recent studies provide evidence that kinase activity of RIPK2 is dispensable for NOD2 signaling, and that

RIPK2 inhibitors inhibit the polyubiquitination of RIPK2 through disrupting the interaction between RIPK2 and XIAP (Goncharov et al., 2018; Hrdinka et al., 2018; Suebsuwong et al., 2020). Therefore, it is likely that RIPK2 inhibitors prevent experimental colitis through the suppression of polyubiquitination of RIPK2.

Mice deficient in NOD2 or RIPK2 are more susceptible to DSS or TNBS-induced colitis; however, the administration of RIPK2 inhibitors ameliorates chronic colonic inflammation. Activation of RIPK2 plays dual roles in the development of experimental colitis. We speculate that the NOD2-RIPK2 and TLRs-RIPK2 pathways play anti-inflammatory and pro-inflammatory roles, respectively, in the development of experimental colitis. This idea is fully supported by our recent report in which NOD1 or NOD2-independent activation of RIPK2 mediates experimental colitis (Watanabe et al., 2019). Expression of RIPK2 and its signaling molecules, such as cIAP2, TRAF6, and TAK1, was markedly elevated in the colonic mucosa of patients with UC or CD compared to that in the healthy colonic mucosa, while the expression of NOD2 decreased (Watanabe et al., 2019). These studies strongly suggest that the interaction between TLRs and RIPK2, rather than that between NOD2 and RIPK2, could be a novel therapeutic target for IBDs. However, the possibility of patients with IBDs being successfully treated with RIPK2 inhibitors awaits the development of RIPK2 inhibitors that inhibit the interaction between TLRs and RIPK2.

CONCLUDING REMARKS

The loss-of-function mutations in *NOD2* and *ATG16L1* are associated with development of CD. Considering that signaling pathways mediated by NOD2 and ATG16L1 merge at the level of RIPK2 in APCs, it is likely that intact NOD2–ATG16L1–RIPK2 pathways maintain intestinal immune homeostasis. Recent studies have provided evidence that the intact NOD2–RIPK2 pathway downregulates colitogenic pro-inflammatory cytokine responses mediated by the TLRs–RIPK2 pathways through the activation of IRF4 and ATG16L1. Mechanistically, IRF4 and ATG16L1 downregulate TLRs-induced pro-inflammatory cytokine responses by inhibiting polyubiquitination of RIPK2. Enhanced activation of RIPK2 was verified in the inflamed colonic mucosa of patients with CD and UC. Small molecules inhibiting RIPK2 have been identified, and their administration successfully treated experimental IBD. These findings strongly suggest that patients with UC and CD might be treated with RIPK2 inhibitors.

AUTHOR CONTRIBUTIONS

HH and TW drafted the manuscript. KK, KM, and MK revised the manuscript. All authors have read and approved the submitted manuscript for publication.

FUNDING

This work was supported by Grants-in-Aid for Scientific Research (19K08455) from the Japan Society for the Promotion of Science as well as by funding from Takeda Science Foundation, Smoking Research Foundation, Yakult Bio-Science Foundation, SENSHIN Medical Research Foundation, and Japan Agency for Medical Research and Development (AMED) for Research on Intractable Diseases.

ACKNOWLEDGMENTS

We would like to thank Yukiko Ueno for her secretarial support.

REFERENCES

Baumgart, D. C., and Sandborn, W. J. (2012). Crohn's disease. *Lancet* 380, 1590–1605. doi:10.1016/s0140-6736(12)60026-9

Bertrand, M. J., Doiron, K., Labbé, K., Korneluk, R. G., Barker, P. A., and Saleh, M. (2009). Cellular inhibitors of apoptosis cIAP1 and cIAP2 are required for innate immunity signaling by the pattern recognition receptors NOD1 and NOD2. *Immunity* 30 (6), 789–801. doi:10.1016/j.immuni.2009.04.011

Bertrand, M. J., Lippens, S., Staes, A., Gilbert, B., Roelandt, R., De Medts, J., et al. (2011). cIAP1/2 are direct E3 ligases conjugating diverse types of ubiquitin chains to receptor interacting proteins kinases 1 to 4 (RIP1-4). *PLoS One* 6 (9), e22356. doi:10.1371/journal.pone.0022356

Biswas, A., Liu, Y. J., Hao, L., Mizoguchi, A., Salzman, N. H., Bevins, C. L., et al. (2010). Induction and rescue of Nod2-dependent Th1-driven granulomatous inflammation of the ileum. *Proc. Natl. Acad. Sci.* 107 (33), 14739–14744. doi:10.1073/pnas.1003363107

Caruso, R., Lo, B. C., and Núñez, G. (2020). Host-microbiota interactions in inflammatory bowel disease. *Nat. Rev. Immunol.* 20 (7), 411–426. doi:10.1038/s41577-019-0268-7

Cavallari, J. F., Fullerton, M. D., Duggan, B. M., Foley, K. P., Denou, E., Smith, B. K., et al. (2017). Muramyl dipeptide-based postbiotics mitigate obesity-induced insulin resistance via IRF4. *Cell Metab.* 25 (5), 1063–1074.e3. doi:10.1016/j.cmet.2017.03.021

Chen, G., Shaw, M. H., Kim, Y. G., and Nuñez, G. (2009). NOD-like receptors: role in innate immunity and inflammatory disease. *Annu. Rev. Pathol. Mech. Dis.* 4, 365–398. doi:10.1146/annurev.pathol.4.110807.092239

Cho, J. H. (2008). The genetics and immunopathogenesis of inflammatory bowel disease. *Nat. Rev. Immunol.* 8 (6), 458–466. doi:10.1038/nri2340

Cooney, R., Baker, J., Brain, O., Danis, B., Pichulik, T., Allan, P., et al. (2010). NOD2 stimulation induces autophagy in dendritic cells influencing bacterial handling and antigen presentation. *Nat. Med.* 16 (1), 90–97. doi:10.1038/nm.2069

Couturier-Maillard, A., Secher, T., Rehman, A., Normand, S., De Arcangelis, A., Haesler, R., et al. (2013). NOD2-mediated dysbiosis predisposes mice to transmissible colitis and colorectal cancer. *J. Clin. Invest.* 123 (2), 700–711. doi:10.1172/JCI62236

Damgaard, R. B., Fiil, B. K., Speckmann, C., Yabal, M., Stadt, U. z., Bekker-Jensen, S., et al. (2013). Disease-causing mutations in the XIAP BIR 2 domain impair NOD 2-dependent immune signalling. *EMBO Mol. Med.* 5 (8), 1278–1295. doi:10.1002/emmm.201303090

Damgaard, R. B., Nachbur, U., Yabal, M., Wong, W. W.-L., Fiil, B. K., Kastirr, M., et al. (2012). The ubiquitin ligase XIAP recruits LUBAC for NOD2 signaling in inflammation and innate immunity. *Mol. Cell* 46 (6), 746–758. doi:10.1016/j.molcel.2012.04.014

Dorsch, M., Wang, A., Cheng, H., Lu, C., Bielecki, A., Charron, K., et al. (2006). Identification of a regulatory autophosphorylation site in the serine-threonine kinase RIP2. *Cell Signal.* 18 (12), 2223–2229. doi:10.1016/j.cellsig.2006.05.005

Fiil, B. K., Damgaard, R. B., Wagner, S. A., Keusekotten, K., Fritsch, M., Bekker-Jensen, S., et al. (2013). OTULIN restricts Met1-linked ubiquitination to control innate immune signaling. *Mol. Cell* 50, 818–830. doi:10.1016/j.molcel.2013.06.004

Fritz, J. H., Girardin, S. E., Fitting, C., Werts, C., Mengin-Lecreulx, D., Caroff, M., et al. (2005). Synergistic stimulation of human monocytes and dendritic cells by Toll-like receptor 4 and NOD1- and NOD2-activating agonists. *Eur. J. Immunol.* 35 (8), 2459–2470. doi:10.1002/eji.200526286

Goncharov, T., Hedayati, S., Mulvihill, M. M., Izrael-Tomasevic, A., Zobel, K., Jeet, S., et al. (2018). Disruption of XIAP-RIP2 association blocks NOD2-mediated inflammatory signaling. *Mol. Cel* 69 (4), 551–565. doi:10.1016/j.molcel.2018.01.016

Haile, P. A., Votta, B. J., Marquis, R. W., Bury, M. J., Mehlmann, J. F., Singhaus, R., Jr., et al. (2016). The identification and pharmacological characterization of 6-(tert-Butylsulfonyl)-N-(5-fluoro-1H-indazol-3-yl)quinolin-4-amine (GSK583), a highly potent and selective inhibitor of RIP2 kinase. *J. Med. Chem.* 59 (10), 4867–4880. doi:10.1021/acs.jmedchem.6b00211

Hall, H. T. L., Wilhelm, M. T., Saibil, S. D., Mak, T. W., Flavell, R. A., and Ohashi, P. S. (2008). RIP2 contributes to Nod signaling but is not essential for T cell proliferation, T helper differentiation or TLR responses. *Eur. J. Immunol.* 38 (1), 64–72. doi:10.1002/eji.200737393

Hasegawa, M., Fujimoto, Y., Lucas, P. C., Nakano, H., Fukase, K., Núñez, G., et al. (2008). A critical role of RICK/RIP2 polyubiquitination in Nod-induced NF-κB activation. *EMBO J.* 27 (2), 373–383. doi:10.1038/sj.emboj.7601962

Hofmann, S. R., Girschick, L., Stein, R., and Schulze, F. (2021). Immune modulating effects of receptor interacting protein 2 (RIP2) in autoinflammation and immunity. *Clin. Immunol.* 223, 108648. doi:10.1016/j.clim.2020.108648

Hollenbach, E., Neumann, M., Vieth, M., Roessner, A., Malfertheiner, P., and Naumann, M. (2004). Inhibition of p38 MAP kinase-and RICK/NF-κB-signaling suppresses inflammatory bowel disease. *FASEB J.* 18 (13), 1550–1552. doi:10.1096/fj.04-1642fje

Hollenbach, E., Vieth, M., Roessner, A., Neumann, M., Malfertheiner, P., and Naumann, M. (2005). Inhibition of RICK/nuclear factor-κb and p38 signaling attenuates the inflammatory response in a murine model of Crohn disease. *J. Biol. Chem.* 280 (15), 14981–14988. doi:10.1074/jbc.m500966200

Homer, C. R., Richmond, A. L., Rebert, N. A., Achkar, J. P., and Mcdonald, C. (2010). ATG16L1 and NOD2 interact in an autophagy-dependent antibacterial pathway implicated in Crohn's disease pathogenesis. *Gastroenterology* 139 (5), 1630–1641. doi:10.1053/j.gastro.2010.07.006

Honjo, H., Watanabe, T., Arai, Y., Kamata, K., Minaga, K., Komeda, Y., et al. (2021). ATG16L1 negatively regulates RICK/RIP2-mediated innate immune responses. *Int. Immunol.* 33 (2), 91–105. doi:10.1093/intimm/dxaa062

Hrdinka, M., Fiil, B. K., Zucca, M., Leske, D., Bagola, K., Yabal, M., et al. (2016). CYLD limits Lys63- and met1-linked ubiquitin at receptor complexes to regulate innate immune signaling. *Cell Rep.* 14, 2846–2858. doi:10.1016/j.celrep.2016.02.062

Hrdinka, M., Schlicher, L., Dai, B., Pinkas, D. M., Bufton, J. C., Picaud, S., et al. (2018). Small molecule inhibitors reveal an indispensable scaffolding role of RIPK2 in NOD2 signaling. *EMBO J.* 37. doi:10.15252/embj.201899372

Inohara, N., Chamaillard, M., McDonald, C., and Nuñez, G. (2005). NOD-LRR proteins: role in host-microbial interactions and inflammatory disease. *Annu. Rev. Biochem.* 74, 355–383. doi:10.1146/annurev.biochem.74.082803.133347

Jostins, L., Ripke, S., Ripke, S., Weersma, R. K., Duerr, R. H., McGovern, D. P., et al. (2012). Host-microbe interactions have shaped the genetic architecture of inflammatory bowel disease. *Nature* 491 (7422), 119–124. doi:10.1038/nature11582

Jun, J. C., Cominelli, F., and Abbott, D. W. (2013). RIP2 activity in inflammatory disease and implications for novel therapeutics. *J. Leukoc. Biol.* 94 (5), 927–932. doi:10.1189/jlb.0213109

Kaser, A., and Blumberg, R. S. (2011). Autophagy, microbial sensing, endoplasmic reticulum stress, and epithelial function in inflammatory bowel disease. *Gastroenterology* 140 (6), 1738–1747. doi:10.1053/j.gastro.2011.02.048

Kim, Y. G., Park, J. H., Shaw, M. H., Franchi, L., Inohara, N., and Núñez, G. (2008). The cytosolic sensors Nod1 and Nod2 are critical for bacterial recognition and host defense after exposure to Toll-like receptor ligands. *Immunity* 28 (2), 246–257. doi:10.1016/j.immuni.2007.12.012

Kobayashi, K., Inohara, N., Hernandez, L. D., Galán, J. E., Núñez, G., Janeway, C. A., et al. (2002). RICK/Rip2/CARDIAK mediates signalling for receptors of the innate and adaptive immune systems. *Nature* 416 (6877), 194–199. doi:10.1038/416194a

Kobayashi, K. S., Chamaillard, M., Ogura, Y., Henegariu, O., Inohara, N., Nunez, G., et al. (2005). Nod2-dependent regulation of innate and adaptive immunity in the intestinal tract. *Science* 307 (5710), 731–734. doi:10.1126/science.1104911

Kuballa, P., Huett, A., Rioux, J. D., Daly, M. J., and Xavier, R. J. (2008). Impaired autophagy of an intracellular pathogen induced by a Crohn's disease associated ATG16L1 variant. *PLoS One* 3 (10), e3391. doi:10.1371/journal.pone.0003391

Lassen, K. G., Kuballa, P., Conway, K. L., Patel, K. K., Becker, C. E., Peloquin, J. M., et al. (2014). Atg16L1 T300A variant decreases selective autophagy resulting in altered cytokine signaling and decreased antibacterial defense. *Proc. Natl. Acad. Sci.* 111 (21), 7741–7746. doi:10.1073/pnas.1407001111

Lu, C., Wang, A., Dorsch, M., Tian, J., Nagashima, K., Coyle, A. J., et al. (2005). Participation of Rip2 in lipopolysaccharide signaling is independent of its kinase activity. *J. Biol. Chem.* 280 (16), 16278–16283. doi:10.1074/jbc.m410114200

Mizushima, N., Levine, B., Cuervo, A. M., and Klionsky, D. J. (2008). Autophagy fights disease through cellular self-digestion. *Nature* 451 (7182), 1069–1075. doi:10.1038/nature06639

Murthy, A., Li, Y., Peng, I., Reichelt, M., Katakam, A. K., Noubade, R., et al. (2014). A Crohn's disease variant in Atg16l1 enhances its degradation by caspase 3. *Nature* 506 (7489), 456–462. doi:10.1038/nature13044

Nachbur, U., Stafford, C. A., Bankovacki, A., Zhan, Y., Lindqvist, L. M., Fiil, B. K., et al. (2015). A RIPK2 inhibitor delays NOD signalling events yet prevents inflammatory cytokine production. *Nat. Commun.* 6, 6442. doi:10.1038/ncomms7442

Negroni, A., Stronati, L., Pierdomenico, M., Tirindelli, D., Di Nardo, G., Mancini, V., et al. (2009). Activation of NOD2-mediated intestinal pathway in a pediatric population with Crohn's disease. *Inflamm. Bowel Dis.* 15 (8), 1145–1154. doi:10.1002/ibd.20907

Neurath, M. F. (2014). New targets for mucosal healing and therapy in inflammatory bowel diseases. *Mucosal Immunol.* 7 (1), 6–19. doi:10.1038/mi.2013.73

Park, J. H., Kim, Y. G., Mcdonald, C., Kanneganti, T. D., Hasegawa, M., Body-Malapel, M., et al. (2007). RICK/RIP2 mediates innate immune responses induced through Nod1 and Nod2 but not TLRs. *J. Immunol.* 178 (4), 2380–2386. doi:10.4049/jimmunol.178.4.2380

Pashenkov, M. V., Murugina, N. E., Budikhina, A. S., and Pinegin, B. V. (2019). Synergistic interactions between NOD receptors and TLRs: mechanisms and clinical implications. *J. Leukoc. Biol.* 105 (4), 669–680. doi:10.1002/jlb.2ru0718-290r

Philpott, D. J., Sorbara, M. T., Robertson, S. J., Croitoru, K., and Girardin, S. E. (2014). NOD proteins: regulators of inflammation in health and disease. *Nat. Rev. Immunol.* 14 (1), 9–23. doi:10.1038/nri3565

Plantinga, T. S., Crisan, T. O., Oosting, M., Van De Veerdonk, F. L., De Jong, D. J., Philpott, D. J., et al. (2011). Crohn's disease-associated ATG16L1 polymorphism modulates pro-inflammatory cytokine responses selectively upon activation of NOD2. *Gut* 60 (9), 1229–1235. doi:10.1136/gut.2010.228908

Saitoh, T., Fujita, N., Jang, M. H., Uematsu, S., Yang, B.-G., Satoh, T., et al. (2008). Loss of the autophagy protein Atg16L1 enhances endotoxin-induced IL-1β production. *Nature* 456 (7219), 264–268. doi:10.1038/nature07383

Salem, M., Ammitzboell, M., Nys, K., Seidelin, J. B., and Nielsen, O. H. (2015). ATG16L1: a multifunctional susceptibility factor in Crohn disease. *Autophagy* 11 (4), 585–594. doi:10.1080/15548627.2015.1017187

Salla, M., Aguayo-Ortiz, R., Danmaliki, G. I., Zare, A., Said, A., Moore, J., et al. (2018). Identification and characterization of novel receptor-interacting serine/threonine-protein kinase 2 inhibitors using structural similarity analysis. *J. Pharmacol. Exp. Ther.* 365 (2), 354–367. doi:10.1124/jpet.117.247163

Shanahan, M. T., Carroll, I. M., Grossniklaus, E., White, A., Von Furstenberg, R. J., Barner, R., et al. (2014). Mouse Paneth cell antimicrobial function is independent of Nod2. *Gut* 63 (6), 903–910. doi:10.1136/gutjnl-2012-304190

Shimada, K., Porritt, R. A., Markman, J. L., O'Rourke, J. G., Wakita, D., Noval Rivas, M., et al. (2018). T-Cell-Intrinsic receptor interacting protein 2 regulates pathogenic T helper 17 cell differentiation. *Immunity* 49 (5), 873–885.e7. doi:10.1016/j.immuni.2018.08.022

Shivaji, U. N., Nardone, O. M., Cannatelli, R., Smith, S. C., Ghosh, S., and Iacucci, M. (2020). Small molecule oral targeted therapies in ulcerative colitis. *Lancet Gastroenterol. Hepatol.* 5 (9), 850–861. doi:10.1016/s2468-1253(19)30414-5

Simms, L. A., Doecke, J. D., Walsh, M. D., Huang, N., Fowler, E. V., and Radford-Smith, G. L. (2008). Reduced -defensin expression is associated with inflammation and not NOD2 mutation status in ileal Crohn's disease. *Gut* 57 (7), 903–910. doi:10.1136/gut.2007.142588

Sorbara, M. T., Ellison, L. K., Ramjeet, M., Travassos, L. H., Jones, N. L., Girardin, S. E., et al. (2013). The protein ATG16L1 suppresses inflammatory cytokines induced by the intracellular sensors Nod1 and Nod2 in an autophagy-independent manner. *Immunity* 39 (5), 858–873. doi:10.1016/j.immuni.2013.10.013

Stafford, C. A., Lawlor, K. E., Heim, V. J., Bankovacki, A., Bernardini, J. P., Silke, J., et al. (2018). IAPs regulate distinct innate immune pathways to Co-ordinate the response to bacterial peptidoglycans. *Cell Rep.* 22 (6), 1496–1508. doi:10.1016/j.celrep.2018.01.024

Strober, W., Asano, N., Fuss, I., Kitani, A., and Watanabe, T. (2014). Cellular and molecular mechanisms underlying NOD2 risk-associated polymorphisms in Crohn's disease. *Immunol. Rev.* 260 (1), 249–260. doi:10.1111/imr.12193

Strober, W., and Fuss, I. J. (2011). Proinflammatory cytokines in the pathogenesis of inflammatory bowel diseases. *Gastroenterology* 140 (6), 1756–1767. doi:10.1053/j.gastro.2011.02.016

Strober, W., Murray, P. J., Kitani, A., and Watanabe, T. (2006). Signalling pathways and molecular interactions of NOD1 and NOD2. *Nat. Rev. Immunol.* 6 (1), 9–20. doi:10.1038/nri1747

Strober, W., Fuss, I., and Mannon, P. (2007). The fundamental basis of inflammatory bowel disease. *J. Clin. Invest.* 117 (3), 514–521. doi:10.1172/jci30587

Strober, W., and Watanabe, T. (2011). NOD2, an intracellular innate immune sensor involved in host defense and Crohn's disease. *Mucosal. Immunol.* 4 (5), 484–495. doi:10.1038/mi.2011.29

Suebsuwong, C., Dai, B., Pinkas, D. M., Duddupudi, A. L., Li, L., Bufton, J. C., et al. (2020). Receptor-interacting protein kinase 2 (RIPK2) and nucleotide-binding oligomerization domain (NOD) cell signaling inhibitors based on a 3,5-diphenyl-2-aminopyridine scaffold. *Eur. J. Med. Chem.* 200, 112417. doi:10.1016/j.ejmech.2020.112417

Takeda, K., and Akira, S. (2005). Toll-like receptors in innate immunity. *Int. Immunol.* 17, 1–14. doi:10.1093/intimm/dxh186

Tao, M., Scacheri, P. C., Marinis, J. M., Harhaj, E. W., Matesic, L. E., and Abbott, D. W. (2009). ITCH K63-ubiquitinates the NOD2 binding protein, RIP2, to influence inflammatory signaling pathways. *Curr. Biol.* 19 (15), 1255–1263. doi:10.1016/j.cub.2009.06.038

Tigno-Aranjuez, J. T., Benderitter, P., Rombouts, F., Deroose, F., Bai, X., Mattioli, B., et al. (2014). *In vivo* inhibition of RIPK2 kinase alleviates inflammatory disease. *J. Biol. Chem.* 289 (43), 29651–29664. doi:10.1074/jbc.m114.591388

Travassos, L. H., Carneiro, L. A. M., Ramjeet, M., Hussey, S., Kim, Y.-G., Magalhães, J. G., et al. (2010). Nod1 and Nod2 direct autophagy by recruiting ATG16L1 to the plasma membrane at the site of bacterial entry. *Nat. Immunol.* 11 (1), 55–62. doi:10.1038/ni.1823

Udden, S. M. N., Peng, L., Gan, J. L., Shelton, J. M., Malter, J. S., Hooper, L. V., et al. (2017). NOD2 suppresses colorectal tumorigenesis via downregulation of the TLR pathways. *Cell Rep.* 19 (13), 2756–2770. doi:10.1016/j.celrep.2017.05.084

Ungaro, R., Mehandru, S., Allen, P. B., Peyrin-Biroulet, L., and Colombel, J. F. (2017). Ulcerative colitis. *Lancet* 389, 1756–1770. doi:10.1016/s0140-6736(16)32126-2

Usluoglu, N., Pavlovic, J., Moelling, K., and Radziwill, G. (2007). RIP2 mediates LPS-induced p38 and IκBα signaling including IL-12 p40 expression in human monocyte-derived dendritic cells. *Eur. J. Immunol.* 37, 2317–2325. doi:10.1002/eji.200636388

Verstockt, B., Ferrante, M., Vermeire, S., and Van Assche, G. (2018). New treatment options for inflammatory bowel diseases. *J. Gastroenterol.* 53 (5), 585–590. doi:10.1007/s00535-018-1449-z

Virgin, H. W., and Levine, B. (2009). Autophagy genes in immunity. *Nat. Immunol.* 10 (5), 461–470. doi:10.1038/ni.1726

Watanabe, T., Asano, N., Murray, P. J., Ozato, K., Tailor, P., Fuss, I. J., et al. (2008). Muramyl dipeptide activation of nucleotide-binding oligomerization domain 2 protects mice from experimental colitis. *J. Clin. Invest.* 118 (2), 545–559. doi:10.1172/JCI33145

Watanabe, T., Asano, N., Fichtner-Feigl, S., Gorelick, P. L., Tsuji, Y., Matsumoto, Y., et al. (2010). NOD1 contributes to mouse host defense against *Helicobacter pylori* via induction of type I IFN and activation of the ISGF3 signaling pathway. *J. Clin. Invest.* 120 (5), 1645–1662. doi:10.1172/jci39481

Watanabe, T., Asano, N., Meng, G., Yamashita, K., Arai, Y., Sakurai, T., et al. (2014). NOD2 downregulates colonic inflammation by IRF4-mediated inhibition of K63-linked polyubiquitination of RICK and TRAF6. *Mucosal. Immunol.* 7 (6), 1312–1325. doi:10.1038/mi.2014.19

Watanabe, T., Kitani, A., Murray, P. J., and Strober, W. (2004). NOD2 is a negative regulator of Toll-like receptor 2-mediated T helper type 1 responses. *Nat. Immunol.* 5 (8), 800–808. doi:10.1038/ni1092

Watanabe, T., Kitani, A., Murray, P. J., Wakatsuki, Y., Fuss, I. J., and Strober, W. (2006). Nucleotide binding oligomerization domain 2 deficiency leads to dysregulated TLR2 signaling and induction of antigen-specific colitis. *Immunity* 25 (3), 473–485. doi:10.1016/j.immuni.2006.06.018

Watanabe, T., Minaga, K., Kamata, K., Sakurai, T., Komeda, Y., Nagai, T., et al. (2019). RICK/RIP2 is a NOD2-independent nodal point of gut inflammation. *Int. Immunol.* 31 (10), 669–683. doi:10.1093/intimm/dxz045

Wehkamp, J., Harder, J., Weichenthal, M., Schwab, M., Schaffeler, E., Schlee, M., et al. (2004). NOD2 (CARD15) mutations in Crohn's disease are associated with diminished mucosal -defensin expression. *Gut* 53 (11), 1658–1664. doi:10.1136/gut.2003.032805

Wehkamp, J., Salzman, N. H., Porter, E., Nuding, S., Weichenthal, M., Petras, R. E., et al. (2005). Reduced Paneth cell -defensins in ileal Crohn's disease. *Proc. Natl. Acad. Sci.* 102 (50), 18129–18134. doi:10.1073/pnas.0505256102

Wullaert, A., Heyninck, K., Janssens, S., and Beyaert, R. (2006). Ubiquitin: tool and target for intracellular NF-κB inhibitors. *Trends Immunol.* 27 (11), 533–540. doi:10.1016/j.it.2006.09.003

Yang, S., Wang, B., Humphries, F., Jackson, R., Healy, M. E., Bergin, R., et al. (2013). Pellino3 ubiquitinates RIP2 and mediates Nod2-induced signaling and protective effects in colitis. *Nat. Immunol.* 14 (9), 927–936. doi:10.1038/ni.2669

Yang, Y., Yin, C., Pandey, A., Abbott, D., Sassetti, C., and Kelliher, M. A. (2007). NOD2 pathway activation by MDP or *Mycobacterium tuberculosis* infection involves the stable polyubiquitination of Rip2. *J. Biol. Chem.* 282 (50), 36223–36229. doi:10.1074/jbc.m703079200

Zhang, H., Zheng, L., Chen, J., Fukata, M., Ichikawa, R., Shih, D. Q., et al. (2017). The protection role of Atg16l1 in CD11c $^{+}$ dendritic cells in murine colitis. *Immunobiology* 222 (7), 831–841. doi:10.1016/j.imbio.2017.03.002

Conflict of Interest: The authors declare that the research was conducted in the absence of any commercial or financial relationships that could be construed as a potential conflict of interest.

frontiers in Pharmacology

REVIEW
published: 12 April 2021
doi: 10.3389/fphar.2021.660040

Role of Leptin in the Digestive System

Min-Hyun Kim[1] *and Hyeyoung Kim*[2]*

[1]Department of Molecular and Integrative Physiology, University of Michigan Medical School, Ann Arbor, MI, United States, [2]Department of Food and Nutrition, College of Human Ecology, Yonsei University, Seoul, Korea

Leptin is a pluripotent peptide hormone produced mainly by adipocytes, as well as by other tissues such as the stomach. Leptin primarily acts on the central nervous system, particularly the hypothalamus, where this hormone regulates energy homeostasis and neuroendocrine function. Owing to this, disruption of leptin signaling has been linked with numerous pathological conditions. Recent studies have also highlighted the diverse roles of leptin in the digestive system including immune regulation, cell proliferation, tissue healing, and glucose metabolism. Of note, leptin acts differently under physiological and pathological conditions. Here, we review the current knowledge on the functions of leptin and its downstream signaling in the gastrointestinal tract and accessory digestive organs, with an emphasis on its physiological and pathological implications. We also discuss the current therapeutic uses of recombinant leptin, as well as its limitations.

Keywords: leptin, digestive system, signal transduction, cytoprotection, immune system

OPEN ACCESS

Edited by:
Thomas Brzozowski, Jagiellonian University Medical College, Poland

Reviewed by:
Oksana Zayachkivska, Danylo Halytsky Lviv National Medical University, Ukraine
Jonathan Flak, Indiana Biosciences Research Institute, United States

***Correspondence:**
Hyeyoung Kim
kim626@yonsei.ac.kr

Specialty section:
This article was submitted to Gastrointestinal and Hepatic Pharmacology, a section of the journal Frontiers in Pharmacology

Received: *28 January 2021*
Accepted: *04 March 2021*
Published: *12 April 2021*

Citation:
Kim M-H and Kim H (2021) Role of Leptin in the Digestive System. Front. Pharmacol. 12:660040. doi: 10.3389/fphar.2021.660040

INTRODUCTION

Leptin, a 16 kDa hormone encoded by the *ob* gene, is mainly produced and secreted by adipocytes (Friedman, 2019). In general, circulating leptin levels reflect body fat mass (Francisco et al., 2018). Leptin is also produced by other tissues, including the stomach, skeletal muscles, pituitary gland, and mammary gland (Reid et al., 2018; Inagaki-Ohara, 2019; Zieba et al., 2020). Leptin was discovered as a central regulator of systemic energy homeostasis (Ahima et al., 1996). Under normal conditions, elevated circulating leptin levels suppress feeding behavior while elevating energy expenditure by modulating multiple neuroendocrine axes (Pandit et al., 2017). On the other hand, decreased circulating leptin levels stimulate feeding behavior while decreasing energy utilization. Adequate levels of functional leptin are required for maintaining several physiological functions, including reproduction, tissue remodeling, growth and development, and the immune system (Ramos-Lobo and Donato Jr, 2017; Maurya et al., 2018; Monteiro et al., 2019; Sengupta et al., 2019).

Leptin function is mediated by its binding with the leptin receptor (LepR), which has multiple isoforms due to alternative splicing of LepR mRNA (Tartaglia et al., 1995; Wauman et al., 2017). Among these, the longest isoform, LepRb, mediates most of the known physiologic functions of leptin (Burguera et al., 2000; Wada et al., 2014) Activated LepRb regulates several downstream signaling pathways. These include the Janus kinase 2 (JAK2)/signal transducer and activator of transcription 3 (STAT3) and STAT5, extracellular-signal-regulated kinase (ERK), and phosphoinositide-3 kinase (PI3K) pathways (Liu et al., 2018). Leptin-mediated STAT3 activation results in feedback inhibition by increasing the expression of suppressor of cytokine signaling 3 (SOCS3) and protein tyrosine phosphatase 1 B (PTP1B), which decreases leptin sensitivity (Zhang et al., 2015). The short isoforms of LepR lack the intracellular domain required for signal transduction (Nunziata et al., 2019). These isoforms seem to be involved in the transport and degradation of leptin in tissues, thereby buffers leptin levels in tissues (Schaab et al., 2015). However, their functional activity is believed to be insignificant compared to the LepRb.

Most of the leptin functions have been attributed to its action in the brain, particularly in the hypothalamus, where LepRb is highly expressed (Van Swieten et al., 2014). In addition to that in the brain, LepRb expression has been widely detected in many other tissues, including immune cells and digestive organs (Wada et al., 2014). In the digestive system, leptin has been shown to play several roles, including regulation of immune responses, supporting cell growth and tissue repair, and regulation of glucose and lipid metabolism (Reidy et al., 2000; Marra, 2007; Fernández-Riejos et al., 2010). Leptin appears to play a complex role in these tissues, acting as either beneficial or deleterious depending on the physiological context. Notably, leptin is a member of the helical cytokine family along with IL-6 and IL-12, and LepR belongs to the group of class I cytokine receptors (Conde et al., 2014; Francisco et al., 2018). Therefore, leptin augments immune responses as a proinflammatory cytokine, which may lead to harmful consequences in inflammatory diseases (La Cava, 2017). Here, we review the current knowledge on the functions of leptin in the digestive system, including the gastrointestinal tract (stomach and intestine) and accessory digestive organs (liver and pancreas), with an emphasis on its physiological and pathological implications. We also discuss the possible therapeutic uses of leptin (to boost leptin signaling) or leptin antagonists (to suppress leptin signaling) in the digestive organs, and its limitations. We searched multiple databases including Pubmed, Scopus, and Web of Science (all dates) to identify relevant studies (total 183 articles identified). We only included peer-reviewed articles with a robust experimental design (28 articles excluded).

STOMACH

Leptin expression is not restricted to adipose tissues; a significant amount of leptin is also produced by the stomach (Kasacka et al., 2019). Bado et al. initially discovered that leptin is expressed in rat stomach epithelium (Bado et al., 1998), and other researchers later observed leptin expression in the human stomach as well (Breidert et al., 1999; Sobhani et al., 2000). The release of gastric leptin is stimulated by food consumption, food digestion, and hormones such as cholecystokinin (CCK), gastrin, or secretin (Camilleri and obesity, 2019; Goyal et al., 2019). Upon secretion, leptin displays resistance to proteolysis in the gastric juice, maintaining its functional structure (Buyse et al., 2001). In the stomach, leptin interacts with CCK to increase vagal afferent activities. This action controls the gastric emptying of ingested food, contributing to satiety (Goyal et al., 2019). Full-length LepRb and four short isoforms are expressed in the membranes of fundic and antral gastric cells (Mix et al., 2000; Sobhani et al., 2000). Despite of the receptor expression, however, a direct action of leptin on gastric epithelial cell function is insufficiently understood. Instead, autonomic activity exerted by leptin's action in the central nervous system (CNS) seems to be more important mechanism to govern physiology of the stomach (Tanida et al., 2019).

Studies using leptin-deficient *ob/ob* mice suggest that normal leptin signaling is critical for healing of gastric injury. In acetic acid-mediated experimental gastric ulcer model, *ob/ob* mice display impaired ulcer healing compared to that in wild-type mice due to the reduced expression of vascular endothelial growth factor (VEGF) and impairment of angiogenesis (Tanigawa et al., 2010). In the same model, restoration of leptin levels in *ob/ob* mice via leptin injection reverses the impaired ulcer healing owing to increased VEGF expression in gastric ulcerous tissue (Tanigawa et al., 2010). In ischemia reperfusion- and ethanol-induced gastric ulceration models, rats administered leptin [10 μg/kg body weight (BW)] showed significantly attenuated gastric lesions (Brzozowski et al., 2001). Notably, the protection conferred by leptin is as effective as that by CCK-8, a potent gastric protector (Mirza et al., 2018). Consistently, in rats with either indomethacin-induced or stress-induced gastric ulcer, leptin treatment (10 μg/kg BW, 6 h) significantly decreased the gastric ulcer index and neutrophil infiltration (Motawi et al., 2008; Khalefa et al., 2010). Several studies using rodent models highlight possible mechanisms. In rats with ulcers, leptin treatment (10 μg/kg BW) supports ulcer healing via production of nitric oxide (NO) and histamine, suppression of oxidative stress, and enhanced expression of transforming growth factor-α (TGF-α), a critical growth promoting factor for the gastric mucosa (Konturek et al., 2001; Erkasap et al., 2003; Motawi et al., 2008).

Nevertheless, unlike its protective effects against gastric injury, leptin appears to accelerate immune responses during gastric inflammation by synergistically interacting with a number of proinflammatory cytokines. Inagaki-Ohara et al. reported that feeding a high-fat diet promotes gastric intestinal metaplasia and atrophic gastritis via the activation of leptin signaling in C57BL6 wild-type mice (Inagaki-Ohara et al., 2016). On the contrary, *ob/ob* mice and LepR-deficient *db/db* mice demonstrate markedly suppressed gastric intestinal metaplasia and expression of proinflammatory cytokines, such as interleukin-6 (IL-6) and IL-11, under the same conditions, indicating that systemic leptin signaling is required to mediate proinflammatory responses (Inagaki-Ohara et al., 2016). Leptin has been implicated in several experimental models of *Helicobacter pylori* infection, which is the major cause of chronic gastritis and peptic ulcer diseases (Kang and Kim, 2017). Several clinical studies have demonstrated that mucosal leptin levels are significantly elevated in *H. pylori*-infected patients compared to those in uninfected individuals (Breidert et al., 1999; Azuma et al., 2001; Nishi et al., 2005; Roper et al., 2008; Romo-González et al., 2017). Using biopsy samples of *H. pylori*-infected patients, Nishi et al. showed that gastric leptin levels are positively correlated with the gastric levels of proinflammatory cytokines, including IL-1β and IL-6, indicating that leptin may modulate inflammatory responses during *H. pylori infection* (Nishi et al., 2005) (**Figure 1**).

INTESTINE

Leptin has been shown to modulate intestinal functions, mostly via its action on CNS as well as its regulation of vagal afferent sensitivity to intestinal signals (Huang et al., 2021). Significant

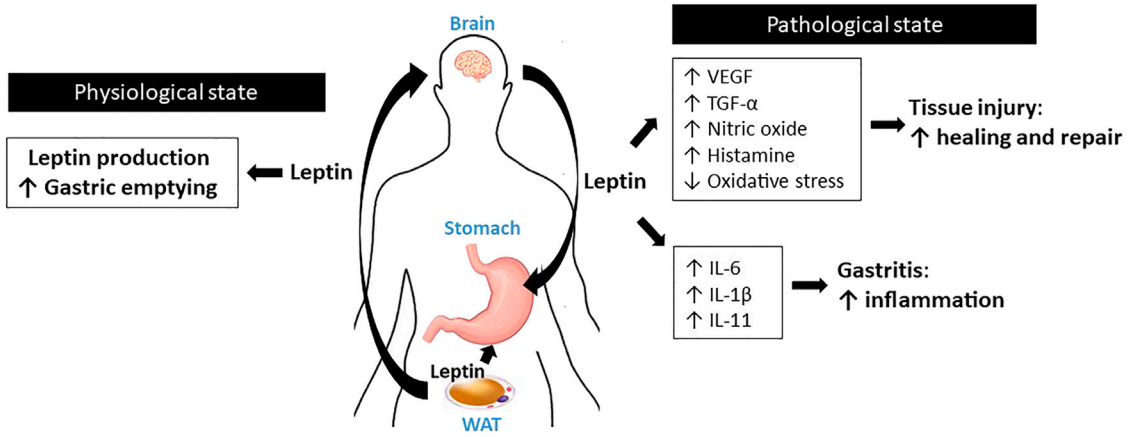

FIGURE 1 | Schematic diagram for the roles of leptin in the stomach.

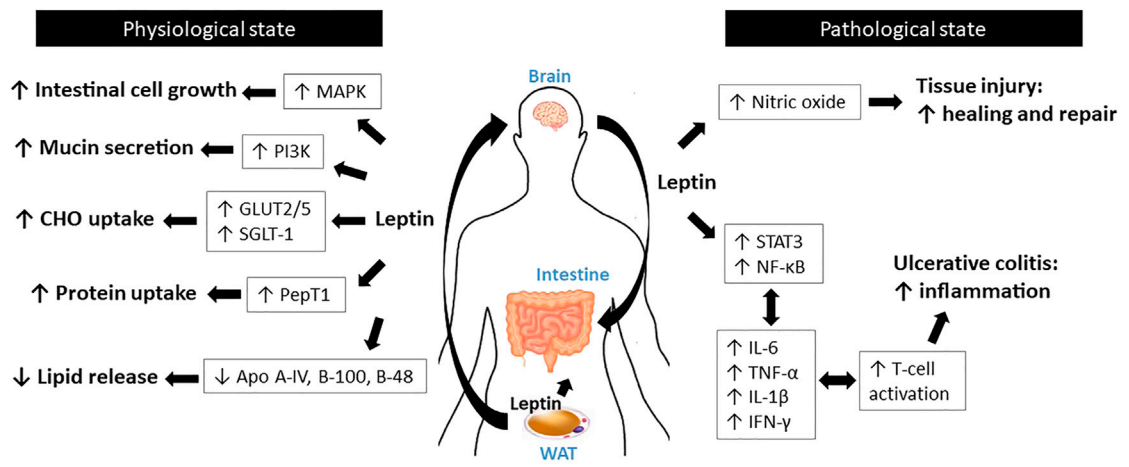

FIGURE 2 | Schematic diagram for the roles of leptin in the intestine.

expression of LepRb, the longest functional isoform, has been detected in Caco-2 and rat intestinal mucosal cells (Buyse et al., 2001), as well as in the brush border, basolateral membrane, and enterocytes of the human intestine (Barrenetxe et al., 2002). In the intestine, leptin has been shown to control the absorption of macronutrients. Although leptin decreases carbohydrate absorption during the pre-prandial state, leptin increases carbohydrate absorption during the postprandial state via increased expression of carbohydrate transporters, glucose transporter 2 (GLUT-2), GLUT-5, and sodium-glucose cotransporter-1 (SGLT-1) (Pearson et al., 2001; Alavi et al., 2002; Sakar et al., 2009). Leptin-mediated upregulation of GLUT2/5 couples with the activation of protein kinase C subunit βII (PKCβII) and 5′AMP-activated protein kinase subunit α (AMPKα), which are the central players in glucose uptake (Sakar et al., 2009). Leptin also increases protein absorption via activation of the proton-dependent di- and tri-peptide transporter PepT1 (Buyse et al., 2001). In contrast, following food ingestion, leptin reduces lipid release into the circulation by suppressing apolipoprotein (Apo) A-IV (Doi et al., 2001), B-100, and B-48 (Stan et al., 2001).

Leptin is required for gut development and maintenance, as it functions as a growth factor for intestinal cells (Martin and Devkota, 2018). Indeed, *ob/ob* and *db/db* mice display diminished intestinal barrier function and increased intestinal permeability relative to wild-type littermates (Thaiss et al., 2018). (Alavi et al., 2020) reported that systemic leptin administration [6.25–43.75 (mu)g/kg/d; total 14 days] to rats enhances mucosal mass, thereby supporting normal gut physiology (Alavi et al., 2002). In C57BL/6 wild-type mice, acute leptin treatment (10 mg/kg BW; 15 h) promotes colonic epithelial cell proliferation. This increased proliferation is mediated by activation of the p42/44 mitogen-activated protein kinase (MAPK) pathway (Hardwick et al., 2001). Several lines of

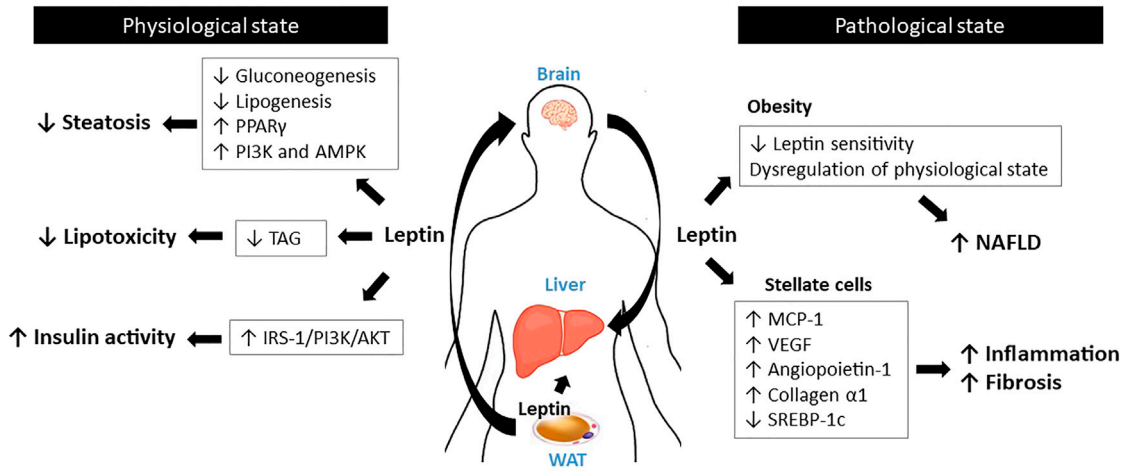

FIGURE 3 | Schematic diagram for the roles of leptin in the liver.

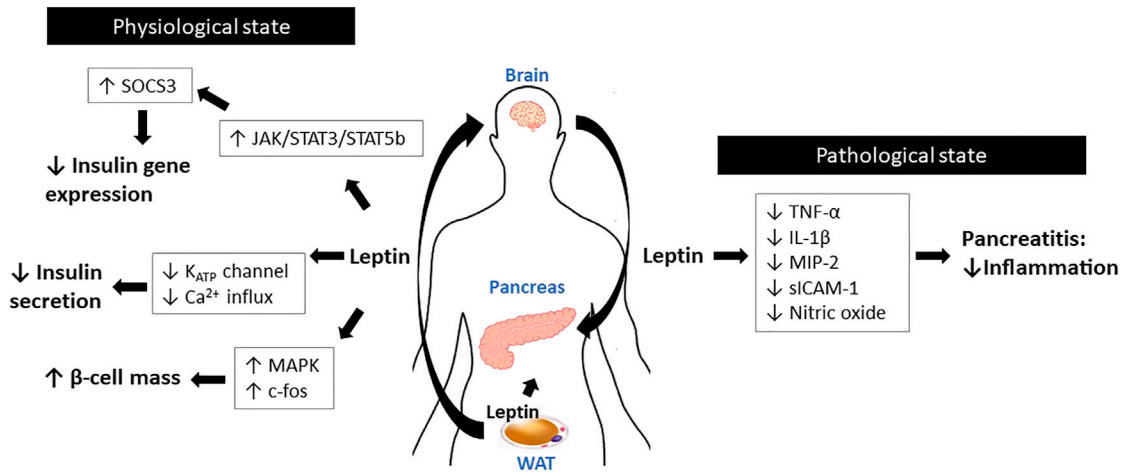

FIGURE 4 | Schematic diagram for the roles of leptin in the pancreas.

evidence indicate that leptin improves tissue injury healing and mucosal defense mechanisms. Leptin stimulates mucin secretion by activating the PKC- and PI3K pathways in human colonic goblet-like HT29-MTX cells (Plaisancie et al., 2006). In rats with anastomotic leaks, leptin administration (1 mg/kg BW, i. p.) leads to increased vascular tissue proliferation, collagen tissue proliferation, and mononuclear leukocyte infiltration, which accelerates the healing of colonic damage (Tasdelen et al., 2004). Similarly, in rats with ischemia-reperfusion injury, leptin treatment (100 μg/kg BW) significantly reduces tissue injury (Hacioglu et al., 2005). A study using rat arteries suggested that the tissue healing effect of leptin may be attributed to its stimulation of nitric oxide production, which mediates vasodilation, which in turn assists wound healing (Kimura et al., 2000).

Inflammatory bowel disease (IBD) comprises Crohn's disease (CD) and ulcerative colitis (UC) (Jarmakiewicz-Czaja et al., 2020). The common features of IBD include body weight loss, anorexia, and higher energy expenditure (Sairenji et al., 2017). As leptin is a central hormone involved in energy homeostasis and neuroendocrine function (Francisco et al., 2018), its involvement in IBD has been examined by many researchers. In both experimental *in vivo* IBD models and in human patients with IBD, serum leptin levels are elevated (Tuzun et al., 2004; Biesiada et al., 2012). In addition, LepR expression is also elevated in the mesenteric adipose tissue of patients with CD and UC (Barbier et al., 2003; Siegmund, 2012; Zulian et al., 2012). These data indicate that systemic leptin signaling is activated in IBD. Multiple researches show that the increased leptin signaling activates immune responses leading to IBD aggravation, resulting in deleterious effects. It should be noted that *ob/ob* and *db/db* mice are more resistant to experimental colitis models than the wild-type littermates (Siegmund et al., 2002). In dextran sulfate sodium (DSS)-

and trinitrobenzene sulfonic acid (TNBS)-induced colitis models, *ob/ob* mice produce significantly low levels of proinflammatory cytokines, such as interferon-γ (IFN-γ), tumor necrosis factor-α (TNF-α), IL-1β, and IL-6, which coincide with reduced STAT3 phosphorylation and cyclooxygenase-2 (COX-2) expression (Siegmund et al., 2002). However, administration of leptin to *ob/ob* mice is able to revert their resistance to colitis. In another study, researchers isolated T-cells from either *db/db* mice or wild-type mice and introduced them into immune-deficient *scid* mice (Siegmund et al., 2004). Strikingly, T-cells isolated from *db/db* mice delayed the development of colitis, indicating that the leptin/LepR axis is required for colitis progression by activating the T lymphocytes (Siegmund et al., 2004). Sitaraman et al., 2004 reported that inflamed colonic epithelial cells express and release leptin into the intestinal lumen (Sitaraman et al., 2004). Luminal leptin then activates nuclear factor kappa B (NF-κB), a potent pro-inflammation stimulator, which results in epithelial wall damage and neutrophil infiltration. Not only proinflammatory responses, leptin may mediates anorexia and body weight loss in IBD. In rats with TNBS-induced colitis, the severity of colitis is associated with circulating leptin levels as well as with anorexia and body weight loss (Barbier et al., 1998). In mice with DSS-induced colitis, delayed puberty is observed in proportion with the changes in serum leptin concentration, food intake, and body weight (Deboer and Li, 2011) (**Figure 2**).

LIVER

Unlike the other tissues discussed above, where the longest form, LepRb, is highly expressed, the liver appears to only express short forms of LepRs (Zhao et al., 2000; Otte et al., 2004). The absence of functional LepRb indicates that liver is unlikely a direct target of leptin. However, leptin has been shown to interact with various hepatic metabolic pathways, such as glucose and lipid metabolism, possibly via its function in the CNS (da Silva et al., 2020). Leptin controls glucose homeostasis by suppressing the hepatic *de novo* gluconeogenesis and lipogenesis and increasing hepatic triglyceride secretion (Denroche et al., 2012; Hackl et al., 2019) as well as modulating insulin activity through the stimulation insulin receptor substrate-1 (IRS-1)-associated PI3K activity (Cohen et al., 1996). Leptin prevents hepatic lipotoxicity by confining the storage of triglycerides to adipocytes (Unger et al., 1999; Engin and Engin, 2017).

Aberrant leptin signaling has been implicated in non-alcoholic fatty liver diseases (NAFLD) such as hepatic steatosis, hepatitis, and fibrosis. Spontaneous liver steatosis develops in *ob/ob* mice and in LepR-mutated *fa/fa* Zucker rats (Laiglesia et al., 2018; Martinelli et al., 2020). Mechanistically, *ob/ob* mice exhibit significantly higher hepatic peroxisome proliferator-activated receptor γ (PPARγ) activation, which elevates hepatic triglyceride levels by targeting the lipid-associated genes such as *Fsp27* (Matsusue et al., 2008). In the liver of *db/db* mice, level of miR-30c-5p is markedly reduced. Since miR-30c-5p is a direct suppressor of fatty acid synthase (FASN) expression, the reduction of miR-30c-5p upregulates fatty acid synthase (FASN), which elevates fatty acid biosynthesis (Fan et al., 2017). Multiple studies conducted in rodents and humans have shown that leptin treatment may ameliorate hepatic fat accumulation, suggesting its anti-steatotic effect (Paz-Filho et al., 2015; Rodríguez et al., 2015; Boutari and Mantzoros, 2020). Leptin also controls hepatic sympathetic nerve activity via activation of PI3K and AMPK signaling, which leads to improvement in the fatty liver disease (Miyamoto et al., 2012; Tanida et al., 2015).

Despite these positive reports on the effect of leptin on the liver, the efficacy of leptin in preventing liver steatosis seems limited by obesity. This is due to leptin resistance, one of the major features observed in obese individuals, where circulating leptin levels are extremely high compared to those in lean individuals (Izquierdo et al., 2019). Despite high concentrations, leptin resistance leads to failure of leptin action, which inhibits the modulation of hepatic glucose metabolism and insulin response (Engin, 2017; Rizwan et al., 2017). Increased fat mass in obesity causes chronic inflammation and increases the expression of numerous adipokines, including leptin. The increased leptin levels in obese status appear to boost hepatic pro-inflammatory and pro-fibrogenic responses, thus damaging the liver (Saxena and Anania, 2015). Indeed, *ob/ob* mice and *fa/fa* Zucker rats fail to develop fibrosis during hepatic steatosis or toxin administration (Leclercq et al., 2002; Ikejima et al., 2005), demonstrating that leptin plays a significant role in this process. The pro-fibrogenic action of leptin involves hepatic stellate cells (HSCs), which are liver-specific pericytes (Tsuchida and Friedman, 2017). Once activated, but not quiescent, HSCs express leptin (Potter et al., 1998). Leptin supports the proliferation and survival of HSCs via ERK- and Akt-dependent phosphorylation pathways (Saxena et al., 2004). In addition, leptin in HSCs stimulates the expression of pro-inflammatory and angiogenic cytokines, such as monocyte chemoattractant protein-1 (MCP-1), VEGF, angiopoietin-1, and collagen α1, which results in higher hepatic collagen expression and inflammation (Aleffi et al., 2005; Yan et al., 2012). Leptin also inhibits the expression of sterol regulatory element-binding protein 1c (SREBP-1c), an inhibitor of fibrogenesis, via the β-catenin pathway in isolated HSCs (Zhai et al., 2013). Despite this evidence in experimental *in vitro* and *in vivo* models, conflicting data have been obtained in human patients with NAFLD, regarding the role of leptin in hepatic inflammation and fibrosis (Polyzos et al., 2015); this has been a major obstacle in testing leptin therapy for this disease. However, leptin therapy has been actively used in patients with lipodystrophy, a disorder characterized by fat loss, severe insulin resistance, and NAFLD and steatohepatitis (NASH) (Akinci et al., 2018). Notably, patients with lipodystrophy display low circulating levels of leptin (hypoleptinemia) (Chong et al., 2010). In 2002, leptin replacement was initially tested in nine female patients with lipodystrophy, and the therapy was shown to be effective in treating the disease (Oral et al., 2002). Specifically, leptin therapy improves glycemic control and decreases triglyceride

levels, thus effectively improving the symptoms of NASH (Polyzos et al., 2019; Baykal et al., 2020) (**Figure 3**).

PANCREAS

Leptin controls glucose homeostasis mainly via its actions on the hypothalamus (D'souza et al., 2017). Pancreatic β-cells are another important target of leptin to regulate glucose metabolism (Marroquí et al., 2012). The functional receptor LepRb is detected in various β-cell lines, including MIN-6, βTC-3, and INS-1 (Kieffer et al., 1996; Tanizawa et al., 1997; Ahren et al., 1999), as well as in the islets of rodents and humans (Emilsson et al., 1997; Poitout et al., 1998; Seufert et al., 1999b). On the contrary, LepR expression is not detected in glucagon-expressing α-cells; thus, leptin action seems limited to β-cells (Soedling et al., 2015). Under steady-state conditions, leptin signaling in the CNS seems to govern pancreas physiology, rather than its direct action in pancreas.

In physiological states, leptin inhibits insulin gene expression in β-cells (Zhao et al., 2020). Insulin inhibition by leptin is mediated by the activation of JAK/STAT3 and STAT5b signaling (Morton and Schwartz, 2011). In INS-1 cells and in human pancreatic islets, Laubner et al. demonstrated that activation of STAT3 and STAT5b induces SOCS3 expression, which in turn suppresses preproinsulin one gene promoter activity (Laubner et al., 2005). This notion was further supported by (Pedroso et al., 2014)who showed that inactivation of SOCS3 in LepR-expressing cells protects mice against diet-induced insulin resistance, indicating that SOCS3 is a critical downstream signaling mediator of leptin to orchestrate glycemic control (Pedroso et al., 2014). In addition to gene expression, leptin inhibits insulin secretion from β-cells by modulating multiple steps of the hormone secretion mechanism (Kulkarni et al., 1997; Kuehnen et al., 2011). Leptin directly inhibits glucose transport into β-cells by inhibiting GLUT2 phosphorylation (Lam et al., 2004). Leptin also inhibits the activation of ATP-dependent potassium channels and the subsequent reduction of Ca^{2+} influx (Kieffer et al., 1997; Seufert et al., 1999a), which interrupts the exocytosis of insulin from β-cells.

Leptin has been shown to contribute to maintaining β-cell mass by modulating the proliferation and apoptosis of β-cells. LepR-deficient *fa/fa* Zucker rats and *db/db* mice develop reduced β-cell mass, which is associated with aging (Lee et al., 1994; Dalbøge et al., 2013), although leptin-deficient *ob/ob* mice exhibit normal islet mass (Bock et al., 2003). In mice, pancreas-specific LepR knockout directly affects β-cell growth and function (Morioka et al., 2007). Leptin treatment enhances cell proliferation in many β-cell lines such as RINm5F and MIN-6, as well as in rat fetal islet cells (Islam et al., 1997; Tanabe et al., 1997; Islam et al., 2000). These proliferative effects of leptin are mediated by activation of the MAPK pathway and c-fos, which are critical regulators of the cell cycle (Zhang and Liu, 2002). In addition, though the results are conflicting, leptin influences β-cell apoptosis. Some studies suggest that leptin suppresses apoptotic β-cell death. In rat islets, leptin increases intracellular fatty acid oxidation, and subsequently depletes triglyceride accumulation in islets, thereby preventing lipotoxicity-induced apoptosis (Shimabukuro et al., 1997).

Mechanistically, *fa/fa* Zucker rats develop reduced β-cell mass due to increased lipotoxicity (Pick et al., 1998; Wang et al., 1998). These results suggest that β-cell lipotoxicity may be a key mediator linking leptin resistance and the development of diabetes (Unger and Roth, 2015; Ercin et al., 2018). In addition, leptin reduces cellular nitric oxide levels by suppressing inducible NO synthase (iNOS) expression (Okuya et al., 2001) and increasing anti-apoptotic Bcl-2 expression in rat pancreatic islets (Shimabukuro et al., 1998), thereby exerting anti-apoptotic effects. However, other studies have shown that leptin enhances β-cell apoptosis. In human islets and INS 832/13 cells, long-term exposure to leptin triggers β-cell apoptosis through activation of the JNK pathway (Maedler et al., 2008). Similarly, chronic exposure of human islets to leptin leads to impaired β-cell function, caspase-3 activation, and apoptosis due to increased IL-1β expression and reduced IL-1 receptor antagonist expression (Maedler et al., 2004). This discrepancy between the anti- and pro-apoptotic effects of leptin may be due to different experimental designs. Indeed, most pro-apoptotic effects were observed when the cells were chronically treated with leptin (Maedler et al., 2004; Maedler et al., 2008), whereas an anti-apoptotic effect was observed with short-term treatment (Okuya et al., 2001).

Several *in vivo* studies have reported that leptin may exert a protective effect on pancreatitis. When acute pancreatitis is induced, *ob/ob* mice exhibit higher pathologic scores and intestinal permeability relative to wild-type mice, indicating that absence of leptin signaling aggravates intestinal inflammation (Ye et al., 2018). In rats with caerulein-induced pancreatitis, leptin administration (1 or 10 μg/kg BW, i. p.) significantly reduced the weight of the pancreas, histological manifestations of inflammation, and the expression of TNF-α and iNOS (Konturek et al., 2002). In the same pancreatitis model, leptin administration (10 μg/kg BW, i. p.) attenuated disease severity, which is mediated by reduced levels of proinflammatory cytokines, such as MIP-2, TNF-α, IL-1β, and sICAM-1, and nitric oxide (Gultekin et al., 2007). In the clinical setting, higher plasma leptin concentrations are associated with acute pancreatitis; thus, leptin may be a possible predictor of disease severity (Konturek et al., 2002; Kerem et al., 2007). Leptin is also associated with persistent hyperglycemia, as shown in the early course of acute pancreatitis (Kennedy et al., 2016). However, no clinical trials have examined exogenous leptin treatment in patients with acute pancreatitis (**Figure 4**).

DISCUSSION

In this section, we discuss the roles of leptin in the digestive system, including the stomach, intestine, liver, and pancreas. The current knowledge indicates that leptin plays critical but complex roles in these tissues, where its action appears to differ in the physiological and pathological states (**Figure 1**-**4**). The functional leptin/LepR axis is required for maintaining normal energy homeostasis and systemic glucose homeostasis. In addition, leptin exerts protective effects by supporting cell proliferation, improving tissue repair, and preventing non-adipocyte lipotoxicity. However, leptin action is not always protective,

particularly during pathologic conditions. Increased leptin and LepR levels are often observed in several inflammation-related diseases, where activated leptin signaling accelerates inflammatory response by promoting T-helper cell responses and supporting the production of proinflammatory cytokines (Fernández-Riejos et al., 2010). Of note, relatively little has been investigated a direct action of leptin in the digestive system. Indeed, most of the studies have examined the effect of central or peripheral leptin administration, which activates leptin signaling in the central nervous system. In that most of the leptin functions have been attributed to its action in the brain, there is no strong evidence to demonstrate leptin acts directly on peripheral tissues by binding receptors expressed in these tissues. Further studies using tissue-specific knockout models to limit the receptor expression are highly warranted.

Leptin replacement therapy is enormously beneficial in individuals with congenital leptin deficiency, which restores their energy homeostasis, neuroendocrine system, and glucose metabolism (Perakakis et al., 2021). As mentioned above, leptin administration is also widely used in patients with lipodystrophy. Since lipodystrophy is a medical condition characterized by degenerative adipose tissue, leptin production in patients is significantly reduced (Grewal et al., 2020). Therefore, administration of human recombinant leptin improves many metabolic defects in patients with lipodystrophy (Petersen et al., 2002). Since its discovery, leptin has been considered an attractive therapeutic target for the treatment of obesity and type 2 diabetes, due to its potency for the endocrine control of energy balance (Friedman, 2019). However, unlike that in congenital leptin deficiency, leptin concentrations are elevated in obesity owing to large fat mass, and systemic leptin signaling is blunted despite high circulating leptin levels. This status has been defined as "leptin resistance", which indicates poor responsiveness to leptin (Gruzdeva et al., 2019). Therefore, exogenous leptin treatment results in no or minimal effects on body weight and neuroendocrine function (Heymsfield et al., 1999; Mantzoros and Flier, 2000). Similarly, leptin therapy only produces modest effects on insulin sensitivity in type 2 diabetes due to leptin resistance (Mittendorfer et al., 2011).

Several *in vivo* experiments have explored the possible use of recombinant leptin or leptin antagonists in digestive organs. As discussed above, leptin augments proinflammatory responses and enhances susceptibility to autoimmune diseases, including UC (La Cava et al., 2004), which implies that neutralizing leptin action using a leptin antagonist may ameliorate the disease symptoms. Indeed, Singh et al. examined a leptin antagonist (PEG-MLA) to treat induced colitis in IL-10 knockout mice (Singh et al., 2013). Interestingly, they reported that PEG-MLA administration reduces systemic and mucosal inflammatory cytokine expression, thereby significantly attenuating the overall clinical features of colitis-associated pathogenesis. However, treatment with leptin or leptin antagonists has not been actively examined in clinical settings, mainly because the underlying mechanisms of leptin action in the digestive system are still unclear. Furthermore, leptin action is multifunctional and complex, which modulates numerous signaling pathways thus increasing the likelihood of an adverse reaction. For example, administration of a leptin antagonist can result in inhibition of the JAK/STAT pathway, a major pathway involved in cell division, cell death, and immunity, which may cause unexpected side effects. In addition, LepR expression is widespread in the body, which makes it difficult to confine the treated leptin/leptin antagonist to the target site. For instance, an excessively high dose of a leptin/leptin antagonist may Singh et al., 2013 cause serious deleterious effects on neuroendocrine function, as the hypothalamus is the most sensitive tissue in response to leptin. Therefore, more information is needed regarding the molecular mechanisms of leptin in the digestive system to consider manipulation of leptin signaling in these tissues as a novel therapeutic approach.

AUTHOR CONTRIBUTIONS

Investigation, and writing-original draft preparation: M-HK; supervision, and writing–review and editing: HK All authors have read and agreed to the published version of the manuscript.

REFERENCES

Ahima, R. S., Prabakaran, D., Mantzoros, C., Qu, D., Lowell, B., Maratos-Flier, E., et al. (1996). Role of leptin in the neuroendocrine response to fasting. *Nature* 382 (6588), 250–252. doi:10.1038/382250a0

Ahrén, B., and Havel, P. J. C. (1999). Integrative, and PhysiologyLeptin inhibits insulin secretion induced by cellular cAMP in a pancreatic B cell line (INS-1 cells). *Am. J. Physiology-Regulatory, Integr. Comp. Physiol.* 277 (4), R959–R966. doi:10.1152/ajpregu.1999.277.4.r959

Akinci, B., Meral, R., and Oral, E. A. J. C. d. r. (2018). Update on therapeutic options in lipodystrophy. *Curr. Diab Rep.*. 18(12), 1–12. doi:10.1007/s11892-018-1100-7

Alavi, K., Schwartz, M. Z., Prasad, R., O'Connor, D., and Funanage, V. (2002). Leptin: a new growth factor for the small intestine. *J. Pediatr. Surg.* 37 (3), 327–330. doi:10.1053/jpsu.2002.30805

Aleffi, S., Petrai, I., Bertolani, C., Parola, M., Colombatto, S., Novo, E., et al. (2005). Upregulation of proinflammatory and proangiogenic cytokines by leptin in human hepatic stellate cells. *Hepatology* 42 (6), 1339–1348. doi:10.1002/hep.20965

Azuma, T., Suto, H., Ito, Y., Ohtani, M., Dojo, M., Kuriyama, M., et al. (2001). Gastric leptin and *Helicobacter pylori* infection. *Gastric leptin and Helicobacter pyloriinfection* 49 (3), 324–329. doi:10.1136/gut.49.3.324

Bado, A., Levasseur, S., Attoub, S., Kermorgant, S., Laigneau, J.-P., Bortoluzzi, M.-N., et al. (1998). The stomach is a source of leptin. *Nature* 394 (6695), 790–793. doi:10.1038/29547

Barbier, M., Vidal, H., Desreumaux, P., Dubuquoy, L., Bourreille, A., Colombel, J. F., et al. (2003). Overexpression of leptin mRNA in mesenteric adipose tissue in inflammatory bowel diseases. *Gastroenterol. Clin. Biol.* 27 (11), 987–991.

Barbier, M., Cherbut, C., Aubé, A. C., Blottière, H. M., and Galmiche, J. P. (1998). Elevated plasma leptin concentrations in early stages of experimental intestinal inflammation in rats. *Gut* 43 (6), 783–790. doi:10.1136/gut.43.6.783

Barrenetxe, J., Villaro, A. C., Guembe, L., Pascual, I., Muñoz-Navas, M., Barber, A., et al. (2002). Distribution of the long leptin receptor isoform in brush border, basolateral membrane, and cytoplasm of enterocytes. *and cytoplasm of enterocytes* 50 (6), 797–802. doi:10.1136/gut.50.6.797

Baykal, A. P., Parks, E. J., Shamburek, R., Syed-Abdul, M. M., Chacko, S., Cochran, E., et al. (2020). Leptin decreases de novo lipogenesis in patients with lipodystrophy. 5(14). doi:10.1172/jci.insight.137180

Biesiada, G., Czepiel, J., Ptak-Belowska, A., Targosz, A., Krzysiek-Maczka, G., Strzalka, M., et al. (2012). Expression and release of leptin and proinflammatory cytokines in patients with ulcerative colitis and infectious diarrhea. *J. Physiol. Pharmacol.* 63 (5), 471–481.

Bock, T., Pakkenberg, B., and Buschard, K. (2003). Increased islet volume but unchanged islet number in ob/ob mice. *Diabetes* 52 (7), 1716–1722. doi:10.2337/diabetes.52.7.1716

Boutari, C., and Mantzoros, C. S. (2020). *Adiponectin and leptin in the diagnosis and therapy of NAFLD*, 103.

Breidert, M., Miehlke, S., Glasow, A., Orban, Z., Stolte, M., Ehninger, G., et al. (1999). Leptin and its receptor in normal human gastric mucosa and in *Helicobacter* pylori-associated gastritis. *Scand. J. Gastroenterol.* 34 (10), 954–961.

Brzozowski, T., Konturek, P. C., Pajdo, R., Kwiecień, S., Ptak, A., Sliwowski, Z., et al. (2001). Brain-gut axis in gastroprotection by leptin and cholecystokinin against ischemia-reperfusion induced gastric lesions. *J. Physiol. Pharmacol.* 52 (4), 583–602.

Buyse, M., Berlioz, F., Guilmeau, S., Tsocas, A., Voisin, T., Péranzi, G., et al. (2001). PepT1-mediated epithelial transport of dipeptides and cephalexin is enhanced by luminal leptin in the small intestine. *J. Clin. Invest.* 108 (10), 1483–1494. doi:10.1172/jci13219

Camilleri, M. (2019). Gastrointestinal hormones and regulation of gastric emptying. *Curr. Opin. Endocrinol. Diabetes Obes.* 26 (1), 3. doi:10.1097/med.0000000000000448

Chong, A. Y., Lupsa, B. C., Cochran, E. K., and Gorden, P. (2010). Efficacy of leptin therapy in the different forms of human lipodystrophy. *Diabetologia* 53 (1), 27–35. doi:10.1007/s00125-009-1502-9

Cohen, B., Novick, D., and Rubinstein, M. (1996). Modulation of insulin activities by leptin. *Science* 274 (5290), 1185–1188. doi:10.1126/science.274.5290.1185

Conde, J., Scotece, M., Abella, V., López, V., Pino, J., Gómez-Reino, J. J., et al. (2014). An update on leptin as immunomodulator. *Expert Rev. Clin. Immunol.* 10 (9), 1165–1170. doi:10.1586/1744666x.2014.942289

D'souza, A. M., Neumann, U. H., Glavas, M. M., and Kieffer, T. J. (2017). The glucoregulatory actions of leptin. *Mol. Metab.* 6 (9), 1052–1065. doi:10.1016/j.molmet.2017.04.011

da Silva, A. A., do Carmo, J. M., and Hall, J. E. J. C. d. r. (2020). CNS regulation of glucose homeostasis: role of the leptin-melanocortin system. 20**,** 1–9. doi:10.1007/s11892-020-01311-1

Dalbøge, L. S., Almholt, D. L., Neerup, T. S., Vassiliadis, E., Vrang, N., Pedersen, L., et al. (2013). Characterisation of age-dependent beta cell dynamics in the male db/db mice. *PLoS ONE* 8 (12), e82813. doi:10.1371/journal.pone.0082813

Deboer, M. D., and Li, Y. (2011). Puberty is delayed in male mice with dextran sodium sulfate colitis out of proportion to changes in food intake, body weight, and serum levels of leptin. *Pediatr. Res.* 69 (1), 34–39. doi:10.1203/pdr.0b013e3181ffee6c

Denroche, H. C., Huynh, F. K., and Kieffer, T. J. (2012). The role of leptin in glucose homeostasis. 3(2)**,** 115–129. doi:10.1111/j.2040-1124.2012.00203.x

Doi, T., Liu, M., Seeley, R. J., Woods, S. C., and Tso, P. C. (2001). Integrative, and PhysiologyEffect of leptin on intestinal apolipoprotein AIV in response to lipid feeding. *Am. J. Physiology-Regulatory, Integr. Comp. Physiol.* 281 (3), R753–R759. doi:10.1152/ajpregu.2001.281.3.r753

Emilsson, V., Liu, Y. L., Cawthorne, M. A., Morton, N. M., and Davenport, M. (1997). Expression of the functional leptin receptor mRNA in pancreatic islets and direct inhibitory action of leptin on insulin secretion. *Diabetes* 46 (2), 313–316. doi:10.2337/diabetes.46.2.313

Engin, A. B., and Engin, A. (2017). *Obesity and lipotoxicity*. Springer.

Engin, A. (2017). *Diet-induced obesity and the mechanism of leptin resistance*, 381–397.

Ercin, M., Sancar-Bas, S., Bolkent, S., and Gezginci-Oktayoglu, S. (2018). Tub and β-catenin play a key role in insulin and leptin resistance-induced pancreatic beta-cell differentiation. *Biochim. Biophys. Acta (Bba) - Mol. Cel Res.* 1865 (12), 1934–1944. doi:10.1016/j.bbamcr.2018.09.010

Erkasap, N., Uzuner, K., Serteser, M., Köken, T., and Aydın, Y. (2003). Gastroprotective effect of leptin on gastric mucosal injury induced by ischemia-reperfusion is related to gastric histamine content in rats. *Peptides* 24 (8), 1181–1187. doi:10.1016/j.peptides.2003.06.007

Fan, J., Li, H., Nie, X., Yin, Z., Zhao, Y., Chen, C., et al. (2017). MiR-30c-5p ameliorates hepatic steatosis in leptin receptor-deficient (db/db) mice via down-regulating FASN. *Oncotarget* 8 (8), 13450. doi:10.18632/oncotarget.14561

Fernández-Riejos, P., Najib, S., Santos-Alvarez, J., Martín-Romero, C., Pérez-Pérez, A., González-Yanes, C., et al. (2010). *Role of leptin in the activation of immune cells*

Francisco, V., Pino, J., Campos-Cabaleiro, V., Ruiz-Fernández, C., Mera, A., Gonzalez-Gay, M. A., et al. (2018). Obesity, fat mass and immune system: role for leptin. 9**,** 640. doi:10.3389/fphys.2018.00640

Friedman, J. M. (2019). Leptin and the endocrine control of energy balance. *Nat. Metab.* 1 (8), 754–764. doi:10.1038/s42255-019-0095-y

Goyal, R. K., Guo, Y., and Mashimo, H. J. N. (2019). *Adv. Physiol. gastric emptying* 31 (4), e13546. doi:10.1111/nmo.13546

Grewal, S., Gubbi, S., Fosam, A., Sedmak, C., Sikder, S., Talluru, H., et al. (2020). Metabolomic analysis of the effects of leptin replacement therapy in patients with lipodystrophy. 4(1)**,** bvz022. doi:10.1210/jendso/bvz022

Gruzdeva, O., Borodkina, D., Uchasova, E., Dyleva, Y., Barbarash, O. J. D. O., et al. (2019). *Leptin resistance: underlying mechanisms and diagnosis*, 12, 191.Metabolic syndrome, targets

Gultekin, F. A., Kerem, M., Tatlicioglu, E., Aricioglu, A., Unsal, C., and Bukan, N. J. W. j. o. g. W. (2007). Leptin treatment ameliorates acute lung injury in rats with cerulein-induced acute pancreatitis. *Wjg* 13 (21), 2932. doi:10.3748/wjg.v13.i21.2932

Hacioglu, A., Algin, C., Pasaoglu, O., Pasaoglu, E., and Kanbak, G. J. B. g. (2005). Protective effect of leptin against ischemia-reperfusion injury in the rat small intestine. 5(1)**,** 1–7. doi:10.1186/1471-230x-5-37

Hackl, M. T., Fürnsinn, C., Schuh, C. M., Krssak, M., Carli, F., Guerra, S., et al. (2019). Brain leptin reduces liver lipids by increasing hepatic triglyceride secretion and lowering lipogenesis. 10(1)**,** 1–13. doi:10.1038/s41467-019-10684-1

Hardwick, J. C. H., Van Den Brink, G. R., Offerhaus, G. J., Van Deventer, S. J. H., and Peppelenbosch, M. P. (2001). Leptin is a growth factor for colonic epithelial cells. *Gastroenterology* 121 (1), 79–90. doi:10.1053/gast.2001.25490

Heymsfield, S. B., Greenberg, A. S., Fujioka, K., Dixon, R. M., Kushner, R., Hunt, T., et al. (1999). Recombinant leptin for weight loss in obese and lean adults. *Jama* 282 (16), 1568–1575. doi:10.1001/jama.282.16.1568

Huang, K.-P., Goodson, M. L., Vang, W., Li, H., Page, A. J., and Raybould, H. E. (2021). Leptin signaling in vagal afferent neurons supports the absorption and storage of nutrients from high-fat diet. *Int. J. Obes.* 45 (2), 348–357. doi:10.1038/s41366-020-00678-1

Ikejima, K., Okumura, K., Lang, T., Honda, H., Abe, W., Yamashina, S., et al. (2005). The role of leptin in progression of non-alcoholic fatty liver disease. *Hepatol. Res.* 33 (2), 151–154. doi:10.1016/j.hepres.2005.09.024

Inagaki-Ohara, K. (2019). Gastric leptin and tumorigenesis: beyond obesity. *Ijms* 20 (11), 2622. doi:10.3390/ijms20112622

Inagaki-Ohara, K., Okamoto, S., Takagi, K., Saito, K., Arita, S., Tang, L., et al. (2016). Leptin receptor signaling is required for high-fat diet-induced atrophic gastritis in mice. 13(1)**,** 1–15. doi:10.1186/s12986-016-0066-1

Islam, M., Sjöholm, Å., and Emilsson, V. (2000). Fetal pancreatic islets express functional leptin receptors and leptin stimulates proliferation of fetal islet cells. *Int. J. Obes.* 24 (10), 1246–1253. doi:10.1038/sj.ijo.0801370

Islam, M. S., Morton, N. M., Hansson, A., Emilsson, V., and communications, b. r. (1997). Rat insulinoma-derived pancreatic β-cells express a functional leptin receptor that mediates a proliferative response. *Biochem. Biophysical Res. Commun.* 238 (3), 851–855. doi:10.1006/bbrc.1997.7399

Izquierdo, A. G., Crujeiras, A. B., Casanueva, F. F., and Carreira, M. C. (2019). Leptin, obesity, and leptin resistance: where are we 25 Years later? *Nutrients* 11 (11), 2704. doi:10.3390/nu11112704

Jarmakiewicz-Czaja, S., Piątek, D., and Filip, R. (2020). *The influence of nutrients on inflammatory bowel diseases*

Kang, H., and Kim, H. (2017). Astaxanthin and β-carotene in *Helicobacter* pylori-induced gastric inflammation: a mini-review on action mechanisms. *J. Cancer Prev.* 22 (2), 57. doi:10.15430/jcp.2017.22.2.57

Kasacka, I., Piotrowska, Ż., Niezgoda, M., and Łebkowski, W. (2019). Differences in leptin biosynthesis in the stomach and in serum leptin level between men and women. *J. Gastroenterol. Hepatol.* 34 (11), 1922–1928. doi:10.1111/jgh.14688

Kennedy, J. I., Askelund, K. J., Premkumar, R., Phillips, A. R., Murphy, R., Windsor, J. A., et al. (2016). Leptin is associated with persistence of hyperglycemia in acute pancreatitis: a prospective clinical study. 95(6). doi:10.1097/md.0000000000002382

Kerem, M., Bedirli, A., Pasaoglu, H., Unsal, C., Yilmaz, T. U., Ofluoglu, E., et al. (2007). Role of ghrelin and leptin in predicting the severity of acute pancreatitis. *Dig. Dis. Sci.* 52 (4), 950–955. doi:10.1007/s10620-006-9150-0

Khalefa, A. A., Abd-Alaleem, D. I., and Attiaa, K. I. (2010). The protective effects of ghrelin and leptin against stress-induced gastric ulcer in rats. *Arab J. Gastroenterol.* 11 (2), 74–78. doi:10.1016/j.ajg.2010.04.005

Kieffer, T. J., Heller, R. S., Habener, J. F., and communications, b. r. (1996). Leptin receptors expressed on pancreatic β-cells. *Biochem. Biophysical Res. Commun.* 224 (2), 522–527. doi:10.1006/bbrc.1996.1059

Kieffer, T. J., Heller, R. S., Leech, C. A., Holz, G. G., and Habener, J. F. (1997). Leptin suppression of insulin secretion by the activation of ATP-sensitive K+ channels in pancreatic -cells. *Diabetes* 46 (6), 1087–1093. doi:10.2337/diab.46.6.1087

Kimura, K., Tsuda, K., Baba, A., Kawabe, T., Boh-oka, S.-i., Ibata, M., et al. (2000). Involvement of nitric oxide in endothelium-dependent arterial relaxation by leptin. *Biochem. Biophysical Res. Commun.* 273 (2), 745–749. doi:10.1006/bbrc.2000.3005

Konturek, P. C., Brzozowski, T., Sulekova, Z., Brzozowska, I., Duda, A., Meixner, H., et al. (2001). Role of leptin in ulcer healing. *Eur. J. Pharmacol.* 414 (1), 87–97. doi:10.1016/s0014-2999(01)00748-8

Konturek, P. C., Jaworek, J., Maniatoglou, A., Bonior, J., Meixner, H., Konturek, S. J., et al. (2002). Leptin modulates the inflammatory response in acute pancreatitis. *Digestion* 65 (3), 149–160. doi:10.1159/000064935

Kuehnen, P., Laubner, K., Raile, K., Schöfl, C., Jakob, F., Pilz, I., et al. (2011). Protein phosphatase 1 (PP-1)-dependent inhibition of insulin secretion by leptin in INS-1 pancreatic β-cells and human pancreatic islets. *Endocrinology. Leptin in INS-1 pancreatic β-cells and human pancreatic islets*, 152, 1800–1808. doi:10.1210/en.2010-1094

Kulkarni, R. N., Wang, Z. L., Wang, R. M., Hurley, J. D., Smith, D. M., Ghatei, M. A., et al. (1997). Leptin rapidly suppresses insulin release from insulinoma cells, rat and human islets and, *in vivo*, in mice. *J. Clin. Invest.* 100 (11), 2729–2736. doi:10.1172/jci119818

La Cava, A., Alviggi, C., and Matarese, G. (2004). Unraveling the multiple roles of leptin in inflammation and autoimmunity. *J. Mol. Med.* 82 (1), 4–11. doi:10.1007/s00109-003-0492-1

La Cava, A. (2017). Leptin in inflammation and autoimmunity. *Cytokine* 98, 51–58. doi:10.1016/j.cyto.2016.10.011

Laiglesia, L. M., Lorente-Cebrián, S., Martínez-Fernández, L., Sáinz, N., Prieto-Hontoria, P. L., Burrell, M. A., et al. (2018). Maresin 1 mitigates liver steatosis in ob/ob and diet-induced obese mice. *Int. J. Obes.* 42 (3), 572–579. doi:10.1038/ijo.2017.226

Lam, N., Cheung, A., Riedel, M., Light, P., Cheeseman, C., and Kieffer, T. (2004). Leptin reduces glucose transport and cellular ATP levels in INS-1 beta-cells. 32(2), 415–424. doi:10.1677/jme.0.0320415

Laubner, K., Kieffer, T. J., Lam, N. T., Niu, X., Jakob, F., and Seufert, J. (2005). Inhibition of preproinsulin gene expression by leptin induction of suppressor of cytokine signaling 3 in pancreatic -cells. *Diabetes* 54 (12), 3410–3417. doi:10.2337/diabetes.54.12.3410

Leclercq, I. A., Farrell, G. C., Schriemer, R., and Robertson, G. R. (2002). Leptin is essential for the hepatic fibrogenic response to chronic liver injury. *J. Hepatol.* 37 (2), 206–213. doi:10.1016/s0168-8278(02)00102-2

Lee, Y., Hirose, H., Ohneda, M., Johnson, J. H., McGarry, J. D., and Unger, R. H. (1994). Beta-cell lipotoxicity in the pathogenesis of non-insulin-dependent diabetes mellitus of obese rats: impairment in adipocyte-beta-cell relationships. *Proc. Natl. Acad. Sci.* 91 (23), 10878–10882. doi:10.1073/pnas.91.23.10878

Liu, J., Yang, X., Yu, S., and Zheng, R. J. N. R. o. M. (2018). *The leptin signaling*, 123–144.

Maedler, K., Schulthess, F. T., Bielman, C., Berney, T., Bonny, C., Prentki, M., et al. (2008). Glucose and leptin induce apoptosis in human β- cells and impair glucose-stimulated insulin secretion through activation of c-Jun N-terminal kinases. *FASEB j.* 22 (6), 1905–1913. doi:10.1096/fj.07-101824

Maedler, K., Sergeev, P., Ehses, J. A., Mathe, Z., Bosco, D., Berney, T., et al. (2004). Leptin modulates cell expression of IL-1 receptor antagonist and release of IL-1 in human islets. *Proc. Natl. Acad. Sci.* 101 (21), 8138–8143. doi:10.1073/pnas.0305683101

Mantzoros, C. S., and Flier, J. S. (2000). Leptin as a therapeutic agent-trials and tribulations. *J. Clin. Endocrinol. Metab.* 85 (11), 4000–4002. doi:10.1210/jcem.85.11.7062

Marra, F. (2007). Leptin and liver tissue repair: do rodent models provide the answers?. *J. Hepatol.* 46 (1), 12–18. doi:10.1016/j.jhep.2006.10.002

Marroquí, L., Gonzalez, A., Ñeco, P., Caballero-Garrido, E., Vieira, E., Ripoll, C., et al. (2012). Role of leptin in the pancreatic β-cell: effects and signaling pathways. 49(1), R9–R17. doi:10.1530/jme-12-0025

Martin, A., and Devkota, S. (2018). Hold the door: role of the gut barrier in diabetes. *Cel Metab.* 27 (5), 949–951. doi:10.1016/j.cmet.2018.04.017

Martinelli, I., Tomassoni, D., Moruzzi, M., Roy, P., Cifani, C., Amenta, F., et al. (2020). Cardiovascular changes related to metabolic syndrome: evidence in obese zucker Rats. *Ijms* 21 (6), 2035. doi:10.3390/ijms21062035

Matsusue, K., Kusakabe, T., Noguchi, T., Takiguchi, S., Suzuki, T., Yamano, S., et al. (2008). Hepatic steatosis in leptin-deficient mice is promoted by the PPARγ target gene Fsp27. *Cel Metab.* 7 (4), 302–311. doi:10.1016/j.cmet.2008.03.003

Maurya, R., Bhattacharya, P., Dey, R., and Nakhasi, H. L. J. F. i. i. (2018). *Leptin functions in infectious diseases*, 9, 2741.

Mirza, K. B., Alenda, A., Eftekhar, A., Grossman, N., Nikolic, K., Bloom, S. R., et al. (2018). Influence of cholecystokinin-8 on compound nerve action potentials from ventral gastric vagus in rats. *Int. J. Neur. Syst.* 28 (09), 1850006. doi:10.1142/s0129065718500065

Mittendorfer, B., Horowitz, J. F., DePaoli, A. M., McCamish, M. A., Patterson, B. W., and Klein, S. (2011). Recombinant human leptin treatment does not improve insulin action in obese subjects with type 2 diabetes. *Diabetes* 60 (5), 1474–1477. doi:10.2337/db10-1302

Mix, H., Widjaja, A., Jandl, O., Cornberg, M., Kaul, A., Göke, M., et al. (2000). Expression of leptin and leptin receptor isoforms in the human stomach. 47(4), 481–486. doi:10.1136/gut.47.4.481

Miyamoto, L., Ebihara, K., Kusakabe, T., Aotani, D., Yamamoto-Kataoka, S., Sakai, T., et al. (2012). Leptin activates hepatic 5′-AMP-activated protein kinase through sympathetic nervous system and α1-adrenergic receptor. *J. Biol. Chem.* 287 (48), 40441–40447. doi:10.1074/jbc.m112.384545

Monteiro, L., Pereira, J. A. d. S., Palhinha, L., and Moraes-Vieira, P. M. M. (2019). Leptin in the regulation of the immunometabolism of adipose tissue-macrophages. *J. Leukoc. Biol.* 106 (3), 703–716. doi:10.1002/jlb.mr1218-478r

Morioka, T., Asilmaz, E., Hu, J., Dishinger, J. F., Kurpad, A. J., Elias, C. F., et al. (2007). Disruption of leptin receptor expression in the pancreas directly affects β cell growth and function in mice. *J. Clin. Invest.* 117 (10), 2860–2868. doi:10.1172/jci30910

Morton, G. J., and Schwartz, M. W. (2011). Leptin and the central nervous system control of glucose metabolism. *Physiol. Rev.* 91 (2), 389–411. doi:10.1152/physrev.00007.2010

Motawi, T. K., Abd Elgawad, H. M., and Shahin, N. N. (2008). Gastroprotective effect of leptin in indomethacin-induced gastric injury. *J. Biomed. Sci.* 15 (3), 405–412. doi:10.1007/s11373-007-9227-6

Nishi, Y., Isomoto, H., Uotani, S., Wen, C. Y., Shikuwa, S., Ohnita, K., et al. (2005). Enhanced production of leptin in gastric fundic mucosa withHelicobacter pyloriinfection. *Wjg* 11 (5), 695. doi:10.3748/wjg.v11.i5.695

Nunziata, A., Funcke, J.-B., Borck, G., von Schnurbein, J., Brandt, S., Lennerz, B., et al. (2019). Functional and phenotypic characteristics of human leptin receptor mutations. 3(1), 27–41. doi:10.1210/js.2018-00123

Okuya, S., Tanabe, K., Tanizawa, Y., and Oka, Y. (2001). Leptin increases the viability of isolated rat pancreatic islets by suppressing apoptosis. 142(11), 4827–4830. doi:10.1210/endo.142.11.8494

Oral, E. A., Simha, V., Ruiz, E., Andewelt, A., Premkumar, A., Snell, P., et al. (2002). Leptin-replacement therapy for lipodystrophy. *N. Engl. J. Med.* 346 (8), 570–578. doi:10.1056/nejmoa012437

Otte, C., Otte, J.-M., Strodthoff, D., Bornstein, S., Fölsch, U., Mönig, H., et al. (2004). Expression of leptin and leptin receptor during the development of liver fibrosis and cirrhosis. *Exp. Clin. Endocrinol. Diabetes* 112 (01), 10–17. doi:10.1055/s-2004-815720

Pandit, R., Beerens, S., and Adan, R. A. J. A. J. o. P.-R. C. (2017). Integrative, and physiology. *Role of leptin in energy expenditure: the hypothalamic perspective*, 312, R938–R947.

Paz-Filho, G., Mastronardi, C. A., and Licinio, J. (2015). Leptin treatment: facts and expectations. *Metabolism* 64 (1), 146–156. doi:10.1016/j.metabol.2014.07.014

Pearson, P. Y., O'Connor, D. M., and Schwartz, M. Z. (2001). Novel effect of leptin on small intestine adaptation. *J. Surg. Res.* 97 (2), 192–195. doi:10.1006/jsre.2001.6153

Pedroso, J. A. B., Buonfiglio, D. C., Cardinali, L. I., Furigo, I. C., Ramos-Lobo, A. M., Tirapegui, J., et al. (2014). Inactivation of SOCS3 in leptin receptor-expressing cells protects mice from diet-induced insulin resistance but does not prevent obesity. *Mol. Metab.* 3 (6), 608–618. doi:10.1016/j.molmet.2014.06.001

Perakakis, N., Farr, O. M., and Mantzoros, C. S. (2021). Leptin in leanness and obesity. *J. Am. Coll. Cardiol.* 77 (6), 745–760. doi:10.1016/j.jacc.2020.11.069

Petersen, K. F., Oral, E. A., Dufour, S., Befroy, D., Ariyan, C., Yu, C., et al. (2002). Leptin reverses insulin resistance and hepatic steatosis in patients with severe lipodystrophy. *J. Clin. Invest.* 109 (10), 1345–1350. doi:10.1172/jci0215001

Pick, A., Clark, J., Kubstrup, C., Levisetti, M., Pugh, W., Bonner-Weir, S., et al. (1998). Role of apoptosis in failure of beta-cell mass compensation for insulin resistance and beta-cell defects in the male Zucker diabetic fatty rat. *Diabetes* 47 (3), 358–364. doi:10.2337/diabetes.47.3.358

Plaisancie, P., Ducroc, R., Homsi, M. E., Tsocas, A., Guilmeau, S., Zoghbi, S., et al. (2006). Luminal leptin activates mucin-secreting goblet cells in the large bowel. *Am. J. Physiology-Gastrointestinal Liver Physiol.* 290 (4), G805–G812. doi:10.1152/ajpgi.00433.2005

Poitout, V., Rouault, C., Guerre-Millo, M., Briaud, I., and Reach, G. (1998). Inhibition of insulin secretion by leptin in normal rodent islets of Langerhans. *Endocrinology* 139 (3), 822–826. doi:10.1210/endo.139.3.5812

Polyzos, S. A., Kountouras, J., and Mantzoros, C. S. (2015). Leptin in nonalcoholic fatty liver disease: a narrative review. *Metabolism* 64 (1), 60–78. doi:10.1016/j.metabol.2014.10.012

Polyzos, S. A., Perakakis, N., and Mantzoros, C. S. (2019). Fatty liver in lipodystrophy: a review with a focus on therapeutic perspectives of adiponectin and/or leptin replacement. *Metabolism* 96, 66–82. doi:10.1016/j.metabol.2019.05.001

Potter, J. J., Womack, L., Mezey, E., Anania, F. A., and communications, b. r. (1998). Transdifferentiation of rat hepatic stellate cells results in leptin expression. *Biochem. Biophysical Res. Commun.* 244 (1), 178–182. doi:10.1006/bbrc.1997.8193

Ramos-Lobo, A. M., and Donato, J., Jr (2017). The role of leptin in health and disease. *Temperature* 4 (3), 258–291. doi:10.1080/23328940.2017.1327003

Reid, I. R., Baldock, P. A., and Cornish, J. (2018). Effects of leptin on the skeleton. *Effects of leptin on the skeleton* 39 (6), 938–959. doi:10.1210/er.2017-00226

Reidy, S. P., Weber, J.-M., Molecular, P. P. A., and Physiology, I. (2000). Leptin: an essential regulator of lipid metabolism. *Comp. Biochem. Physiol. A: Mol. Integr. Physiol.* 125 (3), 285–298. doi:10.1016/s1095-6433(00)00159-8

Rizwan, M., Mehlitz, S., Grattan, D., and Tups, A. J. J. o. n. (2017). Temporal and regional onset of leptin resistance in diet-induced obese mice. 29(10), e12481. doi:10.1111/jne.12481

Rodríguez, A., Moreno, N. R., Balaguer, I., Méndez-Giménez, L., Becerril, S., Catalán, V., et al. (2015). Leptin administration restores the altered adipose and hepatic expression of aquaglyceroporins improving the non-alcoholic fatty liver of ob/ob mice. 5(1), 1–13. doi:10.1038/srep12067

Romo-González, C., Mendoza, E., Mera, R. M., Coria-Jiménez, R., Chico-Aldama, P., Gomez-Diaz, R., et al. (2017). *Helicobacter pylori* infection and serum leptin, obestatin, and ghrelin levels in Mexican schoolchildren. *Pediatr. Res.* 82 (4), 607–613. doi:10.1038/pr.2017.69

Roper, J., Francois, F., Shue, P. L., Mourad, M. S., Pei, Z., Olivares de Perez, A. Z., et al. (2008). Leptin and ghrelin in relation toHelicobacter pyloriStatus in adult males. 93(6), 2350–2357. doi:10.1210/jc.2007-2057

Sairenji, T., Collins, K. L., and Evans, D. V. (2017). An update on inflammatory bowel disease. *Prim. Care Clin. Off. Pract.* 44 (4), 673–692. doi:10.1016/j.pop.2017.07.010

Sakar, Y., Nazaret, C., Lettéron, P., Omar, A. A., Avenati, M., Viollet, B., et al. (2009). Positive regulatory control loop between gut leptin and intestinal GLUT2/GLUT5 transporters links to hepatic metabolic functions in rodents. 4(11), e7935. doi:10.1371/journal.pone.0007935

Saxena, N. K., and Anania, F. A. (2015). Adipocytokines and hepatic fibrosis. *Trends Endocrinol. Metab.* 26 (3), 153–161. doi:10.1016/j.tem.2015.01.002

Saxena, N. K., Titus, M. A., Ding, X., Floyd, J., Srinivasan, S., Sitaraman, S. V., et al. (2004). Leptin as a novel profibrogenic cytokine in hepatic stellate cells: mitogenesis and inhibition of apoptosis mediated by extracellular regulated kinase (Erk) and Akt phosphorylation. *FASEB j.* 18 (13), 1612–1614. doi:10.1096/fj.04-1847fje

Schaab, M., Kratzsch, J., and endocrinology, r. C. (2015). The soluble leptin receptor. *Best Pract. Res. Clin. Endocrinol. Metab.* 29 (5), 661–670. doi:10.1016/j.beem.2015.08.002

Sengupta, P., Bhattacharya, K., and Dutta, S. (2019). Leptin and male reproduction. *Asian Pac. J. Reprod.* 8 (5), 220. doi:10.4103/2305-0500.268143

Seufert, J., Kieffer, T. J., and Habener, J. F. (1999a). Leptin inhibits insulin gene transcription and reverses hyperinsulinemia in leptin-deficient ob/ob mice. *Proc. Natl. Acad. Sci.* 96 (2), 674–679. doi:10.1073/pnas.96.2.674

Seufert, J., Kieffer, T. J., Leech, C. A., Holz, G. G., Moritz, W., Ricordi, C., et al. (1999b). Leptin suppression of insulin secretion and gene expression in human pancreatic islets: implications for the development of adipogenic diabetes Mellitus1. 84(2), 670–676. doi:10.1210/jcem.84.2.5460

Shimabukuro, M., Koyama, K., Chen, G., Wang, M.-Y., Trieu, F., Lee, Y., et al. (1997). Direct antidiabetic effect of leptin through triglyceride depletion of tissues. *Proc. Natl. Acad. Sci.* 94 (9), 4637–4641. doi:10.1073/pnas.94.9.4637

Shimabukuro, M., Wang, M.-Y., Zhou, Y.-T., Newgard, C. B., and Unger, R. H. (1998). Protection against lipoapoptosis of β cells through leptin-dependent maintenance of Bcl-2 expression. *Pnas* 95 (16), 9558–9561. doi:10.1073/pnas.95.16.9558

Siegmund, B., Lehr, H. A., and Fantuzzi, G. (2002). Leptin: a pivotal mediator of intestinal inflammation in mice. *Gastroenterology* 122 (7), 2011–2025. doi:10.1053/gast.2002.33631

Siegmund, B. (2012). Mesenteric fat in Crohn's disease: the hot spot of inflammation?. *Gut* 61 (1), 3–5. doi:10.1136/gutjnl-2011-301354

Siegmund, B., Sennello, J., Jones-Carson, J., Gamboni-Robertson, F., Lehr, H., Batra, A., et al. (2004). Leptin receptor expression on T lymphocytes modulates chronic intestinal inflammation in mice. *Gut* 53 (7), 965–972. doi:10.1136/gut.2003.027136

Singh, U. P., Singh, N. P., Guan, H., Busbee, B., Price, R. L., Taub, D. D., et al. (2013). Leptin antagonist ameliorates chronic colitis in IL-10−/− mice. *Immunobiology* 218 (12), 1439–1451. doi:10.1016/j.imbio.2013.04.020

Sitaraman, S., Liu, X., Charrier, L., Gu, L. H., Ziegler, T. R., Gewirtz, A., et al. (2004). Colonic leptin: source of a novel pro-inflammatory cytokine involved in inflammatory bowel disease. *FASEB j.* 18 (6), 696–698. doi:10.1096/fj.03-0422fje

Sobhani, I., Bado, A., Vissuzaine, C., Buyse, M., Kermorgant, S., Laigneau, J., et al. (2000). Leptin secretion and leptin receptor in the human stomach. *Leptin secretion leptin receptor Hum. stomach* 47 (2), 178–183. doi:10.1136/gut.47.2.178

Soedling, H., Hodson, D. J., Adrianssens, A. E., Gribble, F. M., Reimann, F., Trapp, S., et al. (2015). Limited impact on glucose homeostasis of leptin receptor deletion from insulin- or proglucagon-expressing cells. *Mol. Metab.* 4 (9), 619–630. doi:10.1016/j.molmet.2015.06.007

Stan, S., Levy, E., Bendayan, M., Zoltowska, M., Lambert, M., Michaud, J., et al. (2001). Effect of human recombinant leptin on lipid handling by fully differentiated Caco-2 cells. 508(1), 80–84. doi:10.1016/s0014-5793(01)03032-0

Tanabe, K., Okuya, S., Tanizawa, Y., Matsutani, A., Oka, Y., and communications, b. r. (1997). Leptin induces proliferation of pancreatic β cell line MIN6 through activation of mitogen-activated protein kinase. *Biochem. Biophysical Res. Commun.* 241 (3), 765–768. doi:10.1006/bbrc.1997.7894

Tanida, M., Iwasaki, Y., and Yamamoto, N. (2019). Central injection of leptin increases sympathetic nerve outflows to the stomach and spleen in anesthetized rats. *In Vivo* 33 (6), 1827–1832. doi:10.21873/invivo.11675

Tanida, M., Yamamoto, N., Morgan, D. A., Kurata, Y., Shibamoto, T., and Rahmouni, K. (2015). Leptin receptor signaling in the hypothalamus regulates hepatic autonomic nerve activity via phosphatidylinositol 3-kinase and AMP-activated protein kinase. *J. Neurosci.* 35 (2), 474–484. doi:10.1523/jneurosci.1828-14.2015

Tanigawa, T., Watanabe, T., Otani, K., Nadatani, Y., Machida, H., Okazaki, H., et al. (2010). Leptin promotes gastric ulcer healing via upregulation of vascular endothelial growth factor. *Digestion* 81 (2), 86–95. doi:10.1159/000243719

Tanizawa, Y., Okuya, S., Ishihara, H., Asano, T., Yada, T., and Oka, Y. (1997). Direct stimulation of basal insulin secretion by physiological concentrations of leptin in pancreatic β cells. *Endocrinology* 138 (10), 4513–4516. doi:10.1210/endo.138.10.5576

Tartaglia, L. A., Dembski, M., Weng, X., Deng, N., Culpepper, J., Devos, R., et al. (1995). Identification and expression cloning of a leptin receptor, OB-R. *Cell* 83 (7), 1263–1271. doi:10.1016/0092-8674(95)90151-5

Tasdelen, A., Algin, C., Ates, E., Kiper, H., Inal, M., and Sahin, F. (2004). Effect of leptin on healing of colonic anastomoses in rats. *Hepatogastroenterology* 51 (58), 994–997.

Thaiss, C. A., Levy, M., Grosheva, I., Zheng, D., Soffer, E., Blacher, E., et al. (2018). Hyperglycemia drives intestinal barrier dysfunction and risk for enteric infection. *Science* 359 (6382), 1376–1383. doi:10.1126/science.aar3318

Tsuchida, T., and Friedman, S. L. (2017). Mechanisms of hepatic stellate cell activation. *Nat. Rev. Gastroenterol. Hepatol.* 14 (7), 397. doi:10.1038/nrgastro.2017.38

Tuzun, A., Uygun, A., Yesilova, Z., Ozel, A. M., Erdil, A., Yaman, H., et al. (2004). Leptin levels in the acute stage of ulcerative colitis. *J. Gastroenterol. Hepatol.* 19 (4), 429–432. doi:10.1111/j.1440-1746.2003.03300.x

Unger, R. H., and Roth, M. G. (2015). A new biology of diabetes revealed by leptin. *Cel Metab.* 21 (1), 15–20. doi:10.1016/j.cmet.2014.10.011

Unger, R. H., Zhou, Y.-T., and Orci, L. (1999). Regulation of fatty acid homeostasis in cells: novel role of leptin. *Proc. Natl. Acad. Sci.* 96 (5), 2327–2332. doi:10.1073/pnas.96.5.2327

Van Swieten, M. M. H., Pandit, R., Adan, R. A. H., and Van Der Plasse, G. (2014). The neuroanatomical function of leptin in the hypothalamus. *J. Chem. Neuroanat.* 61-62, 207–220. doi:10.1016/j.jchemneu.2014.05.004

Wada, N., Hirako, S., Takenoya, F., Kageyama, H., Okabe, M., and Shioda, S. (2014). Leptin and its receptors. *J. Chem. Neuroanat.* 61-62, 191–199. doi:10.1016/j.jchemneu.2014.09.002

Wang, M.-Y., Koyama, K., Shimabukuro, M., Newgard, C. B., and Unger, R. H. (1998). OB-Rb gene transfer to leptin-resistant islets reverses diabetogenic phenotype. *Proc. Natl. Acad. Sci.* 95 (2), 714–718. doi:10.1073/pnas.95.2.714

Wauman, J., Zabeau, L., and Tavernier, J. J. F. i. e. (2017). The leptin receptor complex. *heavier than expected?* 8, 30. doi:10.3389/fendo.2017.00030

Yan, K., Deng, X., Zhai, X., Zhou, M., Jia, X., Luo, L., et al. (2012). p38 mitogen-activated protein kinase and liver X receptor-α mediate the leptin effect on sterol regulatory element binding protein-1c expression in hepatic stellate cells. *Mol. Med.* 18 (1), 10–18. doi:10.2119/molmed.2011.00243

Ye, C., Wang, R., Wang, M., Huang, Z., and Tang, C. (2018). Leptin alleviates intestinal mucosal barrier injury and inflammation in obese mice with acute pancreatitis. *Int. J. Obes.* 42 (8), 1471–1479. doi:10.1038/s41366-018-0125-y

Zhai, X., Yan, K., Fan, J., Niu, M., Zhou, Q., Zhou, Y., et al. (2013). The β-catenin pathway contributes to the effects of leptin on SREBP-1c expression in rat hepatic stellate cells and liver fibrosis. *Br. J. Pharmacol.* 169 (1), 197–212. doi:10.1111/bph.12114

Zhang, W., and Liu, H. T. (2002). MAPK signal pathways in the regulation of cell proliferation in mammalian cells. *Cell Res* 12 (1), 9–18. doi:10.1038/sj.cr.7290105

Zhang, Z.-Y., Dodd, G. T., and Tiganis, T. (2015). Protein tyrosine phosphatases in hypothalamic insulin and leptin signaling. *Trends Pharmacol. Sci.* 36 (10), 661–674. doi:10.1016/j.tips.2015.07.003

Zhao, A. Z., Shinohara, M. M., Huang, D., Shimizu, M., Eldar-Finkelman, H., Krebs, E. G., et al. (2000). Leptin induces insulin-like signaling that antagonizes cAMP elevation by glucagon in hepatocytes. *J. Biol. Chem.* 275 (15), 11348–11354. doi:10.1074/jbc.275.15.11348

Zhao, S., Kusminski, C. M., Elmquist, J. K., and Scherer, P. E. (2020). Leptin: less is more. *Diabetes* 69 (5), 823–829. doi:10.2337/dbi19-0018

Zieba, D., Biernat, W., and Barć, J. J. D. a. e. (2020). *Roles of leptin and resistin in metabolism, reproduction, and leptin resistance*, 106472.

Zulian, A., Cancello, R., Micheletto, G., Gentilini, D., Gilardini, L., Danelli, P., et al. (2012). Visceral adipocytes: old actors in obesity and new protagonists in, *Crohn's disease?* 61, 86–94.

Conflict of Interest: The authors declare that the research was conducted in the absence of any commercial or financial relationships that could be construed as a potential conflict of interest.

frontiers in Pharmacology

REVIEW
published: 29 April 2021
doi: 10.3389/fphar.2021.657457

Gaseous Mediators as a Key Molecular Targets for the Development of Gastrointestinal-Safe Anti-Inflammatory Pharmacology

Aleksandra Danielak[1], *John L Wallace*[2], *Tomasz Brzozowski*[1] *and Marcin Magierowski*[1]*

[1]Department of Physiology, Jagiellonian University Medical College, Cracow, Poland, [2]Department of Physiology and Pharmacology, University of Calgary, Calgary, AB, Canada

Non-steroidal anti-inflammatory drugs (NSAIDs) represent one of the most widely used classes of drugs and play a pivotal role in the therapy of numerous inflammatory diseases. However, the adverse effects of these drugs, especially when applied chronically, frequently affect gastrointestinal (GI) tract, resulting in ulceration and bleeding, which constitutes a significant limitation in clinical practice. On the other hand, it has been recently discovered that gaseous mediators nitric oxide (NO), hydrogen sulfide (H_2S) and carbon monoxide (CO) contribute to many physiological processes in the GI tract, including the maintenance of GI mucosal barrier integrity. Therefore, based on the possible therapeutic properties of NO, H_2S and CO, a novel NSAIDs with ability to release one or more of those gaseous messengers have been synthesized. Until now, both preclinical and clinical studies have shown promising effects with respect to the anti-inflammatory potency as well as GI-safety of these novel NSAIDs. This review provides an overview of the gaseous mediators-based NSAIDs along with their mechanisms of action, with special emphasis on possible implications for GI mucosal defense mechanisms.

Keywords: hydrogen sulfide, carbon monoxide, nitric oxide, non-steroidal anti-inflammatory drugs, gastrointestinal safety, inflammation

OPEN ACCESS

Edited by:
Hamid I Akbarali, Virginia Commonwealth University, United States

Reviewed by:
Romain Lefebvre, Ghent University, Belgium
Hasibur Rehman, University of Alabama at Birmingham, United States

***Correspondence:**
Marcin Magierowski
m.magierowski@uj.edu.pl

Specialty section:
This article was submitted to Gastrointestinal and Hepatic Pharmacology, a section of the journal Frontiers in Pharmacology

Received: *22 January 2021*
Accepted: *23 March 2021*
Published: *29 April 2021*

Citation:
Danielak A, Wallace JL, Brzozowski T and Magierowski M (2021) Gaseous Mediators as a Key Molecular Targets for the Development of Gastrointestinal-Safe Anti-Inflammatory Pharmacology. Front. Pharmacol. 12:657457. doi: 10.3389/fphar.2021.657457

INTRODUCTION

Non-steroidal anti-inflammatory drugs (NSAIDs), such as aspirin, ketoprofen, naproxen, indomethacin and others, represent one of the most commonly prescribed medications with a wide spectrum of therapeutic effects. Due to their potent analgesic, anti-inflammatory and antipyretic properties they are commonly used to suppress pain, inflammation as well as fever associated with inflammatory diseases including for instance rheumatoid arthritis and osteoarthritis (Bacchi et al., 2012). Additionally, aspirin, being the most widely used antiplatelet drug, remains crucial in the secondary prevention of cardiovascular diseases (Warner et al., 2011), based on its long-term application (Huang et al., 2011). However, despite considerable advantages of NSAIDs, they are known to exert adverse effects including gastrointestinal (GI) - toxicity, cardiovascular complications and renal failure (Varga et al., 2017). In addition, the risk and panel of complications is further increased by comorbidities and longer time of the NSAIDs treatment, which remains a serious limitation in clinical pharmacotherapy (Harirforoosh et al., 2014). Beneficial and adverse effects of NSAIDs are assumed to result from the inhibition of the enzyme cyclooxygenase (COX), leading to the decreased biosynthesis of prostaglandins (PG), hyperalgesic agents (Bacchi et al.,

2012). COX is known to exist in two main isoforms – COX-1 and COX-2. COX-1 is constitutively expressed and regulates various physiological functions, whereas COX-2 is considered to be an inducible isoform involved in modulation of pain and inflammatory response under pathological conditions (Conaghan, 2012). However, it should be noted, that this mechanism could be oversimplified in the light of recently published data, showing that COX-2 could be also constitutively expressed in certain tissues of human body (Varga et al., 2017).

GI-adverse effects evoked by NSAIDs are well-documented and involve microbleedings, induction of haemorrhagic lesions, gastroduodenal ulcer formation and even perforations (Lanas, 2010). Two main mechanisms have been implicated in the pathogenesis of these adverse effects, on systemic and local level of NSAIDs activity. The topical action is related to direct toxicity of these compounds toward gastric epithelial cells and mucosal surface, whereas among the systemic effects, the inhibition of PGs biosynthesis leading to an impairment of the organ blood flow is particularly crucial (Wallace, 2008). PGI_2 and PGE_2, are mainly produced *via* activity of COX-1 and contribute to the maintenance of gastric mucosal barrier (Konturek, 1985). The following effects have been assumed to be involved in PG-mediated gastroprotection: increased mucosal blood flow, elevated bicarbonate and mucus release, suppression of gastric acid secretion, prevention from leukocyte adherence to the vascular endothelium and downregulation of inflammatory signaling (Wallace, 2008). Therefore, the multifunctional properties of PGs, that embrace both hyperalgesia and GI safety, make this a very challenging prospect to achieve pain and inflammation relief without undesirable GI complications. In recent years many attempts have been undertaken to address this issue and synthesize novel "safer" NSAIDs, which would retain the potent anti-inflammatory action, however, with significantly reduced gastrotoxicity (Sulaieva and Wallace, 2015).

The discovery of second isoform of COX, prompted the development of selective cyclooxygenase-2 inhibitors (coxibs), which were expected to reduce PGs synthesis on the inflammation site, while remaining without such effect in gastric mucosa and thus preserving the potent anti-inflammatory activity with markedly decreased GI-toxicity (Wallace and Muscará, 2001). However, after the enthusiastic introduction of coxibs to the market, serious adverse effects were reported. Although selective COX-2 inhibitors did present improved safety profile in gastric mucosa, generating less ulceration and bleeding, they also exhibited other adverse effects. Precisely, coxibs significantly elevated risk of cardiovascular events such as myocardial infarction, which was a reason for the withdrawal of rofecoxib (Dieppe et al., 2004). This issue raised awareness about important role of COX-2 in the physiological processes in both cardiovascular and renal systems. It has become apparent that inhibition of COX-2 results in suppression of prostacyclin PGI2 synthesis and subsequent imbalance between prothrombotic tromboxane A2 and antithrombotic PGI2, promoting thrombosis and the incidence of cardiovascular events (Mukherjee, 2001). Therefore, despite the preliminary high expectation associated with coxibs and mass promotion of these drugs, they were proved to be of benefit only in a limited group of patients with low risk of cardiovascular death (Topol, 2005).

On the other hand, endogenous gaseous mediators such as nitric oxide (NO), hydrogen sulfide (H_2S) or carbon monoxide (CO) were shown to be involved in the maintenance of GI integrity, to exhibit gastroprotective action, to accelerate ulcer healing and to modulate gastric blood flow and gastro-duodenal secretion. All three molecules were shown to interact each other within GI tract. H_2S-, NO- or CO-releasing pharmacological tools and chemicals were reported to prevent gastric mucosa against the damage induced by exposure of GI-mucosa to stress, ischemia/reperfusion, and the mucosal injury caused by pharmacological agents and drugs such as alendronate or aspirin and other NSAIDs. Therefore, over recent years novel H_2S-, NO- or CO-releasing derivatives of NSAIDs were synthetized (Wallace et al., 2017; Magierowska et al., 2018). Thus, in this review we aimed to provide an update on the recent advances in the development of these novel NSAIDs and their possible molecular mechanisms of action with special emphasis on possible clinical and therapeutic implications.

GASTROENTEROPATHY EVOKED BY NSAIDS

The gastroduodenal toxicity of NSAIDs has been extensively studied so far and the mechanisms beyond it remain largely described. Theoretically, this already recognized pathomechanism of NSAID-induced damage makes these gastric injuries preventable only to limited extent. Gastric acid has been recognized as a crucial pathogenic factor affecting the weakened gastric mucosa due to NSAID-induced PGs inhibition (Wallace, 2012) (**Figure 1**). Therefore, the histamine H_2 receptor antagonists (H2RAs) and proton pump inhibitors (PPIs), both potent acid secretion suppressors have been clinically recommended in prevention of NSAIDs-induced gastric damage (Scheiman et al., 2006). On the other hand, due to the difficulty in diagnosing of small intestine erosions together with its typically subclinical course, NSAID-induced enteropathy constitutes an under-recognized and underestimated clinical problem (Srinivasan and De Cruz, 2017). Development of the small intestine imaging due to the implementation of the capsule endoscopy, revealed that the prevalence of NSAID-induced small intestine injury is far more frequent than it was initially suspected (Graham et al., 2005). Importantly, the incidence of small intestinal damage among healthy subjects receiving NSAIDs combined with PPI over 2 weeks has been estimated at the level of 55–75% (Goldstein et al., 2005; Maiden et al., 2005; Wallace, 2012). As documented by virtual endoscopy, the small bowel injury may be identified as mucosal erythema, erosions, ulcerations and occult GI bleeding, while clinically these damages are manifestated most frequently by iron deficiency anemia (Tai and McAlindon, 2018). Unlike the stomach, there is no proof that gastric acid contributes to the development of intestinal lesions associated with NSAID administration and interestingly, drugs suppressing acid secretion have been shown to even aggravate

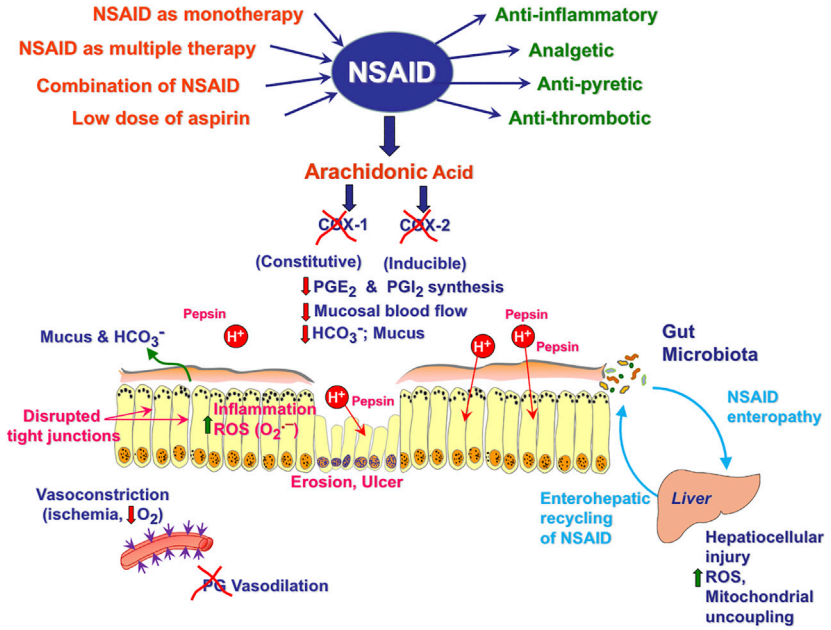

FIGURE 1 | Pathomechanism of NSAIDs-induced gastrointestinal damage.

small bowel injuries (Syer et al., 2015; Tai and McAlindon, 2018). Using capsule endoscopy, Watanabe et al. have reported that among rheumatoid patients treated chronically with NSAIDs, the independent risk factors for severe intestinal damage were the age over 65 years and the use of a PPI along with a H2RA (Watanabe et al., 2013).

Interestingly, the mechanisms underlying the pathogenesis of NSAIDs-enteropathy seem to be complex and distinct from those responsible for gastric damage (Boelsterli et al., 2013). The inhibition of PG biosynthesis has been shown to predispose both, gastric and intestinal mucosa to various injurious factors (**Figure 1**). However, in contrast to NSAIDs gastropathy, the major mechanism responsible for bowel damage appears to be PG-independent (Matsui et al., 2011). Precisely, the enterohepatic circulation of NSAIDs, bile and enteric microbial flora have been all considered as critical pathogenic factors (Syer et al., 2015) (**Figure 1**). Enterohepatic recirculation is assumed to depend upon bacterial β-D-glucuronidase, an enzyme that enhances the resorption of NSAIDs in the ileum, leading in consequence to the harmful re-exposure of the intestinal mucosa to these compounds (Wallace, 2013). Importantly, pharmacological inhibition of bacterial β-glucuronidase has been demonstrated in experimental animal model to reduce the re-exposure of these drugs to intestinal epithelium and thus, remarkably alleviate NSAIDs-induced enteropathy (LoGuidice et al., 2012).

It is also of interest that NSAIDs intake has been shown to elicit significant changes in the quality of enteric microbiota, particularly the elevation in the number of Gram-negative bacteria (Wallace, 2012). The pivotal role of microbiota has been additionally emphasized by the observation that germ-free rats were resistant to the indomethacin-induced enteropathy, and this effect was reversed by intestinal contamination with *E.coli* (Robert and Asano, 1977). There is also a compelling body of evidence suggesting that the profound suppression of acid secretion by PPIs affect the number and diversity of intestinal bacteria, contributing to the exacerbation of intestinal damage (Bruno et al., 2019). For instance, when a PPI (omeprazole or lansoprazole) was administered to rats in combination with NSAID, the significant alterations in the enteric microbiome profile were identified, especially manifested by the reduction in the *Bifidobacterium* content, followed by increased severity of intestinal injury (Wallace et al., 2011).

Additionally, bile acid dysmetabolism has been also implicated in the pathogenesis of small bowel damage associated with gastric acid suppression (Blackler et al., 2014). The study by Shindo et al. revealed that the omeprazole treatment in a group of gastric ulcer patients as well as healthy control volunteers resulted in elevated levels of deconjugated bile acids in both groups, which was attributed to the bacterial overgrowth detected in the jejunum (Shindo et al., 1998). Thus, the deconjugation of bile acids due to bacterial enzymatic activity, which is known to enhance the damaging properties of the bile within intestinal epithelium, could also explain the pathogenesis of enteropathy mediated by long-term acid inhibition due to PPI treatment.

To summarize, until now there is no successful strategy being sufficiently proven to offer a fully effective therapeutic approach either in the prevention or in the treatment of NSAIDs gastroenteropathy. Therefore, there is definitely a need for the development of novel effective therapeutic approaches in this field.

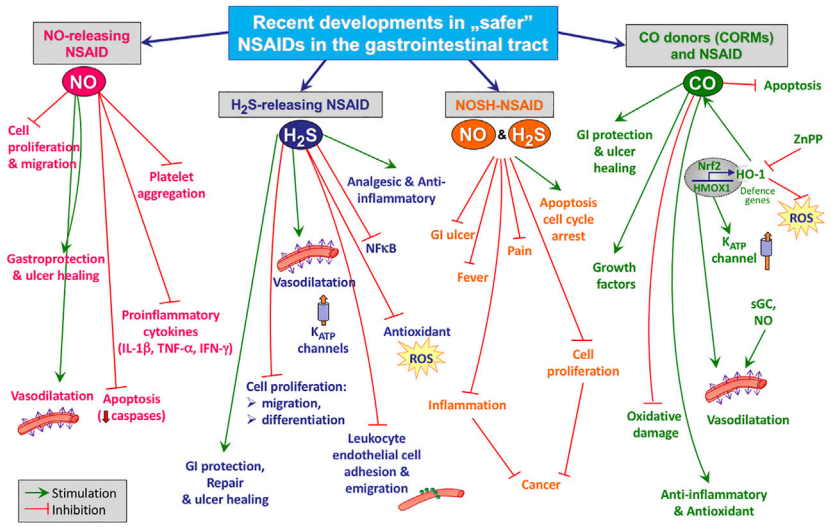

FIGURE 2 | Possible mechanisms of action of NO-, H2S-releasing NSAIDs, NOSH-NSAIDs or NSAIDS applied with CO donors.

GASEOUS MEDIATORS-RELEASING NSAIDS AND GI TRACT

NO-Releasing NSAIDs

NO is a gaseous mediator involved in the regulation of numerous physiological pathways including those responsible for the homeostasis of the GI tract. NO is endogenously produced within esophageal, gastric and intestinal mucosa *via* the enzymatic activity of NO synthases:

- neuronal (nNOS), expressed in the neurons of central and peripheral nervous system,
- endothelial (eNOS) located in both endothelial cells and platelets,
- inducible (iNOS), which is expressed in endothelial cells, smooth vascular muscle, neutrophils and macrophages.

Both nNOS and eNOS are constitutive isoforms responsible for the maintenance of GI mucosal defense due to the constant generation of small amounts of NO (Stanek et al., 2008). According to the recent data, the beneficial actions of NO in GI tract include vasodilatation, crucial for the maintenance of blood flow and mucosal barrier integrity, the enhanced epithelial mucus and bicarbonate secretion, the reduced adherence of neutrophils and their infiltration of gastric tissue resulting in diminished reactive oxygen species (ROS) production and decreased oxidative stress (**Figure 2**) (Magierowski et al., 2015a). Furthermore, NO has been proven to regulate the gastric and intestinal epithelial cells tight junctions through mechanisms involving inhibition of protein and lipid oxidation, modulation of glutathione (GSH/GSSG) ratio, which is crucial for cell survival, and the maintenance of redox homeostasis (Mu et al., 2019). On the other hand, a decrease in NO production has been implicated in the pathogenesis of many diseases including *diabetes mellitus*, hypertension and arteriosclerosis. Moreover, it has been shown that the pharmacologic inhibition of NO-synthase impaired the healing rate of gastric ulcers (Magierowski et al., 2015).

Based on these physiological and pharmacological properties of NO, a new class of NO-releasing NSAIDs (NO-NSAIDs) was developed by chemically binding a NO-releasing moiety with the parent drug (Fiorucci et al., 2001). Importantly, NO-NSAIDs have been shown to exert anti-inflammatory and analgetic effects comparable or even greater to those provided by conventional NSAIDs with markedly lower GI toxicity (Wallace et al., 1995; Wallace et al., 1999; Al-Swayeh et al., 2000; Kato et al., 2001; Fiorucci et al., 2003; Fiorucci et al., 2004; Rolando et al., 2013). The anti-inflammatory activity of NO-NSAIDs have been proved by adding the NO moiety to various derivatives including aspirin, naproxen, ketoprofen, flurbiprofen, ibuprofen, diclofenac, indomethacin, mesalamine, tolfenamic acid, or celecoxib (Pereira-Leite et al., 2017). It is worth mentioning that NCX-4016 (NO-aspirin) and NCX-530 (NO-indomethacin) have been shown to protect gastric mucosa against HCl/ethanol-induced damage (Takeuchi et al., 1998; Takeuchi et al., 2001). Interestingly, in a rodent model, the administration of NCX-530 vs parent indomethacin did not evoke intestinal damage, and the inhibition of bacterial translocation within intestine with this novel NO-NSAID agent has been proposed to explain this phenomenon (Mizoguchi et al., 2001). Additionally, it has been demonstrated, that the prolonged administration of NO-NSAIDs in contrast to classic parent NSAIDs do not delay, but even accelerate the healing of gastric ulcers (Elliott et al., 1995; Brzozowski et al., 2000; Brzozowska et al., 2004). It should be also noticed, that NCX-4016 and NCX-4215, being another derivative of aspirin releasing NO, have been shown to exert increased antithrombotic activity, comparable to that exhibited by aspirin (Wallace et al., 1995; Momi et al., 2000; Bolla et al., 2006).

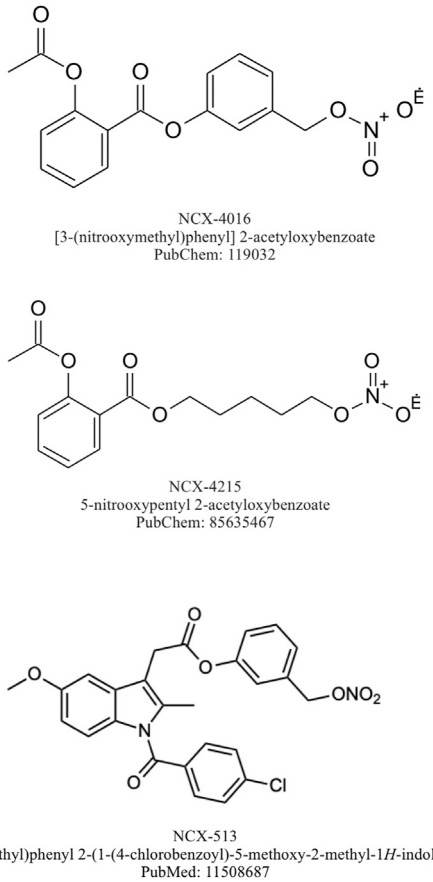

FIGURE 3 | Chemical structures of selected NO-NSAIDs.

These promising results obtained in pre-clinical animal studies provided significant evidence to further explore the assessment of NCX-4016 and nitronaproxen (naproxcinod) in humans. NCX-4016 completed phase 1 clinical trial and entered phase 2, however the further development of this novel NO-NSAID was terminated due to the detected genotoxicity (Di Napoli and Papa, 2003). Naproxcinod successfully completed phase 3 clinical trial and has been shown to be effective in relieving the symptoms of osteoarthritis, while having significantly reduced GI toxicity (Lohmander, 2004; Schnitzer et al., 2005; KARLSSON et al., 2009).

Taking into account that NSAIDs-based pharmacotherapy among elderly diabetic patients correlates with the higher risk of adverse effects such as impaired renal function, excessive fluid retention and aggravated hypertension (Caughey et al., 2010), NO-NSAIDs seemed to be promising alternative but with one essential adverse effect such as the increased risk of NO-mediated hypotension. Pieper et al. (Pieper et al., 2002) documented in their animal study, the protective effect of chronic NCX-4016 treatment against impaired endothelium-dependent relaxation, which is an important feature of human *diabetes mellitus*. Similarly, in another report NCX-4016 treatment in the group of diabetic rats resulted in significantly reduced vascular endothelium damage (Ambrosini et al., 2005). Clearly, the further studies on the usage of NO-NSAID among humans with diabetes are needed to shed more light into the potentially beneficial effects of these novel drugs to counteract some vascular and epithelial aspects of metabolic disorders. Chemical structure of selected NO-NSAIDs are presented on **Figure 3**.

H_2S–Releasing NSAIDs

H_2S, similarly to NO, is an important endogenous gaseous messenger known to modulate the cardiovascular and nervous system functioning, GI defense as well as the inflammatory pathways (Bełtowski, 2015). It is produced within human body due to activity of two enzymes: cystathionine- γ-lyase (CTH) and cystathionine-β-synthetase (CBS) (Huang and Moore, 2015). H_2S could be also generated in mitochondria by the activity mercaptopyruvate sulfurtransferase (MPST) (Kimura, 2014). Additionally, this molecule could be produced and metabolized by microbiota within the gut. The endogenous and exogenous H_2S has been recognized as an anti-inflammatory, anti-oxidative and vasodilatory agent, essentially involved in the modulation of inflammatory cascade and the process of resolution of inflammation (**Figure 2**.) (Wallace, 2010). Furthermore, endogenous and exogenous H_2S released from chemical donors have been implicated in the mechanism of maintenance of gastric mucosal homeostasis and to protect the gastric mucosa against lesions induced by NSAIDs and other noxious factors (Lou et al., 2008; Cipriani et al., 2013; Magierowski et al., 2015; Magierowski et al., 2016; de Araújo et al., 2018; Magierowski et al., 2018). Such a protective effect of H_2S has also been demonstrated in the intestinal mucosa of NSAID-treated rats, which seems to be particularly important due to the current need for an effective therapy against the adverse effects of NSAIDs affecting the intestine (Wallace and Wang, 2015).

A remarkable progress has recently been achieved in the understanding of mechanisms underlying the protective action of H_2S within GI tract, by demonstration that this gaseous molecule enhanced mucosal microcirculation, attenuated the TNF-α signaling along with suppression of pro-inflammatory cytokines expression and leukocyte adherence (Wallace, 2010). Importantly, H_2S released form chemical donors such as NaHS or Lawesson's reagent, as emphasized by many experimental animal studies, decreased the number and severity of gastric mucosal lesions evoked by NSAIDs, ischemia/reperfusion, ethanol and stress (Zanardo et al., 2006; Mard et al., 2012; Magierowski et al., 2015; Magierowski et al., 2016; Sun et al., 2017; Magierowski et al., 2018).

On the other hand, the inhibition of endogenous H_2S production was associated with remarkably elevated adherence of leukocytes to the vessels wall and with aggravated inflammation accompanying induction of paw edema in rats (Zanardo et al., 2006). The study by Fiorucci et al. (2005) revealed that deleterious gastric adverse effects evoked by NSAIDs may be to some extent ascribed to the suppression of endogenous H_2S biosynthesis, which was documented by a decreased CTH mRNA and protein expression during NSAID treatment.

Therefore, numerous derivatives of H_2S-releasing NSAIDs have been developed with improved safety profile of these compounds compared with parent drugs documented in preclinical studies (Magierowski et al., 2015). Promising effects have been achieved with respect to the following novel NSAIDs: H_2S-releasing naproxen (ATB-346), H_2S-releasing diclofenac (ATB-337 and ACS-15), H_2S-releasing ketoprofen (ATB-352) and H_2S-releasing aspirin (ATB-340 and ACS-14). Administration of ATB-337 evoked approximately 90% less intestinal damage, when compared to native diclofenac (Wallace et al., 2007). The possible mechanisms responsible for preventive activity of hydrogen sulfide within intestine seem to involve, at least partially, improvement of intestinal barrier, facilitation of antimicrobial immunity and normalization of enteric microbiota profile (Schroeder et al., 2011; Blackler et al., 2015).

Wallace et al. (Wallace et al., 2007) reported that ATB-337 was less gastrotoxic and produced remarkably less injury within gastric as well as intestinal mucosa in rats as compared to its parent drug. Furthermore, ATB-337 was more effective in decreasing of paw edema evoked by carrageenan. Similarly, S-diclofenac (ACS-15) exhibited augmented anti-inflammatory activity against LPS-induced inflammation in comparison with the parent drug, which could be due to: 1) enhanced ability of S-diclofenac to inhibit LPS-induced upregulation of iNOS expression, 2) Nf-κB pathway suppression – the effect which was not observed in diclofenac treatment (Li et al., 2007). Liu et al. (2012) have demonstrated that H_2S-releasing aspirin (ACS-14) decreased the gastric lesions formation induced by aspirin administration and restored H_2S plasma level, which was substantially reduced in rats subjected to acetylsalicylic acid. Also, H_2S-releasing ketoprofen (ATB-352) reduced the inflammation and concomitant bone resorption in rats in experimental model of periodontitis. This effect was accompanied by a significantly diminished incidence of gastric lesions as compared to rats pretreated with classic ketoprofen (Gugliandolo et al., 2018). In addition, Glowacka et al. (2021) reported that GI toxicity was significantly reduced during chronic treatment with ATB-352 in rats, when compared to parent drug. Furthermore, ketoprofen affected intestinal microbiome profile to much greater extent than ATB-352 and, in sharp contrast to ATB-352, required co-therapy with omeprazole to counteract detrimental alterations within GI tract. Therefore, novel H_2S-releasing ketoprofen could provide improved therapeutic strategy, preventing from the necessity of co-treatment of NSAIDs with PPIs and, in consequence, further impairment of intestinal microbiome induced by PPIs.

Nevertheless, ATB-346 could be considered as the leading drug in this class. This H_2S-releasing derivative of naproxen has been designed for osteoarthritis therapy and it has been confirmed by many animal studies to be as effective as the equimolar doses of its parent drug in terms of COX-1 activity inhibition leading to decreased PGE_2 biosynthesis and alleviation of inflammatory response with significantly decreased GI-toxicity (Blackler et al., 2012; Ekundi-Valentim et al., 2013; Sulaieva and Wallace, 2015; Wallace and Wang, 2015; Magierowski et al., 2017; Van Dingenen et al., 2019). Interestingly, ATB-346 was shown to exert therapeutic effect reflected by the acceleration of gastric ulcers healing in contrast with its parent drug, known not only to exacerbate acute gastric mucosal lesions but also producing a delay in the ulcer healing (Magierowski et al., 2015). Noteworthy, the mechanism of therapeutic properties of this compound has been assumed to involve activation of Nrf-2/HMOX-1/CO pathway, responsible for increased endogenous CO production, since it was observed that protein expression of Nrf-2 and HMOX-1 was significantly elevated in gastric mucosa of rats administered with ATB-346 (Magierowski et al., 2017). Blackler et al. (2012) pointed out that adverse effects of NSAIDs occur especially frequently among elderly patients with co-existing health problems, while most of the studies evaluating the safety of novel drugs is conducted on healthy animals. Based on this, they compared the possible outcomes of ATB-346 and NCX-429 (NO releasing derivative of naproxen) administration among rats afflicted with arthritis, obesity, or hypertension. This study revealed that both novel compounds not only presented similar anti-inflammatory properties comparing to their parent drugs – naproxen and celecoxib, but also they did not evoke mucosal damage within GI tract, suggesting their safety and tolerability by individuals with co-morbidities (Blackler et al., 2012). Recent animal studies have also reported that ATB-346 exerts protective effect on neuroinflammation, neural cell death and brain oxidative stress and may have therapeutic potential to treat traumatic brain injury or neurodegenerative diseases such as Alzheimer's disease (Campolo et al., 2014; Mostafa et al., 2016). Importantly, a phase I clinical trial revealed the safety and good tolerability of ATB-346 (administered in doses ranging from 25 to 2,000 mg). This observation was associated with the significantly lower risk of adverse effects, comparable to that observed in placebo group (Wallace et al., 2018). Interestingly, the plasma half-life of naproxen turned out to be substantially longer in group of patients receiving ATB-346. Recently, ATB-346 has also completed Phase II clinical trial and presented significantly lower rate of GI-tract adverse effects such as ulceration, gastroesophageal reflux, abdominal discomfort or dyspepsia when compared to naproxen (Wallace et al., 2020). Chemical structure of selected H_2S-NSAIDs are presented on **Figure 4**.

NOSH-NSAIDs

Keeping in view the therapeutic properties of NO and H_2S, new compounds integrating both these gaseous mediators have been developed, namely NOSH-NSAIDs. Recent reports documented the promising effects of NOSH-NSAIDs with respect to the growth inhibitory properties in various human cancer cell lines, such as colon, pancreatic, breast, lung, prostate and leukemia cancer cells (**Figure 2**) (Chattopadhyay et al., 2012; Kodela et al., 2012; Kodela et al., 2013; Kashfi, 2015; Kashfi et al., 2015; Vannini et al., 2015a; Chattopadhyay et al., 2020). Interestingly, several studies demonstrated enhanced chemopreventive potential of these novel hybrids compared with parent drugs. For instance, NOSH-ASA was more effective than ASA in HT-29 colon cancer cells (Kodela et al., 2012), whereas NOSH-naproxen (AVT219) was shown to possess improved ability in suppressing the growth of adenomatous,

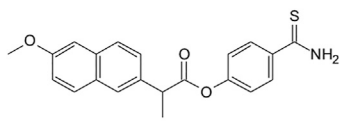

ATB-346
(4-carbamothioylphenyl) 2-(6-methoxynaphthalen-2-yl)propanoate
PubChem: 25065981

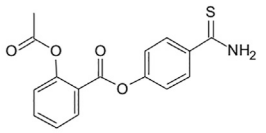

ATB-340
4-(5-thioxo-5H-1,2-dithiol-3-yl)phenyl 2-acetoxybenzoate
PubMed: 32848752

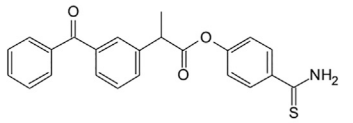

ATB-352
4-carbamothioylphenyl 2-(3-benzoylphenyl)propanoate
PubChem: 25065981

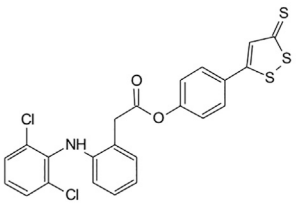

ATB-337
[4-(5-sulfanylidenedithiol-3-yl)phenyl] 2-[2-(2,6-dichloroanilino)phenyl]acetate
PubChem: 11948307

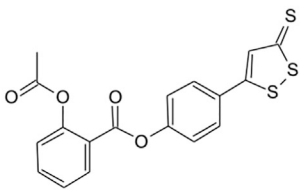

ACS-14
2-acetyloxybenzoic acid 4-(3-thioxo-3H-1,2-dithiol-5-yl)phenyl ester
PubMed: 23029468

FIGURE 4 | Chemical structures of selected H_2S-NSAIDs.

epithelial, and lymphocytic cancer cell lines, as compared to naproxen (Chattopadhyay et al., 2016). Also, a study by Kodela et al. (2013) identified NOSH-naproxen as approximately 8000-fold more effective than the combination of its components in prevention from the growth of human colon cancer cells, implying a remarkable synergistic effect. A similar trend was observed with NOSH-ASA (NBS-1120), being 9000-fold more potent than the sum of its partial molecules in suppressing cell growth (Chattopadhyay et al., 2012). Furthermore, efficacy of NOSH-NSAIDs to influence cancer growth, seems to be dependent on the induction of cell cycle arrest and apoptosis, along with increase in reactive oxygen species (ROS) level, known to promote cell death (Vannini et al., 2015b). Importantly, several animal studies have shown that NOSH-ASA, NOSH-sulindac (AVT-18 A) and NOSH-naproxen, in contrast to their parent drugs, were devoid of GI complications such as ulceration and bleeding, which clearly indicates improved safety profile of these novel compounds (Kashfi, 2015; Chattopadhyay et al., 2016; Chattopadhyay et al., 2020). Additionaly, Kashfi et al. (2015) have demonstrated using a rat model that administration of NOSH-sulindac was associated with decreased lipid peroxidation and increased SOD activity, being an antioxidant marker, in gastric mucosa, as compared to the parent drug sulindac.

On the other hand, NOSH-NSAIDs have also attracted attention as anti-inflammatory agents and as documented in preclinical studies using the carrageenan rat paw edema model, these novel NO and H_2S releasing derivatives exerted similar or even enhanced anti-inflammatory potential than their parent compounds (Kodela et al., 2013; Fonseca et al., 2015; Kashfi, 2015; Kashfi et al., 2015). Furthermore, anti-pyretic, analgesic and anti-platelet properties of NOSH-NSAIDs were comparable to those evoked by conventional NSAIDs (Kashfi et al., 2015). However, we assume that there is a lack of the studies directly comparing these NOSH-NSAIDs not only to the parent NSAID, but also to the respective NO-NSAID and H_2S-NSAID to evaluate whether combining the two gaseous molecules really brings further improvement over the single mediator-releasing NSAID.

Noteworthy, NOSH-NSAIDs have shown promising results in attenuating neuroinflammation and preventing from neuronal death in animal model of ischemic stroke (Lee et al., 2013; Ji et al., 2017). Interestingly, in a human cell model of neuroinflammation the neuroprotective activity of NOSH-ASA was remarkably more potent than NO- or H_2S-releasing ASA, which is consistent with previous observation on synergistic effect of NOSH-NSAIDs (Lee et al., 2013). Thus, NOSH-NSAID may provide new strategies for the treatment of neurodegenerative disorders comprising

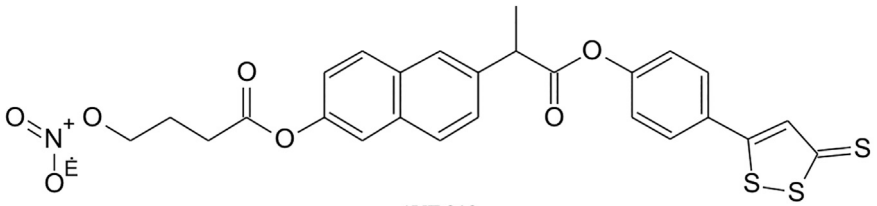

AVT-219
(S)-6-(1-oxo-1-(4-(3-thioxo-3H-1,2-dithiol-5-yl) phenoxy)propan-2-yl)naphthalen-2-yl-4-(nitrooxy)butanoate
PubMed: 24273639

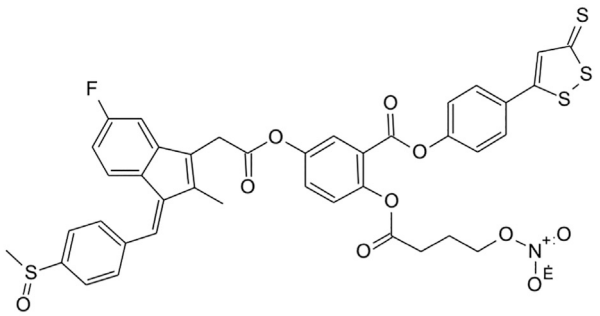

AVT-18A
(Z)-4-(3-thioxo-3H-1,2-dithiol-5-yl)phenyl 5-(2-(5-uoro-2-methyl-1-(4-(methylsulnyl)benzylidene)-1H-inden-3-yl)acetoxy)-2-((4-(nitrooxy)butanoyl)oxy)benzoate
PubMed: 24273639

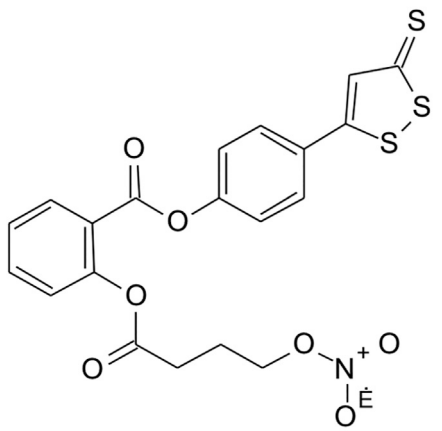

NBS-1120
4-(3-thioxo-3H-1,2-dithiol-5-yl)phenyl 2-((4-(nitrooxy)butanoyl)oxy)benzoate
PubMed: 22366248

FIGURE 5 | Chemical structures of selected NOSH-NSAIDs.

Alzheimer's disease and Parkinson's disease. Chemical structure of selected NOSH-NSAIDs are presented on **Figure 5**.

CO-Releasing Molecules

CO is perceived to be a poisonous 'silent killer' gaseous molecule but it is now receiving increasing attention as an important endogenous messenger constantly produced in small amounts within human body (Wu and Wang, 2005). CO is generated by degradation of free heme to biliverdin *via* the enzymatic activity of heme oxygenases (HMOX) - constitutive HMOX-2 highly expressed in brain and testes, and inducible isoform HMOX-1 (which is also known as heat shock protein 32 – HSP 32), reported to be activated in response to various stressful stimuli such as LPS, inflammatory cytokines or oxidative stress and plays a crucial role in the maintenance of cellular homeostasis (Choi and Alam, 1996; Higuchi et al., 2009; Takahashi et al., 2009). The

well-known cellular targets of CO are soluble guanylyl cyclase (sGC) producing cGMP, cytochrome p-450 and other cytochromes, nitric oxide synthase (NOS), and possibly COXs (Magierowski et al., 2017; Ryter et al., 2018). Importantly, CO seems to upregulate the production of NO in remote tissues suggesting that its supplementation may represent better strategy than molecules liberating NO, which is incapable of being transported to distant targets because of its high reactivity (Motterlini and Otterbein, 2010).

Currently, more light is being shed regarding regulatory functions of CO in many systems including cardiovascular, GI and nervous systems and therapeutic effect of CO-donors on various diseases such as atherosclerosis, hypertension, diabetes, chronic pulmonary disease or gastric ulcers (Motterlini and Otterbein, 2010; Jasnos et al., 2014; Olas, 2014). There is growing data emphasizing potent anti-inflammatory and cytoprotective properties of CO, known to be dependent on multiple pathways involving mitogen-activated protein kinase (MAPK), the elevated cGMP level, the enhanced expression of antioxidant enzymes, and the downregulation of inflammatory Nf-κB pathway (**Figure 2**) (Qin et al., 2015; Sulaieva and Wallace, 2015; Ling et al., 2018).

In the light of these discoveries, several CO-prodrugs, namely CO-releasing molecules (CORMs) were developed to provide safe, manageable way of delivering physiologically efficient quantities of exogenous CO to various tissues and organs. The range of CORMs reported so far is wide and comprises the most investigated ones [Mn2(CO)10] (CORM-1), tricarbonyldichlororuthenium (II) dimer [Ru(CO)3Cl2]2 (CORM-2) and tricarbonylchloro (glycinato)ruthenium (II) (CORM-3) (Kautz et al., 2016). Numerous animal studies have confirmed that CO released from CORMs affords gastroprotection against gastric mucosal injury induced by ethanol, ischemia/reperfusion, stress or NSAIDs and has a beneficial influence by acceleration of gastric ulcers healing (Magierowska et al., 2016; Takagi et al., 2016; Magierowski et al., 2017; Magierowska et al., 2018; Magierowska et al., 2019; Magierowska et al., 2019). What is more, Freitas et al. (2006) have documented in their mice model of acute mesenteric inflammation evoked by carrageenan administration, that dimagnese decacarbonyl DMDC, a CO donor, remarkably decreased leukocyte adhesion and migration to the inflamed tissue and this effect was reversed by a soluble guanylate cyclase (sGC) inhibitor.

Furthermore, combined administration of CORM-2 with aspirin decreased gastric lesion index, increased gastric blood flow (GBF) and attenuated gastric mucosal lipid peroxidation when compared to aspirin administered alone (Magierowski et al., 2018). In another study pretreatment with CORM-2 alleviated aspirin-induced gastric mucosal damage and this beneficial effect was partly dependent on endogenous NO synthesis, but not on H_2S pathway (Magierowski et al., 2016; Magierowska et al., 2018). Interestingly, also novel metal-free organic CO-prodrug, BW-CO-111 has been reported to prevent aspirin-induced gastric damage (Bakalarz et al., 2021). Despite promising effects of combined treatment with CORMs and NSAIDs in order to limit NSAID-induced gastrotoxicity, the chemical synthesis of CO-releasing NSAIDs has not been successful and there is little data published and available on this class of prodrugs. However, the effect of CO-releasing aspirin derivative - (CO-ASS) on malignant pleural mesothelioma (MPM) cell lines was investigated and CO-ASS exerted antiproliferative effect and inhibition of Nf-κB (Zanellato et al., 2013). It was hypothesized by the authors that CO-ASS might be of benefit when used as a CO releasing NSAID novel therapeutic, nevertheless further studies are needed to confirm this theory. Chemical structure of CO-ASS is presented on **Figure 6**.

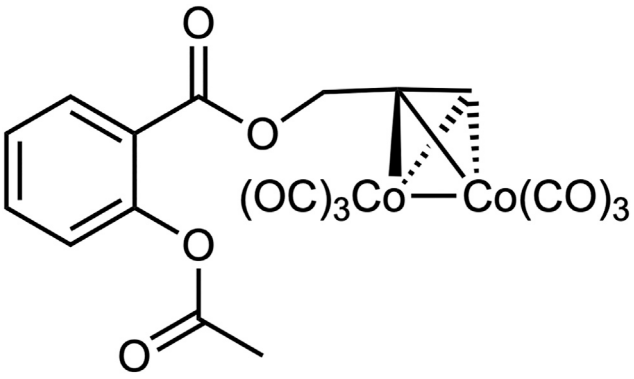

CO-ASS
[2-acetoxy-(2-propynyl)benzoate]hexacarbonyldicobalt
PubMed: 24057048

FIGURE 6 | Chemical structure of CO-ASS.

CARDIOVASCULAR AND RENAL SAFETY OF GASEOUS MEDIATORS-RELEASING NSAIDS

Despite the initial focus on GI adverse effects of NSAIDs, their deleterious impact on cardiac, vascular and renal systems has gained increasing attention, especially when coxibs were introduced and their serious cardiovascular adverse effects were detected. Subsequent studies have confirmed that the widespread use of NSAIDs may be associated with harmful cardiovascular and renal complications including hypertension, myocardial infarction, heart failure as well as acute kidney injury and chronic kidney disease (Bindu et al., 2020). Importantly, NSAIDs have been shown to counteract the effects of antihypertensive drugs, in mechanisms involving PGs biosynthesis inhibition, leading to increased arterial blood pressure (Fournier et al., 2012). Also, given that the usage of NSAIDs is known to advance among elderly patients due to multiple diseases, when at the same time renal function tends to deteriorate in age-related mechanisms, this group seems to be especially vulnerable to renal toxicity (Cabassi et al., 2020).

Cardiovascular and renal adverse effects of NSAIDs constitute therefore a serious limitation to clinical application of this class of drugs, particularly among patients with numerous comorbidities within GI tract, kidneys and cardiovascular system. On the other hand, promising results have been observed with respect to the cardiovascular and renal safety profile of gaseous mediators-releasing NSAIDs. Interestingly, these novel compounds have been even shown to afford protection against various diseases affecting cardiac, vascular and renal systems.

It has been hypothesized that NO-NSAIDs, due to the ability to release NO, could exert therapeutic effects in diseases associated with reduced NO bioavailability such as diabetes mellitus, known to induce endothelial dysfunction (Shi and Vanhoutte, 2017). Consistent with this assumption, it has been demonstrated by Pieper et al. (2002) that NO-donating aspirin NCX-4016 reduced the development of impaired endothelium-dependent relaxation in animal model of chronic diabetes mellitus. Importantly, the endothelium dysfunction has been recognized as a marker of elevated risk of atherosclerosis and cardiovascular events (Bonetti et al., 2003). Additionally, NCX-4016 administration was accompanied by a decrease in plasma isoprostanes levels, suggesting that therapeutic effect of this compound may be related to its antioxidant activity, possibly by NO-dependent reduction of lipid peroxidation. Interestingly, prolonged treatment with NCX-4016 did not induce a nitrate tolerance, which constitutes a pivotal limitation to clinical use of NO-donors such as nitrates (Pieper et al., 2002). Moreover, experiments carried out on isolated rat aortas showed that NO-NSAIDs such as NCX-4215, nitroflurbiprofen and nitroparacetamol caused dose-dependent relaxation of aortic rings precontracted with adrenaline or noradrenaline (Del Soldato et al., 1999; Keeble et al., 2001). Interestingly, this effect seemed to be endothelium-independent, because removal of endothelium even potentiated vasodilatatory properties of nitroflurbiprofen, possibly due to enhanced impact on the smooth muscle cells layer (Keeble et al., 2001). Furthermore, recent animal studies have indicated that NO-NSAIDs are devoid of hypotensive side effects, known to be a common complication during nitrates therapy (Wallace et al., 1995; Fujihara et al., 1998; Keeble et al., 2001). Possible explanation could be that NO-NSAIDs liberate NO at a slower rate in comparison to standard NO donors (Wallace et al., 1995). On the other hand, interesting results have been obtained by Muscará et al. (2001) who reported that NCX-4016 significantly reduced increased arterial blood pressure in hypertnesive rats, but did not affect the blood pressure in normotensive animals. Thus, considering the fact that administration of standard NSAIDs is often complicated by impairment in the efficacy of antihypertensive drugs, NCX-4016 could be promising alternative for patients with hypertension, who require prolonged NSAIDs therapy (Muscará et al., 2001). Moreover, it has been found that pretreatment with NCX-4016 resulted in significant cardioprotection *in vivo* in a model of acute myocardial ischemia as well as *in vitro* based on the model of ischemia/reperfusion myocardial injury, while control treatment with aspirin showed only little or no protection (Rossoni et al., 2000; Rossoni et al., 2001). In detail, NCX-4016 was shown to markedly reduce infarction size and to decrease plasma activity of creatine kinase, which was accompanied by a significant fall in mortality rate (Rossoni et al., 2000; Rossoni et al., 2001). In addition, chronic treatment with NCX-4016 has been demonstrated to exert anti-atherosclerotic and anti-oxidative activity in arteries of hypercholesterolemic mice (Napoli et al., 2002). On the other hand, Napoli et al. (Napoli et al., 2001) investigated the effect of NCX-4016 on the extent of restenosis after balloon angioplasty in mice with concomitant hypercholesterolemia. They revealed that NCX-4016 showed both preventive and therapeutic potency against restenosis, suggesting that it may be a novel therapeutic strategy in reducing restenosis among patients subjected to balloon angioplasty, especially those with hypercholesterolemia (Napoli et al., 2001). Importantly, NCX-4016 has also shown protective effects in a human trial conducted among patients with intermittent claudication, pathology in which physical effort induces endothelial dysfunction in ischemia/reperfusion-dependent mechanisms. NCX-4016 administered orally for four weeks, significantly prevented from the exercise-induced endothelial damage, in contrast to the standard aspirin treatment, which was devoid of such effect (Gresele et al., 2007). On the other hand, another human trial revealed that NCX-4016 markedly reversed insulin resistance and enhanced vascular response to insulin in obese insulin-resistant men (Gresele and Momi, 2006). Clearly, further studies are required to fully evaluate the clinical potential of novel NO-NSAIDs with respect to cardiovascular disorders.

It has been recently demonstrated that also CO and H_2S released from chemical donors may provide protection within the cardiovascular system. Numerous studies have shown that CO- and H_2S-releasing prodrugs exert vasodilatatory and antihypertensive properties (Motterlini et al., 2002; Foresti et al., 2004; Li et al., 2008; Rossoni et al., 2010; Failli et al., 2012; Kulkarni-Chitnis et al., 2015). Rossoni et al. (2010) evaluated the efficacy of H_2S-releasing derivatives of aspirin (ACS-14) and salicylic acid (ACS-21) in modulation of pathological changes related to metabolic syndrome induced by glutathione (GSH) depletion in rats. ACS-14 and ACS-2 but not classic aspirin, significantly restored endothelial dysfunction in aortic tissue and markedly reduced accompanying hypertension along with hyperinsulinemia, most probably in mechanisms dependent on H_2S release (Rossoni et al., 2010). On the other hand, experiments carried out on healthy dogs revealed that administration with H_2S-releasing naproxen, ATB-346, did not produce significant change in arterial blood pressure or heart rate (Wallace et al., 2018). Similarly, phase 1 clinical trial of ATB-346 demonstrated no significant difference in blood pressure between group treated with ATB-346 and placebo control (Wallace et al., 2018). Thus, further research should shed more light into understanding the mechanisms by which H_2S could affect blood pressure under physiological and pathological conditions.

Interestingly, CO-releasing molecules, CORMs, have been also pointed out as potential antihypertensive agents. Preclinical studies demonstrated that treatment with CORM-3 induced

TABLE 1 | Alterations of selected molecular targets by donors of gaseous mediators NO- H_2S- and CO -and NSAID prodrugs.

	Gaseous mediators-relesaing prodrug		
Molecular target	**NO donors and NO-NSAIDs**	**H_2S donors and H_2S-NSAIDs**	**CO donors and NSAIDs**
Nf-κB	Downregulation Bolla et al. (2006)	Downregulation Li et al. (2007)	Downregulation Ling et al. (2018)
Nrf-2	No reports	Upregulation of Nrf-2 expression in gastric mucosa, activation of Nrf-2/HMOX-1/CO pathway Magierowski et al. (2017), Corsello et al. (2018)	Activation of Nrf-2 signaling pathway in mouse macrophages Qin et al. (2015)
ERK/MAPK	Inhibition of MAPK pathway Rigas (2007)	Inhibition of MAPK pathway Guo et al. (2014)	Activation of MAPK pathway Ryter et al. (2018) Modulation of ERK/MAPK in T cells, supressing their profileration Głowacka et al. (2020)
COXs	COX-1 and COX-2 Downregulation Magierowski et al. (2015)	COX-2 downregulation Magierowski et al. (2017)	COX-2 downregulation Ling et al. (2018)
CO biosynthesis	No reports	Upregulatiom of Nrf-2/HMOX-1/CO pathway in gastric mucosa Magierowski et al. (2017)	Upregulation of HMOX-1 expression in gastric mucosa Magierowska et al. (2019)
H_2S biosynthesis	Increase in CTH activation, upregulation of H_2S biosynthesis in cultured aortic smooth muscle cells Zhao et al. (2001) No effect on H_2S biosynthesis in endothelial cells Chen et al. (2014)	No reports	CBS inhibition, regulation of H_2S biosynthesis Głowacka et al. (2020)
NO biosynthesis	iNOS inhibition Rigas (2007)	Inhibition of LPS-induced iNOS overexpression Li et al. (2007), Campolo et al. (2014)	Endothelial NOS activation Ryter et al. (2018), Zuckerbraun et al. (2006)
gut microbiota	No reports	Facilitation of antimicrobial immunity, normalization of enteric microbiota profile Blackler et al. (2015) Restoration of microbiota biofilm Motta et al. (2015)	Modulation of interplay between microbiota and mucosal immune system Głowacka et al. (2020)

relaxation of precontracted aortic rings *ex vivo*, leading to significant vasodilatation with the involvement of potassium channels and guanylate cyclase activity (Motterlini et al., 2002; Foresti et al., 2004; Failli et al., 2012). Additionally, in response to CORM-3 administration, a significant decrease in blood pressure *in vivo* in rats has been noticed, suggesting possible use of CO-donating compounds as alternative therapy for hypertension (Foresti et al., 2004). This seems to be supported by the observation that CORMs showed efficacy to attenuate acute hypertension in animal models (Motterlini et al., 2002). Also, numerous studies have presented protective effects of H_2S-NSAIDs, GYY4137 as chemical donor slowly liberating H_2S, and CORMs against myocardial injury induced by ischemia/reperfusion (Clark et al., 2003; Guo et al., 2004; Varadi et al., 2007; Rossoni et al., 2008; Citi et al., 2018). It is also worth mentioning that in another animal study GYY4137 attenuated atherosclerotic lesions in apoE (-/-) mice, which was accompanied by a significant decrease in vascular inflammation and oxidative profile (Liu et al., 2013). This data seems to be consistent with the observation that atherosclerosis correlates with decreased vascular H_2S level (Liu et al., 2013). Thus, it could be of interest to determine whether H_2S-releasing NSAIDs could be considered as therapeutic agents against atherosclerotic vascular lesions. On the other hand, the clinical implementation of CORMs may by limited due to the risk of cardiomyopathy (Kim and Choi, 2018). Therefore, further studies are still required to fully elucidate the influence of CO released from chemical donors on cardiac tissue.

As it has been mentioned above, chronic treatment with NSAIDs also increases the risk of various forms of kidney injury and concomitant reduction in renal perfusion, secondary to decreased PGs biosynthesis (Whelton, 1999). However, gaseous mediators-releasing NSAIDs could be devoid of renal adverse effects and even exert protective activity against kidney disorders. Wallace et al. (1997) reported that administration of diclofenac to healthy or cirrhotic rats resulted in significant reduction in renal blood flow, while NO-releasing derivative of this drug did not induce such effect. Also, phase 1 clinical trial did not show any significant renal side effects among healthy subjects during therapy with H_2S-releasing ATB-346 [71]. Furthermore, Kodela et al. (2015) hypothesized that NOSH-aspirin may be especially promising with respect to improved renal safety profile, because both NO and H_2S have been recognized as protective factors within renal system. Yet, further studies may confirm and support these conclusions. On the other hand, CO-releasing CORM-A1 applied to healthy mice notably increased renal blood flow, as compared to control group (RYAN et al., 2006). Noteworthy, CORM-A1 has been shown to relax renal interlobar arteries contracted with phenylephrine and this effect was dependent on guanylate cyclase activity together with the opening of potassium

channels (RYAN et al., 2006). In spite of the essential role in physiological processes in kidneys, gaseous mediators released from various donors have been also demonstrated to possess therapeutic properties. In detail, Fujihara et al. (1998) reported that nitroflurbiprofen (HCT-1026) alleviated renal damage in a rat model of 5/6 kidney ablation, contrary to its parent drug, flurbiprofen. In addition, they also observed that HCT-1026 markedly ameliorated albuminuria, interstitial injury, retention of creatinine and hypertension in rats subjected to kidney ablation. In turn, Kim et al. (2020) have examined the therapeutic efficacy of CORM-3 against ischemia-reperfusion renal injury in rats. CORM-3 pretreatment significantly decreased the degree of kidney damage comparing to control group, which could be explained, at least in part, by diminished apoptotic activity evoked by this compound. Similarly, renoprotective potential of CORM-2 has been observed in a mice model of thermal injury (Kim et al., 2020). CO-releasing CORM-2 prevented granulocytes infiltration in renal tissue induced in response to thermal damage, as well as notably decreased NF-κB activation in kidney. To summarize, the numerous effects of gaseous mediators released from chemical donors, involving anti-inflammatory, anti-apoptotic and vasodilatory properties, could account for significant renoprotective action of these compounds, even offering a promising alternative in future therapies against various renal disorders.

CONCLUSIONS AND FURTHER PERSPECTIVES

Overcoming the toxicity of NSAIDs, particularly the well-known GI adverse effects, still remains a target for further studies revolving around different preventive strategies including NSAIDs conjugated with gaseous mediators as one of the most interesting and promising groups. Animal studies as well as clinical trials concerning the efficacy and safety of these novel compounds have shown encouraging results, giving a solid background to prompt the further investigation. These novel NSAIDs or NSAIDs combined with CORMs were shown to modulate several molecular pathways (**Table 1**.).

Both NO-NSADs and H_2S-NSAIDs but also CO donors applied in combination with NSAIDs have been proven to retain the anti-inflammatory activity of their parent drugs, however, with markedly reduced gastrotoxicity and also importantly, with reduced intestinal toxicity, both become subjects of rising clinical underestimated concern (**Figure 2**). The increasing awareness on the deleterious influence of NSAIDs on the intestinal homeostasis confirms the need for the development of novel strategies with diminished toxicity toward intestinal mucosa and quality of enteric microbiota. Importantly, novel gaseous mediator-releasing NSAIDs with greatly limited GI toxicity and more complex molecular activity than parent drugs could be considered to be repurposed into the GI disorders treatment, such as chronic inflammation and pre- and cancerous pathologies. Although some promising results have been achieved with respect to the gaseous mediator-releasing NSAIDs, further studies are still needed to address these interesting and emerging issues.

AUTHOR CONTRIBUTIONS

Conceptualization: MM, Writing—original draft: AD, Writing—review & editing: JW, TB, and MM, Supervision: MM, Funding acquisition: MM.

FUNDING

This work was supported by a grant provided to MM from The National Centre for Research and Development, Poland (LIDER/9/0055/L-8/16/NCBR/2017).

ACKNOWLEDGMENTS

Authors would like to thank to Monika Marcinkowska (Faculty of Pharmacy, Jagiellonian University Medical College) and to Dominik Bakalarz, MSc (Department of Physiology, Jagiellonian University Medical College) for the consultations and assistance regarding chemical structures drawing for the compounds described in the manuscript.

REFERENCES

Al-Swayeh, O. A., Clifford, R. H., Del Soldato, P., and Moore, P. K. (2000). A Comparison of the Anti-inflammatory and Anti-nociceptive Activity of Nitroaspirin and Aspirin. *Br. J. Pharmacol.* 129 (2), 343–350. doi:10.1038/sj.bjp.0703064

Ambrosini, M. V., Mariucci, G., Rambotti, M. G., Tantucci, M., Covarelli, C., Angelis, L. D., et al. (2005). Ultrastructural Investigations on Protective Effects of NCX 4016 (Nitroaspirin) on Macrovascular Endothelium in Diabetic Wistar Rats. *J. Submicrosc Cytol. Pathol.* 37 (2), 205–213. http://www.ncbi.nlm.nih.gov/pubmed/16335593.

Bacchi, S., Palumbo, P., Sponta, A., and Coppolino, M. F. (2012). Clinical Pharmacology of Non-steroidal Anti-inflammatory Drugs: A Review. *Aiaamc* 11 (1), 52–64. doi:10.2174/187152312803476255

Bakalarz, D., Surmiak, M., Yang, X., Wójcik, D., Korbut, E., Śliwowski, Z., et al. (2021). Organic Carbon Monoxide Prodrug, BW-CO-111, in Protection against Chemically-Induced Gastric Mucosal Damage. *Acta Pharmaceutica Sinica B* 11 (2), 456–475. doi:10.1016/j.apsb.2020.08.005

Bełtowski, J. (2015). Hydrogen Sulfide in Pharmacology and Medicine – an Update. *Pharmacol. Rep.* 67 (3), 647–658. doi:10.1016/j.pharep.2015.01.005

Bindu, S., Mazumder, S., and Bandyopadhyay, U. (2020). Non-steroidal Anti-inflammatory Drugs (NSAIDs) and Organ Damage: A Current Perspective. *Biochem. Pharmacol.* 180, 114147. doi:10.1016/j.bcp.2020.114147

Blackler, R., Syer, S., Bolla, M., Ongini, E., and Wallace, J. L. (2012). Gastrointestinal-Sparing Effects of Novel NSAIDs in Rats with Compromised Mucosal Defence. *PLoS One* 7 (4), e35196. doi:10.1371/journal.pone.0035196

Blackler, R. W., De Palma, G., Manko, A., Da Silva, G. J., Flannigan, K. L., Bercik, P., et al. (2015). Deciphering the Pathogenesis of NSAID Enteropathy Using Proton Pump Inhibitors and a Hydrogen Sulfide-Releasing NSAID. *Am. J. Physiology-Gastrointestinal Liver Physiol.* 308 (12), G994–G1003. doi:10.1152/ajpgi.00066.2015

Blackler, R. W., Gemici, B., Manko, A., and Wallace, J. L. (2014). NSAID-gastroenteropathy: New Aspects of Pathogenesis and Prevention. *Curr. Opin. Pharmacol.* 19, 11–16. doi:10.1016/j.coph.2014.05.008

Boelsterli, U. A., Redinbo, M. R., and Saitta, K. S. (2013). Multiple NSAID-Induced Hits Injure the Small Intestine: Underlying Mechanisms and Novel Strategies. *Toxicol. Sci.* 131 (2), 654–667. doi:10.1093/toxsci/kfs310

Bolla, M., Momi, S., Gresele, P., and Del Soldato, P. (2006). Nitric Oxide-Donating Aspirin (NCX 4016): An Overview of its Pharmacological Properties and Clinical Perspectives. *Eur. J. Clin. Pharmacol.* 62 (1), 145–154. doi:10.1007/s00228-005-0026-6

Bonetti, P. O., Lerman, L. O., and Lerman, A. (2003). Endothelial Dysfunction. *Atvb* 23 (2), 168–175. doi:10.1161/01.ATV.0000051384.43104

Bruno, G., Zaccari, P., Rocco, G., Scalese, G., Panetta, C., Porowska, B., et al. (2019). Proton Pump Inhibitors and Dysbiosis: Current Knowledge and Aspects to Be Clarified. *Wjg* 25 (22), 2706–2719. doi:10.3748/wjg.v25.i22.2706

Brzozowska, I., Targosz, A., Sliwowski, Z., Kwiecien, S., Drozdowicz, D., Pajdo, R., et al. (2004). Healing of Chronic Gastric Ulcers in Diabetic Rats Treated with Native Aspirin, Nitric Oxide (NO)-derivative of Aspirin and Cyclooxygenase (COX)-2 Inhibitor. *J. Physiol. Pharmacol.* 55 (4), 773–790. http://www.ncbi.nlm.nih.gov/pubmed/15613743.

Brzozowski, T., Konturek, P. C., Konturek, S. J., Sliwowski, Z., Drozdowicz, D., Kwiecień, S., et al. (2000). Gastroprotective and Ulcer Healing Effects of Nitric Oxide-Releasing Non-steroidal Anti-inflammatory Drugs. *Dig. Liver Dis.* 32 (7), 583–594. doi:10.1016/S1590-8658(00)80840-3

Cabassi, A., Tedeschi, S., Perlini, S., Verzicco, I., Volpi, R., Gonzi, G., et al. (2020). Non-steroidal Anti-inflammatory Drug Effects on Renal and Cardiovascular Function: from Physiology to Clinical Practice. *Eur. J. Prev. Cardiolog* 27 (8), 850–867. doi:10.1177/2047487319848105

Campolo, M., Esposito, E., Ahmad, A., Di Paola, R., Paterniti, I., Cordaro, M., et al. (2014). Hydrogen Sulfide-Releasing Cyclooxygenase Inhibitor ATB-346 Enhances Motor Function and Reduces Cortical Lesion Volume Following Traumatic Brain Injury in Mice. *J. Neuroinflammation* 11 (1), 196. doi:10.1186/s12974-014-0196-1

Caughey, G. E., Roughead, E. E., Vitry, A. I., McDermott, R. A., Shakib, S., and Gilbert, A. L. (2010). Comorbidity in the Elderly with Diabetes: Identification of Areas of Potential Treatment Conflicts. *Diabetes Res. Clin. Pract.* 87 (3), 385–393. doi:10.1016/j.diabres.2009.10.019

Chattopadhyay, M., Kodela, R., Duvalsaint, P. L., and Kashfi, K. (2016). Gastrointestinal Safety, Chemotherapeutic Potential, and Classic Pharmacological Profile of NOSH -naproxen (AVT -219) a Dual NO- and H 2 S-releasing Hybrid. *Pharmacol. Res. Perspect.* 4 (2), e00224. doi:10.1002/prp2.224

Chattopadhyay, M., Kodela, R., Olson, K. R., and Kashfi, K. (2012). NOSH-aspirin (NBS-1120), a Novel Nitric Oxide- and Hydrogen Sulfide-Releasing Hybrid Is a Potent Inhibitor of Colon Cancer Cell Growth In Vitro and in a Xenograft Mouse Model. *Biochem. Biophysical Res. Commun.* 419 (3), 523–528. doi:10.1016/j.bbrc.2012.02.051

Chattopadhyay, M., Kodela, R., Santiago, G., Le, T. T. C., Nath, N., and Kashfi, K. (2020). NOSH-aspirin (NBS-1120) Inhibits Pancreatic Cancer Cell Growth in a Xenograft Mouse Model: Modulation of FoxM1, P53, NF-Kb, iNOS, Caspase-3 and ROS. *Biochem. Pharmacol.* 176, 113857. doi:10.1016/j.bcp.2020.113857

Chen, P.-H., Fu, Y.-S., Wang, Y.-M., Yang, K.-H., Wang, D. L., and Huang, B. (2014). Hydrogen Sulfide Increases Nitric Oxide Production and Subsequent S-Nitrosylation in Endothelial Cells. *Scientific World J.* 2014, 1–8. doi:10.1155/2014/480387

Choi, A. M., and Alam, J. (1996). Heme Oxygenase-1: Function, Regulation, and Implication of a Novel Stress-Inducible Protein in Oxidant-Induced Lung Injury. *Am. J. Respir. Cel Mol Biol* 15 (1), 9–19. doi:10.1165/ajrcmb.15.1.8679227

Cipriani, S., Mencarelli, A., Bruno, A., Renga, B., Distrutti, E., Santucci, L., et al. (2013). Activation of the Bile Acid Receptor GPBAR1 Protects against Gastrointestinal Injury Caused by Non-steroidal Anti-inflammatory Drugs and Aspirin in Mice. *Br. J. Pharmacol.* 168 (1), 225–237. doi:10.1111/j.1476-5381.2012.02128.x

Citi, V., Piragine, E., Testai, L., Breschi, M. C., Calderone, V., and Martelli, A. (2018). The Role of Hydrogen Sulfide and H2S-Donors in Myocardial Protection against Ischemia/Reperfusion Injury. *Cmc* 25 (34), 4380–4401. doi:10.2174/0929867325666180212120504

Clark, J. E., Naughton, P., Shurey, S., Green, C. J., Johnson, T. R., Mann, B. E., et al. (2003). Cardioprotective Actions by a Water-Soluble Carbon Monoxide-Releasing Molecule. *Circ. Res.* 93 (2), e2–8. doi:10.1161/01.RES.0000084381.86567.08

Conaghan, P. G. (2012). A Turbulent Decade for NSAIDs: Update on Current Concepts of Classification, Epidemiology, Comparative Efficacy, and Toxicity. *Rheumatol. Int.* 32 (6), 1491–1502. doi:10.1007/s00296-011-2263-6

Corsello, T., Komaravelli, N., and Casola, A. (2018). Role of Hydrogen Sulfide in NRF2- and Sirtuin-dependent Maintenance of Cellular Redox Balance. *Antioxidants* 7 (10), 129. doi:10.3390/antiox7100129

de Araújo, S., Oliveira, A. P., Sousa, F. B. M., Souza, L. K. M., Pacheco, G., Filgueiras, M. C., et al. (2018). AMPK Activation Promotes Gastroprotection through Mutual Interaction with the Gaseous Mediators H 2 S, NO, and CO. *Nitric Oxide* 78, 60–71. doi:10.1016/j.niox.2018.05.008

Del Soldato, P., Sorrentino, R., and Pinto, A. (1999). NO-aspirins: A Class of New Anti-inflammatory and Antithrombotic Agents. *Trends Pharmacol. Sci.* 20 (8), 319–323. doi:10.1016/S0165-6147(99)01353-X

Di Napoli, M., and Papa, F. (2003). NCX-4016 NicOx. *Curr. Opin. Investig. Drugs* 4 (9), 1126–1139. http://www.ncbi.nlm.nih.gov/pubmed/14582459.

Dieppe, P. A., Ebrahim, S., Martin, R. M., and Jüni, P. (2004). Lessons from the Withdrawal of Rofecoxib: ***. *BMJ* 329 (7471), 867–868. doi:10.1136/bmj.329.7471.867

Ekundi-Valentim, E., Mesquita, F. P., Santos, K. T., de Paula, M. A., Florenzano, J., Zanoni, C. I., et al. (2013). A Comparative Study on the Anti-inflammatory Effects of Single Oral Doses of Naproxen and its Hydrogen Sulfide (H2S)-Releasing Derivative ATB-346 in Rats with Carrageenan-Induced Synovitis. *Med. Gas Res.* 3 (1), 24. doi:10.1186/2045-9912-3-24

Elliott, S. N., McKnight, W., Cirino, G., and Wallace, J. L. (1995). A Nitric Oxide-Releasing Nonsteroidal Anti-inflammatory Drug Accelerates Gastric Ulcer Healing in Rats. *Gastroenterology* 109 (2), 524–530. doi:10.1016/0016-5085(95)90341-0

Failli, P., Vannacci, A., Di Cesare Mannelli, L., Motterlini, R., and Masini, E. (2012). Relaxant Effect of a Water Soluble Carbon Monoxide-Releasing Molecule (CORM-3) on Spontaneously Hypertensive Rat Aortas. *Cardiovasc. Drugs Ther.* 26 (4), 285–292. doi:10.1007/s10557-012-6400-6

Fiorucci, S., Antonelli, E., Burgaud, J.-L., and Morelli, A. (2001). Nitric Oxide??? Releasing NSAIDs. *Drug Saf.* 24 (11), 801–811. doi:10.2165/00002018-200124110-00002

Fiorucci, S., Antonelli, E., Distrutti, E., Rizzo, G., Mencarelli, A., Orlandi, S., et al. (2005). Inhibition of Hydrogen Sulfide Generation Contributes to Gastric Injury Caused by Anti-inflammatory Nonsteroidal Drugs. *Gastroenterology* 129 (4), 1210–1224. doi:10.1053/j.gastro.2005.07.060

Fiorucci, S., Mencarelli, A., Meneguzzi, A., Lechi, A., Renga, B., del Soldato, P., et al. (2004). Co-Administration of Nitric Oxide-Aspirin (NCX-4016) and Aspirin Prevents Platelet and Monocyte Activation and Protects against Gastric Damage Induced by Aspirin in Humans. *J. Am. Coll. Cardiol.* 44 (3), 635–641. doi:10.1016/j.jacc.2004.03.079

Fiorucci, S., Santucci, L., Wallace, J. L., Sardina, M., Romano, M., del Soldato, P., et al. (2003). Interaction of a Selective Cyclooxygenase-2 Inhibitor with Aspirin and NO-Releasing Aspirin in the Human Gastric Mucosa. *Proc. Natl. Acad. Sci.* 100 (19), 10937–10941. doi:10.1073/pnas.1933204100

Fonseca, M. D., Cunha, F. Q., Kashfi, K., and Cunha, T. M. (2015). NOSH-aspirin (NBS-1120), a Dual Nitric Oxide and Hydrogen Sulfide-Releasing Hybrid, Reduces Inflammatory Pain. *Pharmacol. Res. Perspect.* 3 (3), e00133. doi:10.1002/prp2.133

Foresti, R., Hammad, J., Clark, J. E., Johnson, T. R., Mann, B. E., Friebe, A., et al. (2004). Vasoactive Properties of CORM-3, a Novel Water-Soluble Carbon Monoxide-Releasing Molecule. *Br. J. Pharmacol.* 142 (3), 453–460. doi:10.1038/sj.bjp.0705825

Fournier, J.-P., Sommet, A., Bourrel, R., Oustric, S., Pathak, A., Lapeyre-Mestre, M., et al. (2012). Non-steroidal Anti-inflammatory Drugs (NSAIDs) and Hypertension Treatment Intensification: a Population-Based Cohort Study. *Eur. J. Clin. Pharmacol.* 68 (11), 1533–1540. doi:10.1007/s00228-012-1283-9

Freitas, A., Alves-Filho, J. C., Secco, D. D., Neto, A. F., Ferreira, S. H., Barja-Fidalgo, C., et al. (2006). Heme Oxygenase/carbon Monoxide-Biliverdin Pathway Down Regulates Neutrophil Rolling, Adhesion and Migration in Acute Inflammation. *Br. J. Pharmacol.* 149 (4), 345–354. doi:10.1038/sj.bjp.0706882

Fujihara, C. K., Malheiros, D. M. A. C., Donato, J., Poli, A., De Nucci, G., and Zatz, R. (1998). Nitroflurbiprofen, a New Nonsteroidal Anti-inflammatory, Ameliorates Structural Injury in the Remnant Kidney. *Am. J. Physiology-Renal Physiol.* 274 (3), F573–F579. doi:10.1152/ajprenal.1998.274.3.F573

Glowacka, U., Magierowska, K., Wojcik, D., and Hankus, J., Szetela, M., Cieszkowski, J., et al. (2021). Microbiome Profile and Molecular Pathways Alterations in Gastrointestinal Tract by Hydrogen Sulfide-Releasing Non-steroidal Anti-inflammatory Drug (ATB-352). Insight into Possible Safer Polypharmacy. *Antioxid. Redox Signal.* 2020, 8240. doi:10.1089/ars.2020.8240

Goldstein, J. L., Eisen, G. M., Lewis, B., Gralnek, I. M., Zlotnick, S., and Fort, J. G. (2005). Video Capsule Endoscopy to Prospectively Assess Small Bowel Injury with Celecoxib, Naproxen Plus Omeprazole, and Placebo. *Clin. Gastroenterol. Hepatol.* 3 (2), 133–141. doi:10.1016/S1542-3565(04)00619-6

Graham, D. Y., Opekun, A. R., Willingham, F. F., and Qureshi, W. A. (2005). Visible Small-Intestinal Mucosal Injury in Chronic NSAID Users. *Clin. Gastroenterol. Hepatol.* 3 (1), 55–59. doi:10.1016/S1542-3565(04)00603-2

Gresele, P., Migliacci, R., Procacci, A., De Monte, P., and Bonizzoni, E. (2007). Prevention by NCX 4016, a Nitric Oxide-Donating Aspirin, but Not by Aspirin, of the Acute Endothelial Dysfunction Induced by Exercise in Patients with Intermittent Claudication. *Thromb. Haemost.* 97 (03), 444–450. doi:10.1160/TH06-10-0555

Gresele, P., and Momi, S. (2006). Pharmacologic Profile and Therapeutic Potential of NCX 4016, a Nitric Oxide-Releasing Aspirin, for Cardiovascular Disorders. *Cardiovasc. Drug Rev.* 24 (2), 148–168. doi:10.1111/j.1527-3466.2006.00148.x

Gugliandolo, E., Fusco, R., D'Amico, R., Militi, A., Oteri, G., Wallace, J. L., et al. (2018). Anti-inflammatory Effect of ATB-352, a H2S –releasing Ketoprofen Derivative, on Lipopolysaccharide-Induced Periodontitis in Rats. *Pharmacol. Res.* 132, 220–231. doi:10.1016/j.phrs.2017.12.022

Guo, C., Liang, F., Shah Masood, W., and Yan, X. (2014). Hydrogen Sulfide Protected Gastric Epithelial Cell from Ischemia/reperfusion Injury by Keap1 S-Sulfhydration, MAPK Dependent Anti-apoptosis and NF-Kb Dependent Anti-inflammation Pathway. *Eur. J. Pharmacol.* 725 (1), 70–78. doi:10.1016/j.ejphar.2014.01.009

Guo, Y., Stein, A. B., Wu, W.-J., Tan, W., Zhu, X., Li, Q.-H., et al. (2004). Administration of a CO-releasing Molecule at the Time of Reperfusion Reduces Infarct Size In Vivo. *Am. J. Physiology-Heart Circulatory Physiol.* 286 (5), H1649–H1653. doi:10.1152/ajpheart.00971.2003

Głowacka, U., Brzozowski, T., and Magierowski, M. (2020). Synergisms, Discrepancies and Interactions between Hydrogen Sulfide and Carbon Monoxide in the Gastrointestinal and Digestive System Physiology, Pathophysiology and Pharmacology. *Biomolecules* 10 (3), 445. doi:10.3390/biom10030445

Harirforoosh, S., Asghar, W., and Jamali, F. (2014). Adverse Effects of Nonsteroidal Antiinflammatory Drugs: An Update of Gastrointestinal, Cardiovascular and Renal Complications. *J. Pharm. Pharm. Sci.* 16 (5), 821. doi:10.18433/J3VW2F

Higuchi, K., Yoda, Y., Amagase, K., Kato, S., Tokioka, S., Murano, M., et al. (2009). Prevention of NSAID-Induced Small Intestinal Mucosal Injury: Prophylactic Potential of Lansoprazole. *J. Clin. Biochem. Nutr.* 45 (2), 125–130. doi:10.3164/jcbn.SR09-58

Huang, C. W., and Moore, P. K. (2015). H2S Synthesizing Enzymes: Biochemistry and Molecular Aspects. *Handb Exp. Pharmacol.* 230, 3–25. doi:10.1007/978-3-319-18144-8_1

Huang, E. S., Strate, L. L., Ho, W. W., Lee, S. S., and Chan, A. T. (2011). Long-Term Use of Aspirin and the Risk of Gastrointestinal Bleeding. *Am. J. Med.* 124 (5), 426–433. doi:10.1016/j.amjmed.2010.12.022

Jasnos, K., Magierowski, M., Kwiecień, S., and Brzozowski, T. (2014). Carbon Monoxide in Human Physiology - its Role in the Gastrointestinal Tract. *Postepy Hig Med. Dosw* 68, 101–109. doi:10.5604/17322693.1087527

Ji, J., Xiang, P., Li, T., Lan, L., Xu, X., Lu, G., et al. (2017). NOSH-NBP, a Novel Nitric Oxide and Hydrogen Sulfide- Releasing Hybrid, Attenuates Ischemic Stroke-Induced Neuroinflammatory Injury by Modulating Microglia Polarization. *Front. Cel. Neurosci.* 11, 154. doi:10.3389/fncel.2017.00154

Karlsson, J., Pivodic, A., Aguirre, D., and Schnitzer, T. J. (2009). Efficacy, Safety, and Tolerability of the Cyclooxygenase-Inhibiting Nitric Oxide Donator Naproxcinod in Treating Osteoarthritis of the Hip or Knee. *J. Rheumatol.* 36 (6), 1290–1297. doi:10.3899/jrheum.081011

Kashfi, K., Chattopadhyay, M., and Kodela, R. (2015). NOSH-sulindac (AVT-18A) Is a Novel Nitric Oxide- and Hydrogen Sulfide-Releasing Hybrid that Is Gastrointestinal Safe and Has Potent Anti-inflammatory, Analgesic, Antipyretic, Anti-platelet, and Anti-cancer Properties. *Redox Biol.* 6, 287–296. doi:10.1016/j.redox.2015.08.012

Kashfi, K. (2015). Utility of Nitric Oxide and Hydrogen Sulfide-Releasing Chimeras as Anticancer Agents. *Redox Biol.* 5, 420. doi:10.1016/j.redox.2015.09.030

Kato, S., Suzuki, K., Ukawa, H., Komoike, Y., and Takeuchi, K. (2001). Low Gastric Toxicity of Nitric Oxide-Releasing Aspirin, NCX-4016, in Rats with Cirrhosis and Arthritis. *Dig. Dis. Sci.* 46 (8), 1690–1699. doi:10.1023/a:1010601520497

Kautz, A. C., Kunz, P. C., and Janiak, C. (2016). CO-releasing Molecule (CORM) Conjugate Systems. *Dalton Trans.* 45 (45), 18045–18063. doi:10.1039/C6DT03515A

Keeble, J., Al-Swayeh, O. A., and Moore, P. K. (2001). Vasorelaxant Effect of Nitric Oxide Releasing Steroidal and Nonsteroidal Anti-inflammatory Drugs. *Br. J. Pharmacol.* 133 (7), 1023–1028. doi:10.1038/sj.bjp.0704161

Kim, D. K., Shin, S.-J., Lee, J., Park, S. Y., Kim, Y. T., Choi, H. Y., et al. (2020). Carbon Monoxide-Releasing Molecule-3: Amelioration of Renal Ischemia Reperfusion Injury in a Rat Model. *Investig. Clin. Urol.* 61 (4), 441–451. doi:10.4111/icu.2020.61.4.441

Kim, H.-H., and Choi, S. (2018). Therapeutic Aspects of Carbon Monoxide in Cardiovascular Disease. *Ijms* 19 (8), 2381. doi:10.3390/ijms19082381

Kimura, H. (2014). Production and Physiological Effects of Hydrogen Sulfide. *Antioxid. Redox Signaling* 20 (5), 783–793. doi:10.1089/ars.2013.5309

Kodela, R., Chattopadhyay, M., and Kashfi, K. (2012). NOSH-aspirin: A Novel Nitric Oxide-Hydrogen Sulfide-Releasing Hybrid: A New Class of Anti-inflammatory Pharmaceuticals. *ACS Med. Chem. Lett.* 3 (3), 257–262. doi:10.1021/ml300002m

Kodela, R., Chattopadhyay, M., and Kashfi, K. (2013). Synthesis and Biological Activity of NOSH-Naproxen (AVT-219) and NOSH-Sulindac (AVT-18A) as Potent Anti-inflammatory Agents with Chemotherapeutic Potential. *Med. Chem. Commun.* 4 (11), 1472. doi:10.1039/c3md00185g

Kodela, R., Chattopadhyay, M., Velázquez-Martínez, C. A., and Kashfi, K. (2015). NOSH-aspirin (NBS-1120), a Novel Nitric Oxide- and Hydrogen Sulfide-Releasing Hybrid Has Enhanced Chemo-Preventive Properties Compared to Aspirin, Is Gastrointestinal Safe with All the Classic Therapeutic Indications. *Biochem. Pharmacol.* 98 (4), 564–572. doi:10.1016/j.bcp.2015.09.014

Konturek, S. J. (1985). Gastric Cytoprotection. *Scand. J. Gastroenterol.* 20 (5), 543–553. doi:10.3109/00365528509089694

Kulkarni-Chitnis, M., Njie-Mbye, Y. F., Mitchell, L., Robinson, J., Whiteman, M., Wood, M. E., et al. (2015). Inhibitory Action of Novel Hydrogen Sulfide Donors on Bovine Isolated Posterior Ciliary Arteries. *Exp. Eye Res.* 134, 73–79. doi:10.1016/j.exer.2015.04.001

Lanas, A. (2010). A Review of the Gastrointestinal Safety Data-Aa Gastroenterologist's Perspective. *Rheumatology* 49 (Suppl. 2), ii3–ii10. doi:10.1093/rheumatology/keq058

Lee, M., McGeer, E., Kodela, R., Kashfi, K., and McGeer, P. L. (2013). NOSH-aspirin (NBS-1120), a Novel Nitric Oxide and Hydrogen Sulfide Releasing Hybrid, Attenuates Neuroinflammation Induced by Microglial and Astrocytic Activation: A New Candidate for Treatment of Neurodegenerative Disorders. *Glia* 61 (10), 1724–1734. doi:10.1002/glia.22553

Li, L., Rossoni, G., Sparatore, A., Lee, L. C., Del Soldato, P., and Moore, P. K. (2007). Anti-inflammatory and Gastrointestinal Effects of a Novel Diclofenac Derivative. *Free Radic. Biol. Med.* 42 (5), 706–719. doi:10.1016/j.freeradbiomed.2006.12.011

Li, L., Whiteman, M., Guan, Y. Y., Neo, K. L., Cheng, Y., Lee, S. W., et al. (2008). Characterization of a Novel, Water-Soluble Hydrogen Sulfide-Releasing Molecule (GYY4137). *Circulation* 117 (18), 2351–2360. doi:10.1161/CIRCULATIONAHA.107.753467

Ling, K., Men, F., Wang, W.-C., Zhou, Y.-Q., Zhang, H.-W., and Ye, D.-W. (2018). Carbon Monoxide and its Controlled Release: Therapeutic Application, Detection, and Development of Carbon Monoxide Releasing Molecules (CORMs). *J. Med. Chem.* 61 (7), 2611–2635. doi:10.1021/acs.jmedchem.6b01153

Liu, L., Cui, J., Song, C.-J., Bian, J.-S., Sparatore, A., Soldato, P. D., et al. (2012). H(2) S-Releasing Aspirin Protects against Aspirin-Induced Gastric Injury via Reducing Oxidative Stress. *PLoS One* 7 (9), e46301. doi:10.1371/journal.pone.0046301

Liu, Z., Han, Y., Li, L., Lu, H., Meng, G., Li, X., et al. (2013). The Hydrogen Sulfide Donor, GYY4137, Exhibits Anti-atherosclerotic Activity in High Fat Fed

Apolipoprotein E−/−mice. *Br. J. Pharmacol.* 169 (8), 1795–1809. doi:10.1111/bph.12246

LoGuidice, A., Wallace, B. D., Bendel, L., Redinbo, M. R., and Boelsterli, U. A. (2012). Pharmacologic Targeting of Bacterial β-Glucuronidase Alleviates Nonsteroidal Anti-inflammatory Drug-Induced Enteropathy in Mice. *J. Pharmacol. Exp. Ther.* 341 (2), 447–454. doi:10.1124/jpet.111.191122

Lohmander, L. S. (2004). A Randomised, Placebo Controlled, Comparative Trial of the Gastrointestinal Safety and Efficacy of AZD3582 versus Naproxen in Osteoarthritis. *Ann. Rheum. Dis.* 64 (3), 449–456. doi:10.1136/ard.2004.023572

Lou, L-X., Geng, B., Du, J-B., and Tang, C-S. (2008). Hydrogen Sulphide-Induced Hypothermia Attenuates Stress-Related Ulceration in Rats. *Clin. Exp. Pharmacol. Physiol.* 35 (2), 223–228. doi:10.1111/j.1440-1681.2007.04812.x

Magierowska, K., Bakalarz, D., Wójcik, D., Chmura, A., Hubalewska-Mazgaj, M., Licholai, S., et al. (2019a). Time-dependent Course of Gastric Ulcer Healing and Molecular Markers Profile Modulated by Increased Gastric Mucosal Content of Carbon Monoxide Released from its Pharmacological Donor. *Biochem. Pharmacol.* 163, 71–83. doi:10.1016/j.bcp.2019.02.011

Magierowska, K., Brzozowski, T., and Magierowski, M. (2018). Emerging Role of Carbon Monoxide in Regulation of Cellular Pathways and in the Maintenance of Gastric Mucosal Integrity. *Pharmacol. Res.* 129, 56–64. doi:10.1016/j.phrs.2018.01.008

Magierowska, K., Korbut, E., Hubalewska-Mazgaj, M., Surmiak, M., Chmura, A., Bakalarz, D., et al. (2019b). Oxidative Gastric Mucosal Damage Induced by Ischemia/reperfusion and the Mechanisms of its Prevention by Carbon Monoxide-Releasing Tricarbonyldichlororuthenium (II) Dimer. *Free Radic. Biol. Med.* 145, 198–208. doi:10.1016/j.freeradbiomed.2019.09.032

Magierowska, K., Magierowski, M., Surmiak, M., Adamski, J., Mazur-Bialy, A., Pajdo, R., et al. (2016). The Protective Role of Carbon Monoxide (CO) Produced by Heme Oxygenases and Derived from the CO-Releasing Molecule CORM-2 in the Pathogenesis of Stress-Induced Gastric Lesions: Evidence for Non-involvement of Nitric Oxide (NO). *Ijms* 17 (4), 442. doi:10.3390/ijms17040442

Magierowski, M., Magierowska, K., Surmiak, M., and Hubalewska-Mazgaj, M., Kwiecien, S., Wallace, J. L., et al. (2017b). The Effect of Hydrogen Sulfide-Releasing Naproxen (ATB-346) versus Naproxen on Formation of Stress-Induced Gastric Lesions, the Regulation of Systemic Inflammation, Hypoxia and Alterations in Gastric Microcirculation. *J. Physiol. Pharmacol.* 68 (5), 749–756.

Magierowski, M., Hubalewska-Mazgaj, M., Magierowska, K., Wojcik, D., Sliwowski, Z., Kwiecien, S., et al. (2018b). Nitric Oxide, Afferent Sensory Nerves, and Antioxidative Enzymes in the Mechanism of Protection Mediated by Tricarbonyldichlororuthenium(II) Dimer and Sodium Hydrosulfide against Aspirin-Induced Gastric Damage. *J. Gastroenterol.* 53 (1), 52–63. doi:10.1007/s00535-017-1323-4

Magierowski, M., Jasnos, K., Kwiecien, S., Drozdowicz, D., Surmiak, M., Strzalka, M., et al. (2015b). Endogenous Prostaglandins and Afferent Sensory Nerves in Gastroprotective Effect of Hydrogen Sulfide against Stress-Induced Gastric Lesions. *PLoS One* 10 (3), e0118972. doi:10.1371/journal.pone.0118972

Magierowski, M., Magierowska, K., Hubalewska-Mazgaj, M., Adamski, J., Bakalarz, D., Sliwowski, Z., et al. (2016a). Interaction between Endogenous Carbon Monoxide and Hydrogen Sulfide in the Mechanism of Gastroprotection against Acute Aspirin-Induced Gastric Damage. *Pharmacol. Res.* 114, 235–250. doi:10.1016/j.phrs.2016.11.001

Magierowski, M., Magierowska, K., Hubalewska-Mazgaj, M., Sliwowski, Z., Ginter, G., Pajdo, R., et al. (2017a). Carbon Monoxide Released from its Pharmacological Donor, Tricarbonyldichlororuthenium (II) Dimer, Accelerates the Healing of Pre-existing Gastric Ulcers. *Br. J. Pharmacol.* 174 (20), 3654–3668. doi:10.1111/bph.13968

Magierowski, M., Magierowska, K., Hubalewska-Mazgaj, M., Surmiak, M., Sliwowski, Z., Wierdak, M., et al. (2018a). Cross-talk between Hydrogen Sulfide and Carbon Monoxide in the Mechanism of Experimental Gastric Ulcers Healing, Regulation of Gastric Blood Flow and Accompanying Inflammation. *Biochem. Pharmacol.* 149, 131–142. doi:10.1016/j.bcp.2017.11.020

Magierowski, M., Magierowska, K., Kwiecien, S., and Brzozowski, T. (2015a). Gaseous Mediators Nitric Oxide and Hydrogen Sulfide in the Mechanism of Gastrointestinal Integrity, Protection and Ulcer Healing. *Molecules* 20 (5), 9099–9123. doi:10.3390/molecules20059099

Magierowski, M., Magierowska, K., Szmyd, J., Surmiak, M., Sliwowski, Z., Kwiecien, S., et al. (2016b). Hydrogen Sulfide and Carbon Monoxide Protect Gastric Mucosa Compromised by Mild Stress against Alendronate Injury. *Dig. Dis. Sci.* 61 (11), 3176–3189. doi:10.1007/s10620-016-4280-5

Maiden, L., Thjodleifsson, B., Theodors, A., Gonzalez, J., and Bjarnason, I. (2005). A Quantitative Analysis of NSAID-Induced Small Bowel Pathology by Capsule Enteroscopy. *Gastroenterology* 128 (5), 1172–1178. doi:10.1053/j.gastro.2005.03.020

Mard, S. A., Neisi, N., Solgi, G., Hassanpour, M., Darbor, M., and Maleki, M. (2012). Gastroprotective Effect of NaHS against Mucosal Lesions Induced by Ischemia-Reperfusion Injury in Rat. *Dig. Dis. Sci.* 57 (6), 1496–1503. doi:10.1007/s10620-012-2051-5

Matsui, H., Shimokawa, O., Kaneko, T., Nagano, Y., Rai, K., and Hyodo, I. (2011). The Pathophysiology of Non-steroidal Anti-inflammatory Drug (NSAID)-induced Mucosal Injuries in Stomach and Small Intestine. *J. Clin. Biochem. Nutr.* 48 (2), 107–111. doi:10.3164/jcbn.10-79

Mizoguchi, H., Hase, S., Tanaka, A., and Takeuchi, K. (2001). Lack of Small Intestinal Ulcerogenecity of Nitric Oxide-Releasing Indomethacin, NCX-530, in Rats. *Aliment. Pharmacol. Ther.* 15 (2), 257–267. doi:10.1046/j.1365-2036.2001.00916.x

Momi, S., Emerson, M., Paul, W., Leone, M., Mezzasoma, A. M., Del Soldato, P., et al. (2000). Prevention of Pulmonary Thromboembolism by NCX 4016, a Nitric Oxide-Releasing Aspirin. *Eur. J. Pharmacol.* 397 (1), 177–185. doi:10.1016/S0014-2999(00)00223-5

Mostafa, D. K., El Azhary, N. M., and Nasra, R. A. (2016). The Hydrogen Sulfide Releasing Compounds ATB-346 and Diallyl Trisulfide Attenuate Streptozotocin-Induced Cognitive Impairment, Neuroinflammation, and Oxidative Stress in Rats: Involvement of Asymmetric Dimethylarginine. *Can. J. Physiol. Pharmacol.* 94 (7), 699–708. doi:10.1139/cjpp-2015-0316

Motta, J.-P., Flannigan, K. L., Agbor, T. A., Beatty, J. K., Blackler, R. W., Workentine, M. L., et al. (2015). Hydrogen Sulfide Protects from Colitis and Restores Intestinal Microbiota Biofilm and Mucus Production. *Inflamm. Bowel Dis.* 21 (5), 1006–1017. doi:10.1097/MIB.0000000000000345

Motterlini, R., Clark, J. E., Foresti, R., Sarathchandra, P., Mann, B. E., and Green, C. J. (2002). Carbon Monoxide-Releasing Molecules. *Circ. Res.* 90 (2), E17–E24. doi:10.1161/hh0202.104530

Motterlini, R., and Otterbein, L. E. (2010). The Therapeutic Potential of Carbon Monoxide. *Nat. Rev. Drug Discov.* 9 (9), 728–743. doi:10.1038/nrd3228

Mu, K., Yu, S., and Kitts, D. D. (2019). The Role of Nitric Oxide in Regulating Intestinal Redox Status and Intestinal Epithelial Cell Functionality. *Ijms* 20 (7), 1755. doi:10.3390/ijms20071755

Mukherjee, D. (2001). Risk of Cardiovascular Events Associated with Selective COX-2 Inhibitors. *JAMA* 286 (8), 954. doi:10.1001/jama.286.8.954

Muscará, M. N., Lovren, F., McKnight, W., Dicay, M., Soldato, P. d., Triggle, C. R., et al. (2001). Vasorelaxant Effects of a Nitric Oxide-Releasing Aspirin Derivative in Normotensive and Hypertensive Rats. *Br. J. Pharmacol.* 133 (8), 1314–1322. doi:10.1038/sj.bjp.0704209

Napoli, C., Ackah, E., de Nigris, F., Del Soldato, P., D'Armiento, F. P., Crimi, E., et al. (2002). Chronic Treatment with Nitric Oxide-Releasing Aspirin Reduces Plasma Low-Density Lipoprotein Oxidation and Oxidative Stress, Arterial Oxidation-specific Epitopes, and Atherogenesis in Hypercholesterolemic Mice. *Proc. Natl. Acad. Sci.* 99 (19), 12467–12470. doi:10.1073/pnas.192244499

Napoli, C., Cirino, G., Del Soldato, P., Sorrentino, R., Sica, V., Condorelli, M., et al. (2001). Effects of Nitric Oxide-Releasing Aspirin versus Aspirin on Restenosis in Hypercholesterolemic Mice. *Proc. Natl. Acad. Sci.* 98 (5), 2860–2864. doi:10.1073/pnas.041602898

Olas, B. (2014). Carbon Monoxide Is Not Always a Poison Gas for Human Organism: Physiological and Pharmacological Features of CO. *Chemico-Biological Interactions* 222, 37–43. doi:10.1016/j.cbi.2014.08.005

Pereira-Leite, C., Nunes, C., Jamal, S. K., Cuccovia, I. M., and Reis, S. (2017). Nonsteroidal Anti-inflammatory Therapy: A Journey toward Safety. *Med. Res. Rev.* 37 (4), 802–859. doi:10.1002/med.21424

Pieper, G. M., Siebeneich, W., Olds, C. L., Felix, C. C., and Soldato, P. D. (2002). Vascular Protective Actions of a Nitric Oxide Aspirin Analog in Both In Vitro and In Vivo Models of Diabetes Mellitus. *Free Radic. Biol. Med.* 32 (11), 1143–1156. doi:10.1016/S0891-5849(02)00832-8

Qin, S., Du, R., Yin, S., Liu, X., Xu, G., and Cao, W. (2015). Nrf2 Is Essential for the Anti-inflammatory Effect of Carbon Monoxide in LPS-Induced Inflammation. *Inflamm. Res.* 64 (7), 537–548. doi:10.1007/s00011-015-0834-9

Rigas, B. (2007). Novel Agents for Cancer Prevention Based on Nitric Oxide. *Biochem. Soc. Trans.* 35 (5), 1364–1368. doi:10.1042/BST0351364

Robert, A., and Asano, T. (1977). Resistance of Germfree Rats to Indomethacin-Induced Intestinal Lesions. *Prostaglandins* 14 (2), 333–341. doi:10.1016/0090-6980(77)90178-2

Rolando, B., Lazzarato, L., Donnola, M., Marini, E., Joseph, S., Morini, G., et al. (2013). Water-Soluble Nitric-Oxide-Releasing Acetylsalicylic Acid (ASA) Prodrugs. *ChemMedChem* 8 (7), 1199–1209. doi:10.1002/cmdc.201300105

Rossoni, G., Berti, M., Colonna, V. D., Bernareggi, M., Del Soldato, P., and Berti, F. (2000). Myocardial Protection by the Nitroderivative of Aspirin, NCX 4016: In Vitro and In Vivo Experiments in the Rabbit. *Ital. Heart J.* 1 (2), 146–155. http://www.ncbi.nlm.nih.gov/pubmed/10730616.

Rossoni, G., Manfredi, B., Colonna, V. D., Bernareggi, M., and Berti, F. (2001). The Nitroderivative of Aspirin, NCX 4016, Reduces Infarct Size Caused by Myocardial Ischemia-Reperfusion in the Anesthetized Rat. *J. Pharmacol. Exp. Ther.* 297 (1), 380–387. http://www.ncbi.nlm.nih.gov/pubmed/11259566.

Rossoni, G., Manfredi, B., Tazzari, V., Sparatore, A., Trivulzio, S., Del Soldato, P., et al. (2010). Activity of a New Hydrogen Sulfide-Releasing Aspirin (ACS14) on Pathological Cardiovascular Alterations Induced by Glutathione Depletion in Rats. *Eur. J. Pharmacol.* 648 (1-3), 139–145. doi:10.1016/j.ejphar.2010.08.039

Rossoni, G., Sparatore, A., Tazzari, V., Manfredi, B., Soldato, P. D., and Berti, F. (2008). The Hydrogen Sulphide-Releasing Derivative of Diclofenac Protects against Ischaemia-Reperfusion Injury in the Isolated Rabbit Heart. *Br. J. Pharmacol.* 153 (1), 100–109. doi:10.1038/sj.bjp.0707540

Ryan, M., Jernigan, N., Drummond, H., Mclemorejr, G., Rimoldi, J., Poreddy, S., et al. (2006). Renal Vascular Responses to CORM-A1 in the Mouse. *Pharmacol. Res.* 54 (1), 24–29. doi:10.1016/j.phrs.2006.01.012

Ryter, S. W., Ma, K. C., and Choi, A. M. K. (2018). Carbon Monoxide in Lung Cell Physiology and Disease. *Am. J. Physiology-Cell Physiol.* 314 (2), C211–C227. doi:10.1152/ajpcell.00022.2017

Scheiman, J. M., Yeomans, N. D., Talley, N. J., Vakil, N., Chan, F. K. L., Tulassay, Z., et al. (2006). Prevention of Ulcers by Esomeprazole in At-Risk Patients Using Non-selective NSAIDs and COX-2 Inhibitors. *Am. J. Gastroenterol.* 101 (4), 701–710. doi:10.1111/j.1572-0241.2006.00499.x

Schnitzer, T. J., Kivitz, A. J., Lipetz, R. S., Sanders, N., and Hee, A. (2005). Comparison of the COX-Inhibiting Nitric Oxide Donator AZD3582 and Rofecoxib in Treating the Signs and Symptoms of Osteoarthritis of the Knee. *Arthritis Rheum.* 53 (6), 827–837. doi:10.1002/art.21586

Schroeder, B. O., Wu, Z., Nuding, S., Groscurth, S., Marcinowski, M., Beisner, J., et al. (2011). Reduction of Disulphide Bonds Unmasks Potent Antimicrobial Activity of Human β-defensin 1. *Nature* 469 (7330), 419–423. doi:10.1038/nature09674

Shi, Y., and Vanhoutte, P. M. (2017). Macro- and Microvascular Endothelial Dysfunction in Diabetes. *J. Diabetes* 9 (5), 434–449. doi:10.1111/1753-0407.12521

Shindo, K., Machida, M., Fukumura, M., Koide, K., and Yamazaki, R. (1998). Omeprazole Induces Altered Bile Acid Metabolism. *Gut* 42 (2), 266–271. doi:10.1136/gut.42.2.266

Srinivasan, A., and De Cruz, P. (2017). Review Article: a Practical Approach to the Clinical Management of NSAID Enteropathy. *Scand. J. Gastroenterol.* 52 (9), 1–7. doi:10.1080/00365521.2017.1335769

Stanek, A., Gadowska-Cicha, A., Gawron, K., Wielkoszynski, T., Adamek, B., Cieslar, G., et al. (2008). Role of Nitric Oxide in Physiology and Pathology of the Gastrointestinal Tract. *Mrmc* 8 (14), 1549–1560. doi:10.2174/138955708786786462

Sulaieva, O., and Wallace, J. L. (2015). Gaseous Mediator-Based Anti-inflammatory Drugs. *Curr. Opin. Pharmacol.* 25, 1–6. doi:10.1016/j.coph.2015.08.005

Sun, H.-Z., Zheng, S., Lu, K., Hou, F.-T., Bi, J.-X., Liu, X.-L., et al. (2017). Hydrogen Sulfide Attenuates Gastric Mucosal Injury Induced by Restraint Water-Immersion Stressviaactivation of KATPchannel and NF-Kb Dependent Pathway. *Wjg* 23 (1), 87. doi:10.3748/wjg.v23.i1.87

Syer, S. D., Blackler, R. W., Martin, R., de Palma, G., Rossi, L., Verdu, E., et al. (2015). NSAID Enteropathy and Bacteria: a Complicated Relationship. *J. Gastroenterol.* 50 (4), 387–393. doi:10.1007/s00535-014-1032-1

Tai, F. W. D., and McAlindon, M. E. (2018). NSAIDs and the Small Bowel. *Curr. Opin. Gastroenterol.* 34 (3), 175–182. doi:10.1097/MOG.0000000000000427

Takagi, T., Naito, Y., Uchiyama, K., Mizuhima, K., Suzuki, T., Horie, R., et al. (2016). Carbon Monoxide Promotes Gastric Wound Healing in Mice via the Protein Kinase C Pathway. *Free Radic. Res.* 50 (10), 1098–1105. doi:10.1080/10715762.2016.1189546

Takahashi, T., Shimizu, H., Morimatsu, H., Maeshima, K., Inoue, K., Akagi, R., et al. (2009). Heme Oxygenase-1 Is an Essential Cytoprotective Component in Oxidative Tissue Injury Induced by Hemorrhagic Shock. *J. Clin. Biochem. Nutr.* 44 (1), 28–40. doi:10.3164/jcbn.08-210-HO

Takeuchi, K., Ukawa, H., Konaka, A., Kitamura, M., and Sugawa, Y. (1998). Effect of Nitric Oxide-Releasing Aspirin Derivative on Gastric Functional and Ulcerogenic Responses in Rats: Comparison with Plain Aspirin. *J. Pharmacol. Exp. Ther.* 286 (1), 115–121. http://www.ncbi.nlm.nih.gov/pubmed/9655849.

Takeuchi, K., Mizoguchi, H., Araki, H., Komoike, Y., and Suzuki, K. (2001). Lack of Gastric Toxicity of Nitric Oxide-Releasing Indomethacin, NCX-530, in Experimental Animals. *Dig. Dis. Sci.* 46 (8), 1805–1818. doi:10.1023/a:1010638528675

Topol, E. J. (2005). Arthritis Medicines and Cardiovascular Events-"House of Coxibs". *JAMA* 293 (3), 366. doi:10.1001/jama.293.3.366

Van Dingenen, J., Pieters, L., Vral, A., and Lefebvre, R. A. (2019). The H2S-Releasing Naproxen Derivative ATB-346 and the Slow-Release H2S Donor GYY4137 Reduce Intestinal Inflammation and Restore Transit in Postoperative Ileus. *Front. Pharmacol.* 10, 10–116. doi:10.3389/fphar.2019.00116

Vannini, F., Kodela, R., Chattopadhyay, M., and Kashfi, K. (2015a). NOSH-aspirin Inhibits Colon *Cancer* Cell Growth: Effects of Positional Isomerism. *Redox Biol.* 5, 421. doi:10.1016/j.redox.2015.09.033

Vannini, F., MacKessack-Leitch, A. C., Eschbach, E. K., Chattopadhyay, M., Kodela, R., and Kashfi, K. (2015b). Synthesis and Anti-cancer Potential of the Positional Isomers of NOSH-Aspirin (NBS-1120) a Dual Nitric Oxide and Hydrogen Sulfide Releasing Hybrid. *Bioorg. Med. Chem. Lett.* 25 (20), 4677–4682. doi:10.1016/j.bmcl.2015.08.023

Varadi, J., Lekli, I., Juhasz, B., Bacskay, I., Szabo, G., Gesztelyi, R., et al. (2007). Beneficial Effects of Carbon Monoxide-Releasing Molecules on Post-ischemic Myocardial Recovery. *Life Sci.* 80 (17), 1619–1626. doi:10.1016/j.lfs.2007.01.047

Varga, Z., Sabzwariali, S. r. a., and Vargova, V. (2017). Cardiovascular Risk of Nonsteroidal Anti-inflammatory Drugs: An Under-recognized Public Health Issue. *Cureus* 9 (4), e1144. doi:10.7759/cureus.1144

Wallace, J. L., Elliott, S. N., Del Soldato, P., McKnight, W., Sannicolo, F., and Cirino, G. (1997). Gastrointestinal-sparing Anti-inflammatory Drugs: The Development of Nitric Oxide-Releasing NSAIDs. *Drug Dev. Res.* 42 (3-4), 144–149. doi:10.1002/(SICI)1098-2299(199711/12)42:3/4<144::AID-DDR5>3.0.CO;2-Q

Wallace, J. L., Caliendo, G., Santagada, V., Cirino, G., and Fiorucci, S. (2007). Gastrointestinal Safety and Anti-inflammatory Effects of a Hydrogen Sulfide-Releasing Diclofenac Derivative in the Rat. *Gastroenterology* 132 (1), 261–271. doi:10.1053/j.gastro.2006.11.042

Wallace, J. L., Ianaro, A., and de Nucci, G. (2017). Gaseous Mediators in Gastrointestinal Mucosal Defense and Injury. *Dig. Dis. Sci.* 62 (9), 2223–2230. doi:10.1007/s10620-017-4681-0

Wallace, J. L., McKnight, W., Del Soldato, P., Baydoun, A. R., and Cirino, G. (1995). Anti-thrombotic Effects of a Nitric Oxide-Releasing, Gastric-Sparing Aspirin Derivative. *J. Clin. Invest.* 96 (6), 2711–2718. doi:10.1172/JCI118338

Wallace, J. L. (2013). Mechanisms, Prevention and Clinical Implications of Nonsteroidal Anti-inflammatory Drug-Enteropathy. *Wjg* 19 (12), 1861. doi:10.3748/wjg.v19.i12.1861

Wallace, J. L., Muscara, M. N., McKnight, W., Dicay, M., Del Soldato, P., and Cirino, G. (1999). *In Vivo* Antithrombotic Effects of a Nitric Oxide-Releasing Aspirin Derivative, NCX-4016. *Thromb. Res.* 93 (1), 43–50. doi:10.1016/S0049-3848(98)00134-0

Wallace, J. L., and Muscará, M. N. (2001). Selective Cyclo-Oxygenase-2 Inhibitors: Cardiovascular and Gastrointestinal Toxicity. *Dig. Liver Dis.* 33, S21–S28. doi:10.1016/S1590-8658(01)80155-9

Wallace, J. L., Nagy, P., Feener, T. D., Allain, T., Ditrói, T., Vaughan, D. J., et al. (2020). A Proof-of-concept, Phase 2 Clinical Trial of the Gastrointestinal Safety of a Hydrogen Sulfide-releasing Anti-inflammatory Drug. *Br. J. Pharmacol.* 177 (4), 769–777. doi:10.1111/bph.14641

Wallace, J. L. (2012). NSAID Gastropathy and Enteropathy: Distinct Pathogenesis Likely Necessitates Distinct Prevention Strategies. *Br. J. Pharmacol.* 165 (1), 67–74. doi:10.1111/j.1476-5381.2011.01509.x

Wallace, J. L. (2010). Physiological and Pathophysiological Roles of Hydrogen Sulfide in the Gastrointestinal Tract. *Antioxid. Redox Signaling* 12 (9), 1125–1133. doi:10.1089/ars.2009.2900

Wallace, J. L. (2008). Prostaglandins, NSAIDs, and Gastric Mucosal Protection: Why Doesn't the Stomach Digest Itself?. *Physiol. Rev.* 88 (4), 1547–1565. doi:10.1152/physrev.00004.2008

Wallace, J. L., Syer, S., Denou, E., de Palma, G., Vong, L., McKnight, W., et al. (2011). Proton Pump Inhibitors Exacerbate NSAID-Induced Small Intestinal Injury by Inducing Dysbiosis. *Gastroenterology* 141 (4), 1314–1322. doi:10.1053/j.gastro.2011.06.075

Wallace, J. L., Vaughan, D., Dicay, M., MacNaughton, W. K., and de Nucci, G. (2018). Hydrogen Sulfide-Releasing Therapeutics: Translation to the Clinic. *Antioxid. Redox Signaling* 28 (16), 1533–1540. doi:10.1089/ars.2017.7068

Wallace, J. L., and Wang, R. (2015). Hydrogen Sulfide-Based Therapeutics: Exploiting a Unique but Ubiquitous Gasotransmitter. *Nat. Rev. Drug Discov.* 14 (5), 329–345. doi:10.1038/nrd4433

Warner, T. D., Nylander, S., and Whatling, C. (2011). Anti-platelet Therapy: Cyclo-Oxygenase Inhibition and the Use of Aspirin with Particular Regard to Dual Anti-platelet Therapy. *Br. J. Clin. Pharmacol.* 72 (4), 619–633. doi:10.1111/j.1365-2125.2011.03943.x

Watanabe, T., Tanigawa, T., Nadatani, Y., Nagami, Y., Sugimori, S., Okazaki, H., et al. (2013). Risk Factors for Severe Nonsteroidal Anti-inflammatory Drug-Induced Small Intestinal Damage. *Dig. Liver Dis.* 45 (5), 390–395. doi:10.1016/j.dld.2012.12.005

Whelton, A. (1999). Nephrotoxicity of Nonsteroidal Anti-inflammatory Drugs: Physiologic Foundations and Clinical Implications. *Am. J. Med.* 106 (5), 13S–24S. doi:10.1016/S0002-9343(99)00113-8

Wu, L., and Wang, R. (2005). Carbon Monoxide: Endogenous Production, Physiological Functions, and Pharmacological Applications. *Pharmacol. Rev.* 57 (4), 585–630. doi:10.1124/pr.57.4.3

Zanardo, R. C. O., Brancaleone, V., Distrutti, E., Fiorucci, S., Cirino, G., Wallace, J. L., et al. (2006). Hydrogen Sulfide Is an Endogenous Modulator of Leukocyte-mediated Inflammation. *FASEB j.* 20 (12), 2118–2120. doi:10.1096/fj.06-6270fje

Zanellato, I., Bonarrigo, I., Ravera, M., Gabano, E., Gust, R., and Osella, D. (2013). The Hexacarbonyldicobalt Derivative of Aspirin Acts as a CO-releasing NSAID on Malignant Mesothelioma Cells. *Metallomics* 5 (12), 1604. doi:10.1039/c3mt00117b

Zhao, W., Zhang, J., Lu, Y., and Wang, R. (2001). The Vasorelaxant Effect of H2S as a Novel Endogenous Gaseous KATP Channel Opener. *EMBO J.* 20 (21), 6008–6016. doi:10.1093/emboj/20.21.6008

Zuckerbraun, B. S., Chin, B. Y., Wegiel, B., Billiar, T. R., Czsimadia, E., Rao, J., et al. (2006). Carbon Monoxide Reverses Established Pulmonary Hypertension. *J. Exp. Med.* 203 (9), 2109–2119. doi:10.1084/jem.20052267

Conflict of Interest: JW was employed by Antibe Therapeutics, Inc.

The remaining authors declare that the research was conducted in the absence of any commercial or financial relationships that could be construed as a potential conflict of interest.

frontiers in Pharmacology

ORIGINAL RESEARCH
published: 29 April 2021
doi: 10.3389/fphar.2021.667584

Single Capsule Bismuth Quadruple Therapy for Eradication of *H. pylori* Infection: A Real-Life Study

Antonietta G. Gravina†, Kateryna Priadko†, Lucia Granata, Angela Facchiano, Giuseppe Scidà, Rosa Cerbone, Paola Ciamarra and Marco Romano*

Hepatogastroenterology Division, Department of Precision Medicine, University of Campania Luigi Vanvitelli, Naples, Italy

OPEN ACCESS

Edited by:
Thomas Brzozowski, Jagiellonian University Medical College, Poland

Reviewed by:
Stylianos Karatapanis, General Hospital of Rhodes, Greece
Jianzhong Zhang, Chinese Center For Disease Control and Prevention, China
Seng-Kee Chuah, Consultant, China

***Correspondence:**
Antonietta G. Gravina
antoniettagerarda.gravina@unicampania.it

†These authors have contributed equally to this work

Specialty section:
This article was submitted to Gastrointestinal and Hepatic Pharmacology, a section of the journal Frontiers in Pharmacology

Received: *13 February 2021*
Accepted: *17 March 2021*
Published: *29 April 2021*

Citation:
Gravina AG, Priadko K, Granata L, Facchiano A, Scidà G, Cerbone R, Ciamarra P and Romano M (2021) Single Capsule Bismuth Quadruple Therapy for Eradication of H. pylori *Infection: A Real-Life Study. Front. Pharmacol. 12:667584. doi: 10.3389/fphar.2021.667584*

Background and aim: Bismuth quadruple therapy (BQT) or non-bismuth quadruple therapy (i.e., concomitant therapy) (CT) is the first-line regimens to eradicate *H. pylori* infection in areas with high prevalence of clarithromycin (CLA) resistance. Guidelines suggest that in areas of high prevalence of *H. pylori* strains with double resistance (i.e., CLA + metronidazole), BQT should be preferred to CT. The aim of this study was to evaluate the efficacy and safety of BQT administered through the three-in-one pill (Pylera) formulation in a large series of *H. pylori*–infected patients, naive to treatment in a region with high CLA and dual resistance.

Patients and methods: We treated 250 patients (148 F and 102 M, mean age 48.6 years) with H. *pylori* infection naïve to treatment. Patients received esomeprazole 40 mg bid and Pylera 3 tablets qid for 10 days. Diagnosis of H. *pylori* infection was through ^{13}C urea breath test (^{13}C UBT), or stool antigen test or histology, as appropriate. The evaluation of eradication was through ^{13}C UBT at least 45 days after the end of therapy. Incidence of treatment-related adverse events (TRAEs) was assessed through a questionnaire at the end of treatment. Compliance was considered good if at least 90% of medication had been taken. Statistical analysis was per intention-to-treat e per protocol (PP). 95% confidence intervals (CIs) were calculated.

Results: 1) 13 patients (5.2%) discontinued therapy due to side effects; 2) eradication rates in ITT and PP were 227/250 (90.8%; 95% CI 86.3–93.7%) and 226/237 (95.3%; 95% CI 91–99%), respectively; 3) the prevalence of TRAEs was 26.8%; and 4) adherence to treatment was good with compliance greater than 90%.

Conclusion: In this real-life study, we demonstrate that in an area with a high prevalence of *H. pylori* strains with CLA or CLA + metronidazole resistance, BQT using Pylera is an effective therapeutic strategy with ITT eradication rates higher than 90%; this therapy is associated with good compliance and low incidence of side effects.

Keywords: BQT, bismuth quadruple therapy, *H. pylori*, real life, eradication therapy

INTRODUCTION

Helicobacter pylori (*H. pylori*) is a Gram-negative microorganism isolated for the first time in 1982 (Warren and Marshall, 1983). Currently *H. pylori* infection has a worldwide prevalence of about 50%, with the highest prevalence in developing countries related to socioeconomic status within societies and hygiene habits and conditions (Hooi et al., 2017).

H. pylori infection is associated to a number of gastroduodenal pathologic conditions and also extragastric diseases (Kusters et al., 2006; Gravina et al., 2018; Gravina et al., 2020). Up-to-date, *H. pylori* is proved to be main the causative factor of chronic gastritis, peptic ulcer disease, gastric adenocarcinoma, and MALToma (Kusters et al., 2006). Also, dyspepsia associated to *H. pylori* infection is now regarded as an organic form of dyspepsia. The Italian Guidelines and Maastricht V/Florence Consensus recommend test-and-treat strategy in patients with dyspeptic symptoms under the age of 50 years without alarming signs (Zagari et al., 2015; Malfertheiner et al., 2017). H. *pylori* diagnosis should be based on urea breath test (^{13}C) (UBT), monoclonal stool antigen test (SAT), or histology that bear high pre- and posttreatment diagnostic value, while positive serology (i.e., detectable serum levels of IgG against *H. pylori*) does not discriminate past vs. ongoing infection (Zagari et al., 2015; Malfertheiner et al., 2017).

The choice of eradication strategy is another challenging aspect in the management of *H. pylori* infection due to the increasing prevalence of *H. pylori* clinical isolates which are resistant to the antimicrobials currently used to treat the infection. In particular, there is the need of an efficient (i.e., with an eradication rate >90%) first-line empirical therapy because treatment failure leads to an increased prevalence of *H. pylori* resistant strains (Romano et al., 2008). According to Maastricht V/Florence Consensus, the first-line eradication therapy should be based on local prevalence of *H. pylori* strains resistant to clarithromycin (CLA). A country is defined as one with a high CLA resistance when CLA resistance is equal or higher than 15–20% (Malfertheiner et al., 2017). In countries with low resistance to CLA, a 10–14 days triple therapy should be used. On the other side, non-bismuth quadruple (i.e., concomitant) therapy or bismuth quadruple therapy (BQT) should be used in countries with high CLA resistance. Prevalence of *H. pylori* strains with dual resistance to CLA and metronidazole is increasing in many European countries, Italy in particular (De Francesco et al., 2006; Savoldi et al., 2018), thus making it more troublesome to eradicate the infection. While CLA-containing regimens such as concomitant, sequential, or bismuth quadruple therapies are the first-line regimens in regions with CLA resistance over 15%, BQT is the preferred eradication regimen in areas with a high prevalence of dual (CLA + metronidazole) resistance1 (Zagari et al., 2018; Malfertheiner et al., 2017). However, a recent study has demonstrated that concomitant therapy achieves eradication rates comparable to those obtained with BQT (Romano et al., 2020). A recent report based on data collected through the European Registry on *H. pylori* management (Hp-EuReg) on 21,533 patients in various European countries found out that only BQT lasting at least 10 days or optimized 14-day non-bismuth quadruple (i.e., concomitant) therapy is able to achieve eradication rates above 90% (Nyssen et al., 2021).

Besides bacterial resistance, failure of eradication therapy might at least in part be due to an inadequate increase in gastric pH during PPI therapy which leads to a decreased bioavailability of antimicrobials in the gastric lumen in Caucasian subjects in whom prevalence of extensive and intermediate metabolizers of PPI is as high as >95% (Shi and Klotz, 2008). Because of this, it has been suggested (Molina-Infante et al., 2013) to optimize the therapy by doubling the dose of PPI

This study was therefore designed to assess in a large series of patients collected in a single center whether optimized BQT showed high efficacy (i.e., eradication rate over 90%) in the real world, in a region with high CLA and dual resistance. As secondary outcomes, the prevalence of treatment-related adverse events (TRAEs) and compliance to treatment were evaluated

PATIENTS AND METHODS

This is a real-life study performed on consecutive patients referred to the Gastroenterology Unit of University of Campania "L. Vanvitelli" because of dyspeptic symptoms who tested positive for *H. pylori* infection and were naive to treatment from January 2018 to June 2020 (**Figure 1**). Inclusion criteria were as follows: age above 18 years; written informed consent to be enrolled into the study; no previous *H. pylori* eradication treatment; and last use of antibiotics at least four weeks prior to the treatment and/or use of acid suppressing drugs at least two

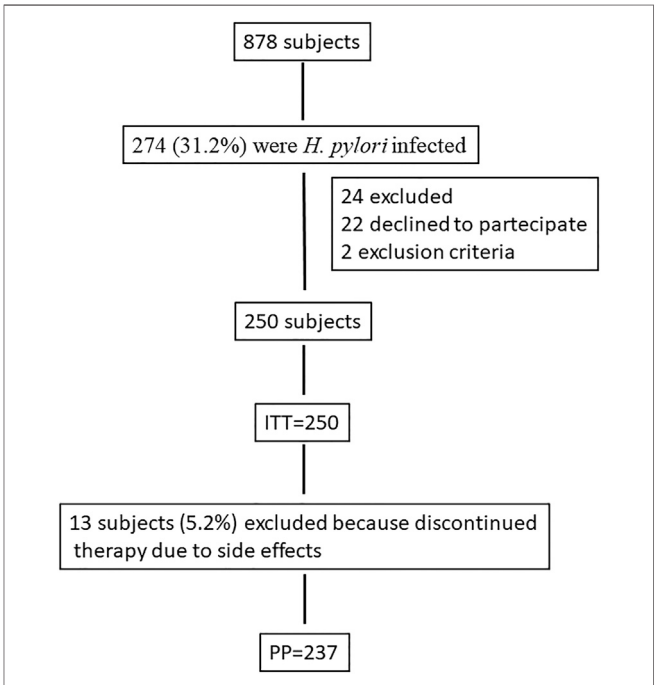

FIGURE 1 | Flow diagram of the study.

TABLE 1 | Baseline information about the study population.

Characteristic	Number (%)
Total subjects	250
Female gender	102 (40.8)
Mean age, years (SD)	48.6 (11.1)
Smoking	82 (32.8)
Test pre-treatment	
^{13}C UBT	143 (57.2)
Histology	89 (35.6)
SAT	10 (4)
SAT + Histology	3 (1.2)
^{13}C UBT + SAT	5 (2)
Test posttreatment	
^{13}C UBT	233 (93.2)
Histology	5 (2)
None	12 (4.8)

weeks prior to treatment. *H. pylori* diagnosis was performed by ^{13}C-urea breath test (^{13}C UBT), stool antigen test (SAT), or histology in those patients who underwent esophagogastroduodenoscopy (EGDS). In particular, for ^{13}C UBT a baseline breath sample was obtained, and 100 mg of ^{13}C urea with citric acid (1.4 g) was administered as an aqueous solution (Expirobacter; SOFAR, Milano, Italy). Another breath sample was collected 30 min later. The test result was considered positive if the difference between the baseline sample and the 30-min sample exceeded 5.0 parts/1,000 of ^{13}CO2 (Federico et al., 2012a). SAT was performed using monoclonal HpSA (HEPY Stool Card Plus, Mascia Brunelli SpA, Milano, Italy).

Assessment of *H. pylori* eradication following the treatment was performed 45 days after the end of treatment in order to minimize the likelihood of false negative results. ^{13}C UBT was used in the vast majority of patients, whereas histology was used only in five patients in whom EGDS was required.

We used single capsule BQT (i.e., Pylera®), approved by the Italian National Health System, for 10 days as an eradication regimen for *H. pylori* infection. Each Pylera capsule contains bismuth subcitrate 140 mg, metronidazole 125 mg, and tetracycline 125 mg. Therapy was as follows: esomeprazole 40 mg before breakfast and dinner + Pylera®three capsules after breakfast, lunch, dinner, and bedtime. The incidence of TRAEs was evaluated via a questionnaire at the end of therapy. Compliance was considered to be good if patients took at least 90% of medications. Patients who did not eradicate the infection were retreated with a 14 days levofloxacin-containing quadruple therapy (i.e., esomeprazole 40 mg bid plus amoxicillin 1 b bid plus levofloxacin 250 mg bid plus tinidazole 500 mg bid).

Statistical Analysis

The primary efficacy variable was the eradication rate of *H. pylori*. We analyzed eradication rates in intention-to-treat (ITT) and per protocol (PP) analysis. ITT analysis included all enrolled subjects who took at least one medicine from the study protocol. PP analysis included only those subjects who strictly adhered to the protocol, received no less than 90% of medications, and underwent eradication confirmatory test that was presented at the follow-up visit. Patients who did not perform eradication test and/or were absent at the follow-up visit were considered lost to follow-up. We calculated mean with standard deviation (SD) for continuous variables and percentages with 95% confidence interval (CI) for categorical variables. A Student t test, chi-squared test, or Fisher exact test, as appropriate, was performed to compare demographic characteristics and eradication rates between treatment groups. A p value of <0.05 was considered statistically significant. All analyses were performed with STATA statistical software (StataCorp).

RESULTS

We screened 878 dyspeptic patients and 274 (31.2%) were *H. pylori* infected. **Figure 1** shows the flow diagram of the study participants. Twenty-four were excluded from the study. A total of 250 patients (148 F and 102 M, mean age 48.6 years) were treated with three-in-one BQT. **Table 1** shows the baseline characteristics of the patients. 13 patients discontinued therapy for side effects (13/250; 5.2%). One of these patients who took therapy for only 7 days, however, underwent ^{13}C UBT, after 45 days from the end of therapy, with a negative result. We calculated eradication rates in ITT and PP analysis, and we obtained eradication in 227/250 (90.8%; 95% CI 86.3–93.7%) in ITT analysis and in 226/237 (95.3%; 95% CI 91–99%) in PP analysis. The prevalence of TRAEs was 26.8% (67/250). Also, 5.2% (13/250) of patients interrupted treatment because experiencing severe TRAE. **Table 2** illustrates TRAE variety and rates. The compliance was good in 237/250 (94.8%) patients who took >90% of prescribed medicines. Ten patients who did not eradicate the infection were retreated with a levofloxacin-containing quadruple therapy and all of them resulted negative 45 days after the end of therapy.

TABLE 2 | Treatment-related adverse events (TRAEs).

TRAEs	n (%)
Patients with TRAEs	67/250 (26.8)
Treatment discontinuation due to TRAEs	13/250 (5.2)
Gastrointestinal disorders	49 (19.6)
Nausea	23/250 (9.2)
Diarrhea	20/250 (8)
Abdominal pain	20/250 (8)
Dyspepsia	10/250 (4)
Vomiting	9/250 (3.6)
Central nervous system	29/250 (11.6)
Dysgeusia	23/250 (9.2)
Headache	11/250 (4.4)
Dizziness	9/250 (3.6)
Sonnolence	2/250 (0.8)
Others	
Asthenia	17/250 (6.8)
Cutaneous itch	3/250 (1.2)

DISCUSSION

Italy is an area with high prevalence of primary resistance toward CLA and metronidazole with a resistance to CLA equal to 30% and a double resistance to CLA and metronidazole as high as 19.3% (Fiorini et al., 2018). In this setting, most of the international guidelines suggest that BQT should be the preferred first-line option (Zagari et al., 2015; Malfertheiner et al., 2017). Recently, a three-in-one pill formulation has been used in place of the conventional BQT, offering the possibility of combining in one pill all of the antimicrobials used in the standard BQT (Di Ciaula et al., 2017; Gómez Rodríguez et al., 2017; Tursi et al., 2017). This formulation has shown to be effective in the treatment of *H. pylori* infection achieving eradication rates ranging from 93 to 98% (Tursi et al., 2017; Gómez Rodríguez et al., 2017). In our single center, real-life study in 250 *H. pylori*–infected patients naive to treatment, we confirm that BQT administered through the novel three-in-one-pill formulation is a highly effective eradication regimen in an area with high prevalence of CLA or double resistance to CLA and metronidazole (Tursi et al., 2017). Eradication rates in ITT analysis were 90.8% (95% CI 86.3–93.7%) and in PP analysis 95.3% (95% CI 91–99%). Our results are therefore similar to those obtained in other studies but on a greater number of patients and in a real-life clinical setting (Romano et al., 2020; Zagari et al., 2018).

Side effects may affect compliance to and efficacy of treatment. In this study, we show that single capsule BQT is associated with good compliance and low incidence of side effects. In our study, compliance was greater than 90% and did not seem to be influenced by the high number of pills which patients had to take daily. Also incidence of TRAEs was of about 26% and only a small percentage of patients (i.e., 5%) discontinued treatment because of severe side effects. This is also in agreement with previous studies (Romano et al., 2020; Fiorini et al., 2018; Gómez Rodríguez et al., 2017; Tursi et al., 2017; Zagari et al., 2018).

Levofloxacin-containing triple therapy has shown efficacy in patients naive to treatment (Federico et al., 2012b). Moreover, Gisbert et al. (2014) showed that levofloxacin-containing eradication regimens are useful as second- or third-line treatment, in particular if bismuth is added. In many countries, such as Italy, bismuth compounds are no longer available, and, therefore, their use in eradication regimens is not possible. According to the recommendations of most international guidelines, we decided to treat patients who failed to eradicate the infection with BQT, using a levofloxacin-containing regimen and decided to increase the efficacy of levofloxacin-containing triple therapy (i.e., the recommended therapy after BQT failure) by adding tinidazole. Although in a small number of subjects, we here demonstrate that a non-bismuth levofloxacin-containing quadruple therapy is highly effective as second-line treatment after failure to eradicate the infection with Pylera. In fact, all of the ten patients who were still positive after single capsule BQT were eradicated of the infection. A study with a larger number of subjects is however necessary to corroborate this result.

The use of PPIs in the eradication of *H. pylori* has demonstrated to increase the eradication rate (Calvet and Gomollón, 2005; Gomollón and Calvet, 2005; McKeage et al, 2008; Baldwin and Keam, 2009; Kirchheiner et al, 2009; McNicholl et al., 2012) by increasing the stability of antibiotics in a less acidic gastric environment thus inducing a higher antibiotic concentration and antibacterial efficacy (McNicholl et al., 2012; Calvet and Gomollón, 2005). Many studies in humans have shown that differences on acid control account for differences in eradication rates and that strong acid inhibition increases the efficacy of *H. pylori* treatments (Boparai et al., 2008; Gisbert et al., 2003). Therefore, in our clinical setting, we decided to optimize therapy by doubling the daily dose of esomeprazole (i.e., 40 mg bid) as already successfully done in previous studies (Romano et al., 2020; McNicholl et al., 2012).

This study has some limitations. First, we do not have a control group of patients treated with a different eradication schedule to compare the efficacy of BQT with. However, in a multicenter study in collaboration with Spain, we demonstrated that 14 days CLA-containing concomitant therapy achieved ITT eradication rates of 91.7% (Molina-Infante et al., 2013). Second, in this real-life study, we do not provide information regarding the prevalence of *H. pylori* antimicrobial resistance, which, according to major guidelines (Zagari et al., 2015; Malfertheiner et al., 2017), should searched for only in case of multiple eradication failures. However, we showed previously that in our region the prevalence of *H. pylori* antimicrobial resistance was 26.1% vs. CLA, 33% vs. metronidazole and 7.1% vs. CLA + metronidazole with no *H. pylori* strains resistant to amoxicillin or tetracycline (Molina-Infante et al., 2013).

In summary, this real-life study in an area of high prevalence of *H. pylori* strains with CLA and double resistance shows that an optimized 10 days BQT through the use of the three-in-one capsule is highly effective in eradicating the infection. Moreover, compliance to treatment was optimal with almost all patients taking more than 90% of prescribed medication. Finally, the incidence of TRAEs was as low as 26% with only a minority of patients experiencing severe side effects.

We conclude that optimized single capsule BQT should be recommended as first-line treatment of *H. pylori* infections in areas with high CLA or dual resistance.

DATA AVAILABILITY STATEMENT

The raw data supporting the conclusions of this article will be made available by the authors, without undue reservation.

ETHICS STATEMENT

The studies involving human participants were reviewed and approved by the Ethics Committee of Univeristy of Campania L. Vanvitelli. The patients/participants provided their written informed consent to participate in this study.

AUTHOR CONTRIBUTIONS

All the authors participated in the preparation of the manuscript. Study concept and design: AG, KP, and MR. Acquisition of data: LG, AF, RC, and PC. Analysis and interpretation of data: AG, KP, and GS. Drafting of the manuscript: AG and KP. Critical revision of the manuscript for important intellectual content: AG, KP, and MR. Statistical analysis: GS and PC. Study supervision: AG, KP, and MR. All authors are responsible for the content of the work.

ACKNOWLEDGMENTS

Research activity of AGG was supported by VALERE Program

REFERENCES

Baldwin, C. M., and Keam, S. J. (2009). Rabeprazole: a review of its use in the management of gastric acid-related diseases in adults. *Drugs* 69 (10), 1373–1401. doi:10.2165/00003495-200969100-00007

Boparai, V., Rajagopalan, J., and Triadafilopoulos, G. (2008). Guide to the use of proton pump inhibitors in adult patients. *Drugs* 68 (7), 925–947. doi:10.2165/00003495-200868070-00004

Calvet, X., and Gomollón, F. (2005). What is potent acid inhibition, and how can it be achieved? *Drugs* 65 (Suppl. 1), 13–23. doi:10.2165/00003495-200565001-00004

De Francesco, V., Margiotta, M., Zullo, A., Hassan, C., Valle, N. D., Burattini, O., et al. (2006). Claritromycin resistance and *Helicobacter pylori* genotypes in Italy. *J. Microbiol.* 44 (6), 660–664.

Di Ciaula, A., Scaccianoce, G., Venerito, M., Zullo, A., Bonfrate, L., Rokkas, T., et al. (2017). Eradication rates in Italian subjects heterogeneously managed for *Helicobacter pylori* infection. Time to abandon empiric treatments in Southern Europe. *Jgld* 26 (2), 129–137. doi:10.15403/jgld.2014.1121.262.itl

Federico, A., Nardone, G., Gravina, A. G., Iovene, M. R., Miranda, A., Compare, D., et al. (2012a). Efficacy of 5-day levofloxacin-containing concomitant therapy in eradication of *Helicobacter pylori* infection. *Gastroenterology* 143 (1), 55–61.e1. doi:10.1053/j.gastro.2012.03.043

Federico, A., Nardone, G., Gravina, A. G., Iovene, M. R., Miranda, A., Compare, D., et al. (2012b). Efficacy of 5-day levofloxacin-containing concomitant therapy in eradication of *Helicobacter pylori* infection. *Gastroenterology* 143 (1), 55–61.e1. doi:10.1053/j.gastro.2012.03.043

Fiorini, G., Zullo, A., Saracino, I. M., Gatta, L., Pavoni, M., and Vaira, D. (2018). Pylera and sequential therapy for first-line Helicobacter pylori eradication: a culture-based study in real clinical practice. *Eur. J. Gastroenterol. Hepatol.* 30 (6), 621–625. doi:10.1097/MEG.0000000000001102

Gómez Rodríguez, B. J., Castro Laria, L., Argüelles Arias, F., Castro Márquez, C., Caunedo Álvarez, Á., and Romero Gómez, M. (2017). A real life study of *Helicobacter pylori* eradication with bismuth quadruple therapy in naïve and previously treated patients. *Rev. Esp Enferm Dig.* 109 (8), 552–558. doi:10.17235/reed.2017.4809/2016

Gisbert, J. P. P., Khorrami, X., Calvet, J. M., and Pajares, J. M. (2003). Systematic review: Rabeprazole-based therapies in *Helicobacter pylori* eradication. *Aliment. Pharmacolther* 17 (6), 751–764. doi:10.1046/j.1365-2036.2003.01450.x

Gisbert, J. P., Perez-Aisa, A., Perez-Aisa, A., Rodrigo, L., Molina-Infante, J., Modolell, I., et al. (2014). Third-line rescue therapy with bismuth-containing quadruple regimen after failure of two treatments (with clarithromycin and levofloxacin) for *H. pylori* infection. *Dig. Dis. Sci.* 59 (2), 383–389. doi:10.1007/s10620-013-2900-x

Gomollón, F., and Calvet, X. (2005). Optimising acid inhibition treatment. *Drugs* 65 (Suppl. 1), 25–33. doi:10.2165/00003495-200565001-00005

Gravina, A. G., Priadko, K., Ciamarra, P., Granata, L., Facchiano, A., Miranda, A., et al. (2020). Extra-gastric manifestations of *Helicobacter pylori* infection. *J Clin Med.* 9 (12), 3887. doi:10.3390/jcm9123887

Gravina, A. G., Zagari, R. M., Musis, C. D., Romano, L., Loguercio, C., and Romano, M. (2018). *Helicobacter* pyloriand extragastric diseases: a review. *World J Gastroenterol.* 24 (29), 3204–3221. doi:10.3748/wjg.v24.i29.3204

Hooi, J. K. Y., Lai, W. Y., Ng, W. K., Suen, M. M. Y., Underwood, F. E., Tanyingoh, D., et al. (2017). Global prevalence of *Helicobacter pylori* infection: systematic review and meta-analysis. *Gastroenterology* 153 (2), 420–429. doi:10.1053/j.gastro.2017.04.022

Kirchheiner, J., Glatt, S., Fuhr, U., Klotz, U., Meineke, I., Seufferlein, T., et al. (2009). Relative potency of proton-pump inhibitors-comparison of effects on intragastric pH. *Eur. J. Clin. Pharmacol.* 65 (1), 19–31. doi:10.1007/s00228-008-0576-5

Kusters, J. G., van Vliet, A. H. M., and Kuipers, E. J. (2006). Pathogenesis of *Helicobacter pylori* infection. *Cmr* 19 (3), 449–490. doi:10.1128/CMR.00054-05

Malfertheiner, P., Megraud, F., O'Morain, C. A., Gisbert, J. P., Kuipers, E. J., Axon, A. T., et al. (2017). Management of *Helicobacter pylori* infection-the Maastricht V/Florence consensus report. *Gut* 66 (1), 6–30. doi:10.1136/gutjnl-2016-312288

McKeage, K., Blick, S. K. A., Croxtall, J. D., Lyseng-Williamson, K. A., and Keating, G. M. (2008). Esomeprazole: a review of its use in the management of gastric acid-related diseases in adults. *Drugs* 68 (11), 1571–1607. doi:10.2165/00003495-200868110-00009

McNicholl, A. G., Linares, P. M., Nyssen, O. P., Calvet, X., and Gisbert, J. P. (2012). Meta-analysis: esomeprazole or rabeprazole vs. first-generation pump inhibitors in the treatment of *Helicobacter pylori* infection. *Aliment. Pharmacol. Ther.* 36 (5), 414–425. doi:10.1111/j.1365-2036.2012.05211.x

Molina-Infante, J., Romano, M., Fernandez-Bermejo, M., Federico, A., Gravina, A. G., Pozzati, L., et al. (2013). Optimized nonbismuth quadruple therapies cure most patients with *Helicobacter pylori* infection in populations with high rates of antibiotic resistance. *Gastroenterology* 145 (1), 121–128.e1. doi:10.1053/j.gastro.2013.03.050

Nyssen, O. P., Bordin, D., Tepes, B., Pérez-Aisa, Á., Pérez-Aisa, Á., Vaira, D., Caldas, M., et al. (2021). European Registry on *Helicobacter pylori* management (Hp-EuReg): patterns and trends in first-line empirical eradication prescription and outcomes of 5 years and 21 533 patients. *Gut* 70 (1), 40–54. doi:10.1136/gutjnl-2020-321372

Romano, M., Iovene, M. R., Russo, M. I., Rocco, A., Salerno, R., Cozzolino, D., et al. (2008). Failure of first-line eradication treatment significantly increases prevalence of antimicrobial-resistant *Helicobacter pylori* clinical isolates. *J. Clin. Pathol.* 61 (10), 1112–1115. doi:10.1136/jcp.2008.060392

Romano, M., Gravina, A. G., Nardone, G., Federico, A., Dallio, M., Martorano, M., et al. (2020). Non-bismuth and bismuth quadruple therapies based on previous clarithromycin exposure are as effective and safe in an area of high clarithromycin resistance: a real-life study. *Helicobacter* 25 (4), e12694. doi:10.1111/hel.12694

Savoldi, A., Carrara, E., Graham, D. Y., Conti, M., and Tacconelli, E. (2018). Prevalence of antibiotic resistance in *Helicobacter pylori*: a systematic review and meta-analysis in world Health organization regions. *Gastroenterology* 155 (5), 1372–1382.e17. doi:10.1053/j.gastro.2018.07.007

Shi, S., and Klotz, U. (2008). Proton pump inhibitors: an update of their clinical use and pharmacokinetics. *Eur. J. Clin. Pharmacol.* 64 (10), 935–951. doi:10.1007/s00228-008-0538-y

Tursi, A., Di Mario, F., Franceschi, M., De Bastiani, R., Elisei, W., Baldassarre, G., et al. (2017). New bismuth-containing quadruple therapy in patients infected with *Helicobacter pylori* : a first Italian experience in clinical practice. *Helicobacter* 22 (3), e12371. doi:10.1111/hel.12371

Warren, J. R, and Marshall, B. (1983). Unidentified curved bacilli on gastric epithelium in active chronic gastritis. *Lancet* 1 (8336), 1273–1275.

Zagari, R. M., Romano, M., Ojetti, V., Stockbrugger, R., Gullini, S., Annibale, B., et al. (2015). Guidelines for the management of *Helicobacter pylori* infection in Italy: the III working group consensus report 2015. *Dig. Liver Dis.* 47 (11), 903–912. doi:10.1016/j.dld.2015.06.010

Zagari, R. M., Romiti, A., Ierardi, E., Gravina, A. G., Panarese, A., Grande, G., et al. (2018). The "three-in-one" formulation of bismuth quadruple therapy forHelicobacter pylorieradication with or without probiotics supplementation: efficacy and safety in daily clinical practice. *Helicobacter* 23 (4), e12502. doi:10.1111/hel.12502

Conflict of Interest: The authors declare that the research was conducted in the absence of any commercial or financial relationships that could be construed as a potential conflict of interest.

frontiers in Pharmacology

REVIEW
published: 04 May 2021
doi: 10.3389/fphar.2021.681417

Chemotherapeutics-Induced Intestinal Mucositis: Pathophysiology and Potential Treatment Strategies

David Dahlgren[1], *Markus Sjöblom*[2], *Per M Hellström*[3] *and Hans Lennernäs*[1]*

[1]Department of Pharmaceutical Biosciences, Uppsala University, Uppsala, Sweden, [2]Department of Neuroscience, Division of Physiology, Uppsala University, Uppsala, Sweden, [3]Department of Medical Sciences, Gastroenterology/Hepatology, Uppsala University, Uppsala, Sweden

The gastrointestinal tract is particularly vulnerable to off-target effects of antineoplastic drugs because intestinal epithelial cells proliferate rapidly and have a complex immunological interaction with gut microbiota. As a result, up to 40–100% of all cancer patients dosed with chemotherapeutics experience gut toxicity, called chemotherapeutics-induced intestinal mucositis (CIM). The condition is associated with histological changes and inflammation in the mucosa arising from stem-cell apoptosis and disturbed cellular renewal and maturation processes. In turn, this results in various pathologies, including ulceration, pain, nausea, diarrhea, and bacterial translocation sepsis. In addition to reducing patient quality-of-life, CIM often leads to dose-reduction and subsequent decrease of anticancer effect. Despite decades of experimental and clinical investigations CIM remains an unsolved clinical issue, and there is a strong consensus that effective strategies are needed for preventing and treating CIM. Recent progress in the understanding of the molecular and functional pathology of CIM had provided many new potential targets and opportunities for treatment. This review presents an overview of the functions and physiology of the healthy intestinal barrier followed by a summary of the pathophysiological mechanisms involved in the development of CIM. Finally, we highlight some pharmacological and microbial interventions that have shown potential. Conclusively, one must accept that to date no single treatment has substantially transformed the clinical management of CIM. We therefore believe that the best chance for success is to use combination treatments. An optimal combination treatment will likely include prophylactics (e.g., antibiotics/probiotics) and drugs that impact the acute phase (e.g., anti-oxidants, apoptosis inhibitors, and anti-inflammatory agents) as well as the recovery phase (e.g., stimulation of proliferation and adaptation).

Keywords: chemotherapeutics-induced mucositis, gastrointestinal physiology, intestinal proliferation, cancer, stem cells, toxicity, mucositis

OPEN ACCESS

Edited by:
Predrag Sikiric,
University of Zagreb, Croatia

Reviewed by:
Pamela Del Carmen Mancha-Agresti,
Federal University of Minas Gerais, Brazil
Oksana Zayachkivska,
Danylo Halytsky Lviv National Medical University, Ukraine

***Correspondence:**
Hans Lennernäs
hans.lennernas@farmbio.uu.se

Specialty section:
This article was submitted to Gastrointestinal and Hepatic Pharmacology, a section of the journal Frontiers in Pharmacology

Received: *16 March 2021*
Accepted: *19 April 2021*
Published: *04 May 2021*

Citation:
Dahlgren D, Sjöblom M, Hellström PM and Lennernäs H (2021) Chemotherapeutics-Induced Intestinal Mucositis: Pathophysiology and Potential Treatment Strategies. Front. Pharmacol. 12:681417. doi: 10.3389/fphar.2021.681417

INTRODUCTION

Chemotherapy is in general associated with extensive anti-tumor effects, but also serious adverse effects and long-term safety issues for both cancer patients and healthcare providers (Sougiannis et al., 2021). One of the more common off-target toxicities is chemotherapeutics-induced intestinal mucositis (CIM), which is a complex gastrointestinal (GI) complication. It affects up to 40–100% of all cancer patients

dosed with chemotherapeutics, depending drug and dosing regimen (Sonis et al., 2015; Villa and Sonis, 2015). The GI tract is particularly vulnerable to antineoplastic drugs that inhibit cell growth and/or cell division, as the intestinal epithelial cells (IEC) proliferate rapidly and have a complex immunological interaction with the gut microbiota. For instance, antineoplastic drugs such as 5-fluorouracil, methotrexate, irinotecan, and doxorubicin target the vulnerable GI tissue by interrupting DNA synthesis, leading to apoptosis. An inability to resist damage and/or rapidly repair and restore the epithelial barrier function after chemotherapy is detrimental to the cancer patient, as it can result in various pathologies, including inflammation, ulceration, pain, nausea, diarrhea, sepsis, and multiple organ dysfunction and failure (Keefe et al., 2004). In addition to reducing the quality-of-life of these patients, CIM often leads to dose-reduction and subsequent decrease of anticancer effect, sometimes even resulting in death.

Despite substantial improvements in cancer treatments and a continuous decline in its incidence in the population, CIM remains a significant and common clinical challenge in many cancer patients (Henley et al., 2020). Consequently, there is a strong consensus that effective strategies are needed for the prevention and treatment of CIM, including new monotherapies and drug combinations (Scarpignato and Bjarnason, 2019; Dahlgren et al., 2020). Crucial to this endeavor is a better understanding of the pathophysiological factors and adaptive processes involved in the regulation and repair of an injured intestinal epithelium (Odenwald and Turner, 2017). For instance, glucagon-like peptide-1 (GLP-1) and -2 (GLP-2) have a central role in the adaptive recovery response in the small intestine (Hytting-Andreasen et al., 2018; Billeschou et al., 2021). Our contribution to this field is the development of relevant *in vivo* models that provide us with a conceptual and rational approach to treat CIM, coupled with a close and rapid collaboration with clinical partners. This review presents an overview of the functions and physiology of the healthy intestinal barrier followed by a summary of the pathophysiological mechanisms involved in the development of CIM. A literature search was performed using the Pub-Med without any time limit for article inclusion, using the following search words: chemotherapeutics-induced intestinal mucositis, intestinal mucositis, chemotherapeutics gut toxicity, chemotherapeutics gastrointestinal side-effects. Finally, we highlight some of the available pharmacological and microbial interventions (prophylactic, acute, and recovery) that have shown clinical potential, with an emphasis on combination treatments. The main objective of this review was to scrutinize and analyze CIM and to discuss and propose a few novel medical strategies.

ANATOMY AND PHYSIOLOGICAL FUNCTIONS OF THE GASTROINTESTINAL TRACT

Anatomy

The morphology of the intestinal barrier varies between regions, but it has a common histology composed of four distinct layers: the mucosa (epithelium, lamina propria, and muscularis mucosae); the submucosa; the muscle layer (circular and longitudinal muscle, and the in-between myenteric nerve plexus); and the serosa. The first barrier between lumen and blood is the mucosal epithelium, which is comprised of columnar IEC covered by a protective mucus layer (Johansson et al., 2013). The IECs are sealed together at the apical surface by tight junction proteins, which form the primary physical barrier to small hydrophilic molecules (approximately less than 250 Da) across the IEC (Fagerholm et al., 1999; Van Itallie and Anderson, 2004). These structurally and biochemically differentiated paracellular regions primarily include tight junctions and anchoring junctions. Tight junctions hold the cells together and form a near leak-proof intercellular seal by fusing adjacent cell membranes, while the anchoring junctions provide essential adhesive and mechanical properties (Andrade et al., 2015). In the small intestine, the mucosa is built up by finger-like villous protrusions that increase the surface area by a factor of about 6 compared to a smooth tube (Helander and Fändriks, 2014). The lamina propria below the IEC layer contains blood vessels, nerve fibers, lymphatic vascular systems, smooth muscle that regulates blood flow and villi movement, and immune cells such as neutrophils, T-regulatory cells, macrophages, and mast cells (about 1 to 10 immune cells per IEC in the epithelium) (Mowat and Agace, 2014). It also contains the most recently identified cells of the innate immune system, the innate lymphoid cells, where they are involved in and coordinate tissue homeostasis during for instance infection, inflammation and cancer by promoting remodeling, healing and repair (Artis and Spits, 2015). The submucosa contains connective tissue with major blood and lymphatic vessels (Bernier-Latmani and Petrova, 2017). The muscle layer contains the submucous plexus, glial cells, cells of Cajal, and circular and longitudinal muscles that control GI movement, while the serosa is mainly composed of connective tissue that supports the GI tract in the abdominal cavity.

The neurons and their nerve fibers in the GI tract are jointly called the enteric nervous system, which is involved in regulation of peristalsis, secretion, digestion and absorption (Furness, 2012). Intestinal microbiota is also sometimes regarded as a part of the GI system, where it is part of a harmonious ecosystem together with the host. It has recently been estimated that the human body hosts up to 10^{13} bacteria, and therefore, about 50% of the cells in our body are non-eukaryotic (Sender et al., 2016). Luminal bacteria and mucosal immune cells show region-related distribution with a higher abundance of bacteria in the distal regions and a more varied immune cell distribution (Mowat and Agace, 2014; Donaldson et al., 2016). Together, they have synergetic roles in maintaining intestinal homeostasis and also the dysregulation associated with intestinal inflammation (Holzapfel et al., 1998).

Physiological Functions

The primary physiological functions of the GI tract are to digest food and to absorb water and nutrients from the intestines and regulate metabolism. In parallel it acts as a dynamic barrier preventing absorption of peptides/proteins/xenobiotics/toxins and translocation of microbes and viruses into the underlying tissue, organs, and systemic circulation (Marchiando et al., 2010). The intestinal mucosa is thus a selective barrier with the complex

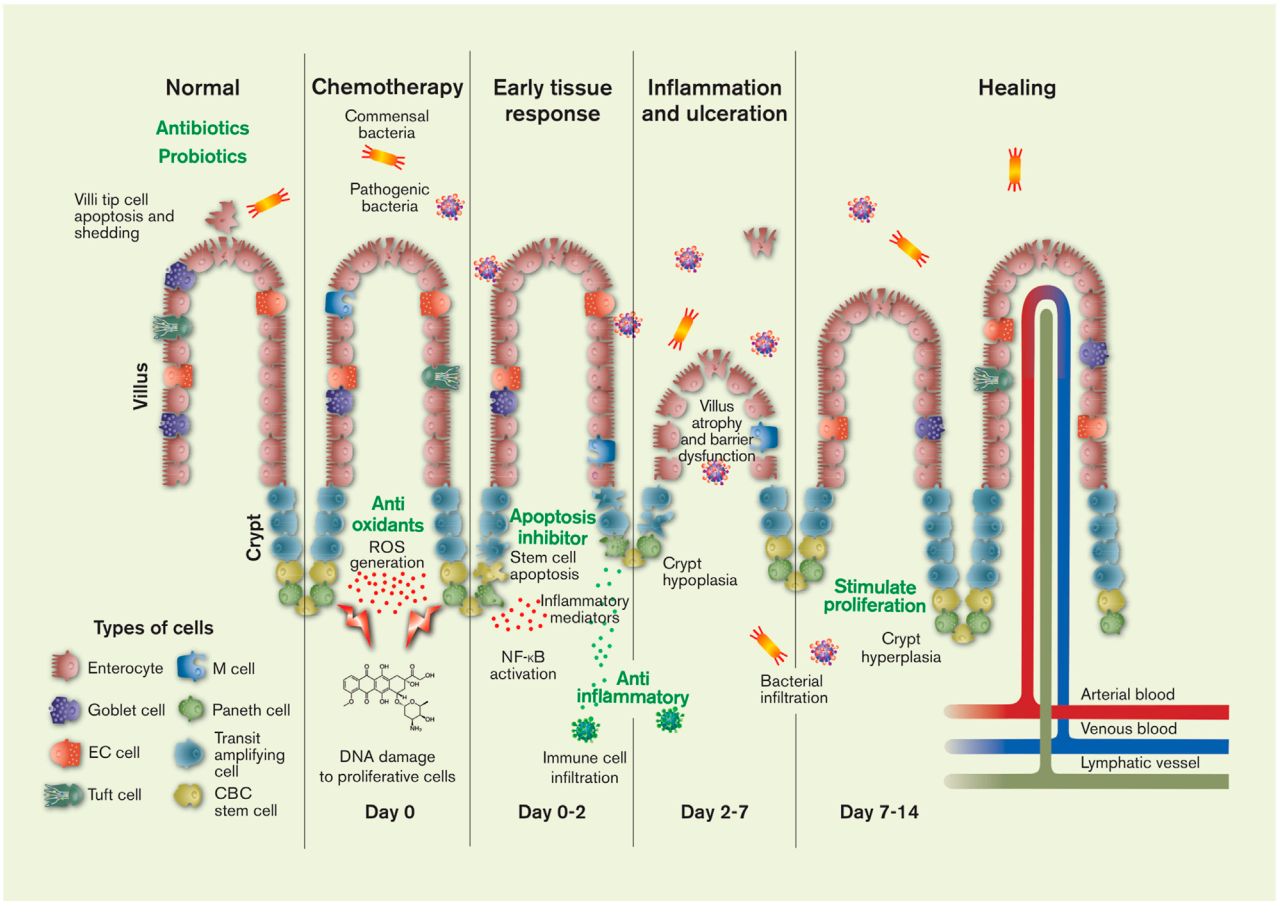

FIGURE 1 | The pathology and timeline of chemotherapeutics-induced intestinal mucositis is primarily related to the effect of cytostatics on stem cells in the proliferation zone of the crypts: crypt base columnar (CBC) stem cells and transit amplifying daughter stem cells. Injury to the DNA of these cells causes apoptosis and initiates of a range of local tissue responses. These include generation of reactive oxygen species (ROS) and inflammation mediators, leading to further injury, inflammation, ulceration, villus and crypt atrophy, and the interstitial infiltration of luminal bacteria (commensal and pathogenic) and immune cells. After about 2 weeks the histology of the intestine is restored in humans (1 week in rodents). The green texts show potential targets for CIM intervention. The figure also shows the six different mature cell types of the intestines, the villi protrusions present in the small intestine, and the lymphatic, venous and arterial vessels. Artwork by Febe Jacobsson. EC = enterochromaffin.

task of simultaneously balancing optimal protection against the harsh biochemical and mechanical luminal environment while allowing efficient nutrient absorption (Dahlgren et al., 2014; Ahluwalia et al., 2017). The GI tract is also a highly specialized chemosensory organ, with the capacity to sense nutrients *via* various receptors from the luminal side to optimize and coordinate digestion, metabolism, and absorption of the diet following ingestion of food and fluids, as well as in the defense response to pathogens present in the lumen. The ingestion of a meal starts neural and hormonal signaling from the GI tract in response to gastric distension and the chemical presence of nutrients in the GI lumen (Steinert et al., 2016).

The permeability and health of the intestinal barrier is strictly regulated by a range of neuroendocrine processes, hormones, and luminal stimuli that jointly aim at upholding homeostasis in conjunction with the different IEC (Chelakkot et al., 2018). The intestinal epithelium contains six mature cell types with distinctly different functions: two absorptive IECs (enterocytes and M cells) and four secretory IECs (goblet cells, enteroendocrine cells, Paneth cells, and tuft cells) (**Figure 1**). The function of the enterocytes is to absorb nutrients, water and ions; they constitute about 80% of the intestinal cells (Gehart and Clevers, 2019). The M-cells are part of the gut-associated lymphoid tissue—the largest immunological tissue in the body—where they allow some uptake of luminal bacteria, thereby triggering or preventing an immunological response depending on the antigen (Ohno, 2016). Thus, the microflora in the intestinal lumen is essential for normal intestinal function and plays an important dynamic role in health and disease progression. Two of the secretory cells primarily secrete into the lumen, where goblet cells secrete protective mucus and the Paneth cells anti-microbial compounds. The other two secretory

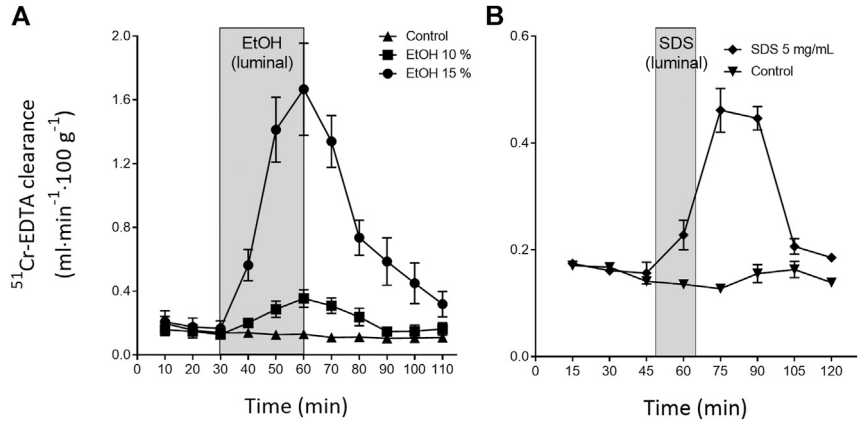

FIGURE 2 | Illustration of the rapid recovery (about 60 min) of the rat small intestinal blood-to-lumen 51Cr-EDTA clearance following local luminal exposure to saline (white area) and two mucosal irritants (grey area): **(A)** ethanol 30 min (Sommansson et al., 2013b) and **(B)** sodium dodecyl sulfate (SDS, anionic surfactant) 15 min (Dahlgren et al., 2018b).

cells secrete primarily into the interstitium as a response to luminal stimuli. The tuft cells are involved in the defense against parasitic infections. The enteroendocrine cells secrete more than 30 different peptide hormones involved in a range of GI and systemic functions, which makes the gut the largest endocrine system in the body (Gribble and Reimann, 2016).

PATHOPHYSIOLOGY OF CHEMOTHERAPEUTICS-INDUCED MUCOSITIS

Normal Injury Response and Mucosal Proliferation

The continuous, everyday mechanical and/or chemical injury to the outer villi sections and epithelium in the lumen is repaired within minutes to hours. This is exemplified in **Figure 2**, which shows the changes in intestinal permeability of the clinical mucosal integrity marker, 51Cr-EDTA (Dahlgren et al., 2017), following luminal exposure of the rat small intestine to ethanol and sodium dodecyl sulfate. This acute repair process re-establishes the tight junctions thereby restoring the intestinal barrier function and avoiding translocation of harmful luminal bacteria and macromolecules into the underlying mucosa. The repair is also crucial for re-establishing other cellular functions, including water regulation and nutrient absorption. The intestinal integrity and local tissue homeostasis is initially upheld by restitution. This is a process in which IEC at the tip of the villi, and injured IEC, undergo different types of cell death, such as anoikis, apoptosis, necroptosis and pyroptosis (Patankar and Becker, 2020). Dead cells slough off, while neighbouring epithelial cells migrate to close the gap. In healthy intestine, this process occurs without any clinically relevant loss of barrier function (Marchiando et al., 2011; Gehart and Clevers, 2019).

A prerequisite for restitution is a continuous renewal of cells from the lower layer of the epithelium. This renewal takes place in the crypts of Lieberkühn, the proliferative region of the intestinal mucosa. These crypts are positioned at the base of the villus protrusions in the small intestine, and directly on the flat surface of the colon. The crypts are invaginations in the epithelium that are protected from mechanical and chemical injury and pathogens, from the luminal side. Each crypt is thought to contain about 15 crypt base columnar stem cells located at cell positions 1-3 (cp1-cp3) from the bottom, wedged between the Paneth cells that secrete anti-microbial compounds. (Potten et al., 2009) These stem cells divide infinitely once every 24 h to initially form a transit population of rapidly dividing progeny cells. These in turn each divide about six times in total, adding up to about 300 new cells per day per crypt (Gehart and Clevers, 2019). As there are about 4–10 crypts per villus depending on small intestinal region (Keefe, 1998), about 1200–3000 cells are shed every day for each villus.

Generation 1 transit population cells at cell position 4 from the bottom (called +4 cell or cp4) to 3 (cp6) divide rapidly and are uncommitted, whereas the transit population cells are committed from generation 4 (cp7) (Duncan and Grant, 2003; Gehart and Clevers, 2019). These committed cells differentiate into the six distinct intestinal cell types, as discussed previously. With the exception of the Paneth cells that travel to the bottom of the crypts, these post-mitotic cells are pushed outward by the constant renewal in the crypts, and they travel along the villus to finally undergo apoptosis and shedding into the lumen at the tip (Gehart and Clevers, 2019). This way only mature cell types face the harsh environment of the lumen, and only for a relative short time; the epithelial surface of the intestine is renewed about every 3–4 days (Darwich et al., 2014). The sources and essential signalling pathways—and their complex interplay in the determination of cell proliferation and differentiation in the intestinal crypts—have been elegantly illustrated by Gehart and Clevers (Gehart and Clevers, 2019). In principal these processes are balanced by two opposing top-to-bottom crypt gradients. In the one gradient, WNT secreted by the Paneth cells and mesenchymal cells in the crypt bottom maintain stem cell function. In the other gradient, bone morphogenetic proteins—secreted by mesenchymal cells higher up in the crypts—counteract the effect of WNT to induce cell maturation.

Wnt signaling is a highly conserved pathway that plays principal regulatory roles in many developmental and biological processes. Besides its crucial role in tissue homeostasis, Wnt signaling is also found to be activated aberrantly in many human diseases, including cancers and metabolic disorders (Novellasdemunt et al., 2015).

Mechanisms for Chemotherapeutics-Induced Mucositis

The DNA of crypt stem cells is well protected from the luminal environment. Fluid flows steadily outwards and interspaced Paneth cells secrete antimicrobial products, making crypts essentially a sterile environment (Nylander and Sjöblom, 2007; Wehkamp and Stange, 2020). However, injury to the DNA in stem cells may arise from events like radiation and cytostatics, causing the cells to go into apoptosis as well as other types of cell death. Still, even when the stem cell pool is completely wiped out it is replenished within a few days. This is possible primarily because initial generations of progeny cells may revert back to the parent stem cell type in the crypt when these are lost. However, others claim that also more committed cells may de-differentiate and repopulate the crypt stem cells upon injury (Buczacki et al., 2013; Yan et al., 2017).

One key issue with chemotherapy is what happens when the cell mitosis and amplification processes in the cryptal stem cells and progenitor cells are compromised by apoptosis. The degree of apoptosis and the local cryptal variations differ depending what cytostatic drug that is used (Ijiri and Potten, 1983). Regardless, normal cell maturation and regeneration of the epithelium is impaired, which means that the continuous (normal) shedding of apoptotic IECs at the tip of the villi is unaccompanied by adequate cellular renewal. In addition, antineoplastic drugs may also be harmful to non-dividing cell populations in the intestine, potentiating any negative effects of an altered cryptal cell renewal. For example, the cytostatic doxorubicin (DOX) is associated with both production of reactive oxygen species and mitochondrial dysfunction (van der Zanden et al., 2020).

Sonis et al. have proposed a general five-stage model for the development of CIM over time (**Figure 1**): 1) initiation, 2) signalling activation and primary damage response, 3) amplification of biological pathways, 4) tissue inflammation and ulceration, and 5) healing (Sonis, 2009; Al-Dasooqi et al., 2013). The *initiation phase* is characterized both by direct DNA injury and the generation of reactive oxygen species. The *primary damage response* starts within seconds of DNA strand breaks and the reactive oxygen species *activate signalling* factors such as Wnt/β-catenin, p53, caspase-1/3, Bcl-2 and NF-κB, and their associated pathways (Bowen et al., 2006; Sukhotnik et al., 2014; Bowen et al., 2019). These effects jointly cause death to the intestinal stem cell population and subsequent breakdown of the intestinal barrier. NF-κB is especially well studied in CIM, because it plays a fundamental role in pathogenesis by regulating a range of cytokines (e.g., TNF-α, IL-6, IL-1, IL-18, and IL-33), stress responders, cell adhesion molecules, as well as apoptosis in normal cell populations (Ribeiro et al., 2016). Many of these effects leads to *signalling amplification*, whereby the positive and negative feedback responses of the initial factors affect the local tissue in a complicated biochemical interplay. For instance, NF-κB activates TNF-α release, which in turn activates more NF-κB. The overall effect of the overwhelming biochemical response is mucosal *inflammation and ulceration*, characterized by an ablation of the epithelial villi, a disruption of IEC adhesion, and an increased translocation of luminal components and immune cells into the lamina propria. This cascade of events leads to even more inflammation. The final stage is the spontaneous *healing* phase in which normal epithelial proliferation, migration, differentiation and maturation are restored.

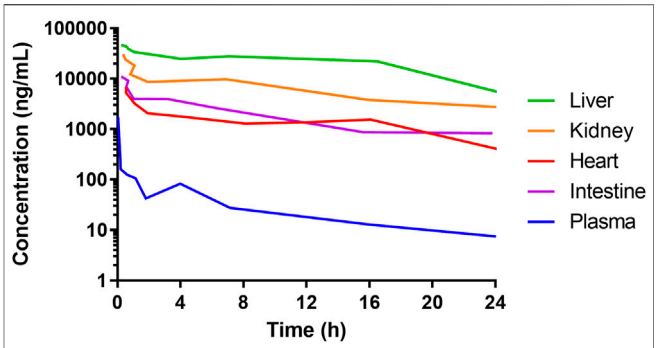

FIGURE 3 | Concentrations of doxorubicin in plasma and liver, heart, kidney, and intestines of mice following 5 mg/mL intravenous administration of a solution. Data from Luo et al. (2017). The high concentration of doxorubicin in all the organs shows that the side-effects of many anti-cancer drugs are not ubiquitously dose-dependent. Rather, they are associated with the tissue-specific cell proliferation rate. This is why cancer tissue and healthy intestinal tissue are typically heavily affected.

The whole alimentary tract is formed from the same structure in the embryo (Stringer et al., 2009), and any effects of chemotherapy should be similar in all regions (oral cavity, stomach, small and large intestine) as the same genes are activated (Yeoh et al., 2007). Nonetheless, there are important physiological and anatomical differences. The mouth and small intestine seem to be most affected by mucositis, and have therefore been the regions most studied (Keefe et al., 2004). The dissimilarity in injury has been attributed to the different regional expression of pro- and anti-apoptotic factors, such as Blc-2, which amplifies apoptosis in the small intestinal crypts (Bowen et al., 2005). Spontaneous apoptosis is 10 times more common in the small intestine than the large intestine, and the small intestine is therefore, not surprisingly, more vulnerable to mucositis induced by chemotherapeutics and radiotherapy (Bowen et al., 2006). The lower apoptosis frequency in the large intestine also contributes to the higher incidence of cancers in the lower compared to the upper intestinal tract.

The time from drug exposure to the epithelial effects varies for different species, doses, administration routes and type of chemotherapeutics, and partly follows species-specific differences in crypt turnover. For instance, after an intravenous dose of DOX, the concentration in the intestine is about 100 times higher than in plasma in animals and humans (Luo et al., 2017; Lee et al., 2020). Although the DOX concentrations in the intestines might be similar as in the liver, kidney, and heart, they cause greater damage to the IECs because these cells have a rapid and extensive proliferation (**Figure 3**) (Luo et al., 2017). In mouse and rat, the cellular apoptosis

TABLE 1 | Potential future treatment options and some examples of specific interventions for CIM. Please see the text for a more detailed description of the proposed treatment strategies.

Treatment options	Examples	Mechanisms
Microbiota	Antibiotics	Reduces pathogenic intestinal bacteria and mucosal infections
	Dihydrotanshinoneon	Restores normal gut microbiota
	Probiotics and fecal microbiota transplantations	Reduces diarrhea, reduce pathogenic bacteria, modulating inflammatory response
Anti-oxidants	Amifostine, melatonin	Detoxifies reactive metabolites of chemotherapeutic agents and scavenges free radicals
Mucosal barrier regulators	Melatonin	Reduces basal and GI injury increases in intestinal permeability
Anti-inflammatory agents	Misoprostol, COX-2 inhibitors	Reduces inflammatory response and propagation
Anti-apoptotic agents	IL-1 receptor antagonist, β-arrestins	Suppression of crypt cell death
Incretins	GLP1 and GLP2	Stimulate growth, promote healing and inhibits epithelial apoptosis
Growth hormones	Keratinocyte growth factor	Stimulates proliferation

in the crypts peaks at about 6–24 h after DOX administration (Thakkar and Potten, 1992), whereas the maximum effects of the villi height and crypt depth peaks at about 72–96 h (Dekaney et al., 2009). This is also the same time interval after DOX treatment at which the cellular renewal process is peaking in the crypts (Dekaney et al., 2009). A complete recovery of the mucosa and its function are restored after about one week in mouse and rat. In humans, these processes are similar to the rodent models, but the peak times are different and the overall time to recovery is about twice as long (Keefe et al., 2004).

CIM not only affects the stem cell population. It also has a complex interplay between the many mucosal cell types (e.g., IEC, immune cells, mesenchymal cells) in the different intestinal compartments (e.g., villus, crypts, intra and extracellular, mucus). These cell types and compartments are important in the injury and healing following cytostatics treatment. For instance, germ-free mice experience the same amount of DOX-induced increase in cryptal apoptosis as normal mice, but the overall intestinal mucosal injury is greater in the normal mice (Rigby et al., 2016). Single intraperitoneal injection of methotrexate (20 mg/kg) to Sprague–Dawley rats (200–250 g) causes severe enterocolitis and death (Mao et al., 1996). However, oral administration of lactobacilli to the treated rats significantly improves their intestinal nutritional status and dynamic barrier function, reduces the number of enteric pathogenic bacteria, and most likely explains the reduction of the bacterial translocation and endotoxemia.

This illustrates the symbiotic interplay between microbiota and the activation of the immune system in maintaining intestinal homeostasis. This is further exemplified by the role of the TLR receptors 2 and 9 that are expressed on a range of intestinal cell types. These receptors recognize bacterial epitopes and determine different responses to commensal and other intestinal bacteria. Mice lacking these receptors display less CIM, most likely as a result of a downregulation of intestinal apoptosis.(Kaczmarek et al., 2012) The extracellular matrix is also important for maintaining tissue morphology and healing. The cancer drug irinotecan is known to affect extracellular matrix protein expression, which contributes to cell cytostasis and apoptosis followed by an increase in collagen deposits partly attributed to changes in the expression of metalloproteinases (Al-Dasooqi et al., 2010; Al-Dasooqi et al., 2011). Furthermore, after cytostatics treatment, it is fundamental for mucosal health that the protective epithelial mucus layer is rebuilt by the mucins. These mucins are involved in cell proliferation, the inhibition of apoptosis, and the overall severity of CIM (Thorpe, 2019).

The multitude of parameters involved in CIM, and our improved understanding of its pathophysiology, give rise to many possible targets for various treatment strategies. Below and in **Table 1** follows a summary of some interesting past and recent studies and potential targets.

POSSIBLE TREATMENT OPTIONS FOR CIM

There is an unmet need to identify and develop efficient drug treatments for GI toxicities caused by chemotherapeutics (Stringer et al., 2009; Sougiannis et al., 2021). The overall aims of any intervention are to reduce the GI related symptoms experienced by cancer patients—this would relieve suffering, enable dose escalation, or avoid dose de-escalation. Interventions can include prophylactic treatments such as probiotics and antibiotics to prepare the GI tract. They may also include anti-oxidants, anti-inflammatory drugs, and apoptosis inhibitors during cytostatics treatment to alleviate some of the immediate toxicities and associated effects. Lastly, treatments such as incretins and growth hormones can be used after cytostatic dosing to benefit the mucosal adaptation and proliferation processes after injury. This section discusses some promising interventions that can be deployed in each of the three stages. Finally, we highlight the usefulness of combining treatment options to tackle CIM from multiple angles.

Microbial and Anti-microbial Treatments

The microbiota can have both detrimental and supportive effects on GI homeostasis and health (Benno et al., 2019). This also holds true for CIM, where luminal bacteria are involved in the regulation of intestinal barrier functions, maintenance of selective intestinal permeability, inflammation and innate immune response, repair mechanisms, cell apoptosis, and oxidative stress (Prisciandaro et al., 2011). The direct or indirect effects of cytostatics on gut microflora dysbiosis also impact the clinical manifestations of CIM, where they contribute to the development of bacteremia and diarrhea. Accordingly, there is an abundance of preclinical CIM rodent models that have

reported positive effects of antibiotics (Hamouda et al., 2017), fecal transplantations (Chang et al., 2020), and probiotics (Yeung et al., 2015; Quaresma et al., 2020). In a mouse model, CIM toxicity has been reduced with dihydrotanshinoneon (a liposoluble plant extract) that restores normal gut microbiota (Wang et al., 2020). In patients undergoing GI surgery, a changed microbial intestinal flora in combination with an altered barrier function may progress to an enhanced inflammatory response. Here probiotics may reduce pathogenic bacteria (Jeppsson et al., 2011). Still, in spite of the vast literature supporting the use of treatments directly or indirectly targeting the luminal microbiota, treatments for CIM that alter the GI microbiome have largely failed in the clinic (Touchefeu et al., 2014), Consequently, there is a need to improve and establish the most suitable composition of type of probiotic bacteria, and its dose and length of treatment. Of special interest is the possibility of combining interventions, such as pre-treatment with antibiotics that target bacterial populations with noxious membrane effects, and beneficial probiotic/fecal microbiota transplantations.

Anti-Oxidants and Mucosal Barrier Regulators

Amifostine is a phosphorylated aminothiol prodrug, which is rapidly hydrolysed *in vivo* by alkaline phosphatase to the active cytoprotective thiol metabolite, WR-1065. This metabolite has a terminal half-life of 90 min (Ranganathan et al., 2018). Intracellularly WR-1065 detoxifies reactive metabolites of chemotherapeutic agents and scavenges free radicals (Bensadoun et al., 2006); it may also accelerate DNA repair and inhibit apoptosis. As such, intravenous administration of WR-1065 may protect intestinal epithelium and connective tissue from various anti-tumor treatments (Grdina et al., 2000). It reduces DOX-induced CIM in rats (Jaćević et al., 2018) and methotrexate-induced CIM in mice, an effect that is potentiated by co-administration of calcium folinate (Chen et al., 2013) The FDA indication for amifostine refers to xerostomia prophylaxis in post-operative head-neck-cancer patients treated with radiotherapy (Antonadou et al., 2002); however, the data are conflicting about its value in oral CIM prevention (Nicolatou-Galitis et al., 2013). Unfortunately, significant side-effects (mainly nausea and hypotension) limit its clinical use.

Melatonin, a serotonin derivative, is a hormone that controls the sleep–wake cycle and is primarily released by the pineal gland at night (Auld et al., 2017). Melatonin is also synthesized and released by the enterochromaffin cells in the intestine, where it binds to the melatonin membrane receptors MT1 and MT2, and to the cytosolic MT3 receptor (Soták et al., 2006; Söderquist et al., 2015). It also scavenges free radicals (Hardeland and Pandi-Perumal, 2005). In rats and mice, melatonin reduces basal intestinal permeability through an inhibitory nicotinic receptor-mediated neural pathway (Sommansson et al., 2013a). This mitigates ethanol-, chemical-, and radiation-induced intestinal damage (Monobe et al., 2005; Sommansson et al., 2013a; Chamanara et al., 2019), as well as methotrexate-induced oxidative stress and injury (Kolli et al., 2013). Clinical trials with melatonin also report positive effects in irritable bowel syndrome and inflammatory bowel disease (Rakhimova, 2010; Siah et al., 2014). In summary, melatonin has a potent effect on mitigating mucosal injury. It should therefore be investigated for limiting CIM, in particular in synergism with other treatments. For example, melatonin dosed with misoprostol abolishes unselective surfactant-induced intestinal injury in rat (Dahlgren et al., 2020).

Anti-Inflammatory and Anti-apoptotic Agents

Pro-inflammatory cytokines, such as IL-1, are involved in the progression of CIM (Kanarek et al., 2014), and their natural antagonists are released upon intestinal injury (Daig et al., 2000). As such, the IL-1 receptor antagonist is repeatedly shown to reduce 5-fluorouracil-induced CIM in mice (Wu et al., 2010; Wu et al., 2011). These effects are attributed to reduced crypt cell death by suppression of p53-dependent apoptosis caused by cytotoxic treatments (Wang et al., 2015). Other mediators in cell apoptosis are β-arrestins that suppress p53 levels (Hara et al., 2011). For example, mice deficient in β-arrestin1 experience increased cell death and injury following cytostatics (Zhan et al., 2016). Other ways to reduce caspase-3 activated cells and apoptosis in mice after 5-fluorouracil-induced mucositis include: a serotonin-receptor antagonist (Yasuda et al., 2013); andrographolide (an herbal extract) (Xiang et al., 2020); and armillariella oral solution (a fungus extract) (Wenqin et al., 2019). These preclinical studies show the potential in targeting cell apoptosis pathways to limit mucosal manifestations and complications in CIM.

The prostaglandin E_1 analogue, misoprostol, is an agonist of G protein-coupled prostaglandin E receptors 1-4 that are involved in epithelial homeostasis and protect against intestinal mucosal damage (Abramovitz et al., 2000). Misoprostol protects by regulating gastric acid and mucus secretion, pro-inflammatory cytokine production, and by activating adaptive cell survival pathways through selective gene repression and splicing (Davies et al., 2001; Field et al., 2018). It is therefore used for the prevention of nonsteroidal anti-inflammatory drug-induced mucosal erosions and ulcers (Graham et al., 1988; Sugimoto and Narumiya, 2007). It is effective at reducing radiation induced injury in animal models (Hanson et al., 1988; Delaney et al., 1994), but its clinical use for treating radiotherapy-induced intestinal and oral mucositis have generated conflicting results, both positive (Hanson et al., 1995) and negative (Duenas-Gonzalez et al., 1996) outcomes. Still, the abundant clinical and preclinical data supporting its cytoprotective effects for a range of GI inflammation and injury models make it a promising drug for further investigations with CIM.

Cyclooxygenase (COX) 1 and 2 are enzymes involved in the formation of prostanoids, which are involved in numerous physiological processes including inflammation (Dahlgren et al., 2018a). COX-1 is expressed and produced

constitutively whereas COX-2 production (prostaglandin E2) is induced at sites of inflammation by pro-inflammatory agents (e.g., IL-1, TNF-α) and transcription factors (e.g., NF-κB) (Turini and Dubois, 2002). The involvement of these mediators in the progression of CIM has led several studies to explore the possible contribution of COX-2 to the amplification phase rather than the acute phase of CIM (Sonis et al., 2004). Accordingly, selective COX-2 inhibition is reported to reduce the overall histopathological changes and/or diarrhoea induced by various cytostatics in rodent models [e.g., 5-fluorouracil (De Miranda et al., 2020) and irinotecan (Javle et al., 2007)]. The same treatments have also been used in the clinics for radiation and chemotherapeutics-induced oral and intestinal mucositis, but with mixed results (Javle et al., 2007; Lalla et al., 2014). Overall, the overlap between effectors in CIM and in inflammatory induction of COX-2 make them a possible adjuvant treatment target.

Incretins and Growth Hormones

Endogenous glucagon-like peptides GLP-1 and GLP-2 are released by the enteroendocrine L-cells into the lamina propria and circulation following oral nutrient ingestion. They stimulate growth, increase absorption, promote healing, maintain intestinal epithelial integrity, and potentially have anti-inflammatory activity (Drucker et al., 1996; Drucker and Yusta, 2014; Ebbesen et al., 2019; Billeschou et al., 2021). The positive effect of luminal food on epithelial growth is also why enteral feeding should be maintained during chemotherapy (Bengmark and Jeppsson, 1995). Plasma levels of GLP-1 correlate with the systemic inflammation in cancer patients receiving chemotherapy; plasma GLP-2 concentrations are significantly elevated 2–5 days following induction of CIM in rats and mice (Kissow et al., 2012; Hytting-Andreasen et al., 2018; Ebbesen et al., 2019). Besides the enhancement of proliferation, exogenous GLP-2 inhibits epithelial apoptosis (Tsai et al., 1997; Boushey et al., 2001). Other studies show GLP-1 and 2 to be central in the adaptive recovery response in the small intestine following CIM (Kissow et al., 2013; Hytting-Andreasen et al., 2018; Billeschou et al., 2021). Thus, GLP-1 and 2, their analogues (semaglutide/exenatide and teduglutide/glepaglutide), or inhibition of their enzymatic-mediated degradation (DPP-IV inhibitors) have great promise for improving mucosal regeneration after CIM, in part by reducing chemotherapy-induced apoptosis (Boushey et al., 2001). GLP-2 analogues also have clinical potential when the integrity or absorptive function of the intestinal mucosa is affected (Salaga et al., 2018).

Another interesting growth factor is the keratinocyte growth factor (KGF), a protein in the fibroblast growth factor family. KGF is a small signalling molecule that binds to fibroblast growth factor receptor 2b which is expressed in the intestine (Song et al., 2020). KGF stimulates proliferation and increases the overall weight of the intestine (Housley et al., 1994). It has been evaluated in rodent models of CIM, but effects have been both positive (Farrell et al., 1998) or absent (Gibson et al., 2002). A human recombinant version of KGF, palifermin, is the only approved (oral) drug treatment for CIM today. As an injection drug, it is used for treating severe oral mucositis in patients receiving myeloablative radiochemotherapy (Nasilowska-Adamska et al., 2007). The cytoprotective effects of palifermin could be expanded to include other indications (Vadhan-Raj et al., 2013).

Combination Treatments

Despite decades of experimental and clinical investigations of CIM, no effective therapeutic interventions are available today for treating it (Ribeiro et al., 2016; Wardill et al., 2019). What treatments that do exist aim at reducing secondary complications to treatment, such as pain and diarrhoea. Consequently, no single treatment to date substantially transforms the clinical management of CIM, despite numerous promising preclinical investigations. This cements the fundamental role of stem cell proliferation in mucosal health and homeostasis, and suggests that its disturbance by chemical agents is so fundamental that no single intervention can readily compensate. Unless any novel breakthrough occurs in this regard, it is our belief that combinations of treatments are necessary to generate any substantial clinical breakthrough in CIM management. A few example of successful additive combinations treatments for alleviating CIM in preclinical models include GLP 1 and 2 (Hytting-Andreasen et al., 2018), troxerutin and celecoxib (De Miranda et al., 2020), amifostine and calcium folinate (Chen et al., 2013). The combinations with the most potential to be successful (high positive ratio of effect/safety) remain to be investigated, validated, and established. An optimal intervention would likely target the pre-treatment phase of CIM with prophylactics (e.g., antibiotics/probiotics), the acute phase with anti-oxidants and anti-inflammatory agents, and the recovery phase, by stimulation of cell proliferation.

CONCLUSIONS

Gastrointestinal injury and symptoms following chemotherapy in cancer patients remains an unsolved clinical issue. As there are currently no effective treatment options for chemotherapeutics-induced intestinal mucositis, there is no way to help these patients other than by lowering the dose of the cytotoxic drug. However, recent progress in the understanding of the molecular and functional pathology of CIM provides many new potential targets and treatment opportunities. We believe that the best possibility for success is to pursue combination treatments that target different aspects of the complex pathological mechanisms involved in intestinal mucositis.

AUTHOR CONTRIBUTIONS

Conceptualization: DD, MS, PH, HL; methodology: DD, HL; investigation: DD, HL; resources: HL; data curation: DD; writing—original draft preparation: DD, HL; writing—review and editing: DD, MS, PH, HL; visualization: DD; funding

acquisition: HL; All authors have read and agreed to the published version of the manuscript.

FUNDING

HL is funded through grants obtained from the Swedish Cancer Foundation (Grant No. CAN2018/602) and Swedish Research Council (Grant Nos. 2018-03301 and 2020-02367).

ACKNOWLEDGMENTS

We thank Febe Jacobsson for her contribution to the artwork.

REFERENCES

Abramovitz, M., Adam, M., Boie, Y., Carrière, M.-C., Denis, D., Godbout, C., et al. (2000). The Utilization of Recombinant Prostanoid Receptors to Determine the Affinities and Selectivities of Prostaglandins and Related Analogs. *Biochim. Biophys. Acta (BBA) - Mol. Cell Biol. Lipids* 1483, 285–293. doi:10.1016/s1388-1981(99)00164-x

Ahluwalia, B., Magnusson, M. K., and Öhman, L. (2017). Mucosal Immune System of the Gastrointestinal Tract: Maintaining Balance between the Good and the Bad. *Scand. J. Gastroenterol.* 52, 1185–1193. doi:10.1080/00365521.2017.1349173

Al-Dasooqi, N., Bowen, J. M., Gibson, R. J., Logan, R. M., Stringer, A. M., and Keefe, D. M. (2011). Irinotecan-induced Alterations in Intestinal Cell Kinetics and Extracellular Matrix Component Expression in the Dark Agouti Rat. *Int. J. Exp. Pathol.* 92, 357–365. doi:10.1111/j.1365-2613.2011.00771.x

Al-Dasooqi, N., Gibson, R. J., Bowen, J. M., Logan, R. M., Stringer, A. M., and Keefe, D. M. (2010). Matrix Metalloproteinases Are Possible Mediators for the Development of Alimentary Tract Mucositis in the Dark agouti Rat. *Exp. Biol. Med. (Maywood)* 235, 1244–1256. doi:10.1258/ebm.2010.010082

Al-Dasooqi, N., Sonis, S. T., Sonis, S. T., Bowen, J. M., Bateman, E., Blijlevens, N., et al. (2013). Emerging Evidence on the Pathobiology of Mucositis. *Support Care Cancer* 21, 2075–2083. doi:10.1007/s00520-013-1810-y

Andrade, M. E. R., Araújo, R. S., De Barros, P. A. V., Soares, A. D. N., Abrantes, F. A., Generoso, S. d. V., et al. (2015). The Role of Immunomodulators on Intestinal Barrier Homeostasis in Experimental Models. *Clin. Nutr.* 34, 1080–1087. doi:10.1016/j.clnu.2015.01.012

Antonadou, D., Pepelassi, M., Synodinou, M., Puglisi, M., and Throuvalas, N. (2002). Prophylactic Use of Amifostine to Prevent Radiochemotherapy-Induced Mucositis and Xerostomia in Head-and-Neck Cancer. *Int. J. Radiat. Oncol. Biol. Phys.* 52, 739–747. doi:10.1016/s0360-3016(01)02683-9

Artis, D., and Spits, H. (2015). The Biology of Innate Lymphoid Cells. *Nature* 517, 293–301. doi:10.1038/nature14189

Auld, F., Maschauer, E. L., Morrison, I., Skene, D. J., and Riha, R. L. (2017). Evidence for the Efficacy of Melatonin in the Treatment of Primary Adult Sleep Disorders. *Sleep Med. Rev.* 34, 10–22. doi:10.1016/j.smrv.2016.06.005

Bengmark, S., and Jeppsson, B. (1995). Gastrointestinal Surface Protection and Mucosa Reconditioning. *J. Parenter. Enteral Nutr.* 19, 410–415. doi:10.1177/0148607195019005410

Benno, P., Norin, E., Midtvedt, T., and Hellström, P. M. (2019). Therapeutic Potential of an Anaerobic Cultured Human Intestinal Microbiota, ACHIM, for Treatment of IBS. *Best Pract. Res. Clin. Gastroenterol.* 40-41, 101607. doi:10.1016/j.bpg.2019.03.003

Bensadoun, R.-J., Schubert, M. M., Lalla, R. V., and Keefe, D. (2006). Amifostine in the Management of Radiation-Induced and Chemo-Induced Mucositis. *Support Care Cancer* 14, 566–572. doi:10.1007/s00520-006-0047-4

Bernier-Latmani, J., and Petrova, T. V. (2017). Intestinal Lymphatic Vasculature: Structure, Mechanisms and Functions. *Nat. Rev. Gastroenterol. Hepatol.* 14, 510–526. doi:10.1038/nrgastro.2017.79

Billeschou, A., Hunt, J. E., Ghimire, A., Holst, J. J., and Kissow, H. (2021). Intestinal Adaptation upon Chemotherapy-Induced Intestinal Injury in Mice Depends on GLP-2 Receptor Activation. *Biomedicines* 9, 46. doi:10.3390/biomedicines9010046

Boushey, R. P., Yusta, B., and Drucker, D. J. (2001). Glucagon-like Peptide (GLP)-2 Reduces Chemotherapy-Associated Mortality and Enhances Cell Survival in Cells Expressing a Transfected GLP-2 Receptor. *Cancer Res.* 61, 687–693.

Bowen, J., Al-Dasooqi, N., Al-Dasooqi, N., Bossi, P., Wardill, H., Van Sebille, Y., et al. (2019). The Pathogenesis of Mucositis: Updated Perspectives and Emerging Targets. *Support Care Cancer* 27, 4023–4033. doi:10.1007/s00520-019-04893-z

Bowen, J. M., Gibson, R. J., Cummins, A. G., and Keefe, D. M. K. (2006). Intestinal Mucositis: the Role of the Bcl-2 Family, P53 and Caspases in Chemotherapy-Induced Damage. *Support Care Cancer* 14, 713–731. doi:10.1007/s00520-005-0004-7

Bowen, J. M., Gibson, R. J., Keefe, D. M., and Cummins, A. G. (2005). Cytotoxic Chemotherapy Upregulates Pro-poptotic Bax and Bak in the Small Intestine of Rats and Humans. *Pathology* 37, 56–62. doi:10.1080/00313020400023461

Buczacki, S. J. A., Zecchini, H. I., Nicholson, A. M., Russell, R., Vermeulen, L., Kemp, R., et al. (2013). Intestinal Label-Retaining Cells Are Secretory Precursors Expressing Lgr5. *Nature* 495, 65–69. doi:10.1038/nature11965

Chamanara, M., Rashidian, A., Mehr, S. E., Dehpour, A.-R., Shirkohi, R., Akbarian, R., et al. (2019). Melatonin Ameliorates TNBS-Induced Colitis in Rats through the Melatonin Receptors: Involvement of TLR4/MyD88/NF-κB Signalling Pathway. *Inflammopharmacol* 27, 361–371. doi:10.1007/s10787-018-0523-8

Chang, C.-W., Lee, H.-C., Li, L.-H., Chiang Chiau, J.-S., Wang, T.-E., Chuang, W.-H., et al. (2020). Fecal Microbiota Transplantation Prevents Intestinal Injury, Upregulation of Toll-like Receptors, and 5-Fluorouracil/oxaliplatin-Induced Toxicity in Colorectal Cancer. *Int. J. Mol. Sci.* 21, 386. doi:10.3390/ijms21020386

Chelakkot, C., Ghim, J., and Ryu, S. H. (2018). Mechanisms Regulating Intestinal Barrier Integrity and its Pathological Implications. *Exp. Mol. Med.* 50, 1–9. doi:10.1038/s12276-018-0126-x

Chen, C., Tian, L., Zhang, M., Sun, Q., Zhang, X., Li, X., et al. (2013). Protective Effect of Amifostine on High-Dose Methotrexate-Induced Small Intestinal Mucositis in Mice. *Dig. Dis. Sci.* 58, 3134–3143. doi:10.1007/s10620-013-2826-3

Dahlgren, D., Cano-Cebrián, M.-J., Hellström, P. M., Wanders, A., Sjöblom, M., and Lennernäs, H. (2020). Prevention of Rat Intestinal Injury with a Drug Combination of Melatonin and Misoprostol. *Int. J. Mol. Sci.* 21, 6771. doi:10.3390/ijms21186771

Dahlgren, D., Roos, C., Lundqvist, A., Tannergren, C., Langguth, P., Sjöblom, M., et al. (2017). Preclinical Effect of Absorption Modifying Excipients on Rat Intestinal Transport of Model Compounds and the Mucosal Barrier Marker51Cr-EDTA. *Mol. Pharmaceutics* 14, 4243–4251. doi:10.1021/acs.molpharmaceut.7b00353

Dahlgren, D., Roos, C., Lundqvist, A., Tannergren, C., Sjöblom, M., Sjögren, E., et al. (2018a). Effect of Absorption-Modifying Excipients, Hypotonicity, and Enteric Neural Activity in an In Vivo Model for Small Intestinal Transport. *Int. J. Pharmaceutics* 549, 239–248. doi:10.1016/j.ijpharm.2018.07.057

Dahlgren, D., Roos, C., Lundqvist, A., Tannergren, C., Sjöblom, M., Sjögren, E., et al. (2018b). Time-dependent Effects on Small Intestinal Transport by Absorption-Modifying Excipients. *Eur. J. Pharmaceutics Biopharmaceutics* 132, 19–28. doi:10.1016/j.ejpb.2018.09.001

Dahlgren, D., Roos, C., Sjögren, E., and Lennernäs, H. (2014). Direct In Vivo Human Intestinal Permeability (Peff) Determined with Different Clinical Perfusion and Intubation Methods. *J. Pharm. Sci.* 104, 2702–2726. doi:10.1002/jps.24258

Daig, R., Rogler, G., Aschenbrenner, E., Vogl, D., Falk, W., Gross, V., et al. (2000). Human Intestinal Epithelial Cells Secrete Interleukin-1 Receptor Antagonist and Interleukin-8 but Not Interleukin-1 or Interleukin-6. *Gut* 46, 350–358. doi:10.1136/gut.46.3.350

Darwich, A. S., Aslam, U., Ashcroft, D. M., and Rostami-Hodjegan, A. (2014). Meta-analysis of the Turnover of Intestinal Epithelia in Preclinical Animal

Species and Humans. *Drug Metab. Dispos* 42, 2016–2022. doi:10.1124/dmd.114.058404

Davies, N. M., Longstreth, J., and Jamali, F. (2001). Misoprostol Therapeutics Revisited. *Pharmacotherapy* 21, 60–73. doi:10.1592/phco.21.1.60.34442

De Miranda, J. A. L., Martins, C. d. S., Fideles, L. d. S., Barbosa, M. L. L., Barreto, J. E. F., Pimenta, H. B., et al. (2020). Troxerutin Prevents 5-fluorouracil Induced Morphological Changes in the Intestinal Mucosa: Role of Cyclooxygenase-2 Pathway. *Pharmaceuticals* 13, 10. doi:10.3390/ph13010010

Dekaney, C. M., Gulati, A. S., Garrison, A. P., Helmrath, M. A., and Henning, S. J. (2009). Regeneration of Intestinal Stem/progenitor Cells Following Doxorubicin Treatment of Mice. *Am. J. Physiology-Gastrointestinal Liver Physiol.* 297, G461–G470. doi:10.1152/ajpgi.90446.2008

Delaney, J. P., Bonsack, M. E., and Felemovicius, I. (1994). Misoprostol in the Intestinal Lumen Protects against Radiation Injury of the Mucosa of the Small Bowel. *Radiat. Res.* 137, 405–409. doi:10.2307/3578717

Donaldson, G. P., Lee, S. M., and Mazmanian, S. K. (2016). Gut Biogeography of the Bacterial Microbiota. *Nat. Rev. Microbiol.* 14, 20–32. doi:10.1038/nrmicro3552

Drucker, D. J., Erlich, P., Asa, S. L., and Brubaker, P. L. (1996). Induction of Intestinal Epithelial Proliferation by Glucagon-like Peptide 2. *Proc. Natl. Acad. Sci.* 93, 7911–7916. doi:10.1073/pnas.93.15.7911

Drucker, D. J., and Yusta, B. (2014). Physiology and Pharmacology of the Enteroendocrine Hormone Glucagon-like Peptide-2. *Annu. Rev. Physiol.* 76, 561–583. doi:10.1146/annurev-physiol-021113-170317

Duenas-Gonzalez, A., Sobrevilla-Calvo, P., Frias-Mendivil, M., Gallardo-Rincon, D., Lara-Medina, F., Aguilar-Ponce, L., et al. (1996). Misoprostol Prophylaxis for High-Dose Chemotherapy-Induced Mucositis: a Randomized Double-Blind Study. *Bone Marrow Transpl.* 17, 809–812.

Duncan, M., and Grant, G. (2003). Oral and Intestinal Mucositis - Causes and Possible Treatments. *Aliment. Pharmacol. Ther.* 18, 853–874. doi:10.1046/j.1365-2036.2003.01784.x

Ebbesen, M. S., Kissow, H., Hartmann, B., Grell, K., Gørløv, J. S., Kielsen, K., et al. (2019). Glucagon-like Peptide-1 Is a Marker of Systemic Inflammation in Patients Treated with High-Dose Chemotherapy and Autologous Stem Cell Transplantation. *Biol. Blood Marrow Transplant* 25, 1085–1091. doi:10.1016/j.bbmt.2019.01.036

Fagerholm, U., Nilsson, D., Knutson, L., and Lennernäs, H. (1999). Jejunal Permeability in Humans In Vivo and Rats In Situ : Investigation of Molecular Size Selectivity and Solvent Drag. *Acta Physiol. Scand.* 165, 315–324. doi:10.1046/j.1365-201x.1999.00510.x

Farrell, C. L., Bready, J. V., Rex, K. L., Chen, J. N., Dipalma, C. R., Whitcomb, K. L., et al. (1998). Keratinocyte Growth Factor Protects Mice from Chemotherapy and Radiation-Induced Gastrointestinal Injury and Mortality. *Cancer Res.* 58, 933–939.

Field, J. T., Martens, M. D., Mughal, W., Hai, Y., Chapman, D., Hatch, G. M., et al. (2018). Misoprostol Regulates Bnip3 Repression and Alternative Splicing to Control Cellular Calcium Homeostasis during Hypoxic Stress. *Cell Death Discov.* 4, 1–20. doi:10.1038/s41420-018-0104-z

Furness, J. B. (2012). The Enteric Nervous System and Neurogastroenterology. *Nat. Rev. Gastroenterol. Hepatol.* 9, 286–294. doi:10.1038/nrgastro.2012.32

Gehart, H., and Clevers, H. (2019). Tales from the Crypt: New Insights into Intestinal Stem Cells. *Nat. Rev. Gastroenterol. Hepatol.* 16, 19–34. doi:10.1038/s41575-018-0081-y

Gibson, R., Keefe, D., Clarke, J., Regester, G., Thompson, F., Goland, G., et al. (2002). The Effect of Keratinocyte Growth Factor on Tumour Growth and Small Intestinal Mucositis after Chemotherapy in the Rat with Breast Cancer. *Cancer Chemother. Pharmacol.* 50, 53–58. doi:10.1007/s00280-002-0460-4

Graham, D., Agrawal, N., and Roth, S. (1988). Prevention of NSAID-Induced Gastric Ulcer with Misoprostol: Multicentre, Double-Blind, Placebo-Controlled Trial. *The Lancet* 332, 1277–1280. doi:10.1016/s0140-6736(88)92892-9

Grdina, D. J., Kataoka, Y., and Murley, J. S. (2000). Amifostine: Mechanisms of Action Underlying Cytoprotection and Chemoprevention. *Drug Metab. Drug interactions* 16, 237–279. doi:10.1515/dmdi.2000.16.4.237

Gribble, F. M., and Reimann, F. (2016). Enteroendocrine Cells: Chemosensors in the Intestinal Epithelium. *Annu. Rev. Physiol.* 78, 277–299. doi:10.1146/annurev-physiol-021115-105439

Hamouda, N., Sano, T., Oikawa, Y., Ozaki, T., Shimakawa, M., Matsumoto, K., et al. (2017). Apoptosis, Dysbiosis and Expression of Inflammatory Cytokines Are Sequential Events in the Development of 5-Fluorouracil-Induced Intestinal Mucositis in Mice. *Basic Clin. Pharmacol. Toxicol.* 121, 159–168. doi:10.1111/bcpt.12793

Hanson, W., Houseman, K., Nelson, A., and Collins, P. (1988). Radiation Protection of the Murine Intestine by Misoprostol, a Prostaglandin E1 Analogue, Given Alone or with WR-2721, Is Stereospecific. *Prostaglandins Leukot. Essent. Fatty Acids* 32, 101–105.

Hanson, W. R., Marks, J. E., Reddy, S. P., Simon, S., Mihalo, W. E., and Tova, Y. (1995). Protection from Radiation-Induced Oral Mucositis by Misoprostol, a Prostaglandin E1 Analog. *Am. J. Ther.* 2, 850–857. doi:10.1097/00045391-199511000-00005

Hara, M. R., Kovacs, J. J., Whalen, E. J., Rajagopal, S., Strachan, R. T., Grant, W., et al. (2011). A Stress Response Pathway Regulates DNA Damage through β2-adrenoreceptors and β-arrestin-1. *Nature* 477, 349–353. doi:10.1038/nature10368

Hardeland, R., and Pandi-Perumal, S. (2005). Melatonin, a Potent Agent in Antioxidative Defense: Actions as a Natural Food Constituent, Gastrointestinal Factor, Drug and Prodrug. *Nutr. Metab.* 2, 1–15. doi:10.1186/1743-7075-2-22

Helander, H. F., and Fändriks, L. (2014). Surface Area of the Digestive Tract - Revisited. *Scand. J. Gastroenterol.* 49, 681–689. doi:10.3109/00365521.2014.898326

Henley, S. J., Ward, E. M., Scott, S., Ma, J., Anderson, R. N., Firth, A. U., et al. (2020). Annual Report to the Nation on the Status of Cancer, Part I: National Cancer Statistics. *Cancer* 126, 2225–2249. doi:10.1002/cncr.32802

Holzapfel, W. H., Haberer, P., Snel, J., Schillinger, U., and Huis in't Veld, J. H. J. (1998). Overview of Gut Flora and Probiotics. *Int. J. Food Microbiol.* 41, 85–101. doi:10.1016/s0168-1605(98)00044-0

Housley, R. M., Morris, C. F., Boyle, W., Ring, B., Biltz, R., Tarpley, J. E., et al. (1994). Keratinocyte Growth Factor Induces Proliferation of Hepatocytes and Epithelial Cells throughout the Rat Gastrointestinal Tract. *J. Clin. Invest.* 94, 1764–1777. doi:10.1172/jci117524

Hytting-Andreasen, R., Balk-Møller, E., Hartmann, B., Pedersen, J., Windeløv, J. A., Holst, J. J., et al. (2018). Endogenous Glucagon-like Peptide-1 and 2 Are Essential for Regeneration after Acute Intestinal Injury in Mice. *PloS one* 13, e0198046. doi:10.1371/journal.pone.0198046

Ijiri, K., and Potten, C. S. (1983). Response of Intestinal Cells of Differing Topographical and Hierarchical Status to Ten Cytotoxic Drugs and Five Sources of Radiation. *Br. J. Cancer* 47, 175–185. doi:10.1038/bjc.1983.25

Jaćević, V., Dragojević-Simić, V., Tatomirović, Ž., Dobrić, S., Bokonjić, D., Kovačević, A., et al. (2018). The Efficacy of Amifostine against Multiple-Dose Doxorubicin-Induced Toxicity in Rats. *Int. J. Mol. Sci.* 19, 2370

Javle, M. M., Cao, S., Durrani, F. A., Pendyala, L., Lawrence, D. D., Smith, P. F., et al. (2007). Celecoxib and Mucosal Protection: Translation from an Animal Model to a Phase I Clinical Trial of Celecoxib, Irinotecan, and 5-fluorouracil. *Clin. Cancer Res.* 13, 965–971. doi:10.1158/1078-0432.ccr-06-0551

Jeppsson, B., Mangell, P., and Thorlacius, H. (2011). Use of Probiotics as Prophylaxis for Postoperative Infections. *Nutrients* 3, 604–612. doi:10.3390/nu3050604

Johansson, M. E. V., Sjövall, H., and Hansson, G. C. (2013). The Gastrointestinal Mucus System in Health and Disease. *Nat. Rev. Gastroenterol. Hepatol.* 10, 352–361. doi:10.1038/nrgastro.2013.35

Kaczmarek, A., Brinkman, B. M., Heyndrickx, L., Vandenabeele, P., and Krysko, D. V. (2012). Severity of Doxorubicin-Induced Small Intestinal Mucositis Is Regulated by the TLR-2 and TLR-9 Pathways. *J. Pathol.* 226, 598–608. doi:10.1002/path.3009

Kanarek, N., Grivennikov, S. I., Leshets, M., Lasry, A., Alkalay, I., Horwitz, E., et al. (2014). Critical Role for IL-1β in DNA Damage-Induced Mucositis. *Proc. Natl. Acad. Sci. USA* 111, E702–E711. doi:10.1073/pnas.1322691111

Keefe, D. M., Gibson, R. J., and Hauer-Jensen, M. (2004). "Gastrointestinal Mucositis," in *Seminars in Oncology Nursing* (Elsevier), 38–47.

Keefe, D. M. K. (1998). *The Effect of Cytotoxic Chemotherapy on the Mucosa of the Small Intestine*. University of Adelaide, Depts. of Gastroenterology and Haematology/Oncology. doi:10.1007/978-1-349-26390-5

Kissow, H., Hartmann, B., Holst, J. J., and Poulsen, S. S. (2013). Glucagon-like Peptide-1 as a Treatment for Chemotherapy-Induced Mucositis. *Gut* 62, 1724–1733. doi:10.1136/gutjnl-2012-303280

Kissow, H., Viby, N.-E., Hartmann, B., Holst, J. J., Timm, M., Thim, L., et al. (2012). Exogenous Glucagon-like Peptide-2 (GLP-2) Prevents Chemotherapy-Induced

Mucositis in Rat Small Intestine. *Cancer Chemother. Pharmacol.* 70, 39–48. doi:10.1007/s00280-012-1882-2

Kolli, V. K., Abraham, P., Isaac, B., and Kasthuri, N. (2013). Preclinical Efficacy of Melatonin to Reduce Methotrexate-Induced Oxidative Stress and Small Intestinal Damage in Rats. *Dig. Dis. Sci.* 58, 959–969. doi:10.1007/s10620-012-2437-4

Lalla, R. V., Choquette, L. E., Curley, K. F., Dowsett, R. J., Feinn, R. S., Hegde, U. P., et al. (2014). Randomized Double-Blind Placebo-Controlled Trial of Celecoxib for Oral Mucositis in Patients Receiving Radiation Therapy for Head and Neck Cancer. *Oral Oncol.* 50, 1098–1103. doi:10.1016/j.oraloncology.2014.08.001

Lee, J. B., Zhou, S., Chiang, M., Zang, X., Kim, T. H., and Kagan, L. (2020). Interspecies Prediction of Pharmacokinetics and Tissue Distribution of Doxorubicin by Physiologically-based Pharmacokinetic Modeling. *Biopharm. Drug Dispos* 41, 192–205. doi:10.1002/bdd.2229

Luo, R., Li, Y., He, M., Zhang, H., Yuan, H., Johnson, M., et al. (2017). Distinct Biodistribution of Doxorubicin and the Altered Dispositions Mediated by Different Liposomal Formulations. *Int. J. pharmaceutics* 519, 1–10. doi:10.1016/j.ijpharm.2017.01.002

Mao, Y., Nobaek, S., Kasravi, B., Adawi, D., Stenram, U., Molin, G., et al. (1996). The Effects of Lactobacillus Strains and Oat Fiber on Methotrexate- Induced Enterocolitis in Rats. *Gastroenterology* 111, 334–344. doi:10.1053/gast.1996.v111.pm8690198

Marchiando, A. M., Graham, W. V., and Turner, J. R. (2010). Epithelial Barriers in Homeostasis and Disease. *Annu. Rev. Pathol. Mech. Dis.* 5, 119–144. doi:10.1146/annurev.pathol.4.110807.092135

Marchiando, A. M., Shen, L., Graham, W. V., Edelblum, K. L., Duckworth, C. A., Guan, Y., et al. (2011). The Epithelial Barrier Is Maintained by In Vivo Tight Junction Expansion during Pathologic Intestinal Epithelial Shedding. *Gastroenterology* 140, 1208–1218. doi:10.1053/j.gastro.2011.01.004

Monobe, M., Hino, M., Sumi, M., Uzawa, A., Hirayama, R., Ando, K., et al. (2005). Protective Effects of Melatonin on γ-ray Induced Intestinal Damage. *Int. J. Radiat. Biol.* 81, 855–860. doi:10.1080/09553000600554804

Mowat, A. M., and Agace, W. W. (2014). Regional Specialization within the Intestinal Immune System. *Nat. Rev. Immunol.* 14, 667–685. doi:10.1038/nri3738

Nasilowska-Adamska, B., Rzepecki, P., Manko, J., Czyz, A., Markiewicz, M., Federowicz, I., et al. (2007). The Influence of Palifermin (Kepivance) on Oral Mucositis and Acute Graft versus Host Disease in Patients with Hematological Diseases Undergoing Hematopoietic Stem Cell Transplant. *Bone Marrow Transpl.* 40, 983–988. doi:10.1038/sj.bmt.1705846

Nicolatou-Galitis, O., Sarri, T., Sarri, T., Bowen, J., Di Palma, M., Kouloulias, V. E., et al. (2013). Systematic Review of Amifostine for the Management of Oral Mucositis in Cancer Patients. *Support Care Cancer* 21, 357–364. doi:10.1007/s00520-012-1613-6

Novellasdemunt, L., Antas, P., and Li, V. S. W. (2015). Targeting Wnt Signaling in Colorectal Cancer. A Review in the Theme: Cell Signaling: Proteins, Pathways and Mechanisms. *Am. J. Physiology-Cell Physiol.* 309, C511–C521. doi:10.1152/ajpcell.00117.2015

Nylander, O., and Sjöblom, M. (2007). Modulation of Mucosal Permeability by Vasoactive Intestinal Peptide or Lidocaine Affects the Adjustment of Luminal Hypotonicity in Rat Duodenum. *Acta Physiol.* 189, 325–335. doi:10.1111/j.1748-1716.2006.01649.x

Odenwald, M. A., and Turner, J. R. (2017). The Intestinal Epithelial Barrier: a Therapeutic Target? *Nat. Rev. Gastroenterol. Hepatol.* 14, 9–21. doi:10.1038/nrgastro.2016.169

Ohno, H. (2016). Intestinal M Cells. *J. Biochem.* 159, 151–160. doi:10.1093/jb/mvv121

Patankar, J. V., and Becker, C. (2020). Cell Death in the Gut Epithelium and Implications for Chronic Inflammation. *Nat. Rev. Gastroenterol. Hepatol.* 17, 543–556. doi:10.1038/s41575-020-0326-4

Potten, C. S., Gandara, R., Mahida, Y. R., Loeffler, M., and Wright, N. A. (2009). The Stem Cells of Small Intestinal Crypts: where Are They? *Cell Prolif.* 42, 731–750. doi:10.1111/j.1365-2184.2009.00642.x

Prisciandaro, L. D., Geier, M. S., Butler, R. N., Cummins, A. G., and Howarth, G. S. (2011). Evidence Supporting the Use of Probiotics for the Prevention and Treatment of Chemotherapy-Induced Intestinal Mucositis. *Crit. Rev. Food Sci. Nutr.* 51, 239–247. doi:10.1080/10408390903551747

Quaresma, M., Damasceno, S., Monteiro, C., Lima, F., Mendes, T., Lima, M., et al. (2020). Probiotic Mixture Containing Lactobacillus Spp. And Bifidobacterium Spp. Attenuates 5-Fluorouracil-Induced Intestinal Mucositis in Mice. *Nutr. Cancer* 72, 1355–1365. doi:10.1080/01635581.2019.1675719

Rakhimova, O. (2010). [Use of Melatonin in Combined Treatment for Inflammatory Bowel Diseases]. *Ter Arkh* 82, 64–68.

Ranganathan, K., Simon, E., Lynn, J., Snider, A., Zhang, Y., Nelson, N., et al. (2018). Novel Formulation Strategy to Improve the Feasibility of Amifostine Administration. *Pharm. Res.* 35, 1–8. doi:10.1007/s11095-018-2386-5

Ribeiro, R. A., Wanderley, C. W. S., Wong, D. V. T., Mota, J. M. S. C., Leite, C. A. V. G., Souza, M. H. L. P., et al. (2016). Irinotecan- and 5-Fluorouracil-Induced Intestinal Mucositis: Insights into Pathogenesis and Therapeutic Perspectives. *Cancer Chemother. Pharmacol.* 78, 881–893. doi:10.1007/s00280-016-3139-y

Rigby, R. J., Carr, J., Orgel, K., King, S. L., Lund, P. K., and Dekaney, C. M. (2016). Intestinal Bacteria Are Necessary for Doxorubicin-Induced Intestinal Damage but Not for Doxorubicin-Induced Apoptosis. *Gut microbes* 7, 414–423. doi:10.1080/19490976.2016.1215806

Salaga, M., Binienda, A., Draczkowski, P., Kosson, P., Kordek, R., Jozwiak, K., et al. (2018). Novel Peptide Inhibitor of Dipeptidyl Peptidase IV (Tyr-Pro-D-Ala-NH2) with Anti-inflammatory Activity in the Mouse Models of Colitis. *Peptides* 108, 34–45. doi:10.1016/j.peptides.2018.08.011

Scarpignato, C., and Bjarnason, I. (2019). Drug-induced Small Bowel Injury: a Challenging and Often Forgotten Clinical Condition. *Curr. Gastroenterol. Rep.* 21, 1–12. doi:10.1007/s11894-019-0726-1

Sender, R., Fuchs, S., and Milo, R. (2016). Revised Estimates for the Number of Human and Bacteria Cells in the Body. *PLoS Biol.* 14, e1002533. doi:10.1371/journal.pbio.1002533

Siah, K. T. H., Wong, R. K. M., and Ho, K. Y. (2014). Melatonin for the Treatment of Irritable Bowel Syndrome. *World J. Gastroenterol.* 20, 2492. doi:10.3748/wjg.v20.i10.2492

Söderquist, F., Hellström, P. M., and Cunningham, J. L. (2015). Human Gastroenteropancreatic Expression of Melatonin and its Receptors MT1 and MT2. *PloS one* 10. e0120195. doi:10.1371/journal.pone.0120195

Sommansson, A., Nylander, O., and Sjöblom, M. (2013a). Melatonin Decreases Duodenal Epithelial Paracellular Permeability *via* a Nicotinic Receptor-dependent Pathway in Rats In Vivo. *J. Pineal Res.* 54, 282–291. doi:10.1111/jpi.12013

Sommansson, A., Saudi, W. S. W., Nylander, O., and Sjöblom, M. (2013b). Melatonin Inhibits Alcohol-Induced Increases in Duodenal Mucosal Permeability in Rats In Vivo. *Am. J. Physiology-Gastrointestinal Liver Physiol.* 305, G95–G105. doi:10.1152/ajpgi.00074.2013

Song, Y., Hu, W., Xiao, Y., Li, Y., Wang, X., He, W., et al. (2020). Keratinocyte Growth Factor Ameliorates Mycophenolate Mofetil-Induced Intestinal Barrier Disruption in Mice. *Mol. Immunol.* 124, 61–69. doi:10.1016/j.molimm.2020.04.012

Sonis, S., Elting, L., Elting, L., Keefe, D., Nguyen, H., Grunberg, S., et al. (2015). Unanticipated Frequency and Consequences of Regimen-Related Diarrhea in Patients Being Treated with Radiation or Chemoradiation Regimens for Cancers of the Head and Neck or Lung. *Support Care Cancer* 23, 433–439. doi:10.1007/s00520-014-2395-9

Sonis, S. T. (2009). Mucositis: the Impact, Biology and Therapeutic Opportunities of Oral Mucositis. *Oral Oncol.* 45, 1015–1020. doi:10.1016/j.oraloncology.2009.08.006

Sonis, S. T., O'donnell, K. E., Popat, R., Bragdon, C., Phelan, S., Cocks, D., et al. (2004). The Relationship between Mucosal Cyclooxygenase-2 (COX-2) Expression and Experimental Radiation-Induced Mucositis. *Oral Oncol.* 40, 170–176. doi:10.1016/s1368-8375(03)00148-9

Soták, M., Mrnka, L., and Pácha, J. (2006). Heterogeneous Expression of Melatonin Receptor MT1 mRNA in the Rat Intestine under Control and Fasting Conditions. *J. Pineal Res.* 41, 183–188. doi:10.1111/j.1600-079x.2006.00355.x

Sougiannis, A. T., Vanderveen, B. N., Davis, J. M., Fan, D., and Murphy, E. A. (2021). Understanding Chemotherapy-Induced Intestinal Mucositis and Strategies to Improve Gut Resilience. *Am. J. Physiology-Gastrointestinal Liver Physiol.* [Epub ahead of print] doi:10.1152/ajpgi.00380.2020

Steinert, R. E., Feinle-Bisset, C., Asarian, L., Horowitz, M., Beglinger, C., and Geary, N. (2016). Ghrelin, CCK, GLP-1, and PYY(3-36): Secretory Controls and Physiological Roles in Eating and Glycemia in Health, Obesity, and After RYGB. *Physiol. Rev.* 97, 411–463. doi:10.1152/physrev.00031.2014

Stringer, A. M., Gibson, R. J., Bowen, J. M., Logan, R. M., Yeoh, A. S., and Keefe, D. M. (2009). Chemotherapy-induced Mucositis: The Role of Gastrointestinal

Microflora and Mucins in the Luminal Environment. *J Support Oncol.* 5(6), 259–67.

Sugimoto, Y., and Narumiya, S. (2007). Prostaglandin E Receptors. *J. Biol. Chem.* 282, 11613–11617. doi:10.1074/jbc.r600038200

Sukhotnik, I., Geyer, T., Pollak, Y., Mogilner, J. G., Coran, A. G., and Berkowitz, D. (2014). The Role of Wnt/β-Catenin Signaling in Enterocyte Turnover during Methotrexate-Induced Intestinal Mucositis in a Rat. *PloS one* 9, e110675. doi:10.1371/journal.pone.0110675

Thakkar, N. S., and Potten, C. S. (1992). Abrogation of Adriamycin Toxicity In Vivo by Cycloheximide. *Biochem. Pharmacol.* 43, 1683–1691. doi:10.1016/0006-2952(92)90697-h

Thorpe, D. (2019). The Role of Mucins in Mucositis. *Curr. Opin. Support. Palliat. Care* 13, 114–118. doi:10.1097/spc.0000000000000423

Touchefeu, Y., Montassier, E., Nieman, K., Gastinne, T., Potel, G., Bruley Des Varannes, S., et al. (2014). Systematic Review: the Role of the Gut Microbiota in Chemotherapy- or Radiation-Induced Gastrointestinal Mucositis - Current Evidence and Potential Clinical Applications. *Aliment. Pharmacol. Ther.* 40, 409–421. doi:10.1111/apt.12878

Tsai, C. H., Hill, M., Asa, S. L., Brubaker, P. L., and Drucker, D. J. (1997). Intestinal Growth-Promoting Properties of Glucagon-like Peptide-2 in Mice. *Am. J. Physiology-Endocrinology Metab.* 273, E77–E84. doi:10.1152/ajpendo.1997.273.1.e77

Turini, M. E., and Dubois, R. N. (2002). Cyclooxygenase-2: a Therapeutic Target. *Annu. Rev. Med.* 53, 35–57. doi:10.1146/annurev.med.53.082901.103952

Vadhan-Raj, S., Goldberg, J. D., Perales, M. A., Berger, D. P., and Van Den Brink, M. R. (2013). Clinical Applications of Palifermin: Amelioration of Oral Mucositis and Other Potential Indications. *J. Cell Mol Med* 17, 1371–1384. doi:10.1111/jcmm.12169

van der Zanden, S. Y., Qiao, X., and Neefjes, J. (2020). New Insights into the Activities and Toxicities of the Old Anticancer Drug Doxorubicin. *FEBS J.* [Epub ahead of print]. doi:10.1111/febs.15583

Van Itallie, C. M., and Anderson, J. M. (2004). The Molecular Physiology of Tight Junction Pores. *Physiology* 19, 331–338. doi:10.1152/physiol.00027.2004

Villa, A., and Sonis, S. T. (2015). Mucositis: Pathobiology and Management. *Curr. Opin. Oncol.* 27, 159–164. doi:10.1097/cco.0000000000000180

Wang, L., Wang, R., Wei, G.-Y., Wang, S.-M., and Du, G.-H. (2020). Dihydrotanshinone Attenuates Chemotherapy-Induced Intestinal Mucositis and Alters Fecal Microbiota in Mice. *Biomed. Pharmacother.* 128, 110262. doi:10.1016/j.biopha.2020.110262

Wang, X., Gao, J., Qian, L., Gao, J., Zhu, S., Wu, M., et al. (2015). Exogenous IL-1Ra Attenuates Intestinal Mucositis Induced by Oxaliplatin and 5-fluorouracil through Suppression of P53-dependent Apoptosis. *Anti-cancer drugs* 26, 35–45. doi:10.1097/cad.0000000000000142

Wardill, H. R., Tissing, W. J. E., Kissow, H., and Stringer, A. M. (2019). Animal Models of Mucositis: Critical Tools for Advancing Pathobiological Understanding and Identifying Therapeutic Targets. *Curr. Opin. Support. Palliat. Care* 13, 119–133. doi:10.1097/spc.0000000000000421

Wehkamp, J., and Stange, E. F. (2020). An Update Review on the Paneth Cell as Key to Ileal Crohn's Disease. *Front. Immunol.* 11, 646. doi:10.3389/fimmu.2020.00646

Wenqin, D., Yaodong, Z., Wanji, S., Fengli, Z., Li, S., Haili, J., et al. (2019). Armillariella Oral Solution Ameliorates Small Intestinal Damage in a Mouse Model of Chemotherapy-Induced Mucositis. *Nutr. Cancer* 71, 1142–1152. doi:10.1080/01635581.2019.1599029

Wu, Z.-Q., Han, X.-D., Wang, Y., Yuan, K.-L., Jin, Z.-M., Di, J.-Z., et al. (2011). Interleukin-1 Receptor Antagonist Reduced Apoptosis and Attenuated Intestinal Mucositis in a 5-fluorouracil Chemotherapy Model in Mice. *Cancer Chemother. Pharmacol.* 68, 87–96. doi:10.1007/s00280-010-1451-5

Wu, Z., Han, X., Qin, S., Zheng, Q., Wang, Z., Xiang, D., et al. (2010). Interleukin 1 Receptor Antagonist Reduces Lethality and Intestinal Toxicity of 5-fluorouracil in a Mouse Mucositis Model. *Biomed. Pharmacother.* 64, 589–593. doi:10.1016/j.biopha.2010.06.006

Xiang, D.-C., Yang, J.-Y., Xu, Y.-J., Zhang, S., Li, M., Zhu, C., et al. (2020). Protective Effect of Andrographolide on 5-Fu Induced Intestinal Mucositis by Regulating P38 MAPK Signaling Pathway. *Life Sci.* 252, 117612. doi:10.1016/j.lfs.2020.117612

Yan, K. S., Gevaert, O., Zheng, G. X. Y., Anchang, B., Probert, C. S., Larkin, K. A., et al. 2017). Intestinal Enteroendocrine Lineage Cells Possess Homeostatic and Injury-Inducible Stem Cell Activity. *Cell stem cell* 21, 78–90.doi:10.1016/j.stem.2017.06.014

Yasuda, M., Kato, S., Yamanaka, N., Iimori, M., Matsumoto, K., Utsumi, D., et al. (2013). 5-HT3receptor Antagonists Ameliorate 5-Fluorouracil-Induced Intestinal Mucositis by Suppression of Apoptosis in Murine Intestinal Crypt Cells. *Br. J. Pharmacol.* 168, 1388–1400. doi:10.1111/bph.12019

Yeoh, A. S. J., Gibson, R. J., Yeoh, E. E. K., Bowen, J. M., Stringer, A. M., Giam, K. A., et al. (2007). A Novel Animal Model to Investigate Fractionated Radiotherapy-Induced Alimentary Mucositis: the Role of Apoptosis, P53, Nuclear Factor-κB, COX-1, and COX-2. *Mol. Cancer Ther.* 6, 2319–2327. doi:10.1158/1535-7163.mct-07-0113

Yeung, C.-Y., Chan, W.-T., Jiang, C.-B., Cheng, M.-L., Liu, C.-Y., Chang, S.-W., et al. (2015). Amelioration of Chemotherapy-Induced Intestinal Mucositis by Orally Administered Probiotics in a Mouse Model. *PloS one* 10, e0138746. doi:10.1371/journal.pone.0138746

Zhan, Y., Xu, C., Liu, Z., Yang, Y., Tan, S., Yang, Y., et al. (2016). β-Arrestin1 Inhibits Chemotherapy-Induced Intestinal Stem Cell Apoptosis and Mucositis. *Cell Death Dis* 7, e2229. doi:10.1038/cddis.2016.136

Conflict of Interest: The authors declare that the research was conducted in the absence of any commercial or financial relationships that could be construed as a potential conflict of interest.

frontiers in Pharmacology

ORIGINAL RESEARCH
published: 10 May 2021
doi: 10.3389/fphar.2021.633403

A Novel Role of $A_{2A}R$ in the Maintenance of Intestinal Barrier Function of Enteric Glia from Hypoxia-Induced Injury by Combining with mGluR5

Lihua Sun†, Xiang Li†, Haidi Guan, Shuaishuai Chen, Xin Fan, Chao Zhou, Hua Yang and Weidong Xiao**

Department of General Surgery, Xinqiao Hospital, Army Medical University, Chongqing, China

OPEN ACCESS

Edited by:
Thomas Brzozowski, Jagiellonian University Medical College, Poland

Reviewed by:
Carmen Diniz, University of Porto, Portugal
Geetha Samak, DVS College of Arts and Science, India

***Correspondence:**
Weidong Xiao
weidong.xiao@126.com
Hua Yang
hwbyang@126.com

†*These authors have contributed equally to this work.*

Specialty section:
This article was submitted to Gastrointestinal and Hepatic Pharmacology, a section of the journal Frontiers in Pharmacology

Received: *10 December 2020*
Accepted: *25 March 2021*
Published: *10 May 2021*

Citation:
Sun L, Li X, Guan H, Chen S, Fan X, Zhou C, Yang H and Xiao W (2021) A Novel Role of $A_{2A}R$ in the Maintenance of Intestinal Barrier Function of Enteric Glia from Hypoxia-Induced Injury by Combining with mGluR5. Front. Pharmacol. 12:633403. doi: 10.3389/fphar.2021.633403

During acute intestinal ischemia reperfusion (IR) injury, the intestinal epithelial barrier (IEB) function is often disrupted. Enteric glial cells (EGCs) play an important role in maintaining the integrity of IEB functions. However, how EGCs regulate IEB function under IR stimulation is unknown. The present study reveals that the adenosine A_{2A} receptor ($A_{2A}R$) is important for mediating the barrier-modulating roles of EGCs. $A_{2A}R$ knockout (KO) experiments revealed more serious intestinal injury in $A_{2A}R$ KO mice than in WT mice after IR stimulation. Moreover, $A_{2A}R$ expression was significantly increased in WT mice when challenged by IR. To further investigate the role of $A_{2A}R$ in IEB, we established an *in vitro* EGC-Caco-2 co-culture system. Hypoxia stimulation was used to mimic the process of *in vivo* IR. Treating EGCs with the CGS21680 $A_{2A}R$ agonist attenuated hypoxia-induced intestinal epithelium damage through up-regulating ZO-1 and occludin expression in cocultured Caco-2 monolayers. Furthermore, we showed that $A_{2A}R$ and metabotropic glutamate receptor 5 (mGluR5) combine to activate the PKCα-dependent pathway in conditions of hypoxia. This study shows, for the first time, that hypoxia induces $A_{2A}R$-mGluR5 interaction in EGCs to protect IEB function via the PKCα pathway.

Keywords: $A_{2A}R$, intestinal epithelial barrier, mGluR5, enteric glial cells, hypoxia

INTRODUCTION

Ischemia-reperfusion (IR) injury of the intestine is a fatal syndrome in abdominal surgeries involving aortic aneurysm, small bowel or liver transplantation, cardiopulmonary bypass, strangulated hernias, and neonatal necrotizing entero colitis (Mallick et al., 2004). Acute intestinal IR injury is one of the most important causes of disruption to the intestinal epithelial barrier (IEB), initiates the systemic inflammatory response syndrome, and leads to multiple organ disorders (Vollmar and Menger, 2011; Lu et al., 2012). For these reasons, increasing attention has been focused on the underlying mechanisms of intestinal IR and promising protective strategies.

Traditionally, enteric glial cells (EGCs), the most abundant cell type in the intestinal nervous system, have been proposed to provide trophic and supportive effects for enteric neurons (Aube et al.,

2006; Ruhl, 2005). However, accumulating evidence reveals that EGCs also play an important role in the regulation of intestinal epithelial proliferation and the intestinal mucosal defense system (Neunlist et al., 2013; Cheadle et al., 2013). EGCs are responsible for enhanced gut permeability and barrier dysfunction in inflammatory bowel disease (IBD) (Zhang et al., 2010; Cabarrocas et al., 2003; von Boyen and Steinkamp, 2010; Neunlist et al., 2008). In transgenic mice, the conditional deletion of EGCs results in the development of fulminant intestinal inflammation with mucosal barrier breakdown (Bush et al., 1998). Previously, we demonstrated that EGCs enhance IEB functions in response to lipopolysaccharide (LPS) stimulation by inhibiting increased iNOS activity (Xiao et al., 2011). We also found that EGC-released glial-derived neurotrophic factor (GDNF) is closely involved in the IEB protective mechanisms of EGCs in acute IR stimulation (Xiao et al., 2014). However, the precise mechanisms by which EGCs regulate IEB in IR injury have not been elucidated.

The Adenosine A_{2A} receptor ($A_{2A}R$), one of four G protein–coupled adenosine receptors (including A_1R, $A_{2A}R$, $A_{2B}R$, and A_3R), binds adenosine and induces activation of adenylate cyclase, promoting cAMP synthesis and producing corresponding biological effects (Welihinda et al., 2016). $A_{2A}R$ is involved in the regulation of several physiological functions, including in the gastrointestinal system (Fornai et al., 2009). $A_{2A}R$ has diverse and important roles in the intestine, including gut motor functions, acetylcholine release, cholinergic contraction modulation, and enteric nervous system regulation (Duarte-Araújo et al., 2004; Antonioli et al., 2006; Fornai et al., 2009; Schriemer et al., 2016). DucoSchriemer et al. revealed that $A_{2A}R$ is a key regulator of terminal neuronal differentiation in GDNF-treated enteric neural crest cells (ENCCs) (Schriemer et al., 2016). However, there is relatively little information about the role of $A_{2A}R$ in EGCs. Therefore, this study was designed to investigate the role of $A_{2A}R$ in EGC-mediated IEB regulation.

MATERIALS AND METHODS

Cell Culture and Co-Culture

Rat EGC/PK060399egfr (CRL-2690™) and human intestinal epithelial cells Caco-2 (HTB-37™) were obtained from the American Type Culture Collection. EGC/PK060399egfr and Caco-2 cells were grown in high glucose DMEM and MEM, respectively, supplemented with 10% FCS, 2 mM L-glutamine, and 100 U/100 μg/ml penicillin–streptomycin. Cells were incubated in a 5% CO_2 humidified incubator at 37°C. The EGC-Caco-2 co-culture system was established as described previously by our laboratory (Xiao et al., 2014). Caco-2 cells were seeded on Millicell®filters (0.4 μm pore diameter; Millipore; Billerica, MA) at a density of 5×10^4 cells/cm^2 for up to 4–5 days. EGCs were seeded at an equal density in 6 or 24 well tissue culture plates to avoid any possible direct cell contact with Caco-2 cells. During the co-culture period, half of the culture medium in the apical and basal compartments was changed daily.

Mice

Global $A_{2A}R$ homozygous KO mice ($A_{2A}R^{-/-}$ mice) with C57BL/6J background were provided by Dr. Yuanguo Zhou (Research Institute of Surgery, Daping Hospital, Army Medical University, Chongqing, China). Specific pathogen-free wild-type (WT) C57BL/6J mice were purchased from the Laboratory Animal Center of the Army Medical University. All mice were housed and maintained in laminar flow cabinets under specific pathogen-free conditions.

In Vitro Hypoxia Experiments

For hypoxia experiments, cells were subjected to hypoxia in a CO_2 incubator (Forma® Series II Water Jacketed CO_2 Incubators; Thermo Scientific) with 94% nitrogen, 5% CO_2, and 1% oxygen and incubated at 37°C for 6 h. Re-oxygenation was initiated by replacing the media and exposing the cell monolayers to 37°C plus 5% $CO_2$for 1 h. Control cells were maintained at 37°C in an atmosphere with 5% CO_2.

Intestinal Ischemia/Reperfusion Model

Male mice (8–10 weeks old) were fasted for 12 h and were free to drink water prior to surgery. The animals were intraperitoneally injected with 40 mg/kg of pentobarbital anesthesia and an aseptic laparotomies dioventral line was placed. The following specific surgical procedures were performed as previously described (Xiao et al., 2014).

Western Blot Analysis

Cells and tissues were lyzed in cold RIPA buffer for 30 min and centrifuged at 13,000× *g* for 30 min at 4°C. Protein concentration was determined using a BCA assay reagent (Beyotime). The primary antibodies used were rabbit anti-ZO-1 (1:800), rabbit anti-Occludin (1:1000), mouse anti-$A_{2A}R$ (1:500), rabbit anti-PKCα (1:1000), rabbit anti-Na+/K+ ATPase (1:1000), and rabbit anti-GAPDH (1:1,000). Protein expression was measured in optical density units and normalized to GAPDH expression.

Immunofluorescence Staining

The small intestine tissues were embedded with OCT compound (Tissue-Tek, Sakura Finetek, Torrance, CA, United States). Consecutive frozen sections (5 μm in thickness) were obtained and fixed in 4% paraformaldehyde for 20 min at room temperature. After 30 min pre-incubation with a blocking solution containing 5% bovine serum albumin, sections were incubated overnight at 4°C with primary antibody against GFAP (Abcam), $A_{2A}R$ (Abcam), or ZO-1 (Abcam). After washing in PBS, sections were incubated with fluorescence-conjugated secondary antibodies at 37°C for 1 h. After washing in PBS, sections were incubated with DAPI nuclear stain solution for 5 min. All images were obtained using a TCS-SP5 confocal microscope (Leica, Germany).

Coimmunoprecipitation

Cells were harvested and lyzed in standard immunoprecipitation (IP) buffer containing either 1% 3-[(3-cholamidopropyl) dimethylammonio] propanesulfonic acid (Chaps) or 1% Triton X-100 (for ERAD substrates), or 2% digitonin (for ERAD machinery) for 1 h on ice. Cells were centrifuged at 16,000 × *g* for 10 min, and the supernatant was used for immunoprecipitation

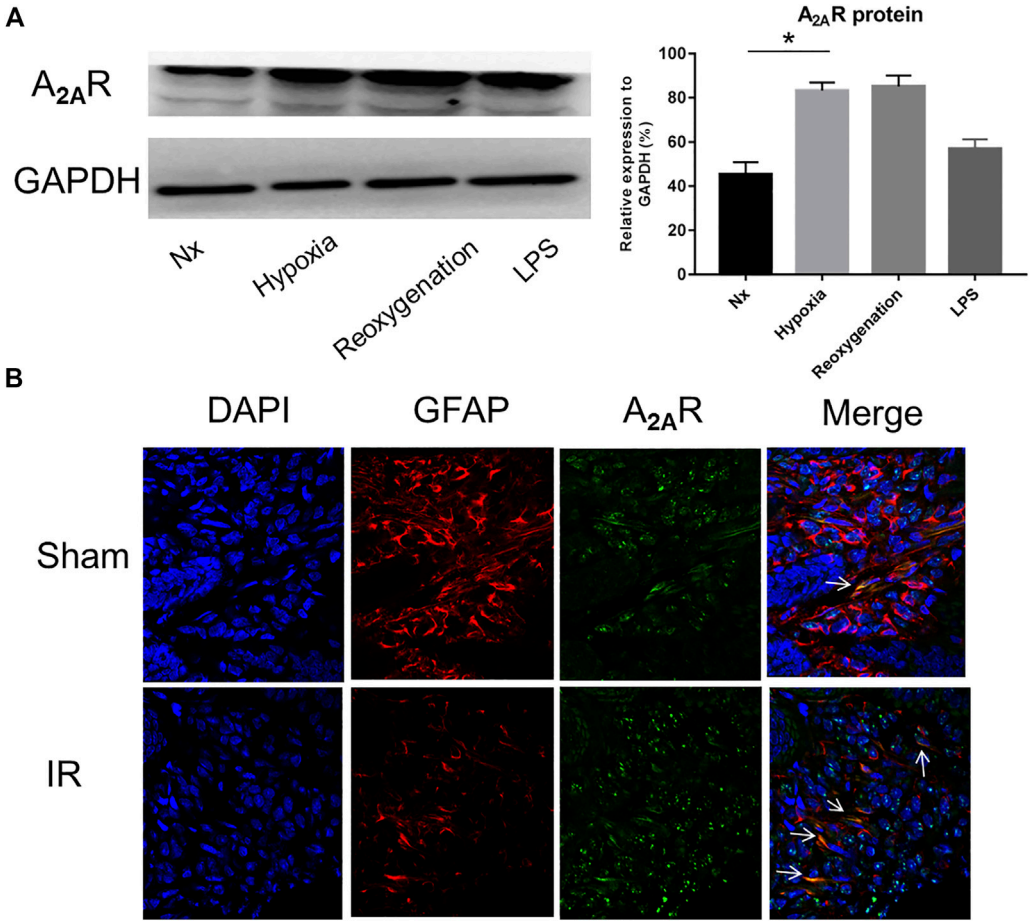

FIGURE 1 | Expression of $A_{2A}R$ in enteric glial cells (EGCs) under hypoxia stimulation. **(A)** Western blot analysis shows a significant increase of $A_{2A}R$ protein level in cultured EGC cells after hypoxia and reoxygenation treatment. GAPDH was used as a standard for cellular protein input. **(B)** Immunofluorescence was used to detect $A_{2A}R$ expression in the small intestine under IR treatment. Red and green signals represent GFAP and $A_{2A}R$, respectively. Results are expressed as mean ± SD (n = 4–6 mice/group) (*$p < 0.05$).

experiments. Co-IP was performed using protein A-agarose beads (EMD Millipore) with anti-$A_{2A}R$ (Santa Cruz Biotechnology, Inc.), anti-mGluR5 antibodies (Cell signaling), or anti-D2R antibodies (Santa Cruz Biotechnology, Inc.) following the usual method.

Transepithelial Electrical Resistance (TER) and Permeability Measurements

The TER of cells was determined via a Millipore electric resistance system (ERS-2; Millipore). Caco-2 cell monolayers were grown in Millicell inserts (0.33 cm^2 area, 0.4 μm pore diameter, and 6.5 mm diameter) and the culture medium was replaced before TER measurement. To calculate the actual resistance of the cell monolayer, the mean resistance of filters without cells was subtracted from the monolayer measurement, and the difference between the filter and monolayer areas was corrected.

The intestinal mucosa TER was measured by Ussing chambers (Physiologic Instruments, San Diego, CA). The excised intestinal tissues were bathed in 5 ml Krebs buffer (110.0 mM NaCl, 3.0 mM$CaCl_2$, 5.5 mM KCl, 1.4 mM KH_2PO_4, 29.0 mM $NaHCO_3$, and 1.2 mM $MgCl_2$, pH 7.4)on both the mucosal and serosal sides. The TER was measured as previously described (Liu et al., 2018).

Statistical Analysis

All experimental data are shown as the Mean ± SD. Statistical significance was determined by unpaired two-tailed Student t test analysis using GraphPad Prism version 7.0 software (San Diego, CA). If not otherwise stated, all experiments included three independent replications in triplicate. $p < 0.05$ was considered statistically significant.

RESULTS

Acute IR Treatment Significantly Activated $A_{2A}R$ Expression in Intestinal Mucosa EGC

To study the effect of $A_{2A}R$ on EGC, we first examined the expression of $A_{2A}R$ in different pathological conditions. Lipopolysaccharide (LPS) and hypoxia treatments were used to

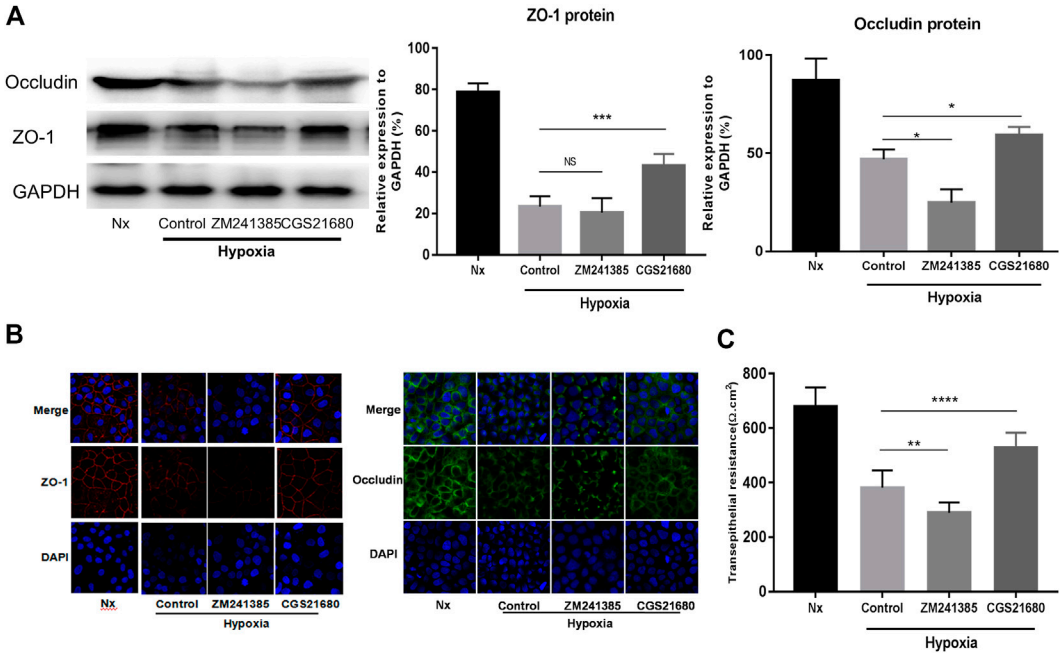

FIGURE 2 | Activation of $A_{2A}R$ in enteric glial cells (EGCs) prevents Caco-2 monolayer barrier dysfunction under hypoxia stimulation. **(A–C)** EGCs were co-cultured with Caco-2 monolayers for 24 h and then treated with ZM241385 (1 μM) and CGS21680 (100 nM) for 6 h respectively under hypoxia conditions. **(A)** Western blot and **(B)** immunofluorescence analyses were used to detect ZO-1 and occludin expression. **(C)** The transepithelial electrical resistance (TER) of Caco-2 monolayers was determined to evaluate intestinal epithelial barrier (IEB) function. Results are expressed as mean ± SD. (**$p < 0.01$; ***$p < 0.001$; ****$p < 0.0001$; NS, not significant.)

stimulate EGCs *in vitro*. As shown in **Figure 1A**, $A_{2A}R$ expression dramatically increased in EGCs following LPS and hypoxia stimulation, with the effect of hypoxia being obvious than that of LPS. Therefore, hypoxia treatment was used to study the effect of $A_{2A}R$. As demonstrated previously, GFAP is a specific marker of activated glial cells (Xiao et al., 2014). $A_{2A}R$ and GFAP immunofluorescent staining colocalization were used to observe changes in $A_{2A}R$ expression in EGCs. Acute IR-treated mice showed a moderate decrease in GFAP-positive intestinal EGCs compared to sham-treated mice (**Figure 1B**). However, the $A_{2A}R$ levels increased significantly in GFAP-positive EGCs after IR treatment. Together, these results indicate that hypoxia stimulation can activate the $A_{2A}R$-mediated signaling pathway in mucosal EGCs in the intestine.

Activation of $A_{2A}R$ in EGCs Efficiently Prevents Barrier Dysfunction of Caco-2 Monolayers Under Hypoxia Stimulation

To further explore the role of $A_{2A}R$ in IEB modulation under acute hypoxia stimulation, we used an $A_{2A}R$ agonist and inhibitor separately in an *in vitro* EGC-Caco-2 co-culture system. The tight junctions (TJs) are primary determinants of IEB function (Lee, 2015). As shown in **Figure 2A**, western blot analysis revealed an almost 50% drop in ZO-1 and occludin expression in the hypoxia group and a similar reduction on ZO-1 and occludin expression in the $A_{2A}R$ inhibitor ZM241385 group. However, the $A_{2A}R$ agonist CGS21680 significantly prevented hypoxia-induced TJs destruction. Further study with immunocytochemistry (ICC) confirmed the western blot results (**Figure 2B**). Additionally, TER measurement analysis produced similar results. CGS21680 pretreatment effectively blocked TER decrease under hypoxia stimulation when compared to the ZM241385 pretreatment group (528.6 ± 18.11 Ω cm^2 vs. 289.6 ± 12.63 Ω cm^2 for the CGS21680 and ZM241385 pretreatment groups, respectively) (**Figure 2C**). Together, these results showed that $A_{2A}R$ plays a protective role in the EGC barrier-protecting effect on the IEC monolayer under hypoxia stimulation.

$A_{2A}R$ Deficiency Aggravates IR-Induced IEB Injury

To further confirm the role of $A_{2A}R$ in the barrier protective of EGCs during hypoxia stimulation, $A_{2A}R$ KO mice were treated with IR. Western blot analysis of ZO-1 and occludin expression was assessed in the small intestine (**Figure 3A**). Acute IR treatment led to a substantial decrease in ZO-1 and occludin expression in $A_{2A}R$ KO mice compared to WT mice. Immunofluorescence analysis also revealed a similar reduction in ZO-1 and occludin expression in the intestinal mucosa after IR stimulation (**Figure 3B**). The functional impact of $A_{2A}R$ knockdown on tight junctions in the small intestine was further evaluated by determining the TER value using Ussing chambers. As shown in **Figure 3E**, intestinal I/R caused a marked TER decrease in $A_{2A}R$ KO mice (78.63 ± 3.407 Ω cm^2) compared with WT mice (94.5 ± 3.151 Ω cm^2). Histological examination of intestinal tissues revealed that IR-treated $A_{2A}R$ KO mice showed more increased intestinal villus fracturing and epithelial removal

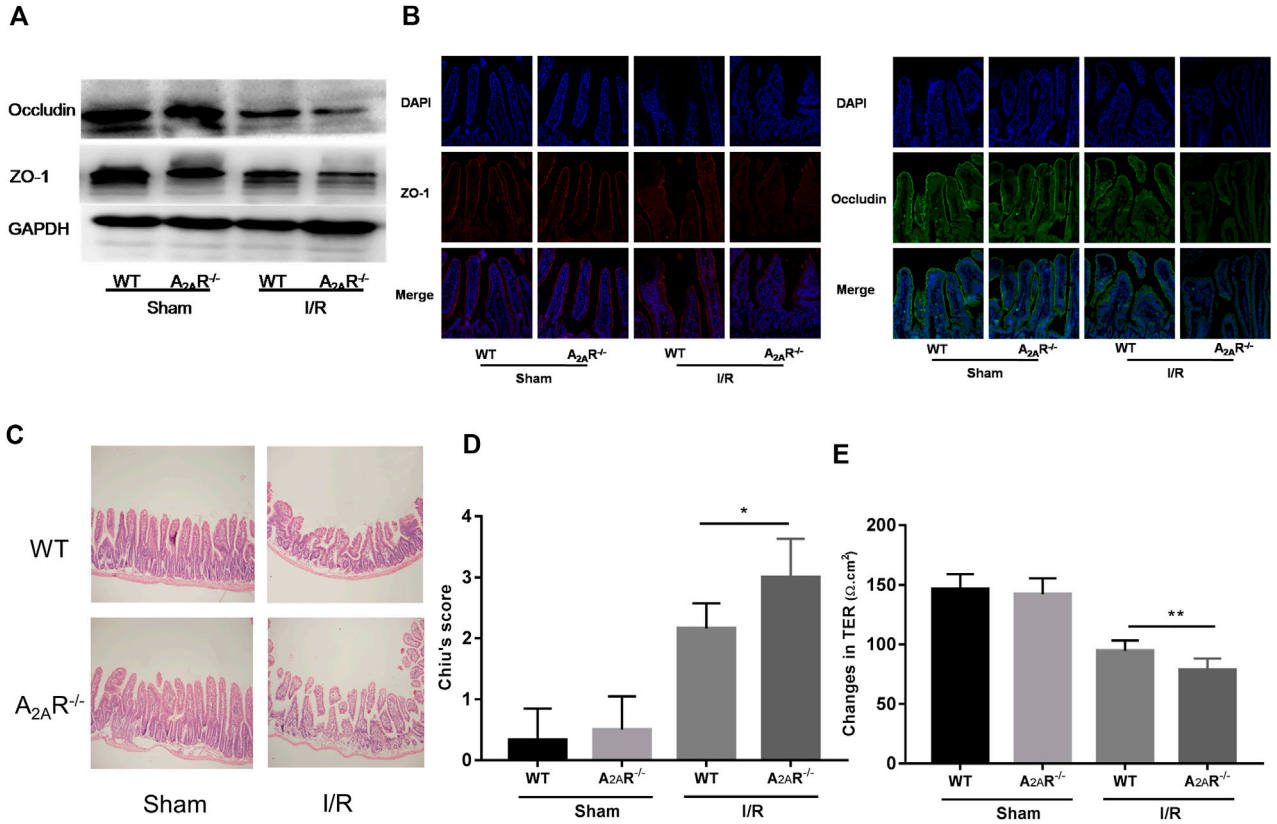

FIGURE 3 | $A_{2A}R$ deficiency aggravates IR-induced intestinal epithelial barrier (IEB) injury. IEB function was assessed in IR-treated WT and $A_{2A}R^{-/-}$ mice by **(A)** ZO-1 and occludin protein expression measured by western blot **(B)**, ZO-1 and occludin protein expression measured by immunofluorescence, and **(E)** the small intestine TER value. The degree of intestinal damage was assessed in IR-treated WT and $A_{2A}R^{-/-}$ mice by **(C)** hematoxylin and eosin staining, and **(D)** Chiu's Score. Results are expressed as mean ± SD (n = 4–6 mice/group. *p < 0.05; **p < 0.01).

than did WT mice (**Figures 3C,D**). Together, these results strongly suggest that $A_{2A}R$ has a significant protective effect in IR-induced IEB injury.

Hypoxia Induces the Interaction between $A_{2A}R$ and mGluR5

There are synergistic interactions between $A_{2A}R$, mGluR5, and the dopamine D2 receptor (D2R) in central nervous system (CNS) related diseases (Ferraro et al., 2012; Fernández-Dueñas et al., 2013). However, whether this relationship exists in the enteric nervous system has yet to be determined. It has been suggested that in micro glial cells, $A_{2A}R$ combines with D2R in low glutamate concentration and combines with mGluR5 in high glutamate concentration (Dai et al., 2010; Beggiato et al., 2016). Therefore, we used high glutamate concentrations as a positive control. We studied the relationship among them under hypoxia in EGCs. When exploring the effect of oxygen concentration, the band corresponding to D2R was coimmunoprecipitated by anti-$A_{2A}R$ antibodies, and an $A_{2A}R$ band was coimmunoprecipitated by anti-D2R antibodies. Together, these results indicate that $A_{2A}R$ and D2R interact in normoxic but not in hypoxic conditions (**Figure 4A**). However, an opposite relationship was observed between $A_{2A}R$ and mGluR5. As shown in **Figure 4B**, the band corresponding to mGluR5 was coimmunoprecipitated by anti-$A_{2A}R$ antibodies, and an $A_{2A}R$ band was also coimmunoprecipitated by anti-mGluR5 antibodies. These results indicate that $A_{2A}R$ and D2R interact in hypoxia but not in normoxia, demonstrating that $A_{2A}R$ interacts with D2R under normoxic conditions and interacts with mGluR5 under hypoxic conditions.

mGluR5 Inhibition Attenuates the Protective Effect of $A_{2A}R$ on the IEB from Hypoxia Induced Damage

To confirm that $A_{2A}R$ regulates the IEB via a mGluR5-dependent pathway, we tested the responsiveness of the IEB to 100 μM of the MPEP selective mGluR5 antagonist under hypoxia. Western blot analysis of ZO-1 and occludin expression revealed that treatment with MPEP significantly inhibited CGS21680-mediated activation of ZO-1 and occludin expression after hypoxia induced damage (**Figure 4C**). Similar results were observed in TER measurements: CGS21680 pretreatment effectively prevented the decrease of TER from hypoxia stimulation, while, MPEP blocked CGS21680-induced potentiation (454.3 ± 15.7 $\Omega\,cm^2$ vs. 391 ± 8.441 $\Omega\,cm^2$) (**Figure 4D**). Together,

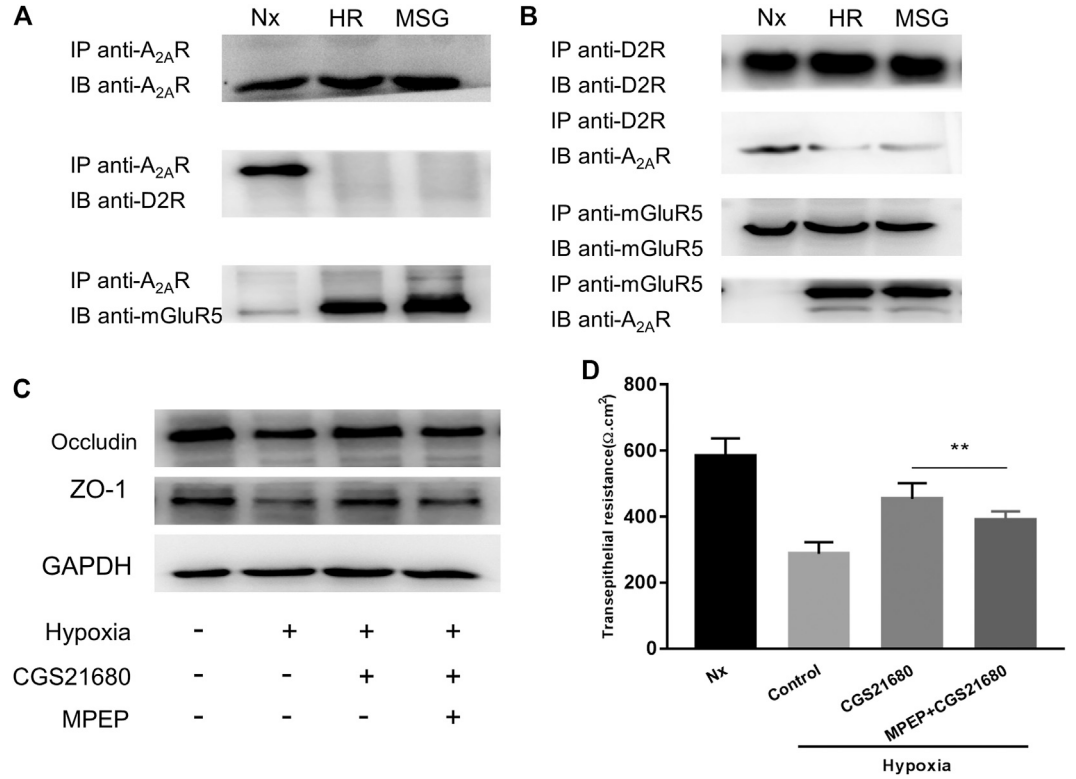

FIGURE 4 | The protective effect of $A_{2A}R$ on the intestinal epithelial barrier (IEB) is mediated by combining with mGluR5. **(A)** Co-IP of $A_{2A}R$ and D2R or mGluR5 in enteric glial cells (EGCs) using an anti-$A_{2A}R$ precipitating antibody. **(B)** Interactions between $A_{2A}R$ and D2R or mGluR5 in EGCs were confirmed by Co-IP using anti- D2R or anti-mGluR5 precipitating antibodies. **(C**,**D)** EGCs were co-cultured with Caco-2 monolayers for 24 h and then treated with MPEP (100 μM) and CGS21680 (100 nM) for 6 h respectively under hypoxia conditions. **(C)** Western blot and **(D)** TER analysis were used to detect the function of IEB. Results are expressed as mean ± SD. (**$p < 0.01$).

these results indicate that the protective effect of $A_{2A}R$on the IEB after hypoxia stimulation is dependent on mGluR5.

The PKCα Signaling Pathway Is Required for the Protective Function of $A_{2A}R$ on IEB

The PKCα signaling pathway is associated with an $A_{2A}R$–mGluR5 interaction-associated proinflammatory effect (Dai et al., 2013; Li et al., 2017). Therefore, we next tested whether PKCα is required for $A_{2A}R$-mediated IEB protection. PKC family isoforms can translocate to multiple subcellular localizations in response to hypoxia in different cell lines (Yu et al., 2015). Consistent with this, western blots showed increased PKCα expression in the membrane after hypoxia stimulation in EGCs (**Figure 5A**). These results were confirmed by immunocytochemistry analysis showing that PKCα translocates from the cytoplasm to the cell membrane in EGCs after hypoxia stimulation (**Figure 5B**). We then used PKCα inhibitor, chelerythrine chloride, to observe whether the protective effect of CGS21680 on IEB was affected. As shown in **Figure 5C**, chelerythrine chloride significantly reduced ZO-1 and occludin protein levels in CGS21680-pretreated EGCs. As expected, chelerythrine chloride pretreatment also blocked CGS21680-promoted TER (533 ± 24.2 Ω cm^2 vs. 390.9 ± 24.14 Ω cm^2) (**Figure 5D**). Together, these results suggest that $A_{2A}R$ exerts its protective effects on IEB via the PKCα signaling pathway.

DISCUSSION

Our research has previously demonstrated that EGCs enhance IEB functions under acute intestinal injury (Xiao et al., 2014). In this context, our data provide the first evidence that EGCs protect IEB by activating $A_{2A}R$. The $A_{2A}R$ agonist significantly improved the barrier functions of Caco-2 monolayers following exposure to HR stimulation. Moreover, in $A_{2A}R$ KO mice, intestinal tissue damage was accelerated, including the structural and mucosal barrier defects, following intestinal I/R. We found that $A_{2A}R$ combines with mGluR5 under hypoxic conditions to exert a protective effect on IEB. This data also shows that $A_{2A}R$ and mGluR5 combine to activate the PKCα-dependent signaling pathway. Together, these results show that $A_{2A}R$ plays a critical role in the barrier protective mechanism of EGCs under acute intestinal hypoxia stimulation.

EGCs are involved in the regulation of IEB function. However, the precise mechanisms by which EGCs function in the regulation

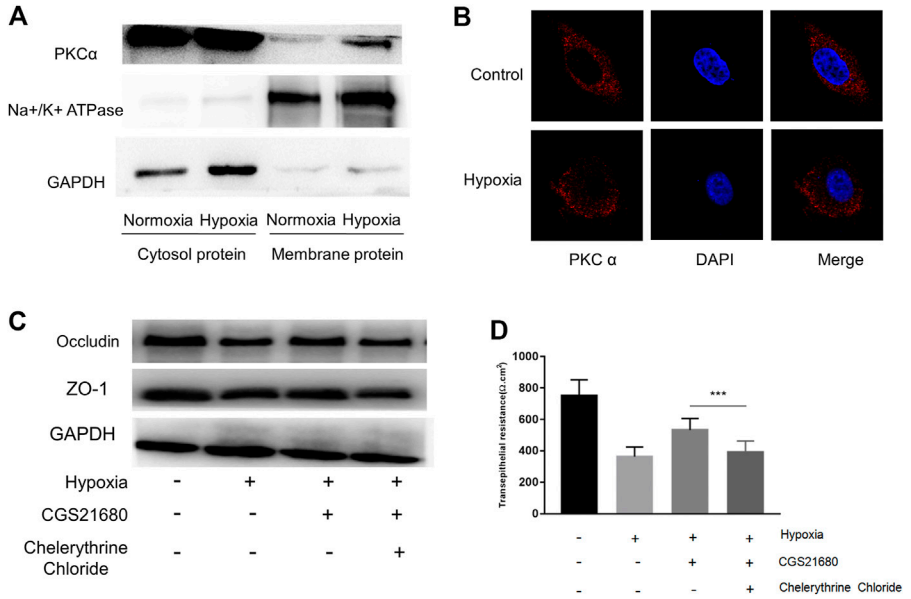

FIGURE 5 | The protective effect of $A_{2A}R$ on IEB is PKCα dependent. PKCα expression was assessed in different enteric glial cells (EGCs) fractions. **(A)** Membrane and cytosol proteins were respectively extracted to detect PKCα change under hypoxia. **(B)** Immunofluorescence was used to visualize PKCα distribution under hypoxia. **(C,D)** EGCs were co-cultured with Caco-2 monolayers for 24 h, then treated with chelerythrine chloride (10 μM) and CGS21680 (100 nM) for 6 h under hypoxic conditions. **(C)** Western blot and **(D)** TER analysis were used to detect the function of IEB. Results are expressed as mean ± SD. (***$p < 0.001$).

of IEB remain unclear. Increasing evidence indicates that EGCs and astrocytes share morphological features and electrophysiological properties and express similar proteins, including GFAP and S100β, leading to the idea that EGCs might share many features of the central nervous system astrocytes (Le Berre-Scoul et al., 2017). The similarities between EGCs and astrocytes indicate that these two glial cell types may regulate barrier functions through common molecular mechanisms (Jiang et al., 2005; Xiao et al., 2014). It is reported that primary cell cultures of either astrocytes or enteric glia can induce barrier properties across endothelia and epithelia (Savidge et al., 2007). Jiang Set al. previously reported that implantation of enteric glia accelerates normal spinal cord vasculature repair processes at the site of injury and promotes functional blood-brain barrier (BBB) induction (Jiang et al., 2005). Additionally, glia promote blood-brain barrier-like properties in peripheral sites including blood-ocular barriers in the eye, the perineurium of peripheral nerves, and the blood myenteric plexus barrier in the gut (Gershon and Bursztajn, 1978; Savidge et al., 2007). Our previous LPS and hypoxia reperfusion stimulation studies showed that EGCs can effectively alleviate IEB damage (Xiao et al., 2011; Xiao et al., 2014). Therefore, we explored the mechanism by which EGCs protect the IEB.

$A_{2A}R$ activation is closely related to a variety of neurological diseases and is an important component of the adenosine signaling pathway (Stone et al., 2009). Recently, many studies have suggested that $A_{2A}R$ also plays an important protective role in enteritis (Warren et al., 2012; Antonioli et al., 2018). However, there is relatively little information about the role of $A_{2A}R$ in intestinal IR damage. $A_{2A}R$ inactivation can prevent IR by regulating the inflammatory response and excitotoxic cascades in the brain, kidney, lung, and blood vessels (Vincent and Okusa, 2015; Li et al., 2013; Mohamed et al., 2012; Mohamed et al., 2016; Gui et al., 2009; Cunha, 2005). Due to the similarities between the brain and the intestine, we speculate that $A_{2A}R$ may also have protective effects on intestinal IR damage. Our data shows that IEB damage is accelerated in $A_{2A}R$ KO mice. However, because there are no mice with selective inactivation of EGCs-derived $A_{2A}R$, we cannot comprehensively show that EGCs protect IEB via the $A_{2A}R$ pathway. We exposed an *in vitro* EGC-Caco-2 co-culture system to hypoxia treatment to detect the role of $A_{2A}R$ in EGCs. Our results show that activation of $A_{2A}R$ in EGCs prevents damage to the IEB during hypoxia.

To clarify the mechanism by which $A_{2A}R$ influences IEB functions under acute intestinal epithelium hypoxia injury, we explored how $A_{2A}R$ works in the brain. Functional $A_{2A}R$-mGluR5 heteromeric complexes have been reported in the central nervous system (Beggiato et al., 2016; Temido-Ferreira et al., 2018). Beggiato et al. found that $A_{2A}R$ and mGlu5R interact synergistically to modulate D2R-mediated control of striatopallidal GABA neurons (Beggiato et al., 2016). Additionally, Dai et al. reported that $A_{2A}R$-mGluR5 interplay is critical for the proinflammatory effect in bone marrow-derived cells (BMDCs) after acute lung injury (Dai et al., 2013). Consistent with our expectation, we observed that $A_{2A}R$ combined with mGluR5 in EGCs suffering from hypoxia.

mGluR5 is a G-protein-coupled receptor that exerts its physiological roles through intracellular chemical-messenger signaling cascades (Power et al., 2016). In general, mGluR5 represents a promising target for studying neuro-protective agents of potential application in neurodegenerative diseases (Li et al., 2017). However, little data exists supporting the function of

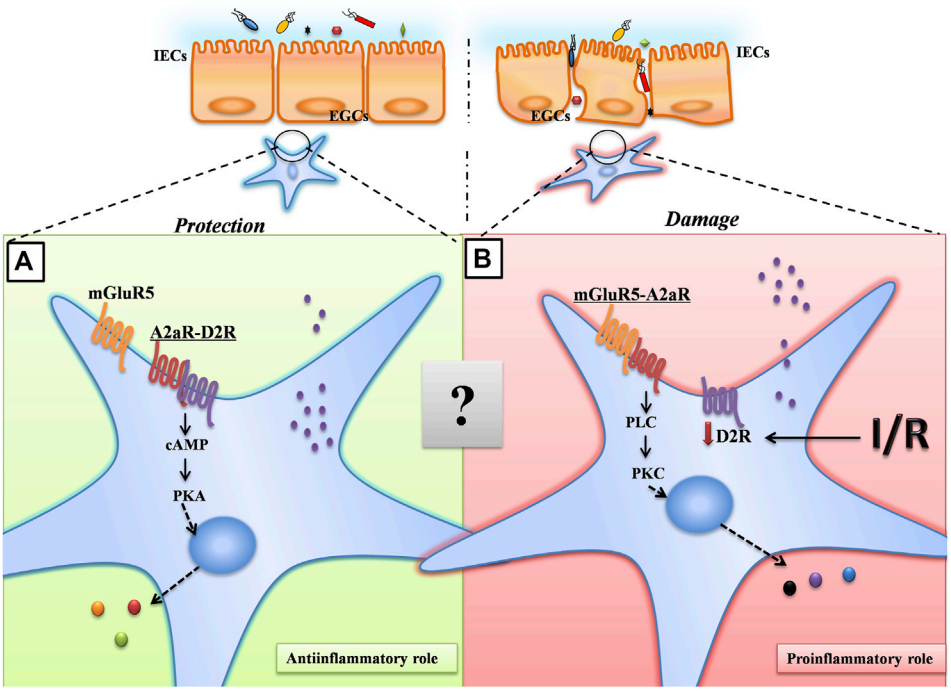

FIGURE 6 | A proposed model for $A_{2A}R$ in the maintenance of intestinal barrier function. Under normoxic conditions, $A_{2A}R$ combines with D2R to maintain the normal physiological activities of EGCs through the PKA signaling pathway. Under hypoxic conditions, $A_{2A}R$ combines with mGluR5 to protect IEB function via the PKCα pathway in EGCs.

mGluR5 in the intestine, especially in relation to its role in IEB regulation. In the intestinal mucosa, mGluR5 is only observed in EGCs (Nasser et al., 2007). EGCs are involved in the occurrence of inflammatory bowel disease through c-Fos and ERK1/2 phosphorylation induced by mGluR5 (Nasser et al., 2007). In the present study, we demonstrated that mGluR5 plays a key role in the protection of IEB by $A_{2A}R$. The proinflammatory effect of mGluR5 is not mediated by PKC signaling, but instead uses the PKA pathway (Dai et al., 2013). Giaroni et al. reported that the PKCα antagonist significantly inhibits intestinal mucosal injury induced by IR (Giaroni et al., 2011). These studies provide further support for our results that $A_{2A}R$ protects the IEB by a PKCα dependent pathway.

Taken together, our results suggest a model for $A_{2A}R$ in the maintenance of intestinal barrier function. Upon intestinal hypoxia injury, $A_{2A}R$ combines with mGluR5 to protect IEB function via the PKCα pathway in EGCs (**Figure 6**). Although there are complex interactions between $A_{2A}R$ and mGluR5 that remain to be fully understood, our findings are important for a better understanding of the role of EGCs in regulating IEB. Additionally, these findings offer new insight into the clinical use of $A_{2A}R$ modulators for IR-induced intestinal injury.

DATA AVAILABILITY STATEMENT

The raw data supporting the conclusions of this article will be made available by the authors, without undue reservation.

ETHICS STATEMENT

The animal study was reviewed and approved by Animal Ethics Committee of the Army Medical University.

AUTHOR CONTRIBUTIONS

LS and XL contributed equally to this work. LS and XL conceived the study and analyzed the data. HG, SC, XF, and CZ performed the research. HY and WX wrote the manuscript.

FUNDING

This research was supported by grants from the National Natural Science Foundation of China (NSFC 81770524 and NSFC 81470803 to WX), and the Program of Changjiang Scholars and Innovative Research (IRT 13050 to HY).

ACKNOWLEDGMENTS

We thank Professor Yuanguo Zhou for providing the $A_{2A}R^{-/-}$ mice.

REFERENCES

Antonioli, L., El-Tayeb, A., Pellegrini, C., Fornai, M., Awwad, O., Giustarini, G., et al. (2018). Anti-inflammatory effect of a novel locally acting A2A receptor agonist in a rat model of oxazolone-induced colitis. *Purinergic Signal.* 14 (1), 27–36. doi:10.1007/s11302-017-9591-2

Antonioli, L., Fornai, M., Colucci, R., Ghisu, N., Blandizzi, C., and Del Tacca, M. (2006). A2a receptors mediate inhibitory effects of adenosine on colonic motility in the presence of experimental colitis. *Inflamm. Bowel Dis.* 12 (2), 117–122. doi:10.1097/01.mib.0000198535.13822.a9

Aube, A.-C., Cabarrocas, J., Bauer, J., Philippe, D., Aubert, P., Doulay, F., et al. (2006). Changes in enteric neurone phenotype and intestinal functions in a transgenic mouse model of enteric glia disruption. *Gut* 55 (5), 630–637. doi:10.1136/gut.2005.067595

Beggiato, S., Tomasini, M. C., Borelli, A. C., Borroto-Escuela, D. O., Fuxe, K., Antonelli, T., et al. (2016). Functional role of striatal A2A, D2, and mGlu5 receptor interactions in regulating striatopallidal GABA neuronal transmission. *J. Neurochem.* 138 (2), 254–264. doi:10.1111/jnc.13652

Bush, T. G., Savidge, T. C., Freeman, T. C., Cox, H. J., Campbell, E. A., Mucke, L., et al. (1998). Fulminant jejuno-ileitis following ablation of enteric glia in adult transgenic mice. *Cell* 93 (2), 189–201. doi:10.1016/s0092-8674(00)81571-8

Cabarrocas, J., Savidge, T. C., and Liblau, R. S. (2003). Role of enteric glial cells in inflammatory bowel disease. *Glia* 41 (1), 81–93. doi:10.1002/glia.10169

Cheadle, G. A., Costantini, T. W., Lopez, N., Bansal, V., Eliceiri, B. P., and Coimbra, R. (2013). Enteric glia cells attenuate cytomix-induced intestinal epithelial barrier breakdown. *PLoS One* 8 (7), e69042. doi:10.1371/journal.pone.0069042

Cunha, R. A. (2005). Neuroprotection by adenosine in the brain: from A1 receptor activation to A2A receptor blockade. *Purinergic Signal.* 1 (2), 111–134. doi:10.1007/s11302-005-0649-1

Dai, S.-S., Wang, H., Yang, N., An, J.-H., Li, W., Ning, Y.-L., et al. (2013). Plasma glutamate-modulated interaction of A2AR and mGluR5 on BMDCs aggravates traumatic brain injury-induced acute lung injury. *J. Exp. Med.* 210 (4), 839–851. doi:10.1084/jem.20122196

Dai, S. S., Zhou, Y. G., Li, W., An, J. H., Li, P., Yang, N., et al. (2010). Local glutamate level dictates adenosine A2A receptor regulation of neuroinflammation and traumatic brain injury. *J. Neurosci.* 30 (16), 5802–5810. doi:10.1523/jneurosci.0268-10.2010

Duarte-Araújo, M., Nascimento, C., Alexandrina Timóteo, M., Magalhães-Cardoso, T., and Correia-de-Sá, P. (2004). Dual effects of adenosine on acetylcholine release from myenteric motoneurons are mediated by junctional facilitatory A2A and extrajunctional inhibitory A1 receptors. *Br. J. Pharmacol.* 141 (6), 925–934. doi:10.1038/sj.bjp.0705697

Fernández-Dueñas, V., Gómez-Soler, M., Morató, X., Núñez, F., Das, A., Kumar, T. S., et al. (2013). Dopamine D2 receptor-mediated modulation of adenosine A2A receptor agonist binding within the A2AR/D2R oligomer framework. *Neurochem. Int.* 63 (1), 42–46. doi:10.1016/j.neuint.2013.04.006

Ferraro, L., Beggiato, S., Tomasini, M. C., Fuxe, K., Antonelli, T., and Tanganelli, S. (2012). A2A/D2 receptor heteromerization in a model of Parkinson's disease. Focus on striatal aminoacidergic signaling. *Brain Res.* 1476, 96–107. doi:10.1016/j.brainres.2012.01.032

Fornai, M., Antonioli, L., Colucci, R., Ghisu, N., Buccianti, P., Marioni, A., et al. (2009). A1and A2areceptors mediate inhibitory effects of adenosine on the motor activity of human colon. *Neurogastroenterol. Motil.* 21 (4), 451–466. doi:10.1111/j.1365-2982.2008.01213.x

Gershon, M. D., and Bursztajn, S. (1978). Properties of the enteric nervous system: limitation of access of intravascular macromolecules to the myenteric plexus and muscularis externa. *J. Comp. Neurol.* 180 (3), 467–487. doi:10.1002/cne.901800305

Giaroni, C., Zanetti, E., Giuliani, D., Oldrini, R., Marchet, S., Moro, E., et al. (2011). Protein kinase C modulates NMDA receptors in the myenteric plexus of the Guinea pig ileum during *in vitro* ischemia and reperfusion. *Neurogastroenterol. Motil.* 23 (2), e91–e103. doi:10.1111/j.1365-2982.2010.01644.x

Gui, L., Duan, W., Tian, H., Li, C., Zhu, J., Chen, J.-F., et al. (2009). Adenosine A2A receptor deficiency reduces striatal glutamate outflow and attenuates brain injury induced by transient focal cerebral ischemia in mice. *Brain Res.* 1297, 185–193. doi:10.1016/j.brainres.2009.08.050

Jiang, S., Khan, M. I., Lu, Y., Werstiuk, E. S., and Rathbone, M. P. (2005). Acceleration of blood-brain barrier formation after transplantation of enteric glia into spinal cords of rats. *Exp. Brain Res.* 162 (1), 56–62. doi:10.1007/s00221-004-2119-3

Le Berre-Scoul, C., Chevalier, J., Oleynikova, E., Cossais, F., Talon, S., Neunlist, M., et al. (2017). A novel enteric neuron-glia coculture system reveals the role of glia in neuronal development. *J. Physiol.* 595 (2), 583–598. doi:10.1113/jp271989

Lee, S. H. (2015). Intestinal permeability regulation by tight junction: implication on inflammatory bowel diseases. *Intest Res.* 13 (1), 11–18. doi:10.5217/ir.2015.13.1.11

Li, C., Chai, S., Ju, Y., Hou, L., Zhao, H., Ma, W., et al. (2017). Pu-erh tea protects the nervous system by inhibiting the expression of metabotropic glutamate receptor 5. *Mol. Neurobiol.* 54 (7), 5286–5299. doi:10.1007/s12035-016-0064-3

Li, J., Zhao, Z., He, X., Zeng, Y-J., and Dai, S.-S. (2013). Sinomenine protects against lipopolysaccharide-induced acute lung injury in mice via adenosine A(2A) receptor signaling. *PLoS One* 8 (3), e59257. doi:10.1371/journal.pone.0059257

Liu, Z., Li, L., Chen, W., Wang, Q., Xiao, W., Ma, Y., et al. (2018). Aryl hydrocarbon receptor activation maintained the intestinal epithelial barrier function through Notch1 dependent signaling pathway. *Int. J. Mol. Med.* 41 (3), 1560–1572. doi:10.3892/ijmm.2017.3341

Lu, Y.-Z., Wu, C.-C., Huang, Y.-C., Huang, C.-Y., Yang, C.-Y., Lee, T.-C., et al. (2012). Neutrophil priming by hypoxic preconditioning protects against epithelial barrier damage and enteric bacterial translocation in intestinal ischemia/reperfusion. *Lab. Invest.* 92 (5), 783–796. doi:10.1038/labinvest.2012.11

Mallick, I. H., Yang, W., Winslet, M. C., and Seifalian, A. M. (2004). Ischemia-reperfusion injury of the intestine and protective strategies against injury. *Dig. Dis. Sci.* 49 (9), 1359–1377. doi:10.1023/b:ddas.0000042232.98927.91

Mohamed, R. A., Agha, A. M., Abdel-Rahman, A. A., and Nassar, N. N. (2016). Role of adenosine A2A receptor in cerebral ischemia reperfusion injury: signaling to phosphorylated extracellular signal-regulated protein kinase (pERK1/2). *Neuroscience* 314, 145–159. doi:10.1016/j.neuroscience.2015.11.059

Mohamed, R. A., Agha, A. M., and Nassar, N. N. (2012). SCH58261 the selective adenosine A2A receptor blocker modulates ischemia reperfusion injury following bilateral carotid occlusion: role of inflammatory mediators. *Neurochem. Res.* 37 (3), 538–547. doi:10.1007/s11064-011-0640-x

Nasser, Y., Keenan, C. M., Ma, A. C., McCafferty, D.-M., and Sharkey, K. A. (2007). Expression of a functional metabotropic glutamate receptor 5 on enteric glia is altered in states of inflammation. *Glia* 55 (8), 859–872. doi:10.1002/glia.20507

Neunlist, M., Van Landeghem, L., Bourreille, A., and Savidge, T. (2008). Neuro-glial crosstalk in inflammatory bowel disease. *J. Intern. Med.* 263 (6), 577–583. doi:10.1111/j.1365-2796.2008.01963.x

Neunlist, M., Van Landeghem, L., Mahé, M. M., Derkinderen, P., des Varannes, S. B., and Rolli-Derkinderen, M. (2013). The digestive neuronal-glial-epithelial unit: a new actor in gut health and disease. *Nat. Rev. Gastroenterol. Hepatol.* 10 (2), 90–100. doi:10.1038/nrgastro.2012.221

Power, E. M., English, N. A., and Empson, R. M. (2016). Are Type 1 metabotropic glutamate receptors a viable therapeutic target for the treatment of cerebellar ataxia? *J. Physiol.* 594 (16), 4643–4652. doi:10.1113/jp271153

Ruhl, A. (2005). Glial cells in the gut. *Neurogastroenterol. Motil.* 17 (6), 777–790. doi:10.1111/j.1365-2982.2005.00687.x

Savidge, T. C., Sofroniew, M. V., and Neunlist, M. (2007). Starring roles for astroglia in barrier pathologies of gut and brain. *Lab. Invest.* 87 (8), 731–736. doi:10.1038/labinvest.3700600

Schriemer, D., Sribudiani, Y., IJpma, A., Natarajan, D., MacKenzie, K. C., Metzger, M., et al. (2016). Regulators of gene expression in enteric neural crest cells are putative Hirschsprung disease genes. *Develop. Biol.* 416 (1), 255–265. doi:10.1016/j.ydbio.2016.06.004

Stone, T. W., Ceruti, S., and Abbracchio, M. P. (2009). Adenosine receptors and neurological disease: neuroprotection and neurodegeneration. *Handb Exp. Pharmacol.* (193), 535–587. doi:10.1007/978-3-540-89615-9_17

Temido-Ferreira, M., Ferreira, D. G., Batalha, V. L., Marques-Morgado, I., Coelho, J. E., Pereira, P., et al. (2018). Age-related shift in LTD is dependent on neuronal adenosine A2A receptors interplay with mGluR5 and NMDA receptors. *Mol. Psychiatry* 25 (8), 1876–1900. doi:10.1038/s41380-018-0110-9

Vincent, I. S., and Okusa, M. D. (2015). Adenosine 2A receptors in acute kidney injury. *Acta Physiol.* 214 (3), 303–310. doi:10.1111/apha.12508

Vollmar, B., and Menger, M. D. (2011). Intestinal ischemia/reperfusion: microcirculatory pathology and functional consequences. *Langenbecks Arch. Surg.* 396 (1), 13–29. doi:10.1007/s00423-010-0727-x

von Boyen, G., and Steinkamp, M. (2010). The role of enteric glia in gut inflammation. *Neuron Glia Biol.* 6 (4), 231–236. doi:10.1017/s1740925x11000068

Warren, C. A., Calabrese, G. M., Li, Y., Pawlowski, S.W., Figler, R. A., Rieger, J., et al. (2012). Effects of adenosine A_2A receptor activation and alanyl-glutamine in *Clostridium difficile* toxin-induced ileitis in rabbits and cecitis in mice. *BMC Infect. Dis.* 12, 13. doi:10.1186/1471-2334-12-13

Welihinda, A. A., Kaur, M., Greene, K., Zhai, Y., and Amento, E. P. (2016). The adenosine metabolite inosine is a functional agonist of the adenosine A2A receptor with a unique signaling bias. *Cell. Signal.* 28 (6), 552–560. doi:10.1016/j.cellsig.2016.02.010

Xiao, W.-D., Chen, W., Sun, L.-H., Wang, W.-S., Zhou, S.-W., and Yang, H. (2011). The protective effect of enteric glial cells on intestinal epithelial barrier function is enhanced by inhibiting inducible nitric oxide synthase activity under lipopolysaccharide stimulation. *Mol. Cell. Neurosci.* 46 (2), 527–534. doi:10.1016/j.mcn.2010.12.007

Xiao, W., Wang, W., Chen, W., Sun, L., Li, X., Zhang, C., et al. (2014). GDNF is involved in the barrier-inducing effect of enteric glial cells on intestinal epithelial cells under acute ischemia reperfusion stimulation. *Mol. Neurobiol.* 50 (2), 274–289. doi:10.1007/s12035-014-8730-9

Yu, H., Yang, Z., Pan, S., Yang, Y., Tian, J., Wang, L., et al. (2015). Hypoxic preconditioning promotes the translocation of protein kinase C ε binding with caveolin-3 at cell membrane not mitochondrial in rat heart. *Cell Cycle* 14 (22), 3557–3565. doi:10.1080/15384101.2015.1084446

Zhang, D. K., He, F. Q., Li, T. K., Pang, X. H., Cui, D. J., Xie, Q., et al. (2010). Glial-derived neurotrophic factor regulates intestinal epithelial barrier function and inflammation and is therapeutic for murine colitis. *J. Pathol.* 222 (2), 213–222. doi:10.1002/path.2749

Conflict of Interest: The authors declare that the research was conducted in the absence of any commercial or financial relationships that could be construed as a potential conflict of interest.

frontiers in Pharmacology

ORIGINAL RESEARCH
published: 21 May 2021
doi: 10.3389/fphar.2021.625543

The Synergistic Effects of 5-Aminosalicylic Acid and Vorinostat in the Treatment of Ulcerative Colitis

*Long He[1,2], Shuting Wen[1,2], Zhuotai Zhong[1], Senhui Weng[1], Qilong Jiang[3], Hong Mi[3] and Fengbin Liu[2,3,4]**

[1]The First Clinical College, Guangzhou University of Chinese Medicine, Guangzhou, China, [2]Lingnan Medical Reserch Center of Guangzhou University of Chinese Medicine, Guangzhou, China, [3]Department of Gastroenterology, The First Affiliated Hospital of Guangzhou University of Chinese Medicine, Guangzhou, China, [4]Baiyun Hospital of the First Affiliated Hospital of Guangzhou University of Chinese Medicine, Guangzhou, China

Background: The drug 5-aminosalicylic acid (5-ASA) is the first-line therapy for the treatment of patients with mild-to-moderate ulcerative colitis (UC). However, in some cases, 5-ASA cannot achieve the desired therapeutic effects. Therefore, patients have to undergo therapies that include corticosteroids, monoclonal antibodies or immunosuppressants, which are expensive and may be accompanied by significant side effects. Synergistic drug combinations can achieve greater therapeutic effects than individual drugs while contributing to combating drug resistance and lessening toxic side effects. Thus, in this study, we sought to identify synergistic drugs that can act synergistically with 5-ASA.

Methods: We started our study with protein-metabolite analysis based on peroxisome proliferator-activated receptor gamma (PPARG), the therapeutic target of 5-ASA, to identify more additional potential drug targets**.** Then, we further evaluated the possibility of their synergy with PPARG by integrating Kyoto Encyclopedia of Genes and Genome (KEGG) pathway enrichment analysis, pathway-pathway interaction analysis, and semantic similarity analysis. Finally, we validated the synergistic effects with *in vitro* and *in vivo* experiments.

Results: The combination of 5-ASA and vorinostat (SAHA) showed lower toxicity and mRNA expression of p65 in human colonic epithelial cell lines (Caco-2 and HCT-116), and more efficiently alleviated the symptoms of dextran sulfate sodium (DSS)-induced colitis than treatment with 5-ASA and SAHA alone.

Conclusion: SAHA can exert effective synergistic effects with 5-ASA in the treatment of UC. One possible mechanism of synergism may be synergistic inhibition of the nuclear factor kappa B (NF-kB) signaling pathway. Moreover, the metabolite-butyric acid may be involved.

Keywords: ulcerative colitis, 5-ASA, SAHA, protein-metabolite interactions, butyric acid, synergistic effects

OPEN ACCESS

Edited by:
Heike Wulff,
University of California, Davis, United States

Reviewed by:
Thomas Brzozowski,
Jagiellonian University Medical College, Poland
Lixin Zhu,
The Sixth Affiliated Hospital of Sun Yat-sen University, China

****Correspondence:***
Fengbin Liu
Liufb163@vip.163.com

Specialty section:
This article was submitted to Gastrointestinal and Hepatic Pharmacology, a section of the journal Frontiers in Pharmacology

Received: *03 November 2020*
Accepted: *10 May 2021*
Published: *21 May 2021*

Citation:
He L, Wen S, Zhong Z, Weng S, Jiang Q, Mi H and Liu F (2021) The Synergistic Effects of 5-Aminosalicylic Acid and Vorinostat in the Treatment of Ulcerative Colitis. Front. Pharmacol. 12:625543. doi: 10.3389/fphar.2021.625543

Abbreviations: 5-ASA, 5-Aminosalicylic Acid; UC, Ulcerative Colitis; PPARG, Peroxisome Proliferator-Activated Receptor Gamma; KEGG, Kyoto Encyclopedia of Genes and Genome; SAHA, vorinostat; NF-kB, Nuclear factor kappaB; TNF, tumor necrosis factor; PPIs, Protein-Protein Interactions; TTD, Therapeutic Target database; HDAC, Histone Deacetylases.

INTRODUCTION

Ulcerative colitis (UC) is a chronic inflammatory disease affecting the colon, with increasing prevalence in recent years (Ungaro et al., 2017). Treatments for UC mainly include 5-aminosalicylic acid (5-ASA) drugs, biological drugs, corticosteroids, and immunosuppressants (Doyle and King, 1989). Among these, 5-ASA drugs are the main choice for the treatment of patients with mild-to-moderate UC (Pedersen and Brynskov, 2010), mainly because of their efficacy and safety. However, a subset of patients may not respond to 5-ASA, therefore, they can only be treated with corticosteroids or biological drugs (Bressler et al., 2015). Patients with UC usually require long-term medication to maintain efficacy, but long-term treatment with corticosteroids may produce acquired drug resistance and significant side effects (Bressler et al., 2015). Biological drugs, such as anti-tumor necrosis factor (TNF)-α therapies, are very expensive. Thus, it is necessary to develop a viable solution to enhance efficacy and reduce drug resistance to 5-ASA.

To treat certain complex diseases, such as cancer, cardiovascular diseases and type II diabetes, drug combinations have been developed (Kreek and Balint, 1980). Enhanced synergistic and antagonistic effects can be created by different types of drug combinations (Jia et al., 2009), and can contribute to combating drug resistance and disease heterogeneity (Hu et al., 2019). Among these, synergistic drug combinations present a prosperous future (Sheng et al., 2018) as they can achieve greater therapeutic effects than the drugs individually (Chou, 2006), while reducing side effects and drug resistance at the same time (Nowak-Sliwinska et al., 2016). Therefore, we hypothesized that identifying synergistic drugs for 5-ASA may be an effective solution to solve the problem of its insufficient efficacy and drug resistance in certain cases.

Based on previous studies, the crucial step for identifying synergistic drugs may be the discovery of potential drug candidates (Sun et al., 2015). In recent years, protein-protein interactions (PPIs) have been considered promising targets in drug discovery (Murakami et al., 2017). This is mainly due to the important roles of proteins in the regulation of biological systems and disease development (Scott et al., 2016). However, proteins can also be associated indirectly with downstream reactions through metabolites (Casas et al., 2019). In addition, recent studies have shown that many metabolites can function intracellularly or act directly as signaling molecules (Husted et al., 2017). For instance, the β-hydroxybutyrate (BHB) ketone can provide pivotal energy when the body's glucose supply is too low (Newman and Verdin, 2017). Furthermore, metabolites can also regulate protein function by acting as protein modifiers (Li et al., 2013). In fact, many signaling events are governed by intermediate metabolites rather than PPIs (Li et al., 2013; Casas et al., 2019). In addition, several studies have reported that metabolites play a vital role in drug discovery (Bertrand et al., 2014; Wishart, 2016). Subsequently, protein-metabolite interactions have emerged as new leads for drug discovery (Casas et al., 2019; Mateus et al., 2020).

In this manuscript, we sought to discover synergistic drugs for 5-ASA to solve the problem of drug resistance and insufficient efficacy that appear in some cases. To identify potential drug candidates, we constructed a network of protein-metabolite interactions and filtered out undruggable targets. Then, we integrated KEGG pathway enrichment analysis, pathway-pathway interaction analysis, and semantic similarity analysis to screen for the most effective targets (**Supplementary Figure S1**). Through the Therapeutic Target database (TTD), we finally identified that SAHA, a histone deacetylase (HDAC) inhibitor (Eckschlager et al., 2017), can work synergistically with 5-ASA. Moreover, we validated their synergistic effects by experiments by *in vitro* and *in vivo* experiments. Notably, PPARG, a key factor in mucosal homeostasis, is the therapeutic target of 5-ASA (Bouguen et al., 2015). Thus, we started our study with protein-metabolite analysis based on PPARG.

RESULTS

Protein-Metabolite Analysis and Network Construction

To identify additional potential drug targets that work synergistically on PPARG, we conducted protein-metabolite interaction analysis through the Human Metabolome Database (HMDB). The HMDB is a database that can provide information about metabolites and their associated proteins (Wishart et al., 2018). In total, with 54 metabolite entries, we established 359 proteins interacting indirectly with PPARG. Next, we further limited the range of potential targets by filtering undruggable target proteins through the TTD (Yang et al., 2016). Subsequently, 63 druggable target proteins (those currently in clinical trials or used in the clinic) were selected (**Supplementary Table S1**). Finally, we integrated the protein-metabolite interactions and built a two-layered network showing the interactions among the associated proteins, metabolite entries, and our seed target-PPARG (**Figure 1**).

KEGG Pathway Enrichment Analysis and Pathway-Pathway Interaction Analysis

Given the potential drug targets, we next evaluated the possibility of synergy between these targets and PPARG. It has been reported that different drug targets involved in the same or associated pathways may produce synergistic effects (Jia et al., 2009). Since PPARG participates in the regulation of UC primarily by inhibiting the nuclear factor-kB (NF-kB) signaling pathway (Cao et al., 2018), drug targets involved in the NF-kB pathway or related pathways can function synergistically with PPARG. Moreover, Chen et al. proposed that pathways can interact with each other by gene-overlapping, functional-related and protein-protein interactions, and gene-overlapping pathway-pathway interactions suggesting more potential for predicting drug synergy (Chen D. et al., 2016). Therefore, we conducted KEGG pathway enrichment analysis on these 63 protein targets (**Figure 2A**). Consequently, pathways such as "Pathways in cancer", "Viral carcinogenesis", "Epstein-Barr virus infection", and "Adipocytokine signaling pathway" were identified to interact with the NF-κB pathway *via* gene-

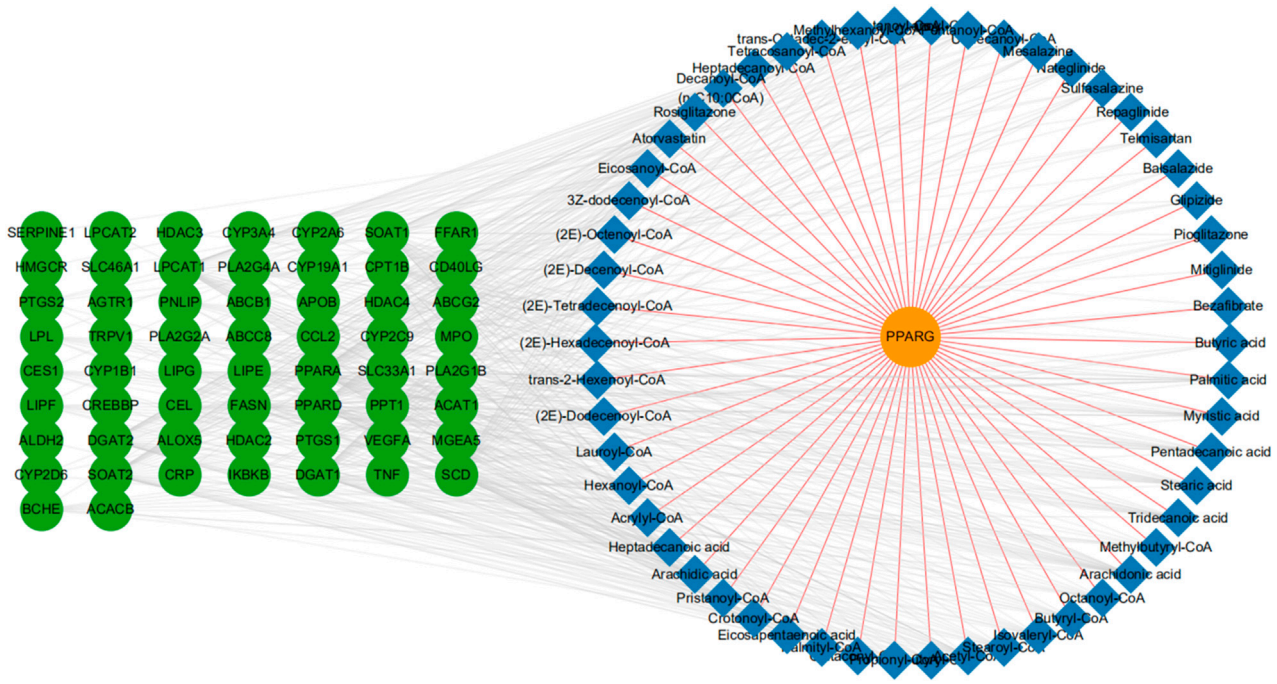

FIGURE 1 | Protein-metabolite network construction. A full network based on the primary protein, PPARG (orange node), associated metabolites (blue node), and related druggable proteins (green node). We also show PPARG-metabolite interactions (brown-yellow edges), and metabolite-protein interactions (light gray edges).

overlapping (**Figure 2B**). Collectively, 20 targets involved in these pathways can function synergistically with PPARG (**Figure 2B**).

Semantic Similarity of Gene Ontology Terms Analysis

Gene Ontology (GO) is a commonly used bioinformatics resource that provides information on the study of protein-protein interactions (Jain and Bader, 2010; Gene Ontology, 2015). Two proteins with similar functions could be further estimated by the geometric mean of semantic similarities in molecular function (MF) and component (CC) of each GO term pair (Wang et al., 2011; Han et al., 2013). Since functional similarity reflects the strength of the relationship between two proteins (Han et al., 2013), by evaluating the functional similarities between each potential target protein and PPARG through the semantic GOSemSim package using the Wang process (Yu et al., 2010), we further narrowed the range of candidate target protein. Finally, we obtained a rank list of functional similarity scores between the candidate target proteins and PPARG (**Figure 2C**; **Supplementary Table S2**).

Peroxisome proliferator-activated receptor alpha (PPARA), peroxisome proliferator-activated receptor delta (PPARD), histone deacetylase 2 (HDAC2), CREB binding protein (CREBBP), histone deacetylase 4 (HDAC4) and histone deacetylase 3 (HDAC3) received the highest scores, suggesting that they were the most likely to synergize with PPARG. However, PPARA is more likely to interfere with the NF-kB pathway in primary smooth muscle cells and hepatocytes rather than intestinal epithelial cells (Bougarne et al., 2018); PPARD is more involved in lipid metabolism; and histone deacetylases (HDACs) are upstream of CREBBP and can inhibit CREBPP (Jia et al., 2018). Thus, HDACs could be ideal candidate target proteins to work synergistically with PPARG in UC. Therefore, we next validated our predictions through experiments.

Validation of the Synergistic Effects of SAHA and 5-ASA in Human Colonic Epithelial Cell Lines

We selected human colon adenocarcinoma cells (Caco-2) and colon cancer cells (HCT-116) to validate the synergistic effects of SAHA and 5-ASA. First, the cytotoxic effects of the PPARG agonist 5-ASA (30 mM) and HDACs inhibitor SAHA (5 μM) on Caco-2 cells were observed after 24 and 48 h of treatment. Notably, the combination of 5-ASA and SAHA from the CCK-8 assay had a lower cytotoxic effect than that of Caco-2 cells treated with 5-ASA or SAHA alone after 48 h of treatment (**Figure 3A**). In addition, when combining 5-ASA with SAHA, the mRNA expression of NF-kB (p65) was significantly reduced compared with that when the cells were individually treated with 5-ASA or SAHA (**Figure 3B**). Similarly, treatment with both 5-ASA and SAHA showed lower cytotoxic effects (**Figure 3C**) and p65 mRNA expression (**Figure 3D**) than individual treatment with 5-ASA or SAHA alone in HCT-116 cells. These findings displayed that the combined use of 5-ASA and SAHA can reduce

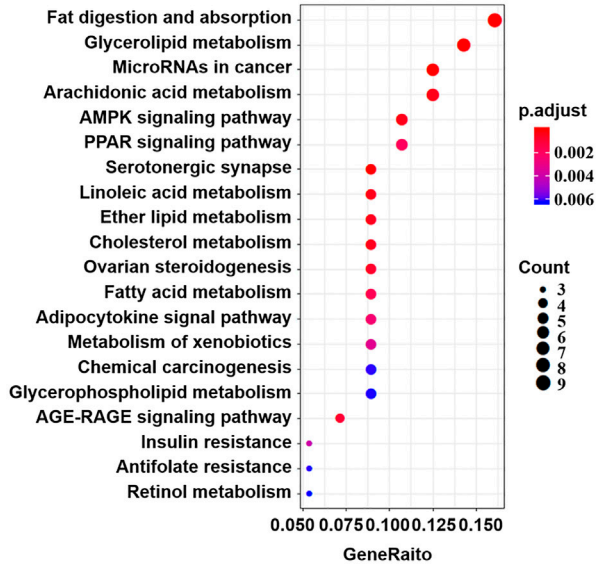

C

UniProt ID	Protein	Semantic similarity
P37231	PPARG	1
Q07869	PPARA	0.84510946
Q03181	PPARD	0.838858749
Q92793	CREBBP	0.727696365
Q92769	HDAC2	0.725939391
P56524	HDAC4	0.714321356
O15379	HDAC3	0.660686007
O00763	ACACB	0.614413542
P35354	PTGS2	0.586432434
O14920	IKBKB	0.578058821

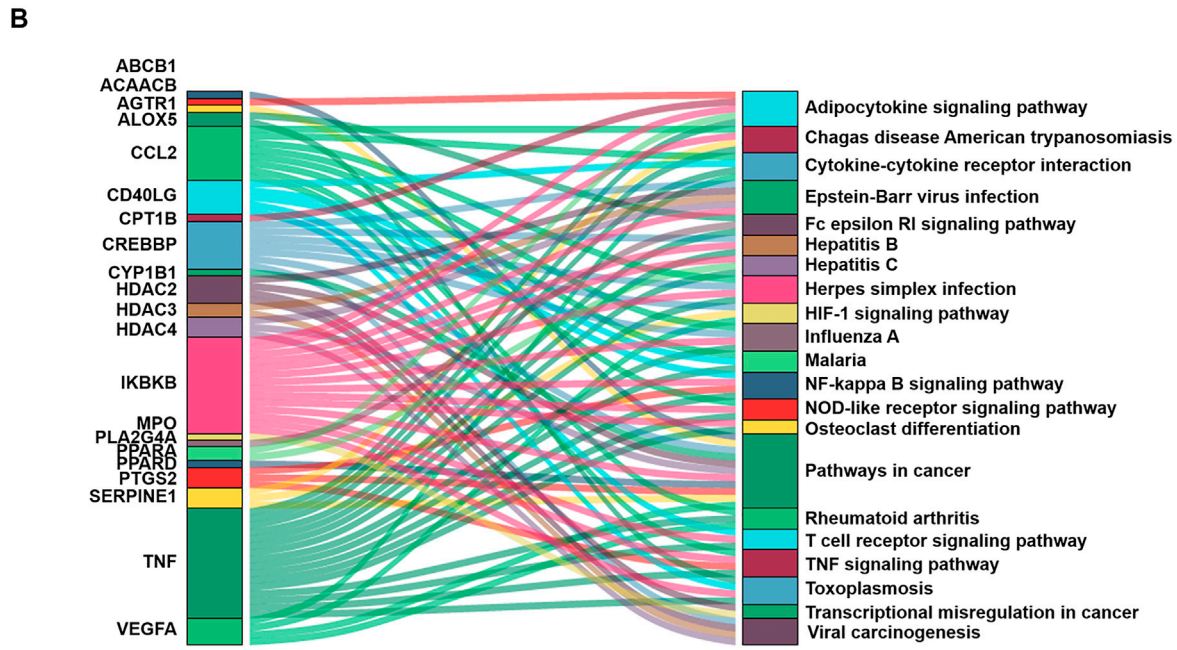

FIGURE 2 | Measurement of the possibility of synergy. **(A)** KEGG pathway enrichment analysis on druggable target proteins. **(B)** Sankey plots of the pathways enriched for the druggable genes. **(C)** The top 10 candidate target proteins with semantic similarity scores and their UniProt IDs.

drug cytotoxicity and synergistically inhibit the NF-kB signaling pathway.

Synergistic Effects of SAHA and 5-ASA in Experimental Colitis

We next further confirmed the synergistic effects of 5-ASA and SAHA in experimental colitis. DSS-induced colitis mice were orally treated with either 5-ASA (100 mg/kg/day) or SAHA (200 mg/kg/day), and 5-ASA and SAHA combined treatment. Treatment with 5-ASA or SAHA reduced DSS-induced colitis symptoms, including weight loss. (**Figure 4A**), disease activity index (DAI) (**Figure 4B**), colon length (**Figure 4C**) and histological score (**Figure 4D**). While combination therapy was more effective in relieving these symptoms, our findings revealed that the combined use of 5-ASA and SAHA in the treatment of experimental colitis had a synergistic impact. We then sought to determine whether 5-ASA and SAHA play a

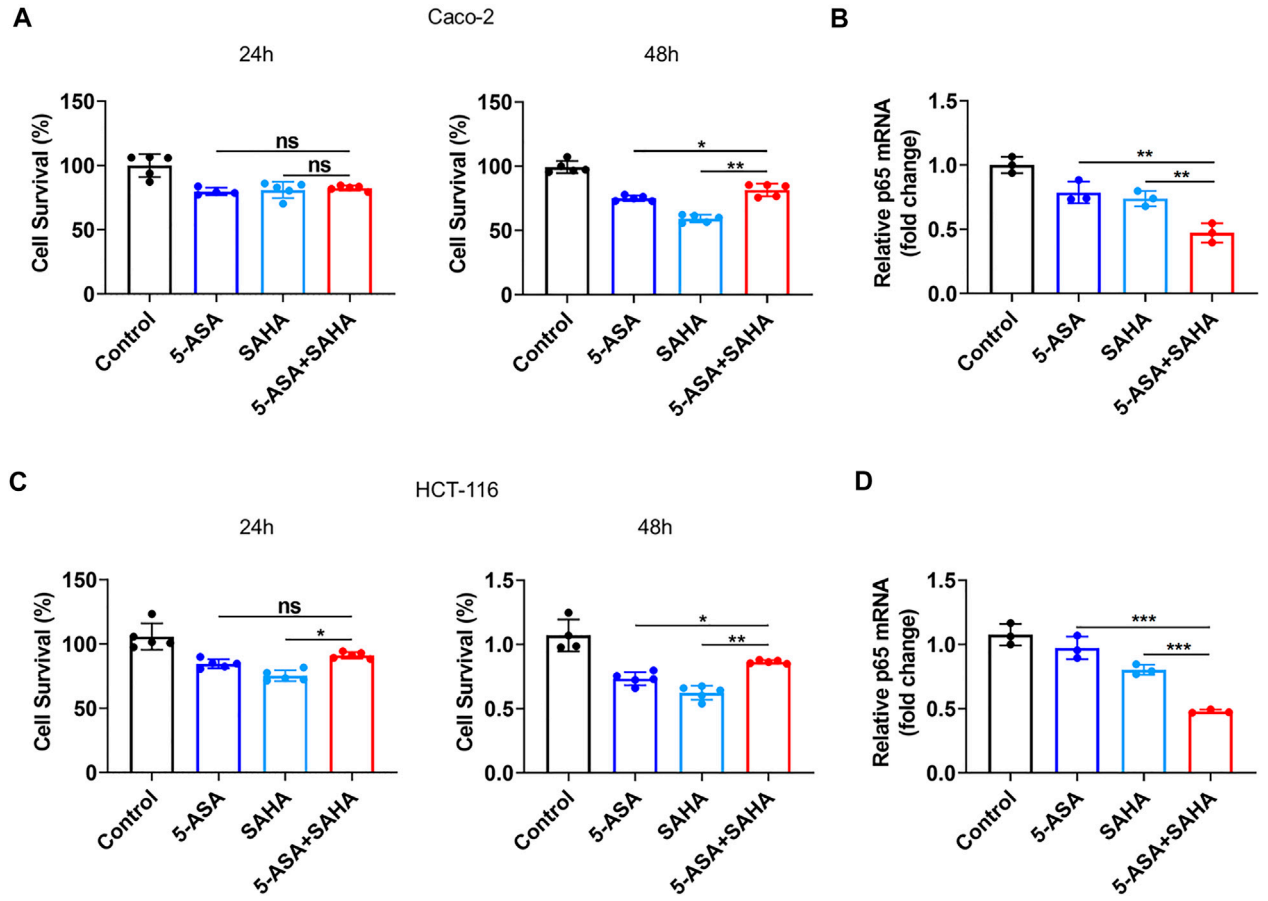

FIGURE 3 | Validation of the prediction results *in vivo*. **(A,C)** CCK eight analysis was performed to evaluate the toxicity of 5-ASA (30 mM) and SAHA (5 μM) alone or in combination in Caco-2 cells or HCT-116 cells after 24 and 48 h of treatment; **(B,D)** The p65 mRNA levels were examined in Caco-2 cells and HCT-116 cells treated with 5-ASA and SAHA in . The data shown are the mean ± SD and represent three independent experiments, *p* values were calculated using an unpaired *t*-test, $^{*}p < 0.05$, $^{**}p < 0.01$, $^{***}p < 0.001$, ns = not significant.

synergistic role in experimental colitis because of their synergistic regulation of the NF-kB signaling pathway. Through immunohistochemical analysis, we detected p65 expression in colon tissues and found that the combined use of 5-ASA and SAHA significantly reduced p65 expression compared with 5-ASA or SAHA (**Figure 4E**). In addition, combined treatment showed lower mRNA expression of p65 compared with the single treatment (**Figure 4F**). The expression levels of downstream inflammatory factors such as IL-6, IL-1β, and TNF-α of the NF-kB signaling pathway were also significantly reduced (**Figure 4G**). Collectively, our findings indicate that SAHA and 5-ASA can exert a synergistic effect in the treatment of experimental colitis by synergistically inhibiting the NF-kB signaling pathway.

Synergistic Effects of SAHA and 5-ASA in the Treatment of Experimental Colitis May be Associated With Butyric Acid

Our network of protein-metabolite analysis results indicated that PPARG and HDACs (HDAC2, HDAC3, HDAC4) can both interact with butyric acid (**Figure 5A**). Furthermore, molecular docking studies suggested that butyric acid can bind to PPARG and HDACs (**Figures 5B,C**). These data demonstrated that PPARG can interact with HDACs through butyric acid. Given the crucial role of metabolites in regulating protein function, we wondered whether butyric acid is upstream of PPARG and HDACs, which may contribute to the synergistic effects of the combination of 5-ASA and SAHA in the treatment of experimental colitis. Thus, we treated Caco-2 cells with butyrate (5 mM) and observed that the mRNA expression of PPARG was upregulated while the expression levels of HDAC2, HDAC3, and HDAC4 were downregulated (**Figure 6A**). In addition, body weight loss (**Figure 6B**), DAI score (**Figure 6C**), colonic shortening (**Figure 6D**) and colon pathology (**Figure 6E**) were improved in DSS-induced mice treated with butyrate (200 mM) compared with those receiving vehicle treatment. Additionally, DSS-induced colonic epithelial cells of mice treated with butyrate exhibited higher expression of PPARG and lower expression of HDAC2, HDAC3, and HDAC4 (**Figure 6F**). These results implied that the metabolite-butyric acid can target both PPARG and HDACs in experimental colitis. Thus, the synergistic effects of 5-ASA and SAHA in the

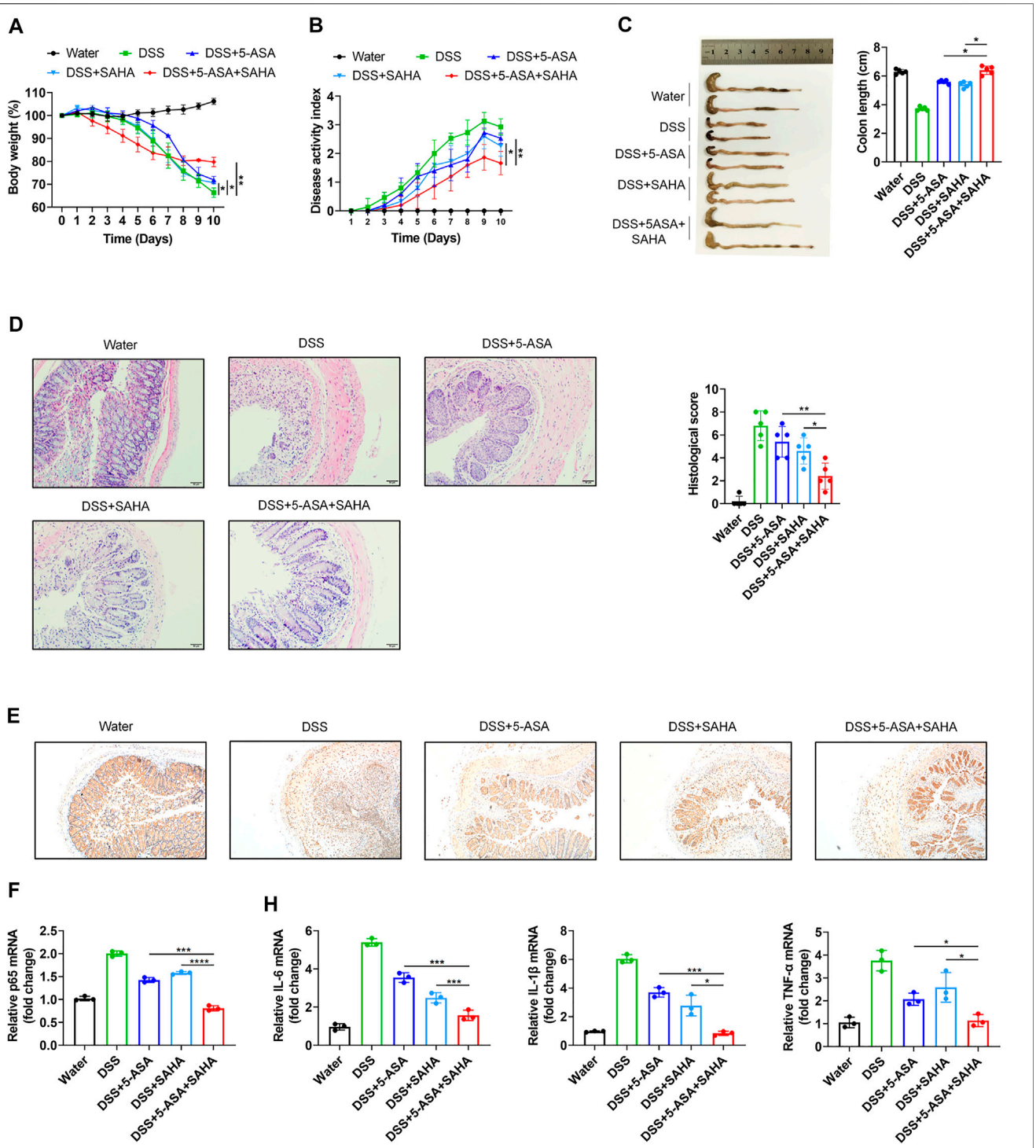

FIGURE 4 | *In vitro* validation of the synergetic effects of 5-ASA and SAHA on DSS-induced colitis mice. B57BL/6 mice were administered 2.5% DSS in drinking water for 7 days, followed by 3 days of water (n = 5 per group). **(A)** Body weight, **(B)** DAI score, **(C)** colon length, **(D)** HE staining (200 × magnification) and histological scores of colitis mice treated with 5-ASA (100 mg/kg/day) and SAHA (200 mg/kg/day) in combination or individually. **(E)** Immunohistochemistry of p65 and **(F)** the p65, **(G)** IL-6, IL-1β, and TNF-α mRNA levels in colonic tissues. The data shown are the mean ± SD and represent three independent experiments, *p* values were calculated using unpaired *t*-test, $^{*}p < 0.05$, $^{**}p < 0.01$, $^{***}p < 0.001$, ns = not significant.

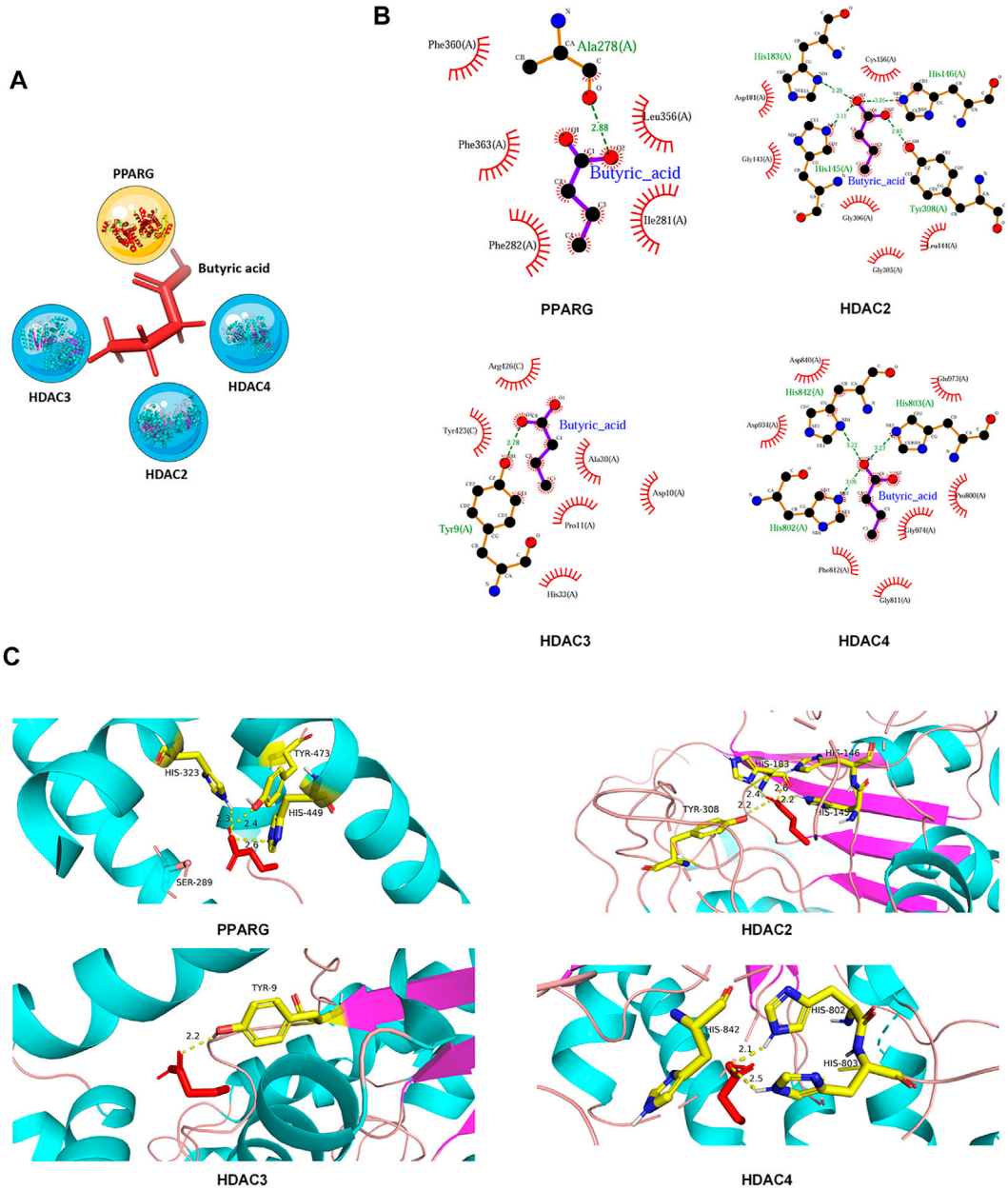

FIGURE 5 | PPARG and HDACs can interact with butyric acid. **(A)** Network of interaction among PPARG, HDACs and the metabolite-butyric acid. **(B)** 2D and **(C)** 3D versions of the molecular docking of butyric acid to PPARG, HDAC2, HDAC3, and HDAC4.

treatment of experimental colitis may be associated with the metabolite- butyric acid.

DISCUSSION

In this study, we sought to identify synergistic drugs for 5-ASA to solve the problem of drug resistance and insufficient efficacy in certain cases. Through protein-metabolite interaction analysis, we identified potential drug targets. Then, we evaluated the possibility of synergistic effects on PPARG, a therapeutic target of 5-ASA, in the treatment of UC. Finally, we identified SAHA can exert synergistic effects with 5-ASA in the treatment of experimental colitis. One possible mechanism of these effects may be synergistic inhibition of the NF-kB signaling pathway. Moreover, the metabolite-butyric acid may participate in the synergistic effect. We validated their synergistic effects both *in vitro* and *in vivo* and the experimental results further demonstrated their synergistic effects.

At present, many in-silico methods have been developed to predict synergistic drug combinations especially in the field of cancer, such as breast cancer, lung cancer (Sun et al., 2015), and gastric cancer (Xiang et al., 2018). Researchers typically use

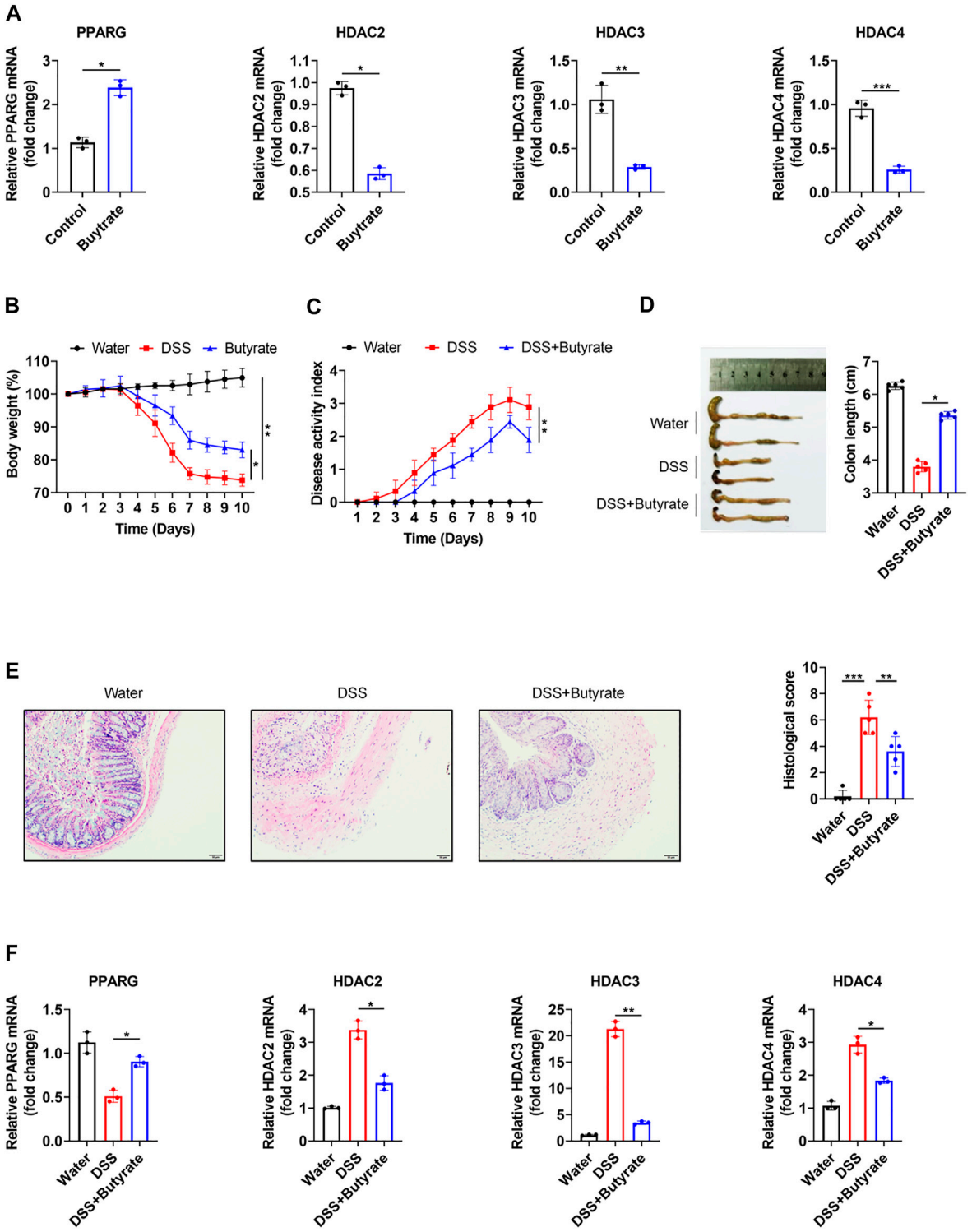

FIGURE 6 | PPARG and HDACs can be regulated by butyrate. **(A)** PPARG, HDAC2, HDAC3 and HDAC4 mRNA levels were determined in Caco-2 cells treated with butyrate (5 mM) for 24 h; B57BL/6 mice were administered 2.5% DSS in drinking water for 7 days, followed by 3 days of water, in the presence or absence of butyrate (200 mM) (n = 5 per group). **(B)** Body weight, **(C)** DAI score, **(D)** colon length, **(E)** HE staining (200 × magnification) and histological scores or vechale. **(F)** PPARG, HDAC2, HDAC3, and HDAC4 mRNA levels in colonic epithelial cells. The data shown are the mean ± SD and represent three independent experiments, *p* values were calculated using unpaired t-test, $^{*}p < 0.05$, $^{**}p < 0.01$, $^{***}p < 0.001$, ns = not significant.

currently known synergistic drug combinations as a seed dataset (Chen X. et al., 2016) and then develop different models or tools such as the Ranking-system of Anti-Cancer Synergy (RACS) (Sun et al., 2015), Network-based Laplacian regularized Least Square Synergistic (NLLSS) (Chen X. et al., 2016) and DrugComboRanker (Huang et al., 2014) to assess the synergistic potential of candidate drug pairs. Consequently, several synergistic drug combinations have been established. For example, the combined use of erlotinib and sorafenib has a major synergistic effect on the inhibition of MCF-7 breast cancer cell proliferation (Sun et al., 2015). However, these techniques may have limitations. 1) Some possible synergistic drugs may be missed due to limited drug pairs; 2) the molecular mechanism of synergistic effects of drug combinations is rarely disclosed; and 3) methods for the prediction of synergistic drug combinations of cancer diseases cannot be applied to other diseases. Therefore, we adopted protein-metabolite interactions to identify more potential drugs, starting with PPARG (**Figure 1**). Given that different drug targets involved in the same or associated pathways may produce synergistic effects (Jia et al., 2009), we further conducted KEGG and pathway-pathway interactions analysis to identify the targets that may participate in the same or a pathway related to PPARG. Then, we evaluated the possibility of synergy of these candidate drug targets and 5-ASA. Finally, we identified that HDAC2, HDAC3, and HDAC4 may exert excellent synergistic effects with PPARG (**Figure 2**). Moreover, PPARG was reported to participate in UC by inhibiting the NF-kB signaling pathway (Cao et al., 2018). Consequently, in our model, HDACs were also thought to regulate the NF-kB signaling pathway and synergize with PPARG. Recent studies have found that HDACs in colonic epithelial cells participate in the progression of colitis (Tsaprouni et al., 2011; Takeshima et al., 2012; Stylianou, 2013). Furthermore, HDAC inhibitors can exert anti-inflammatory effects through inhibiting the NF-kB and TGFβ1 signaling pathways (Chaturvedi et al., 2019; Friedrich et al., 2019).

According to the Therapeutic Target database, there are three approved drugs targeting histone deacetylase (HDAC), which include vorinostat (SAHA), sodium phenylbutyrate (PBA) and valproate (Wang et al., 2020). PBA is derived from the short-chain fatty acid-butyric acid and has been approved for the treatment of spinal muscular atrophy (Sun et al., 2019). Valproate was developed for the treatment of epilepsy (Bedlack et al., 2007). However, both PBA and valproate may cause significant damage to the liver and kidney (Perrine et al., 2007; Lee et al., 2015). Thus, we chose SAHA, an FDA-approved pan-HDACi that is clinically used to treat cutaneous T-cell lymphoma (Podar et al., 2009), as the ideal drug that may exert synergetic effects with 5-ASA. We validated their synergetic effects in UC through *in vivo* and *in vitro* experiments. The combination of 5-ASA and SAHA showed lower toxicity and mRNA expression of p65 in human colonic epithelial cell lines (Caco-2 and HCT-116) (**Figure 3**), and more efficiently alleviated symptoms of DSS-induced colitis than treatment with 5-ASA or SAHA alone (**Figure 4**). Thus, our approach suggests that SAHA combined with 5-ASA can produce synergistic effects in UC through synergistic inhibition of the NF-kB signaling pathway.

Our results demonstrated that butyric acid may bind to active sites of PPARG at His-323, Tyr-473, and His-449. Moreover, butyric acid can also interact with HDAC2 at Tyr-308, His-183, and His-146, interact with HDAC3 at Tyr-9 and interact with HDAC4 at His-842, His-802, and His-803. (**Figure 5**), Butyrate can upregulate the expression of PPARG while downregulating the expression of HDACs (**Figure 6**), which indicated that butyric acid may play an important role in the synergistic effects of 5-ASA and SAHA in the treatment of experimental colitis. Butyric acid is a short-chain fatty acid (SCFA) naturally produced by anaerobic bacteria (Ai et al., 2016). Recent studies have shown that SCFAs may participate in numerous biological processes (Ward et al., 2016). Moreover, a number of drugs have been reported to exert efficacy by influencing the production of SCFAs. For example, the natural plant extract-parthenolide (PTL) can exert a protective effect on DSS-induced colitis by regulating microbiota-derived SCFAs including acetate, propionate and butyrate (Liu et al., 2020). Thus, we wondered whether butyric acid is an intermediate link between 5-ASA targeting PPARG and SAHA targeting HDACs in the treatment of UC, which needs further study.

However, our strategy of identifying drugs that act synergistically with 5-ASA has the following limitations. First, protein-metabolite-protein analysis was conducted through the HMDB. HMDB Version 4.0 contains information on only 5,702 protein sequences and 114,186 associated metabolite entries (Wishart et al., 2018). However, millions of metabolite-protein interactions may exist (Piazza et al., 2018), which implies that not all target proteins can be associated with metabolite entries through the HMDB. Thus, more databases of protein-metabolite interactions should be considered in the future. Second, we focused more on therapeutic effects, but through our approach, side effects and toxicity of drug combinations couldn't be determined. Therefore, the combination of SAHA and 5-ASA needs to be further validated *in vivo* and *in vitro* for toxicity and side effects. Third, through our strategy, we can identify only drug targets rather than direct drugs. Therefore, more combined drug-target networks or databases are needed to obtain the ideal candidate drugs.

In conclusion, our data suggested that the combination of SAHA and 5-ASA can exert significant synergistic effects in the treatment of UC, which may provide a solution for the problem of insufficient efficacy and drug resistance of 5-ASA in certain cases. One possible mechanism of the synergistic effects observed in this study may be their synergistic inhibition of the NF-kB signaling pathway and the metabolite- butyric acid may play a crucial role. In addition, our strategy can be applied to the identification of synergistic drug combinations for other diseases. However, whether the combination of SAHA and 5-ASA is suitable for clinical and the toxicity and side effects need to be further evaluated.

METHODS

Protein-Metabolite Interaction Analysis and Network Construction

To analyze protein-metabolite interactions, we extracted information from the Human Metabolome Database (HMDB) on PPARG related

metabolites and the proteins related to these metabolites. Using the TTD, we littered undruggable targets. Finally, Cystoscope software was used to visualize protein-metabolite interactions.

KEGG Pathway Enrichment Analysis and Semantic Similarity of Gene Ontology Term Analysis

The "clusterProfiler", "enrichplot", and "ggplot2" packages were used to perform KEGG pathway enrichment analyses. Enrichment results with FDR (false discovery rate) < 0.05 were recognized as significant functional categories; The GOSemSim package (Yu et al., 2010) was used to determine semantic similarities of gene ontology terms.

Gene-Overlapping Pathway-Pathway Interactions Analysis

Gene-overlapping pathway-pathway interactions (WWIs) were conducted as previously described (Chen D. et al., 2016). Briefly, when the number of shared genes between two pathways was significant against occasional conditions (by Fisher's exact test, p-values of WWIs should be less than a certain threshold), they are regarded as one gene-overlapping WWI.

Cell Counting Kit-8 (CCK-8) Analysis

The toxicity of 5-ASA and SAHA in Caco-2 or HCT-116 cells was determined by CCK8 assays. The Cell Counting Kit 8 (CCK8, BS350B, Biosharp, China) assay was performed following the manufacturer's protocol. Briefly, at a density of 5,000 per well, Caco-2 or HCT-116 cells were plated onto 96-well plates and incubated overnight. On the second day, the cells were treated in combination or individually with 5-ASA and SAHA for 24 and 48 h. CCK-8 reagent (10 μl) was then added to each well and incubated for 2 h a 37°C in a 5% humidified CO_2 atmosphere. Finally, the absorbance at 450 nm was measured using a microplate reader.

Experimental Animals

C57BL/6 (wild type; WT) mice (male; 8–10 weeks of age; weighing 25–30 g) were purchased from Guangdong Medical Laboratory Animal Center. All mice were maintained under specific pathogen-free conditions (22 ± 2°C with 35–55% relative humidity on a 12-h light/dark cycle) with free access to food and water. All *in vivo* experiments were performed in accordance with protocols approved by the Institutional Animal Ethics Committee of the First Affiliated Hospital, Guangzhou University of Chinese Medicine (Ethics No. TCMF1-2018006).

Induction of Experimental Colitis

Experimental colitis was induced by adding 2.5% DSS (molecular mass 36,000–50,000 Da; MP Biomedicals) to drinking water for 7 days, followed by regular drinking water for another 3 days.

Butyrate Treatments

DSS-induced colitis mice were treated with butyrate (200 mM) in drinking water (Sun et al., 2018); HCT-116 and Caco-2 cells were stimulated with butyrate at a concentration of 5 mM (Olson et al., 2019).

Gene name	Primer sequence
p65 (mice)	Forward: ACTGCCGGGATGGCTACTAT
	Reverse: TCTGGATTCGCTGGCTAATGG
IL-6 (mice)	Forward: CTGCAAGAGACTTCCATCCAG
	Reverse: AGTGGTATAGACAGGTCTGTTGG
IL-1b (mice)	Forward: GAAATGCCACCTTTTGACAGTG
	Reverse: TGGATGCTCTCATCAGGACAG
TNF-a (mice)	Forward: CTGAACTTCGGGGTGATCGG
	Reverse: GGCTTGTCACTCGAATTTTGAGA
PPARG (human)	Forward: CGAGAAGGAGAAGCTGTTG
	Reverse: TCAGCGGGAAGGACTTTA
HDAC2 (human)	Forward: AGTTGCCCTTGATTGTGAG
	Reverse: ATTCTGGAGTGTTCTGGTTTG
HDAC3 (human)	Forward: ATTGGGCTGCTTTAACCTC
	Reverse: GGCAACATTTCGGACAGTA
HDAC4 (human)	Forward: GGGAAAACGCAGCACAG
	Reverse: TCATCTTTGGCGTCGTACA
PPARG (mice)	Forward: CGAGAAGGAGAAGCTGTTG
	Reverse: TCAGCGGGAAGGACTTTA
HDAC2 (mice)	Forward: GGATGAAGGTGAAGGAGGT
	Reverse: CAAGGGTTGCTGAGTTGTT
HDAC3 (mice)	Forward: GCGACCATGACAACGAC
	Reverse: AGACCTGGGGAAACCATAC
HDAC4 (mice)	Forward: CCGCTATGACGATGGGAACT
	Reverse: CCACATCTGGGGCAAACTC

Isolation of Colonic Epithelial Cells (CECs)

Colonic epithelial cells (CECs) were isolated as previously described (Marchiori et al., 2019). Briefly, colon tissues were carefully washed with PBS and cut into 2–3 mm strips. The strips were then incubated for 10 min with 1 mM DTT at room temperature and for 20 min with 5 mM EDTA at 37°C. The CECs were obtained by centrifugation.

Histological Score Analysis

Histological scores were analyzed as previously described (Zhou et al., 2019). Briefly, crypt architecture (normal, 0–severe crypt distortion with loss of entire crypts, 3), degree of inflammatory cell infiltration (normal, 0–dense inflammatory infiltrate, 3), muscle thickening (base of crypt sits on the muscularis mucosae, 0–marked muscle thickening, 3), crypt abscess (absent, 0–present, 1), and goblet cell depletion (absent, 0–present, 1) were recored. The total histological scores were derived by summing each individual score.

Quantitative Real-Time Polymerase Chain Reaction

Trizol reagent was used to extract total RNA from Caco-2 and HCT-116 cells or colonic experimental colitis epithelial cells followed by cDNA synthesis. Using SYBR green gene expression assays on a Bio-Rad iCycler (Bio-Rad, Hercules, CA, United States), quantitative PCRs were performed.

The sequences of the primers used were as follows:

Statistical Analysis

The data were represented as the mean ± SD, and analysis was done using SPSS (version 20.0). To analyze significant differences between three or more classes, a one-way ANOVA test was used. ANOVA and multiple-ANOVA were used to analyze repeated measurement data. Statistical significance was set at $p < 0.05$.

DATA AVAILABILITY STATEMENT

The raw data supporting the conclusions of this article will be made available by the authors, without undue reservation, to any qualified researcher.

ETHICS STATEMENT

The animal study was reviewed and approved by The Institutional Animal Ethics Committee of the First Affiliated Hospital, Guangzhou University of Chinese Medicine (Ethic No. TCMF1-2018006).

AUTHOR CONTRIBUTIONS

FL and LH designed the study; LH and STW performed the bioinformatics analyses; LH, STW, and ZZ conducted the experiments; LH, SHW, and QJ analyzed the data and performed the statistical analyses; LH wrote the manuscript and HM, FL critically revised the article for essential intellectual content. All authors read and approved the final manuscript.

FUNDING

This work was funded by grants from the Science and Technology Program of Guangzhou (No. 201904010234), the Construction of a high-level university Project of Guangzhou University of Chinese Medicine (No. (2017) 10).

SUPPLEMENTARY MATERIAL

The Supplementary Material for this article can be found online at: https://www.frontiersin.org/articles/10.3389/fphar.2021.625543/full#supplementary-material

REFERENCES

Ai, B., Chi, X., Meng, J., Sheng, Z., Zheng, L., Zheng, X., et al. (2016). Consolidated Bioprocessing for Butyric Acid Production from Rice Straw with Undefined Mixed Culture. *Front. Microbiol.* 7, 1648. doi:10.3389/fmicb.2016.01648

Bedlack, R. S., Traynor, B. J., and Cudkowicz, M. E. (2007). Emerging Disease-Modifying Therapies for the Treatment of Motor Neuron Disease/amyotropic Lateral Sclerosis. *Expert Opin. Emerging Drugs* 12, 229–252. doi:10.1517/14728214.12.2.229

Bertrand, S., Bohni, N., Schnee, S., Schumpp, O., Gindro, K., and Wolfender, J.-L. (2014). Metabolite Induction *via* Microorganism Co-culture: a Potential Way to Enhance Chemical Diversity for Drug Discovery. *Biotechnol. Adv.* 32, 1180–1204. doi:10.1016/j.biotechadv.2014.03.001

Bougarne, N., Weyers, B., Desmet, S. J., Deckers, J., Ray, D. W., Staels, B., et al. (2018). Molecular Actions of PPARα in Lipid Metabolism and Inflammation. *Endocr. Rev.* 39, 760–802. doi:10.1210/er.2018-00064

Bouguen, G., Langlois, A., Djouina, M., Branche, J., Koriche, D., Dewaeles, E., et al. (2015). Intestinal Steroidogenesis Controls PPARγ Expression in the colon and Is Impaired during Ulcerative Colitis. *Gut* 64, 901–910. doi:10.1136/gutjnl-2014-307618

Bressler, B., Marshall, J. K., Bernstein, C. N., Bitton, A., Jones, J., Leontiadis, G. I., et al. (2015). Clinical Practice Guidelines for the Medical Management of Nonhospitalized Ulcerative Colitis: the Toronto Consensus. *Gastroenterology* 148, 1035–1058. doi:10.1053/j.gastro.2015.03.001

Cao, H., Liu, J., Shen, P., Cai, J., Han, Y., Zhu, K., et al. (2018). Protective Effect of Naringin on DSS-Induced Ulcerative Colitis in Mice. *J. Agric. Food Chem.* 66, 13133–13140. doi:10.1021/acs.jafc.8b03942

Casas, A. I., Hassan, A. A., Larsen, S. J., Gomez-Rangel, V., Elbatreek, M., Kleikers, P. W. M., et al. (2019). From Single Drug Targets to Synergistic Network Pharmacology in Ischemic Stroke. *Proc. Natl. Acad. Sci. USA* 116, 7129–7136. doi:10.1073/pnas.1820799116

Chaturvedi, L. S., Wang, Q., More, S. K., Vomhof-DeKrey, E. E., and Basson, M. D. (2019). Schlafen 12 Mediates the Effects of Butyrate and Repetitive Mechanical Deformation on Intestinal Epithelial Differentiation in Human Caco-2 Intestinal Epithelial Cells. *Hum. Cel* 32, 240–250. doi:10.1007/s13577-019-00247-3

Chen, D., Zhang, H., Lu, P., Liu, X., and Cao, H. (2016). Synergy Evaluation by a Pathway-Pathway Interaction Network: A New Way to Predict Drug Combination. *Mol. BioSyst.* 12, 614–623. doi:10.1039/c5mb00599j

Chen, X., Ren, B., Chen, M., Wang, Q., Zhang, L., and Yan, G. (2016). NLLSS: Predicting Synergistic Drug Combinations Based on Semi-supervised Learning. *PLoS Comput. Biol.* 12, e1004975. doi:10.1371/journal.pcbi.1004975

Chou, T.-C. (2006). Theoretical Basis, Experimental Design, and Computerized Simulation of Synergism and Antagonism in Drug Combination Studies. *Pharmacol. Rev.* 58, 621–681. doi:10.1124/pr.58.3.10

Doyle, T., and King, K. (1989). Percutaneous Removal of Osteoid Osteomas Using CT Control. *Clin. Radiol.* 40, 514–517. doi:10.1016/s0009-9260(89)80268-5

Eckschlager, T., Plch, J., Stiborova, M., and Hrabeta, J. (2017). Histone Deacetylase Inhibitors as Anticancer Drugs. *Int. J. Mol. Sci.* 18, 1414. doi:10.3390/ijms18071414

Friedrich, M., Gerbeth, L., Gerling, M., Rosenthal, R., Steiger, K., Weidinger, C., et al. (2019). HDAC Inhibitors Promote Intestinal Epithelial Regeneration via Autocrine TGFβ1 Signalling in Inflammation. *Mucosal Immunol.* 12, 656–667. doi:10.1038/s41385-019-0135-7

Gene Ontology, C. (2015). Gene Ontology Consortium: Going Forward. *Nucleic Acids Res.* 43, D1049–D1056. doi:10.1093/nar/gku1179

Han, Y., Yu, G., Sarioglu, H., Caballero-Martinez, A., Schlott, F., Ueffing, M., et al. (2013). Proteomic Investigation of the Interactome of FMNL1 in Hematopoietic Cells Unveils a Role in Calcium-dependent Membrane Plasticity. *J. Proteomics* 78, 72–82. doi:10.1016/j.jprot.2012.11.015

Hu, Y., Chen, C. H., Ding, Y. Y., Wen, X., Wang, B., Gao, L., et al. (2019). Optimal Control Nodes in Disease-Perturbed Networks as Targets for Combination Therapy. *Nat. Commun.* 10, 2180. doi:10.1038/s41467-019-10215-y

Huang, L., Li, F., Sheng, J., Xia, X., Ma, J., Zhan, M., et al. (2014). DrugComboRanker: Drug Combination Discovery Based on Target Network Analysis. *Bioinformatics* 30, i228–i236. doi:10.1093/bioinformatics/btu278

Husted, A. S., Trauelsen, M., Rudenko, O., Hjorth, S. A., and Schwartz, T. W. (2017). GPCR-Mediated Signaling of Metabolites. *Cel Metab.* 25, 777–796. doi:10.1016/j.cmet.2017.03.008

Jain, S., and Bader, G. D. (2010). An Improved Method for Scoring Protein-Protein Interactions Using Semantic Similarity within the Gene Ontology. *BMC Bioinformatics* 11, 562. doi:10.1186/1471-2105-11-562

Jia, D., Augert, A., Kim, D.-W., Eastwood, E., Wu, N., Ibrahim, A. H., et al. (2018). Crebbp Loss Drives Small Cell Lung Cancer and Increases Sensitivity to HDAC Inhibition. *Cancer Discov.* 8, 1422–1437. doi:10.1158/2159-8290.cd-18-0385

Jia, J., Zhu, F., Ma, X., Cao, Z. W., Li, Y. X., Chen, Y. Z., et al. (2009). Mechanisms of Drug Combinations: Interaction and Network Perspectives. *Nat. Rev. Drug Discov.* 8, 111–128. doi:10.1038/nrd2683

Kreek, M. J., and Balint, J. A. (1980). "Skinny Needle" Cholangiography-Results of a Pilot Study of a Voluntary Prospective Method for Gathering Risk Data on New Procedures. *Gastroenterology* 78, 598–604. doi:10.1016/0016-5085(80)90878-1

Lee, S., Cheong, J., Kim, C., and Kim, J. M. (2015). Valproic Acid-Induced Hyperammonemic Encephalopathy as a Cause of Neurologic Deterioration

after Unruptured Aneurysm Surgery. *J. Korean Neurosurg. Soc.* 58, 159–162. doi:10.3340/jkns.2015.58.2.159

Li, F., Xu, W., and Zhao, S. (2013). Regulatory Roles of Metabolites in Cell Signaling Networks. *J. Genet. Genomics* 40, 367–374. doi:10.1016/j.jgg.2013.05.002

Liu, Y.-J., Tang, B., Wang, F.-C., Tang, L., Lei, Y.-Y., Luo, Y., et al. (2020). Parthenolide Ameliorates colon Inflammation through Regulating Treg/Th17 Balance in a Gut Microbiota-dependent Manner. *Theranostics* 10, 5225–5241. doi:10.7150/thno.43716

Marchiori, C., Scarpa, M., Kotsafti, A., Morgan, S., Fassan, M., Guzzardo, V., et al. (2019). Epithelial CD80 Promotes Immune Surveillance of Colonic Preneoplastic Lesions and its Expression Is Increased by Oxidative Stress through STAT3 in colon Cancer Cells. *J. Exp. Clin. Cancer Res.* 38, 190. doi:10.1186/s13046-019-1205-0

Mateus, A., Kurzawa, N., Becher, I., Sridharan, S., Helm, D., Stein, F., et al. (2020). Thermal Proteome Profiling for Interrogating Protein Interactions. *Mol. Syst. Biol.* 16, e9232. doi:10.15252/msb.20199232

Murakami, Y., Tripathi, L. P., Prathipati, P., and Mizuguchi, K. (2017). Network Analysis and In Silico Prediction of Protein-Protein Interactions with Applications in Drug Discovery. *Curr. Opin. Struct. Biol.* 44, 134–142. doi:10.1016/j.sbi.2017.02.005

Newman, J. C., and Verdin, E. (2017). β-Hydroxybutyrate: A Signaling Metabolite. *Annu. Rev. Nutr.* 37, 51–76. doi:10.1146/annurev-nutr-071816-064916

Nowak-Sliwinska, P., Weiss, A., Ding, X., Dyson, P. J., van den Bergh, H., Griffioen, A. W., et al. (2016). Optimization of Drug Combinations Using Feedback System Control. *Nat. Protoc.* 11, 302–315. doi:10.1038/nprot.2016.017

Olson, A. T., Wang, Z., Rico, A. B., and Wiebe, M. S. (2019). A Poxvirus Pseudokinase Represses Viral DNA Replication via a Pathway Antagonized by its Paralog Kinase. *PLoS Pathog.* 15, e1007608. doi:10.1371/journal.ppat.1007608

Pedersen, G., and Brynskov, J. (2010). Topical Rosiglitazone Treatment Improves Ulcerative Colitis by Restoring Peroxisome Proliferator-Activated Receptor-γ Activity. *Am. J. Gastroenterol.* 105, 1595–1603. doi:10.1038/ajg.2009.749

Perrine, S. P., Hermine, O., Small, T., Suarez, F., O'Reilly, R., Boulad, F., et al. (2007). A Phase 1/2 Trial of Arginine Butyrate and Ganciclovir in Patients with Epstein-Barr Virus-Associated Lymphoid Malignancies. *Blood* 109, 2571–2578. doi:10.1182/blood-2006-01-024703

Piazza, I., Kochanowski, K., Cappelletti, V., Fuhrer, T., Noor, E., Sauer, U., et al. (2018). A Map of Protein-Metabolite Interactions Reveals Principles of Chemical Communication. *Cell* 172, 358–372. doi:10.1016/j.cell.2017.12.006

Podar, K., Tai, Y.-T., Hideshima, T., Vallet, S., Richardson, P. G., and Anderson, K. C. (2009). Emerging Therapies for Multiple Myeloma. *Expert Opin. Emerging Drugs* 14, 99–127. doi:10.1517/14728210802676278

Scott, D. E., Bayly, A. R., Abell, C., and Skidmore, J. (2016). Small Molecules, Big Targets: Drug Discovery Faces the Protein-Protein Interaction challenge. *Nat. Rev. Drug Discov.* 15, 533–550. doi:10.1038/nrd.2016.29

Sheng, Z., Sun, Y., Yin, Z., Tang, K., and Cao, Z. (2018). Advances in Computational Approaches in Identifying Synergistic Drug Combinations. *Brief Bioinform* 19, 1172–1182. doi:10.1093/bib/bbx047

Stylianou, E. (2013). Epigenetics. *Curr. Opin. Gastroenterol.* 29, 370–377. doi:10.1097/mog.0b013e328360bd12

Sun, M., Wu, W., Chen, L., Yang, W., Huang, X., Ma, C., et al. (2018). Microbiota-derived Short-Chain Fatty Acids Promote Th1 Cell IL-10 Production to Maintain Intestinal Homeostasis. *Nat. Commun.* 9, 3555. doi:10.1038/s41467-018-05901-2

Sun, W., Zhang, L., Lu, X., Feng, L., and Sun, S. (2019). The Synergistic Antifungal Effects of Sodium Phenylbutyrate Combined with Azoles against Candida Albicans via the Regulation of the Ras-cAMP-PKA Signalling Pathway and Virulence. *Can. J. Microbiol.* 65, 105–115. doi:10.1139/cjm-2018-0337

Sun, Y., Sheng, Z., Ma, C., Tang, K., Zhu, R., Wu, Z., et al. (2015). Combining Genomic and Network Characteristics for Extended Capability in Predicting Synergistic Drugs for Cancer. *Nat. Commun.* 6, 8481. doi:10.1038/ncomms9481

Takeshima, H., Ikegami, D., Wakabayashi, M., Niwa, T., Kim, Y.-J., and Ushijima, T. (2012). Induction of Aberrant Trimethylation of Histone H3 Lysine 27 by Inflammation in Mouse Colonic Epithelial Cells. *Carcinogenesis* 33, 2384–2390. doi:10.1093/carcin/bgs294

Tsaprouni, L. G., Ito, K., Powell, J. J., Adcock, I. M., and Punchard, N. (2011). Differential Patterns of Histone Acetylation in Inflammatory Bowel Diseases. *J. Inflamm.* 8, 1. doi:10.1186/1476-9255-8-1

Ungaro, R., Mehandru, S., Allen, P. B., Peyrin-Biroulet, L., and Colombel, J.-F. (2017). Ulcerative Colitis. *The Lancet* 389, 1756–1770. doi:10.1016/s0140-6736(16)32126-2

Wang, Y., Zhang, S., Li, F., Zhou, Y., Zhang, Y., Wang, Z., et al. (2020). Therapeutic Target Database 2020: Enriched Resource for Facilitating Research and Early Development of Targeted Therapeutics. *Nucleic Acids Res.* 48, D1031–D1041. doi:10.1093/nar/gkz981

Wang, Y., Du, L., Li, X., Zhang, S., Xiao, Y., Gong, B., et al. (2011). Functional Homogeneity in microRNA Target Heterogeneity-A New Sight into Human microRNomics. *OMICS: A J. Integr. Biol.* 15, 25–35. doi:10.1089/omi.2010.0047

Ward, N. L., Phillips, C. D., Nguyen, D. D., Shanmugam, N. K. N., Song, Y., Hodin, R., et al. (2016). Antibiotic Treatment Induces Long-Lasting Changes in the Fecal Microbiota that Protect Against Colitis. *Inflamm. Bowel Dis.* 22, 2328–2340. doi:10.1097/mib.0000000000000914

Wishart, D. S. (2016). Emerging Applications of Metabolomics in Drug Discovery and Precision Medicine. *Nat. Rev. Drug Discov.* 15, 473–484. doi:10.1038/nrd.2016.32

Wishart, D. S., Feunang, Y. D., Marcu, A., Guo, A. C., Liang, K., Vázquez-Fresno, R., et al. (2018). HMDB 4.0: the Human Metabolome Database for 2018. *Nucleic Acids Res.* 46, D608–D617. doi:10.1093/nar/gkx1089

Xiang, Z., Huang, X., Wang, J., Zhang, J., Ji, J., Yan, R., et al. (2018). Cross-Database Analysis Reveals Sensitive Biomarkers for Combined Therapy for ERBB2+ Gastric Cancer. *Front. Pharmacol.* 9, 861. doi:10.3389/fphar.2018.00861

Yang, H., Qin, C., Li, Y. H., Tao, L., Zhou, J., Yu, C. Y., et al. (2016). Therapeutic Target Database Update 2016: Enriched Resource for Bench to Clinical Drug Target and Targeted Pathway Information. *Nucleic Acids Res.* 44, D1069–D1074. doi:10.1093/nar/gkv1230

Yu, G., Li, F., Qin, Y., Bo, X., Wu, Y., and Wang, S. (2010). GOSemSim: an R Package for Measuring Semantic Similarity Among GO Terms and Gene Products. *Bioinformatics* 26, 976–978. doi:10.1093/bioinformatics/btq064

Zhou, J., Huang, S., Wang, Z., Huang, J., Xu, L., Tang, X., et al. (2019). Targeting EZH2 Histone Methyltransferase Activity Alleviates Experimental Intestinal Inflammation. *Nat. Commun.* 10 (1), 2427. doi:10.1038/s41467-019-10176-2

Conflict of Interest: The authors declare that the research was conducted in the absence of any commercial or financial relationships that could be construed as a potential conflict of interest.

frontiers in Pharmacology

ORIGINAL RESEARCH
published: 02 June 2021
doi: 10.3389/fphar.2021.682654

Three-Dimensional Culture of Ameloblast-Originated HAT-7 Cells for Functional Modeling of Defective Tooth Enamel Formation

*Anna Földes[1†], Thanyaporn Sang-Ngoen[1†], Kristóf Kádár[1], Róbert Rácz[1], Ákos Zsembery[1], Pamela DenBesten[2], Martin C. Steward[1,3] and Gábor Varga[1]**

[1]Department of Oral Biology, Semmelweis University, Budapest, Hungary, [2]Department of Orofacial Sciences, University of California San Francisco, San Francisco, CA, United States, [3]School of Medical Sciences, University of Manchester, Manchester, United Kingdom

OPEN ACCESS

Edited by:
Predrag Sikiric,
University of Zagreb, Croatia

Reviewed by:
Michael Lansdell Paine,
University of Southern California, Los Angeles, United States
Paris Simeon,
School of Dental Medicine, Croatia

***Correspondence:**
Gábor Varga
varga.gabor@dent.semmelweis-univ.hu

[†]These authors have contributed equally to this work

Specialty section:
This article was submitted to Gastrointestinal and Hepatic Pharmacology, a section of the journal Frontiers in Pharmacology

Received: 18 March 2021
Accepted: 19 May 2021
Published: 02 June 2021

Citation:
Földes A, Sang-Ngoen T, Kádár K, Rácz R, Zsembery Á, DenBesten P, Steward MC and Varga G (2021) Three-Dimensional Culture of Ameloblast-Originated HAT-7 Cells for Functional Modeling of Defective Tooth Enamel Formation. Front. Pharmacol. 12:682654. doi: 10.3389/fphar.2021.682654

Background: Amelogenesis, the formation of dental enamel, is well understood at the histomorphological level but the underlying molecular mechanisms are poorly characterized. Ameloblasts secrete enamel matrix proteins and Ca^{2+}, and also regulate extracellular pH as the formation of hydroxyapatite crystals generates large quantities of protons. Genetic or environmental impairment of transport and regulatory processes (e.g. dental fluorosis) leads to the development of enamel defects such as hypomineralization.

Aims: Our aims were to optimize the culture conditions for the three-dimensional growth of ameloblast-derived HAT-7 cells and to test the effects of fluoride exposure on HAT-7 spheroid formation.

Methods: To generate 3D HAT-7 structures, cells were dispersed and plated within a Matrigel extracellular matrix scaffold and incubated in three different culture media. Spheroid formation was then monitored over a two-week period. Ion transporter and tight-junction protein expression was investigated by RT-qPCR. Intracellular Ca^{2+} and pH changes were measured by microfluorometry using the fluorescent dyes fura-2 and BCECF.

Results: A combination of Hepato-STIM epithelial cell differentiation medium and Matrigel induced the expansion and formation of 3D HAT-7 spheroids. The cells retained their epithelial cell morphology and continued to express both ameloblast-specific and ion transport-specific marker genes. Furthermore, like two-dimensional HAT-7 monolayers, the HAT-7 spheroids were able to regulate their intracellular pH and to show intracellular calcium responses to extracellular stimulation. Finally, we demonstrated that HAT-7 spheroids may serve as a disease model for studying the effects of fluoride exposure during amelogenesis.

Conclusion: In conclusion, HAT-7 cells cultivated within a Matrigel extracellular matrix form three-dimensional, multi-cellular, spheroidal structures that retain their functional capacity for pH regulation and intracellular Ca^{2+} signaling. This new 3D model will allow us to gain a better understanding of the molecular mechanisms involved in amelogenesis, not

only in health but also in disorders of enamel formation, such as those resulting from fluoride exposure.

Keywords: HAT-7, ameloblast, amelogenesis, bicarbonate transport, intracellular pH, calcium signaling, tight junction, fluoride

INTRODUCTION

Amelogenesis, the formation of dental enamel, is well understood at the histomorphological level, but the underlying molecular mechanisms are poorly characterized (Lacruz et al., 2017; Varga et al., 2018). Ameloblasts, derived from the oral epithelium, are known to secrete proteins and Ca^{2+} into the enamel extracellular matrix. They also regulate extracellular pH as the formation of hydroxyapatite crystals generates large quantities of protons that must be neutralized by HCO_3^- secretion to allow continued crystal growth. Genetic or environmental impairment of transport and regulatory processes (e.g. dental fluorosis) leads to the development of enamel defects such as hypomineralized enamel (Lacruz et al., 2017; Varga et al., 2018).

Ameloblast differentiation and ion transport activities have primarily been investigated by immunohistochemistry and characterization of the enamel phenotypes of knockout mouse models. However, to understand the mechanisms by which environmental factors, such as exposure to high levels of fluoride, affect enamel formation, *in vitro* model systems are needed (Klein et al., 2017).

Culture of primary enamel organ epithelial cells results in two distinct cell shapes: either polygonal or stellate (DenBesten et al., 2005). Stellate cells, which have a phenotype similar to mouse LS8 cells, grow rapidly in 2D culture but cannot be maintained in 3D Matrigel (Li et al., 2006). Polygonal cells are similar in morphology to both ameloblast-like mouse ALC (Nakata et al., 2003) and rat HAT-7 (Kawano et al., 2002) cells. The primary, enamel-originated cells grown in Matrigel alter their morphology in the presence of extracellular calcium (Li et al., 2006; Yan et al., 2006; Chen et al., 2009; He et al., 2010). However, these primary ameloblast-like cells can be passaged only 3 times, and so have limited use in studies of ameloblast function. When transfected by SV40 or telomerase (He et al., 2010; Zheng et al., 2013b; Zheng et al., 2013c), they maintain ameloblast-like characteristics through approximately eight passages (unpublished results), but do not form spheroid structures in Matrigel (Li et al., 2006). This then suggests that these transfected cells are also not a robust model to study ameloblast function (He et al., 2010; Zheng et al., 2013b; Zheng et al., 2013c). While these early studies offer the promise of advanced technologies to more completely regenerate the enamel organ epithelium, further advances are needed to identify cells that retain characteristics similar to primary cells, and that can be scaled up, expanded and standardized. This in turn will allow studies of tooth formation *in vitro*, and investigation of the mechanisms responsible for environmental effects on tooth enamel formation (Klein et al., 2017).

Scaling up of stem cells and progenitors can be performed using three different strategies: 1) monolayer cultures, 2) culturing cells on microspheres and 3) organoid/spheroid production (Silva Couto et al., 2020). Monolayer cultivation is the least effective method. To achieve higher yields of cell expansion, we can use microcarriers, which are principally designed for growing adherent cells in suspension culture systems. The application of microcarriers in dynamic culture systems may provide high yields but it is technically difficult to isolate the cells from their microcarriers (Chen et al., 2015; Lam et al., 2017; Cherian et al., 2020). In organoid/spheroid culture, three-dimensional cell aggregates can be produced under either static or dynamic conditions. This approach is thought to more closely mimic the three-dimensional *in vivo* environment (Wang et al., 2009; Bartosh et al., 2010). An obvious challenge of this strategy is to expand cells under controlled conditions without causing harmful effects on the cells and undesirable cell differentiation (Simoes et al., 2013; Yang et al., 2018a).

In the present study, we have investigated the effects of culture conditions on the three-dimensional growth of HAT-7 cells. These cells, which are derived from rat incisor cervical loop (Kawano et al., 2002), maintain a polygonal shape and exhibit characteristics of maturation-stage ameloblasts, such as the expression of the marker proteins kallikrein-4 and amelotin (Kawano et al., 2002). We have shown previously that HAT-7 cells grown on permeable supports form two-dimensional polarized epithelia which serve as a good experimental model for investigating the molecular physiology of ion transport in ameloblasts (Bori et al., 2016; Racz et al., 2017; Racz et al., 2018; Varga et al., 2018). Furthermore, this cell line has been successfully used in a large number of studies to investigate ameloblast function (Matsumoto et al., 2011; Zheng et al., 2013a; Jalali et al., 2017; Yang et al., 2018b; Takahashi et al., 2019).

In this report we demonstrate that HAT-7 cells can form spheroids similar to those previously obtained in primary cultures of ameloblast-lineage cells. We have compared their capacity to regulate intracellular pH and to show intracellular calcium responses to extracellular stimulation, to our previous findings in 2D culture. To explore the effects of fluoride exposure we have determined the dose at which fluoride exposure disturbs HAT-7 spheroid formation.

MATERIALS AND METHODS

Cell Culture

HAT-7 cells were cultured in "control medium" consisting of DMEM/F12 Ham medium (Sigma-Aldrich, St. Louis, MO, United States) supplemented with 10% HyClone fetal bovine serum (Thermo Scientific, Waltham, MA, United States), 100 U/ml penicillin and 10 μg/ml streptomycin (Sigma-Aldrich). They were incubated in a humidified atmosphere containing 5% CO_2 at

37°C. The cell medium was changed every other day and the cells were subcultured when the cell confluence reached 70–80%.

2D Culture on Permeable Supports

HAT-7 cells were seeded on permeable polyester Transwell culture inserts with 0.4 μm pore size and 1.12 cm^2 surface area (Costar, Corning, NY, United States) and were cultured in "differentiation medium" consisting of control medium, as described above, supplemented with $CaCl_2$ (2.1 mM final concentration) and 10^{-8} M dexamethasone (Sigma-Aldrich) (Arakaki et al., 2012; Bori et al., 2016).

3D Culture with Basement Membrane Matrix

For 3D culture, HAT-7 cells were grown within the gel layer of Matrigel® Basement Membrane Matrix (Corning, NY, United States). For seeding at low density to obtain single cell derived colonies within the Matrigel/, approximately 80,000 HAT-7 cells were resuspended in 160 μl of each following media: 1) control medium, 2) differentiation medium, and 3) Hepato-STIM® (BD Biosciences, San Jose, CA, United States), a commercially available epithelial selection medium, supplemented with 10% HyClone fetal bovine serum (Thermo Scientific), 1% L-glutamine (Sigma-Aldrich), 100 U/ml penicillin and 10 g/ml streptomycin (Bori et al., 2016). Each cell suspension was mixed with 400 μl of Matrigel and 70 μl aliquots were placed in eight individual wells of a 24-well Nunclon Sphera low-attachment plate (Thermo Fisher Scientific, Rochester, NY, United States). The plate was incubated at 37°C to allow the Matrigel to solidify, and then 1 ml of the appropriate medium was added to each well. The culture medium was changed every other day.

Morphology

Spheroid development was assessed in living HAT-7 cell cultures by phase-contrast light microscopy (Nikon Eclipse TE200) and images obtained using a CCD camera (Blackfly USB3 CCD camera, FLIR Systems, Wilsonville, OR, United States). Size distribution was determined using the particle analysis function in ImageJ (NIH, Bethesda, MD, United States).

For histology, spheroids grown for 7 days in Matrigel with Hepato-STIM medium were released from the matrix using 0.25% trypsin/EDTA and fixed in 4% paraformaldehyde. Frozen sections were cut at 5 μm thickness and stained with haematoxylin and eosin.

RT-PCR

Total RNA was isolated from 7-days HAT-7 spheroids and HAT-7 monolayers grown on Transwell permeable supports, using a NucleoSpin RNA XS kit (Macherey-Nagel). The integrity of the RNA was assessed by running the purified RNAs on 1% agarose gels. Only samples in which the amount of 28S rRNA was about twice the intensity of the 18 S rRNA were processed further. Total RNA (1.5 μg/sample) was reverse transcribed using a Maxima First Strand cDNA Synthesis Kit for RT-qPCR (Thermo Scientific). Amplification was performed using QuantStudio 5 with TaqPath qPCR Master Mix, CG (Applied Biosystems, Foster City, CA, United States) and predesigned primers (Life Technologies Magyarország Kft., Budapest): Klk4 (Rn01498536_m1), Cldn1 (Rn00581740_m1), Cldn4 (Rn01196224_s1), Cldn8 (Rn01767199_s1), Tjp1/ZO-1 (Rn02116071_s1), Slc4a2/AE2 (Rn00566910_m1), Slc4a4/NBCe1 (Rn00584747_m1), Slc9a1/NHE1 (Rn00561924_m1), CFTR (Rn01455971_m1), Slc26a4/pendrin (Rn00693043_m1). Acidic ribosomal protein P0 (RPLP0; Rn00821065_g1) was used as internal control. Each sample was measured in three technical parallels. No-template and RT-minus reactions were performed to monitor non-specific and genomic DNA amplifications respectively. Relative fold changes were calculated by the comparative Ct method (2−ΔΔCT).

Microfluorometry

For measurement of intracellular pH (pH_i) and calcium concentration ($[Ca^{2+}]_i$), spheroids cultured in Hepato-STIM medium for one week were released from the Matrigel, using 0.25% Trypsin/EDTA, and plated at low density on 25 mm diameter coverslips coated with 0.01% poly-L-lysine solution (Sigma-Aldrich).

For pH_i measurements, the cells were loaded with BCECF-AM (3 μM, Molecular Probes, Eugene, OR, United States) for 60 min at 37°C. Coverslips were then mounted in a purpose-built perfusion chamber and the spheroids were superfused at 0.9 ml/min with either a HEPES-buffered solution containing (in mM): 137 NaCl, 5 KCl, 1 $CaCl_2$, 1 $MgCl_2$, 10 D-glucose, and 10 HEPES, pH 7.4, gassed with 100% O_2, or a bicarbonate-buffered bath solution containing (in mM): 116 NaCl, 25 $NaHCO_3$, 5 KCl, 1 $CaCl_2$, 1 $MgCl_2$, 10 D-glucose, and 5 HEPES, pH 7.4, gassed with 5% CO_2 in O_2. BCECF fluorescence was measured photometrically at 5-s intervals on an inverted fluorescence microscope (Nikon Eclipse TE200) as described previously (Racz et al., 2017). The ratio of the fluorescence signals obtained with excitation at 490 and 440 nm was converted to pH_i using calibration data obtained with the nigericin/high potassium method (Thomas et al., 1979).

For $[Ca^{2+}]_i$ measurements, the cells were loaded with fura-2AM (4 μM, Molecular Probes) for 45 min at room temperature. The spheroids were then superfused in a custom-made, open perfusion chamber at 2 ml/min with a bath solution containing (in mM): 137 NaCl, 5 KCl, 2 $CaCl_2$, 1 $MgCl_2$, 10 HEPES, and 10 glucose, adjusted to pH 7.4. Fura-2 fluorescence was measured alternately at 340, and 380 nm on an upright fluorescence microscope (Nikon Eclipse E600) using a metal-halide lamp and an internal filter wheel (Lumen 220 Pro, Prior Scientific, Cambridge, United Kingdom) at 1.5-s intervals. Imaging was performed with a cooled sCMOS camera (Prime BSI, Teledyne Photometrics, Tucson, AZ, United States) controlled by NIS AR software (Nikon). Changes in $[Ca^{2+}]_i$ were calculated as the ratio of the emitted fluorescence at the two respective excitation wavelengths (F_{340}/F_{380}) and normalized to the baseline ratio.

Fluoride Exposure

HAT-7 cells were plated in Matrigel and fed with Hepato-STIM medium as described above. There were two experimental

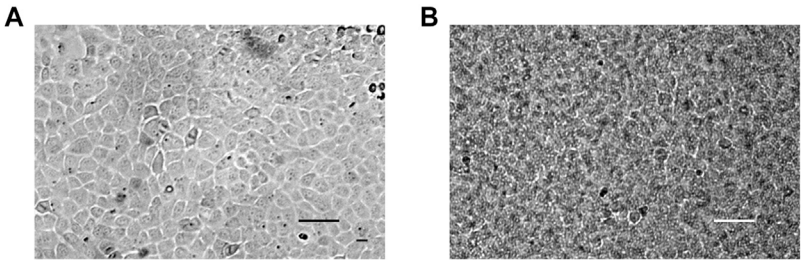

FIGURE 1 | Morphology of 2D HAT-7 cell cultures. **(A)** HAT-7 cells grown in control medium as a conventional monolayer on plastic in a T-25 culture flask for 3 days. **(B)** HAT-7 cells grown in differentiation medium as a polarized monolayer on a Transwell permeable support for 7 days. Also visible are the 0.4 μm pores in the polyester supporting membrane. Scale bars: 100 μm.

groups. In the first group, the culture medium was changed 24 h after seeding to Hepato-STIM containing 0 (control), 0.1, 0.3, 1.0, or 3.0 mM fluoride. In the second group, the culture medium was changed to Hepato-STIM, containing the same range of fluoride concentrations, on day 4 when spheroids were beginning to form. In both groups the medium was refreshed every other day.

Cell growth and spheroid development within the Matrigel layer were assessed by bright-field light microscopy (Nikon Eclipse TE200) and images obtained using a CCD camera (Blackfly USB3 CCD camera, FLIR Systems).

Statistical Analysis

Where appropriate, data are presented as mean ± SEM. Statistical analyses were performed using either one-sample t tests or analysis of variance combined with Tukey's multiple comparison test as appropriate.

RESULTS

HAT-7 Cells in 2D and 3D Culture

For conventional 2D culture on plastic, HAT-7 cells were seeded in T-25 tissue culture flasks and incubated in control medium. As the cells became confluent, they established a fairly uniform polygonal shape, giving a cobblestone appearance typical of epithelial cells (**Figure 1A**). When grown on permeable Transwell supports, their appearance was similar, as shown in **Figure 1B** where the outlines of the 0.4 μm pores in the polyester filter can also be seen.

For 3D culture within the extracellular matrix layer, fully dissociated HAT-7 cells were mixed with Matrigel prior to seeding in low-attachment plate wells. The cells, which were initially quite uniform in size, were then incubated with one of three alternative culture media and imaged after 3 days, 1 week and 2 weeks (**Figure 2A**). The cells cultured in control and differentiation media showed little change in appearance over the first 3 days. After 1 week some of the cells were began to show signs of division. And after 2 weeks a few had formed larger, multicellular spheroids, as depicted in the figure. However, these represented only a small fraction of the population, the rest remaining unchanged in size from their initial seeding.

In contrast, cells cultured in Hepato-STIM medium divided and formed multicellular spherical structures much more rapidly and consistently. Signs of cell division were already evident in most of the cell population after 3 days, and after just one week, many had developed into spheroids approaching 100 μm in diameter. After 2 weeks the spheroids had grown very large and had begun to disintegrate. The change in size distribution of the cells/spheroids over days 4, 5, and 6 (**Figure 2B**) is clearly much more rapid in Hepato-STIM compared with the other media. The yield and size of the spheroids after just one week in Hepato-STIM was much greater than in the control and differentiation media, even when the latter groups were cultured for 2 or more weeks. After culture in Hepato-STIM for one week, numerous HAT-7 spheroids could be released from the Matrigel matrix with trypsin/EDTA, resuspended in physiological salt solutions (**Figure 2C**) and used for a variety of experimental procedures.

The internal structure of the HAT-7 spheroids, cultured in Matrigel with Hepato-STIM medium, was examined in frozen sections stained with haematoxylin and eosin (**Figure 3**). After 7 days in culture, a range of morphologies was observed. The smallest and simplest spheroids consisted of a dense mass of largely undifferentiated cells with occasional extracellular fluid spaces or "lacunae" (**Figure 3A**). At the other end of the range were spheroids consisting of a central cell mass separated from an outer epithelial monolayer by a clear fluid-filled space, thereby showing various degrees of lumen formation (**Figures 3E–H**). The central cell mass could be either disorganized and undifferentiated (**Figures 3E,F**) or lamellar (**Figures 3G,H**) in structure. The spheroids with an intermediate morphology (**Figures 3B–D**) contained significant numbers of lacunae and evidence of an emerging outer epithelial layer that had not yet completely separated from the central cell mass.

RT-qPCR

To examine the expression levels of key structural, functional and marker genes, quantitative RT-PCR was performed using mRNA extracted from HAT-7 spheroids grown in Matrigel with Hepato-STIM medium, and from HAT-7 monolayers grown on Transwell permeable supports. Expression levels in the spheroids were normalised to the monolayer data (**Figure 4**) in order to reveal any significant differences between the 3D

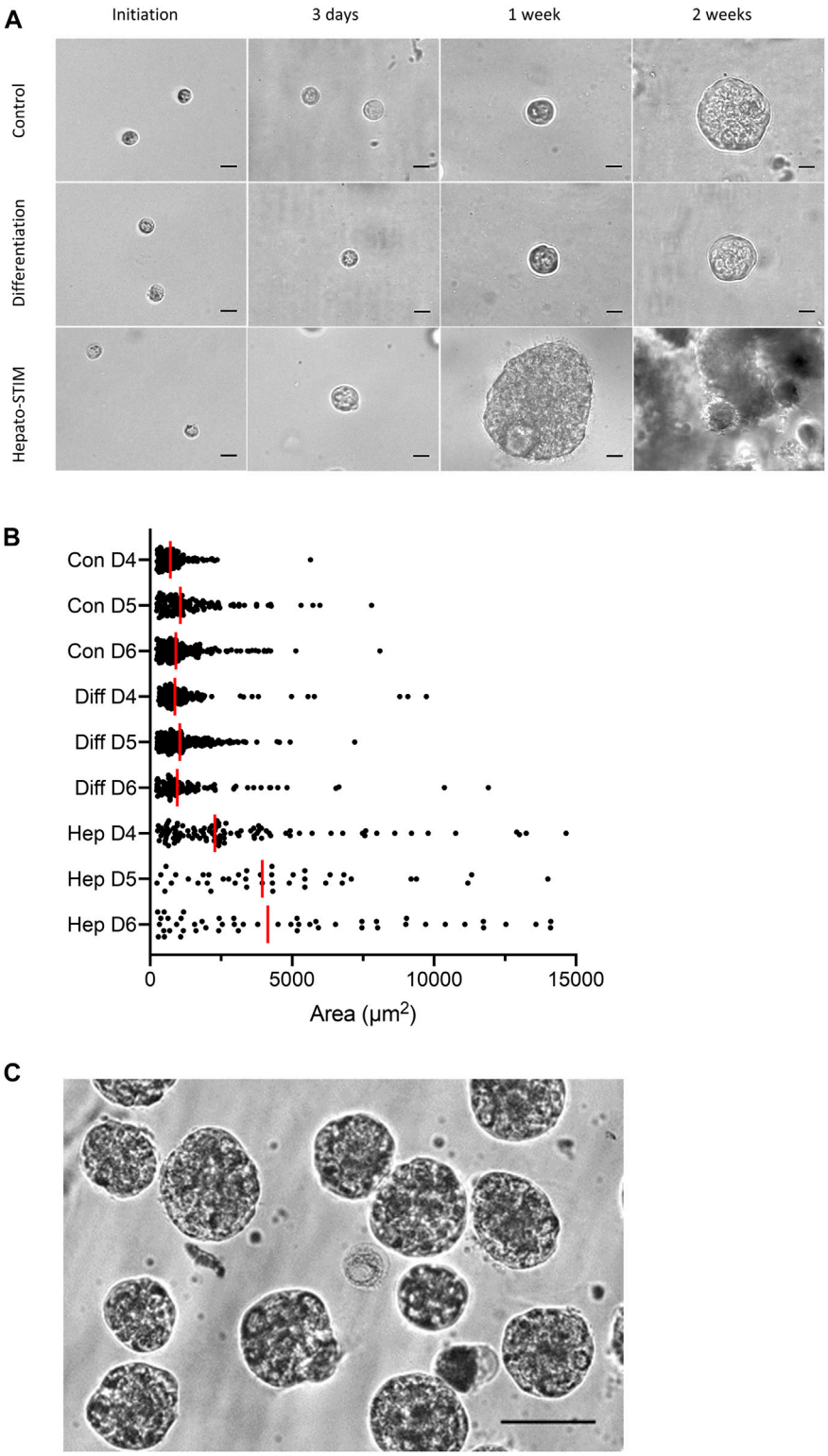

FIGURE 2 | Morphology of 3D HAT-7 cell cultures grown within a Matrigel matrix. **(A)** Time courses of growth and spheroid development when HAT-7 cells were seeded in Matrigel matrix and incubated in three different culture media: control, differentiation and Hepato-STIM. Images were obtained on the day of seeding and then after 3 days, 1 week and 2 weeks. **(B)** Size distribution of HAT-7 cells/spheroids in a representative experiment where growth in the three different culture media was compared on days 4, 5, and 6 (D4-D6). Each point represents the area of a single cell/spheroid and the vertical red bars indicate the median values. **(C)** HAT-7 spheroids isolated from the Matrigel matrix after 7 days of culture in Hepato-STIM and then plated on glass coverslips coated with poly-L-lysine in preparation for microfluorometry experiments to measure intracellular pH and calcium. Scale bars: 20 μm **(A)**, 75 μm **(C)**.

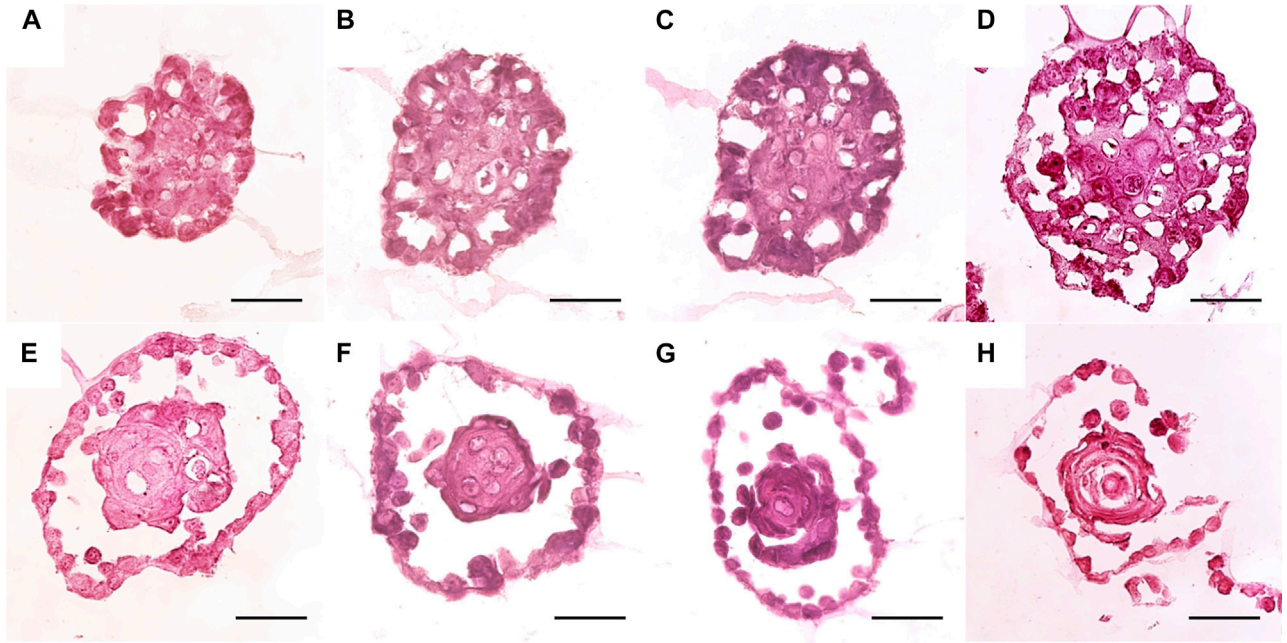

FIGURE 3 | Histology of HAT-7 spheroids grown for 7 days in Matrigel with Hepato-STIM medium. Spheroids were isolated from the matrix using 0.25% trypsin/EDTA. Frozen sections (5 μm) were stained with haematoxylin and eosin. Scale bars: 50 μm.

spheroids and the 2D monolayers used in our previous functional studies (Bori et al., 2016; Racz et al., 2017).

The most striking difference was in the expression of the maturation-stage ameloblast marker Klk4, which was increased approximately 70-fold in the HAT-7 spheroids compared with the monolayers (**Figure 4A**). There were significant decreases in the tight-junction proteins claudin-1, claudin-4 and TJP1/ZO-1, and an increase in claudin-8. Looking at the electrolyte transporters that are involved in HCO_3^- secretion by HAT-7 cells (**Figure 4B**), there were significant reductions in the expression of SLC26A4/pendrin and CFTR (cystic fibrosis transmembrane conductance regulator) in the spheroids–both normally associated with the apical membrane of ameloblasts. Small decreases in the expression of the basolateral transporters NHE1, AE2, and NBCe1 were not statistically significant.

Intracellular pH Regulation

Functional activities of the key transporters involved in HCO_3^- secretion by HAT-7 cells were assessed using BCECF fluorescence to measure intracellular pH changes in small groups of HAT-7 spheroids grown in Matrigel and Hepato-STIM. Standard protocols were used to evaluate the contributions of individual transporters previously shown to be active in 2D cultures of HAT-7 cells (Bori et al., 2016; Racz et al., 2017).

Recovery of pH_i from intracellular acidification was examined by exposing HAT-7 spheroids to NH_4Cl (20 mM) for 3 min, followed by substitution of extracellular Na^+ with $NMDG^+$. In a HCO_3^--free, HEPES-buffered bath solution this resulted in a transient alkalinization of the cells (due to NH_3 entry) followed by a rapid drop in pH_i to a markedly acidic value (**Figure 5A**). This acidification was sustained in the continuing absence of Na^+ indicating that there was no significant Na^+-independent pathway for H^+ extrusion from the cells, such as an H^+-ATPase. When Na^+ was restored to the bath, pH_i recovered rapidly to control values, indicating the presence of an Na^+-dependent H^+ extruder. When Na^+ was restored in the presence of amiloride (0.3 mM)–a selective inhibitor of Na^+/H^+ exchange–the rate of recovery from acidification was greatly reduced. This indicates that an Na^+/H^+ exchanger, most probably NHE1, is active in HAT-7 spheroids. Averaged data for the percentage inhibition of the rate of recovery, compared with the corresponding control in each experiment, is shown in **Figure 5D**.

When the experiment was repeated in the presence of HCO_3^-, the recovery from acidification, when Na^+ was restored to the bath, was less effectively inhibited by amiloride alone (**Figures 5B,D**), indicating the likely contribution of an additional Na^+- and HCO_3^--dependent mechanism. The recovery of pH_i in these conditions was more effectively inhibited (**Figures 5C,D**) by amiloride applied in combination with H_2DIDS (0.5 mM)-an inhibitor of Na^+-HCO_3^- cotransport. It is therefore likely that the HAT-7 spheroids also express an active Na^+-HCO_3^- cotransporter, most probably NBCe1.

The activity of Cl^-/HCO_3^- exchangers in HAT-7 spheroids was examined by substitution of extracellular Cl^- with gluconate$^-$. In the HCO_3^--buffered bath solution, Cl^- substitution evoked a significant rise in pH_i in the spheroid cells (**Figure 5E**), most probably as a result of Cl^- efflux driving an influx of HCO_3^- by Cl^-/HCO_3^- exchange. This rise in pH_i was completely reversed when Cl^- was restored to the bath solution. Furthermore, pre-treatment with DIDS (0.1 mM) - an inhibitor of Cl^-/HCO_3^- exchange-reversibly reduced the rate of change in pH_i resulting

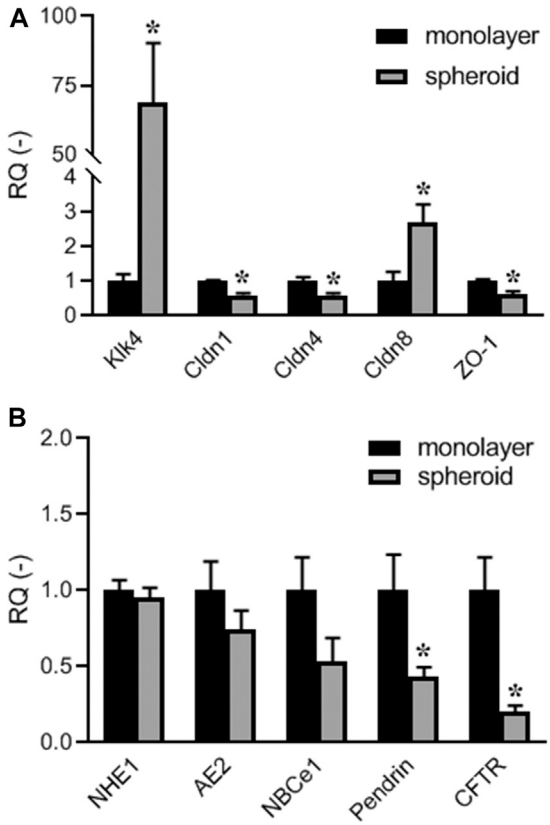

FIGURE 4 | Quantitative RT-PCR data showing expression of: **(A)** maturation-phase ameloblast marker Klk4, and tight-junction protein genes Cldn1, Cldn4, Cldn8 (claudins 1, 4, and 8), and Tjp1 (ZO-1); **(B)** electrolyte transporter genes Slc9a1 (NHE1), Slc4a2 (AE2), Slc4a4 (NBCe1), Slc26a4 (pendrin), and Cftr (CFTR). Expression levels in HAT-7 cells grown in Matrigel with Hepato-STIM medium (spheroid) were normalised to expression levels in HAT-7 cells grown on Transwell permeable supports in differentiation medium (monolayer). Data are mean ± SEM. *$p < 0.05$ (n = 4).

from Cl^- substitution by 72.1 ± 12.1% (n = 4, $p < 0.01$). This indicates that an exchanger of this type, most probably AE2, is active in HAT-7 spheroids.

Calcium Signaling

Previous work has shown that transepithelial HCO_3^- secretion by HAT-7 cells in 2D culture is stimulated by agonists known to elevate intracellular cAMP and Ca^{2+}, such as forskolin and ATP respectively (Bori et al., 2016). In the present study, changes in intracellular Ca^{2+} concentration ($[Ca^{2+}]_i$) were measured in HAT-7 spheroids using fura-2 fluorescence.

To test for the presence of purinergic receptors in the spheroids, we measured the intracellular Ca^{2+} concentration $[Ca^{2+}]_i$ after stimulation with the purinergic agonists ATP (50 μM) and UTP (50 μM). In the presence of external Ca^{2+} (2 mM) ATP and UTP induced similar biphasic Ca^{2+} responses consisting of an initial transient peak and a sustained component. However, in the absence of external Ca^{2+}, both ATP and UTP caused only transient Ca^{2+} responses, suggesting that the sustained component was due to Ca^{2+} influx from the extracellular space (**Figures 6A–C**). Since UTP does not stimulate ionotropic P2X receptors, we speculate that Ca^{2+} entry was due to depletion of intracellular Ca^{2+} stores, which in turn activates store-operated Ca^{2+} channels (SOCCs).

Since acetylcholine (ACh) has been shown to elicit Ca^{2+} signals in freshly isolated rat ameloblasts (Nurbaeva et al., 2018), we also tested the effects of the Ach analog carbachol (100 μM). However, no changes were observed in $[Ca^{2+}]_i$ suggesting that neither muscarinic nor nicotinic functional ACh receptors are expressed in HAT-7 spheroids (**Figure 6D**).

Fluoride Exposure

The effects of fluoride on spheroid formation in the Matrigel matrix were examined in two series of experiments where fluoride, at a range of concentrations, was introduced at two different time points during the culture process.

In the first series, fluoride was added to the Hepato-STIM medium 24 h after the cells had been seeded in Matrigel. The concentrations of fluoride applied were 0.1, 0.3, 1.0, and 3.0 mM, and there was a control group that was not exposed to fluoride. **Figure 7A** shows images of the developing spheroids obtained on days 2 and 7 of culture, and images of spheroids isolated from the Matrigel matrix on day 7. In the absence of fluoride (control), the spheroids developed quickly and uniformly as already seen in **Figure 2A**. HAT-7 cells cultured in 0.1 and 0.3 mM fluoride were also able to form spheroids, with a similar size and appearance to the control group, over a similar time period. When these spheroids were isolated from the Matrigel on day 7, they retained the same shape and appearance as the control group. In other words, spheroid formation did not appear to be significantly affected by 0.1 or 0.3 mM fluoride.

In contrast, HAT-7 cells cultured in Matrigel and Hepato-STIM in the presence of 1 mM fluoride generated only a few small spheroids and significant amounts of cellular debris. The spheroids isolated from the Matrigel on day 7 were few in number and smaller than those obtained at the lower fluoride concentrations and in the control group. As expected, in 3 mM fluoride there were few viable cells remaining after a single day, and no spheroids were formed.

In the second series, fluoride was introduced on day 4, which is the time point when the spheroids start to grow rapidly in Matrigel and Hepato-STIM under control conditions. As can be seen in **Figure 7B**, HAT-7 spheroid development was again largely unaffected by 0.1 and 0.3 mM fluoride. The number, growth rate and final size of the spheroids was similar to those grown in control medium. The higher concentrations of fluoride applied on day 4 had similar effects to what was observed when fluoride was applied after 24 h. The spheroids already present on day 4 gradually decreased in size in the presence of 1 mM fluoride, and by day 7 they were clearly disaggregating. This was particularly noticeable when they were isolated from the Matrigel matrix: few intact spheroids remained and there was a lot of cell debris. In 3 mM fluoride, the death and disintegration of the spheroids proceeded more rapidly and there were none remaining by day 7.

DISCUSSION

In the present study dissociated HAT-7 cells were cultivated within a Matrigel matrix in order to obtain single cell-derived 3D

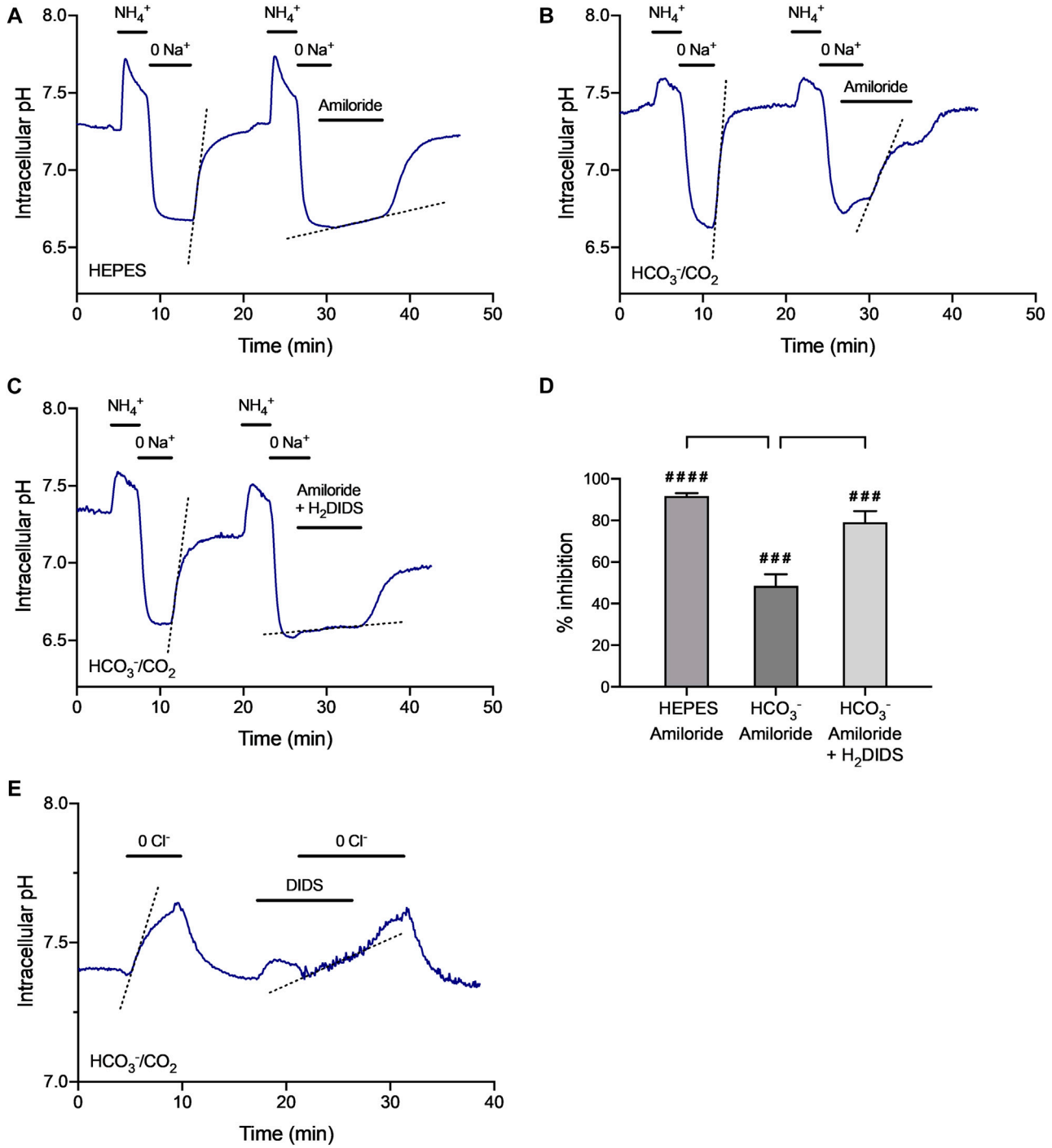

FIGURE 5 | | Regulation of intracellular pH in isolated HAT-7 spheroids. **(A–C)** Recovery of pH_i from intracellular acidification evoked by a 3-min exposure to extracellular NH_4^+ (20 mM) followed by substitution of extracellular Na^+ with $NMDG^+$ (*0 Na^+*): **(A)** in HEPES-buffered bath solution in the absence and presence of the Na^+/H^+ exchange inhibitor amiloride (0.3 mM); **(B)** in HCO_3^--buffered bath solution in the absence and presence of amiloride (0.3 mM); **(C)** in HCO_3^--buffered bath solution in the absence and presence of amiloride (0.3 mM) together with the Na^+-HCO_3^- cotransport inhibitor H_2DIDS (0.5 mM). Dashed lines show the rate of recovery of pH_i when Na^+ was restored to the perfusate. **(D)** Averaged data (mean ± SEM) from 4–6 experiments showing the inhibitory effects of amiloride and H_2DIDS on the rate of recovery of pH_i from acidification in the absence and presence of HCO_3^-. Percentage inhibition was calculated with reference to the internal control in each experiment. ####$p < 0.0001$, ###$p < 0.001$ compared with control (one-sample t test). **$p < 0.01$, ***$p < 0.001$ (ANOVA and Tukey post-hoc test). **(E)** Changes in pH_i evoked by substitution of extracellular Cl^- with gluconate$^-$ (*0 Cl^-*) in HCO_3^--buffered bath solution in the absence and presence of DIDS (0.1 mM). Dashed lines show the rate of recovery of pH_i when Na^+ or Cl^- was restored to the perfusate. Measurements of BCECF fluorescence were pooled from 20–50 HAT-7 spheroids isolated from Matrigel matrix by treatment with 0.25% trypsin/EDTA. Traces are representative of 4–6 experiments.

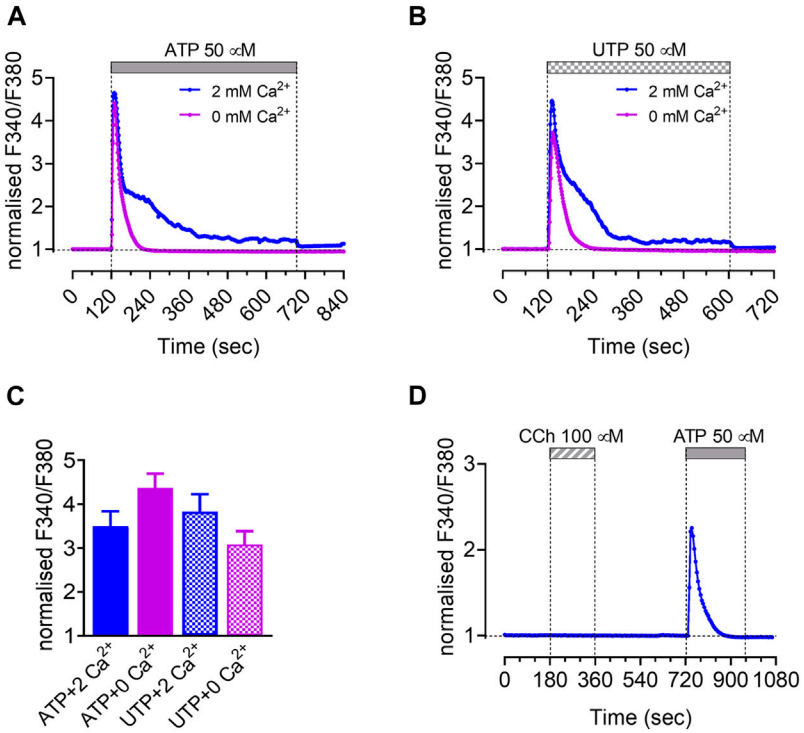

FIGURE 6 | Intracellular Ca^{2+} responses of isolated HAT-7 spheroids to different agonists. Changes in intracellular Ca^{2+} in response to 50 μM ATP (n = 5) **(A)** and 50 μM UTP (n = 3) **(B)** in the presence and absence of extracellular calcium. **(C)** Peak values presented as means ± SEM (no significant difference). **(D)** Effect of carbachol (100 μM, n = 3) on intracellular Ca^{2+} concentration. An ATP stimulus was applied subsequently to test the responsiveness of the spheroids. Panels show representative traces. Data are presented as changes in fura-2 fluorescence ratio normalized to baseline.

colonies. We found that the combination of Hepato-STIM epithelial cell differentiation medium and Matrigel induced cell expansion and 3D spheroid formation. The cells retained epithelial cell morphology and continued to express both ameloblast-specific and ion transport-specific gene expression. Furthermore, like HAT-7 polarized monolayers, the spheroid cells were able to regulate their intracellular pH and to show intracellular calcium responses to extracellular stimulation. Finally, we have demonstrated that HAT-7 spheroids may serve as a disease model for studying the concentration-dependent damaging effects of fluoride exposure on amelogenesis.

The choice of culturing protocols, culture medium and scaffold serve as important selection factors in epithelial cell expansion and 3D culturing (Bajaj et al., 2014). We initially tested three culture media: control medium (standard DMEM/F12 Ham medium supplemented with fetal bovine serum), differentiation medium (control medium supplemented with $CaCl_2$ and dexamethasone) and Hepato-STIM medium (also supplemented with fetal bovine serum). It quickly became apparent that the use of Hepato-STIM medium, rather than the other two media, resulted in a far better outcome, both regarding the number and size of the HAT-7 spheroids. Hepato-STIM is a specialised medium consisting of Williams' E medium supplemented with dexamethasone, insulin, transferrin, selenium, EGF and 1.8 mM Ca^{2+}. These components are all important factors in maintaining an epithelial phenotype (Szlavik et al., 2008a; Maria and Tran, 2011; Hegyesi et al., 2015). This medium was originally designed for the culture of hepatocytes, but has since been used successfully to grow both human primary salivary epithelial cells (Szlavik et al., 2008a; Maria and Tran, 2011; Hegyesi et al., 2015) and lacrimal acinar cells (Schonthal et al., 2000; Tiwari et al., 2018).

In the present work we used Matrigel as a scaffold to induce and promote spheroid formation by HAT-7 cells. Matrigel is a poorly defined basement membrane derivative extracted from Engelbreth–Holm–Swarm mouse sarcoma cells, thus its direct application in regenerative medicine is limited (Huang et al., 2020). However, its use is well established in the culture of spheroids and organoids from various tissues, especially those of epithelial origin. This is mainly because of three key factors: first, the Matrigel provides anchoring molecules such as the arg-gly-asp (RGD) sequence for cell adhesion; second, it has optimal stiffness for housing the cells; and third, it contains laminin-111, an important extracellular component that can independently provide biological signals for spheroid/organoid formation and growth (Huang et al., 2020). Using Matrigel, 3D spheroids and organoids have been created from intestinal epithelial cells (Huang et al., 2019), pancreas (Bakhti et al., 2019; Molnar et al., 2020), lacrimal glands (Schonthal et al., 2000; Massie et al., 2018) and salivary glands (Szlavik et al., 2008a; Szlavik

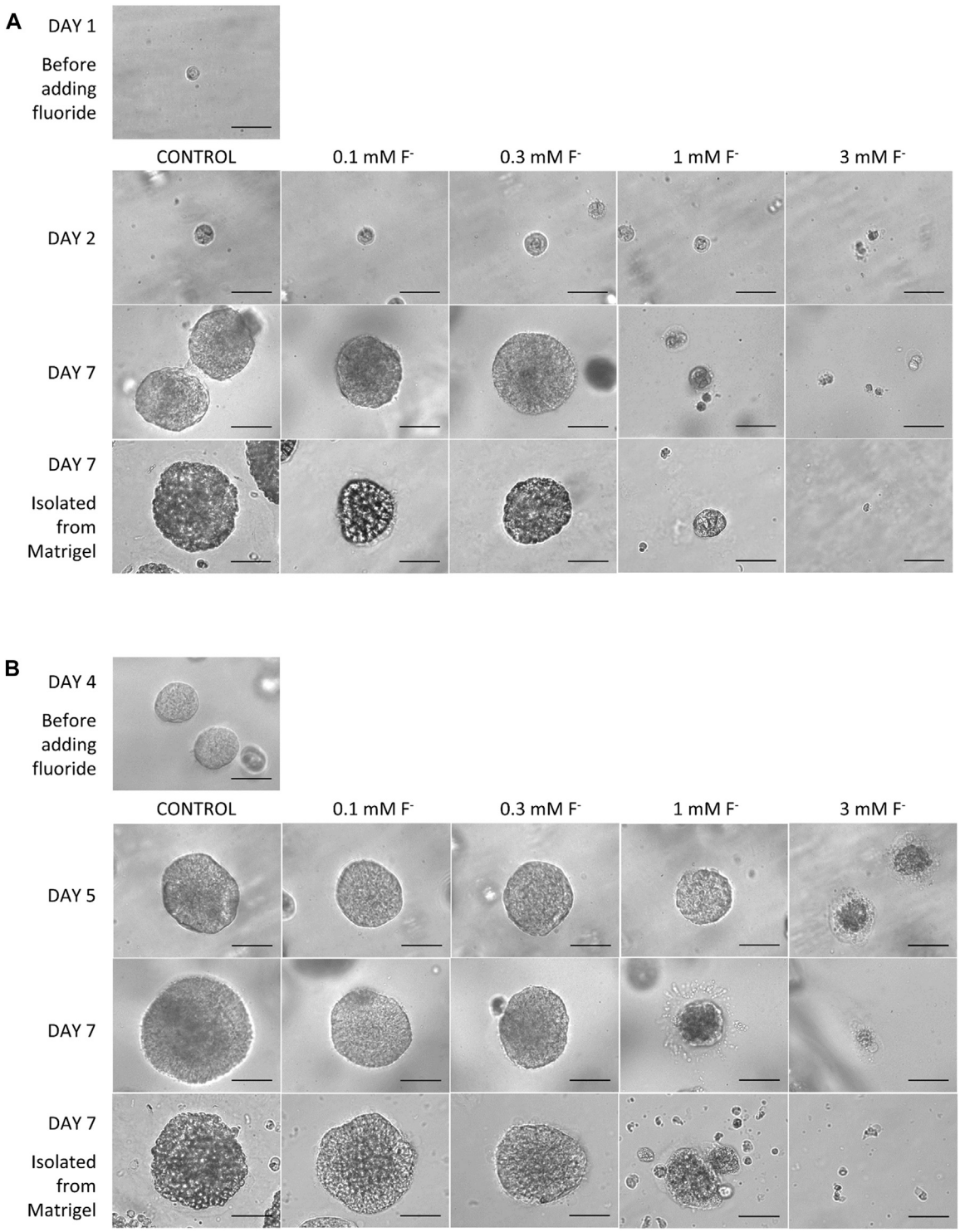

FIGURE 7 | Morphology of HAT-7 spheroids cultured in Matrigel and Hepato-STIM medium in the absence (control) or presence of fluoride (0.1–3.0 mM). **(A)** Spheroid images obtained on days 1, 2, and 7 when fluoride (0, 0.1, 0.3, 1.0, 3.0 mM) was added to the culture medium 24 h after seeding. Also shown are spheroids isolated from the Matrigel on day 7. **(B)** Spheroid images obtained on days 4, 5, and 7 when fluoride (0, 0.1, 0.3, 1.0, 3.0 mM) was added to the culture medium at the time of rapid spheroid growth 4 days after seeding. Also shown are spheroids isolated from the Matrigel on day 7. Scale bars: 70 μm.

et al., 2008b; Maria et al., 2011). Primary culture ameloblast-lineage cells also form 3D spheroids when cultured in Matrigel (Li et al., 2006).

When porcine and human ameloblast-lineage cells (Li et al., 2006; He et al., 2010) are grown in Matrigel, the cells form spherical, acinar-like structures that appeared similar to enamel pearls. Additionally, ameloblast-lineage cells (He et al., 2010) or human embryonic stem cell-derived epithelial cells (Zheng et al., 2013b; Zheng et al., 2013c) pre-cultivated in Matrigel and then cultured together with dental mesenchymal cells result in the formation of tooth-like structures. Finally, when mouse dental epithelial stem cells from the most posterior part of the cervical loop of incisors are isolated, dispersed, and then embedded into Matrigel (Natsiou et al., 2017) spheroids are produced (Natsiou et al., 2017). Our present success in reliably and reproducibly generating 3D HAT-7 spheroids, using Hepato-STIM culture medium and a Matrigel scaffold, are completely in line with those previous observations.

Tight junction proteins ZO-1 and claudins 1, 4, and 8 were all expressed at mRNA level in HAT-7 cells, regardless of whether they were grown on porous Transwell filters or in Matrigel. PCR data normalized to 2D HAT-7 cultivation revealed an increase in Cldn8 while the expression of ZO-1, Cldn1 and Cldn4 claudins were decreased in HAT-7 spheroids. These data are also in accordance with previous studies showing the expression of Cldn1, Cldn4 and Cldn8 in maturation-stage ameloblasts (Inai et al., 2008; Hata et al., 2010). The higher level of Cldn8 expression in the spheroids may reflect the elevated level of paracellular leakage observed when Cldn8 is upregulated (Amasheh et al., 2009).It is important to note that the expression of maturation ameloblast-specific Klk4 was considerably increased, suggesting a shift toward the maturation-type phenotype during 3D organization (Bronckers et al., 2016; Nunez et al., 2016).

The key electrolyte transporters and channels NHE1, AE2, NBCe1, pendrin and CFTR, which are key factors in HCO_3^- secretion and intracellular pH regulation, were all expressed in both HAT-7 monolayers and spheroids, although pendrin and CFTR were significantly decreased in the spheroids. Nonetheless these data are generally in line with previous studies which demonstrated NHE1, AE2, NBCe1, pendrin and CFTR expression in ameloblasts and their involvement in intracellular and extracellular pH regulation (Bronckers et al., 2011; Lacruz et al., 2013; Jalali et al., 2014). The fact that these transporters are present in HAT-7 spheroids suggests that this experimental model, like the polarized 2D HAT-7 monolayer, is suitable for studying ameloblast acid/base transport.

An important function of ameloblasts is to produce hydroxyapatite crystals, comprising Ca^{2+}, phosphate and water, in a process whereby eight moles of protons are liberated during the formation of each mole of hydroxyapatite (Lacruz et al., 2017; Varga et al., 2018). While the Ca^{2+} transport mechanism in these cells is relatively well understood (Lacruz, 2017; Lacruz et al., 2017; Varga et al., 2018), much less is known about the mechanism of phosphate transport into the enamel matrix. Some possibilities include transport into the cells of the enamel via Na^+-phosphate cotransporters of the SLC20 and SLC34 gene families (Merametdjian et al., 2018; Beck, 2019) followed by secretion across the apical membrane or into matrix vesicles (Pandya et al., 2017).

Functional models are needed to better understand how ameloblasts direct Ca^{2+} and phosphate transport into the enamel matrix, and how ameloblasts neutralize the acidity generated as hydroxyapatite crystals form (Lacruz et al., 2017; Varga et al., 2018). HAT-7 cells grown as monolayers on permeable supports express ion transport proteins that mediate the uptake of HCO_3^- ions across the basolateral membrane in order to drive HCO_3^- secretion across the apical membrane (Bori et al., 2016; Racz et al., 2017). Basolateral HCO_3^- uptake is achieved by the H_2DIDS-sensitive Na^+-HCO_3^- cotransporter NBCe1, and indirectly by H^+ extrusion via the amiloride-sensitive Na^+/H^+ exchanger NHE1 works in conjunction with intracellular carbonic anhydrase activity continuously producing H^+ and HCO_3^-. The expansion of these cells into organoid culture systems is an important step toward further studies of ameloblast-mediated ion transport and matrix mineralization.

The pH_i measurements presented here confirm that these transporters are also active in HAT-7 spheroids and that, as in the HAT-7 monolayers, there is no evidence of a basolateral H^+-ATPase contributing to the uptake of HCO_3^- ions. The Cl^- substitution experiments confirm the expression of a DIDS-sensitive Cl^-/HCO_3^- exchanger, most probably AE2, that can contribute to the basolateral uptake of Cl^- ions, which are also required for enamel formation (Bronckers et al., 2015b; Bronckers, 2017). And the RT-qPCR data confirm that all three transporters, NBCe1, NHE1, and AE2, are expressed in HAT-7 spheroids as they are in HAT-7 monolayers.

It was interesting to note that CFTR expression decreased in spheroid culture. *In vivo*, CFTR is highly expressed in maturation-stage ameloblasts with reduced expression in the earlier transition stage and almost no expression in the secretory stage (Bronckers et al., 2010; Bronckers et al., 2015a). In previous studies of primary ameloblast-derived cells in grown in Matrigel, we found increased expression and synthesis of amelogenin protein (He et al., 2010). Amelogenin is a secretory stage protein, and this suggests the possibility that in 3D culture, ameloblast-lineage cells may de-differentiate to an early stage of enamel formation. Further studies and culture media can be used to explore this interesting possibility.

Calcium signaling in HAT-7 spheroids was also investigated in the present study. According to the current classification, adenosine stimulates P1 purinergic receptors whereas the extracellular nucleotides ATP, ADP, UTP, and UDP activate P2 receptors, which are further divided into two subtypes: ionotropic (P2X) and metabotropic (P2Y). In the presence of external Ca^{2+}, both ATP and UTP elicited biphasic Ca^{2+} responses in HAT-7 spheroids, suggesting the activation of metabotropic P2Y2 and/or P2Y4 receptors (Guns et al., 2005). Furthermore, it has been demonstrated that P2Y receptors could regulate the activity of the NCKX4 Ca^{2+} extrusion pathway (Yang and Lytton, 2013) that is known to play a critical role in dental enamel maturation (Nurbaeva et al., 2017). Since ionotropic P2X receptors are insensitive to UTP, the Ca^{2+} entry during the

sustained phase is most likely due to opening of store-operated Ca^{2+} channels. Indeed Nurbaeva and colleagues have recently shown that ATP strongly stimulates store-operated Ca^{2+} entry in maturation but not secretory ameloblasts (Nurbaeva et al., 2018).

Environmental factors, such as exposure to excessive amounts of fluoride, can alter enamel formation. Most studies using ameloblast cell lines have found effects of fluoride only at millimolar concentrations (Li et al., 2006), whereas in primary ameloblast cell cultures fluoride can alter cell characteristics at micromolar levels (Yan et al., 2007; Zhang et al., 2007). In this study, we found that in the presence of 1 mM fluoride applied from day 4, spheroid size gradually decreased, and by day 7 they were clearly disaggregating. Longer term exposure to 1 mM fluoride, between days 2 and 7, resulted in the formation of only a few small spheroids and significant amounts of cellular debris. 3 mM fluoride killed all HAT-7 cells within 2 days.

Exposure to 0.1 and 0.3 mM fluoride for three or six days did not affect spheroid formation compared to controls. These findings are in line with our recent studies on the effect of fluoride using the 2D HAT-7 model, where cells were grown in monolayers on Transwell filters (Racz et al., 2017).

The delay in tight junction formation observed in the 2D monolayer model (Racz et al., 2017) also fits well with our finding that HAT-7 spheroids disintegrated after 3 days of exposure to 1 mM fluoride when isolated from Matrigel using even the most gentle spheroid isolation procedure. The data indicate that 1 mM fluoride not only affects spheroid formation, but it also weakens the cell-cell adhesion structures responsible of maintaining the spheroid structure.

Studies of the effects of micromolar, physiologic levels of fluoride on primary ameloblast culture show that, while there are effects on cell proliferation and apoptosis, there are few to no changes in gene expression (Kubota et al., 2005; Zhang et al., 2006; Yan et al., 2007; Zhang et al., 2007; Sharma et al., 2008; Zhang et al., 2016).

These findings highlight the importance of developing a robust and reproducible culture system to investigate questions such as how fluoride alone, or in combination with other environmental stressors, alters enamel formation and biomineralization. Our finding that HAT-7 cells can form spheroids similar to those formed by primary culture ameloblasts offers the possibility of scaling up this model system to better understand cell-cell and cell-matrix interactions and their importance in enamel formation.

In conclusion, this model system shows that HAT-7 cells cultivated within a Matrigel extracellular matrix form three-dimensional, multi-cellular, spheroidal structures that retain their functional capacity for pH regulation and intracellular Ca^{2+} signaling. They also express protein markers consistent with a maturation-stage ameloblast phenotype. This new 3D model will allow us to gain a better understanding of the molecular mechanisms involved in amelogenesis, not only in health but also in disorders of enamel formation, such as those resulting from environmental factors.

DATA AVAILABILITY STATEMENT

The raw data supporting the conclusions of this article will be made available by the authors, without undue reservation.

AUTHOR CONTRIBUTIONS

AF, and TS-N: contributed to conception, design, data acquisition, analysis and interpretation, and drafted and critically revised manuscript; KK, and RR: contributed to data acquisition, analysis and interpretation, and drafted and critically revised manuscript; ÁZ: contributed to data interpretation and critically revised manuscript; PD: contributed to conception, design, data interpretation, and critically revised manuscript; MS and GV: contributed to conception, design, data interpretation, and drafted and critically revised the manuscript.

FUNDING

This work was supported by the National Institutes of Health (NIH NIDCR grant 1R01DE027971) and by the Hungarian National Research, Development and Innovation Fund (NKFIH K-125161).

REFERENCES

Amasheh, S., Milatz, S., Krug, S. M., Bergs, M., Amasheh, M., Schulzke, J.-D., et al. (2009). Na+ Absorption Defends from Paracellular Back-Leakage by Claudin-8 Upregulation. *Biochem. Biophysical Res. Commun.* 378 (1), 45–50. doi:10.1016/j.bbrc.2008.10.164

Arakaki, M., Ishikawa, M., Nakamura, T., Iwamoto, T., Yamada, A., Fukumoto, E., et al. (2012). Role of Epithelial-Stem Cell Interactions during Dental Cell Differentiation*. *J. Biol. Chem.* 287 (13), 10590–10601. doi:10.1074/jbc.M111.285874

Bajaj, P., Schweller, R. M., Khademhosseini, A., West, J. L., and Bashir, R. (2014). 3D Biofabrication Strategies for Tissue Engineering and Regenerative Medicine. *Annu. Rev. Biomed. Eng.* 16, 247–276. doi:10.1146/annurev-bioeng-071813-105155

Bakhti, M., Scheibner, K., Tritschler, S., Bastidas-Ponce, A., Tarquis-Medina, M., Theis, F. J., et al. (2019). Establishment of a High-Resolution 3D Modeling System for Studying Pancreatic Epithelial Cell Biology *In Vitro*. *Mol. Metab.* 30, 16–29. doi:10.1016/j.molmet.2019.09.005

Bartosh, T. J., Ylostalo, J. H., Mohammadipoor, A., Bazhanov, N., Coble, K., Claypool, K., et al. (2010). Aggregation of Human Mesenchymal Stromal Cells (MSCs) into 3D Spheroids Enhances Their Antiinflammatory Properties. *Proc. Natl. Acad. Sci.* 107 (31), 13724–13729. doi:10.1073/pnas.1008117107

Beck, L. (2019). Expression and Function of Slc34 Sodium-Phosphate Co-transporters in Skeleton and Teeth. *Pflugers Arch. - Eur. J. Physiol.* 471 (1), 175–184. doi:10.1007/s00424-018-2240-y

Bori, E., Guo, J., Rácz, R., Burghardt, B., Földes, A., Kerémi, B., et al. (2016). Evidence for Bicarbonate Secretion by Ameloblasts in a Novel Cellular Model. *J. Dent Res.* 95 (5), 588–596. doi:10.1177/0022034515625939

Bronckers, A., Kalogeraki, L., Jorna, H. J. N., Wilke, M., Bervoets, T. J., Lyaruu, D. M., et al. (2010). The Cystic Fibrosis Transmembrane Conductance Regulator (CFTR) Is Expressed in Maturation Stage Ameloblasts, Odontoblasts and Bone Cells. *Bone* 46 (4), 1188–1196. doi:10.1016/j.bone.2009.12.002

Bronckers, A. L. J. J., Guo, J., Zandieh-Doulabi, B., Bervoets, T. J., Lyaruu, D. M., Li, X., et al. (2011). Developmental Expression of Solute Carrier Family 26A Member 4 (SLC26A4/pendrin) during Amelogenesis in Developing Rodent

Teeth. *Eur. J. Oral Sci.* 119 (Suppl. 1), 185–192. doi:10.1111/j.1600-0722.2011.00901.x

Bronckers, A. L. J. J. (2017). Ion Transport by Ameloblasts during Amelogenesis. *J. Dent Res.* 96 (3), 243–253. doi:10.1177/0022034516681768

Bronckers, A. L. J. J., Lyaruu, D., Jalali, R., Medina, J. F., Zandieh-Doulabi, B., and DenBesten, P. K. (2015a). Ameloblast Modulation and Transport of Cl−, Na+, and K+ during Amelogenesis. *J. Dent Res.* 94 (12), 1740–1747. doi:10.1177/0022034515606900

Bronckers, A. L. J. J., Lyaruu, D. M., Guo, J., Bijvelds, M. J. C., Bervoets, T. J. M., Zandieh-Doulabi, B., et al. (2015b). Composition of Mineralizing Incisor Enamel in Cystic Fibrosis Transmembrane Conductance Regulator-Deficient Mice. *Eur. J. Oral Sci.* 123 (1), 9–16. doi:10.1111/eos.12163

Bronckers, A. L. J. J., Lyaruu, D. M., Jalali, R., and DenBesten, P. K. (2016). Buffering of Protons Released by mineral Formation during Amelogenesis in Mice. *Eur. J. Oral Sci.* 124 (5), 415–425. doi:10.1111/eos.12287

Chen, A. K.-L., Chew, Y. K., Tan, H. Y., Reuveny, S., and Weng Oh, S. K. (2015). Increasing Efficiency of Human Mesenchymal Stromal Cell Culture by Optimization of Microcarrier Concentration and Design of Medium Feed. *Cytotherapy* 17 (2), 163–173. doi:10.1016/j.jcyt.2014.08.011

Chen, J., Zhang, Y., Mendoza, J., and Denbesten, P. (2009). Calcium-mediated Differentiation of Ameloblast Lineage Cells *In Vitro*. *J. Exp. Zool.* 312B (5), 458–464. doi:10.1002/jez.b.21279

Cherian, D. S., Bhuvan, T., Meagher, L., and Heng, T. S. P. (2020). Biological Considerations in Scaling up Therapeutic Cell Manufacturing. *Front. Pharmacol.* 11, 654. doi:10.3389/fphar.2020.00654

DenBesten, P. K., Machule, D., Zhang, Y., Yan, Q., and Li, W. (2005). Characterization of Human Primary Enamel Organ Epithelial Cells *In Vitro*. *Arch. Oral Biol.* 50 (8), 689–694. doi:10.1016/j.archoralbio.2004.12.008

Guns, P.-J. D. F., Korda, A., Crauwels, H. M., Van Assche, T., Robaye, B., Boeynaems, J.-M., et al. (2005). Pharmacological Characterization of Nucleotide P2Y Receptors on Endothelial Cells of the Mouse Aorta. *Br. J. Pharmacol.* 146 (2), 288–295. doi:10.1038/sj.bjp.0706326

Hata, M., Kawamoto, T., Kawai, M., and Yamamoto, T. (2010). Differential Expression Patterns of the Tight junction-associated Proteins Occludin and Claudins in Secretory and Mature Ameloblasts in Mouse Incisor. *Med. Mol. Morphol.* 43 (2), 102–106. doi:10.1007/s00795-009-0482-7

He, P., Zhang, Y., Kim, S. O., Radlanski, R. J., Butcher, K., Schneider, R. A., et al. (2010). Ameloblast Differentiation in the Human Developing Tooth: Effects of Extracellular Matrices. *Matrix Biol.* 29 (5), 411–419. doi:10.1016/j.matbio.2010.03.001

Hegyesi, O., Földes, A., Bori, E., Németh, Z., Barabás, J., Steward, M. C., et al. (2015). Evidence for Active Electrolyte Transport by Two-Dimensional Monolayers of Human Salivary Epithelial Cells. *Tissue Eng. C: Methods* 21 (12), 1226–1236. doi:10.1089/ten.TEC.2014.0614

Huang, J., Jiang, Y., Ren, Y., Liu, Y., Wu, X., Li, Z., et al. (2020). Biomaterials and Biosensors in Intestinal Organoid Culture, a Progress Review. *J. Biomed. Mater. Res.* 108 (7), 1501–1508. doi:10.1002/jbm.a.36921

Huang, J., Ren, Y., Wu, X., Li, Z., and Ren, J. (2019). Gut Bioengineering Promotes Gut Repair and Pharmaceutical Research: a Review. *J. Tissue Eng.* 10, 204173141983984. doi:10.1177/2041731419839846

Inai, T., Sengoku, A., Hirose, E., Iida, H., and Shibata, Y. (2008). Differential Expression of the Tight junction Proteins, Claudin-1, Claudin-4, Occludin, ZO-1, and PAR3, in the Ameloblasts of Rat Upper Incisors. *Anat. Rec.* 291 (5), 577–585. doi:10.1002/ar.20683

Jalali, R., Guo, J., Zandieh-Doulabi, B., Bervoets, T. J. M., Paine, M. L., Boron, W. F., et al. (2014). NBCe1 (SLC4A4) a Potential pH Regulator in Enamel Organ Cells during Enamel Development in the Mouse. *Cell Tissue Res* 358 (2), 433–442. doi:10.1007/s00441-014-1935-4

Jalali, R., Lodder, J. C., Zandieh-Doulabi, B., Micha, D., Melvin, J. E., Catalan, M. A., et al. (2017). The Role of Na:K:2Cl Cotransporter 1 (NKCC1/SLC12A2) in Dental Epithelium during Enamel Formation in Mice. *Front. Physiol.* 8, 924. doi:10.3389/fphys.2017.00924

Kawano, S., Morotomi, T., Toyono, T., Nakamura, N., Uchida, T., Ohishi, M., et al. (2002). Establishment of Dental Epithelial Cell Line (HAT-7) and the Cell Differentiation Dependent on Notch Signaling Pathway. *Connect. Tissue Res.* 43 (2-3), 409–412. doi:10.1080/0300820029000063710.1080/713713488

Klein, O. D., Duverger, O., Shaw, W., Lacruz, R. S., Joester, D., Moradian-Oldak, J., et al. (2017). Meeting Report: a Hard Look at the State of Enamel Research. *Int. J. Oral Sci.* 9 (11), e3. doi:10.1038/ijos.2017.40

Kubota, K., Lee, D. H., Tsuchiya, M., Young, C. S., Everett, E. T., Martinez-Mier, E. A., et al. (2005). Fluoride Induces Endoplasmic Reticulum Stress in Ameloblasts Responsible for Dental Enamel Formation. *J. Biol. Chem.* 280 (24), 23194–23202. doi:10.1074/jbc.M503288200

Lacruz, R. S. (2017). Enamel: Molecular Identity of its Transepithelial Ion Transport System. *Cell Calcium* 65, 1–7. doi:10.1016/j.ceca.2017.03.006

Lacruz, R. S., Habelitz, S., Wright, J. T., and Paine, M. L. (2017). Dental Enamel Formation and Implications for Oral Health and Disease. *Physiol. Rev.* 97 (3), 939–993. doi:10.1152/physrev.00030.2016

Lacruz, R. S., Smith, C. E., Kurtz, I., Hubbard, M. J., and Paine, M. L. (2013). New Paradigms on the Transport Functions of Maturation-Stage Ameloblasts. *J. Dent Res.* 92 (2), 122–129. doi:10.1177/0022034512470954

Lam, A. T.-L., Li, J., Toh, J. P.-W., Sim, E. J.-H., Chen, A. K.-L., Chan, J. K.-Y., et al. (2017). Biodegradable Poly-ε-Caprolactone Microcarriers for Efficient Production of Human Mesenchymal Stromal Cells and Secreted Cytokines in Batch and Fed-Batch Bioreactors. *Cytotherapy* 19 (3), 419–432. doi:10.1016/j.jcyt.2016.11.009

Li, W., Machule, D., Gao, C., and DenBesten, P. K. (2006). Growth of Ameloblast-Lineage Cells in a Three-Dimensional Matrigel Environment. *Eur. J. Oral Sci.* 114 (Suppl. 1), 159–163. doi:10.1111/j.1600-0722.2006.00308.x

Maria, O. M., and Tran, S. D. (2011). Human Mesenchymal Stem Cells Cultured with Salivary Gland Biopsies Adopt an Epithelial Phenotype. *Stem Cell Development* 20 (6), 959–967. doi:10.1089/scd.2010.0214

Maria, O. M., Zeitouni, A., Gologan, O., and Tran, S. D. (2011). Matrigel Improves Functional Properties of Primary Human Salivary Gland Cells. *Tissue Eng. A* 17 (9-10), 1229–1238. doi:10.1089/ten.TEA.2010.0297

Massie, I., Spaniol, K., Barbian, A., Geerling, G., Metzger, M., and Schrader, S. (2018). Development of Lacrimal Gland Spheroids for Lacrimal Gland Tissue Regeneration. *J. Tissue Eng. Regen. Med.* 12 (4), e2001–e2009. doi:10.1002/term.2631

Matsumoto, A., Harada, H., Saito, M., and Taniguchi, A. (2011). Induction of Enamel Matrix Protein Expression in an Ameloblast Cell Line Co-cultured with a Mesenchymal Cell Line *In Vitro*. *Cell.Dev.Biol.-Animal* 47 (1), 39–44. doi:10.1007/s11626-010-9362-7

Merametdjian, L., Beck-Cormier, S., Bon, N., Couasnay, G., Sourice, S., Guicheux, J., et al. (2018). Expression of Phosphate Transporters during Dental Mineralization. *J. Dent Res.* 97 (2), 209–217. doi:10.1177/0022034517729811

Molnár, R., Madácsy, T., Varga, Á., Németh, M., Katona, X., Görög, M., et al. (2020). Mouse Pancreatic Ductal Organoid Culture as a Relevant Model to Study Exocrine Pancreatic Ion Secretion. *Lab. Invest.* 100 (1), 84–97. doi:10.1038/s41374-019-0300-3

Nakata, A., Kameda, T., Nagai, H., Ikegami, K., Duan, Y., Terada, K., et al. (2003). Establishment and Characterization of a Spontaneously Immortalized Mouse Ameloblast-Lineage Cell Line. *Biochem. Biophysical Res. Commun.* 308 (4), 834–839. doi:10.1016/s0006-291x(03)01467-0

Natsiou, D., Granchi, Z., Mitsiadis, T. A., and Jimenez-Rojo, L. (2017). Generation of Spheres from Dental Epithelial Stem Cells. *Front. Physiol.* 8, 7. doi:10.3389/fphys.2017.00007

Núñez, S. M., Chun, Y.-H. P., Ganss, B., Hu, Y., Richardson, A. S., Schmitz, J. E., et al. (2016). Maturation Stage Enamel Malformations in Amtn and Klk4 Null Mice. *Matrix Biol.* 52-54, 219–233. doi:10.1016/j.matbio.2015.11.007

Nurbaeva, M. K., Eckstein, M., Devotta, A., Saint-Jeannet, J.-P., Yule, D. I., Hubbard, M. J., et al. (2018). Evidence that Calcium Entry into Calcium-Transporting Dental Enamel Cells Is Regulated by Cholecystokinin, Acetylcholine and ATP. *Front. Physiol.* 9, 801. doi:10.3389/fphys.2018.00801

Nurbaeva, M. K., Eckstein, M., Feske, S., and Lacruz, R. S. (2017). Ca2+transport and Signalling in Enamel Cells. *J. Physiol.* 595 (10), 3015–3039. doi:10.1113/JP272775

Pandya, M., Rosene, L., Farquharson, C., Millán, J. L., and Diekwisch, T. G. H. (2017). Intravesicular Phosphatase PHOSPHO1 Function in Enamel Mineralization and Prism Formation. *Front. Physiol.* 8, 805. doi:10.3389/fphys.2017.00805

Rácz, R., Földes, A., Bori, E., Zsembery, Á., Harada, H., Steward, M. C., et al. (2017). No Change in Bicarbonate Transport but Tight-Junction Formation Is Delayed

by Fluoride in a Novel Ameloblast Model. *Front. Physiol.* 8, 940. doi:10.3389/fphys.2017.00940

Racz, R., Nagy, A., Rakonczay, Z., Dunavari, E. K., Gerber, G., and Varga, G. (2018). Defense Mechanisms against Acid Exposure by Dental Enamel Formation, Saliva and Pancreatic Juice Production. *Cpd* 24 (18), 2012–2022. doi:10.2174/1381612824666180515125654

Schönthal, A. H., Warren, D. W., Stevenson, D., Schecter, J. E., Azzarolo, A. M., Mircheff, A. K., et al. (2000). Proliferation of Lacrimal Gland Acinar Cells in Primary Culture. Stimulation by Extracellular Matrix, EGF, and DHT. *Exp. Eye Res.* 70 (5), 639–649. doi:10.1006/exer.2000.0824

Sharma, R., Tsuchiya, M., and Bartlett, J. D. (2008). Fluoride Induces Endoplasmic Reticulum Stress and Inhibits Protein Synthesis and Secretion. *Environ. Health Perspect.* 116 (9), 1142–1146. doi:10.1289/ehp.11375

Silva Couto, P., Rotondi, M. C., Bersenev, A., Hewitt, C. J., Nienow, A. W., Verter, F., et al. (2020). Expansion of Human Mesenchymal Stem/stromal Cells (hMSCs) in Bioreactors Using Microcarriers: Lessons Learnt and what the Future Holds. *Biotechnol. Adv.* 45, 107636. doi:10.1016/j.biotechadv.2020.107636

Simões, I. N., Boura, J. S., dos Santos, F., Andrade, P. Z., Cardoso, C. M. P., Gimble, J. M., et al. (2013). Human Mesenchymal Stem Cells from the Umbilical Cord Matrix: Successful Isolation and *Ex Vivo* Expansion Using Serum-/xeno-free Culture media. *Biotechnol. J.* 8 (4), 448–458. doi:10.1002/biot.201200340

Szlávik, V., Szabó, B., Vicsek, T., Barabás, J., Bogdán, S., Gresz, V., et al. (2008a). Differentiation of Primary Human Submandibular Gland Cells Cultured on Basement Membrane Extract. *Tissue Eng. Part A* 14 (11), 1915–1926. doi:10.1089/ten.tea.2007.0208

Szlávik, V., Vág, J., Markó, K., Demeter, K., Madarász, E., Oláh, I., et al. (2008b). Matrigel-induced Acinar Differentiation Is Followed by Apoptosis in HSG Cells. *J. Cel. Biochem.* 103 (1), 284–295. doi:10.1002/jcb.21404

Takahashi, A., Morita, T., Murata, K., Minowa, E., Jahan, A., Saito, M., et al. (2019). Effects of Full-Length Human Amelogenin on the Differentiation of Dental Epithelial Cells and Osteoblastic Cells. *Arch. Oral Biol.* 107, 104479. doi:10.1016/j.archoralbio.2019.07.004

Thomas, J. A., Buchsbaum, R. N., Zimniak, A., and Racker, E. (1979). Intracellular pH Measurements in Ehrlich Ascites Tumor Cells Utilizing Spectroscopic Probes Generated *In Situ*. *Biochemistry* 18 (11), 2210–2218. doi:10.1021/bi00578a012

Tiwari, S., Nair, R. M., Vamadevan, P., Ali, M. J., Naik, M. N., Honavar, S. G., et al. (2018). Establishing and Characterizing Lacrispheres from Human Lacrimal Gland for Potential Clinical Application. *Graefes Arch. Clin. Exp. Ophthalmol.* 256 (4), 717–727. doi:10.1007/s00417-018-3926-8

Varga, G., DenBesten, P., Rácz, R., and Zsembery, Á. (2018). Importance of Bicarbonate Transport in pH Control during Amelogenesis - Need for Functional Studies. *Oral Dis.* 24 (6), 879–890. doi:10.1111/odi.12738

Wang, W., Itaka, K., Ohba, S., Nishiyama, N., Chung, U.-i., Yamasaki, Y., et al. (2009). 3D Spheroid Culture System on Micropatterned Substrates for Improved Differentiation Efficiency of Multipotent Mesenchymal Stem Cells. *Biomaterials* 30 (14), 2705–2715. doi:10.1016/j.biomaterials.2009.01.030

Yan, Q., Zhang, Y., Li, W., and DenBesten, P. K. (2006). Differentiation of Human Ameloblast-Lineage Cells *In Vitro*. *Eur. J. Oral Sci.* 114 (Suppl. 1), 154–158. doi:10.1111/j.1600-0722.2006.00304.x

Yan, Q., Zhang, Y., Li, W., and Denbesten, P. K. (2007). Micromolar Fluoride Alters Ameloblast Lineage Cells *In Vitro*. *J. Dent Res.* 86 (4), 336–340. doi:10.1177/154405910708600407

Yang, X., and Lytton, J. (2013). Purinergic Stimulation of K+-dependent Na+/Ca2+ Exchanger Isoform 4 Requires Dual Activation by PKC and CaMKII. *Biosci. Rep.* 33 (6). doi:10.1042/BSR20130099

Yang, Y.-H. K., Ogando, C. R., Wang See, C., Chang, T.-Y., and Barabino, G. A. (2018b). Changes in Phenotype and Differentiation Potential of Human Mesenchymal Stem Cells Aging *In Vitro*. *Stem Cel Res Ther* 9 (1), 131. doi:10.1186/s13287-018-0876-3

Yang, Y., Li, Z., Chen, G., Li, J., Li, H., Yu, M., et al. (2018a). GSK3β Regulates Ameloblast Differentiation via Wnt and TGF-β Pathways. *J. Cel Physiol* 233 (7), 5322–5333. doi:10.1002/jcp.26344

Zhang, Y., Zhang, K., Ma, L., Gu, H., Li, J., and Lei, S. (2016). Fluoride Induced Endoplasmic Reticulum Stress and Calcium Overload in Ameloblasts. *Arch. Oral Biol.* 69, 95–101. doi:10.1016/j.archoralbio.2016.05.015

Zhang, Y., Li, W., Chi, H. S., Chen, J., and Denbesten, P. K. (2007). JNK/c-Jun Signaling Pathway Mediates the Fluoride-Induced Down-Regulation of MMP-20 *In Vitro*. *Matrix Biol.* 26 (8), 633–641. doi:10.1016/j.matbio.2007.06.002

Zhang, Y., Yan, Q., Li, W., and DenBesten, P. K. (2006). Fluoride Down-Regulates the Expression of Matrix Metalloproteinase-20 in Human Fetal Tooth Ameloblast-Lineage Cells *In Vitro*. *Eur. J. Oral Sci.* 114 (Suppl. 1), 105–110. doi:10.1111/j.1600-0722.2006.00303.x

Zheng, L.-W., Linthicum, L., DenBesten, P. K., and Zhang, Y. (2013c). The Similarity between Human Embryonic Stem Cell-Derived Epithelial Cells and Ameloblast-Lineage Cells. *Int. J. Oral Sci.* 5 (1), 1–6. doi:10.1038/ijos.2013.14

Zheng, L., Seon, Y. J., Mourão, M. A., Schnell, S., Kim, D., Harada, H., et al. (2013a). Circadian Rhythms Regulate Amelogenesis. *Bone* 55 (1), 158–165. doi:10.1016/j.bone.2013.02.011

Zheng, L., Warotayanont, R., Stahl, J., Kunimatsu, R., Klein, O., DenBesten, P. K., et al. (2013b). Inductive Ability of Human Developing and Differentiated Dental Mesenchyme. *Cells Tissues Organs* 198 (2), 99–110. doi:10.1159/000353116

Conflict of Interest: The authors declare that the research was conducted in the absence of any commercial or financial relationships that could be construed as a potential conflict of interest.

frontiers in Pharmacology

ORIGINAL RESEARCH
published: 04 June 2021
doi: 10.3389/fphar.2021.664177

The Nonsteroidal Anti-Inflammatory Drug Ketorolac Alters the Small Intestinal Microbiota and Bile Acids Without Inducing Intestinal Damage or Delaying Peristalsis in the Rat

*Barbara Hutka[1†], Bernadette Lázár[1†], András S. Tóth[1], Bence Ágg[1,2], Szilvia B. László[1], Nóra Makra[3], Balázs Ligeti[4], Bálint Scheich[5], Kornél Király[1], Mahmoud Al-Khrasani[1], Dóra Szabó[3], Péter Ferdinandy[1,2], Klára Gyires[1] and Zoltán S. Zádori[1]**

[1]Department of Pharmacology and Pharmacotherapy, Semmelweis University, Budapest, Hungary, [2]Pharmahungary Group, Szeged, Hungary, [3]Department of Medical Microbiology, Semmelweis University, Budapest, Hungary, [4]Faculty of Information Technology and Bionics, Pázmány Péter Catholic University, Budapest, Hungary, [5]1st Department of Pathology and Experimental Cancer Research, Semmelweis University, Budapest, Hungary

Background: Nonsteroidal anti-inflammatory drugs (NSAIDs) induce significant damage to the small intestine, which is accompanied by changes in intestinal bacteria (dysbiosis) and bile acids. However, it is still a question of debate whether besides mucosal inflammation also other factors, such as direct antibacterial effects or delayed peristalsis, contribute to NSAID-induced dysbiosis. Here we aimed to assess whether ketorolac, an NSAID lacking direct effects on gut bacteria, has any significant impact on intestinal microbiota and bile acids in the absence of mucosal inflammation. We also addressed the possibility that ketorolac-induced bacterial and bile acid alterations are due to a delay in gastrointestinal (GI) transit.

Methods: Vehicle or ketorolac (1, 3 and 10 mg/kg) were given to rats by oral gavage once daily for four weeks, and the severity of mucosal inflammation was evaluated macroscopically, histologically, and by measuring the levels of inflammatory proteins and claudin-1 in the distal jejunal tissue. The luminal amount of bile acids was measured by liquid chromatography-tandem mass spectrometry, whereas the composition of microbiota by sequencing of bacterial 16S rRNA. GI transit was assessed by the charcoal meal method.

Results: Ketorolac up to 3 mg/kg did not cause any signs of mucosal damage to the small intestine. However, 3 mg/kg of ketorolac induced dysbiosis, which was characterized by a loss of families belonging to Firmicutes (*Paenibacillaceae*, *Clostridiales Family XIII*, *Christensenellaceae*) and bloom of *Enterobacteriaceae*. Ketorolac also changed the composition of small intestinal bile by decreasing the concentration of conjugated bile acids and by increasing the amount of hyodeoxycholic acid (HDCA). The level of conjugated bile acids correlated negatively with the abundance of *Erysipelotrichaceae*, *Ruminococcaceae*, *Clostridiaceae 1*, *Muribaculaceae*, *Bacteroidaceae*, *Burkholderiaceae*

OPEN ACCESS

Edited by:
Thomas Brzozowski, Jagiellonian University Medical College, Poland

Reviewed by:
Luca Antonioli, University of Pisa, Italy
Lenard Lichtenberger, University of Texas Health Science Center at Houston, United States
Tetsuya Tanigawa, Osaka City University, Japan
Swapnil Purushottam Borse, Savitribai Phule Pune University, India
Gianfranco Natale, University of Pisa, Italy

***Correspondence:**
Zoltán S. Zádori
zadori.zoltan@med.semmelweis-univ.hu

[†]These authors have contributed equally to this work

Specialty section:
This article was submitted to Gastrointestinal and Hepatic Pharmacology, a section of the journal Frontiers in Pharmacology

Received: 04 February 2021
Accepted: 19 April 2021
Published: 04 June 2021

Citation:
Hutka B, Lázár B, Tóth AS, Ágg B, László SB, Makra N, Ligeti B, Scheich B, Király K, Al-Khrasani M, Szabó D, Ferdinandy P, Gyires K and Zádori ZS (2021) The Nonsteroidal Anti-Inflammatory Drug Ketorolac Alters the Small Intestinal Microbiota and Bile Acids Without Inducing Intestinal Damage or Delaying Peristalsis in the Rat. Front. Pharmacol. 12:664177. doi: 10.3389/fphar.2021.664177

and *Bifidobacteriaceae*. Ketorolac, under the present experimental conditions, did not change the GI transit.

Conclusion: This is the first demonstration that low-dose ketorolac disturbed the delicate balance between small intestinal bacteria and bile acids, despite having no significant effect on intestinal mucosal integrity and peristalsis. Other, yet unidentified, factors may contribute to ketorolac-induced dysbiosis and bile dysmetabolism.

Keywords: ketorolac, nonsteroidal anti-inflammatory drug, enteropathy, microbiota, bile acid, peristalsis, hyodeoxycholic acid

INTRODUCTION

Nonsteroidal anti-inflammatory drugs (NSAIDs) are among the most commonly used prescription and over-the-counter medicines (Lanas and Scarpignato, 2006). They are widely used to treat inflammatory pain and reduce fever, but their use is associated with significant gastrointestinal (GI) adverse events. Besides having the potential to seriously damage the stomach and duodenum, NSAIDs can also damage the small intestine. NSAID enteropathy can occur in up to 70% of chronic NSAID users and may result in a wide variety of complications, ranging from mucosal inflammation and protein loss to ulcers, and even perforations (Maiden et al., 2005). The pathogenesis of enteropathy is complex and still insufficiently understood. It likely involves multiple mechanisms, including topical damaging effects of NSAIDs, inhibition of cyclooxygenase (COX)-mediated prostaglandin (PG) synthesis, and increased toxicity of luminal aggressive factors, like intestinal bacteria and bile acids (Wallace, 2013; Takeuchi and Satoh, 2015; Bjarnason et al., 2018).

The importance of bacteria in NSAID enteropathy has been demonstrated repeatedly by numerous studies. Antibiotic-treated or germ-free animals are largely protected against NSAID-induced small bowel damage (Kent et al., 1969; Robert and Asano, 1977; Uejima et al., 1996). Bacteria may aggravate mucosal damage by several ways, including delayed ulcer healing (Elliott et al., 1998) and increased deconjugation and enterohepatic recirculation of NSAIDs (LoGuidice et al., 2012). It has also long been known that NSAIDs cause marked alterations in the composition of intestinal microbiota (Kent et al., 1969; Dalby et al., 2006; Craven et al., 2012; Blackler et al., 2015; Liang et al., 2015; Rogers and Aronoff, 2016; Maseda et al., 2019). This dysbiosis is typically characterized by a dramatic shift from Gram-positive to Gram-negative organisms, and may exacerbate NSAID-induced mucosal damage as well. Indeed, the abundance of Gram-negative bacteria showed positive correlation with the severity of mucosal injury (Blackler et al., 2015).

Although NSAID-induced dysbiosis is well documented, little is known about the underlying mechanisms. Because inflammation-related perturbations in the microenvironment favor the growth of Gram-negatives, such as *Enterobacteriaceae* (Zeng et al., 2017), NSAID-induced mucosal injury is likely to be a major determinant of dysbiosis. This resonates well with studies showing that microbial alterations appeared in rodents with moderate to severe, but not with minimal or mild enteropathy (Reuter et al., 1997; Craven et al., 2012). In addition, the composition of microbiota changed with time and disease progression (Maseda et al., 2019). However, there is some evidence that certain NSAIDs can induce dysbiosis without any detectable intestinal damage as well (Uejima et al., 1996; Lu et al., 2018), suggesting that other factors than mucosal inflammation may also contribute to NSAID-induced microbial alterations.

Several NSAIDs, such as ibuprofen, naproxen, diclofenac or celecoxib have been reported to possess direct antimicrobial properties *in vitro* (Jiménez-Serna and Hernández-Sánchez, 2011; Thangamani et al., 2015; Chan et al., 2017). It remains unclear whether these effects have any significant relevance in terms of dysbiosis, but it is noteworthy that ibuprofen and celecoxib are active mainly against Gram-positive bacteria *in vitro* (Jiménez-Serna and Hernández-Sánchez, 2011; Obad et al., 2015; Thangamani et al., 2015; Chan et al., 2017), and after chronic treatment both decreased the abundance of Firmicutes (Gram-positives) without any significant or reported intestinal injury *in vivo* (Montrose et al., 2016; Lu et al., 2018). By contrast, chronic treatment with rofecoxib, which lacks direct antibacterial effects, did not cause dysbiosis in the uninflamed gut (Lázár et al., 2019).

Another mechanism by which NSAIDs might change the microbiota is the disturbed GI motility. Several studies have demonstrated that NSAIDs can alter intestinal contractility and/or transit time, although there is still no consensus whether this effect is stimulatory or inhibitory. Indomethacin, for example, was shown to both increase (Takeuchi et al., 2002; Nylander, 2011) and decrease small intestinal contractility in the rat (Lichtenberger et al., 2015). Nevertheless, because GI transit time and gut microbiota are highly interrelated, both accelerated and delayed transit may result in dysbiosis (Kashyap et al., 2013). Of note, slow GI transit in loperamide-treated mice was associated with decreased abundance of Firmicutes (e.g. *Lachnospiraceae*) and expansion of Bacteroidetes (Kashyap et al., 2013; Touw et al., 2017), which were also commonly reported following NSAID treatment (Craven et al., 2012; Blackler et al., 2015; Colucci et al., 2018).

Ketorolac, a COX-1-preferential inhibitor (Warner et al., 1999), is mainly used for the short-term treatment of moderate to severe pain in postoperative or emergency patients (Vadivelu et al., 2015). When given at low doses, ketorolac was shown to spare the rat gastric and intestinal

mucosa (Jamali et al., 1999; Wallace et al., 2000), despite almost complete suppression of gastric prostaglandin synthesis (Wallace et al., 2000). In addition, in a recent study (Maier et al., 2018) ketorolac did not influence the growth of 40 representative gut bacterial strains *in vitro*.

These properties prompted us to use ketorolac as a pharmacological tool to investigate the relationship between mucosal inflammation and dysbiosis. More specifically, we aimed to determine whether chronic treatment with ketorolac, an NSAID lacking direct effect on gut bacteria, has any significant impact on intestinal microbiota in the absence of mucosal inflammation. Because intestinal bacteria and bile acids are closely interrelated (Begley et al., 2005), we also assessed the effect of ketorolac on small intestinal bile acid composition. In addition, we addressed the possibility that ketorolac-induced bacterial and bile acid alterations are due to a delay in small intestinal transit ("stasis").

Here we show that ketorolac given at low, non-damaging dose for 4 weeks caused small intestinal dysbiosis, which resembled that caused by other NSAIDs. Namely, it decreased the abundances of bacterial families belonging to Firmicutes, and increased that of *Enterobacteriaceae*. These changes were accompanied by and correlated with significant bile acid alterations. GI transit was not influenced significantly by ketorolac. These results suggest that besides direct effects on bacteria, intestinal inflammation and stasis also other, yet unidentied, factors may contribute to NSAID-induced dysbiosis and bile dysmetabolism.

MATERIALS AND METHODS

Animals

Experiments were carried out on male Wistar rats weighing 180–240 g (Semmelweis University, Budapest, Hungary). Animals were housed in a temperature (22 ± 2°C)- and humidity-controlled room at a 12-h light/dark cycle. Food and water were available *ad libitum* unless otherwise specified.

Ethical Considerations

All efforts were made to minimize animal suffering and to reduce the number of animals used in the experiments. All procedures conformed to the Directive 2010/63/EU on European Convention for the protection of animals used for scientific purposes. The experiments were approved by the National Scientific Ethical Committee on Animal Experimentation and permitted by the government (Food Chain Safety and Animal Health Directorate of the Government Office for Pest County (PEI/001/1493-4/2015)).

In vivo Studies

Study 1. Evaluating the Effects of Chronic Ketorolac Treatment on Small Intestinal Mucosal Integrity, Microbiota and Bile Acids

40 rats were randomly allocated into 4 experimental groups, with 10 rats in each group. In order to control variations in microbiota composition, before the start of the experiment rats were co-housed for 1 week, and during the experiment all groups were divided and housed in 2-2 individually ventillated cages, with 5 rats per cage, to minimize the cage effect (Laukens et al., 2016).

During the experiment, unfasted rats were treated intragastrically with either vehicle (1% hydroxyethylcellulose) or ketorolac tromethamine (1, 3 and 10 mg/kg) (Sigma, St. Louis, MO, United States of America), in a volume of 0.33 ml/100 g. These doses were chosen based on previous studies, showing that ketorolac at doses of ≤3 mg/kg spared the GI mucosa (Jamali et al., 1999; Wallace et al., 2000; Santos et al., 2007), but inhibited gastric prostaglandin synthesis (Wallace et al., 2000). Of note, ketorolac in this dose range has been reported to possess both analgesic and anti-inflammatory properties (Jett et al., 1999). This was also confirmed by our pilot study, in which a 5-day treatment with 1, 3 and 10 mg/kg ketorolac reduced the concentration of PGE_2 in the carrageenan-airpouch model by 67, 84 and 99%, respectively. Because non-damaging COX-inhibitors (e.g. celecoxib or low-dose ibuprofen) caused intestinal dysbiosis mainly after chronic treatment (1–10 weeks) (Montrose et al., 2016; Lu et al., 2018), we administered ketorolac once daily for 4 weeks. Body weight was measured daily during the course of the treatment. At the end of treatment, 24 h after the final administration of ketorolac, animals were euthanized under CO_2, the small intestines were excised, the content of distal jejunum was quickly collected, snap-frozen in liquid nitrogen and stored at −80°C for analysis of the microbiota and bile acids. The mucosa of the entire small intestine was flushed with cold saline and examined thoroughly for the presence of macroscopic alterations. The length of the whole small intestine was measured, because bowel shortening correlates with the severity of intestinal inflammation. Because NSAID-induced ulcers in the rat occur predominantly in the middle and distal parts of the small intestine (Kent et al., 1969), full-thickness pieces of the distal jejunum were snap-frozen in liquid nitrogen, pulverized and stored at −80°C for further analysis. A further jejunal segment was fixed in 10% formalin for evaluation of microscopic damage.

Study 2. Evaluating the Effect of Ketorolac on GI Transit

Here we aimed to analyze whether ketorolac has any effect on GI peristalsis, which could potentially favor the growth of distinct bacteria and result in dysbiosis after long-term treatment. Rats were treated intragastrically with either vehicle or ketorolac tromethamine (1, 3 and 10 mg/kg) once daily for 5 days, in order to allow any potential drug accumulation or the production of metabolites. On the 5th day, following 18 h fasting and 1 h after the final gavage of vehicle or ketorolac, a charcoal suspension (10% charcoal in 5% gum arabic) was given in a volume of 2 ml/rat per os (Zádor et al., 2020). The timing of charcoal administration was chosen based on pharmacokinetic studies on ketorolac in the rat, showing that maximal blood concentration was achieved within 1 h following per os administration (Granados-Soto et al., 1995; Jamali et al., 1999). 30 min later the rats were euthanized, their entire small intestines were removed and the distance traveled by the charcoal suspension was measured and compared to the total length of small intestine.

Histological Analysis

Samples taken from the distal part of the small intestine were fixed in 10% formalin, embedded in paraffin, sectioned (5 μm), and stained with hematoxylin and eosin. The severity of epithelial damage, edema and cellular infiltration was analysed by an expert pathologist in a blinded fashion as described before (László et al., 2020). The sections were also digitalized by using a PANNORAMIC Digital Slide Scanner (3DHISTECH Ltd., Budapest, Hungary) in order to take representative images.

Measurement of Myeloperoxidase and Tumor Necrosis Factor-α by ELISA

ELISA kits were used to quantify the jejunal protein levels of tumor necrosis factor-α (TNF-α) (Invitrogen, Camirillo, CA) and myeloperoxidase (MPO) (Hycult Biotech, Uden, Netherlands). Tissue samples were homogenized and assayed according to the manufacturers' instructions, in a blinded fashion and in duplicates. The total protein concentration of supernatants was determined by using a bicinchoninic acid assay kit (Thermo Scientific Pierce Protein Research Products, Rockford, United States) with bovine serum albumin as a standard.

Western Blot Analysis of Cyclooxygenase Isoforms and Claudin-1

Distal jejunal tissues were homogenized with a TissueLyser (Qiagen, Venlo, Netherlands) in lysis buffer containing 200 mM NaCl, 5 mM EDTA, 10 mM Tris, 10% glycerine, and 1 μg/ml leupeptin (pH 7.4), supplemented with a protease inhibitor cocktail (cOmplete ULTRA Tablets, Roche, Basel, Switzerland) and PMSF (Sigma, St. Louis, MO, United States). The homogenized lysates were centrifuged twice at 1500 × g and 4°C for 15 min, then the supernatants were collected and their protein concentration was measured by the bicinchoninic acid assay (Thermo Fisher Scientific, Waltham, MA, United States). Equal amount of protein (20 μg) was mixed with Pierce Lane Marker reducing sample buffer (Thermo Fisher Scientific, Waltham, MA, United States), and loaded and separated in a 4–20% precast Tris-glycine SDS polyacrilamide gel (BioRad, Hercules, CA, United States). Proteins were transferred electrophoretically onto a polyvinylidene difluoride membrane (BioRad, Hercules, CA, United States) at 200 mA overnight. Membranes were blocked with 5% nonfat dry milk (BioRad, Hercules, CA, United States) in Tris-buffered saline containing 0.05% Tween-20 (0.05% TBS-T; Sigma, St. Louis, MO, United States) at room temperature for 2 h. Membranes were incubated with primary antibodies against COX-2 (#12282, 1: 500), COX-1 (#4841, 1:500) (Cell Signaling Technology, Danvers, MA, United States) and claudin-1 (ab15098, 1:1000, Abcam, Cambridge, United Kingdom) overnight at 4°C, followed by 2 h incubation at room temperature with anti-rabbit HRP-linked secondary antibody. GAPDH was used to control for sample loading and protein transfer and to normalize the content of target protein. Signals were detected with a chemiluminescence kit (BioRad, Hercules, CA, United States) by Chemidoc XRS+ (BioRad, Hercules, CA, United States).

TABLE 1 | The list of measured bile acids.

Abbreviation	Name	Type
CA	Cholic acid	Primary
CDCA	Chenodeoxycholic acid	Primary
DCA	Deoxycholic acid	Secondary
GCA	Glycocholic acid	Primary, glycine-conjugated
GCDCA	Glycochenodeoxycholic acid	Primary, glycine-conjugated
GDCA	Glycodeoxycholic acid	Secondary, glycine-conjugated
GUDCA	Glycoursodeoxycholic acid	Secondary, glycine-conjugated
HDCA	Hyodeoxycholic acid	Secondary
LCA	Lithocholic acid	Secondary
MCA(α)	α-Muricholic acid	Primary
MCA(β)	β-Muricholic acid	Primary
MCA(ω)	ω-Muricholic acid	Secondary
TCA	Taurocholic acid	Primary, taurine-conjugated
TCDCA	Taurochenodeoxycholic acid	Primary, taurine-conjugated
TDCA	Taurodeoxycholic acid	Secondary, taurine-conjugated
TLCA	Taurolithocholic acid	Secondary, taurine-conjugated
TMCA (α + β)	α- and β-Tauromuricholic acid	Primary, taurine-conjugated
TUDCA	Tauroursodeoxycholic acid	Secondary, taurine-conjugated
UDCA	Ursodeoxycholic acid	Secondary

DNA Isolation, 16S rRNA Gene Library Preparation and MiSeq Sequencing

Bacterial DNA was extracted from 100 mg small intestinal content per sample using the QIAamp PowerFecal DNA Kit (Qiagen, Hilden, Germany) and further purified using AMPure XP beads (Beckman Coulter, Brea, CA, United States) according to the manufacturer's protocols. The concentration of genomic DNA was measured using a Qubit 2.0 Fluorometer with Qubit dsDNA HS Assay Kit (Thermo Fisher Scientific, Waltham, MA, United States). Bacterial DNA was amplified with tagged primers (5′-TCG TCG GCA GCG TCA GAT GTG TAT AAG AGA CAG CCT ACG GGN GGC WGC AG and 5′-GTC TCG TGG GCT CGG AGA TGT GTA TAA GAG ACA GGA CTA CHV GGG TAT CTA ATC C), covering the V3-V4 region of the bacterial 16S rRNA gene. PCR and DNA purifications were performed according to Illumina's demonstrated protocol (Part # 15044223 Rev. B). The PCR product libraries were quantified and qualified by using DNA 1000 Kit on Agilent 2100 Bioanalyzer instrument (Agilent Technologies, Waldbronn, Germany). Equimolar concentrations of libraries were pooled and sequenced on an Illumina MiSeq platform (Illumina, San Diego, CA, United States) using MiSeq Reagent Kit v3 (600 cycles PE).

Essentially the bioinformatic analysis was carried out as described by Mansour et al. (2020). Briefly, the quality of raw reads was assed with FastQC and MultiQC38, the low quality sequences were filtered and trimmed by Trimmomatic (Bolger et al., 2014) and only sequences with minimal length of 36 were kept, and the low quality base calls were discarded (phred score < 20). The SSU Ref NR 99 database (release 132) of SILVA (Quast et al., 2013) was used, which was preprocessed and indexed by the Kraken2 (Wood and Salzberg, 2014) with k-mer = 31. The final microbiome composition was estimated by Bracken (Breitwieser et al., 2019).

Measurement of Small Intestinal Bile Acids by LC-MS/MS

Luminal samples (100 mg on average) obtained from the distal small intestine were sent to Biocrates Life Science AG (Innsbruck, Austria) on dry ice, where metabolomic profiling was performed. Samples were weighed, mixed with the 3-fold volume of extraction buffer (85% ethanol, 15% 0.01 M phosphate buffer (pH 7.4)), and vortexed thoroughly until dissolution. Samples were then sonicated and centrifuged, and the supernatant was used for further analysis. Intestinal luminal bile acids were assessed by electrospray (ESI) mass spectrometry coupled to liquid chromatography (LC) with a tandem mass spectrometry (MS/MS) instrument (SCIEX 4000 QTRAP®,SCIEX, Darmstadt, Germany), by using the commercially available Biocrates® Bile Acids Kit (Biocrates Life Science AG, Innsbruck, Austria), which enabled the absolute quantification of 20 different bile acids (**Table 1**). A highly selective reversed phase high-performance liquid chromatography-tandem mass spectrometry (LC-MS/MS) analysis method in negative ion multiple reaction monitoring detection mode was applied to determine the concentrations of bile acids The experimental metabolomics measurement technique is described in detail by patent US 2007/0004044 (accessible online at http://www.freepatentsonline.com/20070004044.html). For highly accurate quantification, 7-point external calibration curves and 10 stable isotope-labeled internal standards were applied. Data of bile acids were quantified using the appropriate MS software (SCIEX - Analyst) and the results were finally imported into Biocrates MetIDQ software for further analysis.

The mean hydrophobicity index of the luminal content was calculated as a percentage-weighted mean of previously reported hydrophobicities of the individual bile acids (Heuman, 1989; Stenman et al., 2013; Poša, 2014).

Data Analysis

Statistical analysis of the data was performed with Student t test or Mann-Whitney U test (in case of nonparametric values), or with one-way ANOVA, followed by Holm-Sidak post hoc test. Two-way repeated measures ANOVA was employed to compare the time course of weight losses. Outliers detected by Grubb's test were excluded from the analyses. A probability of $p < 0.05$ was considered statistically significant.

Alpha diversities were quantified by using the Shannon index (quantifying entropy of the distribution of taxa proportions). Taxa having at least support of 50 reads were considered as positive, others were discarded from the downstream analysis. Principal component analysis (PCA) was used for visualizing the microbiome composition. The differential abundance tests were performed using ANCOM (Mandal et al., 2015) with Holm-Bonferroni corrected alpha of 0.05 as the rejection threshold. Zero abundance of taxa was replaced by a pseudocount 1.

Associations between bacterial abundances and absolute and relative bile acid concentrations were tested by calculating Spearman's rank correlation coefficients (Rho-value) for each pair of these variables across all samples. Correlation test *p*-values were corrected for type I error by applying the false discovery rate method (FDR; q-value according to Benjamini and Hochberg (1995)), and significant correlations were declared in case of $q < 0.05$. Heat maps with rows and columns ordered by Euclidian distance-based complete linkage clustering and corresponding dendrograms were generated to visualize Rho-values of the pairwise correlation tests. Zero row and column vectors were dropped from the heatmaps. All steps of the correlation analysis were performed with the use of the R software package (version 3.4.4) (R Core Team, 2018).

RESULTS

Ketorolac up to 3 mg/kg did not Cause Significant Damage to the Small Intestinal Mucosa

None of the rats died over the 4-week treatment period, and none of the tested doses of ketorolac caused weight loss compared to vehicle (**Figure 1A**). Upon sacrificing the animals, the mucosa of the entire small intestine was examined thoroughly, but there were no visible morphologic alterations, such as bleeding or ulcers. There were no differences in terms of intestinal lengths, indicating that ketorolac treatment did not cause bowel shortening either (**Figure 1B**). We have also performed a gross examination of the gastric mucosa, but it did not reveal any significant damage (not shown).

The presence of inflammation was assessed by measuring the tissue protein levels of TNF-α, COX-2 and MPO (**Figures 1C,D,F**). COX-2 expression was not detectable by Western blotting in any of the samples, in contrast to the abundant expression of the constitutive COX-1 isoform. Likewise, ketorolac treatment had no effect on the expression of TNF-α, measured by ELISA. The level of MPO, however, was significantly increased in the small intestine of rats treated with the highest dose of ketorolac. Because a decrease in key tight junction proteins, including claudin-1, corresponds to an increase in intestinal permeability (Han et al., 2016; Xiao et al., 2017), we also measured the expression of claudin-1 to assess whether ketorolac treatment has any effect on intestinal barrier. As **Figure 1E** shows, we did not found difference between the claudin-1 expression of vehicle- and ketorolac-treated animals.

Collectively, these data indicate that ketorolac at doses of 1 and 3 mg/kg did not cause significant damage to the small intestine, whereas at a dose of 10 mg/kg ketorolac caused mild inflammation with elevation of MPO. This was also confirmed by histological analysis of the intestinal samples. The structure of villi and epithelium were generally preserved in all rats. Granulocytes were sparsely present in the lamina propria of most samples, but the highest number of cells was noted in the 10 mg/kg group (**Figure 2**).

Ketorolac at a Dose of 3 mg/kg Induced Small Intestinal Dysbiosis

We next examined whether ketorolac at the dose of 3 mg/kg (the highest tested non-damaging dose) has any effect on the composition of small intestinal microbiota. In control rats, the vast majority of taxa belonged to Firmicutes (92.5%), followed by Bacteroidetes (3.9%), Proteobacteria (2.3%) and Actinobacteria

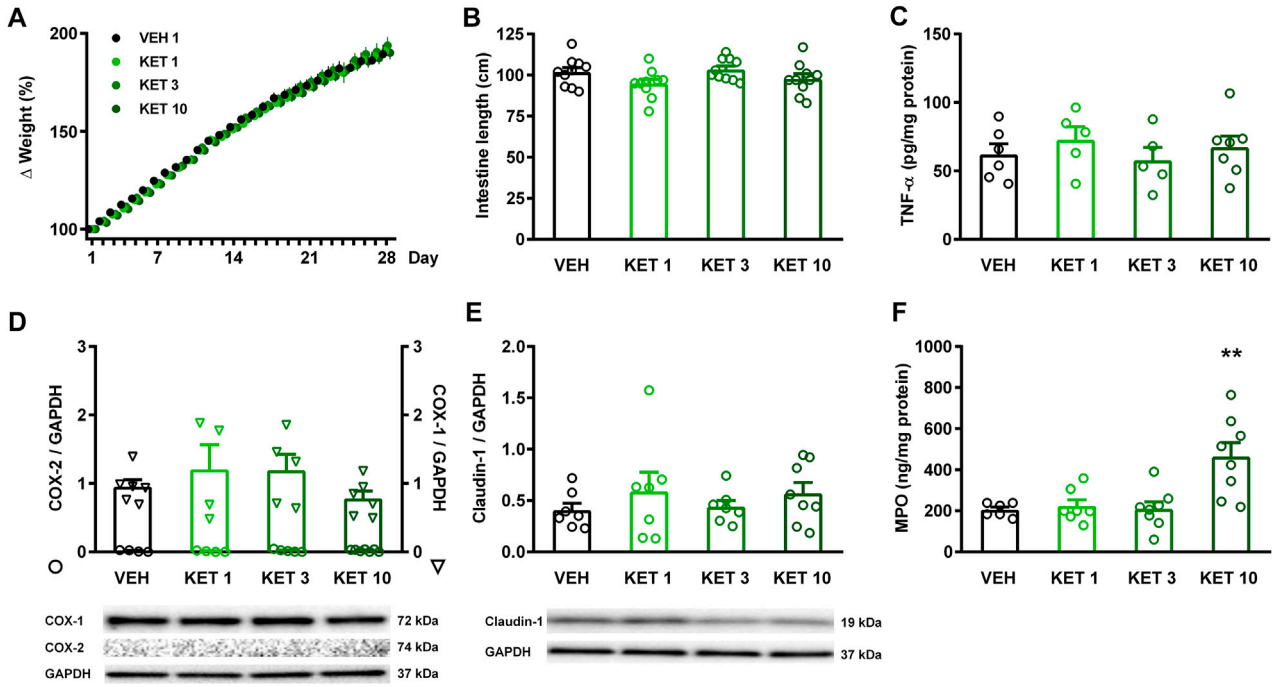

FIGURE 1 | The effect of ketorolac (KET) given at different doses (1, 3 and 10 mg/kg per os, once daily for four weeks) on animal weight, small intestine length, and expression of inflammatory mediators and claudin-1. Panel **A**: results are expressed as the mean + SEM. Panels **B–F**: Circles represent the data of each rat, bars indicate the mean + SEM. For statistical analysis two-way repeated measures ANOVA followed by Holm-Sidak post hoc test **(A)**, and one-way ANOVA with Holm-Sidak post hoc test **(B–F)** were used, n = 4–10/group. $^{**}p < 0.01$ compared to vehicle-treated group.

(0.3%). At the family level, the most abundant bacterial families were *Lactobacillaceae*, *Peptostreptococcaceae* and *Clostridiaceae* (**Figure 3**). Although the same taxa dominated the microbiota of ketorolac-treated rats (**Figure 3**), there were notable differences in their proportions compared to the vehicle group. As **Figure 4** shows, at the phylum level ketorolac increased the abundance of Actinobacteria, and tended to increase that of Bacteroidetes and Proteobacteria. By contrast, the level of Firmicutes tended to decrease, which was mainly due to the decreased level of the families *Paenibacillaceae*, *Clostridiales Family XIII* and *Christensenellaceae*. In addition, ketorolac treatment was associated with higher levels of *Enterobacteriaceae*. Among the identified genera we found significant difference only between the levels of *Ruminococcaceae UCG-014* (**Figure 4**), which was increased in the ketorolac group.

Hence, despite the lack of mucosal injury ketorolac induced significant changes in the composition of small intestinal microbiota. This was also confirmed by principal component analysis (PCA) of the data, in which a clear shift of ketorolac samples was observed on both axes (**Figure 5A**). Bacterial diversities were estimated by calculating the Shannon indices, which were not different between the two groups (**Figure 5B**).

Ketorolac at a Dose of 3 mg/kg Altered the Small Intestinal Bile Acid Composition

The luminal concentration of bile acids in the distal small intestine was measured by LC-MS/MS (**Supplementary Table S1**). As **Figure 6** shows, ketorolac treatment changed neither the total concentration of bile acids, nor the overall hydrophobicity of small intestinal bile. By contrast, it increased dramatically the ratio of unconjugated to total bile acids. This was due to an increase in the concentration of the secondary bile acid hyodeoxycholic acid (HDCA), and a decrease in the levels of glycine- and taurine-conjugated primary and secondary bile acids (**Figure 7**). We found no differences between the concentrations of any other unconjugated primary and secondary bile acids in the two groups.

Ketorolac-Induced Dysbiosis Correlated with the Changes of Bile Acids

Spearman's correlation analysis was performed to explore the associations between ketorolac-induced dysbiosis and bile dysmetabolism, and calculated Rho-values were visualized as heat maps with dendrograms to identify related variables. Some bacterial families, such as *Erysipelotrichaceae*, *Ruminococcaceae*, *Clostridiaceae 1* (all belonging to Firmicutes), *Muribaculaceae*, *Bacteroidaceae* (both belonging to Bacteroidetes), *Burkholderiaceae* and *Bifidobacteriaceae* clustered together and correlated negatively with the absolute concentrations and proportions of glycine- and taurine conjugates (**Figure 8** and **Supplementary Figure S1**). The family *Burkholderiaceae* also showed positive correlation with the percentage of HDCA. By contrast, other Firmicutes bacteria (*Clostridiales Family XI* and *XIII*, *Peptococcaceae*,

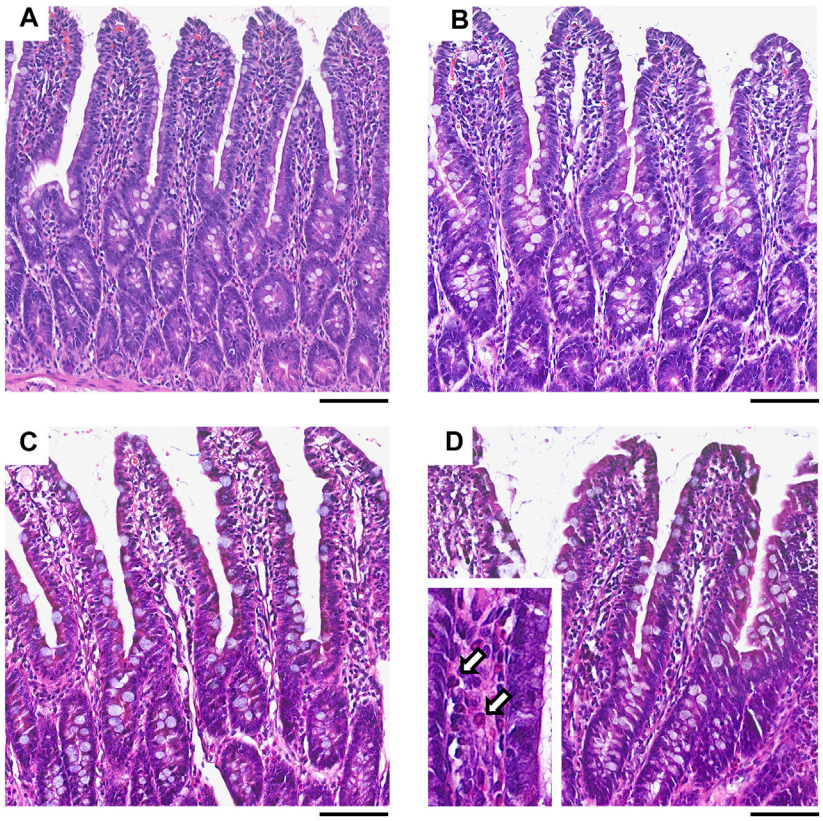

FIGURE 2 | Representative histological micrographs of the distal jejunum of rats treated with vehicle **(A)**, or ketorolac at doses of 1 **(B)**, 3 **(C)** and 10 mg/kg **(D)** for four weeks (scale bar: 100 μM, hematoxylin and eosin staining). White arrows point to neutrophil granulocytes, indicating increased cellularity of the lamina propria.

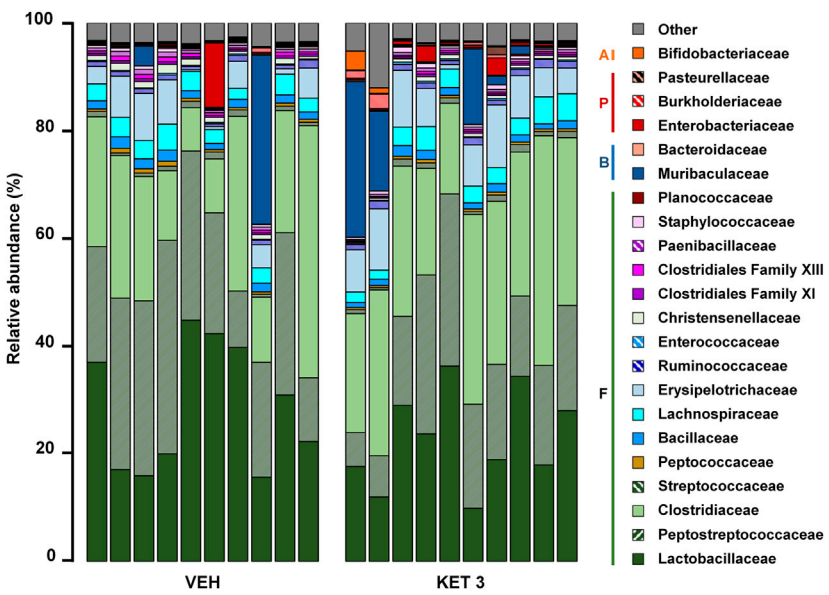

FIGURE 3 | The relative abundance of bacterial families in jejunal samples of rats treated with vehicle (VEH) or ketorolac (KET, 3 mg/kg) for four weeks, determined by sequencing of 16 S rRNA. Each vertical bar represents the sequencing data for one rat. Unclassified families and families with an abundance less than 0.1% are summarized as "Other." Abbreviations: F: Firmicutes, B: Bacteroidetes, P: Proteobacteria, A: Actinobacteria.

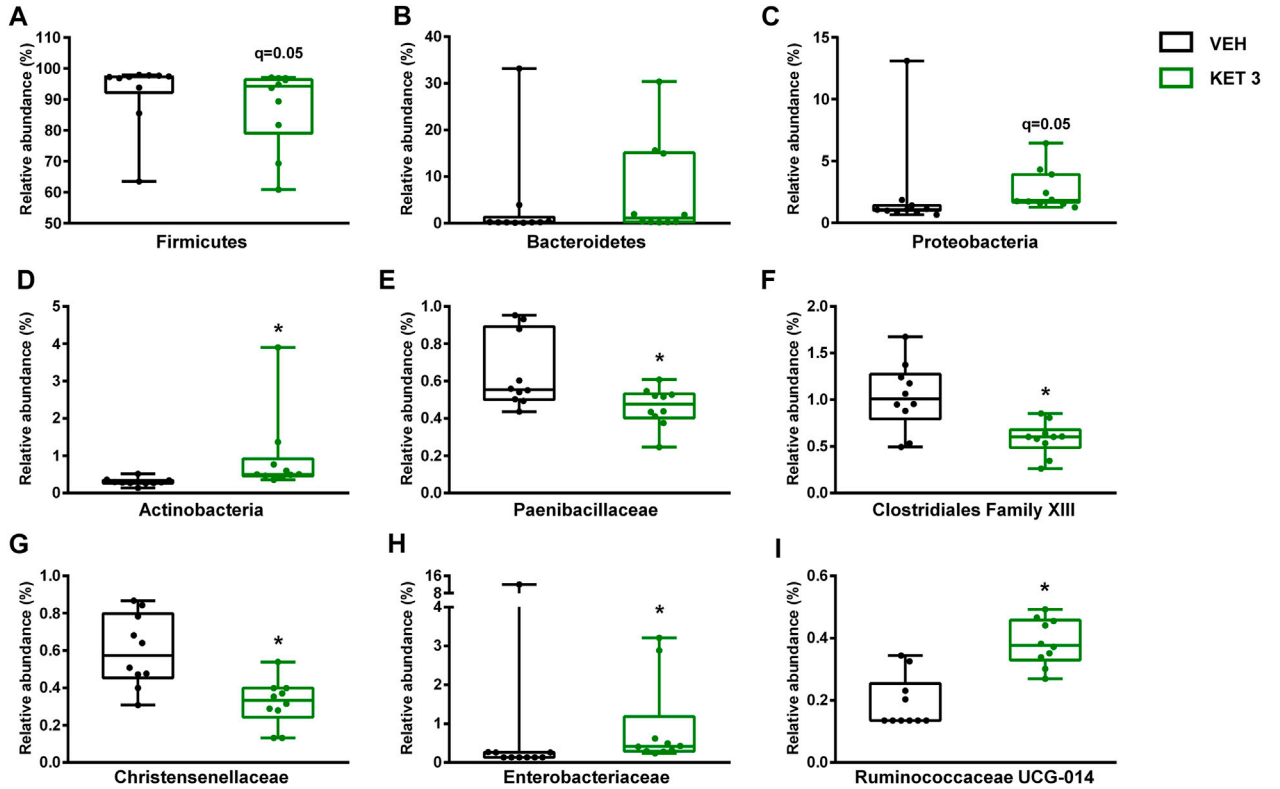

FIGURE 4 | The effect of four-week vehicle (VEH) or ketorolac treatment (KET, 3 mg/kg) on the small intestinal proportion of different bacterial phyla **(A–D)**, families **(E–H)** and the genus *Ruminococcaceae UCG-014* **(I)**. Box and whisker plots indicate the medians, first and third quartiles, and the minimum and maximum values, the points represent individual samples. The differential abundance tests were performed using ANCOM with Holm-Bonferroni correction for multiple comparison, n = 10/group. *q < 0.05 compared to vehicle-treated group.

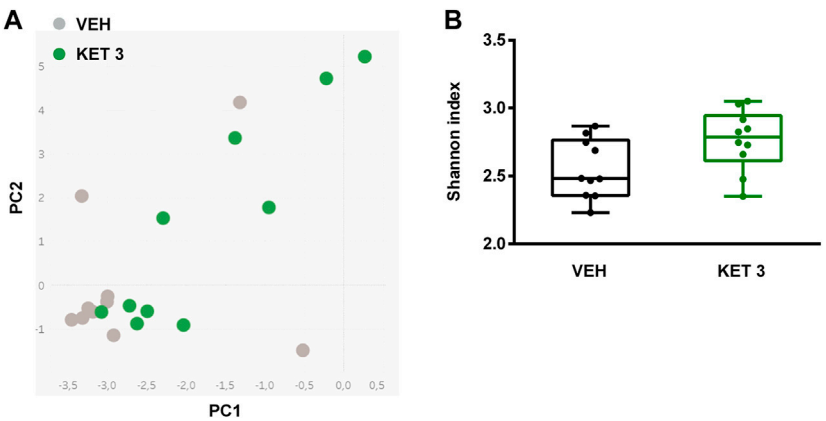

FIGURE 5 | Panel **A**: Principal component analysis (PCA) score plot comparing the small intestinal microbiota composition of rats treated with either vehicle (VEH) or ketorolac (KET, 3 mg/kg) for four weeks. Panel **B**: The effect of ketorolac on small intestinal bacterial diversity, estimated by the Shannon index. Box and whisker plots indicate the medians, first and third quartiles, and the minimum and maximum values, the points represent individual samples. For statistical analysis Mann-Whitney U test was used, n = 10/group.

Peptostreptococcaceae, *Christensenellaceae*) formed another cluster and showed positive correlation with conjugated bile acids, and negative with HDCA (**Figure 8** and **Supplementary Figure S1**).

Ketorolac had no Significant Effect on GI Transit

Small intestinal stasis has long been known to favor the growth of *Bacteroides* and deconjugation of bile acids (Gorbach and

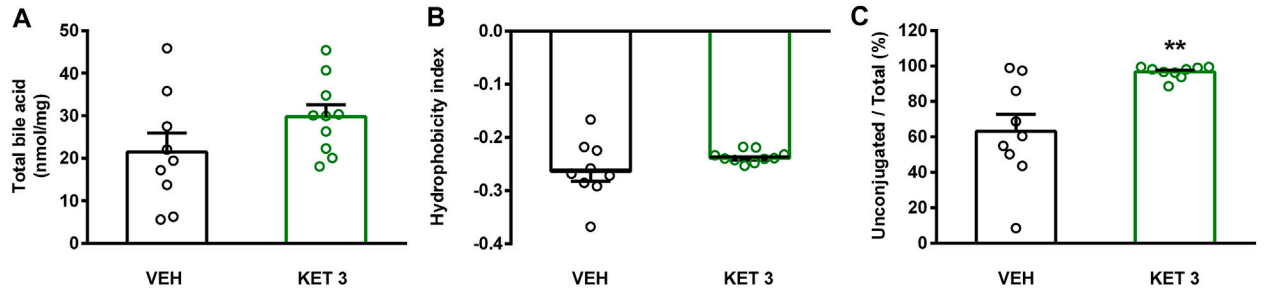

FIGURE 6 | The effect of four-week vehicle (VEH) or ketorolac treatment (KET, 3 mg/kg) on small intestinal total ileal bile acid level **(A)**, mean hydrophobicity index **(B)**, and ratio of conjugated to total ileal bile acids **(C)**. Circles represent the data of each rat, bars indicate the mean + SEM. For statistical analysis Student's t test was used, n = 9–10/group. $^{**}p < 0.01$ compared to vehicle-treated group.

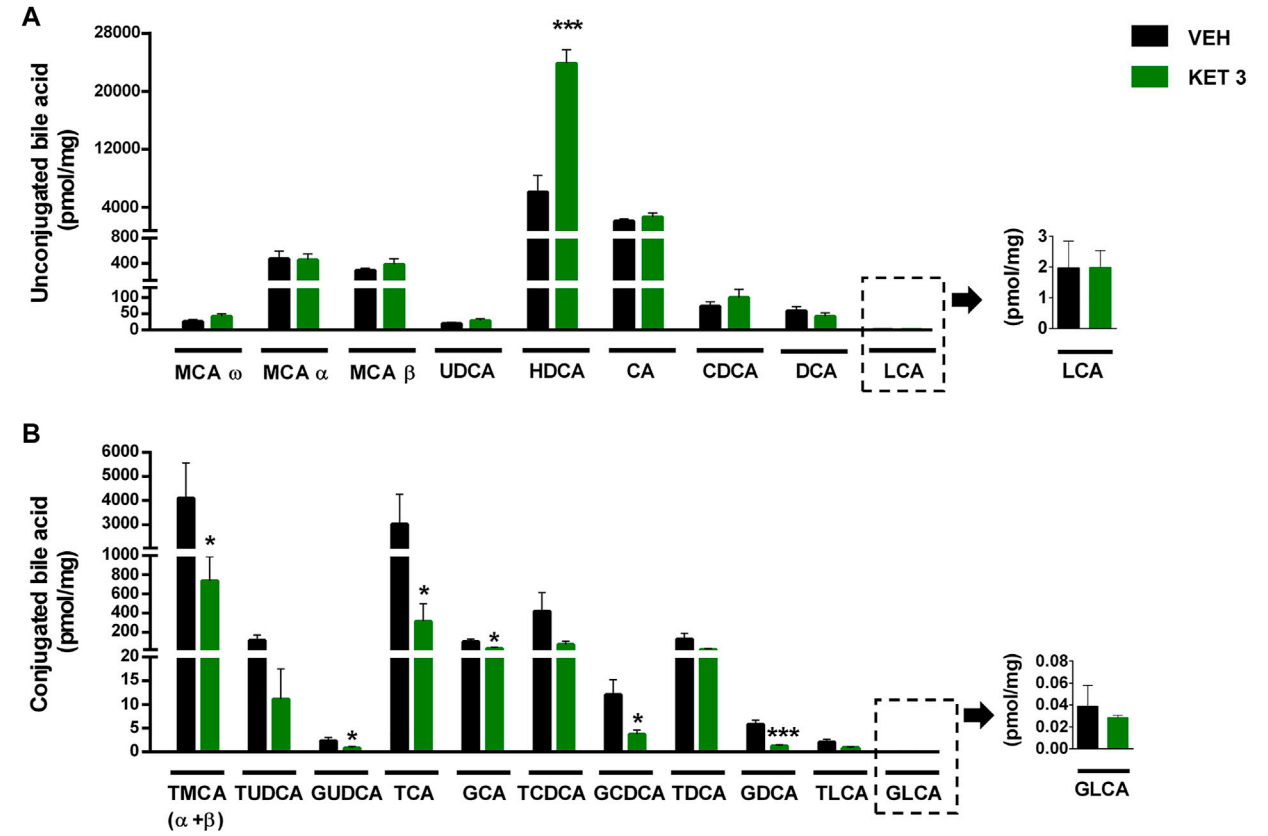

FIGURE 7 | The effect of four-week vehicle (VEH) or ketorolac treatment (KET, 3 mg/kg) on the small intestinal concentration of **(A)** unconjugated and **(B)** conjugated bile acids. Bile acids are ordered by increasing hydrophobicity. Bars indicate the mean + SEM, for statistical analysis Student's t test was used, n = 9–10/group. $^{*}p < 0.05$, $^{***}p < 0.001$ compared to vehicle-treated group. MCA, muricholic acid; UDCA, ursodeoxycholic acid; HDCA, hyodeoxycholic acid; CA, cholic acid; CDCA, chenodeoxycholic acid; DCA, deoxycholic acid; LCA, lithocholic acid; T, respective taurine conjugates; G, respective glycine conjugates.

Tabaqchali, 1969). Therefore, we aimed to investigate whether delayed intestinal peristalsis contributes to the observed changes of bacteria and bile acids. As **Figure 9** shows, ketorolac treatment did not change the GI transit of the charcoal suspension.

DISCUSSION

Here we report that small intestinal dysbiosis developed despite any significant mucosal injury and inflammation in rats treated with low-dose ketorolac, an NSAID lacking direct effects on gut

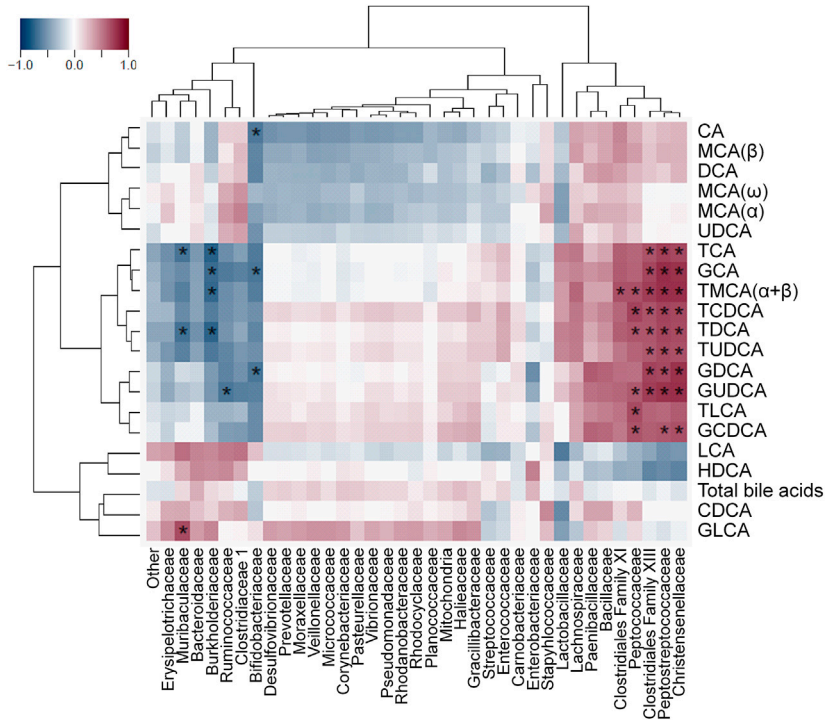

FIGURE 8 | Heat map of Spearman's correlation coefficients between the small intestinal concentration of individual bile acids and the relative abundance of bacterial families. Individual *p* values were corrected by the false discovery rate method according to Benjamini and Hochberg, asterisks indicate q < 0.05.

bacteria. The observed bacterial changes were similar to those reported in previous studies on NSAID enteropathy, characterized by a loss of families belonging to Firmicutes and bloom of *Enterobacteriaceae*. Our results indicate that other factors than mucosal inflammation may contribute to NSAID-induced dysbiosis as well. The role of altered intestinal peristalsis is unlikely, because ketorolac had no significant impact on GI transit. In addition, ketorolac-induced dysbiosis was accompanied by and correlated with significant changes in the intestinal composition of bile acids, which were characterized by reduction of conjugated bile acids and elevation of HDCA.

Although the influence of NSAIDs on the composition of intestinal microbiota is known since several decades (Kent et al., 1969), the underlying mechanism is still poorly understood. Intestinal injury caused by NSAIDs is undoubtedly a major factor driving the changes of microbiota, because the severity of enteropathy correlates with the extent of dysbiosis (Reuter et al., 1997; Craven et al., 2012). Moreover, the inflamed microenvironment promotes the growth of *Enterobacteriaceae* (Zeng et al., 2017), and the expansion of this bacterial family is common following NSAID treatment (Kent et al., 1969; Craven et al., 2012; Terán-Ventura et al., 2014; Blackler et al., 2015). Another factor that may potentially contribute to the NSAID-induced shift in the microbiota toward Gram-negative bacteria is an antibacterial activity against Gram-positives, which has been reported *in vitro* for several NSAIDs, including ibuprofen, diclofenac and celecoxib (Obad et al., 2015; Thangamani et al., 2015; Chan et al., 2017). Of note, ketorolac, a COX-1 preferring NSAID (Warner et al., 1999), had no significant effect on the growth of 40 representative gut bacterial strains *in vitro* (Maier et al., 2018). Our results that chronic treatment with ketorolac at non-damaging dose altered the intestinal microbiota provides evidence for the contribution of additional factors to NSAID-induced dysbiosis.

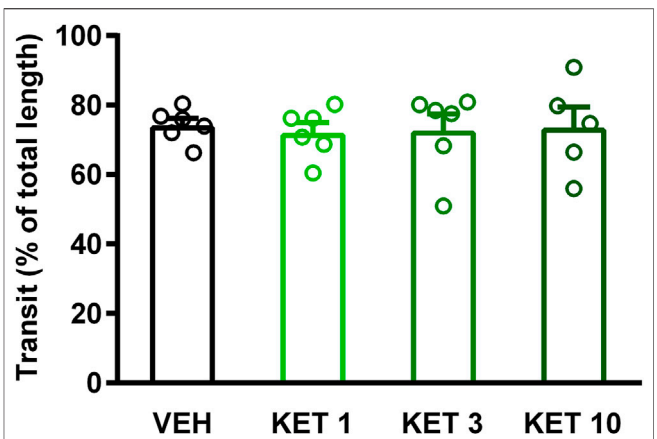

FIGURE 9 | The effect of vehicle (VEH) or ketorolac (KET) given at different doses (1, 3 and 10 mg/kg per os, once daily for five days) on rat gastrointestinal transit. Circles represent the distance traveled by charcoal in each rat, bars indicate the mean + SEM. For statistical analysis one-way ANOVA with Holm-Sidak post hoc test was used, n = 5–6/group.

Although the non-damaging dose of ketorolac (3 mg/kg) used for analysis of bacteria and bile acids was chosen based on previous publications (Jamali et al., 1999; Wallace et al., 2000; Santos et al., 2007), the first and most critical step was to confirm its GI safety. The effect of ketorolac given at different doses on the small intestine was evaluated by macroscopic examination of the entire intestinal mucosa, histological analysis and measurement of inflammatory mediators and claudin-1. Our results that ketorolac at doses up to 3 mg/kg did not cause significant GI damage in the rat correspond to literature data (Jamali et al., 1999; Wallace et al., 2000; Santos et al., 2007). Of note, in cats the same dose of ketorolac induced ulcers in the duodenum, although not in other parts of the small intestine (Satoh et al., 2013), suggesting species differences in its GI tolerability.

Despite no signs of injury we found overt changes in the small intestinal microbiota following ketorolac treatment, which was primarily characterized by a loss of Firmicutes and increased representation of *Enterobacteriaceae*. This result corroborates some previous findings that NSAID-induced dysbiosis can appear without the development of enteropathy as well (Uejima et al., 1996; Liang et al., 2015; Montrose et al., 2016; Lu et al., 2018). These studies, however, focused mainly on the NSAID-induced compositional changes of microbiota, and not on the relationship between inflammation and dysbiosis, therefore only morphological alterations of the intestinal mucosa were assessed. In addition, such NSAIDs were used that may potentially influence the growth of bacteria directly. Our current analysis using ketorolac clearly indicates that NSAID-induced dysbiosis can develop without mucosal inflammation, and based on the *in vitro* results of Maier et al. (2018) also the role of direct effects on gut bacteria is unlikely.

In some (Bennett et al., 1976; Shahbazian et al., 2001; Lichtenberger et al., 2015), but not in other (Takeuchi et al., 2002; Satoh et al., 2009) studies NSAIDs were shown to suppress intestinal motility. Because slower peristalsis was associated with a decrease in Firmicutes and an increase in Bacteroidetes (Kashyap et al., 2013; Touw et al., 2017), we hypothesized that ketorolac induced bacterial changes may be due at least partly to delayed GI peristalsis. However, we found no significant change in GI transit following ketorolac treatment. Of note, in the study of Santos et al. (2007), ketorolac delayed the peristalsis of proximal and medial small intestine. Nevertheless, this effect was detectable only 10 and 20, but not 30, minutes after the application of the test meal. Here we evaluated the transit of test meal 30 min after the gavage, in an attempt to reveal perturbations in peristalsis in more distal parts of the small intestine, at the site of dysbiosis. The lack of effect at this time point (in both studies) indicates that the effect of ketorolac on small intestinal motility at low doses is moderate at best, and does not affect the transit in distal parts of the small intestine. Hence, it is unlikely that altered peristalsis would account for the observed shift in the distal small intestinal microbiota following ketorolac treatment. Similar conclusion was drawn by Hagiwara et al. (2004), who found that DuP-697, a selective COX-2 inhibitor, induced dysbiosis without suppression of peristalsis. A potential limitation of our study is that small intestinal peristalsis was measured only by the charcoal method. Although this simple technique is widely used to assess the net effect of drugs on small intestinal transit, it does not allow to determine the contractile and peristaltic activities of different intestinal segments. Hence, we cannot exclude the possibility that ketorolac had diverse effects on the contractility of proximal, medial and distal parts of the small intestine, resulting in an apparently unchanged transit at the time of evaluation. Further studies are needed to reveal such effects and their potential contribution to small intestinal dysbiosis.

There is a large body of evidence on the close bidirectional relationship between gut bacteria and bile acids. The gut microbiota is capable of producing a wide variety of bile acid metabolites, which may also have diverse effects on the growth of different bacteria (Begley et al., 2005; Ridlon and Bajaj, 2015; Ridlon et al., 2016). Hence, we also aimed to assess whether ketorolac-induced dysbiosis and alterations in the availability of bacterial enzymes had any effect on intestinal bile composition. We found that ketorolac decreased the amount of glycine- and taurine-conjugated primary and secondary bile acids, and increased the concentration of the hydrophilic secondary bile acid HDCA. To date, there is only limited data on the effect of NSAIDs on bile acid composition. Because indomethacin was shown to increase the biliary proportion of hydrophobic bile acids and bile hydrophobicity (Yamada et al., 1996; Uchida et al., 1997), and because the hydrophobicity of bile acids correlates with their cytotoxicity (Heuman, 1989), it was postulated that NSAID-induced small intestinal damage may be partly due to an increased ratio of hydrophobic secondary bile acids (Yamada et al., 1996; Wallace, 2013; Montenegro et al., 2014; Syer et al., 2015). However, in a recent paper focusing mainly on the combined toxicity of ibuprofen and glucocorticoids (Lu et al., 2018), ibuprofen treatment had no effect on the total amount secondary bile acids in the ileum of mice, but increased the amount of primary and conjugated bile acids. Moreover, our recent studies with high-dose indomethacin showed that in severe enteropathy the levels of all conjugated bile acids increased irrespective of their primary or secondary nature, whereas the levels of unconjugated bile acids decreased, except that of HDCA (Lázár et al., submitted manuscript)[1]. Hence, NSAIDs may have diverse effects on small intestinal bile composition, depending on the presence and severity of mucosal damage and the actual microbiota, and the elevation of hydrophobic secondary bile acids is probably not a general consequence of NSAID treatment. On the other hand, NSAIDs can also increase the cytotoxicity of bile due to the formation of more toxic mixed micelles (Barrios and Lichtenberger, 2000; Petruzzelli et al., 2006; Petruzzelli et al., 2007; Zhou et al., 2010; Dial et al., 2015). Therefore, we cannot rule out the possibility that ketorolac treatment increased the toxicity of bile despite having no effect on the overall hydrophobicity of bile acids, but even if this is the case, it still did not cause significant mucosal damage.

The reduced level of conjugated bile acids was likely due to the overgrowth of bacteria involved in bile acid deconjugation. Indeed,

[1]Lázár, B., Brenner, G., Makkos, A., Balogh, M., László, S., Al-Khrasani, M., et al. (2019). Lack of Small Intestinal Dysbiosis Following Long-Term Selective Inhibition of Cyclooxygenase-2 by Rofecoxib in the Rat. Cells 8 (3), 251. doi: 10.3390/cells8030251

deconjugation of bile acids is mainly performed by members of Firmicutes (e.g. *Clostridium*, *Ruminococcus*), Bacteroidetes and *Bifidobacteriaceae* (belonging to Actinobacteria) (Ridlon et al., 2016; Martin et al., 2018), and ketorolac treatment was associated with increased abundance of Actinobacteria and *Ruminococcaceae UCG-014*, and tendency toward elevation of Bacteroidetes. In addition, our correlation analysis revealed negative associations between the levels of conjugated bile acids and the abundance of some Firmicutes (*Erysipelotrichaceae*, *Ruminococcaceae*, *Clostridiaceae 1*), *Muribaculaceae* and *Bacteroidaceae* (both belonging to Bacteroidetes) and *Bifidobacteriaceae*. Although we also found positive correlations between other Firmicutes bacteria (*Clostridiales Family XI* and *XIII*, *Peptococcaceae*, *Peptostreptococcaceae*, *Christensenellaceae*) and conjugated bile acids, these reflect most likely the loss of these bacteria due to ketorolac treatment in parallel with the reduction of conjugated bile acids and lack causality.

At present, little is known about the bacteria involved in the formation of HDCA. Eyssen et al. (1999) reported the isolation of a Gram-positive rod (termed *HDCA-1*) capable to produce HDCA in the presence of an unidentified growth factor produced by a *Ruminococcus productus* strain. Trudeau et al. (2018) recently found positive correlation between the levels of HDCA and *Lachnospiraceae* in pigs. In the present study, the percentage of HDCA showed the strongest positive correlation with the abundance of *Burkholderiaceae*. Whether this association is due to a causal relationship warrants further investigation.

Although the mild changes in small intestinal microbiota and bile acids due to chronic ketorolac treatment were not translated into enteropathy, they may have other important effects on the host. For example, a decreased ratio of Firmicutes to Bacteroidetes may decrease the capacity to harvest energy from the diet (Turnbaugh et al., 2006), and also the increased luminal concentration of HDCA may have glucose-lowering and obesity-preventing effects (Shih et al., 2013). Nevertheless, these potential favourable effects have probably limited, if any, translational relevance due to the GI damaging property and short-term use of ketorolac in humans.

In conclusion, our present study demonstrates that ketorolac, an NSAID lacking direct antibacterial properties, given at low dose caused marked changes in the composition of small intestinal bacteria in rats without inducing significant mucosal inflammation and tissue damage. This dysbiosis was accompanied by and correlated with significant changes in the intestinal composition of bile acids. Our result, that ketorolac had no significant effect on GI peristalsis, suggests that dysbiosis is not likely to be caused by small intestinal stasis, and other, yet unidentified, factors contribute to the observed changes of bacteria and bile acids. Further studies are warranted to reveal the exact mechanisms underlying the associations between NSAIDs, bacteria and bile acids.

DATA AVAILABILITY STATEMENT

The datasets presented in this study can be found in online repositories. The names of the repository/repositories and accession number(s) can be found below: Bioproject: https://www.ncbi.nlm.nih.gov/bioproject/PRJNA705956, Zenodo: https://zenodo.org/record/4601191.

ETHICS STATEMENT

The animal study was reviewed and approved by the National Scientific Ethical Committee on Animal Experimentation and permitted by the government (Food Chain Safety and Animal Health Directorate of the Government Office for Pest County).

AUTHOR CONTRIBUTIONS

BH, BLá, KK, MA, KG, and ZZ contributed to conception and design of the study. BH, BLá, AT, BÁ, SL, NM, BLi, BS, and ZZ organized the database. BH, BLá, AT, BÁ, SL, NM, BLi, BS, and ZZ performed the statistical analysis. BH, BLá, and ZZ wrote the first draft of the manuscript. DS, PF, and KG wrote sections of the manuscript. All authors contributed to manuscript revision, read, and approved the submitted version.

FUNDING

The research was supported by the National Research, Development and Innovation Office of Hungary (NKFI FK 124878: and NKFI K 120650), by the Scientific and Innovative Research Fund of Semmelweis University (SE STIA-KF-17), by the Higher Education Institutional Excellence Program of the Ministry of Human Capacities, within the framework of the Neurology thematic program of the Semmelweis University (FIKP 2018), and by the Research Excellence Program of the National Research, Development and Innovation Office of the Ministry of Innovation and Technology in Hungary (TKP/ITM/NKFIH).

ACKNOWLEDGMENTS

The authors wish to express their thanks to Veronika Pol-Maruzs, Ádám Lakos, Viktor Sajtos, Mirtill Nagy and Petra Sólymos for their technical assistance. The graphical abstract contains artworks produced by Servier Medical Art (http://smart.servier.com).

SUPPLEMENTARY MATERIAL

The Supplementary Material for this article can be found online at: https://www.frontiersin.org/articles/10.3389/fphar.2021.664177/full#supplementary-material

REFERENCES

Barrios, J. M., and Lichtenberger, L. M. (2000). Role of Biliary Phosphatidylcholine in Bile Acid Protection and NSAID Injury of the Ileal Mucosa in Rats. *Gastroenterology* 118 (6), 1179–1186. doi:10.1016/s0016-5085(00)70371-4

Begley, M., Gahan, C. G. M., and Hill, C. (2005). The Interaction between Bacteria and Bile. *FEMS Microbiol. Rev.* 29 (4), 625–651. doi:10.1016/j.femsre.2004.09.003

Benjamini, Y., and Hochberg, Y. (1995). Controlling the False Discovery Rate: A Practical and Powerful Approach to Multiple Testing. *J. R. Stat. Soc. Ser. B (Methodological)* 57 (1), 289–300. doi:10.1111/j.2517-6161.1995.tb02031.x

Bennett, A., Eley, K. G., and Stockley, H. L. (1976). Inhibition of Peristalsis in guinea-pig Isolated Ileum and Colon by Drugs that Block Prostaglandin Synthesis. *Br. J. Pharmacol.* 57 (3), 335–340. doi:10.1111/j.1476-5381.1976.tb07671.x

Bjarnason, I., Scarpignato, C., Holmgren, E., Olszewski, M., Rainsford, K. D., and Lanas, A. (2018). Mechanisms of Damage to the Gastrointestinal Tract from Nonsteroidal Anti-Inflammatory Drugs. *Gastroenterology* 154 (3), 500–514. doi:10.1053/j.gastro.2017.10.049

Blackler, R. W., De Palma, G., Manko, A., Da Silva, G. J., Flannigan, K. L., Bercik, P., et al. (2015). Deciphering the Pathogenesis of NSAID Enteropathy Using Proton Pump Inhibitors and a Hydrogen Sulfide-Releasing NSAID. *Am. J. Physiol.-Gastrointestinal Liver Physiol.* 308 (12), G994–G1003. doi:10.1152/ajpgi.00066.2015

Bolger, A. M., Lohse, M., and Usadel, B. (2014). Trimmomatic: a Flexible Trimmer for Illumina Sequence Data. *Bioinformatics* 30 (15), 2114–2120. doi:10.1093/bioinformatics/btu170

Breitwieser, F. P., Lu, J., and Salzberg, S. L. (2019). A Review of Methods and Databases for Metagenomic Classification and Assembly. *Brief Bioinform* 20 (4), 1125–1136. doi:10.1093/bib/bbx120

Chan, E. W. L., Yee, Z. Y., Raja, I., and Yap, J. K. Y. (2017). Synergistic Effect of Non-steroidal Anti-inflammatory Drugs (NSAIDs) on Antibacterial Activity of Cefuroxime and Chloramphenicol against Methicillin-Resistant Staphylococcus aureus. *J. Glob. Antimicrob. Resist.* 10, 70–74. doi:10.1016/j.jgar.2017.03.012

Colucci, R., Pellegrini, C., Fornai, M., Tirotta, E., Antonioli, L., Renzulli, C., et al. (2018). Pathophysiology of NSAID-Associated Intestinal Lesions in the Rat: Luminal Bacteria and Mucosal Inflammation as Targets for Prevention. *Front. Pharmacol.* 9, 1340. doi:10.3389/fphar.2018.01340

Craven, M., Egan, C. E., Dowd, S. E., McDonough, S. P., Dogan, B., Denkers, E. Y., et al. (2012). Inflammation Drives Dysbiosis and Bacterial Invasion in Murine Models of Ileal Crohn's Disease. *PLoS One* 7 (7), e41594. doi:10.1371/journal.pone.0041594

Dalby, A. B., Frank, D. N., St. Amand, A. L., Bendele, A. M., and Pace, N. R. (2006). Culture-independent Analysis of Indomethacin-Induced Alterations in the Rat Gastrointestinal Microbiota. *Aem* 72 (10), 6707–6715. doi:10.1128/aem.00378-06

Dial, E. J., Dawson, P. A., and Lichtenberger, L. M. (2015). *In vitro* evidence that Phosphatidylcholine Protects against Indomethacin/bile Acid-Induced Injury to Cells. *Am. J. Physiol.-Gastrointestinal Liver Physiol.* 308 (3), G217–G222. doi:10.1152/ajpgi.00322.2014

Elliott, S. N., Buret, A., McKnight, W., Miller, M. J. S., and Wallace, J. L. (1998). Bacteria Rapidly Colonize and Modulate Healing of Gastric Ulcers in Rats. *Am. J. Physiol.-Gastrointestinal Liver Physiol.* 275 (3), G425–G432. doi:10.1152/ajpgi.1998.275.3.G425

Eyssen, H. J., De Pauw, G., and Van Eldere, J. (1999). Formation of Hyodeoxycholic Acid from Muricholic Acid and Hyocholic Acid by an Unidentified Gram-Positive Rod Termed HDCA-1 Isolated from Rat Intestinal Microflora. *Appl. Environ. Microbiol.* 65 (7), 3158–3163. doi:10.1128/aem.65.7.3158-3163.1999

Gorbach, S. L., and Tabaqchali, S. (1969). Bacteria, Bile and the Small Bowel. *Gut* 10 (12), 963–972. doi:10.1136/gut.10.12.963

Granados-Soto, V., López-Muñoz, F. J., Hong, E., and Flores-Murrieta, F. J. (1995). Relationship between Pharmacokinetics and the Analgesic Effect of Ketorolac in the Rat. *J. Pharmacol. Exp. Ther.* 272 (1), 352–356.

Hagiwara, M., Kataoka, K., Arimochi, H., Kuwahara, T., and Ohnishi, Y. (2004). Role of Unbalanced Growth of Gram-Negative Bacteria in Ileal Ulcer Formation in Rats Treated with a Nonsteroidal Anti-inflammatory Drug. *J. Med. Invest.* 51 (1-2), 43–51. doi:10.2152/jmi.51.43

Han, Y.-M., Park, J.-M., Kang, J. X., Cha, J.-Y., Lee, H.-J., Jeong, M., et al. (2016). Mitigation of Indomethacin-Induced Gastrointestinal Damages in Fat-1 Transgenic Mice via Gate-Keeper Action of ω-3-polyunsaturated Fatty Acids. *Sci. Rep.* 6, 33992. doi:10.1038/srep33992

Heuman, D. M. (1989). Quantitative Estimation of the Hydrophilic-Hydrophobic Balance of Mixed Bile Salt Solutions. *J. Lipid Res.* 30 (5), 719–730. doi:10.1016/s0022-2275(20)38331-0

Jamali, F., Lovlin, R., Corrigan, B. W., Davies, N. M., and Aberg, G. (1999). Stereospecific Pharmacokinetics and Toxicodynamics of Ketorolac after Oral Administration of the Racemate and Optically Pure Enantiomers to the Rat. *Chirality* 11 (3), 201–205. doi:10.1002/(sici)1520-636x(1999)11:3<201::aid-chir5>3.0.co;2-z

Jett, M. F., Ramesha, C. S., Brown, C. D., Chiu, S., Emmett, C., Voronin, T., et al. (1999). Characterization of the Analgesic and Anti-inflammatory Activities of Ketorolac and its Enantiomers in the Rat. *J. Pharmacol. Exp. Ther.* 288 (3), 1288–1297.

Jiménez-Serna, A., and Hernández-Sánchez, H. (2011). Effect of Different Antibiotics and Non-steroidal Anti-inflammatory Drugs on the Growth of Lactobacillus Casei Shirota. *Curr. Microbiol.* 62 (3), 1028–1033. doi:10.1007/s00284-010-9819-7

Kashyap, P. C., Marcobal, A., Ursell, L. K., Larauche, M., Duboc, H., Earle, K. A., et al. (2013). Complex Interactions Among Diet, Gastrointestinal Transit, and Gut Microbiota in Humanized Mice. *Gastroenterology* 144 (5), 967–977. doi:10.1053/j.gastro.2013.01.047

Kent, T. H., Cardelli, R. M., and Stamler, F. W. (1969). Small Intestinal Ulcers and Intestinal Flora in Rats Given Indomethacin. *Am. J. Pathol.* 54 (2), 237–249.

Lanas, Á., and Scarpignato, C. (2006). Microbial Flora in NSAID-Induced Intestinal Damage: a Role for Antibiotics? *Digestion* 73 (Suppl. 1), 136–150. doi:10.1159/000089789

László, S. B., Lázár, B., Brenner, G. B., Makkos, A., Balogh, M., Al-Khrasani, M., et al. (2020). Chronic Treatment with Rofecoxib but Not Ischemic Preconditioning of the Myocardium Ameliorates Early Intestinal Damage Following Cardiac Ischemia/reperfusion Injury in Rats. *Biochem. Pharmacol.* 178, 114099. doi:10.1016/j.bcp.2020.114099

Laukens, D., Brinkman, B. M., Raes, J., De Vos, M., and Vandenabeele, P. (2016). Heterogeneity of the Gut Microbiome in Mice: Guidelines for Optimizing Experimental Design. *FEMS Microbiol. Rev.* 40 (1), 117–132. doi:10.1093/femsre/fuv036

Lázár, B., Brenner, G., Makkos, A., Balogh, M., László, S., Al-Khrasani, M., et al. (2019). Lack of Small Intestinal Dysbiosis Following Long-Term Selective Inhibition of Cyclooxygenase-2 by Rofecoxib in the Rat. *Cells* 8 (3), 251. doi:10.3390/cells8030251

Liang, X., Bittinger, K., Li, X., Abernethy, D. R., Bushman, F. D., and FitzGerald, G. A. (2015). Bidirectional Interactions between Indomethacin and the Murine Intestinal Microbiota. *Elife* 4, e08973. doi:10.7554/eLife.08973

Lichtenberger, L. M., Bhattarai, D., Phan, T. M., Dial, E. J., and Uray, K. (2015). Suppression of Contractile Activity in the Small Intestine by Indomethacin and Omeprazole. *Am. J. Physiol.-Gastrointestinal Liver Physiol.* 308 (9), G785–G793. doi:10.1152/ajpgi.00458.2014

LoGuidice, A., Wallace, B. D., Bendel, L., Redinbo, M. R., and Boelsterli, U. A. (2012). Pharmacologic Targeting of Bacterial β-Glucuronidase Alleviates Nonsteroidal Anti-Inflammatory Drug-Induced Enteropathy in Mice. *J. Pharmacol. Exp. Ther.* 341 (2), 447–454. doi:10.1124/jpet.111.191122

Lu, Z., Lu, Y., Wang, X., Wang, F., and Zhang, Y. (2018). Activation of Intestinal GR-FXR and PPARα-UGT Signaling Exacerbates Ibuprofen-Induced Enteropathy in Mice. *Arch. Toxicol.* 92 (3), 1249–1265. doi:10.1007/s00204-017-2139-y

Maiden, L., Thjodleifsson, B., Theodors, A., Gonzalez, J., and Bjarnason, I. (2005). A Quantitative Analysis of NSAID-Induced Small Bowel Pathology by Capsule Enteroscopy. *Gastroenterology* 128 (5), 1172–1178. doi:10.1053/j.gastro.2005.03.020

Maier, L., Pruteanu, M., Kuhn, M., Zeller, G., Telzerow, A., Anderson, E. E., et al. (2018). Extensive Impact of Non-antibiotic Drugs on Human Gut Bacteria. *Nature* 555 (7698), 623–628. doi:10.1038/nature25979

Mandal, S., Van Treuren, W., White, R. A., Eggesbø, M., Knight, R., and Peddada, S. D. (2015). Analysis of Composition of Microbiomes: a Novel Method for

Studying Microbial Composition. *Microb. Ecol. Health Dis.* 26, 27663. doi:10.3402/mehd.v26.27663

Mansour, B., Monyók, Á., Makra, N., Gajdács, M., Vadnay, I., Ligeti, B., et al. (2020). Bladder Cancer-Related Microbiota: Examining Differences in Urine and Tissue Samples. *Sci. Rep.* 10, 11042. doi:10.1038/s41598-020-67443-2

Martin, G., Kolida, S., Marchesi, J. R., Want, E., Sidaway, J. E., and Swann, J. R. (2018). *In Vitro* Modeling of Bile Acid Processing by the Human Fecal Microbiota. *Front. Microbiol.* 9, 1153. doi:10.3389/fmicb.2018.01153

Maseda, D., Zackular, J. P., Trindade, B., Kirk, L., Roxas, J. L., Rogers, L. M., et al. (2019). Nonsteroidal Anti-inflammatory Drugs Alter the Microbiota and Exacerbate *Clostridium difficile* Colitis while Dysregulating the Inflammatory Response. *mBio* 10 (1), e02282. doi:10.1128/mBio.02282-18

Montenegro, L., Losurdo, G., Licinio, R., Zamparella, M., Giorgio, F., Ierardi, E., et al. (2014). Non Steroidal Anti-inflammatory Drug Induced Damage on Lower Gastro-Intestinal Tract: Is There an Involvement of Microbiota?. *Curr. Drug Saf.* 9 (3), 196–204. doi:10.2174/1574886309666140424143852

Montrose, D. C., Zhou, X. K., McNally, E. M., Sue, E., Yantiss, R. K., Gross, S. S., et al. (2016). Celecoxib Alters the Intestinal Microbiota and Metabolome in Association with Reducing Polyp Burden. *Cancer Prev. Res.* 9 (9), 721–731. doi:10.1158/1940-6207.Capr-16-0095

Nylander, O. (2011). The Impact of Cyclooxygenase Inhibition on Duodenal Motility and Mucosal Alkaline Secretion in Anaesthetized Rats. *Acta Physiol. (Oxf)* 201 (1), 179–192. doi:10.1111/j.1748-1716.2010.02196.x

Obad, J., Šušković, J., and Kos, B. (2015). Antimicrobial Activity of Ibuprofen: New Perspectives on an "Old" Non-antibiotic Drug. *Eur. J. Pharm. Sci.* 71, 93–98. doi:10.1016/j.ejps.2015.02.011

Petruzzelli, M., Moschetta, A., Renooij, W., de Smet, M. B. M., Palasciano, G., Portincasa, P., et al. (2006). Indomethacin Enhances Bile Salt Detergent Activity: Relevance for NSAIDs-Induced Gastrointestinal Mucosal Injury. *Dig. Dis. Sci.* 51 (4), 766–774. doi:10.1007/s10620-006-3204-1

Petruzzelli, M., Vacca, M., Moschetta, A., Cinzia Sasso, R., Palasciano, G., van Erpecum, K. J., et al. (2007). Intestinal Mucosal Damage Caused by Non-steroidal Anti-inflammatory Drugs: Role of Bile Salts. *Clin. Biochem.* 40 (8), 503–510. doi:10.1016/j.clinbiochem.2007.01.015

Poša, M. (2014). Heuman Indices of Hydrophobicity of Bile Acids and Their Comparison with a Newly Developed and Conventional Molecular Descriptors. *Biochimie* 97, 28–38. doi:10.1016/j.biochi.2013.09.010

Quast, C., Pruesse, E., Yilmaz, P., Gerken, J., Schweer, T., Yarza, P., et al. (2013). The SILVA Ribosomal RNA Gene Database Project: Improved Data Processing and Web-Based Tools. *Nucleic Acids Res.* 41 (Database issue), D590–D596. doi:10.1093/nar/gks1219

R Core Team (2018). *R: A Language and Environment for Statistical Computing*. Vienna, Austria: R Foundation for Statistical Computing. URL. Available at: http://www.R-project.org/.

Reuter, B., Davies, N., and Wallace, J. (1997). Nonsteroidal Anti-inflammatory Drug Enteropathy in Rats: Role of Permeability, Bacteria, and Enterohepatic Circulation. *Gastroenterology* 112 (1), 109–117. doi:10.1016/s0016-5085(97)70225-7

Ridlon, J. M., and Bajaj, J. S. (2015). The Human Gut Sterolbiome: Bile Acid-Microbiome Endocrine Aspects and Therapeutics. *Acta Pharm. Sin. B* 5 (2), 99–105. doi:10.1016/j.apsb.2015.01.006

Ridlon, J. M., Harris, S. C., Bhowmik, S., Kang, D.-J., and Hylemon, P. B. (2016). Consequences of Bile Salt Biotransformations by Intestinal Bacteria. *Gut Microbes* 7 (1), 22–39. doi:10.1080/19490976.2015.1127483

Robert, A., and Asano, T. (1977). Resistance of Germfree Rats to Indomethacin-Induced Intestinal Lesions. *Prostaglandins* 14 (2), 333–341. doi:10.1016/0090-6980(77)90178-2

Rogers, M. A. M., and Aronoff, D. M. (2016). The Influence of Non-steroidal Anti-inflammatory Drugs on the Gut Microbiome. *Clin. Microbiol. Infect.* 22 (2), 178.e1–178.e9. doi:10.1016/j.cmi.2015.10.003

Santos, c. l., Medeiros, b. a., Palheta-Junior, r. c., Macedo, g. m., Nobre-e-Souza, m. a., Troncon, l. e. a., et al. (2007). Cyclooxygenase-2 Inhibition Increases Gastric Tone and Delays Gastric Emptying in Rats. *Neurogastroenterol Motil.* 19 (3), 225–232. doi:10.1111/j.1365-2982.2007.00913.x

Satoh, H., Amagase, K., Ebara, S., Akiba, Y., and Takeuchi, K. (2013). Cyclooxygenase (COX)-1 and COX-2 Both Play an Important Role in the Protection of the Duodenal Mucosa in Cats. *J. Pharmacol. Exp. Ther.* 344 (1), 189–195. doi:10.1124/jpet.112.199182

Satoh, H., Shiotani, S., Otsuka, N., Hatao, K., and Nishimura, S. (2009). Role of Dietary Fibres, Intestinal Hypermotility and Leukotrienes in the Pathogenesis of NSAID-Induced Small Intestinal Ulcers in Cats. *Gut* 58 (12), 1590–1596. doi:10.1136/gut.2008.156596

Shahbazian, A., Schuligoi, R., Heinemann, A., Peskar, B. A., and Holzer, P. (2001). Disturbance of Peristalsis in the guinea-pig Isolated Small Intestine by Indomethacin, but Not Cyclo-Oxygenase Isoform-Selective Inhibitors. *Br. J. Pharmacol.* 132 (6), 1299–1309. doi:10.1038/sj.bjp.0703940

Shih, D. M., Shaposhnik, Z., Meng, Y., Rosales, M., Wang, X., Wu, J., et al. (2013). Hyodeoxycholic Acid Improves HDL Function and Inhibits Atherosclerotic Lesion Formation in LDLR-knockout Mice. *FASEB J.* 27, 3805–3817. doi:10.1096/fj.12-223008

Stenman, L. K., Holma, R., Forsgård, R., Gylling, H., and Korpela, R. (2013). Higher Fecal Bile Acid Hydrophobicity Is Associated with Exacerbation of Dextran Sodium Sulfate Colitis in Mice. *J. Nutr.* 143 (11), 1691–1697. doi:10.3945/jn.113.180810

Syer, S. D., Blackler, R. W., Martin, R., de Palma, G., Rossi, L., Verdu, E., et al. (2015). NSAID Enteropathy and Bacteria: a Complicated Relationship. *J. Gastroenterol.* 50 (4), 387–393. doi:10.1007/s00535-014-1032-1

Takeuchi, K., Miyazawa, T., Tanaka, A., Kato, S., and Kunikata, T. (2002). Pathogenic Importance of Intestinal Hypermotility in NSAID-Induced Small Intestinal Damage in Rats. *Digestion* 66 (1), 30–41. doi:10.1159/000064419

Takeuchi, K., and Satoh, H. (2015). NSAID-Induced Small Intestinal Damage - Roles of Various Pathogenic Factors. *Digestion* 91 (3), 218–232. doi:10.1159/000374106

Terán-Ventura, E., Aguilera, M., Vergara, P., and Martínez, V. (2014). Specific Changes of Gut Commensal Microbiota and TLRs during Indomethacin-Induced Acute Intestinal Inflammation in Rats. *J. Crohns Colitis* 8 (9), 1043–1054. doi:10.1016/j.crohns.2014.02.001

Thangamani, S., Younis, W., and Seleem, M. N. (2015). Repurposing Celecoxib as a Topical Antimicrobial Agent. *Front. Microbiol.* 6, 750. doi:10.3389/fmicb.2015.00750

Touw, K., Ringus, D. L., Hubert, N., Wang, Y., Leone, V. A., Nadimpalli, A., et al. (2017). Mutual Reinforcement of Pathophysiological Host-Microbe Interactions in Intestinal Stasis Models. *Physiol. Rep.* 5 (6), e13182. doi:10.14814/phy2.13182

Trudeau, M. P., Zhou, Y., Leite, F. L., Gomez, A., Urriola, P. E., Shurson, G. C., et al. (2018). Fecal Hyodeoxycholic Acid Is Correlated with Tylosin-Induced Microbiome Changes in Growing Pigs. *Front. Vet. Sci.* 5, 196. doi:10.3389/fvets.2018.00196

Turnbaugh, P. J., Ley, R. E., Mahowald, M. A., Magrini, V., Mardis, E. R., and Gordon, J. I. (2006). An Obesity-Associated Gut Microbiome with Increased Capacity for Energy Harvest. *Nature* 444, 1027–1031. doi:10.1038/nature05414

Uchida, A., Yamada, T., Hayakawa, T., and Hoshino, M. (1997). Taurochenodeoxycholic Acid Ameliorates and Ursodeoxycholic Acid Exacerbates Small Intestinal Inflammation. *Am. J. Physiology-Gastrointestinal Liver Physiol.* 272 (5 Pt 1), G1249–G1257. doi:10.1152/ajpgi.1997.272.5.G1249

Uejima, M., Kinouchi, T., Kataoka, K., Hiraoka, I., and Ohnishi, Y. (1996). Role of Intestinal Bacteria in Ileal Ulcer Formation in Rats Treated with a Nonsteroidal Antiinflammatory Drug. *Microbiol. Immunol.* 40 (8), 553–560. doi:10.1111/j.1348-0421.1996.tb01108.x

Vadivelu, N., Gowda, A. M., Urman, R. D., Jolly, S., Kodumudi, V., Maria, M., et al. (2015). Ketorolac Tromethamine - Routes and Clinical Implications. *Pain Pract.* 15 (2), 175–193. doi:10.1111/papr.12198

Wallace, J. L., McKnight, W., Reuter, B. K., and Vergnolle, N. (2000). NSAID-induced Gastric Damage in Rats: Requirement for Inhibition of Both Cyclooxygenase 1 and 2. *Gastroenterology* 119 (3), 706–714. doi:10.1053/gast.2000.16510

Wallace, J. L. (2013). Mechanisms, Prevention and Clinical Implications of Nonsteroidal Anti-inflammatory Drug-Enteropathy. *Wjg* 19 (12), 1861–1876. doi:10.3748/wjg.v19.i12.1861

Warner, T. D., Giuliano, F., Vojnovic, I., Bukasa, A., Mitchell, J. A., and Vane, J. R. (1999). Nonsteroid Drug Selectivities for Cyclo-Oxygenase-1 rather Than Cyclo-Oxygenase-2 Are Associated with Human Gastrointestinal Toxicity: a Full In Vitro Analysis. *Proc. Natl. Acad. Sci.* 96 (13), 7563–7568. doi:10.1073/pnas.96.13.7563

Wood, D. E., and Salzberg, S. L. (2014). Kraken: Ultrafast Metagenomic Sequence Classification Using Exact Alignments. *Genome Biol.* 15 (3), R46. doi:10.1186/gb-2014-15-3-r46

Xiao, X., Nakatsu, G., Jin, Y., Wong, S., Yu, J., and Lau, J. Y. W. (2017). Gut Microbiota Mediates Protection against Enteropathy Induced by Indomethacin. *Sci. Rep.* 7, 40317. doi:10.1038/srep40317

Yamada, T., Hoshino, M., Hayakawa, T., Kamiya, Y., Ohhara, H., Mizuno, K., et al. (1996). Bile Secretion in Rats with Indomethacin-Induced Intestinal Inflammation. *Am. J. Physiology-Gastrointestinal Liver Physiol.* 270 (5 Pt 1), G804–G812. doi:10.1152/ajpgi.1996.270.5.G804

Zádor, F., Mohammadzadeh, A., Balogh, M., Zádori, Z. S., Király, K., Barsi, S., et al. (2020). Comparisons of *In Vivo* and *In Vitro* Opioid Effects of Newly Synthesized 14-Methoxycodeine-6-O-Sulfate and Codeine-6-O-Sulfate. *Molecules* 25 (6), 1370. doi:10.3390/molecules25061370

Zeng, M. Y., Inohara, N., and Nuñez, G. (2017). Mechanisms of Inflammation-Driven Bacterial Dysbiosis in the Gut. *Mucosal Immunol.* 10 (1), 18–26. doi:10.1038/mi.2016.75

Zhou, Y., Dial, E. J., Doyen, R., and Lichtenberger, L. M. (2010). Effect of Indomethacin on Bile Acid-Phospholipid Interactions: Implication for Small Intestinal Injury Induced by Nonsteroidal Anti-inflammatory Drugs. *Am. J. Physiol.-Gastrointestinal Liver Physiol.* 298 (5), G722–G731. doi:10.1152/ajpgi.00387.2009

Conflict of Interest: PF is the founder and CEO of Pharmahungary, a group of R&D companies. BA was employed by Pharmahungary Group.

The remaining authors declare that the research was conducted in the absence of any commercial or financial relationships that could be construed as a potential conflict of interest.

frontiers in Pharmacology

ORIGINAL RESEARCH
published: 28 June 2021
doi: 10.3389/fphar.2021.665493

Nicotinamide Riboside Vitamin B3 Mitigated C26 Adenocarcinoma–Induced Cancer Cachexia

Jong Min Park[1], *Young Min Han*[2], *Ho Jae Lee*[3], *Yong Jin Park*[4] *and Ki Baik Hahm*[5,6]*

[1]College of Oriental Medicine, Daejeon University, Daejeon, South Korea, [2]Seoul Center, Korea Basic Science Institute, Seoul, South Korea, [3]Lee Gil Ya Cancer and Diabetes Institute, University of Gachon, Incheon, South Korea, [4]GI Medics, Seoul, South Korea, [5]CHA Cancer Preventive Research Center, CHA Bio Complex, Pangyo, South Korea, [6]Medpacto Research Institute, Medpacto, Seoul, South Korea

Nicotinamide riboside (NR), vitamin B3, is a substrate for nicotinamide adenine dinucleotide (NAD^+)–consuming enzymes and is a coenzyme for hydride-transfer enzymes, including adenosine diphosphate (ADP)–ribose transferases, poly (ADP-ribose) polymerases, cADP-ribose synthases, and sirtuins, which play a central role in the aging process, neurodegenerative processes, and myopathy. Since cancer cachexia is a disease condition presenting with weight loss, skeletal muscle atrophy, and loss of adipose tissue in patients with advanced cancer, we hypothesized that NR intake could ameliorate sarcopenia. In this study, we investigated whether preemptive administration of NR ameliorated C26 adenocarcinoma–induced cancer cachexia and explored anti-cachexic mechanisms focused on the changes in muscle atrophy, cachexic inflammation, and catabolic catastrophe. Dietary intake of the NR-containing pellet diet significantly attenuated cancer cachexia in a mouse model. Starting with significant inhibition of cachexic factors, tumor necrosis factor alpha, and interleukin-6, NR significantly inhibited muscle-specific ubiquitin-proteasome ligases, such as atrogin-1, muscle RING-finger protein-1 (MuRF-1), mitofusin-2, and peroxisome proliferator–activated receptor gamma coactivator-1-alpha (PCG-1α). Significant inhibition of epididymal fat lipolysis was noted with significant inhibition of adipose triglyceride lipase (ATGL) gene. Furthermore, NR administration significantly increased the levels of crucial enzymes involved in the biosynthesis of NAD^+ and nicotinamide phosphoribosyl transferase and significantly inhibited the NAD^+-sensitive deacetylase sirtuin 1 (SIRT1). Preemptive intake of NR in patients vulnerable to cachexia can be a preemptive option to ameliorate cancer cachexia.

Keywords: nicotinamide ribose, cancer cachexia, NAMPT1, sarcopenia, muscle atrophy, inflammation

OPEN ACCESS

Edited by:
Predrag Sikiric,
University of Zagreb, Croatia

Reviewed by:
Gabor Varga,
Semmelweis University, Hungary
Klara Gyires,
Semmelweis University, Hungary

***Correspondence:**
Ki Baik Hahm
hahmkb@hotmail.com
hahmkb@medpacto.com

Specialty section:
This article was submitted to Gastrointestinal and Hepatic Pharmacology, a section of the journal Frontiers in Pharmacology

Received: *08 February 2021*
Accepted: *02 June 2021*
Published: *28 June 2021*

Citation:
Park JM, Han YM, Lee HJ, Park YJ and Hahm KB (2021) Nicotinamide Riboside Vitamin B3 Mitigated C26 Adenocarcinoma–Induced Cancer Cachexia. Front. Pharmacol. 12:665493. doi: 10.3389/fphar.2021.665493

INTRODUCTION

Cancer cachexia is characterized by a significant reduction in body weight, resulting predominantly from loss of skeletal muscle and adipose tissue in patients with advanced cancer. Since complete treatment of cancer as well as the associated and complicated cachexia, except for the early detection of cancer, is not easy, and recovery from the underlying condition causing cancer is impregnable, troublesome cancer cachexia is an unmet medical need. Therefore, as a scientific approach to cancer cachexia, many attempts have been made to inhibit cancer cachexia by targeting the inflammatory cytokines, tumor necrosis factor alpha (TNF-α) and interleukin (IL)-6. Downstream of these cytokine-associated cachexic factors, muscle atrophy–associated genes, such as *muscle RING-*

finger protein-1 (*MuRF-1*) and *atrogin-1*, resulting from the induction of the ubiquitin-proteasome system (UPS) *E3 ligase* genes that mediate the degradation of myofibrillar proteins through the ubiquitin-proteasome pathway, lead to multiple catabolic catastrophes and weaknesses; several approaches are under investigation, for instance, exercise, nutritional intervention, appetite improvement, and some phytochemicals; however, a solution is not available.

The role of nicotinamide adenine dinucleotide (NAD^+) metabolism in health and disease is of increased interest because nicotinamide can protect tissues, and NAD^+ metabolism has been implicated in a variety of disease states in addition to extending the lifespan (Belenky et al., 2007; Sauve, 2008). As a result, enzymes including poly (ADP-ribose) polymerases (PARP), mono-ADP-ribosyltransferases, and *sirtuin* and/or NAD^+ metabolism could be targeted for the therapeutic benefit of patients with cachexia and sarcopenia because the NAD^+ precursor, NR, has been implicated in improving myopathy and muscle atrophy (Bogan and Brenner, 2008).

In this study, under the hypothesis that NR supplementation can ameliorate sarcopenia in relation to cancer cachexia, we administered NR-containing pellet diets preemptively in C26 adenocarcinoma–induced cancer cachexia mice models and found that dietary administration of NR can be a preemptive treatment in patients who are at high risk for cancer cachexia.

MATERIALS AND METHODS

Cell Cultures

Mouse colon carcinoma cells, Colon26 (C26) cells, were obtained from Cell Lines Service GmbH (CLS, Eppelheim, Baden-Württemberg, Germany) and maintained according to the CLS's instructions. C26 cells were maintained in RPMI-1640 medium containing 10% fetal bovine serum (FBS, Sigma-Aldrich, St Louis, MO, United States) and 1% antibiotic antimycotic solution (Sigma-Aldrich, St Louis, MO, United States) at 37°C in a humidified atmosphere composed 5% CO_2 incubator.

Nicotinamide Riboside–Containing Pellet Diets

We administered a mouse diet supplemented with NR at 200 or 400 mg/kg daily for 3 weeks as pellet diet.

Animal Experimental Procedure for Cancer Cachexia

Six-week-old male *Balb/c* mice (total $n = 40$, Orient Animal, Seoul, Korea) were randomly divided into four groups: normal group ($n = 10$), cachectic C26 adenocarcinoma–bearing group ($n = 10$), cachectic C26 adenocarcinoma–bearing group with 200 mg/kg containing pellet diets ($n = 10$), and cachectic C26 adenocarcinoma–bearing group with 400 mg/kg containing pellet diets ($n = 10$). Cachectic C26 adenocarcinoma–bearing groups were shaved on the legs side and injected in their right flank with 1×10^7 C26 cells. According to the method of Acharyya et al. (2004) and Murphy et al. (2013)with minor modifications, cells were counted using a hemocytometer, suspended in 100 µl of sterilized phosphate-buffered saline and then C26 cells were injected into the mice. For 3 weeks, we fed a normal pellet diet or pellet diet with NR with daily measurement of intake. We restricted feeds to 100 g per group to measure reduced food intake due to anorexia. Following this experimental regimen, mice were monitored every 3 days, including body weight and food intake. Leg muscles were isolated and subjected to further histologic examination, enzyme-linked immunosorbent assay (ELISA), Western blotting, and reverse transcription polymerase chain reaction (RT-PCR). Animal studies were carried out in accordance with protocols approved by the Institutional Animal Care and Use Committee of CHA University CHA Bio Complex after IRB approval (IACAC 2019-0601).

Enzyme-Linked Immunosorbent Assay

On day 21 of the experiments, the mice were sacrificed. After the sacrifice of the animals, blood was collected for ELISA assay. After centrifugation at 3,000 rpm, 4°C for 30 min, the IL-6 and TNF-α levels in the supernatant were measured by ELISA, and concentration of IL-6/TNF-α is expressed as pg/mg protein. The process was performed strictly as prescribed in IL-6 or TNF-α ELISA kit manuscript (R&D SYSTEM, Minneapolis, MN, United States). All samples were measured at individual levels, and each sample was analyzed in triplicate manner, taking a mean of the three determinations.

Reverse Transcription-PCR

Total RNA was isolated from leg muscle tissues using TRIzol reagent (Life Technologies, Milan, Italy), and 1–5 mg of each total RNA was transcribed to cDNA using cDNA synthesis kit (TOYOBO, Osaka, Japan). The PCR mixture contained 2× PCR MasterMix (Bioneer, Daejeon, South Korea), autoclaved water, primer (10 pmole/lL), and cDNA in final volume of 20 µl. PCR was performed over 30 cycles of 94°C for 30 s, 52°C for 30 s, and 72°C for 30 s. Oligonucleotide primers were purchased from Bioneer (Daejeon, South Korea). Oligonucleotide primers for IL-6, Atrogin-1, MuRF-1, Mfn-2, and GAPDH are shown in **Table 1**. Each PCR product was directly loaded onto 1.5% agarose gels and stained with Redsafe (iNtRON Biotechnology, Cheonan, South Korea).

Western Blot Analysis and Antibodies

Extracted tissues were washed twice with PBS and then lysed in ice-cold cell lysis buffer (Cell Signaling Technology, Denver, MA, United States) containing 1 mM phenylmethylsulfonyl fluoride (PMSF, Sigma-Aldrich, St Louis, MO, United States). After 20 min of incubation, samples were centrifuged at 10,000 × g for 10 min. Supernatants were then collected. Proteins in lysates were separated by sodium dodecyl sulfate polyacrylamide gel electrophoresis (SDS-PAGE) and transferred to polyvinylidene fluoride (PVDF) membranes, which were incubated with primary

TABLE 1 | Primer sequences in this experiment.

Primer	Forward	Reverse
IL-6	GGGACTGATGCTGGTGACAA	TAACGCACTAGGTTTGCCGA
Mfn-2	GCTCGGAGGCACATGAAAGT	ATCACGGTGCTCTTCCCATT
Atrogin-1	CTGAATAGCATCCAGATCAGCAGG	TTGATAAAGTCTTGAGGGGAAAGTG
MuRF-1	AAATGCTATGGAGAACCTGGA	GTCCTTGGAAGATGCTTTGTAA
GAPDH	AATGTATCCGTTGTGGATCT	TCCACCACCCTGTTGCTGTA

antibodies, washed, incubated with peroxidase-conjugated secondary antibodies, rewashed, and then visualized using an enhanced chemiluminescence (ECL) system (GE Healthcare, Buckinghamshire, United Kingdom) and the relative amounts of proteins associated with specific antibody were quantified using Lumi Vision Imager software (TAITEC). Primary antibodies for Western blotting against NAMPT1, SIRT1, Pax7, ubiquitin, p-p38, ATGL (adipose triglyceride lipase), PARP-1, caspase-8, Bax, and Cyt c were from Cell Signaling Technology (Danvers, MA, United States). Antibodies against MuRF-1 (muscle ring-finger protein-1), Mfn-2 (mitofusin-2), p-AMPKα 1/2, PGC-1α (peroxisome proliferator–activated receptor gamma coactivator-1-alpha), p-JNK, p-ERK, and β-actin were from Santa Cruz Biotechnology (Dallas, TX, United States) Antibody against Atrogin-1 was from ECM biosciences (Versailles, KY, United States). Anti-mouse and anti-rabbit horseradish peroxidase–conjugated secondary antibodies were from Cell Signaling (Danvers, MA, United States).

Statistics

Statistical analysis results are expressed as the mean standard deviation (SD). Statistical analyses were conducted with GraphPad Prism (GraphPad Software, La Jolla, CA, United States) and SPSS software (version 12.0; SPSS Inc., Chicago, IL, United States). Statistical significance between groups was determined by a multivariate test, Kruskal–Wallis test. Statistical significance was accepted at $p < 0.05$.

RESULTS

Nicotinamide Riboside–Containing Pellet Diet Ameliorated C26 Adenocarcinoma–Induced Cancer Cachexia Irrespective of the Size/Volume of Transplanted Tumors

As shown in **Figure1A**, four groups ($n = 10$/group) were included as follows: normal control, cancer cachexia control, and cancer cachexia administered 200 mg/kg NR and 400 mg/kg NR as pellets in their daily diet. The experiments continued until 3 weeks after C26 cell administration because 20% weight loss was noted in the cachexia control group (25–30% weight loss around 4 weeks led to mortality in some). Although there were no significant differences in the transplanted C26 cells between groups, weight changes were significantly different between the control group and the groups administered the NR-containing pellet diet ($p < 0.05$, **Figure 1B**). Significant differences in body weight were evident in both leg muscles and general mouse morphology. As seen in **Figure 1C**, the thigh and gastrocnemius muscles were significantly decreased in the cachexia group 2, whereas they were well-preserved in the NR-administered group, Group 3 and Group 4 ($p < 0.01$, **Figure 1C**). However, when measuring each tumor growth on the buttocks, no significant difference in either tumor volume or tumor size was observed (**Figure 1D**), indicating that the NR diet prevented C26 adenocarcinoma–induced muscle atrophy.

Nicotinamide Riboside Significantly Decreased Cachexic Cytokines, Tumor Necrosis Factor Alpha, and Interleukin-6

TNF-α and IL-6 are well-known cytokines that provoke cancer cachexia in the C26 adenocarcinoma model, where we measured the serum levels of both. As seen in **Figure 2**, the levels of TNF-α and IL-6 were significantly increased in the cachexia control group than in the normal control group ($p < 0.01$). However, groups 3 and 4 that were administered 200 mg or 400 mg/kg NR mixed in pellet diet presented significantly decreased TNF-α and IL-6 levels ($p < 0.01$).

Changes in Mitogen-Activated Protein Kinase and Muscle-specific Mediators

Among mitogen-activated protein kinases (MAPKs), cancer cachexia was significantly associated with the activation of either extracellular-signal regulated kinase 1/2 (ERK1/2) or c-Jun N-terminal kinase (JNK) (**Figure 3A**). ERK1/2 and JNK phosphorylation was significantly increased in group 2, whereas both kinases were significantly inactivated by NR administration (**Figure 3A**). Nicotinamide phosphoribosyl transferase (NAMPT), an enzyme essential for maintaining the NAD^+ pool utilizing nicotinamide riboside kinase 1 (NRK1) to synthesize NAD^+ from NAD^+ precursors (Schondorf et al., 2018), was significantly reduced in group 2, but was restored in the NR group. SIRT1 expression was significantly increased in group 2, but attenuated in the group treated with NR (**Figure 3B**). In contrast, although SIRT1 has been known to stimulate muscle regeneration, in our investigation, SIRT1 was significantly increased in cancer cachexia, whereas its level was significantly decreased in the group treated with NR ($p < 0.001$, **Figure 3C**), reflecting the fact that the elevation of SIRT1 might be due to

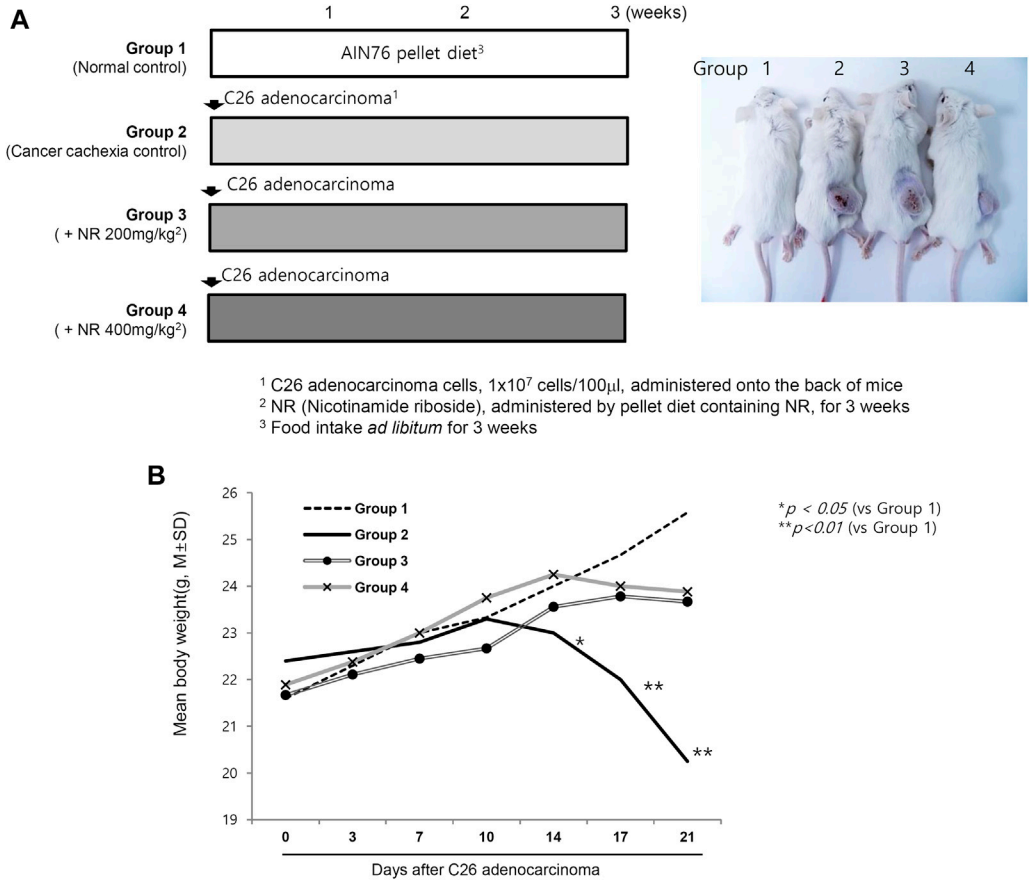

FIGURE 1 | Dietary intake of NR as pellet diet to mitigate C26 adenocarcinoma–induced cancer cachexia. **(A)** Schematic protocol for experiment *Balb/c* mice were administered with 1×10^7 cells/ml on side of abdomen. Right picture shows representational tumors according to the groups. Tumor growth did not differ according to the groups. **(B)** Daily measurement of body weight according to the groups. Body weights after 2 weeks were significantly decreased in Group 2 compared to Group 3 and Group 4. **(C)** Representational gross morphology of thigh including gastrocnemius muscle. Significant atrophy was noted in Group 2 ($p < 0.01$). Using imaging analysis, individual muscle mass of leg was measured and averaged according to the groups. The mean size and volume of resected C26 adenocarcinoma xenograft after 3 weeks. **(D)** Mean tumor volume and tumor masses according to the groups. Though different in body weights and general condition, NR administration did not affect either tumor volume or tumor masses. Though omitted, the mean amounts of daily food intake were not differed according to the groups, suggesting that changes in either appetite or food consumption was not differed according to the groups.

compensatory mechanism against muscle atrophy (Toledo et al., 2011).

Changes in Muscle-specific Ubiquitin-Proteasome System and Muscle-Related Genes

Muscle-specific UPS, *atrogin-1* and *MuRF-1*, were significantly increased in group 2, signifying that muscle-specific ubiquitin-proteasome ligase was enhanced during muscle atrophy in cancer cachexia (**Figure 4A**). NR treatment significantly decreased *atrogin-1* and *MuRF-1*, resulting in decreased ubiquitin ligase activity in the group treated with NR. Pax7, a transcription factor implicated in muscle atrophy, was significantly increased in group 2 but significantly attenuated in the group treated with NR (**Figure 4B**). PCG-1α, a marker for muscle regeneration, was significantly decreased in group 2 but was restored in the group treated with NR (**Figure 4C**). Mitofusin-2, which reflects mitochondrial activity, was significantly increased in group 2, signifying that the degradation of muscle associated with cancer cachexia was significantly increased in group 2, but not in the NR-treated group (**Figure 4D**).

Lipolysis and Anti-Proliferation in Cancer Cachexia and Reversal With Nicotinamide Riboside

Similar to muscle atrophy, significant fat loss is a remarkable finding in cachexia. As shown in **Figure 5A**, the fat mass in the epididymal area was significantly decreased in cancer cachexia group 2 ($p < 0.01$), whereas epididymal fat was significantly preserved in the NR group. Adipose triacylglycerol lipase was significantly increased in group 2, leading to significant lipolysis in cancer cachexia, but was significantly decreased in the NR group (**Figure 5B**). Further exploration of apoptotic executors and substrate revealed the significant increase in caspase-1,

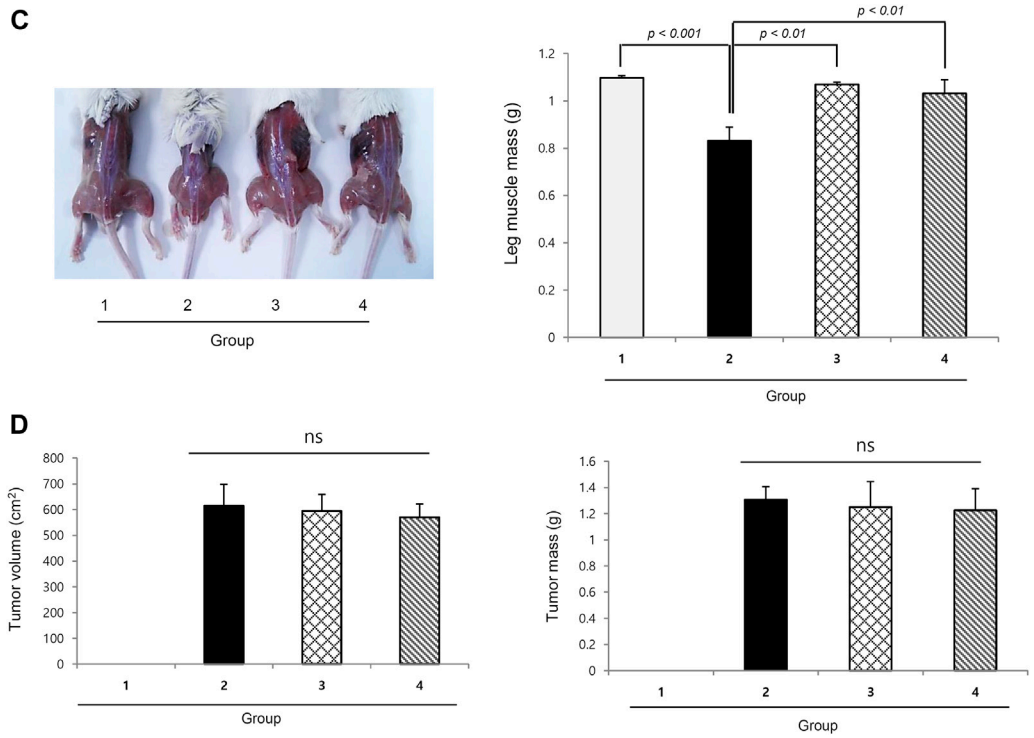

FIGURE 1 | (Continued).

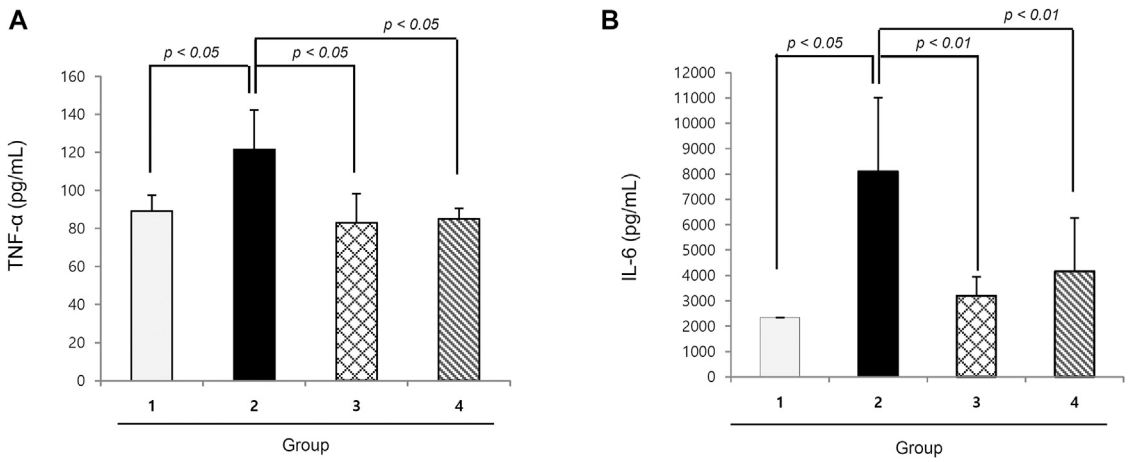

FIGURE 2 | Mean sera levels of cachexic cytokines, TNF-α and IL-6 according to the groups **(A)** TNF-α and **(B)** IL-6. TNF-α and IL-6 were significantly increased in Group 2, cancer cachexia group. Their levels were significantly decreased in the group treated with NR administration.

Bcl-2–associated X protein (Bax), and PARP-1 in group 2, but a significant decrease in the group treated with NR (**Figure 5C**).

DISCUSSION

About half of all cancer patients exhibit cachexia accompanied with anorexia, loss of body fat, and sarcopenia (Suzuki et al., 2013). Cachexia alone indicates poor quality of life, which could lead to severe weight loss during chemotherapy. Many drugs, including appetite stimulants, such as ghrelin (a 28 amino acid orexigenic gut hormone), mimetics (Khatib et al., 2018; Mohammadi et al., 2019), thalidomide, cytokine inhibitors, such as MABp1 [a natural IgG1k human monoclonal antibody against IL-1α (Prado and Qian, 2019)], steroids, such as progesterone (Gharahdaghi et al., 2019; Solomon et al., 2019),

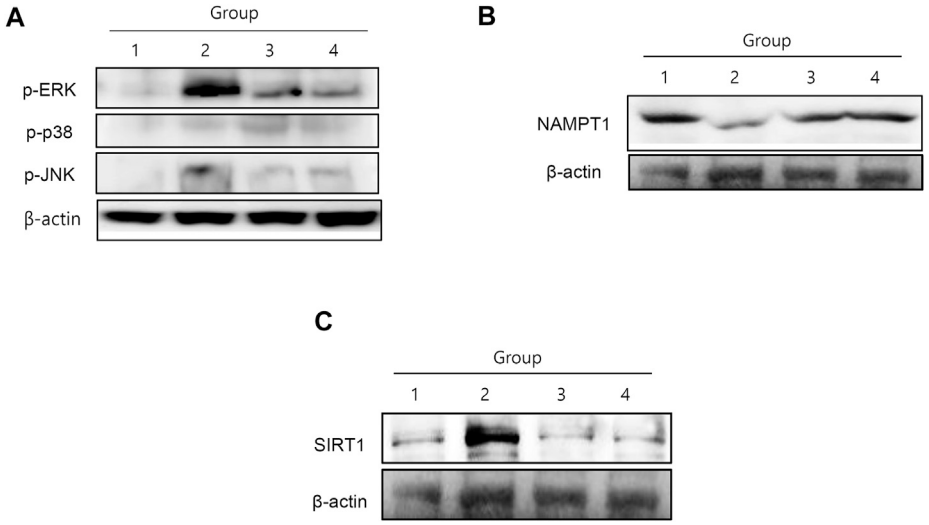

FIGURE 3 | MAPKs, NAMPT, and SIRT1 changes according to the group. **(A)** C26-induced cancer cachexia was associated either ERK and JNK activation, then NR administration significantly inactivated these cachexia-associated MAPKs. **(B)** NAMPT1 was significantly decreased in cancer cachexia group, suggesting incomplete conversion of NAD^+ in cancer cachexia, whereas NR administration maintained NAMPT1 expression. **(C)** SIRT1 was significantly increased in cancer cachexia group, but not in the NR-treated group, suggesting that NR administration did not affect SIRT1-mediated muscle atrophy.

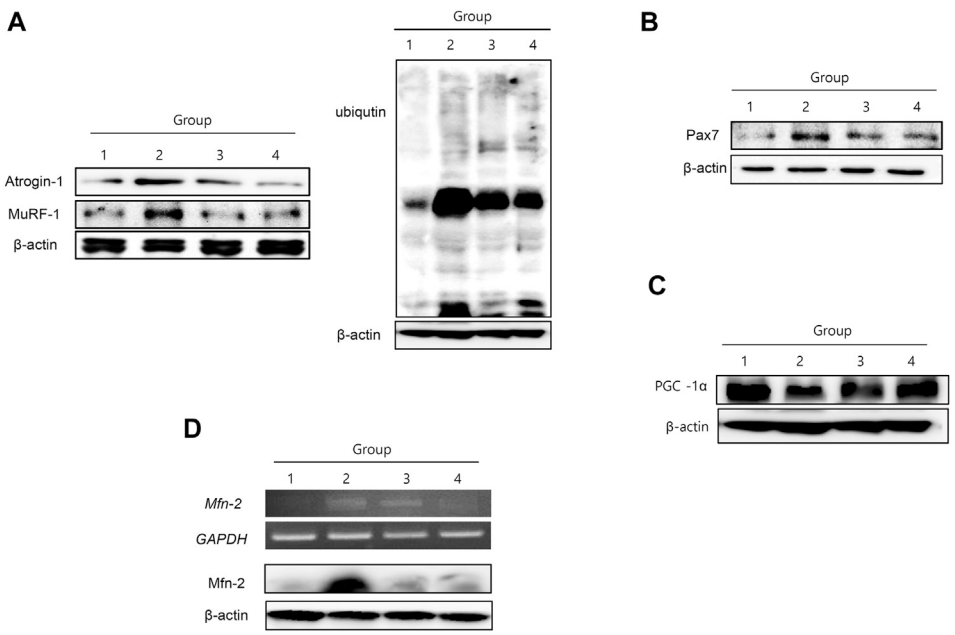

FIGURE 4 | Changes of muscle-specific UPS ligase atrogin-1 and MuRF-1, Pax 7, PCG-1α, and mitofucin-2. **(A)** Western blot for atrogin-1 and MuRF-1 according to the groups **(I)** and UPS ligase according to the groups blotted with ligase **(II)**. **(B)** Western blot for Pax7 and **(C)** Western blot for PCG-1α **(D)** RT-PCR and Western blot for mitofucin-2.

nonsteroidal anti-inflammatory drugs, such as celecoxib (Mantovani et al., 2010; Solheim et al., 2013), and branched-chain amino acids, such as leucine 2–4 g/day or eicosapentaenoic acids (Pappalardo et al., 2015; Prado et al., 2020; Storck et al., 2020), have been investigated in the clinic, whereas others are still under investigation (Ravasco, 2019). Although great progress has been made in understanding the underlying biological mechanisms of cachexia, further development is still awaited. In this miserable state, our current study clearly revealed the efficacious contribution of

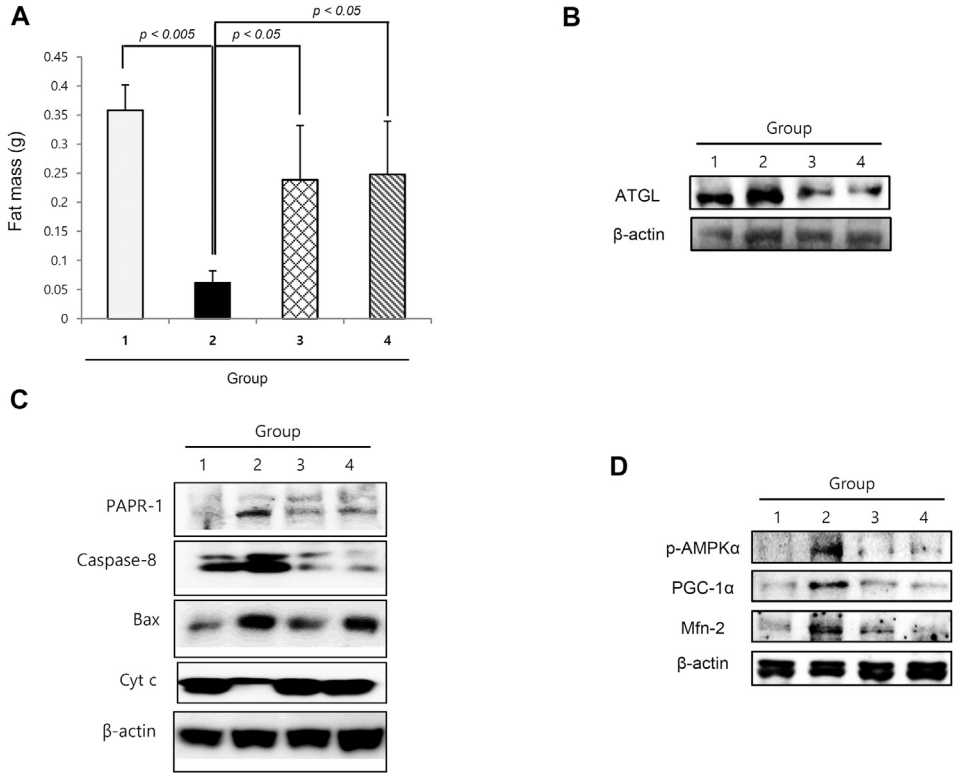

FIGURE 5 | Changes of fat status according to the groups. **(A)** Epididymal fat mass according to the groups. **(B)** Western blot for ATGL. **(C)** Western blot for apoptotic executors according to the groups. **(D)** Western blot for p-AMPKα, PCG-1α, and Mfn-2.

dietary NR supplementation in a cancer cachexia model in a preemptive manner (**Figure 6**).

Since NAD^+ availability may protect skeletal muscle from age-related metabolic decline, dietary supplementation with nicotinamide mononucleotide (NMN) and NR as NAD^+ precursors appears efficacious in elevating muscle NAD^+ (Fletcher et al., 2017). Therefore, skeletal muscle cells require NAMPT to maintain NAD^+ availability. NAMPT catalyzes the conversion of nicotinamide to NMN, which is associated with most of the NAD^+ formation.

As the pathogenesis of age- or cachexia-associated muscle declines, two key NAD^+ intermediates, including NR and NMN, have been studied over the past several years (Yoshino et al., 2018) because supplementation using these NAD^+ intermediates has shown preventive and therapeutic effects against aging and sarcopenia. Although not measured in this investigation, NRK1 is a rate-limiting enzyme for the use of exogenous NR for NAD^+ synthesis (Ratajczak et al., 2016). Since mammalian cells require the conversion of extracellular NMN to NR for cellular uptake and NAD^+ synthesis, we measured the changes in SIRT1 instead of NRK because NAD^+ is a vital redox cofactor and a substrate required for the activity of various enzyme families, including *sirtuin*s and PARP.

Since NR and NAD^+ also play important roles in the regulation of NAD^+-consuming enzymes, including *sirtuin*s, PARPs, and CD38/157 ectoenzymes, and NAD^+ biosynthesis mediated by NAMPT and SIRT1 function together to regulate metabolism, NAD^+ levels decline during cachexia, causing defects in mitochondrial functions and resulting in sarcopenia (Imai and Guarente, 2014). As seen in our investigation (**Figure 3B**), NAMPT expression in the cachexia group was significantly increased with NR administration, whereas SIRT1 levels decreased. Restoring NAD^+ by supplementing NR could dramatically ameliorate cachexia-associated sarcopenia and counteract cancer cachexia (Imai, 2010).

In **Figures 3B,C**, the contribution of dietary NR administration against cancer cachexia is shown through the changes in NAMPT and SIRT1. Curiously, NR administration decreased SIRT1 expression, which was unexpectedly increased in the cachexia group, a contradictory finding, because of the lack of muscle regeneration during muscle wasting in tumor-bearing animals *via* SIRT1 (Toledo et al., 2011). Pharmacological blockade of NADPH oxidase 4 (nox4), a key regulator of reactive oxygen species in muscle, significantly abrogated cancer cachexia in mice; targeting the SIRT1-nox4 axis seems to be an effective therapeutic intervention for mitigating cancer cachexia (Dasgupta et al., 2020). As an effect of SIRT1, nuclear factor kappa B (NF-κB) signaling is inhibited by deacetylation of the p65 subunit of NF-κB complex and stimulation of oxidative energy production via the activation of AMP-activated protein kinase, peroxisome proliferator–activated receptor-alpha,

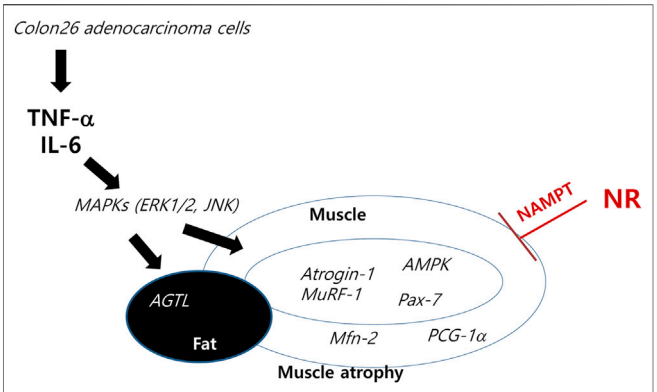

FIGURE 6 | Schematic presentation telling how NR intake tackles the cachexic process. Anti-cachexic effect of preemptive dietary intake of NR vitamin B3 in C26 adenocarcinoma–induced cancer cachexia. Preemptive administration of NR exerted significant protection from muscle atrophy, inflammation, and catabolic disaster featured in cancer cachexia.

and peroxisome proliferator–activated receptor gamma coactivator-1-alpha. Therefore, although SIRT1 inhibition disrupts oxidative energy metabolism and stimulates NF-κB-induced inflammatory responses, SIRT1 inhibition is associated with muscle preservation (Kauppinen et al., 2013).

Recently, Hulmi et al. reported about disturbed muscle NAD^+ homeostasis in experimental cancer cachexia (Hulmi et al., 2020). Muscle proteomics in C26 tumor–bearing (TB) cachectic mice revealed downregulated signatures for mitochondrial oxidative phosphorylation (OXPHOS) and increased acute-phase response (APR). These were accompanied by muscle NAD^+ deficiency, alterations in NAD^+ biosynthesis, and decreased muscle protein synthesis. Our findings supported these results such as NAD^+ depletion, muscle protein degradation, and the elevation of inflammatory cytokine in TB-mice. However, the induction of enzymes of the NAD^+ biosynthesis pathway such as NAMPT and the reduction of SIRT1, a conserved protein NAD^+-dependent deacetylase, in TB-mice are inconsistent with our study. Hulmi et al. collected samples 11 days after the C26 cell inoculation, but we collected samples 21 days after the C26 cell inoculation. In our study, the elevation of SIRT1 might be due to compensatory mechanism against muscle atrophy. Further research should also examine by time dependent manner.

The basic action of NR in mitigating cancer cachexia with NR administration, as shown in **Figure 2**, is significantly decreasing the levels of IL-6 and TNF-α. Different kinds of cancer cells are known to secrete IL-6, a candidate mediator of cachexia, and IL-6 levels correlate with weight loss in some cancer patients (Scott et al., 1996; Moses et al., 2009); moreover, increasing levels of IL-6 in tumor-bearing mice correlated with the development of cachexia (Strassmann et al., 1992). Even better than IL-6, TNF-α is a key inflammatory cytokine in cancer cachexia (Tracey and Cerami, 1994; Lu et al., 2020).

"Preemptive administration" is usually employed for pain control (Szedlak et al., 2018), including the application of multifactorial synergistic medication before pain development. In this condition, the absence of biomarkers that cause cachexia has currently led to a dependence on clinical findings. However, there had been several publications suggesting poor prognosis because of poor muscle mass, weight loss, and poor performance in cancer patients. To date, our study may be the only study showing preemptive efficacy in ameliorating cancer cachexia.

Lipolysis is also a prominent event implicated in cancer cachexia. Inadera et al. (2002) clarified the biological characteristics of a lipid-depleting factor in both 3T3-L1 adipocytes and C26-inoculated mouse cachexia model and found that a reduced quantity of mature sterol regulatory element–binding transcription factor-1, without affecting peroxisome proliferator-activated receptor (PPAR)-γ and CCAAT/enhancer binding protein (C/EBP)-α, resulted in increased lipolysis and reduced lipogenesis. SREBP-1 and C/EBP-alpha are key transcriptional factors involved in lipogenesis. SREBP-1 is a transcription factor that regulates lipid and fatty acid synthesis, energy storage, and acts as intercellular signaling nodes of convergence/divergence. C/EBP-alpha plays a significant role in adipocyte differentiation. For example, the transcription factor C/EBP-alpha is considered to be essential master regulators of adipogenesis. Similar findings were noted in the current study, but dietary NR significantly restored cachexia-induced fat loss under the same molecular changes. In another study by Bing et al. (2006) using a similar cachexia model of MAC16 tumors, adipose tissues from cachexic mice contained shrunken adipocytes and increased fibrosis, with similar findings observed in muscle tissue, causing shrinkage in size, decreased muscle bundles, and some fibrotic changes. Genetic analysis revealed major reductions in mRNA levels of adipogenic transcription factors, such as C/EBP-α and C/EBP-β, PPAR-γ, fatty acid synthase, acetyl-CoA carboxylase, stearoyl-CoA desaturase 1, glycerol-3-phosphate acyltransferase, and sterol regulatory element–binding transcription factor-1.

In conclusion, we found that preemptive dietary intake of NR in preclinical models of cancer cachexia can be a potential regimen to inhibit the occurrence of a catabolic catastrophe, cachexic inflammation, and muscle atrophy. A well-designed randomized clinical trial should be developed to study whether dietary intake of NR can cover the unmet medical needs in cancer cachexia.

In this study, we documented that dietary intake of NR, a vitamin B3, can be a feasible preemptive intervention in patients with advanced cancer who are vulnerable to cachexia. As summarized in **Figure 6**, C26 adenocarcinoma led to significant cancer cachexia accompanied by muscle degeneration with disturbed muscle regeneration, high TNF-α and IL-6 levels, MAPK activation leading to increased *atrogin-1*/*MuRF-1* levels, and lipolysis. However, preemptive administration of NR led to significant rescue from cancer cachexia. Considering the fact that more than 30% of patients with chronic illness die due to cachexia and more than 50% of patients with cancer because of cachexia, but not due to chemotherapeutic drugs or agents, our investigation revealed that preemptive and dietary intake of NR in patients at high risk of developing cancer cachexia can be a potential regimen to inhibit the occurrence of a catabolic catastrophe, cachexia inflammation, and muscle atrophy. However, well-designed RCTs should be developed for the unmet medical needs in cancer cachexia.

DATA AVAILABILITY STATEMENT

The raw data supporting the conclusion of this article will be made available by the authors, without undue reservation, to any qualified researcher.

ETHICS STATEMENT

The animal study was reviewed and approved by the Institutional Animal Care and Use Committee of CHA University CHA Bio Complex after IRB approval (IACAC 2019-0601).

AUTHOR CONTRIBUTIONS

Conceptualization and methodology, JP and HL; investigation, JP, YH, and HL; data analysis and interpretation, YP; writing and original draft preparation, KH.

FUNDING

This research was supported by the Daejeon University Research Grants (2019).

REFERENCES

Acharyya, S., Ladner, K. J., Nelsen, L. L., Damrauer, J., Reiser, P. J., Swoap, S., et al. (2004). Cancer Cachexia Is Regulated by Selective Targeting of Skeletal Muscle Gene Products. *J. Clin. Invest.* 114 (3), 370–378. doi:10.1172/JCI2017410.1172/jci200420174

Belenky, P., Bogan, K. L., and Brenner, C. (2007). NAD+ Metabolism in Health and Disease. *Trends Biochem. Sci.* 32 (1), 12–19. doi:10.1016/j.tibs.2006.11.006

Bing, C., Russell, S., Becket, E., Pope, M., Tisdale, M. J., Trayhurn, P., et al. (2006). Adipose Atrophy in Cancer Cachexia: Morphologic and Molecular Analysis of Adipose Tissue in Tumour-Bearing Mice. *Br. J. Cancer* 95 (8), 1028–1037. doi:10.1038/sj.bjc.6603360

Bogan, K. L., and Brenner, C. (2008). Nicotinic Acid, Nicotinamide, and Nicotinamide Riboside: A Molecular Evaluation of NAD+Precursor Vitamins in Human Nutrition. *Annu. Rev. Nutr.* 28, 115–130. doi:10.1146/annurev.nutr.28.061807.155443

Dasgupta, A., Shukla, S. K., Vernucci, E., King, R. J., Abrego, J., Mulder, S. E., et al. (2020). SIRT1-NOX4 Signaling axis Regulates Cancer Cachexia. *J. Exp. Med.* 217 (7). doi:10.1084/jem.20190745

Fletcher, R. S., Ratajczak, J., Doig, C. L., Oakey, L. A., Callingham, R., Da Silva Xavier, G., et al. (2017). Nicotinamide Riboside Kinases Display Redundancy in Mediating Nicotinamide Mononucleotide and Nicotinamide Riboside Metabolism in Skeletal Muscle Cells. *Mol. Metab.* 6 (8), 819–832. doi:10.1016/j.molmet.2017.05.011

Gharahdaghi, N., Rudrappa, S., Brook, M. S., Idris, I., Crossland, H., Hamrock, C., et al. (2019). Testosterone Therapy Induces Molecular Programming Augmenting Physiological Adaptations to Resistance Exercise in Older Men. *J. Cachexia, Sarcopenia Muscle* 10 (6), 1276–1294. doi:10.1002/jcsm.12472

Hulmi, J. J., Penna, F., Pöllänen, N., Nissinen, T. A., Hentilä, J., Euro, L., et al. (2020). Muscle NAD+ Depletion and Serpina3n as Molecular Determinants of Murine Cancer Cachexia-The Effects of Blocking Myostatin and Activins. *Mol. Metab.* 41, 101046. doi:10.1016/j.molmet.2020.101046

Imai, S.-i. (2010). A Possibility of Nutriceuticals as an Anti-aging Intervention: Activation of Sirtuins by Promoting Mammalian NAD Biosynthesis. *Pharmacol. Res.* 62 (1), 42–47. doi:10.1016/j.phrs.2010.01.006

Imai, S.-i., and Guarente, L. (2014). NAD+ and Sirtuins in Aging and Disease. *Trends Cel Biol.* 24 (8), 464–471. doi:10.1016/j.tcb.2014.04.002

Inadera, H., Nagai, S., Dong, H.-Y., and Matsushima, K. (2002). Molecular Analysis of Lipid-Depleting Factor in a colon-26-inoculated Cancer Cachexia Model. *Int. J. Cancer* 101 (1), 37–45. doi:10.1002/ijc.10578

Kauppinen, A., Suuronen, T., Ojala, J., Kaarniranta, K., and Salminen, A. (2013). Antagonistic Crosstalk between NF-Kb and SIRT1 in the Regulation of Inflammation and Metabolic Disorders. *Cell Signal.* 25 (10), 1939–1948. doi:10.1016/j.cellsig.2013.06.007

Khatib, M. N., Gaidhane, A., Gaidhane, S., and Quazi, Z. S. (2018). Ghrelin as a Promising Therapeutic Option for Cancer Cachexia. *Cell Physiol Biochem* 48 (5), 2172–2188. doi:10.1159/000492559

Lu, S., Zhang, Y., Li, H., Zhang, J., Ci, Y., and Han, M. (2020). Ginsenoside Rb1 Can Ameliorate the Key Inflammatory Cytokines TNF-α and IL-6 in a Cancer Cachexia Mouse Model. *BMC Complement. Med. Ther.* 20 (1), 11. doi:10.1186/s12906-019-2797-9

Mantovani, G., Macciò, A., Madeddu, C., Serpe, R., Antoni, G., Massa, E., et al. (2010). Phase II Nonrandomized Study of the Efficacy and Safety of COX-2 Inhibitor Celecoxib on Patients with Cancer Cachexia. *J. Mol. Med.* 88 (1), 85–92. doi:10.1007/s00109-009-0547-z

Mohammadi, E. N., Pietra, C., Giuliano, C., Fugang, L., and Greenwood-Van Meerveld, B. (2019). A Comparison of the Central versus Peripheral Gastrointestinal Prokinetic Activity of Two Novel Ghrelin Mimetics. *J. Pharmacol. Exp. Ther.* 368 (1), 116–124. doi:10.1124/jpet.118.250738

Moses, A. G., Maingay, J., Sangster, K., Fearon, K. C., and Ross, J. A. (2009). Pro-inflammatory Cytokine Release by Peripheral Blood Mononuclear Cells from Patients with Advanced Pancreatic Cancer: Relationship to Acute Phase Response and Survival. *Oncol. Rep.* 21 (4), 1091–1095. doi:10.3892/or_00000328

Murphy, K. T., Chee, A., Trieu, J., Naim, T., and Lynch, G. S. (2013). Inhibition of the Renin-Angiotensin System Improves Physiological Outcomes in Mice with Mild or Severe Cancer Cachexia. *Int. J. Cancer* 133 (5), 1234–1246. doi:10.1002/ijc.28128

Pappalardo, G., Almeida, A., and Ravasco, P. (2015). Eicosapentaenoic Acid in Cancer Improves Body Composition and Modulates Metabolism. *Nutrition* 31 (4), 549–555. doi:10.1016/j.nut.2014.12.002

Prado, B. L., and Qian, Y. (2019). Anti-cytokines in the Treatment of Cancer Cachexia. *Ann. Palliat. Med.* 8 (1), 67–79. doi:10.21037/apm.2018.07.06

Prado, C. M., Purcell, S. A., and Laviano, A. (2020). Nutrition Interventions to Treat Low Muscle Mass in Cancer. *J. Cachexia, Sarcopenia Muscle* 11 (2), 366–380. doi:10.1002/jcsm.12525

Ratajczak, J., Joffraud, M., Trammell, S. A. J., Ras, R., Canela, N., Boutant, M., et al. (2016). NRK1 Controls Nicotinamide Mononucleotide and Nicotinamide Riboside Metabolism in Mammalian Cells. *Nat. Commun.* 7, 13103. doi:10.1038/ncomms13103

Ravasco, P. (2019). Nutrition in Cancer Patients. *Jcm* 8 (8), 1211. doi:10.3390/jcm8081211

Sauve, A. A. (2008). NAD+and Vitamin B3: From Metabolism to Therapies. *J. Pharmacol. Exp. Ther.* 324 (3), 883–893. doi:10.1124/jpet.107.120758

Schöndorf, D. C., Ivanyuk, D., Baden, P., Sanchez-Martinez, A., De Cicco, S., Yu, C., et al. (2018). The NAD+ Precursor Nicotinamide Riboside Rescues Mitochondrial Defects and Neuronal Loss in iPSC and Fly Models of Parkinson's Disease. *Cel Rep.* 23 (10), 2976–2988. doi:10.1016/j.celrep.2018.05.009

Scott, H., McMillan, D., Crilly, A., McArdle, C., and Milroy, R. (1996). The Relationship between Weight Loss and Interleukin 6 in Non-small-cell Lung Cancer. *Br. J. Cancer* 73 (12), 1560–1562. doi:10.1038/bjc.1996.294

Solheim, T. S., Fearon, K. C. H., Blum, D., and Kaasa, S. (2013). Non-steroidal Anti-inflammatory Treatment in Cancer Cachexia: a Systematic Literature Review. *Acta Oncologica* 52 (1), 6–17. doi:10.3109/0284186X.2012.724536

Solomon, Z. J., Mirabal, J. R., Mazur, D. J., Kohn, T. P., Lipshultz, L. I., and Pastuszak, A. W. (2019). Selective Androgen Receptor Modulators: Current Knowledge and Clinical Applications. *Sex. Med. Rev.* 7 (1), 84–94. doi:10.1016/j.sxmr.2018.09.006

Storck, L. J., Ruehlin, M., Gaeumann, S., Gisi, D., Schmocker, M., Meffert, P. J., et al. (2020). Effect of a Leucine-Rich Supplement in Combination with Nutrition and Physical Exercise in Advanced Cancer Patients: A Randomized Controlled Intervention Trial. *Clin. Nutr.* 39, 3637–3644. doi:10.1016/j.clnu.2020.04.008

Strassmann, G., Fong, M., Kenney, J. S., and Jacob, C. O. (1992). Evidence for the Involvement of Interleukin 6 in Experimental Cancer Cachexia. *J. Clin. Invest.* 89 (5), 1681–1684. doi:10.1172/JCI115767

Suzuki, H., Asakawa, A., Amitani, H., Nakamura, N., and Inui, A. (2013). Cancer Cachexia-Pathophysiology and Management. *J. Gastroenterol.* 48 (5), 574–594. doi:10.1007/s00535-013-0787-0

Szedlák, B., Mitre, C., and Fülesdi, B. (2018). Preemptív És Preventív Analgesia - a Perioperatív Fájdalomcsillapítás Fontos Eleme. *Orvosi Hetilap* 159 (17), 655–660. doi:10.1556/650.2018.31045

Toledo, M., Busquets, S., Ametller, E., López-Soriano, F. J., and Argilés, J. M. (2011). Sirtuin 1 in Skeletal Muscle of Cachectic Tumour-Bearing Rats: a Role in Impaired Regeneration?. *J. Cachexia Sarcopenia Muscle* 2 (1), 57–62. doi:10.1007/s13539-011-0018-6

Tracey, K. J., and Cerami, A. (1994). Tumor Necrosis Factor: a Pleiotropic Cytokine and Therapeutic Target. *Annu. Rev. Med.* 45, 491–503. doi:10.1146/annurev.med.45.1.491

Yoshino, J., Baur, J. A., and Imai, S.-i. (2018). NAD+ Intermediates: The Biology and Therapeutic Potential of NMN and NR. *Cel Metab.* 27 (3), 513–528. doi:10.1016/j.cmet.2017.11.002

Conflict of Interest: Although Author YP was employed by the company GI medis, the author has and decleares that no support, financial or otherwise, has been received from any organization that may have an interest in the submitted work.

The remaining authors declare that the research was conducted in the absence of any commercial or financial relationships that could be construed as a potential conflict of interest.

frontiers in Pharmacology

REVIEW
published: 29 June 2021
doi: 10.3389/fphar.2021.627533

Stable Gastric Pentadecapeptide BPC 157 and Wound Healing

*Sven Seiwerth[1], Marija Milavic[1], Jaksa Vukojevic[2], Slaven Gojkovic[2], Ivan Krezic[2], Lovorka Batelja Vuletic[1], Katarina Horvat Pavlov[1], Andrea Petrovic[1], Suncana Sikiric[1], Hrvoje Vranes[2], Andreja Prtoric[3], Helena Zizek[2], Tajana Durasin[2], Ivan Dobric[3], Mario Staresinic[3], Sanja Strbe[2], Mario Knezevic[2], Marija Sola[2], Antonio Kokot[4], Marko Sever[3], Eva Lovric[1], Anita Skrtic[1], Alenka Boban Blagaic[2] and Predrag Sikiric[2]**

[1]Department of Pathology, School of Medicine, University of Zagreb, Zagreb, Croatia, [2]Department of Pharmacology, School of Medicine, University of Zagreb, Zagreb, Croatia, [3]Department of Surgery, School of Medicine, University of Zagreb, Zagreb, Croatia, [4]Department of Anatomy and Neuroscience, School of Medicine Osijek, University of Osijek, Osijek, Croatia

Significance: The antiulcer peptide, stable gastric pentadecapeptide BPC 157 (previously employed in ulcerative colitis and multiple sclerosis trials, no reported toxicity (LD1 not achieved)), is reviewed, focusing on the particular skin wound therapy, incisional/excisional wound, deep burns, diabetic ulcers, and alkali burns, which may be generalized to the other tissues healing.

Recent Advances: BPC 157 has practical applicability (given alone, with the same dose range, and same equipotent routes of application, regardless the injury tested).

Critical Issues: By simultaneously curing cutaneous and other tissue wounds (colocutaneous, gastrocutaneous, esophagocutaneous, duodenocutaneous, vesicovaginal, and rectovaginal) in rats, the potency of BPC 157 is evident. Healing of the wounds is accomplished by resolution of vessel constriction, the primary platelet plug, the fibrin mesh which acts to stabilize the platelet plug, and resolution of the clot. Thereby, BPC 157 is effective in wound healing much like it is effective in counteracting bleeding disorders, produced by amputation, and/or anticoagulants application. Likewise, BPC 157 may prevent and/or attenuate or eliminate, thus, counteract both arterial and venous thrombosis. Then, confronted with obstructed vessels, there is circumvention of the occlusion, which may be the particular action of BPC 157 in ischemia/reperfusion.

Future Directions: BPC 157 rapidly increases various genes expression in rat excision skin wound. This would define the healing in the other tissues, that is, gastrointestinal tract, tendon, ligament, muscle, bone, nerve, spinal cord, cornea (maintained transparency), and blood vessels, seen with BPC 157 therapy.

Keywords: stable gastric pentadecapeptide BPC 157, fistula, bleeding disorder, concept practical applicability, wound healing

OPEN ACCESS

Edited by:
Gabor Varga,
Semmelweis University, Hungary

Reviewed by:
Alexandra Mikó,
University of Pécs, Hungary
Zoltán S. Zádori,
Semmelweis University, Hungary

****Correspondence:***
Predrag Sikiric
sikiric@mef.hr

Specialty section:
This article was submitted to Gastrointestinal and Hepatic Pharmacology, a section of the journal Frontiers in Pharmacology

Received: *09 November 2020*
Accepted: *03 February 2021*
Published: *29 June 2021*

Citation:
Seiwerth S, Milavic M, Vukojevic J, Gojkovic S, Krezic I, Vuletic LB, Pavlov KH, Petrovic A, Sikiric S, Vranes H, Prtoric A, Zizek H, Durasin T, Dobric I, Staresinic M, Strbe S, Knezevic M, Sola M, Kokot A, Sever M, Lovric E, Skrtic A, Blagaic AB and Sikiric P (2021) Stable Gastric Pentadecapeptide BPC 157 and Wound Healing. Front. Pharmacol. 12:627533. doi: 10.3389/fphar.2021.627533

SCOPE AND SIGNIFICANCE

This stable gastric pentadecapeptide BPC 157 review (Seiwerth et al., 2018; Sikiric et al., 2020a; Sikiric et al., 2020b) is focused on the particular skin wound therapy, incisional/excisional wound (Seiwerth et al., 1997), deep burns (Mikus et al., 2001), diabetic ulcer (Tkalecevic et al., 2007), alkali burns (Huang et al., 2015), and healing of various other tissue types (Staresinic et al., 2003; Staresinic et al., 2006; Sever et al., 2009; Masnec et al., 2015; Becejac et al., 2018). The defensive system pertaining to

BPC 157 beneficial activities was already appraised in several reviews (Sikiric et al., 1993; Sikiric et al., 2006; Sikiric et al., 2010; Sikiric et al., 2011; Sikiric et al., 2012; Sikiric et al., 2013; Seiwerth et al., 2014; Sikiric et al., 2014; Sikiric et al., 2016; Sikiric et al., 2017; Kang et al., 2018; Seiwerth et al., 2018; Sikiric et al., 2018; Gwyer et al., 2019; Park et al., 2020; Sikiric et al., 2020a; Sikiric et al., 2020b). A particular topic is its role in mediating Robert gastric cytoprotection and endothelial maintenance (Sikiric et al., 2010; Sikiric et al., 2011; Sikiric et al., 2017; Sikiric et al., 2018), as well as its therapeutic effect in the gastrointestinal tract (Sikiric et al., 2010; Sikiric et al., 2011; Sikiric et al., 2012; Sikiric et al., 2017; Seiwerth et al., 2018; Sikiric et al., 2018; Sikiric et al., 2020a; Sikiric et al., 2020b), additionally acting as membrane stabilizer (Park et al., 2020), with particular reference to ulcerative colitis (Sikiric et al., 2011). Recently, to approach particular skin wound therapy, we and others reviewed the significance of its beneficial effect on muscle, tendon, ligament, and bone injuries (Gwyer et al., 2019; Seiwerth et al., 2018).

TRANSLATIONAL RELEVANCE

A special point confronts BPC 157 effectiveness with standard growth angiogenic factors, and their healing effects on the tendon, ligament, muscle, and bone lesions vs. their healing effects on gastrointestinal tract lesions (Seiwerth et al., 2018). Only BPC 157 has the same regimens, as used in the gastrointestinal healing studies, improving these lesions healing, accurately implementing its own healing angiogenic effect (Seiwerth et al., 2018). Additionally, we reviewed its particular effects, such as the non-steroidal anti-inflammatory drugs (NSAIDs) toxicity counteraction (Sikiric et al., 2013; Park et al., 2020), its relationship to the nitric oxide (NO)-system (Sikiric et al., 2014), and blood vessels (Sikiric et al., 2006; Seiwerth et al., 2014; Sikiric et al., 2018), and its role in the brain–gut and gut–brain axis (Sikiric et al., 2016), along with its CNS-disturbances therapy (Sikiric et al., 2016) and stress disorders (Sikiric et al., 2017; Sikiric et al., 2018).

CLINICAL RELEVANCE

As mentioned, the significance of its particular skin wound therapy was not especially reviewed. Namely, BPC 157 is always applied alone (i.e., its own effect ascribed only to the peptide (for review, see Sikiric et al., 1993; Sikiric et al., 2006; Sikiric et al., 2010; Sikiric et al., 2011; Sikiric et al., 2012; Sikiric et al., 2013; Seiwerth et al., 2014; Sikiric et al., 2014; Sikiric et al., 2016; Sikiric et al., 2017; Seiwerth et al., 2018; Kang et al., 2018; Sikiric et al., 2018; Gwyer et al., 2019; Sikiric et al., 2020a; Sikiric et al., 2020b). Unlike growth factors peptides, which need carrier(s) addition, and are rapidly degraded in human gastric juice, BPC 157, as an antiulcer peptide, is native and resistant to human gastric juice exciding one day period (Sikiric et al., 1993; Sikiric et al., 2006; Sikiric et al., 2010; Sikiric et al., 2011; Sikiric et al., 2012; Sikiric et al., 2013; Seiwerth et al., 2014; Sikiric et al., 2014; Sikiric et al., 2016; Sikiric et al., 2017; Kang et al., 2018; Seiwerth et al., 2018; Sikiric et al., 2018; Gwyer et al., 2019; Park et al., 2020; Sikiric et al., 2020a; Sikiric et al., 2020b). Therefore, BPC 157 practical applicability (given alone, with the same dose range, and the same equipotent routes of application, regardless of the injury tested) could be clearly generalized and used in the wound healing therapy.

BACKGROUND OR OVERVIEW

Stable gastric pentadecapeptide BPC 157 is still far less investigated (Sikiric et al., 1993; Sikiric et al., 2006; Sikiric et al., 2010; Sikiric et al., 2011; Sikiric et al., 2012; Sikiric et al., 2013; Seiwerth et al., 2014; Sikiric et al., 2014; Sikiric et al., 2016; Sikiric et al., 2017; Kang et al., 2018; Seiwerth et al., 2018; Sikiric et al., 2018; Gwyer et al., 2019; Park et al., 2020; Sikiric et al., 2020a; Sikiric et al., 2020b) than the generally established angiogenic growth factors, epidermal growth factor (EGF), basic fibroblast growth factor (bFGF), and vascular endothelial growth factor (VEGF) (Tarnawski and Ahluwalia, 2012; Deng et al., 2013). Originally, BPC 157 appears as a cytoprotective antiulcer peptide, stable in human gastric juice, previously employed in ulcerative colitis clinical trials and now in those concerning multiple sclerosis (Sikiric et al., 1993; Sikiric et al., 2006; Sikiric et al., 2010; Sikiric et al., 2011; Sikiric et al., 2012; Sikiric et al., 2013; Seiwerth et al., 2014; Sikiric et al., 2014; Sikiric et al., 2016; Sikiric et al., 2017; Kang et al., 2018; Seiwerth et al., 2018; Sikiric et al., 2018; Park et al., 2020; Sikiric et al., 2020a; Sikiric et al., 2020b) without toxicity (lethal dose 1 (LD1) could be not obtained) (Sikiric et al., 1993; Sikiric et al., 2006; Sikiric et al., 2010; Sikiric et al., 2011; Sikiric et al., 2012; Sikiric et al., 2013; Seiwerth et al., 2014; Sikiric et al., 2014; Sikiric et al., 2016; Sikiric et al., 2017; Kang et al., 2018; Seiwerth et al., 2018; Sikiric et al., 2018; Gwyer et al., 2019; Park et al., 2020; Sikiric et al., 2020a; Sikiric et al., 2020b). As a cytoprotective agent, mediating Robert's cytoprotection, it maintains endothelium integrity and has a particular angiomodulatory effect (Sikiric et al., 1993; Sikiric et al., 2006; Sikiric et al., 2010; Sikiric et al., 2011; Sikiric et al., 2012; Sikiric et al., 2013; Seiwerth et al., 2014; Sikiric et al., 2014; Sikiric et al., 2016; Sikiric et al., 2017; Kang et al., 2018; Seiwerth et al., 2018; Sikiric et al., 2018; Park et al., 2020; Sikiric et al., 2020a; Sikiric et al., 2020b) (in various wound models, VEGF, factor VIII, CD34 peak appear in the early interval, while later depressed (Brcic et al., 2009)). In the sponge assay, BPC 157 exhibits an angiogenic effect greater than the standard antiulcer agents (Sikiric et al., 1999a). Besides, when we consider the general wound principles in tissue damage as a dynamic equilibrium between negative and positive events (i.e., necrosis and possibly pus formation *vs.* activation of macrophages and fibroblasts), BPC 157 shows the particular full extent of its healing actions (Seiwerth et al., 1997). This includes in addition to the skin lesions, the concomitant lesions counteraction, that is, burn stress gastric lesions in severely burned mice (Mikus et al., 2001). As an extending point, there appears to be fistula healing (i.e., simultaneous healing of the skin and other tissues wounds) (Klicek et al., 2008; Skorjanec et al., 2009; Cesarec et al., 2013; Skorjanec et al., 2015; Baric et al., 2016; Grgic

et al., 2016; Sikiric et al., 2020a). Illustratively, there are particular distinctions from the platelet-derived growth factor (PDGF-BB) activity (Seveljevic-Jaran et al., 2006; Tkalcevic et al., 2007). In contrast to PDGF-BB, in diabetic wounds, induced by alloxan application, BPC 157 largely promoted mature collagen in granulation tissue (Seveljevic-Jaran et al., 2006) (note, previously, BPC 157 healed alloxan-induced gastric lesions in rats (Petek et al., 1999)). In addition, BPC 157 has a particular beneficial effect when confronted with the major vessel occlusion (Duzel et al., 2017; Amic et al., 2018; Drmic et al., 2018; Vukojevic et al., 2018; Sever et al., 2019; Berkopic Cesar et al., 2020; Gojkovic et al., 2020; Kolovrat et al., 2020; Vukojevic et al., 2020). BPC 157 rapidly attenuates the major vessel occlusion severe consequences by rapidly activating collateral pathways occlusion (Duzel et al., 2017; Amic et al., 2018; Drmic et al., 2018; Vukojevic et al., 2018; Sever et al., 2019; Berkopic Cesar et al., 2020; Gojkovic et al., 2020; Kolovrat et al., 2020; Vukojevic et al., 2020). With permanent vessel obstruction, once the therapeutic effect begins, the beneficial action proceeds without further reappearance of the adverse effects of vessel obstruction (Duzel et al., 2017; Amic et al., 2018; Drmic et al., 2018; Vukojevic et al., 2018; Sever et al., 2019; Gojkovic et al., 2020; Kolovrat et al., 2020; Vukojevic et al., 2020). Likewise, reestablished blood flow may certainly contribute to the rapid recovery effect noted.

This particular balanced modulatory action, which rapidly appears, along with this pentadecapeptide's particular characteristics, will be especially reviewed. It may be even more interesting and more effective than that of comparative standard agents (Sikiric et al., 1993; Sikiric et al., 2006; Sikiric et al., 2010; Sikiric et al., 2011; Sikiric et al., 2012; Sikiric et al., 2013; Seiwerth et al., 2014; Sikiric et al., 2014; Sikiric et al., 2016; Sikiric et al., 2017; Kang et al., 2018; Seiwerth et al., 2018; Sikiric et al., 2018; Gwyer et al., 2019; Park et al., 2020; Sikiric et al., 2020a; Sikiric et al., 2020b), the silver sulfadiazine cream (Mikus et al., 2001) or systemic corticosteroids (Sikiric et al., 2003), for possible wound healing therapy (i.e., incisional/excisional wound, deep burns, diabetic ulcer, and alkali burns) (Seiwerth et al., 1997; Mikus et al., 2001; Sikiric et al., 2003; Xue et al., 2004a; Bilic et al., 2005; Seveljevic-Jaran et al., 2006; Tkalcevic et al., 2007; Huang et al., 2015). Additionally, BPC 157 administration counteracted various free radical–induced lesions and increased free radical formation in other organs (Sikiric et al., 1993; Ilic et al., 2010; Belosic Halle et al., 2017; Duzel et al., 2017; Luetic et al., 2017; Amic et al., 2018; Drmic et al., 2018; Vukojevic et al., 2018; Sever et al., 2019; Sucic et al., 2019; Berkopic Cesar et al., 2020; Kolovrat et al., 2020). The carboxylic groups of the pentadecapeptide BPC 157 may contribute to its role as an antioxidant. The cumulative antioxidant activity could be very high with the reactivation of the carboxylic groups (e.g., glutathione or enzymes). Additionally, BPC 157 is present in most tissues (Seiwerth et al., 2018), where it can bind reactive free radicals and inactivate them at crucial positions not reachable by other antioxidants (Sikiric et al., 1993; Sikiric et al., 2006; Sikiric et al., 2010; Sikiric et al., 2011; Sikiric et al., 2012; Sikiric et al., 2013; Seiwerth et al., 2014; Sikiric et al., 2014; Sikiric et al., 2016; Sikiric et al., 2017; Kang et al., 2018; Seiwerth et al., 2018; Sikiric et al., 2018; Gwyer et al., 2019; Park et al., 2020; Sikiric et al., 2020a; Sikiric et al., 2020b).

Skin Wounds

This particular balanced modulatory action was indicated in the initial manuscript (Seiwerth et al., 1997). This study already established that the combined triad of collagen-inflammatory cells–angiogenesis was accordingly upgraded, appearing at earlier intervals, more rapid, and advanced with BPC 157 therapy (Seiwerth et al., 1997). Quantitative analysis of collagen development as well as granulation tissue formation and angiogenesis was performed *in vivo* models, incisional skin wounds, colon–colon anastomoses, and synthetic sponge implants (Seiwerth et al., 1997). The applied rationale of skin and colon wounds (Seiwerth et al., 1997) covers the different healing patterns and dynamics of these organs related to their collagen structures (Eyre et al., 1984; Eckersley and Dudley, 1988; Hendriks and Mastboom, 1990). The noted wide effectiveness in all of these models postulates a quite general wound healing effect (Seiwerth et al., 1997). Thereby, the subsequent burn studies were on the burns covering 20% of total body area on the back of mice, open flame for 5 or 7 s (Mikus et al., 2001; Sikiric et al., 2003). The accelerated healing in burns of treated mice includes the activity of the pentadecapeptide BPC 157 (**Figure 1**), given locally (as a cream) or systemically (ip), on the inflammatory cells, edema, reticulin, collagen, necrosis, blood vessel formation, number of preserved follicles, re-epithelization, tensile breaking strength, and water content in burned skin. BPC 157 regimens also attenuated burn stress-gastric lesions (Mikus et al., 2001). Note, there is apparently smaller extent of the silver sulfadiazine cream effect (Mikus et al., 2001). Further positive outcome appears in the corticosteroid animals with severe burns (Mikus et al., 2001; Sikiric et al., 2003). With BPC 157 additional therapy, there are no characteristic corticosteroid adverse effects in the corticosteroid animals (Sikiric et al., 2003). As a beneficial property, inhibition of the inflammatory response did not impair wound healing and did not induce failed collagen synthesis (Mikus et al., 2001; Sikiric et al., 2003). In this, pentadecapeptide BPC 157 consistently (grossly, microscopically, and biomechanically) cured burn injuries, and counteracted corticosteroid (6α-methylprednisolone 1.0 or 10 mg/kg/day ip for 21 days)-induced impairment of burn healing (Mikus et al., 2001; Sikiric et al., 2003). With pentadecapeptide BPC 157, less edema and less inflammatory cells, re-epithelization, tensile breaking force, relative elongation of the burned part skin appear together, and inhibition of inflammation and beneficial effects. This chain of events fails to occur in the corticosteroids animals after initial inflammation inhibition (Sikiric et al., 2003). Even more importantly, BPC 157 accordingly inhibited corticosteroid-induced immunosuppression (Sikiric et al., 2003). *In vitro*, in comparison with control, healthy animals, the assessment of splenic cells (day 21) demonstrated that the 6α-methylprednisolone animals had declined reactivity to nitrogen, while the addition of BPC 157 (1 μg/g cream) returned cell reactivity to normal values (Mikus et al., 2001; Sikiric et al., 2003). A similar outcome appears in the CO_2 laser injury on the dorsal skin mice (Bilic et al., 2005).

To find out a specific mechanism, a comparison with the becaplermin (recombinant human platelet–derived growth factor

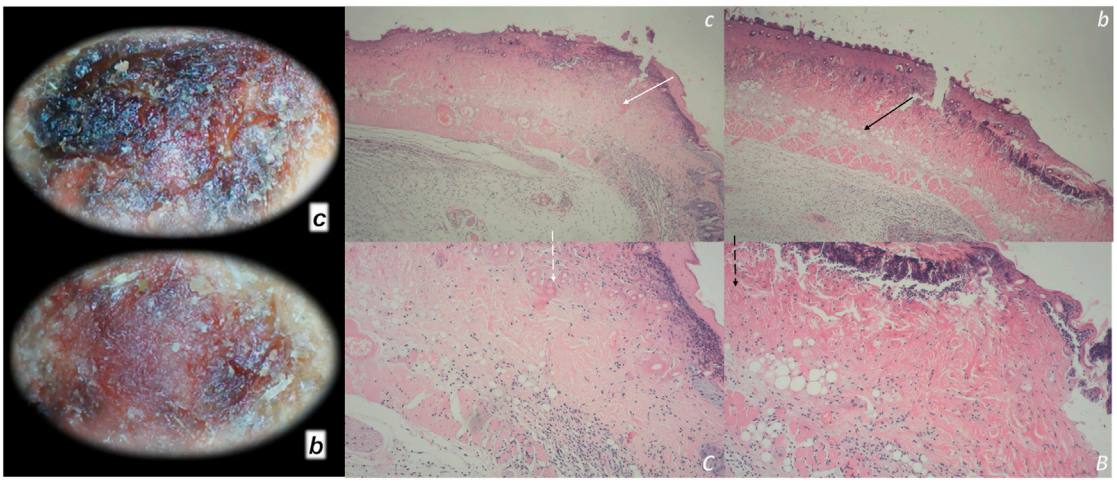

FIGURE 1 | Burn skin lesions in mice and BPC 157 therapy effect. The effects of the gastric pentadecapeptide BPC 157 were investigated on deep partial skin thickness burns (1.5 × 1.5 cm) covering 20% of the total body area, when administered topically or systemically in burned mice (Mikus et al., 2001). Characteristic wound presentation at one week after injury, grossly, the poor healing in the untreated control or mice treated with vehicle only (*c (black letter)*) was completely reversed in BPC 157 cream–treated mice (*b (black letter)*) (1 μg/g neutral cream thin layer once time daily). Likewise, BPC 157 mice exhibited an increased breaking strength and relative elongation of burned skin and reduced water content in burned skin. Contrarily, silver sulfadiazine regimen did not achieve these healing effects. Microscopically **(lower)**, at the postinjury day 3, in control mice, the burned area exhibits severe edema in the dermis and subcutis as well as an exudate with abundant edematous fluid on the surface (white arrow). Coagulated blood vessel walls and a proportion of vessels with fibrin clots (dashed white arrow) (HE, x4 (*c*), x10 (*C*)). Contrarily, BPC 157 mice have much less pronounced edema (black arrow), weak cellular infiltrate, and exudate, and the blood vessels walls seem to be more preserved (dashed black arrow) and in more vessels, endothelial cell can be observed. Almost no arterial clots (HE, x4 (*b*), x10 (*B*)) were observed.

homodimer of B chains, PDGF-BB) was the focus of the two additional studies using excisional wounds in diabetic rats and mice (**Figure 2**) (Seveljevic-Jaran et al., 2006; Tkalcevic et al., 2007). Increased expression of the immediate response gene, early growth response gene-1 (egr-1), was shown in Caco-2 cells *in vitro* (Tkalcevic et al., 2007). These studies, even in diabetic conditions (Seveljevic-Jaran et al., 2006; Tkalcevic et al., 2007), revealed increased stimulation of early collagen organization in BPC 157 therapy. Importantly, BPC 157, but not PDGF-BB, stimulated earlier maturation of granulation tissue, soluble collagen concentration in the exudates (using sponge implantation), and organized collagen significantly more in wounds (i.e., on day 12 after daily treatment) (Tkalcevic et al., 2007). As a rationale, the study proposed the evidence that stimulation of the Caco-2 cells with 10–100 μM BPC 157 resulted in an earlier, reproducible stimulation of the expression of mRNA for egr-1, with a peak after 15 min. The peak expression of mRNA for the egr-1 co-repressor, nerve growth factor 1-A binding protein-2 (nab2), was observed 30 min after BPC 157 stimulation (Tkalcevic et al., 2007). This favors the possible controlling role of the BPC 157. Namely, we should consider egr-1 gene both positive and negative association. The beneficial significance of the egr-1 gene implies the healing process (i.e., trans-activation of many cognate target genes in healing tissue, including growth factors and cytokines (Braddock et al., 1999; Braddock, 2001), the transcription of other genes, including those for collagen II (α1) and PDGF (Alexander et al., 2002). Likewise, there is its negative association (i.e., elevated egr-1 levels associated with cardiovascular pathobiology (Khachigian, 2006) or cholestatic liver injury (Kim et al., 2006; Zhang et al., 2011). It may be that BPC 157 rapid activation of the egr-1 and its co-repressor, nab2, means an essential operating healing BPC 157 feedback axis controlling egr-1 levels along with nab2.

Finally, BPC 157 administration cured the alkali burn-induced skin injury (Huang et al., 2015). There were faster granulation tissue formation, re-epithelialization, dermal remodeling, and collagen deposition through extracellular signal–regulated kinases (ERK)1/2 signaling pathway as well as its downstream targets, including c-Fos, c-Jun, and egr-1. Likewise, there is greater proliferation of human umbilical vein endothelial cells (HUVECs), significantly promoted migration of HUVECs (transwell assay), and the upregulated expression of VEGF-a, and accelerated vascular tube formation *in vitro* (Huang et al., 2015).

Finally, this effect is apparently not species specific, and it was seen in the bigger animals as well. A similar finding (i.e., rehabilitation of skin wound and maturation of granulation tissue markedly promoted by BPC 157) was obtained in small-type pigs (Xue et al., 2004a). Note, the same group also reported a therapy with a prominent beneficial effect on various stomach lesions after administration of BPC 157 (Xue et al., 2004b).

Practical Application as Support

The evidence reported for the BPC 157 is the effectiveness with peptide given alone (Sikiric et al., 1993; Sikiric et al., 2006; Sikiric et al., 2010; Sikiric et al., 2011; Sikiric et al., 2012; Sikiric et al., 2013; Seiwerth et al., 2014; Sikiric et al., 2014; Sikiric et al., 2016; Sikiric et al., 2017; Kang et al., 2018; Seiwerth et al., 2018; Sikiric

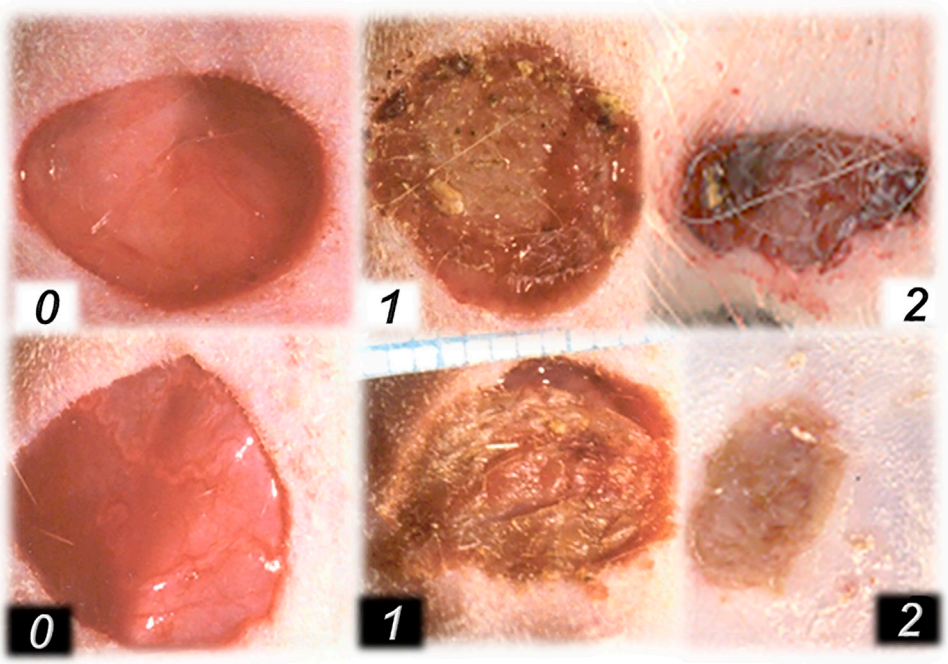

FIGURE 2 | Excisional wound in diabetic rats (0, 1) and in rats with ligation of the right iliac artery and vein (2) **(upper)** and BPC 157 therapy **(lower)**. At 3 days before wounding, alloxan (300 mg/kg sc), thin layer of the BPC 157 cream (1 μg/1 g neutral cream) (white number), or neutral cream (black number) was immediately given upon wounding (*0, 0*). Advanced wound healing presentation at 24 h in BPC 157 rats (*1, white*), but not in controls (*1, black*). Likewise, advanced healing in the rats with ligated right iliac arteries and veins, when ingested BPC 157 through drinking water (10 μg/kg, 10 ng/kg, 0.16 μg/ml, 0.16 ng/ml, and 12 ml/rat/day) at postsurgery day 4 (*2, white*), but not in controls (*2, black*).

et al., 2018; Gwyer et al., 2019; Park et al., 2020; Sikiric et al., 2020a; Sikiric et al., 2020b). Contrarily, when there is a peptide carrier, far more investigated and commonly implied angiogenic standard growth factors in the growth factor healing concept (Tarnawski and Ahluwalia, 2012; Deng et al., 2013) have several limitations (i.e., local application, carrier addition, and weak and uncertain peptide activity of its own (Seiwerth et al., 2018)), delaying practical realization of the growth factor healing concept.

Illustratively, in the mentioned laser-wound studies, human albumin solder supplemented with transforming growth factor (TGF)-β1 only, but not with HB-EGF or bFGF, increased the early postoperative strength of laser-welded wounds (Poppas et al., 1996), even though the superpulsed CO_2 laser enhanced fibroblast replication and appeared to stimulate bFGF and inhibit TGF-β1 secretion (Nowak et al., 2000). Likewise, an essential problem with regard to the active (and effective) peptide is the continuous search for new delivery systems and new carriers, and new carriers and delivery systems together, with all standard angiogenic growth factors to improve their efficacy, although they are very extensive and highly sophisticated (for review, see Saghazadeh et al., 2018; Jee et al., 2019). Obviously, it may be unclear which one of the parts of peptide + carrier complex would be responsible for the activity (for review, see Urist, 1996). Thereby, this pitfall (i.e., the more carriers, the less own peptide activity) is commonly not considered (Saghazadeh et al., 2018; Jee et al., 2019), despite the fact it is recognized (Urist, 1996), and eventually jeopardizes the conclusions about these peptide activities and significance (Tarnawski and Ahluwalia, 2012; Deng et al., 2013). Obviously, the effects of one growth factor could be not unified when obtained with addition (and help) of different carriers (Seiwerth et al., 2018), and regardless given highly sophisticated evidence (Tarnawski and Ahluwalia, 2012; Deng et al., 2013), they could make the erroneous conclusions. Thus, it may be that ignoring these attribution problems jeopardizes the current growth factor healing concept (Tarnawski and Ahluwalia, 2012; Deng et al., 2013) since the needed certainty that the full healing evidence was correctly ascribed to the given peptid, is obviously lacking. For example, FGF studies in 1990s (Damien et al., 1993; Thorén and Aspenberg, 1993; Siegall et al., 1994; Walter et al., 1996; Wang and Aspenberg, 1996; Yu et al., 1998; Tabata et al., 1999) are illustrative for the pertinence of the poorly resolved problem, illustrative for the diversity of the carriers (i.e., hyaluronate gel carrier (Wang and Aspengberg, 1996), alginate/heparin–sacharose microspheres and films (Yu et al., 1998), cellulose gel (Thorén and Aspenberg, 1993), defective form of *Pseudomonas* exotoxin (Siegall et al., 1994), fibrin adhesive carrier (Walter et al., 1996), biodegredable hydrogen gelatin (Tabata et al., 1999), natural coral, and collagen (Damien et al., 1993)). Obviously, as indicated (Sikiric et al., 2018), there is an inescapable diversity of the carriers and thereby, an evident diversity of the obtained beneficial effects, and disable conclusion. Likewise, for bone morphogenic proteins (BMPs),

at that time, besides bone matrix, the following biomaterials have been tested as carriers: calcium phosphate, collagen, gelatin, and starch (Miyamoto et al., 1992; Gao et al., 1993; Katoh et al., 1993; Kawai et al., 1993; Cook et al., 1994; Kato et al., 1995; Kawakami et al., 1997). Some carriers (true ceramics and pure titanium) remain in the bone tissue, whereas others (collagen and synthetic polymers) are absorbed. Some are absorbed so quickly that there is no enough time for a population of host cells to gather (Kawakami et al., 1997). Finally, the statement of Marshall Urist, the BMPs concept founder, about the mechanism of the release from BMP delivery system to mesenchymal cell receptor mechanisms as obscure and under intensive investigation in academic and industrial laboratories (Urist, 1996) is true also nowadays, and it can be generally applied to any of the peptide + carrier complexes.

Contrarily, BPC 157 has a general healing argument as general application protocol. Namely, it is always applied alone (Sikiric et al., 1993; Sikiric et al., 2006; Sikiric et al., 2010; Sikiric et al., 2011; Sikiric et al., 2012; Sikiric et al., 2013; Seiwerth et al., 2014; Sikiric et al., 2014; Sikiric et al., 2016; Sikiric et al., 2017; Kang et al., 2018; Seiwerth et al., 2018; Sikiric et al., 2018; Gwyer et al., 2019; Park et al., 2020; Sikiric et al., 2020a; Sikiric et al., 2020b). Unlike other growth factors, which need carrier(s) addition, and are rapidly destroyed in human gastric juice, BPC 157 is native and stable in human gastric juice for more than 24 h (Sikiric et al., 2018; Sikiric et al., 2020a; Sikiric et al., 2020b). As BPC 157 counteracts lesions in the whole gastrointestinal tract produced by various noxious procedures (Sikiric et al., 1993; Sikiric et al., 2006; Sikiric et al., 2010; Sikiric et al., 2011; Sikiric et al., 2012; Sikiric et al., 2013; Seiwerth et al., 2014; Sikiric et al., 2014; Sikiric et al., 2016; Sikiric et al., 2017; Kang et al., 2018; Seiwerth et al., 2018; Sikiric et al., 2018; Gwyer et al., 2019; Park et al., 2020; Sikiric et al., 2020a; Sikiric et al., 2020b), it may be indeed that it may endogenously maintain gastrointestinal mucosa integrity (Sikiric et al., 1993; Sikiric et al., 2006; Sikiric et al., 2010; Sikiric et al., 2011; Sikiric et al., 2012; Sikiric et al., 2013; Seiwerth et al., 2014; Sikiric et al., 2014; Sikiric et al., 2016; Sikiric et al., 2017; Kang et al., 2018; Seiwerth et al., 2018; Sikiric et al., 2018; Gwyer et al., 2019; Park et al., 2020; Sikiric et al., 2020a; Sikiric et al., 2020b). Consequently, BPC 157 may have beneficial activity with the same dose range, and same equipotent routes of application, regardless of injury tested (Sikiric et al., 1993; Sikiric et al., 2006; Sikiric et al., 2010; Sikiric et al., 2011; Sikiric et al., 2012; Sikiric et al., 2013; Seiwerth et al., 2014; Sikiric et al., 2014; Sikiric et al., 2016; Sikiric et al., 2017; Kang et al., 2018; Seiwerth et al., 2018; Sikiric et al., 2018; Gwyer et al., 2019; Park et al., 2020; Sikiric et al., 2020a; Sikiric et al., 2020b). Therefore, this could be clearly generalized, and thus, its own effect unmistakably ascribed only to the given peptide (for review, see Seiwerth et al., 2018). Besides, as indicated specifically in skin wound healing (Tkalcevic et al., 2007), BPC 157 half-life is long enough to exert a therapeutically stimulating effect on connective tissue growth (Tkalcevic et al., 2007). In sponge exudates, it remains active at the site of wounds for several hours (Tkalcevic et al., 2007).

The generalization of the skin wound healing therapy (Seiwerth et al., 1997; Mikus et al., 2001; Sikiric et al., 2003; Xue et al., 2004a; Bilic et al., 2005; Seveljevic-Jaran et al., 2006; Tkalcevic et al., 2007; Huang et al., 2015) as a particular point, will be illustrated with the subsequent successful healing of the various fistulas (thereby, the simultaneous healing of the different tissues) (Klicek et al., 2008; Skorjanec et al., 2009; Cesarec et al., 2013; Skorjanec et al., 2015; Baric et al., 2016; Grgic et al., 2016; Sikiric et al., 2020a) (see *Fistula Healing as Support*). Next, its particular therapeutic result on wound healing is decreased bleeding (Stupnisek et al., 2012; Stupnisek et al., 2015), and during wounding and recovery, all four major events in clot formation and dissolution were accomplished (Stupnisek et al., 2012). This was illustrated in the therapy of the bleeding disorders (Stupnisek et al., 2012; Stupnisek et al., 2015) (see *Therapy of Bleeding Disorders as Support*).

Fistula Healing as Support

BPC 157 application successfully cured various fistulas (Sikiric et al., 2020a). Anastomoses between two defects in the corresponding tissues (i.e., in esophagus and skin (Cesarec et al., 2013), stomach and skin (Skorjanec et al., 2009), duodenum and skin (Skorjanec et al., 2015), colon and skin (Klicek et al., 2008), colon and bladder (Grgic et al., 2016), and rectum and vagina (Baric et al., 2016)) depict the various fistulas (Sikiric et al., 2020a). Likewise, these defects of the controlled size may fairly illustrate accelerated or enabled healing (i. e., closure) and wound/gastrointestinal ulcer relation (Sikiric et al., 2020a).

Of note, the methodology of this healing evidence (Klicek et al., 2008; Skorjanec et al., 2009; Cesarec et al., 2013; Skorjanec et al., 2015; Baric et al., 2016; Grgic et al., 2016; Sikiric et al., 2020a) may contrast with the miscellaneous underlying fistula causes, various origin and location and different occurrences (Orangio, 2010; Visschers et al., 2012; Tonolini and Magistrelli, 2017). Likewise, this approach may contrast with therapeutic tactics for fistulas, which depend on their location and severity of occurrence (Orangio, 2010; Visschers et al., 2012; Tonolini and Magistrelli, 2017). Also, it opposes the nowadays aggressive wound management if it considers in fistulas healing mostly local skin protection (Orangio, 2010; Visschers et al., 2012; Tonolini and Magistrelli, 2017). On the other hand, this healing evidence as such (Klicek et al., 2008; Skorjanec et al., 2009; Cesarec et al., 2013; Skorjanec et al., 2015; Baric et al., 2016; Grgic et al., 2016; Sikiric et al., 2020a) may accommodate and resolve the mentioned fistula diversity (Orangio, 2010; Visschers et al., 2012; Tonolini and Magistrelli, 2017) as a common healing denominator providing simultaneous healing of different tissues.

Consequently, we hold fistulas commonality (Klicek et al., 2008; Skorjanec et al., 2009; Cesarec et al., 2013; Skorjanec et al., 2015; Baric et al., 2016; Grgic et al., 2016; Sikiric et al., 2020a) and thereby, the revealing common resolution (Sikiric et al., 2020a). There are two different tissues simultaneously affected and a healing process that would organize synchronized healing (Sikiric et al., 2020a). Thus, the main implication of the fistula healing model as wounds with abnormal connections is the verification of the effectiveness of the skin wound healing as understood with BPC 157 effects in the skin wound models (Seiwerth et al., 1997; Mikus et al., 2001; Sikiric et al., 2003; Xue et al., 2004a; Bilic et al., 2005; Seveljevic-Jaran et al., 2006; Tkalcevic et al., 2007; Huang

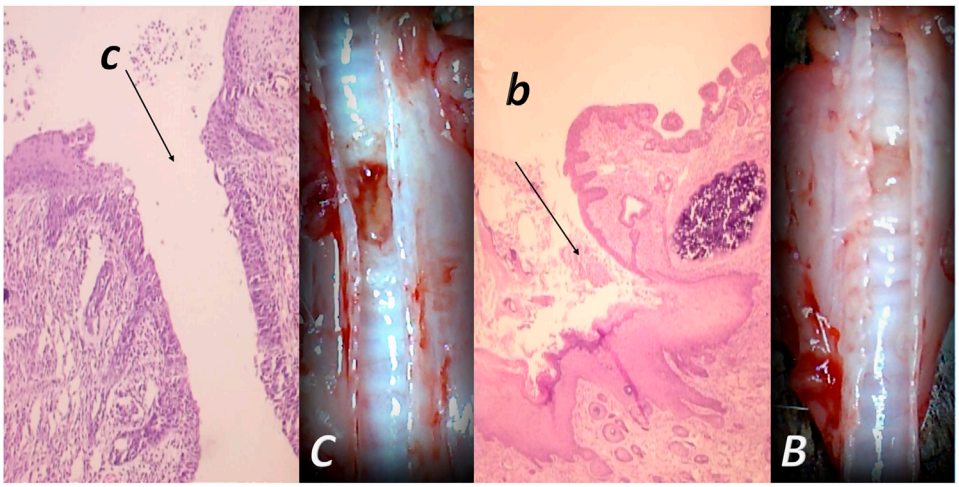

FIGURE 3 | Tracheocutaneous fistulas and BPC 157 therapy. After injury induction, BPC 157 dissolved in saline (10 μg, 10 ng/kg body weight) given per-orally in drinking water till the sacrifice (0.16 μg/ml, 0.16 ng/ml, and 12 ml/day/rat). At postsurgery day 7, fistula closure, closed tracheal defect, and closed skin defect (*B, b*) (arrow) were observed in BPC 157 rats. Contrarily, in controls, fistula remained open, fistulous channel was formed in the skin, and open tracheal defects were observed (*C, c*) (arrow) (HE, x4).

et al., 2015). That healing may be smoothly generalized simultaneously to the other tissues (**Figure 3**), and this particular balanced modulatory action may have the general significance, with the eventual healing of the affected tissues (**Figure 4**) (Klicek et al., 2008; Skorjanec et al., 2009; Cesarec et al., 2013; Skorjanec et al., 2015; Baric et al., 2016; Grgic et al., 2016; Sikiric et al., 2020a). Otherwise, the healing of the different tissues, which are normally not connected, would hardly provide a simultaneous wound healing effect, particularly in the most critical circumstances (Klicek et al., 2008; Skorjanec et al., 2009; Cesarec et al., 2013; Skorjanec et al., 2015; Baric et al., 2016; Grgic et al., 2016; Sikiric et al., 2020a). Note that due to the relative small size of the rats, rat fistulas regularly appeared as large and complex, and thereby, in this respect, corresponded to the worst presentation in the patients (Klicek et al., 2008; Skorjanec et al., 2009; Cesarec et al., 2013; Skorjanec et al., 2015; Baric et al., 2016; Grgic et al., 2016; Sikiric et al., 2020a). Harmful disturbances and poor healing of rectovaginal fistulas in patients (Baric et al., 2016) may occur also in rats (i.e., fecal leaking through the vagina). Rats could not endure more than 4 days with esophagocutaneous fistulas (Cesarec et al., 2013). However, with BPC 157 therapy, both skin and esophageal defect may be closed without mortality (Cesarec et al., 2013). Thereby, that healing in rat fistulas in these experiments should be highly relevant (Klicek et al., 2008; Skorjanec et al., 2009; Cesarec et al., 2013; Skorjanec et al., 2015; Baric et al., 2016; Grgic et al., 2016; Sikiric et al., 2020a). Obviously, a distinctive correlation follows with the major systems generally involved in the healing processes (Sikiric et al., 2020a).

Basically, closure of fistulas may be a measure of particular agent's capacity to cure, at the same time, the skin wound and other corresponding tissues' wound (Klicek et al., 2008; Skorjanec et al., 2009; Cesarec et al., 2013; Skorjanec et al., 2015; Baric et al., 2016; Grgic et al., 2016; Sikiric et al., 2020a). The healing of the skin and colon defect, as colocutaneous fistulas, stable gastric pentadecapeptide BPC 157, and the therapy regimens (per-oral, in drinking water; or intraperitoneal (once time daily) for 28 days) may serve as a prototype (for review, see Sikiric et al., 1993; Sikiric et al., 2006; Sikiric et al., 2010; Sikiric et al., 2011; Sikiric et al., 2012; Sikiric et al., 2013; Seiwerth et al., 2014; Sikiric et al., 2014; Sikiric et al., 2016; Sikiric et al., 2017; Kang et al., 2018; Seiwerth et al., 2018; Sikiric et al., 2018; Gwyer et al., 2019; Sikiric et al., 2020a; Sikiric et al., 2020b).

Also, a similar protocol was successful in the therapy of the other fistulas, that is, gastrocutaneous (Skorjanec et al., 2009), esophagocutaneous (Cesarec et al., 2013), duodenocutaneous (Skorjanec et al., 2015), vesicovaginal (Grgic et al., 2016), and rectovaginal (Baric et al., 2016) in rats. Noteworthy, as shown in separate studies, BPC 157 counteracts the known lesions in the skin (Seiwerth et al., 1997; Mikus et al., 2001; Sikiric et al., 2003; Xue et al., 2004a; Bilic et al., 2005; Seveljevic-Jaran et al., 2006; Tkalcevic et al., 2007; Huang et al., 2015), stomach (Sikiric et al., 1997a; Petek et al., 1999; Mikus et al., 2001; Xue et al., 2004b; Becejac et al., 2018; Ilic et al., 2009; Ilic et al., 2011a), duodenum (Sikiric et al., 1994; Sikiric et al., 1997b; Sikiric et al., 2001; Bedekovic et al., 2003; Amic et al., 2018), esophagus (Sikiric et al., 1999b; Petrovic et al., 2006; Dobric et al., 2007; Djakovic et al., 2016), colon (Sikiric et al., 2001; Klicek et al., 2013), rectum (Sikiric et al., 2001; Klicek et al., 2013), bladder (Sucic et al., 2019), and vagina (Jandric et al., 2013), whereas the fistula studies show an additional combining healing effect, providing different combinations of the lesions that were simultaneously included (**Figures 3**, **4**), thereby a proof of the concept for a quite general healing effect (Klicek et al., 2008; Skorjanec et al., 2009; Cesarec et al., 2013; Skorjanec et al., 2015; Baric et al., 2016; Grgic et al., 2016; Sikiric et al., 2020a). A particular relationship was established with the NO-system, and the advantage of the BPC 157 over the corresponding standard agents (i.e., corticosteroids,

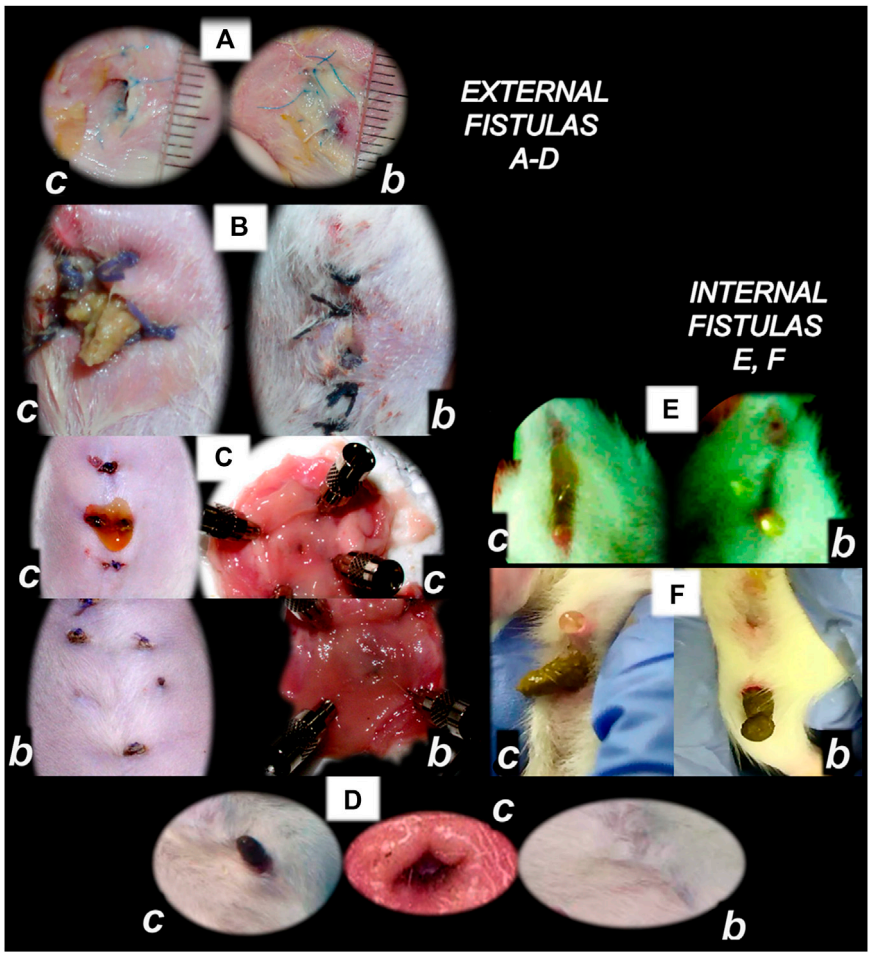

FIGURE 4 | BPC 157 and fistulas closing. External **(A–D)** and internal **(E, F)** fistulas. External fistulas. **(A)** Persistent esophagocutaneous fistula and BPC 157 therapy effect. BPC 157 was given per-orally, in drinking water (10 μg/kg, 10 ng/kg, i.e., 0.16 μg/ml, 0.16 ng/ml, 12 ml/rat/day) until sacrifice, or intraperitoneally (10 μg/kg, 10 ng/kg) with first application at 30 min after surgery, last at 24 h before sacrifice. To establish NO-system involvement, L-NAME (5 mg/kg i.p.) (worsening) and/or L-arginine (100 mg/kg i.p.) (beneficial effect) were given alone or together; first application at 30 min after surgery, last at 24 h before sacrifice. BPC 157 (10 μg/kg, i.p. or p.o.) given with L-NAME (5 mg/kg i.p.) and/or L-arginine (100 mg/kg i.p.) and it maintained its original beneficial effect. A closely interrelated process of unhealed skin, esophageal defects, unhealed fistulas (upregulated eNOS, iNOS, and COX2 mRNA levels), usually lethal, particularly NO-system–related and therapy dependent, illustrate a largely open skin defect in controls at day 3 (*c*) and a closed skin defect in BPC 157 rats (*b*) (Ceserec et al., 2013). **(B)** Initial presentation of the persistent gastrocutaneous fistula and BPC 157 therapy effect. Huge gastrocutaneous fistula leaking at 1st postoperative day in control rats (*c*) and dried fistula without any leakage in BPC 157 rats (*b* (Skorjanec et al., 2009). The rats received pentadecapeptide BPC 157 (0.16 μg/ml) in drinking water (12 ml/rat) until sacrifice or drinking water only. A comparative study of the BPC 157 beneficial effect was done with intraperitoneal application, once daily, intraperitoneally (per kg body weight) 10 μg, 10 ng, or 10 pg BPC 157, while standard agents 10 mg atropine, 50 mg ranitidine, and 50 mg omeprazole provide only a weak effect. 6-alpha-methylprednisolone (1 mg/kg intraperitoneally, once daily) was given alone which produced a considerable worsening and was completely eliminated with coadministration of BPC 157 10 μg/kg intraperitoneally. **(C)** Persistent duodenocutaneous fistula and BPC 157 therapy effect. BPC 157 was given per-orally, in drinking water (10 μg/kg, 10 ng/kg, i.e., 0.16 μg/ml, 0.16 ng/ml, and 12 ml/rat/day) till sacrifice, or alternatively, 10 μg/kg and 10 ng/kg intraperitoneally; first application at 30 min after surgery, last at 24 h before sacrifice. To establish a connection with the NO-system, L-NAME (5 mg/kg intraperitoneally) (worsening) and/or L-arginine (100 mg/kg intraperitoneally) (beneficial effect) were given alone or together; first application at 30 min after surgery, last at 24 h before sacrifice. BPC 157 10 μg/kg, intraperitoneally or per-orally, was given with L-NAME (5 mg/kg intraperitoneally) and/or L-arginine (100 mg/kg intraperitoneally) and it maintained its original beneficial effect. Controls simultaneously received an equivolume of saline (5.0 ml/kg intraperitoneally) or water only. Duodenal fistula leaking through skin defect and still open duodenal defect at 2 weeks following fistula creation by anastomosis between the skin and duodenum defect (*c*). Closed both skin and duodenal defect in BPC 157 rats (fistula closed, *b*) (Skorjanec et al., 2015). **(D)** Persistent colocutaneous fistula and BPC 157 therapy effect. BPC 157 accelerated parenterally or per-orally the healing of colonic and skin defect, leading to the suitable closure of the fistula, macro/microscopically, biomechanically, and functionally (larger water volume sustained without fistula leaking) (Klicek et al., 2013). In anesthetized rats, we created the colocutaneous fistula at 5 cm from the anus, colon defect of 5 mm, and skin defect of 5 mm. The rats received pentadecapeptide BPC 157 (0.16 μg/ml) or nothing in the drinking water (12.0 ml/rat) until the sacrifice or once daily, intraperitoneally BPC 157 10.0 μg/kg, 10.0 ng/kg, or saline (5.0 ml/kg b.w.); first application at 30 min after surgery, final 24 h before sacrifice. For comparison, sulfasalazine (50 mg/kg intraperitoneally, once daily) (moderately effective) or 6-α-methylprednisolone (1.0 mg/kg intraperitoneally, once daily) (aggravation) was given. To establish connection with the NO-system, L-NAME (5.0 mg/kg) (worsening) and L-arginine (200.0 mg/kg) (effective only with blunted NO-synthesis, but not alone) were given intraperitoneally alone or in combination (D-arginine 200.0 mg/kg was not effective, data not shown). BPC 157 given with NO-agents, which maintained its original effect. Initial colon defect presentation at 4 weeks following fistula creation by anastomosis between the skin and colon defect (c, middle). Presentation after next 2 weeks (*c, b*): in control rats, drinking water was continuously given (12 ml/day/rat)

(*Continued*)

FIGURE 4 | (defecation through fistula, *c*) and in BPC 157 rats, BPC 157 (10 μg/kg/day) was given in drinking water (0.16 μg/ml/day/rat) (fistula closed, *b*). Internal fistulas. **(E)** Persistent colovesical fistula and BPC 157 therapy effect. With internal fistulas in the colon and the bladder, with BPC 157 therapy, the colon and bladder defects showed simultaneous healing effects, including closing of the colovesical fistula in a matching healing process (Grgic et al., 2016). BPC 157 was given per-orally in drinking water (10 μg/kg, 12 ml/rat/day) until sacrifice, or 10 μg/kg or 10 ng/kg was given intraperitoneally once daily, with the first application at 30 min after surgery and the last application at 24 h before sacrifice. The controls simultaneously received an equivolume of saline (5.0 ml/kg ip) or water only (12 ml/rat/day). At postoperative day 28, voiding through fistula in controls (fecaluria) (*c*) and a normal voiding in BPC 157-rats (*b*). **(F)** Persistent rectovaginal fistula and BPC 157 therapy effect. We suggest BPC 157 healing of the rats' rectovaginal fistulas (since spontaneous only poor healing as those in humans) as a realization of the internal fistula-healing concept, an efficient "wound-healing capability" as the therapy of the complicated internal fistula healing. BPC 157 was given per-orally, in drinking water (10 μg/kg or 10 ng/kg, 0.16 μg/ml, or 0.16 ng/ml 12 ml/rat/day) till sacrifice, or alternatively, 10 μg/kg and 10 ng/kg intraperitoneally once daily; first application at 30 min after surgery, last at 24 h before sacrifice. Controls simultaneously received an equivolume of saline (5.0 ml/kg ip) or water only (12 ml/rat/day). At postoperative day 21, defecation through vagina in controls (*c*) and a normal defecation in BPC 157 rats (*b*) (Baric et al., 2016).

sulfasalazine, H2 blockers, anticholinergics, and proton pump inhibitors) which showed only weak, if any, effect on these fistulas closing (Klicek et al., 2008; Skorjanec et al., 2009; Cesarec et al., 2013; Skorjanec et al., 2015; Baric et al., 2016; Grgic et al., 2016; Sikiric et al., 2020a).

Gastrocutaneous (Skorjanec et al., 2009) and/or duodenocutaneous (Skorjanec et al., 2015) fistulas, as persistent lesions, are another instructive prototype of the "two-ways" model. Often, the peptic ulcers' inability to heal is taken as analogous to the chronic skin wound inability to heal; thus, resistant peptic ulcers equal to resistant chronic skin ulcers, both unable to heal (Skorjanec et al., 2009). Contrary to the use of the gastrocutaneous fistula for the secretory studies only (Skorjanec et al., 2009), the wound/gastrointestinal ulcer relation of these gastrocutaneous fistulas healing exemplifies the reported particular "self-controlling healing system" (Skorjanec et al., 2009). Only the simultaneous healing of the skin defect and the stomach defect would lead to the fistula closure (Skorjanec et al., 2009). Since classic models are not combined, gastric/duodenal ulcer models (Selye and Szabo, 1973; Robert, 1979; Okabe and Amagase, 2005) would define agents' action. Likewise, skin defect models (Rantfors and Cassuto, 2003; Numata et al., 2006; Rao et al., 2007) would explain agents' action ("one-way" model). Thus, there is a practical advantage of the composed effects of the administered agents, and the gastrocutaneous fistulas as a combined ("two-ways") model. For example, for mutual definition (model → agent; agent → model), there are prostaglandins analogues—ethanol model (Robert, 1979) relationships, NSAIDs—acetic acid model (Okabe and Amagase, 2005) relationships, dopamine agonists—cysteamine model (Selye and Szabo, 1973) relationships, and H_2 blockers—cysteamine model (Selye and Szabo, 1973) relationships. Thereby, studies of gastrocutaneous fistulas (Skorjanec et al., 2009) may resolve in the wound/gastrointestinal ulcer relation. This may be the improvement or aggravation that tested agents can exhibit of healing. This may be healing of the skin or gastric wound, or both, or neither of them, simultaneously or not. This may identify the so-called parallel or non-parallel healing actions, with the final end result, positive (fistula closing) or negative (fistula remains open) (Skorjanec et al., 2009). Besides, BPC 157 promptly ameliorates both skin and stomach mucosa healing and induces closure of fistulas, with no leakage after up to 20 ml water intragastrically, including also counteraction of 6-alpha-methylprednisolone aggravation (Skorjanec et al., 2009).

Therapy of Bleeding Disorders as Support

The BPC 157 therapy of the bleeding disorders can be considered as an implementation and support of its wound healing effect (Seiwerth et al., 1997; Mikus et al., 2001; Sikiric et al., 2003; Xue et al., 2004a; Bilic et al., 2005; Seveljevic-Jaran et al., 2006; Tkalcevic et al., 2007; Huang et al., 2015) that can be purposefully extended (Stupnisek et al., 2012; Stupnisek et al., 2015). This particular balanced modulatory action in wound healing, which rapidly appears, along with this pentadecapeptide particular characteristics, may be even more interesting and more effective to be demonstrated in relation that in wounding, it decreases the bleeding. Namely, as curing of the wounds includes resolution of vessel constriction, the primary platelet plug, the secondary plug, and resolution of the clot (Stupnisek et al., 2012; Stupnisek et al., 2015) stabilize gastric pentadecapeptide BPC 157, which is effective in wound healing (**Figures 1–6**) (Seiwerth et al., 1997; Mikus et al., 2001; Sikiric et al., 2003; Xue et al., 2004a; Bilic et al., 2005; Seveljevic-Jaran et al., 2006; Tkalcevic et al., 2007; Huang et al., 2015); it also counteracts the bleeding disorders, amputation, organ perforation, and/or anti-coagulants application or major vessel occlusion (Stupnisek et al., 2012; Stupnisek et al., 2015; Drmic et al., 2018; Vukojevic et al., 2018; Gojkovic et al., 2020; Kolovrat et al., 2020). This reversal was seen also on the background of the disturbed prostaglandins- and NO-systems, prostaglandins synthesis inhibition as well as NO-overstimulation (NOS-substrate L-arginine) or NO-blockade (N(G)-nitro-L-arginine methyl ester (L-NAME)) (Stupnisek et al., 2012; Stupnisek et al., 2015). This should be taken along with its endothelium maintenance as the follow-up of its cytoprotection capability (Robert, 1979; Sikiric et al., 2010; Sikiric et al., 2018), along with the evidence that pentadecapeptide BPC 157 may prevent and/or attenuate or eliminate, thus, counteract both developing and already formed both arterial thrombosis (Hrelec et al., 2009; Gojkovic et al., 2020; Kolovrat et al., 2020), and venous thrombosis (Vukojevic et al., 2018; Gojkovic et al., 2020; Kolovrat et al., 2020). This therapy rapidly reversed the hind legs failure after abdominal aorta anastomosis (Hrelec et al., 2009). After occlusion of the inferior caval vein, accordingly, BPC 157 counteracts the whole Virchow triad (Vukojevic et al., 2018) and inferior caval vein syndrome (Vukojevic et al., 2018). At a particular point, venography demonstrated a rapid recruitment of the collaterals to bypass occlusion and reestablish blood flow (Vukojevic et al., 2018). In the rats with infrarenally occluded inferior caval vein, the left ovarian vein is

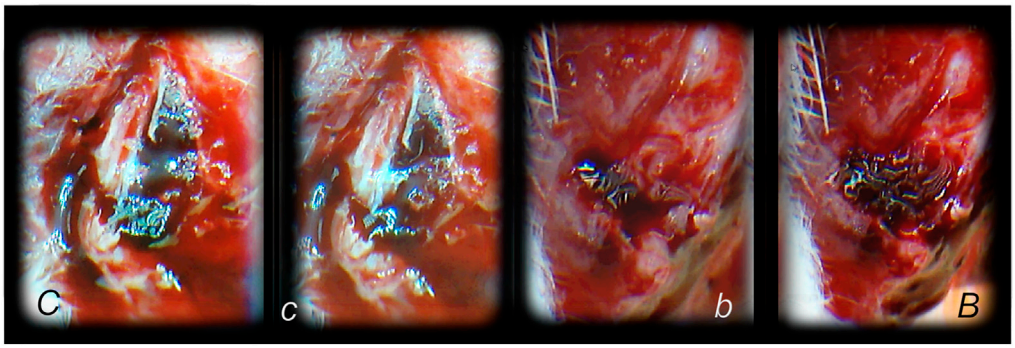

FIGURE 5 | Hematoma formation following tibial diaphysis fracture and BPC 157 therapy effect, in analogy with accomplished all four events (vessel constriction, the primary platelet plug, the secondary plug, and resolution of the clot) that occur in a set order following the loss of vascular integrity (Stupnisek et al., 2012) involved in the wound healing. We suggest BPC 157 healing starting with a rapid formation of the adequate hematoma as a connective scaffold between the stumps. BPC 157 (10 ng/kg) was given as a 1-ml bath to the injury, immediately after injury induction. Controls simultaneously received an equal of saline as a bath to the injury. At 1 min after application, hematoma within fracture gap (*b*) further progressed at 2 min (*B*) in BPC 157 rats. Diffuse bleeding in controls at 1 min (*c*) and 2 min (*C*), weak hematoma formed outside of the fracture gap.

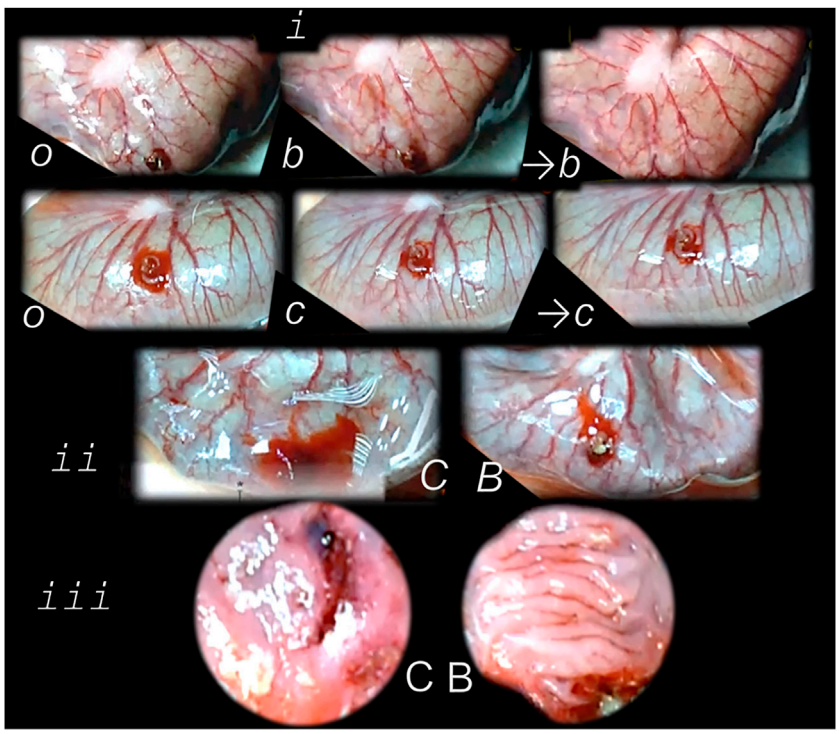

FIGURE 6 | Perforated cecum defect and BPC 157 therapy effect. *i*. Presentation of the perforated cecum defect (*o*-immediately after perforation, before therapy) as an illustration of the rapid healing effect immediately after wounding, with vessels "running" toward the defect augmented by BPC 157 bath application (10 μg/kg) (USB microcamera). *b*—vessels recruitment presentation immediately under the immersion of the BPC 157 bath, which had been applied at the cecum, and presentation immediately thereafter →*b*) with corresponding controls (saline bath 1 ml/rat) presentation *c*, →*c*). *ii*. Resultant bleeding from the perforated defect (*C* (controls), decreased in BPC 157 rats (B). *iii*. Final failure of the perforated defect healing in controls (C) (postinjury day 7) and completely healed defect in BPC 157 rats (B). This beneficial effect goes along with counteraction of the worsening effect of both NOS-blocker L-NAME (5 mg/kg), or NOS substrate L-arginine (100 mg/kg) (directly applied to the perforated cecum, alone or combined, and spread through the abdominal cavity), and normalization of the increased MDA- and NO-values in the cecum (Drmic et al., 2018).

rapidly presented as the major pathway (**Figure 7**). The other veins (such as epigastric veins, intercostal veins, mammary veins, iliolumbar veins, paraumbilical vein, azygos vein, and right ovarian vein) accordingly appear. Together, this means rapidly activated efficient compensatory pathways and the ligation stop at the inferior caval vein efficiently bypassed (Vukojevic et al., 2018).

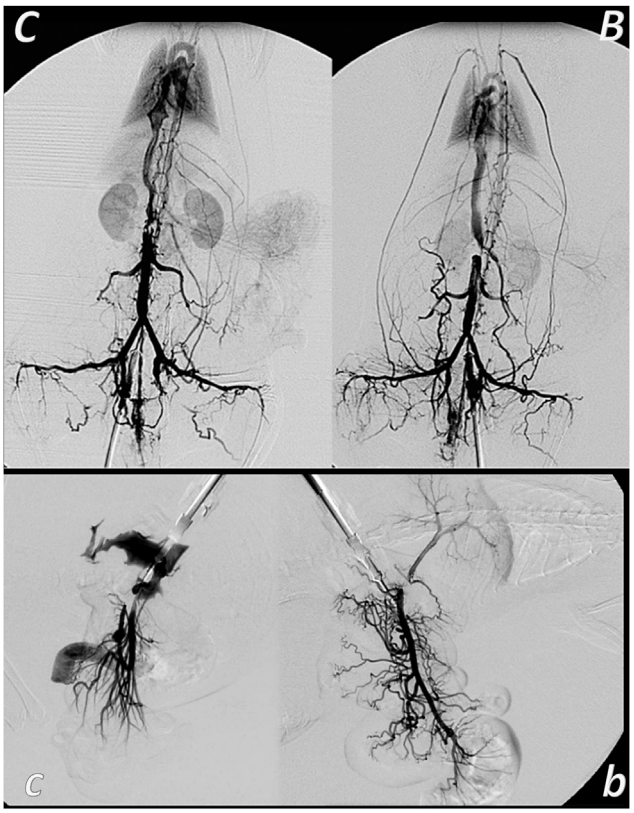

FIGURE 7 | Venous occlusion and BPC 157 therapy. Given BPC 157 (as an abdominal bath) immediately before venography, at a particular point, venography demonstrated a rapid recruitment of the collaterals to bypass occlusion and reestablish blood flow. In the rats with infrarenally occluded inferior caval vein, venography in the inferior caval vein below the ligation shows that the left ovarian vein is rapidly presented as the major pathway. The other veins (such as epigastric veins, intercostal veins, mammary veins, iliolumbar veins, paraumbilical vein, azygos vein, and right ovarian vein) accordingly appear in BPC 157 rats (*B*), unlike in controls (*C*). Together, this means rapidly activated efficient compensatory pathways and the ligation-stop at the inferior caval vein efficiently bypassed (Vukojevic et al., 2018). Both kidneys and canal systems and confluence of the inferior caval vein to the right heart demonstrated that redistribution of otherwise trapped blood volume was rapidly achieved (Vukojevic et al., 2018). In the rats with occluded superior mesenteric vein, occlusion was made at the end of the superior mesenteric vein. Venography in superior mesenteric vein below the ligation shows that bypassing through inferior anterior pancreaticoduodenal vein and superior anterior pancreaticoduodenal vein to the pyloric vein toward the portal vein rapidly occurs in BPC 157 rats (*b*), unlike failed bypassing presentation in controls with occluded superior mesenteric vein (*c*).

Both kidneys and canal systems and confluence of the inferior caval vein to the right heart demonstrated that the trapped blood volume is rapidly redistributed (Vukojevic et al., 2018). This commonly occurred with all of the used BPC 157 therapeutic regimens as well as at both early and advanced stages (Vukojevic et al., 2018). There is a similar beneficial effect in the rats with the Pringle maneuver, ischemia, reperfusion, and suprahepatic inferior caval vein occlusion (Budd–Chiari syndrome) (Gojkovic et al., 2020; Kolovrat et al., 2020). Thus, confronted with major vessels occlusion, BPC 157 commonly alleviates the peripheral vascular occlusion disturbances (Vukojevic et al., 2018; Gojkovic et al., 2020; Kolovrat et al., 2020) rapidly activating alternative bypassing pathways to adequately reestablish the blood flow (Duzel et al., 2017; Amic et al., 2018; Drmic et al., 2018; Vukojevic et al., 2018; Gojkovic et al., 2020; Kolovrat et al., 2020). Once the therapeutic effect begun, the therapeutic effect is continuous, and neither of the continuous ligation-induced disturbances reappeared (Vukojevic et al., 2018; Gojkovic et al., 2020; Kolovrat et al., 2020). Furthermore, direct vein injury, thrombosis, thrombocytopenia, and prolonged bleeding were all counteracted (Vukojevic et al., 2018; Gojkovic et al., 2020; Kolovrat et al., 2020). Trapped blood volume redistribution rapidly occurred throughout rapid presentation of collaterals (Vukojevic et al., 2018; Gojkovic et al., 2020; Kolovrat et al., 2020). Venous hypertension and arterial hypotension and tachycardia, rapidly presented, which were collectively attenuated or counteracted, emphasize BPC 157s therapeutic effects (Vukojevic et al., 2018; Gojkovic et al., 2020; Kolovrat et al., 2020). All these events mean that the counteraction of the full syndrome occurs (Vukojevic et al., 2018; Gojkovic et al., 2020; Kolovrat et al., 2020). This also means the counteracted oxidative stress was as a result of the lysis of endothelial cells (Vukojevic et al., 2018). Counteracted low NO-level in inferior caval vein and particular gene expression (i.e. *Egr, Nos, Srf, Vegfr, Akt1, Plcɣ*, and *Kras*) provide a likely special point to explain how the dysfunction and its counteraction is causal to, or result of (Vukojevic et al., 2018) (see *Genes Expression as Support*).

Finally, therapy as the recovering effect it has on occluded vessels (Duzel et al., 2017; Amic et al., 2018; Drmic et al., 2018; Vukojevic et al., 2018; Gojkovic et al., 2020; Kolovrat et al., 2020) bypassing the occlusion (Duzel et al., 2017; Amic et al., 2018; Drmic et al., 2018; Vukojevic et al., 2018; Gojkovic et al., 2020; Kolovrat et al., 2020) appears as the specific effect of BPC 157 in ischemia/reperfusion (Duzel et al., 2017; Amic et al., 2018; Drmic et al., 2018; Vukojevic et al., 2018; Gojkovic et al., 2020; Kolovrat et al., 2020). There is benefit in the inferior caval vein occlusion (Vukojevic et al., 2018; Gojkovic et al., 2020), also in colitis ischemia/reperfusion (Duzel et al., 2017), duodenal venous congestion lesions (Amic et al., 2018), and cecum perforation (Drmic et al., 2018), arising from BPC 157 therapy in addition to the deep vein thrombosis (Vukojevic et al., 2018; Gojkovic et al., 2020; Kolovrat et al., 2020). Recently, in the bile duct ligation-induced liver cirrhosis (Sever et al., 2019), no portal hypertension development and reversal of the already preexisting portal hypertension to normal values (Sever et al., 2019) have become possible.

Besides, BPC 157 had no effect on clotting parameters as shown in the previous amputation and/or anticoagulant studies (Stupnisek et al., 2012; Stupnisek et al., 2015; Vukojevic et al., 2018), while counteracting prolonged bleeding and thrombocytopenia (Stupnisek et al., 2012; Stupnisek et al., 2015; Vukojevic et al., 2018). Consistently, it was shown that BPC 157 maintains thrombocytes' function (Konosic et al., 2019).

Here, the concluding evidence may be that BPC 157 counteracted adhesion formation after abdominal wall injury. Additionally, its counteracting effect occurred even with pre-existing adhesions (Berkopic Cesar et al., 2020).

Thus, with the damage of the peritoneum, two damaged peritoneal surfaces come into contact with each other, and the coagulation cascade is activated (Fortin et al., 2015). Contrarily, BPC 157 counteracts the whole Virchow triad (Vukojevic et al., 2018; Gojkovic et al., 2020; Kolovrat et al., 2020), venous thrombosis (Vukojevic et al., 2018; Gojkovic et al., 2020; Kolovrat et al., 2020), and arterial thrombosis (Hrelec et al., 2009; Gojkovic et al., 2020; Kolovrat et al., 2020). Also, BPC 157 administration attenuates prolonged bleeding and thrombocytopenia after amputation, organ perforation, and anticoagulant use or prolonged major vessel occlusion (Stupnisek et al., 2012; Stupnisek et al., 2015; Drmic et al., 2018; Vukojevic et al., 2018). Consequently, it may be likely that BPC 157 may also interfere with and reverse the process that would result in fusion to form a connection, for example, adhesion (Berkopic Cesar et al., 2020). Therefore, less adhesion formation as well as reversing existing adhesions, the restoration of normal tissue structure and function, suggest that BPC 157 may act with the temporary role of fibrin in healing without adhesions that must be purposefully degraded by the fibrinolytic system (Collen, 1980; Davey and Maher, 2017).

Gene Expression as Support

In general, as before (Vukojevic et al., 2018), our focus was on the early and very early periods providing the general understanding of the precise coordination of cellular events, the formation and modification of the vascular system, and molecular signaling by numerous molecules which are responsible for fast activation and modulation of these events (Vukojevic et al., 2018).

For this purpose, the findings obtained in the rats with infrarenal occlusion of the inferior caval vein may be noteworthy (Vukojevic et al., 2018). The investigation was done at two particular intervals, at 1 and 24 h. Assessed were the inferior caval vein (which was occluded), right ovarian vein (which appears as blind vessel due to the infrarenal occlusion), and left ovarian vein (which serves as a bypassing pathway) (Vukojevic et al., 2018). With BPC 157 administration, these beneficial effects were combined with particular specificities with the altered genes' expression (*Egr, Nos, Srf, Vegr, Plc*ɣ, and *Kras*) or no change (*Akt1* continuously remained unchanged) (Vukojevic et al., 2018).

BPC 157 administration raises several questions regarding its therapeutic role in the process occurring in rats with obstructed vessels (Sikiric et al., 2014; Duzel et al., 2017; Vukojevic et al., 2018; Gojkovic et al., 2020; Kolovrat et al., 2020) and with vessels that used to be obstructed (Duzel et al., 2017; Kolovrat et al., 2020; Vukojevic et al., 2020). Rapid endothelial restoration and activation of the major collaterals (in addition, there are abundant anastomoses between individual vessels on both surfaces of the large intestine (Kachlik, et al., 2010)) may reorganize blood flow (Duzel et al., 2017; Vukojevic et al., 2018; Gojkovic et al., 2020; Kolovrat et al., 2020). Additionally, the rapid therapeutic effect of BPC 157 is evidenced by rapid reversal of the negative chain of events (Vukojevic et al., 2018). This included circumvention of the complex downhill syndrome, as well as a sudden decrease of blood supply, decreased NO levels in the inferior caval vein tissue, an immediate heavy loss of endothelial cells from the vascular wall, a lower eNOS production ability (Berra-Romani et al., 2013), and finally, the elimination of oxidative stress due to endothelial cell lysis (Rangan and Bulkley, 1993; Schiller et al., 1993). BPC 157 has been able to restore endothelial integrity and reverse most oxidative stress-induced damage (Duzel et al., 2017; Amic et al., 2018; Drmic et al., 2018; Vukojevic et al., 2018; Sever et al., 2019). Moreover, it largely interacts with the NO-system (Sikiric et al., 2014), the endothelium being significant in that demonstrates increased plasma NO-values, but normalized 3,4-methylenedioxyamphetamine (MDA)-values, as well as adequate endothelial NO-synthase (eNOS) system function (Duzel et al., 2017; Amic et al., 2018; Drmic et al., 2018; Vukojevic et al., 2018; Sever et al., 2019) and blood supply. After consideration of the aforementioned BPC 157–induced changes, several applications of BPC 157 with respect to its therapeutic effects on rats with preexisting (Duzel et al., 2017; Kolovrat et al., 2020; Vukojevic et al., 2020) or existing vessel obstruction (Sikiric et al., 2014; Duzel et al., 2017; Vukojevic et al., 2018; Gojkovic et al., 2020; Kolovrat et al., 2020) can be foreseen.

More specifically, this may be observed with respect to certain genes, including *Egr, Nos, Srf, Vegr, Akt1, Plc*ɣ, and *Kras* genes (Vukojevic et al., 2018), all of which are responsible for the synthesis of factors necessary for a diverse set of processes. The factors have proadhesive, proinflammatory, and prothromobic roles, all of which become pertinent after vascular injury (Schweighofer et al., 2007; Ansari et al., 2015; Hinterseher et al., 2015). In these, the described BPC 157 efficacy is considered as an important demonstration of the confirmation that BPC 157 could ensure a particular specificity within the *Egr, Nos, Srf, Vegfr, Akt1, Plc*ɣ, and *Kras* pathways (Vukojevic et al., 2018). After administering BPC 157 to rats with a ligated inferior caval vein, the beneficial effects induced by BPC 157 were complemented with altered *Egr, Nos, Srf, Vegr*, and *Kras* gene expression. Specifically, this included increased (*Egr, Nos, Srf,* and *Kras*) or decreased (*Egr, Vegfr,* and *Plc*ɣ) gene expression, while *Akt1* gene expression remained unchanged (Vukojevic et al., 2018). These changes in gene expression are dependent on the time interval during which the genes were analyzed, as well as the type of vessel investigated. For example, increased levels of the *Egr* gene were observed at 1 h, *Nos*, *Srf*, and *Kras* genes demonstrated increased expression at 1 and 24 h in all vessels, and *Egr* expression was increased at 24 h in both ovarian veins. Likewise, decreased gene expression of *Egr* was evident at 24 h in the inferior caval vein, *Vegfr* expression was decreased at 1 h and 24 h in all vessels, and *Plc*ɣ gene expression was decreased at 24 h in the inferior caval vein. *Akt1* remained unchanged in the inferior caval vein, as well as in the right ovarian vein and left ovarian vein (Vukojevic et al., 2018). Consequently, the aforementioned data suggest that particular pathways may have both local and systemic relevance. Collectively, these pathways may be responsible for the novel balance (of gene expression) achieved and ultimately, maintained. Finally, we should emphasize the rapid presentation of all of these effects. Obviously, they occurred before the initiation of angiogenesis (Sikiric et al., 1993; Sikiric et al., 2006; Sikiric et al., 2010; Sikiric et al., 2011; Sikiric et al., 2012; Sikiric et al., 2013; Seiwerth et al.,

Gene symbol	Synonyms	2 min	5 min	10 min
Akt1	*PKB, RAC*	▲	▲	▲
Grb2	*Ash-psi*	▲	▲	▲
Nos3	*cNOS, eNos*	▲	▲	▲
Pik3cd	*LOC366508*	▲	▲	▲
Prkcg	*PKC, Prkc*	▲	▲	▲
Ptk2	*FAK, FADK1, FRNK*	▲	▲	▲
Src	*c-Src, p60-Src*	▲	▲	▲
Braf	*B-Raf*	○	▲	▲
Egfr	*ERBB1*	○	▲	▲
Egr1	*NGFI-A, Krox-24, Zif268*	○	▲	▲
Hdac7	*HD7*	○	▲	▲
Mapk1	*Erk2, ERT1, p42mapk*	○	▲	▲
Mapk3	*Erk-1, ERT2, p44*	○	▲	▲
Mapk14	*CRK1, p38, Mxi2*	○	▲	▲
Plcg1	*PLC148, PLC-II, PPLCA*	○	▲	▲
Pxn	*LOC360820*	○	▲	▲
Srf	*LOC501099*	○	▲	▲
Vegfa	*VEGF-A, VPF*	○	▲	▲
Kras	*Ki-Ras, Kras2*	○	○	▲

FIGURE 8 | Gene expression analysis and BPC 157 therapy. With the therapy done immediately after wounding, we performed the *Akt1, Braf, Egfr, Egr1, Grb2, Hdac7, Kras, Mapk1, Mapk3, Mapk14, Nos3, Pik3cd, Plcg1, Prkcg, Ptk2, Pxn, Src, Srf*, and *Vegfa* genes expression analysis (○, no significant change in gene expression; ▲, increased gene expression) in the rats' excision wound and in the skin and subcutaneous tissue, done at 2, 5, and 10 min following BPC 157 application. Thus, considering the quite rapid presentation of the BPC 157 beneficial effect in the wound healing, it is likely indicative that the expression of all of the genes *Akt1, Braf, Egfr, Egr1, Grb2, Hdac7, Kras, Mapk1, Mapk3, Mapk14, Nos3, Pik3cd, Plcg1, Prkcg, Ptk2, Pxn, Src, Srf,* and *Vegfa* is increased at the 10-min interval. An additional indicative point is sequential involvement. The increased expression of the *Akt1, Grb2, Nos3, Pik3cd, Prkcg, Ptk2,* and *Src* appears immediately at 2-min interval. *Braf, Egfr, Egr1, Hdac7, Mapk1, Mapk3, Mapk14, Plcg1, Prkcg, Ptk2, Pxn, Src, Srf,* and *Vegfa* increased expression is noted at 5 min. The increased expression of the *Kras* appears at 10 min. Of note, an enormous number of the interactions between the genes involved prevents a more definitive understanding of function insight outcome. However, the evidence is obtained that BPC 157 action initially affects expression of particular genes (i.e., *Akt1, Grb2, Nos3, Pik3cd, Prkcg, Ptk2, Src*). Then, it involves other set of the genes (*Braf, Egfr, Egr1, Hdac7, Mapk1, Mapk3, Mapk14, Plcg1, Prkcg, Ptk2, Pxn, Src, Srf,* and *Vegfa*). Subsequently, it concludes with additional genes set (i.e., *Kras*). Together, these may likely represent the complex way how the action, which will eventually resolve the lesion, may start and progress.

2014; Sikiric et al., 2014; Sikiric et al., 2016; Sikiric et al., 2017; Kang et al., 2018; Seiwerth et al., 2018; Sikiric et al., 2018; Gwyer et al., 2019; Park et al., 2020; Sikiric et al., 2020a; Sikiric et al., 2020b). Thus, we can assume that pathways additional to those involved in angiogenesis (Vukojevic et al., 2018) are associated with the increased expression, internalization of VEGFR2, and the activation of the VEGFR2-Akt-eNOS signaling pathway (Hsieh et al., 2017).

Furthermore, we additionally challenged the most immediate period after injury induction (skin defect) (i.e., 2, 5, and 10 min) (**Figure 8**) due to the evidence that BPC 157 did ensure a particular specificity within the pathways (at least, *Egr, Nos, Srf, Vegr, Akt1, Plcγ*, and *Kras* genes) (Vukojevic et al., 2018). We emphasize the immediate relationship of the pentadecapeptide BPC 157 with the genes involved in cellular signaling pathways important for the regulation of angiogenesis. That point is supported with the extensive gene expression analysis. With the therapy done immediately after wounding, we performed the *Akt1, Braf, Egfr, Egr1, Grb2, Hdac7, Kras, Mapk1, Mapk3, Mapk14, Nos3, Pik3cd, Plcg1, Prkcg, Ptk2, Pxn, Src, Srf*, and *Vegfa* genes expression analysis in the rats' excision wounds, in the skin, and subcutaneous tissue, done at 2, 5, and 10 min following BPC 157 application (**Figure 8**). Thus, considering the quite rapid presentation of the beneficial effect of BPC 157 in wound healing, it is likely indicative that the expression of all of the genes *Akt1, Braf, Egfr, Egr1, Grb2, Hdac7, Kras, Mapk1, Mapk3, Mapk14, Nos3, Pik3cd, Plcg1, Prkcg, Ptk2, Pxn, Src, Srf,* and *Vegfa* is increased at the 10-min interval. An additional indicative point is sequential involvement. The increased expression of the *Akt1, Grb2, Nos3, Pik3cd, Prkcg, Ptk2,* and *Src* appears immediately at 2-min interval. Increased expression of *Braf, Egfr, Egr1, Hdac7, Mapk1, Mapk3, Mapk14, Plcg1, Prkcg, Ptk2, Pxn, Src, Srf,* and *Vegfa* is noted at 5 min. The increased expression of the *Kras* appears at 10 min. Of note, an enormous number of the interactions between the genes involved obscure the final outcome. However, the evidence is obtained that BPC 157 action initially affects expression of particular genes (i.e., *Akt1, Grb2, Nos3, Pik3cd, Prkcg, Ptk2,* and *Src*). Then, it involves other set of the genes (*Braf, Egfr, Egr1, Hdac7, Mapk1, Mapk3, Mapk14, Plcg1, Prkcg, Ptk2, Pxn, Src, Srf,* and *Vegfa*). Subsequently, it concludes with additional set of genes (i.e., *Kras*). Together, these may likely represent the complex way of how the action, which will eventually resolve the lesion, may start and progress.

The Effect on Other Tissues Healing as Support

Defining of the adequate skin wound healing effect (Seiwerth et al., 1997; Mikus et al., 2001; Sikiric et al., 2003; Xue et al., 2004a; Bilic et al., 2005; Seveljevic-Jaran et al., 2006; Tkalcevic et al., 2007; Huang et al., 2015) indicates its essential application in the other tissues healing, particularly, the muscle (**Figures 9–12**), tendon (**Figure 12**), ligament, and bone (**Figure 13**) (Sikiric et al., 1993; Sikiric et al., 2006; Sikiric et al., 2010; Sikiric et al., 2011; Sikiric et al., 2012; Sikiric et al., 2013; Seiwerth et al., 2014; Sikiric et al., 2014; Sikiric et al., 2016; Sikiric et al., 2017; Kang et al., 2018; Seiwerth et al., 2018; Sikiric et al., 2018; Gwyer et al., 2019; Park et al., 2020; Sikiric et al., 2020a; Sikiric et al., 2020b). Especially, BPC 157 exhibits both special muscle healing (i.e., after transection of major muscle (**Figures 9**, **11**, **12**), crush (**Figure 10**), and denervation (**Figure 11**) (Staresinic et al., 2006; Novinscak et al., 2008; Mihovil et al., 2009; Pevec et al., 2010)), and tendon healing (Staresinic et al., 2003; Krivic et al., 2006; Krivic et al., 2008) (i.e., after the Achilles tendon transection and detachment from calcaneal bone), or ligament healing (Cerovecki et al., 2010) (i.e., medial collateral ligament transection). In addition, along with function recovery (**Figure 11**), BPC 157 counteracts muscle disability related to various noxious procedures, after abdominal aorta anastomosis (Hrelec et al., 2009), L2-L3 compression (Perovic et al., 2019), severe electrolytes disturbances (Baric et al., 2016; Medvidovic-Grubisic et al., 2017), application of the succinylcholine (Stambolija et al., 2016), neuroleptics (Jelovac et al., 1999; Belosic Halle et al., 2017), or neurotoxin (MPTP, cuprizone)

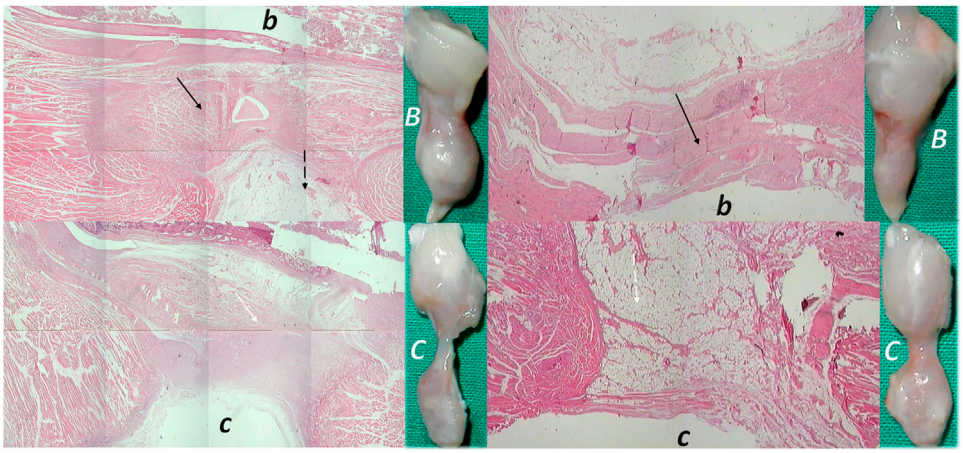

FIGURE 9 | (Left, 14 days) **(right**, 28 days). Transected muscle and BPC 157 therapy (Staresinic et al., 2006). Quadriceps muscle was completely transected transversely 1.0 cm proximal to the patella means a definitive defect that cannot be compensated in rat. BPC 157 (10 μg, 10 ng, and 10 pg/kg) is given intraperitoneally, once daily; the first application 30 min posttransection, the final 24 h before sacrifice. Throughout the whole 72-day period, BPC 157 consistently improves all muscle-healing parameters (biomechanic, function, macro/microscopy/immunochemistry, finally presentation close to normal non-injured muscle, and no postsurgery leg contracture). Controls exhibit stumps grossly weakly connected (*C*), at postsurgery day 14 and 28, microscopically (HE, x10), at postsurgery day 14, gap filled with fibrous tissue (white arrow) (*c*), and at postsurgery day 28, a gap filled with fat tissue (dashed white arrow); incorporating few collagen strands is interposed between the transection stumps and unsuccessful attempts of muscle fibers to cross the gap can be observed (*c*). Contrarily, BPC 157 rats exhibit stumps grossly well connected, approaching to presentation of the normal non-injured muscle (*B*), microscopically, at postsurgery day 14 and at postsurgery day 28, broad muscle (black arrow) fibers connecting the stumps, while the fat tissue is much less present (*b*) (dashed black arrow).

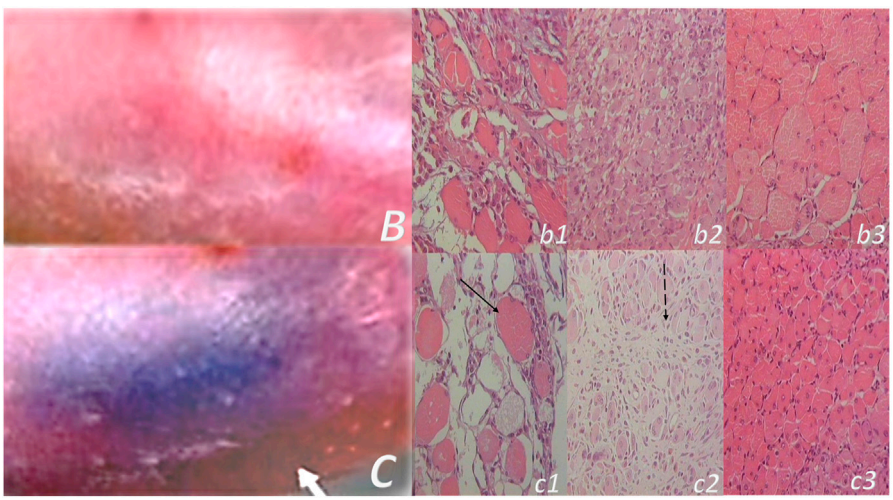

FIGURE 10 | Muscle crush injury and BPC 157 therapy (Novinscak et al., 2008; Pevec et al., 2010). Force delivered was of 0.727 Ns/cm^2 (impulse force 0.4653 Ns, kinetic energy 0.7217 J), to a maximum diameter of gastrocnemius muscle complex (GMC), about 2 cm proximal to the insertion of the Achilles tendon. Regimens with similar effectiveness included (i) BPC 157 dissolved in saline (10 μg, 10 ng/kg body weight), (ii) pentadecapeptide BPC 157 in neutral cream (1.0 or 0.01 μg dissolved in distilled water/g commercial neutral cream). Controls received saline (5.0 ml/kg) applied intraperitoneally and or commercial neutral cream applied as a thin cream layer at the site of injury. All animals were treated only once, immediately after injury, if killed and assessed after 2 h. Alternatively, the animals were treated once daily, receiving a final dose 24 h before death and/or assessment (walking, muscle function, and a macroscopic analysis) at days 1, 2, 4, 7, and 14. Gross posttraumatic hematoma presentation at 2 h after injury induction (*C*-control (white arrow), *B*-BPC 157 rats (thin cream layer at the site of the injury immediately after injury induction)). Microscopy assessment (*c1, b1* (postinjury day 4), *c2, b2* (postinjury day 7), and *c3, b3* (postinjury day 14)). HE, x10. Controls. Severe atrophy with severe reduction of myocytes (black arrow) and no regeneration attempt, pronounced perimyocytic edema (postinjury day 4, *c1*); scarce to moderate regeneratory attempts in muscle with maturing granulation tissue (dashed black arrow) (postinjury day 7, *c2*); pronounced regeneration with a high number of smaller myocytes and some areas of scarring (postinjury day 14, *c3*). BPC 157. Clearly visible regenerative activity and less edema (postinjury day 4, *b1*); florid regenerative activity in myocytes with high number of relatively small myocytes and no scarring (postinjury day 7, *b2*); well-regenerated myocytes of appropriate size and very little scarring (postinjury day 14, *b3*).

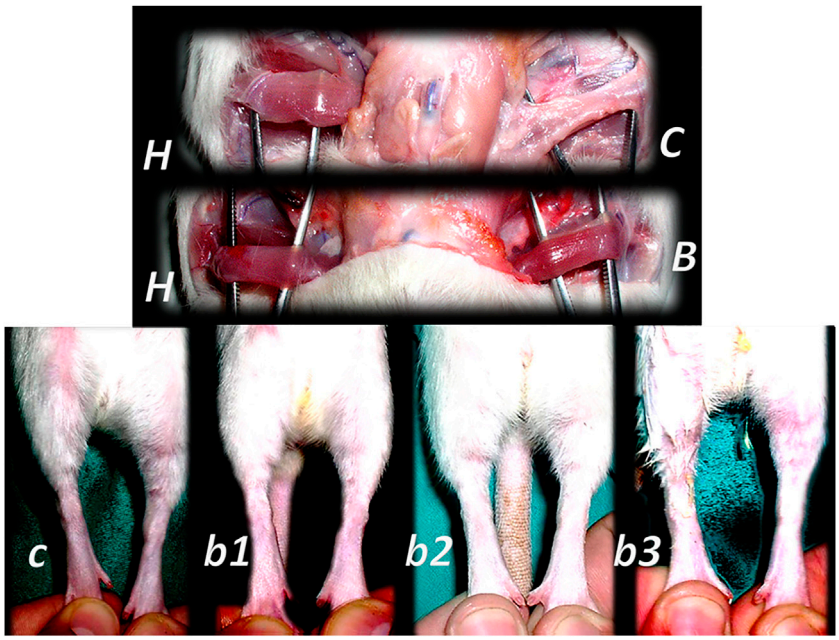

FIGURE 11 | Denervated gracilis muscle and BPC 157 therapy **(upper)** (Mihovil et al., 2009). Transected muscle induced injured leg function failure as induced leg contracture and BPC 157 therapy **(lower)** (Staresinic et al., 2006). Presentation of the denervated gracilis muscle (*B, C*) and normal healthy gracilis muscle (*H*) in rats at 1 year after denervation. Characteristic denervated muscle presentation in controls (*C*). Counteraction by BPC 157 (10 μg/kg) therapy given per-orally, in drinking water (0.16 μg/ml, 12 ml/rat/day) till the sacrifice (*B*). Quadriceps muscle was completely transected transversely 1.0 cm proximal to patella to present a definitive defect that cannot be compensated in rats with a considerable injured leg contracture as presented at postsurgery day 21 in controls with maximal leg extension (*c*). Counteraction by various regimens of the BPC 157 (10 μg, 10 ng) therapy. Given intraperitoneally, once daily; the first application 30 min posttransection, the final 24 h before sacrifice (*b1*); per-orally, in drinking water (0.16 μg/ml, 0.16 ng/ml, and 12 ml/rat/day) till the sacrifice (*b2*); locally, thin layer of neutral cream 1 μg/1 g neutral cream once daily; the first application 30 min post-transection, the final 24 h before sacrifice (*b3*).

(Sikiric et al., 1999c; Klicek et al., 2013). Also, BPC 157 counteracts tumor cachexia (Kang et al., 2018). There are counteracted muscle wasting, significantly corrected deranged muscle proliferation as well as myogenesis, counteracted increase of the proinflammatory cytokines such as IL-6 and TNF-α, looking at muscle metabolism relevant to cancer cachexia as well as the changes in the expression of FoxO3a, p-AKT, p-mTOR, and P-GSK-3β (Kang et al., 2018). To illustrate the success of the application and the way of application efficacy, it may be instructive to mention the noted effect in the recovery of the transected sciatic nerve injury (providing the efficacy of the once intraperitoneal, intragastric application much like the application into the tube with inserted nerve stumps) (Gjurasin et al., 2010). In support, recently BPC 157 increased the survival rate of cultured enteric neurons and the proliferation rate of cultured enteric glial cells (Wang et al., 2019).

In the aforementioned study by Hsieh and collaborators (Hsieh et al., 2017) that focused on the ischemic muscle model (achieved via removal of the femoral artery), the pro-angiogenic effects of BPC 157 are evident, given the increased expression, internalization of vascular endothelial growth factor receptor 2 (VEGFR2), and the activation of the VEGFR2-Akt-eNOS signaling pathway (Hsieh et al., 2017). BPC 157 promotes angiogenesis in the chick choriallantoic membrane (CAM) assay and tube formation assay (Hsieh et al., 2017). Additionally, it counteracts rat hind limb ischemia by accelerating blood flow recovery and vessel number (Hsieh et al., 2017). BPC 157 upregulates VEGFR2 expression in rats with hind limb ischemia and endothelial cell culture. BPC 157–induced VEGFR2 internalization is combined with VEGFR2-Akt-eNOS activation. Of note, that BPC 157 effect is particular (i.e., activated the phosphorylation of VEGFR2, Akt, and eNOS signaling pathway) and does not need other known ligands or shear stress (Hsieh et al., 2017).

Also, this tissue-specific effect is demonstrated in tendon tissue-specific healing, which occurs without side effects that are present with other peptides (Seiwerth et al., 2018). For instance, ossicle formation in Achilles tendon tissue appears with osteogenic protein 1 (OP-1) (Forslund and Aspenberg, 1998). Contrary to this, it does not induce ossicle formation in tendon or ligament tissue (Staresinic et al., 2003; Krivic et al., 2006; Krivic et al., 2008). Specifically, BPC 157 accelerates tendon- and (Staresinic et al., 2003; Krivic et al., 2006; Krivic et al., 2008) ligament-healing (Cerovecki et al., 2010) and has a strong osteogenic effect the in non-union model (Sebecic et al., 1999) (and in other models, such as is observed with rat femoral head osteonecrosis (Gamulin et al., 2013), or alveolar bone loss (Keremi et al., 2009). Of note, in the tendon studies (Chang et al., 2011; Chang et al., 2014), BPC 157–induced promotion of the *ex vivo* outgrowth of tendon fibroblasts from tendon explants, cell survival under stress, and the *in vitro* migration of tendon fibroblasts are the effects mediated by the activation of the

focal adhesion kinase (FAK)–paxillin pathway (Chang et al., 2011; Chang et al., 2014). Janus kinase (JAK) 2, the downstream signal pathway of growth hormone receptor, was activated in a time-dependent fashion via stimulation of the BPC 157–treated tendon fibroblasts with a growth hormone (Chang et al., 2011; Chang et al., 2014). Thus, the BPC 157–induced increase of growth hormone receptor in tendon fibroblasts may potentiate the proliferative effect of growth hormone and contribute to tendon healing (Chang et al., 2011; Chang et al., 2014).

Similarly, as the next wound-healing focus with BPC 157 therapy (Sever et al., 2019) administered per-orally, continuously in drinking water, or intraperitoneally, alleviated rats showed bile duct ligation (BDL) and counteracted BDL-induced liver cirrhosis (Sever et al., 2019). BPC 157 normalized MDA and NO-levels in the liver of BDL rats (Sever et al., 2019) and wound-healing response to chronic liver injury that may be accordingly modified (**Figure 12**) (Albanis and Friedman, 2001; Aller et al., 2008; Wynn, 2008; Sever et al., 2019). There were cured jaundice, weight loss, liver enlargement, microscopy (i.e., piecemeal necrosis, focal lytic necrosis, apoptosis and focal inflammation, and disturbed cell proliferation (Ki-67-staining), cytoskeletal structure in the hepatic stellate cell (α-SMA staining), collagen presentation (Mallory staining), and biochemistry presentation (Sever et al., 2019), and counteracted the increased NOS3 expression, interleukin (IL)-6, tumor necrosis factor (TNF)-α, and IL-1β levels. There were both prophylactic and therapy effects. Developing portal hypertension as well as established portal hypertension were both rapidly counteracted in BDL rats (i.e., BPC 157 per-orally, in drinking water, since the end of week 4) (Sever et al., 2019). The balanced collagen synthesis and counteracted hepatic fibrosis (considered as a model of the wound-healing response to chronic liver injury), are along with BPC 157s particular interaction with several molecular pathways (Tkalcevic et al., 2007; Chang et al., 2011; Cesarec et al., 2013; Chang et al., 2014; Huang et al., 2015; Hsieh et al., 2017; Kang et al., 2018; Vukojevic et al., 2018; Sever et al., 2019; Park et al., 2020; Vukojevic et al., 2020). In addition, there is a likely analogy (see for review i.e., (Seiwerth et al., 2018)) with the attenuated fibrosis and scar formation in other tissues (i.e., the skin, muscle, tendon, and ligament) (Mikus et al., 2001; Sikiric et al., 2003; Staresinic et al., 2003; Krivic et al., 2006; Staresinic et al., 2006; Krivic et al., 2008; Cerovecki et al., 2010). Also, they regained the dermal, muscle, tendon, and ligament functions (Mikus et al., 2001; Sikiric et al., 2003; Staresinic et al., 2003; Krivic et al., 2006; Staresinic et al., 2006; Krivic et al., 2008; Cerovecki et al., 2010). These, as mentioned before, occur in the BPC 157s healing of the severe injuries, such as the skin burns (Mikus et al., 2001; Sikiric et al., 2003) or muscle (Staresinic et al., 2006) or tendon (Staresinic et al., 2003; Krivic et al., 2006; Krivic et al., 2008) or ligament (Cerovecki et al., 2010) transection.

In this issue, the already mentioned Tkalcevic and collaborators' study may be illustrative (Seveljevic-Jaran et al., 2006; Tkalcevic et al., 2007). A clear demonstration was obtained that BPC 157 stimulated both the egr-1 gene (critical in proliferation, differentiation, and inflammation during cholestatic liver injury, cytokine and growth factor generation, and early extracellular matrix (collagen) formation) (Kim et al., 2006; Zhang et al., 2011) and its co-repressor gene nab2 (Seveljevic-Jaran et al., 2006; Tkalcevic et al., 2007). Consequently, as also indicated in our other liver studies (Ilic et al., 2009; Ilic et al., 2010; Ilic et al., 2011a; Ilic et al., 2011b), BPC 157 (with nab2) may be a particular feedback-controlling mechanism.

The final point of the wound-healing focus with BPC 157 therapy (Seiwerth et al., 1997; Mikus et al., 2001; Sikiric et al., 2003; Xue et al., 2004a; Bilic et al., 2005; Seveljevic-Jaran et al., 2006; Tkalcevic et al., 2007; Huang et al., 2015) belongs to the

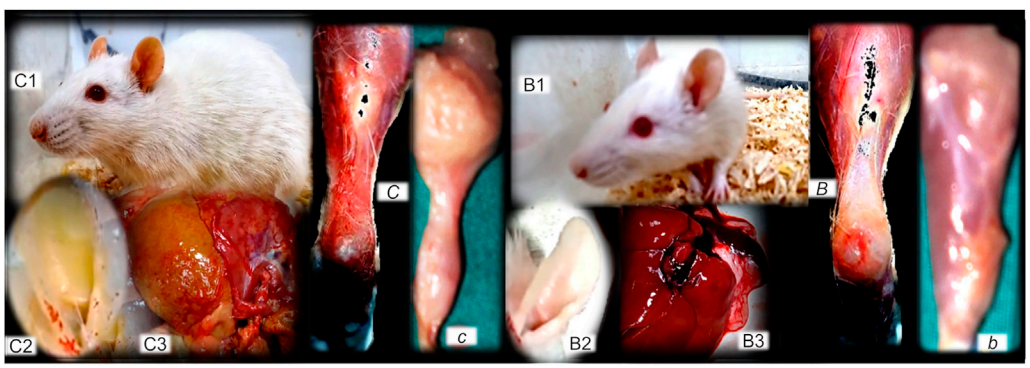

FIGURE 12 | (Left, control), **(right**, BPC 157). Fibrosis and BPC 157 therapy. Summarized gross evidence. Presentation of the bile duct ligation rats ("yellow rats") following 4 months of occlusion (as a model of the wound-healing response to chronic liver injury), gross rat presentation (C1), and after sacrifice, yellow ears (C2), and liver presentation (C3) (Sever et al., 2019). Possible analogy goes with the dermal, muscle (proximal and distal stump of quadriceps muscle poorly connected at day 72 after transection (*c*)), tendon (gap after tendon detached from calcaneus (*C*)) and ligament fibrosis and scar formation, and failed function (Mikus et al., 2001; Krivic et al., 2006; Staresinic et al., 2006; Cerovecki et al., 2010). In rats with bile duct ligation, BPC 157 counteracts cirrhosis and portal hypertension (gross rat presentation (B1), and after sacrifice, normal ears (B2), and liver presentation (B3)) much like it attenuates dermal, muscle (well-formed quadriceps muscle at day 72 after transection (*b*), tendon (tendon reattached to the calcaneous after detachement (*B*)), and ligament fibrosis and scar formation, and regained function (Mikus et al., 2001; Krivic et al., 2006; Staresinic et al., 2006; Cerovecki et al., 2010).

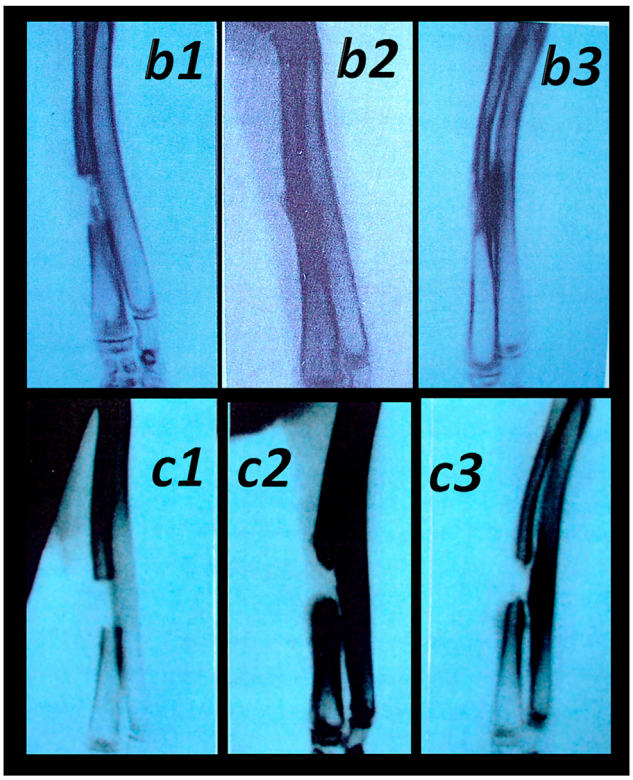

FIGURE 13 | Healing of the segmental osteoperiosteal bone defect (0.8 cm, in the middle of the left radius) in rabbits (Sebecic et al., 1999). Incompletely healed defect in all controls (assessed during 6 weeks, in 2-weeks intervals (*c1* (week 2), *c2* (week 4), and *c3* (week 6)). Pentadecapeptide BPC 157 beneficial effect was consistently obtained (either percutaneously given locally (10 μg/kg) into the bone defect, or applied intramuscularly (intermittently, at postoperative days 7, 9, 14, and 16 at 10 μg/kg) or continuously (once per day, postoperative days 7–21 at 10 microg or 10 ng/kg)) (*b1* (week 2), *b2* (week 4), and *b3* (week 6)). Comparative regimens included percutaneous administration of autologous bone marrow locally (2 ml, postoperative day 7) as well as an autologous cortical graft inserted in the bone defect immediately after its formation. Saline-treated (2 ml intramuscularly (i.m.) and 2 ml locally into the bone defect), injured animals were used as controls (Sebecic et al., 1999).

controlling role of the pentadecapeptide BPC 157, considering that all of the described healing effects should avoid possible harmful outrage.

Illustratively, BPC 157 may interfere with NO-system activities (Sikiric et al., 2014) and counteract harmful events, arising from either NO-blockade (L-NAME-application) or L-arginine (NOS-substrate-application) (Sikiric et al., 2014). As an indicative example, without its own effect on normal blood pressure, it counteracts L-NAME hypertension as well as L-arginine hypotension (Sikiric et al., 1997a). Also, BPC 157 counteracts chronic heart failure (Lovric Bencic et al., 2004) or venous occlusion (Vukojevic et al., 2018)–induced hypotension (Lovric Bencic et al., 2004; Vukojevic et al., 2018) as well as hyperkalemia-induced hypertension (Barisic et al., 2013). Accordingly, BPC 157 provides the counteraction of the opposite effects of L-NAME (prothrombotic) and L-arginine (antithrombotic) application (Stupnisek et al., 2015). Likewise, BPC 157 may interfere with prostaglandin system activities, that is, it strongly counteracts NSAIDs toxicity (Sikiric et al., 2013), much like it counteracts developing and already formed adjuvant arthritis in rats (Sikiric et al., 1997c). Also, it strongly counteracts corticosteroid-induced adverse effects (i.e., eventual healing failure (Klicek et al., 2008; Krivic et al., 2008; Skorjanec et al., 2009; Pevec et al., 2010) and worsening, and immunosuppression (Sikiric et al., 2003).

That controlling point is also recognized in the most recent reviews (Gwyer et al., 2019; Sikiric et al., 2018). As indicated, despite the tumor-promoting effects of many growth factors and peptides (Gwyer et al., 2019; Sikiric et al., 2018), BPC 157 has been shown to inhibit and counteract uncontrolled cell proliferation (Ki-67 overproduction counteracted) and increased expression of VEGF and subsequent signaling pathways (Radeljak et al., 2004; Sever et al., 2019), thus avoiding and directly counteracting VEGF tumorigenesis (Radeljak et al., 2004). Furthermore, as mentioned (Gwyer et al., 2019), BPC 157 inhibits the growth of several tumor lines and can counteract tumor cachexia (Kang et al., 2018), a point combined, as mentioned, with counteracted pro-inflammatory and pro-cachectic cytokines such as IL-6, TNF-α, cancer cachexia–related pathways expression (i.e., FoxO3a, p-AKT, p-mTOR, and P-GSK-3β) (Kang et al., 2018). Also, BPC 157 may counteract cyclophosphamide toxicity (Luetic et al., 2017; Sucic et al., 2019), and in particular, BPC 157 consistently decreased elevated MDA values, while MDA itself, owing to its high cytotoxicity and inhibitory action on protective enzymes, is suggested to act as a tumor promoter and a cocarcinogenic agent (Seven et al., 1999; Bakan et al., 2002).

Moreover, BPC 157 therapy generated from its distinctive healing effects in various tissues also functions as an eye drops therapy that heals perforating corneal ulcers in rats and rapidly regains corneal transparency (**Figures 14**, **15**) (Masnec et al., 2015). Epithelial defects completely healed within three or four days (2 μg or 2 ng regimens, respectively), aqueous cells were not present after four or five days after injury. Regularly, in control rats, developed new vessels grew from the limbus to the penetrated area. Contrarily, generally no new vessels grew in BPC 157–treated rats (i.e., those that did form in the limbus did not make contact with the penetrated area) (Masnec et al., 2015), showing that BPC 157 therapy may acknowledge also "the angiogenic privilege" of the corneal avascularity as essential for corneal wound healing (Tshionyi et al., 2012). This may be the clue that to regain the tissue integrity after wounding, BPC 157 may accommodate the healing depending on the tissue and injury conditions.

SUMMARY

In conclusion, since the wound healing therapy with the standard angiogenic growth factors may be of essential importance, we presented an overview of the stable gastric pentadecapeptide BPC 157 and wound-healing issue.

Ultimately, this review challenges the general strategy that the skin wound healing (Seiwerth et al., 1997; Mikus et al., 2001;

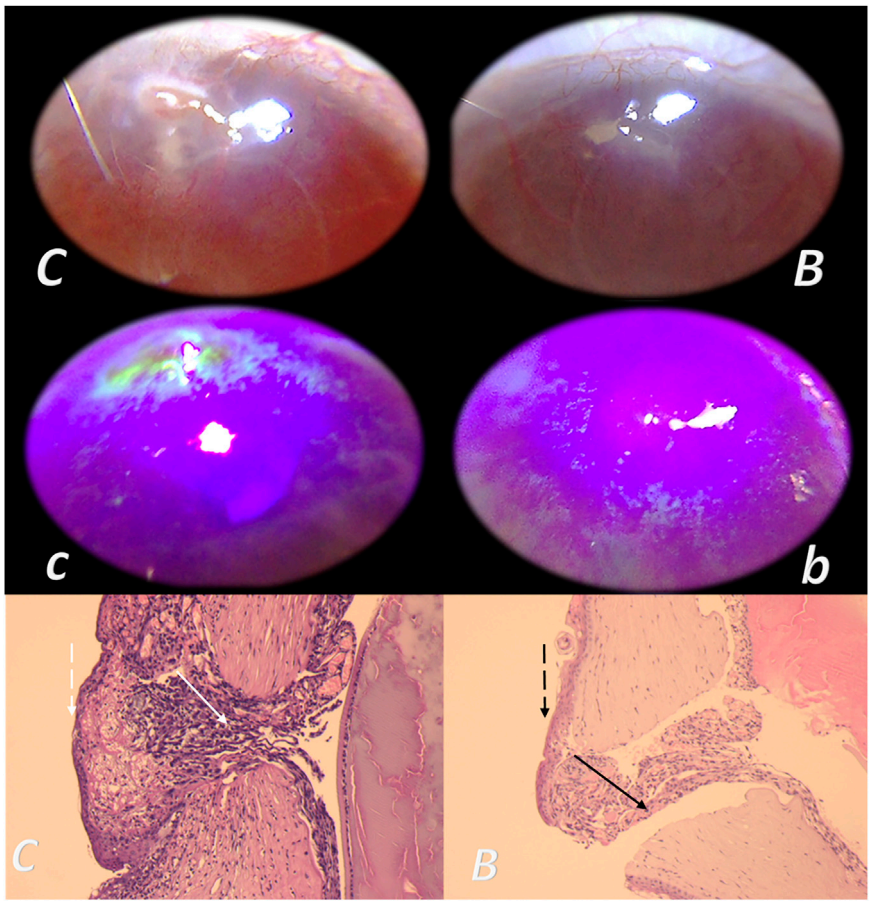

FIGURE 14 | Corneal ulcer and BPC 157 therapy, ophthalmoscopy and microscopy presentation (Masnec et al., 2015). In deeply anesthetized rats, a penetrant linear 2-mm incision was made and two drops of 0.4% oxybuprocaine topical anesthetic were given (to inhibit possible eyelid reflex) in the paralimbal region of the left cornea at the 5 o'clock position with a 20-gauge MVR incision knife at 45° under an operating microscope. BPC 157 was dissolved in distilled water at 2 pg/ml, 2 ng/ml, and 2 μg/ml, and two eye drops were administered to the left eye in each rat immediately after induction of the injury and then every 8 h up to 120 h; controls received an equal volume of distilled water. Characteristic microscopy presentation (HE, x4) at 48 h after injury induction in control rats was much wider gap, not maturing and abundant granulation tissue, edematous with a lot of fibrin (clot-like) at the surface (white arrow). The surface epithelium is relatively unorganized and progressing over the gap showing a basal cell-like morphology (*C*) (dashed white arrow). In BPC 157–treated animals, the perforation channel is narrow, partly filled with well-vascularized but maturing, non-edematous granulation tissue (black arrow). The superficial epithelium progressing over the gap looks stratified (*B*) (dashed black arrow).

Sikiric et al., 2003; Xue et al., 2004a; Bilic et al., 2005; Seveljevic-Jaran et al., 2006; Tkalcevic et al., 2007; Huang et al., 2015), if properly accomplished, may be the principle largely generalized (see *Skin Wounds*). The success of such an undertaking depends, however, on a few particular, both practical and theoretical, considerations.

With the BPC 157 application (Sikiric et al., 1993; Sikiric et al., 2006; Sikiric et al., 2010; Sikiric et al., 2011; Sikiric et al., 2012; Sikiric et al., 2013; Seiwerth et al., 2014; Sikiric et al., 2014; Sikiric et al., 2016; Sikiric et al., 2017; Kang et al., 2018; Seiwerth et al., 2018; Sikiric et al., 2018; Gwyer et al., 2019; Park et al., 2020; Sikiric et al., 2020a; Sikiric et al., 2020b), this provides overcoming (Seiwerth et al., 2018) of the technical and practical limitations now presented as shortage in the corresponding standard angiogenic growth factors applicability and diverse delivery and carrier systems (see *Practical Application as Support*). In this, for the BPC 157 wound healing, we initially provided consistent argumentation for the accomplished successful skin wound healing (i.e., the combined triad collagen–inflammatory cells–angiogenesis was accordingly upgraded, appearing at earlier intervals, and the formation of granulation tissue containing mature collagen) (Seiwerth et al., 1997; Mikus et al., 2001; Sikiric et al., 2003; Xue et al., 2004; Bilic et al., 2005; Seveljevic-Jaran et al., 2006; Tkalcevic et al., 2007; Huang et al., 2015) (see *Skin Wounds*). With the consistent application of the peptide alone, this skin-healing evidence (Seiwerth et al., 1997; Mikus et al., 2001; Sikiric et al., 2003; Xue et al., 2004a; Bilic et al., 2005; Seveljevic-Jaran et al., 2006; Tkalcevic et al., 2007; Huang et al., 2015) was successfully applied to the other tissues healing (and thereby avoiding all shortages related to the peptide + carrier complex(es) (standard angiogenic growth factors application with diverse carriers)) (see *Practical Application as Support*). The arguments include the same dose range and same equipotent routes of application, regardless of the

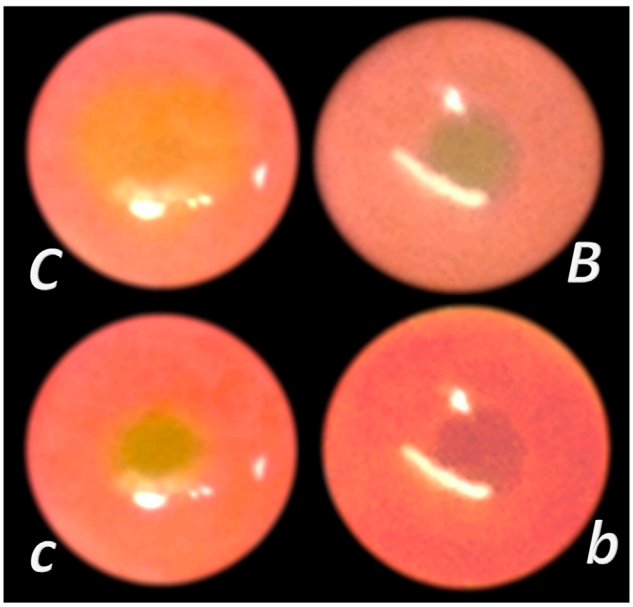

FIGURE 15 | Total debridement of corneal epithelium and BPC 157 therapy (Lazic et al., 2005). Total debridement of corneal epithelium preformed in rats unilaterally and lesions stained (green) and photographed. Medication was distilled water (control group) or BPC 157 2 pg/ml, 2 ng/ml, and 2 μg/ml, two drops/rat eye started immediately after injury induction, every 8 h up to 40 h (i.e., at 0, 8, 16, 24, 32, and 40 h). Lesions presentation at 24 h in controls (*C*) and lesions attenuation in BPC 157 rats (*B*), lesions presentation at 32 h in controls (*C*) and lesions disappearance in BPC 157 rats (*B*).

injury tested (Sikiric et al., 1993; Sikiric et al., 2006; Sikiric et al., 2010; Sikiric et al., 2011; Sikiric et al., 2012; Sikiric et al., 2013; Seiwerth et al., 2014; Sikiric et al., 2014; Sikiric et al., 2016; Sikiric et al., 2017; Kang et al., 2018; Seiwerth et al., 2018; Sikiric et al., 2018; Gwyer et al., 2019; Park et al., 2020; Sikiric et al., 2020a; Sikiric et al., 2020b), to induce a simultaneous healing, even in different tissues (and therefore the healing of diverse fistulas (Klicek et al., 2008; Skorjanec et al., 2009; Cesarec et al., 2013; Skorjanec et al., 2015; Baric et al., 2016; Grgic et al., 2016; Sikiric et al., 2020a)). This also can be applied to the healing of anastomoses, as evidenced by the simultaneous healing of both stumps of the anastomosis (i.e., various gastrointestinal anastomoses (Sikiric et al., 1993; Sikiric et al., 2006; Sikiric et al., 2010; Sikiric et al., 2011; Sikiric et al., 2012; Sikiric et al., 2013; Seiwerth et al., 2014; Sikiric et al., 2014; Sikiric et al., 2016; Sikiric et al., 2017; Kang et al., 2018; Seiwerth et al., 2018; Sikiric et al., 2018; Gwyer et al., 2019; Park et al., 2020; Sikiric et al., 2020a; Sikiric et al., 2020b), even those with large part of the bowel removal (Sever et al., 2009; Lojo et al., 2016), but also other tissue anastomoses, i.e., vessels (Numata et al., 2006) or nerve (Jelovac et al., 1999)) that occurs with the application of BPC 157. In addition, in BPC 157 short-bowel rats, the counteraction of the escalating short bowel syndrome provides that all three intestinal wall layers accordingly adapt in parallel with reaching the same weight gain as in normal rats (Sever et al., 2009) (see *Fistula Healing as Support*). The further proof of the concept includes much like the skin wound healing (Seiwerth et al., 1997; Mikus et al., 2001; Sikiric et al., 2003; Xue et al., 2004a; Bilic et al., 2005; Seveljevic-Jaran et al., 2006; Tkalcevic et al., 2007; Huang et al., 2015), the muscle, tendon, ligament, and bone healing (Sebecic et al., 1999; Staresinic et al., 2003; Krivic et al., 2006; Staresinic et al., 2006; Krivic et al., 2008; Novinscak et al., 2008; Keremi et al., 2009; Mihovil et al., 2009; Cerovecki et al., 2010; Pevec et al., 2010; Chang et al., 2011; Gamulin et al., 2013; Chang et al., 2014; Hsieh et al., 2017) (see *The Effect on Other Tissues Healing as Support*). The combining clue may be also the particular effect on blood vessels as the follow-up of its cytoprotection capability (Robert, 1979; Sikiric et al., 2010; Sikiric et al., 2018) (see *Therapy of Bleeding Disorders as Support*). The accomplishment of wound healing includes resolution of all four major events (vessel constriction, the primary platelet plug, the secondary plug, and resolution of the clot) (Stupnisek et al., 2012; Stupnisek et al., 2015). Therefore, stable gastric pentadecapeptide BPC 157 is effective in wound healing (Seiwerth et al., 1997; Mikus et al., 2001; Sikiric et al., 2003; Xue et al., 2004a; Bilic et al., 2005; Seveljevic-Jaran et al., 2006; Tkalcevic et al., 2007; Huang et al., 2015), much like it is effective also in counteracting bleeding disorders (Stupnisek et al., 2012; Stupnisek et al., 2015; Vukojevic et al., 2018), produced by amputation, and/or anti-coagulants application, or major vessel occlusion, along with the evidence that pentadecapeptide BPC 157 may prevent and/or attenuate or eliminate, thus, counteracting both arterial thrombosis (Hrelec et al., 2009; Gojkovic et al., 2020; Kolovrat et al., 2020) and venous thrombosis (Vukojevic et al., 2018; Gojkovic et al., 2020; Kolovrat et al., 2020). Consequently, the therapy signifies the recovering effect BPC 157 has on occluded vessels (Vukojevic et al., 2018; Gojkovic et al., 2020; Kolovrat et al., 2020; Vukojevic et al., 2020), bypassing the occlusion (Duzel et al., 2017; Amic et al., 2018; Drmic et al., 2018; Vukojevic et al., 2018; Gojkovic et al., 2020; Kolovrat et al., 2020; Vukojevic et al., 2020), appears as the specific effect of BPC 157 in ischemia/reperfusion (Duzel et al., 2017; Amic et al., 2018; Drmic et al., 2018; Vukojevic et al., 2018; Gojkovic et al., 2020; Kolovrat et al., 2020; Vukojevic et al., 2020). Finally, they reflect pathways likely additional to those involved in the angiogenesis (Vukojevic et al., 2018), recently associated in particular with the increased expression, internalization of VEGFR2, and the activation of the VEGFR2-Akt-eNOS signaling pathway (Hsieh et al., 2017) (see *Genes Expression as Support*), given the rapid presentation of all of these effects, which occurred before the process of angiogenesis could be initiated (Sikiric et al., 1993; Sikiric et al., 2006; Sikiric et al., 2010; Sikiric et al., 2011; Sikiric et al., 2012; Sikiric et al., 2013; Seiwerth et al., 2014; Sikiric et al., 2014; Sikiric et al., 2016; Sikiric et al., 2017; Kang et al., 2018; Seiwerth et al., 2018; Sikiric et al., 2018; Gwyer et al., 2019; Park et al., 2020; Sikiric et al., 2020a; Sikiric et al., 2020b). Thus, in rats with occluded blood vessels, at 1 and 24 h, BPC 157 demonstrated a particular specificity within the pathways (at least, *Egr, Nos, Srf, Vegfr, Akt1, Plcγ*, and *Kras*) and vessels involved (Vukojevic et al., 2018). In the most immediate period after injury induction (skin defect) (i.e., 2, 5, and 10 min), BPC 157 increases *Akt1, Braf, Egfr, Egr1, Grb2, Hdac7, Kras, Mapk1, Mapk3, Mapk14, Nos3, Pik3cd, Plcg1, Prkcg, Ptk2, Pxn, Src, Srf,* and *Vegfa* gene expression in rats' excision wounds in the skin. Finally, based on the noted beneficial

effect, BPC 157 may balance collagen synthesis and affect hepatic fibrosis, as a model of the wound-healing response to chronic liver injury, which was modified (Albanis and Friedman, 2001; Aller et al., 2008; Wynn, 2008; Sever et al., 2019). Namely, the BPC 157 effect, in addition to the counteracted BDL-induced liver cirrhosis and portal hypertension (Sever et al., 2019) is also the attenuated dermal, muscle, tendon, and ligament fibrosis and scar formation, and regained function (Mikus et al., 2001; Sikiric et al., 2003; Staresinic et al., 2003; Staresinic et al., 2006; Krivic et al., 2008; Cerovecki et al., 2010) (see *The Effect on Other Tissues Healing as Support*). Controlling the role of BPC 157 likely involves its particular interaction with the major systems involved in wound healing, such as the NO-system (counteracted harmful events, arising from either NO-blockade or NOS-substrate application) (Sikiric et al., 2014) and the prostaglandins system (i.e., large extent of the counteracted NSAIDs toxicity (Sikiric et al., 2013) as well as counteracted developing and already formed adjuvant arthritis in rats (Sikiric et al., 1997c)). For corticosteroid-related systems, we should emphasize the counteracted eventual healing failure (Klicek et al., 2008; Krivic et al., 2008; Skorjanec et al., 2009; Pevec et al., 2010) and worsening, as well as immunosuppression (Sikiric et al., 2003). Finally, there is the evidence of BPC 157 generation of NO in *ex vivo* condition (Sikiric et al., 1997a; Turkovic et al., 2004), resistant to L-NAME, even in conditions when L-arginine does not work, which has some physiologic importance (Sikiric et al., 1997; Turkovic et al., 2004). Consequently, since it is formed constitutively in the gastric mucosa, stable, and present in human gastric juice (Sikiric et al., 1993; Sikiric et al., 2006; Sikiric et al., 2010; Sikiric et al., 2011; Sikiric et al., 2012; Sikiric et al., 2013; Seiwerth et al., 2014; Sikiric et al., 2014; Sikiric et al., 2016; Sikiric et al., 2017; Kang et al., 2018; Seiwerth et al., 2018; Sikiric et al., 2018; Park et al., 2020; Sikiric et al., 2020a; Sikiric et al., 2020b), along with suggested significance of NO-synthase and the basal formation of NO in stomach mucosa, greater than that seen in other tissues (Whittle et al., 1992), BPC 157 exhibits a general, effective competing with both L-arginine analogs (i.e., L-NAME) and L-arginine (Sikiric et al., 2014). Additionally, there is a controlling role of the pentadecapeptide BPC 157 against the tumor-promoting effects of many growth factors and peptides (Gwyer et al., 2019; Sikiric et al., 2018) as well as counteracting harmful escape from the initial healing effect (i.e., angiogenesis). VEGF tumorigenesis was avoided and counteracted (Sikiric et al., 1997c), and inhibition of the growth of several tumor lines and counteraction of tumor cachexia (Kang et al., 2018) and counteraction of the uncontrolled cell proliferation (Ki-67 overexpression counteracted) (Sever et al., 2019) were observed. BPC 157 stimulated both egr-1 and its co-repressor gene nab2 (Tkalcevic et al., 2007). Since egr-1 is critical in proliferation, differentiation, and inflammation during cholestatic liver injury, cytokine and growth factor generation and early extracellular matrix (collagen) formation (Kim et al., 2006; Zhang et al., 2011), BPC 157 (with nab2) may have an essential role as a particular feedback-controlling mechanism. In these terms, indicative is the rat corneal ulcer successfully closed with the BPC 157 eye drops and maintained corneal transparency (**Figure 14**) (Masnec et al., 2015). With BPC 157, corneal transparency was maintained and regained after total debridement of corneal epithelium (**Figure 15**) and dry eye syndrome in rats when BPC 157 counteracts the damaging effects of lacrimal gland extirpation (Lazic et al., 2005; Kralj et al., 2017).

Together, these findings indicate that with regard to wounds in operating instances, a BPC 157–defensive system exists that may accommodate the healing depending on the tissue and injury conditions. Of note, the possible contribution of the particular counteracting effect on the intravenous dextran- or egg white–induced anaphylactoid reaction (Duplancic et al., 2014) should also be considered, although not specifically mentioned in this review. Unlike histamine receptor antagonists (H1 and H2), BPC 157 has a strong beneficial effect in both rats and mice. Upper and lower lip and snout edema, as well as extreme cyanosis and edema of paws and scrotum were markedly attenuated. Poor respiration and fatalities were not observed (Duplancic et al., 2014). However, it remains to be seen when this particular balanced modulatory action will have further application in therapy.

AUTHOR CONTRIBUTIONS

MS, SG, IK, and SS: conceptualization and methodology. ID, AK, HZ, and MK: validation. SS, AP, TD, and HV: formal analysis. LB, AP, KP, and EL: investigation. MS, AB, and MM: resources. JV, AS, SS, and PS: writing—original draft, review, and editing.

FUNDING

This study is supported by the University of Zagreb, Zagreb, Croatia, grant number 099.

REFERENCES

Albanis, E., and Friedman, S. L. (2001). Hepatic fibrosis. Pathogenesis and principles of therapy. *Clin. Liver Dis.* 5 (2), 315. doi:10.1016/s1089-3261(05)70168-9

Alexander, D., Judex, M., Meyringer, R., Weis-Klemm, M., Gay, S., Müller-Ladner, U., et al. (2002). Transcription factor Egr-1 activates collagen expression in immortalized fibroblasts or fibrosarcoma cells. *Biol. Chem.* 383 (12), 1845–1853. doi:10.1515/BC.2002.208

Aller, M. A., Arias, J. L., García-Domínguez, J., Arias, J. I., Durán, M., and Arias, J. (2008). Experimental obstructive cholestasis: the wound-like inflammatory liver response. *Fibrogenesis Tissue Repair* 1 (1), 6. doi:10.1186/1755-1536-1-6

Amic, F., Drmic, D., Bilic, Z., Krezic, I., Zizek, H., Peklic, M., et al. (2018). Bypassing major venous occlusion and duodenal lesions in rats, and therapy with the stable gastric pentadecapeptide BPC 157, L-NAME and L-arginine. *World J. Gastroenterol.* 24 (47), 5366–5378. doi:10.3748/wjg.v24.i47.5366

Ansari, D., Ansari, D., Andersson, R., and Andrén-Sandberg, Å. (2015). Pancreatic cancer and thromboembolic disease, 150 years after Trousseau. *Hepatobiliary Surg. Nutr.* 4, 325–335. doi:10.3978/j.issn.2304-3881.2015.06.08

Bakan, E., Taysi, S., Polat, M. F., Dalga, S., Umudum, Z., Bakan, N., et al. (2002). Nitric oxide levels and lipid peroxidation in plasma of patients with gastric cancer. *Jpn. J. Clin. Oncol.* 32 (5), 162–166. doi:10.1093/jjco/hyf035

Baric, M., Sever, A. Z., Vuletic, L. B., Rasic, Z., Sever, M., Drmic, D., et al. (2016). Stable gastric pentadecapeptide BPC 157 heals rectovaginal fistula in rats. *Life Sci.* 148, 63–70. doi:10.1016/j.lfs.2016.02.029

Barisic, I., Balenovic, D., Klicek, R., Radic, B., Nikitovic, B., Drmic, D., et al. (2013). Mortal hyperkalemia disturbances in rats are NO-system related. The life saving effect of pentadecapeptide BPC 157. *Regul. Pept.* 181, 50–66. doi:10.1016/j.regpep.2012.12.007

Becejac, T., Cesarec, V., Drmic, D., Hirsl, D., Madzarac, G., Djakovic, Z., et al. (2018). An endogeous defensive concept, renewed cytoprotection/adaptive cytoprotection: intra(per)-oral/intraastric strong alcohol in rat. Involvement of pentadecapeptide BPC 157 and nitric oxide system. *J. Physiol. Pharmacol.* 69 (3), 429–440. doi:10.26402/jpp.2018.3.11

Bedekovic, V., Mise, S., Anic, T., Staresinic, M., Gjurasin, M., Kopljar, M., et al. (2003). Different effect of antiulcer agents on rat cysteamine-induced duodenal ulcer after sialoadenectomy, but not gastrectomy. *Eur. J. Pharmacol.* 477 (1), 73–80. doi:10.1016/j.ejphar.2003.08.013

Belosic Halle, Z., Vlainic, J., Drmic, D., Strinic, D., Luetic, K., Sucic, M., et al. (2017). Class side effects: decreased pressure in the lower oesophageal and the pyloric sphincters after the administration of dopamine antagonists, neuroleptics, anti-emetics, L-NAME, pentadecapeptide BPC 157 and L-arginine. *Inflammopharmacology* 25, 511–522. doi:10.1007/s10787-017-0358-8

Berkopic Cesar, L., Gojkovic, S., Krezic, I., Malekinusic, D., Zizek, H., Batelja Vuletic, L., et al. (2020). Bowel adhesion and therapy with the stable gastric pentadecapeptide BPC 157, L-NAME and L-arginine in rats. *World J. Gastrointest. Pharmacol. Ther.* 11 (5). 93–109. doi:10.4292/wjgpt.v11.i5.93

Berra-Romani, R., Avelino-Cruz, J. E., Raqeeb, A., Della Corte, A., Cinelli, M., Montagnani, S., et al. (2013). Ca^{2+}-dependent nitric oxide release in the injured endothelium of excised rat aorta: a promising mechanism applying in vascular prosthetic devices in aging patients. *BMC Surg.* 13 (2), S40. doi:10.1186/1471-2482-13-S2-S40

Bilic, M., Bumber, Z., Blagaic, A. B., Batelja, L., Seiwerth, S., and Sikiric, P. (2005). The stable gastric pentadecapeptide BPC 157, given locally, improves CO2 laser healing in mice. *Burns* 31 (3), 310–315. doi:10.1016/j.burns.2004.10.013

Braddock, M., Campbell, C. J., and Zuder, D. (1999). Current therapies for wound healing: electrical stimulation, biological therapeutics, and the potential for gene therapy. *Int. J. Dermatol.* 38 (11), 808–817. doi:10.1046/j.1365-4362.1999.00832.x

Braddock, M. (2001). The transcription factor Egr-1: a potential drug in wound healing and tissue repair. *Ann. Med.* 33 (5), 313–318. doi:10.3109/07853890109002083

Brcic, L., Brcic, I., Staresinic, M., Novinscak, T., Sikiric, P., and Seiwerth, S. (2009). Modulatory effect of gastric pentadecapeptide BPC 157 on angiogenesis in muscle and tendon healing. *J. Physiol. Pharmacol.* 60 (7), 191–196.

Cerovecki, T., Bojanic, I., Brcic, L., Radic, B., Vukoja, I., Seiwerth, S., et al. (2010). Pentadecapeptide BPC 157 (PL 14736) improves ligament healing in the rat. *J. Orthop. Res.* 28 (9), 1155–1161. doi:10.1002/jor.21107

Cesarec, V., Becejac, T., Misic, M., Djakovic, Z., Olujic, D., Drmic, D., et al. (2013). Pentadecapeptide BPC 157 and the esophagocutaneous fistula healing therapy. *Eur. J. Pharmacol.* 701 (1-3), 203–212. doi:10.1016/j.ejphar.2012.11.055

Chang, C. H., Tsai, W. C., Hsu, Y. H., and Pang, J. H. (2014). Pentadecapeptide BPC 157 enhances the growth hormone receptor expression in tendon fibroblasts. *Molecules* 19 (11), 19066–19077. doi:10.3390/molecules191119066

Chang, C. H., Tsai, W. C., Lin, M. S., Hsu, Y. H., and Pang, J. H. (2011). The promoting effect of pentadecapeptide BPC 157 on tendon healing involves tendon outgrowth, cell survival, and cell migration. *J. Appl. Physiol.* 110 (3), 774–780. doi:10.1152/japplphysiol.00945.2010

Collen, D. (1980). On the regulation and control of fibrinolysis. Edward Kowalski Memorial Lecture. *Thromb. Haemost.* 43, 77–89. doi:10.1055/s-0038-1650023

Cook, S. D., Baffes, G. C., Wolfe, M. W., Sampath, T. K., and Rueger, D. C. (1994). Recombinant human bone morphogenetic protein-7 induces healing in a canine long-bone segmental defect model. *Clin. Orthop. Relat. Res.* 301, 302–312. doi:10.1097/00003086-199404000-00046

Damien, C. J., Christel, P. S., Benedict, J. J., Patat, J. L., and Guillemin, G. (1993). A composite of natural coral, collagen, bone protein and basic fibroblast growth factor tested in a rat subcutaneous model. *Ann. Chir Gynaecol. Suppl.* 207, 117–128.

Davey, A. K., and Maher, P. J. (2007). Surgical adhesions: a timely update, a great challenge for the future. *J. Minim. Invasive Gynecol.* 14, 15–22. doi:10.1016/j.jmig.2006.07.013

Deng, X., Szabo, S., Khomenko, T., Tolstanova, G., Paunovic, B., French, S. W., et al. (2013). Novel pharmacologic approaches to the prevention and treatment of ulcerative colitis. *Curr. Pharm. Des.* 19 (1), 17–28. doi:10.2174/13816128130105

Djakovic, Z., Djakovic, I., Cesarec, V., Madzarac, G., Becejac, T., Zukanovic, G., et al. (2016). Esophagogastric anastomosis in rats: improved healing by BPC 157 and L-arginine, aggravated by L-NAME. *World J. Gastroenterol.* 22 (41), 9127–9140. doi:10.3748/wjg.v22.i41.9127

Dobric, I., Drvis, P., Petrovic, I., Shejbal, D., Brcic, L., Blagaic, A. B., et al. (2007). Prolonged esophagitis after primary dysfunction of the pyloric sphincter in the rat and therapeutic potential of the gastric pentadecapeptide BPC 157. *J. Pharmacol. Sci.* 104 (1), 7–18. doi:10.1254/jphs.fp0061322

Drmic, D., Samara, M., Vidovic, T., Malekinusic, D., Antunovic, M., Vrdoljak, B., et al. (2018). Counteraction of perforated cecum lesions in rats: effects of pentadecapeptide BPC 157, L-NAME and L-arginine. *World J. Gastroenterol.* 24 (48), 5462–5476. doi:10.3748/wjg.v24.i48.5462

Duplancic, B., Stambolija, V., Holjevac, J., Zemba, M., Balenovic, I., Drmic, D., et al. (2014). Pentadecapeptide BPC 157 and anaphylactoid reaction in rats and mice after intravenous dextran and white egg administration. *Eur. J. Pharmacol.* 727, 75–79. doi:10.1016/j.ejphar.2014.01.046

Duzel, A., Vlainic, J., Antunovic, M., Malekinusic, D., Vrdoljak, B., Samara, M., et al. (2017). Stable gastric pentadecapeptide BPC 157 in the treatment of colitis and ischemia and reperfusion in rats: new insights. *World J. Gastroenterol.* 23 (48), 8465–8488. doi:10.3748/wjg.v23.i48.8465

Eckersley, J. R., and Dudley, H. A. (1988). Wounds and wound healing. *Br. Med. Bull.* 44 (2), 423–436. doi:10.1093/oxfordjournals.bmb.a072259

Eyre, D. R., Paz, M. A., and Gallop, P. M. (1984). Cross-linking in collagen and elastin. *Annu. Rev. Biochem.* 53, 717–748. doi:10.1146/annurev.bi.53.070184.003441

Forslund, C., and Aspenberg, P. (1998). OP-1 has more effect than mechanical signals in the control of tissue differentiation in healing rat tendons. *Acta Orthop. Scand.* 69 (6), 622–626. doi:10.3109/17453679808999268

Fortin, C. N., Saed, G. M., and Diamond, M. P. (2015). Predisposing factors to post-operative adhesion development. *Hum. Reprod. Update* 21, 536–551. doi:10.1093/humupd/dmv021

Gamulin, O., Serec, K., Bilić, V., Balarin, M., Kosović, M., Drmić, D., et al. (2013). Monitoring the healing process of rat bones using Raman spectroscopy. *J. Mol. Struct.* 1044, 308–313. doi:10.1016/j.molstruc.2013.01.049

Gao, T. J., Lindholm, T. S., Marttinen, A., and Puolakka, T. (1993). Bone inductive potential and dose-dependent response of bovine bone morphogenetic protein combined with type IV collagen carrier. *Ann. Chir Gynaecol. Suppl.* 207, 77–84.

Gjurasin, M., Miklic, P., Zupancic, B., Perovic, D., Zarkovic, K., Brcic, L., et al. (2010). Peptide therapy with pentadecapeptide BPC 157 in traumatic nerve injury. *Regul. Pept.* 160 (1-3), 33–41. doi:10.1016/j.regpep.2009.11.005

Gojkovic, S., Krezic, I., Vrdoljak, B., Malekinusic, D., Barisic, I., Petrovic, A., et al. (2020). Pentadecapeptide BPC 157 resolves suprahepatic occlusion of the inferior caval vein, Budd-Chiari syndrome model in rats. *World J. Gastrointest. Pathophysiol* 11 (1), 1–19. doi:10.4291/wjgp.v11.i1.1

Grgic, T., Grgic, D., Drmic, D., Sever, A. Z., Petrovic, I., Sucic, M., et al. (2016). Stable gastric pentadecapeptide BPC 157 heals rat colovesical fistula. *Eur. J. Pharmacol.* 780, 1–7. doi:10.1016/j.ejphar.2016.02.038

Gwyer, D., Wragg, N. M., and Wilson, S. L. (2019). Gastric pentadecapeptide body protection compound BPC 157 and its role in accelerating musculoskeletal soft tissue healing. *Cell Tissue Res* 377 (2), 153–159. doi:10.1007/s00441-019-03016-8

Hendriks, T., and Mastboom, W. J. (1990). Healing of experimental intestinal anastomoses. Parameters for repair. *Dis. Colon Rectum* 33, 891–901. doi:10.1007/BF02051930

Hinterseher, I., Schworer, C. M., Lillvis, J. H., Stahl, E., Erdman, R., Gatalica, Z., et al. (2015). Immunohistochemical analysis of the natural killer cell cytotoxicity pathway in human abdominal aortic aneurysms. *Int. J. Mol. Sci.* 16, 11196–11212. doi:10.3390/ijms160511196

Hrelec, M., Klicek, R., Brcic, L., Brcic, I., Cvjetko, I., Seiwerth, S., et al. (2009). Abdominal aorta anastomosis in rats and stable gastric pentadecapeptide BPC 157, prophylaxis and therapy. *J. Physiol. Pharmacol.* 60 (7), 161–165.

Hsieh, M. J., Liu, H. T., Wang, C. N., Huang, H. Y., Lin, Y., Ko, Y. S., et al. (2017). Therapeutic potential of pro-angiogenic BPC157 is associated with VEGFR2 activation and up-regulation. *J. Mol. Med.* 95 (3), 323–333. doi:10.1007/s00109-016-1488-y

Huang, T., Zhang, K., Sun, L., Xue, X., Zhang, C., Shu, Z., et al. (2015). Body protective compound-157 enhances alkali-burn wound healing *in vivo* and promotes proliferation, migration, and angiogenesis *in vitro*. *Drug Des. Devel Ther.* 9, 2485–2499. doi:10.2147/DDDT.S82030

Ilic, S., Brcic, I., Mester, M., Filipovic, M., Sever, M., Klicek, R., et al. (2009). Over-dose insulin and stable gastric pentadecapeptide BPC 157. Attenuated gastric ulcers, seizures, brain lesions, hepatomegaly, fatty liver, breakdown of liver glycogen, profound hypoglycemia and calcification in rats. *J. Physiol. Pharmacol.* 60 (7), 107–114.

Ilic, S., Drmic, D., Franjic, S., Kolenc, D., Coric, M., Brcic, L., et al. (2011a). Pentadecapeptide BPC 157 and its effects on a NSAID toxicity model: diclofenac-induced gastrointestinal, liver, and encephalopathy lesions. *Life Sci.* 88 (11-12), 535–542. doi:10.1016/j.lfs.2011.01.015

Ilic, S., Drmic, D., Zarkovic, K., Kolenc, D., Brcic, L., Radic, B., et al. (2011b). Ibuprofen hepatic encephalopathy, hepatomegaly, gastric lesion and gastric pentadecapeptide BPC 157 in rats. *Eur. J. Pharmacol.* 667 (1-3), 322–329. doi:10.1016/j.ejphar.2011.05.038

Ilic, S., Drmic, D., Zarkovic, K., Kolenc, D., Coric, M., Brcic, L., et al. (2010). High hepatotoxic dose of paracetamol produces generalized convulsions and brain damage in rats. A counteraction with the stable gastric pentadecapeptide BPC 157 (PL 14736). *J. Physiol. Pharmacol.* 61 (2), 241–250.

Jandric, I., Vrcic, H., Jandric Balen, M., Kolenc, D., Brcic, L., Radic, B., et al. (2013). Salutary effect of gastric pentadecapeptide BPC 157 in two different stress urinary incontinence models in female rats. *Med. Sci. Monit. Basic Res.* 19, 93–102. doi:10.12659/MSMBR.883828

Jee, J. P., Pangeni, R., Jha, S. K., Byun, Y., and Park, J. W. (2019). Preparation and *in vivo* evaluation of a topical hydrogel system incorporating highly skin-permeable growth factors, quercetin, and oxygen carriers for enhanced diabetic wound-healing therapy. *Int. J. Nanomedicine* 14, 5449–5475. doi:10.2147/IJN.S213883

Jelovac, N., Sikiric, P., Rucman, R., Petek, M., Marovic, A., Perovic, D., et al. (1999). Pentadecapeptide BPC 157 attenuates disturbances induced by neuroleptics: the effect on catalepsy and gastric ulcers in mice and rats. *Eur. J. Pharmacol.* 379 (1), 19–31. doi:10.1016/s0014-2999(99)00486-0

Kachlik, D., Baca, V., and Stingl, J. (2010). The spatial arrangement of the human large intestinal wall blood circulation. *J. Anat.* 216 (3), 335–343. doi:10.1111/j.1469-7580.2009.01199.x

Kang, E. A., Han, Y. M., An, J. M., Park, Y. J., Sikiric, P., Kim, D. H., et al. (2018). BPC157 as potential agent rescuing from cancer cachexia. *Curr. Pharm. Des.* 24 (18), 1947–1956. doi:10.2174/1381612824666180614082950

Kato, N., Kawai, T., Maeda, H., Nagao, T., Murakami, H., Miyazawa, K., et al. (1995). A study of thecarrier of BMP – osteoinductive activity of polysaccharide-BMP–complex. *J. Hard Tissue Biol.* 4, 15–22.

Katoh, T., Sato, K., Kawamura, M., Iwata, H., and Miura, T. (1993). Osteogenesis in sintered bone combined with bovine bone morphogenetic protein. *Clin. Orthop. Relat. Res.* 287, 266–275. doi:10.1097/00003086-199302000-00042

Kawai, T., Mieki, A., Ohno, Y., Umemura, M., Kataoka, H., Kurita, S., et al. (1993). Osteoinductive activity of composites of bone morphogenetic protein and pure titanium. *Clin. Orthop. Relat. Res.* 290, 296–305. doi:10.1097/00003086-199305000-00038

Kawakami, T., Kawai, T., Takei, N., Kise, T., Eda, S., and Urist, M. R. (1997). Evaluation of heterotopic bone formation induced by squalane and bone morphogenetic protein composite. *Clin. Orthop. Relat. Res.* 337, 261–266. doi:10.1097/00003086-199704000-00029

Keremi, B., Lohinai, Z., Komora, P., Duhaj, S., Borsi, K., Jobbagy-Ovari, G., et al. (2009). Antiinflammatory effect of BPC 157 on experimental periodontitis in rats. *J. Physiol. Pharmacol.* 60 (7), 115–122.

Khachigian, L. M. (2006). Early growth response-1 in cardiovascular pathobiology. *Circ. Res.* 98 (2), 186–191. doi:10.1161/01.RES.0000200177.53882.c3

Kim, N. D., Moon, J. O., Slitt, A. L., and Copple, B. L. (2006). Early growth response factor-1 is critical for cholestatic liver injury. *Toxicol. Sci.* 90 (2), 586–595. doi:10.1093/toxsci/kfj111

Klicek, R., Kolenc, D., Suran, J., Drmic, D., Brcic, L., Aralica, G., et al. (2013). Stable gastric pentadecapeptide BPC 157 heals cysteamine-colitis and colon-colon-anastomosis and counteracts cuprizone brain injuries and motor disability. *J. Physiol. Pharmacol.* 64 (5), 597–612.

Klicek, R., Sever, M., Radic, B., Drmic, D., Kocman, I., Zoricic, I., et al. (2008). Pentadecapeptide BPC 157, in clinical trials as a therapy for inflammatory bowel disease (PL14736), is effective in the healing of colocutaneous fistulas in rats: role of the nitric oxide-system. *J. Pharmacol. Sci.* 108 (1), 7–17. doi:10.1254/jphs.fp0072161

Kolovrat, M., Gojkovic, S., Krezic, I., Malekinusic, D., Vrdoljak, B., Kasnik Kovac, K., et al. (2020). Pentadecapeptide BPC 157 resolves Pringle maneuver in rats, both ischemia and reperfusion. *World J. Hepatol.* 12 (5), 184–206. doi:10.4254/wjh.v12.i5.184

Konosic, S., Petricevic, M., Ivancan, V., Konosic, L., Goluza, E., Krtalic, B., et al. (2019). Intragastric application of aspirin, clopidogrel, cilostazol, and BPC 157 in rats: platelet aggregation and blood clot. *Oxid Med. Cell Longev* 2019, 9084643. doi:10.1155/2019/9084643

Kralj, T., Kokot, A., Kasnik, K., Drmic, D., Zlatar, M., Seiwerth, S., et al. (2017). Effects of pentadecapeptide BPC 157 on experimental rat model of dry eye. *FASEB J.* 31 (1), 993.3. doi:10.1096/fasebj.31.1_supplement.993.3Abstract retrieved fromExperimental Biology 2017 Meeting

Krivic, A., Anic, T., Seiwerth, S., Huljev, D., and Sikiric, P. (2006). Achilles detachment in rat and stable gastric pentadecapeptide BPC 157: promoted tendon-to-bone healing and opposed corticosteroid aggravation. *J. Orthop. Res.* 24 (5), 982–989. doi:10.1002/jor.20096

Krivic, A., Majerovic, M., Jelic, I., Seiwerth, S., and Sikiric, P. (2008). Modulation of early functional recovery of Achilles tendon to bone unit after transection by BPC 157 and methylprednisolone. *Inflamm. Res.* 57 (5), 205–210. doi:10.1007/s00011-007-7056-8

Lazic, R., Gabric, N., Dekaris, I., Bosnar, D., Boban-Blagai, A., and Sikiric, P. (2005). Gastric pentadecapeptide BPC 157 promotes corneal epithelial defects healing in rats. *Coll. Antropol* 29 (1), 321–325.

Lojo, N., Rasic, Z., Zenko Sever, A., Kolenc, D., Vukusic, D., Drmic, D., et al. (2016). Effects of diclofenac, L-NAME, L-arginine, and pentadecapeptide BPC 157 on gastrointestinal, liver, and brain lesions, failed anastomosis, and intestinal adaptation deterioration in 24 hour-short-bowel rats. *PLoS One* 11 (9), e0162590. doi:10.1371/journal.pone.0162590

Lovric-Bencic, M., Sikiric, P., Hanzevacki, J. S., Seiwerth, S., Rogic, D., Kusec, V., et al. (2004). Doxorubicine-congestive heart failure-increased big endothelin-1 plasma concentration: reversal by amlodipine, losartan, and gastric pentadecapeptide BPC157 in rat and mouse. *J. Pharmacol. Sci.* 95, 19–26. doi:10.1254/jphs.95.19

Luetic, K., Sucic, M., Vlainic, J., Halle, Z. B., Strinic, D., Vidovic, T., et al. (2017). Cyclophosphamide induced stomach and duodenal lesions as a NO-system disturbance in rats: L-NAME, L-arginine, stable gastric pentadecapeptide BPC 157. *Inflammopharmacology* 25 (2), 255–264. doi:10.1007/s10787-017-0330-7

Masnec, S., Kokot, A., Zlatar, M., Kalauz, M., Kunjko, K., Radic, B., et al. (2015). Perforating corneal injury in rat and pentadecapeptide BPC 157. *Exp. Eye Res.* 136, 9–15. doi:10.1016/j.exer.2015.04.016

Medvidovic-Grubisic, M., Stambolija, V., Kolenc, D., Katancic, J., Murselovic, T., Plestina-Borjan, I., et al. (2017). Hypermagnesemia disturbances in rats, NO-related: pentadecapeptide BPC 157 abrogates, L-NAME and L-arginine worsen. *Inflammopharmacology* 25 (4), 439–449. doi:10.1007/s10787-017-0323-6

Mihovil, I., Radic, B., Brcic, L., Brcic, I., Vukoja, I., Ilic, S., et al. (2009). Beneficial effect of pentadecapeptide BPC 157 on denervated muscle in rats. *J. Physiol. Pharmacol.* 60 (2), 69.

Mikus, D., Sikiric, P., Seiwerth, S., Petricevic, A., Aralica, G., Druzijancic, N., et al. (2001). Pentadecapeptide BPC 157 cream improves burn-wound healing and attenuates burn-gastric lesions in mice. *Burns* 27 (8), 817–827. doi:10.1016/s0305-4179(01)00055-9

Miyamoto, S., Takaoka, K., Okada, T., Yoshikawa, H., Hashimoto, J., Suzuki, S., et al. (1992). Evaluation of polylactic acid homopolymers as carriers for bone morphogenetic protein. *Clin. Orthop. Relat. Res.* 278, 274–285.

Novinscak, T., Brcic, L., Staresinic, M., Jukic, I., Radic, B., Pevec, D., et al. (2008). Gastric pentadecapeptide BPC 157 as an effective therapy for muscle crush injury in the rat. *Surg. Today* 38 (8), 716–725. doi:10.1007/s00595-007-3706-2

Nowak, K. C., McCormack, M., and Koch, R. J. (2000). The effect of superpulsed carbon dioxide laser energy on keloid and normal dermal fibroblast secretion of growth factors: a serum-free study. *Plast. Reconstr. Surg.* 105 (6), 2039–2048. doi:10.1097/00006534-200005000-00019

Numata, Y., Terui, T., Okuyama, R., Hirasawa, N., Sugiura, Y., Miyoshi, I., et al. (2006). The accelerating effect of histamine on the cutaneous wound-healing process through the action of basic fibroblast growth factor. *J. Invest. Dermatol.* 126 (6), 1403–1409. doi:10.1038/sj.jid.5700253

Okabe, S., and Amagase, K. (2005). An overview of acetic acid ulcer models–the history and state of the art of peptic ulcer research. *Biol. Pharm. Bull.* 28 (8), 1321–1341. doi:10.1248/bpb.28.1321

Orangio, G. R. (2010). Enterocutaneous fistula: medical and surgical management including patients with Crohn's disease. *Clin. Colon Rectal Surg.* 23 (3), 169–175. doi:10.1055/s-0030-1262984

Park, J. M., Lee, H. J., Sikiric, P., and Hahm, K. B. (2020). BPC 157 rescued NSAID-cytotoxicity via stabilizing intestinal permeability and enhancing cytoprotection. *Curr. Pharm. Des.* 26 (25), 2971–2981. doi:10.2174/1381612826666200523180301

Perovic, D., Kolenc, D., Bilic, V., Somun, N., Drmic, D., Elabjer, E., et al. (2019). Stable gastric pentadecapeptide BPC 157 can improve the healing course of spinal cord injury and lead to functional recovery in rats. *J. Orthop. Surg. Res.* 14 (1), 199. doi:10.1186/s13018-019-1242-6

Petek, M., Sikiric, P., Anic, T., Buljat, G., Separovic, J., Stancic-Rokotov, D., et al. (1999). Pentadecapeptide BPC 157 attenuates gastric lesions induced by alloxan in rats and mice. *J. Physiol. Paris* 93 (6), 501–504. doi:10.1016/s0928-4257(99)00120-5

Petrovic, I., Dobric, I., Drvis, P., Shejbal, D., Brcic, L., Blagaic, A. B., et al. (2006). An experimental model of prolonged esophagitis with sphincter failure in the rat and the therapeutic potential of gastric pentadecapeptide BPC 157. *J. Pharmacol. Sci.* 102 (3), 269–277. doi:10.1254/jphs.fp0060070

Pevec, D., Novinscak, T., Brcic, L., Sipos, K., Jukic, I., Staresinic, M., et al. (2010). Impact of pentadecapeptide BPC 157 on muscle healing impaired by systemic corticosteroid application. *Med. Sci. Monit.* 16 (3), 81–88.

Poppas, D. P., Massicotte, J. M., Stewart, R. B., Roberts, A. B., Atala, A., Retik, A. B., et al. (1996). Human albumin solder supplemented with TGF-beta 1 accelerates healing following laser welded wound closure. *Lasers Surg. Med.* 19 (3), 360–368. doi:10.1002/(SICI)1096-9101(1996)19:3<360::AID-LSM13>3.0.CO;2–8

Radeljak, S., Seiwerth, S., and Sikiric, P. (2004). BPC 157 inhibits cell growth and VEGF signalling via the MAPK kinase pathway in the human melanoma cell line. *Melanoma Res.* 14, 14–15.

Rangan, U., and Bulkley, G. B. (1993). Prospects for treatment of free radical-mediated tissu injury. *Br. Med. Bull.* 49 (3), 700–718. doi:10.1093/oxfordjournals.bmb.a072641

Rantfors, J., and Cassuto, J. (2003). Role of histamine receptors in the regulation of edema and circulation postburn. *Burns* 29 (8), 769–777. doi:10.1016/s0305-4179(03)00203-1

Rao, K. S., Patil, P. A., and Malur, P. R. (2007). Promotion of cutaneous wound healing by famotidine in Wistar rats. *Indian J. Med. Res.* 125 (2), 149–154.

Robert, A. (1979). Cytoprotection by prostaglandins. *Gastroenterology* 77 (4), 761–767.

Saghazadeh, S., Rinoldi, C., Schot, M., Kashaf, S. S., Sharifi, F., Jalilian, E., et al. (2018). Drug delivery systems and materials for wound healing applications. *Adv. Drug Deliv. Rev.* 127, 138–166. doi:10.1016/j.addr.2018.04.008

Schiller, H. J., Reilly, P. M., and Bulkley, G. B. (1993). Tissue perfusion in critical illnesses. Antioxidant therapy. *Crit. Care Med.* 21 (1), 92–102.

Schweighofer, B., Schultes, J., Pomyje, J., and Hofer, E. (2007). Signals and genes induced by angiogenic growth factors in comparison to inflammatory cytokines in endothelial cells. *Clin. Hemorheol. Microcirc.* 37, 57–62.

Sebecic, B., Nikolic, V., Sikiric, P., Seiwerth, S., Sosa, T., Patrlj, L., et al. (1999). Osteogenic effect of a gastric pentadecapeptide BPC 157, on the healing of segmental bone defect in rabbits. A comparison with bone marrow and autologous cortical bone implantation. *Bone* 24 (3), 195–202. doi:10.1016/s8756-3282(98)00180-x

Seiwerth, S., Brcic, L., Vuletic, L. B., Kolenc, D., Aralica, G., Misic, M., et al. (2014). BPC 157 and blood vessels. *Curr. Pharm. Des.* 20 (7), 1121–1125. doi:10.2174/13816128113199990421

Seiwerth, S., Rucman, R., Turkovic, B., Sever, M., Klicek, R., Radic, B., et al. (2018). BPC 157 and standard angiogenic growth factors. Gastrointestinal tract healing, lessons from tendon, ligament, muscle and bone healing. *Curr. Pharm. Des.* 24 (18), 1972–1989. doi:10.2174/1381612824666180712110447

Seiwerth, S., Sikiric, P., Grabarevic, Z., Zoricic, I., Hanzevacki, M., Ljubanovic, D., et al. (1997). BPC 157's effect on healing. *J. Physiol. Paris* 91 (3-5), 173–178. doi:10.1016/s0928-4257(97)89480-6

Selye, H., and Szabo, S. (1973). Experimental model for production of perforating duodenal ulcers by cysteamine in the rat. *Nature* 244 (5416), 458–459. doi:10.1038/244458a0

Seveljevic-Jaran, D., Cuzic, S., Dominis-Kramaric, M., Glojnaric, I., Ivetic, V., Radosevic, S., et al. (2006). Accelerated healing of excisional skin wounds by PL 14736 in alloxan-hyperglycemic rats. *Skin Pharmacol. Physiol.* 19 (5), 266–274. doi:10.1159/000093982

Seven, A., Civelek, S., Inci, E., Inci, F., Korkut, N., and Burcak, G. (1999). Evaluation of oxidative stress parameters in blood of patients with laryngeal carcinoma. *Clin. Biochem.* 32 (5), 369–373. doi:10.1016/s0009-9120(99)00022-3

Sever, A. Z., Sever, M., Vidovic, T., Lojo, N., Kolenc, D., Vuletic, L. B., et al. (2019). Stable gastric pentadecapeptide BPC 157 in the therapy of the rats with bile duct ligation. *Eur. J. Pharmacol.* 847, 130–142. doi:10.1016/j.ejphar.2019.01.030

Sever, M., Klicek, R., Radic, B., Brcic, L., Zoricic, I., Drmic, D., et al. (2009). Gastric pentadecapeptide BPC 157 and short bowel syndrome in rats. *Dig. Dis. Sci.* 54 (10), 2070–2083. doi:10.1007/s10620-008-0598-y

Siegall, C. B., Gawlak, S. L., Chace, D. F., Merwin, J. R., and Pastan, I. (1994). *In vivo* activities of acidic fibroblast growth factor-Pseudomonas exotoxin fusion proteins. *Bioconjug. Chem.* 5 (1), 77–83. doi:10.1021/bc00025a010

Sikiric, P., Drmic, D., Sever, M., Klicek, R., Blagaic, A. B., Tvrdeic, A., et al. (2020a). Fistulas healing. Stable gastric pentadecapeptide BPC 157 therapy. *Curr. Pharm. Des.* 26 (25), 2991–3000. doi:10.2174/1381612826666200424180139

Sikiric, P., Hahm, K. B., Blagaic, A. B., Tvrdeic, A., Pavlov, K. H., Petrovic, A., et al. (2020b). Stable gastric pentadecapeptide BPC 157, Robert's stomach cytoprotection/adaptive cytoprotection/organoprotection, and Selye's stress coping response: progress, achievements, and the future. *Gut Liver* 14 (2), 153–167. doi:10.5009/gnl18490

Sikiric, P., Jadrijevic, S., Seiwerth, S., Sosa, T., Deskovic, S., Perovic, D., et al. (1999b). Long-lasting cytoprotection after pentadecapeptide BPC 157, ranitidine, sucralfate or cholestyramine application in reflux oesophagitis in rats. *J. Physiol. Paris* 93 (6), 467–477. doi:10.1016/s0928-4257(99)00124-2

Sikiric, P., Marovic, A., Matoz, W., Anic, T., Buljat, G., Mikus, D., et al. (1999c). A behavioural study of the effect of pentadecapeptide BPC 157 in Parkinson's disease models in mice and gastric lesions induced by 1-methyl-4-phenyl-1,2,3,6-tetrahydrophyridine. *J. Physiol. Paris* 93 (6), 505–512. doi:10.1016/s0928-4257(99)00119-9

Sikiric, P., Mikus, D., Seiwerth, S., Grabarevic, Z., Rucman, R., Petek, M., et al. (1997b). Pentadecapeptide BPC 157, cimetidine, ranitidine, bromocriptine, and atropine effect in cysteamine lesions in totally gastrectromized rats: a model for cytoprotective studies. *Dig. Dis. Sci.* 42 (5), 1029–1037. doi:10.1023/a:1018893220943

Sikiric, P., Petek, M., Rucman, R., Seiwerth, S., Grabarevic, Z., Rotkvic, I., et al. (1993). A new gastric juice peptide, BPC. An overview of the stomach-stress-organoprotection hypothesis and beneficial effects of BPC. *J. Physiol. Paris* 87 (5), 313–327. doi:10.1016/0928-4257(93)90038-u

Sikiric, P., Rucman, R., Turkovic, B., Sever, M., Klicek, R., Radic, B., et al. (2018). Novel cytoprotective mediator, stable gastric pentadecapeptide BPC 157. Vascular recruitment and gastrointestinal tract healing. *Curr. Pharm. Des.* 24 (18), 1990–2001. doi:10.2174/1381612824666180608101119

Sikiric, P., Seiwerth, S., Brcic, L., Blagaic, A. B., Zoricic, I., Sever, M., et al. (2006). Stable gastric pentadecapeptide BPC 157 in trials for inflammatory bowel disease (PL-10, PLD-116, PL 14736, Pliva, Croatia). Full and distended stomach, and vascular response. *Inflammopharmacology* 14 (5-6), 214–221. doi:10.1007/s10787-006-1531-7

Sikiric, P., Seiwerth, S., Brcic, L., Sever, M., Klicek, R., Radic, B., et al. (2010). Revised Robert's cytoprotection and adaptive cytoprotection and stable gastric

pentadecapeptide BPC 157. Possible significance and implications for novel mediator. *Curr. Pharm. Des.* 16 (10), 1224–1234. doi:10.2174/138161210790945977

Sikiric, P., Seiwerth, S., Grabarevic, Z., Balen, I., Aralica, G., Gjurasin, M., et al. (2001). Cysteamine-colon and cysteamine-duodenum lesions in rats. Attenuation by gastric pentadecapeptide BPC 157, cimetidine, ranitidine, atropine, omeprazole, sulphasalazine and methylprednisolone. *J. Physiol. Paris* 95 (1-6), 261–270. doi:10.1016/s0928-4257(01)00036-5

Sikiric, P., Seiwerth, S., Grabarevic, Z., Petek, M., Rucman, R., Turkovic, B., et al. (1994). The beneficial effect of BPC 157, a 15 amino acid peptide BPC fragment, on gastric and duodenal lesions induced by restraint stress, cysteamine and 96% ethanol in rats. A comparative study with H2 receptor antagonists, dopamine promotors and gut peptides. *Life Sci.* 54 (5), 63–68. doi:10.1016/0024-3205(94)00796-9

Sikiric, P., Seiwerth, S., Grabarevic, Z., Rucman, R., Petek, M., Jagic, V., et al. (1997c). Pentadecapeptide BPC 157 positively affects both non-steroidal anti-inflammatory agent-induced gastrointestinal lesions and adjuvant arthritis in rats. *J. Physiol. Paris* 91 (3-5), 113–122. doi:10.1016/s0928-4257(97)89474-0

Sikiric, P., Seiwerth, S., Grabarevic, Z., Rucman, R., Petek, M., Jagic, V., et al. (1997a). The influence of a novel pentadecapeptide, BPC 157, on N(G)-nitro-L-arginine methylester and L-arginine effects on stomach mucosa integrity and blood pressure. *Eur. J. Pharmacol.* 332 (1), 23–33. doi:10.1016/s0014-2999(97)01033-9

Sikiric, P., Seiwerth, S., Mise, S., Staresinic, M., Bedekovic, V., Zarkovic, N., et al. (2003). Corticosteroid-impairment of healing and gastric pentadecapeptide BPC-157 creams in burned mice. *Burns* 29 (4), 323–334. doi:10.1016/s0305-4179(03)00004-4

Sikiric, P., Seiwerth, S., Rucman, R., Drmic, D., Stupnisek, M., Kokot, A., et al. (2017). Stress in gastrointestinal tract and stable gastric pentadecapeptide BPC 157. Finally, do we have a solution? *Curr. Pharm. Des.* 23 (27), 4012–4028. doi:10.2174/1381612823666170220163219

Sikiric, P., Seiwerth, S., Rucman, R., Kolenc, D., Vuletic, L. B., Drmic, D., et al. (2016). Brain-gut *Axis* and pentadecapeptide BPC 157: theoretical and practical implications. *Curr. Neuropharmacol.* 14 (8), 857–865. doi:10.2174/1570159x13666160502153022

Sikiric, P., Seiwerth, S., Rucman, R., Turkovic, B., Rokotov, D. S., Brcic, L., et al. (2012). Focus on ulcerative colitis: stable gastric pentadecapeptide BPC 157. *Curr. Med. Chem.* 19 (1), 126–132. doi:10.2174/092986712803414015

Sikiric, P., Seiwerth, S., Rucman, R., Turkovic, B., Rokotov, D. S., Brcic, L., et al. (2014). Stable gastric pentadecapeptide BPC 157-NO-system relation. *Curr. Pharm. Des.* 20 (7), 1126–1135. doi:10.2174/13816128113190990411

Sikiric, P., Seiwerth, S., Rucman, R., Turkovic, B., Rokotov, D. S., Brcic, L., et al. (2011). Stable gastric pentadecapeptide BPC 157: novel therapy in gastrointestinal tract. *Curr. Pharm. Des.* 17 (16), 1612–1632. doi:10.2174/138161211796196954

Sikiric, P., Seiwerth, S., Rucman, R., Turkovic, B., Rokotov, D. S., Brcic, L., et al. (2013). Toxicity by NSAIDs. Counteraction by stable gastric pentadecapeptide BPC 157. *Curr. Pharm. Des.* 19 (1), 76–83. doi:10.2174/13816128130111

Sikiric, P., Separovic, J., Anic, T., Buljat, G., Mikus, D., Seiwerth, S., et al. (1999a). The effect of pentadecapeptide BPC 157, H2-blockers, omeprazole and sucralfate on new vessels and new granulation tissue formation. *J. Physiol. Paris* 93 (6), 479–485. doi:10.1016/s0928-4257(99)00123-0

Skorjanec, S., Dolovski, Z., Kocman, I., Brcic, L., Blagaic Boban, A., Batelja, L., et al. (2009). Therapy for unhealed gastrocutaneous fistulas in rats as a model for analogous healing of persistent skin wounds and persistent gastric ulcers: stable gastric pentadecapeptide BPC 157, atropine, ranitidine, and omeprazole. *Dig. Dis. Sci.* 54 (1), 46–56. doi:10.1007/s10620-008-0332-9

Skorjanec, S., Kokot, A., Drmic, D., Radic, B., Sever, M., Klicek, R., et al. (2015). Duodenocutaneous fistula in rats as a model for "wound healing-therapy" in ulcer healing: the effect of pentadecapeptide BPC 157, L-nitro-arginine methyl ester and L-arginine. *J. Physiol. Pharmacol.* 66 (4), 581–590.

Stambolija, V., Stambolija, T. P., Holjevac, J. K., Murselovic, T., Radonic, J., Duzel, V., et al. (2016). BPC 157: the counteraction of succinylcholine, hyperkalemia, and arrhythmias. *Eur. J. Pharmacol.* 781, 83–91. doi:10.1016/j.ejphar.2016.04.004

Staresinic, M., Petrovic, I., Novinscak, T., Jukic, I., Pevec, D., Suknaic, S., et al. (2006). Effective therapy of transected quadriceps muscle in rat: gastric pentadecapeptide BPC 157. *J. Orthop. Res.* 24 (5), 1109–1117. doi:10.1002/jor.20089

Staresinic, M., Sebecic, B., Jadrijevic, S., Suknaic, S., Perovic, D., Aralica, G., et al. (2003). Gastric pentadecapeptide BPC 157 accelerates healing of transected rat Achilles tendon and *in vitro* stimulates tendocytes growth. *J. Orthop. Res.* 21 (6), 976–983. doi:10.1016/S0736-0266(03)00110-4

Stupnisek, M., Franjic, S., Drmic, D., Hrelec, M., Kolenc, D., Radic, B., et al. (2012). Pentadecapeptide BPC 157 reduces bleeding time and thrombocytopenia after amputation in rats treated with heparin, warfarin or aspirin. *Thromb. Res.* 129 (5), 652–659. doi:10.1016/j.thromres.2011.07.035

Stupnisek, M., Kokot, A., Drmic, D., Hrelec Patrlj, M., Zenko Sever, A., Kolenc, D., et al. (2015). Pentadecapeptide BPC 157 reduces bleeding and thrombocytopenia after amputation in rats treated with heparin, warfarin, L-NAME and L-arginine. *PLoS One* 10 (4), e0123454. doi:10.1371/journal.pone.0123454

Sucic, M., Luetic, K., Jandric, I., Drmic, D., Sever, A. Z., Vuletic, L. B., et al. (2019). Therapy of the rat hemorrhagic cystitis induced by cyclophosphamide. Stable gastric pentadecapeptide BPC 157, L-arginine, L-NAME. *Eur. J. Pharmacol.* 861, 172593. doi:10.1016/j.ejphar.2019.172593

Tabata, Y., Nagano, A., and Ikada, Y. (1999). Biodegradation of hydrogel carrier incorporating fibroblast growth factor. *Tissue Eng.* 5 (2), 127–138. doi:10.1089/ten.1999.5.127

Tarnawski, A. S., and Ahluwalia, A. (2012). Molecular mechanisms of epithelial regeneration and neovascularization during healing of gastric and esophageal ulcers. *Curr. Med. Chem.* 19 (1), 16–27. doi:10.2174/092986712803414088

Thorén, K., and Aspenberg, P. (1993). Effects of basic fibroblast growth factor on bone allografts. A study using bone harvest chambers in rabbits. *Ann. Chir Gynaecol. Suppl.* 207, 129–135.

Tkalcevic, V. I., Cuzic, S., Brajsa, K., Mildner, B., Bokulic, A., Situm, K., et al. (2007). Enhancement by PL 14736 of granulation and collagen organization in healing wounds and the potential role of egr-1 expression. *Eur. J. Pharmacol.* 570 (1-3), 212–221. doi:10.1016/j.ejphar.2007.05.072

Tonolini, M., and Magistrelli, P. (2017). Enterocutaneous fistulas: a primer for radiologists with emphasis on CT and MRI. *Insights Imaging* 8 (6), 537–548. doi:10.1007/s13244-017-0572-3

Tshionyi, M., Shay, E., Lunde, E., Lin, A., Han, K. Y., Jain, S., et al. (2012). Hemangiogenesis and lymphangiogenesis in corneal pathology. *Cornea* 31 (1), 74–80. doi:10.1097/ICO.0b013e31821dd986

Turkovic, B., Sikiric, P., Seiwerth, S., Mise, S., Anic, T., Petek, M., et al. (2004). Stable gastric pentadecapeptide BPC 157 studied for inflammatory bowel disease (PLD-116, PL14736, Pliva) induces nitric oxide synthesis. *Gastroenterology* 126, 287.

Urist, M. R. (1996). The first three decades of bone morphogenetic protein. *Osteologie* 4, 207–233.

Visschers, R. G., van Gemert, W. G., Winkens, B., Soeters, P. B., and Olde Damink, S. W. (2012). Guided treatment improves outcome of patients with enterocutaneous fistulas. *World J. Surg.* 36 (10), 2341–2348. doi:10.1007/s00268-012-1663-4

Vukojevic, J., Siroglavic, M., Kasnik, K., Kralj, T., Stancic, D., Kokot, A., et al. (2018). Rat inferior caval vein (ICV) ligature and particular new insights with the stable gastric pentadecapeptide BPC 157. *Vascul Pharmacol.* 106, 54–66. doi:10.1016/j.vph.2018.02.010

Vukojevic, J., Vrdoljak, B., Malekinusic, D., Siroglavic, M., Milavic, M., Kolenc, D., et al. (2020). The effect of pentadecapeptide BPC 157 on hippocampal ischemia/reperfusion injuries in rats. *Brain Behav.* 10 (8), e01726. doi:10.1002/brb3.1726

Walter, M. A., Toriumi, D. M., Patt, B. S., Bhattacharyya, T. K., O'Grady, K., Caulfield, J. B., et al. (1996). Fibroblast growth factor-induced motor end plate regeneration in atrophic muscle. *Arch. Otolaryngol. Head Neck Surg.* 122 (4), 425–430. doi:10.1001/archotol.1996.01890160065012

Wang, J. S., and Aspenberg, P. (1996). Basic fibroblast growth factor promotes bone ingrowth in porous hydroxyapatite. *Clin. Orthop. Relat. Res.* 333, 252–260.

Wang, X. Y., Qu, M., Duan, R., Shi, D., Jin, L., Gao, J., et al. (2019). Cytoprotective mechanism of the novel gastric peptide BPC157 in gastrointestinal tract and cultured enteric neurons and glial cells. *Neurosci. Bull.* 35 (1), 167–170. doi:10.1007/s12264-018-0269-8

Whittle, B. J. R., Boughton-Smith, N. K., and Moncada, S. (1992). Biosynthesis and role of the endothelium-derived vasodilator, nitric oxide in gastric mucosa. *Ann. NY Acad. Sci.* 664, 126–139. doi:10.1111/j.1749-6632.1992.tb39755.x

Wynn, T. A. (2008). Cellular and molecular mechanisms of fibrosis. *J. Pathol.* 214 (2), 199–210. doi:10.1002/path.2277

Xue, X. C., Wu, Y. J., Gao, M. T., Li, W. G., Zhao, N., Wang, Z. L., et al. (2004a). Protective effects of pentadecapeptide BPC 157 on gastric ulcer in rats. *World J. Gastroenterol.* 10 (7), 1032–1036. doi:10.3748/wjg.v10.i7.1032

Xue, X. C., Wu, Y. J., Gao, M. T., Li, W. G., Zhao, N., Wang, Z. L., et al. (2004b). Study of the protective effects of pentadecapeptide BPC 157 on skin cut wounds in small type pigs. *Chin. J. New Drugs* 13, 602–605.

Yu, C., Cunningham, M., Rogers, C., Dinbergs, I. D., and Edelman, E. R. (1998). The biologic effects of growth factor-toxin conjugates in models of vascular injury depend on dose, mode of delivery, and animal species. *J. Pharm. Sci.* 87 (11), 1300–1304. doi:10.1021/js980086i

Zhang, Y., Bonzo, J. A., Gonzalez, F. J., and Wang, L. (2011). Diurnal regulation of the early growth response 1 (Egr-1) protein expression by hepatocyte nuclear factor 4alpha(HNF4alpha) and small heterodimer partner (SHP) cross-talk in liver fibrosis. *J. Biol. Chem.* 286 (34), 29635–29643. doi:10.1074/jbc.M111.253039

Conflict of Interest: The authors declare that the research was conducted in the absence of any commercial or financial relationships that could be construed as a potential conflict of interest.

frontiers in Pharmacology

ORIGINAL RESEARCH
published: 27 July 2021
doi: 10.3389/fphar.2021.719581

MALAT1: A Pivotal lncRNA in the Phenotypic Switch of Gastric Smooth Muscle Cells *via* the Targeting of the miR-449a/DLL1 Axis in Diabetic Gastroparesis

Yanjuan Wang[1†], Yan Wang[1†], Boqian Zhu[2], Ying Zhu[3], Ya Jiang[1], Wenjie Xiong[1], Lin Lin[1] and Yaoyao Gong[1*]*

[1]Department of Gastroenterology, The First Affiliated Hospital of Nanjing Medical University, Nanjing, China, [2]Department of Cardiology, Affiliated Hospital of Nanjing University of Chinese Medicine, Nanjing, China, [3]Department of Gastroenterology, Northern Jiangsu People's Hospital, Yangzhou, China

Diabetic gastroparesis (DGP) is a common complication of diabetes mellitus (DM). Our previous study suggested that the expression of the long non-coding RNA (lncRNA) metastasis-associated lung adenocarcinoma transcript 1 (MALAT1) is closely related to DGP. However, the role of MALAT1 in DGP pathogenesis remains unclear. Here, we aim to characterize the role of MALAT1 in DGP. First, we analyzed the lncRNA expression profiles through lncRNA sequencing. Next, we detected MALAT1 expression in the stomach tissues of DGP model mice and diabetic patients. Then, we investigated the role and mechanisms of MALAT1 in the proliferation, migration, phenotypic switch, and carbachol-induced intracellular Ca^{2+} changes in human gastric smooth muscle cells (HGSMCs) under high glucose (HG) conditions, using short hairpin RNA technology, RNA immunoprecipitation, and dual-luciferase reporter assays. We show that MALAT1 expression was upregulated in the gastric tissues of DGP model mice, the adjacent healthy tissues collected from diabetic gastric cancer patients with DGP symptoms, and in HGSMCs cultured under HG conditions. Functionally, MALAT1 knockdown *in vitro* impacted the viability, proliferation, migration and promoted the phenotypic switch of HGSMCs under HG conditions. Additionally, we show that MALAT1 sponged miR-449a, regulating Delta-like ligand 1 (DLL1) expression in HGSMCs; any disturbance of the MALAT1/miR-449a/DLL1 pathway affects the proliferation, migration, phenotypic switch, and carbachol-induced Ca^{2+} transient signals in HGSMCs under HG conditions. Collectively, our data highlight a novel regulatory signaling pathway, the MALAT1/miR-449a/DLL1 axis, in the context of DGP.

Keywords: gastroparesis, myocytes, smooth muscle, RNA, long noncoding, diabetes, phenotypic switch

OPEN ACCESS

Edited by:
Duan Chen,
Norwegian University of Science and Technology, Norway

Reviewed by:
Hui Yang,
The Second Affiliated Hospital of Guangzhou Medical University, China
Xianju Huang,
South-Central University for Nationalities, China

****Correspondence:***
Yaoyao Gong
ygong@njmu.edu.cn
Lin Lin
lin9100@aliyun.com

[†]These authors have contributed equally to this work

Specialty section:
This article was submitted to Gastrointestinal and Hepatic Pharmacology, a section of the journal Frontiers in Pharmacology

Received: *02 June 2021*
Accepted: *13 July 2021*
Published: *27 July 2021*

Citation:
Wang Y, Wang Y, Zhu B, Zhu Y, Jiang Y, Xiong W, Lin L and Gong Y (2021) MALAT1: A Pivotal lncRNA in the Phenotypic Switch of Gastric Smooth Muscle Cells via the Targeting of the miR-449a/DLL1 Axis in Diabetic Gastroparesis. Front. Pharmacol. 12:719581. doi: 10.3389/fphar.2021.719581

INTRODUCTION

Diabetic gastroparesis (DGP), defined as the objectively delayed gastric emptying without mechanical obstruction, is a severe complication of diabetes mellitus (DM); it causes early satiety, nausea, vomiting, bloating, heartburn, and abdominal pain, as well as significant morbidity (Vanormelingen et al., 2013; Camilleri et al., 2017). Although the exact prevalence of DGP remains unknown, gastric emptying disorders reportedly occur in approximately one-third of diabetic patients (De Block et al., 2006; Bharucha et al., 2019). Notably, more than to affect the quality of life, DGP significantly impacts the patients' self-management of diabetes (Kumar et al., 2018). Of note, not only hyperglycemia but also immune disorders, hormonal disturbances, autonomic neuropathy, autonomic or enteric neuropathy, gastric smooth muscle lesions, and injury of the interstitial cells of Cajal (ICCs) may result in DGP (Camilleri et al., 2011; Bharucha et al., 2019). Previous studies have demonstrated that patients with DGP show the thickening of the basal lamina around smooth muscle cells (SMCs), together with smooth muscle degeneration and fibrosis, suggesting that gastric smooth muscle lesions play a pivotal role in DGP formation (Kashyap and Farrugia 2010; Camilleri et al., 2011; Faussone-Pellegrini et al., 2012). However, the mechanisms underlying the formation of smooth muscle lesions remain unclear.

Normal gastric emptying is coordinated by SMCs, nerve cells, ICCs, glial cells, and hormones (Horvath et al., 2014). Of note, SMCs show plasticity, characterized by the reversible phenotype switch from a contractile (differentiated) to synthetic (dedifferentiated) phenotype when stimulated by some agents, such as inflammatory cytokines (Nair et al., 2011; Grover et al., 2011; Scirocco et al., 2016). This process is associated with a reduced expression of contractile markers, such as SM myosin heavy chain (MHC), calponin, α-SMA, SM22α, and smoothelin (Scirocco et al., 2016).Although this process has been more thoroughly studied in vascular SMCs, recent studies have found the plasticity of SMCs also exists in the gastrointestinal (GI) tract (Nair et al., 2011; Scirocco et al., 2016). Grover and colleagues found that SMC contractile protein smoothelin expression decreased in the gastric tissue of patients with DGP (Grover et al., 2011). Our laboratory has also reported that the expression of SMC contractile proteins was markedly reduced in the stomach tissues of a DM rat model (Yu et al., 2017).

Long non-coding ribonucleic acids (lncRNAs) are RNAs with lengths exceeding 200 bp without known protein-coding functions (Wilusz et al., 2009; Bunch, 2018). lncRNAs impact many biological processes, such as cell proliferation, migration, and differentiation (Bharucha et al., 2015; Gong et al., 2018). However, few studies have evaluated the function of lncRNAs in the pathogenesis of GI motility disorders. Our previous study found that the levels of metastasis-associated lung adenocarcinoma transcript 1 (MALAT1), a lncRNA located at the human chromosome 11q13, were elevated in the gastric tissues of patients with DM and DGP symptoms (Gong et al., 2018). Besides, we found that MALAT1 may be involved in the pathogenesis of DGP, impacting the SMC phenotypic transition (Gong et al., 2018). However, the underlying mechanisms of MALAT1 in the context of the SMC phenotypic transition and the pathogenesis of DGP remain largely unclear.

This study aimed to investigate the role of the lncRNA MALAT1 in the pathogenesis of DGP and the specific mechanism by which MALAT1 regulates the phenotypic transition of gastric SMCs. First, we detected the increased MALAT1 using lncRNA sequencing and verified that the expression of MALAT1 in the stomach tissues of a DGP mouse model and diabetic patients was indeed increased. Subsequently, we investigated the role and mechanisms of MALAT1 in human gastric SMCs (HGSMCs) under high glucose (HG) conditions, using the short hairpin RNA (shRNA) technology. Here we demonstrate that MALAT1 is upregulated under HG conditions, interacting with miR-449a, leading to the upregulation of Delta-like ligand 1 (DLL1); this ultimately leads to the phenotypic transition of SMCs and the development of DGP. Besides, as smooth muscle contraction in response to agonists is related to the increase in the intracellular Ca^{2+} concentration $[Ca^{2+}]_i$, we also detected the effects of the MALAT1/miR-499a/DLL1 pathway on the carbachol (CCh)-induced $[Ca^{2+}]_i$. Altogether, our data clarify the mechanism behind DGP, providing potential new targets for the development of novel prophylactic and therapeutic approaches in the context of DGP.

MATERIALS AND METHODS

Tissue Specimens

All specimens were obtained from the Human Tissue Specimen Research Bank of the First Affiliated Hospital, Nanjing Medical University. Stomach specimens were collected from the adjacent normal area of the stomach of ten patients with gastric cancer and diabetes with symptoms of DGP who underwent gastrectomy. Additionally, control samples were obtained from the stomachs of ten non-diabetic gastric cancer patients with no symptoms of DGP. The collection standards for gastric specimens were as described previously (Gong et al., 2018).

Animals and Gastric Emptying Test

Male C57BL/6J mice (6 weeks old, 20–26 g) were randomly divided into two groups: control (n = 10) and diabetic (n = 10). Diabetes was induced and diagnosed as described elsewhere (Yu et al., 2017). The solid gastric emptying experiment was performed 8 weeks after streptozotocin injection. Briefly, the mice were fasted for 16 h with free access to water and then were allowed to feed on a solid food pellet for 30 min. Then, mice were fasted again for 2 h. All mice were sacrificed at the end of fasting. The stomach was excised, and its contents were air-dried for 48 h before weighing. The gastric emptying rate was calculated using the following equation:

$$\text{Gastric emptying rate}(\%) = \left[1 - \left(\text{dried gastric content in g}\right)/ \times \left(\text{food intake in g}\right)\right] \times 100$$

RNA Sequencing and Analysis and Pathway and Gene Ontology Analysis

Total RNA was extracted from tissues using the Trizol reagent (Invitrogen, Carlsbad, CA, United States) and measured using the NanoDrop 1000 spectrophotometer (Thermo Fisher Scientific, Waltham, MA, United States). RNA sequencing and data analysis and pathway and gene ontology analysis was performed by Aksomics (Aksomics, Shanghai, China).

In vitro Studies of Gastric Antral Contractility

Three circular muscle strips (approximately 2 mm × 10 mm) were taken from each murine gastric antral specimen and placed in Tyrode solution (37°C, 5% CO_2 + 95% O_2). The tension signal was recorded and analyzed using a multi-channel data acquisition and analysis system (Techman Software Co., Chengdu, China). A preload of 1 g tension was set. After tissues were equilibrated for 0.5 h, the contraction tension was recorded by the stimulation of CCh (Apexbio Technology, Houston, TX, United States). The maximum contraction tension was calculated as the maximum post-stimulation tension minus the average pre-stimulation value.

Cell Culture

HGSMCs were cultured in Dulbecco's modified Eagle's medium (DMEM, Gibco, Carlsbad, CA, United States) with 10% fetal bovine serum (Gibco) and 1% penicillin-streptomycin (Hyclone, South Logan, UT, United States). All cells were cultured in an incubator with 5% CO_2 at 37°C.

RNA Knockdown and Cell Transfection

ShRNAs targeting MALAT1 (shMALAT1) and DLL1 (shDLL1) were designed and synthesized by GenePharma (Shanghai, China). The relevant sequences are as follows: shMALAT1-1: 5′-GCAGCCCGAGACTTCTGTAAA-3'. shMALAT1-2, sense: 5′-GCCCGAGACTTCTGTAAAGGA-3'. shMALAT1-3, sense: 5′-GCTCTAAATTGTTGTGGTTCT-3'. shDLL1-1: 5′-GGT ACTGTGACGAGTGTATCC-3'. shDLL1-2, sense: 5′-GCT CTTCACCCTGTTCTAATG-3'. shDLL1-3, sense: 5′- GAT GAGTGCGTCATAGCAACT-3′.

The miR-449a mimic, miR-449a inhibitor, and the respective negative controls (NC) were purchased from Sangon Biotech Co., Ltd (Shanghai, China). Transfections were carried out using Lipofectamine-2000 (Invitrogen, Carlsbad, CA, United States) following the manufacturer's instructions.

RNA Extraction and Quantitative Real-Time Polymerase Chain Reaction

Total RNA was extracted from tissues and HGSMCs using the Trizol reagent (Invitrogen, Carlsbad, CA, United States) and measured using the NanoDrop 1000 spectrophotometer (Thermo Fisher Scientific, Waltham, MA, United States). Total RNA (1 μg) was reversely transcribed into cDNA using the PrimeScript RT Reagent Kit (Takara, Dalian, China). qPCR was performed with the SYBR Green I mix (Junxin Biotech Co., Suzhou, China) using the ABI 7500 Fast real-time PCR system (Applied Biosystems, Foster City, CA, United States). Gene expression was normalized to the expression of β-Actin or U6. Data were analyzed using the $2^{-\Delta\Delta Ct}$ method. The primers used in this study were all synthesized by Sangon Biotech Co., Ltd. The primer sequences used are listed in Supplementary Material (**Table 1**).

Western Blot Analysis

Proteins were extracted from tissues and HGSMCs with the Radio-Immunoprecipitation Assay Buffer (RAPI, Junxin Biotech). Western blot analysis was carried out as described previously (Yu et al., 2017). The antibodies used were as follows: anti-α-SMA (1:1000, Ab108424, Abcam, Cambridge, United Kingdom), anti-SM22α (1:1000, D123178, Sangon Biotech Co., Ltd, Shanghai, China), anti-MHC (1:1000, Ab23990, Abcam), anti-DLL1 (1:1000, Ab10554, Abcam), anti-β-Actin (1:4000, K200058M, Solarbio, Beijing, China), HRP-conjugated goat anti-rabbit IgG (1:4000, D110058, Sangon Biotech), and HRP-conjugated goat anti-mouse IgG (1:4000, D110087, Sangon Biotech). An enhanced chemiluminescence detection kit (Junxin Biotech) was used to observe the immunoreactivity, and the Gelpro analyzer software (Infaimon S.L., Barcelona, Spain) was used for data analysis.

Cell Viability Assay

HGSMCs were seeded into 96-well plates (4×10^3 cells/well) and subjected to different treatments. Cell viability was examined with the Cell Counting Kit-8 (CCK-8, Junxin Biotech). The cells were then cultured in an incubator containing 5% CO_2 at 37°C for 2 h. The optical density was examined at a wavelength of 450 nm using a microplate spectrophotometer (Thermo Fisher Scientific).

Cell Proliferation Assay

HGSMCs were seeded into 48-well plates (5×10^4 cells/well) and subjected to different treatments. Cell proliferation was detected using a 5-ethynyl-2′-deoxyuridine (EdU) kit (Junxin Biotech). Briefly, the cells were incubated with 200 μL EdU in a CO_2 incubator at 37°C for 2 h. The cells were then rinsed once in cold phosphate-buffered saline (PBS), fixed with 4% paraformaldehyde, and treated with 0.5% Triton X-100. After being rinsed in PBS, the cells were incubated with carboxytetramethylrhodamine (TAMRA) and then stained with Hoechst 33,342. Stained cells were photographed using a fluorescence microscope (Olympus CKX53, Japan).

Cell Migration Assay

Cell migration was investigated using the Transwell invasion assay (Corning, NY, United States). HGSMCs were re-suspended in 100 μL serum-free medium and then transferred into the top chamber; 600 μL DMEM containing 10% serum was added to the lower chamber. After incubation for 18 h, the cells in the upper chamber of the filter were carefully removed. Then, 4% paraformaldehyde and 0.1% crystal violet were applied to fix and stain the cells invading through the membrane, respectively. Cells were then imaged using a light microscope and counted.

TABLE 1 | Primers used in this study.

Gene	Primer	Sequence
Human MALAT1	Forward	5′- GTCATAACCAGCCTGGCAGT -3′
	Reverse	5′- CGAAACATTGGCACACAGCA-3′
Murine MALAT1	Forward	5′- TGCAGTGTGCCAATGTTTCG -3′
	Reverse	5′- GGCCAGCTGCAAACATTCAA -3′
Human DLL1	Forward	5′- GTTTCCCGAGGTTGCCTTTCC -3′
	Reverse	5′- CTCTCCTTAGAACAGCGGCG-3′
Murine DLL1	Forward	5′- TGATCGTGGACAACACGGAG -3′
	Reverse	5′- TCGTCTGGCTTTCAGTCCAC-3′
Human β-actin	Forward	5′- CATTCCAAATATGAGATGCGTTGT -3′
	Reverse	5′- TGTGGACTTGGGAGAGGACT -3′
Murine β-actin	Forward	5′- GGCTGTATTCCCCTCCATCG -3′
	Reverse	5′- CCAGTTGGTAACAATGCCATGT -3′
Human U6	Forward	5′- CTCGCTTCGGCAGCACA-3′
	Reverse	5′- AACGCTTCACGAATTTGCGT-3′
Murine U6	Forward	5′- ACGGCTACCTCTCAATCCCA-3′
	Reverse	5′- GATGCCCGTTGTAGGTCTCC-3′
Human miR-449a	Forward	5′- GTGCTGTGGCAGTGTATTGTTA-3′
	RT	5′-GTCGTATCCAGTGCAGGGTCCGAGGTATTCGCACTGGATACGACACCAGC-3′
Human miR-25-3p	Forward	5′- GCCATTGCACTTGTCTCG-3′
	RT	5′-GTCGTATCCAGTGCAGGGTCCGAGGTATTCGCACTGGATACGACTCAGAC-3′
Human miR-34a-5p	Forward	5′- GTGCTGGCAGTGTCTTAGC-3′
	RT	5′-GTCGTATCCAGTGCAGGGTCCGAGGTATTCGCACTGGATACGACACAACC-3′
Human miR-429	Forward	5′- GCGGTCTAATACTGTCTGGTAAAAC-3′
	RT	5′-GTCGTATCCAGTGCAGGGTCCGAGGTATTCGCACTGGATACGACACGGTTT-3′
Human miR-92a-3p	Forward	5′- GTCTATTGCACTTGTCCCGG-3′
	RT	5′-GTCGTATCCAGTGCAGGGTCCGAGGTATTCGCACTGGATACGACACAGGC-3′
Human miR-32-5p	Forward	5′- GCGGTGTATTGCACATTACTAAG-3′
	RT	5′-GTCGTATCCAGTGCAGGGTCCGAGGTATTCGCACTGGATACGACTGCAAC-3′
Human miR-92b-3p	Forward	5′- GTTATTGCACTCGTCCCGG-3′
	RT	5′-GTCGTATCCAGTGCAGGGTCCGAGGTATTCGCACTGGATACGACGGAGGC-3′
Human miR-363-3p	Forward	5′- GCGAGCAATTGCACGGTATCCAT-3′
	RT	5′-GTCGTATCCAGTGCAGGGTCCGAGGTATTCGCACTGGATACGACTACAGA-3′

Measurement of the Intracellular Ca^{2+} Levels

The Fluo-3/AM calcium indicator (Solarbio Science & Technology Co., Beijing, China) was used to detect intracellular Ca^{2+} levels. HGSMCs were seeded into glass-bottom dishes and subjected to different treatments. Cells were then incubated with Fluo-3/AM (5 μmol/L) in a CO_2 incubator at 37°C for 30 min and rinsed twice in PBS. Calcium fluorescence intensity was examined using a confocal laser scanning microscope (LSM510, Carl Zeiss, Oberkochen, Germany) at an excitation wavelength of 488 nm and an emission wavelength of 525 nm. The changes in Ca^{2+} fluorescence intensity are expressed as F/F0, where F0 is the basal fluorescence intensity before stimulation. CCh was used as a stimulant to generate Ca^{2+} transient signals.

Luciferase Reporter Assays

To investigate the relationship between the lncRNA MALAT1 or DLL1 and miR-449a, we used dual-Luciferase reporter assays. The respective amplified DNA sequences were inserted into the psiCheck2 luciferase reporter vector to form the MALAT1 luciferase vector (Luciferase-MALAT1-wt), the mutated MALAT1 luciferase vector (Luciferase-MALAT1-mut), the DLL1 3′ UTR luciferase vector (Luciferase-DLL1-wt), and the mutated DLL1 3′ UTR luciferase vector (Luciferase-DLL1-mut). Then, to detect the effect of MALAT1 on miR-449a, HGSMCs were co-transfected with Luciferase-NC, Luciferase-MALAT1-wt, or Luciferase-MALAT1-mut together with the miR-449a mimic or the respective NC using Lipofectamine-2000 (Invitrogen) according to the manufacturer's instructions. Moreover, to detect the effect of miR-449a on DLL1, cells were co-transfected with Luciferase-NC, Luciferase-DLL1-wt, or Luciferase-DLL1-mut together with the miR-449a mimic or the respective NC. 48 h after transfection, the luciferase activity was tested using the Dual-Luciferase Assay System (Promega, Madison, WI, United States) according to the manufacturer's protocol.

RNA Immunoprecipitation

According to the manufacturer's instructions, RIP was carried out using the Magna RIP Kit (Millipore, Bedford, MA, United States). In brief, HGSMCs under different treatments were harvested and lysed. Then, the lysates were incubated with an anti-Argonaute two antibody (AGO2, Ab32381, Abcam) or control IgG (Ab172730, Abcam) and protein A/G beads (Biolinkedin, Shanghai, China). qPCR was used to examine the enrichment of MALAT1, miR-449a, and DLL1.

Statistical Analysis

All experimental data are presented as the mean ± standard deviation (SD) from at least three independent experiments.

TABLE 2 | Comparison of fasting blood glucose, gastric emptying rate and gastric muscle strip contractility in STZ group and normal group.

Group	*N*	Fasting blood glucose (mmol/L)	Gastric emptying rate (%)	Muscle strip contractility (g)
Control group	10	6.231 ± 0.725	71.111 ± 6.333	1.829 ± 1.316
STZ group	10	20.806 ± 3.339**	42.778 ± 3.993**	0.650 ± 0.145**

**p < *0.01*.

Statistical differences were evaluated using the ANOVA or Student's *t* test; the SPSS 11.0 software was used. *p* values <0.05 were considered statistically significant.

RESULTS

Metastasis-Associated Lung Adenocarcinoma Transcript 1 Is Highly Expressed in Both Clinical Samples and Diabetic Gastroparesis Model Mice

To systematically screen the functional lncRNAs in DGP, we established a mouse model of DGP. Notably, the blood glucose levels, gastric emptying profiles, and gastric muscle strip contractility of the diabetic and control mice were measured (Supplementary Material **Table 2**). The gastric emptying rate and muscle strip contractility (**Figure 1A**) of the mice in the diabetic group were significantly lower than those of mice in the control group.

Then, lncRNA sequencing was conducted in three pairs of gastric tissues from DGP mice and the respective control group to investigate the profile of lncRNA expression. **Figure 1B** shows the hierarchical cluster and volcano analysis of the expression profile of lncRNA. Compared with the control group, a total of 585 lncRNAs (210 down-regulated and 375 upregulated) were differently expressed in DGP tissues (fold change >2.0 and $p < 0.05$), indicating that these lncRNAs may be involved in the development of DGP. In order to verify the reliability of the sequencing results, top ten upregulated and down-regulated candidate lncRNAs were selected for qPCR, and the results were consistent with those of the sequencing analysis (**Figure 1C**). Next, we quantified MALAT1 expression using qPCR in the DGP mice and respective control groups. The qPCR results showed that the expression of MALAT1 in mice with DGP was significantly increased compared with that in control mice ($p < 0.01$; **Figure 1D**). Therefore, we focused on lncRNA MALAT1 further in the study.

To further determine the role of MALAT1 in DGP, we obtained the adjacent normal tissues from the stomach of diabetic gastric cancer patients with DGP symptoms and normal tissues from the stomach of non-diabetic gastric cancer patients without DGP symptoms. Interestingly, the expression of MALAT1 was significantly upregulated in samples from diabetic patients with DGP symptoms compared to in control individuals ($p < 0.01$; **Figure 1E**).

Altogether, these results indicate that MALAT1 is upregulated in the context of DGP.

Metastasis-Associated Lung Adenocarcinoma Transcript 1 Knockdown Reverses the Phenotypic Switching of Human Gastric SMCs Under High Glucose Conditions

Based on the above experimental results, we hypothesized that MALAT1 might modulate the function of HGSMCs. To test this hypothesis, we examined MALAT1 expression in HGSMCs under HG conditions; qPCR results showed that MALAT1 was upregulated in HGSMCs under HG (**Figure 2A**). Then, we designed and synthesized three shRNAs specifically targeting MALAT1 (shMALAT1) and transfected them along with the respective control RNA (shNC) into HGSMCs. 48 h later, qPCR analysis showed that all three shMALAT1 could effectively downregulate MALAT1 expression in HGSMCs; shMALAT1-1 was selected for subsequent experiments (**Figure 2B**).

Then, four groups of HGSMCs were generated and analyzed: normal glucose (NG)+shNC group, high glucose (HG)+shNC group, NG + shMALAT1 group, and HG + shMALAT1 group. The CCK-8 assay results indicated that MALAT1 silencing reduced cell viability and prevented the effect of HG in the context of HGSMCs (**Figure 2C**). Furthermore, EdU analysis results revealed that MALAT1 knockdown inhibited cell proliferation and attenuated the HG-induced elevation of cell proliferation in HGSMCs (**Figure 2D**). Transwell assay results showed that MALAT1 knockdown suppressed cell migration and alleviated the HG-induced promotion of cell migration in HGSMCs (**Figure 2E**).

Next, we examined contractile markers' expression to define the relationship between MALAT1 and the phenotypic switching in HGSMCs. The qPCR and western blot analyses demonstrated that MALAT1 knockdown increased the expression of the contractile markers α-SMA, SM22α, and MHC at both the RNA and protein levels, alleviating the HG-induced reduction of the expression of these genes in HGSMCs (**Figures 2F,G**).

In summary, these observations suggest that the silencing of MALAT1 affects the HG-induced promotion of cell viability, proliferation, migration, and phenotype switching in HGSMCs.

Metastasis-Associated Lung Adenocarcinoma Transcript 1 Interacts With miR-449a in Human Gastric SMCs

To further investigate the molecular mechanisms of MALAT1 in HGSMCs under HG conditions, we utilized the online miRcode database (http://www.mircode.org) to screen for miRNAs with MALAT1 sequence complementarity. We found that miR-449a, miR-25-3p, miR-34a-5p, miR-429, miR-92a-3p, miR-32-5p, miR-

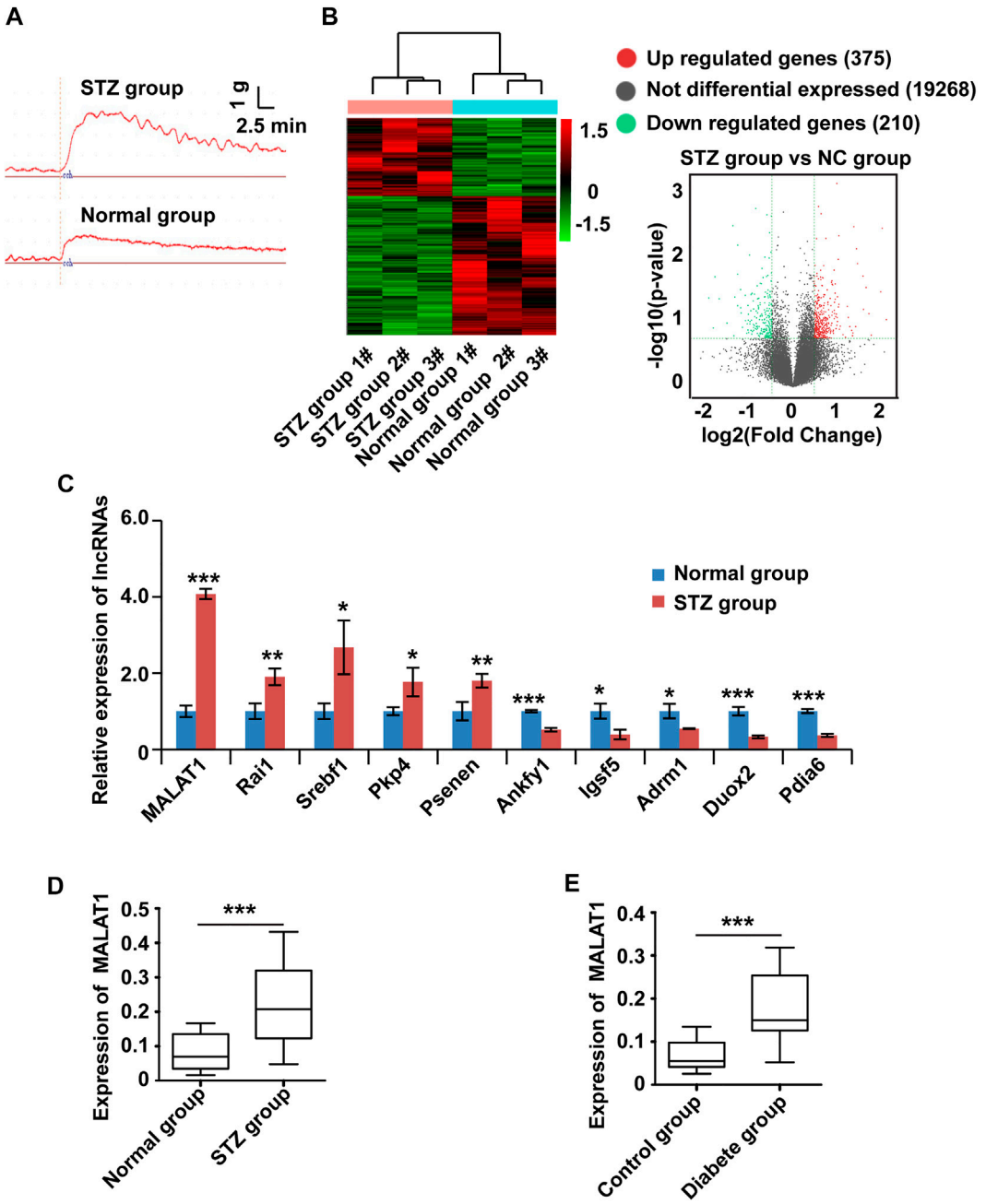

FIGURE 1 | The expression of MALAT1 is upregulated in clinical samples and a murine model of DGP. **(A)** Contractility of circular gastric muscle strips from streptozotocin-induced diabetic and respective control mice after administration of 100 μmol/L CCh. **(B)** The hierarchical clustering and volcano analysis of differentially expressed lncRNAs. Here, 585 differentially expressed lncRNAs (210 downregulated and 375 upregulated) from hierarchical clustering were identified between DGP mice and the respective control group. The expression level of lncRNA is represented in red if it is above the average value of the gene in all samples. Conversely, green indicates that the expression level of lncRNA is below the average value. **(C)** qPCR was used to validate significantly differentially expressed lncRNAs, and lncRNA MALAT1 was significantly up-regulated in DGP mice. **(D)** qPCR analysis of the expression of MALAT1 in gastric tissues from a DGP mouse model (and control mice; n = 10 per group). **(E)** qPCR analysis of the expression of MALAT1 in (adjacent) normal stomach tissues from patients who underwent gastrectomy with or without DM and DGP symptoms (n = 10 per group). β-Actin was used as an internal control. ***p < 0.001, **p < 0.01, *p < 0.05.

92b-3p, and miR-363-3p were complementary with MALAT1. To filter out functional miRNAs in HGSMCs under HG, we performed qPCR and observed that the expression of miR-449a was downregulated in HGSMCs under HG conditions (**Figure 3A**). Then, we cloned the MALAT1 cDNA containing the intact binding site of miR-449a and the MALAT1 cDNA with a mutated binding site into luciferase reporter plasmids (Luciferase-MALAT1-wt, and Luciferase-MALAT1-mut, respectively). Luciferase-

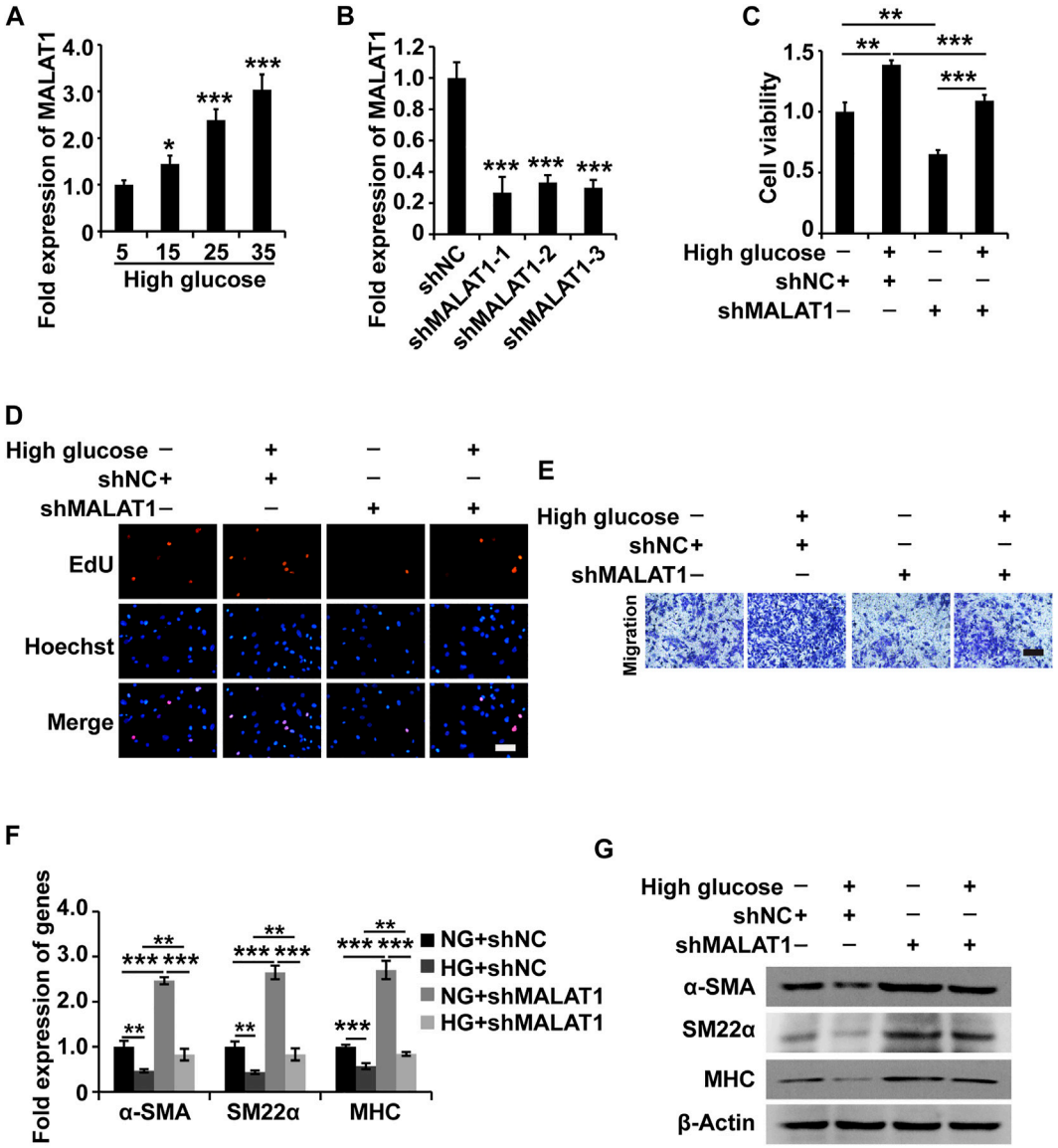

FIGURE 2 | MALAT1 knockdown attenuates the HG-induced promotion of cell viability, proliferation, migration, and phenotypic switching in HGSMCs. **(A)** qPCR analysis of the expression of MALAT1 in HGSMCs treated with different concentrations of glucose (5, 15, 25, and 35 mM) for 48 h. **(B)** qPCR analysis of the expression of MALAT1 in HGSMCs 48 h after transfection with shMALAT1s and shNC. **(C–E)** The CCK8, EdU, and Transwell assays were carried out to analyze the viability, proliferation, and migration of HGSMCs under different treatments. **(F–G)** qPCR and western blot analyses of SMC contractile markers (α-SMA, SM22α, and MHC) in HGSMCs under different treatments. For **(C–G)**, four groups of cells were used: NG + shNC group, HG + shNC group, NG + shMALAT1 group, and HG + shMALAT1 group. β-Actin was used as an internal control. ***$p < 0.001$, **$p < 0.01$, *$p < 0.05$.

MALAT1-wt, Luciferase-MALAT1-mut, and the respective control plasmids (Luciferase-NC) were transfected into HGSMCs together with a miR-449a mimic or the respective mimic NC, and luciferase activities were detected. Remarkably luciferase activity of cells transfected with the Luciferase-MALAT1-wt plasmid was significantly decreased by miR-449a mimic, while no effect occurred in Luciferase-NC- or Luciferase-MALAT1-mut-transfected cells, suggesting an interaction between MALAT1 and miR-449a (**Figures 3B,C**). The RIP analysis also revealed that endogenous MALAT1 pulled-down by AGO2 was specifically enriched in miR-449a-transfected cells, further confirming the interaction between MALAT1 and miR-449a (**Figure 3D**). Taken together, these results prove that MALAT1 directly targets miR-449a.

Delta-Like Ligand 1 is a Target of Metastasis-Associated Lung Adenocarcinoma Transcript 1 *via* miR-449a

To explore the target of the MALAT1-miR-449a complex, the online miRNA target-prediction tool TargetScan was used. The *in silico* analysis revealed that the DLL1 3′ UTR contains a binding site for miR-449a. We transfected a miR-449a mimic, a miR-449a inhibitor,

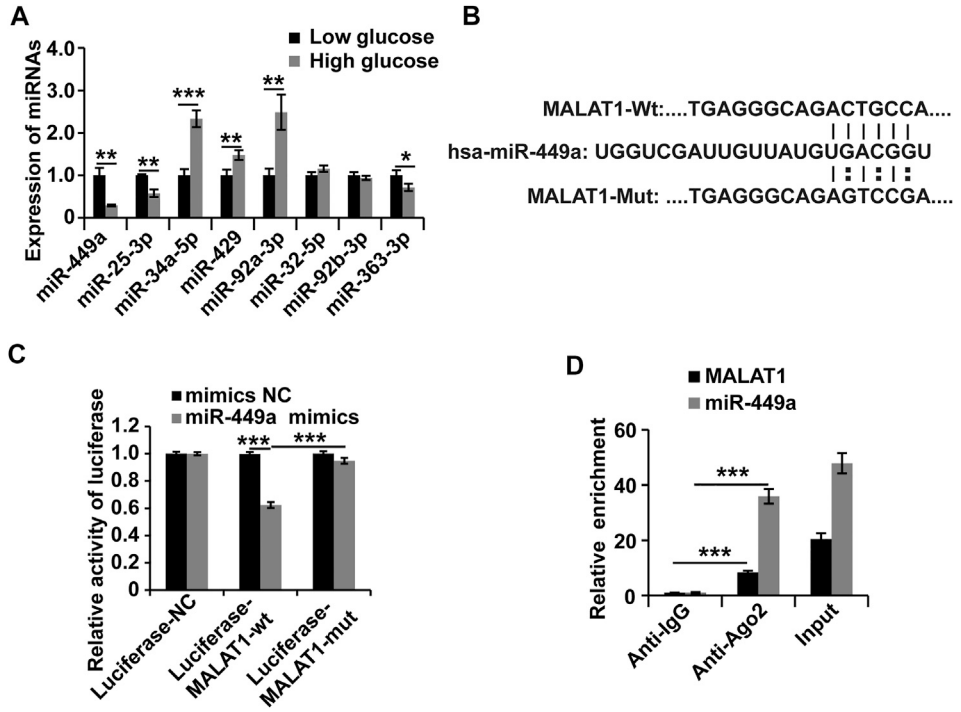

FIGURE 3 | MALAT1 interacts with miR-449a in HGSMCs. **(A)** qPCR analysis was conducted to detect the endogenous microRNAs associated with MALAT1 in HGSMCs under HG conditions for about 48 h. **(B)** Predicted binding site of miR-449a in the MALAT1 sequence. **(C)** luciferase reporter assay analysis of the interaction between MALAT1 and miR-449a. **(D)** RIP assay analysis of the interaction between MALAT1 and miR-449a. U6 was used as an internal control. ***$p < 0.001$, **$p < 0.01$, *$p < 0.05$.

and the respective controls into HGSMCs to validate this result. The results of qPCR and western blot analyses 48 h later revealed that the miR-449a mimic inhibited the expression of DLL1 and, conversely, the miR-449a inhibitor promoted the expression of DLL1 in HGSMCs (**Figures 4A,B**). Furthermore, we cloned the DLL1 3′ UTR containing the exact binding site of miR-449a as well as the DLL1 3′ UTR with a mutated sequence into luciferase reporter plasmids (Luciferase-DLL1-wt, and Luciferase-DLL1-mut, respectively) and co-transfected them with the miR-449a mimic into HGSMCs. Luciferase activity was inhibited by miR-449a mimic in the context of Luciferase-DLL1-wt and restored in Luciferase-DLL1-mut-transfected cells (**Figures 4C,D**). A RIP analysis further proved the interaction between miR-449a and DLL1 (**Figure 4E**). Thus, we conclude that DLL1 is a direct target of miR-449a in HGSMCs.

Delta-Like Ligand 1 Knockdown Reverses the Phenotypic Switching of Human Gastric SMCs Under High Glucose Conditions

To understand the role of DLL1 in DGP, we first measured the expression of DLL1 in the clinical samples, DGP model mice, and in HGSMCs under HG conditions. The qPCR and western blot results showed that DLL1 was upregulated in both the clinical samples and the DGP mouse model (**Figures 5A,B**). Furthermore, the results of qPCR and western blot analyses showed that the expression of DLL1 was increased in HGSMCs under HG conditions (**Figure 5C**).

Next, we designed and synthesized three shRNAs specific to DLL1 (shDLL1s) and transfected them, along with the respective control RNA (shNC), into HGSMCs. The qPCR analysis 48 h after revealed that all three shDLL1s could sufficiently downregulate the expression of DLL1 in HGSMCs; shDLL1-2 was chosen for subsequent experiments (**Figure 5D**).

Four groups of HGSMCs were generated and analyzed: NG + shNC, HG + shNC, NG + shDLL1, and HG + shDLL1. The results of the CCK-8, EdU, and Transwell assays showed that DLL1 knockdown led to a reduction in the cell viability, proliferation, and migration and the reversion of the HG-induced effects in HGSMCs (**Figures 5E–G**). Furthermore, the results of qPCR and western blot analyses revealed that DLL1 knockout suppressed the HG-induced phenotype switching in HGSMCs (**Figures 5H,I**). These results collectively show that the inhibition of DLL1 abrogates the impact of HG conditions on the viability, proliferation, migration, and phenotype switching of HGSMCs.

The Metastasis-Associated Lung Adenocarcinoma Transcript 1/miR-449a/Delta-Like Ligand 1 Pathway Regulates Human Gastric SMCs Under High Glucose Conditions

As mentioned above, we proved that MALAT1 could target miR-449a and that miR-449a could target DLL1 in HGSMCs. Additionally, we found that MALAT1 and DLL1 impacted the viability, proliferation, migration, and phenotype switching of HGSMCs. Therefore, we wondered whether MALAT1 would

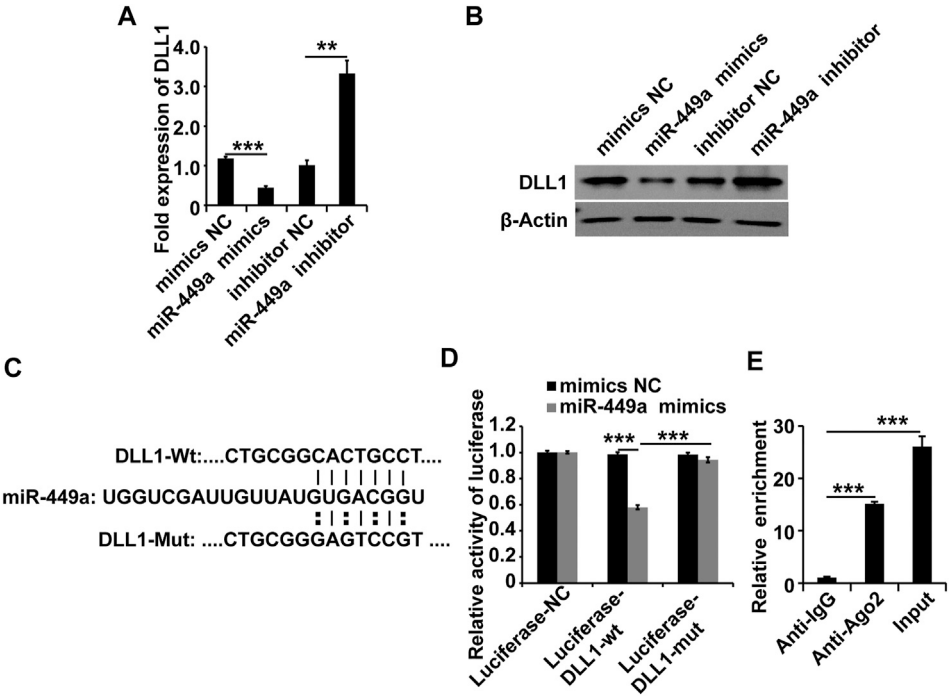

FIGURE 4 | miR-449a targets DLL1. **(A–B)** HGSMCs were transfected with a miR-449a mimic, a miR-449a inhibitor, or the respective controls (NC), and 48 h later, the DLL1 mRNA and protein levels were detected by qPCR and western blotting. **(C)** Predicted binding site of miR-449a on the 3′ UTR of DLL1. **(D)** luciferase reporter assay analysis of the interaction between miR-449a and DLL1. **(E)** RIP assay analysis of the interaction between miR-449a and DLL1. U6 or β-Actin was used as an internal control. ***$p < 0.001$, **$p < 0.01$, *$p < 0.05$.

exert its function *via* the modulation of the miR-449a/DLL1 pathway in HGSMCs under HG conditions. To answer this question, we constructed five new groups of HGSMCs: NG + shNC, HG + shNC, HG + shMALAT1, HG + shMALAT1+miR-449a inhibitor, and HG + shMALAT1+miR-449a inhibitor + shDLL1. The CCK-8, EdU, and Transwell assays showed that the MALAT1/miR-449a/DLL1 axis modulation affected the viability, proliferation, and migration of HGSMCs under HG conditions (**Figures 6A–C**). Moreover, the results of qPCR and western blot analyses revealed that any disturbance of the MALAT1/miR-449a/DLL1 pathway affected the phenotype switching of HGSMCs under HG conditions (**Figures 6D,E**). Altogether, our data suggest that a new lncRNA-based regulatory axis is behind the pathogenesis of DGP: MALAT1/miR-449a/DLL1.

MALAT1/miR-449a/DLL1 axis effects on CCh-induced Ca^{2+} transient signals in HGSMCs.

To further demonstrate the effects of the MALAT1/miR-449a/DLL1 pathway axis on HGSMC contractility, we detected the $[Ca^{2+}]_i$ in the context of the above five groups under 100 μmol/L CCh treatment. As shown in **Figures 6F,G**, in the NG + shNC group, CCh significantly increased the mean $[Ca^{2+}]_i$. In the HG + shNC group, the CCh-induced Ca^{2+} response was weaker than that in the NG + shNC group. Additionally, in the HG + shMALAT1 and HG + shMALAT1+miR-449 inhibitor + shDLL1 groups, the CCh-induced $[Ca^{2+}]_i$ enhancement was significantly higher than that in the HG + shNC group.

DISCUSSION

While various studies have shown that lncRNAs are involved in the pathogenesis of many diseases, the influence of lncRNAs on GI motility-related diseases remains unclear. Our previous study (Gong et al., 2018) showed that the lncRNA MALAT1 participates in the pathogenesis of DGP. However, the roles and underlying molecular mechanisms remain elusive. Several major observations were made in this study. First, we introduced the lncRNA array to systematically screen the lncRNAs differentially expressed in the DGP mouse model and demonstrated that MALAT1 was upregulated in both DGP mice and clinical samples. Next, we proved that HG enhanced cell viability, proliferation, and migration of HGSMCs, and promoted their phenotype switching; importantly, MALAT1 knockdown reversed this phenotype. Then, we demonstrated that MALAT1 exerted its role *via* sponging miR-449a in HGSMCs. Finally, we found out that DLL1 is the downstream target of miR-449a. Thus, our research highlights a new regulatory axis (MALAT1/miR-449a/DLL1) in the context of DGP. The model diagram is shown in **Figure 7**.

As one of the common complications of diabetes, DGP leads to many upper GI symptoms. Of note, these symptoms can be severe and affect the patients' glycemic control (Camilleri et al., 2017; Bharucha et al., 2015). Since the pathogenic mechanism of DGP has not been fully elucidated, there is a lack of effective treatments. It is currently believed that DGP is probably associated with neuropathy,

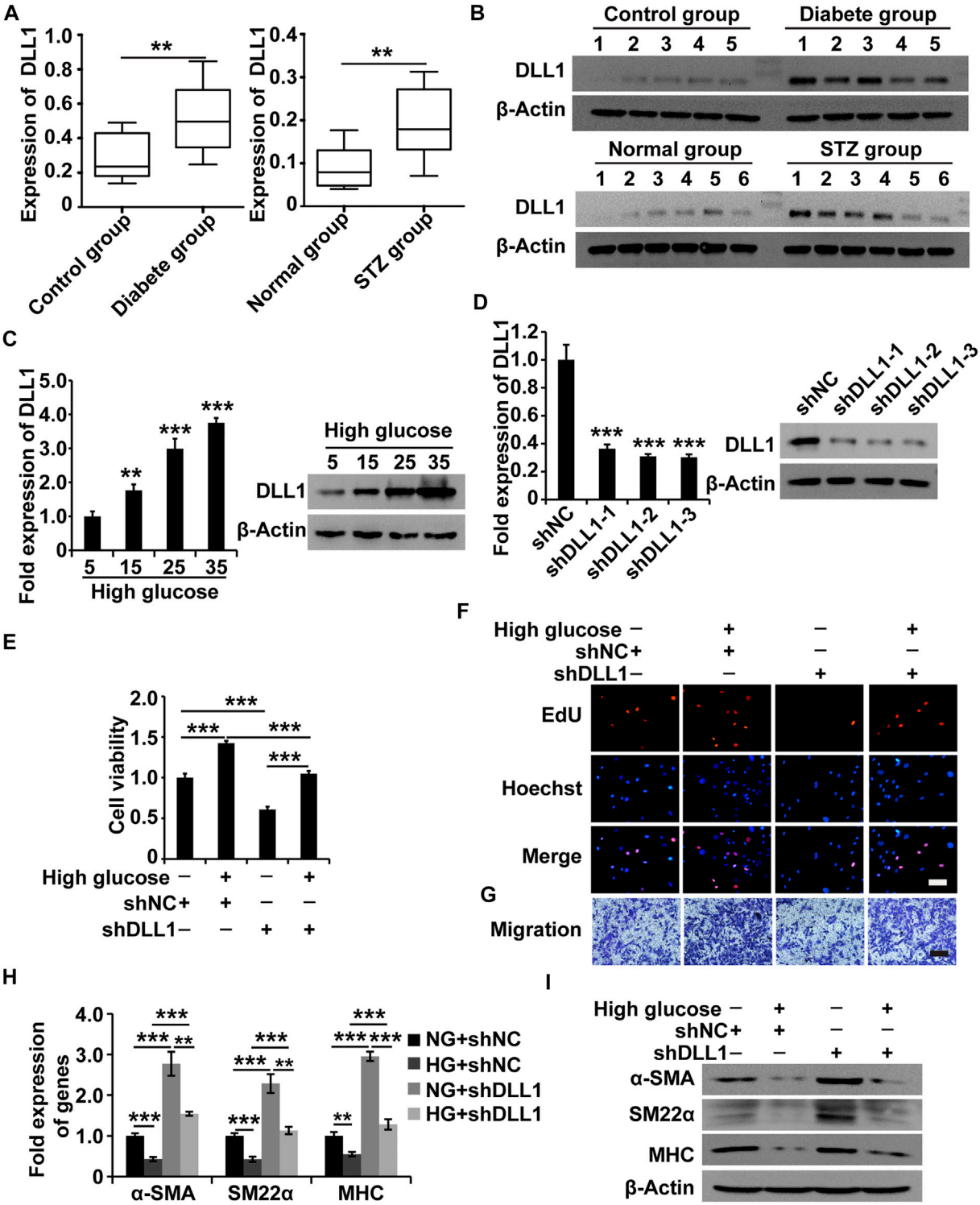

FIGURE 5 | DLL1 is a target of MALAT1 *via* miR-449a. **(A)** qPCR analysis of DLL1 expressions in the adjacent normal tissues from the stomach of patients who underwent gastrectomy with or without DM and DGP symptoms (n = 10 per group) as well as in the gastric tissues from DGP and control mice (n = 10 per group). **(B)** Western blot analysis shows that the expression levels of DLL1 proteins were significantly upregulated in the gastric tissues of DGP clinical samples and DGP model mice. **(C)** qPCR and western blot analyses of the expression of DLL1 in HGSMCs treated with different concentrations of glucose (5, 15, 25, and 35 mM) for 48 h. **(D)** qPCR and western blot analyses of the expression of DLL1 in HGSMCs transfected with shDLL1s and shNC. **(E–G)** CCK8, EdU, and Transwell assays to analyze the viability, proliferation, and migration of HGSMCs under different treatments. **(H–I)** qPCR and western blot analyses of SMC contractile markers (α-SMA, SM22α, and MHC) in HGSMCs under different treatments. For **(E–I)** four groups were analyzed: NG + shNC group, HG + shNC group, NG + shDLL1 group, and HG + shDLL1 group. β-Actin was used as an internal control. ***$p < 0.001$, **$p < 0.01$, *$p < 0.05$.

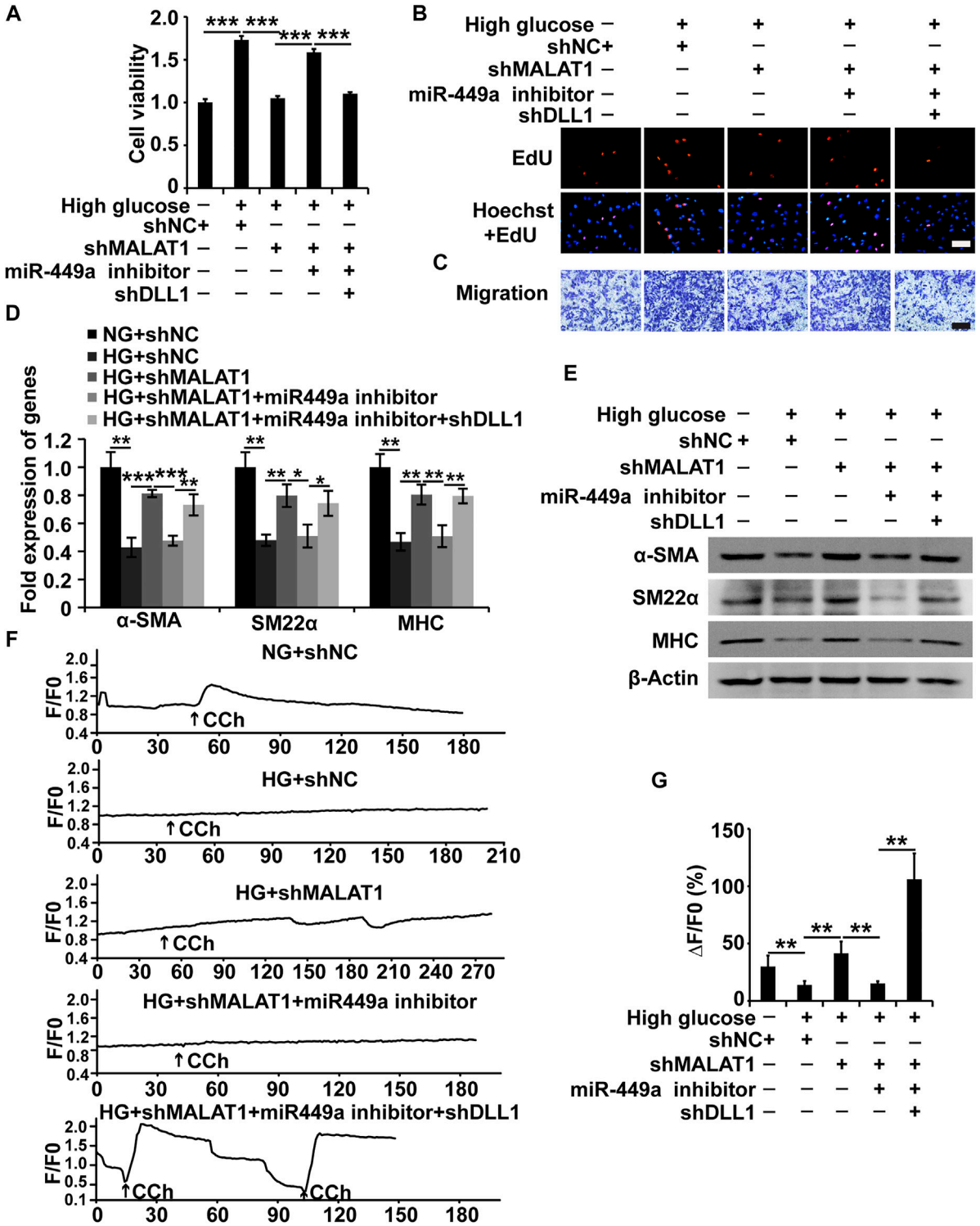

FIGURE 6 | The MALAT1/miR-499a/DLL1 pathway regulates the cellular processes, phenotypic switch and CCh-induced Ca2+ transient signals in HGSMCs under HG conditions. **(A–C)** CCK8, EdU, and Transwell assays for the analysis of the viability, proliferation, and migration of HGSMCs under different treatments. **(D–E)** qPCR and western blot analyses of SMC contractile markers (α-SMA, SM22α, and MHC) in HGSMCs under different treatments. **(F)** CCh (100 μmol/L)—induced $[Ca^{2+}]_i$ changes in HGSMCs under different treatments. Changes in Ca^{2+} fluorescence intensity are expressed as F/F0, where F0 is the basal fluorescence intensity before stimulation. **(G)** Histogram analysis of the $[Ca^{2+}]_i$ changes, where ΔF is the fluorescent intensity of the response minus F0. For **(A–G)**, five groups were analyzed: NG + shNC group, HG + shNC group, HG + shMALAT1 group, HG + shMALAT1+miR-449a inhibitor, HG + shMALAT1+miR-449a inhibitor + shDLL1 group. β-Actin was used as an internal control. ***$p < 0.001$, **$p < 0.01$, *$p < 0.05$.

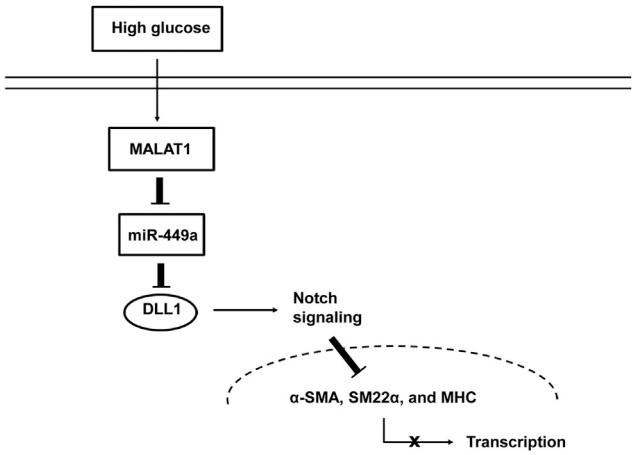

FIGURE 7 | Proposed mechanism by which MALAT1 regulates the phenotypic switch of HGSMCs under HG condition.

ICC injury, smooth muscle abnormalities, acute fluctuations in blood glucose, and changes in gastrointestinal hormones (Bharucha et al., 2019; Camilleri et al., 2011). SMCs are behind the contraction process and are essential for regular gastric emptying; of note, the contractile ability of SMCs depends on a contractile phenotype (Scirocco et al., 2016; Sanders et al., 2012). As mentioned above, SMCs have intrinsic plasticity, being capable of undergoing reversible changes in phenotype, a process referred to as "phenotypic switch" under different stimuli (Scirocco et al., 2016). This phenomenon has been more thoroughly studied in vascular SMCs; in response to injury, the expression of genes related to contractility is suppressed, whereas the expression of genes related to synthetic, migratory, and proliferative functions is upregulated (Scirocco et al., 2016). However, the phenotypic switch of GI SMCs in the context of GI motility diseases and the regulatory signaling pathways behind them remains poorly investigated. Our previous study found that the expression of contractile markers markedly decreased in the gastric tissues of diabetic patients with DGP symptoms (Gong et al., 2018). This study verified that HG could cause an abnormal proliferation, migration, and phenotype switching of HGSMCs, which may lead to DGP-related smooth muscle abnormalities.

Several studies have shown that lncRNAs play an important role in the pathogenesis of diabetes and its complications (Zhang et al., 2020; He et al., 2020). We demonstrated that MALAT1 was elevated in the tissue samples from diabetic patients with DGP symptoms as well as in a murine model of DGP. Furthermore, we clarified that MALAT1 mediates the proliferation, migration, phenotypic switching, and CCh-induced $[Ca^{2+}]_i$ changes of HGSMCs in the context of HG conditions. LncRNAs have been proposed to function as competing endogenous RNAs, absorbing miRNAs and regulating their downstream signaling pathways (Salmena et al., 2011; Tay et al., 2014; Thomson and Dinger, 2016). In the present study, we found that MALAT1 could control the levels of miR-449a precisely by acting as a sponge. Of note, the downregulation of miR-449a promoted the expression of DLL1. Therefore, MALAT1 exerted its function *via* the miR-449a/DLL1 signaling pathway. Notably, the MALAT1/miR-449a/DLL1 regulatory axis is a novel regulatory pathway in DGP.

DLL1 is a mammalian ligand of Notch receptors; interactions between DLL1 and Notch regulate the Notch signaling pathway (Dyczynska et al., 2007). Accumulating evidence shows that the Notch signaling pathway plays a pivotal role in controlling the differentiation and phenotypic switching of vascular SMCs (Morrow et al., 2008; Liu et al., 2018). Here, we found that DLL1 is a direct target of miR-449a; of note, the inhibition of DLL1 reversed the effects of HG. We speculate that DLL1 regulates the phenotypic switching of HGSMCs under HG conditions *via* the activation of the Notch signaling pathway.

A limitation of this study was that the clinical specimens analyzed were frozen (stored at -80°C) tissues obtained from the Human Tissue Specimen Research Bank; thus, we were unable to associate pathological characteristics in patient tissue with the expression of MALAT1.

In conclusion, here we show that the expression of MALAT1 is upregulated in the gastric tissues of a DGP mouse model, the adjacent normal gastric tissues collected from diabetic gastric cancer patients with DGP symptoms and in HGSMCs cultured under HG conditions. The upregulation of MALAT1 promotes the phenotype switching of HGSMCs under HG conditions *via* the miR-449a/DLL1 axis. These findings highlight a novel regulatory signaling pathway in the context of DGP that deserves to be further characterized in the quest for new diagnostic biomarkers and treatment approaches for DGP.

DATA AVAILABILITY STATEMENT

Data for experiment are available from the corresponding author (YG) upon reasonable request. The RNA sequencing data presented in this study can be found in online repository. The name of the repository and accession number can be found below: NCBI Sequence Read Archive PRJNA743433.

ETHICS STATEMENT

The studies involving human participants were reviewed and approved by the Research Ethics Committee of the First Affiliated Hospital of Nanjing Medical University. The patients/participants provided their written informed consent to participate in this study. The animal study was reviewed and approved by the Institutional Animal and Use Committee of Nanjing Medical University.

AUTHOR CONTRIBUTIONS

YG and LL contributed to the study conception and design. Material preparation, data collection and analysis were performed by YJW, YW, BZ, YZ, YJ, WX, and YG. The first draft of the manuscript was written by YG and all authors commented on previous versions of the manuscript. All authors read and approved the final manuscript.

FUNDING

This study was supported by the National Natural Science Foundation of China (Research Grant # 81800478) and Natural Science Foundation of Jiangsu Province (Research Grant # BK20181082).

REFERENCES

Bharucha, A. E., Batey-Schaefer, B., Cleary, P. A., Murray, J. A., Cowie, C., Lorenzi, G., et al. (2015). Delayed Gastric Emptying Is Associated with Early and Long-Term Hyperglycemia in Type 1 Diabetes Mellitus. *Gastroenterology* 149, 330–339. doi:10.1053/j.gastro.2015.05.007

Bharucha, A. E., Kudva, Y. C., and Prichard, D. O. (2019). Diabetic Gastroparesis. *Diabetic Gastroparesis Endocr. Rev.* 40, 1318–1352. doi:10.1210/er.2018-00161

Bunch, H. (2018). Gene Regulation of Mammalian Long Non-coding Rna. *Mol. Genet. Genomics* 293, 1–15. doi:10.1007/s00438-017-1370-9

Camilleri, M., Bharucha, A. E., and Farrugia, G. (2011). Epidemiology, Mechanisms, and Management of Diabetic Gastroparesis. *Clin. Gastroenterol. Hepatol.* 9, 5–12. doi:10.1016/j.cgh.2010.09.022

Camilleri, M., McCallum, R. W., Tack, J., Spence, S. C., Gottesdiener, K., and Fiedorek, F. T. (2017). Efficacy and Safety of Relamorelin in Diabetics with Symptoms of Gastroparesis: A Randomized, Placebo-Controlled Study. *Gastroenterology* 153, 1240–1250. doi:10.1053/j.gastro.2017.07.035

De Block, C., De Leeuw, I., Pelckmans, P., and Van Gaal, L. (2006). Current Concepts in Gastric Motility in Diabetes Mellitus. *Curr. Diabetes Rev.* 2, 113–130. doi:10.2174/157339906775473662

Dyczynska, E., Sun, D., Yi, H., Sehara-Fujisawa, A., Blobel, C. P., and Zolkiewska, A. (2007). Proteolytic Processing of delta-like 1 by Adam Proteases. *J. Biol. Chem.* 282, 436–444. doi:10.1074/jbc.m605451200

Faussone-Pellegrini, M. S., Grover, M., Pasricha, P. J., Bernard, C. E., Lurken, M. S., Smyrk, T. C., et al. (2012). Ultrastructural Differences between Diabetic and Idiopathic Gastroparesis. *J. Cel Mol Med* 16, 1573–1581. doi:10.1111/j.1582-4934.2011.01451.x

Gong, Y., Zhu, Y., Zhu, B., Si, X., Heng, D., Tang, Y., et al. (2018). Lncrna Malat1 Is Up-Regulated in Diabetic Gastroparesis and Involved in High-Glucose-Induced Cellular Processes in Human Gastric Smooth Muscle Cells. *Biochem. Biophysical Res. Commun.* 496, 401–406. doi:10.1016/j.bbrc.2018.01.038

Grover, M., Farrugia, G., Lurken, M. S., Bernard, C. E., Faussone–Pellegrini, M. S., Smyrk, T. C., et al. (2011). Cellular Changes in Diabetic and Idiopathic Gastroparesis. *Gastroenterology* 140, 1575–1585. doi:10.1053/j.gastro.2011.01.046

He, Y., Dan, Y., Gao, X., Huang, L., Lv, H., and Chen, J. (2020). Dnmt1-mediated Lncrna Meg3 Methylation Accelerates Endothelial-Mesenchymal Transition in Diabetic Retinopathy through the Pi3k/akt/mtor Signaling Pathway. *Am. J. Physiol. Endocrinol. Metab.* 320, E598. doi:10.1152/ajpendo.00089.2020

Horvath, V. J., Izbeki, F., Lengyel, C., Kempler, P., and Várkonyi, T. (2014). Diabetic Gastroparesis: Functional/morphologic Background, Diagnosis, and Treatment Options. *Curr. Diab Rep.* 14, 527. doi:10.1007/s11892-014-0527-8

Kashyap, P., and Farrugia, G. (2010). Diabetic Gastroparesis: what We Have Learned and Had to Unlearn in the Past 5 years: Figure 1. *Gut* 59, 1716–1726. doi:10.1136/gut.2009.199703

Kumar, M., Chapman, A., Javed, S., Alam, U., Malik, R. A., and Azmi, S. (2018). The Investigation and Treatment of Diabetic Gastroparesis. *Clin. Ther.* 40, 850–861. doi:10.1016/j.clinthera.2018.04.012

Liu, Z., Wang, Y., Zhu, H., Qiu, C., Guan, G., Wang, J., et al. (2018). Matrine Blocks Ages- Induced Hcsmcs Phenotypic Conversion via Suppressing Dll4-Notch Pathway. *Eur. J. Pharmacol.* 835, 126–131. doi:10.1016/j.ejphar.2018.07.051

Morrow, D., Guha, S., Sweeney, C., Birney, Y., Walshe, T., O'Brien, C., et al. (2008). Notch and Vascular Smooth Muscle Cell Phenotype. *Circ. Res.* 103, 1370–1382. doi:10.1161/circresaha.108.187534

Nair, D. G., Han, T. Y., Lourenssen, S., and Blennerhassett, M. G. (2011). Proliferation Modulates Intestinal Smooth Muscle Phenotype *In Vitro* and in Colitis *In Vivo*. *Am. J. Physiology-Gastrointestinal Liver Physiol.* 300, G903–G913. doi:10.1152/ajpgi.00528.2010

Salmena, L., Poliseno, L., Tay, Y., Kats, L., and Pandolfi, P. P. (2011). A Cerna Hypothesis: The Rosetta Stone of a Hidden Rna Language? *Cell* 146, 353–358. doi:10.1016/j.cell.2011.07.014

Sanders, K. M., Koh, S. D., Ro, S., and Ward, S. M. (2012). Regulation of Gastrointestinal Motility-Insights from Smooth Muscle Biology. *Nat. Rev. Gastroenterol. Hepatol.* 9, 633–645. doi:10.1038/nrgastro.2012.168

Scirocco, A., Matarrese, P., Carabotti, M., Ascione, B., Malorni, W., and Severi, C. (2016). Cellular and Molecular Mechanisms of Phenotypic Switch in Gastrointestinal Smooth Muscle. *J. Cel. Physiol* 231, 295–302. doi:10.1002/jcp.25105

Tay, Y., Rinn, J., and Pandolfi, P. P. (2014). The Multilayered Complexity of Cerna Crosstalk and Competition. *Nature* 505, 344–352. doi:10.1038/nature12986

Thomson, D. W., and Dinger, M. E. (2016). Endogenous Microrna Sponges: Evidence and Controversy. *Nat. Rev. Genet.* 17, 272–283. doi:10.1038/nrg.2016.20

Vanormelingen, C., Tack, J., and Andrews, C. N. (2013). Diabetic Gastroparesis. *Br. Med. Bull.* 105, 213–230. doi:10.1093/bmb/ldt003

Wilusz, J. E., Sunwoo, H., and Spector, D. L. (2009). Long Noncoding RNAs: Functional Surprises from the RNA World. *Genes Develop.* 23, 1494–1504. doi:10.1101/gad.1800909

Yu, T., Zheng, Y., Wang, Y., Xiong, W., and Lin, L. (2017). Advanced Glycation End Products Interfere with Gastric Smooth Muscle Contractile Marker Expression via the AGE/RAGE/NF-κB Pathway. *Exp. Mol. Pathol.* 102, 7–14. doi:10.1016/j.yexmp.2016.12.002

Zhang, C., Gong, Y., Li, N., Liu, X., Zhang, Y., Ye, F., et al. (2020). Long Non-coding Rna Kcnq1ot1 Promotes Sc5b-9-Induced Podocyte Pyroptosis by Inhibiting Mir-486a-3p and Upregulating Nlrp3. *Am. J. Physiol. Cel Physiol* 320, C355. doi:10.1152/ajpcell.00403.2020

Conflict of Interest: The authors declare that the research was conducted in the absence of any commercial or financial relationships that could be construed as a potential conflict of interest.

frontiers in Pharmacology

SYSTEMATIC REVIEW
published: 06 August 2021
doi: 10.3389/fphar.2021.682656

Orally Administered Probiotics Decrease *Aggregatibacter actinomycetemcomitans* but Not Other Periodontal Pathogenic Bacteria Counts in the Oral Cavity: A Systematic Review and Meta-Analysis

Thanyaporn Sang-Ngoen[1], László Márk Czumbel[1], Wuttapon Sadaeng[1], Alexandra Mikó[2], Dávid István Németh[2], Péter Mátrai[2], Péter Hegyi[2,3,4], Barbara Tóth[5], Dezső Csupor[2,5], István Kiss[6], Andrea Szabó[7], Gábor Gerber[8], Gábor Varga[1†] and Beáta Kerémi[1†]*

[1]Department of Oral Biology, Semmelweis University, Budapest, Hungary, [2]Szentágothai Research Centre, Institute for Translational Medicine, Medical School, University of Pécs, Pécs, Hungary, [3]Centre for Translational Medicine, Semmelweis University, Budapest, Hungary, [4]Division of Pancreatic Diseases, Heart and Vascular Center, Semmelweis University, Budapest, Hungary, [5]Department of Clinical Pharmacy, Faculty of Pharmacy, University of Szeged, Szeged, Hungary, [6]Department of Public Health Medicine, Medical School, University of Pécs, Pécs, Hungary, [7]Department of Public Health, Faculty of Medicine, University of Szeged, Szeged, Hungary, [8]Department of Anatomy, Histology and Embryology, Semmelweis University, Budapest, Hungary

Introduction: At the initial part of the gastrointestinal tract, multiple tissues serve the normal function of food delivery. Periodontal structures are integral elements of these. When they deteriorate, it is extremely challenging to regenerate and reconstruct them. The conventional intervention for periodontal disease is scaling and root planning with the aim of reducing pathogenic bacteria. However, periodontal pathogens can rapidly recolonize treated areas. Probiotics have been proposed as novel tools for managing oral health by suppressing pathogenic bacteria through their anti-inflammatory effect, but the available data are controversial.

Aim: Therefore, we performed a meta-analysis to study the effect of probiotics on periodontal pathogenic bacteria.

Methods: The study was registered in PROSPERO under registration number CRD42018094903. A comprehensive literature search from four electronic databases (PubMed, Cochrane CENTRAL, Embase, and Web of Science) yielded nine eligible records for statistical analysis. Studies measuring bacterial counts in saliva and supra- and subgingival plaque were included. Bacterial counts were analyzed using standard mean difference (SMD) and by a random effects model with the DerSimonian–Laird estimation.

Results: The results showed a significant decrease in the overall count of *Aggregatibacter actinomycetemcomitans* in the probiotic-treated group compared to the control at 4 weeks (SMD: −0.28; 95% CI: −0.56–−0.01; p = 0.045) but not later. Analyzing the

OPEN ACCESS

Edited by:
Predrag Sikiric,
University of Zagreb, Croatia

Reviewed by:
Rinaldo Pellicano,
Molinette Hospital, Italy
Dan-Lucian Dumitrașcu,
Iuliu Hațieganu University of Medicine and Pharmacy, Romania

***Correspondence:**
Beáta Kerémi
keremi.beata@dent.semmelweis-univ.hu

†These authors have contributed equally to this work and share last authorship

Specialty section:
This article was submitted to Pharmacology of Infectious Diseases, a section of the journal Frontiers in Pharmacology

Received: *18 March 2021*
Accepted: *01 July 2021*
Published: *06 August 2021*

Citation:
Sang-Ngoen T, Czumbel LM, Sadaeng W, Mikó A, Németh DI, Mátrai P, Hegyi P, Tóth B, Csupor D, Kiss I, Szabó A, Gerber G, Varga G and Kerémi B (2021) Orally Administered Probiotics Decrease Aggregatibacter actinomycetemcomitans *but Not Other Periodontal Pathogenic Bacteria Counts in the Oral Cavity: A Systematic Review and Meta-Analysis. Front. Pharmacol. 12:682656. doi: 10.3389/fphar.2021.682656*

bacterial counts in subgroups, namely, in saliva and supra- and subgingival plaque, separately, yielded no significant difference. Probiotics had no significant effect on the overall count of *Porphyromonas gingivalis* at 4 weeks (SMD: −0.02; 95% CI: −0.35–0.31; $p = 0.914$) or later. Subgroup analysis also revealed no significant difference between treatment and control groups nor did probiotics significantly decrease the overall and subgroup bacterial counts of *Prevotella intermedia*, *Tannerella forsythia*, and *Fusobacterium nucleatum*.

Conclusion: Our data support the beneficial effect of probiotics in reducing *A. actinomycetemcomitans* counts, but not of other key periodontal pathogenic bacteria in periodontal disease patients. However, due to the complex mechanism associated with periodontal disease and the limitations of the available studies, there is a further need for well-designed randomized clinical trials to assess the efficacy of probiotics.

Keywords: probiotics, *Aggregatibacter actinomycetemcomitans*, periodontal disease, bacterium, *Porphyromonas gingivalis*, *Tannerella forsythia*, *Prevotella intermedia*, *Fusobacterium nucleatum*

INTRODUCTION

In the oral cavity, at the entrance to the gastrointestinal tract, multiple tissues serve the normal function of food delivery. Periodontal structures are integral elements of these. It is extremely challenging to regenerate and reconstruct them when deteriorated. Periodontal disease is a multifactorial, bacteria-induced inflammatory disease of the tooth-supporting structures (Darveau, 2010). Approximately 20–50% of the population are affected worldwide (Nazir, 2017). In susceptible patients, due to bacterial dysbiosis, an uncontrolled and exaggerated inflammatory process develops, which eventually leads to gingival recession, bone resorption, and, consequently, tooth mobility and tooth loss (Windisch et al., 2002; Costalonga and Herzberg, 2014; Hajishengallis, 2014).

The bacteria closely related to periodontal disease are mostly Gram-negative, such as *Porphyromonas gingivalis* (*P. gingivalis*), *Treponema denticola* (*T. denticola*), *Tannerella forsythia* (*T. forsythia*), *Prevotella intermedia* (*P. intermedia*), *Fusobacterium nucleatum* (*F. nucleatum*), and *Aggregatibacter actinomycetemcomitans* (*A. actinomycetemcomitans*) (Roberts and Darveau, 2002; Darveau, 2010; Costalonga and Herzberg, 2014; Hajishengallis, 2014). In addition to the bacteria, host response also plays a key role in the etiology of periodontal disease (Genco, 1992). After bacterial infection, inflammatory mediators are secreted from host immune cells to combat and limit the infected area around the dental tissues (Silva et al., 2015). In addition, smoking, uncontrolled diabetes, and old age, among other important factors, contribute to the inflammation process of the disease (Van Dyke and Sheilesh, 2005). The conventional treatment of periodontal disease includes scaling and root planning as well as the improvement of oral hygiene. These methods target the removal of sub- and supragingival plaque and calculus (Cobb, 2002; Roberts and Darveau, 2002; Claffey et al., 2004). In some cases, because of deep pocket sites in multirooted teeth, scaling and root planning alone are not sufficient, and additional advanced therapies, such as periodontal surgery and the use of antibiotics, are required (Claffey et al., 2004; Cobb, 2008).

Periodontal treatments aim to reduce the number of pathogenic bacteria and remove infected tissue, thereby provoking periodontal tissue healing (Zappa et al., 1991; Cobb, 2002; Claffey et al., 2004). However, periodontopathogens could rapidly recolonize at the previously treated sites even when antibiotics or antiseptics are applied (Cobb, 2002; Quirynen et al., 2005). Thus, scaling and root planning must be performed periodically during the maintenance phase of periodontal disease treatment (Cobb, 2002). Unfortunately, there is insufficient evidence to determine the superiority of different antibiotic protocols (Manresa et al., 2018; Mcgowan et al., 2018). The effectiveness of antibiotic treatments can be very limited, owing to the different antibiotic resistance of the individual species of bacteria and the fact that some bacteria persist intracellularly (Rudney et al., 2005; Teughels et al., 2007; Muniz et al., 2013). Due to these difficulties, there is an increasing need for new treatment modalities to maintain and prolong well-balanced oral microflora and succeed in the therapy of periodontal disease.

Probiotics have been of increasing interest following their success in the treatment of gastrointestinal diseases (Devine and Marsh, 2009). Probiotics are defined as live microorganisms, which, when administered in adequate amounts, confer a health benefit on the host (Sanders, 2008). In dentistry, probiotics have been studied and proposed as a promising alternative treatment to manage oral diseases due to their antimicrobial and anti-inflammatory effects, which may lead to the enrichment of beneficial bacteria (Devine and Marsh, 2009; Allaker and Stephen, 2017). Some clinical trials have reported the favorable effect of probiotics on controlling dental caries, halitosis, and periodontal disease (Burton et al., 2006a; Burton et al., 2006b; Teughels et al., 2013; Vestman et al., 2013; Tekce et al., 2015). On the contrary, other studies have suggested that probiotic treatments do not significantly alter pathogenic flora in the oral cavity (Ahola et al., 2002; Montalto et al., 2004; Montero et al., 2017). Recently published reviews and meta-analyses on this topic have focused on the improvement of clinical periodontal parameters

but not on the possible shift in bacterial species in response to probiotics (Yanine et al., 2013; Martin-Cabezas et al., 2016; Akram et al., 2020; Vives-Soler and Chimenos-Küstner, 2020).

Only a few original articles have attempted to study the effect of probiotics on periodontal pathogens in periodontal diseases. Because of the relatively small sample number used and other limitations of these studies, evidence provided is very weak (Gruner et al., 2016; Seminario-Amez et al., 2017; Ikram et al., 2018; Ho et al., 2020). Therefore, in the present meta-analysis, we aimed to study the effect of probiotics on periodontal pathogenic bacteria based on the data from available randomized clinical trials (RCTs).

MATERIALS AND METHODS

Protocol and Registration

This meta-analysis was reported according to the Preferred Reporting Items for Systematic Reviews and Meta-Analyses (PRISMA) statement (Liberati et al., 2009) using the same strategy as in our other recent oral cavity/upper GI-related studies (Czumbel et al., 2019; Keremi et al., 2020; Ruksakiet et al., 2020). The content of this meta-analysis is summarized using the PRISMA checklist (**Supplementary Table 1**). The study was registered in the international prospective register of systematic reviews, PROSPERO, under the registration number CRD42018094903. There was no deviation from the study protocol.

Eligibility Criteria

A PICO (patient, intervention, control, and outcome) format was constructed following the clinical question: do orally administered probiotics decrease the quantity of harmful periodontal bacteria in saliva or supra- or subgingival plaque? The PICO framework was the following: patients: periodontal diseases; intervention: orally administered probiotics; control: placebo or no orally administered probiotics. The outcome was the quantity of periodontal pathogenic bacteria in saliva and supragingival and subgingival plaque.

Inclusion and Exclusion Criteria

Studies that met the following eligibility criteria were included: 1) RCTs, 2) periodontal disease patients, 3) orally administered probiotics, and 4) existing control group. Studies that lacked periodontal pathogenic bacteria counts were excluded. Another exclusion criterion was the application of antibiotics.

Search Strategy and Information Sources

A systematic search was performed in four electronic databases [MEDLINE (via PubMed), Cochrane Central Register of Controlled Trials (CENTRAL), Embase, and Web of Science] up to June 7, 2020. The electronic search was supplemented by a manual search of bibliographic references from included articles and related review articles. The keyword used for the search was [*probiotic and* (*"periodontal disease" or periodontitis or gingivitis or plaque or saliva*)]. The detailed search string can be found in **Supplementary Table 2**.

Study Selection

After duplicate removal, the titles and abstracts in each record were screened by two authors (TS-N and WS) independently. Full texts of the individual records were further assessed by those two authors (TS-N and WS) independently. Disagreements between the reviewers were resolved after discussion or by consulting a third reviewer (GV).

Data Collection Process and Data Items

Data were collected on the following on predefined data collection spreadsheets: first author, year of publication, number and characteristics of patients, pretreatment, probiotic strain, dose, form, instruction and duration, comparator, and number of periodontal pathogens, such as *A. actinomycetemcomitans*, *P. gingivalis*, *P. intermedia*, *F. nucleatum*, and *T. forsythia* in saliva and supra- and subgingival plaque.

Risk of Bias Assessment

The Cochrane Risk of Bias Tool for assessing the risk of bias in randomized controlled trials was used. Assessment was performed by two of the authors (TS-N and WS) independently. Disagreements were resolved by consulting a third reviewer (GV). Studies were assessed according to six major domains: random sequence generation (selection bias), allocation concealment (selection bias), blinding of participants and personnel (performance bias), blinding of outcome assessment (detection bias), incomplete outcome data (attrition bias), and selective reporting (reporting bias). Risk of bias in each domain was categorized into low risk, unclear, and high risk (Higgins et al., 2019).

Summary Measures and Synthesis of Results—Statistical Analysis

Extracted data were pooled using the random effects model with the DerSimonian–Laird estimation and displayed in forest plots as standardized mean difference (SMD) for different methods of measurement. Summary mean estimation, p value, and 95% confidence interval (CI) were calculated. $p < 0.05$ was considered as a significant difference from summary mean = 0. Statistical heterogeneity was analyzed using the I^2 statistic and the chi-square test to ascertain probability values; $p < 0.1$ was defined indicating significant heterogeneity (Higgins et al., 2019).

Risk of Bias Across Studies and Additional Analyses

The confidence in the body of evidence was graded using the GRADEpro GDT program (McMaster University). Each outcome was assessed following the study design, risk of bias, inconsistency, indirectness, imprecision, and publication bias. A high, moderate, low, or very low grade was assigned to each outcome (Schünemann et al., 2013).

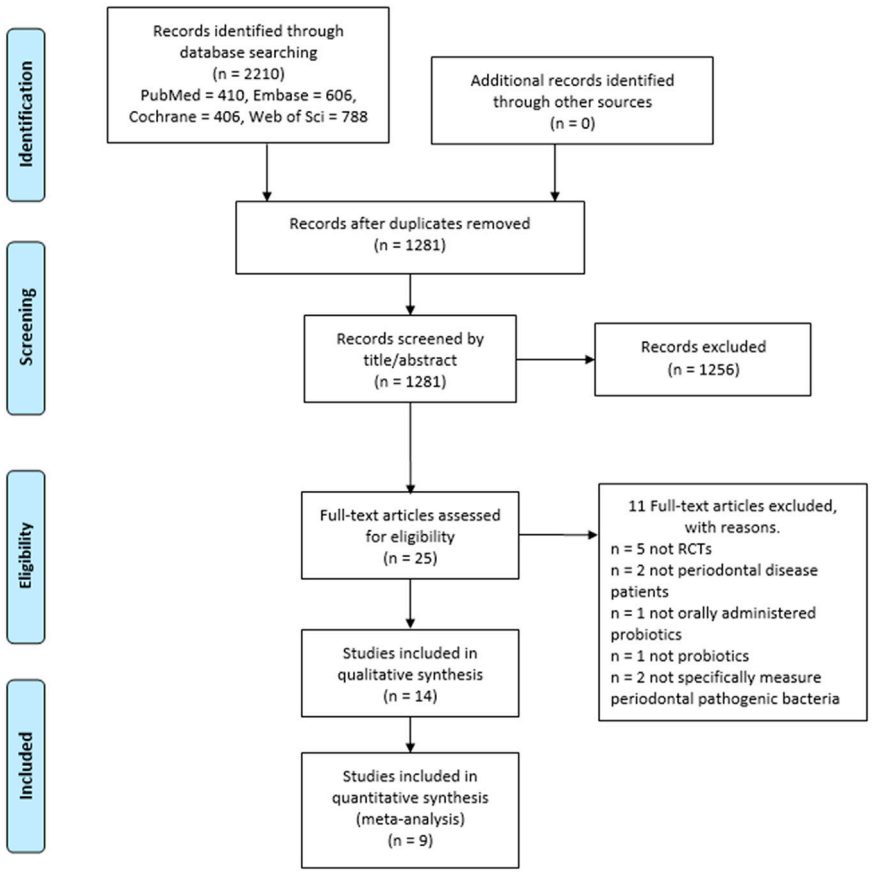

FIGURE 1 | PRISMA flowchart presents the process of study selection.

RESULTS

Study Selection

The comprehensive search from four electronic databases (PubMed, Cochrane Central, Embase, and Web of Science) supplemented by a manual search yielded 1,281 records after duplicate removal. Twenty-five articles were potentially eligible after removing duplicate records and screening by titles and abstracts. After full-text reviews, 14 articles were included in the qualitative analysis, and nine were suitable for the quantitative synthesis (**Figure 1**).

Reasons for Exclusions on Full-Text Assessment

In the course of assessing the full-text articles, eleven articles were excluded for good reasons. Out of these, five studies (Zahradnik et al., 2009; Iwamoto et al., 2010; Imran et al., 2015; Kaklamanos et al., 2019; Elsadek et al., 2020) were excluded due to nonrandomized controlled study designs. Six other studies were ineligible owing to their study characteristics. Two articles (Hallstrom et al., 2013; Becirovic et al., 2018) did not investigate periodontal disease patients. Another (Boyeena et al., 2019) used subgingivally delivered probiotics. Tobita and coworkers (Tobita et al., 2018) used killed bacteria, which does not meet the definition of probiotics. Two other studies (Tekce et al., 2015; Swarna Meenakshi and Varghese, 2018) measured total bacterial numbers and obligate anaerobes, which do not fit the purpose of our study. For the quantitative meta-analysis, five studies were excluded for the following reasons. One (Mayanagi et al., 2009) reported periodontal pathogen numbers in graphs which cannot be used in our statistical method. An email requesting the exact number of bacteria was sent to the corresponding author of the study; however, no reply was received. One study (Goyal et al., 2019) did not specify whether the participants had periodontal disease, and another (Vivekananda et al., 2010) waited 21 days before administering probiotics to the participants. Finally, two other investigations (Shah et al., 2013; Shah et al., 2017) combined probiotics with antibiotics.

Characteristics of the Studies Included

Eight of the 14 studies (Mayanagi et al., 2009; Teughels et al., 2013; Laleman et al., 2015; Montero et al., 2017; Alanzi et al., 2018; Invernici et al., 2018; Morales et al., 2018; Laleman et al., 2019) were randomized, double-blind, placebo-controlled parallel trials. The other four investigations (Shah et al., 2013; Dhaliwal et al.,

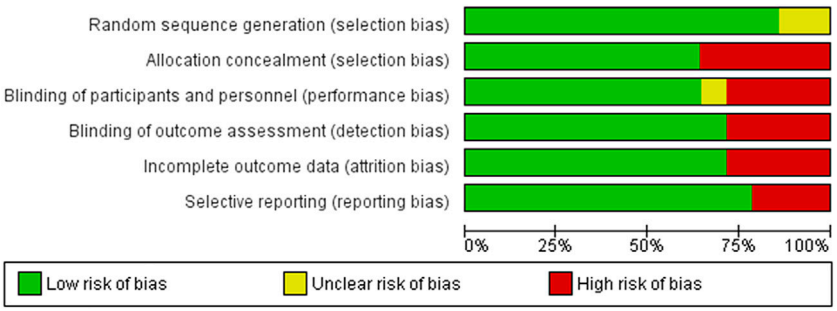

FIGURE 2 | Risk of bias graph presented each risk of bias item as percentages across all included studies.

2017; Shah et al., 2017; Goyal et al., 2019) were randomized, open, controlled parallel trials. The work of Iniesta and coworkers (Iniesta et al., 2012) was a randomized, double-blind, placebo-controlled, crossover clinical trial. An additional one (Vivekananda et al., 2010) had a randomized, placebo-controlled, double-blind, split-mouth design. The age of participants varied from adolescent to elderly.

Different probiotic strains and doses are used for intervention (**Supplementary Table 3**). Commonly used forms of probiotics are tablets or lozenges. However, other formulations, such as mouthwash or a sachet, are also in use. Instructions for use depended on the probiotic products (**Supplementary Table 3**). The duration of use ranged from 4 weeks to 3 months. In most studies, the investigated periodontal pathogenic bacteria were *A. actinomycetemcomitans*, *P. gingivalis*, *P. intermedia*, *T. forsythia*, and *F. nucleatum*.

Risk of Bias Assessment

Biases in the 14 included studies were assessed by using the Cochrane Risk of Bias Tool for randomized trials. All included studies identified or explained the randomization method, except one (Goyal et al., 2019), which did not specify the method. Allocation concealment was determined as high in five studies because the staff who assigned the participants to the groups was not blinded. Most of the included studies had a double-blind design, and the performance and detection biases were evaluated as low. However, four studies (Shah et al., 2013; Dhaliwal et al., 2017; Shah et al., 2017; Goyal et al., 2019) were open trials; the performance and detection biases of these were therefore determined as high. One study (Morales et al., 2018) was assessed as having an unclear risk in performance bias for microbiological parameters because the sample collector was not blinded. Four studies (Dhaliwal et al., 2017; Montero et al., 2017; Morales et al., 2018; Goyal et al., 2019) incompletely reported microbiological data with no explanation. High reporting bias was found in three studies (Laleman et al., 2015; Montero et al., 2017; Morales et al., 2018) because they did not report all prespecified outcomes. The result of the risk of bias assessment can be found in **Figure 2** and **Supplementary Figure 1**, and the details of assessment in each included study can be found in **Supplementary Table 4**.

Results of the Meta-Analysis

Out of the five investigated periodontal pathogenic bacteria, *A. actinomycetemcomitans* exhibited the greatest response to probiotics treatment. When subgingival and supragingival changes were examined together with salivary bacteria counts, the overall *A. actinomycetemcomitans* bacteria counts were significantly lower in the probiotic-treated group than in the control at 4 weeks (SMD: −0.28; 95% CI: −0.56–−0.01; $p = 0.045$). There were no significant heterogeneity differences between the studies ($I^2 = 36.5\%$; $p = 0.150$). However, the subgroup analysis revealed no difference in *A. actinomycetemcomitans* between the probiotics group and the control (**Figure 3**). *A. actinomycetemcomitans* values in subgingival plaque taken from three studies (Iniesta et al., 2012; Teughels et al., 2013; Dhaliwal et al., 2017) involving a total of 97 participants (49 subjects in the treated group and 48 people in the control) showed no significant difference between the probiotics group and the control group (SMD: −0.34; 95% CI: −0.99–0.30; $p = 0.297$), but, in this respect, significant heterogeneity was found among the studies ($I^2 = 60\%$, $p = 0.082$). As regards supragingival plaque and saliva, two studies (Teughels et al., 2013; Alanzi et al., 2018) involving 131 participants (67 probiotic-treated and 64 control subjects) showed no significant difference between the two groups either (SMD: −0.29; 95% CI: −0.80–0.22; $p = 0.262$; and SMD: −0.24; 95% CI: −0.81–0.34; $p = 0.420$, respectively). Significant heterogeneity among the studies was found again for both supragingival plaque and saliva values ($I^2 = 40.3\%$, $p = 0.195$; $I^2 = 51.8\%$, $p = 0.150$, respectively).

Eight weeks after the initiation of probiotics treatment, when subgingival, supragingival, and saliva bacteria counts were combined, the overall *A. actinomycetemcomitans* bacteria counts showed a tendency to decrease, but this difference fell short of significance between the probiotic-treated and the control groups (SMD: −0.16; 95% CI: −0.45–0.13; $p = 0.271$) with no significant heterogeneity ($I^2 = 0.0\%$, $p = 0.650$). Similarly, the subgroup analysis showed no significant difference in subgingival plaque (SMD: −0.13; 95% CI: −0.48–0.23; $p = 0.474$) and no significant heterogeneity ($I^2 = 2.1\%$; $p = 0.382$) in supragingival plaque (SMD: −0.12; 95% CI: −0.84–0.59; $p = 0.733$) and in saliva (SMD: −0.34; 95% CI: −1.06–0.39; $p = 0.362$) (**Figure 4**).

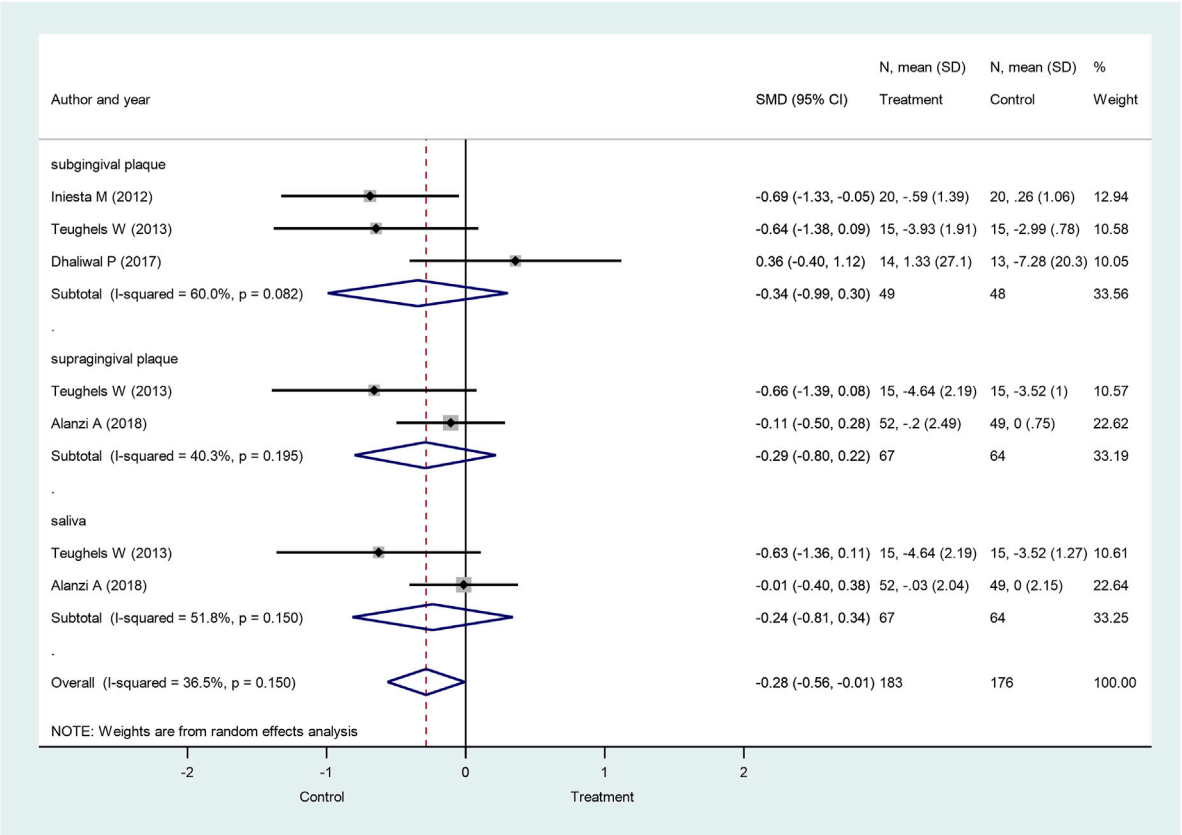

FIGURE 3 | Forest plot analysis of the change in *Aggregatibacter actinomycetemcomitans* at 4 weeks. The overall result presented a significant decrease of *Aggregatibacter actinomycetemcomitans* in the treatment group compared to the control group (SMD: −0.28; 95% CI: −0.56–−0.01; $p = 0.045$).

Another pathogenic bacterium regarded as a key factor in the development of periodontitis is *P. gingivalis*. When subgingival and supragingival changes were combined with salivary bacteria counts, the overall *P. gingivalis* bacteria counts were not significantly different between the probiotic-treated and the control groups at 4 weeks (SMD: −0.02; 95% CI: −0.35–0.31; $p = 0.914$) (**Figure 5**), 8 weeks (SMD: −0.01; 95% CI: −0.53–0.52; $p = 0.977$) (**Supplementary Figure 2**), and 12 weeks after treatment initiation (SMD: −0.23; 95% CI: −0.90–0.43; $p = 0.488$) (**Supplementary Figure 3**).

When only subgingival plaque *P. gingivalis* values were involved, again, no significant differences were observed between the probiotic-treated group and the control at 4 weeks (SMD: −0.15; 95% CI: −0.83–0.54; $p = 0.670$) (**Figure 5**), 8 weeks (SMD: −0.04; 95% CI: −0.61–0.52; $p = 0.877$) (**Supplementary Figure 2**), and 12 weeks after treatment initiation (SMD: −0.08; 95% CI: −1.15–0.98; $p = 0.876$) (**Supplementary Figure 3**). We also analyzed *P. gingivalis* counts in supragingival plaque. Similar to the findings above, the bacteria counts were not significantly different between the probiotic-treated and the control group at 4 weeks (SMD: 0.28; 95% CI: −0.70–1.27; $p = 0.570$) (**Figure 5**), 8 weeks (SMD: 0.41; 95% CI: −2.43–3.25; $p = 0.779$) (**Supplementary Figure 2**), and 12 weeks after treatment initiation (SMD: −0.21; 95% CI: −1.96–1.54; $p = 0.813$) (**Supplementary Figure 3**). Similar results were found for *P. gingivalis* bacteria numbers in saliva, yielding no significant differences between the probiotic-treated and the control groups at 4 weeks (SMD: −0.09; 95% CI: −0.35–0.18; $p = 0.519$) (**Figure 5**), 8 weeks (SMD: −0.20; 95% CI: −0.87–0.47; $p = 0.564$) (**Supplementary Figure 2**), and 12 weeks after treatment initiation (SMD: −0.42; 95% CI: −1.52–0.68; $p = 0.455$) (**Supplementary Figure 3**).

We also studied the bacteria count changes investigating three additional pathogenic bacteria, *P. intermedia*, *F. nucleatum*, and *T. forsythia*, which are also assumed to play a crucial role in the course of periodontitis development. When subgingival, supragingival, and salivary bacteria counts were combined, the overall *P. intermedia* bacteria counts did not significantly differ between the probiotic-treated group and the control group at 4 weeks (SMD: 0.01; 95% CI: −0.16–0.19; $p = 0.874$) (**Figure 6**), 8 weeks (SMD: −0.01; 95% CI: −0.24–0.21, $p = 0.912$) (**Supplementary Figure 4**), and 12 weeks after treatment initiation (SMD: −0.00; 95% CI: −0.30–0.29; $p = 0.981$) (**Supplementary Figure 5**). Similar observations were made in subgroup analysis, when subgingival, supragingival, and salivary *P. intermedia* bacteria counts were investigated separately, showing no significant differences between the treatment groups.

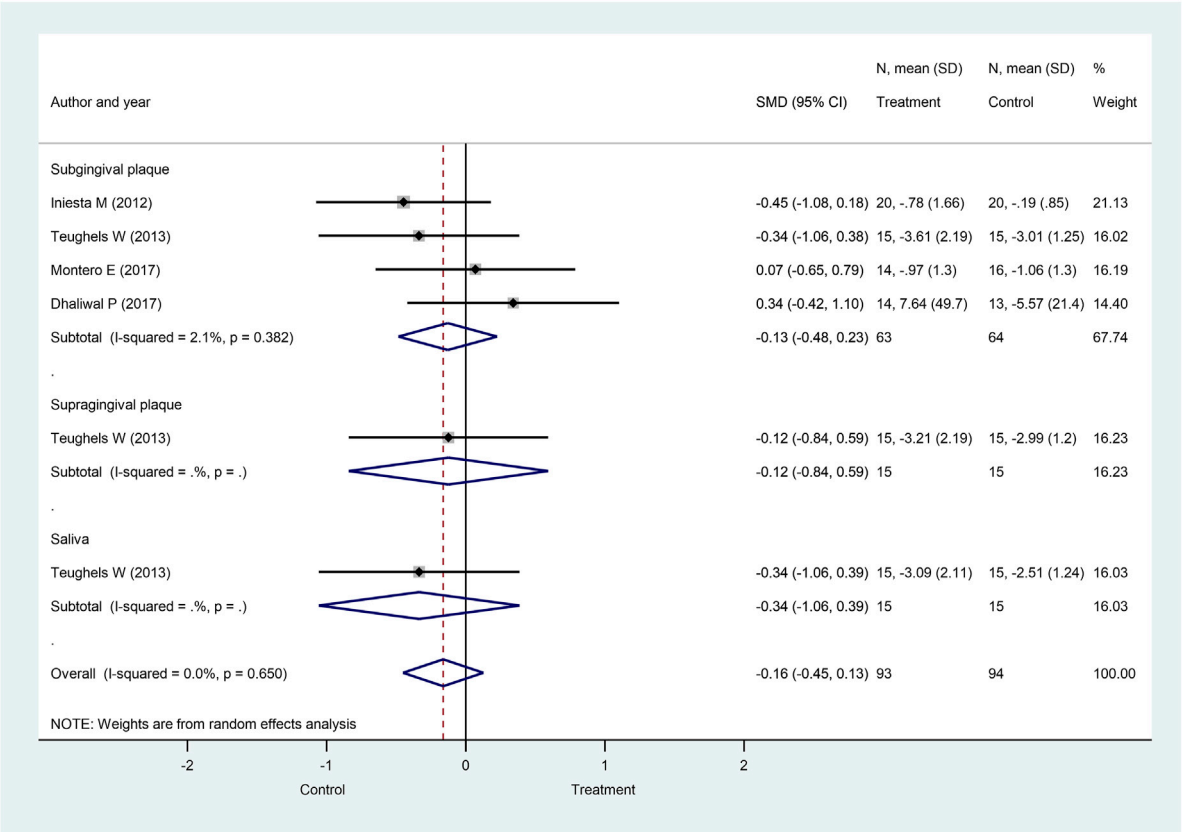

FIGURE 4 | Forest plot analysis of the change in *Aggregatibacter actinomycetemcomitans* at 8 weeks. The overall result presented no significant difference of bacterial decrease when both treatment and control groups were compared (SMD: −0.16; 95% CI: −0.45–0.13; p = 0.271).

For *F. nucleatum*, combined subgingival, supragingival, and salivary bacteria counts yielded no significantly different results between the probiotic-treated group and the control group at 4 weeks (SMD: −0.10; 95% CI: −0.27–0.07; p = 0.256) (**Figure 7**), 8 weeks (SMD: 0.12; 95% CI: −0.09–0.32; p = 0.270) (**Supplementary Figure 6**), and 12 weeks after treatment initiation (SMD: −0.06; 95% CI: −0.27–0.15; p = 0.580) (**Supplementary Figure 7**). When subgingival, supragingival, and salivary count changes were investigated separately, subgroup analysis also demonstrated the lack of significant differences between treatment groups.

Finally, when subgingival and supragingival counts were combined with salivary bacteria counts, the overall *T. forsythia* bacteria counts were not significantly different between the probiotic-treated group and the control group at 4 weeks (SMD: −0.32; 95% CI: −1.25–0.62) (**Figure 8**) and 8 weeks (SMD: 0.05; 95% CI: −0.19–0.30) (**Supplementary Figure 8**). Similarly, no significant differences were found between the treatment groups using subgroup analysis, investigating subgingival, supragingival, and salivary counts separately.

The Quality of Evidence

The GRADE assessment of periodontal pathogen outcomes was very low due to serious risk bias, inconsistency, and imprecision (**Table 1**). The details of grading the results can be seen in **Supplementary Table 5**. According to the certainty classification of the GRADE system, the low level indicates that further research is very likely to have an important impact on our confidence in estimating effect and is likely to change the estimate. The very low level of certainty suggests that any estimate of effect is very uncertain.

DISCUSSION

Summary of Evidence

In the present work, we conducted a meta-analysis comparing periodontal pathogenic bacteria counts between probiotic-treated and placebo-treated control groups of patients suffering from periodontal diseases. In our analysis, the primary focus was to study the effect of probiotics by evaluating the colony-forming unit (CFU) counts of pathogenic bacteria. Five different species at three anatomical sites (saliva, supragingival, and subgingival areas) were analyzed. To strengthen the grade of evidence, only RCTs were included in our study. We found a significant decrease in *A. actinomycetemcomitans* counts in the probiotic-treated group compared to the control group at 4 weeks after treatment initiation, but the difference fell short of significance

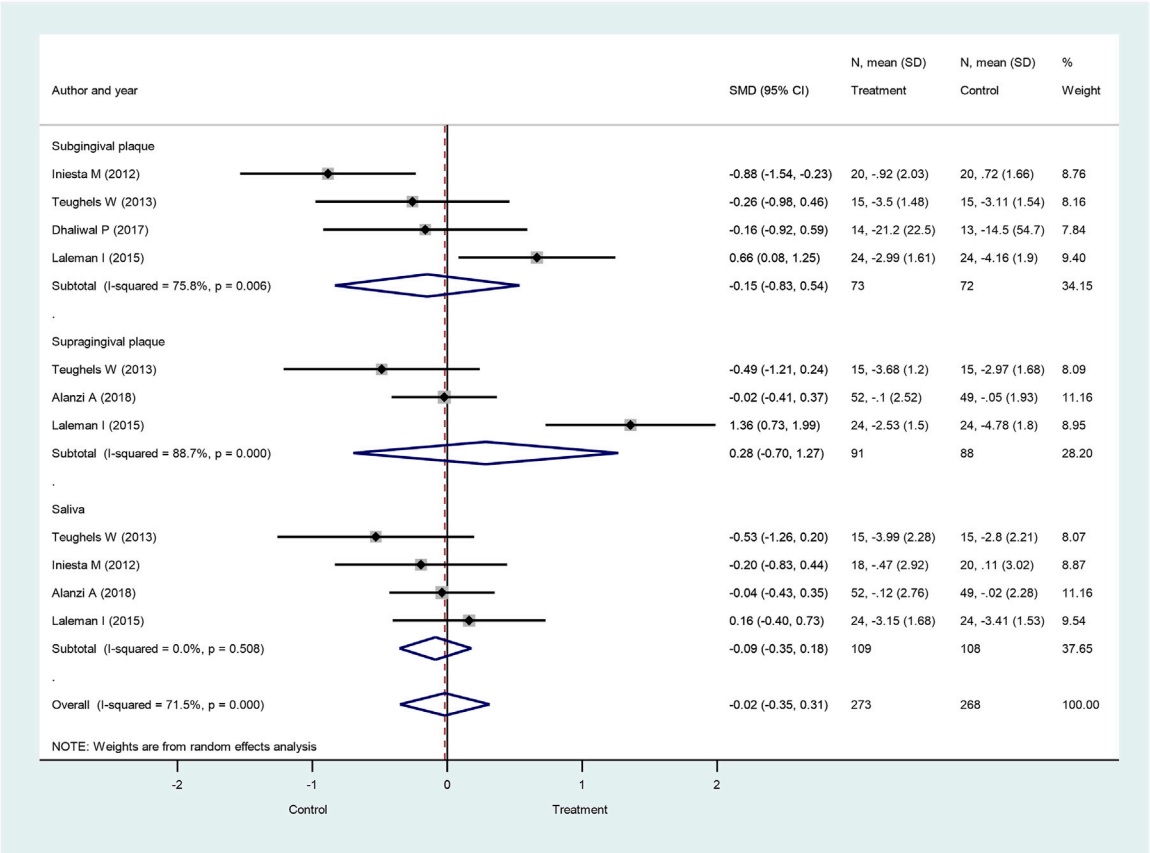

FIGURE 5 | Forest plot analysis of the change in *Porphyromonas gingivalis* at 4 weeks. The overall result presented no significant difference of bacterial decrease when both treatment and control groups were compared (SMD: –0.02; 95% CI: –0.35–0.31; p = 0.914).

after 8 weeks. There were no significant differences in the other four periodontal pathogenic bacteria, *P. gingivalis, P. intermedia, F. nucleatum*, and *T. forsythia*, at any time points when counts were compared between the two groups.

Up until now, three systematic reviews and one meta-analysis have investigated the effect of probiotics on periodontal pathogens. Among these, two published articles claimed that it was impossible to draw definite conclusions about the effectiveness of probiotics due to the limited number of available studies (Seminario-Amez et al., 2017; Ikram et al., 2018). One systematic review did not specify the investigated periodontal pathogens but claimed that probiotics do not cause a diminishing effect on periodontal pathogens (Seminario-Amez et al., 2017). Only one meta-analysis (Gruner et al., 2016) used only two RCT studies for meta-analysis, which are obviously not sufficient to perform an analysis with acceptable statistical power. That work reported the diminishing effect of probiotics on *A. actinomycetemcomitans* and no effect on *P. gingivalis* and *P. intermedia*. Although these results can only be regarded as qualitative, they clearly show similarities to our data, which were drawn from far more studies and therefore much higher sample numbers. However, there are some differences between their work and our studies. Gruner and coinvestigators (Gruner et al., 2016) in the two included studies used bacteria numbers which were only obtained at the latest follow-up time points, combining eight- and twelve-week results. In contrast, we included more studies, more samples, and more time points. Another article also reported an analysis which was only based on two original articles (Ho et al., 2020), also reporting no significant effects on *P. gingivalis*, *P. intermedia*, *F. nucleatum*, and *T. forsythia* in response to probiotic treatment.

Our study included all types of periodontal diseases in our meta-analysis in order to primarily focus on the change in periodontal pathogen counts during periodontal diseases. Additionally, we included studies using different strains of probiotics to yield conclusive results. Among these included studies, four (Vivekananda et al., 2010; Iniesta et al., 2012; Teughels et al., 2013; Laleman et al., 2019) used *L. reuteri*. Two studies (Alanzi et al., 2018; Goyal et al., 2019) employed a mixture of *L. reuteri* with other beneficial bacteria. The remaining RCTs used other probiotic strains. The most commonly used probiotic, *L. reuteri*, was reported to show a potency to overcome pathogenic microorganisms because of its antimicrobial compounds, reuterin and reutericyclin, and it was also described as having an immunomodulatory effect on the host (Britton, 2017).

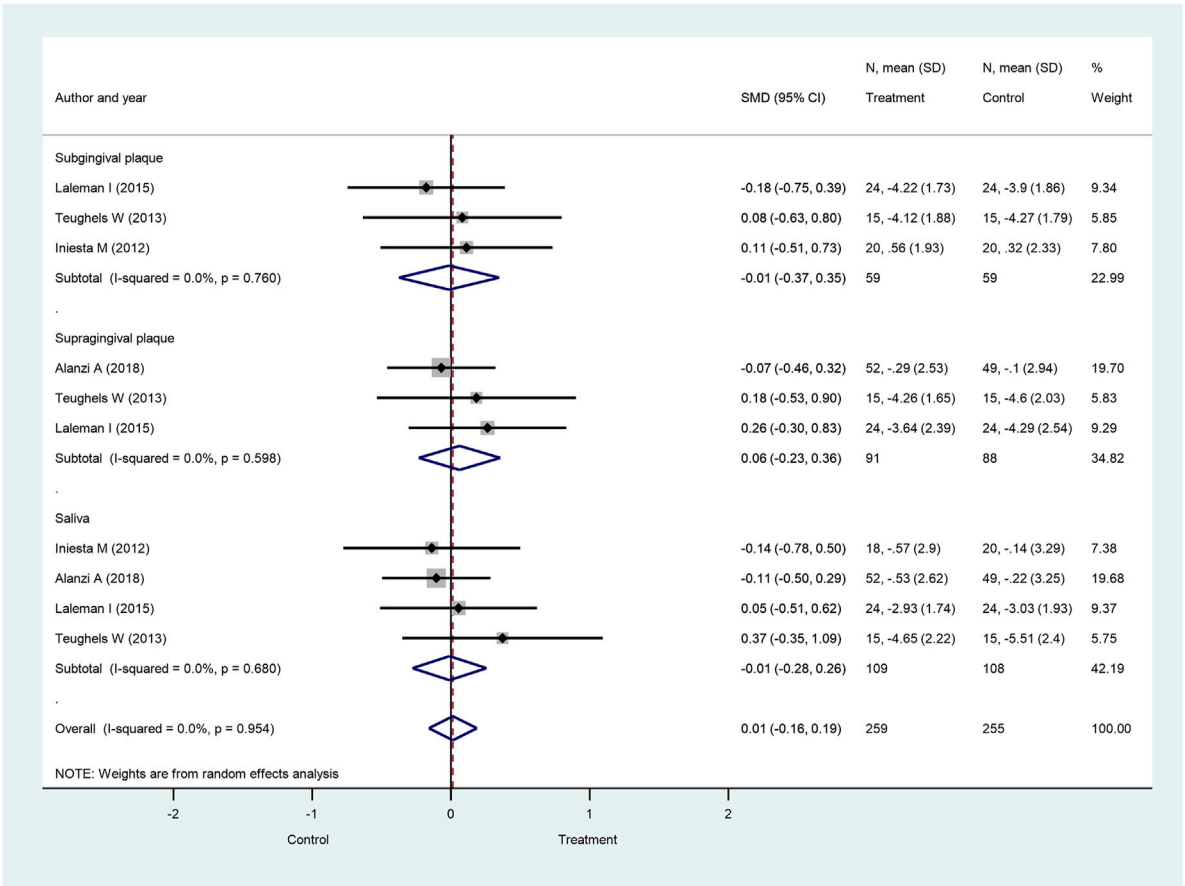

FIGURE 6 | Forest plot analysis of the change in *Prevotella intermedia* at 4 weeks. The overall result presented no significant difference of bacterial decrease when both treatment and control groups were compared (SMD: 0.01; 95% CI: −0.16–0.19; p = 0.874).

Some clinical trials included in our article investigated the antibacterial effects of *L. reuteri* and showed a reduction in the number of periodontal pathogens, such as *A. actinomycetemcomitans*, *P. gingivalis*, and *T. forsythia*, in patients with periodontal diseases (Vivekananda et al., 2010; Iniesta et al., 2012; Teughels et al., 2013; Goyal et al., 2019). Additionally, this antimicrobial effect is supported by three *in vitro* experiments (Kang et al., 2011; Baca-Castan et al., 2014; Santos et al., 2020). One included study (Goyal et al., 2019) used a mixture of *L. reuteri*, *L. rhamnosus*, *B. longum*, and *B. bifidum* and showed the beneficial effect at 24 weeks, while another included study (Laleman et al., 2019) showed no beneficial effect of probiotics on periodontal pathogens at 12 and 24 weeks. This might suggest that long-term use of *L. reuteri* can limit the antibacterial effect, and a mixture of *L. reuteri* was possibly used in the long term to prolong the antibacterial effect. The dose of *L. reuteri* used in three trials (Vivekananda et al., 2010; Iniesta et al., 2012; Teughels et al., 2013) was at least 2×10^8 CFU per day, which seems to be an effective dose.

Three previous meta-analyses reported a specific effect of *L. reuteri* on clinical periodontal parameters (Martin-Cabezas et al., 2016; Ikram et al., 2018; Akram et al., 2020). Martin-Cabesaz and coinvestigators (Martin-Cabezas et al., 2016) reported beneficial effects of probiotics on improving CAL gain and reducing PPD in both moderate and deep pockets. Moreover, they described a significant reduction of BOP in the probiotic group in the short term (combining 6- and 12-week results). Another meta-analysis (Ikram et al., 2018) suggested the effectiveness of probiotics on CAL gain in chronic periodontitis compared to controls; however, they were not able to demonstrate this for PPD reduction. Another meta-analysis (Akram et al., 2020) investigated the effect of *L. reuteri* in gingivitis patients and suggested no statistically significant difference in GI and PI between the probiotic-treated and control groups. These three meta-analyses of periodontal diseases report quite diverse responses to *L. reuteri* treatment.

Another previous meta-analysis (Ho et al., 2020) reported significant CAL gain and PPD reduction in chronic periodontitis at 3 months. Additionally, published reviews indicated variable results, either supporting or questioning the effectiveness of probiotics on the clinical parameters of periodontal diseases (Deepa and Mehta, 2009; Yanine et al., 2013; Matsubara et al., 2016; Seminario-Amez et al., 2017; Barboza et al., 2020; Vives-Soler and Chimenos-Küstner, 2020). The reason for the

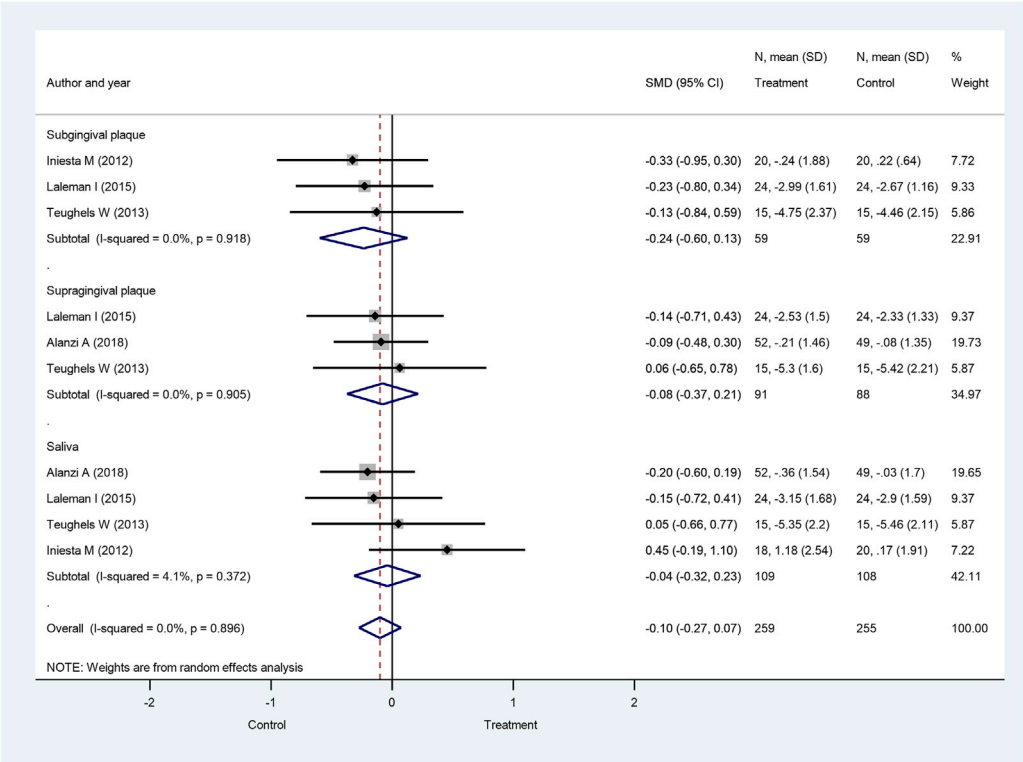

FIGURE 7 | Forest plot analysis of the change in *Fusobacterium nucleatum* at 4 weeks. The overall result presented no significant difference of bacterial decrease when both treatment and control groups were compared (SMD: −0.10; 95% CI: −0.27–0.07; $p = 0.256$).

controversial results may depend on a number of factors, including the pooling of very different follow-up times of the included RCTs, the use of a wide variety of probiotics and their dosage in the included RCTs, and variations in patient characteristics.

The efficacy of probiotics probably relies on the actual bacteria strain, dose, and follow-up time, as described in the management of gastrointestinal tract disorders (Verna and Lucak, 2010; Ciorba, 2012; Kechagia et al., 2013). Various probiotic species may have divergent effects on pathogenic bacteria (Schrezenmeir and de Vrese, 2001; Verna and Lucak, 2010). In addition to the bacteria strain of probiotics, the dose of consumption is also important. The minimum effective doses of probiotics are still controversial; however, it is generally accepted that probiotic products should be consumed daily for a total of 10^8—10^9 probiotic microorganisms (Ciorba, 2012). Additionally, the characteristics of patients should also be considered as different gastrointestinal tract diseases caused by different pathogenic bacteria could be cured by different probiotic strains (Verna and Lucak, 2010). The occurrence of different pathogenic bacteria related to each type of periodontal diseases may also be different (Ardila et al., 2012; Farias et al., 2012). Thus, the type of periodontal disease could be important for the selection of probiotics in future studies.

The safety of probiotics is also important. Three studies (Mayanagi et al., 2009; Vivekananda et al., 2010; Dhaliwal et al., 2017) reported no adverse effects of probiotics during the trial, while two studies (Iniesta et al., 2012; Montero et al., 2017) described abdominal pain resulting from increased intestinal motility, which can be considered as a mild side effect. Another study (Laleman et al., 2019) reported altered sensations in the oral cavity.

Considering our findings on microbiological data, *A. actinomycetemcomitans* has been shown to induce bone loss, periodontal pocket formation, and clinical attachment loss during periodontitis (Mooney and Kinane, 1994; Fine et al., 2007). Furthermore, successful periodontal treatment is often based on the reduction of depth of the periodontal pocket (Donos, 2018). Therefore, our results could suggest that probiotics decrease *A. actinomycetemcomitans*, allowing the healing of tooth-supporting tissues and resulting in clinical parameters in cases when the high count of this bacterium plays a significant pathological role in the course of periodontal disease.

Limitations

The present meta-analysis provides evidence-based answers through appropriately selected articles and processed data. Bacteria numbers on a continuous scale were used for statistical analysis; the change in the bacteria number thus clearly demonstrated, analyzed, and accurately indicated the results. Nevertheless, some unavoidable limitations are present in our study. The major limitation is the low number of included

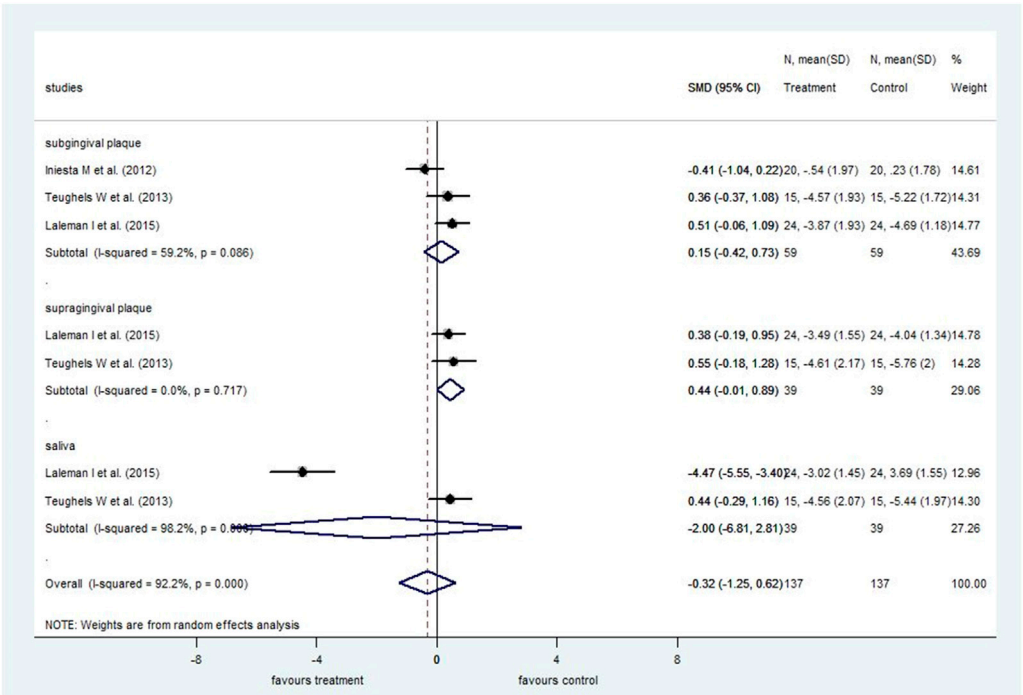

FIGURE 8 | Forest plot analysis of the change in *Tannerella forsythia* at 4 weeks. The overall result presented no significant difference of bacterial decrease when both treatment and control groups were compared (SMD: −0.32; 95% CI: −1.25–0.62).

TABLE 1 | Summary of **s**tatistical analysis for the microbiological outcomes.

Outcomes	No. of studies in meta-analysis	Patients (n)	Results		Heterogeneity		Quality
			Meta-analysis overall estimate (95%CI)	*p*	I^2 (%)	*p*	
A. actinomycetemcomitans at 4 weeks	4	198	SMD: −0.28 (−0.56, −0.01)	0.045	36.5	0.150	⊕OOO
A. actinomycetemcomitans at 8 weeks	4	127	SMD: −0.16 (−0.45, 0.13)	0.271	0.00	0.650	⊕OOO
P. gingivalis at 4 weeks	5	246	SMD: −0.02 (−0.35, 0.31)	0.914	71.5	0.000	⊕OOO
P. gingivalis at 8 weeks	5	196	SMD: −0.01 (−0.53, 0.52)	0.977	84.3	0.000	⊕OOO
P. gingivalis at 12 weeks	3	117	SMD: −0.23 (−0.90, 0.43)	0.488	88.7	0.000	⊕OOO
P. intermedia at 4 weeks	4	219	SMD: 0.01 (−0.16, 0.19)	0.874	0.00	0.954	⊕OOO
P. intermedia at 8 weeks	3	118	SMD: −0.01 (−0.24, 0.21)	0.912	0.00	0.814	⊕OOO
P. intermedia at 12 weeks	4	144	SMD: −0.00 (−0.30, 0.29)	0.981	51.3	0.030	⊕OOO
F. nucleatum at 4 weeks	5	267	SMD: −0.10 (−0.27, 0.07)	0.256	0.00	0.896	⊕OOO
F. nucleatum at 8 weeks	4	170	SMD: 0.12 (−0.09, 0.32)	0.270	0.00	0.791	⊕OOO
F. nucleatum at 12 weeks	3	117	SMD: −0.06 (−0.27, 0.15)	0.580	0.00	0.933	⊕OOO
T. forsythia at 4 weeks	3	128	SMD: −0.32 (−1.25, 0.62)	0.851	92.2	0.000	⊕OOO
T. forsythia at 8 weeks	4	167	SMD: 0.05 (−0.19, 0.30)	0.685	18.8	0.281	⊕OOO

trials and the relatively high heterogeneity. Only nine articles were included in the statistical analysis. These articles used different probiotic strains; a clear outcome for specific probiotic strains could therefore not be produced. The heterogeneity of the included studies, for example, different probiotic strains, doses, and forms, was ignored to yield sufficient data for statistical analysis. We diminished these differences by using means and standard deviations for result synthesis. However, some hidden confounding factors could have affected the results, such as the microbial culture count, subjective decision on the plaque index and gingival index, and the probing pressure used. Furthermore, according to Matsubara et al. (2016), each probiotic strain may have a different effect on each pathogenic species. Furthermore, studies were conducted in different regions of the world, thus creating diverse environmental factors. The different genetic and genomic background of the patients may also have interfered with the efficacy of probiotic strains and have had an overall altering effect

on treatment. Additionally, oral hygienic instructions and cleaning of teeth or scaling and root planning could vary across studies, which may also have led to the heterogeneity of the results.

In conclusion, based on the included data, orally administered probiotics decrease *A. actinomycetemcomitans* counts. In contrast, no beneficial effect of probiotics was observed for the other investigated periodontal pathogens. Our study highlights the heterogeneity among the available RCTs and the need for standardized clinical protocols in the future to evaluate the effect of various probiotics on periodontal pathogens.

AUTHOR CONTRIBUTIONS

TS-N, LCM, WS, PH, GV, and BK devised the project, the main conceptual ideas, and planned the research. TS-N, LCM, WS, BT, DC, GV, and BK worked out the methodology. TS-N, WS, LCM, BK, and GV performed the data collection: literature search, study selection, and data extraction. LCM, AM, and PM also organized and maintained research data for analysis. PM performed analytic calculations and applied statistical models for synthetizing data. AM, DIN, IK, and AS also aided the research by interpretation of raw and synthetized data. PM visualized synthetized data into forest plots. TS-N, WS, and LCM worked on summarizing results into figures and tables. GG, BK, and GV were responsible for managing and coordinating the research activity. PH, GV, and BK took leadership responsibility for the research activity, provided resources, and acquired financial support for the research project. GG, PH, GV, and BK validated reproducibility of the results. TS-N, LCC, PM, GV, and BK wrote the manuscript with input from all authors. WS, AM, DIN, IK, AS, BT, DC, PH, GG, GV, and BK extensively reviewed the work and further edited the manuscript.

FUNDING

This study was funded by the Hungarian Human Resources Development Operational Programme (EFOP-3.6.2-16-2017-00006). Additional funding was received from the Thematic Excellence Programme (2020-4.1.1.-TKP2020) of the Ministry for Innovation and Technology in Hungary within the framework of the Therapy thematic programme at Semmelweis University. Support was also received from an Economic Development and Innovation Operative Programme Grant (GINOP 2.3.2-15-2016-00048) and an Institutional Developments for Enhancing Intelligent Specialization Grant (EFOP-3.6.1-16-2016-00022) from the National Research, Development and Innovation Office. All funds were provided by the Hungarian government with the cooperation of the European Union. The funders played no role in the research. Open access publication support was received through the Central Library of Semmelweis University.

SUPPLEMENTARY MATERIAL

The Supplementary Material for this article can be found online at: https://www.frontiersin.org/articles/10.3389/fphar.2021.682656/full#supplementary-material

REFERENCES

Ahola, A. J., Yli-Knuuttila, H., Suomalainen, T., Poussa, T., Ahlström, A., Meurman, J. H., et al. (2002). Short-term Consumption of Probiotic-Containing Cheese and its Effect on Dental Caries Risk Factors. *Arch. Oral Biol.* 47 (11), 799–804. doi:10.1016/s0003-9969(02)00112-7

Akram, Z., Shafqat, S., Aati, S., Kujan, O., and Fawzy, A. (2020). Clinical Efficacy of Probiotics in the Treatment of Gingivitis: A Systematic Review and Meta-analysis. *Aust. Dent J.* 65 (1), 12–20. doi:10.1111/adj.12733

Alanzi, A., Honkala, S., Honkala, E., Varghese, A., Tolvanen, M., and Söderling, E. (2018). Effect of Lactobacillus Rhamnosus and Bifidobacterium Lactis on Gingival Health, Dental Plaque, and Periodontopathogens in Adolescents: a Randomised Placebo-Controlled Clinical Trial. *Beneficial Microbes* 9 (4), 593–602. doi:10.3920/BM2017.0139

Allaker, R. P., and Stephen, A. S. (2017). Use of Probiotics and Oral Health. *Curr. Oral Health Rep.* 4 (4), 309–318. doi:10.1007/s40496-017-0159-6

Ardila, C., Alzate, J., and Guzmán, I. (2012). Relationship between Gram Negative Enteric Rods, Aggregatibacter Actinomycetemcomitans, and Clinical Parameters in Periodontal Disease. *J. Indian Soc. Periodontol.* 16, 65–69. doi:10.4103/0972-124X.94607

Baca-Castan, M. L., Alczar-Pizaa, A. G., De La Garza-Ramos, M., García, E. E., Njera-Snchez, R. I., and Medina-De La Garza, C. (2014), Antimicrobial Effect of Lactobacillus Reuteri on Bacteria: Periodontal-Disease and Dental-Caries. *AADR Annual Meeting and Exhibition*. Charlotte, North Carolina: IADR.

Barboza, E. P., Arriaga, P. C., Luz, D. P., Montez, C., and Vianna, K. C. (2020). Systematic Review of the Effect of Probiotics on Experimental Gingivitis in Humans. *Braz. Oral Res.* 34, e031. doi:10.1590/1807-3107bor-2020.vol34.0031

Becirovic, A., Abdi-Dezfuli, J. F., Hansen, M. F., Lie, S. A., Vasstrand, E. N., and Bolstad, A. I. (2018). The Effects of a Probiotic Milk Drink on Bacterial Composition in the Supra- and Subgingival Biofilm: A Pilot Study. *Beneficial Microbes* 9 (6), 865–874. doi:10.3920/BM2018.0009

Boyeena, L., Koduganti, R. R., Panthula, V. R., and Jammula, S. P. (2019). Comparison of Efficacy of Probiotics versus Tetracycline Fibers as Adjuvants to Scaling and Root Planing. *J. Indian Soc. Periodontol.* 23 (6), 539–544. doi:10.4103/jisp.jisp_590_18

Britton, R. A. (2017). "Lactobacillus Reuteri," in *The Microbiota in Gastrointestinal Pathophysiology*. Editors M. H. Floch, Y. Ringel, and W. Allan Walker (Boston: Academic Press), 89–97. doi:10.1016/b978-0-12-804024-9.00008-2

Burton, J. P., Chilcott, C. N., Moore, C. J., Speiser, G., and Tagg, J. R. (2006a). A Preliminary Study of the Effect of Probiotic Streptococcus Salivarius K12 on Oral Malodour Parameters. *J. Appl. Microbiol.* 100 (4), 754–764. doi:10.1111/j.1365-2672.2006.02837.x

Burton, J. P., Wescombe, P. A., Moore, C. J., Chilcott, C. N., and Tagg, J. R. (2006b). Safety Assessment of the Oral Cavity Probiotic Streptococcus Salivarius K12. *Appl. Environ. Microbiol.* 72 (4), 3050–3053. doi:10.1128/AEM.72.4.3050-3053.2006

Ciorba, M. A. (2012). A Gastroenterologist's Guide to Probiotics. *Clin. Gastroenterol. Hepatol.* 10 (9), 960–968. doi:10.1016/j.cgh.2012.03.024

Claffey, N., Polyzois, I., and Ziaka, P. (2004). An Overview of Nonsurgical and Surgical Therapy. *Periodontol. 2000* 36, 35–44. doi:10.1111/j.1600-0757.2004.00073.x

Cobb, C. M. (2002). Clinical Significance of Non-surgical Periodontal Therapy: an Evidence-Based Perspective of Scaling and Root Planing. *J. Clin. Periodontol.* 29 (Suppl. 2), 6–16. doi:10.1034/j.1600-051x.29.s2.4.x

Cobb, C. M. (2008). Microbes, Inflammation, Scaling and Root Planing, and the Periodontal Condition. *Am. Dental Hygienists Assoc.* 82 (Suppl. 2), 4.

Costalonga, M., and Herzberg, M. C. (2014). The Oral Microbiome and the Immunobiology of Periodontal Disease and Caries. *Immunol. Lett.* 162 (2 Pt A), 22–38. doi:10.1016/j.imlet.2014.08.017

Czumbel, L. M., Kerémi, B., Gede, N., Mikó, A., Tóth, B., Csupor, D., et al. (2019). Sandblasting Reduces Dental Implant Failure Rate but Not Marginal Bone Level Loss: A Systematic Review and Meta-Analysis. *PLoS One* 14 (5), e0216428. doi:10.1371/journal.pone.0216428

Darveau, R. P. (2010). Periodontitis: a Polymicrobial Disruption of Host Homeostasis. *Nat. Rev. Microbiol.* 8 (7), 481–490. doi:10.1038/nrmicro2337

Deepa, D., and Mehta, D. (2009). Is the Role of Probiotics Friendly in the Treatment of Periodontal Diseases !!. *J. Indian Soc. Periodontol.* 13 (1), 30–31. doi:10.4103/0972-124x.51892

Devine, D. A., and Marsh, P. D. (2009). Prospects for the Development of Probiotics and Prebiotics for Oral Applications. *J. Oral Microbiol.* 1. doi:10.3402/jom.v3401i3400.194910.3402/jom.v1i0.194910.3402/jom.v1i0.1949

Dhaliwal, P. K., Grover, V., Malhotra, R., and Kapoor, A. (2017). Clinical and Microbiological Investigation of the Effects of Probiotics Combined with Scaling and Root Planing in the Management of Chronic Periodontitis: A Randomized, Controlled Study. *J. Int. Acad. Periodontol.* 19 (3), 101–108.

Donos, N. (2018). The Periodontal Pocket. *Periodontol. 2000* 76 (1), 7–15. doi:10.1111/prd.12203

Elsadek, M. F., Ahmed, B. M., Alkhawtani, D. M., and Zia Siddiqui, A. (2020). A Comparative Clinical, Microbiological and Glycemic Analysis of Photodynamic Therapy and Lactobacillus Reuteri in the Treatment of Chronic Periodontitis in Type-2 Diabetes Mellitus Patients. *Photodiagnosis Photodynamic Ther.* 29, 101629. doi:10.1016/j.pdpdt.2019.101629

Farias, B. C., Souza, P. R. E., Ferreira, B., Melo, R. S. A., Machado, F. B., Gusmão, E. S., et al. (2012). Occurrence of Periodontal Pathogens Among Patients with Chronic Periodontitis. *Braz. J. Microbiol.* 43 (3), 909–916. doi:10.1590/S1517-83822012000300009

Fine, D. H., Markowitz, K., Furgang, D., Fairlie, K., Ferrandiz, J., Nasri, C., et al. (2007). Aggregatibacter Actinomycetemcomitans and its Relationship to Initiation of Localized Aggressive Periodontitis: Longitudinal Cohort Study of Initially Healthy Adolescents. *J. Clin. Microbiol.* 45 (12), 3859. doi:10.1128/JCM.00653-07

Genco, R. J. (1992). Host Responses in Periodontal Diseases: Current Concepts. *J. Periodontol.* 63 (4S), 338–355. doi:10.1902/jop.1992.63.4s.338

Goyal, N., Shamanna, P. U., Varughese, S. T., Abraham, R., Antony, B., Emmatty, R., et al. (2019). Effects of Amine Fluoride and Probiotic Mouthwash on Levels of Porphyromonas Gingivalis in Orthodontic Patients: A Randomized Controlled Trial. *J. Indian Soc. Periodontol.* 23 (4), 339–344. doi:10.4103/jisp.jisp_551_18

Gruner, D., Paris, S., and Schwendicke, F. (2016). Probiotics for Managing Caries and Periodontitis: Systematic Review and Meta-Analysis. *J. dentistry* 48, 16–25. doi:10.1016/j.jdent.2016.03.002

Hajishengallis, G. (2014). Immunomicrobial Pathogenesis of Periodontitis: Keystones, Pathobionts, and Host Response. *Trends Immunology* 35 (1), 3–11. doi:10.1016/j.it.2013.09.001

Hallström, H., Lindgren, S., Yucel-Lindberg, T., Dahlén, G., Renvert, S., and Twetman, S. (2013). Effect of Probiotic Lozenges on Inflammatory Reactions and Oral Biofilm during Experimental Gingivitis. *Acta Odontologica Scand.* 71 (3-4), 828–833. doi:10.3109/00016357.2012.734406

Higgins, J., Thomas, J., Chandler, J., Cumpston, M., Li, T., Page, M., et al. (2019). in *Cochrane Handbook for Systematic Reviews of Interventions* (Cochrane. version 6.0updated July, 2019).

Ho, S. N., Acharya, A., Sidharthan, S., Li, K. Y., Leung, W. K., Mcgrath, C., et al. (2020). A Systematic Review and Meta-Analysis of Clinical, Immunological, and Microbiological Shift in Periodontitis after Nonsurgical Periodontal Therapy with Adjunctive Use of Probiotics. *J. Evid. Based Dental Pract.* 20 (1), 101397. doi:10.1016/j.jebdp.2020.101397

Ikram, S., Hassan, N., Raffat, M. A., Mirza, S., and Akram, Z. (2018). Systematic Review and Meta-analysis of Double-blind, Placebo-controlled, Randomized Clinical Trials Using Probiotics in Chronic Periodontitis. *J. Invest. Clin. Dent* 9 (3), e12338. doi:10.1111/jicd.12338

Imran, F., Das, S., Padmanabhan, S., Rao, R., Suresh, A., and Bharath, D. (2015). Evaluation of the Efficacy of a Probiotic Drink Containing Lactobacillus Casei on the Levels of Periodontopathic Bacteria in Periodontitis: A Clinico-Microbiologic Study. *Indian J. Dent Res.* 26 (5), 462–468. doi:10.4103/0970-9290.172033

Iniesta, M., Herrera, D., Montero, E., Zurbriggen, M., Matos, A. R., Marín, M. J., et al. (2012). Probiotic Effects of Orally administeredLactobacillus Reuteri-Containing Tablets on the Subgingival and Salivary Microbiota in Patients with Gingivitis. A Randomized Clinical Trial. *J. Clin. Periodontol.* 39 (8), 736–744. doi:10.1111/j.1600-051X.2012.01914.x

Invernici, M. M., Salvador, S. L., Silva, P. H. F., Soares, M. S. M., Casarin, R., Palioto, D. B., et al. (2018). Effects of Bifidobacterium Probiotic on the Treatment of Chronic Periodontitis: A Randomized Clinical Trial. *J. Clin. Periodontol.* 45 (10), 1198–1210. doi:10.1111/jcpe.12995

Iwamoto, T., Suzuki, N., Tanabe, K., Takeshita, T., and Hirofuji, T. (2010). Effects of Probiotic Lactobacillus Salivarius WB21 on Halitosis and Oral Health: An Open-Label Pilot Trial. *Oral Surg. Oral Med. Oral Pathol. Oral Radiol. Endodontology* 110 (2), 201–208. doi:10.1016/j.tripleo.2010.03.032

Kaklamanos, E. G., Nassar, R., Kalfas, S., Al Halabi, M., Kowash, M., Hannawi, H., et al. (2019). A Single-centre Investigator-Blinded Randomised Parallel Group Clinical Trial to Investigate the Effect of Probiotic strainsStreptococcus salivariusM18 andLactobacillus Acidophiluson Gingival Health of Paediatric Patients Undergoing Treatment with Fixed Orthodontic Appliances: Study Protocol. *BMJ Open* 9 (9), e030638. doi:10.1136/bmjopen-2019-030638

Kang, M.-S., Oh, J.-S., Lee, H.-C., Lim, H.-S., Lee, S.-W., Yang, K.-H., et al. (2011). Inhibitory Effect of Lactobacillus Reuteri on Periodontopathic and Cariogenic Bacteria. *J. Microbiol.* 49 (2), 193–199. doi:10.1007/s12275-011-0252-9

Kechagia, M., Basoulis, D., Konstantopoulou, S., Dimitriadi, D., Gyftopoulou, K., Skarmoutsou, N., et al. (2013). Health Benefits of Probiotics: A Review. *ISRN Nutr.* 2013, 1–7. doi:10.5402/2013/481651

Kerémi, B., Márta, K., Farkas, K., Czumbel, L. M., Tóth, B., Szakács, Z., et al. (2020). Effects of Chlorine Dioxide on Oral Hygiene - A Systematic Review and Meta-Analysis. *Cpd* 26 (25), 3015–3025. doi:10.2174/1381612826666200515134450

Laleman, I., Pauwels, M., Quirynen, M., and Teughels, W. (2019). A Dual-strain Lactobacilli Reuteri Probiotic Improves the Treatment of Residual Pockets: A Randomized Controlled Clinical Trial. *J. Clin. Periodontol.* 47, 43–53. doi:10.1111/jcpe.13198

Laleman, I., Yilmaz, E., Ozcelik, O., Haytac, C., Pauwels, M., Herrero, E. R., et al. (2015). The Effect of a Streptococci Containing Probiotic in Periodontal Therapy: a Randomized Controlled Trial. *J. Clin. Periodontol.* 42 (11), 1032–1041. doi:10.1111/jcpe.12464

Liberati, A., Altman, D. G., Tetzlaff, J., Mulrow, C., Gøtzsche, P. C., Ioannidis, J. P. A., et al. (2009). The PRISMA Statement for Reporting Systematic Reviews and Meta-Analyses of Studies that Evaluate Health Care Interventions: Explanation and Elaboration. *Plos Med.* 6 (7), e1000100. doi:10.1371/journal.pmed.1000100

Manresa, C., Sanz-Miralles, E. C., Twigg, J., and Bravo, M. (2018). Supportive Periodontal Therapy (SPT) for Maintaining the Dentition in Adults Treated for Periodontitis. *Cochrane Database Syst. Rev.* 1, Cd009376. doi:10.1002/14651858.CD009376.pub2

Martin-Cabezas, R., Davideau, J.-L., Tenenbaum, H., and Huck, O. (2016). Clinical Efficacy of Probiotics as an Adjunctive Therapy to Non-surgical Periodontal Treatment of Chronic Periodontitis: a Systematic Review and Meta-Analysis. *J. Clin. Periodontol.* 43 (6), 520–530. doi:10.1111/jcpe.12545

Matsubara, V. H., Bandara, H. M. H. N., Ishikawa, K. H., Mayer, M. P. A., and Samaranayake, L. P. (2016). The Role of Probiotic Bacteria in Managing Periodontal Disease: a Systematic Review. *Expert Rev. Anti-infective Ther.* 14 (7), 643–655. doi:10.1080/14787210.2016.1194198

Mayanagi, G., Kimura, M., Nakaya, S., Hirata, H., Sakamoto, M., Benno, Y., et al. (2009). Probiotic Effects of Orally administeredLactobacillus salivariusWB21-Containing Tablets on Periodontopathic Bacteria: a Double-Blinded, Placebo-Controlled, Randomized Clinical Trial. *J. Clin. Periodontol.* 36 (6), 506–513. doi:10.1111/j.1600-051X.2009.01392.x

Mcgowan, K., Mcgowan, T., and Ivanovski, S. (2018). Optimal Dose and Duration of Amoxicillin-Plus-Metronidazole as an Adjunct to Non-surgical Periodontal Therapy: A Systematic Review and Meta-Analysis of Randomized, Placebo-Controlled Trials. *J. Clin. Periodontol.* 45 (1), 56–67. doi:10.1111/jcpe.12830

Mcmaster University, D.B.E.P.. GRADEpro GDT: GRADEpro Guideline Development Tool [Software], Inc..

Montalto, M., Vastola, M., Marigo, L., Covino, M., Graziosetto, R., Curigliano, V., et al. (2004). Probiotic Treatment Increases Salivary Counts of Lactobacilli: A Double-Blind, Randomized, Controlled Study. *Digestion* 69 (1), 53–56. doi:10.1159/000076559

Montero, E., Iniesta, M., Rodrigo, M., Marín, M. J., Figuero, E., Herrera, D., et al. (2017). Clinical and Microbiological Effects of the Adjunctive Use of Probiotics in the Treatment of Gingivitis: A Randomized Controlled Clinical Trial. *J. Clin. Periodontol.* 44 (7), 708–716. doi:10.1111/jcpe.12752

Mooney, J., and Kinane, D. F. (1994). Humoral Immune Responses to Porphymmonas Gingivalis and Actinobacillus Actinomycetemcomitans in Adult Periodontitis and Rapidly Progressive Periodontitis. *Oral Microbiol. Immunol.* 9 (6), 321–326. doi:10.1111/j.1399-302x.1994.tb00281.x

Morales, A., Gandolfo, A., Bravo, J., Carvajal, P., Silva, N., Godoy, C., et al. (2018). Microbiological and Clinical Effects of Probiotics and Antibiotics on Nonsurgical Treatment of Chronic Periodontitis: a Randomized Placebo-Controlled Trial with 9-month Follow-Up. *J. Appl. Oral Sci.* 26, e20170075. doi:10.1590/1678-7757-2017-0075

Muniz, F. W. M. G., de Oliveira, C. C., de Sousa Carvalho, R., Moreira, M. M. S. M., de Moraes, M. E. A., and Martins, R. S. (2013). Azithromycin: A New Concept in Adjuvant Treatment of Periodontitis. *Eur. J. Pharmacol.* 705, 135–139. doi:10.1016/j.ejphar.2013.02.044

Nazir, M. A. (2017). Prevalence of Periodontal Disease, its Association with Systemic Diseases and Prevention. *Int. J. Health Sci. (Qassim)* 11 (2), 72–80.

Quirynen, M., Vogels, R., Pauwels, M., Haffajee, A. D., Socransky, S. S., Uzel, N. G., et al. (2005). Initial Subgingival Colonization of 'pristine' Pockets. *J. Dent Res.* 84 (4), 340–344. doi:10.1177/154405910508400409

Roberts, F. A., and Darveau, R. P. (2002). Beneficial Bacteria of the Periodontium. *Periodontol. 2000* 30, 40–50. doi:10.1034/j.1600-0757.2002.03004.x

Romani Vestman, N., Hasslöf, P., Keller, M. K., Granström, E., Roos, S., Twetman, S., et al. (2013). Lactobacillus Reuteri Influences Regrowth of Mutans Streptococci after Full-Mouth Disinfection: A Double-Blind, Randomised Controlled Trial. *Caries Res.* 47 (4), 338–345. doi:10.1159/000347233

Rudney, J. D., Chen, R., and Zhang, G. (2005). Streptococci Dominate the Diverse Flora within Buccal Cells. *J. Dent Res.* 84 (12), 1165–1171. doi:10.1177/154405910508401214

Ruksakiet, K., Hanák, L., Farkas, N., Hegyi, P., Sadaeng, W., Czumbel, L. M., et al. (2020). Antimicrobial Efficacy of Chlorhexidine and Sodium Hypochlorite in Root Canal Disinfection: A Systematic Review and Meta-Analysis of Randomized Controlled Trials. *J. Endodontics* 46 (8), 1032–1041.e1037. doi:10.1016/j.joen.2020.05.002doi:

Sanders, M. E. (2008). Probiotics: Definition, Sources, Selection, and Uses. *Clin. Infect. Dis.* 46 (Suppl. 2), S58–S61. doi:10.1086/523341

Santos, T. A., Scorzoni, L., Correia, R., Junqueira, J. C., and Anbinder, A. L. (2020). Interaction between Lactobacillus Reuteri and Periodontopathogenic Bacteria Using *In Vitro* and *In Vivo* (G. Mellonella) Approaches. *Pathog. Dis.* 78. doi:10.1093/femspd/ftaa044

Schrezenmeir, J., and De Vrese, M. (2001). Probiotics, Prebiotics, and Synbiotics-Approaching a Definition. *Am. J. Clin. Nutr.* 73 (2 Suppl. l), 361s–364s. doi:10.1093/ajcn/73.2.361s

Schünemann, H., Brozek, J., Guyatt, G., and Oxman, A. (2013). in *GRADE Handbook for Grading Quality of Evidence and Strength of Recommendations* (The GRADE Working Group).

Seminario-Amez, M., Lopez-Lopez, J., Estrugo-Devesa, A., Ayuso-Montero, R., and Jane-Salas, E. (2017). Probiotics and Oral Health: A Systematic Review. *Med. Oral* 22 (3), E282–E288. doi:10.4317/medoral.21494

Shah, M., Gujjari, S., and Chandrasekhar, V. (2018). Long-term Effect of Lactobacillus Brevis CD2 (Inersan) And/or Doxycycline in Aggressive Periodontitis. *J. Indian Soc. Periodontol.* 21 (4), 341–343. doi:10.4103/jisp.jisp_215_17

Shah, M. P., Gujjari, S. K., and Chandrasekhar, V. S. (2013). Evaluation of the Effect of Probiotic (Inersan®) Alone, Combination of Probiotic with Doxycycline and Doxycycline Alone on Aggressive Periodontitis - a Clinical and Microbiological Study. *J. Clin. Diagn. Res.* 7 (3), 595–600. doi:10.7860/JCDR/2013/5225.2834

Silva, N., Abusleme, L., Bravo, D., Dutzan, N., Garcia-Sesnich, J., Vernal, R., et al. (2015). Host Response Mechanisms in Periodontal Diseases. *J. Appl. Oral Sci.* 23 (3), 329–355. doi:10.1590/1678-775720140259

Swarna Meenakshi, S., and Varghese, S. (2018). Adjunctive Effect of Probiotic (Lactobacillus Casei Shirota) to Scaling and Root Planing in the Management of Chronic Periodontitis. *Drug Invention Today* 10 (8), 1381–1386.

Tekce, M., Ince, G., Gursoy, H., Dirikan Ipci, S., Cakar, G., Kadir, T., et al. (2015). Clinical and Microbiological Effects of Probiotic Lozenges in the Treatment of Chronic Periodontitis: a 1-year Follow-Up Study. *J. Clin. Periodontol.* 42 (4), 363–372. doi:10.1111/jcpe.12387

Teughels, W., Durukan, A., Ozcelik, O., Pauwels, M., Quirynen, M., and Haytac, M. C. (2013). Clinical and Microbiological Effects of Lactobacillus Reuteri Probiotics in the Treatment of Chronic Periodontitis: a Randomized Placebo-controlled Study. *J. Clin. Periodontol.* 40 (11), 1025–1035. doi:10.1111/jcpe.12155

Teughels, W., Kinder Haake, S., Sliepen, I., Pauwels, M., Van Eldere, J., Cassiman, J.-J., et al. (2007). Bacteria Interfere with A. Actinomycetemcomitans Colonization. *J. Dent Res.* 86 (7), 611–617. doi:10.1177/154405910708600706

Tobita, K., Watanabe, I., Tomokiyo, M., and Saito, M. (2018). Effects of Heat-Treated Lactobacillus Crispatus KT-11 Strain Consumption on Improvement of Oral Cavity Environment: A Randomised Double-Blind Clinical Trial. *Beneficial Microbes* 9 (4), 585–592. doi:10.3920/BM2017.0137

Van Dyke, T. E., and Sheilesh, D. (2005). Risk Factors for Periodontitis. *J. Int. Acad. Periodontol.* 7 (1), 3–7.

Verna, E. C., and Lucak, S. (2010). Use of Probiotics in Gastrointestinal Disorders: what to Recommend?. *Therap Adv. Gastroenterol.* 3 (5), 307–319. doi:10.1177/1756283X10373814

Vivekananda, M. R., Vandana, K. L., and Bhat, K. G. (2010). Effect of the probioticLactobacilli reuteri(Prodentis) in the Management of Periodontal Disease: a Preliminary Randomized Clinical Trial. *J. Oral Microbiol.* 2, 5344. doi:10.3402/jom.v2i0.5344

Vives-Soler, A., and Chimenos-Küstner, E. (2020). Effect of Probiotics as a Complement to Non-surgical Periodontal Therapy in Chronic Periodontitis: A Systematic Review. *Med. Oral* 25 (2), e161–e167. doi:10.4317/medoral.23147

Windisch, P., Sculean, A., Klein, F., Tóth, V., Gera, I., Reich, E., et al. (2002). Comparison of Clinical, Radiographic, Histometric Measurements Following Treatment with Guided Tissue Regeneration or Enamel Matrix Proteins in Human Periodontal Defects. *J. Periodontol.* 73 (4), 409–417. doi:10.1902/jop.2002.73.4.409

Yanine, N., Araya, I., Brignardello-Petersen, R., Carrasco-Labra, A., González, A., Preciado, A., et al. (2013). Effects of Probiotics in Periodontal Diseases: a Systematic Review. *Clin. Oral Invest.* 17 (7), 1627–1634. doi:10.1007/s00784-013-0990-7

Zahradnik, R. T., Magnusson, I., Walker, C., Mcdonell, E., Hillman, C. H., and Hillman, J. D. (2009). Preliminary Assessment of Safety and Effectiveness in Humans of ProBiora3 , a Probiotic Mouthwash. *J. Appl. Microbiol.* 107 (2), 682–690. doi:10.1111/j.1365-2672.2009.04243.x

Zappa, U., Smith, B., Simona, C., Graf, H., Case, D., and Kim, W. (1991). Root Substance Removal by Scaling and Root Planing. *J. Periodontol.* 62 (12), 750–754. doi:10.1902/jop.1991.62.12.750

Conflict of Interest: The authors declare that the research was conducted in the absence of any commercial or financial relationships that could be construed as a potential conflict of interest.

Publisher's Note: All claims expressed in this article are solely those of the authors and do not necessarily represent those of their affiliated organizations, or those of the publisher, the editors and the reviewers. Any product that may be evaluated in this article, or claim that may be made by its manufacturer, is not guaranteed or endorsed by the publisher.

frontiers in Pharmacology

ORIGINAL RESEARCH
published: 18 August 2021
doi: 10.3389/fphar.2021.675443

Rejuvenation of *Helicobacter pylori*–Associated Atrophic Gastritis Through Concerted Actions of Placenta-Derived Mesenchymal Stem Cells Prevented Gastric Cancer

Jong Min Park[1], *Young Min Han*[2] *and Ki Baik Hahm*[3,4]*

[1]College of Oriental Medicine, Daejeon University, Daejeon, Korea, [2]Western Seoul Center, Korea Basic Science Institute, Seoul, Korea, [3]Medpacto Research Institute, Medpacto, Seoul, Korea, [4]CHA Cancer Preventive Research Center, CHA Bio Complex, Seongnam, Korea

Chronic *Helicobacter pylori* infection causes gastric cancer via the progression of precancerous chronic atrophic gastritis (CAG). Therefore, repairing gastric atrophy could be a useful strategy in preventing *H. pylori*–associated gastric carcinogenesis. Although eradication of the bacterial pathogen offers one solution to this association, this study was designed to evaluate an alternative approach using mesenchymal stem cells to treat CAG and prevent carcinogenesis. Here, we used human placenta-derived mesenchymal stem cells (PD-MSCs) and their conditioned medium (CM) to treat *H. pylori*–associated CAG in a mice/cell model to explore their therapeutic effects and elucidate their molecular mechanisms. We compared the changes in the fecal microbiomes in response to PD-MSC treatments, and chronic *H. pylori*–infected mice were given ten treatments with PD-MSCs before being sacrificed for end point assays at around 36 weeks of age. These animals presented with significant reductions in the mean body weights of the control group, which were eradicated following PD-MSC treatment ($p < 0.01$). Significant changes in various pathological parameters including inflammation, gastric atrophy, erosions/ulcers, and dysplastic changes were noted in the control group ($p < 0.01$), but these were all significantly reduced in the PD-MSC/CM-treated groups. Lgr5+, Ki-67, H^+/K^+-ATPase, and Musashi-1 expressions were all significantly increased in the treated animals, while inflammatory mediators, MMP, and apoptotic executors were significantly decreased in the PD-MSC group compared to the control group ($p < 0.001$). Our model showed that *H. pylori*–initiated, high-salt diet–promoted gastric atrophic gastritis resulted in significant changes in the fecal microbiome at the phylum/genus level and that PD-MSC/CM interventions facilitated a return to more normal microbial communities. In conclusion, administration of PD-MSCs or their conditioned medium may present a novel rejuvenating agent in preventing the progression of *H. pylori*–associated premalignant lesions.

Keywords: *H pylori*, chronic atrophic gastritis, placenta-derived mesenchymal stem cell, rejuvenation, cell therapy, inflammation

OPEN ACCESS

Edited by:
Predrag Sikiric,
University of Zagreb, Croatia

Reviewed by:
Rinaldo Pellicano,
Molinette Hospital, Italy
Francesco Di Mario,
University of Parma, Italy

***Correspondence:**
Ki Baik Hahm
hahmkb@medpacto.com

Specialty section:
This article was submitted to Gastrointestinal and Hepatic Pharmacology, a section of the journal Frontiers in Pharmacology

Received: *03 March 2021*
Accepted: *22 June 2021*
Published: *18 August 2021*

Citation:
Park JM, Han YM and Hahm KB (2021) Rejuvenation of Helicobacter pylori*–Associated Atrophic Gastritis Through Concerted Actions of Placenta-Derived Mesenchymal Stem Cells Prevented Gastric Cancer. Front. Pharmacol. 12:675443. doi: 10.3389/fphar.2021.675443*

INTRODUCTION

There has been a broad paradigm shift in our understanding of gastric cancer prevention over the last three decades. Gastric cancers are the second leading cause of cancer-related deaths worldwide (Koulis et al., 2019), and their development is strongly associated with gastric ulcerations. The high number of gastric cancer deaths and the clear link between gastric cancers and *Helicobacter pylori* infections have led to the identification of several pathways for preventing pathogenesis. These include the possibility of reversing the pathogenesis of premalignant lesions by rejuvenating chronic atrophic gastritis (CAG), the total eradication of *Helicobacter* colonization and the concomitant reduction in mutagenic inflammation/oxidative stress, and the directed alteration of the tumor microenvironment and the mucosal immune response via engineering of the microbiota (Yashima et al., 2010; Chen et al., 2016; Liu et al., 2016) or some combination of these interventions. Most gastric carcinomas follow a documented and easily discernable cascade of precursor lesions, slowly progressing from the premalignant stages of CAG, to intestinal metaplasia (IM), and dysplasia to gastric carcinoma (de Vries et al., 2007; Moss, 2017), and since most of these lesions are a direct result of the chronic inflammation of gastric mucosa associated with *H. pylori* infection, multiple clinical interventions and trials have been implemented to prevent this cascade and detour the progression of this disease (Sipponen and Kimura, 1994; Correa and Piazuelo, 2012; Correa, 2013; Piazuelo and Correa, 2013; Rugge et al., 2013). These interventions all rely on the theory that gastric cancers associated with *H. pylori* infection can be prevented by the application of antioxidants or equivalent therapies via their reduction of the premalignant lesions including CAG with IM and their so-called suspension of the gastric precancerous cascade.

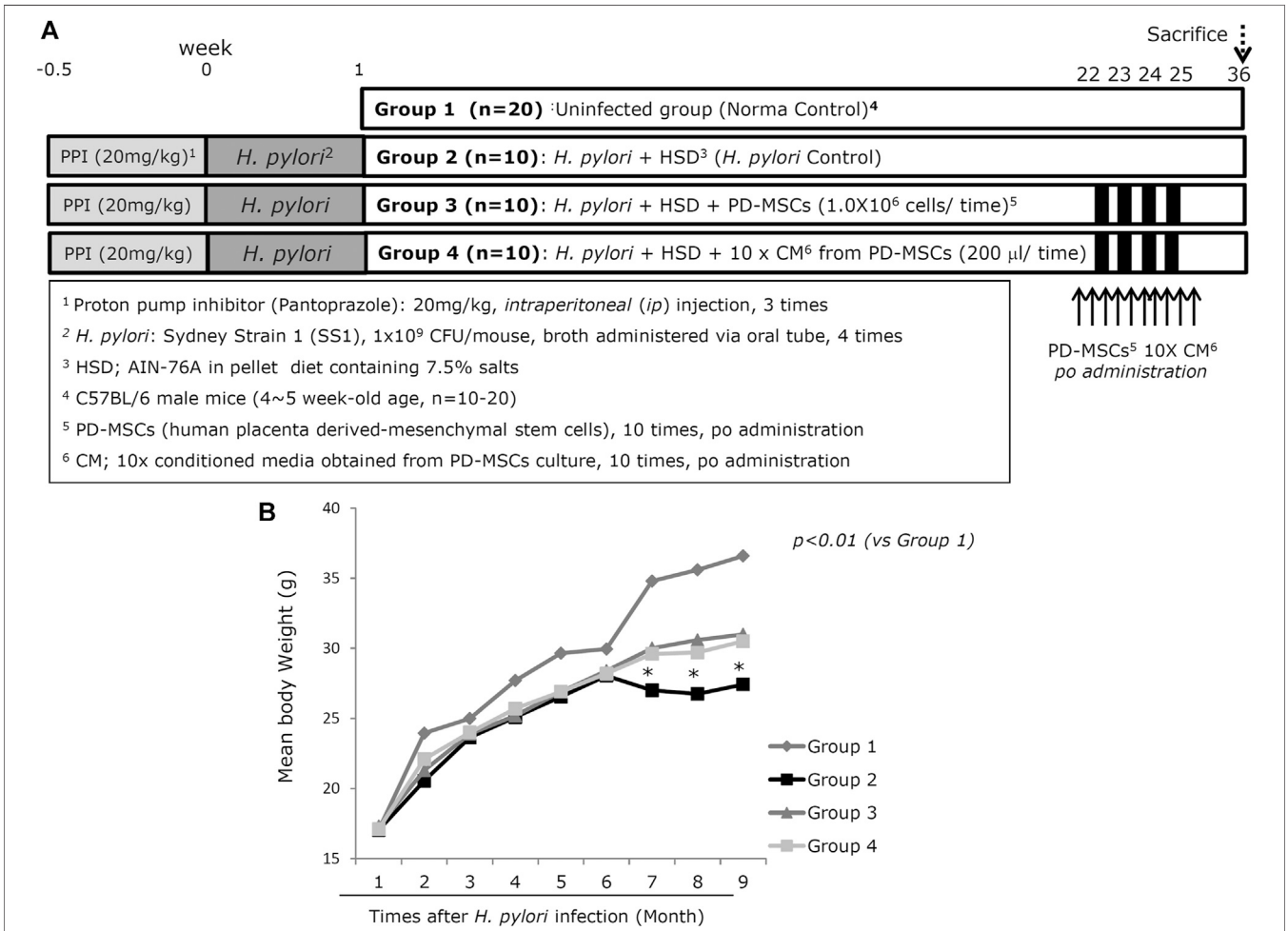

FIGURE 1 | Influence of PD-MSCs or their CM on an *H. pylori*–initiated, high-salt diet–promoted CAG mice model (36 weeks). **(A)** Scheme for groups: Group 1, normal control; Group 2, *H. pylori*–associated CAG disease control; Group 3, disease control treated with $1x10^6$ PD-MSCs (100 μl), 10 times during 22–25 weeks; and Group 4, disease control treated with 10x concentrated CM (200 μl). **(B)** Body weight changes according to groups. Body weights were measured every 3 days in all mice. **(C)** Representative photo of the resected stomach and mean gross lesion scores according to groups, see **Supplementary Table 1** for the scoring system. **(D)** Representational pathology and mean pathological scores according to groups, see **Supplementary Table 2** for the scoring system. All data represent mean ± SD (n = 10).

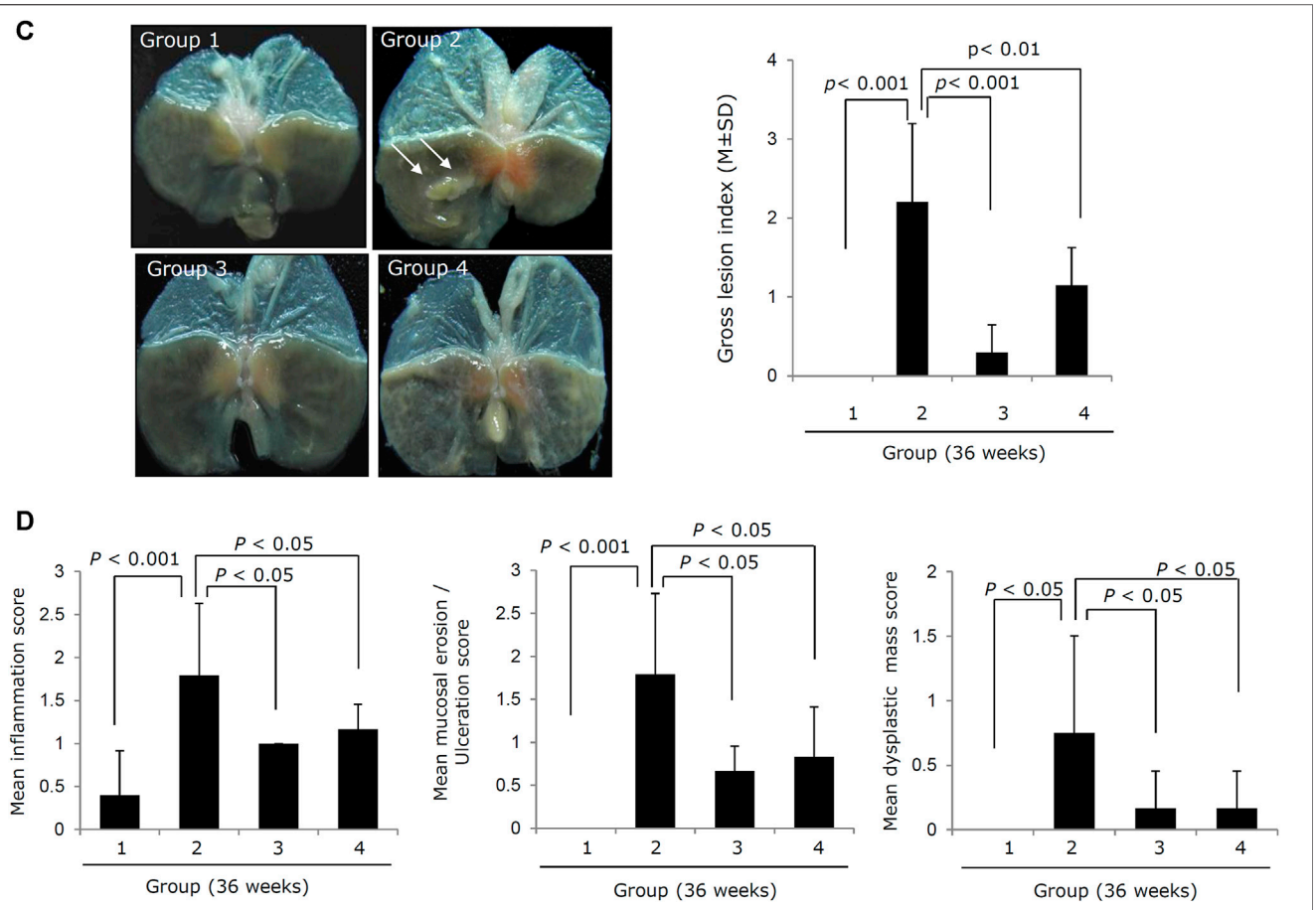

Figure 1. | (Continued).

In addition to interventions such as antioxidants, phytoceuticals, and natural products, stem cells, including embryonic stem cells (ESCs), somatic cell–derived induced pluripotent stem cells (*i*PSCs), and mesenchymal stem cells (MSCs), are well-known therapeutic agents possessing unlimited self-renewal capacity and great potential to differentiate into various cell types from any of the three embryonic germ layers, including ectodermal, mesodermal, and endodermal lineages (Gumucio et al., 2008; Wang H. et al., 2020). Given this, we hypothesize that the administration of MSCs or their conditioned medium (CM) prior to irreversible dysplasia could facilitate the therapeutic rejuvenation of CAG. Therapeutic use of human placenta-derived MSCs (PD-MSCs) has been shown to exhibit enormous clinical potential as a source of regenerative medicine, with relatively low immunogenicity, easy producibility, and high stability. These attributes make MSCs uniquely qualified to support the regeneration of injured or diseased organs which is modeled by the CAG phenotypes in this study (Lu and Zhao, 2013; Quan and Wang, 2014).

The ability to replace defective cells in the stomach with cells that can engraft, integrate, and restore a functional epithelium could potentially cure atrophic gastritis. Stem cells or the factors included in their CM could serve as an attractive therapeutic strategy for dealing with *H. pylori*–associated gastric precancerous cascades. Efforts to identify efficient therapeutic agents or strategies capable of either rejuvenating *H. pylori*–associated gastric atrophy or preventing gastric cancer via their regulation of class I carcinogen *H. pylori* infection (Vogiatzi et al., 2007) remain a top priority. However, in addition to eradication, non-anti-microbial approaches, including the use of antioxidants, probiotics, vitamin E, *Artemisia*, and green tea, among others, have been evaluated. It is from these strategies that we selected the administration of PD-MSCs or their CM since multiple clinical trials involving MSCs in a range of human diseases or as the primary cell source in cell therapies and regenerative medicine strategies are already underway (Bunpetch et al., 2017; Kimbrel and Lanza, 2020; Maqsood et al., 2020; Shariati et al., 2020). In this study, we investigated whether PD-MSCs or their concentrated CM administered during *H. pylori*–associated CAG could induce a rejuvenating effect on CAG and facilitate a reversion of these lesions to their premalignant state while allowing us to explore the molecular mechanisms underlying these actions.

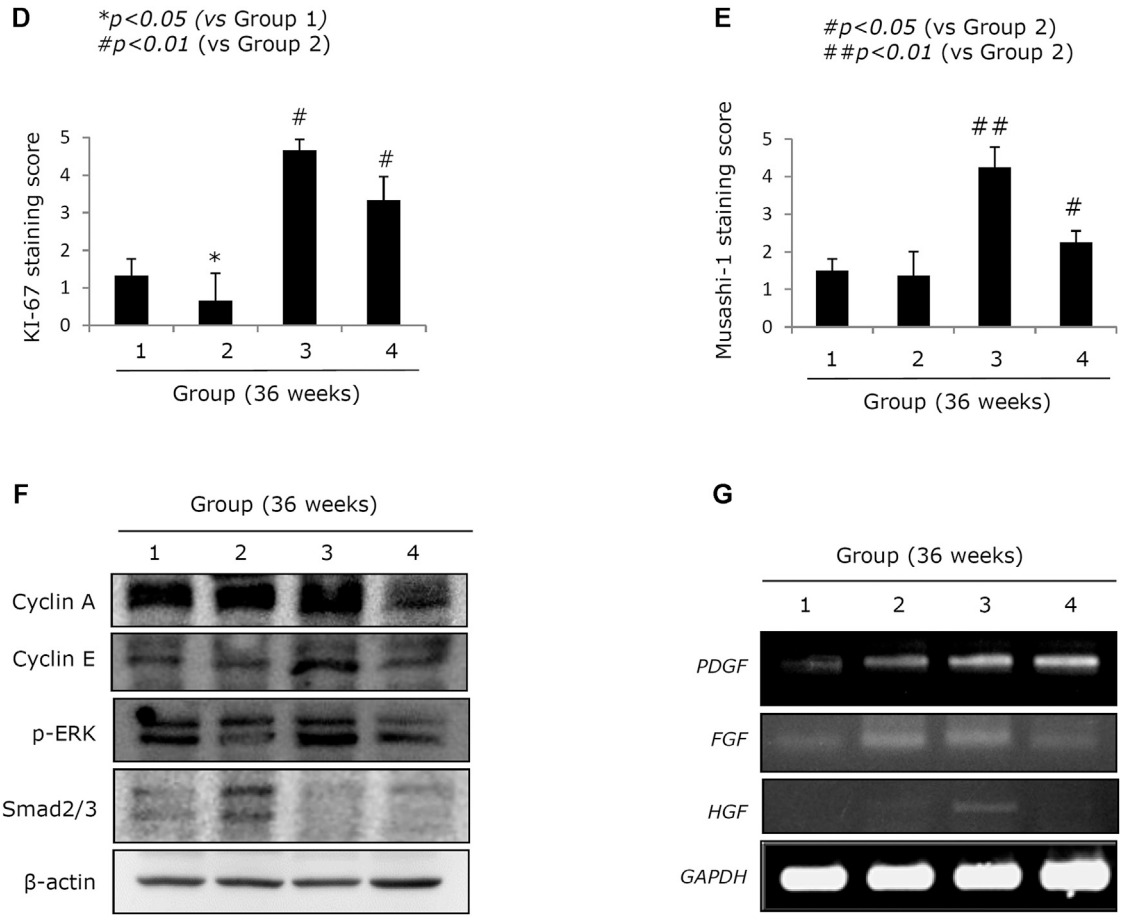

FIGURE 2 | Changes of stemness according to groups relevant to gastric atrophy. **(A)** Scores for gastric atrophy: left, representational pathology of Group 2 showing significant changes of CAG featured with a loss of parietal cells, gastric inflammation, and a loss of gastric glands with some foci of erosions; right, scores according to groups. See **Supplementary Table 2** for the scoring system. **(B)** Immunohistochemical staining of the proton pump with antibody of H^+/K^+-ATPase. **(C)** Confocal staining with LGR5+ antibody: left, representational staining with LGR5+, x100 magnification; right, mean scoring according to groups. **(D)** Immunohistochemical staining of Ki-67 antibody and the mean positive scoring according to groups. **(E)** Immunohistochemical staining of Musashi-1 antibody and the mean positive scoring according to groups. **(F)** Western blot for cell cycle, ERK among MAPK, and smad2/3. **(G)** RT-PCR for *PDGF*, *FGF*, and *HGF* mRNA. All data represent mean ± SD (n = 10).

MATERIALS AND METHODS

Cell Culture

PD-MSCs were obtained from CHA University (Prof. Yong Soo Choi, CHA University, Seongnam, Korea). The PD-MSC line was cultured in α-MEM containing 1 μg/ml heparin, 25 mg/ml fibroblast growth factor, 10% (*v*/*v*) fetal bovine serum, and 100 U/ml penicillin. The cells were maintained at 37°C in a humidified atmosphere containing 5% CO_2. The rat gastric mucosal cells, RGM-1, were kindly given by Prof. Hirofumi Matsui (University of Tsukuba, Japan) and were maintained at 37°C in a humidified atmosphere containing 5% CO_2. RGM-1 cells were cultured in Dulbecco's modified Eagle's medium containing 10% (v/v) fetal bovine serum, 100 U/ml penicillin, and 100 μg/ml streptomycin. For co-culture experiments, PD-MSCs were seeded in a six-well transwell system and cultured for 24 h before co-culture with RGM-1 cells. Just prior to co-culture, PD-MSCs were washed with PBS three times and co-cultured with RGM-1 in the RGM-1 cell culture medium.

H. pylori Culture

H. pylori strain ATCC43504 (American Type Culture Collection, *cag*A+ and *vac*A s1-m1 type strain) was used for the *in vitro* cell model and Sydney strain (SS1, a *cag*A+ and *vac*A s2-m2 strain adapted for mice infection) for the *in vivo* model. *H. pylori* bacteria (**Figure 1A** and **Figure 4A**) were cultured at 37°C in a BBL Trypticase soy (TS) agar plate with 5% sheep blood (TSAII; BD Biosciences, Franklin Lakes, NJ) under microaerophilic conditions (BD GasPaK EZ Gas Generating Systems, BD Biosciences) for 3 days. The bacteria were harvested in clean TS broth, centrifuged at 3,000×*g* for 5 min, and resuspended in the broth at a final concentration of 10^9 colony-forming units (CFUs)/ml. In all experiments, cultures grown for 72 h on TS agar plates were used.

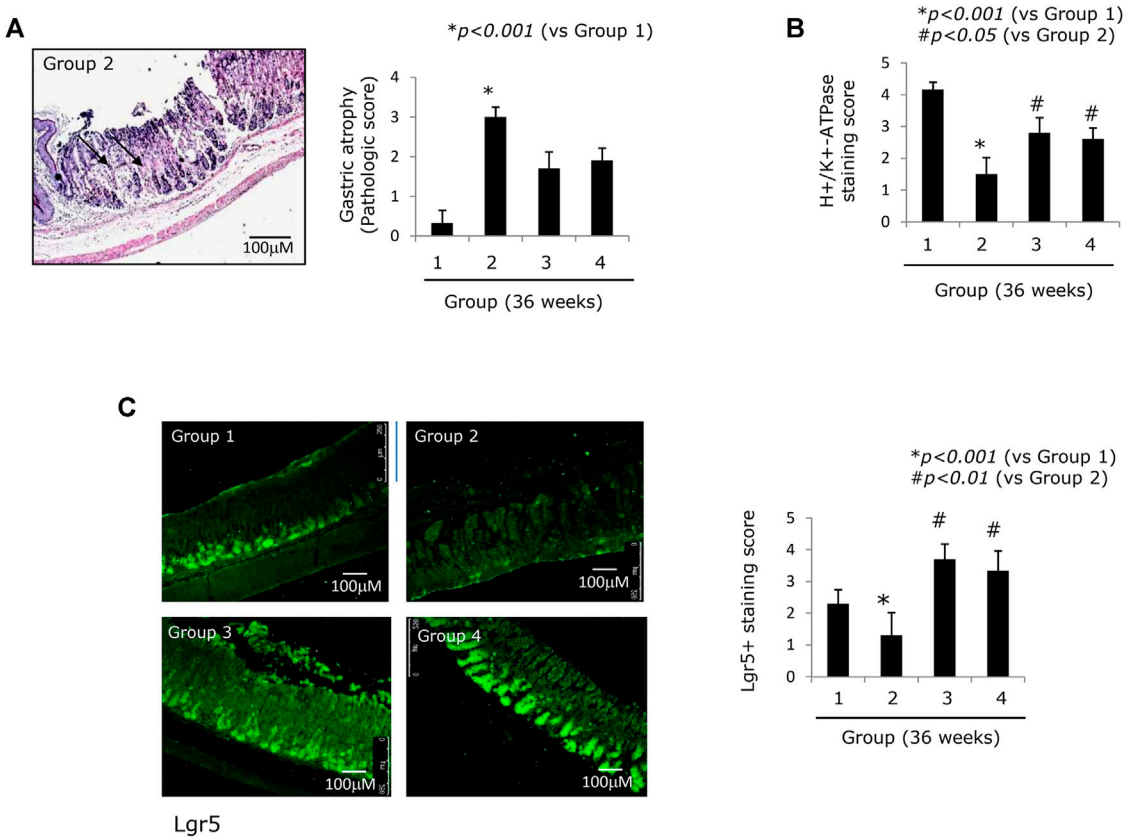

Figure 2. | (Continued).

Animals and Study Protocol: Experimental Protocol of *H. pylori*–Infected Mice Model

Five-week-old male C57BL/6 mice (WT mice) were purchased from Orient (Seoul, Korea), and they were housed in a cage maintained in a 12 h/12 h light/dark cycle under specific-pathogen-free conditions (n = 50). C57BL/6 mice were purchase from Central Lab Animal Inc. (Seoul, Korea). Six-week-old female C57BL/6 mice were fed sterilized commercial pellet diets (Biogenomics, Seoul, South Korea) and sterile water *ad libitum* and housed in an air-conditioned biohazard room at a temperature of 24°C. We divided 50 mice into four groups: Group 1 (n = 10), WT mice in the vehicle control group; Group 2 (n = 20), WT mice in the *H. pylori*–infected disease control group; Group 3 (n = 10), WT mice in the *H. pylori*–infected disease group administered $1x10^7$/100 ml PD-MSCs; and Group 4 (n = 10), WT mice in the *H. pylori*–infected disease group administered CM obtained from PD-MSCs, 100 μl concentrated from PD-MSC culture. We maintained these four groups up to 36 weeks, respectively. All groups were given intraperitoneal injections of pantoprazole, 20 mg/kg (Amore-Pacific Pharma, Seoul, Korea), as the proton pump inhibitor (PPI), three times per week, to increase successful *H. pylori* colonization through lowered gastric acidity, and then, each mouse was intragastrically inoculated with a suspension of *H. pylori* containing 10^8 CFUs/ml or with an equal volume (100 μl) of clean TS broth using gastric intubation needles. The *H. pylori*–infected mice were fed a special pellet diet based on AIN-46A containing 7.5% NaCl (high-salt diet, Biogenomics, Seongnam, Korea) for a total of 36 weeks (**Figure 1A** and **Figure 4A**) to promote the *H. pylori*–induced carcinogenic process in all infected animals. Randomized groups of mice (n = 10) were sacrificed after 36 weeks of *H. pylori* infection, respectively, based on our previous experience that CAG was generated at 24 weeks and gastric tumorigenesis was generated after 36 weeks (Park et al., 2014). The body weight was checked in all mice every 3 days up to observational periods. The stomachs of mice were opened along the greater curvature and washed with ice-cold PBS. The numbers of either erosions/ulcers or protruded nodule/mass were determined under the magnified photographs (**Figure 1C**). Stomachs were isolated and subjected to histologic examination, ELISA, western blotting, and RT-PCR. All animal studies were carried out in accordance with protocols approved by the Institutional Animal Care and Use Committee (IACUC) of CHA University, CHA Cancer Institute, after IRB approval (IRB 17-0901).

Statistical Analysis

The results are expressed as mean (standard deviation (SD)). Statistical analyses were conducted with GraphPad Prism (GraphPad Software, La Jolla, CA) and SPSS software (version 12.0; SPSS Inc., Chicago, IL). Statistical significance between groups was determined by a multi-variate Kruskal–Wallis test. Statistical significance was accepted at $p < 0.05$.

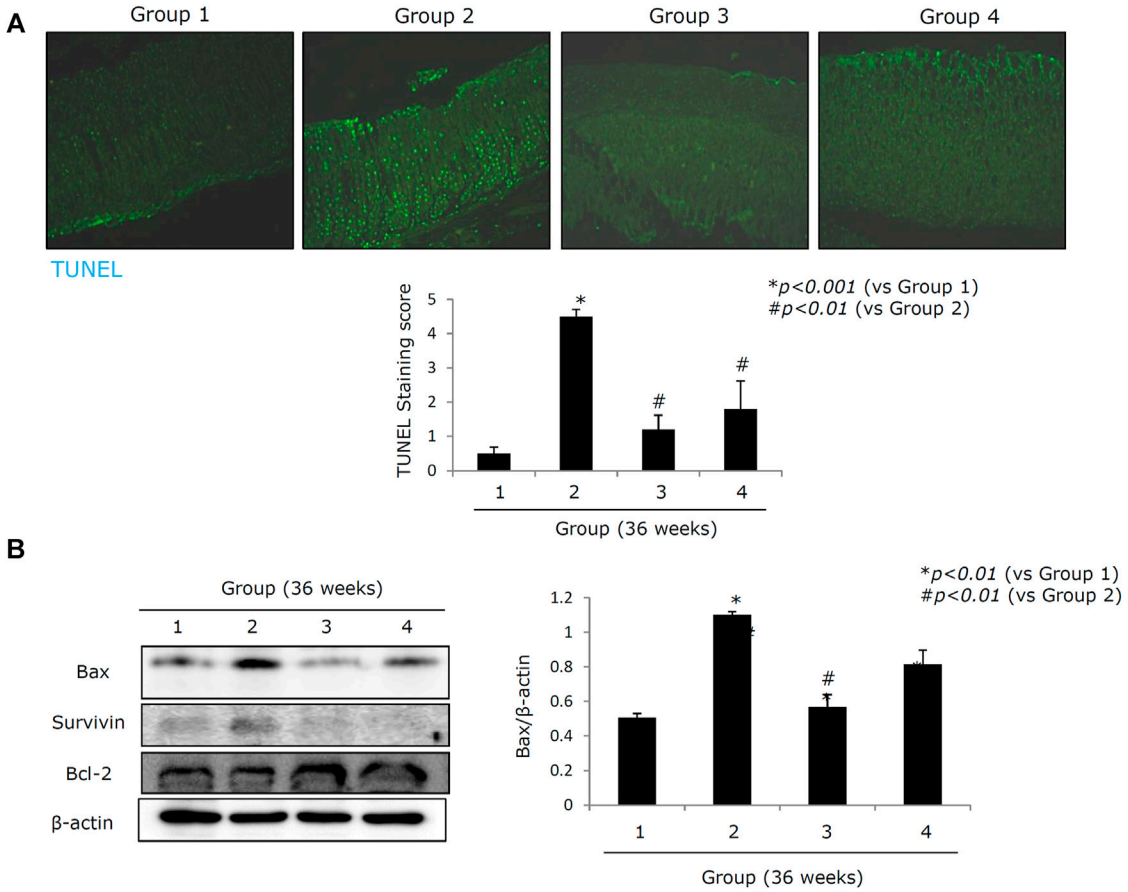

FIGURE 3 | Apoptotic status according to groups. **(A)** TUNEL staining with apoptotic index according to groups, x100 magnification. **(B)** Western blot for apoptotic executors, Bax, surviving, and Bcl-2. **(C)** Changes of RGM-1 cells' viability after *H. pylori* infection in a different time point and different POI in a transwell co-culture system. Cell counting using a hemocytometer and trypan blue for measuring cell viability was done after 24 hr of *H. pylori* infection in the absence or presence of PD-MSCs. **(D)** Western blot for apoptotic executors in the presence or absence of PD-MSCs under *H. pylori* infection, 100 MOI, 24 hr. **(E)** Western blot for autophagy, Beclin1, cleaved Beclin1, ATG5, and LC3B in the presence or absence of PD-MSCs under *H. pylori* infection, 100 MOI, 24 hr. **(F)** Confocal imaging of LC3B after CM administration. **(G)** Cell viability after PD-MSCs in the presence of *H. pylori* infection in mock cells and LC3B siRNA transfection. All data represent mean ± SD (n = 10).

Supplementary Information

Detailed experimental procedures for gross lesion index, index of histopathologic injury, immunohistochemical staining, terminal deoxynucleotidyl transferase–mediated dUTP nick-end labeling (TUNEL) staining, RT-PCR, western blotting, cytokine protein array, preparation of cytosolic and nuclear extracts, RNA interference, zymography, bacterial DNA extraction from mouse stool samples, bacterial metagenomic analysis using DNA from stool samples, and analysis of bacterial composition in the microbiota can be found in the Supplementary Materials.

RESULTS

Placenta-Derived Mesenchymal Stem Cells (PD-MSCs) or Their Conditioned Medium Ameliorates *H. pylori*–Associated CAG

Since we already have an established *H. pylori*–induced CAG mouse, which relies on an *H. pylori* infection–initiated, high-salt diet–promoted mouse model (Nam et al., 2004a; Nam et al., 2004b; Park et al., 2014; Jeong et al., 2015; Han et al., 2016; An et al., 2019), we went on to design this experiment to document the ameliorating action of PD-MSCs or their conditioned medium (CM) against *H. pylori*–induced CAG. We administered ten doses of PD-MSCs or their CM following 22 weeks of *H. pylori* infection and then evaluated these animals over a nine-week period until they were terminated for end point analysis at 36 weeks (**Figure 1A**). Our CAG model was initiated following four PPI injections, which facilitates the successful colonization of *H. pylori* in the lowered gastric pH and of cultured *H. pylori* into mice who were then fed a 7.5% salt AIN-76A pellet diet until 20–24 weeks, when the control mice (Group 2) showed significant changes in CAG, manifested with erosions, ulcers, and a very thin atrophied gastric wall (**Figure 1C**). To encourage the rejuvenating effects of the PD-MSCs (1×10^7/100 µl PD-MSCs, Group 3) or their concentrated CM (100 µl, concentrated from PD-MSC culture), they were were administered to groups of mice via the *oral* route approximately 10 times before the mice were

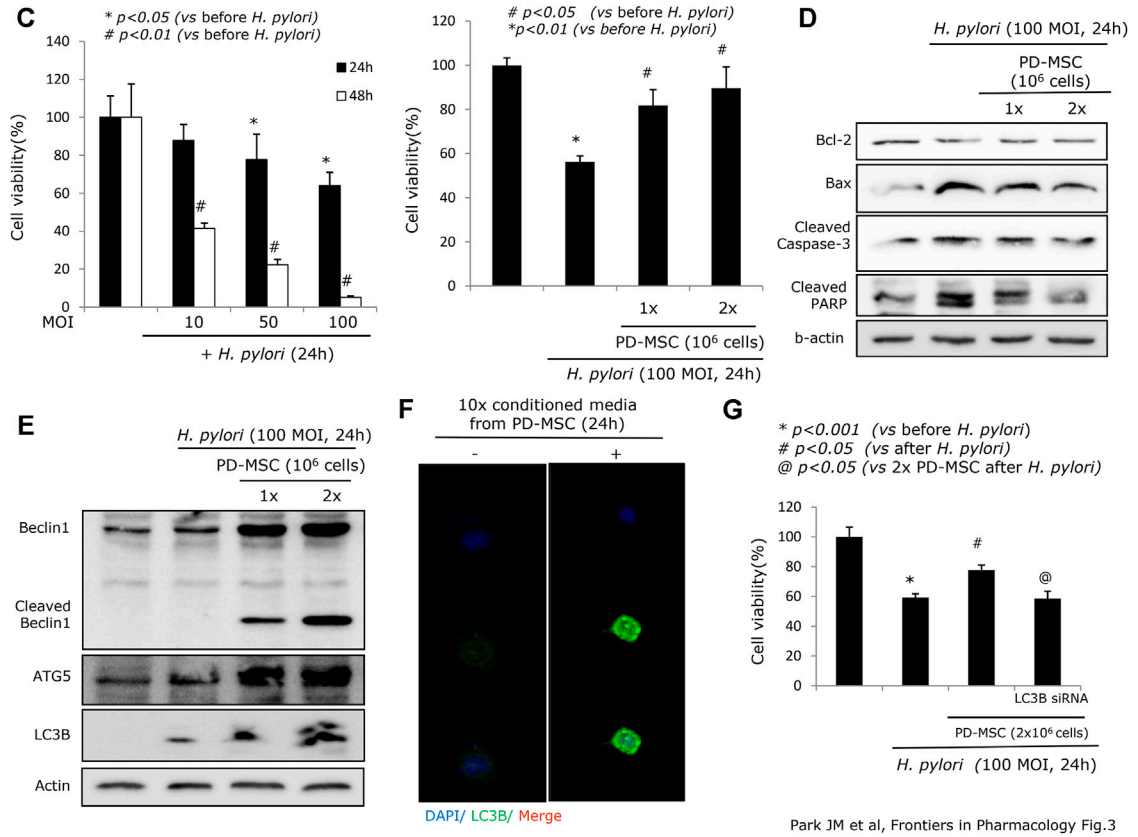

Figure 3. | (Continued).

sacrificed at 36 weeks and subjected to histological examination. In addition, each mouse was evaluated for body weight over the total course of treatment as this is an effective marker for atrophic gastritis. **Figure 1B** clearly shows that the mean body weights of the *H. pylori* control mice significantly decreased between week 24 and the end point of the experiment ($p < 0.01$), while there were no significant changes in body weight in the groups treated with PD-MSCs or their CM. There were also significant changes in the gross lesions of the stomach in the control animals at 36 weeks, with these animals presenting with multiple scattered nodular and elevated mass-like lesions, thinned corpus and pylorus walls, and some scattered nodular changes, signifying the development of typical CAG. The gross lesion index revealed that there were significant changes in the *H. pylori*–infected stomach and that intervention with PD-MSCs or their concentrated CM ($p < 0.01$) significantly ameliorated the severity of these lesions (**Supplementary Table 1**; Group 4, $p < 0.01$, **Figure 1C**). The resected stomachs from each group were also subjected to pathological evaluation, and the total pathological scores describing gastric inflammation, gastric atrophy, and tumorigenesis were significantly decreased in the PD-MSC–treated group compared to the control group (**Supplementary Table 2**; $p < 0.001$, **Figure 1D**). Gastric atrophy is generally associated with a loss of parietal cells and gastric glands and increased inflammatory cell infiltration. Our evaluations revealed that Group 2 demonstrated a typical increase in these parameters ($p < 0.001$), but that intervention with PD-MSCs or their CM significantly ameliorated these effects ($p < 0.05$, **Figure 2A**; **Supplementary Figure 1A**). Further investigation of the proton pump in the parietal cells, analyzed via immunostaining of H^+/K^+-ATPase, revealed a significant decrease in its expression in the control group ($p < 0.01$) but an increase in its expression in Groups 3 and 4 ($p < 0.05$, **Figure 2B**; **Supplementary Figure 1B**). These results suggest that PD-MSCs and their CM exert a significant mitigating effect on *H. pylori*–induced CAG.

Mitigated CAG in Response to PD-MSC Treatment Is Closely Associated With an Enrichment in the Number of Lgr5+ Cells

Lgr5+ cells have been identified as a possible source of stemness in the stomach (Hata et al., 2018; Sigal et al., 2019; Tang et al., 2019). **Figure 2C** shows that the expression of Lgr5+ was significantly decreased in Group 2 ($p < 0.05$, **Figure 2C**) and that there was a loss of leucine-rich repeat-containing G-protein–coupled receptor 5+ (Lgr5+) cells following chronic *H. pylori* infection. On the contrary, this trend was reversed following treatment with either PD-MSCs or their CM ($p < 0.01$, **Figure 2C**). Ki-

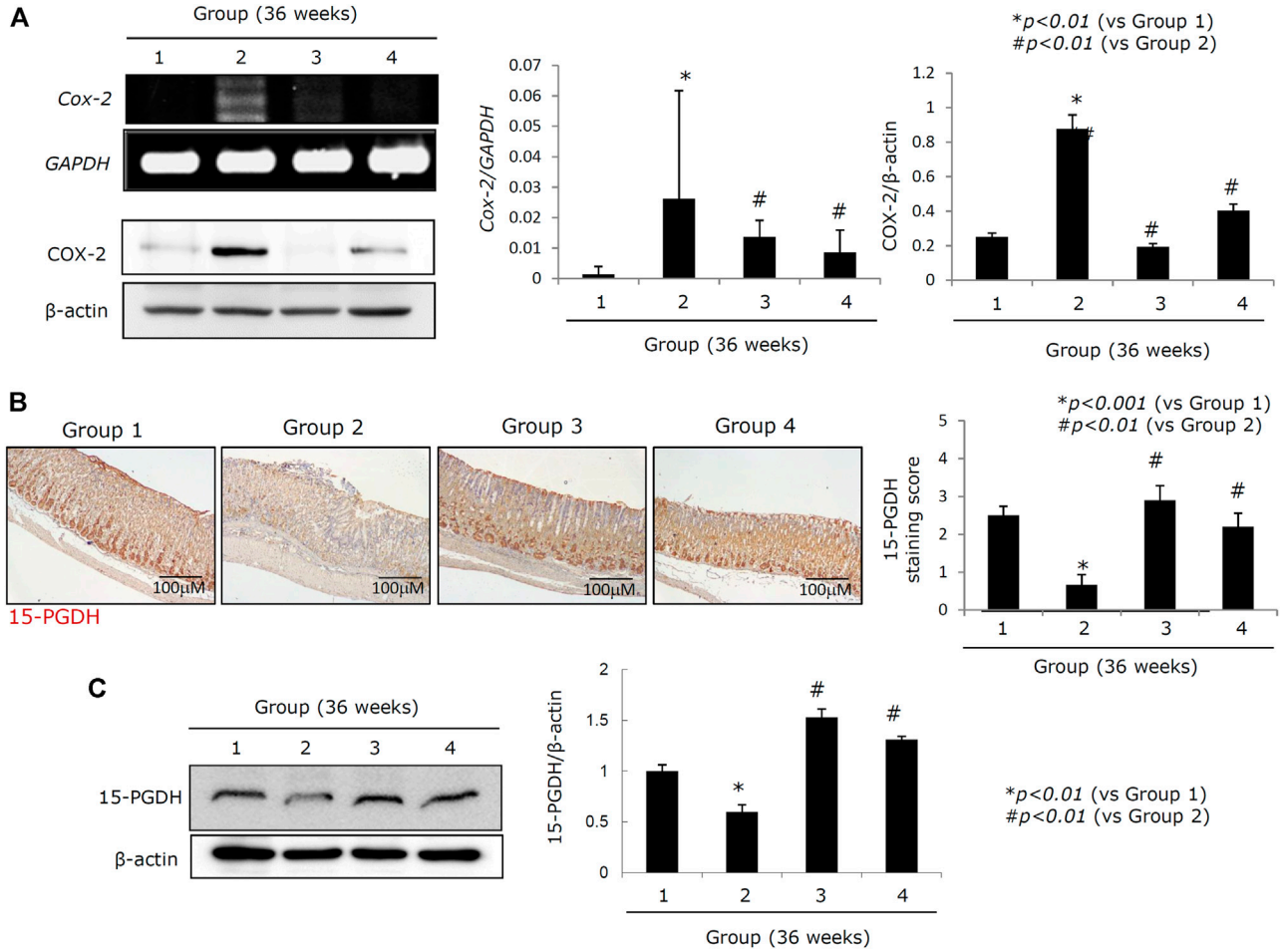

FIGURE 4 | Changes of COX-2 and 15-PGDH according to groups. **(A)** RT-PCR for *COX-2* mRNA and western blot for COX-2. **(B)** Left: immunohistochemical staining for 15-PGDH, x100 magnification; right: mean expressions according to groups. **(C)** Western blot for 15-PGDH. All data represent mean ± SD (n = 10).

67–mediated evaluation of cellular proliferation revealed that there were significantly fewer Ki-67 cells in the control group when compared to the healthy control. However, Groups 3 and 4 showed significant increases in Ki-67 expression ($p < 0.01$, **Figure 2D**; **Supplementary Figure 1C**). Musashi-1 expression in the stomach reflects stemness. Musashi-1 expression was increased in Groups 3 and 4 ($p < 0.05$, **Figure 2E**). In addition, the expressions of cyclin A, cyclin E, p-ERK, and smad2/3, which are all implicated in the pathogenesis of *H. pylori*–associated CAG, were evaluated in response to treatment with PD-MSCs or their CM. PD-MSCs significantly increased cyclin E expression, and PD-MSCs and their concentrated CM significantly decreased cell growth suppressive *smad*2/3 expression (**Figure 2F**; **Supplementary Figure 2**). The expression of *PDGF* mRNA in the resected stomach tissues was significantly increased in response to treatment with either PD-MSCs or their concentrated CM. The expression of HGF mRNA was increased in response to treatment with PD-MSCs (**Figure 2G**).

PD-MSC Treatment Induces Preemptive Amelioration of Apoptosis and Protease Inhibition Alleviating CAG in the Mouse Model

Chronic *H. pylori* infection induces considerable levels of apoptosis, a loss of parietal cells in the corpus, decreased somatostatin-secreting D cells in the antrum, and robust apoptosis in the epithelial cells, which are responsible for atrophic gastritis, peptic ulcer disease, and mucosal erosions (Alzahrani et al., 2014; Zhao et al., 2020). **Figure 3A** shows that 36 weeks of chronic *H. pylori* infection led to considerable levels of apoptosis ($p < 0.001$). However, animals treated with PD-MSCs showed significantly decreased levels of apoptosis, even during chronic *H. pylori* infection ($p < 0.01$, **Figure 3A**). Western blot against the central apoptosis-related molecules showed a significant increase in Bax in response to CAG conditions (Group 2). However, the levels of Bcl-2 were significantly increased and Bax was significantly decreased in Group 3 ($p < 0.05$, **Figure 3B**). Given this, we extended our investigation to include an exploration of the anti-apoptotic

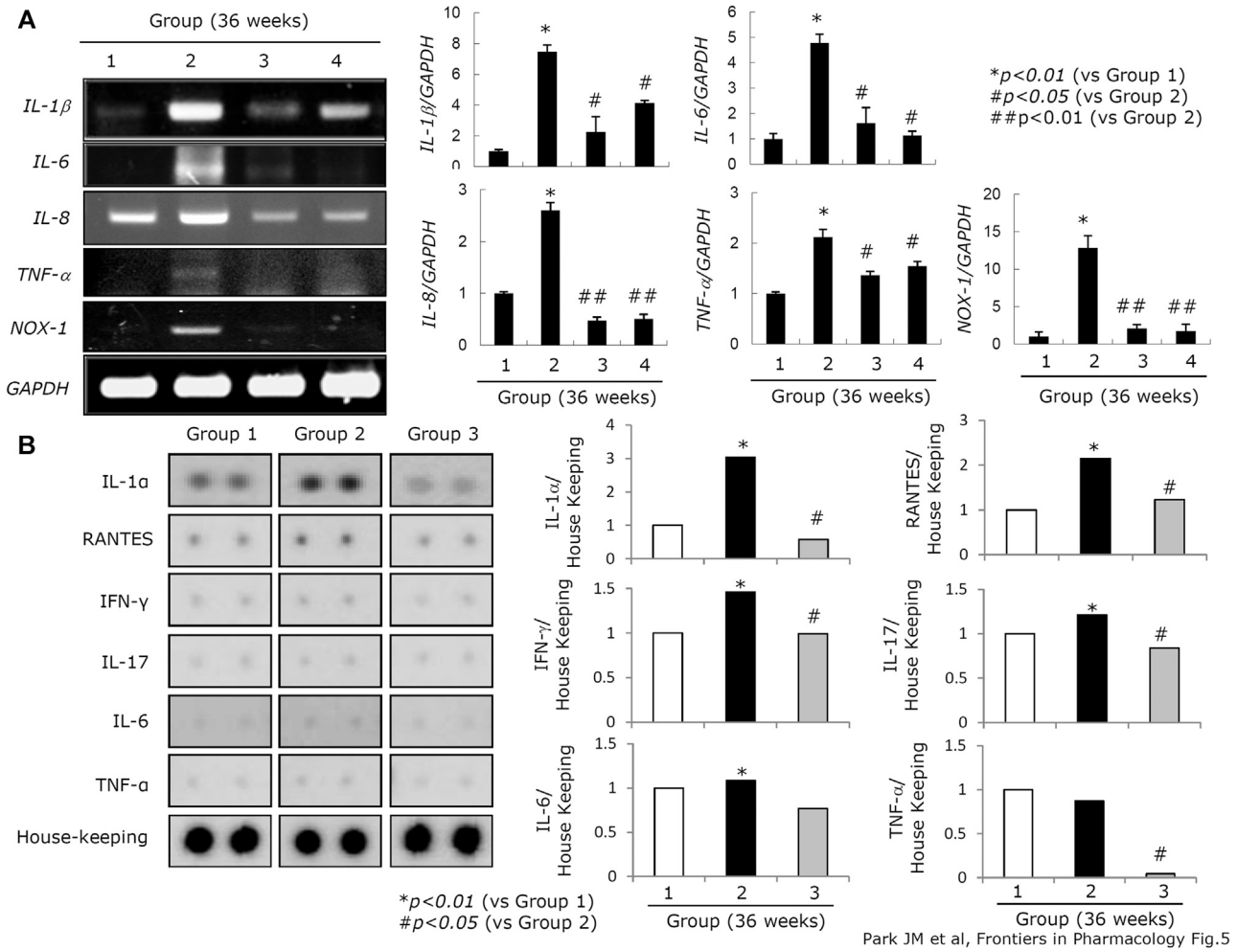

FIGURE 5 | Changes of inflammatory mediators according to groups. **(A)** Left: RT-PCR for *IL-1β*, *IL-6*, *IL-8*, *TNF-α*, and *NOX-1* according to groups; right: mean expressions according to inflammatory genes. **(B)** Left: protein array for inflammatory proteins including IL-1α, RANTES, IFN-γ, IL-17, IL-6, and TNF-α; right: mean changes of individual inflammatory proteins on the protein array panel. **(C)** Western blot for p-NF-κB p65 and p-STAT3. **(D)** Immunohistochemical staining for NF-κB p65 according to groups. **(E)** Immunohistochemical staining for F4/80 denoting the status of macrophages according to groups, x100 magnification. All data represent mean ± SD (n = 10).

effects of PD-MSCs using a transwell co-culture system. **Figures 3C,D** demonstrate that *H. pylori* infection significantly decreased RGM-1 cell viability, while the addition of PD-MSCs significantly decreased the expression of *H. pylori*–induced apoptotic executors. Further evaluations of the autophagy response in cells treated with PD-MSCs or their CM demonstrated that there was a significant increase in LC3B-II and ATG5 autophagosomes (**Figures 3E,F**; **Supplementary Figure 3**) and that this increase was lost in response to LC3B siRNAs (**Figure 3G**).

PD-MSC–Mediated Preservation of 15-PGDH Afforded These Treatments' Anti-Tumorigenic Effects and Alleviated CAG

Increased expression of COX-2 is known to be responsible for perpetuated gastric inflammation and gastric carcinogenesis in chronic *H. pylori* infections (Resende et al., 2011; Thiel et al., 2011; Cheng and Fan, 2013; Echizen et al., 2016). When we measured *COX-2* mRNA and COX-2 protein expressions (**Figure 4A**), we noted a significant increase in both *COX-2* mRNA and COX-2 protein in Group 2 ($p < 0.001$). However, COX-2 expression was significantly decreased in both Groups 3 and 4 ($p < 0.01$, **Figure 4A**). COX induction can lead to an increase in 15-PGDH as part of the hormetic response designed to retain homeostasis. Expression of 15-PGDH is known to exert some tumor suppressive effects and has been linked to reducing tumorigenesis in response to *H. pylori*–mediated CAG. However, the mean expression of 15-PGDH in Group 2 was significantly lower than that in Group 1 ($p < 0.01$; **Figure 4B**), while 15-PGDH levels were significantly increased in Groups 3 and 4 compared to Group 2 ($p < 0.05$, **Figure 4B**). The results of the immunohistochemical staining of 15-PGDH were further confirmed by western blot against this protein in each group ($p < 0.01$, **Figure 4C**).

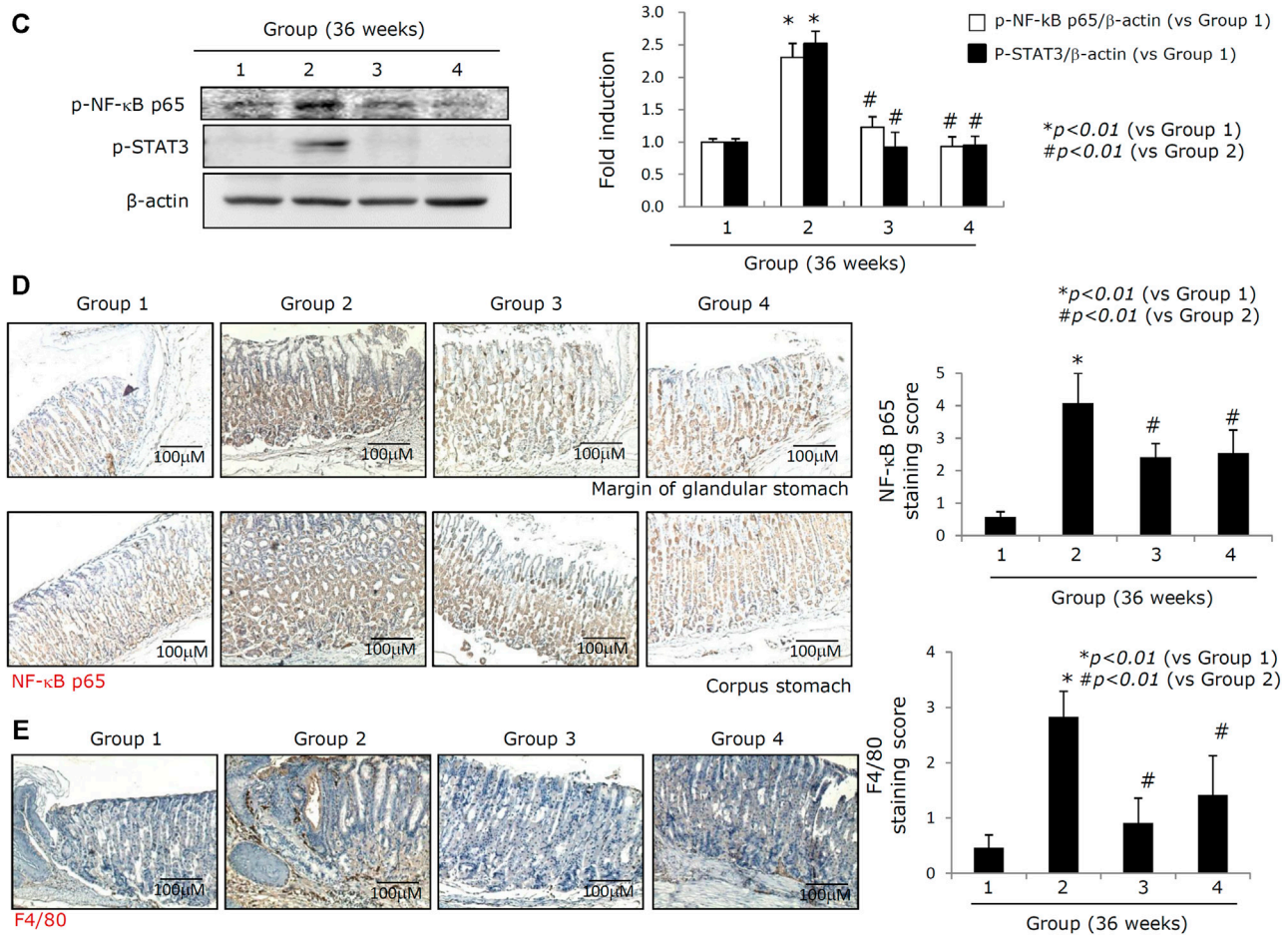

Figure 5. | (Continued).

PD-MSCs Exert an Anti-Inflammatory Effect Which Lowers Mutagenic Inflammation and Counteracts *H. pylori*–Induced Atrophy

Oncogenic perpetuated gastric inflammation following *H. pylori* infection is the root cause of both CAG and gastric carcinogenesis (Piazuelo et al., 2010; Kim E.-H. et al., 2011). The expressions of inflammatory mediators such as IL-1β, IL-6, IL-8, TNF-α, and NOX-1 were all significantly increased in Group 2. However, administration of either the PD-MSCs or their concentrated CM led to a significant decrease in the expression of these inflammatory mediators (**Figure 5**). In this experiment, a protein array comprising several cytokines and chemokines was compared between the groups. The expressions of IL-1β, RANTES, IFN-γ, IL-17, IL-6, and TNF-α were all significantly increased in Group 2, but their expressions were all consistently attenuated in Group 3, signifying the contribution of the PD-MSCs to both the anti-inflammatory and anti-mutagenesis responses (**Figure 5A**). The RT-PCR evaluating the expression of the inflammatory mediators was then validated using a protein array experiment (**Figure 5B**). NF-κB activation and STAT3 phosphorylation are known to be involved in the progression of gastric inflammation following *H. pylori* infection. When we compare the expression of NF-κB and the phosphorylation of STAT3 between the groups (**Figure 5C**), we observed a significant increase in the activation of NF-κB κ and STAT3 in Group 2 and that the addition of PD-MSCs or their CM reversed these effects almost entirely. Infiltrating macrophages are the primary source of these inflammatory mediators following transcriptional activation, and we examined the expression of NF-κB, p65, and F4/80 through immunohistochemical staining. **Figures 5C,D** show that the highest expression levels of NF-κB and F4/80 (**Figure 5E**) were seen in Group 2 and that their expression was significantly decreased in Groups 3 and 4 ($p < 0.01$).

Changes in the Activation and Expression of IL-10, IL-1β, and MMP Are All Critical in the Rejuvenation of CAG Tissues in Response to PD-MSC Treatment

Acute and chronic *H. pylori* infection leads to significant changes in atrophic gastritis (Correa and Piazuelo, 2008; Piazuelo et al., 2010; Correa and Piazuelo, 2011; Wroblewski et al., 2015), and *H.*

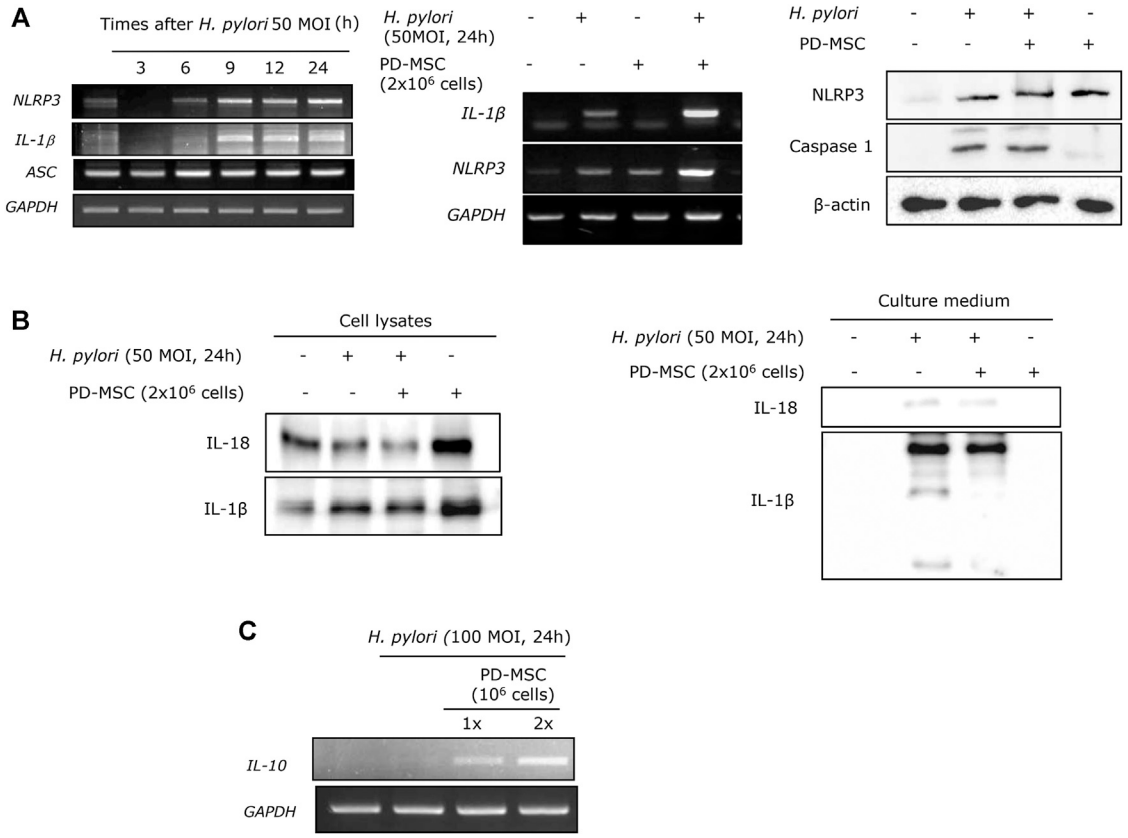

FIGURE 6 | Inflammasomes relevant to *H. pylori* infection and PD-MSC influence. **(A)** Left: RT-PCR for *NLRP3*, *IL-1β*, and *ASC*. RT-PCR for *IL-1β* and *NLRP3* mRNA was repeated in the presence of PD-MSCs in RGM-1 cells using a transwell co-culture system. Right: western blot for NLRP3 and caspase-1 in the presence of PD-MSCs. **(B)** Western blot for IL-1β and IL-18 in cell lysate and cultured media in the presence of PD-MSCs. **(C)** IL-10 expressions according to PD-MSC RT-PCR for IL-10 mRNA. **(D)** IL-1β expression under *H. pylori* in the presence of PD-MSCs. **(E)** Left: IL-1β fold changes under *H. pylori* in the presence of PD-MSCs; right: IL-1β ELISA levels under *H. pylori* in the presence of PD-MSCs. **(F)** Upper: RT-PCR for *MMP-2*; lower: zymography for MMP-2. **(G)** Protein array for MMP-2. All data represent mean ± SD (n = 10).

pylori infection is defined as a class I carcinogen. Although eradication of *H. pylori* and non-anti-microbial interventions have been evaluated in the prevention of gastric cancer, the data suggest that the rejuvenation of precancerous atrophic gastritis seems to be the best way to prevent malignancy. Homeostasis seems to be very important in achieving rejuvenation in these tissues, and we hypothesize that IL-10 and the regulation of the inflammasome are critical to the success of therapeutic interventions using PD-MSCs. *H. pylori* infection is associated with increased inflammasome activity (**Figure 6A**; **Supplementary Figure 4A**) as *H. pylori* infection leads to increased NOD, LRR, and pyrin domain–containing protein 3 (NLRP3) and IL-1β expressions. PD-MSCs significantly increased inflammasome activation in the presence of *H. pylori* infection in the transwell co-culture system. However, *H. pylori* infection led to a significant decrease in IL-1β/IL-18 activity, while the administration of PD-MSCs in the presence of *H. pylori* infection led to significant inhibition of IL-18 and IL-1β secretion (**Figure 6B**; **Supplementary Figure 4B**). Under these conditions, IL-10 mRNA expression was significantly induced in response to PD-MSCs (**Figure 6C**; **Supplementary Figure 4C**), and where IL-10 induction was not feasible, the inhibitory action of PD-MSCs on IL-1β was significantly reduced (**Figures 6D,E**). This suggests that the significant anti-inflammatory actions of PD-MSCs were largely reliant on the concerted activity of various mechanisms for maintaining homeostasis. These actions were further supported by the significant inhibitory action of PD-MSCs on MMP, as seen in **Figures 6F,G**, which revealed a significant attenuation in *H. pylori*–induced MMP activity in response to these cells. Activated proteases, especially matrix metalloprotease (MMP), have been implicated in the propagation and aggravation of gastritis and the development of CAG or ulcers. This is supported by the fact that the expressions of MMP-2 and MMP-2 activity are significantly increased in Group 2 ($p < 0.001$). The protein array revealed that the expression of TIMP-1 was significantly increased in Group 3 ($p < 0.001$, **Figure 6G**), and these results were validated by a significant decrease in the expression of *MMP-2* mRNA and MMP-2 activity in the RT-PCR and zymography assays (**Figure 6F**).

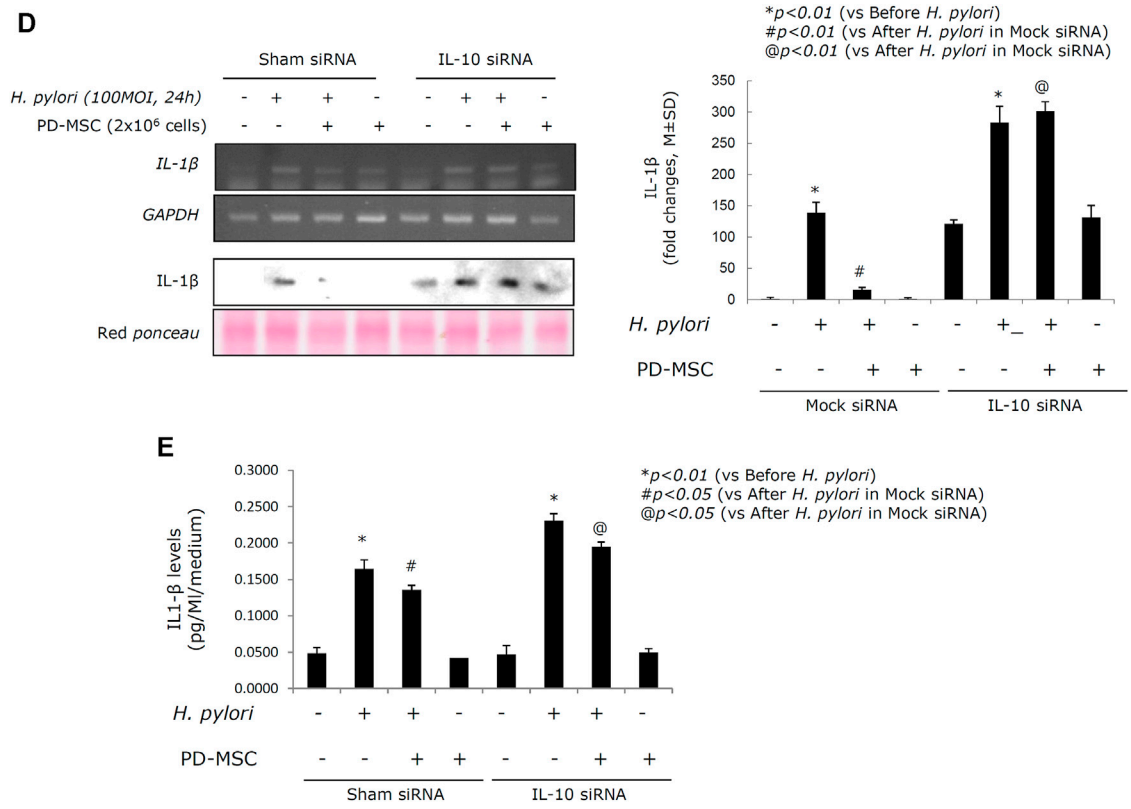

Figure 6. | (Continued).

Changes in the Microbiome Reflect the Rejuvenation of *H. pylori*–Associated Atrophic Gastritis in Response to PD-MSC Treatment

Changes in the microbiome in response to *H. pylori* infection are responsible for various gastric pathologies as bacterial overgrowth is closely associated with the changes in gastric atrophy and decreased gastric acidity (Huang et al., 2020; Lahner et al., 2020; Stewart et al., 2020; Ye et al., 2020). Although not clearly defined, overt changes in the intestinal microbiota do occur as the gastric pathology progresses toward atrophic gastritis. **Figure 7A** shows that the changes in the microbiota can be defined according to the group. Clear delineation was observed in PDA. Phylum analysis clearly showed that the phyla in Group 2 were quite different from those in Group 1 and Groups 3 and 4. Since the average gastric pathology was CAG, we speculated that the genera in Group 2 were also different from those in Group 1. However, Groups 3 and 4 showed a similar pattern to Group 1, suggesting that changes in CAG in Groups 3 and 4 might improve the community composition of the microbiome in these mice and facilitate their return to a more normal profile (**Figure 7B,C**). A detailed analysis of the genera in these samples (**Figure 7D**) revealed significant changes in the gastric microbiota in Group 2, but not in Groups 3 and 4 when compared to Group 1. The heatmap in **Figure 7E** and **Supplementary Table 3** summarize the detailed changes in the gastric microbiota of these animals. We concluded that the administration of PD-MSCs and their CM significantly rejuvenated *H. pylori*–associated CAG, leading to the expectation that MSCs can be used as potential cell therapeutics to reverse precancerous atrophic changes after chronic *H. pylori* infection.

DISCUSSION

This study sheds light on the potential of using PD-MSCs or their CM as therapeutics to rejuvenate precancerous atrophic gastritis in order to reduce pathogenic progression. In addition to the basic proliferative, restorative, anti-inflammatory, immunomodulatory, and regenerative effects of the MSCs, treatment with these agents induces the expression of LGR5+ (Mills and Shivdasani, 2011; Ye et al., 2018) and Musashi-1 (Murata et al., 2008) and promotes Ki-67–mediated proliferation (Kim et al., 2004) and anti-apoptotic effects while reducing NF-κB expression (Ralhan et al., 2009) and inhibiting oncogenic STAT3 expression (Balic et al., 2020). The application of PD-MSCs also promotes the cross-talk between the inflammasome and autophagy pathways and 15-PGDH in a chronic *H. pylori* infection model (Figure 8).

PD-MSCs have multiple properties, including strong self-renewal, multi-potent differentiation, immunomodulatory, anti-inflammatory, antioxidative, and regenerative capabilities

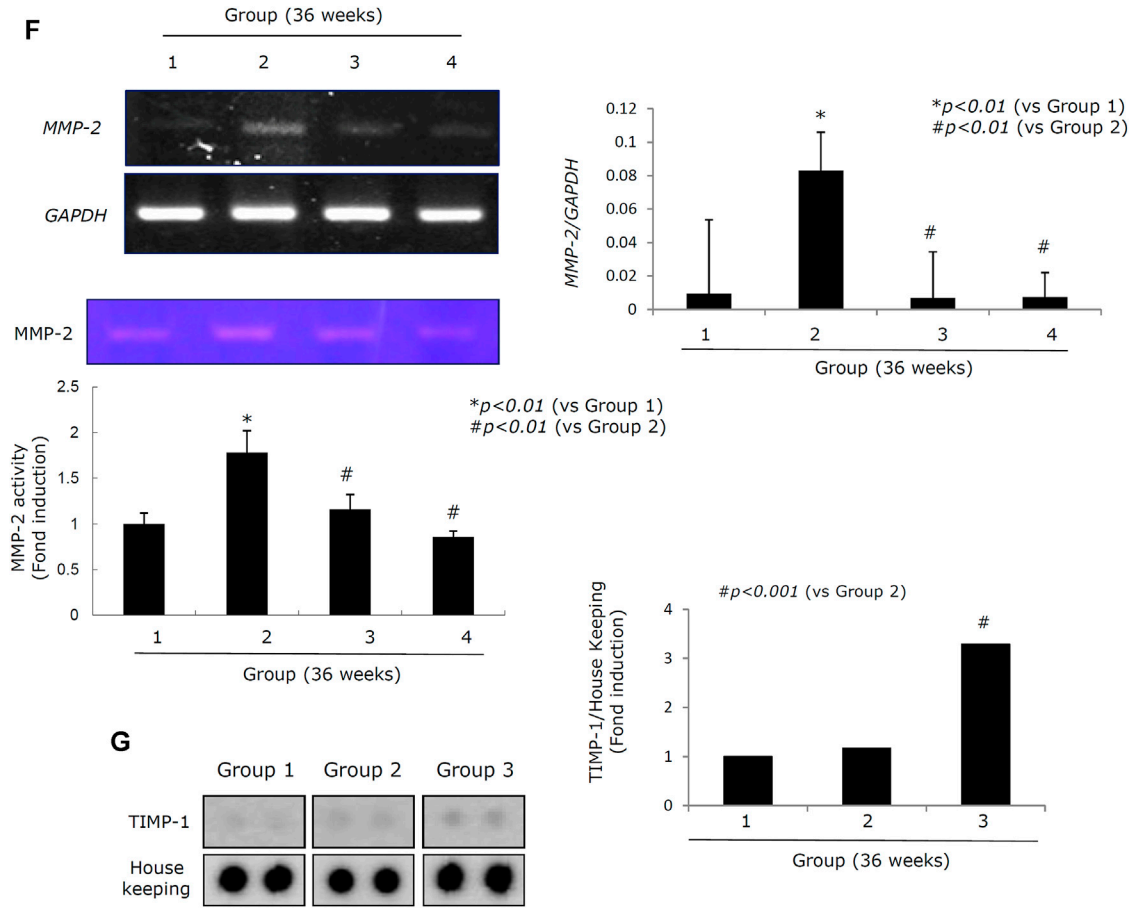

Figure 6. | (Continued).

(Kim M. J. et al., 2011; Seok et al., 2020a; Chou and Chen, 2020; Saleh et al., 2020; Yuan et al., 2020). Among the various types of MSCs, including umbilical cord–derived MSCs, chorionic plate–derived MSCs, adipose-derived MSCs, and bone marrow–derived MSCs, PD-MSCs are best known for their secretion of various cytokines, including growth factors such as G-CSF; regulated upon activation, normal T cell expressed and secreted (RANTES); and immunomodulators such as IL-6, IL-8, and IL-10, and have been linked to the effective treatment of various degenerative and destructive diseases (Lee et al., 2010; Lee et al., 2012; Jung et al., 2013; Munir et al., 2019; Seok et al., 2020b). The reasons why the MSCs have emerged among the most promising regenerative tools are closely linked to their multi-differentiation potential and immunosuppressive capacity. PD-MSCs are preferred within the MSC cohort because of their superior proliferation capacity, lower immunogenicity, and likely lower mutation rates than other kinds of MSCs originating from the amniotic membrane (AM), umbilical cord (UC), *decidua parietalis*, and chorionic plate (CP) (Wu et al., 2018; Chen et al., 2019; Guan et al., 2019; Ma et al., 2019).

Robust apoptosis after *H. pylori* infection is one of the core mechanisms responsible for atrophic gastritis (**Figures 3A,B**). Multiple studies have attempted to clarify the related autophagy mechanisms underlying apoptosis, clearing of damaged organelles, cell debris, and external pathogens needed to maintain the genomic integrity of cells, supply more energy, maintain cell or tissue homeostasis, inhibit endoplasmic reticulum (ER) stress, maintain ER function by degrading unfolded protein aggregates, and promote cell growth and proliferation in response to CAG (Lum et al., 2005; Karantza-Wadsworth et al., 2007; Hu et al., 2020). In **Figures 3E–G**, we clearly document the contribution of PD-MSCs to the protective actions of induced autophagy as part of relieving *H. pylori*–associated CAG for the first time, although multiple reports have revealed modulating autophagy as a primary mechanism in the protective effects of MSCs used to prevent hypoxia and ischemia or infection-induced post-injury toxicity in affected organs (Golpanian et al., 2016; Hu and Li, 2018; Hu et al., 2019; Zhang et al., 2019). Although the impacts of the autophagic processes are different, that is, protective against *H. pylori*, determining the intracellular fate of *H. pylori*, and carcinogenic in infected cells (Wang et al., 2009; Chu et al., 2010; Deen et al., 2013; Pott et al., 2018), our study clearly shows the therapeutic potential of autophagic processing of PD-MSCs at the CAG stage of gastric cancer lesion development.

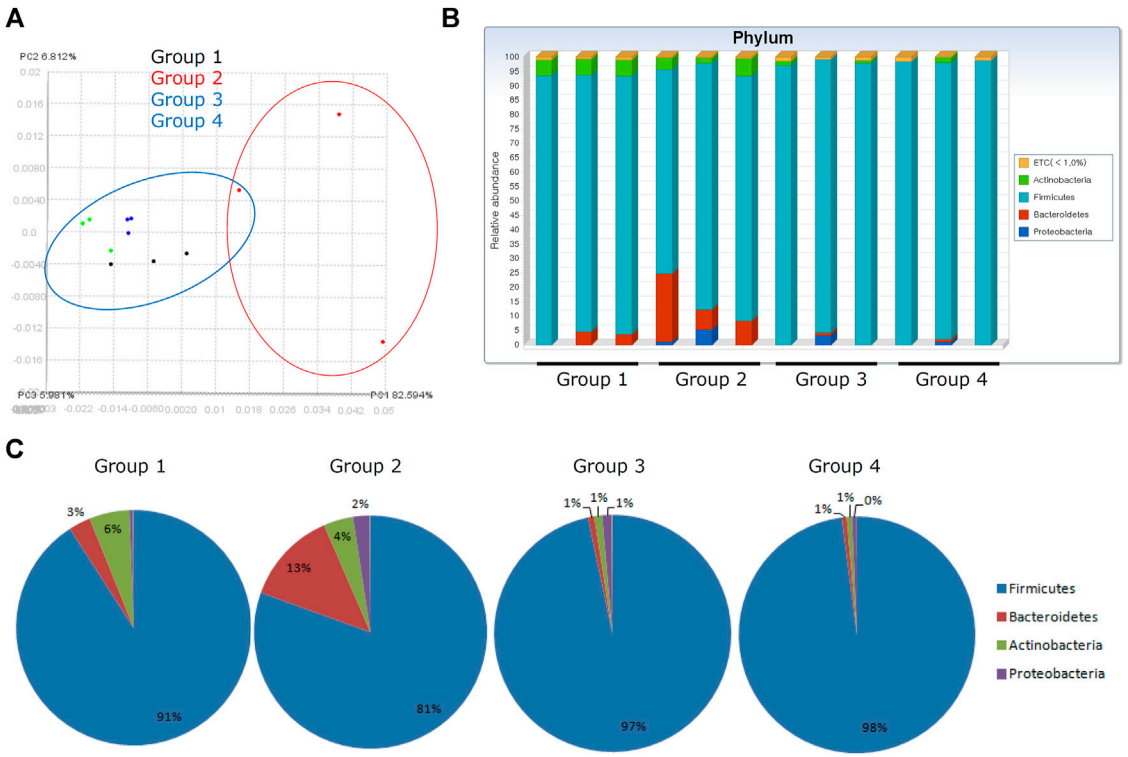

FIGURE 7 | Fecal microbiota changes according to groups. **(A)** Principal coordinate analysis (PCoA) showing definite discrimination of microbiota according to PD-MSC administration, that is, between PD-MSC–treated and non-treated groups under *H. pylori*–induced CAG. **(B)** Phyla changes showing bar display. **(C)** Phyla level change. **(D)** Genus level changes with bar display. **(E)** Heatmap with microbiota nomination.

In this study, PD-MSCs exerted a significant rejuvenating effect against *H. pylori*–induced atrophic gastritis by regulating the inflammasomes associated with autophagy induction and inducing a significant increase in anti-inflammatory IL-10 production (**Figure 6**). Cross-talk between the inflammasomes and the autophagy pathways plays an important role in intracellular homeostasis, inflammation, immunity, and pathology, after which the dysregulation of these processes is often associated with the pathogenesis of numerous cancers, including *H. pylori*–associated pro-tumor and gastric cancer (Chung et al., 2020). Inflammasomes are multi-protein complexes that assemble in the cytosol of cells upon detection of pathogen- or danger-associated molecular patterns (PAMP/DAMP) (Broz and Monack, 2011; Russo et al., 2018; Seveau et al., 2018). A critical outcome of inflammasome assembly is the activation of serine protease caspase-1, which activates the pro-inflammatory cytokine precursors pro-IL-1β and pro-IL-18, as shown in **Figure 6**. However, in the presence of *H. pylori* infection, PD-MSCs significantly inhibited secretion of IL-1β via their active secretion of anti-inflammatory IL-10.

The question of whether the reversal of gastric atrophy following *H. pylori* eradication is possible was not answered before 1998 (Domellof, 1998), but extensive evaluations, research, and nationwide trials in Japan have shown that it may be possible to repair the damage associated with *H. pylori* infection and prevent gastric cancer (Sugano et al., 2015; Tsuda et al., 2017; Choi et al., 2018; Choi et al., 2020). Furthermore, the non-microbial approach including the application of phytochemicals, probiotics, *n*-3 polyunsaturated fatty acids (*n*-3 PUFAs), walnut, and fermented kimchi (Chung and Hahm, 2010; Kim et al., 2010; Jeong et al., 2015; Lee et al., 2015; Park et al., 2015; Han et al., 2016; Jeong et al., 2016) can rejuvenate CAG. Given this success, this study was designed to evaluate the application of stem cells or their conditioned medium as candidates for clinically relevant therapeutic intervention in CAG and the downstream prevention of gastric cancer. We tried to apply stem cells at the atrophic gastritis stage as the above non-microbial approaches were usually implemented before CAG development and independent from *H. pylori* eradication (Oh et al., 2006; Giannakis et al., 2008; Kim, 2019).

Moreover, in this study, we reported that PD-MSCs induced more Lgr5+ cells, thereby facilitating the recovery from CAG induced by *H. pylori*. A stem cell niche includes both Wnt and BMP signaling pathways, and the balance between their signaling is important within the intestine. In our recent study, the Wnt signaling pathway has emerged as a potential regulator of self-renewal for intestinal stem cells by PD-MSCs (Han et al., 2017). Furthermore, induction of Wnt/β-catenin and growth factor signaling rescues liver dysfunction through the induction of Lgr5+ cells (Lin et al., 2017). PD-MSCs in the current study

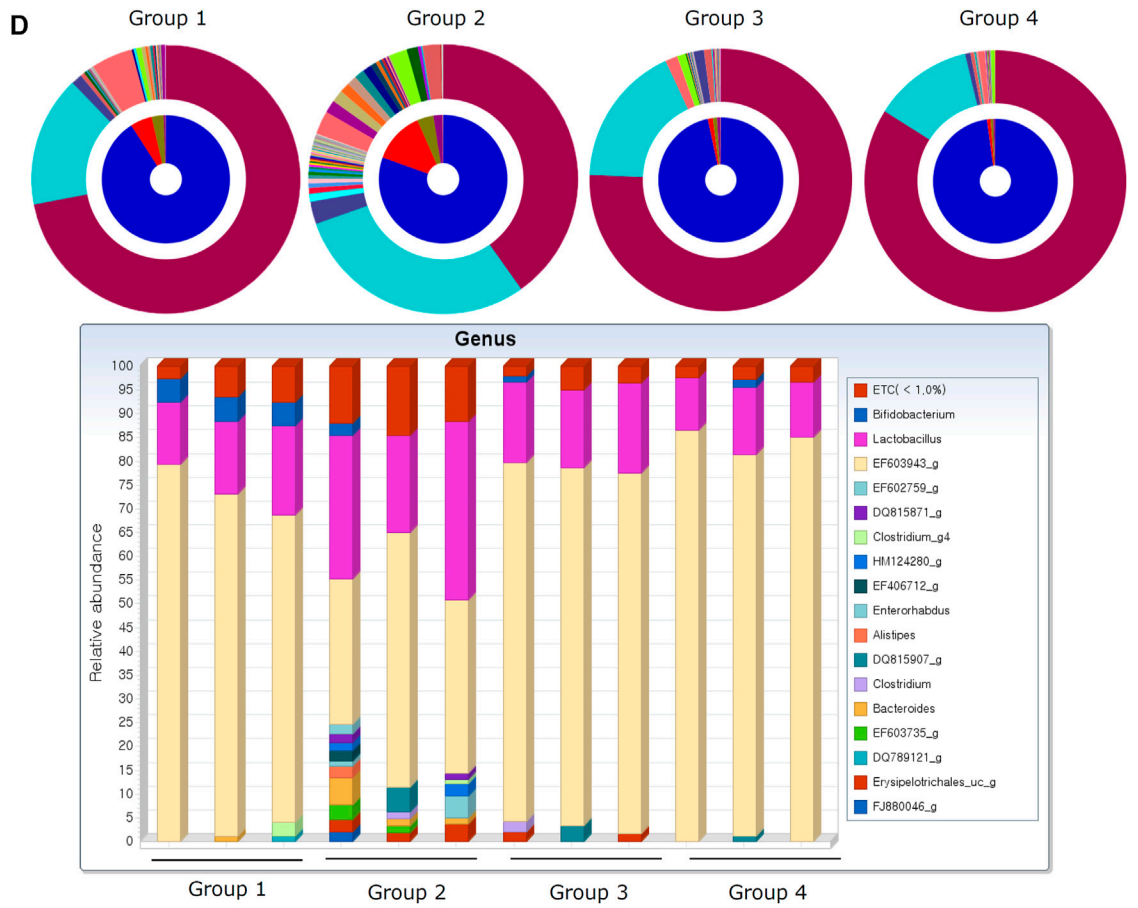

Figure 7. | (Continued).

faithfully contributed to the regeneration of the ulcerated tissue structure. PD-MSCs effectively enhanced or maintained the regeneration process along with significantly concerted actions of anti-inflammation, anti-apoptosis, and induction of autophagy and inflammasomes.

Lastly, this study revealed several interesting observations related to the fecal microbiome and its ability to reflect improvements in CAG associated with PD-MSC treatment. **Figure 7** clearly shows the changes in the distribution of the phyla and genera in each group, with significant changes in the composition of the microbiota noted in Group 2 when compared with that in Group 1, signifying a relationship between this microbiome and atrophic changes in the gastric tissues. However, these microbiome changes could be reversed following the application of either the PD-MSCs or their CM. Detailed microbiomes are presented in **Supplementary Table 3** and support our conclusion that PD-MSCs afforded some repair to the microenvironment producing one that is more favorable to supporting non-atrophic conditions. Although the exact changes in the gastric microbiome across stages of neoplastic progression remain poorly understood, the study by Wang *et al.*(Wang Z. et al., 2020) showed that the bacterial diversity and abundance of Armatimonadetes, Chloroflexi, Elusimicrobia, Nitrospirae, Planctomycetes, Verrucomicrobia, and WS3 decrease as atrophy progresses and Actinobacteria, *Bacteroides*, Firmicutes, Fusobacteria, SR1, and TM7 were enriched in the intestinal metaplasia (Coker et al., 2018; Park et al., 2019; Yu et al., 2020). The results of our fecal microbiota analysis according to therapeutic intervention to rejuvenate CAG increased the potential MSCs or their CM as therapeutics, similar to cosmetics for aged skin. Among the microbes in the stomach, *H. pylori* remains the single most important risk factor for gastric disease, its capacity to shape the collective gastric microbiota as well as its contribution to pathogenesis should be further elucidated (Rajilic-Stojanovic et al., 2020), and current results suggest a definite role for this pathogen in CAG since the addition of PD-MSCs significantly changed the fecal microbiome.

In this study, we have shown that oral administration of PD-MSCs or their CM rejuvenated the *H. pylori*–associated CAG by stimulation of gastric stem cells, induction of autophagy, inhibition of inflammation, and induction of inflammasomes. As a non-microbial approach for *H. pylori*–associated CAG, supplementation or treatment with

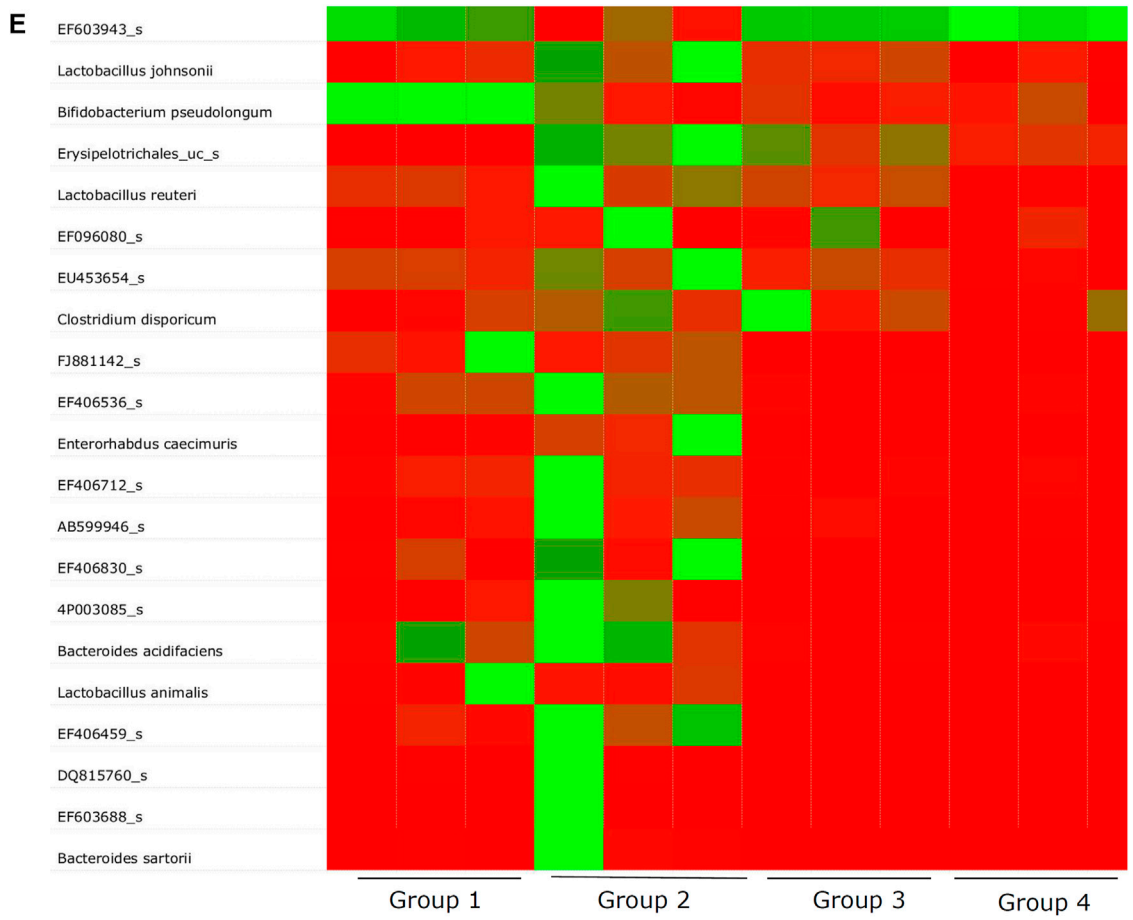

Figure 7. | (Continued).

long-term phytochemicals, antioxidants, and probiotics was proven to be very efficacious in the prevention of *H. pylori*–associated CAG and carcinogenesis. These treatment strategies were supported by anti-inflammation and cytoprotection activities by targeting small molecules or regulating signaling cascades. Although MSC administration has a significant inhibitory effect on the inflammatory response, there remain problems in clinical trials of stem cell therapy, including embolism risk and immunogenic adverse effect. Therefore, a lot of studies have been conducted to know the effect and underlying mechanism of MSC–CM on inflammation-related diseases. Factors secreted by MSC have been reported to include inflammatory modulators such as transforming growth factor-β (TGF-β), TNF-stimulated gene-6 (TSG-6), prostaglandin E2 (PGE2), and hepatocyte growth factor (HGF). However, to the best of our knowledge, the effect of oral administration of MSCs and CM on inflammatory diseases has not yet been reported. The data obtained suggested the use of MSCs and CM to treat inflammatory diseases without any cell transplantation.

In conclusion, this study shows that the administration of PD-MSCs or their CM at the CAG stage can produce a significant rejuvenation of the gastric tissues and help to prevent or revert the *H. pylori*–induced pro-tumor conditions in these tissues. Our evaluations revealed several novel mechanisms facilitating these effects which add to the basic proliferative, self-renewal, and regenerative capability of these cells. PD-MSCs exerted inflammasomes/autophagy/15-PGDH induction/IL-10 induction (Figure 8). The next step is to evaluate these effects in careful clinical trials.

DATA AVAILABILITY STATEMENT

The datasets presented in this study can be found in online repositories. The names of the repository/repositories and accession number(s) can be found in the article/**Supplementary Material**.

ETHICS STATEMENT

The animal study was reviewed and approved by the Institutional Animal Care and Use Committee of CHA

University, CHA Bio Complex, after IRB approval (IACUC 2019-0601).

AUTHOR CONTRIBUTIONS

JP and KH conceptualized and designed the study and involved in data analysis and interpretation. JP and YH involved in collection and/or assembly of data. JP, YH, and KH wrote the manuscript. KH approved the final manuscript.

SUPPLEMENTARY MATERIAL

The Supplementary Material for this article can be found online at: https://www.frontiersin.org/articles/10.3389/fphar.2021.675443/full#supplementary-material

REFERENCES

Alzahrani, S., Lina, T. T., Gonzalez, J., Pinchuk, I. V., Beswick, E. J., and Reyes, V. E. (2014). Effect ofHelicobacter Pylorion Gastric Epithelial Cells. *World. J. Gasteroentrol.* 20 (36), 12767–12780. doi:10.3748/wjg.v20.i36.12767

An, J. M., Kang, E. A., Han, Y.-M., Oh, J. Y., Lee, D. Y., Choi, S. H., et al. (2019). Dietary Intake of Probiotic Kimchi Ameliorated IL-6-driven Cancer Cachexia. *J. Clin. Biochem. Nutr.* 65 (2), 109–117. doi:10.3164/jcbn.19-10

Balic, J. J., Saad, M. I., Dawson, R., West, A. J., McLeod, L., West, A. C., et al. (2020). Constitutive STAT3 Serine Phosphorylation Promotes Helicobacter-Mediated Gastric Disease. *Am. J. Pathol.* 190 (6), 1256–1270. doi:10.1016/j.ajpath.2020.01.021

Broz, P., and Monack, D. M. (2011). Molecular Mechanisms of Inflammasome Activation during Microbial Infections. *Immunol. Rev.* 243 (1), 174–190. doi:10.1111/j.1600-065X.2011.01041.x

Bunpetch, V., Wu, H., Zhang, S., and Ouyang, H. (2017). From "Bench to Bedside": Current Advancement on Large-Scale Production of Mesenchymal Stem Cells. *Stem Cell Develop.* 26 (22), 1662–1673. doi:10.1089/scd.2017.0104

Chen, H.-N., Wang, Z., Li, X., and Zhou, Z.-G. (2016). *Helicobacter pylori* Eradication Cannot Reduce the Risk of Gastric Cancer in Patients with Intestinal Metaplasia and Dysplasia: Evidence from a Meta-Analysis. *Gastric Cancer* 19 (1), 166–175. doi:10.1007/s10120-015-0462-7

Chen, L., Qu, J., Cheng, T., Chen, X., and Xiang, C. (2019). Menstrual Blood-Derived Stem Cells: toward Therapeutic Mechanisms, Novel Strategies, and Future Perspectives in the Treatment of Diseases. *Stem Cel Res Ther* 10 (1), 406. doi:10.1186/s13287-019-1503-7

Cheng, J., and Fan, X. M. (2013). Role of Cyclooxygenase-2 in Gastric Cancer Development and Progression. *World. J. Gasteroentrol.* 19 (42), 7361–7368. doi:10.3748/wjg.v19.i42.7361

Choi, I. J., Kim, C. G., Lee, J. Y., Kim, Y.-I., Kook, M.-C., Park, B., et al. (2020). Family History of Gastric Cancer and *Helicobacter pylori* Treatment. *N. Engl. J. Med.* 382 (5), 427–436. doi:10.1056/NEJMoa1909666

Choi, I. J., Kook, M.-C., Kim, Y.-I., Cho, S.-J., Lee, J. Y., Kim, C. G., et al. (2018). *Helicobacter pylori* Therapy for the Prevention of Metachronous Gastric Cancer. *N. Engl. J. Med.* 378 (12), 1085–1095. doi:10.1056/NEJMoa1708423

Chou, H.-C., and Chen, C.-M. (2020). Human Placenta-Derived Mesenchymal Stem Cells Attenuate Established Hyperoxia-Induced Lung Injury in Newborn Rats. *Pediatr. Neonatal.* 61, 498–505. doi:10.1016/j.pedneo.2020.05.012

Chu, Y.-T., Wang, Y.-H., Wu, J.-J., and Lei, H.-Y. (2010). Invasion and Multiplication of *Helicobacter pylori* in Gastric Epithelial Cells and Implications for Antibiotic Resistance. *Infect. Immun.* 78 (10), 4157–4165. doi:10.1128/IAI.00524-10

Chung, C., Seo, W., Silwal, P., and Jo, E.-K. (2020). Crosstalks between Inflammasome and Autophagy in Cancer. *J. Hematol. Oncol.* 13 (1), 100. doi:10.1186/s13045-020-00936-9

Chung, J.-W., and Hahm, K.-B. (2010). Rejuvenation of Atrophic Gastritis in the Elderly. *J. Gastroenterol. Hepatol.* 25 (3), 434–435. doi:10.1111/j.1440-1746.2010.06251.x

Coker, O. O., Dai, Z., Nie, Y., Zhao, G., Cao, L., Nakatsu, G., et al. (2018). Mucosal Microbiome Dysbiosis in Gastric Carcinogenesis. *Gut* 67 (6), 1024–1032. doi:10.1136/gutjnl-2017-314281

Correa, P., and Piazuelo, M. B. (2011). *Helicobacter pylori* Infection and Gastric Adenocarcinoma. *US Gastroenterol. Hepatol. Rev.* 7 (1), 59–64 .

Correa, P. (2013). Gastric Cancer. *Gastroenterol. Clin. North America* 42 (2), 211–217. doi:10.1016/j.gtc.2013.01.002

Correa, P., and Piazuelo, M. B. (2008). Natural History of *Helicobacter pylori* Infection. *Dig. Liver Dis.* 40 (7), 490–496. doi:10.1016/j.dld.2008.02.035

Correa, P., and Piazuelo, M. B. (2012). The Gastric Precancerous cascade. *J. Dig. Dis.* 13 (1), 2–9. doi:10.1111/j.1751-2980.2011.00550.x

de Vries, A. C., Haringsma, J., and Kuipers, E. J. (2007). The Detection, Surveillance and Treatment of Premalignant Gastric Lesions Related to *Helicobacter pylori* Infection. *Helicobacter* 12 (1), 1–15. doi:10.1111/j.1523-5378.2007.00475.x

Deen, N. S., Huang, S. J., Gong, L., Kwok, T., and Devenish, R. J. (2013). The Impact of Autophagic Processes on the Intracellular Fate ofHelicobacter Pylori. *Autophagy* 9 (5), 639–652. doi:10.4161/auto.23782

Domellöf, L. (1998). Reversal of Gastric Atrophy after *Helicobacter pylori* Eradication: Is it Possible or Not? *Am. J. Gastroenterol.* 93 (9), 1407–1408. doi:10.1111/j.1572-0241.1998.01407.x

Echizen, K., Hirose, O., Maeda, Y., and Oshima, M. (2016). Inflammation in Gastric Cancer: Interplay of the COX-2/prostaglandin E 2 and Toll-like receptor/MyD88 Pathways. *Cancer Sci.* 107 (4), 391–397. doi:10.1111/cas.12901

Giannakis, M., Chen, S. L., Karam, S. M., Engstrand, L., and Gordon, J. I. (2008). *Helicobacter pylori* Evolution during Progression from Chronic Atrophic Gastritis to Gastric Cancer and its Impact on Gastric Stem Cells. *Proc. Natl. Acad. Sci.* 105 (11), 4358–4363. doi:10.1073/pnas.0800668105

Golpanian, S., Wolf, A., Hatzistergos, K. E., and Hare, J. M. (2016). Rebuilding the Damaged Heart: Mesenchymal Stem Cells, Cell-Based Therapy, and Engineered Heart Tissue. *Physiol. Rev.* 96 (3), 1127–1168. doi:10.1152/physrev.00019.2015

Guan, Y. T., Xie, Y., Li, D. S., Zhu, Y. Y., Zhang, X. L., Feng, Y. L., et al. (2019). Comparison of Biological Characteristics of Mesenchymal Stem Cells Derived from the Human Umbilical Cord and Decidua Parietalis. *Mol. Med. Rep.* 20 (1), 633–639. doi:10.3892/mmr.2019.10286

Gumucio, D. L., Fagoonee, S., Qiao, X. T., Liebert, M., Merchant, J. L., Altruda, F., et al. (2008). Tissue Stem Cells and Cancer Stem Cells: Potential Implications for Gastric Cancer. *Panminerva Med.* 50 (1), 65–71.

Han, Y.-M., Kim, K.-J., Jeong, M., Park, J.-M., Go, E.-J., Kang, J. X., et al. (2016). Suppressed Helicobacter Pylori-Associated Gastric Tumorigenesis in Fat-1 Transgenic Mice Producing Endogenous ω-3 Polyunsaturated Fatty Acids. *Oncotarget* 7 (41), 66606–66622. doi:10.18632/oncotarget.11261

Han, Y.-M., Park, J.-M., Choi, Y. S., Jin, H., Lee, Y.-S., Han, N.-Y., et al. (2017). The Efficacy of Human Placenta-Derived Mesenchymal Stem Cells on Radiation Enteropathy along with Proteomic Biomarkers Predicting a Favorable Response. *Stem Cel Res Ther* 8 (1), 105. doi:10.1186/s13287-017-0559-5

Hata, M., Hayakawa, Y., and Koike, K. (2018). Gastric Stem Cell and Cellular Origin of Cancer. *Biomedicines* 6 (4), 100. doi:10.3390/biomedicines6040100

Hu, C., and Li, L. (2018). Preconditioning Influences Mesenchymal Stem Cell Properties *In Vitro* and *In Vivo*. *J. Cel. Mol. Med.* 22 (3), 1428–1442. doi:10.1111/jcmm.13492

Hu, C., Zhao, L., Shen, M., Wu, Z., and Li, L. (2020). Autophagy Regulation Is an Effective Strategy to Improve the Prognosis of Chemically Induced Acute Liver Injury Based on Experimental Studies. *J. Cel Mol Med* 24 (15), 8315–8325. doi:10.1111/jcmm.15565

Hu, C., Zhao, L., Wu, D., and Li, L. (2019). Modulating Autophagy in Mesenchymal Stem Cells Effectively Protects against Hypoxia- or Ischemia-Induced Injury. *Stem Cel Res Ther* 10 (1), 120. doi:10.1186/s13287-019-1225-x

Huang, R., Ju, Z., and Zhou, P.-K. (2020). A Gut Dysbiotic Microbiota-Based Hypothesis of Human-To-Human Transmission of Non-communicable Diseases. *Sci. Total Environ.* 745, 141030. doi:10.1016/j.scitotenv.2020.141030

Jeong, M., Park, J.-M., Han, Y.-M., Kangwan, N., Kwon, S.-O., Kim, B.-N., et al. (2016). Dietary Intervention ofArtemisiaand Green Tea Extracts to RejuvenateHelicobacter Pylori-Associated Chronic Atrophic Gastritis and to Prevent Tumorigenesis. *Helicobacter* 21 (1), 40–59. doi:10.1111/hel.12229

Jeong, M., Park, J.-M., Han, Y.-M., Park, K. Y., Lee, D. H., Yoo, J.-H., et al. (2015). Dietary Prevention of Helicobacter Pylori-Associated Gastric Cancer with Kimchi. *Oncotarget* 6 (30), 29513–29526. doi:10.18632/oncotarget.4897

Jung, J., Choi, J. H., Lee, Y., Park, J.-W., Oh, I.-H., Hwang, S.-G., et al. (2013). Human Placenta-Derived Mesenchymal Stem Cells Promote Hepatic Regeneration in CCl4-Injured Rat Liver Model via Increased Autophagic Mechanism. *Stem Cells* 31 (8), 1584–1596. doi:10.1002/stem.1396

Karantza-Wadsworth, V., Patel, S., Kravchuk, O., Chen, G., Mathew, R., Jin, S., et al. (2007). Autophagy Mitigates Metabolic Stress and Genome Damage in Mammary Tumorigenesis. *Genes Develop.* 21 (13), 1621–1635. doi:10.1101/gad.1565707

Kim, E.-H., Hong, K.-S., Hong, H., and Hahm, K. B. (2011a). Detouring the Undesired Route of Helicobacter Pylori-Induced Gastric Carcinogenesis. *Cancers* 3 (3), 3018–3028. doi:10.3390/cancers3033018

Kim, K. M., Oh, Y. L., Ko, J. S., Choe, Y. H., and Seo, J. K. (2004). Histopathology and Expression of Ki-67 and Cyclooxygenase-2 in Childhood *Helicobacter pylori* Gastritis. *J. Gastroenterol.* 39 (3), 231–237. doi:10.1007/s00535-003-1282-9

Kim, M. J., Shin, K. S., Jeon, J. H., Lee, D. R., Shim, S. H., Kim, J. K., et al. (2011b). Human Chorionic-Plate-Derived Mesenchymal Stem Cells and Wharton's Jelly-Derived Mesenchymal Stem Cells: a Comparative Analysis of Their Potential as Placenta-Derived Stem Cells. *Cell Tissue Res* 346 (1), 53–64. doi:10.1007/s00441-011-1249-8

Kim, N. (2019). Chemoprevention of Gastric Cancer byHelicobacter Pylorieradication and its Underlying Mechanism. *J. Gastroenterol. Hepatol.* 34 (8), 1287–1295. doi:10.1111/jgh.14646

Kim, Y. J., Chung, J. W., Lee, S. J., Choi, K. S., Kim, J. H., and Hahm, K. B. (2010). Progression from Chronic Atrophic Gastritis to Gastric Cancer; Tangle, Toggle, Tackle with Korea Red Ginseng. *J. Clin. Biochem. Nutr.* 46 (3), 195–204. doi:10.3164/jcbn.10-03

Kimbrel, E. A., and Lanza, R. (2020). Next-generation Stem Cells - Ushering in a new era of Cell-Based Therapies. *Nat. Rev. Drug Discov.* 19 (7), 463–479. doi:10.1038/s41573-020-0064-x

Koulis, A., Buckle, A., and Boussioutas, A. (2019). Premalignant Lesions and Gastric Cancer: Current Understanding. *World. J. Gasteroentrol. Oncol.* 11 (9), 665–678. doi:10.4251/wjgo.v11.i9.665

Lahner, E., Conti, L., Annibale, B., and Corleto, V. D. (2020). Current Perspectives in Atrophic Gastritis. *Curr. Gastroenterol. Rep.* 22 (8), 38. doi:10.1007/s11894-020-00775-1

Lee, J. M., Jung, J., Lee, H.-J., Jeong, S. J., Cho, K. J., Hwang, S.-G., et al. (2012). Comparison of Immunomodulatory Effects of Placenta Mesenchymal Stem Cells with Bone Marrow and Adipose Mesenchymal Stem Cells. *Int. Immunopharmacology* 13 (2), 219–224. doi:10.1016/j.intimp.2012.03.024

Lee, M.-J., Jung, J., Na, K.-H., Moon, J. S., Lee, H.-J., Kim, J.-H., et al. (2010). Anti-fibrotic Effect of Chorionic Plate-Derived Mesenchymal Stem Cells Isolated from Human Placenta in a Rat Model of CCl4-Injured Liver: Potential Application to the Treatment of Hepatic Diseases. *J. Cel. Biochem.* 111 (6), 1453–1463. doi:10.1002/jcb.22873

Lee, S. H., Park, J. M., Han, Y. M., Ko, W. J., and Hahm, K. B. (2015). Unpleasant Journey fromHelicobacter Pylori-Associated Gastritis to Gastric Cancer: Cancer Prevention by Taking a Detour. *Korean J. Gastroenterol.* 66 (6), 303–311. doi:10.4166/kjg.2015.66.6.303

Lin, Y., Fang, Z.-P., Liu, H.-J., Wang, L.-J., Cheng, Z., Tang, N., et al. (2017). HGF/R-spondin1 Rescues Liver Dysfunction through the Induction of Lgr5+ Liver Stem Cells. *Nat. Commun.* 8 (1), 1175. doi:10.1038/s41467-017-01341-6

Liu, K. S.-H., Wong, I. O., and Leung, W. K. (2016). Helicobacter Pyloriassociated Gastric Intestinal Metaplasia: Treatment and Surveillance. *World. J. Gasteroentrol.* 22 (3), 1311–1320. doi:10.3748/wjg.v22.i3.1311

Lu, X., and Zhao, T. (2013). Clinical Therapy Using iPSCs: Hopes and Challenges. *Genomics, Proteomics & Bioinformatics* 11 (5), 294–298. doi:10.1016/j.gpb.2013.09.002

Lum, J. J., Bauer, D. E., Kong, M., Harris, M. H., Li, C., Lindsten, T., et al. (2005). Growth Factor Regulation of Autophagy and Cell Survival in the Absence of Apoptosis. *Cell* 120 (2), 237–248. doi:10.1016/j.cell.2004.11.046

Ma, J., Wu, J., Han, L., Jiang, X., Yan, L., Hao, J., et al. (2019). Comparative Analysis of Mesenchymal Stem Cells Derived from Amniotic Membrane, Umbilical Cord, and Chorionic Plate under Serum-free Condition. *Stem Cel Res Ther* 10 (1), 19. doi:10.1186/s13287-018-1104-x

Maqsood, M., Kang, M., Wu, X., Chen, J., Teng, L., and Qiu, L. (2020). Adult Mesenchymal Stem Cells and Their Exosomes: Sources, Characteristics, and Application in Regenerative Medicine. *Life Sci.* 256, 118002. doi:10.1016/j.lfs.2020.118002

Mills, J. C., and Shivdasani, R. A. (2011). Gastric Epithelial Stem Cells. *Gastroenterology* 140 (2), 412–424. doi:10.1053/j.gastro.2010.12.001

Moss, S. F. (2017). The Clinical Evidence Linking *Helicobacter pylori* to Gastric Cancer. *Cell Mol. Gastroenterol. Hepatol.* 3 (2), 183–191. doi:10.1016/j.jcmgh.2016.12.001

Munir, F., Jamshed, M. B., Shahid, N., Muhammad, S. A., Ghanem, N. B., and Qiyu, Z. (2019). Current Status of Diagnosis and Mesenchymal Stem Cells Therapy for Acute Pancreatitis. *Physiol. Rep.* 7 (21), e14170. doi:10.14814/phy2.14170

Murata, H., Tsuji, S., Tsujii, M., Nakamura, T., Fu, H. Y., Eguchi, H., et al. (2008). *Helicobacter pylori* Infection Induces Candidate Stem Cell Marker Musashi-1 in the Human Gastric Epithelium. *Dig. Dis. Sci.* 53 (2), 363–369. doi:10.1007/s10620-007-9858-5

Nam, K. T., Hahm, K.-B., Oh, S.-Y., Yeo, M., Han, S.-U., Ahn, B., et al. (2004a). The Selective Cyclooxygenase-2 Inhibitor Nimesulide Prevents Helicobacter Pylori-Associated Gastric Cancer Development in a Mouse Model. *Clin. Cancer Res.* 10 (23), 8105–8113. doi:10.1158/1078-0432.CCR-04-0896

Nam, K. T., Oh, S. Y., Ahn, B., Kim, Y. B., Jang, D. D., Yang, K. H., et al. (2004b). Decreased *Helicobacter pylori* Associated Gastric Carcinogenesis in Mice Lacking Inducible Nitric Oxide Synthase. *Gut* 53 (9), 1250–1255. doi:10.1136/gut.2003.030684

Oh, J. D., Kling-Bäckhed, H., Giannakis, M., Engstrand, L. G., and Gordon, J. I. (2006). Interactions between Gastric Epithelial Stem Cells and *Helicobacter pylori* in the Setting of Chronic Atrophic Gastritis. *Curr. Opin. Microbiol.* 9 (1), 21–27. doi:10.1016/j.mib.2005.12.013

Park, C. H., Lee, A.-r., Lee, Y.-r., Eun, C. S., Lee, S. K., and Han, D. S. (2019). Evaluation of Gastric Microbiome and Metagenomic Function in Patients with Intestinal Metaplasia Using 16S rRNA Gene Sequencing. *Helicobacter* 24 (1), e12547. doi:10.1111/hel.12547

Park, J.-M., Jeong, M., Kim, E.-H., Han, Y.-M., Kwon, S. H., and Hahm, K.-B. (2015). Omega-3 Polyunsaturated Fatty Acids Intake to RegulateHelicobacter Pylori-Associated Gastric Diseases as Nonantimicrobial Dietary Approach. *Biomed. Res. Int.* 2015, 1–11. doi:10.1155/2015/712363

Park, J.-M., Park, S.-H., Hong, K.-S., Han, Y.-M., Jang, S.-H., Kim, E.-H., et al. (2014). Special Licorice Extracts Containing Lowered Glycyrrhizin and Enhanced Licochalcone A PreventedHelicobacter Pylori-Initiated, Salt Diet-Promoted Gastric Tumorigenesis. *Helicobacter* 19 (3), 221–236. doi:10.1111/hel.12121

Piazuelo, M. B., and Correa, P. (2013). Gastric Cáncer: Overview. *Colomb Med. (Cali)* 44 (3), 192–201 .doi:10.25100/cm.v44i3.1263

Piazuelo, M. B., Epplein, M., and Correa, P. (2010). Gastric Cancer: an Infectious Disease. *Infect. Dis. Clin. North America* 24 (4), 853–869. doi:10.1016/j.idc.2010.07.010

Pott, J., Kabat, A. M., and Maloy, K. J. (2018). Intestinal Epithelial Cell Autophagy Is Required to Protect against TNF-Induced Apoptosis during Chronic Colitis in Mice. *Cell Host Microbe* 23 (2), 191–202. doi:10.1016/j.chom.2017.12.017

Quan, Y., and Wang, D. (2014). Clinical Potentials of Human Pluripotent Stem Cells in Lung Diseases. *Clin. Translational Med.* 3, 15. doi:10.1186/2001-1326-3-15

Rajilic-Stojanovic, M., Figueiredo, C., Smet, A., Hansen, R., Kupcinskas, J., Rokkas, T., et al. (2020). Systematic Review: Gastric Microbiota in Health and Disease. *Aliment. Pharmacol. Ther.* 51 (6), 582–602. doi:10.1111/apt.15650

Ralhan, R., Pandey, M. K., and Aggarwal, B. B. (2009). Nuclear Factor-Kappa B Links Carcinogenic and Chemopreventive Agents. *Front. Biosci.* 1, 45–60. doi:10.2741/e6

Resende, C., Thiel, A., Machado, J. C., and Ristimäki, A. (2011). Gastric Cancer: Basic Aspects. *Helicobacter* 16 (Suppl. 1), 38–44. doi:10.1111/j.1523-5378.2011.00879.x

Rugge, M., Capelle, L. G., Cappellesso, R., Nitti, D., and Kuipers, E. J. (2013). Precancerous Lesions in the Stomach: from Biology to Clinical Patient Management. *Best Pract. Res. Clin. Gastroenterol.* 27 (2), 205–223. doi:10.1016/j.bpg.2012.12.007

Russo, A. J., Behl, B., Banerjee, I., and Rathinam, V. A. K. (2018). Emerging Insights into Noncanonical Inflammasome Recognition of Microbes. *J. Mol. Biol.* 430 (2), 207–216. doi:10.1016/j.jmb.2017.10.003

Saleh, M., Taher, M., Sohrabpour, A. A., Vaezi, A. A., Nasiri Toosi, M., Kavianpour, M., et al. (2020). Perspective of Placenta Derived Mesenchymal Stem Cells in Acute Liver Failure. *Cell Biosci* 10, 71. doi:10.1186/s13578-020-00433-z

Seok, J., Jung, H. S., Park, S., Lee, J. O., Kim, C. J., and Kim, G. J. (2020a). Alteration of Fatty Acid Oxidation by Increased CPT1A on Replicative Senescence of Placenta-Derived Mesenchymal Stem Cells. *Stem Cel Res Ther* 11 (1), 1. doi:10.1186/s13287-019-1471-y

Seok, J., Park, H., Choi, J. H., Lim, J.-Y., Kim, K. G., and Kim, G. J. (2020b). Placenta-Derived Mesenchymal Stem Cells Restore the Ovary Function in an Ovariectomized Rat Model via an Antioxidant Effect. *Antioxidants* 9 (7), 591. doi:10.3390/antiox9070591

Seveau, S., Turner, J., Gavrilin, M. A., Torrelles, J. B., Hall-Stoodley, L., Yount, J. S., et al. (2018). Checks and Balances between Autophagy and Inflammasomes during Infection. *J. Mol. Biol.* 430 (2), 174–192. doi:10.1016/j.jmb.2017.11.006

Shariati, A., Nemati, R., Sadeghipour, Y., Yaghoubi, Y., Baghbani, R., Javidi, K., et al. (2020). Mesenchymal Stromal Cells (MSCs) for Neurodegenerative Disease: A Promising Frontier. *Eur. J. Cel Biol.* 99 (6), 151097. doi:10.1016/j.ejcb.2020.151097

Sigal, M., Reinés, M. d. M., Müllerke, S., Fischer, C., Kapalczynska, M., Berger, H., et al. (2019). R-spondin-3 Induces Secretory, Antimicrobial Lgr5+ Cells in the Stomach. *Nat. Cel Biol* 21 (7), 812–823. doi:10.1038/s41556-019-0339-9

Sipponen, P., and Kimura, K. (1994). Intestinal Metaplasia, Atrophic Gastritis and Stomach Cancer: Trends over Time. *Eur. J. Gastroenterol. Hepatol.* 6 Suppl 1 (Suppl. 1), S79–S83.

Stewart, O. A., Wu, F., and Chen, Y. (2020). The Role of Gastric Microbiota in Gastric Cancer. *Gut Microbes* 11 (5), 1220–1230. doi:10.1080/19490976.2020.1762520

Sugano, K., Tack, J., Kuipers, E. J., Graham, D. Y., El-Omar, E. M., Miura, S., et al. (2015). Kyoto Global Consensus Report onHelicobacter Pylorigastritis. *Gut* 64 (9), 1353–1367. doi:10.1136/gutjnl-2015-309252

Tang, Y., Yang, G., Zhang, J., Li, X., Zhang, C., Wang, Y., et al. (2019). E-cadherin Is Required for the Homeostasis of Lgr5+ Gastric Antral Stem Cells. *Int. J. Biol. Sci.* 15 (1), 34–43. doi:10.7150/ijbs.28879

Thiel, A., Mrena, J., and Ristimäki, A. (2011). Cyclooxygenase-2 and Gastric Cancer. *Cancer Metastasis Rev.* 30 (3-4), 387–395. doi:10.1007/s10555-011-9312-1

Tsuda, M., Asaka, M., Kato, M., Matsushima, R., Fujimori, K., Akino, K., et al. (2017). Effect on *Helicobacter pylori* Eradication Therapy against Gastric Cancer in Japan. *Helicobacter* 22 (5), e12415. doi:10.1111/hel.12415

Vogiatzi, P., Cassone, M., Luzzi, I., Lucchetti, C., Otvos, L., Jr., and Giordano, A. (2007). *Helicobacter pylori* as a Class I Carcinogen: Physiopathology and Management Strategies. *J. Cel. Biochem.* 102 (2), 264–273. doi:10.1002/jcb.21375

Wang, H., Wu, R., Xie, D., Ding, L., Lv, X., Bian, Y., et al. (2020). A Combined Phytochemistry and Network Pharmacology Approach to Reveal the Effective Substances and Mechanisms of Wei-Fu-Chun Tablet in the Treatment of Precancerous Lesions of Gastric Cancer. *Front. Pharmacol.* 11, 558471. doi:10.3389/fphar.2020.558471

Wang, Y.-H., Wu, J.-J., and Lei, H.-Y. (2009). The Autophagic Induction in Helicobacter Pylori-Infected Macrophage. *Exp. Biol. Med. (Maywood)* 234 (2), 171–180. doi:10.3181/0808-RM-252

Wang, Z., Gao, X., Zeng, R., Wu, Q., Sun, H., Wu, W., et al. (2020). Changes of the Gastric Mucosal Microbiome Associated with Histological Stages of Gastric Carcinogenesis. *Front. Microbiol.* 11, 997. doi:10.3389/fmicb.2020.00997

Wroblewski, L. E., Piazuelo, M. B., Chaturvedi, R., Schumacher, M., Aihara, E., Feng, R., et al. (2015). Helicobacter Pyloritargets Cancer-Associated Apical-Junctional Constituents in Gastroids and Gastric Epithelial Cells. *Gut* 64 (5), 720–730. doi:10.1136/gutjnl-2014-307650

Wu, C., Chen, L., Huang, Y.-z., Huang, Y., Parolini, O., Zhong, Q., et al. (2018). Comparison of the Proliferation and Differentiation Potential of Human Urine-, Placenta Decidua Basalis-, and Bone Marrow-Derived Stem Cells. *Stem Cell Int.* 2018, 1–11. doi:10.1155/2018/7131532

Yashima, K., Sasaki, S., Koda, M., Kawaguchi, K., Harada, K., and Murawaki, Y. (2010). Premalignant Lesions in Gastric Cancer. *Clin. J. Gastroenterol.* 3 (1), 6–12. doi:10.1007/s12328-009-0130-8

Ye, Q., Shao, X., Shen, R., Chen, D., and Shen, J. (2020). Changes in the Human Gut Microbiota Composition Caused by *Helicobacter pylori* Eradication Therapy: A Systematic Review and Meta-analysis. *Helicobacter* 25 (4), e12713. doi:10.1111/hel.12713

Ye, W., Takabayashi, H., Yang, Y., Mao, M., Hibdon, E. S., Samuelson, L. C., et al. (2018). Regulation of Gastric Lgr5+ve Cell Homeostasis by Bone Morphogenetic Protein (BMP) Signaling and Inflammatory Stimuli. *Cell Mol. Gastroenterol. Hepatol.* 5 (4), 523–538. doi:10.1016/j.jcmgh.2018.01.007

Yu, C., Su, Z., Li, Y., Li, Y., Liu, K., Chu, F., et al. (2020). Dysbiosis of Gut Microbiota Is Associated with Gastric Carcinogenesis in Rats. *Biomed. Pharmacother.* 126, 110036. doi:10.1016/j.biopha.2020.110036

Yuan, W., Song, H. Y., Xiong, J., Jiang, W. L., Kang, G. J., Huang, J., et al. (2020). Placenta derived Mesenchymal Stem Cells Ameliorate Lipopolysaccharideinduced Inflammation in RAW264.7 Cells and Acute Lung Injury in Rats. *Mol. Med. Rep.* 22 (2), 1458–1466. doi:10.3892/mmr.2020.11231

Zhang, F., Chen, C., Hu, J., Su, R., Zhang, J., Han, Z., et al. (2019). Molecular Mechanism of Helicobacterpyloriinduced Autophagy in Gastric Cancer (Review). *Oncol. Lett.* 18 (6), 6221–6227. doi:10.3892/ol.2019.10976

Zhao, Y., Zhang, J., Cheng, A. S. L., Yu, J., To, K. F., and Kang, W. (2020). Gastric Cancer: Genome Damaged by Bugs. *Oncogene* 39 (17), 3427–3442. doi:10.1038/s41388-020-1241-4

Conflict of Interest: The author KH was employed by the company Medpacto, Inc.

The remaining authors declare that the research was conducted in the absence of any commercial or financial relationships that could be construed as a potential conflict of interest.

Publisher's Note: All claims expressed in this article are solely those of the authors and do not necessarily represent those of their affiliated organizations, or those of the publisher, the editors and the reviewers. Any product that may be evaluated in this article, or claim that may be made by its manufacturer, is not guaranteed or endorsed by the publisher.

frontiers in Pharmacology

ORIGINAL RESEARCH
published: 24 August 2021
doi: 10.3389/fphar.2021.729414

Naringin Exerts Therapeutic Effects on Mice Colitis: A Study Based on Transcriptomics Combined With Functional Experiments

Jianyi Dong[1†], Yuanyuan Chen[1†], Fang Yang[1†], Weidong Zhang[1], Kun Wei[1], Yongjian Xiong[2], Liang Wang[1], Zijuan Zhou[1], Changyi Li[1], Jingyu Wang[3] and Dapeng Chen[1]**

[1]Comparative Medicine Department of Researching and Teaching, Dalian Medical University, Dalian, China, [2]Central Laboratory, First Affiliated Hospital of Dalian Medical University, Dalian, China, [3]Labarotary Animal Center, Dalian Medical University, Dalian, China

OPEN ACCESS

Edited by:
Predrag Sikiric, University of Zagreb, Croatia

Reviewed by:
Hong-Ping Guan, Rezubio Pharmaceuticals Co. Ltd., China
Md. Areeful Haque, International Islamic University Chittagong, Bangladesh

***Correspondence:**
Jingyu Wang
wangjingyus@163.com
Dapeng Chen
cdp.9527@163.com

[†]These authors have contributed equally to this work and share first authorship

Specialty section:
This article was submitted to Gastrointestinal and Hepatic Pharmacology, a section of the journal Frontiers in Pharmacology

Received: *23 June 2021*
Accepted: *12 August 2021*
Published: *24 August 2021*

Citation:
Dong J, Chen Y, Yang F, Zhang W, Wei K, Xiong Y, Wang L, Zhou Z, Li C, Wang J and Chen D (2021) Naringin Exerts Therapeutic Effects on Mice Colitis: A Study Based on Transcriptomics Combined With Functional Experiments. Front. Pharmacol. 12:729414. doi: 10.3389/fphar.2021.729414

Naringin has been shown to exert protective effects in an animal model of ulcerative colitis, but detailed mechanisms remain unclear. This study aimed to investigate function and signaling mechanisms underlying naringin-induced therapeutic effects on colitis. Two mouse models were established to mimic human Inflammatory bowel disease (IBD) by treating drinking water with dextran sodium sulphate or intra-colonic administration of 2, 4, 6-trinitrobenzene sulfonic acid. Transcriptomics combined with functional experiments were used to investigate underlying mechanisms. Colitis symptoms, including weight loss and high disease activity index were significantly reversed by naringin. The inflammatory response, oxidative reactions, and epithelial cell apoptosis that occur with colitis were also alleviated by naringin. After naringin treatment, transcriptomics results identified 753 differentially expressed mRNAs that were enriched in signaling pathways, including the neuroactive ligand-receptor interaction, calcium signaling, and peroxisome proliferator-activated receptor (PPAR) signaling. The naringin-induced alleviation of colitis was significantly inhibited by the PPAR-γ inhibitor BADGE. In IEC-6 and RAW264.7 cells incubated with lipopolysaccharide (LPS), NF-κB-p65, a downstream protein of PPAR-γ, was significantly increased. Naringin suppressed LPS-induced high expression of NF-κB-p65, which was inhibited by small interfering RNA targeting PPAR-γ. Our study clarifies detailed mechanisms underlying naringin-induced therapeutic effects on mice colitis, and PPAR-γ was found to be the main target of naringin by functional experiments both *in vivo* and *in vitro*. Our study supplies new scientific information for the use of naringin in colitis treatment.

Keywords: naringin, inflammatory bowel disease, RNA sequencing, peroxisome proliferator-activated receptor-γ, NF-κB

Abbreviations: BSA, bovine serum albumin; CD, Crohn's disease; Cl-caspase3, cleaved caspase3; DAI, disease activity index; DSS, dextran sodium sulphate; H and E, hematoxylin-eosin; IBD, inflammatory bowel disease; IF, immunofluorescent; IHC, immunohistochemical; IL, interleukins; INF, interferon; LPS, lipopolysaccharide; PBS, phosphate-buffered saline; PBST, PBS containing Tween-20; p-NF-κB-p65, phosphorylated NF-κB-p65; PPAR, peroxisome proliferator-activated receptor; qRT-PCR, quantitative real-time polymerase chain reaction; RNA-seq, RNA sequencing; SASP, Sulfasalazine; siRNA, interfering RNA; TNBS, 2, 4, 6-trinitrobenzene sulfonic acid; TNF, tumor necrosis factor; UC, ulcerative colitis.

INTRODUCTION

Inflammatory bowel disease (IBD) is an array of chronic inflammatory disorders within the gastrointestinal tract and includes primarily ulcerative colitis (UC) and Crohn's disease (CD). CD affects the entire gastrointestinal tract from mouth to anus, whereas UC mainly affects colon (Sairenji et al., 2017). Since 2000, incidence ranges of CD are 6–11/100,000 and that of UC are 6–15/100,000 in the Western world (Kaplan and Windsor, 2021). The main symptoms of IBD include diarrhea, abdominal pain, mucus stool and bloody stool, which can be accompanied by a variety of intestinal and parenteral complications, such as intestinal obstruction, stenosis, fibrosis, and joint lesions. Moderate and severe UC or colonic CD is a high-risk factor for colon cancer (Grivennikov, 2013). IBD has become one of the most complex and refractory intestinal diseases which bring a heavy economic and social burden to the health systems of various countries all over the world.

The IBD pathogenesis is still under investigation, recent studies have suggested that both genetic and environmental factors are involved. Current drugs include sulfasalazine, 5-aminosalicylic acid, broad spectrum antibiotics, and corticosteroids are often applied in the treatment of IBD (Abraham et al., 2017). However, many side effects like nausea, anorexia, cytopenia, myalgia, and malfunctions of the kidney, liver, and lungs have been reported (Abraham et al., 2017). Although biopharmaceuticals have been shown to exert good therapeutic effects on IBD, a large part of patients do not respond or lose response to biopharmaceuticals over time (Yanai and Hanauer, 2011). In addition, biologic therapy may increase the risk of serious infections and malignancies (Holmer and Singh, 2019). Therefore, it is valuable to screen or develop new drugs to expand therapy options.

In recent years, herbal medicines with multi-target actions have been widely used in the treatment of complex inflammatory diseases. Citrus peel is a kind of herbal medicine and is used as an anti-inflammatory drug in China. Naringin (4′,5,7-trihydroxyflavanone-7-rhamnoglucoside) is a major and active flavanone glycoside isolated from citrus fruit species (Ali and El Kader, 2004). Naringin has been found to exert anti-inflammatory, anti-oxidative, and anti-cancer effects (Jeon et al., 2001; Zhang et al., 2016). Cao et al. find that naringin exerts protective effects on dextran sodium sulphate (DSS)-induced colitis *via* modulation of PPAR-γ activity (Cao et al., 2018). However, the detailed mechanisms of naringin on colitis are still not fully understood because multiple targets may be involved. In addition, naringin-induced modulation of PPAR-γ should also be confirmed in cells and other animal models of colitis.

In this study, transcriptomics and functional experiments are used to uncover the detailed mechanisms of naringin-induced therapeutic effects on colitis. RNA sequencing (RNA-seq) is a deep-sequencing approach in transcriptome profiling that provides an impartial and accurate method for measuring the levels of transcripts and their isoforms (Kukurba and Montgomery, 2015). Two mouse models are established to mimic human IBD by treating drinking water with DSS or intra-colonic administration of 2, 4, 6-trinitrobenzene sulfonic acid (TNBS).

MATERIALS AND METHODS

Materials

Naringin (purity ≥ 98%) was purchased from Beijing Solarbio Co. Ltd. (Beijing, China). Sulfasalazine (SASP) was purchased from Tian-jin Kingyork Group Co. Ltd. (Tianjin, China). Antibodies against PPAR-γ (A0270) were from ABclonal Co. Ltd. (Wuhan, China). Antibodies against caspase-3 (19677-1-AP), cleaved caspase3 (cl-caspase3) (19677-1-AP), and iNOS (14142-1-AP) were from Proteintech Co. Ltd. (Wuhan, China). Antibodies against NF-κB-p65 (66535-1-Ig), phosphorylated NF-κB-p65 (p-NF-κB-p65) (WL02169) and PPAR-α (WL00978) were from Wanleibio Co. Ltd. (Shenyang, China). A cell counting kit-8 (WLA074b) was from Wanleibio Co. Ltd. BADGE (B6691) was obtained from Apexbio (Houston, TX, United States). Chemicals were obtained from Sigma–Aldrich (St. Louis, MO, United States), unless otherwise indicated.

Animals

Eighty male C57BL/6 mice (6–8 weeks old, weighing 18–20 g) were obtained from the laboratory animal center, Dalian Medical University, Dalian city, China [Certificate of Conformity: No. SYXK (Liao) 2018–0007]. The experimental protocol was approved by Dalian Medical University Animal Care and Ethics Committee (No. AEE20046). The animals were acclimatized to laboratory conditions (23°C, 12 h/12 h light/dark, 50% humidity, ad libitum access to food, and water) for 2 weeks prior to experiments. The animal protocol was designed to minimize pain and discomfort to the animals. Mice were housed one per cage and were deprived of food for 12 h before experiments. All mice were euthanized by barbiturate overdose (intravenous injection, 150 mg/kg pentobarbital sodium) for intestinal tissue collection. All animal experiments were carried out in accordance with the National Institutes of Health guide for the care and use of laboratory animals. Animal studies are reported in compliance with the ARRIVE guidelines (Kilkenny et al., 2010). All applicable institutional and/or national guidelines for the care and use of animals were followed.

Cell Culture and Cell Transfection

Murine RAW264.7 cells and rat intestinal IEC-6 epithelial cells were purchased from the cell bank of the Shanghai Institute (Shanghai, China). Cells used in this study were evaluated before conducting experiments, and no significant interspecies variations in PPAR-γ signaling that might have affected the results of the current study were observed in preliminary tests. The cells were maintained at 37°C in a 5% CO_2 environment. The RAW264.7 cells were cultured in RPMI-1640 medium with 10% top fetal bovine serum. Rat intestinal IEC-6 epithelial cells were cultured in DMEM (Invitrogen, Waltham, MA, United States) medium with 4.5 mg/ml glucose, 50 U/mL penicillin, 50 U/mL streptomycin, 4 mM glutamine, 25 mM HEPES, and 10% fetal bovine serum (Invitrogen) (Sui et al., 2020). RAW264.7 and IEC-6 cells were transfected using Lipofectamine 2000 (Invitrogen) with PPAR-γ-targeted or control small interfering

RNA (siRNA) oligos (GenePharma, Suzhou, China), according to the manufacturer's instructions (Takara Biotechnology (Dalian) Co., Ltd.). The siRNA sequences for PPAR-γ interfering RAW264.7 cells and IEC-6 cells, respectively were:

Sense: 5′-GGUGCUAAGAGAUUGCCUUTT-3′;
Antisense: 5′-AAGGCAAUCUCUUAGCACCTT-3′;
Sense: 5′-CCAUCCGAUUGAAGCUUAUTT-3′;
Antisense: 5′-AUAAGCUUCAAUCGGAUGGTT-3′.
The efficiency of gene silencing was confirmed by western blotting.

Experimental Design

For the DSS–colitis model, mice were divided randomly into five groups of six mice each. The mice were treated as follows: group I was a sham-operated control with gavage administration of saline; group II was untreated colitis; and groups III, IV, and V were treated with the following: SASP (500 mg/kg body weight, gavage administration, dissolved in saline), low-dose naringin (20 mg/kg body weight, gavage administration, dissolved in saline), and high-dose naringin (40 mg/kg body weight, gavage administration, dissolved in saline), respectively. All treatments occurred 1 day after colitis induction with DSS. SASP is an anti-inflammatory drug that is, widely used for the clinical treatment of diseases such as IBD and, therefore, it was used as a positive control for the effects of naringin on colitis. Mice in group III, IV, and V were administered SASP or naringin by gavage once a day for seven successive days. Mice in groups II–V were given drinking water containing DSS (4% w/v) dissolved in autoclaved distilled water, to induce colitis symptoms (Feng et al., 2020). Control group I mice were given autoclaved distilled water and otherwise, treated in the same way. No abnormal moribund mice were found during the study. Food intake and bodyweight of mice were recorded once a day. On the 8th day, mice in group I–V were given autoclaved distilled water as drinking water. On the 9th day, distal colon samples in groups I–V were harvested for biochemical studies. Mice in the PPAR-γ inhibition group were injected intraperitoneally with 30 mg/kg BADGE solution per day for seven consecutive days, the experimental designs are the same as above.

For the TNBS–colitis model study, mice were divided randomly into five groups of six mice each. The mice were treated as follows: group I was a sham-operated control with gavage administration of saline; group II was untreated colitis; and groups III, IV, and V were treated with the following: SASP (500 mg/kg body weight, gavage administration, dissolved in saline), low-dose naringin (20 mg/kg body weight, gavage administration, dissolved in saline), and high-dose naringin (40 mg/kg body weight, gavage administration, dissolved in saline), respectively. All treatments occurred 1 day after colitis induction. Mice in group III, IV, and V were administered SASP (Xiong et al., 2017), naringin by gavage once a day for seven successive days. Colitis was induced with TNBS, as described previously (Dong et al., 2020). A catheter was inserted through the anus to approximately the level of the splenic flexure under urethane anesthesia. The colon was then infused with 0.1 ml of TNBS dissolved in ethanol (50% v/v) at a dose of 125 mg/kg. The mice could eat and drink ad libitum starting 1 h after the operation. On the 8th day, mice in groups I–V were given autoclaved distilled water as drinking water. On the 9th day, distal colon samples in groups I–V were harvested for biochemical studies. Protein extraction, western blotting, and ELISA were performed as previously described (Dong et al., 2020).

Assessment of Disease Activity Index

Mice body weights were monitored daily. The DAI scores were assessed according to our previous study (Melgar et al., 2005). Briefly, an observer blinded to the treatments combined the scores for weight loss, stool bleeding, and stool consistency on the last day.

Isolation of Colonic Epithelial Cells

Colonic epithelial cells were isolated according to a previous study (Dong et al., 2020). Briefly, distal colons were isolated from euthanized mice and immediately rinsed with ice-cold phosphate-buffered saline (PBS) to clear luminal contents. The distal colon was then opened longitudinally along the mesenteric border. Tissue was cut into approximately 2 mm long pieces and submerged in 40 ml of ice-cold PBS with 5 mM EDTA in a 50 ml Falcon tube. The pieces of tissue in PBS-EDTA were then incubated at 37°C with gentle rocking for 30 min. Following incubation, colonic tissue was vigorously shaken to disperse colonic crypts and surface epithelium in solution. Supernatant was then loaded into 1.5 ml microcentrifuge tubes and spun at 1×10^3 g for 5 min to pellet suspended cells. The isolated epithelial cells were used in downstream applications.

RNA-Seq and Bioinformatics

Three naringin treated DSS-induced C57BL/6 mice, three DSS-induced C57BL/6 mice and three untreated mice were used for mRNA profile detection. Total RNA was extracted using TRIzol reagent (Invitrogen), and quality was evaluated using the RNA Nano 6000 Assay Kit of the Bioanalyzer 2,100 system (Agilent Technologies, CA, United States).

A total of 3 μg RNA per sample was used to generate an mRNA sequencing library using NEBNext® Ultra™ RNA Library Prep Kit for Illumina® (NEB, United States) following manufacturer's recommendations and index codes were added to each sample for identification (Gao et al., 2012). Briefly, mRNA was purified and fragmented. Then, first and second strand cDNA was synthesized, ends were repaired and adenylated, adapters were ligated, and fragments were enriched with PCR amplification. Library quality was assessed on the Agilent Bioanalyzer 2,100 system. Libraries were sequenced on an Illumina platform.

Raw data (raw reads) of fastqc format were first processed through Trimmomatic (Bolger et al., 2014). In this step, clean data (clean reads) were obtained by removing reads containing adapter, reads containing poly-N, and low-quality reads from raw data. Reference genome and gene model annotation files were downloaded from the genome website directly. Index of the reference genome was built and paired-end clean reads were aligned to the reference genome using Hisat2 (v2.0.5), the selected mapping tool. The mapped reads of each sample were assembled

TABLE 1 | mRNA sequences obtained from the NCBI database.

Gene name	Forward primer sequence (5'–>3')	Reverse primer sequence (5'–>3')<
Mus-Ppar-α	tatggccgagaagacgcttg	attctgtgagctccgtgacg
Mus-Ppar-γ	atccaagacaacctgctgca	caaggaggacagcatcgtga
Mus-Ppar-δ	gcccaagttcgagtttgctg	acctggggcacattcatgag
Mus-Scd1	ttctcagaaacacacgccga	tccagttttccgcccttctc
Mus-Hmgcs2	gcccaaacgtctagactccc	ttgcttgtgtctccaggtgg

by StringTie (v1.3.3b) in a reference-based approach. FeatureCounts v1.5.0-p3 was used to count the reads mapped to each gene. Then, FPKM of each gene was calculated based on the length of the gene and read counts mapped to this gene (Conesa et al., 2016). FPKM, expected number of Fragments Per Kilobase of transcript sequence per Million base pairs sequenced, considers the effect of sequencing depth and gene length for the read counts at the same time. Differential expression analysis of two conditions/groups (two biological replicates per condition) was performed using the DESeq2 R package (1.16.1). The resulting *p*-values were adjusted using the Benjamini and Hochberg approach. Genes with an adjusted *p*-value < 0.05 found by DESeq2 were assigned as differentially expressed. We used the clusterProfiler R package to test the statistical enrichment of differential expression genes in KEGG pathways. The raw sequencing data sets were deposited in the Sequence Read Archive of the NCBI (https://www.ncbi.nlm. nih. gov/sra) under accession number PRJNA741857.

Quantitative Real-Time Polymerase Chain Reaction

Validation of differentially expressed genes was performed by qRT-PCR using SuperReal PreMix Plus (SYBR Green, FP205, Tiangen) with an Applied Biosystems StepOnePlus Real-Time PCR System, according to the manufacturer's instructions. Total RNA was isolated from colonic epithelial cells using RNAiso Plus (9108, TaKaRa) and reverse-transcribed to single-stranded cDNA using a reverse transcription system (KR116, Tiangen). Primer sequences are listed in **Table 1**. A separate qRT-PCR using a primer for the detection of GAPDH was used as a control.

Hematoxylin-Eosin, Immunohistochemical and Immunofluorescent Analysis

Colon tissues were fixed with 4% paraformaldehyde at 4°C. The samples were dehydrated, embedded in paraffin, and sectioned into 3-μm-thick transverse sections. For H and E staining, the sections were dewaxed, rehydrated, and stained with hematoxylin and eosin. After being washed with distilled water and dehydrated, the sections were treated with xylene. Colitis activity scores were assessed in a blinded fashion, by combining the scores of inflammation severity, inflammation extent, crypt damage, and percent involvement (Kihara et al., 2003). Inflammation severity score was assessed according to the following criteria: 0: none; 1: mild; 2: moderate; and 3: severe. Inflammation extent score was assessed according to the following: 0: none; 1: mucosa; 2: submucosa; and 3: transmural. Crypt damage score was assessed by the following criteria: 0: none; 1: basal 1/3 damage; 2: basal 2/3 damage; 3: crypt lost; surface epithelium present; and 4: crypt and surface epithelium lost. Percent involvement score was determined as follows: 0: 0%; 1: 1–25%; 2: 26–50%; 3: 51–75%; and 4: 76–100%. For IHC staining, the sections were dewaxed, rehydrated, and washed with distilled water three times. The sections were then treated with 3% H_2O_2 for 10 min, washed in PBS containing Tween-20 (PBST), treated with 5% bovine serum albumin (BSA) (Solarbio, A8020) and then incubated with rabbit anti-PPAR-γ (ABclonal, A0270) (1:100 dilution) overnight at 4°C. After three washes with PBST, the sections were incubated with secondary antibody for 30 min at 37°C. After being rinsed, the sections were incubated with diaminobenzidine. After counterstaining with hematoxylin, washing with distilled water, and dehydration, the sections were treated with xylene. For IF staining, sections were dewaxed, dehydrated, and subjected to antigen retrieval. 3% BSA (Solarbio, A8020) was utilized to block nonspecific binding. Then, the sections were incubated with rabbit anti-PPAR-γ (ABclonal, A0270) (1:100 dilution) overnight at 4°C. Later, these sections were rinsed with PBS and incubated with Alexa Fluor 488 (FITC) secondary antibody (Proteintech, SA00013-2) in the dark for 60 min at room temperature. 4,6-diamidino-2-phenylindole (Invitrogen, P36941) was later applied to dye the nuclei. Fluorescence photographs were obtained under a fluorescence microscope DM5000 B (Leica, Germany).

Statistical Analysis

The animal experiments, *in vitro* experiments, and data analysis were conducted according to a single-blind study design. Data were compared between three or more groups using one-way ANOVA, and between two groups using Student's t-test. Data were expressed as the mean ± standard deviation. Data were normally distributed, and each group showed similar variances. Further evaluation was carried out using Kruskal–Wallis rank sum tests. All experiments were repeated at least three times and a p value < 0.05 was considered statistically significant.

RESULTS AND DISCUSSION

Effects of Naringin on Normal Mice and Cells

The chemical structure of naringin is shown in **Figure 1A**. Naringin had no significant effect on body weight or food intake in normal mice (**Figures 1B,C**). Cytokine profiles [TNF-α, interleukins (IL)-1β, and interferon (INF)-γ] in colon tissue were not affected by naringin (**Figures 1D–F**). There was no significant effect on expression of PPAR-γ in colon tissue after gavage administration of 10 and 40 mg/kg naringin for 7 days, while the expression of PPAR-γ was decreased by 160 mg/kg naringin (**Figure 1G**). Naringin (5–160 μM, 12 h) did not significantly affect cell viability in RAW264.7 cells. Naringin (5–80 μM, 12 h) exerted no significant effects on cell viability in IEC6 cells, while 160 μM significantly inhibited cell viability (**Figure 1H**). According to our preliminary experiments and

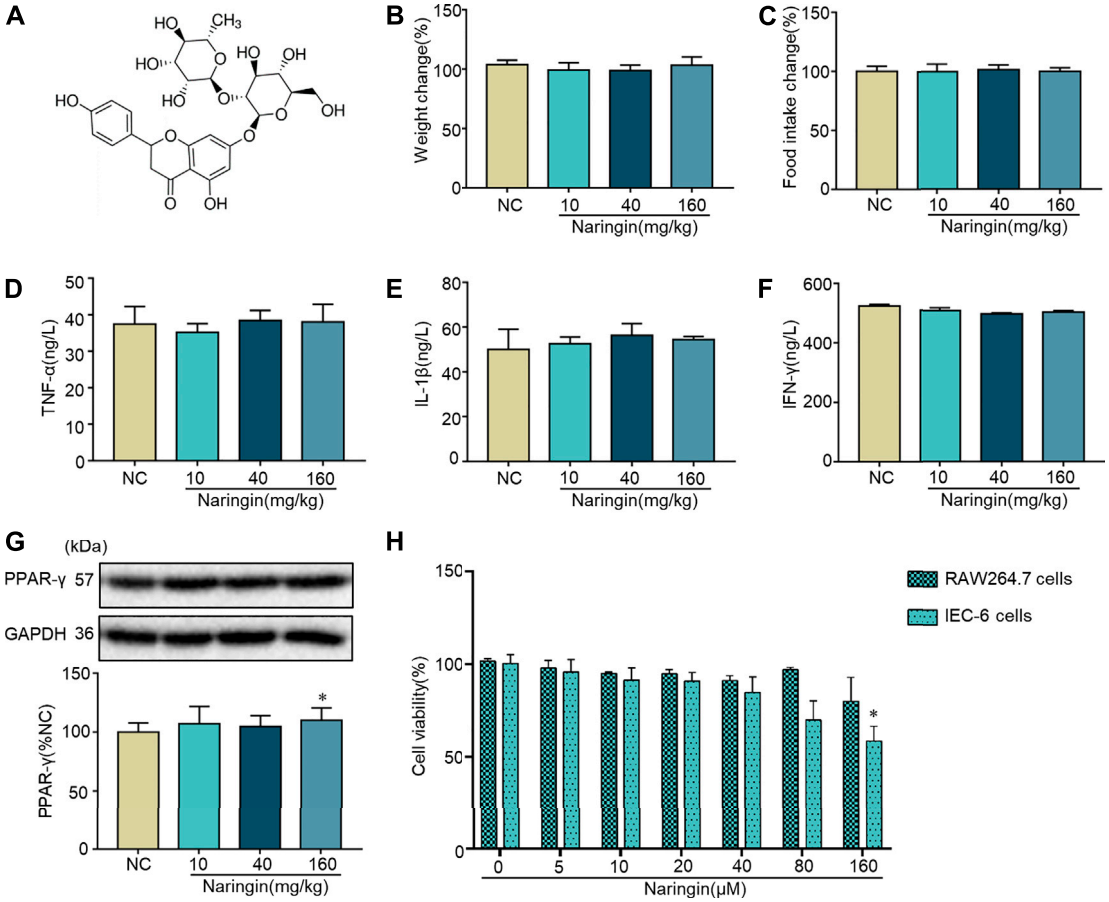

FIGURE 1 | Toxicity of naringin in normal cells and mice. **(A)** Chemical structure of naringin. Naringin was administered to mice by gavage once a day for seven consecutive days. Effects of naringin on **(B)** body weight and **(C)** food intake. Expression levels of the colonic cytokines **(D)** TNF-α, **(E)** IL-1β, and **(F)** INF-γ were examined by ELISA, and expression levels of **(G)** PPAR-γ were examined by western blotting. **(H)** Cytotoxicity of naringin was studied by CCK8 assay in RAW 264.7 and IEC-6 cells. Data are expressed as the mean ± SD. Values in the normal control (NC) group are set to 100%, and other values are given relative to the NC group. *p <0.05 compared with NC group. n = 3 samples in western blotting experiments; n = 6 samples for other experiments. These blots are cropped, and the full-length blots are presented is in the **Supplementary Figure S1**.

previous reports (Ahmad et al., 2015; Cao et al., 2018), the maximum doses of naringin were 40 mg/kg *in vivo* and 20 μM *in vitro*.

Naringin Ameliorates DSS-Colitis Symptoms

The significant weight loss, high colon weight-to-length ratio, decreased food intake and high DAI scores in the untreated model group showed that instillation of DSS to the colon resulted in reproducible colitis in mice (**Figures 2A–D**). The overall morphology of the colon is shown in **Figure 2E**. Histopathological damage was characteristically induced by DSS (**Figures 2F,G**). A variety of colitis symptoms, including damaged villi structure (green ring), infiltration of inflammatory cells (black arrow), submucosal edema (blue ring), and muscle fiber separation (blue arrow) were visible in the H and E staining (**Figure 2G**). Naringin and SASP reversed the pathological changes in colitis.

Effects of Naringin on Inflammation and Apoptosis in DSS-Colitis

As shown in **Figures 3A–D**, MPO activity and expression of pro-inflammatory factors (TNF-α, IL-1β, and INF-γ) were significantly increased in DSS-colitis, and naringin significantly reversed these changes. DSS-induced colitis up-regulated inflammation-related proteins (iNOS and p-NF-κB-p65) and an apoptosis-related protein cl-caspase3 expression. Finally, an attenuated trend was observed in groups treated with naringin (**Figures 3E–G**). These results confirmed that naringin has anti-inflammatory and anti-apoptotic activities in DSS-colitis.

High-Throughput Transcriptome Sequencing and KEGG Pathway Enrichment Analysis

We applied transcriptome sequencing to investigate the possible mechanisms of naringin in the treatment of colitis. A total of 753 differentially expressed mRNAs before and after naringin

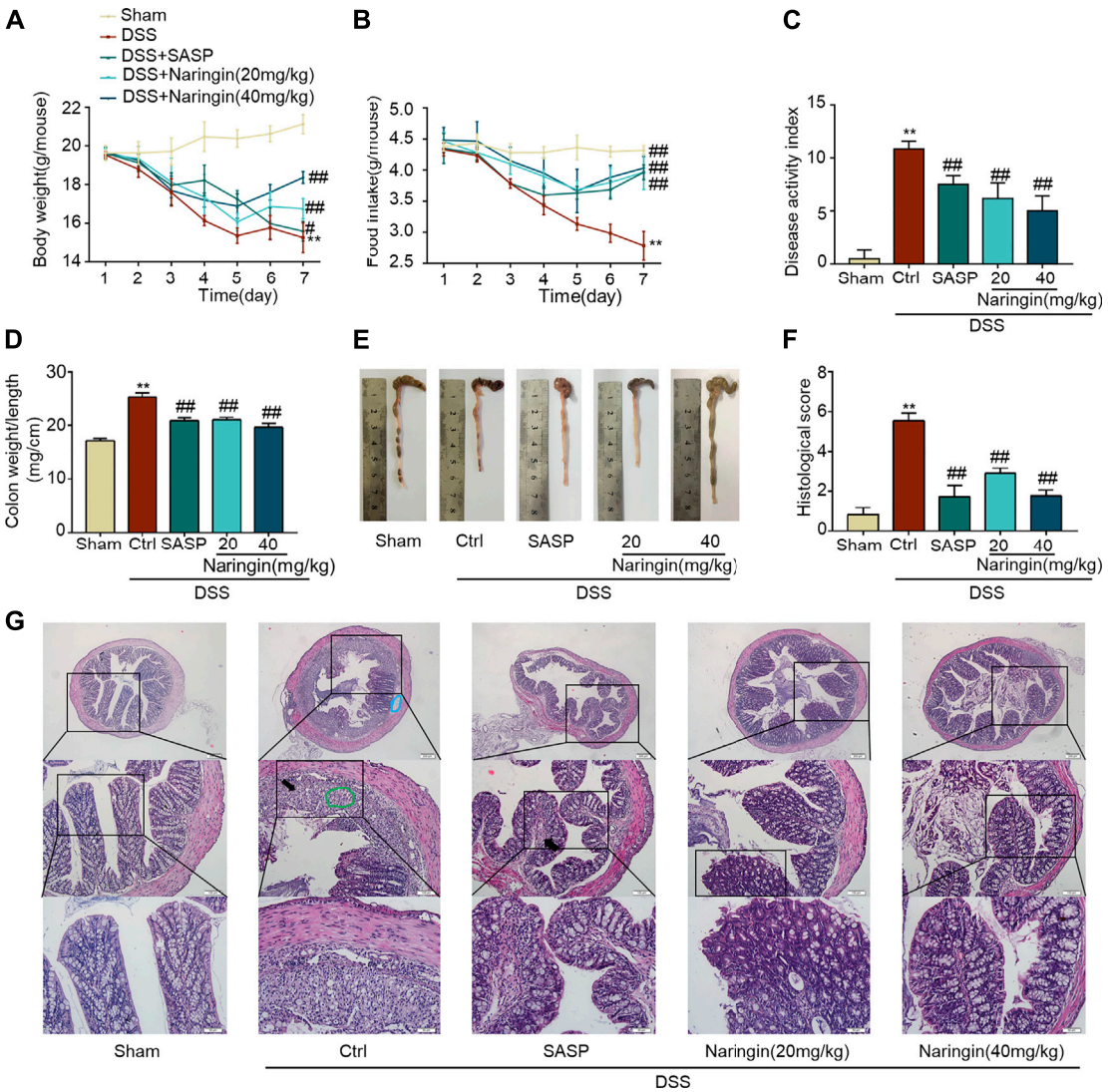

FIGURE 2 | Naringin ameliorates DSS-colitis symptoms. Colitis symptoms were recorded after 7 days of naringin treatment. Effects of naringin on **(A)** body weight, **(B)** food intake, **(C)** DAI, **(D)** colon weight-to-length ratio, and **(E)** gross morphology of colon tissue. **(F)** Total histological score was calculated as the sum of epithelial damage and histological score. **(G)** H and E staining of mice colonic tissue. Scale bars, 200, 100, 50 μm. Green ring indicates damaged villi structure; black arrow indicates infiltration of inflammatory cells; blue ring indicates submucosal edema. Data are expressed as mean ± SD. Values in the sham group are set to 100%, and other values are given relative to the sham group. $^{**}p < 0.01$ compared with sham group; $^{\#\#}p < 0.01$ compared with DSS-colitis group; $n = 6$ samples.

treatment were identified with fold changes > 2 and $p < 0.05$ and some representative genes were shown in heatmap (**Figures 4A,B**). In addition, compared with the control group, 834 differentially expressed mRNAs were observed in the model group (**Figure 5A**).

The KEGG enrichment results showed the top 20 enriched KEGG pathways in the model group vs. naringin treatment group (**Figure 4C**) and the control group vs. model group (**Figure 5B**). There are three common enriched KEGG pathways including the neuroactive ligand-receptor interaction, calcium signaling, and PPAR signaling among the top 20 enriched KEGG pathways between the model group vs. naringin treatment group and the control group vs. model group (**Figure 4C**, **Figure 5B**). Based on the genes contained in the top 11 pathways, we constructed a KEGG-target network of naringin-induced treatment including 133 targets (**Figure 4D**). Most targets were associated with different pathways, suggesting synergistic effects are involved in naringin-induced treatment. Therefore, naringin may target different pathways and targets.

Effects of Naringin on PPAR-γ

According to reference validation, we subsequently studied proteins in the PPAR signaling pathways to uncover naringin-induced treatment effects on colitis. We used qRT-PCR to detect the roles of some mRNAs in PPAR signaling pathways, including PPAR-α, PPAR-γ, PPAR-δ, Scd1, and Hmgcs2 in naringin-

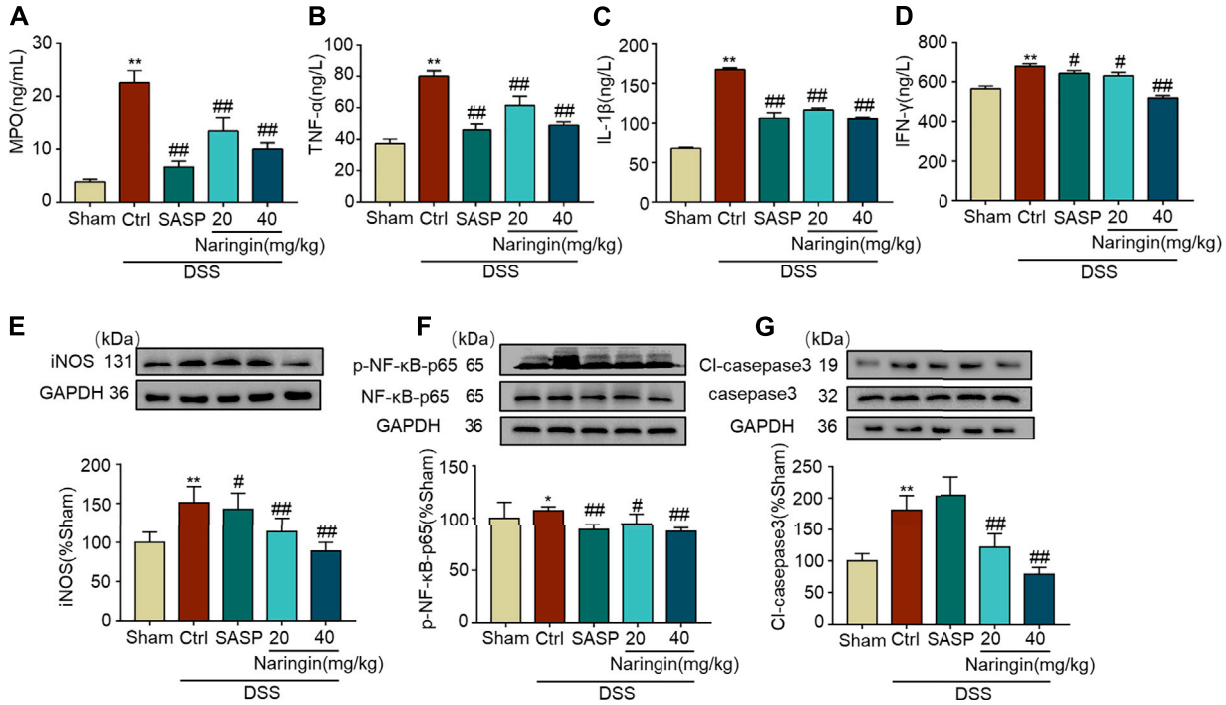

FIGURE 3 | Effects of naringin on inflammation and apoptosis in DSS-colitis. Expression levels of the colonic cytokines **(A)** MPO, **(B)** TNF-α, **(C)** IL-1β, and **(D)** IFN-γ were determined by ELISA. Western blotting analysis of inflammation-related proteins **(E)** iNOS, **(F)** p-NF-κB-p65 (calculated as p-NF-κB-p65/NF-κB-p65); apoptosis-related protein **(G)** cl-caspase3, calculated as cl-caspase3/caspase3. Data are expressed as mean ± SD. Values in the sham group are set to 100% and other values are given relative to those in the sham group, $^{*}p < 0.05$, $^{**}p < 0.01$ compared with sham group; $^{\#}p < 0.05$, $^{\#\#}p < 0.01$ compared with DSS-colitis group; $n = 3$ samples in western blotting experiments; $n = 6$ samples for other experiments. These blots are cropped, and the full-length blots are presented is in the **Supplementary Figures S2–S9**.

induced treatment effects (**Figure 6**). There were significant differences in the expressions of PPAR-α and PPAR-γ between the naringin treatment and DSS-colitis groups. The expressions of PPAR-δ, Scd1, and Hmgcs2 were not significantly affected by naringin in the colitis model.

We further studied the protein expressions of PPAR-α and PPAR-γ. Compared with the sham group, PPAR-γ expression was significantly decreased in DSS-colitis, but naringin treatment significantly stimulated PPAR-γ expression (**Figures 7B–D**). However, naringin treatment did not significantly affect PPAR-α protein expression (**Figure 7A**). The results suggest that PPAR-α and PPAR-γ may be involved in naringin-induced treatment effects, however, PPAR-γ plays a more important role.

Next, we examined the role of PPAR-γ for naringin-induced treatment effects. *In vivo*, the PPAR-γ inhibitor BADGE was used to investigate the role of PPAR-γ in naringin-induced improvement of colitis. As shown in **Figure 8A**, PPAR-γ expression was significantly inhibited by BADGE, and BADGE significantly exacerbated colitis symptoms including weight loss (**Figure 8B**), high DAI, increased colon weight-to-length ratio, and histological score (**Figures 8C,D,F**). The overall morphology of the colon is shown in **Figure 8E**. Every colitis symptom was reversed by naringin, but this affect was significantly inhibited by BADGE.

Both RAW264.7 and IEC-6 cells were used to confirm the stimulatory effects of naringin on PPAR-γ. In RAW264.7 cells, pro-inflammatory cytokines, including TNF-α, IL-1β, and INF-γ, were significantly increased by LPS, and the increase was reversed by naringin (**Figures 9A–C**). P-NF-κB-p65, a target gene of PPAR-γ, was also significantly increased by LPS (**Figures 9D–F**). The LPS induced increase in p-NF-κB-p65 was significantly reversed by naringin, but was significantly inhibited by siRNA targeting PPAR-γ. Similar results were also obtained using IEC-6 cells (**Figures 9G–I**). These results suggested that PPAR-γ is a potential target of naringin.

Effects of Naringin on TNBS-Colitis

A TNBS-colitis model was also established to study the effects of naringin. Compared with the sham group, significant weight loss, high colon weight-to-length ratio, lower food intake, high DAI scores, and increased histological score were observed in the untreated colitis model group (**Figures 10A–D,F**). The overall morphology of the colon is shown in **Figure 10E**. Naringin significantly reversed these colitis symptoms. Higher levels of MPO activity and the expression of pro-inflammatory cytokines (IL-1β, INF-γ, and TNF-α) were also reversed by naringin treatment (**Figures 10H–K**). Naringin ameliorated the above colitis symptoms as evidenced by H and E staining (**Figure 10G**). Damaged villi structure (green ring), infiltration

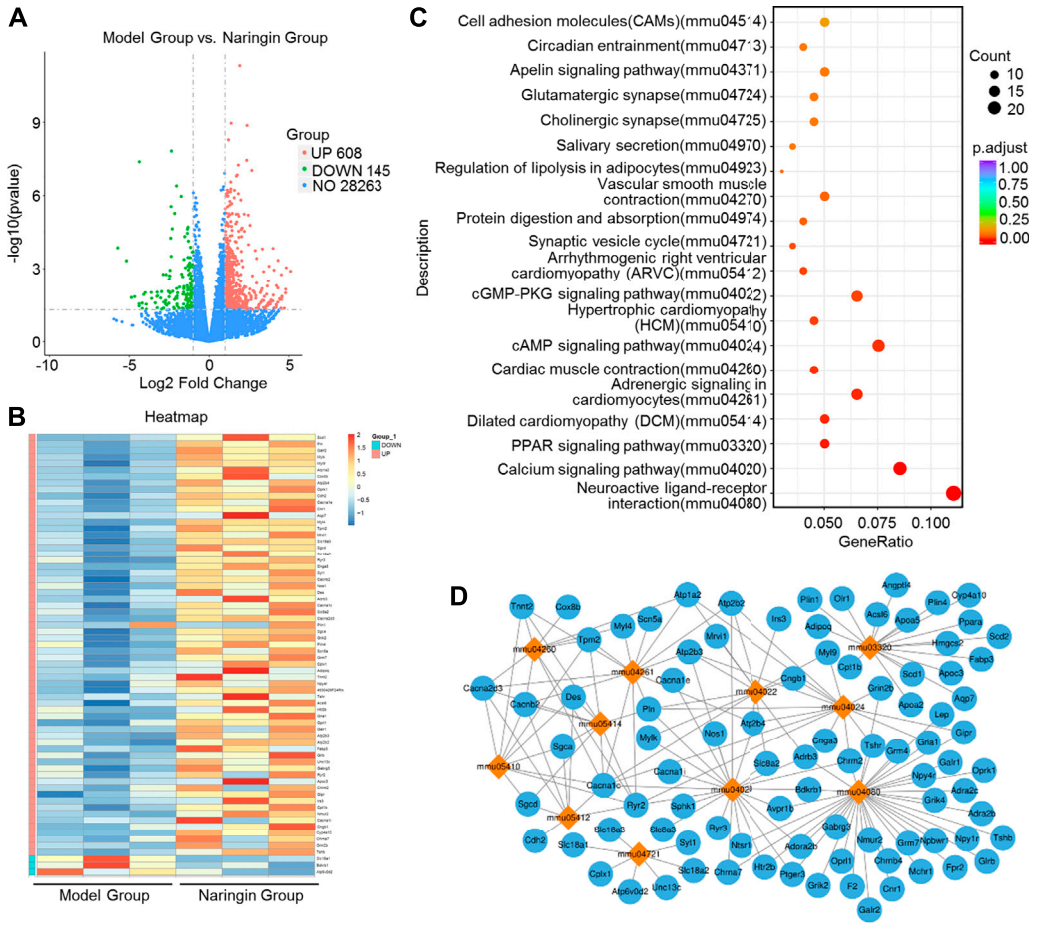

FIGURE 4 | High-throughput transcriptome sequencing and KEGG pathway enrichment analysis. Naringin (40 mg/kg) was administered to mice by gavage once a day for seven consecutive days and total RNA was extracted from colonic epithelial cells. **(A)** Volcano plot of differentially expressed mRNAs in model group vs. naringin treatment group. **(B)** Heatmap of some representative genes. **(C)** The scatter plots showing the top 20 enriched KEGG pathways in model group vs. naringin group. The Rich factor is the ratio of differentially expressed gene numbers annotated in this pathway term to all gene number annotated in this pathway term. Greater rich factor means greater intensiveness. Q-value is corrected *p* value ranging from 0 to 1. **(D)** Target-pathway network including candidate 133 targets and 11 KEGG pathways.

of inflammatory cells (black arrow), and submucosal edema (blue ring) shown in H and E staining were alleviated by naringin.

Naringin can reverse the increasing expression of inflammation-related proteins (iNOS and p-NF-κB-p65), and apoptosis-related protein cl-caspase3 in TNBS-colitis (**Figures 11D–F**). Furthermore, decreased PPAR-γ expression in TNBS-colitis was also stimulated by gastric administration of naringin (**Figures 11A–C**). In accordance with our DSS-colitis results, naringin also significantly alleviated TNBS-colitis.

DISCUSSION

In this study, we examined the effects and detailed mechanisms of naringin on mouse colitis. We showed that naringin had therapeutic effects on both DSS- and TNBS-induced colitis. Colitis symptoms, including neutrophil infiltration, cytokine profiles, and epithelial barrier dysfunction were significantly ameliorated by naringin. In this study, PPAR-γ was found to be an important target for naringin-induced improvement of colitis.

Based on RNA-seq analysis, 753 mRNAs were identified that differed between untreated colitis and naringin treated groups. We identified 11 important pathways involved using a KEGG-target network. Some of these pathways have previously been shown to be involved in colitis. For example, the disruption of Ca^{2+} homeostasis is associated with colonic dysmotility in UC (Wang et al., 2016a). cAMP/PKA-dependent and independent pathways can reduce the expression of inflammatory mediators and attenuate p38 phosphorylation to treat TNBS-colitis (Sun et al., 2017). The activation of PPAR-α, PPAR-δ, and Scd1 has been shown to play a role in DSS-colitis, and Hmgcs2 has an effect in TNBS-colitis (Bassaganya-Riera et al., 2004; Wang et al., 2016b; Wang et al., 2017; Liu et al., 2018). Cnr1, part of the neuroactive ligand-receptor interaction, is reported to be

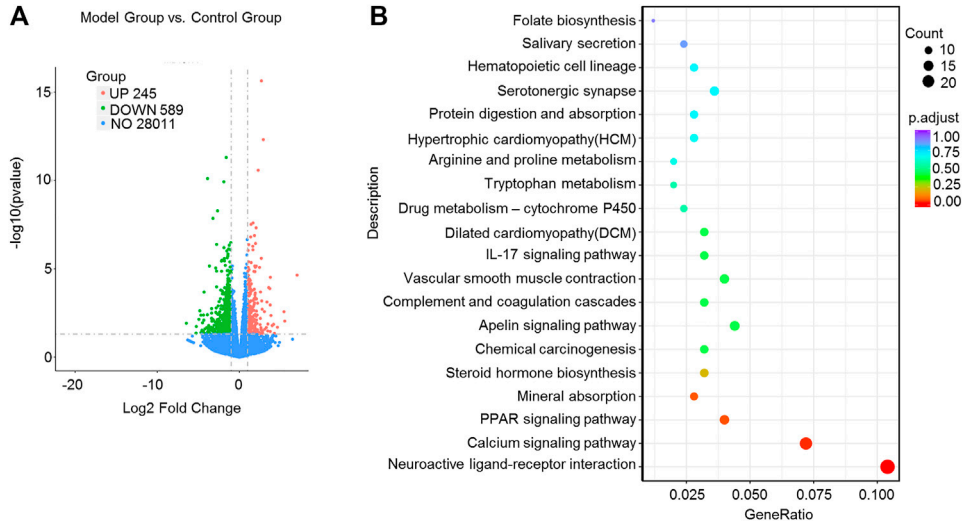

FIGURE 5 | High-throughput transcriptome sequencing and KEGG pathway enrichment analysis. Naringin (40 mg/kg) was administered to mice by gavage once a day for seven consecutive days and total RNA was extracted from colonic epithelial cells. **(A)** Volcano plot of differentially expressed mRNAs in model group vs. control group. **(B)** The scatter plots showing the top 20 enriched KEGG pathways in model group vs. control group. The Rich factor is the ratio of differentially expressed gene numbers annotated in this pathway term to all gene number annotated in this pathway term. Greater rich factor means greater intensiveness. Q-value is corrected *p* value ranging from 0 to 1.

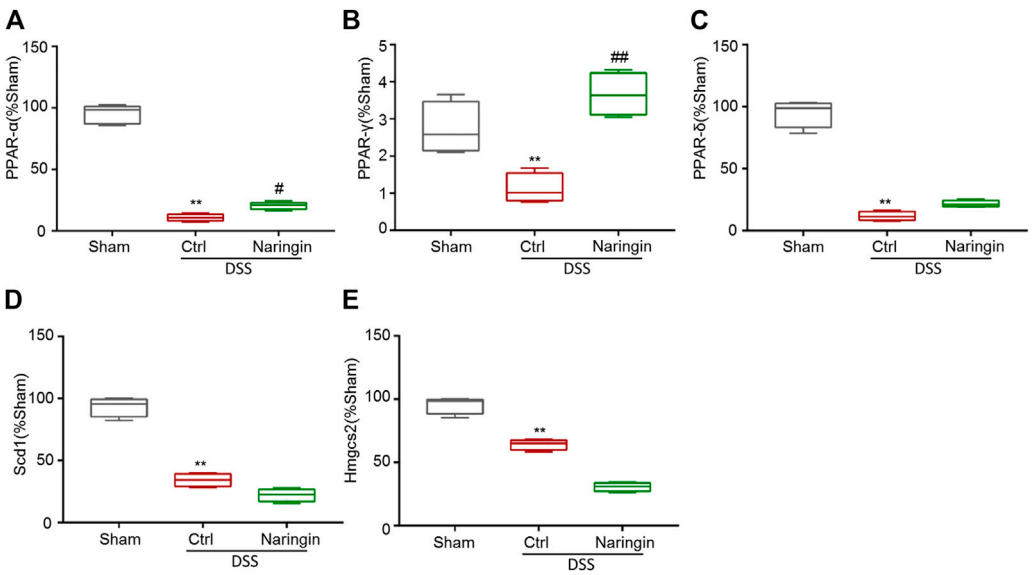

FIGURE 6 | The effect of naringin on some mRNAs in PPAR signaling pathways detected by qRT-PCR. Naringin (40 mg/kg) was administered to mice by gavage once a day for seven consecutive days. The expression levels of some mRNAs in PPAR signaling pathways including **(A)** PPAR-α, **(B)** PPAR-γ, **(C)** PPAR-δ, **(D)** Scd1, and **(E)** Hmgcs2 were detected by qRT-PCR (means ± SD, $n = 3$). $^{**}p < 0.01$ compared with sham group; $^{\#}p < 0.05$, $^{\#\#}p < 0.01$ compared with DSS-colitis group.

associated with IBD symptoms (Storr et al., 2010). The expression of Mylk in the calcium signaling pathway is a molecular marker of intestinal fibrosis, a critical complication of CD (Rodansky et al., 2015). In our study, PPAR-α, PPAR-γ, PPAR-δ, Scd1, and Hmgcs2 involved in PPAR signaling pathways were selected for preliminary research. Although we found that PPAR-γ is the main target for naringin-induced improvement of colitis, there are multiple targets involved. The other potential targets of naringin will be studied in the future.

PPAR-γ is a transcription factor that plays an important role in anti-inflammation, antioxidant, and phagocyte-mediated cleanup processes and is highly expressed in colonic epithelium and adipose tissue (Lefebvre et al., 1999;

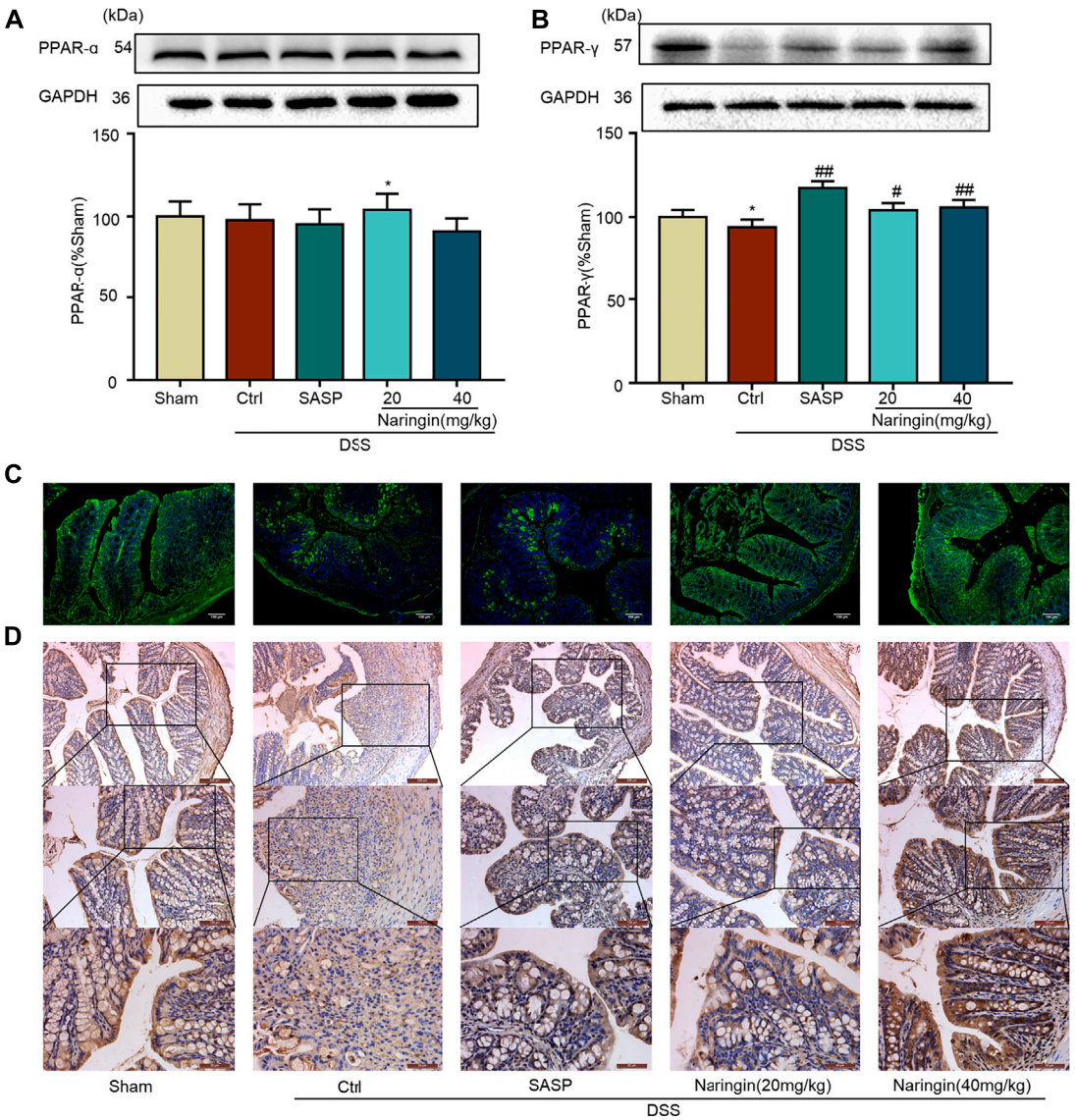

FIGURE 7 | Effects of naringin on PPAR-γ expression in DSS-colitis. Naringin was administered to mice by gavage once a day for seven consecutive days. **(A)** Western blotting analysis of PPAR-α. **(B)** Western blotting analysis of PPAR-γ. **(C)** IF staining of PPAR-γ in colonic epithelium. Scale bars, 100 μm. **(D)** IHC staining of PPAR-γ in colonic epithelium. Scale bars, 200, 100, and 50 μm. Data are expressed as mean ± SD. Values in the sham group are set to 100% and other values are given relative to those in the sham group. $^{**}p < 0.01$ compared with sham group; $^{\#}p < 0.05$, $^{\#\#}p < 0.01$ compared with DSS-colitis group; $n = 3$ samples in western blotting experiments; $n = 6$ samples for other experiments. These blots are cropped, and the full-length blots are presented is in the **Supplementary Figures S10–S13**.

Dubuquoy et al., 2002). Several studies have demonstrated that expression of PPAR-γ is reduced in UC patients (Dubuquoy et al., 2003; Pedersen and Brynskov, 2010). In the present study, PPAR-γ expression was significantly decreased in both DSS- and TNBS-induced colitis. Reduced PPAR-γ expression may lead to an increase in expression of nuclear transcription factor NF-κB. PPAR-γ can directly bind to NF-κB p50/NF-κB p65 dimer and inhibit the degradation of IκBα, thereby blocking the activation of NF-κB and its nuclear translocation (Chen et al., 2014). Gavage administration of naringin significantly alleviated colitis symptoms in two animal models. Increased MPO activity and higher levels of pro-inflammatory factors (TNF-α, IL-1β, and INF-γ) in colitis were significantly reversed by naringin. High expression of the inflammation-related protein iNOS in colitis was significantly decreased by naringin. Naringin also significantly reduced cl-caspase3 expression to maintain epithelial barrier. Naringin induced alleviation of colitis symptoms was abolished by PPAR-γ inhibitor BADGE, which suggests that PPAR-γ may be a target for naringin induced therapeutic effects on colitis.

In RAW264.7 cells, higher levels of pro-inflammatory factors (TNF-α, IL-1β, and INF-γ) were significantly reversed by naringin. In IEC-6 cells and RAW264.7 cells, LPS-induced high expression of NF-

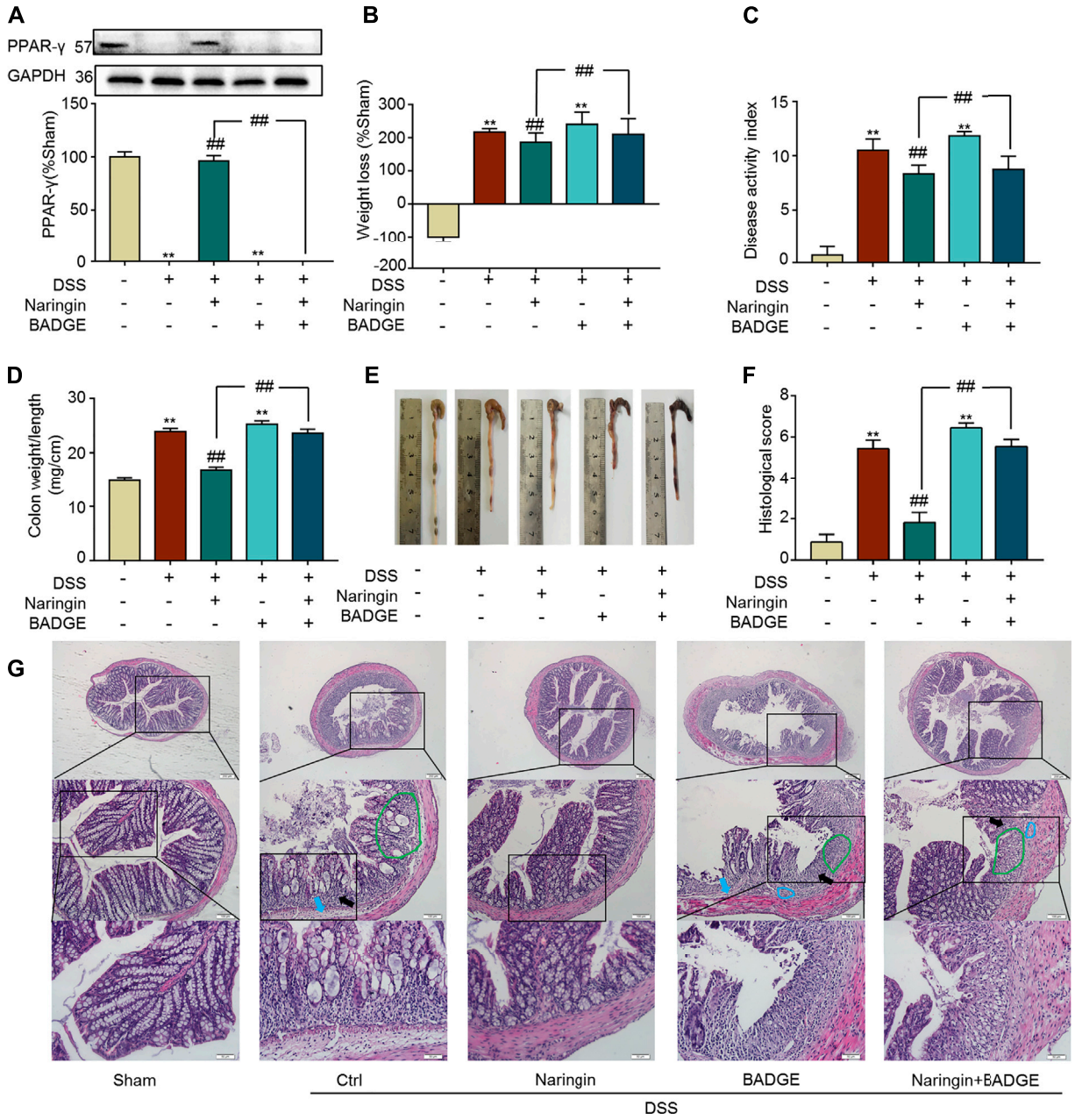

FIGURE 8 | Effects of PPAR-γ inhibitor BAGDE (30 mg/kg) on naringin induced treatment. **(A)** PPAR-γ expression in the presence of PPAR-γ inhibitor BAGDE. Effects of naringin (40 mg/kg) on **(B)** weight loss, **(C)** DAI, **(D)** colon weight-to-length ratio and **(E)** gross morphology of colon tissue. **(F)** Total histological score was calculated as the sum of epithelial damage and histological score. **(G)** H and E staining analysis of the aggravated symptoms with BADGE. Scale bars, 200, 100, and 50 μm. Green ring indicates damaged villi structure; black arrow indicates infiltration of inflammatory cells; blue ring indicates submucosal edema, blue arrow indicates muscle fiber separation. Data are expressed as mean ± SD. Values in the sham group are set to 100% and other values are given relative to those in the sham group. $^{**}p < 0.01$ compared with sham group; $^{\#\#}p < 0.01$ compared with DSS-colitis group; $n = 3$ samples in western blotting experiments; $n = 6$ samples for other experiments. These blots are cropped, and the full-length blots are presented is in the **Supplementary Figures S14–S15**.

κB-p65 was significantly reduced by naringin, and the reduction was inhibited by siRNA targeting PPAR-γ. All these results suggests that naringin exert treatment effects on colitis through inducing PPAR-γ activation. It has been reported that some PPAR-γ agonists, such as rosiglitazone, pioglitazone, exert inhibitory effects on inflammatory responses (Nitta et al., 2013; Zhou et al., 2021). In this study, we aimed to search and identify natural products which may serve as PPAR-γ agonists. Compared with chemical drugs, naringin is a monomer isolated from citrus fruit species with better safety.

The two animal models of colitis were used in this study to confirm the treatment effects of naringin. DSS-colitis is a type of acute injury and it is caused by disrupting the integrity of the mucosal barrier.

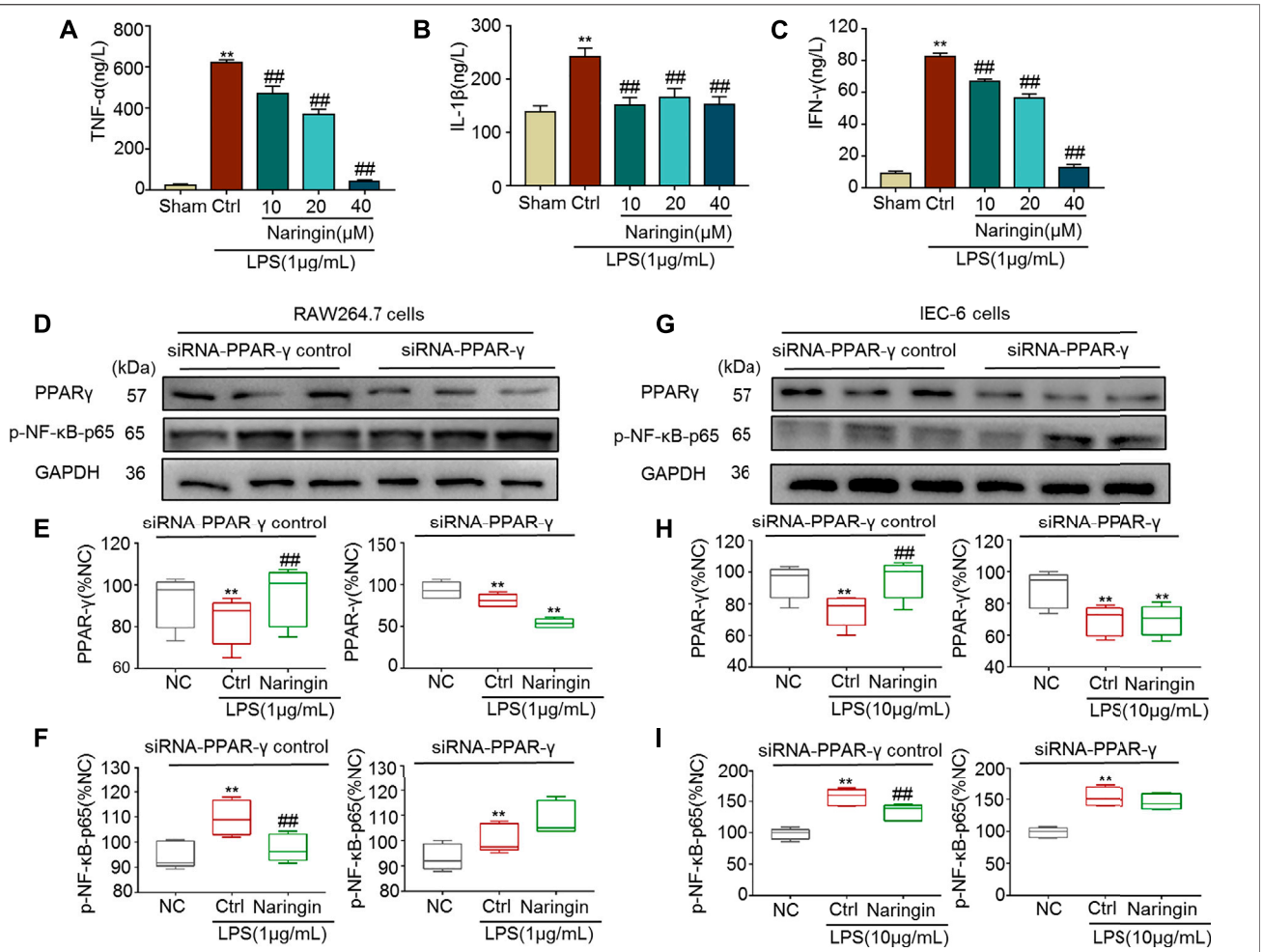

FIGURE 9 | The anti-inflammatory effect of naringin (20 μM) was eliminated by siRNA targeting PPAR-γ. Expression levels of the colonic cytokines **(A)** TNF-α, **(B)** IL-1β, **(C)** IFN-γ in DSS-induced RAW264.7 cells were determined by ELISA. Expression of PPAR-γ and p-NF-κB-p65 in the absence and presence of siRNA targeting PPAR-γ in **(D–F)** RAW 264.7 and **(G–I)** IEC-6 cells. Data are expressed as mean ± SD. Values in corresponding sham or normal control (NC) group are set to 100% and other values are given relative to the control values. $^{**}p < 0.01$ compared with sham/NC group; $^{\#\#}p < 0.01$ compared with DSS/LPS control group or as indicated; $n = 3$ samples in western blotting experiments; $n = 6$ samples for other experiments. These blots are cropped, and the full-length blots are presented is in the **Supplementary Figures S16–S21**.

TNBS-colitis is characterized by T-cell-mediated immunity against haptenized proteins and luminal antigens (Gadaleta et al., 2017). More or less, DSS-induced intestinal inflammation is mainly mediated by an excessive Th1 T-cell response (CD-like IBD), while TNBS-induced intestinal inflammation is a Th2-mediated inflammation (UC-like IBD) (Strober et al., 2002). PPAR-γ activation can inhibit the inflammatory response by inhibiting NF-κB. It is also known that PPAR-γ upregulating tight junction improves the integrity of intestinal mucosal barrier (Huang et al., 2020). In this study, naringin had a good therapeutic effect on both types of colitis through activating PPAR-γ. We used transcriptome sequencing to detect the expression of genes only in naringin treated DSS-induced C57BL/6 mice. Whether the mechanisms of naringin treatment of TNBS-colitis is the same as that of DSS-colitis still needs further investigation.

In conclusion, we uncovered the drug target net of naringin for alleviating DSS- and TNBS-induced colitis. We established a KEGG-target network to explore detailed mechanisms involved in naringin-induced amelioration of colitis symptoms. PPAR-γ may be a main potential target of naringin. There are still some limitations for our study, for example, the interaction between naringin and PPAR-γ is not clearly studied. The future plan is to extensively explore the interaction between naringin and PPAR-γ, including the exact binding site of PPAR-γ for naringin. The chemical structure of monomers isolated from Chinese medicinal plants is complex, and they can exert pharmacological effects through multiple targets. RNA-seq may be a good method to help researchers to construct the drug target net for monomers isolated from Chinese medicinal plants.

DATA AVAILABILITY STATEMENT

The datasets presented in this study can be found in online repositories. The names of the repository/repositories and accession number(s) can be found below: BioProject accession: PRJNA741857.

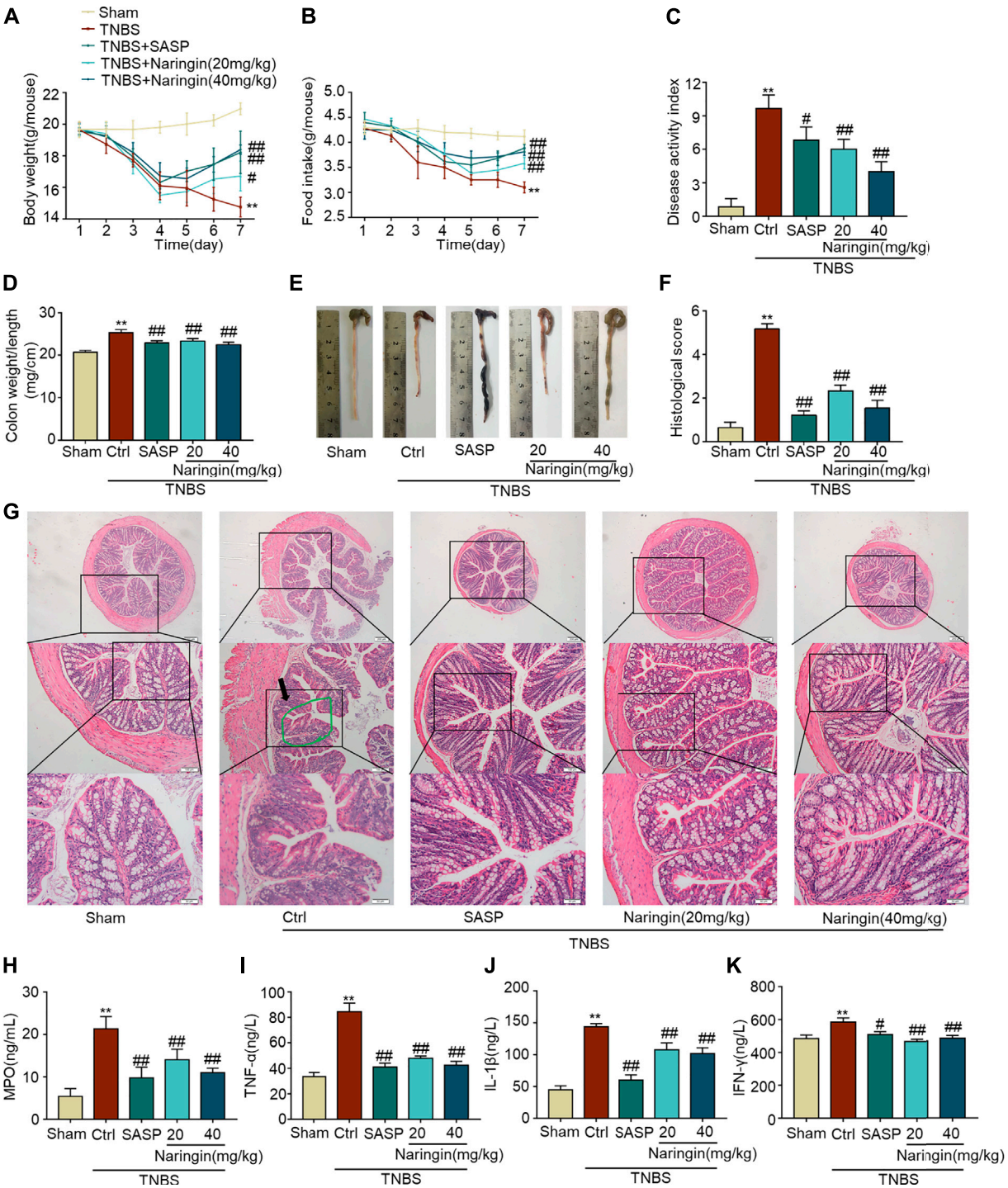

FIGURE 10 | Effects of naringin on TNBS-colitis. Naringin was administered to mice by gavage once a day for seven consecutive days. Effects of naringin on **(A)** body weight, **(B)** food intake, **(C)** DAI, **(D)** colon weight-to-length ratio, and **(E)** gross morphology of colon tissue. **(F)** Total histological score was calculated as the sum of epithelial damage and histological score. **(G)** H and E staining of mice colonic tissue. Scale bars, 200, 100, and 50 μm. Green ring indicates damaged villi structure; black arrow indicates infiltration of inflammatory cells. Expression levels of the colonic cytokines **(H)** MPO, **(I)** TNF-α, **(J)** IL-1β, and **(K)** IFN-γ were determined by ELISA. Data are expressed as mean ± SD. Values in the sham group are set to 100% and other values are given relative to those in the sham group. $^{**}p < 0.01$ compared with sham group; $^{\#}p < 0.05$, $^{\#\#}p < 0.01$ compared with TNBS-colitis group; $n = 6$ samples.

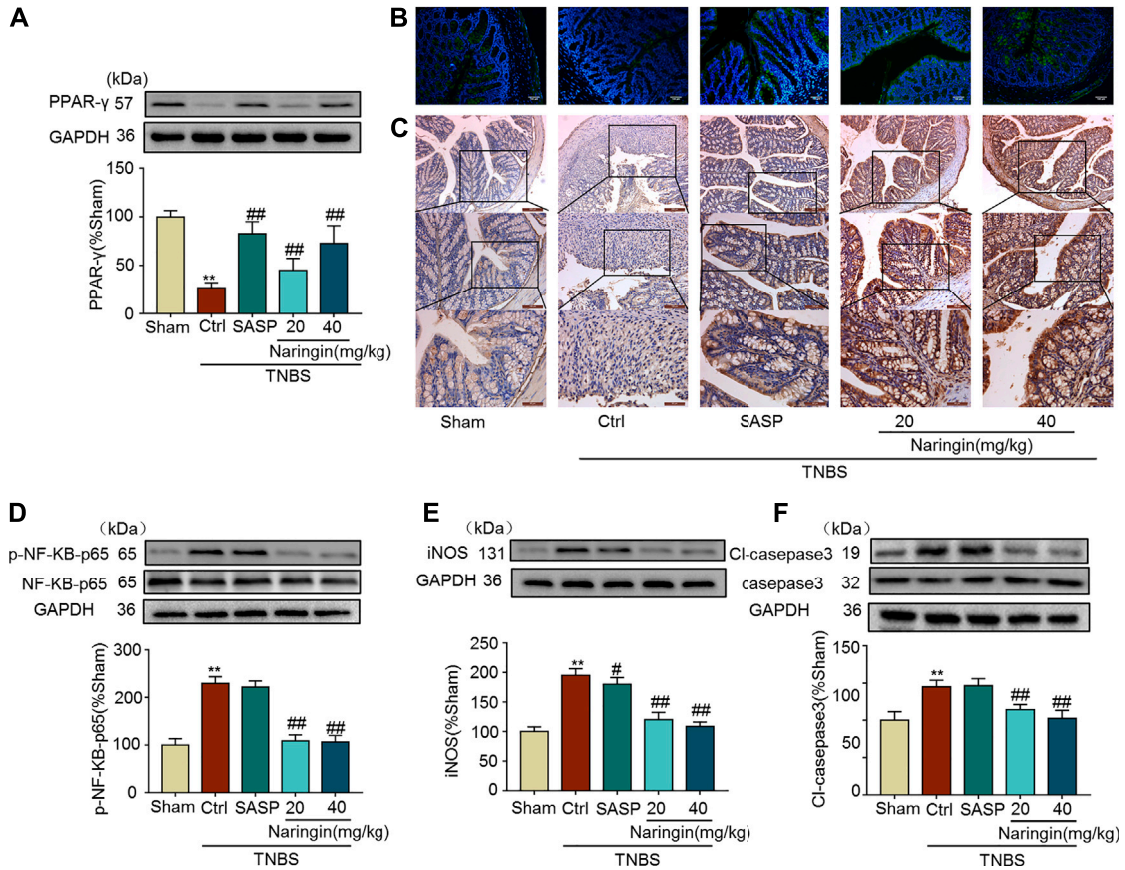

FIGURE 11 | Effects of naringin on PPAR-γ expression, inflammation and apoptosis in TNBS-colitis mouse model. **(A)** Western blotting analysis of PPAR-γ. **(B)** IF staining of PPAR-γ in colonic epithelium. Scale bars, 100 μm. **(C)** IHC staining of PPAR-γ in colonic epithelium. Scale bars, 200, 100, and 50 μm. Western blotting analysis of inflammation-related proteins **(D)** p-NF-κB-p65 (calculated as p-NF-κB-p65/ NF-κB-p65), **(E)** iNOS; apoptosis-related protein **(F)** cl-caspase3, calculated as cl-caspase3/caspase3. Data are expressed as mean ± SD. Values in the sham group are set to 100% and other values are given relative to those in the sham group. $^{**}p < 0.01$ compared with sham group; $^{\#}p < 0.05$, $^{\#\#}p < 0.01$ compared with TNBS-colitis group; $n = 3$ samples in western blotting experiments; $n = 6$ samples for other experiments. These blots are cropped, and the full-length blots are presented is in the **Supplementary Figures S22–S31**.

ETHICS STATEMENT

The animal study was reviewed and approved by the Laboratory Animal Ethics Committee of Dalian Medical University. Written informed consent was obtained from the owners for the participation of their animals in this study.

AUTHOR CONTRIBUTIONS

JD: Conceptualization, Methodology, Validation, Formal analysis, Visualization. YC: Formal analysis, Resources, Writing—original draft, Visualization. FY: Formal analysis, Resources, Visualization. WZ: Software, Formal analysis, Visualization. KW: Validation, Visualization. YX: Validation, Visualization. LW: Validation, Resources. ZZ: Formal analysis, Visualization. CL: Validation, Visualization. DC: Conceptualization, Methodology, Resources, Writing—review and editing, Supervision, Project administration. JW: Conceptualization, Resources, Writing—review and editing, Supervision, Funding acquisition.

FUNDING

The authors acknowledge the financial support received from the National Natural Science Foundation of China (Grant No. 81600440); Basic research projects of Liaoning Province Universities (Grant No. LQ2017042); Dalian high level talent support program (No. 2017RQ017); and National Key Research and Development Project of China (2017YFD050160203).

SUPPLEMENTARY MATERIAL

The Supplementary Material for this article can be found online at: https://www.frontiersin.org/articles/10.3389/fphar.2021.729414/full#supplementary-material

REFERENCES

Abraham, B. P., Ahmed, T., and Ali, T. (2017). Inflammatory Bowel Disease: Pathophysiology and Current Therapeutic Approaches. *Handb Exp. Pharmacol.* 239, 115–146. doi:10.1007/164_2016_122

Ahmad, S. F., Attia, S. M., Bakheet, S. A., Zoheir, K. M., Ansari, M. A., Korashy, H. M., et al. (2015). Naringin Attenuates the Development of Carrageenan-Induced Acute Lung Inflammation through Inhibition of NF-Kb, STAT3 and Pro-inflammatory Mediators and Enhancement of IκBα and Anti-inflammatory Cytokines. *Inflammation* 38, 846–857. doi:10.1007/s10753-014-9994-y

Ali, M. M., and El Kader, M. A. (2004). The Influence of Naringin on the Oxidative State of Rats with Streptozotocin-Induced Acute Hyperglycaemia. *Z. Naturforsch C J. Biosci.* 59, 726–733. doi:10.1515/znc-2004-9-1018

Bassaganya-Riera, J., Reynolds, K., Martino-Catt, S., Cui, Y., Hennighausen, L., Gonzalez, F., et al. (2004). Activation of PPAR Gamma and delta by Conjugated Linoleic Acid Mediates protection from Experimental Inflammatory Bowel Disease. *Gastroenterology* 127, 777–791. doi:10.1053/j.gastro.2004.06.049

Bolger, A. M., Lohse, M., and Usadel, B. (2014). Trimmomatic: a Flexible Trimmer for Illumina Sequence Data. *Bioinformatics* 30, 2114–2120. doi:10.1093/bioinformatics/btu170

Cao, H., Liu, J., Shen, P., Cai, J., Han, Y., Zhu, K., et al. (2018). Protective Effect of Naringin on DSS-Induced Ulcerative Colitis in Mice. *J. Agric. Food Chem.* 66, 13133–13140. doi:10.1021/acs.jafc.8b03942

Chen, K., Li, J., Wang, J., Xia, Y., Dai, W., Wang, F., et al. (2014). Erratum to "15-Deoxy-Γ12,14-Prostaglandin J2 Reduces Liver Impairment in a Model of ConA-Induced Acute Hepatic Inflammation by Activation of PPARγ and Reduction in NF-Kb Activity". *PPAR Res.* 2014, 864839. doi:10.1155/2014/864839

Conesa, A., Madrigal, P., Tarazona, S., Gomez-Cabrero, D., Cervera, A., McPherson, A., et al. (2016). A Survey of Best Practices for RNA-Seq Data Analysis. *Genome Biol.* 17, 13. doi:10.1186/s13059-016-0881-8

Dong, J.-y., Xia, K.-j., Liang, W., Liu, L.-l., Yang, F., Fang, X.-s., et al. (2020). Ginsenoside Rb1 Alleviates Colitis in Mice via Activation of Endoplasmic Reticulum-Resident E3 Ubiquitin Ligase Hrd1 Signaling Pathway. *Acta Pharmacol. Sin*. doi:10.1038/s41401-020-00561-9

Dubuquoy, L., Dharancy, S., Nutten, S., Pettersson, S., Auwerx, J., and Desreumaux, P. (2002). Role of Peroxisome Proliferator-Activated Receptor Gamma and Retinoid X Receptor Heterodimer in Hepatogastroenterological Diseases. *Lancet* 360, 1410–1418. doi:10.1016/s0140-6736(02)11395-x

Dubuquoy, L., Jansson, E. A., Deeb, S., Rakotobe, S., Karoui, M., Colombel, J. F., et al. (2003). Impaired Expression of Peroxisome Proliferator-Activated Receptor Gamma in Ulcerative Colitis. *Gastroenterology* 124, 1265–1276. doi:10.1016/s0016-5085(03)00271-3

Feng, P. P., Fang, X. S., Zhao, S. H., Fu, J. Y., Zhang, H. T., Yi, Y. L., et al. (2020). Salvianolic Acid B Decreases Interleukin-1β-Induced Colitis Recurrence in Mice. *Chin. Med. J. (Engl)* 133, 1436–1444. doi:10.1097/cm9.0000000000000773

Gadaleta, R. M., Garcia-Irigoyen, O., and Moschetta, A. (2017). Exploration of Inflammatory Bowel Disease in Mice: Chemically Induced Murine Models of Inflammatory Bowel Disease (IBD). *Curr. Protoc. Mouse Biol.* 7, 13–28. doi:10.1002/cpmo.20

Gao, F., Liu, X., Wu, X. P., Wang, X. L., Gong, D., Lu, H., et al. (2012). Differential DNA Methylation in Discrete Developmental Stages of the Parasitic Nematode *Trichinella spiralis*. *Genome Biol.* 13, R100. doi:10.1186/gb-2012-13-10-r100

Grivennikov, S. I. (2013). Inflammation and Colorectal Cancer: Colitis-Associated Neoplasia. *Semin. Immunopathol* 35, 229–244. doi:10.1007/s00281-012-0352-6

Holmer, A., and Singh, S. (2019). Overall and Comparative Safety of Biologic and Immunosuppressive Therapy in Inflammatory Bowel Diseases. *Expert Rev. Clin. Immunol.* 15, 969–979. doi:10.1080/1744666X.2019.1646127

Huang, Y., Wang, C., Tian, X., Mao, Y., Hou, B., Sun, Y., et al. (2020). Pioglitazone Attenuates Experimental Colitis-Associated Hyperalgesia through Improving the Intestinal Barrier Dysfunction. *Inflammation* 43, 568–578. doi:10.1007/s10753-019-01138-3

Jeon, S. M., Bok, S. H., Jang, M. K., Lee, M. K., Nam, K. T., Park, Y. B., et al. (2001). Antioxidative Activity of Naringin and Lovastatin in High Cholesterol-Fed Rabbits. *Life Sci.* 69, 2855–2866. doi:10.1016/s0024-3205(01)01363-7

Kaplan, G. G., and Windsor, J. W. (2021). The Four Epidemiological Stages in the Global Evolution of Inflammatory Bowel Disease. *Nat. Rev. Gastroenterol. Hepatol.* 18, 56–66. doi:10.1038/s41575-020-00360-x

Kihara, N., de la Fuente, S. G., Fujino, K., Takahashi, T., Pappas, T. N., and Mantyh, C. R. (2003). Vanilloid Receptor-1 Containing Primary Sensory Neurones Mediate Dextran Sulphate Sodium Induced Colitis in Rats. *Gut* 52, 713–719. doi:10.1136/gut.52.5.713

Kilkenny, C., Browne, W., Cuthill, I. C., Emerson, M., and Altman, D. G. (2010). Animal Research: Reporting *In Vivo* Experiments: the ARRIVE Guidelines. *J. Physiol.* 588, 2519–2521. doi:10.1113/jphysiol.2010.192278

Kukurba, K. R., and Montgomery, S. B. (2015). RNA Sequencing and Analysis. *Cold Spring Harb Protoc.* 2015, 951–969. doi:10.1101/pdb.top084970

Lefebvre, M., Paulweber, B., Fajas, L., Woods, J., McCrary, C., Colombel, J. F., et al. (1999). Peroxisome Proliferator-Activated Receptor Gamma Is Induced during Differentiation of colon Epithelium Cells. *J. Endocrinol.* 162, 331–340. doi:10.1677/joe.0.1620331

Liu, X., Yu, X., Xu, X., Zhang, X., and Zhang, X. (2018). The Protective Effects of Poria Cocos-Derived Polysaccharide CMP33 against IBD in Mice and its Molecular Mechanism. *Food Funct.* 9, 5936–5949. doi:10.1039/c8fo01604f

Melgar, S., Karlsson, A., and Michaëlsson, E. (2005). Acute Colitis Induced by Dextran Sulfate Sodium Progresses to Chronicity in C57BL/6 but Not in BALB/c Mice: Correlation between Symptoms and Inflammation. *Am. J. Physiol. Gastrointest. Liver Physiol.* 288, G1328–G1338. doi:10.1152/ajpgi.00467.2004

Nitta, Y., Tahara, N., Tahara, A., Honda, A., Kodama, N., Mizoguchi, M., et al. (2013). Pioglitazone Decreases Coronary Artery Inflammation in Impaired Glucose Tolerance and Diabetes Mellitus: Evaluation by FDG-PET/CT Imaging. *JACC Cardiovasc. Imaging* 6, 1172–1182. doi:10.1016/j.jcmg.2013.09.004

Pedersen, G., and Brynskov, J. (2010). Topical Rosiglitazone Treatment Improves Ulcerative Colitis by Restoring Peroxisome Proliferator-Activated Receptor-Gamma Activity. *Am. J. Gastroenterol.* 105, 1595–1603. doi:10.1038/ajg.2009.749

Rodansky, E. S., Johnson, L. A., Huang, S., Spence, J. R., and Higgins, P. D. (2015). Intestinal Organoids: a Model of Intestinal Fibrosis for Evaluating Anti-fibrotic Drugs. *Exp. Mol. Pathol.* 98, 346–351. doi:10.1016/j.yexmp.2015.03.033

Sairenji, T., Collins, K. L., and Evans, D. V. (2017). An Update on Inflammatory Bowel Disease. *Prim. Care* 44, 673–692. doi:10.1016/j.pop.2017.07.010

Storr, M., Emmerdinger, D., Diegelmann, J., Pfennig, S., Ochsenkühn, T., Göke, B., et al. (2010). The Cannabinoid 1 Receptor (CNR1) 1359 G/A Polymorphism Modulates Susceptibility to Ulcerative Colitis and the Phenotype in Crohn's Disease. *PloS one* 5, e9453. doi:10.1371/journal.pone.0009453

Strober, W., Fuss, I. J., and Blumberg, R. S. (2002). The Immunology of Mucosal Models of Inflammation. *Annu. Rev. Immunol.* 20, 495–549. doi:10.1146/annurev.immunol.20.100301.064816

Sui, J., Zhang, C., Fang, X., Wang, J., Li, Y., Wang, J., et al. (2020). Dual Role of Ca2+-Activated Cl- Channel Transmembrane Member 16A in Lipopolysaccharide-Induced Intestinal Epithelial Barrier Dysfunction *In Vitro*. *Cell Death Dis* 11, 404. doi:10.1038/s41419-020-2614-x

Sun, W., Cai, Y., Zhang, X. X., Chen, H., Lin, Y. D., and Li, H. (2017). Osthole Pretreatment Alleviates TNBS-Induced Colitis in Mice via Both cAMP/PKA-dependent and Independent Pathways. *Acta Pharmacol. Sin* 38, 1120–1128. doi:10.1038/aps.2017.71

Wang, L., Xie, H., Xu, L., Liao, Q., Wan, S., Yu, Z., et al. (2017). rSj16 Protects against DSS-Induced Colitis by Inhibiting the PPAR-α Signaling Pathway. *Theranostics* 7, 3446–3460. doi:10.7150/thno.20359

Wang, R., Gu, X., Dai, W., Ye, J., Lu, F., Chai, Y., et al. (2016). A Lipidomics Investigation into the Intervention of Celastrol in Experimental Colitis. *Mol. Biosyst.* 12, 1436–1444. doi:10.1039/c5mb00864f

Wang, Y., Li, J. X., Ji, G. J., Zhai, K., Wang, H. H., and Liu, X. G. (2016). The Involvement of Ca(2+) Signal Pathways in Distal Colonic Myocytes in a Rat Model of Dextran Sulfate Sodium-Induced Colitis. *Chin. Med. J. (Engl)* 129, 1185–1192. doi:10.4103/0366-6999.181968

Xiong, Y., Shi, L., Wang, L., Zhou, Z., Wang, C., Lin, Y., et al. (2017). Activation of Sirtuin 1 by Catalpol-Induced Down-Regulation of microRNA-132 Attenuates Endoplasmic Reticulum Stress in Colitis. *Pharmacol. Res.* 123, 73–82. doi:10.1016/j.phrs.2017.05.030

Yanai, H., and Hanauer, S. B. (2011). Assessing Response and Loss of Response to Biological Therapies in IBD. *Am. J. Gastroenterol.* 106, 685–698. doi:10.1038/ajg.2011.103

Zhang, Y. S., Li, Y., Wang, Y., Sun, S. Y., Jiang, T., Li, C., et al. (2016). Naringin, a Natural Dietary Compound, Prevents Intestinal Tumorigenesis in Apc (Min/+) Mouse Model. *J. Cancer Res. Clin. Oncol.* 142, 913–925. doi:10.1007/s00432-015-2097-9

Zhou, J. P., Yang, X. N., Song, Y., Zhou, F., Liu, J. J., Hu, Y. Q., et al. (2021). Rosiglitazone Alleviates Lipopolysaccharide-Induced Inflammation in RAW264.7 Cells via Inhibition of NF-Kb and in a PPARγ-dependent Manner. *Exp. Ther. Med.* 22, 743. doi:10.3892/etm.2021.10175

Conflict of Interest: The authors declare that the research was conducted in the absence of any commercial or financial relationships that could be construed as a potential conflict of interest.

Publisher's Note: All claims expressed in this article are solely those of the authors and do not necessarily represent those of their affiliated organizations, or those of the publisher, the editors and the reviewers. Any product that may be evaluated in this article, or claim that may be made by its manufacturer, is not guaranteed or endorsed by the publisher.

frontiers in Pharmacology

ORIGINAL RESEARCH
published: 30 August 2021
doi: 10.3389/fphar.2021.693100

Hydrogen Sulfide Prevents Mesenteric Adipose Tissue Damage, Endothelial Dysfunction, and Redox Imbalance From High Fructose Diet-Induced Injury in Aged Rats

*Oleh Revenko[1], Yaroslav Pavlovskiy[1], Maryana Savytska[1], Antonina Yashchenko[2], Vasyl Kovalyshyn[2], Ilona Chelpanova[2], Olena Varyvoda[3] and Oksana Zayachkivska[1]**

[1]Department of Physiology, Danylo Halytsky Lviv National Medical University, Lviv, Ukraine, [2]Department of Histology, Cytology and Embryology, Danylo Halytsky Lviv National Medical University, Lviv, Ukraine, [3]Department of Pathological Anatomy and Forensic Medicine, Danylo Halytsky Lviv National Medical University, Lviv, Ukraine

OPEN ACCESS

Edited by:
Sven Seiwerth,
University of Zagreb, Croatia

Reviewed by:
Luis Enrique Gomez-Quiroz,
Autonomous Metropolitan University, Mexico
Alaaeldin Ahmed Hamza,
National Organization for Drug Control and Research (NODCAR), Egypt

***Correspondence:**
Oksana Zayachkivska
ozayachkivska@gmail.com

Specialty section:
This article was submitted to Gastrointestinal and Hepatic Pharmacology, a section of the journal Frontiers in Pharmacology

Received: *09 April 2021*
Accepted: *22 July 2021*
Published: *30 August 2021*

Citation:
Revenko O, Pavlovskiy Y, Savytska M, Yashchenko A, Kovalyshyn V, Chelpanova I, Varyvoda O and Zayachkivska O (2021) Hydrogen Sulfide Prevents Mesenteric Adipose Tissue Damage, Endothelial Dysfunction, and Redox Imbalance From High Fructose Diet-Induced Injury in Aged Rats. Front. Pharmacol. 12:693100. doi: 10.3389/fphar.2021.693100

A high fructose diet (HFD) and advanced age are key factors for the gradual loss of physiological integrity of adipose tissue. Endogenous hydrogen sulfide (H_2S) has beneficial effects on cytoprotection and redox balance. But its interactive effects on age-related damage of mesenteric vessels and connective and adipose tissues (MA) during HFD which could be the base of the development of effective physiological-based therapeutic strategy are unknown. The aim of study was to investigate age- and HFD-induced mesenteric cellular changes and activities of enzymes in H_2S synthesis and to test the effects of sodium hydrosulfide (NaHS) which is considered an H_2S donor on them. Adult and aged male rats on a standard diet (SD) or 4-week HFD were exposed to acute water-immersion restraint stress (WIRS) for evaluation of mesenteric subcellular and cellular adaptive responses by electron microscopy. The effects of exogenous NaHS (5.6 mg/kg/day for 9 days) versus vehicle on mesentery changes were investigated. Serum glucose level, thiobarbituric acid reactive substances (TBARS), and activities of cystathionine γ-lyase (CSE) and cystathionine β-synthase (CBS), thiosulfate-dithiol sulfurtransferase (TST), and sulfite oxidase (SO) were examined by spectrophotometry. In both adult and aged SD groups, treatment with NaHS protected mesenteric cells after WIRS. In both groups, the treatment with NaHS also protected MA mitochondria, microvascular endothelial and sub-endothelial structures, and fibroblasts versus the vehicle-treated group that had signs of damage. HFD increased MA injury and mitochondrial changes in both aged and adult rats. HFD-associated malfunction is characterized by low activities of CSE, CBS, TST, SO, and increased TBARS. Finally, we demonstrated that pretreatment with NaHS inhibited MA and mitochondria alterations in aged rats exposed to HFD and WIRS, lowered TBARS, and enhanced H_2S enzyme

Abbreviations: CECs: capillary endothelial cells; CBS: cystathionine beta-synthase; CSE: cystathionine gamma-lyase; H_2S: hydrogen sulfide; HFD: high fructose diet; MA: mesenteric white adipocyte; NaHS: sodium hydrosulfide; NSAIDs: nonsteroidal anti-inflammatory drugs; SD: standard diet; SO: sulfite oxidase; TST: thiosulfate-dithiol sulfurtransferase; TBARS: thiobarbituric acid reactive substances; WIRS: water-immersion restraint stress.

activities in contrast to the vehicle-treated group. Mitochondrial integrity alterations, endothelial damage, and redox imbalance are key factors for rat mesenteric adipose tissue damage during advanced age. These alterations and MA hypertrophic changes retain the central for HFD-induced damage. Moreover, H_2S signaling contributes to MA and mitochondria redox balance that is crucial for advanced age and HFD injury. The future study of H_2S donors' effects on mesenteric cells is fundamental to define novel therapeutic strategies against metabolic changes.

Keywords: white adipocyte, mitochondria, mesentery, H_2S (hydrogen sulfide), high fructose consumption, age-related, NaHS

INTRODUCTION

There is growing evidence that suggests the importance of the functional roles of adipose tissue. This includes white adipocytes, brown adipocytes, and beige adipocytes, which differ in morphology and functions (Hilton et al., 2015; Shimizu et al., 2015; Lee et al., 2019). These cells are unique in their ability to collect and integrate thousands of different types of input and to translate them into signaling pathways that are responsible for pleiotropic expression contributing to the risk of numerous metabolic disorders related to obesity, type 2 diabetes, and gastrointestinal and cardiovascular diseases processes (Li et al., 2018; Scheja et al., 2019; Zhu et al., 2019). Recent clinical data has shown that markers of both obesity and the COVID-19 had severe negative outcomes when these cofactors are present in older age, leading to multi-organ dysfunction (Korakas et al., 2020; Tamara et al., 2020).

Since the visceral, gonadal, and subcutaneous white adipose tissues have different physiological and metabolic functions and adaptive potential, these tissues have diverse roles in metabolism regulation (Wronska and Kmiec, 2012; Do et al., 2019). It is widely understood that maintaining mitochondrial homeostasis and its quality is crucial for varied signaling pathways for cytoprotection, apoptosis, or inflammation (Cedikova et al., 2016; Kiriyama et al., 2018; He et al., 2020). Moreover, ultrastructural studies of white adipocytes are helpful to determine the shape, quality, and quantity of their mitochondria, focusing on them as a target for novel therapy strategies (Miliotis et al., 2019). The recent discovery has noted visceral fat tissue that contains white adipocytes physiologically active in the mesentery, newly described as separate organs in the abdominal cavity (Coffey et al., 2020). Adipocytes in the mesentery (MA) have a poor blood capillary supply and intrinsically low antioxidant enzyme defenses which make them vulnerable to hypoxia and free radical damage (Kredel et al., 2014). Since it has been reported that the accumulation of a mesenteric adipocyte tissue (known as creeping fat) is the driving force for transmural inflammation, interaction MA and fibrosis may play role in the pathogenesis of several diseases, like Crohn's disease (Mao et al., 2019; Rivera et al., 2019). However, the exact mechanism of adipose tissue damage which is defined as the gradual loss of physiological integrity with both quantitative and qualitative changes in adipocyte numbers and stromal-vascular cell composition is not yet entirely understood (Wang et al., 2018; Conte et al., 2019; Streich et al., 2020). Recently, in the previous study, we have obtained results of MA changes during exposure to a high fructose diet (HFD) (Revenko et al., 2020). Moreover, the link between mesenteric white adipocytes damage during aging and the chronic overload nutrition of glycemic carbohydrates still remains incomplete; thus, in this report, we demonstrate that mesenteric cells can change in advanced age and have compared their change during HFD.

The vasodilatory, anti-inflammatory, antioxidant properties of endogenous hydrogen sulfide (H_2S) have beneficial effects as H_2S donors on cytoprotection during metabolic dysregulation in numerous studies (Suzuki et al., 2011; Shibuya and Kimura, 2013). The impact of H_2S signaling and redox balance on mitochondria has recently been demonstrated as a critical control point between the physiological and pathological states (Murphy et al., 2019; Paul et al., 2020). However, little is known about the effect of H_2S on mitochondria dynamics in mesenteric white adipocytes during metabolic states related to aging and the chronic overnutrition of glycemic carbohydrates which has a crucial impact on oxidative damage (Mezouari et al., 2020). Recently, it has been shown that chronic fructose overload causes metabolic disorders and comorbidities (Bidwell, 2017; de Farias Lelis et al., 2020). There is a pressing need for translational research to study the link of MA damage as the gradual loss of physiological integrity and redox system during aging and the chronic overnutrition of glycemic carbohydrates. This will help develop effective target-focused therapy. Since H_2S may also control the processes important for redox balance, we hypothesized that, by studying biomarkers of lipid peroxidation products based on levels of thiobarbituric acid reactive substances (TBARS) and activities of enzymes involved in H_2S synthesis, we will clarify the mechanism of H_2S effects on mesenteric white cells during aging and in an experimental metabolic model using rat fed with high fructose diet (HFD). These enzymes include cystathionine γ-lyase (CSE), cystathionine β-synthase (CBS), thiosulfate-dithiol sulfurtransferase (TST), and sulfite oxidase (SO) which control the redox system on an intracellular and intercellular basis. Thus, the objectives of this study are 1) to have a closer look at early age-related changes in mesenteric adipocytes in rats fed with SD and during HFD and 2) to investigate mesenteric white adipocyte tissue damage characteristics focusing on the mitochondria-centered picture during stress induction and stimulation of the endogenous H_2S bioavailability by exogenous NaHS administration.

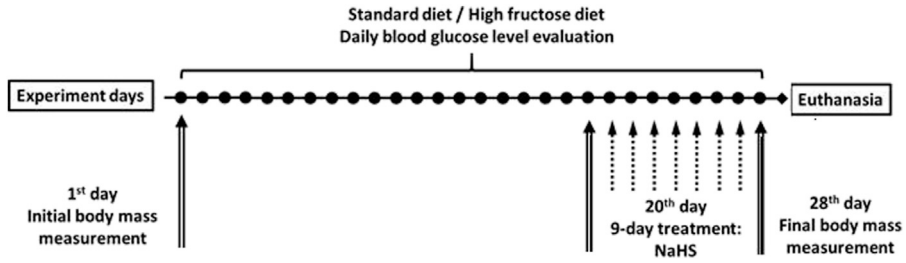

FIGURE 1 | Overview of the study.

METHODS

Ethical Approval

All experiments were approved by the local animal care committee at the Danylo Halytsky Lviv National Medical University Ethics Committee (protocol April 23, 2018, № 4) and were carried out in accordance with the National Institute of Health Guide for the Care and Use of Laboratory Animals (NIH Publications No. 80-23) revised 1996 or the United Kingdom Animals (Scientific Procedures) Act 1986 and associated guidelines, or the European Communities Council Directive of November 24, 1986 (86/609/EEC). All efforts were made to minimize animal suffering and to reduce the number of animals used.

Overall Study Design and Experimental Animals

All experiments were performed on male adult (age = 12–14 weeks, $n = 36$) and aged Wistar rats (age = 42–46 weeks, $n = 36$). Animals were maintained under a constant 12 h light and dark cycle and an ambient temperature of 21–23°C with 50 ± 10% relative humidity. All animals were kept in raised mesh-bottom cages to prevent coprophagy and subdivided into groups ($n = 6$). **Figure 1** shows the design of the study. Rats were randomly assigned to nine experimental groups. Adult and aged rats in the control groups had free access to water and were fed a standard diet (SD). Animals in the experimental groups were fed a high fructose diet (HFD) by receiving 28-day unrestricted access to a 40% solution of fructose ad libitum and fed at the same time SD (Pavlovskiy et al., 2020). To investigate adaptive reactions to acute injury on the 29th day of study, acute stress was induced by the model of Takagi Takagi and Okabe (1968) that involves short-term exposure to water-immersion restraint stress (WIRS). For this intervention, the rats were placed in restraint cages and immersed vertically to the level of the xiphoid process in a water bath of 23°C for 3.5 h. Food deprivation for 12 h before the end of experiments has been performed for all rats. Daily animal health checks were performed by laboratory or institutional laboratory animal staff, under the supervision of the institutional veterinarian.

Weights were recorded at the beginning and end of the study by an RN 10C13U, 100 g–10 kg, ±5 g (Vaga, Kyiv, Ukraine). Rat blood glucose concentrations were measured daily after 15 h of fasting (18:00–9:00) by a glucometer (Achtung TD-4207, Munich, Germany) using a blood sample from the tail vein. The data in each group were compared at the beginning and end of the study and with the results from control rats. At the end of the experiment, the rats were deeply anesthetized with an intramuscular injection of ketamine (60 mg/kg; Biovet, Bila Tserkva, Ukraine) and sacrificed, and after that, blood was collected and the samples of the mesentery tissue associated were resected. After thoroughly washing with saline, sections of the mesentery were taken for histological examination and the establishment of macroscopic signs of damage. Samples for histological cellular and subcellular analysis by electron microscopy were obtained from the mesentery associated with the small intestine.

The Cellular and Subcellular Investigation *via* Electron Microscopy

We directed electron microscope evaluation of the mesentery to assess adipocytes, vascular changes, fibroblasts, and collagen fibers. For the cellular and subcellular analysis, the mesenteric material was fixed with a 2% solution of osmium oxide (OsO_4) eV 0.10 mol/L phosphate buffer. Subsequently, mesenteric material was processed according to generally accepted methods.

Ultrathin sections (30–60 nm) were made using an ultramicrotome UTMTP-3M (Sumy Electron Optics PKF, Sumy, Ukraine). After Reynolds staining, sections were photographed and examined using an electron microscope «UEMV-100K» (Sumy Electron Optics PKF, Sumy, Ukraine) at a magnification of 4,000, 6,000, and 10,000x. Histological analyses were performed by at least two independent people blinded to the identity of the samples. About 15 different cells in each sample were analyzed per rat. A single researcher that was unaware of the experimental groups performed the analysis. The state of histopathological mesentery changes in each group in comparison with that of the other groups was determined by protocol-blinded researchers.

Biochemical Analysis

Blood glucose concentrations were measured daily by a glucometer (Achtung TD-4207, Munich, Germany) using a blood sample from the tail vein.

On the 29th day of the study, animals were sacrificed, and the samples from rat blood and mesentery which belong to the intestinal mucosa were evaluated for the serum TBARS levels and catalytic activities of CBS (EC 4.2.1.22), CSE (EC 4.4.1.1), SO

(EC 1.8.3.1), and TST (EC 2.8.1.5). The resected material was washed with cold 1.15% potassium chloride solution, after which the mucous membrane was separated and homogenized in a medium of 1.15% potassium chloride in a ratio of 1:4. The mesenteric homogenates were centrifuged at 600 g and 40°C for 30 min to obtain a post-nuclear fraction.

Determination of Metabolic and Redox Balance Parameters by TBARS Levels and CBS, CSE, SO, and TST Activities

Plasma TBARS levels, as a biomarker of systemic effect of lipid peroxidation and oxidative damage Montes-Nieto et al. (2017), were evaluated by assaying reaction with thiobarbituric acid. The resulting lipid peroxidation products from a red-stained complex are extracted with butanol. The test tubes containing the serum were cooled at room temperature and maximum light absorbance was measured at 535 nm using a UV-visible spectrophotometer (Apel PD-303, Saitama, Japan) (Zaichko et al., 2009; Zaichko et al., 2014). We evaluated CBS, CSE, SO, and TST activities in mesenteric homogenates (nmol/min*1 mg of protein), using a modified version of the Stipanuk M.H. and Beck P.W. method as previous (Stipanuk et al., 1982; Pavlovskiy et al., 2020). Substrate and cofactor concentrations, pH, and incubation time, which could provide optimal conditions for enzyme activity determination, were selected in advance.

Treatment Groups

The animals were subdivided into control groups of adult rats and aged rats with consuming normal rodent chow (SD) and experimental groups receiving 28-day hypercaloric HFD, without and with acute stress. To evaluate the role of H_2S from the 19th day of the experiment, both adult and aged animals group days were treated for 9 days intragastrically by saline (as the vehicle), with NaHS at a dose of 5.6 mg/kg/day and NaHS, 5.6 mg/kg/day and stress induction. The administration of NaHS was performed in doses tested previously.

Data and Statistical Analysis

All results were evaluated using Statistical Analysis System and visualization program « Statistica 7.0» (StatSoft, Informer Technologies, Inc.) and expressed as mean ± standard deviation for a series of experiments. A paired Mann–Whitney *U* test was used for comparisons of paired treatments between two groups, and one-way ANOVA using Dunnett's test was performed to compare different experimental groups with control. Statistical significance was set to p values ≤0.05.

RESULTS

Effect of 4-Week High Fructose Diet on Adult and Aged Rats Fed With Standard Diet and High Fructose Diet

Basal metabolic characteristics from adult and aged rats fed with SD were body weight: 198 ± 20 g and 256 ± 28 g and fasting glucose: 6.3 ± 0.2 nmol/L and 6.5 ± 0.2 nmol/L, respectively. Aged rats' basal body weight was 29% more than adult rats ($p < 0.05$). There were no differences in adult rat body weight between the vehicle group and supplemented NaHS. At the end of the experiment rats fed with HFD had 32% increased final body weight in the aged group in comparison to the adult group ($p < 0.05$). Administration of NaHS did not affect final adult rat body weight fed with HFD. There were no differences in adult animals fed SD basal fasting glucose between groups supplemented with vehicle and NaHS. After 4 weeks of HFD administration in adult animals, fasting glucose levels were increased by 25% ($p < 0.05$) versus adults on SD; however, no differences were noted between the vehicle group and supplemented NaHS. At the end of the experiment, aged rats fed HFD exhibited increased fasting glucose levels by 29%. NaHS also did not affect final fasting glucose in aged rats fed with HFD.

Rats fed with HFD for 28 days exhibited an elevation of fasting blood glucose levels (from 6.3 ± 0.2 mmol/L to 7.9 ± 0.7 mmol/L for adult rats; from 6.5 ± 0.3 mmol/L to 8.4 ± 0.7 mmol/L for aged rats ($p < 0.05$ vs. rats with SD)) and about 67% (adult rats) and 71% (aged rats) gain in body weight (342 ± 31 g for adult rats; 451 ± 32 g for aged rats) over that of the control rats with SD (200 ± 21 g for adult rats; 270 ± 28 g for aged rats; $p \geq 0.001$).

The Ultrastructural Differences of Mesenteric White Adipocytes and Microvessels in Adult and Aged Rats

The obtained mesenteric material of adult and aged rats from the area associated with the small intestine fed with SD and treated with vehicle exhibited age-related differences in ultrastructural appearance represented in **Figure 2**. The representative photomicrographs of few adipocyte fragments without signs of fat fragmentation and well-preserved capillary endothelial cells (CECs) with erythrocyte in the lumen in adult rats fed with SD demonstrated data in **Figure 2A**. Examination of the mesenteric material of aged rats on SD revealed the degenerating adipocyte with signs in the cytoplasm of fat fragmentation and different shaped mitochondria demonstrated in **Figure 2B.** This image shows the age-related different mitochondrial morphological changes, including the round-shaped mitochondria in the act of cross talk with other mitochondria in the cytoplasm of white adipocytes.

Effect of H_2S on Ultrastructural Changes of Mesenteric White Adipocytes, Microvessels, and Connective Tissue in Aged Rats Exhibited 4-Week HFD and Acute Stress

To assess the effect of H_2S on the adaptive changes of mesenteric white adipocytes in aged rats fed with HFD, the treatment by NaHS and exposition to WIRS was used. Representative images of various kinds of changes in white adipocytes in aged rats fed with HFD with belonged stromal-vascular cells are shown in **Figure 3**. The differences of mesenteric white adipocytes in aged rats fed HFD and vehicle were observed (**Figure 3A, B**) in comparison to the group of aged rats fed HFD with NaHS treatment (**Figure 3C, D**). The adipocyte in aged rats fed HFD and vehicle were with signs of fat fragmentation and disrupted basal membrane, with many small lipid drops in the cytoplasm and different shaped mitochondria (**Figure 3A**). Many smallest

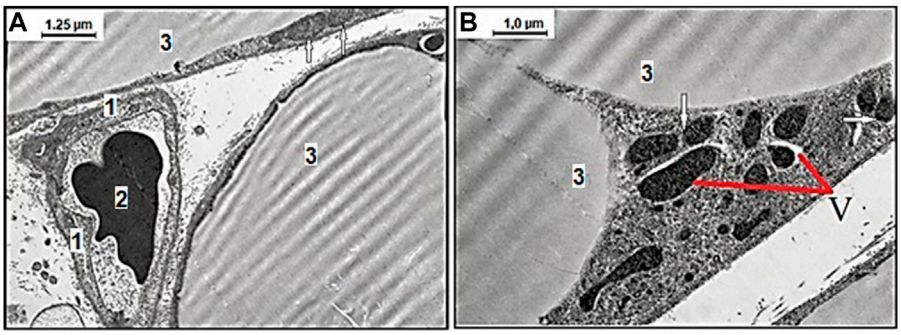

FIGURE 2 | Representative electron microscopy images of the age-related effect of ultrastructural examination of mesenteric material harvested from the area associated with the small intestine of adult **(A)** and aged **(B)** rats with the standard diet. **(A)** Among the connective tissues, there are well preserved capillary endothelial cells (CECs), 1) with erythrocyte 2) in the lumen surrounded with few adipocytes 3) without signs of fat fragmentation, and normal mitochondria (arrows mark) (original magnification × 8,000). **(B)** The degenerating adipocyte with signs of vacuolization in the cytoplasm (V) and differently shaped electron-dense mitochondria. The defective mitochondria in an act of cross talk with other mitochondria (arrows mark) (original magnification × 10,000).

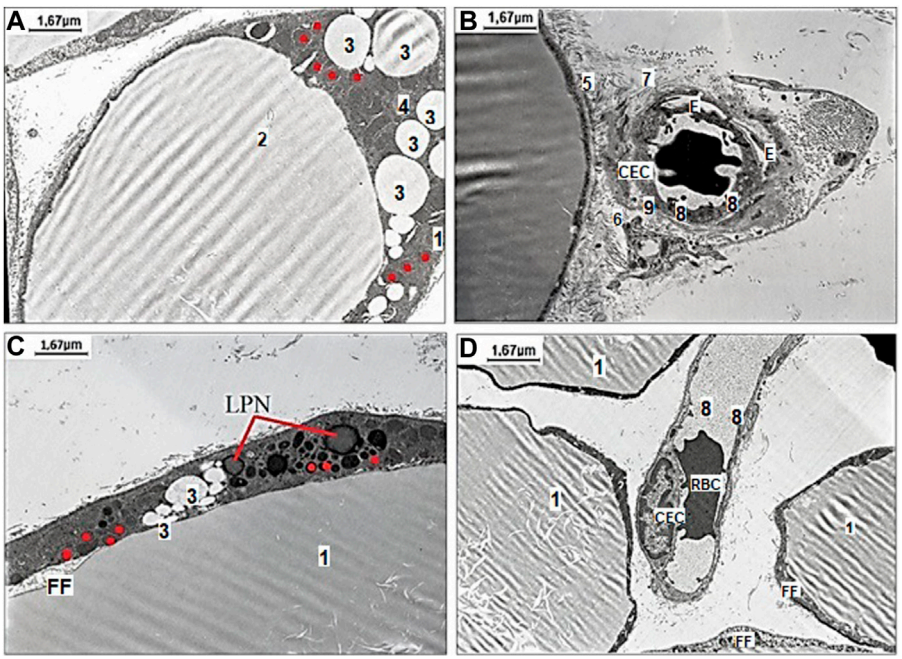

FIGURE 3 | Representative pictures of the effect of fructose-feeding and stress induction on ultrastructural examination of mesenteric material harvested from the area associated with the small intestine of aged rats with vehicle **(A–B)** and NaHS **(C,D)** treatment. **(A)** The degenerating adipocyte 1) with signs of fat fragmentation 2), with small lipid drops 3) in the cytoplasm 4) of adipocytes and different shaped mitochondria (original magnification × 6,000). **(B)** Evidence of adipocyte damage includes disrupted basal membrane 5), cell debris in the interstitium 6), disorganized collagen fibers 7), and changes the microarchitecture of the capillary endothelial cells (CEC) with microvilli 8), destruction of basal membrane 9), and edema **(E)** around the capillary space with destructive red blood cell (RBC) in the lumen (original magnification × 6,000). **(C)** The adipocyte with signs of fat fragmentation, smaller drops of fat in the cytoplasm of adipocytes, lipid-laden phagolysosomes (LPN) and detective ring-like mitochondria (original magnification × 6,000). **(D)** Well preserved capillary endothelial cells with destructive erythrocyte (RBC) adhered to endotheliocytes in the lumen surrounded with few adipocytes without signs of fat fragmentation (FF) (original magnification × 6,000). Red dots mark ring-like mitochondria.

peripheral lipid droplets are present in the marginal cytoplasm of adipocytes with defective mitochondria and lipid-laden phagolysosomes. Adipocyte collagen fibers were disorganized, and the changes in the microarchitecture of the capillary endothelial cells which have microvilli were observed (**Figure 3B**). The destruction of the capillary basal membrane and submembrane edema with destructive red blood cells in the lumen was detected (**Figure 3B**). These results suggested that

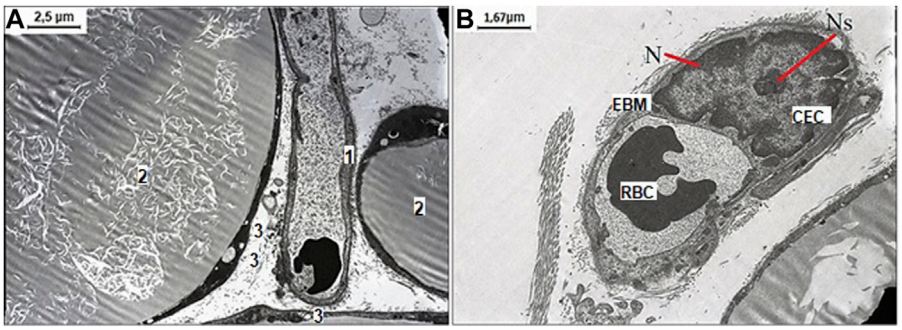

FIGURE 4 | Representative pictures of the effect of NaHS fructose-fed and stress induction on ultrastructural examination of mesenteric material harvested from the area associated with the small intestine of aged rats. **(A)** The well-preserved capillary 1) between three white monovacuolar adipocytes 2) with single lipid droplets 3) (original magnification ×4,000). **(B)** The capillary with the endothelial cells (CEC) with an optimally developed nucleus (N) and nucleolus (Ns), and thickened and edematous basal membrane (EBM) with altered red blood cell (RBC) in its lumen (original magnification ×6,000).

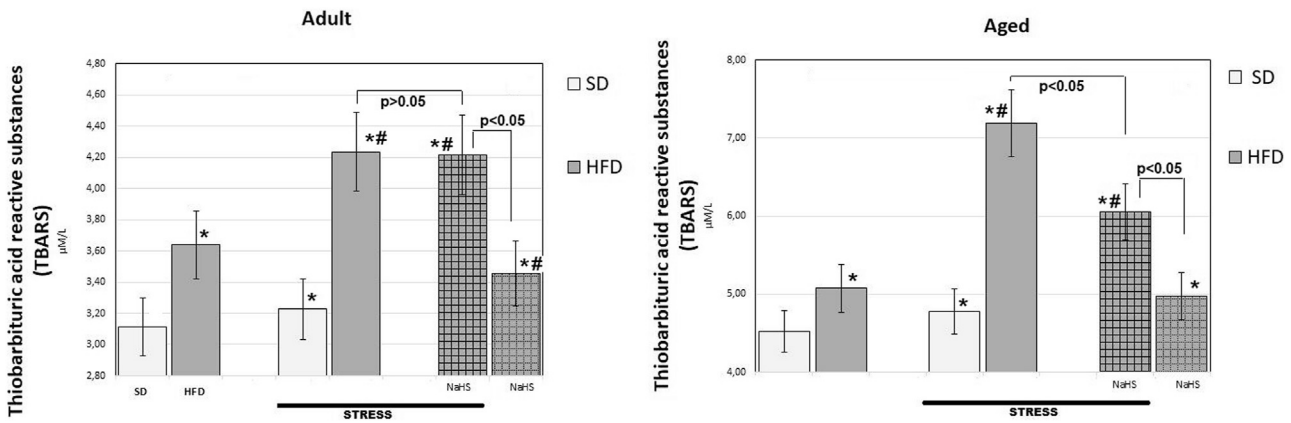

FIGURE 5 | TBARS levels in adult and aged rats fed with a standard diet (SD) or high fructose diet (HFD) without and with H_2S releasing therapy (NaHS) and induction of acute stress (n = 6); *p < 0.05 vs. SD; #p < 0.05 vs. HFD.

HFD affects MA, inducing its defragmentation, mitochondrial dysfunction, and endothelial damage in aged rats.

The results of exogenous stimulation of H_2S by NaHS showed that the adipocyte had fewer signs of fat fragmentation (smaller drops of fat in the cytoplasm of adipocytes) and showed a tendency to decrease the number of its detective mitochondria (**Figure 3D**). Under the changes induced by NaHS, well-preserved capillary basal membrane, endothelial cells, and destructive erythrocyte in the lumen were detected in the microvessel (**Figure 3E**). Our data showed that HFD and age-related alterations of MA, its mitochondria, and mesenteric connective tissue are reversible under the influence of H_2S donor—NaHS. There was a remarkable difference in mesenteric endotheliocytes' condition that confirms the cytoprotective effect of H_2S donors.

After NaHS administration and WIRS induction, the enlarged monovacuolar fat cells were with a few smaller drops on the periphery. The released fat drops and well-preserved capillary without sign of endothelial dysfunction with an optimally developed nucleus and nucleolus are detected in interstitial space, which suggested mesenteric cells tended to recover under influence of increased H_2S bioavailability (**Figure 4**).

NaHS, an H_2S Releasing Donor, Reduces HFD Stimulated TBARS Production in Both Adult and Aged Rats Without and With Acute Stress

To further understand the exact stimulation effects of endogenous H_2S on age- and HFD-related changes on oxidative damage in the mesentery, the TBARS levels (**Figure 5**) and CBS, CSE, SO, and TST activities (**Figures 6**, **7**) involved in the biosynthesis of H_2S mobilization were investigated.

In groups of adult and aged rats fed SD, the TBARS content was 3.11 ± 0.14 µM/L in adult rats and 4.52 ± 0.25 µM/L in aged rats (p < 0.01), we see an age-related increase in TBARS. In HFD-fed rats treated with saline, the levels of TBARS increased by 17%

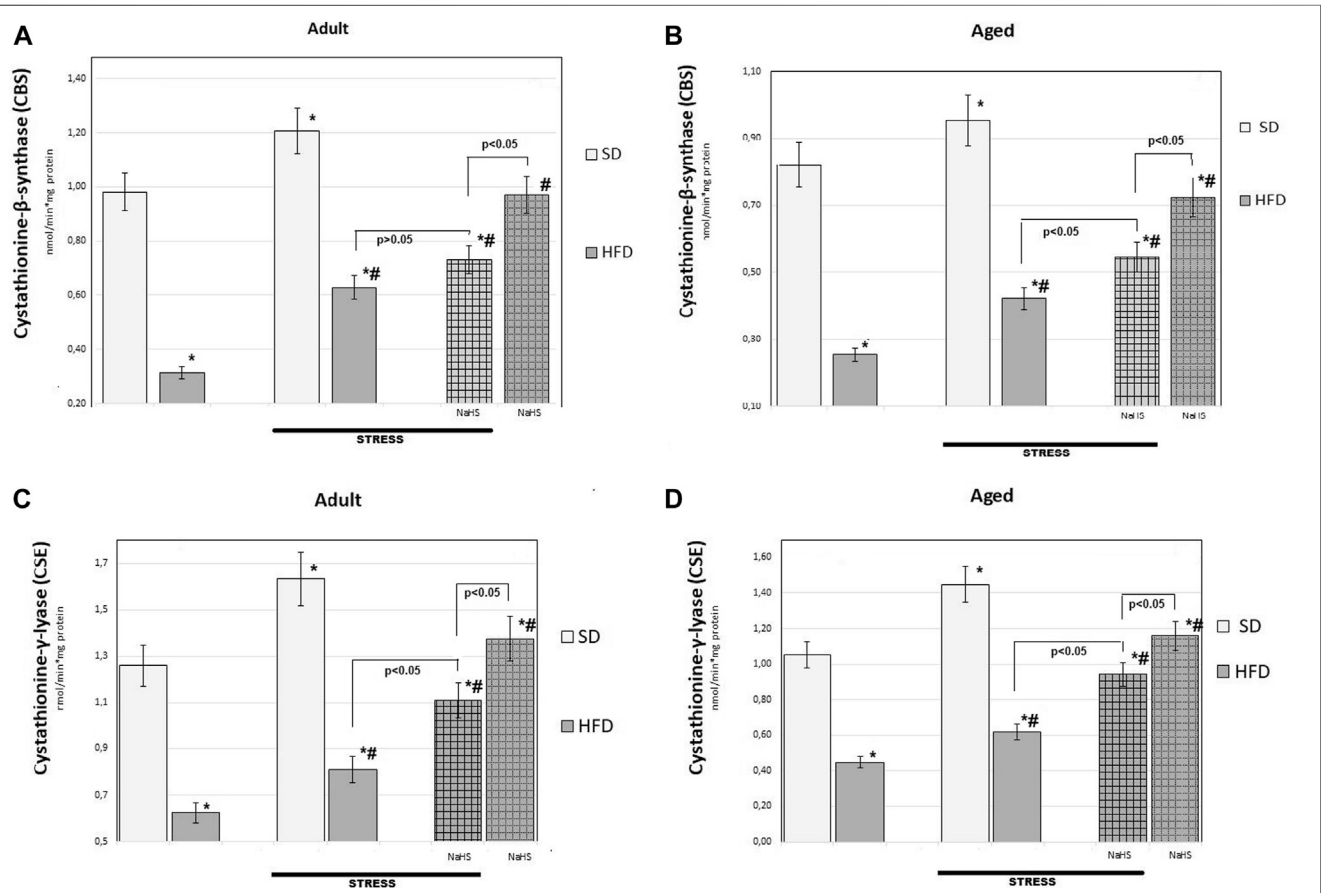

FIGURE 6 | Activities of cystathionine-β-synthase (CBS) **(A,B)**, cystathionine-γ-lyase (CSE) **(C,D)** in adult **(A,C)** and aged rats **(B and D)** (n = 6) fed with a standard diet (SD) or high fructose diet (HFD) without and with H_2S releasing molecule compound therapy (NaHS) and induction of acute stress; *p < 0.05 vs. SD; #p < 0.05 vs. HFD.

adult groups (3.64 ± 0.3 μM/L) and 12% aged groups (5.08 ± 0.17 μM/L) over results of the SD-fed groups (p < 0.05), and there was a significant increase in the level of TBARS in HFD. The effects of WIRS caused changes in the content of TBARS, and age differences were noted. Aged rats treated by being fed HFD under acute stress showed a 41% increase in TBARS (up to 7.19 ± 0.36 μM/L) and in adults, by 16% (up to 4.24 ± 0.15 μM/L) compared with animals without stress. In adult rats, administration of NaHS did not cause a significant reduction in TBARS in groups fed HFD without and with stress induction (p < 0.001). It was also found that conducting hydrogen sulfide modulation by the introduction of NaHS in aged rats, exposed to stress, significantly reduced TBARS by 16% compared with placebo-treated animals and without stress induction (p < 0.001). This effect of NaHS could be interpreted as anti-oxidative stress.

To further understand the exact influence of H_2S donor administration, NaHS, on age- and HFD-related effects on mesentery, the expressions of CBS, CSE, TST, and SO activities involved in endogenous H_2S mobilization were investigated (**Figures 6**, **7**). In intact adult control rats on SD, the activities of CBS, CSE, TST, and SO were reaching 0.98 ± 0.06 nmol/min*1, 1.26 ± 0.08 nmol/min*1, 1.16 ± 0.09 nmol/min*1, and 2.9 ± 0.14 nmol/min*1 mg of protein, respectively. There were age-related differences in their enzyme activities. In intact aged rats on SD, the activities of CBS, CSE, TST, and SO were reaching 0.82 ± 0.06 nmol/min*1, 1.05 ± 0.07 nmol/min*1, 1.01 ± 0.04 nmol/min*1, and 4.15 ± 0.1 nmol/min*1 mg of protein, respectively. In HFD-fed groups, there were decreased enzyme activities (CBS, CSE, TST) and increased activity of SO in rats compared to SD-fed rats. There was also a significant difference in enzyme activities between adult and aged rats on HFD versus SD. Adult rats on HFD had much lower activity of CBS–69%, CSE–51%, and TST–53%; aged rats on HFD had much lower activity of CBS–70%, CSE–57%, and TST–50%, compared to the SD group (p < 0.05). The results showed increased activity SO in both groups: in adult rats up to 11% and in aged rats up to 15%. In contrast, the expression of CBS, CSE, and TST showed a tendency to decrease in the aged rats on HDF which have lower enzyme activities of CBS, CSE, and TST versus aged rats on SD. Notably, the increased activities of all H_2S-related enzymes during induction WIRS were recorded, except for SO, which

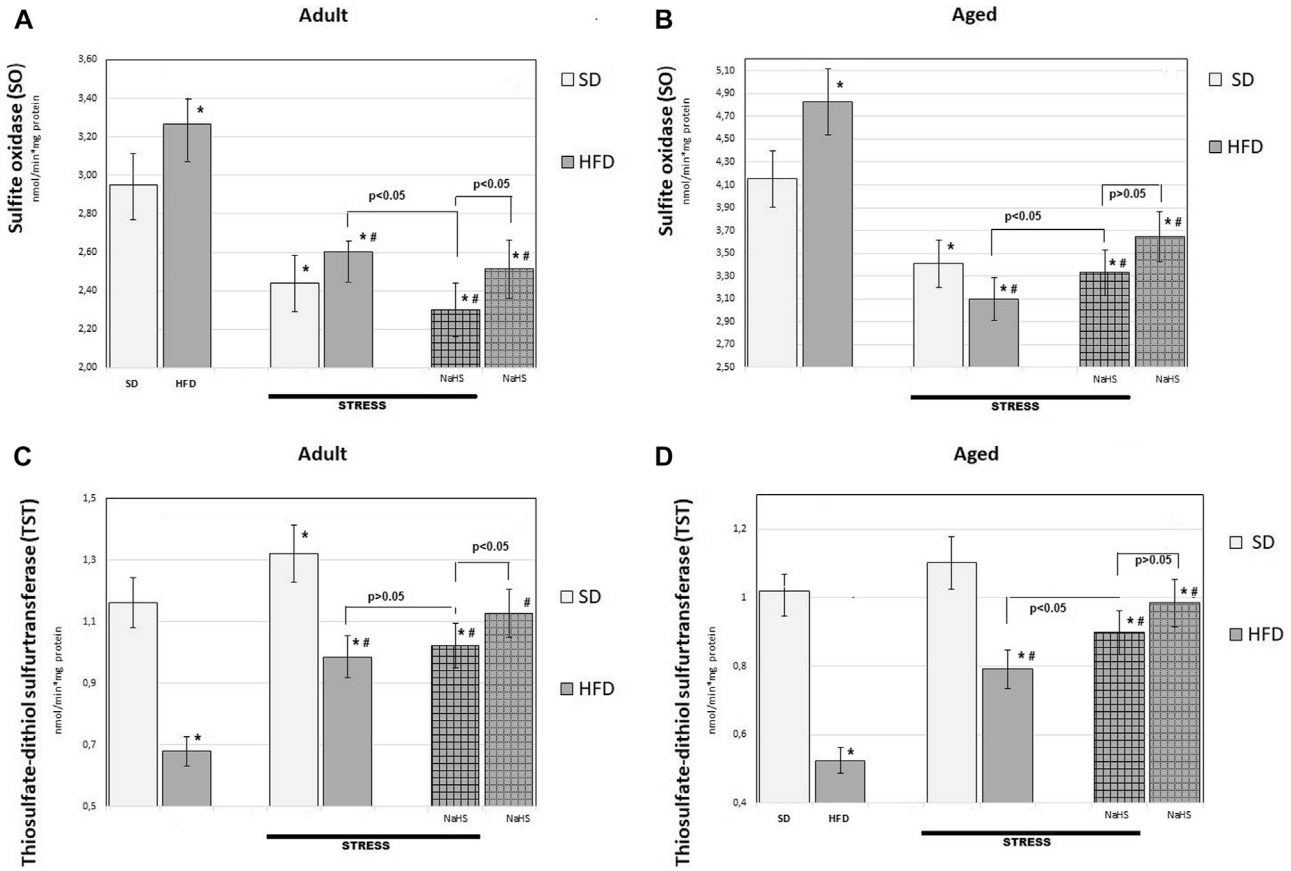

FIGURE 7 | Activities of sulfide oxidase **(A,B)** and thiosulfate-dithiol sulfurtransferase (TST) **(C,D)** in adult **(A,C)** and aged rats **(B,D)** (n = 6) fed with a standard diet (SD) or high fructose diet (HFD) without and with H_2S releasing molecule compound therapy (NaHS) and induction of acute stress; *p < 0.05 vs. SD; #p < 0.05 vs. HFD.

decreased (**Figure 7A, B**). We found that treatment by NaHS in adult rats exposed to stress on HFD resulted in increased activities of CBS–16%, CSE–37%, and TST by 5% over adult rats which did not receive NaHS (p < 0.01) and aged rats, CBS–28%, CSE–51%, and TST–13% (p < 0.01). These results indicate NaHS has the potential for regulating redox imbalance on mesenteric injury in rats induced by advanced age and HFD.

DISCUSSION

In modern times, the prevalence of metabolic disorders in the world has pandemic levels. Among them, obesity has similarly faced an upward trend, with the older population showing more susceptibility to obesity and related disorders than younger adults (Ponti et al., 2020). One interpretation of the ability of adipose tissue to reprogram whole-body physiology is their mitochondria which integrate several processes, including oxidative phosphorylation, ATP synthesis, and ROS generation that could cause metabolic signals for obesity Boudina and Graham (2014) and vascular disorders (Zhou et al., 2021). We have limited understanding of H_2S signaling effects on metabolic disorders based on mesenteric adipocytes tissue damage and MA mitochondrial function, as well as other mesenteric vessels and fibroblasts. The physiological implication of H_2S impacts our understanding of redox balance, cell homeostasis, and death, synthesis of pro-inflammatory molecules into the cytoplasm, and has potential for target therapy (Cedikova et al., 2016). In light of recent advances, the ultrastructural mitochondrial changes could be investigated by methods of classical transmission electron microscopy or 3D reconstruction of serial block-face scanning (Vincent et al., 2016). The electron microscopy results in the current experimental study demonstrating that age-related changes of mesenteric white adipocytes and endothelial condition are characterized by hypertrophic changes of MA with signs of fat degradation, different shaped and defective mitochondria, endothelial dysfunction, and abnormal basal membrane integrity. Numerous experimental studies have shown that epigenetic factors contribute to the risk of numerous metabolic disorders related to obesity, type 2 diabetes, and non-alcoholic fatty liver (Pichette et al., 2016; Melino et al., 2019). Both human and animal studies have reflected the potentially negative effects of glycemic and resistant carbohydrates on metabolic physiology (Law et al.,

2017; Henry et al., 2021; Omar et al., 2021). Consumption of a high amount of dietary fructose or other types of sugars in sweetened foods and aging could cause adipocyte tissue damage which might be related to metabolic and obesity-related disorders (Crescenzo et al., 2014; Pinnick et al., 2019). Human studies reveal the tendency of mesenteric fat wrapping or visceral adiposities and may act as a "red flag" in patients much earlier than symptom-onset (Li et al., 2021).

In the present study, we used animal models for induction metabolic disorders based on 28 days of consumption of HFD and compared age-related changes of mesenteric cells to rats fed with SD. The choice of induction of acute WIRS was important to study adaptive changes of mesenteric cells during acute injury. This model of WIRS was originally designed to study gastroprotection Takagi and Okabe (1968) and it quickly became widely useful for better understanding cytoprotective effects. Our report of results of MA ultrastructural study obtained from rats fed with HFD has shown mesenteric white adipocyte damage which is characterized by the disrupted basal membrane of MA, intracellular fat fragmentation with many smallest lipid drops in the cytoplasm, and different shaped mitochondria. There were signs of mesenteric capillary endothelial cell injury and fibroblast damage in adult rats fed with HFD during stress induction. These results confirm that metabolic disorders may cause similar changes as during accelerated aging (Salvestrini et al., 2019). The ultrastructural changes of MA in aged rats exhibiting HFD reflected ring-like mitochondria and many small drops of fat in the cytoplasm of adipocytes. Wide range effects of H_2S signaling on the resolution of inflammation, inhibition of leucocyte-endothelial adhesion, mitochondrial dynamics in cell homeostasis, and redox balance have been extensively studied over the last 2 decades and implemented in novel therapeutic strategies (Papapetropoulos et al., 2020). Furthermore, a recent study demonstrated that stimulation of endogenous H_2S biosynthesis can preserve adipocyte physiology in humans (Comas et al., 2019).

In our study, the dysfunctional mesenteric cells in aged rats fed with HFD induce increased TBARS production and decreased activity of H_2S signaling was recorded, while stimulation endogenous H_2S by NaHS caused MA and capillary endothelial cells' cytoprotection, decreased TBARS level, and increased catalytic activity of H_2S enzymes that regulate redox system via several intercellular and intracellular pathways (Pavlovskiy et al., 2018; Mezouari et al., 2020). These results for the first time indicate that H_2S signaling is an important mesenteric mitoprotective factor that facilitates the dysregulation redox balance operated by intracellular and extracellular activities of CBS, CSE, TST, and SO. It would be of interest to study the defects in MA mitochondrial functions via mitochondrial redox balance by free radicals, glutamate/glutamine, indicators of programmed death, or the amount of ATP determination in the future. There are several explanations of the link between white adipocytes, inflammation, and redox balance which is essential to maintain metabolic homeostasis and structural-functional integrity of adipocytes, capillary endothelial cells, and fibroblasts in the mesentery (Lefranc et al., 2018; Ma et al., 2018; Magnuson et al., 2020). It has been suggested that dysregulated adipocyte-to-macrophage mitochondria transfer axis leads to obesity (Miliotis et al., 2019; Brestoff et al., 2020). Taken into account that, in the healthy state, secretory factors from adipocytes are responsible for preserving metabolism homeostasis and integrity in adipose tissue, our results show that endogenous H_2S signaling in mesenteric white adipocytes is involved in age-related physiological changes. As such, these findings have potential as a therapeutic tool. It was interesting to note that stimulation production of endogenous H_2S by NaHS demonstrated decreased mesenteric adipose tissue damage, mitochondrial impairment, and redox imbalance in aged rats with SD and both adult and aged rats exhibiting HFD.

In conclusion, the identification of the stimulation of endogenous hydrogen sulfide synthesis which inhibits mesenteric white adipocyte tissue, vessels, and fibroblasts damage after the overload of fructose in aged rats will be suggesting a possible future therapeutic application. Abolishment of mitochondrial dysfunction in the mesenteric adipocytes and stromal-vascular subcellular adaptive changes and redox imbalance seems to play an important role in the H_2S effect on age-related and high fructose-induced mesenteric injury.

DATA AVAILABILITY STATEMENT

The data from this study are not publicly available but are available from the corresponding author on reasonable request.

ETHICS STATEMENT

The animal study was reviewed and approved by the Local Animal Care Committee at the Danylo Halytsky Lviv National Medical University Ethics Committee (protocol April 23, 2018, No. 4).

AUTHOR CONTRIBUTIONS

OZ designed the study. OR, YP, and MS, performed experiments and data analysis. Histological evaluation was done by AY, VK, IC, OV, and OR. OR, AY, VK, and OZ interpreted the findings and prepared and completed the manuscript. All authors contributed to the article and approved the submitted version.

FUNDING

This work has been supported in part by Danylo Halytsky Lviv National Medical University under the project "Role of Systemic and Local Mechanisms in Cytoprotection under the Extreme Influence" (the state registration ID 0116U004510).

ACKNOWLEDGMENTS

We thank Zaichko N. (National Pirogov Memorial Medical University, Vinnytsia, Ukraine) for her expert suggestions.

REFERENCES

Bidwell, A. (2017). Chronic Fructose Ingestion as a Major Health Concern: Is a Sedentary Lifestyle Making it Worse? A Review. *Nutrients* 9 (6), 549. doi:10.3390/nu9060549

Boudina, S., and Graham, T. E. (2014). Mitochondrial Function/Dysfunction in White Adipose Tissue. *Exp. Physiol.* 99 (9), 1168–1178. doi:10.1113/expphysiol.2014.081414

Brestoff, J. R., Wilen, C. B., Moley, J. R., Li, Y., Zou, W., Malvin, N. P., and Teitelbaum, S. L. (2020). Intercellular Mitochondria Transfer to Macrophages Regulates White Adipose Tissue Homeostasis and Is Impaired in Obesity. *Cel. Metab.* 33, 270. doi:10.1016/j.cmet.2020.11.008

Cedikova, M., Kripnerová, M., Dvorakova, J., Pitule, P., Grundmanova, M., Babuska, V., and Kuncova, J. (2016). Mitochondria in white, Brown, and Beige Adipocytes. *Stem Cell Int.* 2016, 6067349. doi:10.1155/2016/6067349

Coffey, J. C., Walsh, D., Byrnes, K. G., Hohenberger, W., and Heald, R. J. (2020). Mesentery - a 'New' Organ. *Emerging Top. Life Sci.* 4 (2), 191–206. doi:10.1042/etls20200006

Comas, F., Latorre, J., Ortega, F., Arnoriaga Rodríguez, M., Kern, M., Lluch, A., and Moreno-Navarrete, J. M. (2021). Activation of Endogenous H_2S Biosynthesis or Supplementation with Exogenous H_2S Enhances Adipose Tissue Adipogenesis and Preserves Adipocyte Physiology in Humans. *Antioxidants and Redox Signaling* 10, 319–340. doi:10.1089/ars.2020.8206

Conte, M., Martucci, M., Sandri, M., Franceschi, C., and Salvioli, S. (2019). The Dual Role of the Pervasive "Fattish" Tissue Remodeling with Age. *Front. Endocrinol.* 10, 114. doi:10.3389/fendo.2019.00114

Crescenzo, R., Bianco, F., Coppola, P., Mazzoli, A., Valiante, S., Liverini, G., et al. (2014). Adipose Tissue Remodeling in Rats Exhibiting Fructose-Induced Obesity. *Eur. J. Nutr.* 53 (2), 413–419. doi:10.1007/s00394-013-0538-2

Do, T. T. H., Marie, G., Héloïse, D., Dorothée, G., Marthe, M., Bruno, F., et al. (2019). Glucocorticoid-Induced Insulin Resistance Is Related to Macrophage Visceral Adipose Tissue Infiltration. *J. Steroid Biochem. Mol. Biol.* 185, 150–162. doi:10.1016/j.jsbmb.2018.08.010

He, Z., Ning, N., Zhou, Q., Khoshnam, S. E., and Farzaneh, M. (2020). Mitochondria as a Therapeutic Target for Ischemic Stroke. *Free Radic. Biol. Med.* 146, 45–58. doi:10.1016/j.freeradbiomed.2019.11.005

Henry, C. J., Quek, R. Y. C., Kaur, B., Shyam, S., and Singh, H. K. G. (2021). A Glycaemic Index Compendium of Non-Western Foods. *Nutr. Diabetes* 11 (1), 1–36. doi:10.1038/s41387-020-00145-w

Hilton, C., Karpe, F., and Pinnick, K. E. (2015). Role of Developmental Transcription Factors in White, Brown and Beige Adipose Tissues. *Biochim. Biophys. Acta (Bba) - Mol. Cel. Biol. Lipids* 1851 (5), 686–696. doi:10.1016/j.bbalip.2015.02.003

Kiriyama, Y., and Nochi, H. (2018). Intra- and Intercellular Quality Control Mechanisms of Mitochondria. *Cells* 7 (1), 1. doi:10.3390/cells7080095

Korakas, E., Ikonomidis, I., Kousathana, F., Balampanis, K., Kountouri, A., Raptis, A., et al. (2020). Obesity and COVID-19: Immune and Metabolic Derangement as a Possible Link to Adverse Clinical Outcomes. *Am. J. Physiology-Endocrinology Metab.* 319 (1), E105–E109. doi:10.1152/ajpendo.00198.2020

Kredel, L. I., and Siegmund, B. (2014). Adipose-Tissue and Intestinal Inflammation–Visceral Obesity and Creeping Fat. *Front. Immunol.* 5, 462. doi:10.3389/fimmu.2014.00462

Law, M., Huot, P. S. P., Lee, Y. T., Vien, S., Luhovyy, B. L., and Anderson, G. H. (2017). The Effect of Dairy and Nondairy Beverages Consumed with High Glycemic Cereal on Subjective Appetite, Food Intake, and Postprandial Glycemia in Young Adults. *Appl. Physiol. Nutr. Metab.* 42 (11), 1201–1209. doi:10.1139/apnm-2017-0135

Lee, J. H., Park, A., Oh, K. J., Lee, S. C., Kim, W. K., and Bae, K. H. (2019). The Role of Adipose Tissue Mitochondria: Regulation of Mitochondrial Function for the Treatment of Metabolic Diseases. *Int. J. Mol. Sci.* 20 (19), 4924. doi:10.3390/ijms20194924

Lefranc, C., Friederich-Persson, M., Palacios-Ramirez, R., and Nguyen Dinh Cat, A. (2018). Mitochondrial Oxidative Stress in Obesity: Role of the Mineralocorticoid Receptor. *J. Endocrinol.* 238 (3), R143–R159. doi:10.1530/joe-18-0163

Lelis, D. d. F., Andrade, J. M. O., Almenara, C. C. P., Broseguini-Filho, G. B., Mill, J. G., and Baldo, M. P. (2020). High Fructose Intake and the Route towards Cardiometabolic Diseases. *Life Sciences* 259, 118235. doi:10.1016/j.lfs.2020.118235

Li, X. H., Feng, S. T., Cao, Q. H., Coffey, J. C., Baker, M. E., Huang, L., and Mao, R. (2021). Degree of Creeping Fat Assessed by CT Enterography Is Associated with Intestinal Fibrotic Stricture in Patients with Crohn's Disease: A Potentially Novel Mesenteric Creeping Fat Index. *J. Crohn's Colitis* 15, 1161. doi:10.1093/ecco-jcc/jjab005

Li, Z., Hardij, J., Bagchi, D. P., Scheller, E. L., and MacDougald, O. A. (2018). Development, Regulation, Metabolism and Function of Bone Marrow Adipose Tissues. *Bone* 110, 134–140. doi:10.1016/j.bone.2018.01.008

Ma, X., Wang, D., Zhao, W., and Xu, L. (2018). Deciphering the Roles of PPARγ in Adipocytes via Dynamic Change of Transcription Complex. *Front. Endocrinol.* 9, 473. doi:10.3389/fendo.2018.00473

Magnuson, A. M., Regan, D. P., Booth, A. D., Fouts, J. K., Solt, C. M., Hill, J. L, and Foster, M. T. (2020). High-fat Diet Induced central Adiposity (Visceral Fat) Is Associated With Increased Fibrosis and Decreased Immune Cellularity of the Mesenteric Lymph Node in Mice. *Eur. J. Nutr.* 59 (4), 1641–1654.

Mao, R., Kurada, S., Gordon, I. O., Baker, M. E., Gandhi, N., McDonald, C., et al. (2019). The Mesenteric Fat and Intestinal Muscle Interface: Creeping Fat Influencing Stricture Formation in Crohn's Disease. *Inflamm. Bowel Dis.* 25 (3), 421–426. doi:10.1093/ibd/izy331

Melino, S., Leo, S., and Papajani, V. (2019). Natural Hydrogen Sulfide Donors from Allium Sp. As a Nutraceutical Approach in Type 2 Diabetes Prevention and Therapy. *Nutrients* 11 (7), 1581. doi:10.3390/nu11071581

Mezouari, A., Nangia, R., and Gagnon, J. (2020). The Protective Role of Hydrogen Sulfide against Obesity-Associated Cellular Stress in Blood Glucose Regulation. *Antioxidants* 9 (11), 1038. doi:10.3390/antiox9111038

Miliotis, S., Nicolalde, B., Ortega, M., Yepez, J., and Caicedo, A. (2019). Forms of Extracellular Mitochondria and Their Impact in Health. *Mitochondrion* 48, 16–30. doi:10.1016/j.mito.2019.02.002

Montes-Nieto, R., Insenser, M., Murri, M., Fernández-Durán, E., Ojeda-Ojeda, M., Martínez-García, M. Á., and Escobar-Morreale, H. F. (2017). Plasma Thiobarbituric Acid Reactive Substances (TBARS) in Young Adults: Obesity Increases Fasting Levels Only in Men whereas Glucose Ingestion, and Not Protein or Lipid Intake, Increases Postprandial Concentrations Regardless of Sex and Obesity. *Mol. Nutr. Food Res.* 61 (11), 1700425. doi:10.1002/mnfr.201700425

Murphy, B., Bhattacharya, R., and Mukherjee, P. (2019). Hydrogen Sulfide Signaling in Mitochondria and Disease. *FASEB J.* 33 (12), 13098–13125. doi:10.1096/fj.201901304r

Omar, N. A. M., Frank, J., Kruger, J., Bello, F. D., Medana, C., Collino, M., and Landberg, R. (2021). Effects of High Intakes of Fructose and Galactose, with or without Added Fructooligosaccharides, on Metabolic Factors, Inflammation, and Gut Integrity in a Rat Model. *Mol. Nutr. Food Res.* 65, e2001133. doi:10.1002/mnfr.202001133

Papapetropoulos, A., Wallace, J. L., and Wang, R. (2020). From Primordial Gas to the Medicine Cabinet. *Br. J. Pharmacol.* 177 (4), 715–719. doi:10.1111/bph.14929

Paul, B. D., Snyder, S. H., and Kashfi, K. (2020). Effects of Hydrogen Sulfide on Mitochondrial Function and Cellular Bioenergetics. *Redox Biol.* 38, 101772. doi:10.1016/j.redox.2020.101772

Pavlovskiy, Y., Lutsyk, M., Zayachkivska, O., Lutsyk, M., Yashchenko, A., Zaichko, N., et al. (2018). Atb 340 (A Modulator of Sulfite Oxidase Activity) Reduces Oxidative Stress During Hyperglycemia and in Stress Exposed Gastric Mucosa in Old Rats. *Ntsn Ms.* 52 (2), 33–41. doi:10.25040/ntsh2018.02.033

Pavlovskiy, Y., Yashchenko, A., and Zayachkivska, O. (2020). H_2S Donors Reverse Age-Related Gastric Malfunction Impaired Due to Fructose-Induced Injury via CBS, CSE, and TST Expression. *Front. Pharmacol.* 11, 1134. doi:10.3389/fphar.2020.01134

Pichette, J., and Gagnon, J. (2016). Implications of Hydrogen Sulfide in Glucose Regulation: How H2S Can Alter Glucose Homeostasis through Metabolic Hormones. *Oxid. Med. Cell Longev.* 2016, 3285074. doi:10.1155/2016/3285074

Pinnick, K. E., and Hodson, L. (2019). Challenging Metabolic Tissues with Fructose: Tissue-specific and Sex-specific Responses. *J. Physiol.* 597 (14), 3527–3537. doi:10.1113/jp277115

Ponti, F., Santoro, A., Mercatelli, D., Gasperini, C., Conte, M., Martucci, M., and Bazzocchi, A. (2020). Aging and Imaging Assessment of Body Composition: from Fat to Facts. *Front. Endocrinol.* 10, 861. doi:10.3389/fendo.2019.00861

Revenko, O., Zaichko, N., Wallace, J., and Zayachkivska, O. (2020). Exogenous Hydrogen Sulfide for the Treatment of Mesenteric Damage Associated with Fructose-Induced Malfunctions via Inhibition of Oxidative Stress. *Ukr. Biochem. J.* 92 (2), 86–97. doi:10.15407/ubj92.02.086

Rivera, E. D., Coffey, J. C., Walsh, D., and Ehrenpreis, E. D. (2019). The Mesentery, Systemic Inflammation, and Crohn's Disease. *Inflamm. Bowel Dis.* 25 (2), 226–234. doi:10.1093/ibd/izy201

Salvestrini, V., Sell, C., and Lorenzini, A. (2019). Obesity May Accelerate the Aging Process. *Front. Endocrinol.* 10, 266. doi:10.3389/fendo.2019.00266

Scheja, L., and Heeren, J. (2019). The Endocrine Function of Adipose Tissues in Health and Cardiometabolic Disease. *Nat. Rev. Endocrinol.* 15 (9), 507–524. doi:10.1038/s41574-019-0230-6

Shibuya, N., and Kimura, H. (2013). Production of Hydrogen Sulfide From D-Cysteine and its Therapeutic Potential. *Front. Endocrinol.* 4, 87. doi:10.3389/fendo.2013.00087

Shimizu, I., and Walsh, K. (2015). The Whitening of Brown Fat and its Implications for Weight Management in Obesity. *Curr. Obes. Rep.* 4 (2), 224–229. doi:10.1007/s13679-015-0157-8

Stipanuk, M. H., and Beck, P. W. (1982). Characterization of the Enzymic Capacity for Cysteine Desulphhydration in Liver and Kidney of the Rat. *Biochem. J.* 206 (2), 267–277. doi:10.1042/bj2060267

Streich, K., Smoczek, M., Hegermann, J., Dittrich-Breiholz, O., Bornemann, M., Siebert, A., et al. (2020). Dietary Lipids Accumulate in Macrophages and Stromal Cells and Change the Microarchitecture of Mesenteric Lymph Nodes. *J. Adv. Res.* 24, 291–300. doi:10.1016/j.jare.2020.04.020

Suzuki, K., Olah, G., Modis, K., Coletta, C., Kulp, G., Gerö, D., et al. (2011). Hydrogen Sulfide Replacement Therapy Protects the Vascular Endothelium in Hyperglycemia by Preserving Mitochondrial Function. *Proc. Natl. Acad. Sci.* 108 (33), 13829–13834. doi:10.1073/pnas.1105121108

Takagi, K., and Okabe, S. (1968). The Effects of Drugs on the Production and Recovery Processes of the Stress Ulcer. *Jpn. J. Pharmacol.* 18 (1), 9–18. doi:10.1254/jjp.18.9

Tamara, A., and Tahapary, D. L. (2020). Obesity as a Predictor for a Poor Prognosis of COVID-19: A Systematic Review. *Diabetes Metab. Syndr. Clin. Res. Rev.* 14 (4), 655–659. doi:10.1016/j.dsx.2020.05.020

Vincent, A. E., Ng, Y. S., White, K., Davey, T., Mannella, C., Falkous, G., and Picard, M. (2016). The Spectrum of Mitochondrial Ultrastructural Defects in Mitochondrial Myopathy. *Scientific Rep.* 6 (1), 1–12. doi:10.1038/srep30610

Wang, Q., and Wu, H. (2018). T Cells in Adipose Tissue: Critical Players in Immunometabolism. *Front. Immunol.* 9, 2509. doi:10.3389/fimmu.2018.02509

Wronska, A., and Kmiec, Z. (2012). Structural and Biochemical Characteristics of Various white Adipose Tissue Depots. *Acta Physiol.* 205 (2), 194–208. doi:10.1111/j.1748-1716.2012.02409.x

Zaichko, N., Pentyuk, N., and Melnik, A. (2009). The Formation of Hydrogen Sulfide in the Organs of Rats. *Med. Chem.* (4), 10–11.

Zaichko, N. V., Melnik, A. V., Yoltukhivskyy, M. M., Olhovskiy, A. S., and Palamarchuk, I. V. (2014). Hydrogen Sulfide: Metabolism, Biological and Medical Role. *Ukrainian Biochem. J.* 86 (No 5), 5–25. doi:10.15407/ubj86.05.005

Zhou, Y., Li, H., and Xia, N. (2021). The Interplay between Adipose Tissue and Vasculature: Role of Oxidative Stress in Obesity. *Front. Cardiovasc. Med.* 8, 131. doi:10.3389/fcvm.2021.650214

Zhu, Q., Glazier, B. J., Hinkel, B. C., Cao, J., Liu, L., Liang, C., et al. (2019). Neuroendocrine Regulation of Energy Metabolism Involving Different Types of Adipose Tissues. *Int. J. Mol. Sci.* 20 (11), 2707. doi:10.3390/ijms20112707

Conflict of Interest: The authors declare that the research was conducted in the absence of any commercial or financial relationships that could be construed as a potential conflict of interest.

Publisher's Note: All claims expressed in this article are solely those of the authors and do not necessarily represent those of their affiliated organizations, or those of the publisher, the editors, and the reviewers. Any product that may be evaluated in this article, or claim that may be made by its manufacturer, is not guaranteed or endorsed by the publisher.

frontiers in Pharmacology

ORIGINAL RESEARCH
published: 08 September 2021
doi: 10.3389/fphar.2021.680167

Triptolide Downregulates the Expression of NRF2 Target Genes by Increasing Cytoplasmic Localization of NRF2 in A549 Cells

Le Ba Nam[1], *Won Jun Choi*[1] *and Young-Sam Keum*[1,2]*

[1]College of Pharmacy and Integrated Research Institute for Drug Development, Dongguk University, Goyang, South Korea, [2]Panacea Co., Goyang, South Korea

We have identified triptolide as a novel NRF2 inhibitor, which significantly attenuates ARE-luciferase activity at nanomolar concentrations. Triptolide did not affect the level of NRF2, but significantly inhibited the expression of NRF2 target genes in A549 cells. We found that NRF2 possesses a previously unrecognized NES in the Neh2 domain, and that triptolide promotes an interaction between NRF2 and CRM1. Triptolide also decreased nuclear accumulation of NRF2, suggesting that it promotes nuclear export of NRF2. In addition, we show that triptolide decreased the expression of NRF2 target genes and increased intracellular oxidative stress, suppressing invasion and promoting cisplatin-induced apoptosis in A549 cells. Finally, oral administration of triptolide suppressed the growth of A549 xenografts in athymic mice by decreasing the expression of NRF2 target genes and promoting oxidative damages via the nuclear export of NRF2 and CRM1 *in vivo*. To the best of our knowledge, triptolide is the first type of compound to inhibit NRF2 by increasing cytoplasmic localization of NRF2.

Keywords: triptolide, NF-E2-related factor 2 (Nrf2), chromosomal maintenance 1 (CRM1), leptomycin B (LMB), nuclear export signal (NES)

OPEN ACCESS

Edited by:
Thomas Brzozowski, Jagiellonian University Medical College, Poland

Reviewed by:
Susana Chaves, University of Minho, Portugal
Pengjuan Xu, Tianjin University of Traditional Chinese Medicine, China
Ousman Tamgue, University of Douala, Cameroon
Jiaqi Pang, Sun Yat-sen University, China

***Correspondence:**
Young-Sam Keum
keum03@dongguk.edu

Specialty section:
This article was submitted to Pharmacology of Anti-Cancer Drugs, a section of the journal Frontiers in Pharmacology

Received: *15 March 2021*
Accepted: *25 August 2021*
Published: *08 September 2021*

Citation:
Nam LB, Choi WJ and Keum Y-S (2021) Triptolide Downregulates the Expression of NRF2 Target Genes by Increasing Cytoplasmic Localization of NRF2 in A549 Cells. Front. Pharmacol. 12:680167. doi: 10.3389/fphar.2021.680167

INTRODUCTION

NF-E2-related factor 2 (NRF2) is responsible for transcriptional activation of phase II cytoprotective enzymes by binding to the antioxidant response element (ARE), a *cis*-acting motif that exists in the promoter of NRF2 target genes (Itoh et al., 1997). The stability of NRF2 is controlled by Kelch-like ECH-associated protein 1 (KEAP1), an adaptor for Cullin 3 (CUL3)-based E3 ubiquitin ligase under basal conditions: CUL3/KEAP1 E3 ubiquitin ligase promotes poly-ubiquitination of NRF2 in the cytosol (Kobayashi et al., 2004). Oxidants and electrophiles halts poly-ubiquitination of NRF2 by inactivating KEAP1, which allows NRF2 to rapidly accumulate, translocate to the nucleus, and activate transcription of NRF2 target genes by forming a heterodimer with small musculoaponeurotic fibrosarcomas (MAFs) (Taguchi et al., 2011). While NRF2 activators provide beneficial therapeutic effects in a variety of stress-related diseases (Cuadrado et al., 2019), aberrant NRF2 activation is often observed in many types of tumors and is closely correlated with poor prognosis because NRF2 activation confers significant advantages towards the growth, proliferation, and metastasis of cancer (Rojo De La Vega et al., 2018).

Cancer genome sequencing studies have identified frequent gain of function mutations in the KEAP1/NRF2 pathway in human non-small cell lung carcinoma (NSCLC) (La Fleur et al., 2019).

Specifically, the KEAP1/NRF2 pathway is significantly altered in human lung squamous carcinoma (LUSC) accounting for 34% of genomic alterations, such as somatic mutations and copy number variations (Cancer Genome Atlas Research Network, 2012). Similarly, 23% of human lung adenocarcinoma (LUAD) harbors genomic alterations in the KEAP1/NRF2 pathway (Cancer Genome Atlas Research Network, 2014). While Keap1 mutations are widely distributed, a unique feature of Nrf2 mutations is that they are exclusively clustered in the KEAP1 binding motifs (Taguchi et al., 2011). In addition, the exon 2 in the Nrf2 locus is recurrently lost via alternative splicing and this contributes to the production of NRF2 isoform lacking the Neh2 domain, suggesting an alternative mechanism how NRF2 is activated in lung cancer cells that do not bear mutations in the KEAP1/NRF2 pathway (Goldstein et al., 2016). Taken together, these studies provide evidence that the release of NRF2 from KEAP1 is important for the survival and the proliferation of lung cancer (Taguchi and Yamamoto, 2017).

Considering the abundance of lung tumors exhibiting NRF2 activation and the limited number of available NRF2 inhibitors, the development of NRF2 inhibitors is of a great therapeutic advantage (Jung et al., 2018). Because the structural information of NRF2 is lacking, however, it is impossible to perform the *in silico* analysis of small molecules that might dock to the relevant domains of NRF2. Therefore, scientists have performed the ARE-luciferase assay to identify new NRF2 inhibitors. After discovering brusatol as the first NRF2 inhibitor (Ren et al., 2011), subsequent studies have reported various NRF2 inhibitors with different chemical structures (Robledinos-Anton et al., 2019). Our group identified the Na^+/K^+-ATPase inhibitors (Nam and Keum, 2020) and homoharringtonine (Kang et al., 2019) as novel NRF2 inhibitors, suggesting that the Na^+/K^+-ATPase and the G-quadruplex structure in the Nrf2 mRNA can be targeted for the development of NRF2 inhibitors (Kang et al., 2020). In an attempt to further develop NRF2 inhibitors, we have observed that triptolide inhibits NRF2 with a distinct mechanism of action compared with other NRF2 inhibitors: triptolide does not affect the level of NRF2, but suppresses the expression of NRF2 target genes by facilitating cytoplasmic localization of NRF2 in A549 cells. In addition, we have identified a novel nuclear export signal (NES) existing in the Neh2 domain of NRF2.

MATERIALS AND METHODS

Cell Culture, Chemicals, and Antibodies

Human lung adenocarcinoma A549 cells, human non-small cell lung carcinoma H1299 cells and human embryonic kidney 293Tcells were cultured in Dulbecco's Modified Eagle Medium (DMEM) supplemented with 10% fetal bovine serum (FBS) and 1% penicillin/streptomycin (Pen/Strep). DMEM and FBS were purchased from GenDEPOT (Austin, TX, United States). Phosphate-buffered saline (PBS) and Pen/Strep were purchased from WELGENE (Daegu, Korea). Triptolide and cisplatin were obtained from Tokyo Chemical Industry (Tokyo, Japan). The natural compound library was purchased from MedChemExpress (South Brunswick, NJ, United States). FLAG antibody (M2), FLAG-HRP, anti-FLAG beads, anti-HA beads, paraformaldehyde and bovine serum albumin (BSA) were purchased from Sigma-Aldrich (St. Louis, MO, United States). Leptomycin B (LMB) was purchased from Santa Cruz Biotechnology (Santa Cruz, CA, United States). The antibody against HO-1 was purchased from Enzo Life Science (Farmingdale, NY, United States). Antibodies against NQO1 and 4-HNE were purchased from Abcam (Cambridge, MA, United States). Antibodies against actin, CRM1, and 8-OHdG were purchased from Santa Cruz Biotechnology (Santa Cruz, CA, United States). Antibodies against NRF2, cleaved poly (ADP-ribose) polymerase (PARP), cleaved Caspase-3, and HA-HRP were purchased from Cell Signaling Technology (Danvers, MA, United States). JetPEI was purchased from Polyplus transfection (New York, NY, United States).

Transfection of siRNAs

Transfection of siRNAs was performed according to the manufacturer's instructions. When cells reached approximately 70% confluence, they were transfected with siRNAs using JetPEI, allowed to grow for additional 48 h, and harvested for biochemical analyses. The Crm1 siRNA sequences are as follows: Sense: CUCUCUGAAGUGCCUCACU; Antisense: AGUGAGGCACUUCAGAGAG. The Nrf2 siRNA sequences are as follows: Sense: GAGACUACCAUGGUUCCAA; Antisense: UUGGAACCAUGGUAGUCUC.

Firefly Luciferase Assay

A549-ARE-GFP-luciferase and H1299-ARE-GFP-luciferase cells were previously established in our laboratory (Lee et al., 2018b). After treatment, the cells were washed three times with ice-cold 1x PBS and lysed with luciferase lysis buffer (100 mM potassium phosphate buffer at pH 7.8, 1% Triton X-100, 1 mM DTT, and 2 mM EDTA) for 1 h. The cell lysates were collected by centrifugation and the luciferase activity was monitored using the GLOMAX Multi-system (Promega, Madison, WI, United States) followed by normalization of the protein concentration.

MTT Assay

The cells were seeded in 96-well culture plates. After treatment, the cells were washed three times with ice-cold 1x PBS and incubated in a mixture of 180 μl DMEM and 20 μl MTT solution (500 μg/ml) for 4 h. The cells were lysed with 100 μl DMSO for 30 min, and absorbance was measured by spectrophotometer at a wavelength of 560 nm.

Trypan Blue Exclusion Assay

The cells were plated in quadruplicate in 6-well culture plates and exposed to various concentrations of triptolide for 24 h. The cells were washed with 1x PBS and collected by trypsinization. After washing with 1x PBS, the cells were stained with 0.4% trypan blue solution for 3 min at room temperature. The number of viable cells was counted with a hemocytometer.

Immunofluorescence

A549 cells were grown on a slice glass and incubated with blocking serum (1% BSA) for 30 min. After washing with 1× PBS, the cells were fixed in paraformaldehyde and hybridized with primary antibodies overnight at 4 C. The slides were washed with 1× PBS and probed with fluorescein isothiocyanate (FITC)-conjugated anti-rabbit or anti-mouse secondary antibodies (Jackson-ImmunoResearch, West Grove, PA, United States). The fluorescent images were obtained with C2 confocal microscope (Nikon Korea, Seoul, Korea).

Fractionation of the Nucleus and the Cytosol

Cells were washed with 1x PBS and lysed with cell lysis buffer A (50 mM Tris-HCl, 10 mM NaCl, 5 mM $MgCl_2$, and 0.5% NP-40, pH 8.0). The lysates were centrifuged at 13,000 rpm for 10 min and the supernatant was collected as the cytosolic fraction. After washing the remnant pellets twice with cell lysis buffer A, they were resuspended in high salt buffer B (20 mM HEPES, 0.5 M NaCl, 1 mM EDTA, and 1 mM dithiothreitol, pH 7.9) and centrifuged for 15 min after brief sonication. The supernatant was collected as the nuclear fraction. The nuclear and cytosolic fractions were subjected to Western blot analysis after the quantification of protein concentration. Glyceraldehyde 3-phosphate dehydrogenase (GAPDH) and histone H3 (H3) were used as the cytosolic and nuclear fraction markers, respectively. The antibody against GAPDH was purchased from Santa Cruz Biotechnology and the antibody against histone H3 was purchased from Cell Signaling Technology.

Western Blot Analysis

After treatment, the cells were washed three times with 1x PBS and the cell pellets were collected by centrifugation. The pellets were resuspended in 1x RIPA lysis buffer [50 mM Tris-HCl at pH 8.0, 150 mM NaCl, 1% NP-40, 0.5% deoxycholic acid, 0.1% sodium dodecyl sulfate (SDS), 1 mM Na_3VO_4, 1 mM DTT, and 1 mM phenylmethylsulfonyl fluoride (PMSF)] and incubated on ice for 1 h. After cell lysates were collected, the protein concentration was measured using the BCA protein assay kit (Thermo-Fisher Scientific, Waltham, MA, United States). Cell lysates were resolved by SDS-PAGE and transferred to PVDF membranes (Merck-Millipore Korea, Daejeon, Korea). The membranes were incubated in blocking buffer (5% skim milk in 1x PBS-0.1% Tween-20, and 1x PBST) for 1 h and hybridized with appropriate primary antibodies in 1x PBS overnight at 4°C. After washing three times with 1x PBST for 30 min, the membrane was hybridized with horseradish peroxidase (HRP)-conjugated secondary antibody (Thermo-Fischer Scientific) for 1 h at 4 C. The membranes were washed three times with 1x PBST for 30 min and visualized using an enhanced chemiluminescence (ECL) detection system.

Real-Time Reverse Transcription-Polymerase Chain Reaction

Total RNA was extracted with the Hybrid-R RNA extraction kit (GeneAll, Seoul, Korea). Total RNA was subjected to reverse transcription and PCR amplification, using the PrimeScript RT-PCR kit (TAKARA Korea, Seoul, Korea). The real-time RT-PCR analysis was performed using SYBR Mix on a CFX384 Real-time System as recommended by the manufacturer (BioRad Laboratories, Hercules, CA, United States). The mRNA levels of individual genes were normalized by that of GAPDH. The real-time RT-PCR primer sequences are listed in **Table 1**.

TABLE 1 | Real-time RT-PCR primers

Genes	Forward	Reverse
Nrf2	CGGTATGCAACAGGACATTG	ACTGGTTGGGGTCTTCTGTG
Ho-1	GGGAATTCTCTTGGCTGGCT	CACGCATGGCTCAAAAACCA
Nqo1	GGTTTGGAGTCCCTGCCATT	GCCTTCTTACTCCGGAAGGG
Gapdh	CCATGGGGAAGGTGAAGGTC	TGATGACCCTTTTGGCTCCC

Generation of Stable Cells

Stable A549 cells were generated by transfection of pcDNA3-puro-HA-NRF2 or pcDNA3-HA-NRF2 mutant plasmids, followed by selection of transfected cells with puromycin selection (1 μg/ml) for 48 h. Human Nrf2 and Crm1 cDNAs were amplified from 293T cells using RT-PCR and ligated into pcDNA3-HA-puro and pcDNA3-FLAG-puro vectors. Mutant Nrf2 plasmids were created by overlapping PCR. The sequences of the plasmids were confirmed by DNA sequencing.

Invasion Assay

Invasion assay was conducted using the Costar Transwell System (Corning Inc., Corning, NY, United States), which bears an 8.0 μm pore size membrane in a plastic ware. The Watrigel Matrix (Corning Inc., Corning, NY, United States) was laid on the membrane in the upper chamber for 12 h. A549 cells were seeded at a density of 5×10^4 cells/well with serum-free DMEM into the upper chamber in the absence or presence of triptolide. After 24 h, cells that invaded in the lower chamber were fixed in 3.7% formaldehyde for 2 min, permeabilized with methanol for 10 min, and stained with Mayer's Hematoxylin for 15 min. The number of invaded cells was counted in selected random fields of wells using the Eclipse Ti-U inverted microscope (Nikon, Tokyo, Japan).

A549 Xenograft Study

Six-week old Balb/c nude mice were purchased from Daehan Biolink Co. (Eumseong, Korea). After 1 week acclimation, the mice were subcutaneously injected with A549 cells (5×10^6 cells/mouse) into right the dorsal flank. After 1 week, the mice were orally administered with triptolide everyday (10, 20, and 30 nmol/mouse/day). The weight of the mice and the sizes of the tumors were measured every 3 days during the experiment. The mice were sacrificed by asphyxiation with CO_2, and the tumors were excised and weighed. The tumor samples were stored either for biochemical analyses or for immunohistochemistry. The animal experiment was performed under the Institutional Animal Care and Use Committee-approved Protocol (IACUC-2020-026-1) of Dongguk University (Seoul, Korea).

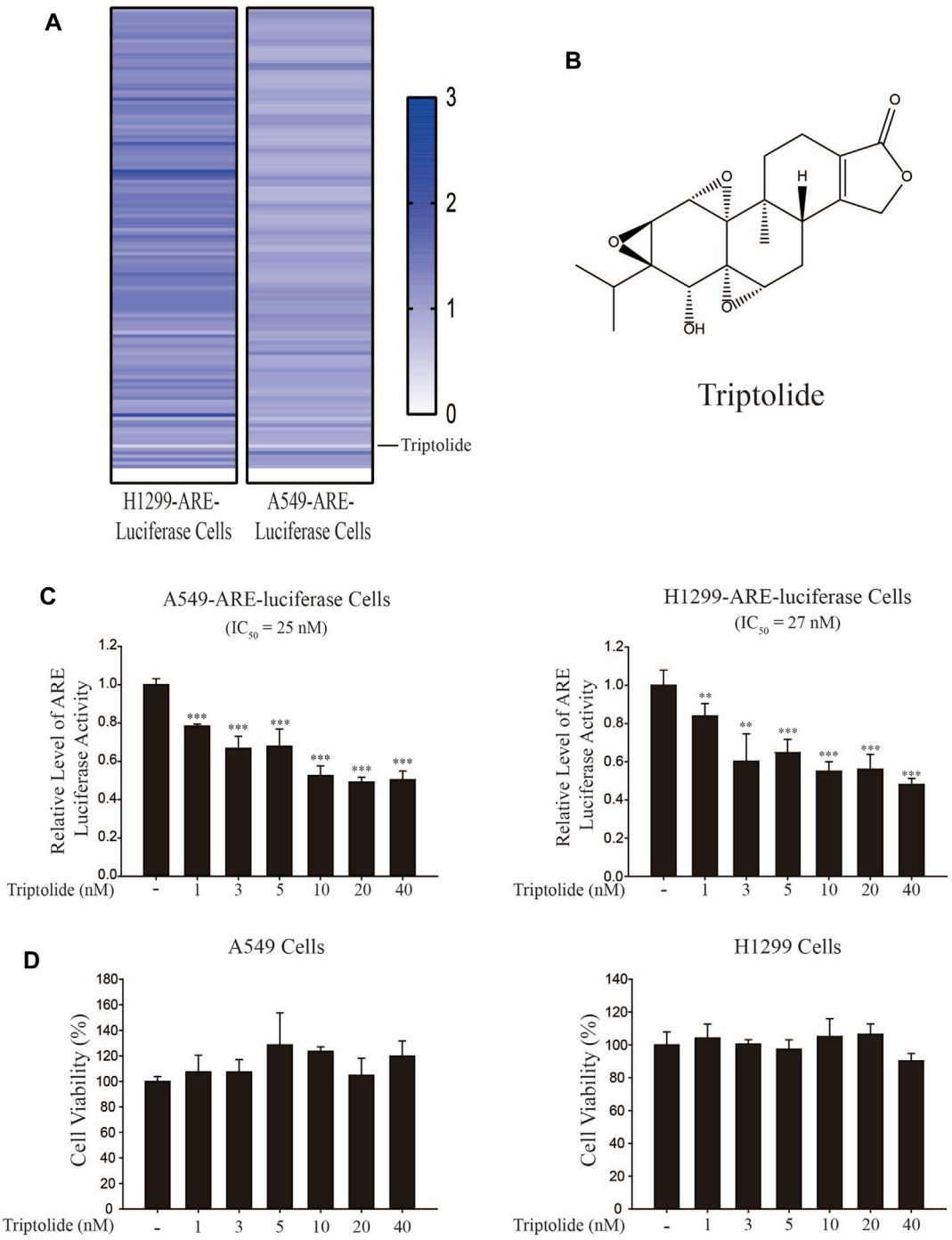

FIGURE 1 | Identification of triptolide as an NRF2 inhibitor. **(A)** Experimental setup for NRF2 inhibitor screening. Triptolide was identified as the strongest ARE-luciferase inhibitor in H1299-ARE-luciferase and A549-ARE-luciferase cells. **(B)** Chemical structure of triptolide. **(C)** Triptolide inhibits ARE-luciferase activity in A549-ARE-luciferase cells (Left Panel) and H1299-ARE-luciferase cells (Right Panel) in a dose-dependent manner. A549-ARE-GFP-luciferase and H1299-ARE-GFP-luciferase cells were seeded in 24-well culture plates (2×10^5 cells/well) and exposed to triptolide at multiple concentrations for 24 h. Cells were collected and the luciferase activity was measured. Asterisks indicate a statistical significance ($n = 3$): $^{**}p < 0.01$ and $^{***}p < 0.001$. **(D)** Triptolide does not affect the viability of A549 cells (Left Panel) and H1299 cells (Right Panel) at concentrations up to 40 nM. A549 and H1299 cells were seeded in 96-well culture plates (4×10^4 cells/well) and MTT assay was conducted ($n = 3$) after triptolide was added for 24 h.

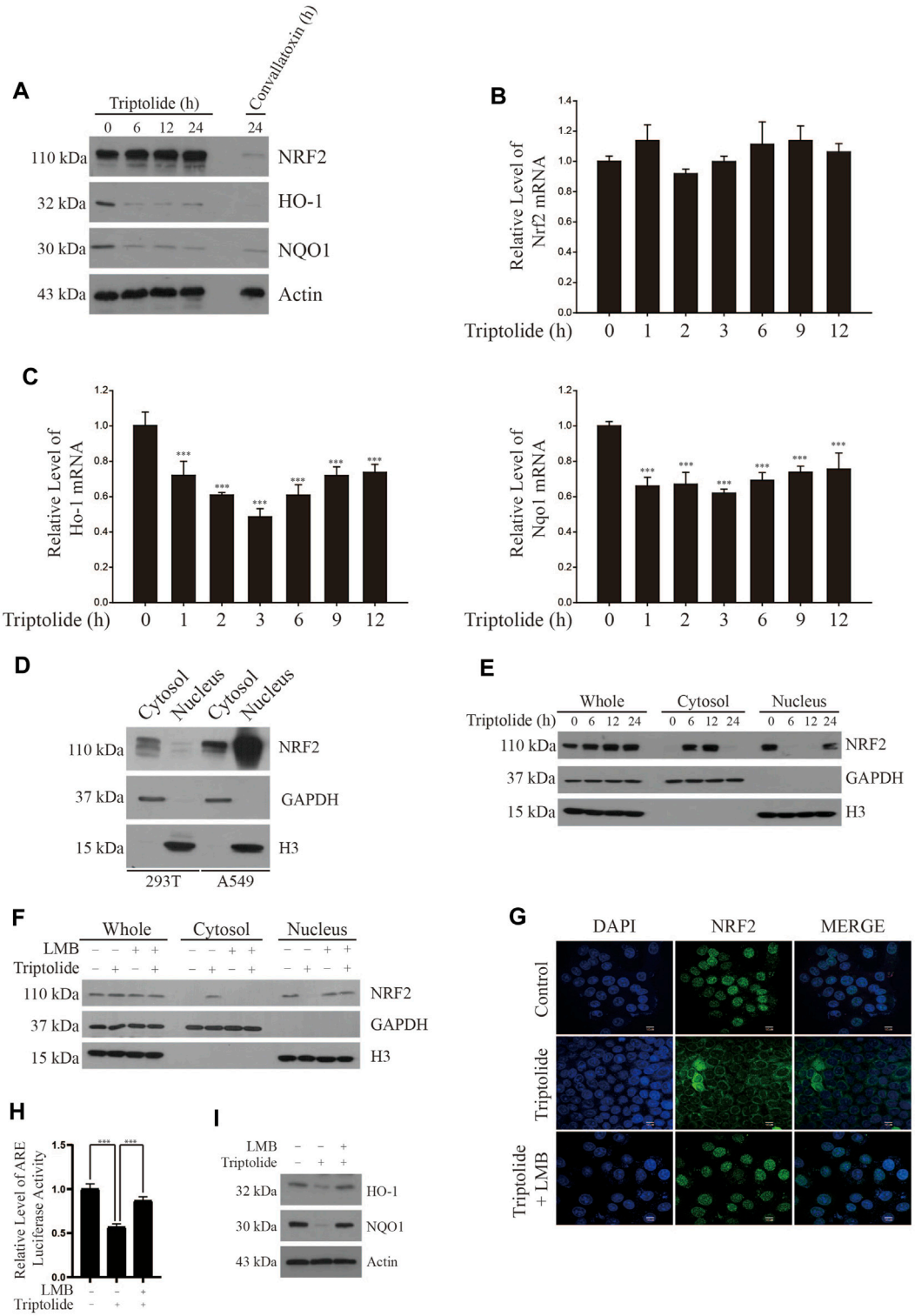

FIGURE 2 | Triptolide increases cytoplasmic localization of NRF2 in A549 cells. **(A)** Triptolide does not affect the level of NRF2, but suppress the expression of HO-1 and NQO1 in A549 cells. Convallatoxin was included as a positive control. A549 cells were seeded in 100 mm culture plates (2×10^6 cells) and exposed to triptolide (20 nM) for various amounts of time. Western blot analysis was performed against NRF2, HO-1, NQO1, and actin **(B)** Triptolide does not affect the level of Nrf2 mRNA in A549 cells. A549 cells were seeded in 6-well culture plates (2.0×10^5 cells/well) and exposed to triptolide (20 nM) for various amounts of time. Real-time RT-PCR was performed against Nrf2 mRNA ($n = 4$). **(C)** Triptolide significantly inhibits the mRNA levels of Ho-1 (Left Panel) and Nqo1 (Right Panel) in A549 cells. A549 cells were seeded in 6-well culture plates (2.0×10^5 cells/well) and exposed to triptolide (20 nM) for various amounts of time. Real-time RT-PCR was performed against Ho-1 and

(*Continued*)

FIGURE 2 | Nqo1 mRNAs. Asterisks indicate a statistical significance ($n = 4$): $^{*}p < 0.05$ and $^{***}p < 0.001$. **(D)** NRF2 abundantly exists in the nucleus of A549 cells. 293T and A549 cells were seeded in 100 mm culture plates (4×10^6 cells). The cytosol and the nucleus were separated, and they were subjected to Western blot analysis. GAPDH and H3 were used as markers for the cytosol and the nucleus, respectively. **(E)** Triptolide promotes the nuclear exclusion of NRF2 in A549 cells. A549 cells were seeded in 100 mm culture plates (2×10^6 cells/well) and exposed to triptolide (20 nM) for various amounts of time. The cytosol and the nucleus were separated and subjected to Western blot analysis. GAPDH and H3 were used as markers for the cytosol and the nucleus, respectively. **(F)** LMB abrogates the nuclear export of NRF2 by triptolide in A549 cells. A549 cells were seeded in 100 mm culture plates (2×10^6 cells) and exposed to triptolide (20 nM) for 6 h in the absence or presence of LMB (20 ng/ml). Western blot analysis was performed against NRF2. GAPDH and H3 were used as markers for the cytosol and the nucleus, respectively. **(G)** Triptolide promotes the nuclear exclusion of NRF2 in A549 cells. A549 cells were seeded in slice glasses (7.5×10^4 cells/glass) and exposed to triptolide (20 nM) for 6 h in the absence or presence of LMB (20 ng/ml). A549 cells were subjected to immunofluorescence using the NRF2 antibody. The nucleus was stained with DAPI. **(H)** LMB abrogates the inhibition of ARE-luciferase activity by triptolide in A549-ARE-luciferase cells. A549-ARE-GFP-luciferase cells were seeded in 24-well culture plates (2×10^5 cells/well) and exposed to triptolide in the absence or presence of LMB (20 ng/ml) for 24 h. The luciferase assay was performed and asterisks indicate a statistical significance ($n = 3$): $^{***}p < 0.001$. **(I)** LMB abrogates the inhibition of NRF2 expression by triptolide in A549 cells. A549 cells were seeded in 100 mm culture plates (2×10^6 cells) and exposed to triptolide (20 nM) in the absence or presence of LMB (20 ng/ml) for 24 h. Western blot analysis was performed against HO-1, NQO1, and actin.

Immunohistochemistry

Tissue samples were fixed in formalin solution at room temperature. The fixed samples were embedded in paraffin and sectioned at 8 μm with the microtome. The tissue slices were mounted on slides and deparaffinized with xylene, followed by multiple hydration steps with increasing concentrations of ethanol. Citrate buffer (pH 6.0) was used for antigen retrieval, and the slides were heated in a microwave for 15 min. The slides were blocked with the IHC blocking solution (ScyTek, Logan, Utah, United States) and incubated with primary antibodies. After hybridization with primary antibodies, the slides were washed multiple times with 1x PBS and incubated with UltraTEk anti-rabbit or anti-mouse HRP-conjugated secondary antibodies (ScyTek, Logan, Utah, United States). The slides were developed with the DAB Kit (GBI Labs, Mukilteo, WA, United States) and counterstained with hematoxylin and eosin. Alternatively, the slides were washed with 1× PBS after hybridization with primary antibodies and probed with FITC-conjugated anti-rabbit or anti-mouse secondary antibodies (Jackson-ImmunoResearch, West Grove, PA, United States). The fluorescent images were obtained with the C2 confocal microscope (Nikon Korea, Seoul, Korea).

Statistical Analysis

The statistical analysis was conducted using one-way analysis of variance (ANOVA). The asterisks indicate a statistical significance: $^{*}p < 0.05$, $^{**}p < 0.01$, and $^{***}p < 0.01$.

RESULTS

Triptolide Inhibits NRF2 Target Genes by Increasing Cytoplasmic Localization of NRF2 in A549 Cells

In an attempt to find out a novel NRF2 inhibitor, we have exposed A549-ARE-GFP-luciferase cells and H1299-ARE-GFP-luciferase cells to 10 nM of 2,650 chemicals from a natural compound library for 24 h (**Figure 1A**). As a result, we found that triptolide (**Figure 1B**) significantly inhibited ARE-luciferase activity in A549-ARE-GFP-luciferase cells (IC_{50} = 25 nM) and H1299-ARE-GFP-luciferase cells (IC_{50} = 27 nM) (**Figure 1C**). Concentrations up to 40 nM of triptolide did not affect the metabolic activity of A549 cells and H1299 cells, as assessed by MTT assay (**Figure 1D**). Trypan blue exclusion assay also indicated that the viability of A549 and H1299 cells was unaffected by triptolide at concentrations up to 40 nM (**Supplementary Figure S1**). We have previously identified that convallatoxin inhibits NRF2 and sensitizes A549 cells to cisplatin-induced apoptosis (Lee et al., 2018a). Using convallatoxin as a prototypical NRF2 inhibitor, we exposed A549 cells to triptolide, and examined the expression of NRF2 and its target proteins, heme oxygenase-1 (HO-1) and NAD [P]H: quinone oxidoreductase-1 (NQO1) by Western blot analysis. As a result, we observed that triptolide suppressed the expression of HO-1 and NQO1, but it failed to downregulate the expression of NRF2 in A549 cells (**Figure 2A**). Real-time RT-PCR analysis also indicates that triptolide failed to affect the level of Nrf2 mRNA (**Figure 2B**), but significantly inhibited the levels of Ho-1 (Left Panel) and Nqo1 (Right Panel) mRNAs in A549 cells (**Figure 2C**).

A549 cells are derived from an adenocarcinoma of human alveolar basal epithelium and exhibit aberrant activation of NRF2 owing to two mechanisms: one is a somatic mutation in Keap1 at G333C (Singh et al., 2006) and the other is the epigenetic silencing by methylation in the promoter of Keap1 (Wang et al., 2008). To investigate the molecular mechanisms underlying how triptolide inhibits the expression of NRF2 target genes without affecting the level of NRF2, we exposed A549 cells to triptolide and fractionated the nucleus and cytosol. We observed that, unlike 293T cells, NRF2 was abundantly located in the nucleus of A549 cells during basal condition (**Figure 2D**). Our results also show that triptolide promoted cytoplasmic localization of NRF2 in A549 cells (**Figure 2E**) and this event was suppressed by cotreatment of leptomycin B (LMB), a nuclear export inhibitor (Fung and Chook, 2014), as examined by Western blot analysis (**Figure 2F**) and immunofluorescence (**Figure 2G**). Consistent with these observations, LMB abrogated the inhibition of ARE-luciferase activity (**Figure 2H**) and that of HO-1 and NQO1 (**Figure 2I**) by triptolide. Together, these results illustrate that triptolide inhibits the expression of NRF2 target genes by reducing the nuclear accumulation of NRF2 in A549 cells.

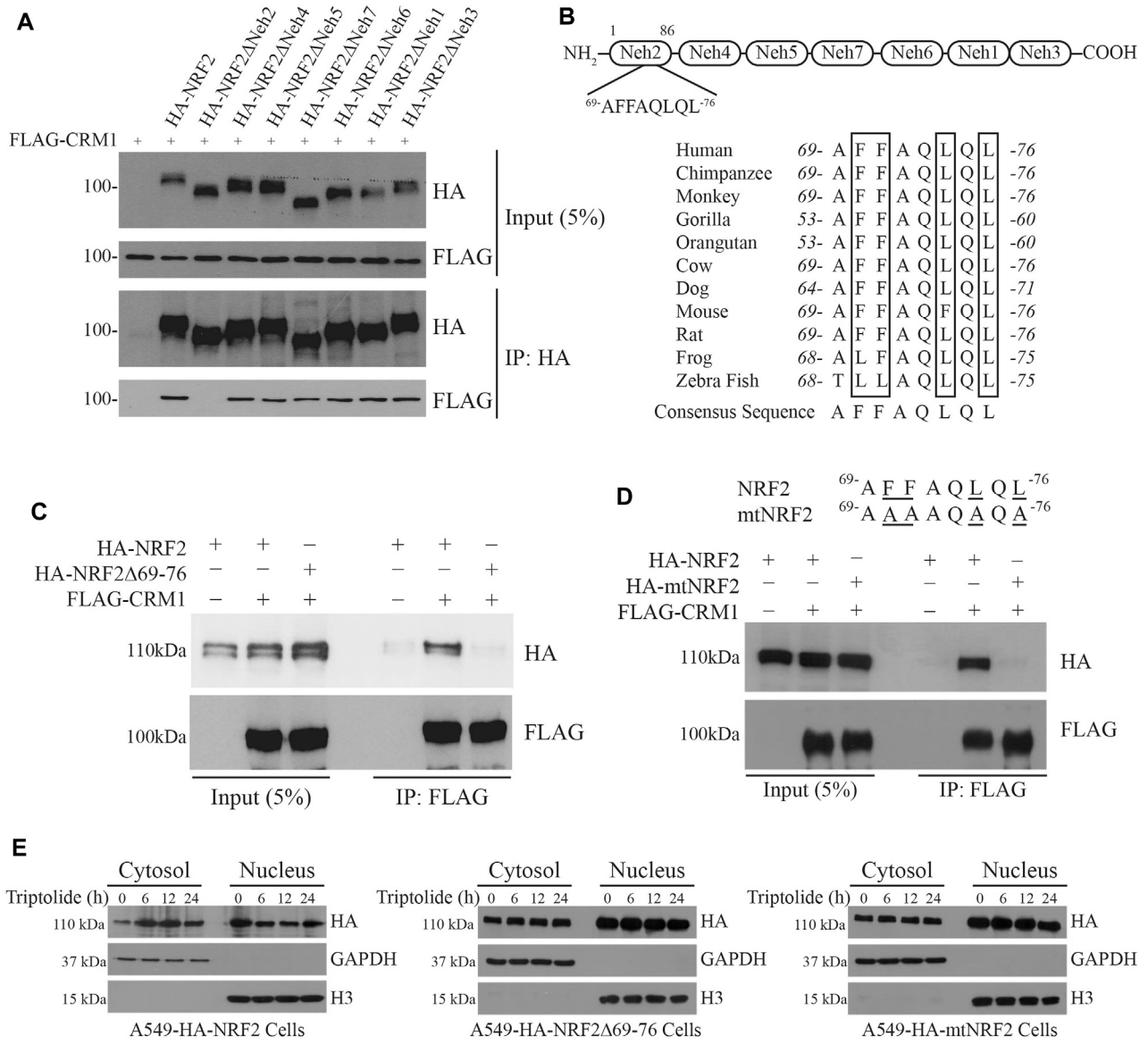

FIGURE 3 | Identification of a novel nuclear export signal (NES) in the Neh2 domain. **(A)** The Neh2 domain is responsible for binding to CRM1. pcDNA3-FLAG-CRM1 plasmid (1 μg) was cotransfected with pcDNA3-HA-NRF2 (1 μg) or pcDNA3-HA-NRF2 plasmids deleted with the individual Neh domains (1 μg) in 293T cells. The cell lysates were collected and immunoprecipitated with anti-HA beads. After immunoprecipitation, Western blot analysis was performed using HA-HRP and FLAG-HRP antibodies. **(B)** Domain architecture of the Neh domains in NRF2 (Upper Panel) and the existence of the NES-like sequence in the Neh2 domain, which is highly preserved across the species (Lower Panel). **(C)** NRF2 deleted with the NES-like sequence in the Neh2 domain fails to bind to CRM1. pcDNA3-FLAG-CRM1 plasmid (1 μg) was cotransfected with pcDNA3-HA-NRF2 (1 μg) or pcDNA3-NRF2Δ69-76 deletion mutant (1 μg) in 293T cells for 24 h. The cells lysates were collected and immunoprecipitated with anti-FLAG beads. After immunoprecipitation, Western blot analysis was performed using FLAG-HRP and HA-HRP antibodies. **(D)** NRF2 mutated in the NES-like sequence in the Neh2 domain (mtNRF2) fails to bind to CRM1. pcDNA3-FLAG-CRM1 plasmid (1 μg) was cotransfected with pcDNA3-HA-NRF2 (1 μg) or pcDNA3-mtNRF2 (1 μg) plasmids in 293T cells for 24 h. The cell lysates were collected and immunoprecipitated with anti-FLAG beads. After immunoprecipitation, Western blot analysis was performed using FLAG-HRP and HA-HRP antibodies. **(E)** Triptolide promotes the nuclear exclusion of HA-NRF2, but not that of NRF2Δ69-76 or HA-mtNRF2. Stable A549-HA-NRF2, A549-HA-NRF2Δ69-76 and A549-HA-mutNRF2 cells were seeded in 100 mm culture plates (2×10^6 cells), and they were exposed to triptolide (20 nM) for various amounts of time. The cytosol and the nucleus were separated, and Western blot analysis was performed against HA. GAPDH and H3 were used as markers for the cytosol and the nucleus, respectively.

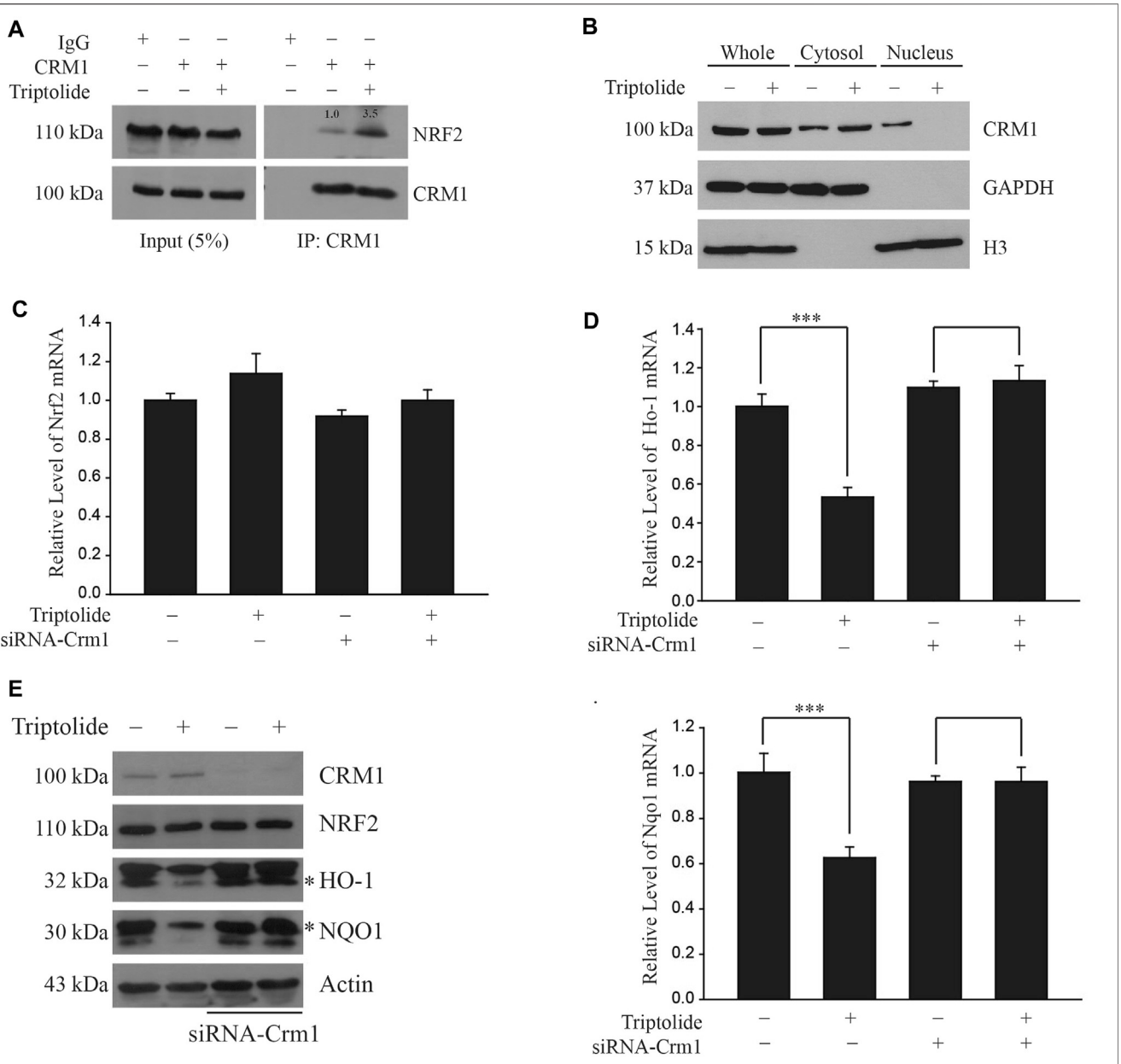

FIGURE 4 | Triptolide promotes the interaction between NRF2 and CRM1 in A549 cells. **(A)** Triptolide promotes the endogenous interaction between NRF2 and CRM1 in A549 cells. A relative density of bands is illustrated inside the figure. A549 cells were seeded in 100 mm culture plates (2×10^6 cells) and exposed to triptolide (20 nM) for 24 h. Cell lysates were collected and incubated with IgG (1 μg) or CRM1 antibody (1 μg) overnight at 4°C. After immunoprecipitation with protein A/G beads, the samples were washed with NP-40 lysis buffer and Western blot analysis was performed against NRF2 and CRM1. **(B)** Triptolide increases cytoplasmic localization of CRM1 in A549 cells. A549 cells were seeded in 100 mm culture plates (2×10^6 cells) and exposed to triptolide (20 nM) for 24 h. After separation of the cytosol and the nucleus, Western blot analysis was performed against CRM1. GAPDH and H3 were used as markers for the cytosol and the nucleus, respectively. **(C)** Triptolide does not affect the level of Nrf2 mRNA regardless of CRM1. A549 cells were seeded in 60 mm plates (2.0×10^5 cells) and exposed to triptolide (20 nM) for 3 h in the absence or presence of siRNA against Crm1 (100 nM). Total RNA was prepared and real-time RT-PCR was performed using Nrf2]specific primers ($n = 4$). **(D)** Suppression of transcription of Ho-1 (Left Panel) and Nqo1 (Right Panel) by triptolide is dependent on CRM1. A549 cells were seeded in 60 mm plates (2.0×10^5 cells) and exposed to triptolide (20 nM) for 3 h in the absence or presence of siRNA against Crm1 (100 nM). Total RNA was prepared and real-time RT-PCR was conducted using specific primers against Ho-1 and Nqo1. Asterisks indicate a statistical significance ($n = 4$): $^{***}p < 0.01$. **(E)** Suppression of HO-1 and NQO1 by triptolide is dependent on CRM1. A549 cells were seeded in 60 mm plates (2.0×10^5 cells) and exposed to triptolide (20 nM) in the absence or presence of siRNA against Crm1 (100 nM) for 24 h. Cell lysates were collected and Western blot analysis was performed.

Triptolide Promotes the Nuclear Exclusion of NRF2 by CRM1

Chromosomal Maintenance 1 (CRM1, also known as Exportin 1) is a major mammalian export protein that facilitates the transport of large macromolecules including RNA and proteins across the nuclear membrane into the cytosol (Hutten and Kehlenbach, 2007). While a previous study provided a clue that CRM1 can bind to and regulate the activity of NRF2 (Velichkova and Hasson, 2005), the mode of interaction is still unclear. To address this issue, we cotransfected FLAG-CRM1 plasmid with HA-NRF2 plasmid or with HA-NRF2 plasmids lacking the individual Neh domains in 293T cells and performed immunoprecipitation with HA-agarose beads followed by Western blot analysis: 293T cells were used to monitor the interaction between two epitope-tagged plasmids due to the ease of transfection. Our results show that FLAG-CRM1 failed to bind to HA-NRF2ΔNeh2, suggesting that CRM1 binds to the Neh2 domain of NRF2 (**Figure 3A**).

A close examination of the amino acid sequence in the Neh2 domain illustrated that the Neh2 domain contains a highly conserved and previously unrecognized nuclear export signal (NES) across the species (**Figure 3B**). To examine whether this putative NES is critical for the interaction between NRF2 and CRM1, we created the HA-NRF2 plasmid lacking the NES (referred to as HA-NRF2Δ69-76) or a mutant NRF2 plasmid in which all phenylalanine (F) and leucine (L) residues in the putative NES were mutated into alanine (A) (referred to as mtNRF2), and cotransfected them with FLAG-CRM1 in 293T cells followed by immunoprecipitation with HA-agarose beads and Western blot analysis. Our results show that FLAG-CRM1 failed to bind to HA-NRF2Δ69-76 (**Figure 3C**) and HA-mtNRF2 (**Figure 3D**), suggesting that this putative NES is critical for the binding of NRF2 to CRM1. To examine whether this putative NES plays a role in the nuclear export of NRF2 by triptolide, we created stable A549 cells overexpressing HA-NRF2, HA-NRF2Δ69-76 and HA-mtNRF2, and exposed them to triptolide. Our results show that triptolide promoted the nuclear export of HA-NRF2, but not that of HA-NRF2Δ69-76 and HA-mtNRF2 (**Figure 3E**), suggesting that this putative NES is critical for the nuclear export of NRF2 by triptolide.

The Inhibition of NRF2 Target Genes by Triptolide Is Dependent on CRM1 in A549 Cells

We observed that triptolide increased an endogenous interaction between NRF2 and CRM1 in A549 cells (**Figure 4A**). Triptolide also promoted cytoplasmic localization of CRM1 in A549 cells (**Figure 4B**). To examine whether the inhibition of NRF2 target genes by triptolide is dependent on CRM1, we knocked down Crm1 in A549 cells and exposed them to triptolide. While triptolide failed to affect the level of Nrf2 mRNA (**Figure 4C**), knocking down Crm1 abrogated the inhibition of Ho-1 (Upper Panel) and Nqo1 mRNAs (Lower Panel) by triptolide (**Figure 4D**). Consistent with this observation, knocking-down Crm1 abrogated the inhibition of HO-1 and NQO1 by triptolide (**Figure 4E**). Together, these results illustrate that the inhibition of NRF2 target genes by triptolide is dependent on CRM1 in A549 cells.

Triptolide Increases Oxidative Stress, Inhibits Invasion, and Sensitizes Cisplatin-Induced Apoptosis in A549 Cells

We found that triptolide promoted the generation of intracellular oxidative stress in A549 cells, as illustrated by an increase in the levels of 8-hydroxydeoxyguanine (8-OHdG, Left Panel) and 4-hydroxynonenal (4-HNE, Right Panel) (**Figure 5A**). Triptolide also inhibited invasion of A549 cells, but this event was attenuated when Nrf2 was silenced by siRNA (**Figure 5B**). In addition, triptolide potentiated cisplatin-induced cell death (**Figure 5C**) and increased cisplatin-induced caspase-3 activation, an indicator of apoptosis (**Figure 5D**). Together, these results illustrate that the inhibition of NRF2 by triptolide is associated with promoting oxidative stress, suppressing invasion, and potentiating cell death and apoptosis in A549 cells.

Triptolide Inhibits the Growth of A549 Xenografts *In Vivo*

In order to examine whether the inhibition of NRF2 by triptolide exerts inhibitory effects on the growth of lung tumors *in vivo*, we injected A549 cells into the flank of athymic nude mice and orally administered them with triptolide (**Figure 6A**). While triptolide did not affect the body weight of mice during the course of study (**data not shown**), it significantly decreased the growth of A549 xenografts after 12 and 15 days (**Figure 6B**). At sacrifice, we noticed that triptolide significantly decreased the weight of A549 cell xenografts in a dose-dependent manner (**Figure 6C**). Immunohistochemistry studies illustrate that triptolide promoted cytoplasmic localization of NRF2 and CRM1 (**Figure 6D**), inhibited the expression of HO-1 and NQO1 (**Figure 6E**), and increased the generation of oxidative stress markers (8-OHdG and 4-HNE) in A549 xenografts (**Figure 6E**). These results illustrate that the inhibition of the growth of A549 xenografts by triptolide is associated with the inhibition of NRF2 target genes, cytoplasmic localization of NRF2 and CRM1, and the generation of oxidative stress *in vivo*.

DISCUSSION

Triptolide was first isolated from *Tripterygium wilfordii* Hook F, also known as Lei Gong Teng or Thunder God Vine (Kupchan et al., 1972). Thereafter, a number of studies have demonstrated that triptolide is effective against various diseases, including cancer. Because triptolide is a lipophilic compound, its clinical efficacy is limited. Therefore, many attempts to develop triptolide derivatives with higher efficacy, enhanced water solubility, and lower toxicity have been made in the last two decades and two triptolide derivatives (minnelide and F60008) are currently under the clinical trials (Noel et al., 2019). Triptolide is known to affect a

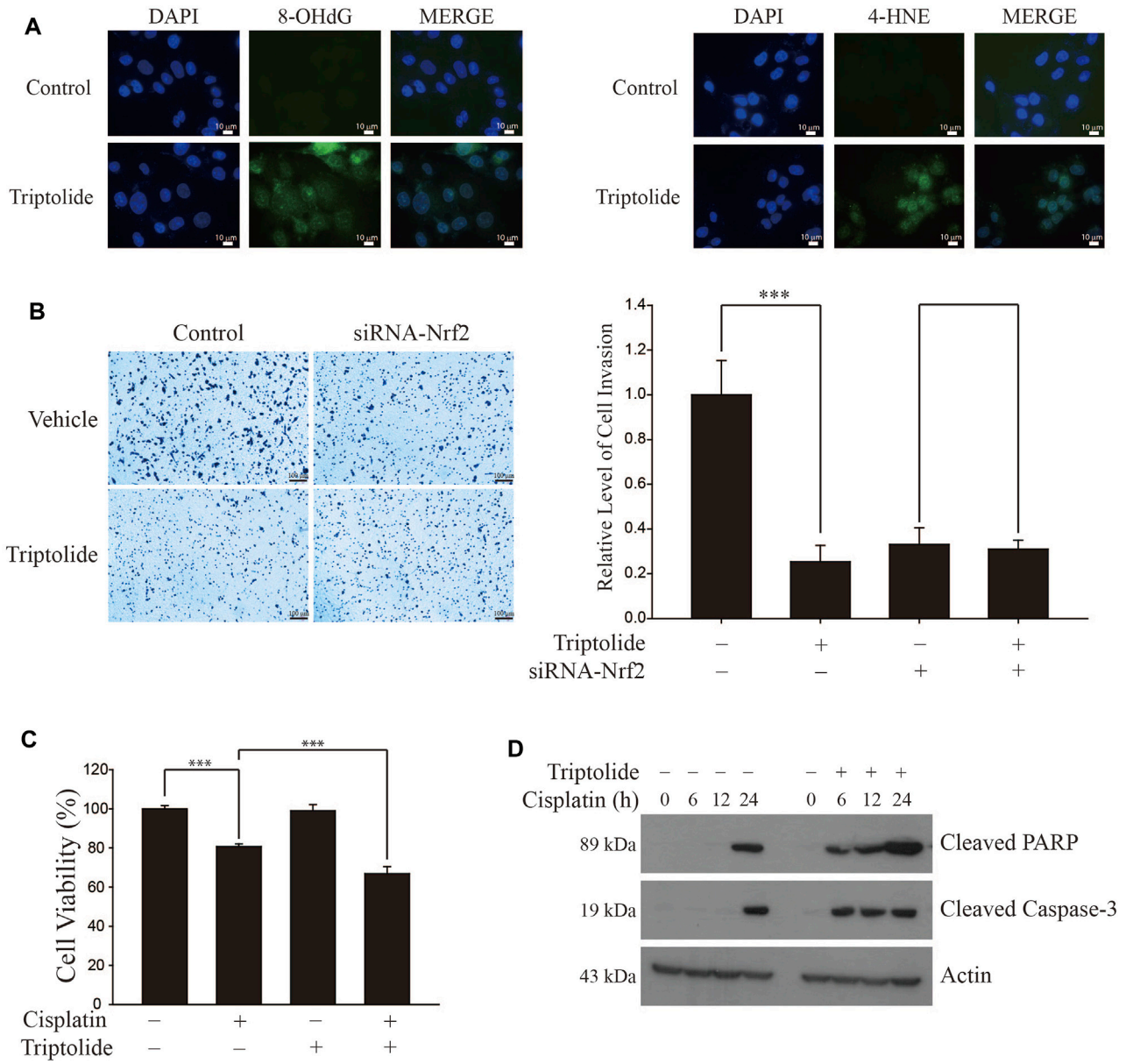

FIGURE 5 | Triptolide induces oxidative stress, inhibits invasion, and sensitizes cisplatin-induced cell death in A549 cells. **(A)** Triptolide induces intracellular oxidative stress. After treatment of triptolide (20 nM) for 24 h, the levels of the oxidative stress markers 8-OHdG (Left Panel) and 4-HNE (Right Panel) were measured by immunofluorescence in A549 cells. **(B)** Triptolide suppresses invasion in A549 cells. The invasion assay was conducted with A549 cells in the absence or presence of triptolide (20 nM) for 24 h. Representative figures are provided (Left Panel) and asterisks indicate a statistical significance with ***$p < 0.001$ (Right Panel, $n = 4$). **(C)** Triptolide potentiates cisplatin-induced cell death in A549 cells. A549 cells were seeded in 96-well culture plates (4×10^4 cells/well) and exposed to cisplatin (20 μM) in the absence or presence of triptolide (20 nM) for 24 h. MTT assay was conducted to measure the cell viability and asterisks indicate a statistical significance ($n = 3$): ***$p < 0.001$. **(D)** Triptolide sensitizes cisplatin-induced apoptosis in A549 cells. A549 cells were seeded in 60 mm plates (2.0×10^5 cells/well) and exposed to cisplatin (20 μM) alone or together with triptolide (20 nM). Western blot analysis was conducted using Cleaved PARP, Cleaved Caspase-3, and actin antibodies.

number of cellular proteins and intracellular kinase pathways to exhibit anti-carcinogenic effects (Chen et al., 2018). In addition, it is assumed that nuclear hormone receptors could be putative targets for the inhibition of NRF2 by triptolide because triptolide possesses a diterpenoid structure similar to several lipophilic hormones (Liu et al., 2015). However, the mechanistic linkage between the nuclear receptors and NRF2 is currently lacking.

Triptolide has a hydroxyl group deemed important for its anti-tumorigenic activity (Li et al., 2009). Triptolide also possesses four reactive chemical groups that may covalently react with cellular targets: the butenolide moiety in the five-membered lactone ring and the three epoxides. While direct cellular targets for the hydroxyl and the butenolide groups of triptolide are unclear, He *et al.* demonstrated that the epoxide

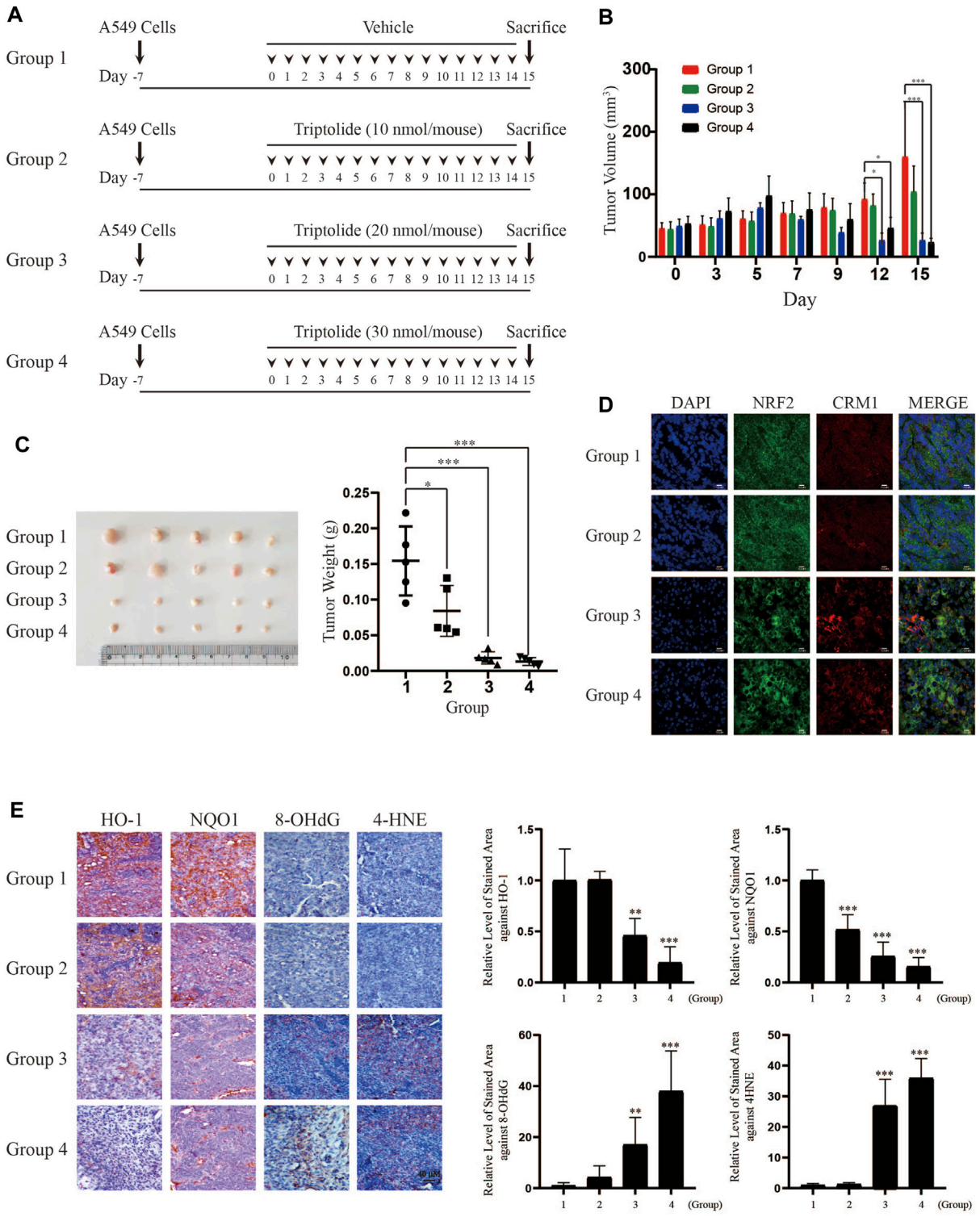

FIGURE 6 | Triptolide inhibits the growth of A549 xenografts in nude mice. **(A)** Experimental scheme of A549 xenograft experiment. **(B)** Triptolide suppresses the growth of A549 xenografts in nude mice. During the experiment, the volume of A549 xenografts was measured by caliper every 3 days and calculated based on the formula, $V = LxW^2/2$ (L: Length, W: Width). Asterisks indicate a statistical significance ($n = 5$): $^*p < 0.05$ and $^{***}p < 0.001$. **(C)** Triptolide suppresses the weight of A549 xenografts in nude mice. The weight of A549 xenografts was measured at sacrifice. Asterisks indicate a statistical significance ($n = 5$): $^*p < 0.05$ and $^{***}p < 0.001$. **(D)** Triptolide promotes nuclear exclusion of NRF2 *in vivo*. Tissue samples of A549 xenografts were subjected to immunofluorescence using NRF2 and CRM1 antibodies. Representative slides of each group are provided. **(E)** Triptolide suppresses the expression of NRF2 target proteins (HO-1 and NQO1) and promotes oxidative stress (8-OHdG and 4-HNE) *in vivo*. The representative images of proteins stained with individual antibodies are provided (Left Panel) and the relative levels of stained area are provided (Right Panel). Asterisks indicate a statistical significance ($n = 5$): $^{**}p < 0.01$ and $^{***}p < 0.001$, compared with the control (Group 1).

in triptolide targets the XBP1 subunit of transcription factor TFIIH (Titov et al., 2011) and inhibits transcription and nucleotide excision repair activity of RNA polymerase II *via* a covalent modification at Cys342 (He et al., 2015). Zhao *et al.* showed that triptolide targets the peroxiredoxin I (Prx I) and inhibits its chaperone activity, but not peroxidase activity, in an analogous manner: the epoxide in triptolide prevents formation of the Prx I homodecamer via covalent modifications at Cys83 and Cys173 (Zhao et al., 2015). It is unclear whether and, if so, which moieties in triptolide is required for NRF2 inhibition and we are currently conducting the structure-activity relationship (SAR) studies to address this issue. While the roles of the XBP1 subunit and Prx I in the regulation of NRF2 target genes by triptolide is unknown, we observed that knocking down Nrf2 in A549 cells abrogated the inhibition of HO-1 and NQO1 (**Supplementary Figure S2A**), and that of Ho-1 and Nqo1 mRNAs (**Supplementary Figure S2B**) by triptolide. In addition, triptolide failed to affect the level of Ho-1 and Nqo1 mRNAs in 293T cells (**Supplementary Figure S3**). These results suggest that NRF2 plays a major role in the inhibition of NRF2 target genes by triptolide in A549 cells.

In the present study, we have identified that triptolide is a novel NRF2 inhibitor (**Figure 1**). The unique feature of NRF2 inhibition by triptolide is that, unlike other NRF2 inhibitors, triptolide inhibits the expression of NRF2 target genes without affecting the level of NRF2 (**Figure 2**). The nuclear export of NRF2 and the inhibition of NRF2 target genes by triptolide was observed *in vitro* (**Figure 2**) and *in vivo* (**Figure 6D**). While the detailed molecular mechanisms remain to be further investigated, we observed that triptolide promoted the nuclear exclusion of NRF2 in A549 cells and increased the interaction between NRF2 and CRM1 in whole cell extracts (**Figures 3**, **4**). In addition, we have identified that NRF2 possesses a previously unrecognized NES in the Neh2 domain where CRM1 can bind to and promote the nuclear export of NRF2 (**Figure 3**). Because the NES in the Neh2 domain lacks potential amino acid residues susceptible to post-translational modifications, it is unlikely that the induction of post-translational modification in the NES promoted the interaction between NRF2 and CRM1 caused by triptolide. We are rather tempted to speculate that triptolide might induce post-translational modification(s) in CRM1 and/or its regulatory proteins to affect cytoplasmic localization of NRF2. Indeed, there exist studies demonstrating post-translational modifications affect the activities of CRM1 (Wu et al., 2013) and its regulatory protein, Ran-GTPase (De Boor et al., 2015). However, due to the lack of appropriate antibodies indicative of post-translational modifications of CRM1 and Ran-GTPase, we could not examine this hypothesis. Collectively, we propose that triptolide has an advantage compared with other NRF2 inhibitors in that it downregulates the expression of NRF2 target genes without affecting NRF2, which could be used to treat lung cancer cells regardless of mutation status in the Keap1/Nrf2 pathway. Understanding the detailed molecular mechanisms how triptolide promotes the nuclear exclusion of NRF2 will provide us a clue to develop NRF2 inhibitors with higher efficacy and lower toxicity.

DATA AVAILABILITY STATEMENT

The raw data supporting the conclusions of this article will be made available by the authors, without undue reservation.

ETHICS STATEMENT

The animal study was reviewed and approved by the Dongguk University.

AUTHOR CONTRIBUTIONS

LBN, WJC and Y-SK conceived the idea and designed the experiments. LBN conducted all the experiments and Y-SK wrote the manuscript.

FUNDING

This work was supported by Basic Science Research Program through the National Research Foundation of Korea (NRF) funded by the Ministry of Education (NRF-2016R1D1A1B01010116) and National Research Foundation of Korea (NRF) grants funded by the Korean government (MSIT) (NRF-2018R1A5A2023127).

SUPPLEMENTARY MATERIAL

The Supplementary Material for this article can be found online at: https://www.frontiersin.org/articles/10.3389/fphar.2021.680167/full#supplementary-material.

Supplementray Figure S1 | Triptolide does not affect the viability of A549 cells (Left Panel) and H1299 cells (Right Panel) at concentrations up to 40 nM. A549 cells and H1299 cells were seeded in 96-well culture plates ($4x10^4$ cells/well) and trypan blue exclusion assay was conducted (n = 4) after treatment of triptolide at multiple concentrations for 24 h.

Supplementray Figure S2 | Suppression of NRF2 target genes by triptolide requires NRF2 in A549 cells. **(A)** Triptolide fails to suppress the expression of HO-1 and NQO1 in A549 cells when Nrf2 is silenced by siRNA**.** A549 cells were seeded in 100 mm culture plates ($2x10^6$ cells) and exposed to triptolide (20 nM) for 24 h in the absence or presence of siRNA against Nrf2 (100 nM). Western blot analysis was performed using NRF2, HO-1, NQO1, and actin antibodies. **(B)** Suppression of Ho-1 (Left Panel) and Nqo1 (Right Panel) mRNAs by triptolide is dependent on NRF2. A549 cells were seeded in 60 mm plates ($2.0x10^5$ cells) and exposed to triptolide (20 nM) for 3 h in the absence or presence of siRNA against Nrf2 (100 nM). Total RNA was prepared and real-time RT-PCR was conducted using specific primers against Ho-1 and Nqo1. Asterisks indicate a statistical significance (n = 4): $^{***}P<0.01$.

Supplementray Figure S3 | Triptolide does not affect the levels of Ho-1 and Nqo1 mRNAs in 293T cells. 293T cells were exposed to triptolide (10 nM) for 3 h. Total RNA of 293T cells and A549 cells was prepared and real-time RT-PCR was conducting specific primers against Ho-1 and Nqo1. Asterisks indicate a statistical significance (n = 4): $^{***}P<0.01$.

REFERENCES

Cancer Genome Atlas Research Network (2012). Comprehensive Genomic Characterization of Squamous Cell Lung Cancers. *Nature* 489, 519–525. doi:10.1038/nature11404

Cancer Genome Atlas Research Network (2014). Comprehensive Molecular Profiling of Lung Adenocarcinoma. *Nature* 511, 543–550. doi:10.1038/nature13385

Chen, S. R., Dai, Y., Zhao, J., Lin, L., Wang, Y., and Wang, Y. (2018). A Mechanistic Overview of Triptolide and Celastrol, Natural Products from Tripterygium Wilfordii Hook F. *Front. Pharmacol.* 9, 104. doi:10.3389/fphar.2018.00104

Cuadrado, A., Rojo, A. I., Wells, G., Hayes, J. D., Cousin, S. P., Rumsey, W. L., et al. (2019). Therapeutic Targeting of the NRF2 and KEAP1 Partnership in Chronic Diseases. *Nat. Rev. Drug Discov.* 18, 295–317. doi:10.1038/s41573-018-0008-x

De Boor, S., Knyphausen, P., Kuhlmann, N., Wroblowski, S., Brenig, J., Scislowski, L., et al. (2015). Small GTP-Binding Protein Ran Is Regulated by Posttranslational Lysine Acetylation. *Proc. Natl. Acad. Sci. U S A.* 112, E3679–E3688. doi:10.1073/pnas.1505995112

Fung, H. Y., and Chook, Y. M. (2014). Atomic Basis of CRM1-Cargo Recognition, Release and Inhibition. *Semin. Cancer Biol.* 27, 52–61. doi:10.1016/j.semcancer.2014.03.002

Goldstein, L. D., Lee, J., Gnad, F., Klijn, C., Schaub, A., Reeder, J., et al. (2016). Recurrent Loss of NFE2L2 Exon 2 Is a Mechanism for Nrf2 Pathway Activation in Human Cancers. *Cell Rep* 16, 2605–2617. doi:10.1016/j.celrep.2016.08.010

He, Q. L., Titov, D. V., Li, J., Tan, M., Ye, Z., Zhao, Y., et al. (2015). Covalent Modification of a Cysteine Residue in the XPB Subunit of the General Transcription Factor TFIIH through Single Epoxide Cleavage of the Transcription Inhibitor Triptolide. *Angew. Chem. Int. Ed. Engl.* 54, 1859–1863. doi:10.1002/anie.201408817

Hutten, S., and Kehlenbach, R. H. (2007). CRM1-Mediated Nuclear Export: To the Pore and Beyond. *Trends Cel Biol* 17, 193–201. doi:10.1016/j.tcb.2007.02.003

Itoh, K., Chiba, T., Takahashi, S., Ishii, T., Igarashi, K., Katoh, Y., et al. (1997). An Nrf2/Small Maf Heterodimer Mediates the Induction of Phase II Detoxifying Enzyme Genes through Antioxidant Response Elements. *Biochem. Biophys. Res. Commun.* 236, 313–322. doi:10.1006/bbrc.1997.6943

Jung, B. J., Yoo, H. S., Shin, S., Park, Y. J., and Jeon, S. M. (2018). Dysregulation of NRF2 in Cancer: From Molecular Mechanisms to Therapeutic Opportunities. *Biomol. Ther. (Seoul)* 26, 57–68. doi:10.4062/biomolther.2017.195

Kang, J. S., Lee, J., Nam, L. B., Yoo, O. K., Pham, K. T., Duong, T. H., et al. (2019). Homoharringtonine Stabilizes Secondary Structure of Guanine-Rich Sequence Existing in the 5'-Untranslated Region of Nrf2. *Bioorg. Med. Chem. Lett.* 29, 2189–2196. doi:10.1016/j.bmcl.2019.06.049

Kang, J. S., Nam, L. B., Yoo, O. K., and Keum, Y. S. (2020). Molecular Mechanisms and Systemic Targeting of NRF2 Dysregulation in Cancer. *Biochem. Pharmacol.* 177, 114002. doi:10.1016/j.bcp.2020.114002

Kobayashi, A., Kang, M. I., Okawa, H., Ohtsuji, M., Zenke, Y., Chiba, T., et al. (2004). Oxidative Stress Sensor Keap1 Functions as an Adaptor for Cul3-Based E3 Ligase to Regulate Proteasomal Degradation of Nrf2. *Mol. Cel Biol* 24, 7130–7139. doi:10.1128/MCB.24.16.7130-7139.2004

Kupchan, S. M., Court, W. A., Dailey, R. G., Jr., Gilmore, C. J., and Bryan, R. F. (1972). Triptolide and Tripdiolide, Novel Antileukemic Diterpenoid Triepoxides from Tripterygium Wilfordii. *J. Am. Chem. Soc.* 94, 7194–7195. doi:10.1021/ja00775a078

La Fleur, L., Falk-Sörqvist, E., Smeds, P., Berglund, A., Sundström, M., Mattsson, J. S., et al. (2019). Mutation Patterns in a Population-Based Non-Small Cell Lung Cancer Cohort and Prognostic Impact of Concomitant Mutations in KRAS and TP53 or STK11. *Lung Cancer* 130, 50–58. doi:10.1016/j.lungcan.2019.01.003

Lee, J., Kang, J. S., Nam, L. B., Yoo, O. K., and Keum, Y. S. (2018a). Suppression of NRF2/ARE by Convallatoxin Sensitises A549 Cells to 5-FU-Mediated Apoptosis. *Free Radic. Res.* 52, 1416–1423. doi:10.1080/10715762.2018.1489132

Lee, J., Mailar, K., Yoo, O. K., Choi, W. J., and Keum, Y. S. (2018b). Marliolide Inhibits Skin Carcinogenesis by Activating NRF2/ARE to Induce Heme Oxygenase-1. *Eur. J. Med. Chem.* 150, 113–126. doi:10.1016/j.ejmech.2018.02.068

Li, Z., Zhou, Z. L., Miao, Z. H., Lin, L. P., Feng, H. J., Tong, L. J., et al. (2009). Design and Synthesis of Novel C14-Hydroxyl Substituted Triptolide Derivatives as Potential Selective Antitumor Agents. *J. Med. Chem.* 52, 5115–5123. doi:10.1021/jm900342g

Liu, X., Wang, K., Duan, N., Lan, Y., Ma, P., Zheng, H., et al. (2015). Computational Prediction and Experimental Validation of Low-Affinity Target of Triptolide and its Analogues. *RSC Adv.* 5, 34572–34579. doi:10.1039/c4ra17009a

Nam, L. B., and Keum, Y. S. (2020). Regulation of NRF2 by Na+/K+-ATPase: Implication of Tyrosine Phosphorylation of Src. *Free Radic. Res.* 54 (11-12), 883–893. doi:10.1080/10715762.2020.1735633

Noel, P., Von Hoff, D. D., Saluja, A. K., Velagapudi, M., Borazanci, E., and Han, H. (2019). Triptolide and its Derivatives as Cancer Therapies. *Trends Pharmacol. Sci.* 40, 327–341. doi:10.1016/j.tips.2019.03.002

Ren, D., Villeneuve, N. F., Jiang, T., Wu, T., Lau, A., Toppin, H. A., et al. (2011). Brusatol Enhances the Efficacy of Chemotherapy by Inhibiting the Nrf2-Mediated Defense Mechanism. *Proc. Natl. Acad. Sci. U S A.* 108, 1433–1438. doi:10.1073/pnas.1014275108

Robledinos-Antón, N., Fernández-Ginés, R., Manda, G., and Cuadrado, A. (2019). Activators and Inhibitors of NRF2: A Review of Their Potential for Clinical Development. *Oxid Med. Cel Longev* 2019, 9372182. doi:10.1155/2019/9372182

Rojo De La Vega, M., Chapman, E., and Zhang, D. D. (2018). NRF2 and the Hallmarks of Cancer. *Cancer Cell* 34, 21–43. doi:10.1016/j.ccell.2018.03.022

Singh, A., Misra, V., Thimmulappa, R. K., Lee, H., Ames, S., Hoque, M. O., et al. (2006). Dysfunctional KEAP1-NRF2 Interaction in Non-Small-Cell Lung Cancer. *Plos Med.* 3, e420. doi:10.1371/journal.pmed.0030420

Taguchi, K., and Yamamoto, M. (2017). The KEAP1-NRF2 System in Cancer. *Front. Oncol.* 7, 85. doi:10.3389/fonc.2017.00085

Taguchi, K., Motohashi, H., and Yamamoto, M. (2011). Molecular Mechanisms of the Keap1–Nrf2 Pathway in Stress Response and Cancer Evolution. *Genes Cells* 16, 123–140. doi:10.1111/j.1365-2443.2010.01473.x

Titov, D. V., Gilman, B., He, Q. L., Bhat, S., Low, W. K., Dang, Y., et al. (2011). XPB, a Subunit of TFIIH, Is a Target of the Natural Product Triptolide. *Nat. Chem. Biol.* 7, 182–188. doi:10.1038/nchembio.522

Velichkova, M., and Hasson, T. (2005). Keap1 Regulates the Oxidation-Sensitive Shuttling of Nrf2 into and Out of the Nucleus via a Crm1-Dependent Nuclear Export Mechanism. *Mol. Cel Biol* 25, 4501–4513. doi:10.1128/MCB.25.11.4501-4513.2005

Wang, R., An, J., Ji, F., Jiao, H., Sun, H., and Zhou, D. (2008). Hypermethylation of the Keap1 Gene in Human Lung Cancer Cell Lines and Lung Cancer Tissues. *Biochem. Biophys. Res. Commun.* 373, 151–154. doi:10.1016/j.bbrc.2008.06.004

Wu, Z., Jiang, Q., Clarke, P. R., and Zhang, C. (2013). Phosphorylation of Crm1 by CDK1-Cyclin-B Promotes Ran-Dependent Mitotic Spindle Assembly. *J. Cel Sci* 126, 3417–3428. doi:10.1242/jcs.126854

Zhao, Q., Ding, Y., Deng, Z., Lee, O. Y., Gao, P., Chen, P., et al. (2015). Natural Products Triptolide, Celastrol, and Withaferin A Inhibit the Chaperone Activity of Peroxiredoxin I. *Chem. Sci.* 6, 4124–4130. doi:10.1039/c5sc00633c

Conflict of Interest: Y-SK was employed by Panacea Co.

The remaining authors declare that the research was conducted in the absence of any commercial or financial relationships that could be construed as a potential conflict of interest.

Publisher's Note: All claims expressed in this article are solely those of the authors and do not necessarily represent those of their affiliated organizations, or those of the publisher, the editors and the reviewers. Any product that may be evaluated in this article, or claim that may be made by its manufacturer, is not guaranteed or endorsed by the publisher.

frontiers in Pharmacology

ORIGINAL RESEARCH
published: 20 October 2021
doi: 10.3389/fphar.2021.682643

Non-Invasive Remote Ischemic Preconditioning May Protect the Gastric Mucosa Against Ischemia-Reperfusion-Induced Injury Through Involvement of Glucocorticoids

Ludmila Filaretova, Olga Komkova, Maria Sudalina and Natalia Yarushkina*

Laboratory of Experimental Endocrinology, Pavlov Institute of Physiology, Russian Academy of Sciences, St. Petersburg, Russia

OPEN ACCESS

Edited by:
Thomas Brzozowski, Jagiellonian University Medical College, Poland

Reviewed by:
Edoardo Bindi, Salesi Hospital Foundation, Italy
Leonid Maslov, Tomsk National Research Medical Center (RAS), Russia

***Correspondence:**
Ludmila Filaretova
filaretovalp@infran.ru

Specialty section:
This article was submitted to Gastrointestinal and Hepatic Pharmacology, a section of the journal Frontiers in Pharmacology

Received: *18 March 2021*
Accepted: *30 September 2021*
Published: *20 October 2021*

Citation:
Filaretova L, Komkova O, Sudalina M and Yarushkina N (2021) Non-Invasive Remote Ischemic Preconditioning May Protect the Gastric Mucosa Against Ischemia-Reperfusion-Induced Injury Through Involvement of Glucocorticoids. Front. Pharmacol. 12:682643. doi: 10.3389/fphar.2021.682643

Remote ischemic preconditioning (RIPC) is one of the most effective approaches to attenuate tissue injury caused by severe ischemia-reperfusion (I/R). Experimental studies have demonstrated that RIPC is capable of producing a protective effect not only on heart, but also on brain, lungs, kidneys, liver, intestine, and stomach. We previously demonstrated that glucocorticoids participate in protective effect of local gastric ischemic preconditioning against I/R-induced gastric injury. In the present study we investigated whether RIPC may protect the gastric mucosa against I/R-induced injury through involvement of glucocorticoids. Anesthetized fasted Sprague Dawley male rats were exposed to prolonged gastric I/R (30 min occlusion of celiac artery followed by 3 h of reperfusion) alone or with preliminary brief RIPC (10 min non-invasive occlusion of right hind limb blood flow followed by reperfusion for 30 min). First, we investigated the effect of RIPC on I/R-induced injury by itself. Then to study the role of glucocorticoids similar experiments were carried out: 1) in rats pretreated with the inhibitor of glucocorticoid synthesis, metyrapone (30 mg/kg, i.p), and in control animals; 2) in adrenalectomized rats without or with corticosterone replacement (4 mg/kg, s.c.) and in sham-operated animals; 3) in rats pretreated with glucocorticoid receptor antagonist RU-38486 (20 mg/kg, s.c.) and in control animals. I/R induced corticosterone rise and resulted in the gastric erosion formation. RIPC significantly reduced the erosion area in control animals. Metyrapone injected shortly before RIPC caused a decrease in plasma corticosterone levels and prevented the gastroprotective effect of RIPC and, moreover, further aggravated the deleterious effect of I/R. Adrenalectomy performed 1 week before experiment created long-lasting corticosterone deficiency and had no effect on the gastroprotective effect of RIPC. Nevertheless, corticosterone replacement which mimics the corticosterone rise, similar to RIPS, significantly reduced erosion areas of gastric mucosa in adrenalectomized

Abbreviations: CGRP, calcitonin gene-related peptide; CRF, corticotropin-releasing factor; I/R, ischemia-reperfusion; IPC, ischemic preconditioning; HPA axis, hypothalamic-pituitary-adrenocortical axis; PGs, prostaglandins; RIPC, remote ischemic preconditioning.

rats supporting the role of glucocorticoids in gastroprotection. RU-38486, which occupied glucocorticoid receptors, similar to metyrapone prevented the gastroprotective effect of RIPC and, moreover, further aggravated the deleterious effect of I/R. The results of the present study demonstrate for the first time that RIPC may protect the gastric mucosa against I/R-induced injury through involvement of glucocorticoids.

Keywords: gastric injury, ischemia-reperfusion, gastroprotection, remote ischemic preconditioning, glucocorticoids

INTRODUCTION

Ischemic preconditioning (IPC) is an adaptive phenomenon, in which a tissue becomes more resistant to prolonged exposure of ischemia or ischemia reperfusion (I/R) after one or more brief preconditioning ischemia-reperfusion episodes (Aggarwal et al., 2016; McDonough and Weinstein, 2020). The phenomenon of IPC was first depicted as early as 1986 by Murry et al. (1986). It has been shown in dogs that multiple brief ischemic episodes protect the heart from a subsequent sustained ischemic insult (Murry et al., 1986). Later a similar model of ischemic tolerance was also described in rat, rabbit and pig hearts (Kloner and Jennings, 2001). The concept of IPC was supported in humans (Kloner and Yellon, 1994).

Although early IPC studies were related with the heart, the protective effects IPC has been demonstrated in multiple organ systems and shown to be effective. Various organs including kidneys (Fuller et al., 2005), lungs (Soncul et al., 1999), liver (Fernández et al., 2002), stomach (Pajdo et al., 2001) or brain (Li et al., 2017) also respond to brief ischemia exposures with an increased resistance to severe ischemia.

Initially the effect of IPC was assumed to implement only within the tissue subjected to prolonged ischemia and, in this case, IPC is considered as local or regional phenomenon. But in 1993 Karin Przyklenk with colleagues showed in canine model that brief episodes of ischemia in one vascular bed may protect remote myocardium from subsequent sustained coronary artery occlusion (Przyklenk et al., 1993). This phenomenon was termed as remote ischemic preconditioning (RIPC) (Przyklenk et al., 1993). There is growing experimental and clinical evidence supporting that RIPS elicits cardioprotection. It is considered as the most practical, non-invasive, cost-free, and clinically compatible, secure procedure for reducing I/R-induced injury. The use of a conventional blood pressure cuff on the upper or lower limb in eliciting cardioprotection has expedited its clinical applicability (Uutela et al., 2020).

After discovery by Karin Przyklenk RIPC phenomenon regarding heart, it was demonstrated that RIPC similar to local IPC is common physiological phenomenon. Indeed, experimental studies found that it was possible to protect non-cardiac organs and tissues from acute I/R injury (Lim and Hausenloy, 2012; Wang et al., 2015).

The findings suggest that RIPC represents a form of systemic protection against acute I/R injury and may provide non-invasive endogenous therapeutics strategy for protection organs against acute I/R (Lim and Hausenloy, 2012; Heusch and Gersh, 2016). RIPC and the mechanisms underlying this phenomenon have been extensively studied in animal models and cardiac surgery, as well as in solid organ transplantation (Uutela et al., 2020). Three main pathways for transmitting the protective signal from the organ or tissue, in which the RIPC stimulus is applied, to the target organ or tissue, are considered: neural pathway, the release of circulating humoral factors (humoral pathway) and activation of a systemic protective effect (systemic response) (Lim and Hausenloy, 2012).

Injury caused by ischemia or I/R plays a significant role in the abdominal organ diseases, in the gastric mucosal injury in particular, and development new approaches to attenuate or prevent the pathology is extremely important. RIPC is one of the most effective non-invasive approaches to attenuate tissue gastric injury caused by severe I/R. RIPC-induced gastroprotection was first demonstrated by Brzozowski et al. (2004a) using a rat model of gastric I/R-caused injury. The authors showed that RIPC applied to the heart or liver significantly improved gastric blood flow and reduced gastric injury via the mechanisms involving prostaglandin E2 (PGs) production and the activation of sensory nerves releasing calcitonin gene-related peptide (CGRP) combined with the suppression of plasma proinflammatory cytokines (IL-1β and TNFα) levels (Brzozowski et al., 2004a; Brozowski et al., 2004b).

No study so far has been undertaken to verify whether glucocorticoids may participate in realization of protective effect of RIPC against I/R-induced gastric injury. Glucocorticoids are key hormonal factors providing systemic response to stressor. Taking into consideration this fact together with the facts that humoral pathway and systemic response are two main pathways for the transmitting the RIPC-induced protective signals (Lim and Hausenloy, 2012) it is reasonable to propose a participation of glucocorticoids in realization of gastroprotective effect of RIPC. Our previous findings about gastroprotective role of glucocorticoids also allowed us to assume that glucocorticoids may contribute to gastroprotective effect of RIPC (Filaretova et al., 1998; Filaretova et al., 2004; Filaretova et al., 2007; Filaretova et al., 2008, Filaretova et al., 2012; Filaretova, 2011; Filaretova, 2017; Filaretova and Bagaeva, 2016). Additionally it is important to note that we previously demonstrated participation of glucocorticoids in protective effect of local gastric ischemic preconditioning against I/R-induced gastric injury (Bobryshev et al., 2009).

In the present study we investigated whether RIPC may protect the gastric mucosa against IR-induced injury through involvement of glucocorticoids.

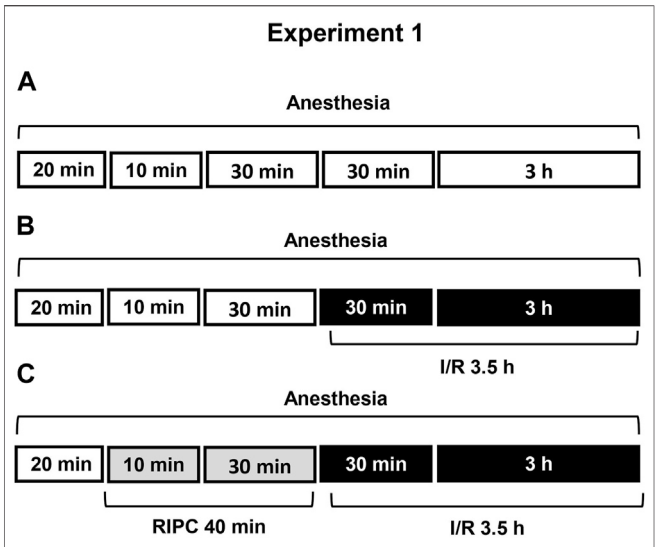

FIGURE 1 | Design of Experiment 1: effect of RIPC on I/R-induced gastric erosions and plasma corticosterone levels. Three groups of rats were used: control rats without any exposures (I/R or/and RIPC) **(A)**; rats which were subjected I/R alone **(B)** or preliminary RIPC before I/R **(C)**.

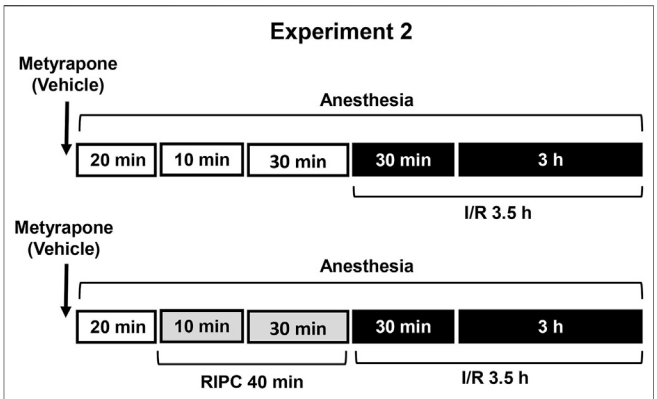

FIGURE 2 | Design of Experiment 2: effect of metyrapone pretreatment on gastroprotective action of RIPC and plasma corticosterone levels. Four groups of rats were used: rats pretreated with metyrapone (30 mg/kg, i.p.) or its vehicle which were subjected to I/R alone and rats pretreated with metyrapone or its vehicle which were subjected to preliminary RIPC before I/R.

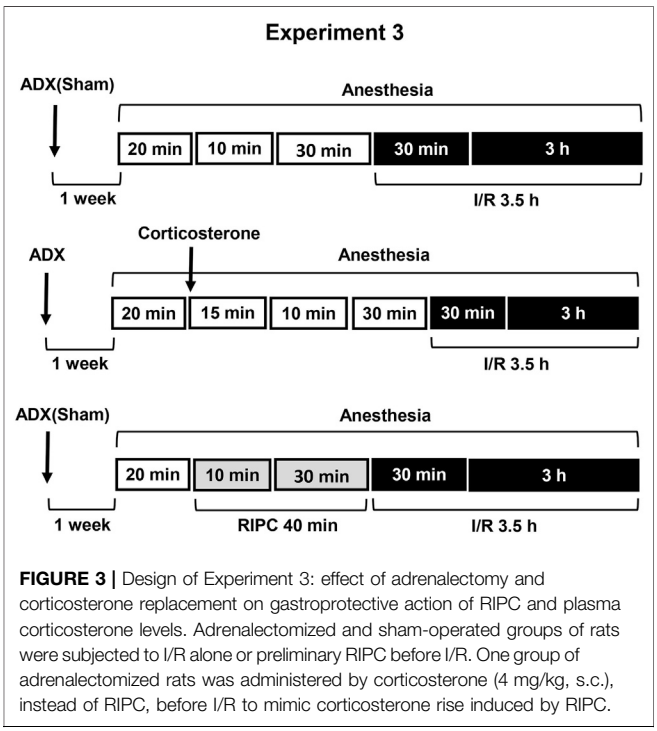

FIGURE 3 | Design of Experiment 3: effect of adrenalectomy and corticosterone replacement on gastroprotective action of RIPC and plasma corticosterone levels. Adrenalectomized and sham-operated groups of rats were subjected to I/R alone or preliminary RIPC before I/R. One group of adrenalectomized rats was administered by corticosterone (4 mg/kg, s.c.), instead of RIPC, before I/R to mimic corticosterone rise induced by RIPC.

MATERIALS AND METHODS

Animals

Male Sprague-Dawley rats (Stolbovoe, Moscow, Russia) weighing about 250–300 g were housed six animals per cage and have been acclimated to the standard laboratory conditions (12:12-h light-dark cycle, temperature 20 ± 1°C, free access to food and water) for a week. The animals were fasted 24 h before the experiment but given free access to drinking water. The care and treatment of animals were done in accordance with ARRIVE guidelines and EU Directive 2010/63/EU for animal experiments and was reviewed and approved by the Institutional Animal Care and Use Committee of the Pavlov Institute of Physiology RAS.

Production of Gastric Lesions Induced by Ischemia/Reperfusion

Gastric erosions were produced by prolonged I/R in preliminary (24 h) fasted anesthetized rats. We used a well known experimental model of I/R to produce gastric erosions (Wada et al., 1996). Animals were given with tiletamine/zolazepam (Zoletil ®, «Virbac», Carros, France, 7.5 mg/kg, ip) and xylazine hydrochloride (Rometar, «SPOFA», Luberec, Czech Republic, 10 mg/kg, ip) in a volume of 0.5 ml/kg for general anaesthesia. Additionally, Zoletil (4 mg/kg) was administered every 40 min to maintain an adequate level of anesthesia. Under anesthesia, the abdomen was opened, the celiac artery clamped with a small vascular clamp for 30 min followed by removal of this clamp to obtain reperfusion for 3 h (in total 3.5 h). Sham-operated animals subjected to the same surgical procedure but the celiac artery was not occluded. After completion of 3.5 h I/R, anesthetized animals were euthanized, and the stomachs were removed for examination of gastric lesions (the area in mm 2). The area of lesions developed in the corpus mucosa was measured using computer program ImageJ, summed per stomach, and used as a lesion score.

Remote Ischemic Preconditioning

In our study we used hind limb ischemic preconditioning as RIPC (Souza Filho et al., 2009). RIPC included 10 min non-invasive occlusion of right hind limb blood flow followed by reperfusion for 30 min (in total 40 min). Non-invasive occlusion of hind limb blood flow was produced by placing a forceps to the quadriceps femoris muscle; then, they were removed for reperfusion.

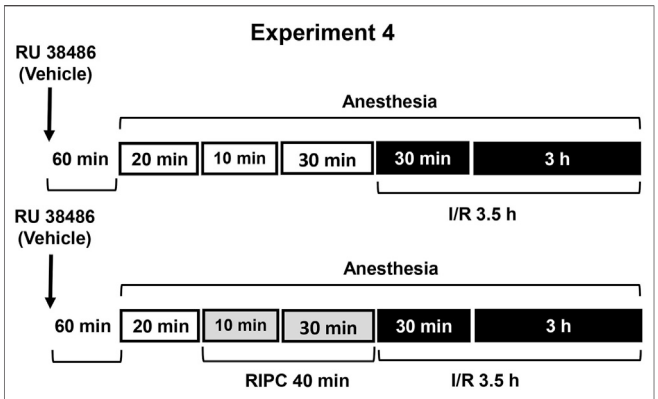

FIGURE 4 | Design of Experiment 4: effect of RU-38486 pretreatment on gastroprotective action of RIPC and plasma corticosterone levels. Four groups of rats were used: rats pretreated with RU-38486 (20 mg/kg, s.c.) or its vehicle which were subjected to I/R alone and rats pretreated with RU-38486 or its vehicle which were subjected to preliminary RIPC before I/R.

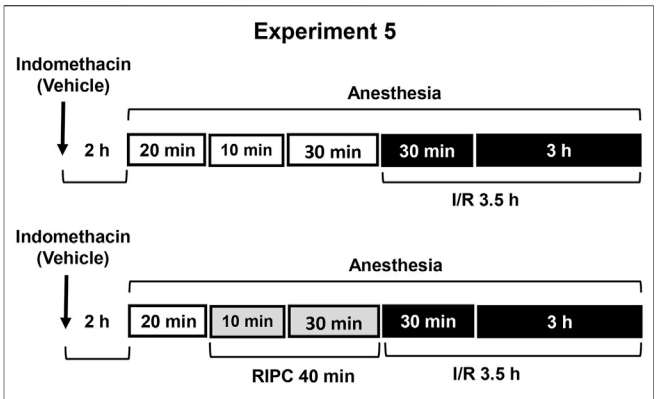

FIGURE 5 | Design of Experiment 5: effect of indomethacin on gastroprotective action of RIPC and plasma corticosterone levels. Four groups of rats were used: rats pretreated with indomethacin (5 mg/kg, s.c.) or its vehicle which were subjected to I/R alone and rats pretreated with indomethacin or its vehicle which were subjected to preliminary RIPC before I/R.

Approaches

First, we examined the protective effect of RIPC against I/R-induced gastric erosion formation (**Experiment 1**) (**Figure 1**). To verify whether glucocorticoids contribute to protective effect of RIPC against I/R-induced gastric injury we compared the effects of RIPC in rats with normal and deficient corticosterone production as well as in rats with normal and occupied glucocorticoid receptors. Glucocorticoid deficiency was created by inhibition of glucocorticoid synthesis by metyrapone (**Experiment 2**) (**Figure 2**) or adrenalectomy (**Experiment 3**) (**Figure 3**). Corticosterone replacement was used to mimic corticosterone rise in adrenalectomized rats (**Experiment 3**) (**Figure 3**). The antagonist of glucocorticoid receptors RU-38486 was used for occupation of glucocorticoid receptors (**Experiment 4**) (**Figure 4**). To estimate the contribution of prostaglandins to gastroprotective action of RIPC, we compared the effects of RIPC against the I/R-induced gastric erosion in rats with normal and deficient prostaglandin production (**Experiment 5**) (**Figure 5**). Deficiency of prostaglandins was created by non-selective inhibitor of cyclooxygenase 1 and 2 indomethacin administered at the non-ulcerogenic dose.

Experiment 1. Effect of RIPC on I/R-Induced Gastric Erosions and Plasma Corticosterone Levels.

Figure 1 is showing design of experiment. Twenty minutes after the onset of anesthesia, fasted rats were exposed to prolonged gastric I/R (30 min occlusion of celiac artery followed by 3 h of reperfusion) alone or with preliminary brief RIPC (10 min non-invasive occlusion of right hind limb blood flow followed by reperfusion for 30 min). Control animals were anesthetized and kept at the same conditions, but did not subject any surgery or RIPC.

Experiment 2. Effect of Metyrapone Pretreatment on Gastroprotective Action of RIPC and Plasma Corticosterone Levels.

Metyrapone (Sigma-Aldrich, Steinheim, Germany), inhibitor of glucocorticoid synthesis, was injected at the dose of 30 mg/kg (in 5 ml/kg 0.9% normal saline with drop of Tween-80, i.p.) 20 min before RIPC (**Figure 2**). Control rats were received vehicle of metyrapone. Immediately after metyrapone or vehicle injection all animals were anesthetized. Twenty minutes later one half each group was exposed to RIPC for 40 min, other half each group kept at the same conditions, but without RIPC. Then, all animals were exposed to I/R for 3.5 h. After completion of I/R anesthetized animals were decapitated.

Experiment 3. Effect of Adrenalectomy and Corticosterone Replacement on Gastroprotective Action of RIPC and Plasma Corticosterone Levels.

Adrenalectomy as well as sham operation was performed 1 week before experiment under ether anesthesia. Sham-operated rats were subjected to the same surgical procedure, but the adrenals were not removed (**Figure 3**). After surgery adrenalectomized rats were provided with a 0.9% NaCl solution in addition to tap water in the home cage. Corticosterone replacement was performed by injecting corticosterone (Sigma, Steinheim, Germany, 4 mg/kg in 1 ml/kg 1,2-propylene glycol s.c.) to adrenalectomized rats 55 min before I/R.

The experiment was carried out in sham-operated and adrenalectomized rats: one half each group was exposed to RIPC for 40 min, other half each group kept at the same conditions, but without RIPC. Then, all animals were exposed to I/R for 3.5 h and decapitated after completion of I/R.

Experiment 4. Effect of RU-38486 Pretreatment on Gastroprotective Action of RIPC and Plasma Corticosterone Levels.

The antagonist of glucocorticoid receptors RU-38486 (Sigma, Saint Louis, United States) was injected at the dose of 20 mg/kg (in 5 ml/kg 1,2-propylene glycol, s.c.) 1 h 20 min before RIPC (**Figure 4**). Control rats were received vehicle of RU-38486. The experiment was carried out in rats pretreated with RU-38486 or its vehicle. One half each group was exposed to RIPC for 40 min, other half each group kept at the same conditions, but without RIPC. Then, all animals were exposed to I/R for 3.5 h and decapitated after completion of I/R.

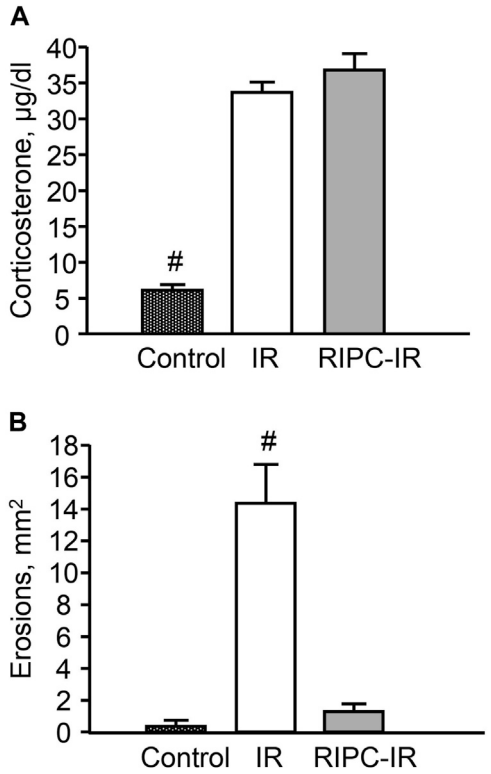

FIGURE 6 | Effect of remote ischemic preconditioning (RIPC) on ischemia-reperfusion (I/R)-induced plasma corticosterone levels **(A)** and gastric erosions (**B**) in rats. Significant differences at $p < 0.05$; # from all groups; number of rats per group (n): Control (n = 6); I/R (n = 10); RIPC-I/R (n = 11).

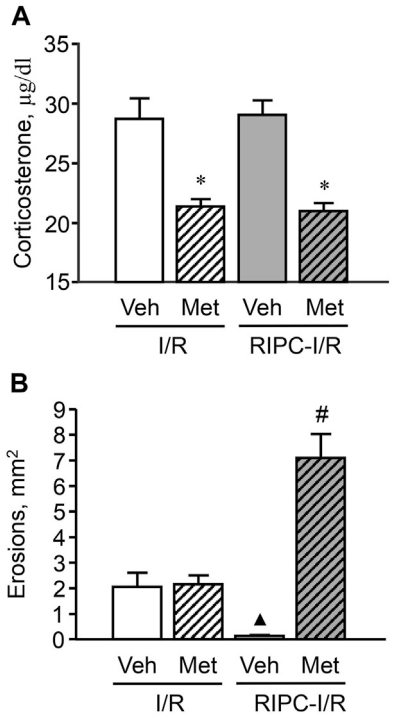

FIGURE 7 | Effect of pretreatment with metyrapone on ischemia-reperfusion (I/R)-induced plasma corticosterone levels **(A)** and gastric erosions **(B)** in rats with and without remote ischemic preconditioning (RIPC). Significant differences at $p < 0.05$; * vs. corresponding vehicle (Veh) group; ▲ vs. "Veh + I/R" group; # from all groups; number of rats per group (n): Veh + I/R (n = 11); Met + I/R (n = 16); Veh + RIPC-I/R (n = 15); Met + RIPC-I/R (n = 16).

Experiment 5. Effect of Indomethacin on Gastroprotective Action of RIPC and Plasma Corticosterone Levels.

To evaluate the contribution of prostaglandins, non-selective inhibitor of cyclooxygenase 1 and 2 indomethacin at the non-ulcerogenic dose (5 mg/kg, in 5 ml/kg 0.9% normal saline with drop of Tween-80, s.c.) was administered 2 h 20 min before RIPC **(Figure 5)**. Control rats were received vehicle of indomethacin. The experiment was carried out in rats pretreated with indomethacin or its vehicle: one half each group was exposed to RIPC for 40 min, other half each group kept at the same conditions, but without RIPC. Then, all animals were exposed to I/R for 3.5 h and decapitated after completion of I/R.

Collection of Blood Samples and Determination of Plasma Corticosterone Levels

Blood samples were collected from trunk vessels after decapitation. Plasma samples were obtained by blood centrifugation at 3,000 revolutions/min, for 15 min at 4°C. Samples were stored at −20°C until further analysis. The concentration of corticosterone in plasma was determined using commercial ELISA kits (K210R, "HEMA", Russia). Detection level was 5 nmol/L according to the manufacturer.

Statistical Analysis

Data was expressed as mean ± SEM. Data was analyzed with ANOVA module of the MedCalc Version 12.7.0.0. (Statictics for biomedical research, MedCalc Software, Belgium). Statistical significances were tested by one way ANOVA followed by a post hoc Student-Neuman-Keuls. Levene's test was applied before post hoc test for validation of the equality of variances. In case of different variances Kruskal-Wallis test was used. In each case, the required level for significance was considered to be $p < 0.05$.

RESULTS

Effect of Remote Ischemic Preconditioning on Plasma Corticosterone Levels and Gastric Erosion Induced by Ischemia-Reperfusion

I/R significantly ($p < 0.05$) increased plasma corticosterone level as compared to control animals (**Figure 6A**) [H (2; 27) = 13,9263; p = 0.0009]. RIPC did not further influence on I/R-induced corticosterone rise: there were no significant differences in I/R-induced corticosterone levels between the groups subjected to I/R alone (without RIPC) and with preliminary RIPC (**Figure 6A**).

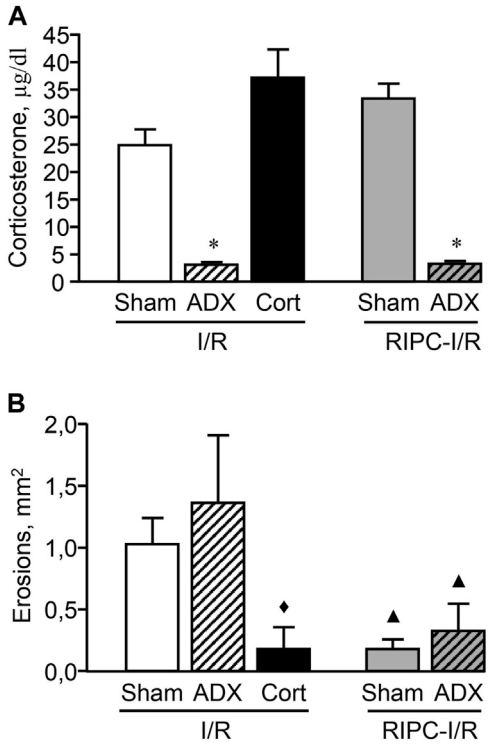

FIGURE 8 | Effect of adrenalectomy and corticosterone replacement on ischemia-reperfusion (I/R)-induced plasma corticosterone levels (**A**) and gastric erosions (**B**) in rats with and without remote ischemic preconditioning (RIPC). Significant differences at $p < 0.05$; * vs sham-operated (Sham) group (A); ▲ vs. corresponding Sham or ADX (adrenalectomy) groups in rats without RIPC; ◆ vs. "ADX + I/R" group (B); Cort–corticosterone replacement; number of rats per group (n): Sham + I/R ($n = 11$); ADX + I/R ($n = 10$); Cort + I/R ($n = 7$); Sham + RIPC-I/R ($n = 8$); ADX + RIPC-I/R ($n = 9$).

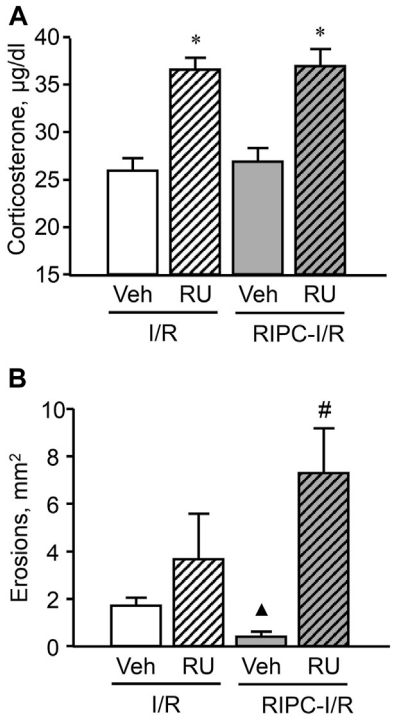

FIGURE 9 | Effect of pretreatment with RU-38486 on ischemia-reperfusion (I/R)-induced plasma corticosterone levels (**A**) and gastric erosions (**B**) in rats with and without remote ischemic preconditioning (RIPC). Significant differences at $p < 0.05$; * vs. vehicle (Veh) group; ▲ vs. "Veh + IR" group; # from all groups; number of rats per group (n): Veh + I/R ($n = 14$); RU + I/R ($n = 12$); Veh + RIPC-I/R ($n = 14$); RU + RIPC-I/R ($n = 12$).

Exposure to I/R for 3.5 h produced gastric erosion in preliminary fasted rats. The hemorrhagic erosion occurred mostly in the corpus mucosa. RIPC significantly ($p < 0.05$) reduced the I/R-induced gastric erosion (gastroprotective effect) [H (2; 27) = 17,5574; $p = 0.0002$] (**Figure 6B**).

There were no gastric erosion in the pre-starved control animals without I/R or/and RIPC (**Figure 6B**).

Effect of Pretreatment With Metyrapone on Gastroprotective Action of Remote Ischemic Preconditioning

In rats pretreated with vehicle of metyrapone (**Figure 7A**) I/R-induced plasma corticosterone levels were as high as corticosterone levels in rats treated with I/R alone (**Figure 6A**). RIPC did not change plasma corticosterone levels in vehicle-treated rats (**Figure 7A**). Metyrapone injected shortly before RIPC caused a decrease ($p < 0.05$) of corticosterone response to I/R (**Figure 7A**) in both rats with and without RIPC [H (3; 58) = 31,1791; $p = 0,0001$].

Metyrapone had no effect on I/R-induced gastric injury by itself. However, it prevented the gastroprotective effect of RIPC. Moreover, further aggravated the deleterious effect of I/R (**Figure 7B**). Indeed, the average area of gastric lesion caused by I/R in metyrapone-pretreated animals with RIPC was significantly greater ($p < 0.05$) than that in the vehicle- and metyrapone-pretreated groups without RIPC [H (3; 58) = 32,7465; $p = 0.0001$].

Effect of Adrenalectomy on Gastroprotective Action of Remote Ischemic Preconditioning

Adrenalectomy performed 1 week before experiment created long-lasting corticosterone deficiency (**Figure 8A**). The adrenalectomized rats subjected I/R alone as well as with preliminary RIPC had lower ($p < 0.05$) plasma corticosterone levels compared to sham-operated animals [H (4; 45) = 33,7527; $p = 0.0001$]. Corticosterone replacement mimicked I/R-induced corticosterone rise in adrenalectomized rats (**Figure 8A**). There were no differences in I/R-induced plasma corticosterone levels in adrenalectomized rats and sham-operated animals after corticosterone replacement.

Adrenalectomy had no effect on I/R-induced gastric injury as well as the gastroprotective effect of RIPC. RIPC attenuated ($p < 0.05$) I/R-induced gastric injury in sham-operated as well as adrenalectomized rats [H (4; 45) = 14,2686; $p = 0.0065$]

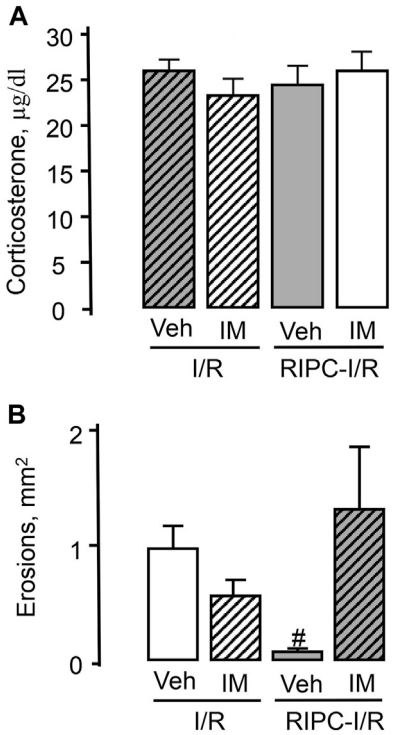

FIGURE 10 | Effect of pretreatment with indomethacin on ischemia-reperfusion (I/R)-induced plasma corticosterone levels **(A)** and gastric erosions **(B)** in rats with and without remote ischemic preconditioning (RIPC). Significant differences at $p < 0.05$; # from all groups; number of rats per group (n): Veh + I/R ($n = 27$); IM + I/R ($n = 24$); Veh + RIPC-I/R ($n = 12$); IM + RIPC-I/R ($n = 13$).

(**Figure 8B**). Nevertheless, corticosterone replacement which mimics the corticosterone rise, similar to RIPS, significantly ($p < 0.05$) reduced erosion areas of gastric mucosa in adrenalectomized rats supporting the role of glucocorticoids in gastroprotection (**Figure 8B**).

Effect of Pretreatment With RU-38486 on Gastroprotective Action of Remote Ischemic Preconditioning

Pretreatment with the antagonist of glucocorticoid receptors RU-38486 potentiated an increase of the I/R-induced corticosterone level in rats with as well as without RIPC [$F(3; 48) = 16{,}7952$; $p = 0.0001$] (**Figure 9A**). The increased plasma corticosterone level in RU-38486-pretreated rats can be considered as an evidence of occupation of glucocorticoid receptors by their antagonist.

RU-38486, which occupied glucocorticoid receptors, had no effect on I/R-induced gastric injury by itself but similar to metyrapone prevented the gastroprotective effect of RIPC and, moreover, further aggravated the deleterious effect of IR (**Figure 9B**). Specifically, the mean area of I/R-induced gastric injury after RIPC was significantly ($p < 0.05$) greater in rats pretreated with RU-38486 than in rats pretreated with RU-38486 vehicle subjected I/R alone or with preliminary RIPC ($H(3; 52) = 22{,}4574$; $p = 0{,}0001$).

Effect of Pretreatment With Indomethacin on the Gastroprotective Action of Remote Ischemic Preconditioning

Pretreatment with indomethacin at the non-ulcerogenic dose (5 mg/kg, s.c.) that suppressed mucosal generation of prostaglandins did not affect I/R-induced plasma corticosterone levels in rats subjected I/R alone or in combination with RIPC (**Figure 10A**).

Indomethacin had no significant effect on I/R-induced gastric injury by itself. However, indomethacin pretreatment prevented the gastroprotective effect of RIPC (**Figure 10B**). Indeed, RIPC reduced ($p < 0.05$) the area of I/R-induced gastric lesion in indomethacin vehicle pretreated rats, whereas in indomethacin-pretreated rats this area did not differ the area of I/R-induced gastric lesion without RIPC and was significantly ($p < 0.05$) greater compared to that in vehicle-treated rats with preliminary RIPC [$H(3; 76) = 15.72$; $p = 0.001$] (**Figure 10B**).

DISCUSSION

The results of the present study show that 3.5 h I/R, which resulted in the gastric erosion formation, markedly increased plasma corticosterone level in rats. RIPC significantly reduced the erosion area in control animals. The gastroprotective effect of RIPC was eliminated by the pretreatment rats with metyrapone, inhibitor glucocorticoid synthesis, as well as with RU-38486, glucocorticoid receptor antagonist. The data suggest that glucocorticoids may be involved in gastroprotective effect of RIPC against I/R-induced gastric injury.

Gastroprotective effect of RIPC demonstrated in our study is consistent with the data of literature (Brzozowski et al., 2004a), but it should be noted that in our study the effect was more pronounced.

A new knowledge revealed in this study is the fact of the involvement of glucocorticoids in the implementation of the gastroprotective effect of RIPC.

It is the first study aimed to verify whether glucocorticoids may participate in realization of protective effect of RIPC against IR-induced gastric injury. It was not assumed before to verify the participation of glucocorticoids in gastroprotective effect of RIPS, apparently due to the prevailing traditional point of view on ulcerogenic action of glucocorticoids released during stress. Nevertheless, our previous findings suggest that glucocorticoids released during acute stress-induced activation of the hypothalamic-pituitary-adrenocortical (HPA) axis are naturally occurring protective factors that play an important role in maintenance of the gastric mucosal integrity (Filaretova et al., 1998; Filaretova et al., 2012; Filaretova 2011; Filaretova and Bagaeva 2016). It was demonstrated that glucocorticoids released during preconditioning mild stress contribute to the protective effect of this stress on gastric mucosa against cold-restraint-induced gastric lesions (Filaretova et al., 2008; Filaretova,

2017). Moreover, we found that glucocorticoids produced in response to various ulcerogenic stimuli such as I/R, indomethacin, aspirin, ethanol, acetic acid also play gastroprotective role (Bobryshev et al., 2009; Filaretova 2011). Gastroprotective effects of glucocorticoids may be mediated by multiple actions, including maintenance of gastric mucosal blood flow, mucus production, and attenuation of enhanced gastric motility and microvascular permeability (Filaretova et al., 2004; Filaretova 2011). In addition, glucocorticoids released during activation of the HPA axis may contribute to protection of the gastric mucosa by maintaining general body homeostasis, including glucose levels and systemic blood pressure, which could be a basis for their beneficial influence on gastric mucosal integrity (Filaretova et al., 2004). Furthermore, glucocorticoids exert a compensatory gastroprotective role in the case of impaired gastroprotective mechanisms provided by PGs, nitric oxide (NO), and capsaicin-sensitive sensory neurons (Filaretova et al., 2007). Taking into consideration beneficial action of glucocorticoids on the gastric mucosa, gastric blood flow particularly, and general body homeostasis (Filaretova et al., 2004) first we supposed that glucocorticoids may contribute to gastroprotective effect of local ischemic preconditioning. The results obtained indeed confirmed that glucocorticoids participate in protective effect of gastric IPC against IR-induced gastric injury (Bobryshev et al., 2009; Filaretova 2017). In the present study we moved further demonstrating a participation of glucocorticoids in gastroprotective effect RIPC too. The present findings are additional strong support of gastroprotective nature of glucocorticoids.

To test the participation of glucocorticoids in RIPC-induced gastroprotection the three approaches were used in the present study.

Adrenalectomy has frequently been used for studying the role of glucocorticoids in gastric erosions, with conflicting results. Adrenalectomy has been used to understand effects of stress-produced glucocorticoids on the gastric mucosa and mechanisms of gastroprotective action of corticotropin-releasing factor (CRF) and results obtained in adrenalectomized rats (in cold-restrained ulcerogenic model) do not support gastroprotective role of glucocorticoids produced in stress as well as participation of glucocorticoids in gastroprotective action of CRF. Nevertheless, using several other approaches for creating glucocorticoid deficiency, not interfering with adrenomedullary catecholamines, we obtained convincing results about gastroprotective role glucocorticoids released during activation of HPA axis (Filaretova et al., 1998; Filaretova et al., 2004; Filaretova et al., 2008; Filaretova, 2011; Filaretova, 2017; Filaretova and Bagaeva, 2016) and their participation in gastroprotective action of CRF (Filaretova et al., 2012).

One reason for the inconsistent effects of adrenalectomy may be the removal of adrenomedullary catecholamines that can provoke acute gastric lesions in experimental animals and we discussed it (see Filaretova et al., 1998). Additionally to a lack of catecholamines, long-lasting glucocorticoid deficiency triggers systemic homeostatic shifts as well as protective processes including an increase in CRF production which may attenuate negative effects of glucocorticoid deficiency (Filaretova et al., 2012).

In the present study glucocorticoid deficiency caused by adrenalectomy led to an exacerbation of inflammation in gastric mucosa, but had no effect on the gastroprotective effect of RIPC. The excessive production of CRF caused by the lack of glucocorticoids within the HPA feedback loop (Uchoa et al., 2014) could be one of the reasons. Additional studies with CRF receptor antagonists are necessary to check this suggestion. Nevertheless, corticosterone replacement which mimics the corticosterone rise, similar to RIPS, significantly reduced erosion areas of gastric mucosa in adrenalectomized rats supporting the role of glucocorticoids in gastroprotection.

Pretreatment with metyrapone, the inhibitor of glucocorticoid synthesis was the most suitable approach because of a short-lasting inhibiting effect of the drug (Mikics et al., 2004). Metyrapone pretreatment allowed us to prevent the acute corticosterone response and avoid the long-lasting effects of glucocorticoid deficiency. Metyrapone injected shortly before RIPC caused a decrease in plasma corticosterone levels and prevented the gastroprotective effect of RIPC and, moreover, further aggravated the deleterious effect of I/R. The results support a participation of corticosterone in a realization of gastroprotective effect of RIPC in rats.

Further support for participation of glucocorticoids in the protective effects of RIPC against I/R-induced gastric injury comes from our experiments with pretreatment by glucocorticoid receptor antagonist RU-38486. Since the RU-38486 is a high affinity antagonist of glucocorticoid receptors and prevents their translocation to the nucleus, it was applied to interrupt genomic signaling pathways of glucocorticoids (Alexandrová, 1994; Bartholomew et al., 1997). A blockade of glucocorticoid receptors increases corticosterone level by activating negative feedback (Filaretova et al., 2002) and we observed this increase in our experiments as a marker of an occupation of glucocorticoid receptors by their antagonist. RIPC-caused gastroprotective effect was not observed in the rats pretreated by RU-38486. RU-38486 similar to metyrapone not only prevented the gastroprotective effect of RIPC but, moreover, further aggravated the deleterious effect of I/R. The results obtained using metyrapone and RU-38486 pretreatments taken together argue for the participation of glucocorticoids in gastroprotective effect of RIPC. It is important to note that in our experimental conditioning we reproduced well known effect of PG deficiency on RIPC-caused gastroprotective effect: indomethacin pretreatment at non-ulcerogenic dose similar to metyrapone or RU-38486 also prevented the gastroprotective effect of RIPC.

In general, the natural gastric mucosal defensive mechanisms that counteract ulcerogenic stimuli are not completely elucidated, however a significant number of factors that participate in realization of these mechanisms were found; there are well known PGs, NO, glucocorticoids, heat shock proteins, trefoil peptides, growth factors, sensory innervation among them (Filaretova et al., 1998; Filaretova et al., 2002; Brzozowski et al., 2004a; Brzozowski et al., 2004b; Kobata et al., 2007; Filaretova, 2011; Gyires et al., 2015; Luetic et al., 2017). Most of these factors are possible participants of local IPC as well as RIPC-caused gastroprotection.

In most cases, I/R arise during trauma or surgery, when a temporary cessation or reduction of blood flow is inevitable. I/R represents a blood circulation recovery in ischemic organ or tissue which exacerbate the injury caused by ischemia by itself (Parks and Granger, 1988). I/R leads to an excessive production of reactive oxygen species and gastrin reducing simultaneously the local microcirculation provoking acute erosions and ulcer in gastric mucosa (Konturek et al., 2004).

Understanding of I/R pathogenesis and gastroprotective mechanisms as well as gastroprotective strategies is critical in the field of vascular surgery and pharmacology. Among such strategies special attention is paid to RIPC. RIPC represents a form of systemic protection against acute I/R injury and may provide non-invasive endogenous therapeutics strategy for protection organs against acute I/R (Kharbanda et al., 2002; Lim and Hausenloy, 2012; Heusch and Gersh, 2016). Although the phenomenon of RIPC has been known for a long time, its mechanisms are still partly unclear. Since glucocorticoid receptors are presented in almost all organs and tissues (Kanemasa et al., 1999), glucocorticoids could provide connection between preconditioned organ and target one. This connection can be provided not only by direct contact but also through the central effects like glucose level, blood pressure and vascular permeability or temperature homeostasis (Filaretova, 2011). Taking into consideration our previous findings demonstrating a compensatory gastroprotective role of glucocorticoids in the case of impaired gastroprotective mechanisms provided by PGs, NO, and capsaicin-sensitive sensory neurons (Filaretova et al., 2007) as well as the data on a participation of PGs, NO, and capsaicin-sensitive sensory neurons in realization of gastroprotective effect of RIPC (Brzozowski et al., 2004a; Brzozowski et al., 2004b) we assume a close interaction between these important gastroprotective factors in an implementation of RIPC-induced gastroprotection.

RIPC can exert the protective action against on I/R-induced injury in gastrointestinal tract through the reduction of inflammation (Zhu et al., 2021). Decrease of intestinal I/R induced damages after RIPC was accompanied by reduced mRNA expression of tumor necrosis factor α (TNF-α) and interleukin-6 (IL-6) (Zhu et al., 2021). Glucocorticoids, as anti-inflammatory drugs, inhibit the expression of multiple inflammatory genes including cytokines and, therefore, these hormones may provide the gastroprotective effect after RIPC through an inhibition of inflammation. A verification of this suggestion is the task for our future study.

Thus, the results of the present study demonstrate for the first time that non-invasive RIPC may protect the gastric mucosa against I/R-induced injury through involvement of glucocorticoids.

DATA AVAILABILITY STATEMENT

The raw data supporting the conclusion of this article will be made available by the authors, without undue reservation.

ETHICS STATEMENT

The animal study was reviewed and approved by the Institutional Animal Care and Use Committee of the Pavlov Institute of Physiology RAS.

AUTHOR CONTRIBUTIONS

LF—conception and design of the study, interpretation of data and manuscript writing; NY—data analysis and manuscript writing; OK—performance of experiments and collection of data; MS—data analysis and generation of figures. All authors listed contributed to the manuscript and approved the submitted version.

FUNDING

The study was supported by grant of Russian Science Foundation (RSF) 19-15-00430.

REFERENCES

Aggarwal, S., Randhawa, P. K., Singh, N., and Jaggi, A. S. (2016). Preconditioning at a Distance: Involvement of Endothelial Vasoactive Substances in Cardioprotection against Ischemia-Reperfusion Injury. *Life Sci.* 151, 250–258. doi:10.1016/j.lfs.2016.03.021

Alexandrová, M. (1994). Stress Induced Tyrosine Aminotransferase Activity via Glucocorticoid Receptor. *Horm. Metab. Res.* 26, 97–99. doi:10.1055/s-2007-1000781

Bartholomew, J. S., Glenville, S., Sarkar, S., Burt, D. J., Stanley, M. A., Ruiz-Cabello, F., et al. (1997). Integration of High-Risk Human Papillomavirus DNA Is Linked to the Down-Regulation of Class I Human Leukocyte Antigens by Steroid Hormones in Cervical Tumor Cells. *Cancer Res.* 57, 937–942.

Bobryshev, P., Bagaeva, T., and Filaretova, L. (2009). Ischemic Preconditioning Attenuates Gastric Ischemia-Reperfusion Injury through Involvement of Glucocorticoids. *J. Physiol. Pharmacol.* 60 (Suppl. 7), 155–160.

Brzozowski, T., Konturek, P. C., Konturek, S. J., Pajdo, R., Kwiecien, S., Pawlik, M., et al. (2004a). Ischemic Preconditioning of Remote Organs Attenuates Gastric Ischemia-Reperfusion Injury through Involvement of Prostaglandins and Sensory Nerves. *Eur. J. Pharmacol.* 499, 201–213. doi:10.1016/j.ejphar.2004.07.072

Brzozowski, T., Konturek, P. C., Pajdo, R., Kwiecień, S., Sliwowski, Z., Drozdowicz, D., et al. (2004b). Importance of Brain-Gut axis in the Gastroprotection Induced by Gastric and Remote Preconditioning. *J. Physiol. Pharmacol.* 55, 165–177. doi:10.1016/j.ejphar.2004.07.072

Fernández, L., Heredia, N., Grande, L., Gómez, G., Rimola, A., Marco, A., et al. (2002). Preconditioning Protects Liver and Lung Damage in Rat Liver Transplantation: Role of Xanthine/xanthine Oxidase. *Hepatology* 36, 562–572. doi:10.1053/jhep.2002.34616

Filaretova, L., Bagaeva, T., and Makara, G. B. (2002). Aggravation of Nonsteroidal Antiinflammatory Drug Gastropathy by Glucocorticoid Deficiency or Blockade of Glucocorticoid Receptors in Rats. *Life Sci.* 71, 2457–2468. doi:10.1016/s0024-3205(02)02078-7

Filaretova, L., Bagaeva, T., and Morozova, O. (2012). Stress and the Stomach: Corticotropin-Releasing Factor May Protect the Gastric Mucosa in Stress through Involvement of Glucocorticoids. *Cell. Mol. Neurobiol.* 32, 829–836. doi:10.1007/s10571-012-9800-z

Filaretova, L., and Bagaeva, T. (2016). The Realization of the Brain-Gut Interactions with Corticotropin-Releasing Factor and Glucocorticoids. *Curr. Neuropharmacol.* 14, 876–881. doi:10.2174/1570159x14666160614094234

Filaretova, L., Bobryshev, P., Bagaeva, T., Podvigina, T., and Takeuchi, K. (2007). Compensatory Gastroprotective Role of Glucocorticoid Hormones during Inhibition of Prostaglandin and Nitric Oxide Production and Desensitization of Capsaicin-Sensitive Sensory Neurons. *Inflammopharmacology* 15, 146–153. doi:10.1007/s10787-007-1589-x

Filaretova, L. (2017). Gastroprotective Effect of Stress Preconditioning: Involvement of Glucocorticoids. *Curr. Pharm. Des.* 23, 3923–3927. doi:10.2174/1381612823666170215145125

Filaretova, L. (2011). Glucocorticoids Are Gastroprotective under Physiologic Conditions. *Ther. Adv. Chronic Dis.* 2, 333–342. doi:10.1177/2040622311412420

Filaretova, L. P., Bagaeva, T. R., Amagase, K., and Takeuchi, K. (2008). Contribution of Glucocorticoids to Protective Influence of Preconditioning Mild Stress against Stress-Induced Gastric Erosions. *Ann. N. Y Acad. Sci.* 1148, 209–212. doi:10.1196/annals.1410.005

Filaretova, L. P., Filaretov, A. A., and Makara, G. B. (1998). Corticosterone Increase Inhibits Stress-Induced Gastric Erosions in Rats. *Am. J. Physiol.* 274, G1024–G1030. doi:10.1152/ajpgi.1998.274.6.G1024

Filaretova, L. P., Podvigina, T. T., Bagaeva, T. R., Tanaka, A., and Takeuchi, K. (2004). Mechanisms Underlying the Gastroprotective Action of Glucocorticoids Released in Response to Ulcerogenic Stress Factors. *Ann. N. Y Acad. Sci.* 1018, 288–292. doi:10.1196/annals.1296.034

Fuller, T. F., Freise, C. E., Feng, S., and Niemann, C. U. (2005). Ischemic Preconditioning Improves Rat Kidney Graft Function after Severe Ischemia/reperfusion Injury. *Transpl. Proc.* 37, 377–378. doi:10.1016/j.transproceed.2004.12.274

Gyires, K., Toth, V. E., and Zadori, Z. S. (2015). Gastric Mucosal protection: from the Periphery to the central Nervous System. *J. Physiol. Pharmacol.* 66, 319–329.

Heusch, G., and Gersh, B. J. (2016). The Pathophysiology of Acute Myocardial Infarction and Strategies of protection beyond Reperfusion: a Continual challenge. *Eur. Heart J.* 38, 774–784. doi:10.1093/eurheartj/ehw224

Kanemasa, H., Ozawa, H., Konishi, H., Ito, T., Nishi, M., Mitsufuji, S., et al. (1999). Distribution of Glucocorticoid Receptor Immunoreactivity in Gastric Mucosa of normal and Adrenalectomized Rats. *Dig. Dis. Sci.* 44, 2081–2087. doi:10.1023/a:1026686705421

Kharbanda, R. K., Mortensen, U. M., White, P. A., Kristiansen, S. B., Schmidt, M. R., Hoschtitzky, J. A., et al. (2002). Transient Limb Ischemia Induces Remote Ischemic Preconditioning *In Vivo*. *Circulation* 106, 2881–2883. doi:10.1161/01.cir.0000043806.51912.9b

Kloner, R. A., and Jennings, R. B. (2001). Consequences of Brief Ischemia: Stunning, Preconditioning, and Their Clinical Implications: Part 1. *Circulation* 104, 2981–2989. doi:10.1161/hc4801.100038

Kloner, R. A., and Yellon, D. (1994). Does Ischemic Preconditioning Occur in Patients? *J. Am. Coll. Cardiol.* 24, 1133–1142. doi:10.1016/0735-1097(94)90880-X

Kobata, A., Kotani, T., Komatsu, Y., Amagase, K., Kato, S., and Takeuchi, K. (2007). Dual Action of Nitric Oxide in the Pathogenesis of Ischemia/reperfusion-Induced Mucosal Injury in Mouse Stomach. *Digestion* 75, 188–197. doi:10.1159/000108590

Konturek, P. C., Brzozowski, T., Burnat, G., Kwiecien, S., Pawlik, T., Hahn, E. G., et al. (2004). Role of Brain-Gut axis in Healing of Gastric Ulcers. *J. Physiol. Pharmacol.* 55, 179–192.

Li, S., Hafeez, A., Noorulla, F., Geng, F., and Takeuchi, K. (2007). Dual Action of Nitric Oxide in the Pathogenesis of Ischemia/reperfusion-Induced Mucosal Injury in Mouse Stomach. *Digestion* 75, 188–197. doi:10.1159/000108590

Lim, S. Y., and Hausenloy, D. J. (2012). Remote Ischemic Conditioning: From Bench to Bedside. *Front. Physiol.* 3, 27. doi:10.3389/fphys.2012.00027

Luetic, K., Sucic, M., Vlainic, J., Halle, Z. B., Strinic, D., Vidovic, T., et al. (2017). Cyclophosphamide Induced Stomach and Duodenal Lesions as a NO-System Disturbance in Rats: L-NAME, L-Arginine, Stable Gastric Pentadecapeptide BPC 157. *Inflammopharmacology* 25, 255–264. doi:10.1007/s10787-017-0330-7

McDonough, A., and Weinstein, J. R. (2020). The Role of Microglia in Ischemic Preconditioning. *Glia* 68, 455–471. doi:10.1002/glia.23695

Mikics, E., Kruk, M. R., and Haller, J. (2004). Genomic and Non-genomic Effects of Glucocorticoids on Aggressive Behavior in Male Rats. *Psychoneuroendocrinology* 29, 618–635. doi:10.1016/S0306-4530(03)00090-8

Murry, C. E., Jennings, R. B., and Reimer, K. A. (1986). Preconditioning with Ischemia: a Delay of Lethal Cell Injury in Ischemic Myocardium. *Circulation* 74, 1124–1136. doi:10.1161/01.cir.74.5.1124

Pajdo, R., Brzozowski, T., Konturek, P. C., Kwiecien, S., Konturek, S. J., Sliwowski, Z., et al. (2001). Ischemic Preconditioning, the Most Effective Gastroprotective Intervention: Involvement of Prostaglandins, Nitric Oxide, Adenosine and Sensory Nerves. *Eur. J. Pharmacol.* 427, 263–276. doi:10.1016/s0014-2999(01)01246-8

Parks, D. A., and Granger, D. N. (1988). Ischemia-reperfusion Injury: A Radical View. *Hepatology* 8, 680–682. doi:10.1002/hep.1840080341

Przyklenk, K., Bauer, B., Ovize, M., Kloner, R. A., and Whittaker, P. (1993). Regional Ischemic 'preconditioning' Protects Remote virgin Myocardium from Subsequent Sustained Coronary Occlusion. *Circulation* 87, 893–899. doi:10.1161/01.cir.87.3.893

Soncul, H., Öz, E., and Kalaycioglu, S. (1999). Role of Ischemic Preconditioning on Ischemia-Reperfusion Injury of the Lung. *Chest* 115, 1672–1677. doi:10.1378/chest.115.6.1672

Souza Filho, M. V., Loiola, R. T., Rocha, E. L., Simão, A. F., Gomes, A. S., Souza, M. H., et al. (2009). Hind Limb Ischemic Preconditioning Induces an Anti-inflammatory Response by Remote Organs in Rats. *Braz. J. Med. Biol. Res.* 42, 921–929. doi:10.1590/s0100-879x2009005000025

Uchoa, E. T., Aguilera, G., Herman, J. P., Fiedler, J. L., Deak, T., and de Sousa, M. B. (2014). Novel Aspects of Glucocorticoid Actions. *J. Neuroendocrinol.* 26, 557–572. doi:10.1111/jne.12157

Uutela, A., Helanterä, I., Lemström, K., Passov, A., Syrjälä, S., Åberg, F., et al. (2020). Randomised Sham-Controlled Double-Blind Trial Evaluating Remote Ischaemic Preconditioning in Solid Organ Transplantation: A Study Protocol for the RIPTRANS Trial. *BMJ Open* 10, e038340. doi:10.1136/bmjopen-2020-038340

Wada, K., Kamisaki, Y., Kitano, M., Kishimoto, Y., Nakamoto, K., and Itoh, T. (1996). A New Gastric Ulcer Model Induced by Ischemia-Reperfusion in the Rat: Role of Leukocytes on Ulceration in Rat Stomach. *Life Sci.* 59, PL295–301. doi:10.1016/0024-3205(96)00500-0

Wang, Z., Ji, Y., Wang, S., Wang, R., Li, Z., Kang, A., et al. (2015). Protective Effect of Intestinal Ischemic Preconditioning on Ischemia Reperfusion-Caused Lung Injury in Rats. *Inflammation* 38, 424–432. doi:10.1007/s10753-014-0047-3

Zhu, H., Li, B., Bindi, E., Lee, C., Alganabi, M., Lok, M. J., et al. (2021). Remote Ischemic Conditioning Avoids the Development of Intestinal Damage after Ischemia Reperfusion by Reducing Intestinal Inflammation and Increasing Intestinal Regeneration. *Pediatr. Surg. Int.* 37, 333–337. doi:10.1007/s00383-020-04831-9

Conflict of Interest: The authors declare that the research was conducted in the absence of any commercial or financial relationships that could be construed as a potential conflict of interest.

Publisher's Note: All claims expressed in this article are solely those of the authors and do not necessarily represent those of their affiliated organizations, or those of the publisher, the editors and the reviewers. Any product that may be evaluated in this article, or claim that may be made by its manufacturer, is not guaranteed or endorsed by the publisher.

frontiers in Pharmacology

ORIGINAL RESEARCH
published: 11 November 2021
doi: 10.3389/fphar.2021.756259

The Protective Effect of *Panax notoginseng* Mixture on Hepatic Ischemia/Reperfusion Injury in Mice *via* Regulating NR3C2, SRC, and GAPDH

Wen Hou[1], *Bao Wei*[2] *and Hong Sheng Liu*[1]*

[1]NHC Key Laboratory of Critical Care Medicine, Tianjin First Central Hospital, Tianjin, China, [2]Department of Surgery, Children's Hospital, Tianjin, China

Panax notoginseng mixture (PNM) has the characteristics of multicomponent, multitarget, and multieffect, which can cope with the multidirectional and multidimensional complex pathological process caused by hepatic ischemia/reperfusion injury (HIRI). Our animal experiments showed that PNM composed of notoginseng, dogwood, and white peony root could significantly reduce the level of aspartate transaminase and alanine aminotransferase in the blood of mice with HIRI, indicating that this preparation had a protective effect on HIRI in mice. Therefore, on this basis, the molecular mechanism of PNM intervention in HIRI was further explored by network pharmacology. First, target genes corresponding to active components and HIRI were obtained through databases such as TCMSP, Pharm Mapper, Swiss Target Prediction, GeneCards, and so on. All target genes were standardized by Uniprot database, and a total of 291 target genes with their intersection were obtained. Then, Kyoto Encyclopedia of Genes and Genomes (KEGG) pathways and biological processes (BPs) of 291 target genes were obtained through the online public platform of DAVID. A total of 177 KEGG pathways and 337 BPs were obtained by setting $p < 0.01$ and false discovery rate <0.05. The network mapping map of components and disease targets was drawn by Cytoscape, and the top 10 Hub target genes related to HIRI were obtained. At the same time, the String database was used to obtain the protein–protein interaction dataset, which was imported into Cytoscape, and the first 10 Hub target genes were obtained. The Hub target genes obtained by the above two methods were molecular docking with their corresponding small molecule compounds through DockThor online tool. The results showed that the docking of paeoniflorin with glyceraldehyde 3-phosphate dehydrogenase (GAPDH), paeoniflorin and loganin with SRC, ginsenoside Rb1 with NR3C2, ursolic acid and oleanolic acid with IL-6, paeoniflorin docking VEGFA, and MMP9. Finally, NR3C2, SRC, and GAPDH were identified as target genes in this study by referring to relevant literature reports. After verification by immunohistochemical experiments, compared with the sham group, the above three target genes were highly expressed in the HIRI group ($p < 0.01$). Compared with the HIRI group, the expression of three target genes in

OPEN ACCESS

Edited by:
Sven Seiwerth,
University of Zagreb, Croatia

Reviewed by:
Xianju Huang,
South-Central University for Nationalities, China
Azna Zuberi,
Northwestern University, United States

***Correspondence:**
Hong Sheng Liu
lhswmg@sina.com

Specialty section:
This article was submitted to Gastrointestinal and Hepatic Pharmacology, a section of the journal Frontiers in Pharmacology

Received: *10 August 2021*
Accepted: *13 October 2021*
Published: *11 November 2021*

Citation:
Hou W, Wei B and Liu HS (2021) The Protective Effect of Panax notoginseng *Mixture on Hepatic Ischemia/Reperfusion Injury in Mice* via *Regulating NR3C2, SRC, and GAPDH. Front. Pharmacol. 12:756259. doi: 10.3389/fphar.2021.756259*

the PNM + HIRI group was significantly decreased ($p < 0.01$). The results showed that PNM could protect mouse HIRI by decreasing the expression of NR3C2, SRC, and GAPDH.

Keywords: mineralocorticoid receptor, glyceraldehyde-3-phosphate dehydrogenase liver, tyrosine-protein kinase, notoginseng mixture, hepatic ischemia/reperfusion injury

INTRODUCTION

Hepatic ischemia/reperfusion injury (HIRI) refers to the process of hepatic cells undergoing different degrees of apoptosis and necrosis during blood reperfusion after the temporary loss of blood supply, which aggravates hepatic function damage. It is commonly seen in the process of hepatic transplantation, hepatic resection, hemorrhagic shock or trauma, and so on (Ito et al., 2019; Zhang et al., 2019). HIRI is a key factor in hepatic failure and death after surgery (Kim and Ha, 2010). Therefore, HIRI has been one of the hot topics that medical researchers have been exploring and solving in recent years. It is very important to find ways to reduce the adverse consequence of HIRI for improving the success rate of hepatic surgery.

HIRI is a common pathophysiological phenomenon in clinical practice, and its pathogenesis remains unknown. There is no good prevention and treatment method (Shinoda et al., 2002). In recent years, intervention methods for HIRI mainly include ischemic preconditioning, drug intervention, monoclonal antibodies, signaling pathway inhibitors, cytokine antagonists, gene knockout and RNA interference, and so on (Peng et al., 2015). At present, the mechanisms of HIRI mainly include oxidative stress, complement activation, inflammatory cell infiltration, release of inflammatory factors, and cell apoptosis (Lee et al., 2014; Liu et al., 2015; Kim et al., 2016). However, most of these research ideas and methods are still in the stage of research and development, and there is still a long way to go before they can be really used in clinical practice to weaken or eliminate the efficacy of HIRI.

Recent studies have shown that monomer components of traditional Chinese medicine as pretreatment drugs play a certain mitigating role in the development of HIRI. Lin reported that ginsenoside Rg1 improved HIRI by inhibiting the mitochondrial apoptosis pathway mediated by cyclophilin D protein (Lin et al., 2020). Jawan et al. reported that magnolol had a protective effect on warm HIRI by upregulation of antiapoptotic Bcl-XL gene and inhibition of Bcl-XS gene (Jawan et al., 2003). Li et al. reported that galangin alleviated HIRI in rats by mediating the PI3K/Akt pathway (Li et al., 2018), Jiang et al. reported that oxymatrine played a protective role on warm HIRI by inhibiting apoptosis (Jiang et al., 2005). Zhang et al. reported that *Atractylodes macrocephala* on polysaccharides inhibited the expression of nuclear factor κB, inhibition of enzyme activity, and reduction of the generation of oxygen free radicals reducing HIRI (Zhang et al., 2010). However, HIRI is a complex pathological process, and its pathogenesis is multifaceted. Therefore, the study on the mechanism of a single component corresponding to a single target cannot completely solve the negative effects of HIRI in liver surgery, that is, the limited drug action model of a single component corresponding to a single target. However, the multicomponent, multitarget, and multieffect characteristics of traditional Chinese medicine exactly correspond to the multidimensional and multidimensional complex pathological process caused by HIRI; thus, this study was conducted.

The concept of network pharmacology was proposed by the British pharmacologist Hopkins (2007), which clarified that the occurrence of diseases is the result of the disruption of the dynamic balance of the interactions of multiple genes, multifunctional proteins, and multipathways in the human body; that is, the molecular basis for the occurrence of diseases is multidimensional. It is suggested that the mechanism of some single chemical drugs acting on a single disease target is not comprehensive enough. Network pharmacology can analyze the characteristics of a single component of a drug acting on different targets, cells, and organs at the molecular and genetic levels and systematically predict and reveal the action and mechanism of a drug, so as to evaluate the efficacy and adverse reactions of a drug and find new drugs with high efficiency and low toxicity. Therefore, this research method has brought great opportunities and hopes for the research and development of traditional Chinese medicine (Wang et al., 2021).

Panax notoginseng mixture (PNM) is based on the advice of senior clinical experts of traditional Chinese medicine and reference to the relevant Chinese medicine pharmacology books. The whole formula consists of notoginseng radix et rhizoma (notoginseng), corni fructus (dogwood), and Paeoniae radix alba (white peony root). Li et al. reported that the TCM syndrome differentiation diagnosis of HIRI was mainly blood stasis syndrome (Li, 2008). Notoginseng is a plant of the Araliaceae family, with the effect of dispersing stasis and relieving pain, reducing swelling, and relieving pain. Since ancient times, its remarkable effect of promoting blood circulation and removing blood stasis has been reputed as "priceless" (Yang et al., 2020). Thus, the effect of notoginseng on promoting blood circulation is very strong. White peony root is derived from the root of herbaceous peony cultivated in Ranunculaceae. It has the functions of nourishing blood, softening liver, and relieving pain. It is the best medicine for the treatment of chest, abdomen, waist, and rib pain in Chinese folks (Wu, 1985). Pharmacological studies have shown that white peony root has immunomodulatory, hepatoprotective, vascular dilatation, anti-inflammatory, and other effects (Wang et al., 1999). Dogwood is derived from the dried and mature pulp of *Cornus officinalis* and has the effect of tonifying the liver and kidney. Modern pharmacology shows that dogwood has functions such as liver protection, antioxidant effects,

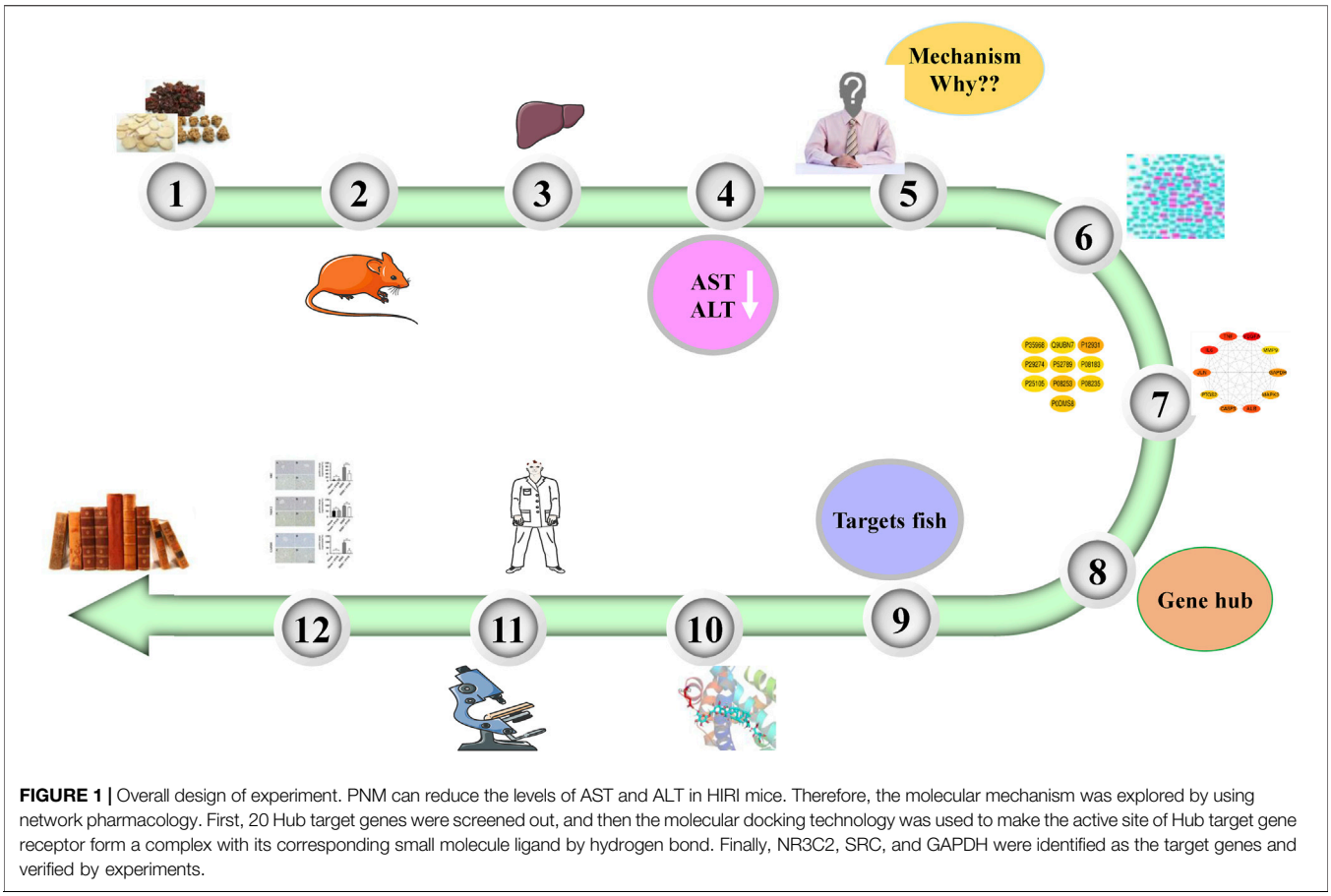

FIGURE 1 | Overall design of experiment. PNM can reduce the levels of AST and ALT in HIRI mice. Therefore, the molecular mechanism was explored by using network pharmacology. First, 20 Hub target genes were screened out, and then the molecular docking technology was used to make the active site of Hub target gene receptor form a complex with its corresponding small molecule ligand by hydrogen bond. Finally, NR3C2, SRC, and GAPDH were identified as the target genes and verified by experiments.

neuroprotection, and myocardial protection (Nan et al., 2018). Therefore, the efficacy of notoginseng and white peony root for promoting blood circulation and removing blood stasis, for softening the liver and relieving pain, and the efficacy of dogwood for tonifying liver and kidney and regulating immunity were combined to observe the efficacy of intervening mouse HIRI by PNM.

The animal experiments showed that PNM could effectively reduce the expressions of aspartate transaminase (AST) and alanine aminotransferase (ALT) in the blood of HIRI mice model group, and there was a significant difference compared with the sham group ($p < 0.01$), indicating that PNM could effectively intervene in the occurrence of HIRI in mice. Therefore, the potential mechanism of PNM alleviating HIRI in mice using bioinformation network pharmacology is described in detail in the following. The overall design of this study is shown in **Figure 1**.

MATERIALS AND METHODS

Animals and Drug Treatment

The animals used in our study were obtained from the Institute of Medical Laboratory Animals, Chinese Academy of Medical Sciences (Beijing, China), license no. SCXK (Beijing) 2014-0004. Male C57BL mice, weighing 19–21 g and aged 5–6 weeks, were raised in a specific pathogen-free environment with air-conditioning at a controlled temperature of 23.5°C ± 1.0°C and a relative humidity of 65 ± 20%. The mice were fed optionally with laboratory chow and water.

PNM (containing loganin 2.502 mg/L and paeoniflorin 6.422 mg/L) was provided by the Key Laboratory of Critical Care Emergency Medicine of the National Health Commission (Tianjin, China). It was administered intragastrically (10 mg/g, raw drug/body weight of mice).

Animal Surgery

Twenty-eight mice were randomly divided into four groups with seven mice in each group, which were sham, sham + PNM, HIRI, and HIRI + PNM, respectively. Among them, sham + PNM and HIRI + PNM were given intragastric administration PNM for 14 days, once a day. The other sham and HIRI were given the same amount of normal saline by intragastric administration. One hour after the last administration of preconditioning, animals were anesthetized by injection intraperitoneally with pentobarbital sodium (40 ng/g). The abdominal cavity is opened in the middle of the upper abdomen, carefully exposing the liver, and the hilar ligament is dissociated. In HIRI and HIRI + PNM groups, the left lobe and middle lobe of the liver were clipped to block blood flow, and the clipping was

loosened 1 h later to restore blood flow. The sham group only dissociated the hilum without blocking the blood flow. Six hours after reperfusion, eyeballs were removed for blood collection, and parts of the liver tissues were separated and stored at −80°C, whereas the remaining liver tissues were stored in formalin.

Blood Biochemical Analyses and Liver Histological Examination

The collected blood was placed at room temperature for 60 min and centrifuged at 3,000 revolutions/min for 20 min. The serum was separated, and AST and ALT in the blood of mice were determined using an automatic clinical biochemical analyzer (Sysmex Chemix-180) from the First Central Hospital of Tianjin, China. Liver specimens for histopathological analysis were obtained 6 h after reperfusion. Samples were fixed in 4% paraformaldehyde buffer solution and then embedded in paraffin. The samples were sliced into 5-μm sections, dewaxed with xylene and ethanol, and stained with hematoxylin and eosin (HE), followed by dehydration. Then the slices were observed with microscope inspection. Histological changes were evaluated in randomly chosen histological fields at 400× magnification.

Collection, Screening, and Target Prediction of Active Components of PNM

In traditional Chinese medicine database and analysis platform system pharmacology TCMSP (http://tcmspw.com./tcmsp.php), refer to the related literature for collecting the chemical component information of notoginseng, dogwood, and white peony root in PNM formula. Oral bioavailability (OB) ≥30% and drug-like drug (DL) ≥0.18 (Zhang M. et al., 2020) were the screening criteria for obtaining small molecule compounds, and applying the PharmMapper (http://lialb-ecust.cn/pharmmapper/) and Swiss Target Prediction (http://www.swisstarget.progress.ch/) database predicts the corresponding target genes. After the elimination of duplication, the target genes were unified in the Uniprot (http://www.uniprot.org/) service platform for correction and transformation and finally represented by Uniprot ID to establish the target database of active ingredients of PNM.

Construction of Active Ingredient-HIRI Target Gene Network

In GeneCards (http://www.genecards.org/) database, "hepatic ischemia reperfusion injury" was used as keywords to predict the target genes associated with HIRI, and correction and transformation were performed in the Uniprot service platform. Finally, it is represented by Uniprot IDs. A total of 291 target genes with the intersection of components and HIRI were collected by using the function of finding duplicates in Excel, and their Uniprot IDs were imported into Cytoscape 3.7.2 software to construct a visual network diagram of active components and target genes of HIRI disease. Then, the first 10 Hub target genes were obtained by using the MCC function of Cytoscape 3.7.2 plug-in cytoHubba.

Protein–Protein Interaction Analysis of Target Gene With Intersection

Gene symbol of 219 target genes with intersection was imported into the String (https://string-db.org/) service platform, and the limited species was *Homo sapiens* to construct a protein–protein interaction (PPI) network. Meanwhile, the PPI dataset was imported into Cytoscape 3.7.2, and the top 10 Hub target genes of PPI were obtained by using the MCC function of cytoHubba plug-in.

Kyoto Encyclopedia of Genes and Genomes Pathway and Biological Processes Analysis

The Kyoto Encyclopedia of Genes and Genomes (KEGG) and biological process (BP) analysis were performed using DAVID (https://david.ncifcrf.gov/) on 291 target genes with the OFFICIAL_GENE SYMBOL as the select identifier, and the species as *H. sapiens*. KEGG and BP enrichment datasets were obtained using $p < 0.01$ and false discovery rate (FDR) <0.05 as screening conditions, and their results were presented by bar plots.

Molecular Docking Analysis

First, the Hub target genes (Hub target genes obtained through MCC and PPI) and their corresponding active components were applied to PDB (http://www.rcsb.org/) and the PubChem database (https://pubchem.ncbi.nlm.nih.gov/) to download the structure of protein and small molecule compounds and use the DockThor (https://dockthor.lncc.br/v2/) online tool for molecular docking. According to the molecular docking results and literature review, three target genes, NR3C2, SRC, and glyceraldehyde 3-phosphate dehydrogenase (GAPDH), were finally selected for experimental verification to reveal the molecular mechanism of PNM intervention in HIRI.

Immunohistochemistry

First, the slices were successively put into xylene, anhydrous ethanol, and distilled water to complete the dewaxing of paraffin slices to water. The tissue sections were then placed in a box filled with citric acid (pH 6.0) solution and put into a microwave oven for antigen repair. The box was heated for 8 min to boil, then held fire for 8 min, and then heated at medium and low heat for 7 min. After natural cooling, the sections were placed in PBS (pH 7.4) and washed by shaking on a decolorizing bed for three times, 5 min each. The slices were then incubated in 3% hydrogen peroxide solution at room temperature and protected from light for 25 min to block endogenous peroxidase. Then, 3% bovine serum albumin was added evenly in the section ring and sealed at room temperature for 30 min. Then, the blocking fluid was gently removed; PBS diluted antibody (NR3C2 [1:500]), SRC (1:500), and GAPDH (1:1,000) were added to the sections, respectively. The sections were placed flat in the wet box and incubated overnight at 4°C. On the second day, the sections were washed with PBS, and the secondary antibody (horseradish peroxidase label) corresponding to the primary antibody was added to cover the tissues in the circle, and the tissues were

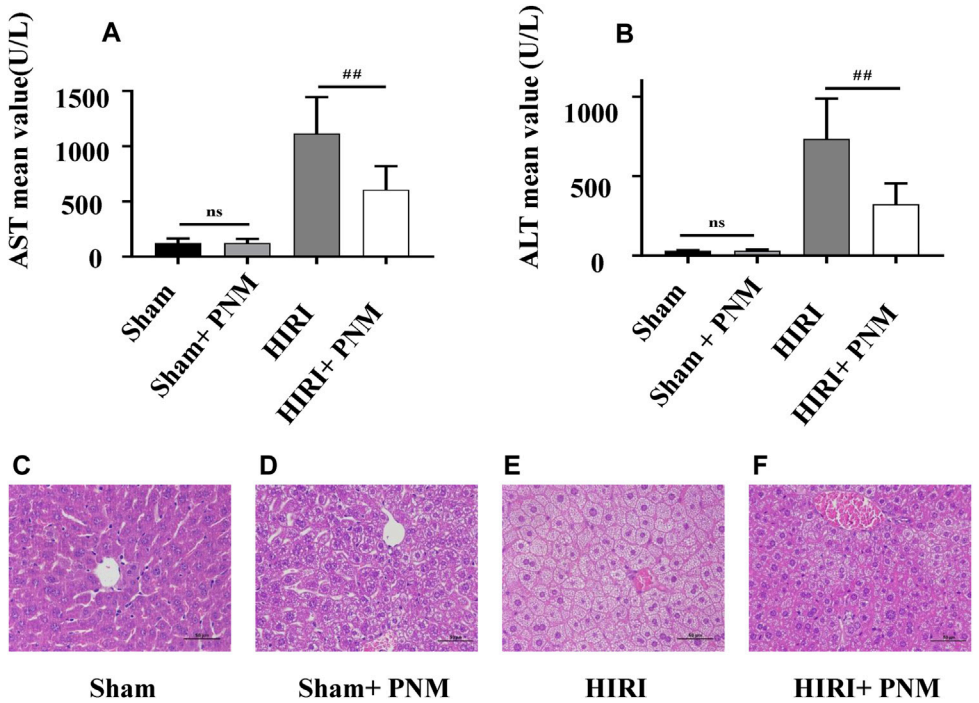

FIGURE 2 | Effects of PNM on AST and ALT in serum of HIRI mice. Figure **(A,B)** shows that the expressions of AST and ALT in serum of mice in the HIRI group were significantly higher than those in the sham group ($p < 0.01$), indicating successful modeling. Compared with the HIRI group, the expressions of AST and ALT in the serum of mice in the HIRI + PNM group were significantly decreased ($^{\#\#}p < 0.01$), indicating that PNM had a protective effect on HIRI in mice. There was no significant difference in serum AST and ALT between the sham and sham + PNM groups ($p > 0.05$), indicating that PNM does not cause damage to healthy mice, which proves the safety of PNM (n = 7). **(C–F)** Results of HE staining experiment. **(C)** The mouse liver tissue was intact. **(D)** Liver tissue was largely intact. **(E)** Liver tissue showed varying degrees of swelling/necrosis, steatosis, inflammatory cell infiltration, and so on. **(F)** The pathological changes of mouse liver tissue were improved, indicating that PNM had a protective effect on HIRI mice. The scale is 50 μm, and the magnification is 400 times.

incubated at room temperature for 50 min. Then, after washing the slices with PBS, the newly prepared DAB chromogenic solution was added into the ring. The chromogenic time was controlled under the microscope, and the positive color was brown-yellow. The chromogenic process was terminated by washing the slices with tap water. Finally, the nuclei were recolored with hematoxylin and sealed by dehydration.

Data Analysis

Immunohistochemical assay was performed to quantitatively analyze the positive staining intensity of 3 sections ($n = 3$) in each group by histochemistry score (H-score) method. One-way analysis of variance and Tukey *post hoc* statistics were used to analyze the differences between groups. $p < 0.05$ was considered statistically significant.

RESULTS

Effects of PNM on AST and ALT in Serum of HIRI Mice

Mice were randomly divided into four groups, with seven mice in each group, which were sham, sham + PNM, HIRI, and HIRI + PNM, respectively. Sham + PNM and HIRI + PNM groups were given intragastric administration PNM for 14 days, once a day, whereas the sham and HIRI groups were given normal saline by intragastric administration for 14 days, once a day. For the HIRI and HIRI + PNM groups, operation was performed for 1-h liver ischemia and 6-h reperfusion, whereas for the sham and sham + PNM group, only the hilum was dissociated without blocking the blood flow. The serum samples of the four groups of animal experiments were detected by automatic clinical biochemical analyzer; compared with the sham group, the serum ALT and AST levels in the HIRI model group were significantly increased ($p < 0.01$), indicating successful modeling. Compared with the HIRI model group, the serum ALT and AST levels in the PNM group were significantly decreased ($p < 0.01$), indicating that PNM had a protective effect on HIRI mice. There was no statistical significance in the changes of ALT and AST in the serum between the sham and sham + PNM groups, indicating that PNM would not cause damage to normal mice, proving the safety of PNM (**Figures 2A,B**). At the same time, HE staining was performed on the liver tissue sections of mice. The results of the four groups showed that, compared with the sham group, the liver tissue of mice in the HIRI group showed swelling/necrosis, steatosis, inflammatory cell infiltration, and so on, at different degrees. Compared with the HIRI group, the pathological changes of liver tissue of mice in the HIRI + PNM group were improved, indicating that PNM had a protective effect on HIRI in mice. The liver tissues of mice in the sham and sham + PNM

TABLE 1 | Basic information of PNM compounds.

Compound code	Compound name	OB/%	DL	Medicine
MOL008457	Tetrahydroalstonine	32.42	0.81	Dogwood
MOL007487	Notoginsenosider1	5.42	0.13	Notoginseng
MOL007488	Notoginsenosider2	7.69	0.28	Notoginseng
MOL007476	Ginsenoside Rb1	6.29	0.04	Notoginseng
MOL007475	Ginsenoside F2	36.43	0.25	Notoginseng
MOL005531	Telocinobufagin	69.99	0.79	Dogwood
MOL005530	Hydroxygenkwanin	36.47	0.27	Dogwood
MOL005503	Cornudentanone	39.6	0.33	Dogwood
MOL005489	3,6-Digalloylglucose	31.42	0.66	Dogwood
MOL005486	3,4-Dehydrolycopen-16-al	46.64	0.49	Dogwood
MOL005481	2,6,10,14,18-Pentaene	33.40	0.24	Dogwood
MOL005360	Malkangunin	57.71	0.63	Dogwood
MOL005344	Ginsenoside rh2	36.32	0.56	Notoginseng
MOL003137	Leucanthoside	32.12	0.78	Dogwood
MOL002883	Ethyl oleate (NF)	32.40	0.19	Dogwood
MOL002879	Diop	43.59	0.39	Dogwood, notoginseng
MOL001933	Oxypaeoniflorin	21.88	0.78	White peony root
MOL001930	Benzoyl paeoniflorin	31.77	0.75	White peony root
MOL001928	Albiflorin_qt	66.64	0.33	White peony root
MOL001927	Albiflorin	12.09	0.77	White peony root
MOL001925	Paeoniflorin_qt	68.18	0.40	White peony root
MOL001924	Paeoniflorin	53.87	0.79	White peony root
MOL001921	Lactiflorin	49.12	0.80	White peony root
MOL001911	Albiflorin R1	21.29	0.82	White peony root
MOL000874	Paeonol	28.74	0.04	White peony root
MOL001792	DFV	32.76	0.18	Notoginseng
MOL001771	Poriferast-5-en-3β-ol	36.91	0.75	Dogwood
MOL001680	Loganin	59.00	0.44	Dogwood
MOL001495	Ethyl linolenate	46.10	0.20	Dogwood
MOL001494	Mandenol	42.00	0.19	Dogwood, notoginseng
MOL000554	Gallicacid-3-O-(6′-O-galloyl)-glucoside	30.25	0.67	Dogwood
MOL000511	Ursolic acid	16.77	0.75	Dogwood
MOL000492	(+)-Catechin	54.8	0.24	White peony root
MOL000449	Stigmasterol	43.8	0.75	Dogwood, notoginseng
MOL000422	Kaempferol	41.88	0.24	White peony root
MOL000359	Sitosterol	36.91	0.75	White peony root
MOL000358	β-Sitosterol	36.90	0.75	White peony root, dogwood, notoginseng
MOL000263	Oleanolic acid	29.02	0.76	White peony root, dogwood
MOL000211	Mairin	55.38	0.24	White peony root
MOL000098	Quercetin	46.43	0.28	Notoginseng
MOL000069	Palmitic acid	19.30	0.10	Dogwood

groups were basically unchanged, indicating that PNM basically did not cause damage to the liver tissues of normal mice (**Figures 2C–F**).

Collection, Screening, and Target Prediction of Active Components of PNM

Through TCMSP database and taking OB ≥30% and DL ≥0.18 as screening conditions, the active ingredients of the three drugs were obtained. Among them, notoginseng has 9 components, dogwood has 20 components, and white peony root has 11 components. In addition, according to literature reports, candidates of active ingredients that were not included in the screening criteria but had important biological activities and pharmacological effects were also incorporated (Chen et al., 2019) including three components of notoginseng, three components of dogwood, and four components of white peony root. After combining the common ingredients, a total of 41 active ingredients were finally obtained (**Table 1**).

The chemical composition structure was uploaded to the Pharm Mapper service platform in MOL2 format for target prediction. The SMILES of chemical composition is uploaded to the Swiss Target Prediction database platform for target prediction. After collecting targets, sorting out, and removing duplicate items, they were represented by Uniprot ID. Finally, a total of 2,677 predicted targets corresponding to the components of three drugs were obtained.

Construction of Active Ingredient–HIRI Target Gene Network and Acquisition of Hub Target

A total of 1,117 target genes were obtained from Genecards database based on the keywords of "hepatic ischemia reperfusion injury" and expressed as Uniprot ID.2677

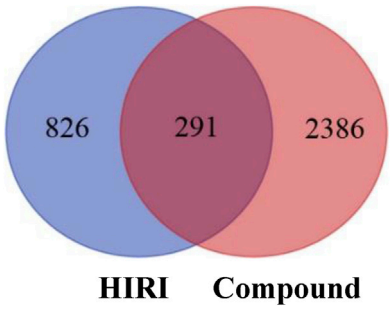

FIGURE 3 | Intersection diagram of components and disease targets. The blue part in the figure represents the number of HIRI target genes obtained, that is, 1,117, and the red part represents the number of constituent target genes obtained, that is, 2,677. There were 291 target genes in the intersection between components and HIRI.

components, and from the predicted target genes in the intersection, 291 intersection target genes were obtained, and the Venn diagram (http://bioinformatics.psb.ugent.be/webtools/Venn/) software was used for its visualization, as shown in (**Figure 3**). The composition–HIRI visual network diagram was drawn by using Cytoscape 3.7.2 software. A pink rectangle represents the composition, a blue oval represents the target gene, and a light blue line represents the intersection line between the component and the target gene (**Figure 4**). Then, the first 10 Hub target genes were obtained by using the MCC function of Cytoscape3.7.2 plug-in cytoHubba. They were P12931 (SRC), P08253 (MMP2), P0DMS8 (ADORA3), P35968 (KDR), P52789 (HK2), P29274 (ADORA2a), P08235 (NR3C2), P25105 (PTAFR), P08183 (ABCB1), and Q9UBN7 (HDAC6), as shown in (**Figure 5**).

Hub Target Genes Were Obtained From the String Database

Two hundred ninety-one intersection target genes were imported into the String database to obtain the PPI dataset, the top 10 Hub target genes of PPI were obtained by Cytoscape. They were P15692 (VEGFA), P05231 (IL-6), P01375 (TNF), P02768 (ALB), P05412 (JUN), P42574 (CASP3), P04406 (GAPDH), P27361 (MAPK3), P35354 (PTGS2), and P14780 (MMP9), respectively, as shown in (**Figure 6**).

Outcome Analysis of KEGG Pathways and Biological Processes

The selection conditions of $p < 0.01$ and FDR <0.05 were set, and 117 KEGG pathways and 337 BP-enriched datasets of 291 target genes with intersection were obtained from DAVID database and were presented by bar plots. KEGG pathways mainly include TNF signaling pathway, HIF-1 signaling pathway, VEGF signaling pathway, PI3K-Akt signaling pathway, and so on (**Figure 7**). BP mainly includes inflammatory response, response to hypoxia,

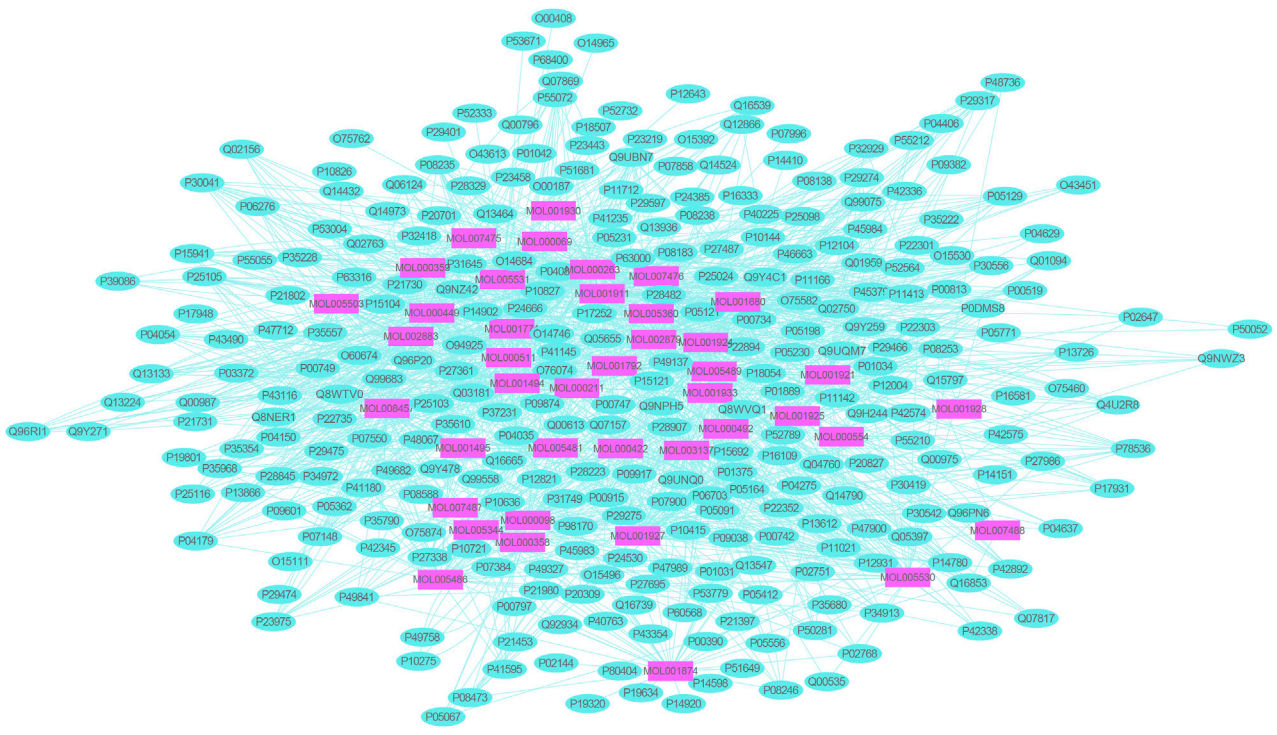

FIGURE 4 | Network diagram of mutual mapping between components and HIRI. In the figure, the pink rectangle represents the component target gene, the blue oval represents the HIRI target gene, and the light blue color line represents the intersection line between the component and the target gene.

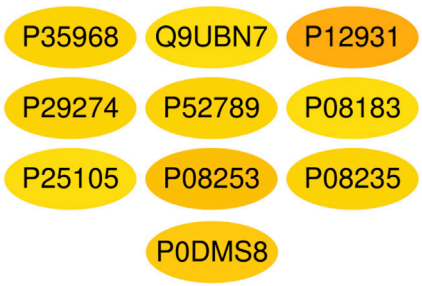

FIGURE 5 | Top 10 Hub target genes of HIRI obtained through the MCC function. The color gradually changes from yellow to red; the closer to the red target gene, the more important it is. They are, respectively, P15692 (VEGFA), P05231 (IL-6), P01375 (TNF), P02768 (Alb), P05412 (Jun), P42574 (Casp3), P04406 (GAPDH), MAPK3 (P27361), P35354 (PTGS2), and MMP9 (P14780).

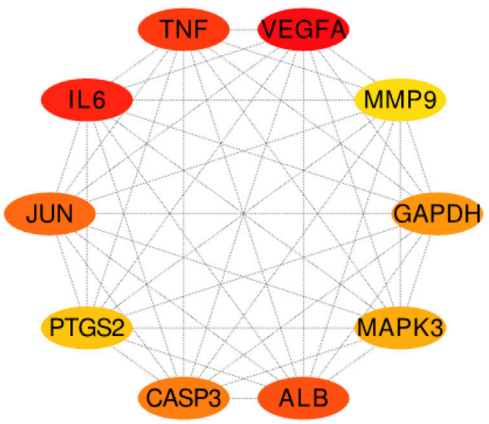

FIGURE 6 | The top 10 Hub target genes of PPI were obtained through MCC function. The color gradually changes from yellow to red; the closer to the red target gene, the more important it is. They are, respectively, P15692 (VEGFA), P05231 (IL-6), P01375 (TNF), P02768 (ALB), P05412 (JUN), P42574 (CASP3), P04406 (GAPDH), MAPK3 (P27361), P35354 (PTGS2), and MMP9 (P14780).

platelet activation, protein phosphorylation, and so on, as shown in (**Figure 8**).

Analysis of Molecular Docking Results

In the first step, Hub target genes obtained through the MCC and PPI were applied to the PDB database to obtain their protein crystal structures and then uploaded to the DockThor online molecular docking tool. The second step is to upload the 3D structure of small molecule compounds downloaded from PubChem database to the DockThor online tool in the form of sdf. The procedure was as follows: After adding H, click "send to DockThor." Step 3: Click the blind docking to identify the active site. In the fourth step, click "dock" for molecular docking. Finally, eight pairs of Hub target genes obtained above were successfully docked with their corresponding small molecule compounds, respectively; loganin and paeoniflorin were docked with SRC, ginsenoside

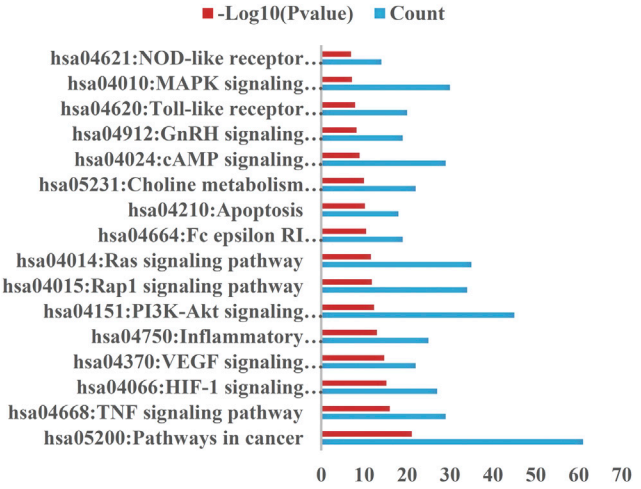

FIGURE 7 | KEGG pathway. Setting the screening conditions of $p < 0.01$ and FDR <0.05, 117 KEGG pathways were obtained from 291 target genes with intersection in DAVID database, and only 16 major pathways are shown in this figure.

Rb1 was docked with NR3C2, paeoniflorin was docked with GAPDH, oleanolic acid and ursolic acid docked with IL-6, paeoniflorin docked with MMP9, and paeoniflorin docked with VEGFA, as shown in (**Table 2**). According to the docking results and literature reports, three target genes, NR3C2, SRC, and GAPDH, were finally selected for experimental verification. Their docking results with their corresponding small molecule compounds are shown in (**Figure 9**).

Analysis of Immunohistochemical Test Results

The sections of sham, sham + PNM, HIRI, and HIRI + PNM groups (n = 3) were immunostained with NR3C2 (1:500), SRC (1:500), and GAPDH (1:1,000), respectively. The positive number and staining intensity in each section were converted into corresponding values by H-score, so as to achieve the semiquantitative purpose of tissue staining. H-score is between 0 and 300, and the greater the value, the stronger the comprehensive positive intensity (Guo et al., 2019; Paschalis et al., 2019). The results showed that the expressions of NR3C2, SRC, and GAPDH were significantly increased in the HIRI group compared with the sham group ($p < 0.001$), indicating that the expression of these three target genes was low in normal liver tissue and high in HIRI. Compared with the HIRI group, the expressions of NR3C2, SRC, and GAPDH in the HIRI + PNM group were significantly decreased ($p < 0.01$), indicating that PNM can protect mouse HIRI through the expression of these three target genes. There were no significant differences in the expressions of NR3C2, SRC, and GAPDH in the sham and sham + PNM groups ($p > 0.05$), indicating that PNM did not cause damage to normal liver tissue of mice, as shown in (**Figure 10**).

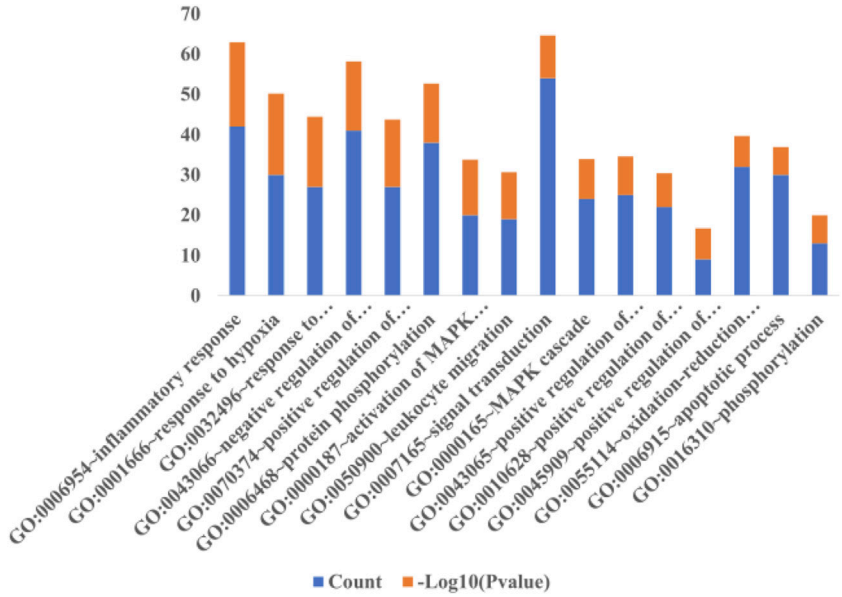

FIGURE 8 | Biological process. When the screening conditions of $p < 0.01$ and FDR <0.05 were set, 337 BP enriched datasets were obtained from 291 intersection target genes in DAVID database, and only 16 major BP results are shown in this figure.

TABLE 2 | Molecular docking information table.

Genes	PDB ID	Compound	Score
VEGFA	5t89	Paeoniflorin	−7.274
SRC	3el8	Loganin	−6.834
SRC	3el8	Paeoniflorin	−7.417
NR3C2	6ggg	Ginsenoside Rb1	−10.776
MMP9	1gkd	Paeoniflorin	−7.321
IL-6	1alu	Oleanolic acid	−7.543
IL-6	1alu	Ursolic acid	−7.715
GAPDH	1ihy	Paeoniflorin	−8.314

DISCUSSION

Partial hepatectomy and liver transplantation are the most effective methods for the treatment of liver malignant tumors and end-stage liver disease. HIRI is a common pathological process during these operations and one of the important causes of perioperative liver failure and death. Therefore, it is of great significance to explore and intervene in the pathogenesis and defense means of HIRI. Notoginseng, dogwood, and white peony root, which make up PNM, are commonly used Chinese medicines in clinical practice, and they are safe and effective. Modern pharmacological studies have shown that these three drugs have regulatory effects as anti-inflammatory, immunomodulatory, antioxidant, anti-tumor, and so on (Liao et al., 2015; Liu et al., 2021; Chen et al., 2021). Previous animal experiments have shown that the HIRI + PNM group can significantly reduce the expressions of AST and ALT in serum of mice in the HIRI group, and AST and ALT are two of the examination indexes reflecting the physiological function of the liver, and the higher their values are, the more serious the damage of the liver cells is (Asbaghi et al., 2021). As PNM can intervene in the occurrence of HIRI by reducing AST and ALT, we continued to use bioinformation network pharmacology to explore the molecular mechanism of PNM's protection of HIRI.

Twenty Hub target genes related to HIRI were obtained by applying many online pharmacological public databases and various analysis software, as shown in **Figures 5**, **6**. DockThor online tool was used to carry out molecular docking of these target gene receptors and their corresponding small molecule conjugated ligands, and the results are shown in **Table 2**. Cao et al. (2017) recently reported that before bone marrow–derived endothelial progenitor cell transplantation, exogenous liposome delivery of VEGF gene may be an effective strategy to reduce orthotopic liver transplantation–induced HIRI. Jiao et al. (2021) reported that VEGF and IL-6 play an important role in the study of the potential of mesenchymal stem cell secretome to promote liver regeneration after hepatic ischemia/reperfusion combined with partial resection. Kato et al. (2014), Huang et al. (2019) reported that inhibition of the expression of MMP9 gene will greatly affect the process of HIRI, indicating that it is a good way to treat or alleviate HIRI research. Therefore, VEGFA, MMP9, and IL-6 have been reported in the studies of liver ischemia/reperfusion injury–related diseases, so the molecular mechanism of these target genes will not be discussed here.

SRC is a nonreceptor tyrosine protein kinase, which is the first proto-oncogene existing in a normal cell state in the body, and plays an important role in maintaining normal physiological functions of the body (Kaplan et al., 1990). The experimental results of this study showed that the expression of immunohistochemical SRC was increased in the HIRI group compared with the sham group ($p < 0.01$). Compared with the HIRI group, the expression of SRC in the PNM + HIRI group was decreased ($p < 0.01$). There was no statistical significance in the expression of SRC in sham and

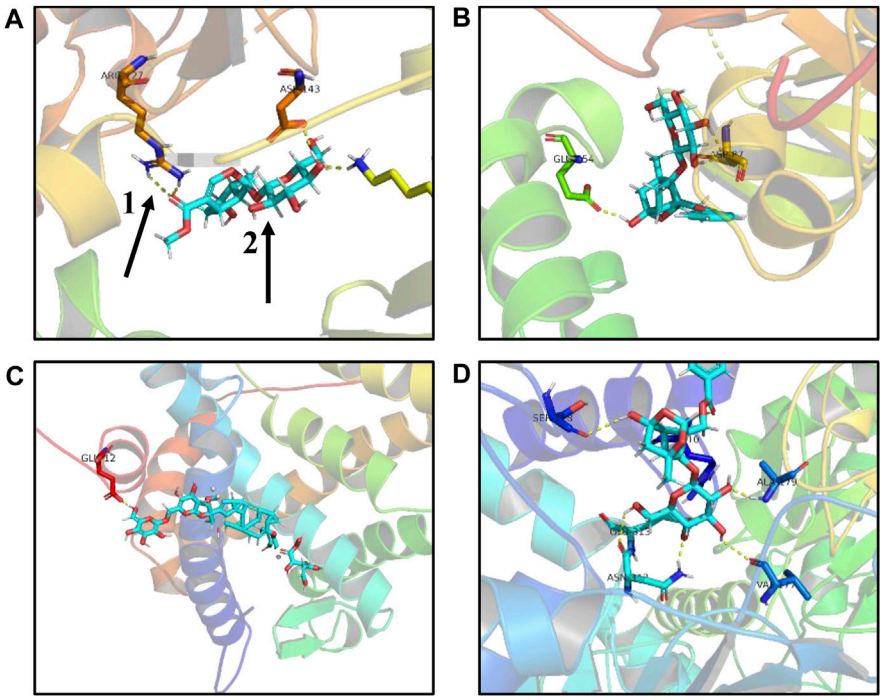

FIGURE9 | Schematic diagram of molecular docking results. **(A)** Loganin is linked to the SRC active site through two hydrogen bonds to form a complex. **(B)** Paeoniflorin is linked to the SRC active site through two hydrogen bonds to form a complex. **(C)** Ginsenoside Rb1 is linked to the NR3C2 active site through one hydrogen bond to form a complex. **(D)** Paeoniflorin is linked to the GAPDH active site through three hydrogen bonds to form a complex, one for hydrogen bond, and two for small compound ligand.

sham + PNM groups ($p > 0.05$). The above experimental results indicate that PNM can reduce the occurrence of HIRI in mice by down-regulating the expression of SRC and the low expression of SRC in normal tissues. This result is consistent with literature reports that SRC is precisely regulated in normal cells and tissues, but is highly expressed in a variety of human tumors, such as lung cancer, colon cancer, nausea and hematologic diseases, and breast cancer (Wang et al., 2021). SRC is a 60-kDa nonreceptor tyrosine kinase family. At present, a total of nine different family members have been found in vertebrate cells. In the SRC kinase family, SRC proto-oncogene is mainly studied, and its changes in the occurrence and development of various diseases are mainly discussed (Wheeler et al., 2009). In this study, the small molecule ligand loganin and paeoniflorin in PNM were connected to the active site of SRC through hydrogen bond to form a complex, thereby inhibiting the activation of SRC to reduce the effect of ischemia/reperfusion injury.

NR3C2 (mineralocorticoid receptor [MR]) is nuclear receptor subfamily 3 group C member 2. It belongs to the adrenocortical receptor family with glucocorticoid receptor. MR is expressed not only in the epithelial tissues of liver and kidney, but also in human and mouse tissues such as large intestine, salivary glands, airway, sweat glands, and inner ear (Viengchareun et al., 2007). Inactivated MR mainly exists in the cytoplasm. Once MR binds to its ligand aldosterone, the MR configuration changes can occur. It can activate the nuclear localization signal, make the activated receptor–ligand complex quickly transfer to the nucleus, participate in the reaction of gene promoter or interact with other transcription factors, and induce the activation or inhibition of transcription and to regulate MR-related signaling pathways and a variety of physiological and pathological responses (Bouarab et al., 2021). Our experimental results showed that compared with the sham group, the expression of MR was increased in the HIRI group ($p < 0.01$). Compared with the HIRI group, the expression of MR in the HIRI + PNM group was significantly decreased ($p < 0.01$). The expression of MR in the sham and sham + PNM groups was not statistically significant ($p > 0.05$), and its expression content was low. The above experimental results indicate that PNM can reduce the occurrence of HIRI in mice by reducing the expression of MR, and the expression of MR is low in normal tissues. Moreover, PNM did not cause damage to normal mouse liver tissue. The expression of MR mRNA in the hypothalamus of Lewis spontaneous kidney-Yang deficiency rats was slightly increased compared with that of normal Wistar rats. Interfering with the Chinese medicine *Cordyceps sinensis* could inhibit the expression of MR mRNA in the hypothalamus of Lewis spontaneous kidney-Yang deficiency rats (Zhang L. et al., 2020). It was found that MR was highly expressed in renal tissues of rats with obstructive nephropathy, and traditional Chinese medicine for invigorating qi and activating blood could reduce the expression of MR in renal tissues by regulating protein kinase-1 (SGK-1) (Chai et al., 2020). These reports are consistent with our findings that inhibiting the expression of MR in tissues can improve the pathophysiological status of the body. In this study, ginsenoside Rb1, a small molecular compound in PNM, was linked to the active site of MR through hydrogen bonds to form a complex, thereby

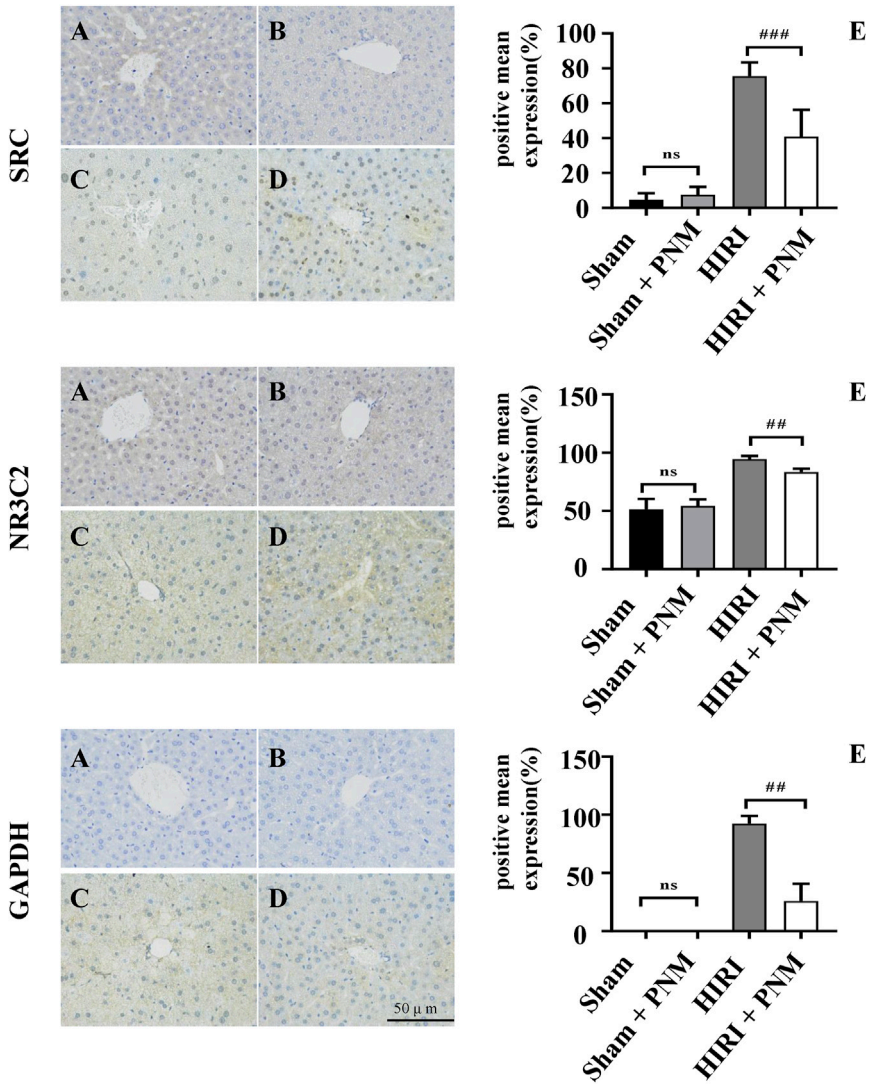

FIGURE 10 | Expression of NR3C2, SRC, and GAPDH in HIRI of mice verified by immunohistochemical assay **(A)** = sham, **(B)** = sham + PNM, **(C)** = HIRI, **(D)** = HIRI + PNM. Diagram scale is 50 μm, magnified 400 times. **(E)** is a bar chart made by analyzing the differences between groups by one-way analysis of variance and Tukey *post hoc* statistical methods according to H-score (n = 3). Bar chart **(E)** shows that the expressions of NR3C2, SRC, and GAPDH were significantly increased in the HIRI group compared with the sham group (##$p < 0.01$). Compared with the HIRI group, the expressions of NR3C2, SRC, and GAPDH in the HIRI + PNM group were significantly decreased (##$p < 0.01$). There was no statistical significance in the expression of the three target genes in the sham and sham + PNM groups ($p > 0.05$). The experimental results showed that PNM protected HIRI in mice by down-regulating the expression of NR3C2, SRC, and GAPDH.

inhibiting the activation of MR to reduce the effect of ischemia/reperfusion injury.

GAPDH is a key enzyme in the glycolytic pathway that catalyzes the conversion of glyceraldehyde 3-phosphate to 1, 3-phosphate glycerate. As a multifunctional enzyme, GAPDH also plays roles in gene expression regulation, DNA repair and replication, neurodegeneration, pathogenic mechanism, regulation of apoptosis and autophagy, and so on (Butera et al., 2019). GAPDH plays an important role in various diseases mainly through aggregation, nuclear translocation, and binding to specific proteins. Our results showed that the expression of GAPDH was increased in the HIRI group compared with the sham group ($p < 0.01$). Compared with the HIRI group, the expression of GAPDH was significantly decreased in the HIRI + PNM group ($p < 0.01$). The expression of GAPDH in the sham and sham + PNM groups was not statistically significant ($p > 0.05$), and its expression content was low. The experimental results indicated that PNM could reduce the occurrence of HIRI in mice by reducing the expression of GAPDH, and the expression of GAPDH was low in normal tissues. The results of this study are consistent with the findings of these scholars on the expression of GAPDH in these diseases. Darusman et al. report that levels of GAPDH were significantly higher in patients with Alzheimer disease neurodegenerative disease than in healthy cynomolgus monkeys (Darusman et al., 2021). Galbiati et al. reported that inhibition of GAPDH expression could be used as a strategy for the development

of drugs against various tumors and parasites (Galbiati et al., 2020). Wang et al. reported that GAPDH was highly expressed in lung adenocarcinoma tissues (Wang et al., 2020). Hao et al. reported that their clinical tissue studies showed that GAPDH protein levels were significantly upregulated in lung squamous cell carcinoma tissues compared with the adjacent normal lung tissues, and this was confirmed by Western blotting and immunohistochemistry. *In vitro*, GAPDH knockdown by siRNA can significantly reduce the proliferation, migration, and invasion of lung squamous cell carcinoma cells (Hao et al., 2020). In this study, paeoniflorin, a small molecular compound in PNM formed a complex with the active site of GAPDH through hydrogen bond, which effectively inhibited the expression of GAPDH in mouse HIRI and alleviated the occurrence of HIRI. However, whether the decrease of GAPDH expression is caused by inhibiting its aggregation, nuclear translocation, or preventing the binding with specific proteins still needs further discussion.

CONCLUSION

In short, HIRI is an urgent clinical problem to be solved, so it is of great clinical significance to carry out relevant research. In this study, small molecular compounds in PNM, such as ginsenoside Rb1, paeoniflorin, and loganin, formed complexes with NR3C2, GAPDH, and SRC, respectively, to reduce the expression of these target genes in HIRI, thus achieving the protection of mouse HIRI. There are many targets associated with the occurrence of HIRI. Our study confirmed that NR3C2, GAPDH, and SRC are also important target genes in the prevention and treatment of HIRI. In the future, we will further explore the molecular mechanism of these target genes against HIRI. Inhibitors through NR3C2, GAPDH, and SRC will be developed by ginsenoside Rb1, paeoniflorin, and loganin, making these three target genes promising target genes to weaken or stop the development of HIRI disease.

DATA AVAILABILITY STATEMENT

The original contributions presented in the study are included in the article/**Supplementary Material**, further inquiries can be directed to the corresponding author.

ETHICS STATEMENT

The animal study was reviewed and approved by Animal Ethics Committee of Nankai University.

AUTHOR CONTRIBUTIONS

WH and HL designed the study. HL conducted network pharmacological data mining and analysis. BW conducted animal and immunohistochemical experiments. HL and WH conducted molecular docking simulation. WH prepared the first draft of the manuscript. HL modified the manuscript. All authors approved the final version of the manuscript.

FUNDING

This work was financially supported by the Health Commission of Tianjin, China (ZC20169).

SUPPLEMENTARY MATERIAL

The Supplementary Material for this article can be found online at: https://www.frontiersin.org/articles/10.3389/fphar.2021.756259/full#supplementary-material

REFERENCES

Asbaghi, O., Kashkooli, S., Mardani, M., Rezaei Kelishadi, M., Fry, H., Kazemi, M., et al. (2021). Effect of green Coffee Bean Extract Supplementation on Liver Function and Inflammatory Biomarkers: A Meta-Analysis of Randomized Clinical Trials. *Complement. Ther. Clin. Pract.* 43, 101349. doi:10.1016/j.ctcp.2021.101349

Bouarab, C., Roullot-Lacarrière, V., Vallée, M., Le Roux, A., Guette, C., Mennesson, M., et al. (2021). PAI-1 Protein Is a Key Molecular Effector in the Transition from normal to PTSD-like Fear Memory. *Mol. Psychiatry*. doi:10.1038/s41380-021-01024-1

Butera, G., Mullappilly, N., Masetto, F., Palmieri, M., Scupoli, M. T., Pacchiana, R., et al. (2019). Regulation of Autophagy by Nuclear GAPDH and its Aggregates in Cancer and Neurodegenerative Disorders. *Int. J. Mol. Sci.* 20 (9), 2062. doi:10.3390/ijms20092062

Cao, D., Wang, M., Gong, J., Wei, S., Gong, J., and Li, J. (2017). Exogenous Vascular Endothelial Growth Factor Delivery Prior to Endothelial Precursor Cell Transplantation in Orthotopic Liver Transplantation-Induced Hepatic Ischemia/reperfusion Injury. *Liver Transpl.* 23 (6), 804–812. doi:10.1002/lt.24745

Chai, Y.-n., Ma, X.-l., Hao, J., Zhang, Y.-x., Zhao, Q.-y., Gao, X.-m., et al. (2020). Inhibition of Mineralocorticoid Receptor Activation by Eplerenone to Reduce Autophagy in Obstructive Nephropathy. *Chin. Pharmacol. Bull.* 36 (2), 256–259. doi:10.3969/j.issn.1001-1978.2020.02.020

Chen, Q., He, X. Y., Zhou, M. J., Liao, G. H., and Cheng, R. B. (2021). Research Progress on Chemical Components, Pharmacological Effects Andclinical Application of Radix Paeoniae Alba[J]. *Clin. Med. Res. Pract.* 6 (11), 187–189.

Chen, W. L., Fan, H. L., Zhao, L., Wen, L. N., Zhu, Y. S., Zhan, Z. D., et al. (2019) Protective Effects of Cornus Officinalis Extract on Hepatic Ischemia-Reperfusion Injury and SIRT1-P53 Pathway in Rats [J]. *Central South Pharmacy*. 17(05), 651–655.

Darusman, H. S., Saepuloh, U., Mariya, S. S., Sajuthi, D., Schapiro, S. J., and Hau, J. (2021). Increased Expression of GAPDH in Cynomolgus Monkeys with Spontaneous Cognitive Decline and Amyloidopathy Reminiscent of an Alzheimer's-type Disease Is Reflected in the Circulation. *Am. J. Primatol* 83 (11), e23296. doi:10.1002/ajp.23296

Galbiati, A., Zana, A., and Conti, P. (2020). Covalent Inhibitors of GAPDH: From Unspecific Warheads to Selective Compounds. *Eur. J. Med. Chem.* 207, 112740. doi:10.1016/j.ejmech.2020.112740

Guo, R., Berry, L. D., Aisner, D. L., Sheren, J., Boyle, T., Bunn, P. A., et al. (2019). MET IHC Is a Poor Screen for MET Amplification or MET Exon 14 Mutations in Lung Adenocarcinomas: Data from a Tri-institutional Cohort of the Lung Cancer Mutation Consortium. *J. Thorac. Oncol.* 14 (9), 1666–1671. doi:10.1016/j.jtho.2019.06.009

Hao, L., Zhou, X., Liu, S., Sun, M., Song, Y., Du, S., et al. (2020). Elevated GAPDH Expression Is Associated with the Proliferation and Invasion of Lung and Esophageal Squamous Cell Carcinomas. *Proteomics* 20 (12), e2070084. doi:10.1002/pmic.202070084

Hopkins, A. L. (2007). Network Pharmacology. *Nat. Biotechnol.* 25 (10), 1110–1111. doi:10.1038/nbt1007-1110

Huang, S., Ju, W., Zhu, Z., Han, M., Sun, C., Tang, Y., et al. (2019). Comprehensive and Combined Omics Analysis Reveals Factors of Ischemia-Reperfusion Injury in Liver Transplantation. *Epigenomics* 11 (5), 527–542. doi:10.2217/epi-2018-0189

Ito, T., Nakamura, K., Kageyama, S., Korayem, I. M., Hirao, H., Kadono, K., et al. (2019). Impact of Rifaximin Therapy on Ischemia/Reperfusion Injury in Liver Transplantation: A Propensity Score-Matched Analysis. *Liver Transpl.* 25 (12), 1778–1789. doi:10.1002/lt.25633

Jawan, B., Goto, S., Pan, T. L., Lai, C. Y., Luk, H. N., Eng, H. L., et al. (2003). The Protective Mechanism of Magnolol, a Chinese Herb Drug, against Warm Ischemia-Reperfusion Injury of Rat Liver. *J. Surg. Res.* 110 (2), 378–382. doi:10.1016/s0022-4804(03)00034-9

Jiang, H., Meng, F., Li, J., and Sun, X. (2005). Anti-apoptosis Effects of Oxymatrine Protect the Liver from Warm Ischemia Reperfusion Injury in Rats. *World J. Surg.* 29 (11), 1397–1401. doi:10.1007/s00268-005-7885-y

Jiao, Z., Ma, Y., Zhang, Q., Wang, Y., Liu, T., Liu, X., et al. (2021). The Adipose-Derived Mesenchymal Stem Cell Secretome Promotes Hepatic Regeneration in Miniature Pigs after Liver Ischaemia-Reperfusion Combined with Partial Resection. *Stem Cel Res Ther* 12 (1), 218. doi:10.1186/s13287-021-02284-y

Kaplan, J. M., Varmus, H. E., and Bishop, J. M. (1990). The SRC Protein Contains Multiple Domains for Specific Attachment to Membranes. *Mol. Cel Biol* 10 (3), 1000–1009. doi:10.1128/mcb.10.3.1000

Kato, H., Kuriyama, N., Duarte, S., Clavien, P. A., Busuttil, R. W., and Coito, A. J. (2014). MMP-9 Deficiency Shelters Endothelial PECAM-1 Expression and Enhances Regeneration of Steatotic Livers after Ischemia and Reperfusion Injury. *J. Hepatol.* 60 (5), 1032–1039. doi:10.1016/j.jhep.2013.12.022

Kim, I. D., and Ha, B. J. (2010). The Effects of Paeoniflorin on LPS-Induced Liver Inflammatory Reactions. *Arch. Pharm. Res.* 33 (6), 959–966. doi:10.1007/s12272-010-0620-8

Kim, J., Oh, C. H., Jeon, J., Baek, Y., Ahn, J., Kim, D. J., et al. (2016). Molecular Phenotyping Small (Asian) versus Large (Western) Plaque Psoriasis Shows Common Activation of IL-17 Pathway Genes but Different Regulatory Gene Sets. *J. Invest. Dermatol.* 136 (1), 161–172. doi:10.1038/jid.2015.378

Lee, H., Ko, E. H., Lai, M., Wei, N., Balroop, J., Kashem, Z., et al. (2014). Delineating the Relationships Among the Formation of Reactive Oxygen Species, Cell Membrane Instability and Innate Autoimmunity in Intestinal Reperfusion Injury. *Mol. Immunol.* 58 (2), 151–159. doi:10.1016/j.molimm.2013.11.012

Li, M. (2008). *Study on the Intervention of HSP70 Expression in Hepatic Ischemia-Reperfusion Injuries of Rats by Traditional Chinese Medicine of Promoting Blood Circulation and Removing Stasis* (Chongqing: Master's Thesis), 19.

Li, Y., Tong, L., Zhang, J., Zhang, Y., and Zhang, F. (2018). Galangin Alleviates Liver Ischemia-Reperfusion Injury in a Rat Model by Mediating the PI3K/AKT Pathway. *Cell Physiol Biochem* 51 (3), 1354–1363. doi:10.1159/000495553

Liao, C. L., Lin, J. H., Lien, J. C., Hsu, S. C., Chueh, F. S., Yu, C. C., et al. (2015). The Crude Extract of Corni Fructus Inhibits the Migration and Invasion of U-2 OS Human Osteosarcoma Cells through the Inhibition of Matrix Metalloproteinase-2/-9 by MAPK Signaling. *Environ. Toxicol.* 30 (1), 53–63. doi:10.1002/tox.21894

Lin, J., Huang, H. F., Yang, S. K., Duan, J., Qu, S. M., Yuan, B., et al. (2020). The Effect of Ginsenoside Rg1 in Hepatic Ischemia Reperfusion (I/R) Injury Ameliorates Ischemia-Reperfusion-Induced Liver Injury by Inhibiting Apoptosis. *Biomed. Pharmacother.* 129, 110398. doi:10.1016/j.biopha.2020.110398

Liu, C., Yang, Y., Sun, D., Wang, C., Wang, H., Jia, S., et al. (2015). Total Saponin from Anemone Flaccida Fr. Schmidt Prevents Bone Destruction in Experimental Rheumatoid Arthritis via Inhibiting Osteoclastogenesis. *Rejuvenation Res.* 18 (6), 528–542. doi:10.1089/rej.2015.1688

Liu, Y. C., Zhang, T. J., Guo, H. B., Xu, B., Lin, J., Zhang, H. B., et al. (2021). Research progress on Notoginseng Radix et Rhizoma and predictive analysis on its Q-Marker [J]. *Chin. Traditional Herbal Drugs* 52 (9), 2733–2743.

Nan, M. J., Tang, K., Zhang, H. W., Cui, C. L., and Deng, C. (2018). Liver Protective Effect of Extracts from Different Parts of Cornus Officinalis on Acute Liver Injury Model Mice [J]. *Chin. Pharm.* 29(17),2385–2389.

Paschalis, A., Sheehan, B., Riisnaes, R., Rodrigues, D. N., Gurel, B., Bertan, C., et al. (2019). Prostate-specific Membrane Antigen Heterogeneity and DNA Repair Defects in Prostate Cancer. *Eur. Urol.* 76 (4), 469–478. doi:10.1016/j.eururo.2019.06.030

Peng, F. Y., and Li, B. (2015). Research Progress on Mechanism of Hepatic Ischemia Reperfusion Injury and Corresponding Protective Measures [J]. *Mod. Med. Health* 12 (3), 1821–1823.

Shinoda, M., Shimazu, M., Wakabayashi, G., Tanabe, M., Hoshino, K., and Kitajima, M. (2002). Tumor Necrosis Factor Suppression and Microcirculatory Disturbance Amelioration in Ischemia/reperfusion Injury of Rat Liver after Ischemic Preconditioning. *J. Gastroenterol. Hepatol.* 17 (11), 1211–1219. doi:10.1046/j.1440-1746.2002.02864.x

Viengchareun, S., Le Menuet, D., Martinerie, L., Munier, M., Lombes, L., and Lombès, M. (2007). The Mineralocorticoid Receptor: Insights into its Molecular and (Patho)physiological Biology. *Nucl. Recept Signal.* 5, e012. doi:10.1621/nrs.05012

Wang, C. H., and Mi, Z. D. (1999). Study on Chemical Constituents and Pharmacology of Paeonia Lactiflora L [J]. *Shizhen Med. Mater. Med. Res.* 7 (10), 544–546.

Wang, Q., Liu, L., Le, Y., and Yan, L. J. (2021). Research Progress of SRC Kinase Inhibitors [J]. *Chin. J. Med. Chem.* 31 (4), 312–319.

Wang, X., Shi, D., Zhao, D., and Hu, D. (2020). Aberrant Methylation and Differential Expression of SLC2A1, TNS4, GAPDH, ATP8A2, and CASZ1 Are Associated with the Prognosis of Lung Adenocarcinoma. *Biomed. Res. Int.* 2020, 1–8. doi:10.1155/2020/1807089

Wang, X., Wang, Z.-Y., Zheng, J.-H., and Li, S. (2021). TCM Network Pharmacology: A New Trend towards Combining Computational, Experimental and Clinical Approaches. *Chin. J. Nat. Medicines* 19 (1), 1–11. doi:10.1016/s1875-5364(21)60001-8

Wheeler, D. L., Iida, M., and Dunn, E. F. (2009). The Role of SRC in Solid Tumors. *Oncologist* 14 (7), 667–678. doi:10.1634/theoncologist.2009-0009

Wu, C. F. (1985). Pharmacological Study of Paeonia Lactiflora and its Chemical Constituents [J]. *Traditional Chin. Med. J.* 10 (6), 43.

Yang, F., Ma, Q., Matsabisa, M. G., Chabalala, H., Braga, F. C., and Tang, M. (2020). Panax Notoginseng for Cerebral Ischemia: A Systematic Review. *Am. J. Chin. Med.* 48 (6), 1331–1351. doi:10.1142/s0192415x20500652

Zhang, L., Lang, J., Jin, L., Jin, L., Cao, B., Shao, X., et al. (2020). Effect of Hirsutella Sinensis Fungus on the Hypothalamic-Pituitary-Adrenal Axis in Lewis Rats with Kidney-Yang Deficiency Syndrome. *Evidence-Based Complement. Altern. Med.* 2020, 1–10. doi:10.1155/2020/5952612

Zhang, M., Yuan, Y., Zhou, W., Qin, Y., Xu, K., Men, J., et al. (2020). Network Pharmacology Analysis of Chaihu Lizhong Tang Treating Non-alcoholic Fatty Liver Disease. *Comput. Biol. Chem.* 86, 107248. doi:10.1016/j.compbiolchem.2020.107248

Zhang, P. J., Jin, C., and Lang, J. (2010). Effect of Atractylodes Macrocephalaon Polysaccharides for Reducing Liver Ischemia/reperfusion Injury in Rats after Orthotopic Liver Autotransplantation. *Zhongguo Zhong Xi Yi Jie He Za Zhi* 30 (11), 1193–1196.

Zhang, T., Gu, J., Guo, J., Chen, K., Li, H., and Wang, J. (2019). Renalase Attenuates Mouse Fatty Liver Ischemia/Reperfusion Injury through Mitigating Oxidative Stress and Mitochondrial Damage via Activating SIRT1. *Oxidative Med. Cell Longevity* 2019, 1–21. doi:10.1155/2019/7534285

Conflict of Interest: The authors declare that the research was conducted in the absence of any commercial or financial relationships that could be construed as a potential conflict of interest.

Publisher's Note: All claims expressed in this article are solely those of the authors and do not necessarily represent those of their affiliated organizations, or those of the publisher, the editors and the reviewers. Any product that may be evaluated in this article, or claim that may be made by its manufacturer, is not guaranteed or endorsed by the publisher.

frontiers in Pharmacology

PERSPECTIVE
published: 12 November 2021
doi: 10.3389/fphar.2021.733526

Advantages of Tailored Isotretinoin Treatment in Moderate to Severe Acne: Real-Life Data

*Nevena Skroza, Ersilia Tolino *, Veronica Balduzzi, Nicoletta Bernardini, Alessandra Mambrin, Anna Marchesiello, Federica Marraffa, Giovanni Rossi, Salvatore Volpe, Ilaria Proietti and Concetta Potenza*

Dermatology Unit "Daniele Innocenzi", "A. Fiorini" Hospital, Terracina, Italy

This retrospective single-center study analyzes the efficacy and safety of isotretinoin for the treatment of moderate to severe acne in real-life clinical practice, particularly with regard to acne severity, isotretinoin cumulative dosage, and patients' gender. The results suggest the opportunity of an early isotretinoin systemic treatment in patients affected by moderate acne and emphasize the importance of an appropriate dose adjustment in order to minimize adverse events.

Keywords: isotretinoin, efficacy, safety, acne severity, gender

OPEN ACCESS

Edited by:
Predrag Sikiric,
University of Zagreb, Croatia

Reviewed by:
Chiara Resnati,
University of Campania Luigi Vanvitelli, Italy
Salma Samir,
Alexandria University, Egypt
Vincenzo Bettoli,
University of Ferrara, Italy

****Correspondence:***
Ersilia Tolino
ersiliatolino@gmail.com

Specialty section:
This article was submitted to Translational Pharmacology, a section of the journal Frontiers in Pharmacology

Received: *30 June 2021*
Accepted: *27 September 2021*
Published: *12 November 2021*

Citation:
Skroza N, Tolino E, Balduzzi V, Bernardini N, Mambrin A, Marchesiello A, Marraffa F, Rossi G, Volpe S, Proietti I and Potenza C (2021) Advantages of Tailored Isotretinoin Treatment in Moderate to Severe Acne: Real-Life Data. Front. Pharmacol. 12:733526. doi: 10.3389/fphar.2021.733526

INTRODUCTION

Isotretinoin (13-cis-retinoic acid, a derivative of vitamin A) was approved by the Food and Drug Administration (FDA) for the systemic treatment of nodulocystic acne in 1982. At first, it was reserved to patients affected by severe nodulocystic or conglobate acne. Nowadays, it is also indicated for patients with moderate acne, resistant to oral antibiotics associated with topical therapy (Cunliffe et al., 1997; Layton, 2010). Isotretinoin is the only therapy acting on four acne principal pathogenic mechanisms: reducing sebaceous glands' dimensions and excretion rate, normalizing infundibular keratinization, decreasing drastically *Cutibacterium acnes* population, and, consequently, inflammation (Nast et al., 2010; Bagatin and Costa, 2020; Landis, 2020).

Moreover, it modulates inflammation working on cellular targets and normalizing innate immune responses mediated by Toll-like receptors, which are hyperactive in acne (Falcon et al., 1986; Coates et al., 1997). In the early phase of therapy, isotretinoin induces apoptosis of sebocytes by activation of tumor suppressor genes, downregulation of genes implicated in lipid metabolism, and upregulation of genes which codify for collagen and fibronectin (Dispenza et al., 2012).

Most common oral isotretinoin adverse events are cheilitis, xerosis, eczema, and blefaroconjuntivitis. They are predictable, dose-dependent, and easily manageable with emollients, lubricants, and moisturizing agents (Nelson et al., 2009; Layton, 2010).

Mild increase of transaminases is also frequent, but reversible, with a fast return to pre-treatment levels following isotretinoin discontinuation (Rademaker, 2013). Other reported adverse events are headache, intracranial hypertension, depression, myalgias, arthralgias, and teratogenicity (Jones et al., 1983; Hull and Demkiw-Bartel, 2000). A transient clinical worsening of acne occurring in 6% of patients has also been reported, during the first month of treatment (Demirci Saadet, 2021).

MATERIALS AND METHODS

The retrospective single-center study was carried on patients affected by moderate or severe acne who had been treated with oral isotretinoin from January 2016 to December 2020. Isotretinoin daily dosages were determined according to body weight, and all cumulative doses at the end of the first treatment cycle were estimated. Therapy was tailored on personal basis, starting with lower doses to the maximum tolerated dosage. The Global Acne Grading System (GAGS) score and Assessment of Quality of Life (AQoL) questionnaire were calculated at baseline and at the end of the first treatment cycle, in order to evaluate overall improvement. Adverse events occurring during the treatment period were registered in order to evaluate tolerability. Primary endpoints of the study were isotretinoin efficacy (estimated as reduction of GAGS score and increase of AQoL value) at the end of the first treatment cycle; isotretinoin efficacy related to its cumulative dose; isotretinoin tolerability; and recurrence rate after the end of the first treatment cycle. The patients were observed from the end of the first cycle until the end of the study. We performed pelvic echography and hormonal profile for all the female subjects; no alterations that could interfere with the treatment were found. Secondary endpoints were comparisons of isotretinoin efficacy and tolerability in male and female patients at the end of the first treatment cycle.

Quantitative parameters were analyzed by calculating the mean, the median, and the standard deviation. Also, pre- and post-treatment absolute variations (delta) of these quantitative parameters were compared. Statistical analyses were made using a software program (MedCalc). The results were analyzed using the chi-squared test, Student's *t*-test, the analysis of variance (ANOVA) test, the Mann–Whitney *U*-test, and the Wilcoxon test. The statistical significance level was 95% ($p < 0.05$).

RESULTS

A total of 140 patients (mean age 22 years, age range 16–52 years) were enrolled; 46% of them were male (65 patients, mean age 20 years, age range 16–33 years), and 54% were female (75 patients, mean age 24 years, age range 17–52 years). At baseline, 88 patients (63%) were affected by moderate papulopustular acne previously resulted resistant to oral antibiotics: 37 of them were female (42%) and 51 were male (58%). Instead, 52 patients (37%) were affected by severe nodulocystic acne: 28 (54%) females and 24 (46%) males. The average duration of first therapy cycle was 5.6 months (23 weeks). The average daily dosage was 0.41 mg/kg (range 0.2–0.6 mg/kg): 0.39 mg/kg in males (range 0.2–0.6 mg/kg) and 0.43 mg/kg in females (range 0.2–0.6 mg/kg). The average cumulative dosage was 75,36 mg/kg: 72.8 mg/kg in males and 78,2 mg/kg in females.

At baseline, the mean GAGS score was 27 (95% CI 26–28) and mean AQoL value was 60 (95% CI 50–60). At the end of the first treatment cycle, the mean GAGS score was 2 (95% CI 2-3) and mean AQoL value was 90 (95% CI 89-90). Thus, the improvement was assessed as a decrease of GAGS score by 93% and increase of AQoL value by 50%. In the severe acne group, the mean delta GAGS score was 30 (95% CI 30-30), while in the moderate acne group, it was 22 (95% CI 20–23) ($p < 0.0001$). In the severe acne group, the mean delta AQoL value was 59 (95% CI 56–63), while in the moderate acne group, it was 66 (95% CI 65-66) ($p < 0.0001$). GAGS score improvement was significantly greater in patients treated with a medium/high to high isotretinoin cumulative dosage (100–120 mg/kg, >120 mg/kg) than in patients treated with a medium/low to low cumulative dosage (80–100 mg/kg, <80 mg/kg). No significant differences in isotretinoin efficacy were observed between males and females. Otherwise, any significant relationship between AQoL value improvement and isotretinoin cumulative dosage was not observed. Finally, no significant differences were observed in acne recurrence between groups treated with medium/high and high isotretinoin cumulative dosages ($p > 0.005$).

During isotretinoin treatment, 16 (11%) patients developed laboratory parameter abnormalities: 7 (44%) males and 9 (56%) females. In particular, 10 (7%) patients developed hypertransaminasemia and 5 (4%) patients developed hypercholesterolemia. All the laboratory abnormalities were of low grade and reverted with isotretinoin discontinuation.

Most of patients (76%, 55 males and 52 females) presented at least one adverse event: 72 (51%) patients (40 males and 32 females) presented only one adverse event, 30 (21%) patients (18 females and 12 males) presented two adverse events, and 5 (4%) patients (2 males and 3 females) presented four adverse events. In the low isotretinoin cumulative dosage group, 60 (77%) patients presented adverse events: 45 (57%) patients presenting only one, 13 (17%) patients two, and 2 (3%) patients three adverse events. In the medium/low isotretinoin cumulative dosage group, 19 (65%) patients presented adverse events: 16 (55%) patients presenting only one and 3 (10%) patients two adverse events. In the medium/high isotretinoin cumulative dosage group, 13 (87%) patients presented adverse events: 8 (53%) patients presenting only one and 5 (34%) patients two adverse events. In the high isotretinoin cumulative dosage group, 15 (83%) patients presented adverse events: 3 (17%) patients presenting only one, 9 (50%) patients two, and 3 (17%) patients three adverse events. The most common adverse events were cheilitis (60 patients: 33 males and 27 females) and xerosis (62 patients: 31 males and 31 females). Other adverse events observed were epistaxis, headache, tachycardia, decrease in visual acuity, chalazion, scalp dermatitis, somnolence, and keratitis.

The demographic and clinical characteristics of the patients are summarized in **Table 1**.

DISCUSSION

This study puts in evidence that oral isotretinoin efficacy, estimated in terms of GAGS score increase, results to be significantly greater in patients affected by severe acne than in patients affected by moderate acne. Nevertheless, advanced quality of life (increase of AQoL value) due to oral isotretinoin treatment was significantly greater in patients affected by moderate acne than in patients affected by severe acne.

TABLE 1 | Cumulative dose.

—	Cumulative dose			
	<80 mg/kg	80–100 mg/kg	100–120 mg/kg	>120 mg/kg
Patients, *n*	78	29	15	18
Age, mean (range)	23 (16–52)	22 (17–31)	20 (18–30)	20 (17–20)
Female, *n* (%)	33 (42)	12 (41)	67 (10)	50% (9)
Male, *n* (%)	45 (58)	17 (59)	5 (33)	9 (50)
GAGS, mean (range)	2 (59–38)	25 (12–33)	31 (26–35)	33 (31–36)
AQoL, mean (range)	60 (14–92)	62 (34–95)	50 (35–70)	45 (35–90)
Laboratory parameter abnormalities, *n* (%)	5 (6)	1 (3)	5 (33)	5 (28)
Hypertransaminasemia, *n* (%)	4 (5)	0	2 (13)	4 (22)
Thrombocytopenia, *n* (%)	1 (1)	0	0	0
Hypercholesterolemia, *n* (%)	0	1 (3)	3 (20)	1 (6)
Adverse effects, *n* (%)	60 (77)	19 (65)	13 (87)	15 (83)
Cheilitis, *n* (%)	33 (42)	10 (34)	5 (33)	10 (56)
Xerosis, *n* (%)	33 (42)	10 (34)	9 (60)	8 (44)
Relapse, *n* (%)	7 (9)	1 (3)	3 (20)	4 (22)

In terms of different doses, no statistically significant differences were observed in GAGS score improvement, AQoL value increase, and acne recurrence rate between patients treated with a medium/high cumulative dosage (100–120 mg/kg) and patients treated with a high cumulative dosage (>120 mg/kg). It confirms that the isotretinoin cumulative dosage lower than that recommended (120 mg/kg) does not determine a higher recurrence probability, as reported by Rademaker (2013).

The sample size was greater in the group of patients receiving low isotretinoin cumulative dosage because this group also encompassed all patients who required dose adjustment because of the development of adverse events. In addition, the results showed how adverse events are dose-dependent: low doses are more tolerable but require longer periods of treatment to obtain the same clinical improvement. A limit of the study can be the small sample size; furthermore, we did not perform a multivariate analysis to calculate the relative impact of demographic and clinical variables.

In summary, our study highlights that, in the era of antibiotic resistance, an early systemic isotretinoin treatment should be taken in consideration in those patients affected not only by severe but also by moderate acne. Furthermore, our data show that there is not any clinical advantage of an isotretinoin cumulative dosage higher than 120 mg/kg, which is conversely associated with an increased risk of adverse events that could result in compliance reduction. In conclusion, given the chronic-relapsing course of acne, it is crucial to adopt a tailored therapeutic approach, taking advantage of dose adjustment in order to gain good clinical outcomes, minimize side effects, and improve patient compliance and adherence (Zomerdijk et al., 2014; Choi et al., 2021; Clark and Cunliffe, 1995).

DATA AVAILABILITY STATEMENT

The raw data supporting the conclusions of this article will be made available by the authors, without undue reservation.

AUTHOR CONTRIBUTIONS

NS, ET, VB, and CP conceptualized the study. NS, ET, VB, AM, FM, GR, and SV wrote the original draft. NS, ET, VB, NB, AM, and IP reviewed and edited the paper. NB, AM, IP, and CP supervised the work. CP was involved in project administration. All authors read and agreed to the published version of the manuscript.

REFERENCES

Bagatin, E., and Costa, C. S. (2020). The Use of Isotretinoin for Acne - an Update on Optimal Dosing, Surveillance, and Adverse Effects. *Expert Rev. Clin. Pharmacol.* 13 (8), 885–897. doi:10.1080/17512433.2020.17966310.1080/17512433.2020.1796637

Choi, E. J., Kim, N., Kwak, H. S., Han, H. J., Chun, K. C., Kim, Y. A., et al. (2021). The Rates of Major Malformations after Gestational Exposure to Isotretinoin: a Systematic Review and Meta-Analysis. *Obstet. Gynecol. Sci.* 64 (4), 364–373. doi:10.5468/ogs.20373

Clark, S. M., and Cunliffe, W. J. (1995). Acne Flare and Isotretinoin - Incidence and Treatment. *Br. J. Dermatol.* 133 (Suppl. 45), 26.

Coates, P., Adams, C. A., Cunliffe, W. J., McGinley, K. T., Eady, E. A., Leyden, J. J., et al. (1997). Does Oral Isotretinoin Prevent Propionibacterium Acnes Resistance. *Dermatology* 195 (Suppl. 1), 4–40. doi:10.1159/000246012

Cunliffe, W. J., Van de Kerkhof, P. C., Caputo, R., Cavicchini, S., Cooper, A., Fyrand, O. L., et al. (1997). Roaccutane Treatment Guidelines: Results of an International Survey. *Dermatology* 194 (4), 351–357. doi:10.1159/000246134

Demirci Saadet, E. (2021). Investigation of Relapse Rate and Factors Affecting Relapse after Oral Isotretinoin Treatment in Patients with Acne Vulgaris. *Dermatol. Ther.*, e15109. doi:10.1111/dth.15109

Dispenza, M. C., Wolpert, E. B., Gilliland, K. L., Dai, J. P., Cong, Z., Nelson, A. M., et al. (2012). Systemic Isotretinoin Therapy Normalizes Exaggerated TLR-2-Mediated Innate Immune Responses in Acne Patients. *J. Invest. Dermatol.* 132 (9), 2198–2205. doi:10.1038/jid.2012.111

Falcon, R. H., Lee, W. L., Shalita, A. R., Suntharalingam, K., and Fikrig, S. M. (1986). *In Vitro* effect of Isotretinoin on Monocyte Chemotaxis. *J. Invest. Dermatol.* 86 (5), 550–552. doi:10.1111/1523-1747.ep12355006

Hull, P. R., and Demkiw-Bartel, C. (2000). Isotretinoin Use in Acne: Prospective Evaluation of Adverse Events. *J. Cutan. Med. Surg.* 4 (2), 66–70. doi:10.1177/120347540000400205

Jones, D. H., King, K., Miller, A. J., and Cunliffe, W. J. (1983). A Dose-Response Study of I3-Cis-Retinoic Acid in Acne Vulgaris. *Br. J. Dermatol.* 108 (3), 333–343. doi:10.1111/j.1365-2133.1983.tb03973.x

Landis, M. N. (2020). Optimizing Isotretinoin Treatment of Acne: Update on Current Recommendations for Monitoring, Dosing, Safety, Adverse Effects, Compliance, and Outcomes. *Am. J. Clin. Dermatol.* 21 (3), 411–419. doi:10.1007/s40257-020-00508-0

Layton, A. M. (2010). "Disorders of Sebaceous Glands". In: T. Burns, S. Breathnach, N. Cox, and C. Griffiths, editors *Rook's Textbook of Dermatology*. 8th Edition, Vol. 2. Oxford: Blackwell Publishing, 38–66.

Nast, A., Bayerl, C., Borelli, C., Degitz, K., Dirschka, T., Erdmann, R., et al. (2010). S2k-guideline for Therapy of Acne. *J. Dtsch Dermatol. Ges* 8 Suppl 2 (9813), s1–59. doi:10.1111/j.1610-0387.2010.07466.x

Nelson, A. M., Zhao, W., Gilliland, K. L., Zaenglein, A. L., Liu, W., and Thiboutot, D. M. (2009). Temporal Changes in Gene Expression in the Skin of Patients Treated with Isotretinoin Provide Insight into its Mechanism of Action. *Dermatoendocrinol* 1 (3), 177–187. doi:10.4161/derm.1.3.8258

Rademaker, M. (2013). Isotretinoin: Dose, Duration and Relapse. What Does 30 Years of Usage Tell Us. *Australas. J. Dermatol.* 54 (3), 157–162. doi:10.1111/j.1440-0960.2012.00947.x

Zomerdijk, I. M., Ruiter, R., Houweling, L. M., Herings, R. M., Sturkenboom, M. C., Straus, S. M., et al. (2014). Isotretinoin Exposure during Pregnancy: a Population-Based Study in The Netherlands. *BMJ Open* 4 (11), e005602. doi:10.1136/bmjopen-2014-005602

Conflict of Interest: The authors declare that the research was conducted in the absence of any commercial or financial relationships that could be construed as a potential conflict of interest.

Publisher's Note: All claims expressed in this article are solely those of the authors and do not necessarily represent those of their affiliated organizations, or those of the publisher, the editors, and the reviewers. Any product that may be evaluated in this article, or claim that may be made by its manufacturer, is not guaranteed or endorsed by the publisher.

frontiers in Pharmacology

ORIGINAL RESEARCH
published: 17 November 2021
doi: 10.3389/fphar.2021.682614

Claudins: Beyond Tight Junctions in Human IBD and Murine Models

Snježana Čužić[1], Maja Antolić[1], Anja Ognjenović[1], Darija Stupin-Polančec[1], Adriana Petrinić Grba[1], Boška Hrvačić[1], Miroslava Dominis Kramarić[1], Sanja Musladin[1], Lidija Požgaj[1], Ivo Zlatar[1], Denis Polančec[1], Gorana Aralica[2,3], Marko Banić[2,4,5], Marija Urek[2,3], Brankica Mijandrušić Sinčić[5,6], Aleksandar Čubranić[5,6], Ines Glojnarić[1], Martina Bosnar[1] and Vesna Eraković Haber[1,5]**

[1]Fidelta, Zagreb, Croatia, [2]School of Medicine, University Zagreb, Zagreb, Croatia, [3]Department of Pathology Clinical Hospital Dubrava, Zagreb, Croatia, [4]Department of Internal Medicine Clinical Hospital Dubrava, Zagreb, Croatia, [5]Faculty of Medicine, University of Rijeka, Rijeka, Croatia, [6]Department of Internal Medicine, Clinical Hospital Center Rijeka, Rijeka, Croatia

Claudins are transmembrane proteins constituting one of three tight junction protein families. In patients with inflammatory bowel disease (IBD), disease activity–dependent changes in expression of certain claudins have been noted, thus making certain claudin family members potential therapy targets. A study was undertaken with the aim of exploring expression of claudins in human disease and two different animal models of IBD: dextrane sulfate sodium–induced colitis and adoptive transfer model of colitis. The expression of sealing claudin-1, claudin-3, claudin-4, and claudin-8, and pore-forming claudin-2 in humans and rodents has been evaluated by immunohistochemistry and quantitative polymerase chain reaction. Claudins were expressed by epithelial and cells of mesodermal origin and were found to be situated at the membrane, within the cytoplasm, or within the nuclei. Claudin expression by human mononuclear cells isolated from lamina propria has been confirmed by Western blot and flow cytometry. The claudin expression pattern in uninflamed and inflamed colon varied between species and murine strains. In IBD and both animal models, diverse alterations in claudin expression by epithelial and inflammatory cells were recorded. Tissue mRNA levels for each studied claudin reflected changes within cell lineage and, at the same time, mirrored the ratio between various cell types. Based on the results of the study, it can be concluded that 1) claudins are not expressed exclusively by epithelial cells, but by certain types of cells of mesodermal origin as well; 2) changes in the claudin mRNA level should be interpreted in the context of overall tissue alterations; and 3) both IBD animal models that were analyzed can be used for investigating claudins as a therapy target, respecting their similarities and differences highlighted in this study.

Keywords: claudins, inflammatory bowel disease, dextran sodium sulfate colitis model, adoptive transfer colitis model, ulcerative colitis, Crohn's disease

OPEN ACCESS

Edited by:
Thomas Brzozowski, Jagiellonian University Medical College, Poland

Reviewed by:
Antonella Fazio, University Medical Center Hamburg-Eppendorf, Germany
Gabor Varga, Semmelweis University, Hungary
George Grant, University of Aberdeen, United Kingdom
Irina Leonardi, Cornell University, United States
Carol Aherne, University College Dublin, Ireland
Gabriela Fonseca-Camarillo, Instituto Nacional De Ciencias Médicas y Nutrición Salvador Zubirán (INCMNSZ), Mexico

***Correspondence:**
Snježana Čužić
snjezana.cuzic@fidelta.eu
Vesna Eraković Haber
vesna.erakovichaber@fidelta.eu

Specialty section:
This article was submitted to Gastrointestinal and Hepatic Pharmacology, a section of the journal Frontiers in Pharmacology

Received: *18 March 2021*
Accepted: *11 October 2021*
Published: *17 November 2021*

Citation:
Čužić S, Antolić M, Ognjenović A, Stupin-Polančec D, Petrinić Grba A, Hrvačić B, Dominis Kramarić M, Musladin S, Požgaj L, Zlatar I, Polančec D, Aralica G, Banić M, Urek M, Mijandrušić Sinčić B, Čubranić A, Glojnarić I, Bosnar M and Eraković Haber V (2021) Claudins: Beyond Tight Junctions in Human IBD and Murine Models. Front. Pharmacol. 12:682614. doi: 10.3389/fphar.2021.682614

INTRODUCTION

Tight junctions (TJs), together with adherens junctions and gap junctions, constitute the intestinal epithelial barrier that regulates paracellular permeability (Lee et al., 2018). Apart from building up TJs, TJ proteins are involved in regulation of other cell functions, such as maintenance of cell polarity, proliferation, and differentiation (Farkas et al., 2012).

Inflammatory bowel disease (IBD), which comprises Crohn disease (CD) and ulcerative colitis (UC), is characterized by damage of the intestinal epithelium and prolonged chronic inflammation. Altered TJ function and TJ-protein expression in IBD have attracted the attention of the scientific community due to increased permeability of the intestinal epithelial barrier being one of the hallmarks of IBD, presenting even before onset of overt inflammation in CD patients (Chelakkot et al., 2018; Keita et al., 2018).

As rising incidence of IBD (Ng et al., 2017) has kindled significant drug discovery research efforts aimed at controlling IBD clinical manifestations, animal models of IBD play an important role in the testing cascade of new therapeutics. The aim of this study was to evaluate the potential use of animal models of intestinal inflammation in studying expression of claudins and constitutive TJ proteins, relevant for IBD in humans. Colon expression of sealing claudin-1, claudin-3, claudin-4, and claudin-8 and pore-forming claudin-2 in IBD patients, IBD models, and their nondiseased controls was examined.

Animal models of two different pathophysiology were chosen for the study. The first model was dextrane sulfate sodium (DSS)–induced colitis caused by epithelial barrier disruption, leading to antigen leakage and finally inflammation (Pickert et al., 2009). The second model was adoptive transfer colitis induced by transfer of $CD4^+CD25^-CD62L^+$ T lymphocytes into immunodeficient mice causing T_H17-mediated mucosal inflammation and reactive epithelial proliferation (Mars et al., 2009; Brockman et al., 2017; Kempski et al., 2017).

MATERIALS AND METHODS

Patients

Formalin-fixed paraffin-embedded (FFPE) colon samples were obtained from IBD patients who underwent small intestine/colon resection due to the severity of disease. There were eight patients with CD (four female and four male patients, 27–84 years of age [average age, 45 years]) and five patients with UC (four female and one male patients, 18–51 years of age [average age, 38 years]). Control FFPE colon samples were obtained from patients undergoing colon resection due to carcinoma (eight non-IBD control subjects: one female and seven male control subjects, 50–90 years of age [average age, 72 years]). Disease activity in IBD patients was evaluated using a published histologic score method (Naini and Cortina, 2012), excluding neuroendocrine hyperplasia (**Supplementary Table S1A**). Human tissue specimens used for lamina propria mononuclear cell (LPMC) isolation for Western blot and flow cytometry analysis included surgical colon resections and mucosal biopsies from 5 UC patients (four female and one male patients, 39–77 years of age [average age, 53 years]) and two CD patients (male, aged 35 and 67 years).

Animal Models

Two DSS experiments were included into the study. Ten C57Bl6N male mice (Charles River, Italy) were exposed to 3% DSS (MP Biomedicals, 38–50 kDa) in drinking water every working day for 3 weeks (5 days a week DSS and 2 days without DSS). Nine control animals were drinking only water. At the beginning of the studies, mice were 7–8 weeks old and weighed 19–22 g (median, 21 g). Disease activity in the DSS model was evaluated using a histologic score method published by Nishitani et al. (2009) (**Supplementary Table S1B**).

Three adoptive transfer experiments have been performed. An adoptive transfer model of chronic colitis was induced in C.B-17 female SCID mice (Charles River, France). At the beginning of the experiments, mice were 7–10 weeks old and weighed 15–21 g (median, 18 g). Purified $CD4^+CD25^-CD62L^+$ T cells were isolated from spleen cells of female BALB/c mice (Charles River) using "CD4+CD25$^-$CD62L$^+$ T Cell Isolation Kit II, mouse" (Miltenyi Biotec) according to manufacturer instructions. Purified $CD4^+CD25^-CD62L^+$ cells (>95% pure and >90% viable) were resuspended in sterile phosphate-buffered saline (PBS) (5×106 cells/mL) and transferred into SCID mice intraperitoneally (i.p.). Mice with more than 5% of $CD4^+$ T cells within total blood leukocytes at day 14 (D14) after transfer were included in the study. Twenty control SCID naive animals and 35 diseased animals were sacrificed at 4, 6, and 8 weeks after transfer. Disease activity in the adoptive transfer model was evaluated using a histologic score method published by Laroux et al. (2004) (**Supplementary Table S1C**).

Immunohistochemistry

Immunohistochemistry (IHC) was performed on FFPE tissue using the following primary antibodies: claudin-1 (Abcam, ab56417, 1:250), claudin-2 (Abcam, ab125293, 1:75), claudin-3 (GeneTex, GTX15102, 1:50), claudin-4 (Abcam, ab53156, 1:1,000), and claudin-8 (Abcam, ab183738, 1:1,000) followed by DAKO EnVision Detection System Kit or R&D System Kit (**Supplementary Figure S1**). Whole slide for each human sample/animal sample was evaluated. Human samples were at least 1 cm long. Animal samples represented the whole colon. Colon was sampled as proximal and distal parts; each part was cut into three to four pieces; whole material was embedded. On one slide, there have been three to four transversal cuts from proximal colon and three to four cuts from the distal colon.

Quantitative Polymerase Chain Reaction

Total RNA was isolated from the FFPE blocks with the use of RNeasy FFPE Kit, as recommended by manufacturer (Qiagen). First-strand cDNA was obtained by reverse transcription using a commercial SuperScript III First-Strand Synthesis System according to the manufacturer's protocol (Invitrogen) and random hexamers as primers.

Quantitative real-time polymerase chain reaction (qRT-PCR) for detection of claudin-1, claudin-2, claudin-3, claudin-4, and claudin-8 mRNA expression was performed on an Applied Biosystems 7300 Real-Time PCR system using the TaqMan method and glycerin-aldehyde-3-phosphate (GAPDH) as a housekeeping gene. Only expression of human claudin-3 expression was measured using SyberGreen technology. Primers and probes (**Table 1**) were designed in Primer Express software version 3.0 and used at validated concentrations. All primers and TaqMan probes were used at a final concentration of 100 nM qRT-PCR was performed in a

TABLE 1 | Sequences of primers and probes used for qPCR.

Human		
Gene		Sequence
GAPDH	F	ACCCACTCCTCCACCTTTGAC
	R	CATACCAGGAAATGAGCTTGACAA
	P	CTGGCATTGCCCTCAACGACCA
Claudin-1	F	ACGAATTTGGTCAGGCTCTCT T
	R	AAGTAGGGCACCTCCCAGAAG
	P	ACTGGCTGGGCTGCTGCTTCTCTC T
Claudin-2	F	TCTGTGGTGGGCATGAGATG
	R	TGCTACCGCCACTCTGTC TTT
	P	ACAGTCTTCTGCCAGGAATCCCGAGC
Claudin-3	F	AGCGAGTCGTACACCTTGCA
	R	CATCATCACGTCGCAGAACAT
	P	—
Claudin-4	F	GGCTGCTTTGCTGCAACTG
	R	CAGAGCGGGCAGCAGAATA
	P	CCACCCCGCACAGACAAGCCTTACT
Claudin-8	F	TGCAACGAAAAGAGCAGTAGCT
	R	TTCCGGTGTGATAACTTTTTTGG
	P	CAGATACTCGATACCTTCCCATCGCACAA
Mouse		
Gene		Sequence
GAPDH	F	TGTGTCCGTCGTGGATCTGA
	R	CCTGCTTCACCACCTTCTTGA
	P	CCGCCTGGAGAAACCTGCCAAGTATG
Claudin-1	F	ATCTACGAGGGACTGTGGATGTC
	R	AGCAAGGAGTCGAAGACTTTGC
	P	CGTTTCGCAAAGCACCGGGC
Claudin-2	F	GCCCCAGGGCAATCGT
	R	GGAGAGCTCCTAGTGGCAAGAG
	P	CCAACTACTATGATGGCTACCAGGCCCAG
Claudin-3	F	GCGCCTTGCTGTGTTGCT
	R	AGAGGATCTTGGTGGGTGCAT
	P	CTGCCCACCGCGCGACAAG
Claudin-4	F	CGTGGCAAGCATGCTGATTA
	R	GTCGCGGATGACGTTGTG
	P	TGCCCGTGTCCTGGACCGC
Claudin-8	F	GGGACGATGAGAACGTGAAGA
	R	CCAAGCCGGTGATGAAGAA
	P	CGCATCTTGCTGACAGCCGGAAT

F, forward; P, TaqMan probe; R, reverse.

30 µL final volume containing 1× Applied Biosystems TaqMan PCR Master Mix or 1× Applied Biosystems SYBR Green PCR Master Mix, 100 nM primers and probes, and 1 µL of cDNA. Amplification was performed using the following cycling conditions: 2 min at 50°C, 10 min at 95°C, and 45 two-step cycles of 15 s at 95°C and 60 s at 60°C. Triplicate qRT-PCR analyses were executed for each sample, and the obtained threshold cycle (CT/Ct) values were averaged. The relative level of tested genes mRNA was then normalized to the GAPDH CT value to give the ΔCT value for each sample.

Isolation of Lamina Propria Mononuclear Cells From Human Colonic Mucosa, Western Blot Analysis, and Flow Cytometry

Isolation of LPMCs was performed using a lamina propria dissociation kit (Miltenyi Biotec, 130-097-410) following the manufacturer's instructions. Briefly, the method consisted of epithelial cell removal by incubation of tissue in a solution containing 1 mM DTT and 5 mM EDTA, followed by enzymatic digestion (enzymes included in the kit) and mechanical dissociation using a gentle MACS dissociator (Miltenyi Biotec, 130-093-235). In case of resection specimens, from which higher cell yield was obtained, mononuclear cells were further purified by Lymphoprep density gradient centrifugation. Isolated cells were cryopreserved in medium containing 70% fetal bovine serum (FBS), 20% RPMI 1640, and 10% dimethyl sulfoxide, following the protocol described previously for PBMCs (Kreher et al., 2003).

For Western blot analysis, LPMCs were lysed in PBS with 1% Triton-X (Sigma, T9284), phosphatase inhibitor (Roche, 04906837001), and protease inhibitor (Roche, 04693124001). Protein concentration in lysates was determined using Pierce BCA Protein Assay Kit (23,225; Thermo Fisher Scientific, Waltham, MA, USA) and adjusted to 0.5 mg/mL. Claudin-1, claudin-2, and claudin-4 and GAPDH protein expression was determined by use of Wes System, Wes separation 12–230 kDa capillary cartridges (SM-W004), and standard pack (PS-ST01EZ-8) (all from Protein Simple) according to manufacturer's instructions. The following primary antibodies were used: GAPDH (Abcam, ab9485, 1:1,000), claudin-1 (Abcam, ab15098, 1:50), claudin-2 (Abcam, ab53032, 1:100) and claudin-4 (Abcam, ab53156, 1:100).

For flow cytometry, LPMCs were thawed and plated in 96-well U-bottom plates for staining. Cells were washed twice with PBS and stained for live/dead discrimination using Invitrogen LIVE/DEAD Fixable Aqua dead cell stain kit (Thermo Fisher Scientific). Blocking of Fc receptors was performed using Human BD Fc Block (Becton–Dickinson, Franklin Lakes, NJ, USA) and was followed by surface staining. Cells were stained with fluorescently labeled monoclonal antibodies directed to claudin-1 BV421 (clone 421203, BD), CD56 BV605 (clone HCD56; BioLegend, San Diego, CA, USA), CD19 BV711 (clone 2H7; BioLegend), CD4 PerCP-Cy5.5 (clone RPA-T4; Thermo Fisher Scientific), claudin-2 PE (polyclonal; Lifespan Biosciences, Seattle, WA, USA), claudin-3 PE (clone REA751; Miltenyi Biotech, Bergisch Gladbach, Germany), claudin-4 PE (clone REA898; Miltenyi Biotech), HLA-DR PE-Cy7 (clone LN3; Thermo Fisher Scientific), CD3 APC (clone SK7; Thermo Fisher Scientific), CD14 AF700 (clone HCD14; BioLegend), and CD45 APC-Cy7 (clone HI30; BioLegend) at 4°C for 30 min. After staining, cells were washed in PBS with 2% FBS and 2 mM EDTA and acquired immediately. Fluorescence-minus-one (FMO) controls were prepared for each claudin. Gates were set using FMO controls with <1% background accepted. Gating strategy for flow cytometry analysis is given in (**Supplementary Figure S2**). Data were collected using an Attune NxT flow cytometer (Thermo Fisher Scientific) and then analyzed using FlowJo software version 10.7 (FlowJo LLC, Ashland, OR, USA). Graphs were generated using GraphPad Prism software version 9.1 (GraphPad Software, San Diego, CA, USA).

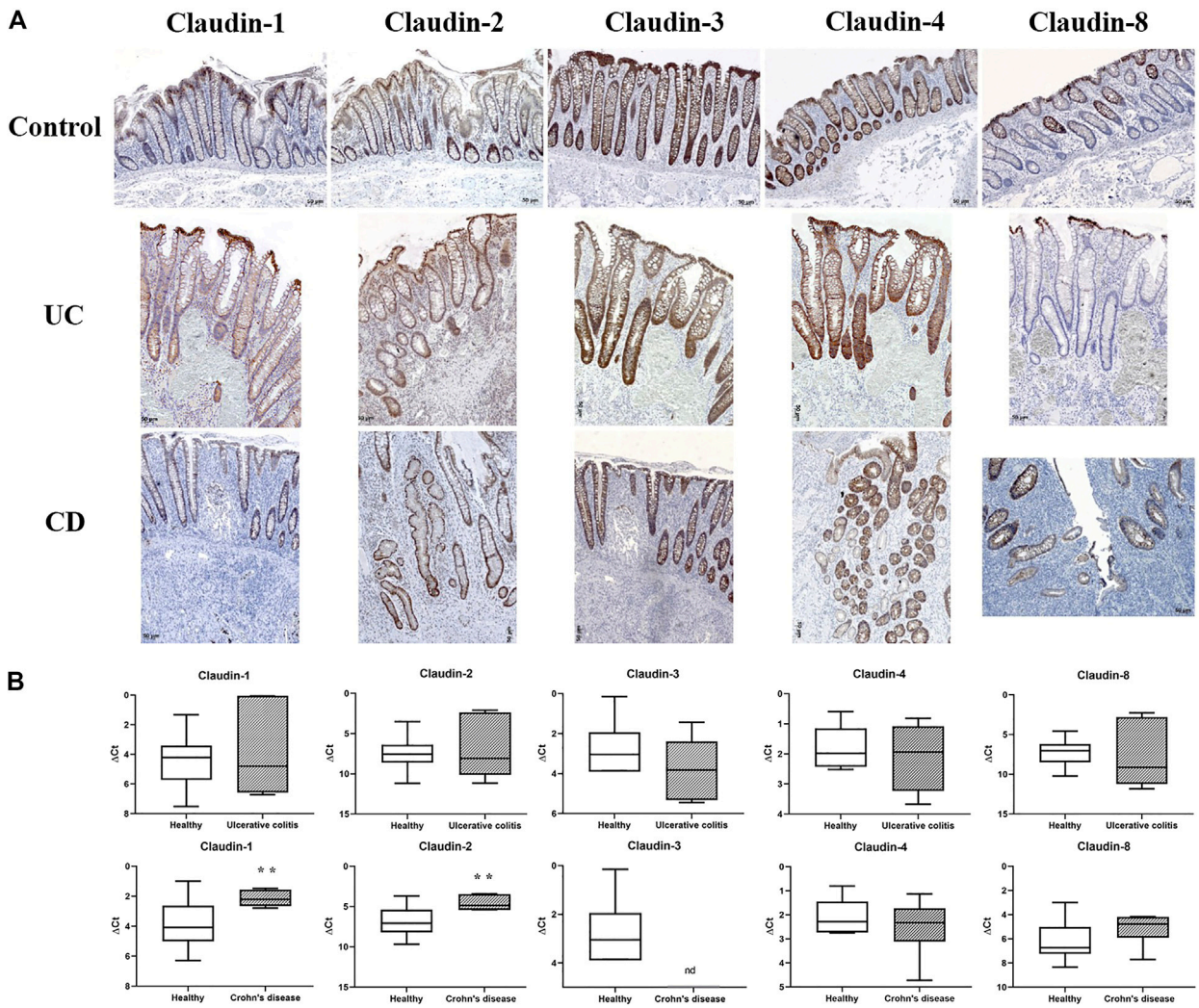

FIGURE 1 | Claudin-1, claudin-2, claudin-3, claudin-4, and claudin-8 expression in control human colon and colon of IBD patients. **(A)** Overview of claudin-1, claudin-2, claudin-3, claudin-4, and claudin-8 expression pattern (IHC); **(B)** claudin mRNA expressed as ΔCT value from claudin CT normalized to the GAPDH CT. Data are presented as box-and-whisker plots, with median and whiskers extending from 5 to 95 percentiles (eight non-IBD, five UC, and eight CD). ND, below detection limit. *t* Test, $p < 0.05$ vs. non-IBD; CD, Crohn disease; UC, ulcerative colitis.

Statistical Analysis

The Mann–Whitney nonparametric test was used for statistical evaluation of histology score data. Differences in claudin gene expression between healthy and UC or CD patients, as well as between naive animals and animals with induced colitis, were deduced using *t* test. The level of significance was set to $p < 0.05$ in all cases. GraphPad Prism Software (San Diego, CA, USA) was employed.

RESULTS

Claudin Expression in Human Colon and IBD

In control human colon, TJ proteins claudin-1, claudin-2, claudin-3, claudin-4, and claudin-8 were variably expressed along the crypt axis and differently distributed along the epithelial cell membrane, reflecting the differences of claudin expression by absorptive and secretory epithelial cells (**Figure 1A**-Control). Claudin-3 and claudin-4 were expressed along the whole crypt axis, whereas claudin-1 and claudin-8 expression increased toward crypt surface (**Figure 1A**, Control). Claudin-2 was variably present in colon tissue from different donors and ranged from faint to strong. Absorptive cells expressed claudin-1 (**Figure 2A**), claudin-3 (**Figure 2B**), claudin-4 (**Figure 2C**; **Supplementary Figure S3D**), and claudin-8 (**Figure 2D**; **Supplementary Figure S3E**) at TJs and along basolateral membranes. Claudin-3, claudin-4, claudin-8 (**Supplementary Figure S3F**), and focally claudin-1 (**Supplementary Figures S3B,C**) formed TJs of goblet cells. In addition, claudin-3 and claudin-4 (**Figures 2B,C**), as well focally claudin-1 (**Supplementary Figure S3C**) and claudin-8, were

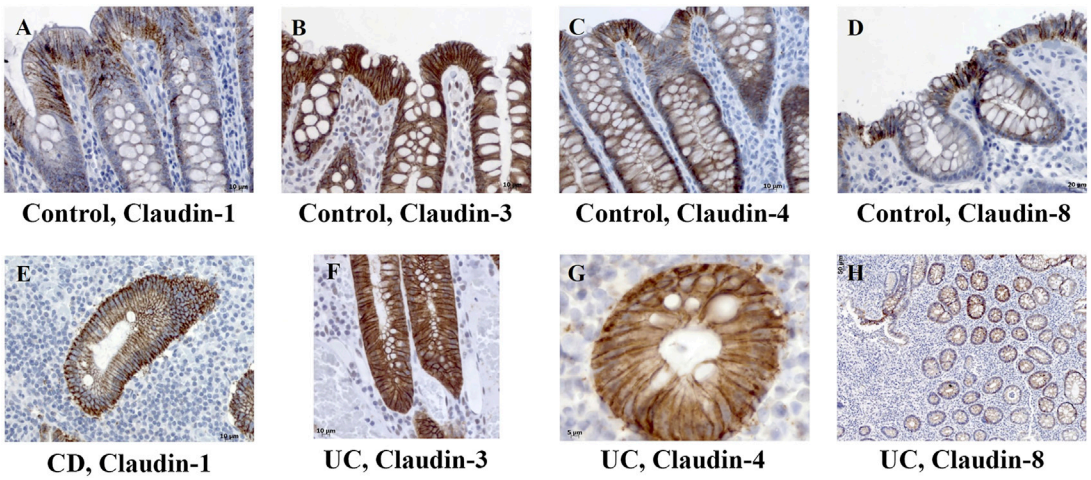

FIGURE 2 | Claudin-1, claudin-3, claudin-4, and claudin-8 expression patterns of absorptive cells in control human colon and colon of IBD patients. **(A)** Claudin-1 (IHC), control human colon; **(B)** claudin-3 (IHC), control human colon; **(C)** claudin-4 (IHC), control human colon; **(D)** claudin-8 (IHC), control human colon; **(E)** claudin-1 (IHC), CD; **(F)** claudin-3 (IHC), UC; **(G)** claudin-4 (IHC), UC; **(H)** claudin-8 (IHC), UC. CD, Crohn disease, UC, ulcerative colitis.

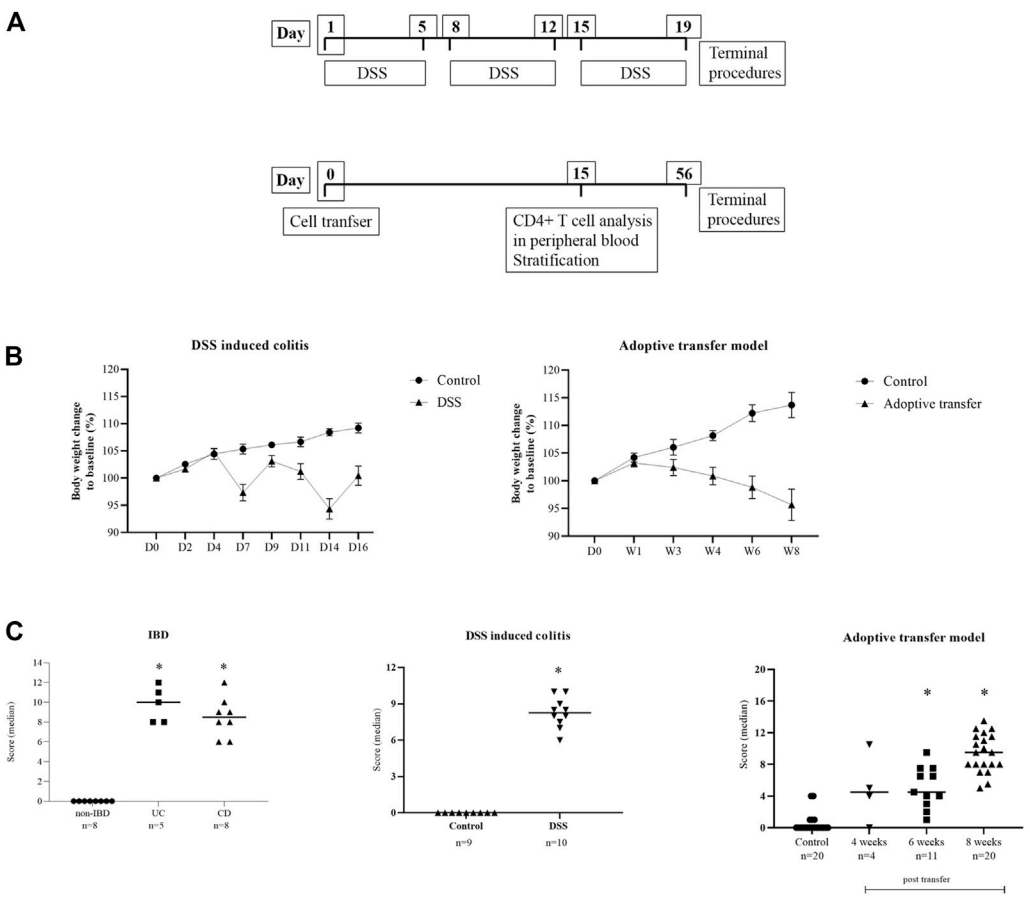

FIGURE 3 | (A) Diagrams of the experimental protocols for the induction of DSS colitis and adoptive transfer model in mice. **(B)** Body weight change in animal models. Data are presented as mean ± SEM (D, day; W, week). **(C)** Disease activity score. Score is given as group median; Mann–Whitney nonparametric test; $p < 0.05$ vs. control; IBD (Naini and Cortina, 2012), DSS (Nishitani et al., 2009), adoptive transfer model (Laroux et al., 2004).

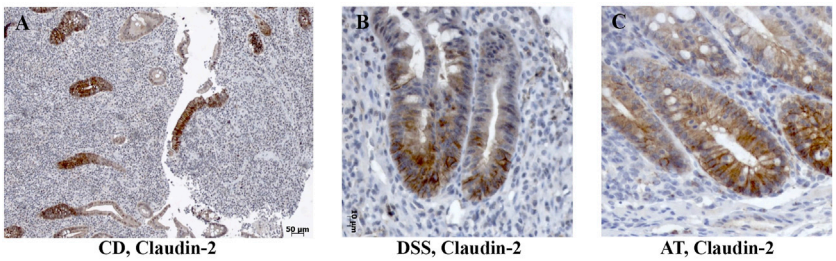

FIGURE 4 | Claudin-2 expression within enlarged proliferative zone in human IBD colon tissue and IBD animal models. **(A)** Claudin-2 (IHC), CD; **(B)** claudin-2 (IHC), DSS-model; **(C)** claudin-2 (IHC); Adoptive transfer model, 4 weeks after transfer. CD, Crohn disease, AT, adoptive transfer model.

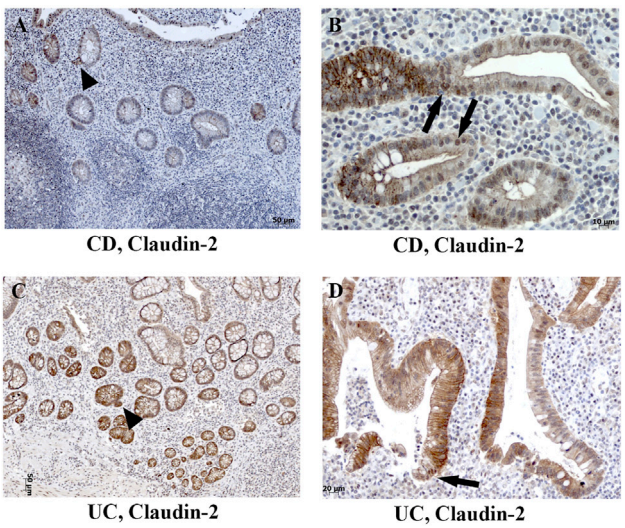

FIGURE 5 | Heterogeneous claudin-2 expression pattern in human IBD colon tissue. **(A)** Claudin-2 (IHC) positive cells at sites of "crypt budding," CD; **(B)** claudin-2 (IHC) expressed along cell membranes and within nuclei, CD; **(C)** claudin-2 (IHC) positive cells at sites of "crypt budding," UC; **(D)** claudin-2 (IHC) expressed along membranes and within nuclei, UC. Highlighted features: "crypt budding" (arrowheads) and claudin-2 positive nuclei (arrows). CD, Crohn disease; UC, ulcerative colitis.

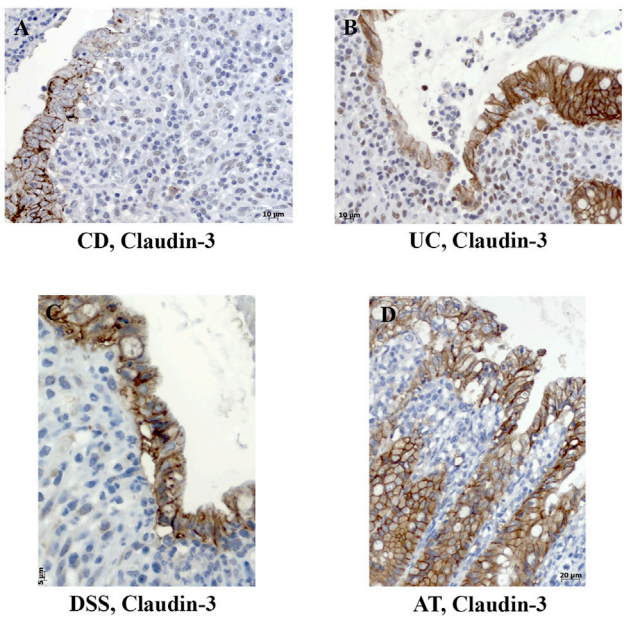

FIGURE 6 | Decreased membranous expression and internalization of claudin-3 in colon tissue of IBD patients and IBD animal models. **(A)** Claudin-3 (IHC), CD; **(B)** claudin-3 (IHC), UC; **(C)** claudin-3 (IHC), DSS; **(D)** claudin-3 (IHC), adoptive transfer model, 8 weeks after transfer. CD, Crohn disease; UC, ulcerative colitis; AT, adoptive transfer model.

expressed linearly along the basolateral membrane of goblet cells. Interindividual differences were noted in focal/segmental claudin-1 and claudin-8 expression by goblet cells. Tuft cells were positive for claudin-1 (**Supplementary Figure S3A**). Apart from epithelial cells, claudins were expressed by cells of mesoderm origin. Claudin-2 was expressed by mononuclear cells in lamina propria, a subset of lymphocytes within lymphoid tissue and endothelial cells. Claudin-3 was expressed by a subset of cells within the germinal center of lymphoid follicles (**Supplementary Figures S3G,H**) and high endothelial venules' (HEVs') endothelial cells (**Supplementary Figure S3I**).

In severe IBD cases analyzed in this study (**Figure 3C**; **Supplementary Table S1A**), the epithelial proliferation rate and cell differentiation were profoundly disturbed. This was manifested through a plethora of crypt phenotypes, each characterized by a different claudin signature (**Figure 1A**, UC, CD). Nevertheless, some characteristic patterns were still observed. Lineage claudin expression signature was not altered by the shift of differentiation toward absorptive cells (**Figures 2E–H**). Claudin-2 was preponderantly, but not exclusively, expressed by cells within an enlarged crypt proliferative zone (**Figure 4A**) and at sites of "budding" (**Figures 5A,C**). Claudin-2 expression pattern was heterogeneous and varied among crypts, even between morphologically identical cells within the same crypt (**Figures 5B,D**). On the other hand, decreased claudin expression by epithelial cells was observed at sites of neutrophil infiltration. Furthermore, intestinal surface epithelium in a vicinity of mucosal erosions and ulcers, in addition to decreased membranous claudin-3 expression, showed internalization of claudin-3 (**Figures 6A,B**) and claudin-8 into the cell cytoplasm.

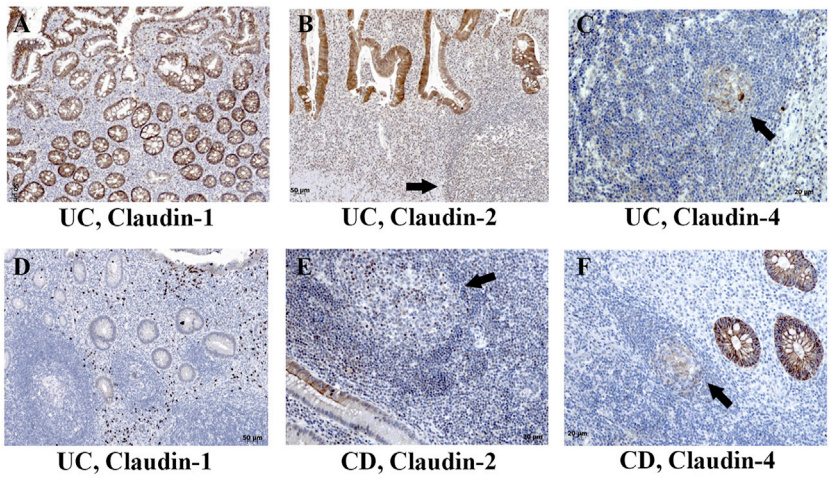

FIGURE 7 | Claudin-1, claudin-2, and claudin-4 expression by mononuclears and within tertian lymph nodes in colon of IBD patients. **(A)** Claudin-1 (IHC), UC; **(B)** claudin-2 (IHC), UC; **(C)** claudin-4 (IHC), UC; **(D)** claudin-1 (IHC), UC; **(E)** claudin-2 (IHC), CD; **(F)** claudin-4 (IHC), CD. Highlighted features: claudin positive cells within tertian lymph nodes (arrows). CD, Crohn disease; UC, ulcerative colitis.

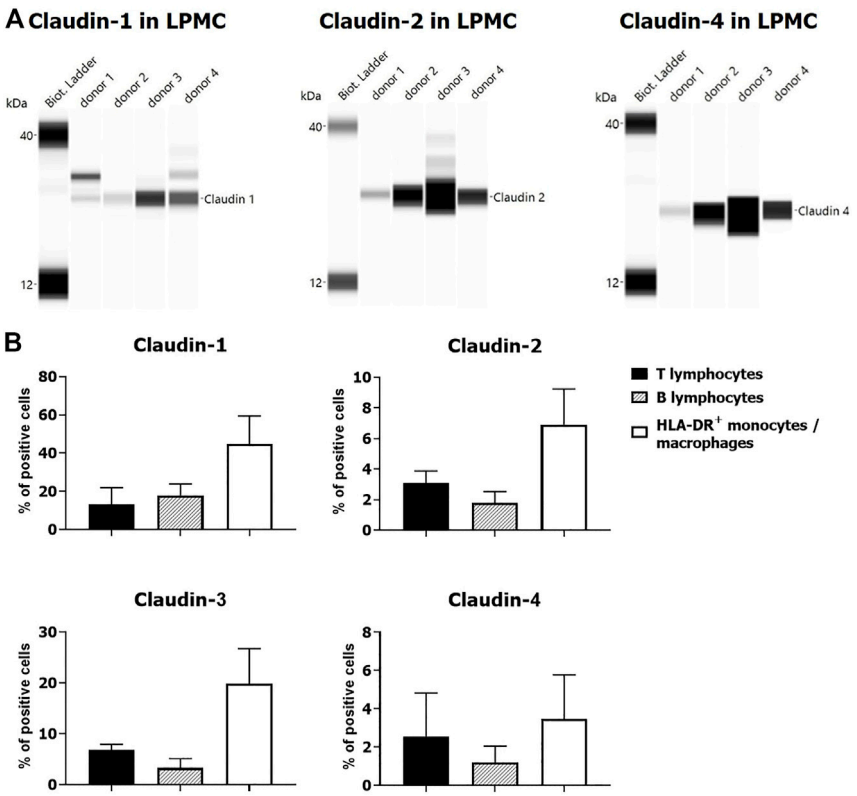

FIGURE 8 | Claudin expression by LPMCs: **(A)** Western blot, four UC donors (colon); **(B)** flow cytometry: percentage of claudin positive cells (mean ± SD) within individual LPMC subpopulations: two UC (colon) and two CD (terminal ileum) donors.

Expression of claudin-1 (**Figures 7A,D**), claudin-2 (**Figures 7B,E**), and claudin-4 (**Figures 7C,F**) by inflammatory cells infiltrating into IBD mucosa was noticed in tissue examined by IHC. Protein expression of claudins in isolated LPMCs was confirmed by Western blot analysis and flow cytometry of biopsies obtained from seven IBD donors (**Figure 8**). Within

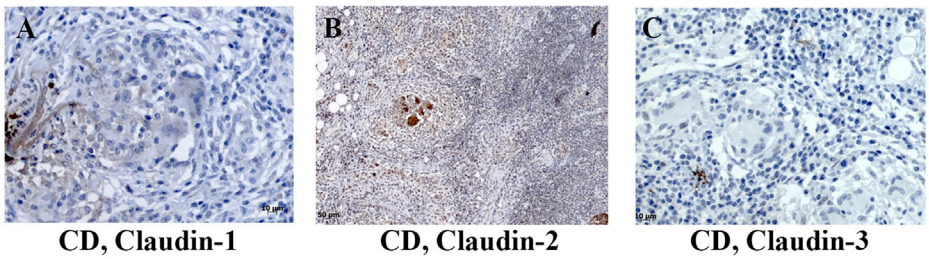

FIGURE 9 | Claudin-1, claudin-2, and claudin-3 expression by granuloma cells in colon of CD patients. **(A)** Claudin-1 (IHC), CD; **(B)** claudin-2 (IHC), CD; **(C)** claudin-3 (IHC), CD. CD, Crohn disease.

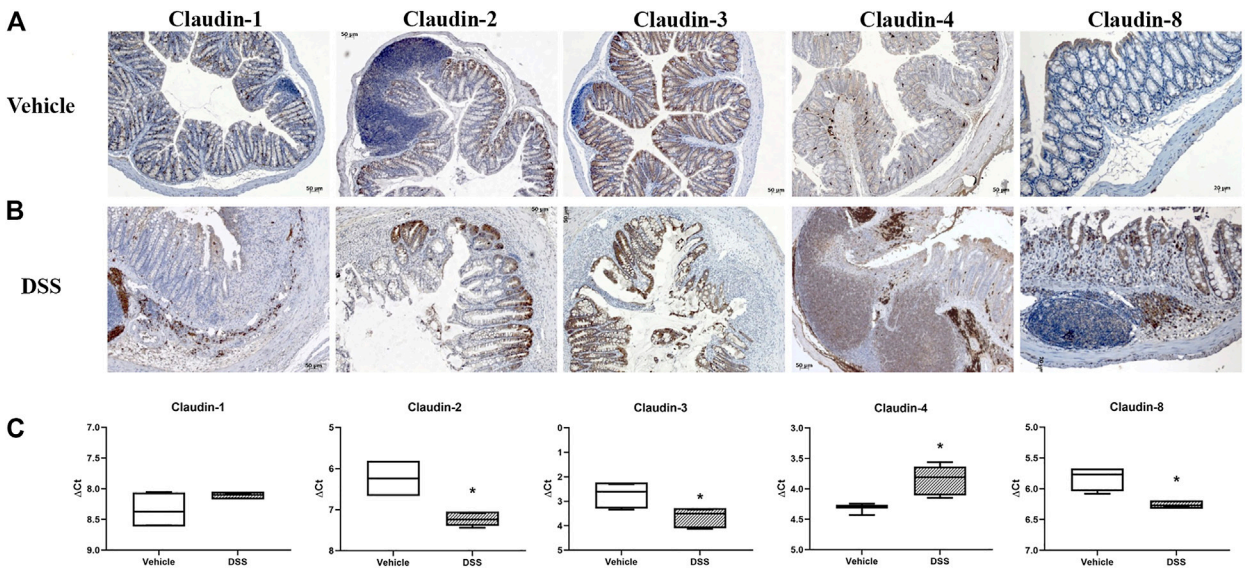

FIGURE 10 | Claudin-1, claudin-2, claudin-3, claudin-4, and claudin-8 expression in DSS-induced colitis, a murine model of IBD. **(A)** Overview of claudin-1, claudin-2, claudin-3, claudin-4, and claudin-8 expression pattern (IHC) in naive C57Bl6N mice; **(B)** overview of claudin-1, claudin-2, claudin-3, claudin-4, and claudin-8 expression pattern (IHC) in DSS-treated mice; **(C)** claudin mRNA expressed as ΔCT value from claudin CT normalized to the GAPDH CT. Data are presented as box-and-whisker plots, with median and whiskers extending from 5 to 95 percentiles (one representative experiment: four naive animals and five animals exposed to DSS). *t* Test, $p < 0.05$ vs. naive mice.

ectopic tertiary lymphoid tissue, claudin-2 was expressed by lymphocyte subpopulation(s) (**Figures 7B,E**), and claudin-3– and claudin-4–positive cells were found in germinal centers (**Figures 7C,F**). In CD, epithelioid macrophages and multinuclear giant cells within granuloma expressed claudin-2 (**Figure 9B**), while being claudin-1 (**Figure 9A**) and claudin-3 (**Figure 9C**) negative.

In surgically removed intestine from patients with CD, claudin-1 and claudin-2 mRNA levels (**Figure 1B**) were significantly higher than in non-IBD control intestine. Levels of claudin-4 and claudin-8 mRNA remained unchanged (**Figure 1B**). Claudin-3 mRNA was below detection level in all CD samples. In resected colon samples obtained from patients with UC, claudin-1, claudin-2, claudin-4, and claudin-8 mRNA levels were comparable to non-IBD control intestine (**Figure 1B**). On the other hand, a tendency toward the lower level of claudin-3 mRNA was observed in UC patients (**Figure 1B**).

Claudin Expression in C57Bl/6N Mice and DSS Model

In C57Bl/6N naive colon (**Figure 10A**), absorptive epithelial cells expressed claudin-3 along lateral membranes, claudin-4 was present at a very low level within the cytoplasm, and claudin-8 was expressed unevenly within the cytoplasm and/or along lateral membranes. Colon absorptive epithelial cells in C57Bl/6N mice did not express claudin-1. Claudin-1 was present within the cytoplasm of crypt secretory cells. All cell types within crypt expressed claudin-3 along the whole length of the basolateral membranes. Claudin-2 was positive in the stem cell niche at the crypt base, situated at TJs and along the basolateral membrane. The claudin-4 expression pattern in crypt was more pronounced in the proliferative region. Claudin-8 was mostly absent from crypt cells. Furthermore, claudin-4 was unevenly expressed by epithelial cells overlying mucosa-associated lymphoid tissue (MALT). The cell

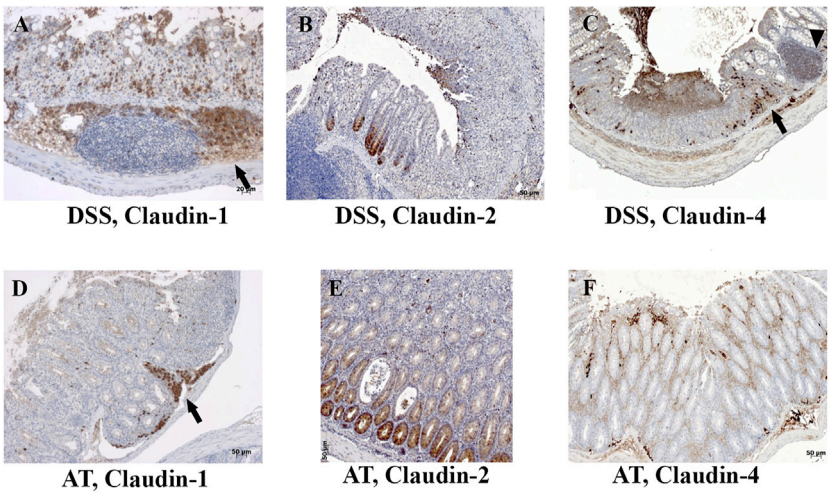

FIGURE 11 | Claudin-1, claudin-2, and claudin-4 expression by mononuclears and within lymph nodes in IBD animal models. **(A)** Claudin-1 (IHC), DSS; **(B)** claudin-2 (IHC), DSS; **(C)** claudin-4 (IHC), DSS; **(D)** claudin-1 (IHC), adoptive transfer, 6 weeks after transfer; **(E)** claudin-2 (IHC), adoptive transfer, 6 weeks after transfer; **(F)** claudin-4 (IHC), adoptive transfer, 8 weeks after transfer. Highlighted features: lymphoid follicle (arrowhead) and accumulation of macrophages (arrows). AT, adoptive transfer model.

subpopulation within MALT expressed claudin-2 and/or claudin-4. The macrophages in lamina propria were strongly claudin-4 positive. Endothelial cells were claudin-2 positive, but claudin-1, claudin-3, claudin-4, and claudin-8 negative.

DSS-induced murine chronic colitis (**Figure 3A**) was characterized by weight loss (**Figure 3B**), colon shortening and chronic active inflammation, mucosa erosions, and formation of ulcers that was reflected through a total histology activity score (**Figure 3C**, **Supplementary Table S1B**). Epithelial cells situated at the edge of epithelial defects were claudin-1 and claudin-3 positive along membranes and within the cytoplasm (**Figure 6C**). In noninflamed mucosa, claudin-3 occasionally formed small intracytoplasmic vacuoles within absorptive epithelial cells. In majority of the epithelial cells, claudin-4 was present at a relatively low level, whereas claudin-8 expression level within epithelial cell compartment increased (**Figure 10B**). Within the crypt proliferative zone, claudin-2 was overexpressed (**Figure 4B**; **Figure 10B**), claudin-3 was localized along lateral membranes, whereas claudin-8 was moderately expressed within the subset of the crypts (**Figure 10B**). Lymph follicles were strongly claudin-4 positive (**Figure 10B**; **Figure 11C**), whereas various infiltrating inflammatory cells in lamina propria were either claudin-1 (**Figure 10B**; **Figure 11A**), claudin-2 (**Figure 11B**), claudin-4 (**Figure 11C**), or claudin-8 positive (**Figure 10B**); among those, macrophages expressed claudin-1 (**Figure 10B**; **Figure 11A**), claudin-4 (**Figure 10B**; **Figure 11C**), and claudin-8 (**Figure 10B**). qRT-PCR analysis of the mouse colon revealed significantly greater expression of claudin-4 and significantly lower expression of claudin-2, claudin-3, and claudin-8 in DSS-treated mice versus healthy controls when expressed over housekeeping gene (**Figure 10C**).

Claudin Expression in SCID Mice and Adoptive Transfer Model of Colitis

In SCID murine nondiseased colon, absorptive epithelial cells expressed claudin-1 and claudin-3 along the lateral membranes (**Figure 12A**). Claudin-8 was unevenly expressed among surface and crypt cells, mainly within the cytoplasm. All crypt cell-types showed membranous claudin-3 expression (**Figure 12A**). Cells in the proliferative zone, unlike other crypt cells, were strongly claudin-2 positive. Claudin-2 was situated at TJs, along the whole lateral membrane or within the cytoplasm of cells in crypt proliferative zone (**Figure 12A**). Microfold (M) cells within the epithelium covering the lymphoid tissue expressed claudin-4 along the lateral membranes and occasionally within the cytoplasm, whereas MALT cells were claudin-4 negative (**Figure 12A**). On the other hand, MALT-associated epithelial cells and lymphoid cells within the MALT were claudin-8 positive (**Figure 12A**). Claudin-8 was mainly found within the cell cytoplasm. Endothelial cells were claudin-2 positive.

$CD4^+CD25^-CD62L^+$ T cell transfer into SCID mice induced colitis (**Figure 3A**) that was manifested by weight loss (**Figure 3B**), colon elongation, and by mucosal inflammation accompanied by crypt loss due to lymphoid infiltration into the crypt epithelium, diffuse crypt elongation with increased crypt proliferative zone, and reduced goblet cell number (**Figure 12B**) and was reflected through a total histology activity score (**Figure 3C**; **Supplementary Table S1C**). Absorptive cells lining mucosa surface expressed claudin-1 and claudin-3 along the basolateral membranes (**Figure 12B**). From 4 weeks after transfer onward, cells lining elongated crypts that were lacking goblet cells acquired claudin-1 and claudin-3 expression pattern

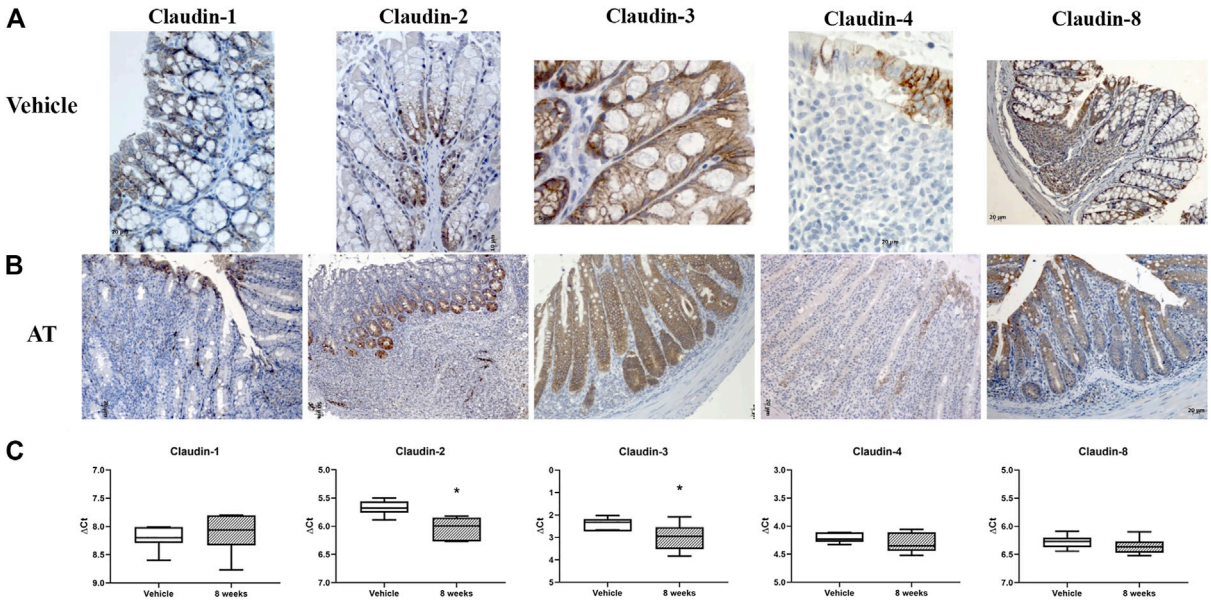

FIGURE 12 | Claudin-1, claudin-2, claudin-3, claudin-4, and claudin-8 expression in adoptive transfer murine model of IBD. **(A)** Overview of claudin-1, claudin-2, claudin-3, claudin-4, and claudin-8 expression pattern (IHC), in naive SCID mice; **(B)** overview of claudin-1, claudin-2, claudin-3, claudin-4, and claudin-8 expression pattern (IHC) in adoptive transfer model, 8 weeks after transfer; **(C)** claudin mRNA expressed as ΔCT value from claudin CT normalized to the GAPDH CT. Data are presented as box-and-whisker plots, with median and whiskers extending from 5 to 95 percentiles (one representative experiment: seven naive animals and nine animals sacrificed 8 weeks after transfer). *t* Test, $p < 0.05$ vs. naive mice; AT, adoptive transfer model.

characteristic for surface absorptive cells (**Figure 12B**). Most of the surface, crypt body, and crypt base epithelial cells retained cytoplasmic claudin-8 positivity at variable levels (**Figure 12B**). Claudin-8 translocated toward the membrane in a subset of those cells. In diseased animals, M cells remained claudin-4 positive. Claudin-4–positive cells "outside" MALT-covering epithelium were found. Among epithelial cells covering mucosa surface and in crypts, small clusters of epithelial cells expressed claudin-4 along basolateral membrane (**Figure 12B**). The crypt proliferative zone was steadily increasing over the posttransfer observation period and was strongly claudin-2 positive (**Figure 4C**; **Figure 11E**; **Figure 12B**). At sites of lymphocytic invasion, epithelial cells lost claudin expression. In adoptive transfer model of IBD subsets of infiltrating mononuclear cells, among other macrophages were claudin-1 (**Figure 11D**; **Figure 12B**), claudin-2 (**Figure 11E**; **Figure 12B**), claudin-4 (**Figure 11F**), and/or claudin-8 positive. qRT-PCR analysis of the mouse colon revealed lower expression of claudin-2 and claudin-3 mRNA in mice with adoptive transfer versus healthy controls when expressed over housekeeping gene, whereas claudin-1, claudin-4, and claudin-8 mRNA expression did not significantly change (**Figure 12C**).

DISCUSSION

Our study has confirmed that claudin-1, claudin-2, claudin-3, claudin-4, and claudin-8 are constitutive epithelial membrane proteins in nondiseased control human colon with variable distribution pattern along the crypt axis (Lu et al., 2013; Luissint et al., 2016; Garcia-Hernandez et al., 2017). Results obtained in this study highlighted interstrain difference in claudin expression pattern between C57Bl6 and C.B.17/lcr SCID mice (congenic to BALB/c mice; Janvier Labs). Claudin distribution along the crypt axis recorded in either murine strain examined does not completely reflect distribution noted in humans.

Although claudins are primarily regarded as TJ proteins, their distribution outside TJs, along lateral membrane and within the cytoplasm or nucleus of intestinal epithelial cells, in both human and mice was documented in this study. Observed claudin-1 and claudin-3 expression along the whole length of colonocyte basolateral membrane is in line with previous reports in healthy human colon mucosa and IBD, as well as in mice (Prasad et al., 2005; Guttman et al., 2006; Barrmeyer et al., 2015; Hagen, 2017). It has been proposed that claudins situated at basolateral membrane contribute to intestinal homeostasis (Luissint et al., 2016) by forming integrin–claudin adhesion complexes between epithelial cells and extracellular matrix, thus playing a role in cell migration and epithelial–mesenchymal transdifferentiation (Hagen, 2017).

In severe IBD cases analyzed in this study, claudin-2 translocation into the nucleus of epithelial cells was observed. Existence of claudins that shuttle from the membrane to the cytoplasm and even the nucleus has been reported earlier in different malignancies including colorectal adenocarcinoma cells (Dhawan et al., 2005; Ikari et al., 2014; Tokuhara et al., 2017; Torres-Martinez et al., 2017; Hagen, 2017; Chang et al., 2018). To

the best of our knowledge, nuclear localization of claudins in nondiseased control intestine or IBD was never reported in the literature. In addition to nuclear claudin expression, increased membranous claudin-2 staining of single cells, as well as increased number of cells expressing claudin-2, was detected regularly in proliferative zone of elongated crypts in resected intestine tissue from IBD patients, as well as in both examined animal models. This phenomenon was described previously by some authors analyzing biopsy tissue from IBD patients (Prasad et al., 2005; Barmeyer et al., 2015; Chang et al., 2018) and adoptive transfer colitis model (Su et al., 2013). It has been shown that apart from contributing to the epithelial barrier function, claudin-2, a Wnt-target gene itself, plays a role in cell proliferation and differentiation. It has been noted that claudin-2–positive cells express Ki67, cyclin D1, and c-Myc (Mankertz et al., 2004; Dhawan et al., 2005; Dhawan et al., 2011; Ikari et al., 2014; Barmeyer et al., 2015; Mah et al., 2016; Ahmad et al., 2017; Torres-Martinez et al., 2017).

In IBD patients and in both animal models studied, the presence of crypts lined by a single epithelial cell type, characterized by strain-specific claudin expression pattern of either absorptive or goblet cells, was observed. Differentiation of intestinal cells into absorptive and secretory cell lineage is regulated, among others, by Notch signaling pathway (VanDussen et al., 2012; Bankaitis et al., 2018). Certain claudins can influence Notch pathway, and in return, claudin expression level lies under Notch control. It has been reported that claudin-1 regulates Notch signaling, thus influencing shift toward absorptive cell lineage differentiation (Pope et al., 2014). Loss of Notch-1 signaling induced claudin-2 expression (Dahan et al., 2011) and differentiation shift toward secretory lineage (VanDussen et al., 2012).

In inflammatory milieu, claudin expression level/pattern by epithelial cells was altered. Although CD and UC do not entirely share pathophysiology, with CD being characterized by granulomatous inflammation, whereas UC is T_H2-driven (Ramos and Papadakis, 2019), certain similarities are present. One of the common IBD hallmarks is neutrophilic inflammation and mucosal defects due to necrosis, ranging from erosions to ulcer formation. In examined IBD cases, neutrophilic infiltration of mucosa was accompanied by a lower expression of claudin by enterocyte, a phenomenon that was described in IBD previously by Kucharzik (2001). In IBD patient and animal model colon tissue, not only a decrease of claudin expression level has been documented, but also a disruption of continuous claudin-3 expression along the lateral membranes and its internalization into the cytoplasm of cells in the vicinity of mucosal defects in the IBD and DSS model. Translocation of certain claudins from the enterocyte membrane into the cytoplasm was observed in a murine model of necrotizing colitis induced by commensal bacteria (Bergmann et al., 2013). It has also been shown that claudin-1 and claudin-3 relocate from the membrane into the cell cytoplasm following infection with certain pathogens (Guttman et al., 2006). In particular, *Clostridium perfringens* enterotoxin is able to bind claudin-3 and induce its internalization (Luissint et al., 2016).

In the adoptive transfer model, a lack of claudin epithelial staining at sites of intraepithelial lymphocyte infiltration was noted. Loss of claudin expression could be linked to the inflammatory environment. It is known from the *in vitro* studies that cytokines can alter epithelial claudin expression and hence influence permeability of intestinal epithelial barrier (Albert-Bayo et al., 2019). Tumor necrosis factor (TNF-α), interleukin 1β (IL-1β), and interferon γ, all playing a role in IBD (Guan and Zhang, 2017; Ramos and Papadakis, 2019) and IBD animal models (Lyons et al., 2018; Yan-Hong et al., 2018), downregulate claudin-3 and claudin-4 expression by epithelial cells, whereas IL-23 and IL-9 downregulate claudin-8 (Prasad et al., 2005; Zhu et al., 2019). On the other hand, TNF-α, IL-6, IL-13, and IL-17 upregulate claudin-2 expression (Kinugasa et al., 2000; Prasad et al., 2005; Weber et al., 2010), thus increasing barrier permeability. As discussed previously, upregulation of claudin-2 expression by cytokines could influence not only the function of the epithelial barrier, but also cell proliferation.

In nondiseased SCID mice, claudin-4 was exclusively expressed by the follicle-associated epithelium covering MALT, known as M cells. In C57Bl/6 mice, M cells were claudin-4 positive, as previously reported (Tamagawa et al., 2003), but this was not such a striking characteristic as in SCID mice, since in C57Bl/6 mice, other epithelial cells were also expressing claudin-4. M cells are specialized for antigen uptake from the intestine lumen into lymphoid tissue (Nakamura et al., 2018) and have a role in the development of gut immune tolerance and microbial-pathogen defense (Jung et al., 2010). Induction of claudin-4–positive epithelial cells apart from MALT-covering epithelium, but not necessarily overlying lymphoid infiltrate, was evident after T-cell transfer in the adoptive transfer model. Such small clusters of claudin-4 epithelial cells were found also in the DSS model. The true lineage of these cells, absorptive versus M-cell, cannot be deduced from the results of our study.

In addition to claudin expression by epithelial cells, we could confirm claudin expression by cells originating from mesoderm, both in humans and mice. The claudin expression pattern differed among examined species in healthy and diseased intestine. In our report, we concentrated on claudin-expression by endothelial and myeloid cells. Specific claudin signatures were documented for different species and vessel-type endothelial cells. In humans, C57Bl/6 and SCID mice endothelial cells of colon vessels expressed claudin-2. On the other hand, HEVs in humans were claudin-3 positive, while negative in both murine strains. These data are in concordance with an earlier publication on claudin expression on endothelial/HEV cells in C57Bl/6 mice (Pfeiffer et al., 2008) and support literature reports on the lack of overlap among claudin signatures of various endothelial cell types (Komarova et al., 2017). Among claudins studied in our work, claudin-2 was identified as the most widely expressed among cells of myeloid origin in human colon. Claudin-1–, claudin-2–, and claudin-4–positive mononuclear cells in human IBD colon mucosa have been documented by IHC. Protein expression of claudins was confirmed by Western blot analysis and flow cytometry of LPMCs isolated from colon mucosal samples obtained from IBD patients. Furthermore, we also report that epithelioid macrophages and multinucleated giant cells, found

within granuloma in CD, express claudin-2. Monocyte-derived macrophages and tissue resident macrophages can transform into epithelioid macrophages under the influence of various cytokines and consequently fuse to form multinucleated giant cells (Timmermans et al., 2016; Brooks et al., 2019). Our findings are, to a certain extent, in line with earlier reported claudin-2 expression by CD163-positive macrophages in noncancerous human colon mucosa (Mezheyeuski et al., 2018). Apart from macrophages, dendritic cells were reported to express claudin-1 and claudin-2 (Rescigno et al., 2001; Van den Bossche et al., 2012). In contrast to humans, lymphocytes in colon lamina propria of naive C57Bl/6N and SCID mice did not express any of the studied claudins. Claudin-2– and claudin-4–positive cells within MALT tissue were found in C57Bl/6N, but not SCID mice. In both IBD models examined in our study, infiltrating myeloid cells, among others macrophages, showed claudin-1, claudin-2, claudin- 4, and claudin-8 positivity. Claudin-1, claudin-2, and claudin-8 expression by alternatively activated macrophages was observed *in vitro* and in murine *in vivo* models (Van den Bossche et al., 2012). In this study, various claudin expression patterns by diverse myeloid cell types in IBD and IBD-models have been documented, but it is beyond the scope of our work to discuss their role upon activation under different inflammatory stimuli.

Next to the examination of claudin expression by IHC, we have evaluated claudin mRNA expression in neighboring tissue slices of the same paraffin blocks. In this study, increased claudin-1 and claudin-2 mRNA levels in colon resection specimens from patients with severe CD were observed. Oshima et al. (2008) reported increased claudin-2 mRNA level in rectal biopsies from UC patients. Differently to observed increase in claudin-2 mRNA expression in human IBD, a decrease of claudin-2 mRNA was observed in both animal models. An increase of claudin-1 mRNA expression observed in CD patient colon tissue was not detected in either of animal models, whereas an increase of claudin-4 mRNA and decrease of claudin-8 mRNA were observed only in the DSS model. A decrease of claudin-3 mRNA detected in IBD patient colon tissue and tissue from both animal models was in line with observed histological changes reflecting relative decrease of claudin-3–positive epithelial cell population versus claudin-3–negative myeloid cell population. Based on the results gained in this study, it can be stated that changes in claudin mRNA level are not a mere consequence of alteration in claudin expression by epithelial cells (Mennigen et al., 2009), as an influx of claudin-1–, claudin-2–, and claudin-4–positive inflammatory cells into mucosa was documented by IHC, Western blot, and flow cytometry. Changes in claudin mRNA isolated from the whole tissue samples reflect overall dynamic of claudin protein synthesis within epithelial and lamina propria compartment: loss of epithelial cells, proliferation of epithelial cells, influx of claudin positive/negative inflammatory cells, and finally relative proportion of certain cell types in analyzed tissue samples. As underlined in this study, mRNA level should be interpreted based on tissue morphology.

Claudins are emerging drug targets; thus, evaluation of their expression in human disease and animal models is crucial for the scientists working in the field of drug discovery. Results of the presented study emphasize the variety of claudin expression patterns among cells of epithelial and myeloid lineage, thus urging for overwhelming and throughout investigation of potential drug effects on claudin expression/function in a wide spectrum of cells in inflamed intestine that is not based solely on quantitative measure of mRNA/protein level within tissue or isolated cell population. Even the alteration of claudin expression in the single cells within highly organized structures such as lymph follicles could have profound downstream consequences for the disease development. Therefore, 1) claudins should not be regarded solely as TJ proteins involved exclusively in the intestinal barrier function, and expression of claudins by inflammatory cells in inflamed mucosa should be considered; 2) differences and similarities in claudin expression pattern by intestinal epithelial cells, in noninflamed and inflamed mucosa, between humans and mice, as well as between murine strains and animal models, should be respected; 3) results of quantitative measurements of claudin level in the tissue should be interpreted with caution and in the context of tissue alterations.

In summary, claudin expression pattern in uninflamed and inflamed colon varies between species, but at the same time, some common characteristics are noted. Claudins are not expressed solely by epithelial cells and are not exclusively TJ proteins. Claudin expression by LPMCs has been confirmed by IHC, flow cytometry, and Western blot. Noted changes at claudin mRNA tissue level in IBD and in either model reflected complex alterations in claudin expression by epithelial cells and relative relation between claudin-positive epithelial cells and claudin bearing inflammatory cells.

DATA AVAILABILITY STATEMENT

The original contributions presented in the study are included in the article/**Supplementary Material**, further inquiries can be directed to the corresponding author.

ETHICS STATEMENT

The studies involving human participants were reviewed and approved by Ethics Committee of Clinical Hospital Centre Rijeka and Ethics Committee of Clinical Hospital Dubrava. The patients/participants provided their written informed consent to participate in this study. The animal study was reviewed and approved by Committee for Animal Research

Ethics—Zagreb (CARE-ZG) in Fidelta Ltd. and the Croatian Ministry of Agriculture.

AUTHOR CONTRIBUTIONS

SČ, IG, MBo, and VEH created a study concept and design. SČ, MA, and AO analysed claudin expression in human tissue and tissue obtained from animal models by using IHC and have performed histological analysis of the tissue samples. DS-P did qPCR analysis and data interpretation. BH and MDK conducted *in vivo* animal experiments. SM and LP performed isolation of LPMCs. APG has performed Western blot analysis and IZ flow cytometry analysis of LPMs. IZ and DP isolated lymphocytes and performed flow cytometry in adoptive transfer model. GA has performed pathohistological diagnosis of human samples. MBa, MU, BMS, and AČ recruited donors, established clinical diagnosis and collected clinical samples. All authors have contributed to the discussion of results and manuscript drafting. VEH did final manuscript approval.

FUNDING

This research has been funded by Fidelta Ltd.

ACKNOWLEDGMENTS

Authors would like to acknowledge the contributions of Ms. Irineja Ćubela and Ms. Božana Maleta for technical support in preparation of histological slides, Steve Price for critical reading of the manuscript and Vuk Milutinović for the help with the picture formatting.

SUPPLEMENTARY MATERIAL

The Supplementary Material for this article can be found online at: https://www.frontiersin.org/articles/10.3389/fphar.2021.682614/full#supplementary-material

Supplementary Figure S1 | Negative control for immunohistochemistry: tissue stained without primary antibody. **(A)** R&D System Kit CTS002, control mouse tissue; **(B)** R&D System Kit CTS005, control mouse tissue; **(C)** R&D System Kit CTS008, control mouse tissue; **(D)** DAKO EnVision System Detection Kit, Human control tissue

Supplementary Figure S2 | Gating strategy for flow cytometry analysis. Time vs. forward scatter-height (FSC-H) was used to check the quality of the sample acquire followed by exclusion of doublets on FSC-H vs FSC- Width (FSC-W) and FSC-H vs FSC-Area (FSC-A). Side scatter-area (SSC-A) vs red-FL3-A APC-Cy7 CD45 was done to gate $CD45^+$ leukocytes. From live $CD45^+$ leukocytes gate B and T lymphocytes were gated followed by a gate from double-negative population ($CD20^-CD3^-$) was used for gating HLA-DR^+CD14^+ monocytes/macrophages cells. Each claudin (claudin-1, claudin-2, claudin-3, and claudin-4) was gated on histogram plots for each cell type population. Fluorescence-minus-one (FMO) controls were used for setting the gates.

Supplementary Figure S3 | Claudin-1, claudin-4, and claudin-8 expression in absorptive/ secretory epithelial cells and claudin-3 expression within lymphoid follicle in control human colon tissue. **(A)** Claudin-1 (IHC), control, tuft cells; **(B)** claudin-1 (IHC), control, goblet cells; **(C)** claudin-1 (IHC), control, goblet cells; **(D)** claudin-4 (IHC), control, absorptive cells; **(E)** claudin-8 (IHC), control, absorptive cells; **(F)** claudin-8 (IHC), control, goblet cells; **(G)** claudin-3 (IHC), control, epithelium, and lymphoid follicle; **(H)** claudin-3 (IHC), control, germinal center; **(I)** claudin-3 (IHC), control, HEV.

Supplementary Table S1 | Criteria for histological evaluation of disease activity in IBD and animal models of IBD. **(A)** Histologic score for disease activity in IBD patients modified from the method published by Naini and Cortina (2012) **(B)** Histologic score for disease activity in DSS animal model published by Nishitani et al. (2009) **(C)** Histologic score method for disease activity in adoptive transfer animal model published by Laroux et al. (2004).

REFERENCES

Ahmad, R., Kumar, B., Pan, K., Dhawan, P., and Singh, A. B. (2017). HDAC-4 Regulates Claudin-2 Expression in EGFR-Erk1/2 Dependent Manner to Regulate Colonic Epithelial Cell Differentiation. *Oncotarget* 8, 87718–87736. doi:10.18632/oncotarget.21190

Albert-Bayo, M., Paracuellos, I., González-Castro, A. M., Rodríguez-Urrutia, A., Rodríguez-Lagunas, M. J., Alonso-Cotoner, C., et al. (2019). Intestinal Mucosal Mast Cells: Key Modulators of Barrier Function and Homeostasis. *Cells* 8, 135. doi:10.3390/cells8020135

Bankaitis, E. D., Ha, A., Kuo, C. J., and Magness, S. T. (2018). Reserve Stem Cells in Intestinal Homeostasis and Injury. *Gastroenterology* 155, 1348–1361. doi:10.1053/j.gastro.2018.08.016

Barmeyer, C., Schulzke, J. D., and Fromm, M. (2015). Claudin-related Intestinal Diseases. *Semin. Cel Dev. Biol.* 42, 30–38. doi:10.1016/j.semcdb.2015.05.006

Bergmann, K. R., Liu, S. X., Tian, R., Kushnir, A., Turner, J. R., Li, H. L., et al. (2013). Bifidobacteria Stabilize Claudins at Tight Junctions and Prevent Intestinal Barrier Dysfunction in Mouse Necrotizing Enterocolitis. *Am. J. Pathol.* 182, 1595–1606. doi:10.1016/j.ajpath.2013.01.013

Brockmann, L., Giannou, A. D., Gagliani, N., and Huber, S. (2017). Regulation of TH17 Cells and Associated Cytokines in Wound Healing, Tissue Regeneration, and Carcinogenesis. *Int. J. Mol. Sci.* 18, 1033. doi:10.3390/ijms18051033

Brooks, P. J., Glogauer, M., and McCulloch, C. A. (2019). An Overview of the Derivation and Function of Multinucleated Giant Cells and Their Role in Pathologic Processes. *Am. J. Pathol.* 189, 1145–1158. doi:10.1016/j.ajpath.2019.02.006

Chang, M., Chang, L., Chang, H. M., and Chang, F. (2018). Intestinal and Extraintestinal Cancers Associated with Inflammatory Bowel Disease. *Clin. Colorectal Cancer* 17, e29–e37. doi:10.1016/j.clcc.2017.06.009

Chelakkot, C., Ghim, J., and Ryu, S. H. (2018). Mechanisms Regulating Intestinal Barrier Integrity and its Pathological Implications. *Exp. Mol. Med.* 50, 103–109. doi:10.1038/s12276-018-0126-x

Dahan, S., Rabinowitz, K. M., Martin, A. P., Berin, M. C., Unkeless, J. C., and Mayer, L. (2011). Notch-1 Signaling Regulates Intestinal Epithelial Barrier Function, through Interaction with CD4+ T Cells, in Mice and Humans. *Gastroenterology* 140, 550–559. doi:10.1053/j.gastro.2010.10.057

Dhawan, P., Ahmad, R., Chaturvedi, R., Smith, J. J., Midha, R., Mittal, M. K., et al. (2011). Claudin-2 Expression Increases Tumorigenicity of Colon Cancer Cells: Role of Epidermal Growth Factor Receptor Activation. *Oncogene* 30, 3234–3247. doi:10.1038/onc.2011.43

Dhawan, P., Singh, A. B., Deane, N. G., No, Y., Shiou, S. R., Schmidt, C., et al. (2005). Claudin-1 Regulates Cellular Transformation and Metastatic Behavior in colon Cancer. *J. Clin. Invest.* 115, 1765–1776. doi:10.1172/JCI24543

Farkas, A. E., Capaldo, C. T., and Nusrat, A. (2012). Regulation of Epithelial Proliferation by Tight junction Proteins. *Ann. N. Y. Acad. Sci.* 1258, 115–124. doi:10.1111/j.1749-6632.2012.06556.x

Garcia-Hernandez, V., Quiros, M., and Nusrat, A. (2017). Intestinal Epithelial Claudins: Expression and Regulation in Homeostasis and Inflammation. *Ann. N. Y. Acad. Sci.* 1397, 66–79. doi:10.1111/nyas.13360

Guan, Q., and Zhang, J. (2017). Recent Advances: The Imbalance of Cytokines in the Pathogenesis of Inflammatory Bowel Disease. *Mediators Inflamm.* 2017, 4810258. doi:10.1155/2017/4810258

Guttman, J. A., Li, Y., Wickham, M. E., Deng, W., Vogl, A. W., and Finlay, B. B. (2006). Attaching and Effacing Pathogen-Induced Tight junction Disruption *In Vivo*. *Cell. Microbiol.* 8, 634–645. doi:10.1111/j.1462-5822.2005.00656.x

Hagen, S. J. (2017). Non-canonical Functions of Claudin Proteins: Beyond the Regulation of Cell-Cell Adhesions. *Tissue Barriers* 5, e1327839. doi:10.1080/21688370.2017.1327839

Ikari, A., Watanabe, R., Sato, T., Taga, S., Shimobaba, S., Yamaguchi, M., et al. (2014). Nuclear Distribution of Claudin-2 Increases Cell Proliferation in Human Lung Adenocarcinoma Cells. *Biochim. Biophys. Acta* 1843, 2079–2088. doi:10.1016/j.bbamcr.2014.05.017

Jung, C., Hugot, J.-P., and Barreau, F. (2010). Peyer's Patches: The Immune Sensors of the Intestine. *Int. J. Inflam.* 2010, 1–12. doi:10.4061/2010/823710

Keita, Å. V., Lindqvist, C. M., Öst, Å., Magana, C. D. L., Schoultz, I., and Halfvarson, J. (2018). Gut Barrier Dysfunction-A Primary Defect in Twins with Crohn's Disease Predominantly Caused by Genetic Predisposition. *J. Crohns Colitis* 12, 1200–1209. doi:10.1093/ecco-jcc/jjy045

Kempski, J., Brockmann, L., Gagliani, N., and Huber, S. (2017). TH17 Cell and Epithelial Cell Crosstalk during Inflammatory Bowel Disease and Carcinogenesis. *Front. Immunol.* 8, 1373. doi:10.3389/fimmu.2017.01373

Kinugasa, T., Sakaguchi, T., Gu, X., and Reinecker, H. C. (2000). Claudins Regulate the Intestinal Barrier in Response to Immune Mediators. *Gastroenterology* 118, 1001–1011. doi:10.1016/S0016-5085(00)70351-9

Komarova, Y. A., Kruse, K., Mehta, D., and Malik, A. B. (2017). Protein Interactions at Endothelial Junctions and Signaling Mechanisms Regulating Endothelial Permeability. *Circ. Res.* 120, 179–206. doi:10.1161/CIRCRESAHA.116.306534

Kreher, C. R., Dittrich, M. T., Guerkov, R., Boehm, B. O., and Tary-Lehmann, M. (2003). CD4+ and CD8+ Cells in Cryopreserved Human PBMC Maintain Full Functionality in Cytokine ELISPOT Assays. *J. Immunol. Methods* 278, 79–93. doi:10.1016/S0022-1759(03)00226-6

Kucharzik, T., Walsh, S. V., Chen, J., Parkos, C. A., and Nusrat, A. (2001). Neutrophil Transmigration in Inflammatory Bowel Disease Is Associated with Differential Expression of Epithelial Intercellular junction Proteins. *Am. J. Pathol.* 159, 2001–2009. doi:10.1016/S0002-9440(10)63051-9

Laroux, F. S., Norris, H. H., Houghton, J., Pavlick, K. P., Bharwani, S., Merrill, D. M., et al. (2004). Regulation of Chronic Colitis in Athymic Nu/nu (Nude) Mice. *Int. Immunol.* 16, 77–89. doi:10.1093/intimm/dxh006

Lee, B., Moon, K. M., and Kim, C. Y. (2018). Tight junction in the Intestinal Epithelium: Its Association with Diseases and Regulation by Phytochemicals. *J. Immunol. Res.* 2018, 2645465. doi:10.1155/2018/2645465

Lu, Z., Ding, L., Lu, Q., and Chen, Y. H. (2013). Claudins in Intestines: Distribution and Functional Significance in Health and Diseases. *Tissue Barriers* 1, e24978. doi:10.4161/tisb.24978

Luissint, A. C., Parkos, C. A., and Nusrat, A. (2016). Inflammation and the Intestinal Barrier: Leukocyte-Epithelial Cell Interactions, Cell Junction Remodeling, and Mucosal Repair. *Gastroenterology* 151, 616–632. doi:10.1053/j.gastro.2016.07.008

Lyons, J., Ghazi, P. C., Starchenko, A., Tovaglieri, A., Baldwin, K. R., Poulin, E. J., et al. (2018). The Colonic Epithelium Plays an Active Role in Promoting Colitis by Shaping the Tissue Cytokine Profile. *Plos Biol.* 16, e2002417. doi:10.1371/journal.pbio.2002417

Mah, A. T., Yan, K. S., and Kuo, C. J. (2016). Wnt Pathway Regulation of Intestinal Stem Cells. *J. Physiol.* 594, 4837–4847. doi:10.1113/JP271754

Mankertz, J., Hillenbrand, B., Tavalali, S., Huber, O., Fromm, M., and Schulzke, J. D. (2004). Functional Crosstalk between Wnt Signaling and Cdx-Related Transcriptional Activation in the Regulation of the Claudin-2 Promoter Activity. *Biochem. Biophys. Res. Commun.* 314, 1001–1007. doi:10.1016/j.bbrc.2003.12.185

Mars, L. T., Araujo, L., Kerschen, P., Diem, S., Bourgeois, E., Van, L. P., et al. (2009). Invariant NKT Cells Inhibit Development of the T_H17 Lineage. *Proc. Natl. Acad. Sci. U. S. A.* 106, 6238–6243. doi:10.1073/pnas.0809317106

Mennigen, R., Nolte, K., Rijcken, E., Utech, M., Loeffler, B., Senninger, N., et al. (2009). Probiotic Mixture VSL#3 Protects the Epithelial Barrier by Maintaining Tight junction Protein Expression and Preventing Apoptosis in a Murine Model of Colitis. *Am. J. Physiol. Gastrointest. Liver Physiol.* 296, G1140–G1149. doi:10.1152/ajpgi.90534.2008

Mezheyeuski, A., Strell, C., Hrynchyk, I., Guren, T. K., Dragomir, A., Doroshenko, T., et al. (2018). Treatment-related Survival Associations of Claudin-2 Expression in Fibroblasts of Colorectal Cancer. *Virchows Arch.* 472, 395–405. doi:10.1007/s00428-017-2263-3

Naini, B. V., and Cortina, G. (2012). A Histopathologic Scoring System as a Tool for Standardized Reporting of Chronic (Ileo)colitis and Independent Risk Assessment for Inflammatory Bowel Disease. *Hum. Pathol.* 43, 2187–2196. doi:10.1016/j.humpath.2012.03.008

Nakamura, Y., Kimura, S., and Hase, K. (2018). M Cell-dependent Antigen Uptake on Follicle-Associated Epithelium for Mucosal Immune Surveillance. *Inflamm. Regen.* 38, 15. doi:10.1186/s41232-018-0072-y

Ng, S. C., Shi, H. Y., Hamidi, N., Underwood, F. E., Tang, W., Benchimol, E. I., et al. (2017). Worldwide Incidence and Prevalence of Inflammatory Bowel Disease in the 21st century: a Systematic Review of Population-Based Studies. *Lancet* 390, 2769–2778. doi:10.1016/S0140-6736(17)32448-0

Nishitani, Y., Tanoue, T., Yamada, K., Ishida, T., Yoshida, M., Azuma, T., et al. (2009). Lactococcus Lactis Subsp. Cremoris FC Alleviates Symptoms of Colitis Induced by Dextran Sulfate Sodium in Mice. *Int. Immunopharmacol.* 9, 1444–1451. doi:10.1016/j.intimp.2009.08.018

Oshima, T., Miwa, H., and Joh, T. (2008). Changes in the Expression of Claudins in Active Ulcerative Colitis. *J. Gastroenterol. Hepatol.* 23 (2), S146–S150. doi:10.1111/j.1440-1746.2008.05405.x

Pfeiffer, F., Kumar, V., Butz, S., Vestweber, D., Imhof, B. A., Stein, J. V., et al. (2008). Distinct Molecular Composition of Blood and Lymphatic Vascular Endothelial Cell Junctions Establishes Specific Functional Barriers within the Peripheral Lymph Node. *Eur. J. Immunol.* 38, 2142–2155. doi:10.1002/eji.200838140

Pickert, G., Neufert, C., Leppkes, M., Zheng, Y., Wittkopf, N., Warntjen, M., et al. (2009). STAT3 Links IL-22 Signaling in Intestinal Epithelial Cells to Mucosal Wound Healing. *J. Exp. Med.* 206, 1465–1472. doi:10.1084/jem.20082683

Pope, J. L., Bhat, A. A., Sharma, A., Ahmad, R., Krishnan, M., Washington, M. K., et al. (2014). Claudin-1 Regulates Intestinal Epithelial Homeostasis through the Modulation of Notch-Signalling. *Gut* 63, 622–634. doi:10.1136/gutjnl-2012-304241

Prasad, S., Mingrino, R., Kaukinen, K., Hayes, K. L., Powell, R. M., MacDonald, T. T., et al. (2005). Inflammatory Processes Have Differential Effects on Claudins 2, 3 and 4 in Colonic Epithelial Cells. *Lab. Invest.* 85, 1139–1162. doi:10.1038/labinvest.3700316

Ramos, G. P., and Papadakis, K. A. (2019). Mechanisms of Disease: Inflammatory Bowel Diseases. *Mayo Clin. Proc.* 94, 155–165. doi:10.1016/j.mayocp.2018.09.013

Rescigno, M., Urbano, M., Valzasina, B., Francolini, M., Rotta, G., Bonasio, R., et al. (2001). Dendritic Cells Express Tight junction Proteins and Penetrate Gut Epithelial Monolayers to Sample Bacteria. *Nat. Immunol.* 2, 361–367. doi:10.1038/86373

Su, L., Nalle, S. C., Shen, L., Turner, E. S., Singh, G., Breskin, L. A., et al. (2013). TNFR2 Activates MLCK-dependent Tight junction Dysregulation to Cause Apoptosis-Mediated Barrier Loss and Experimental Colitis. *Gastroenterology* 145, 407–415. doi:10.1053/j.gastro.2013.04.011

Tamagawa, H., Takahashi, I., Furuse, M., Yoshitake-Kitano, Y., Tsukita, S., Ito, T., et al. (2003). Characteristics of Claudin Expression in Follicle-Associated Epithelium of Peyer's Patches: Preferential Localization of Claudin-4 at the apex of the Dome Region. *Lab. Invest.* 83, 1045–1053. doi:10.1097/01.LAB.0000078741.55670.6E

Timmermans, W. M., van Laar, J. A., van Hagen, P. M., and van Zelm, M. C. (2016). Immunopathogenesis of Granulomas in Chronic Autoinflammatory Diseases. *Clin. Transl Immunol.* 5, e118. doi:10.1038/cti.2016.75

Tokuhara, Y., Morinishi, T., Matsunaga, T., Sakai, M., Sakai, T., Ohsaki, H., et al. (2017). Nuclear Expression of Claudin-3 in Human Colorectal Adenocarcinoma Cell Lines and Tissues. *Oncol. Lett.* 15, 99–108. doi:10.3892/ol.2017.7281

Torres-Martínez, A. C., Gallardo-Vera, J. F., Lara-Holguin, A. N., Montaño, L. F., and Rendón-Huerta, E. P. (2017). Claudin-6 Enhances Cell Invasiveness through Claudin-1 in AGS Human Adenocarcinoma Gastric Cancer Cells. *Exp. Cel Res.* 350, 226–235. doi:10.1016/j.yexcr.2016.11.025

Van den Bossche, J., Laoui, D., Morias, Y., Movahedi, K., Raes, G., de Baetselier, P., et al. (2012). Claudin-1, Claudin-2 and Claudin-11 Genes Differentially Associate with Distinct Types of Anti-inflammatory Macrophages *In Vitro* and with Parasite- and Tumour-Elicited Macrophages *In Vivo*. *Scand. J. Immunol.* 75, 588–598. doi:10.1111/j.1365-3083.2012.02689.x

VanDussen, K. L., Carulli, A. J., Keeley, T. M., Patel, S. R., Puthoff, B. J., Magness, S. T., et al. (2012). Notch Signaling Modulates Proliferation and Differentiation of Intestinal Crypt Base Columnar Stem Cells. *Development* 139, 488–497. doi:10.1242/dev.070763

Weber, C. R., Raleigh, D. R., Su, L., Shen, L., Sullivan, E. A., Wang, Y., et al. (2010). Epithelial Myosin Light Chain Kinase Activation Induces Mucosal Interleukin-

13 Expression to Alter Tight junction Ion Selectivity. *J. Biol. Chem.* 285, 12037–12046. doi:10.1074/jbc.M109.064808

Yan-Hong, L., Rosenstein, A., Colombel, J. F., and Bian, Z. X. (2018). A Characterization of Pro-inflammatory Cytokines in Dextran Sulfate Sodium-Induced Chronic Relapsing Colitis Mice Model. *Int. Immunopharmacol.* 60, 194–201. doi:10.1016/j.intimp.2018.05.001

Zhu, L., Han, J., Li, L., Wang, Y., Li, Y., and Zhang, S. (2019). Claudin Family Participates in the Pathogenesis of Inflammatory Bowel Diseases and Colitis-Associated Colorectal Cancer. *Front. Immunol.* 10, 1441. doi:10.3389/fimmu.2019.01441

Conflict of Interest: SČ, MA, AO, DS-P, APG, BH, MDK, SM, LP, IZ, DP, IG, MBo, and VEH have been employed by Fidelta d.o.o.

The remaining authors declare that the research was conducted in the absence of any commercial or financial relationships that could be construed as a potential conflict of interest.

Publisher's Note: All claims expressed in this article are solely those of the authors and do not necessarily represent those of their affiliated organizations, or those of the publisher, the editors and the reviewers. Any product that may be evaluated in this article, or claim that may be made by its manufacturer, is not guaranteed or endorsed by the publisher.

frontiers in Pharmacology

ORIGINAL RESEARCH
published: 13 December 2021
doi: 10.3389/fphar.2021.718147

Stable Gastric Pentadecapeptide BPC 157 Therapy for Primary Abdominal Compartment Syndrome in Rats

Marijan Tepes[1,2,3,4], Slaven Gojkovic[4], Ivan Krezic[4], Helena Zizek[4], Hrvoje Vranes[4], Zrinko Madzar[5], Goran Santak[6], Lovorka Batelja[7], Marija Milavic[7], Suncana Sikiric[7], Ivica Kocman[4], Karol Simonji[8], Mariam Samara[4], Mario Knezevic[4], Ivan Barisic[4], Eva Lovric[7], Sanja Strbe[4], Antonio Kokot[9], Ivica Sjekavica[10], Toni Kolak[11], Anita Skrtic[7], Sven Seiwerth[7], Alenka Boban Blagaic[4] and Predrag Sikiric[4]**

[1]Department of Surgery, General Hospital Nasice, Nasice, Croatia, [2]Department of Clinical Medicine, Faculty of Dental Medicine and Health Osijek, Osijek, Croatia, [3]PhD Program Translational Research in Biomedicine—TRIBE, School of Medicine, University of Split, Split, Croatia, [4]Department of Pharmacology, School of Medicine, University of Zagreb, Zagreb, Croatia, [5]Clinical Department of Surgery, Sestre Milosrdnice University Hospital Center, Zagreb, Croatia, [6]Department of Surgery, Faculty of Medicine, University of Osijek, Osijek, Croatia, [7]Department of Pathology, School of Medicine, University of Zagreb, Zagreb, Croatia, [8]Internal Diseases Clinic, Faculty of Veterinary Medicine Zagreb, Zagreb, Croatia, [9]Department of Anatomy and Neuroscience, Faculty of Medicine, J.J. Strossmayer University of Osijek, Osijek, Croatia, [10]Department of Diagnostic and Interventional Radiology, University Hospital Centre, Zagreb, Croatia, [11]Department of Surgery, School of Medicine, University of Zagreb, Zagreb, Croatia

OPEN ACCESS

Edited by:
Fan Jiang,
Shandong University, China

Reviewed by:
Dechang Chen,
Shanghai Jiao Tong University, China
Ying Li,
Xi'an Jiaotong University, China

***Correspondence:**
Predrag Sikiric
sikiric@mef.hr
Anita Skrtic
skrtic.anita@gmail.com

Specialty section:
This article was submitted to Translational Pharmacology, a section of the journal Frontiers in Pharmacology

Received: *09 June 2021*
Accepted: *17 November 2021*
Published: *13 December 2021*

Citation:
Tepes M, Gojkovic S, Krezic I, Zizek H, Vranes H, Madzar Z, Santak G, Batelja L, Milavic M, Sikiric S, Kocman I, Simonji K, Samara M, Knezevic M, Barisic I, Lovric E, Strbe S, Kokot A, Sjekavica I, Kolak T, Skrtic A, Seiwerth S, Boban Blagaic A and Sikiric P (2021) Stable Gastric Pentadecapeptide BPC 157 Therapy for Primary Abdominal Compartment Syndrome in Rats. Front. Pharmacol. 12:718147. doi: 10.3389/fphar.2021.718147

Recently, the stable gastric pentadecapeptide BPC 157 was shown to counteract major vessel occlusion syndromes, i.e., peripheral and/or central occlusion, while activating particular collateral pathways. We induced abdominal compartment syndrome (intra-abdominal pressure in thiopental-anesthetized rats at 25 mmHg (60 min), 30 mmHg (30 min), 40 mmHg (30 min), and 50 mmHg (15 min) and in esketamine-anesthetized rats (25 mmHg for 120 min)) as a model of multiple occlusion syndrome. By improving the function of the venous system with BPC 157, we reversed the chain of harmful events. Rats with intra-abdominal hypertension (grade III, grade IV) received BPC 157 (10 μg or 10 ng/kg sc) or saline (5 ml) after 10 min. BPC 157 administration recovered the azygos vein via the inferior–superior caval vein rescue pathway. Additionally, intracranial (superior sagittal sinus), portal, and caval hypertension and aortal hypotension were reduced, as were the grossly congested stomach and major hemorrhagic lesions, brain swelling, venous and arterial thrombosis, congested inferior caval and superior mesenteric veins, and collapsed azygos vein; thus, the failed collateral pathway was fully recovered. Severe ECG disturbances (i.e., severe bradycardia and ST-elevation until asystole) were also reversed. Microscopically, transmural hyperemia of the gastrointestinal tract, intestinal mucosa villi reduction, crypt reduction with focal denudation of superficial epithelia, and large bowel dilatation were all inhibited. In the liver, BPC 157 reduced congestion and severe sinusoid enlargement. In the lung, a normal presentation was observed, with no alveolar membrane focal thickening and no lung congestion or edema, and severe intra-alveolar hemorrhage was absent. Moreover, severe heart congestion, subendocardial infarction, renal hemorrhage, brain edema, hemorrhage, and neural damage were prevented. In conclusion, BPC 157 cured primary abdominal compartment syndrome.

Keywords: gastric pentadecapeptide BPC 157, primary abdominal compartment syndrome, rats, brain edema, lung edema

INTRODUCTION

We suggest that abdominal compartment syndrome (Depauw et al., 2019) is a multiple occlusion syndrome. Therefore, it is thought that by improving the function of the venous system with the stable gastric pentadecapeptide BPC 157 (Vukojevic et al., 2018; Gojkovic et al., 2020; Kolovrat et al., 2020; Gojkovic et al., 2021a; Knezevic et al., 2021a; Knezevic et al., 2021a; Gojkovic et al., 2021b; Knezevic et al., 2021b; Strbe et al., 2021), the chain of harmful events in abdominal compartment syndrome can be reversed.

The stable gastric pentadecapeptide BPC 157 was chosen and tested in this study due to its beneficial effects in major vessel occlusion syndromes (Vukojevic et al., 2018; Gojkovic et al., 2020; Kolovrat et al., 2020; Gojkovic et al., 2021a; Knezevic et al., 2021a; Knezevic et al., 2021a; Gojkovic et al., 2021b; Knezevic et al., 2021b; Strbe et al., 2021) and as a prototypic cytoprotective peptide (for review, see Sikiric et al., 1993a; Sikiric et al., 2006; Sikiric et al., 2010; Sikiric et al., 2011; Sikiric et al., 2012; Sikiric et al., 2013; Sikiric et al., 2014; Sikiric et al., 2016; Sikiric et al., 2017; Sikiric et al., 2018; Sikiric et al., 2020a; Sikiric et al., 2020b; Seiwerth et al., 2014; Seiwerth et al., 2018; Seiwerth et al., 2021; Kang et al., 2018; Park et al., 2020; Gwyer et al., 2019, Vukojevic et al., 2022).

To fully model intra-abdominal hypertension syndrome (continuous intraperitoneal insufflation of ordinary air), these occlusion syndromes have been induced peripherally (Vukojevic et al., 2018; Gojkovic et al., 2020; Kolovrat et al., 2020; Knezevic et al., 2021a; Knezevic et al., 2021a; Knezevic et al., 2021b) or centrally (Gojkovic et al., 2021a) and both peripherally and centrally (Gojkovic et al., 2021b; Strbe et al., 2021). Specific occlusion syndrome induction can be performed by the occlusion of a major vein (Vukojevic et al., 2018; Gojkovic et al., 2020; Gojkovic et al., 2021a; Knezevic et al., 2021b) or an artery (Knezevic et al., 2021a), or with both artery and vein occlusion (Kolovrat et al., 2020; Knezevic et al., 2021a), or by intragastric application of absolute alcohol (Gojkovic et al., 2021b) and intraperitoneal application of lithium overdose (Strbe et al., 2021).

Considering the effects of BPC 157 therapy peripherally and centrally (Vukojevic et al., 2018; Gojkovic et al., 2020; Kolovrat et al., 2020; Gojkovic et al., 2021a; Knezevic et al., 2021a; Knezevic et al., 2021a; Gojkovic et al., 2021b; Knezevic et al., 2021b; Strbe et al., 2021), in rats with severely increased intra-abdominal pressure, i.e., primary abdominal compartment syndrome, we attempted to introduce a therapy for compressed essential vessel tributaries, both arterial and venous (peripherally and centrally), due to occluded major veins and arteries, in order to prevent the consequent noxious syndrome, both peripherally and centrally. Otherwise, intra-abdominal hypertension adversely affects many organs, such as the brain, heart, lungs, kidneys, and gastrointestinal tract (Cullen et al., 1989), progressing to lethal levels. As abdominal compartment syndrome leads to organ failure at an intra-abdominal pressure of 20 mmHg (Hunter and Damani, 2004; Hedenstierna and Larsson, 2012), to assess the degree of severity that can be treated with this therapy, higher intra-abdominal pressures of 25, 30, 40, and 50 mmHg were also used. It was found that systemic and splanchnic blood flow and afferent hepatic flow were reduced as the intra-abdominal pressure rose; i.e., liver blood flow decreased by 39% when pneumoperitoneum increased from 10 to 15 mmHg and liver ischemic injury occurred (Chen et al., 2017).

Furthermore, as an immediate effect, the abdominal, thoracic, and cranial cavities interact with each other (Depauw et al., 2019), and increased intra-abdominal pressure causes an increase in intracranial pressure (Malbrain and Wilmer, 2007; Scalea et al., 2007; Youssef et al., 2012; Chen et al., 2020). Increased intra-abdominal pressure also increases intrathoracic pressure, which is rapidly transmitted up through the venous system, thereby further increasing intracranial pressure (Malbrain and Wilmer, 2007; Scalea et al., 2007; Youssef et al., 2012; Chen et al., 2020). Thus, although not specifically indicated, these findings support the rapid improvement of venous system function as an essential common point to prevent and reverse the noxious chain of events and attenuate all harmful consequences.

Thus, it may be that maintained increased intra-abdominal pressure causes widespread dysfunction, which would be similar to the severe syndromes observed in rats with the occlusion of peripheral vessels (Vukojevic et al., 2018; Gojkovic et al., 2020; Kolovrat et al., 2020; Knezevic et al., 2021a; Knezevic et al., 2021a; Knezevic et al., 2021b) and central vessels (Gojkovic et al., 2021a) or after the intragastric application of absolute alcohol (Gojkovic et al., 2021b) and intraperitoneal application of the lithium overdose (Strbe et al., 2021). These peripheral and central deficits can include severe gastrointestinal lesions, intracranial (superior sagittal sinus) hypertension, brain swelling and lesions, portal and caval hypertension, aortic hypotension, peripheral and central thrombosis, inferior caval vein and superior mesenteric vein congestion, azygos vein failure, electrocardiogram (ECG) disturbances, and heart, lung, liver, and kidney lesions (Vukojevic et al., 2018; Gojkovic et al., 2020; Kolovrat et al., 2020; Gojkovic et al., 2021a; Knezevic et al., 2021a; Knezevic et al., 2021a; Gojkovic et al., 2021b; Knezevic et al., 2021b; Strbe et al., 2021). Syndrome development and treatment with BPC 157 have been demonstrated in a variety of procedures inducing vessel occlusion (Vukojevic et al., 2018; Gojkovic et al., 2020; Kolovrat et al., 2020; Gojkovicc et al., 2021a; Knezevic et al., 2021a; Knezevic et al., 2021a; Gojkovic et al., 2021b; Knezevic et al., 2021b; Strbe et al., 2021). These syndromes, specifically those induced by vessel occlusion and subsequently treated with BPC 157, include inferior caval vein syndrome (Vukojevic et al., 2018), Pringle maneuver ischemia, reperfusion (Kolovrat et al., 2020), Budd–Chiari syndrome (Gojkovic et al., 2020), superior sagittal sinus occlusion (Gojkovic et al., 2021a), and superior mesenteric artery and/or vein occlusion (Knezevic et al., 2021a; Knezevic et al., 2021a; Knezevic et al., 2021b). The bypassing loops appear to be reliant on the corresponding injurious occlusion and reestablish blood flow to compensate for vessel occlusion and to reduce syndrome severity (Vukojevic et al., 2018; Gojkovic et al., 2020; Kolovrat et al., 2020; Gojkovic et al., 2021a; Knezevic et al., 2021a; Knezevic et al., 2021a; Gojkovic et al., 2021b; Knezevic et al., 2021b; Strbe et al., 2021). Previously, we showed this for the left ovarian vein (i.e., inferior caval vein syndrome (Vukojevic et al., 2018)), the inferior mesenteric vein in

the portocaval shunt (Kolovrat et al., 2020), and the azygos vein in the superior-inferior caval vein shunt (Gojkovic et al., 2020; Gojkovic et al., 2021a; Gojkovic et al., 2021b; Strbe et al., 2021). More specifically, the superior mesenteric vein, inferior and superior anterior pancreaticoduodenal, pyloric vein, and portal vein in the superior mesenteric vein-portal vein shunt reestablish the interrupted superior mesenteric and portal vein pathway (the occluded end of the superior mesenteric vein) (Knezevic et al., 2021b). The inferior mesenteric artery and inferior anterior pancreaticoduodenal artery are alternative pathways in the case of an occluded superior mesenteric artery (Knezevic et al., 2021a). With simultaneous occlusion of both superior mesenteric vessels, i.e., the artery and the vein, both pathways, arterial and venous, are activated (Knezevic et al., 2021a). Centrally (para)sagittal venous collateral circulation appears with an occluded superior sagittal sinus (Gojkovic et al., 2021a). It has been theorized that BPC 157 therapy could likely represent a "bypassing key," by rapidly activating bypassing pathways and abrogating the complex syndrome induced by simultaneous occlusion of essential arterial and venous tributaries. Likewise, it has been theorized that this "bypassing key" appears to be an effect of the essential endothelial protective capacity of BPC 157. BPC 157, as a novel and relevant cytoprotective mediator, rapidly activates collateral bypassing pathways and alleviates vessel occlusion syndromes (Vukojevic et al., 2018; Gojkovic et al., 2020; Kolovrat et al., 2020; Gojkovic et al., 2021a; Knezevic et al., 2021a; Knezevic et al., 2021a; Gojkovic et al., 2021b; Knezevic et al., 2021b; Strbe et al., 2021). As such, with BPC 157 therapy, endothelial protection (as a shared effect of cytoprotective agents (Robert, 1979; Szabo et al., 1985)) and the cytoprotection theory maxim "endothelium maintenance → epithelium maintenance" (Robert, 1979; Szabo et al., 1985) may have additional significance. Namely, Robert's and Szabo's original maxim ("endothelium maintenance → epithelium maintenance") may be further promoted. Therefore, we reported evidence about blood vessel recruitment and activation ("running") toward the site of injury, also described as bypassing occlusion via alternative pathways (Vukojevic et al., 2018; Gojkovic et al., 2020; Kolovrat et al., 2020; Gojkovic et al., 2021a; Knezevic et al., 2021a; Knezevic et al., 2021a; Gojkovic et al., 2021b; Knezevic et al., 2021b; Strbe et al., 2021). Consequently, compensatory activated collateral blood vessels and reorganized blood flow following BPC 157 treatment in rats with the occluded major peripheral vessel(s) or central vessels reduced superior sagittal sinus, portal and caval hypertension, aortal hypotension, progressive venous and arterial thrombosis peripherally and centrally, and ECG disturbances. Markedly, multiple organ lesions in the heart, lung, liver, kidney, and gastrointestinal tract, in particular, as well as brain lesions, were attenuated, and oxidative stress was reduced in tissues (Vukojevic et al., 2018; Gojkovic et al., 2020; Kolovrat et al., 2020; Gojkovic et al., 2021a; Knezevic et al., 2021a; Knezevic et al., 2021a; Knezevic et al., 2021b; Strbe et al., 2021).

The many blood vessels identified as being activated by specific pathways following a given vessel injury require a regularly applicable therapy, with beneficial effects dependent on, but not limited to, occlusion of a particular vessel (Sikiric et al., 2018). With BPC 157 therapy, this point was envisaged by the consistent reduction of the whole "occlusive-like" syndrome that regularly follows the intragastric application of absolute alcohol in rats (Gojkovic et al., 2021b) and intraperitoneal application of the lithium overdose (Strbe et al., 2021). Consequently, we observed that this beneficial effect, after direct injury (permanent ligation) applied to one or two major vessels, could instantly oppose more general damage (maintained intra-abdominal hypertension, either high (grade III) or very high (grade IV)), as all blood vessels which can be compressed with increased intra-abdominal pressure. Therefore, a "bypassing key," i.e., an activated azygos vein as a rescuing pathway, avoiding both the lung and liver and also noted in Budd–Chiari syndrome (i.e., suprahepatic occlusion of the inferior caval vein) (Gojkovic et al., 2020), combines the inferior caval vein and superior caval vein via direct blood delivery. Thus, activated azygos vein shunt could reorganize blood flow and instantly attenuate the consequences of maintained high intra-abdominal pressure, both peripherally and centrally.

BPC 157s endothelial effects and its function as a "bypassing key" (Sikiric et al., 2018) are strongly supported by its interaction with the nitric oxide (NO) system (for a review, see Sikiric et al., 2014). The most recent demonstration of the impact of BPC 157 on vasomotor tone was carried out through BPC 157-specific activation of the Src-caveolin-1-endothelial NO synthase (eNOS) pathway (Hsieh et al., 2020). BPC 157 acts as a membrane stabilizer and free radical scavenger and reduces leaky gut syndrome, as shown in gastrointestinal tract cytoprotective studies (Park et al., 2020). BPC 157 also has a curative effect due to interactions with several molecular pathways (Tkalcević et al., 2007; Chang et al., 2011, 2014; Huang et al., 2015; Hsieh et al., 2017; Kang et al., 2018; Vukojevic et al., 2018; Wang et al., 2019; Cesarec et al., 2013; Hsieh et al., 2020; Park et al., 2020; Vukojevic et al., 2020; Wu et al., 2020).

Thus, we assessed BPC 157 therapy as a curative principle in rats with established permanent intra-abdominal hypertension. As confirmation, we used the crisis that occurred with the high intra-abdominal pressure-induced syndrome, in which intra-abdominal hypertension simultaneously affected all abdominal vessels and organs for a considerable period and restrained the ability to recruit alternative pathways, such that a deadly situation was created before therapy initiation.

MATERIALS AND METHODS

Animals

This study was conducted with 12-week-old, 200 g body weight, male Albino Wistar rats, randomly assigned at six rats/group/interval. Rats were bred in-house at the Animal Pharmacology Facility, School of Medicine, Zagreb, Croatia. The animal facility is registered with the Veterinary Directorate (Reg. No: HR-POK-007). Laboratory rats were acclimated for five days and randomly assigned to their respective treatment groups. Laboratory animals were housed in polycarbonate (PC) cages under conventional laboratory conditions at 20–24°C, relative humidity of

40–70%, and noise level of 60 dB. Each cage was identified with dates, number of studies, group, dose, number, and sex of each animal. Fluorescent lighting provided illumination 12 h per day. Standard good laboratory practice (GLP) diet and fresh water were provided *ad libitum*. Animal care was in compliance with standard operating procedures (SOPs) of the Animal Pharmacology Facility and the European Convention for the Protection of Vertebrate Animals used for Experimental and Other Scientific Purposes (ETS 123).

This study was approved by the local ethics committee. Ethical principles of the study complied with the European Directive 010/63/E, the Law on Amendments to the Animal Protection Act (Official Gazette 37/13), the Animal Protection Act (Official Gazette 135/06), the ordinance on the protection of animals used for scientific purposes (Official Gazette 55/13), Federation of European Laboratory Animal Science Associations (FELASA) recommendations, and the recommendations of the Ethics Committee of the School of Medicine, University of Zagreb. The experiments were assessed by observers blinded as to the treatment.

Drugs

Medication was administered as described previously (Vukojevic et al., 2018; Gojkovic et al., 2020; Kolovrat et al., 2020; Gojkovic et al., 2021a; Knezevic et al., 2021a; Knezevic et al., 2021a; Gojkovic et al., 2021b; Knezevic et al., 2021b), without the use of a carrier or peptidase inhibitor, for stable gastric pentadecapeptide BPC 157 (10 μg or 10 ng/kg subcutaneously), a partial sequence of the human gastric juice protein BPC, which is freely soluble in water at pH 7.0 and in saline. BPC 157 (GEPPPGKPADDAGLV, molecular weight 1,419; Diagen, Slovenia) was prepared as a peptide with 99% high-performance liquid chromatography (HPLC) purity, with 1-des-Gly peptide being the main impurity. The dose and application regimens were as described previously (Duzel et al., 2017; Amic et al., 2018; Drmic et al., 2018; Vukojevic et al., 2018; Sever et al., 2019; Cesar et al., 2020; Gojkovic et al., 2020; Kolovrat et al., 2020; Vukojevic et al., 2020).

Experimental Protocol

In deeply anesthetized rats (intraperitoneal (ip) injected 40 mg/kg thiopental (Rotexmedica, Germany) and 10 mg/kg diazepam (Apaurin; Krka, Slovenia)), we induced abdominal compartment syndrome by intraperitoneal insufflation of ordinary air controlled by a manual and digital manometer with a data logger connected to a computer (DD890, Dostmann Electronic GmbH, Germany) and maintained high abdominal pressure at 25 mmHg for 120 min before sacrifice, with a pressure measurement interval of 1 s. High abdominal pressure at 25, 30, 40, or 50 mmHg was maintained until sacrifice at 60 min (25 mmHg), 30 min (30 mmHg, 40 mmHg), or 15 min (50 mmHg). Rats received BPC 157 (10 μg or 10 ng/kg subcutaneously) or saline (5 ml) at 10 min abdominal compartment syndrome-time. Alternatively, using esketamine anesthesia (40 mg/kg esketamine (Rotexmedica, Germany) and 10 mg/kg diazepam (Apaurin; Krka, Slovenia) intraperitoneally), we induced abdominal compartment syndrome as described before and maintained high abdominal pressure at 25 mmHg for 120 min before sacrifice. Medication (BPC 157 (10 μg or 10 ng/kg sc) or saline (5 ml)) was given after 10 min of high abdominal pressure.

Recordings of brain swelling were performed in rats before sacrifice after complete calvariectomy was performed (Gojkovic et al., 2021a; Knezevic et al., 2021a; Knezevic et al., 2021a; Knezevic et al., 2021b). Briefly, six burr holes were drilled in three horizontal lines, all of them medially to the superior temporal lines and temporalis muscle attachments. The two rostral burr holes were placed just basal from the posterior interocular line, the two basal burr holes were placed just rostral to the lambdoid suture (and transverse sinuses) on both sides, respectively, and the two middle burr holes were placed in line between the basal and rostral burr holes.

Rats were laparatomized before sacrifice for the corresponding presentation of the peripheral vessels (azygos vein, superior mesenteric vein, portal vein, inferior caval vein, and abdominal aorta). The recording was performed with a camera attached to a VMS-004 Discovery Deluxe USB microscope (Veho, United States) at the end of the experiment and assessed as before (Gojkovic et al., 2021a; Knezevic et al., 2021a; Knezevic et al., 2021a; Knezevic et al., 2021b; Strbe et al., 2021).

Superior Sagittal Sinus, Portal, Superior Mesenteric, and Caval Vein, and Abdominal Aorta Pressure Recording

As described before (Vukojevic et al., 2018; Gojkovic et al., 2020; Kolovrat et al., 2020; Gojkovic et al., 2021a; Knezevic et al., 2021a; Knezevic et al., 2021a; Gojkovic et al., 2021b; Knezevic et al., 2021b; Strbe et al., 2021), recordings were made in deeply anesthetized rats with a cannula (BD Neoflon™ Cannula) connected to a pressure transducer (78534C MONITOR/TERMINAL; Hewlett Packard, United States), inserted into the portal vein, inferior caval vein, and superior sagittal sinus, as well as the abdominal aorta at the level of the bifurcation at 15, 30, 60, or 120 min ACS-time. For superior sagittal sinus pressure recording, we made a single burr hole in the rostral part of the sagittal suture, above the superior sagittal sinus, and cannulated the superior sagittal sinus anterior part using a Braun intravenous cannula; then, we laparatomized the rat for portal vein, inferior vena cava, and abdominal aorta pressure recording.

Notably, normal rats exhibited a superior sagittal sinus pressure of −24 to −27 mmHg and superior mesenteric pressure and portal pressure of 3–5 mmHg similar to that of the inferior vena cava, though with values at least 1 mmHg higher in the portal vein. By contrast, abdominal aorta blood pressure values were 100–120 mm Hg at the level of the bifurcation (Vukojevic et al., 2018; Gojkovic et al., 2020; Kolovrat et al., 2020; Gojkovic et al., 2021a; Knezevic et al., 2021a; Knezevic et al., 2021a; Gojkovic et al., 2021b; Knezevic et al., 2021b; Strbe et al., 2021).

ECG Recording

ECGs were recorded continuously in deeply anesthetized rats for all three main leads, by positioning stainless steel electrodes on all four limbs using an ECG monitor with a 2090 programmer (Medtronic, United States) connected to a Waverunner LT342 digital oscilloscope (LeCroy, United States) at 30 min ligation time. This arrangement enabled precise recordings, measurements, and analysis of ECG parameters (Vukojevic et al., 2018; Gojkovic et al., 2020; Kolovrat et al., 2020; Gojkovic et al., 2021a; Knezevic et al., 2021a; Knezevic et al., 2021a; Gojkovic et al., 2021b; Knezevic et al., 2021b; Strbe et al., 2021). The time until extreme bradycardia and asystole was assessed.

Thrombus Assessment

Following sacrifice, the superior sagittal sinus and peripherally the portal vein, external jugular vein, inferior caval vein, superior mesenteric vein, hepatic vein, superior mesenteric artery, hepatic artery, and abdominal aorta were removed from the rats, and the clots were weighed (Vukojevic et al., 2018; Gojkovic et al., 2020; Kolovrat et al., 2020; Gojkovic et al., 2021a; Knezevic et al., 2021a; Knezevic et al., 2021a; Gojkovic et al., 2021b; Knezevic et al., 2021b; Strbe et al., 2021).

Brain Volume and Vessel Presentation

Brain volume and vessel presentation were proportional to the change in the brain or vessel surface area. The presentation of the brain and peripheral vessels (superior mesenteric vein, portal vein, inferior caval vein, azygos vein, and abdominal aorta) was recorded in deeply anesthetized rats, with a camera attached to a VMS-004 Discovery Deluxe USB microscope (Veho, United States) (Gojkovic et al., 2021a; Knezevic et al., 2021a; Knezevic et al., 2021a; Gojkovic et al., 2021b; Knezevic et al., 2021b; Strbe et al., 2021). The border of the brain in the image was marked using ImageJ software and then the surface area of the brain was measured. This was done with brain images for both the control (saline) group and treated (BPC 157) group of rats at same intervals after the application and at the time of sacrifice. The arithmetic mean of the surface areas was calculated for both groups. Then, the ratio of these two areas was calculated as $(\frac{A_{con}}{A_{bpc}})$, where A_{con} is the arithmetic mean brain area of the control group and A_{bpc} is the arithmetic mean brain area of the treated group. Starting from the square-cube law equations *[1] [2]*, an equation for the change in brain volume proportional to the change in brain surface area *[6]* was derived. In expressions [*1–5*], *l* is defined as any arbitrary one-dimensional length of the brain (for example, rostrocaudal length of the brain), used only for defining the one-dimensional proportion (l_2/l_1) between two observed brains and as an inter-factor (and because of that not measured *[6]*) for deriving final expression *[6]*. The procedure was as follows: $A_2 = A_1 \times (\frac{l_2}{l_1})^2$ *[1]* (square-cube law), $V_2 = V_1 \times (\frac{l_2}{l_1})^3$ *[2]* (square-cube law), $\frac{A_2}{A_1} = (\frac{l_2}{l_1})^2$ [3] (from [1], after dividing both sides by A_1), $\frac{l_2}{l_1} = \sqrt{\frac{A_2}{A_1}}$ *[4]* (from *[3]*, after taking the square root of both sides), $\frac{V_2}{V_1} = (\frac{l_2}{l_1})^3$ *[5]* (from *[2]*, after dividing both sides by V_1), and $\frac{V_2}{V_1} = (\sqrt{\frac{A_2}{A_1}})^3$ *[6]* (after incorporating expression *[4]* into equation *[5]*).

Gross Assessment of Gastrointestinal Lesions

A camera attached to a VMS-004 Discovery Deluxe USB microscope (Veho, United States) was used for recording. In deeply anesthetized rats, laparatomized before sacrifice, we assessed the gross lesions in the gastrointestinal tract and in the stomach (sum of the longest diameters, mm) (Gojkovic et al., 2020; Kolovrat et al., 2020; Gojkovic et al., 2021a; Knezevic et al., 2021a; Knezevic et al., 2021a; Gojkovic et al., 2021b; Knezevic et al., 2021b; Strbe et al., 2021).

Liver and Spleen Weights

Liver and spleen weights are expressed as a percentage of total body weight (for normal rats, liver, 3.2–4.0%; spleen, 0.20–0.26%).

MICROSCOPY

From rats, at end of the experiment, the brain, liver, kidney, stomach, duodenum, jejunum, colon, rectum, lungs, and heart were fixed in 10% neutral buffered formalin (pH 7.4) at room temperature for 24 h. Representative tissue specimens were embedded in paraffin, sectioned at 4 μm, stained with hematoxylin and eosin (H&E), and evaluated by light microscopy using an Olympus 71 digital camera and an Olympus BX51 microscope (Japan) acquiring digital images saved as uncompressed 24-bit RGB TIFF files.

Analysis of Central Nervous System Karyopyknotic Cells

Modified Bielschowsky's silver staining and Klüver–Barrera staining (using Klüver–Barrera Luxol fast blue) were performed to demonstrate argentophilic neurites, axonal spheroids, and neuronal cell bodies, particularly in brain karyopyknotic areas (https://journals.sagepub.com/doi/pdf/10.1038/jcbfm.1995.128) (file:///F:/ACS%20manuscript/CVI_rat_phd_nedergaard1987.pdf).

The brain was dissected according to NTP-7 at Levels 3 and 6 with neuroanatomic subsites presented in certain brain sections using coronal sections with three mandatory sections (Eustis et al., 2017; Gojkovic et al., 2021a; Knezevic et al., 2021a; Knezevic et al., 2021a; Gojkovic et al., 2021b; Knezevic et al., 2021b; Strbe et al., 2021) and analyzed using a semiquantitative neuropathological scoring system, as previously described (Bona et al., 1998; Gojkovic et al., 2021a; Knezevic et al., 2021a; Knezevic et al., 2021a; Gojkovic et al., 2021b; Knezevic et al., 2021b; Strbe et al., 2021), the and combined score (0–8) = the sum of the analyzed affected areas (0–4) and karyopyknotic cells in the brain areas (0–4), as follows. Specifically, analyzed were the affected brain areas (0–4), cerebral (NTP-7, Level 3), cerebellar cortex

(NTP-7, Level 6), and hippocampus, thalamus, and hypothalamus (NTP-7, Level 3) as follows (score 0 indicates no histopathologic change): score 1: small, patchy, complete, or incomplete infarcts (≤10% of the area affected); score 2: partly confluent or incomplete infarcts (20–30% of the area affected); score 3: large confluent complete infarcts (40–60% of the area affected); score 4: in cortex total disintegration of the tissue and the hypothalamus, thalamus, and hippocampus large complete infarcts (˃75% of the area affected). Analyzed were karyopyknotic cells in the affected brain areas (0–4), cerebral (NTP-7, Level 3), cerebellar cortex (NTP-7, Level 6), and hippocampus, thalamus, and hypothalamus (NTP-7, Level 3) as follows (score 0 indicates no change): score 1: a few karyopyknotic of neuronal cells (≤20%); score 2: patchy areas of karyopyknotic cells (50%); score 3: more extensive karyopyknotic areas (75%); score 4: complete infarction (100%).

The neuronal pathological changes were also observed in the acquired digital images saved as uncompressed 24-bit RGB TIFF files in the software program AnalySIS (Olympus Soft Imaging System GmbH, Münster, Germany) performing quantitative analysis of neuronal damage in the karyopyknotic areas. The neurons of the cortical cerebral, cerebellar region, hippocampus, and hypothalamus were counted in 10 different high-powered fields (HPF, 400x) and 3 to 5 serial sections of each sample were used to do the count as described in https://www.ncbi.nlm.nih.gov/pmc/articles/PMC5303860/. The field size was 0.24 μm^2.

Lung histology. A scoring system was used to grade the degree of lung injury in lung tissue analysis (Gojkovic et al., 2021a; Knezevic et al., 2021a; Knezevic et al., 2021a; Gojkovic et al., 2021b; Knezevic et al., 2021b). Features included focal thickening of the alveolar membranes, congestion, pulmonary edema, intra-alveolar hemorrhage, interstitial neutrophil infiltration, and intra-alveolar neutrophil infiltration. Each feature was assigned a score from 0 to 3 based on its absence (0) or presence to a mild (1), moderate (2), or severe (3) degree, and a final histology score was determined (Murao et al., 2003).

Renal, liver, and heart histology. The criteria renal injury was based on the degeneration of Bowman's space and glomeruli, degeneration of the proximal and distal tubules, vascular congestion, and interstitial edema (Gojkovic et al., 2021a; Knezevic et al., 2021a; Knezevic et al., 2021a; Gojkovic et al., 2021b; Knezevic et al., 2021b; Strbe et al., 2021). The criteria for liver injury were vacuolization of hepatocytes and pyknotic hepatocyte nuclei, activation of Kupffer cells, and enlargement of sinusoids. Each specimen was scored using a scale ranging 0–3 (0: none; 1: mild; 2: moderate; 3: severe) for each criterion, and a final histology score was determined (Ibrahim, et al., 2010; Gojkovic et al., 2021a; Gojkovic et al., 2021b; Knezevic et al., 2021a; Knezevic et al., 2021b; Knezevic et al., 2021a; Strbe et al., 2021). Cardiac lesion estimation was based on the dilatation and congestion of blood vessels within the myocardium and coronary arteries using a scale ranging 0–3 (0: none; 1: mild; 2: moderate; 3: severe) (Gojkovic et al., 2021a; Knezevic et al., 2021a; Knezevic et al., 2021a; Gojkovic et al., 2021b; Knezevic et al., 2021b; Strbe et al., 2021).

Gastrointestinal histology. As previously described (Gojkovic et al., 2020; Kolovrat et al., 2020; Gojkovic et al., 2021a; Knezevic et al., 2021a; Knezevic et al., 2021a; Gojkovic et al., 2021b; Knezevic et al., 2021b; Strbe et al., 2021), intestinal tissue damage was analyzed using a histologic scoring scale adapted from Chui and coworkers (Chui et al., 1970) on a scale of 0–5 (normal to severe) in three categories (mucosal injury, inflammation, and hyperemia/hemorrhage) for a total score of 0–15, as described by Lane and coworkers (Lane et al., 1997). Morphologic features of mucosal injury were based on different grades of epithelial lifting, villi denudation, and necrosis; grades of inflammation were graded from focal to diffuse according to lamina propria infiltration or subendothelial infiltration; hyperemia/hemorrhage was graded from focal to diffuse according to lamina propria or subendothelial localization. In addition, the villi height was assessed as well (normal villi height as indicated before (Sever et al., 2009; Teshfam et al., 2010)).

Statistical Analysis

Statistical analysis was performed by parametric one-way analysis of variance (ANOVA), with the Newman–Keuls *post hoc* test or the non-parametric Kruskal–Wallis test and subsequently the Mann–Whitney *U* test to compare groups. Values are presented as the mean ± standard deviation (SD) and as the minimum/median/maximum. To compare the frequency difference between groups, the chi-squared test or Fischer's exact test was used. $p < 0.05$ was considered statistically significant.

RESULTS

We revealed that, despite permanently increased intra-abdominal hypertension (grade III and grade IV), a perilous syndrome occurred peripherally and centrally, the reversal of the abdominal compartment syndrome induced by the stable gastric pentadecapeptide BPC 157 application was quite consistent. With sustained increased intra-abdominal pressures and pentadecapeptide BPC 157 application, otherwise imminent abdominal compartment syndrome (i.e., 25 mmHg or 30 mmHg, or 40 mmHg or 50 mmHg for 25, 30, and 60 min (thiopental) and for 120 min (esketamine)) did not appear. This was seen with the portal, caval, aortal, and superior sagittal sinus pressure assessment, reduced major ECG disturbances, nearly abrogated arterial and vein thrombosis, and preserved presentation of the brain, heart, lungs, liver, kidneys, and gastrointestinal tract, with no lethal outcomes despite the permanent maintenance of high intra-abdominal pressure. Both BPC 157 regimens (μg and ng) provided a similar therapeutic effect in all of the investigated protocols of abdominal compartment syndrome.

Commonly, all increased intra-abdominal pressures (i.e., 25, 30, 40, and 50 mmHg) produced a highly noxious syndrome, which occurred both peripherally and centrally. This noxious syndrome resembled the major vessel occlusion-induced syndromes (Vukojevic et al., 2018; Gojkovic et al., 2020; Kolovrat et al., 2020; Gojkovic et al., 2021a; Knezevic et al., 2021a; Knezevic et al., 2021a; Knezevic et al., 2021b) or "occlusion-like" syndromes that appear after intragastric

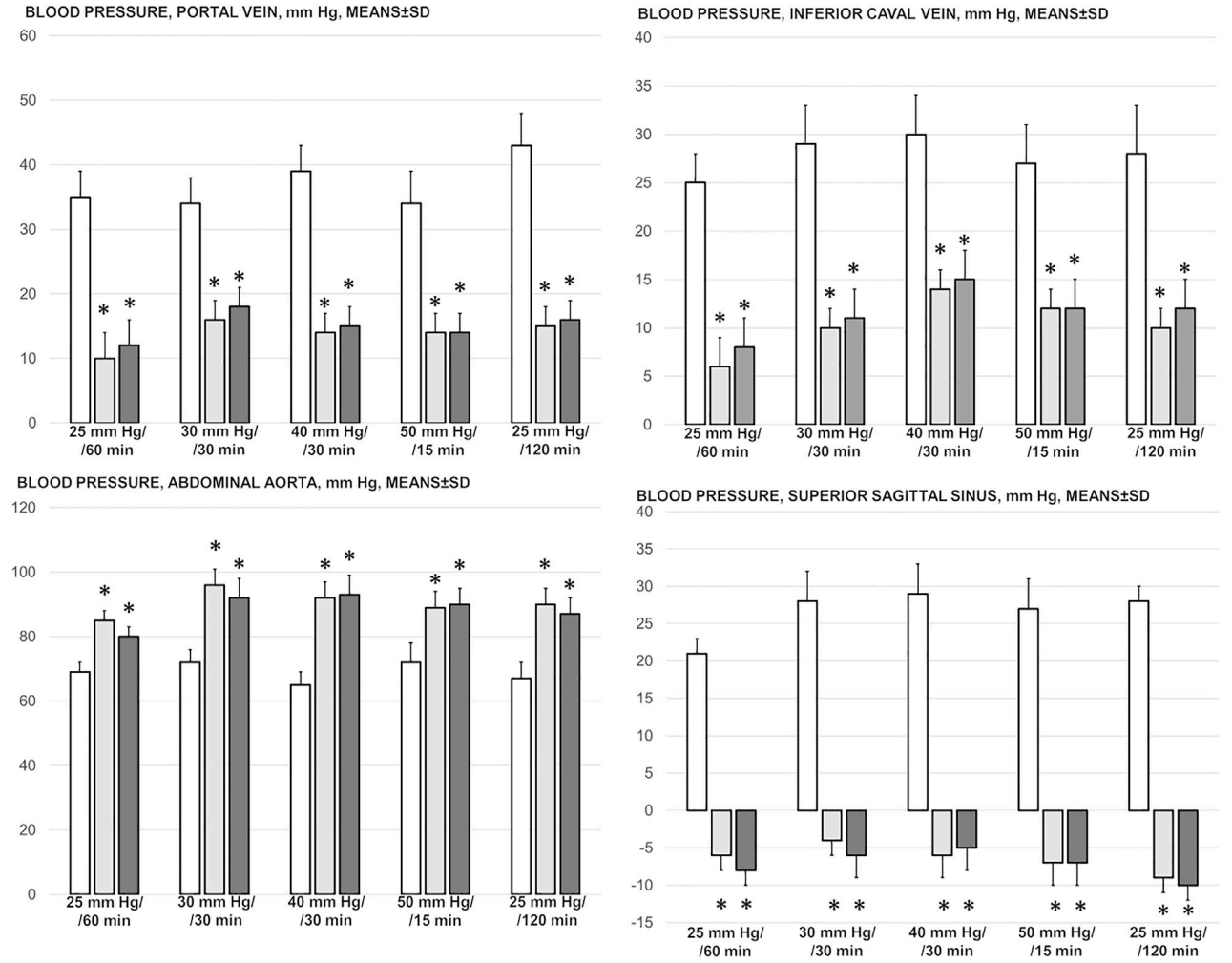

FIGURE 1 | Blood pressure, mmHg (in the superior sagittal sinus (SSS), portal vein (PV), abdominal aorta (AA), inferior caval vein (ICV)), in the thiopental-anesthetized rats with the increased intra-abdominal pressures at 50 mmHg for 25 min, at 30 mmHg or 40 mmHg for 30 min, and at 25 mmHg for 60 min increased intra-abdominal pressures-time, and in the esketamine-anesthetized rats with the increased intra-abdominal pressures at the 25 mmHg for 120 min increased intra-abdominal pressures-time, following medication (BPC 157 10 μg/kg (light gray bars), 10 ng/kg (dark gray bars); saline 5 ml/kg (white bars)) given subcutaneously at 10 min increased intra-abdominal pressures-time. Means ± SD, *P<0.05, vs. control.

application of absolute alcohol (Gojkovic et al., 2021b) and intraperitoneal application of lithium overdose (Strbe et al., 2021), in particular, similar to the acute Budd–Chiari syndrome and acute suprahepatic inferior caval vein occlusion (Gojkovic et al., 2020). Contrarily, in rats with high intra-abdominal pressure, the application of BPC 157 had a considerable therapeutic effect. For this effect, in all BPC 157-treated rats, the common key finding may be the rapidly activated azygos vein collateral pathway, which combined the inferior caval vein and left superior caval vein, to reverse the rapid presentation of this deadly syndrome.

Blood Pressure Disturbances

Perceived as a cause-consequence relation, the important evidence is that BPC 157 reduced blood pressure disturbances that were induced by increased intra-abdominal pressures, shown to be quite severe and noted peripherally (portal and caval hypertension, aortal hypotension) as well centrally (superior sagittal sinus hypertension) (**Figure 1**). The severely increased pressure values in the portal vein, inferior caval vein, and superior sagittal sinus, as well as the decreased pressure values in the abdominal aorta, were markedly attenuated with BPC 157 application.

Collateral Pathways, Blood Vessels, and Brain Gross Presentation

As a follow-up to the attenuation of blood pressure disturbances, peripherally and centrally, there was a reduction in blood stasis by activating the collateral pathway to compensate for major vessel occlusion due to mechanical compression. Consequently, there were particular effects of BPC 157 on the relative volume of the vessels and

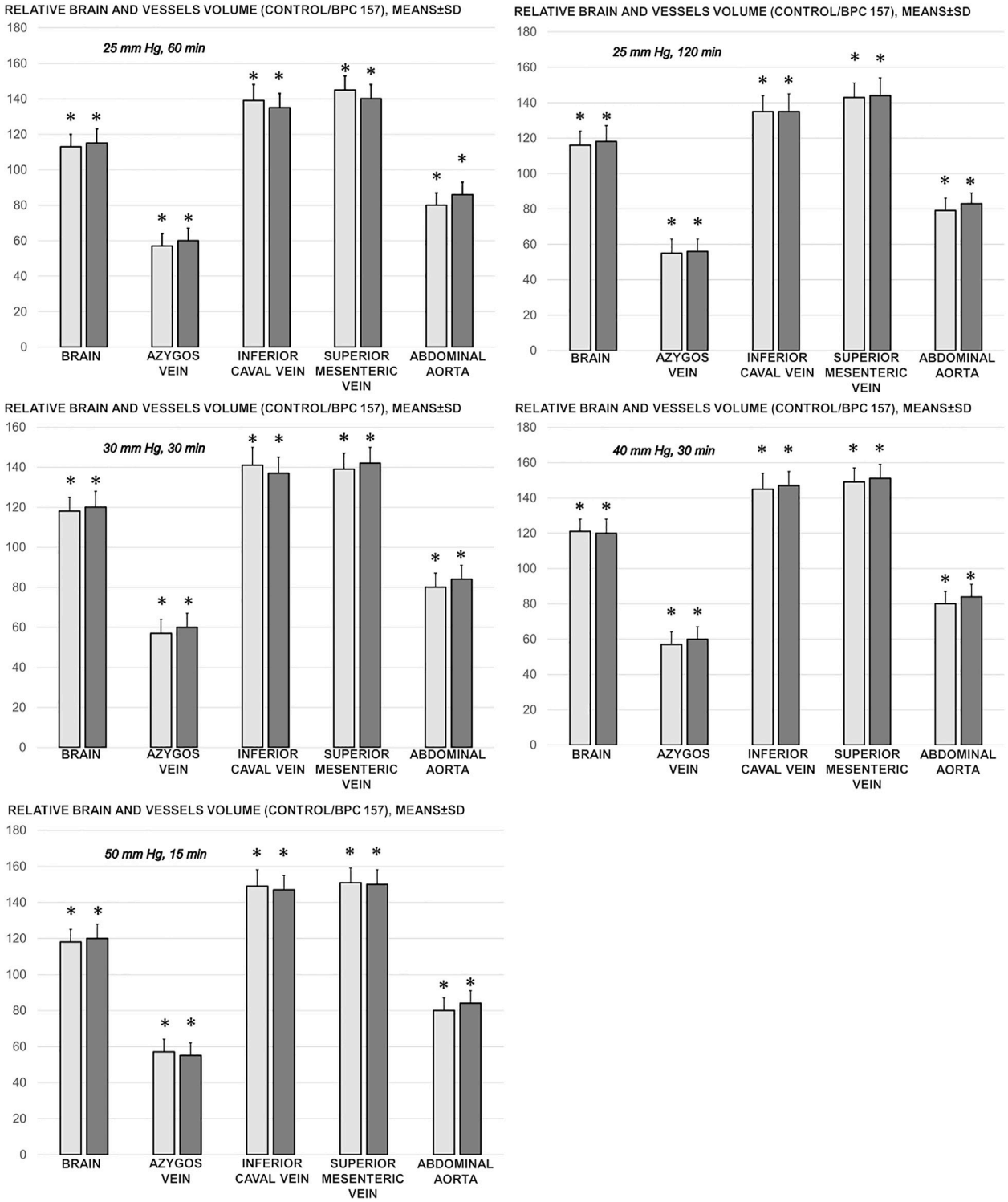

FIGURE 2 | Relative brain and vessels volume (volume control/volume BPC 157, %) in the thiopental-anesthetized rats with the increased intra-abdominal pressures at 50 mmHg for 25 min, at 30 mmHg or 40 mmHg for 30 min, and at 25 mmHg for 60 min increased intra-abdominal pressures-time, and in the esketamine-anesthetized rats with the increased intra-abdominal pressures at 25 mmHg for 120 min increased intra-abdominal pressures-time, following medication (BPC 157 10 μg/kg (light gray bars), 10 ng/kg (dark gray bars); saline 5 ml/kg (not shown, control/control as control, 100% for comparison)) given subcutaneously at 10 min increased intra-abdominal pressures-time. Means ± SD, *P˂0.05, vs. control.

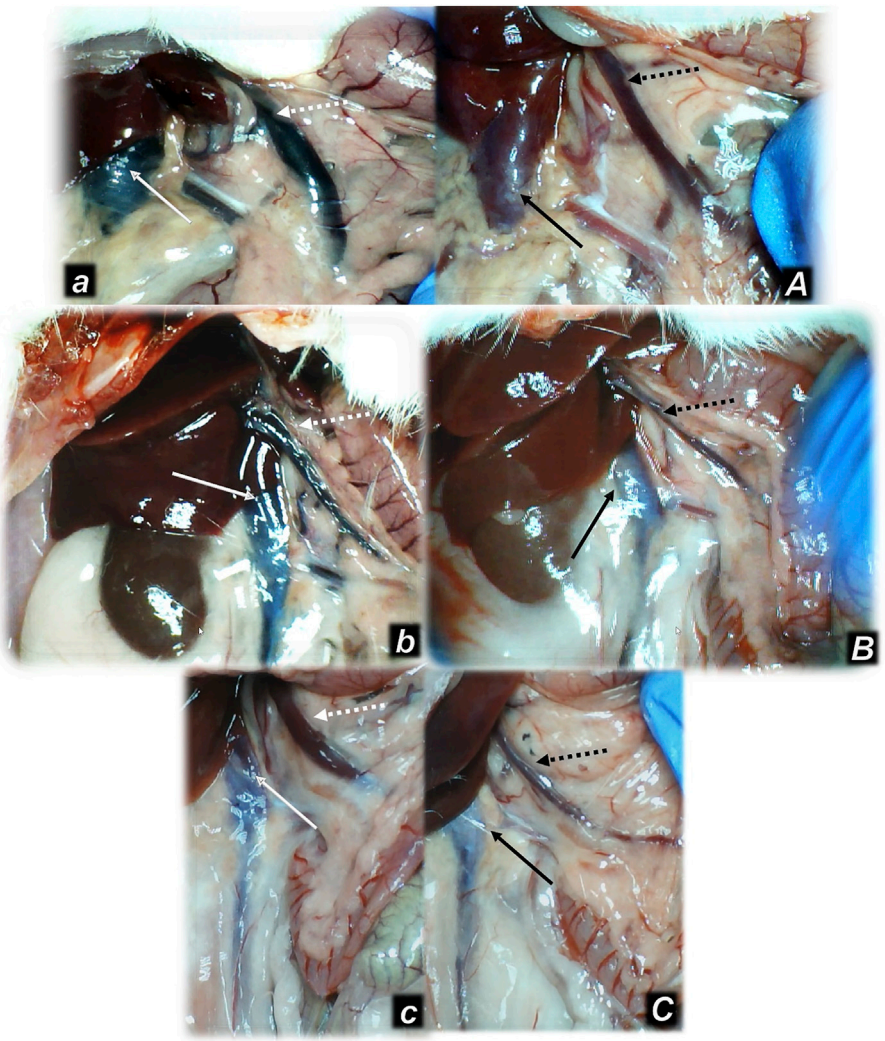

FIGURE 3 | Illustrative presentation of the inferior caval vein (full arrows) and superior mesenteric vein (dashed arrows) after the increased intraabdominal pressure and medication (sc) (saline (5 ml/kg) (white arrows, small letters, congested veins *a, b, c*) or BPC 157 (10 ng/kg) (black arrows, capitals, non-congested veins *A, B, C*): 25 mmHg (60 min) (*a, A*), 40 mmHg (30 min) (*b, B*), and 50 mmHg (30 min) (*c, C*). A camera attached to a VMS-004 Discovery Deluxe USB microscope (Veho, United States).

brain that may be indicative of the activated defensive response (**Figures 2**, **3**, **4**, **5**). BPC 157 may decrease the relative volume of the superior mesenteric vein and inferior caval vein and brain (**Figures 2**, **4**, **5**). These veins appeared congested (**Figures 3**, **4**), likely due to failed vessels and trapped blood volume (note that the liver and spleen relative weights were increased, along with hemorrhagic lesions in the stomach) (**Figures 9**, **10**) (**Figures 3**, **4**, **5**). Evidently, as a particular effect on blood vessels, congestion was reduced by activating the collateral bridging pathway, i.e., the azygos vein (**Figure 2**), as BPC 157 increased the azygos vein relative volume (**Figures 2**, **4**). In this way, BPC 157 combined the inferior caval vein and left superior caval vein to reestablish blood flow. Finally, regarding brain swelling and increased volume (associated with considerable brain injuries) (**Figures 2**, **5**), BPC 157 rapidly induced a considerable decrease toward normal brain presentation (**Figures 2**, **5**).

Thrombosis

Likewise, in the cause-consequence course of the therapy, BPC 157 reduced thrombosis, both peripherally and centrally. Without therapy, thrombosis imminently occurred along with high intra-abdominal pressure, peripherally in veins (i.e., portal vein and inferior caval vein, superior mesenteric vein, hepatic veins, and external jugular vein) and in arteries (i.e., superior mesenteric artery, hepatic artery and abdominal aorta) and centrally (i.e., superior sagittal sinus) (**Figure 6**). Note that, without therapy, while thrombosis was present in all investigated vessels, with an initial increase of 25 mm, the most prominent clots appeared in the hepatic veins. With further pressure increases (30, 40, and 50 mmHg), clot formation generally increased, and prominent clots also appeared in the portal vein and inferior caval vein and in the abdominal aorta.

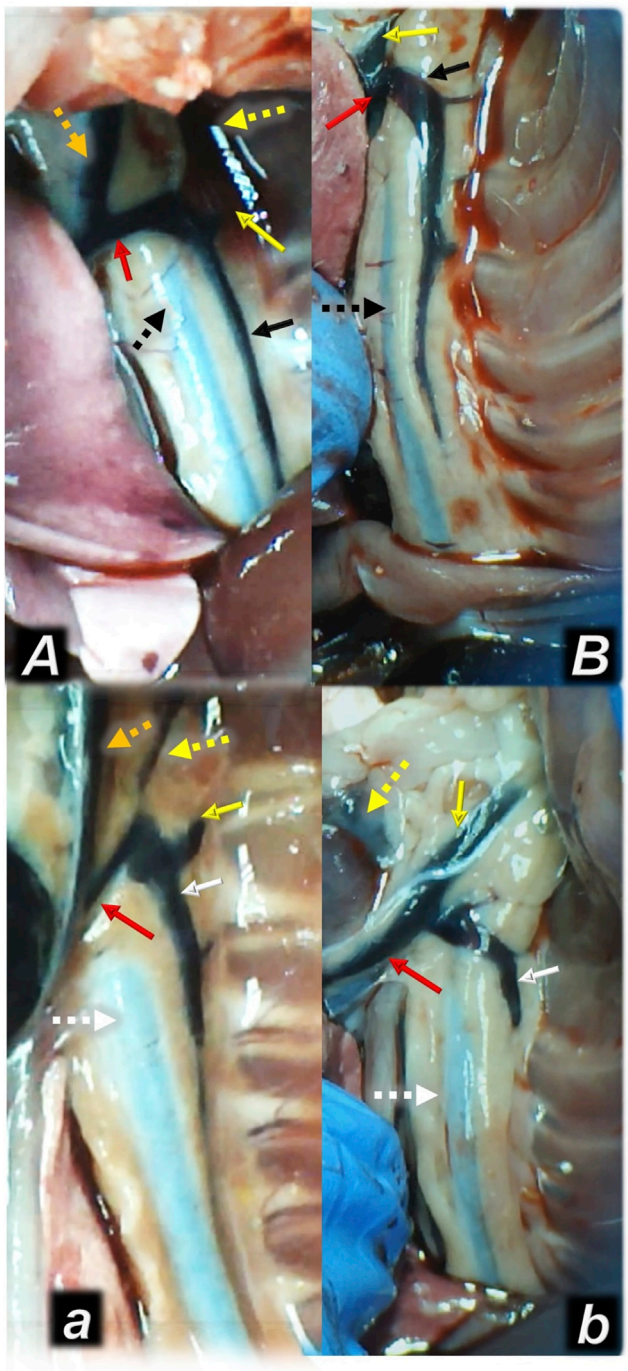

FIGURE 4 | Illustrative presentation of the azygos veins after the increased intraabdominal pressure and medication (sc) (full white arrow, saline (5 ml/kg, low, poor azygos vein presentation a, b) or BPC 157 (full black arrow, 10 ng/kg, upper, functioning azygos vein A, B): 40 mmHg (30 min) (a, A) and 50 mmHg (25 min) (b, B). Aorta (dashed arrows (white (control), black (BPC 157), axillar vein (full yellow arrow), left superior caval vein (red arrow), eternal jugular vein (dashed yellow arrow), internal jugular vein (dark yellow dashed arrow). A camera attached to a VMS-004 Discovery Deluxe USB microscope (Veho, United States).

Heart and ECG Disturbances

Commonly, high intra-abdominal pressures were timely along with the nodal rhythm, with dominant ST-elevation and bradycardia. Extreme bradycardia and asystole appeared as the ultimate outcome, at 20 ± 2 min (50 mmHg), 25 ± 5 min and 28 ± 2 min (30 mmHg and 40 mmHg), and 55 ± 8 min (25 mmHg) in control rats under thiopental anesthesia and at 110 ± 25 min in esketamine-anesthetized control rats. However, the evidence shows that despite continuously maintaining high intra-abdominal pressure, in all BPC 157-treated rats, heart function was consistently maintained, with fewer ECG disturbances. The sinus rhythm was preserved, with occasional first-degree AV block, but with no ST-elevation. Extreme bradycardia and asystole were not observed. This occurred along with normal heart microscopic presentation, unlike the myocardial congestion and sub-endocardial infarction observed in controls (**Figure 11**).

Gastrointestinal, Lung, Liver, Kidney, and Heart Lesions

Consequently, as part of the cause-consequence therapeutic course, i.e., reduced intracranial (superior sagittal sinus), portal, and caval hypertension, reduced aortal hypotension, and activated collateral pathway, BPC 157 reduced the severity of lesions in the gastrointestinal tract and other organs commonly noted in the untreated rats with high intra-abdominal pressures (**Figures 7**, **8**, **9**, **10**, **11**; **Supplementary Figures S1, S2**).

With an increase in severity from the upper toward the lower part of the gastrointestinal tract, control rats demonstrated transmural hyperemia of the entire gastrointestinal tract, stomach, duodenum, and small and large bowel wall, along with a reduction in the villi in the intestinal mucosa, crypt reduction with focal denudation of superficial epithelia, and dilatation of the large bowel (**Figures 7**, **8**, **9**, **10**, **11**; **Supplementary Figures S1, S2**). Regularly, in BPC 157-treated rats, we noted no or minimal congestion in the gastrointestinal mucosa with well-preserved intestinal villi and colonic crypts with no dilatation of the large bowel. Considering intra-abdominal hypertension at grade III and grade IV and the therapeutic effect, it was not surprising to find a considerable decrease in villi height in all control rats with high intra-abdominal pressure (**Figures 7**, **9**; **Supplementary Figures S1, S2**) and preserved villi height in the BPC 157-treated rats (similar to the villi height in healthy rats, indicating preserved intestinal function despite high intra-abdominal pressure).

Without therapy, severe lesions were observed in the rats with high intra-abdominal pressures, characterized by marked congestion of the myocardium and subendocardial infarcts (**Figure 11**), marked congestion and large areas of intra-alveolar hemorrhage in the lung (**Figure 10**), vascular dilation of the liver parenchyma (**Figure 10**), and renal congestion (**Figure 11**). In contrast, as a result of treatment, the equally high intra-abdominal pressures in BPC 157-treated rats led to only mild congestion in the gastrointestinal tract, liver, and kidney (**Figures 7**, **8**, **9**, **10**, **11**), particularly with high intra-

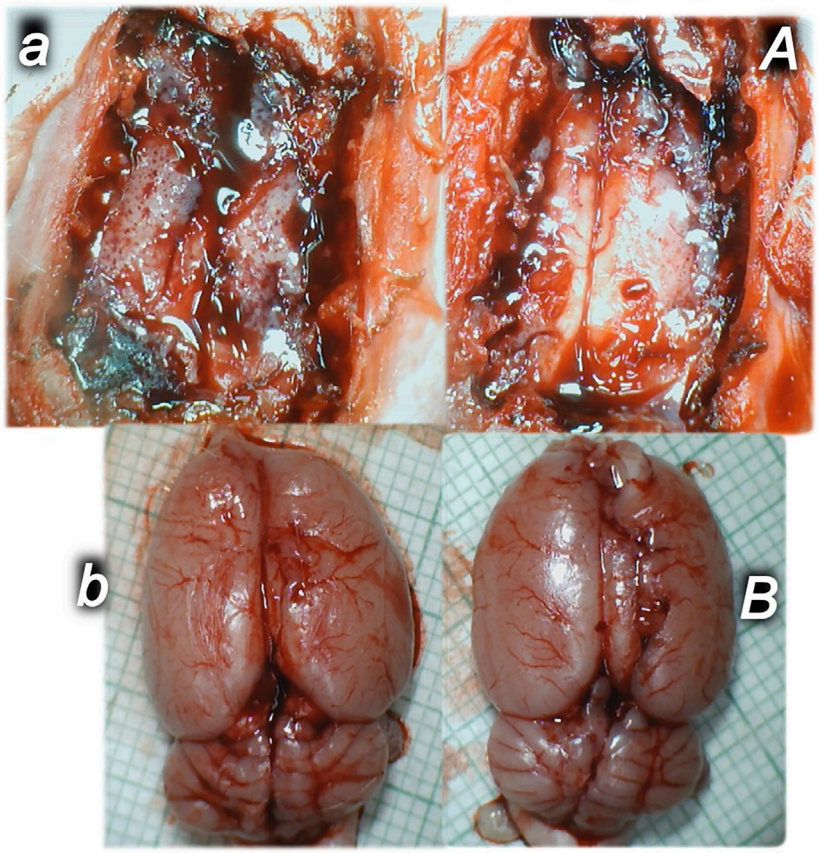

FIGURE 5 | Illustrative brain presentation in the rats with the increased intra-abdominal pressure (50 mm Hg). In calvarial window **(upper)**, at 15 min increased pressure time and medication saline (5 ml/kg ip) **(upper, left, control, *a*)** or BPC 157 (10 ng/kg sc) **(upper, right, *A*)**, at 10 min increased intra-abdominal pressure time. After sacrifice **(low)**, at the 25 min increased intra-abdominal pressure time (saline (5 ml/kg ip) **(low, left, control, *b*)** or BPC 157 (10 ng/kg sc) **(low, right, *B*)** at 10 min increased intra-abdominal pressure time. Prominent brain swelling in control rats **(left)**, completely reversed in BPC 157 rats **(right)**. A camera attached to a VMS-004 Discovery Deluxe USB microscope (Veho, United States).

abdominal pressures at 40 and 50 mmHg (otherwise, no changes in the liver and renal parenchyma were observed). The myocardium was preserved, with no change in the lung parenchyma (**Figure 8**, **10**, **11**).

Brain Lesions, Cerebral and Cerebellar Cortex, Hypothalamus/Thalamus, and Hippocampus

Without therapy, the consistently downhill course of intra-abdominal hypertension in rats with high intra-abdominal pressures led to multiple organ lesions, widespread thrombosis, disturbed ECG and blood pressure, portal and caval hypertension, aortal hypotension, and, in particular, intracranial (superior sagittal sinus) hypertension (**Figures 1–15**) along with severe brain lesions (**Figures 12**, **13**, **14**, **15**). Moreover, evidently, the brain was consistently swollen (**Figures 1**, **5**), resulting in brain damage in all investigated areas (**Figures 12**, **13**, **14**, **15**).

In general, congestion of the cerebral and cerebellar cortex, hypothalamus/thalamus, and hippocampus was observed, with edema and large areas with increased numbers of karyopyknotic cells, as well as intracerebral hemorrhage, mostly in the infratentorial space, affecting the cerebello angle/area (**Figures 12**, **13**, **14**, **15**). We noted an increased number of karyopyknotic cells in all four regions, i.e., the cerebral and cerebellar cortex, hippocampus, and hypothalamus/thalamus (**Figure 14**). Especially, there was karyopyknosis and degeneration of Purkinje cells of the cerebellar cortex and marked karyopyknosis of pyramidal cells in the hippocampus. In particular, these brain lesions appeared to be distinctively affected by high intra-abdominal pressure; i.e., the most progressive hippocampal neuronal damage was found with the highest intra-abdominal pressure. Contrarily, as a cause-consequence of BPC 157 therapy, i.e., reduced intracranial (superior sagittal sinus) hypertension and gross brain swelling, along with reduced portal and caval hypertension, aortal hypotension, abrogated thrombosis, and an activated collateral pathway, these lesions were largely reduced in BPC 157-treated rats, with a highly protected cortex, hypothalamus/thalamus, and hippocampus, as well as healthy Purkinje cells in the

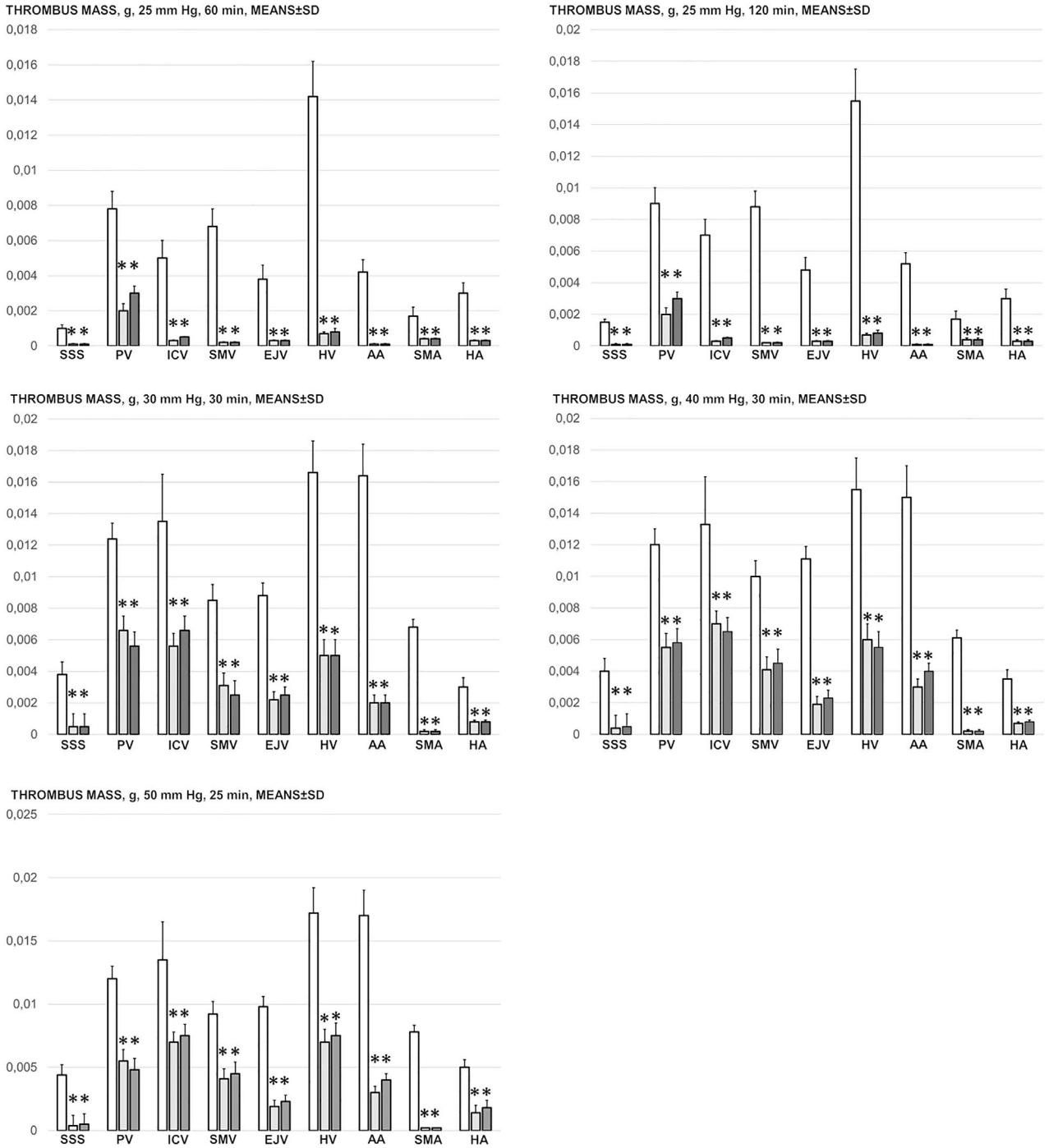

FIGURE 6 | Thrombus mass, g (in the superior sagittal sinus (SSS), portal vein (PV), inferior caval vein (ICV), superior mesenteric vein (SMV), external jugular vein (EJV), hepatic veins (HV), abdominal aorta (AA), superior mesenteric artery (SMA) and hepatic artery (HA)) in the thiopental-anesthetized rats with the increased intra-abdominal pressures at 50 mmHg for 25 min, at 30 mmHg or 40 mmHg for 30 min, at 25 mmHg for 60 min increased intra-abdominal pressures-time and in the esketamine-anesthetized rats with the increased intra-abdominal pressures at 25 mmHg for 120 min increased intra-abdominal pressures-time, following medication (BPC 157 10 μg/kg (light gray bars), 10 ng/kg (dark gray bars); saline 5 ml/kg (white bars)) given subcutaneously at 10 min increased intra-abdominal pressures-time. Means ± SD, *P<0.05, vs. control.

cerebellar cortex. BPC 157-treated rats showed a few karyopyknotic neuronal cells in the analyzed neuroanatomic structures.

Quantitative analysis of neuronal damage in the karyopyknotic areas in all four neuroanatomic structures showed no or only a few karyopyknotic neural cells

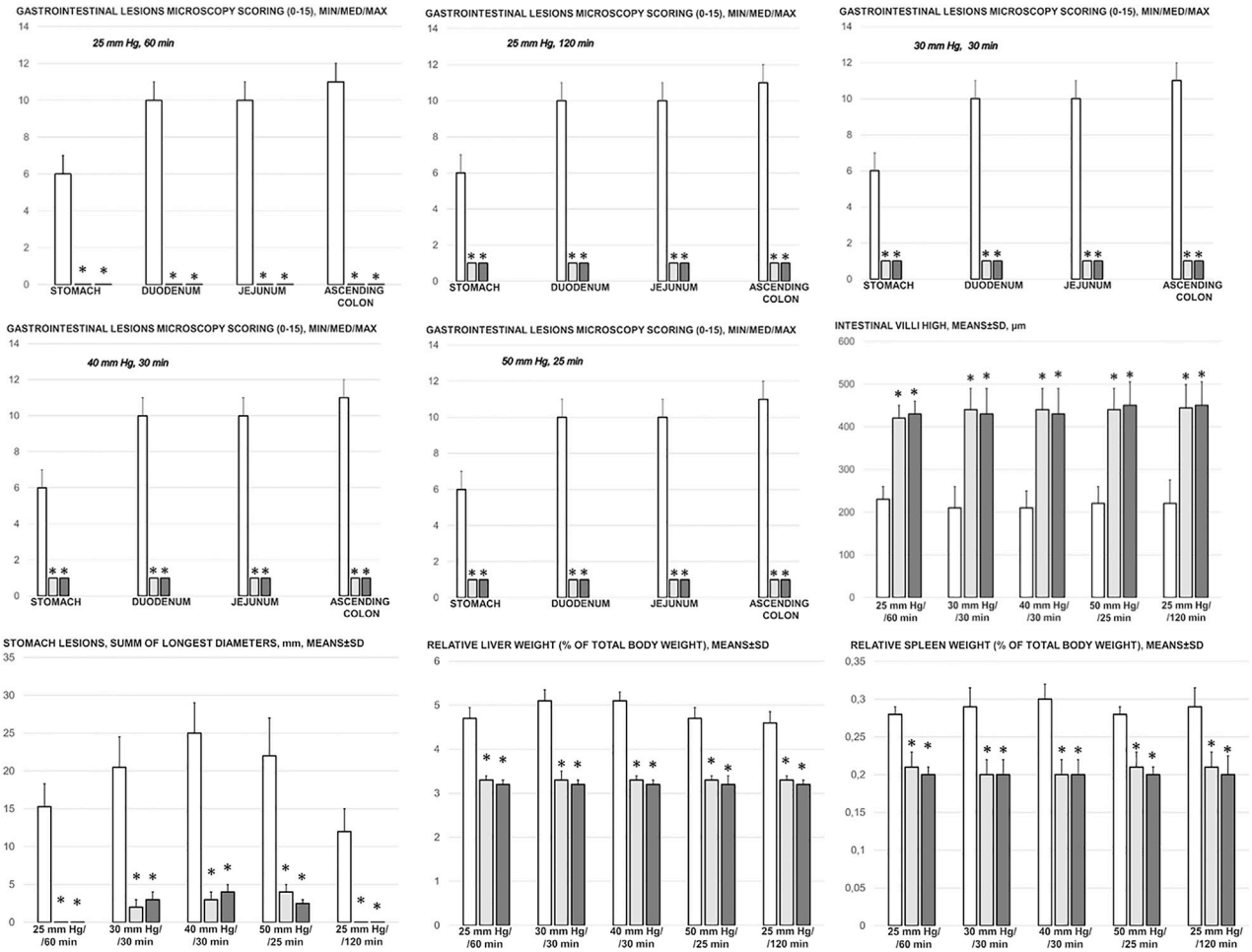

FIGURE 7 | Gastrointestinal lesions microscopy scoring (0–15), stomach, duodenum, jejunum, ascending colon and intestinal villi high, µm, and stomach lesions (sum of longest lesions diameters, mm), relative liver weight (% of total body weight), relative spleen weight (% of total body weight) in the thiopental-anesthetized rats with the increased intra-abdominal pressures at 50 mmHg for 25 min, at 30 mmHg or 40 mmHg for 30 min, at 25 mmHg for 60 min increased intra-abdominal pressures-time, and in the esketamine-anesthetized rats with the increased intra-abdominal pressures at 25 mmHg for 120 min increased intra-abdominal pressures-time, following medication (BPC 157 10 µg/kg (light gray bars), 10 ng/kg (dark gray bars); saline 5 ml/kg (white bars)) given subcutaneously at 10 min increased intra-abdominal pressures-time. Minimum (min), maximum (max), median (med), means ± SD, *P<0.05, vs. control.

(**Figure 12**). The white matter was more vulnerable to chronic cerebral injury. No white matter lesions were found in both groups of animals using modified Bielschowsky silver staining and Klüver–Barrera staining.

In summary, after BPC 157 therapy, rats with high intra-abdominal pressures (grade III and grade IV) exhibited markedly attenuated portal and caval hypertension, ameliorated aortal hypotension, and markedly attenuated superior sagittal sinus hypertension. Additionally, venous and arterial thrombosis was attenuated, both peripherally and centrally, which markedly mitigated stasis and moreover reduced brain, heart, lung, liver, kidney, and gastrointestinal lesions as the untreated result. These reductions were ascribed to the key finding of an activated particular collateral pathway, i.e., the azygos vein, which combined the inferior caval vein and left superior vein to reorganize blood flow.

DISCUSSION

We investigated the reversal of abdominal compartment syndrome induced by the stable gastric pentadecapeptide BPC 157 due to its previously observed therapeutic effect noted in vessel occlusion syndromes (Vukojevic et al., 2018; Gojkovic et al., 2020; Kolovrat et al., 2020; Gojkovic et al., 2021a; Knezevic et al., 2021a; Knezevic et al., 2021a; Gojkovic et al., 2021b; Knezevic et al., 2021b; Strbe et al., 2021).

With the applied procedure (i.e., 25, 30, 40, or 50 mmHg intra-abdominal hypertension), there was a regular downhill chain of events, regardless of the type of anesthesia (i.e., esketamine, as ketamine is an antioxidant (Xingwei et al., 2014) that may provide a more prolonged survival period than thiopental). The abdominal wall compliance threshold was crossed mechanically, with no further stretch of the abdomen; this

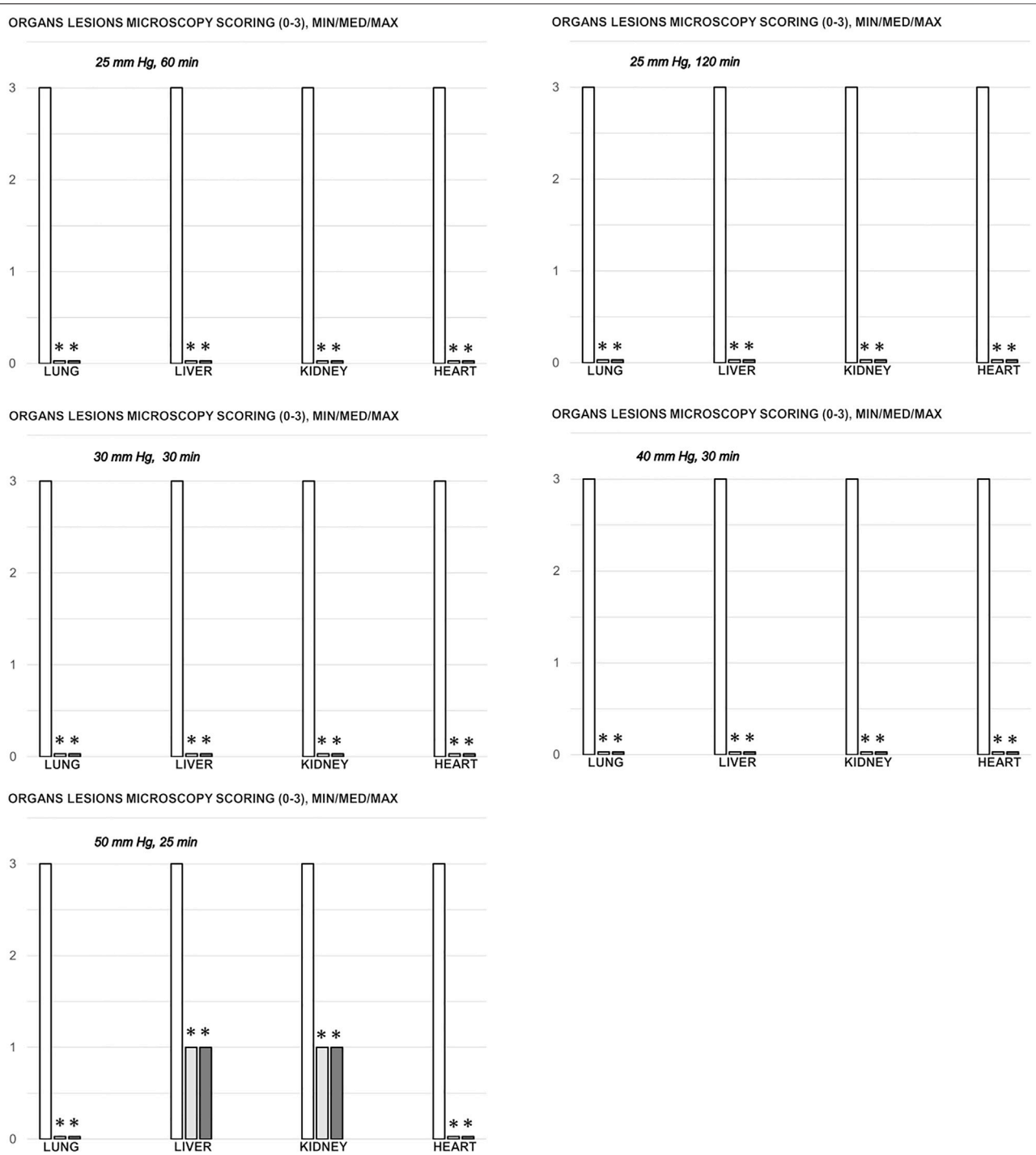

FIGURE 8 | Organs (lung, liver, kidney, heart) microscopy scoring (0–3), in the thiopental-anesthetized rats with the increased intra-abdominal pressures at 50 mmHg for 25 min, at 30 mmHg or 40 mmHg for 30 min, at 25 mmHg for 60 min increased intra-abdominal pressures-time, and in the esketamine-anesthetized rats with the increased intra-abdominal pressures at 25 mmHg for 120 min increased intra-abdominal pressures-time, following medication (BPC 157 10 μg/kg (light gray bars), 10 ng/kg (dark gray bars); saline 5 ml/kg (white bars)) given subcutaneously at 10 min increased intra-abdominal pressures-time. Minimum (min), maximum (max), median (med), *P<0.05, vs. control. **Figure 9**. Illustrative presentation of gross and microscopic presentation. Gross presentation. Stomach (*a, A*) and liver (*b,B*) (white letters) after the increased intraabdominal pressure and medication (sc) (saline (5 ml/kg, left, stomach and duodenum with multiple small hemorrhagic lesions (*a*), and congested liver (*b*) presentation) or BPC 157 (10 ng/kg, right, stomach and duodenum, and liver *A, B*): 25 mmHg (30 min) (*a, A*) and 40 mmHg (30 min) (*b, B*). A camera attached to a VMS-004 Discovery Deluxe USB microscope (Veho, United States). Microscopy presentation. Stomach (*a, A*) and colon (*b, B*) (black letters) presentation in rats with the increased intra-abdominal pressure at 50 mmHg for 25 min treated at 10 min increased intra-abdominal pressure time with saline (control, *a, b*) or BPC 157 (*A, B*). The control group showed marked hyperemia and congestion of the stomach wall (*a*) and a reduction of the colonic crypts with focal denudation of the superficial epithelia (*b*). BPC 157-treated rats exhibit presentation close to normal gastrointestinal tract presentation (*A, B*). (HE; *a, A*, magnification ×100, scale bar 200 μm; *b, B*, magnification ×200, scale bar 100 μm).

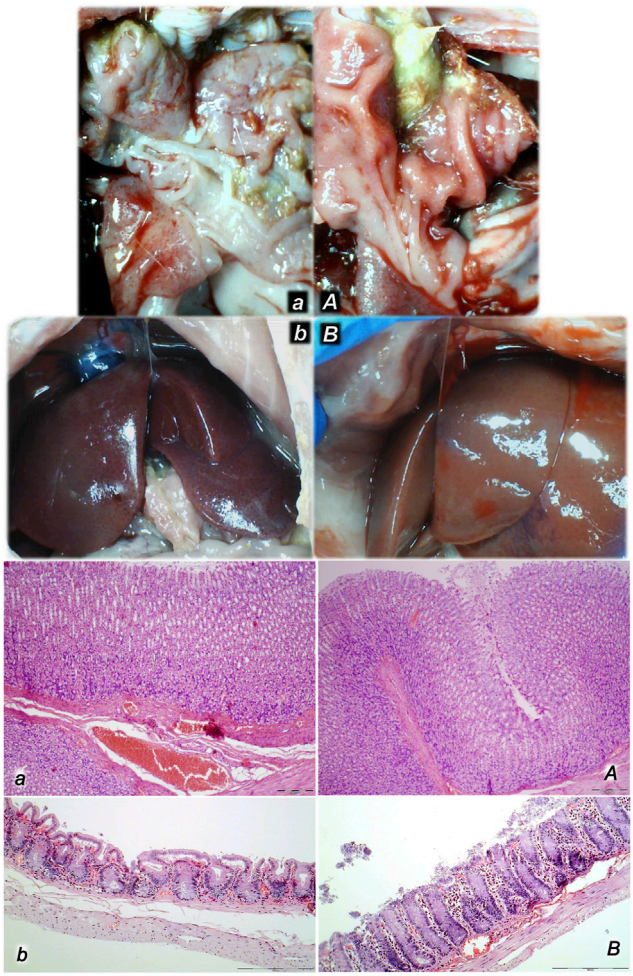

FIGURE 9 | Illustrative presentation of gross and microscopic presentation. Gross presentation. Stomach (a, A) and liver (b,B) (white letters) after the increased intraabdominal pressure and medication (sc) (saline (5 ml/kg, left, stomach and duodenum with multiple small hemorrhagic lesions (a), and congested liver (b) presentation) or BPC 157 (10 ng/kg, right, stomach and duodenum, and liver A, B): 25 mmHg (30 min) (a, A), and 40 mmHg (30 min) (b, B). The camera attached to a VMS-004 Discovery Deluxe USB microscope (Veho, United States). Microscopy presentation. Stomach (a, A) and colon (b, B) (black letters) presentation in rats with the increased intra-abdominal pressure at 50 mmHg for 25 min treated at 10 min increased intra-abdominal pressure time with saline (control, a, b) or BPC 157 (A, B). The control group showed marked hyperemia and congestion of the stomach wall (a) and a reduction of the colonic crypts with focal denudation of the superficial epithelia (b). BPC 157-treated rats exhibit presentation close to normal gastrointestinal tract presentation (A, B). (HE; a, A, magnification ×100, scale bar 200 μm; b, B, magnification ×200, scale bar 100 μm).

increased intra-abdominal pressure, compressed vessels and organs, and pushed up the diaphragm as a predetermined definitive outcome (Depauw et al., 2019). Abdominal compartment syndrome appeared as a multiple occlusion syndrome that could not be avoided unless therapy was given. Regularly, reciprocal changes in the abdominal, thoracic, and brain cavities (Depauw et al., 2019) rapidly appeared as determinants of vascular failure. Therefore, in the rats with intra-abdominal hypertension, multiorgan failure (i.e., gastrointestinal, brain, heart, liver, and kidney lesions), portal and caval hypertension, aortal hypotension, intracranial (superior sagittal sinus) hypertension, and generalized thrombosis appeared. This led to generalized stasis, generalized Virchow triad presentation, and severe ECG disturbances; therapy was able to provide adequate compensation (i.e., activation of collateral pathways to reestablish blood flow), both rapid and sustained, as demonstrated with BPC 157 therapy. As a prime and practical confirmation, rats with major vessel ligation and occlusion, in either artery and/or vein, and either peripherally or centrally, exhibited a similar syndrome (Vukojevic et al., 2018; Gojkovic et al., 2020; Kolovrat et al., 2020; Gojkovic et al., 2021a; Knezevic et al., 2021a; Knezevic et al., 2021a; Knezevic et al., 2021b). Thus, there may be a shared inability to react, leading to innate vascular failure upon major vessel occlusion (ligation) (Vukojevic et al., 2018; Gojkovic et al., 2020; Kolovrat et al., 2020; Gojkovic et al., 2021a; Knezevic et al., 2021a; Knezevic et al., 2021a; Knezevic et al., 2021b) as well as upon the induction of high intra-abdominal pressure, with all vessels compressed. Likewise, with BPC 157 therapy, there may be a shared curative effect, with consistent beneficial evidence in all of the rats with major vessel occlusion (Vukojevic et al., 2018; Gojkovic et al., 2020; Kolovrat et al., 2020; Gojkovic et al., 2021a; Knezevic et al., 2021a; Knezevic et al., 2021a; Knezevic et al., 2021b). Activation of the collateral pathway following occlusion injury fully reduces occlusion syndrome (Vukojevic et al., 2018; Gojkovic et al., 2020; Kolovrat et al., 2020; Gojkovic et al., 2021a; Knezevic et al., 2021a; Knezevic et al., 2021a; Knezevic et al., 2021b). Together, this evidence strongly supports a comparable beneficial effect (i.e., a "bypassing key") in rats with intra-abdominal hypertension and multiple vessel compression. As a follow-up, fully reduced abdominal compartment syndrome appeared as a confirmative conceptual result.

To reverse abdominal compartment syndrome as a multiple occlusion syndrome disaster, we improved the function of the venous system with the stable gastric pentadecapeptide BPC 157. Considering the multitude of vessels that had been directly compressed, this improvement should be greater than that in specific vessel occlusion syndromes (Vukojevic et al., 2018; Gojkovic et al., 2020; Kolovrat et al., 2020; Gojkovic et al., 2021a; Knezevic et al., 2021a; Knezevic et al., 2021a; Knezevic et al., 2021b) or with an intragastric application of absolute alcohol and intraperitoneal application of lithium overdose, which induce an "occlusion-like" syndrome (Gojkovic et al., 2021b; Strbe et al., 2021). This abdominal compartment syndrome therapy addresses more than one known initial target, i.e., single vessel occlusion (ligation) (Vukojevic et al., 2018; Gojkovic et al., 2020; Kolovrat et al., 2020; Gojkovic et al., 2021a; Knezevic et al., 2021a; Knezevic et al., 2021a; Knezevic et al., 2021b) vs. intragastric application of absolute alcohol (Gojkovic et al., 2021b) and intraperitoneal application of lithium overdose (Strbe et al., 2021) vs. all vessels compressed (increased intra-abdominal hypertension). Thus, by resolving and compensating for damaged functions, the reversal of the chain of harmful consequences of high intra-abdominal pressure can be achieved and abdominal compartment syndrome recovery

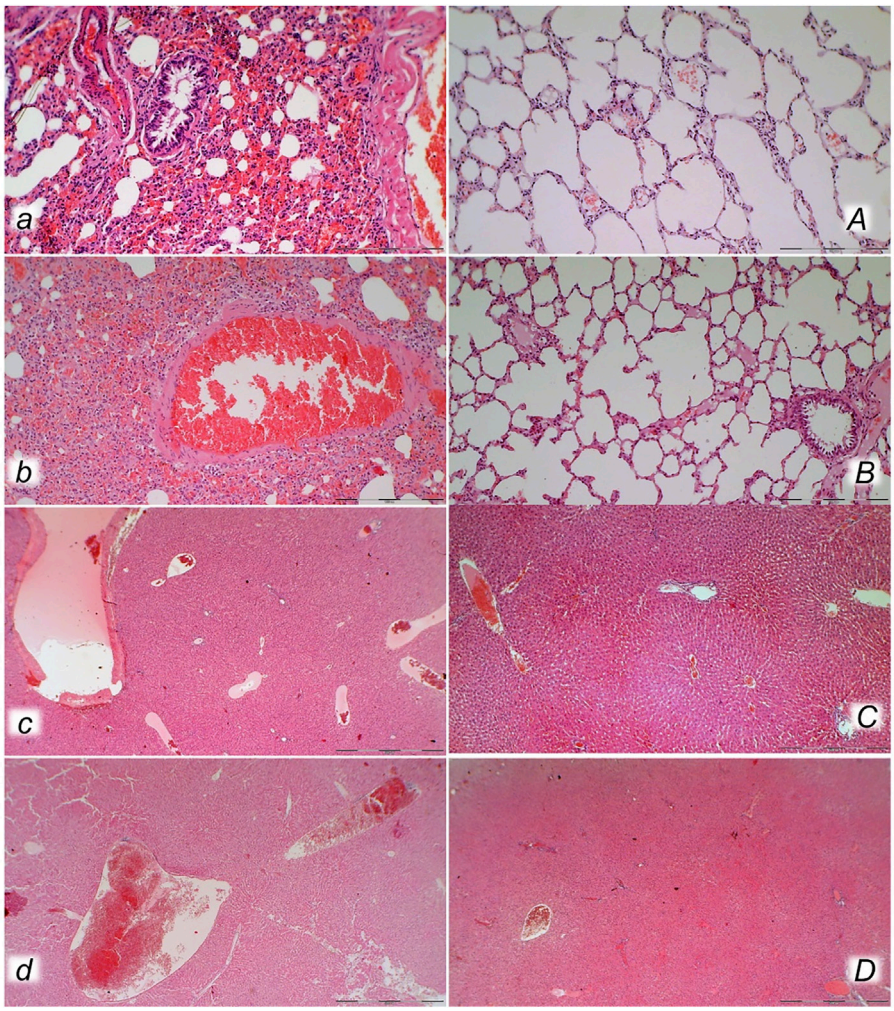

FIGURE 10 | Lung (*a, A, b, B*) and liver (*c, C, d, D*) presentation in rats with the increased intra-abdominal pressure at 25 mmHg for 60 min (*a, A, c, C*) or at 50 mmHg for 25 min (*b, B, d, D*), treated at 10 min increased intra-abdominal pressure time with saline (control, *a, b, c, d*) or BPC 157 (*A, B, C, D*). *a, b*. Lung parenchyma with marked congestion and large areas of intra-alveolar hemorrhage in control rats. *A, B*. Normal lung parenchyma in BPC 157-treated rats. *c, d*. Vascular dilatation of liver parenchyma in controls, normal architecture in BPC 157 treated rats (C) and slight congestion of liver parenchyma (*D*). (HE; magnification ×200, scale bar 100 μm (*a, A, b, B*); magnification ×100, scale bar 500 μm (*c, C, d, D*)).

can occur. Thus, the beneficial findings in rats with severely increased intra-abdominal pressure given the stable gastric pentadecapeptide BPC 157 (for review, see Sikiric et al., 2018) likely occurred due to the effect on compressed essential vessel tributaries, both arterial and venous, peripherally and centrally. As a likely rescue pathway, as seen in the rat Budd–Chiari syndrome (Gojkovic et al., 2020), superior sagittal sinus occlusion syndrome (Gojkovic et al., 2021a), and intragastric application of absolute alcohol (Gojkovic et al., 2021b) or intraperitoneal application of lithium overdose (Strbe et al., 2021), we identified the activated azygos vein pathway and the inferior vena cava–azygos vein–left superior vena cava pathway. The azygos vein pathway was fully activated in BPC 157-treated rats (and thereby provided additional direct blood flow delivery), while it was collapsed in control saline-treated rats with intra-abdominal hypertension.

There may be, however, other activated bypassing loops (Vukojevic et al., 2018; Gojkovic et al., 2020; Kolovrat et al., 2020; Gojkovic et al., 2021a; Knezevic et al., 2021a; Knezevic et al., 2021a; Gojkovic et al., 2021b; Knezevic et al., 2021b). With the harmful effects of intra-abdominal hypertension, peripherally but also centrally, rats with an occluded superior sagittal sinus may be an illustrative example (Gojkovic et al., 2021a). Therefore, we identified central shunts through the ophthalmic vein, angularis vein, facial anterior and posterior veins, and facial vein, as well as the superior cerebral veins, the superior and inferior sinus cavernosus, the sinus petrosus, the sinus transversus, the external jugular vein, the subclavian vein, and the superior vena cava (Gojkovic et al., 2021a). Moreover, with BPC 157 therapy delivered topically to the swollen brain, intraperitoneally or intragastrically, a rapid attenuation of brain swelling was observed (Gojkovic et al., 2021a). A similar syndrome also

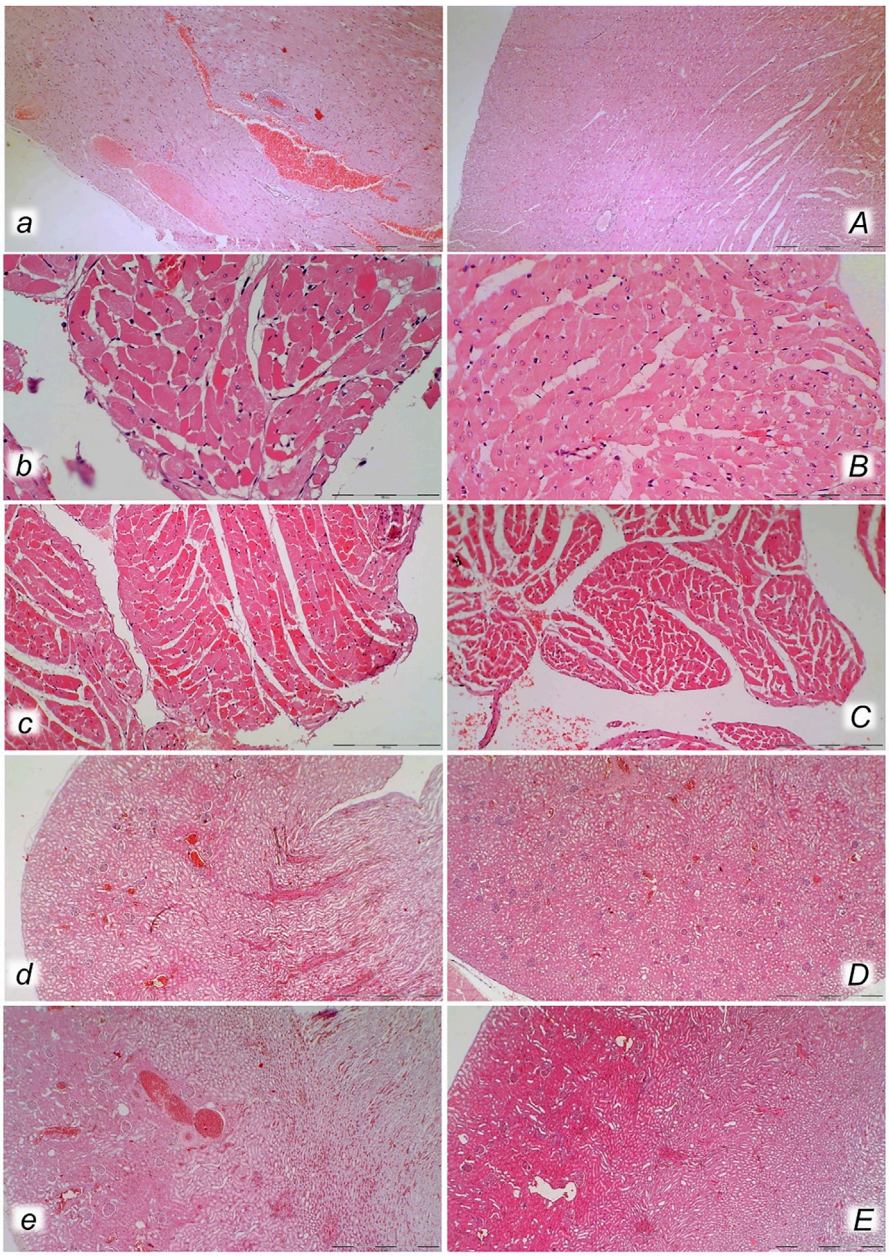

FIGURE 11 | Heart (*a, A, b, B, c, C*) and kidney (*d, D, e, E*) presentation in the rats with the increased intra-abdominal pressure at 25 mmHg for 60 min (*a, A, b, B, d, D*) or at 50 mmHg for 25 min (*c, C, e, E*), treated at 10 min increased intra-abdominal pressure time with saline (control, *a, b, c, d, e*) or BPC 157 (*A, B, C, D, E*). Marked congestion of myocardium of control rats, with subendocardial infract found in all control rats at 25 mmHg (*a, b*), and at 50 mmHg of intra-abdominal pressure (*c*), while myocardium was preserved in all BPC 157- treated rats (*A, B, C*). Severe congestion of renal tissue was found in control rats at 25 mmHg (*d*) and at 50 mmHg of intra-abdominal pressure (*e*), while in BPC 157- treated rats, no changes were found at 25 mmHg intra-abdominal pressure (*D*) and only discrete congestion was found at 50 mmHg of intra-abdominal pressure (*E*). (HE; magnification ×200, scale bar 100 μm (*a, A*); x400, scale bar 50 μm (*b, B, c, C*); x100, scale bar 500 μm (*d, D, e, E*)).

appeared with peripherally induced syndromes, i.e., an occluded superior mesenteric artery (Knezevic et al., 2021a) or vein (Knezevic et al., 2021b), or both artery and vein (Knezevic et al., 2021a). Commonly, as in the present study, BPC 157 therapy rapidly eliminated the increased pressure in the superior sagittal sinus, severe portal and vena caval hypertension, and aortal hypotension and moreover quickly recruited collateral vessels, which abrogated venous and arterial thrombosis (Gojkovic et al., 2021a; Knezevic et al., 2021a; Knezevic et al., 2021a; Gojkovic et al., 2021b; Knezevic et al., 2021b; Strbe et al., 2021). This was interpreted as a widespread resolution of the Virchow triad (endothelium injury, hypercoagulability, and stasis), which allowed recovery from organ lesions (Vukojevic et al., 2018; Gojkovic et al., 2020;

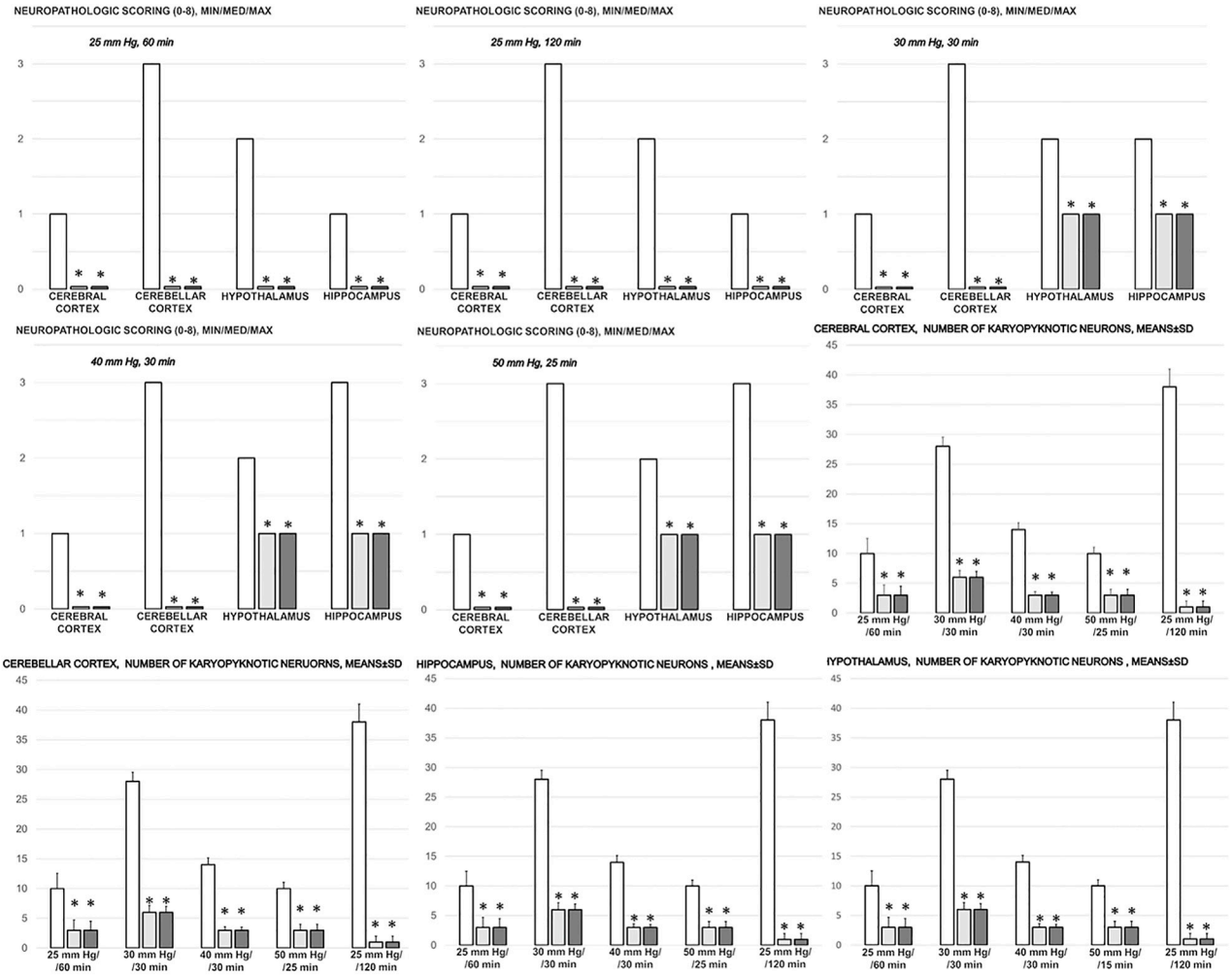

FIGURE 12 | Neuropathologic scoring (0–8), cerebral cortex, cerebellar cortex, hypothalamus, hippocampus, and the number of karyopyknotic cells, cerebral cortex, cerebellar cortex, hypothalamus, hippocampus, in the thiopental-anesthetized rats with the increased intra-abdominal pressures at 50 mmHg for 25 min, at 30 mmHg or 40 mmHg for 30 min, at 25 mmHg for 60 min increased intra-abdominal pressures-time, and in the esketamine-anesthetized rats with the increased intra-abdominal pressures at the 25 mmHg at the 120 min increased intra-abdominal pressures-time, following medication (BPC 157 10 μg/kg (light gray bars), 10 ng/kg (dark gray bars); saline 5 ml/kg (white bars)) given subcutaneously at 10 min increased intra-abdominal pressures-time. Minimum (min), maximum (max), median (med), means ± SD, *P<0.05, vs. control.

Kolovrat et al., 2020; Gojkovic et al., 2021a; Knezevic et al., 2021a; Knezevic et al., 2021a; Gojkovic et al., 2021b; Knezevic et al., 2021b; Strbe et al., 2021). Evidently, in the resolution of damage due to increased intra-abdominal hypertension, peripherally (Vukojevic et al., 2018; Gojkovic et al., 2020; Kolovrat et al., 2020; Knezevic et al., 2021a; Knezevic et al., 2021a; Knezevic et al., 2021b), centrally (Gojkovic et al., 2021a), or both peripherally and centrally (Gojkovic et al., 2021b; Strbe et al., 2021), there is a common therapeutic point from which BPC 157 operates.

Moreover, as BPC 157 therapy also works in advance, the properly reactivated azygos vein pathway and improved functioning of the combined inferior caval vein and left superior caval vein may resist even higher intra-abdominal hypertension (25 mmHg<30 mmHg<40 mmHg<50 mmHg) and prolonged intra-abdominal pressures increases (25–120 min). There were no lethal outcomes despite the permanent maintenance of high intra-abdominal pressures (note that abdominal compartment syndrome with a sustained level of 25 mmHg may be fatal within 1 h (Strang et al., 2020)). As an accurate conceptual analogy with the similar therapeutic effect in occlusion syndromes (Vukojevic et al., 2018; Gojkovic et al., 2020; Kolovrat et al., 2020; Gojkovic et al., 2021a; Knezevic et al., 2021a; Knezevic et al., 2021a; Knezevic et al., 2021b) or alcohol and lithium intoxication (Gojkovic et al., 2021b; Strbe et al., 2021), BPC 157 therapy is effective against severe bradycardia and ST-elevation until asystole, myocardial congestion, and infarction before death. This beneficial effect meant that, with more severe intra-abdominal hypertension, BPC 157 rats still exhibited normal microscopic presentation of the heart. Thus, as before (Vukojevic et al., 2018; Gojkovic et al., 2020; Kolovrat et al., 2020;

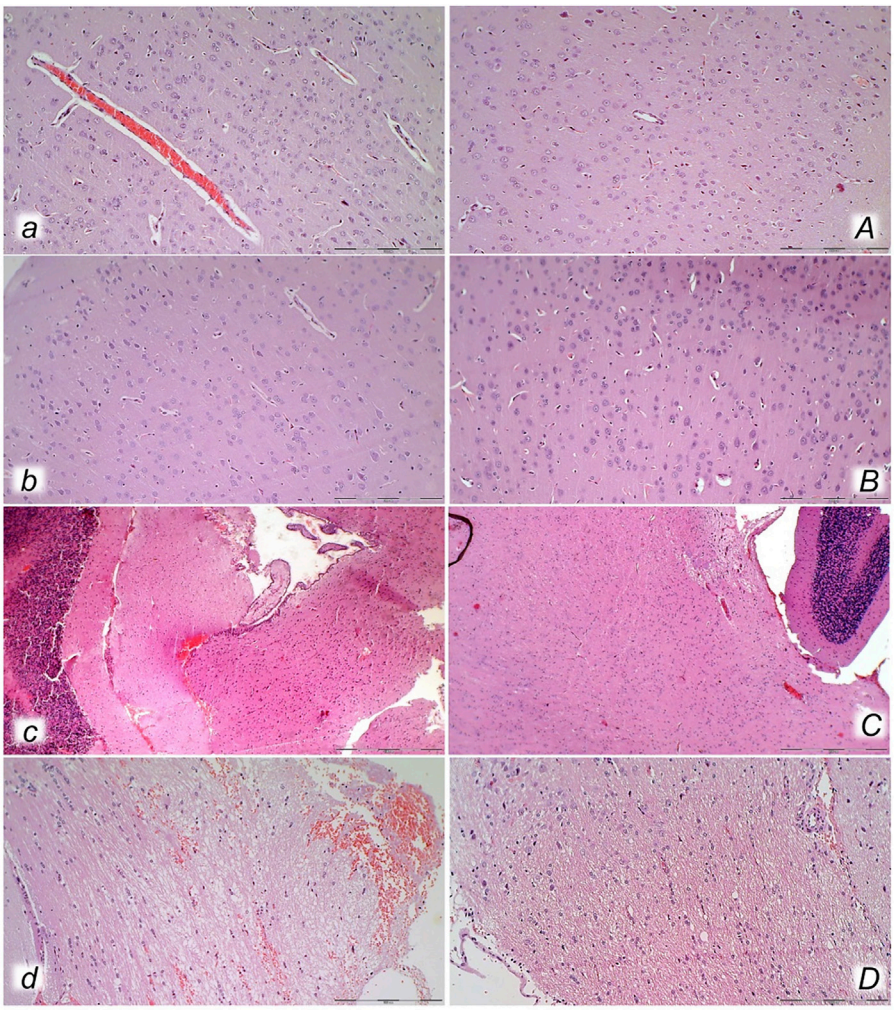

FIGURE 13 | Neuropathological changes of the cerebral cortex (*a, A, b, B*), cerebellar cortex (*c, C*) and pons (*d, D*) in rats with the increased intra-abdominal pressure at 25 mmHg for 60 min (*a, A, c, C*) or at 50 mmHg for 25 min (*b, B, d, D*), treated at 10 min increased intraabdominal pressure time with saline (control, *a, b, c, d*) or BPC 157 (*A, B, C, D*). Generalized edema and congestion (*a, b, c, d*) with an increased number of karyopyknotic cells were found in the cerebral cortex (*a, b*) that was significantly different from the cortex area in BPC 157-treated rats (*A, B*). In control rats, intracerebral hemorrhage was found in infratentorial space (*d*), mostly in cerebellopontine angle/area (*c*) with generalized edema and congestion of central nervous system, while no hemorrhage (*C*) and only mild edema was found in treated animals, mostly at 50 mmHg intra-abdominal pressure (*D*). (HE; magnification ×200, scale bar 100 μm (*a, A, b, B, d, D);* magnification ×100, scale bar 200 μm (*c, C*)).

Gojkovic et al., 2021a; Knezevic et al., 2021a; Knezevic et al., 2021a; Gojkovic et al., 2021b; Knezevic et al., 2021b; Strbe et al., 2021), this activated alternative blood flow was provided continuously maintained heart function, leading to near-normal lung, liver, and kidney presentation, unlike the extreme congestion and hemorrhage observed in control rats. Collectively, these findings implicate that the heart, lungs, liver, and kidney are BPC 157 therapeutic targets.

Thus, despite increased intra-abdominal pressure, BPC 157 therapy normalized portal and caval pressure and aortal pressure, as well as portal vein and inferior caval vein and aorta presentation. This maintenance may be essentially important. Otherwise, high portal and caval hypertension, aortal hypotension, exaggerated congestion of both the inferior caval and superior mesenteric veins, and a narrowed aorta all appear along with the most severe organ lesions. This clear damage has also been seen in other vessel occlusion studies (Vukojevic et al., 2018; Gojkovic et al., 2020; Kolovrat et al., 2020; Gojkovic et al., 2021a; Knezevic et al., 2021a; Knezevic et al., 2021a; Gojkovic et al., 2021b; Knezevic et al., 2021b; Strbe et al., 2021). Conceptually, the gastrointestinal, liver, and kidney lesions described here are illustrative cause-consequence relationships indicative of an uninterrupted injurious course. Vice versa, when the lesions are absent/abrogated, they clearly illustrate the therapeutic effect of BPC 157 and an interrupted injurious course.

Thus, specific conceptual support in rats with high intra-abdominal pressures is provided by gastrointestinal tract failure, hemorrhagic lesions in the stomach, transmural hyperemia of the entire gastrointestinal tract, stomach, duodenum, and small and large bowel wall. The reduction of

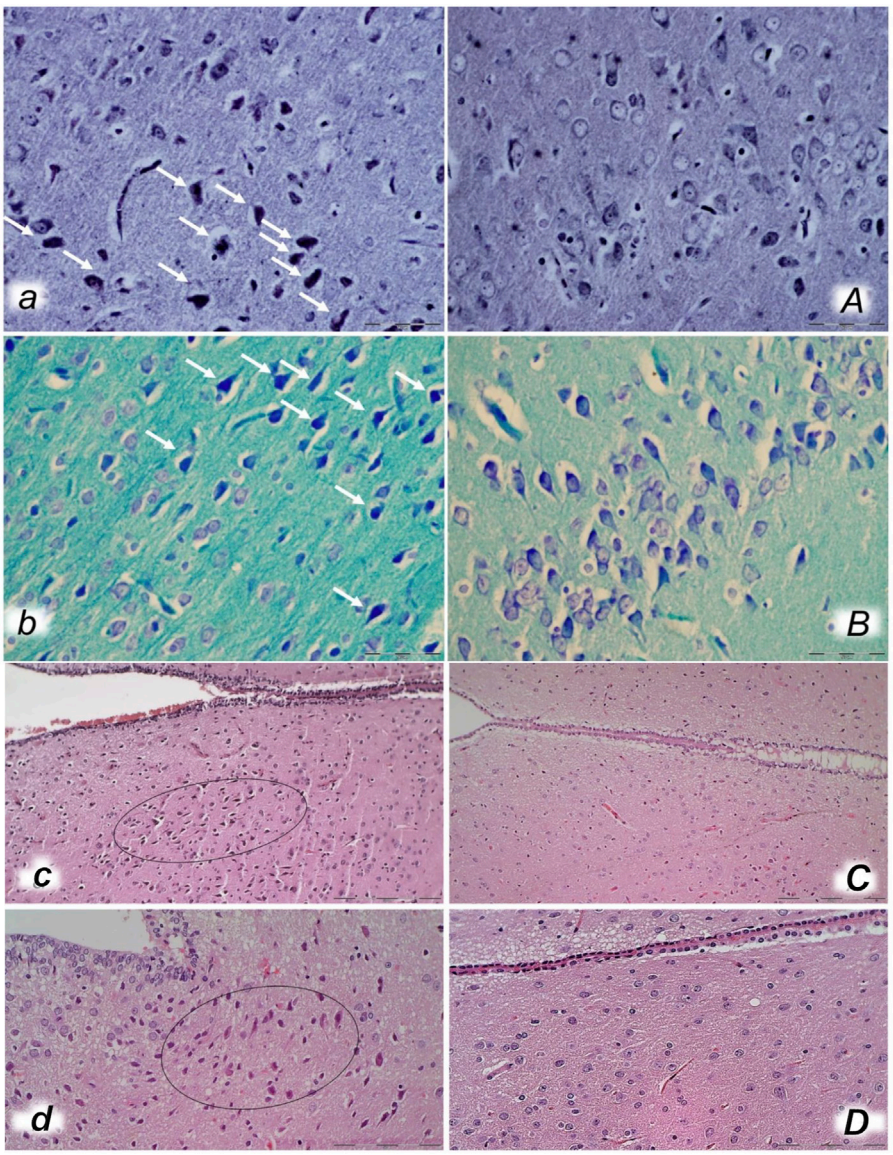

FIGURE 14 | Bielschowsky and Klüver–Barrera histochemical staining presenting neuropathological changes of cerebral cortex in rats with the increased intra-abdominal pressure at 30 mmHg for 30 min (*a, A, b, B*) treated at 10 min increased intraabdominal pressure time with saline (control *a, b*) or BPC 157 (*A, B*). In control rats, an increased number of karyopyknotic cells was found in the cerebral cortex (white arrows) (*A, B*) that was significantly different from the cortex area in BPC 157-treated rats (*a, b*). (Bielschowsky staining (*a, A*); Klüver–Barrera staining (*b, B*); magnification ×600, scale bar 50 μm). Neuropathological changes of hypothalamic/thalamic area (*c, C, d, D*) presentation in rats with the increased intra-abdominal pressure at 25 mmHg for 60 min (*c, C*) or at 50 mmHg for 25 min (*d, D*), treated at 10 min increased intra-abdominal pressure time with saline (control, *c, d*) or BPC 157 (*C, D*). A marked karyopyknosis was found in all control rats (marked in oval) (*c,* 25 mmHg/60 min); *d,* 50 mmHg/25 min) while preserved brain tissue was found in BPC 157-treated rats (*C,* 25 mmHg/60 min); *D,* 50 mmHg/25 min). (HE; magnification ×400, scale bar 50 μm).

villi in the intestinal mucosa and crypt reduction with focal denudation of superficial epithelia and dilatation of the large bowel illustrate vascular failure (Chan et al., 2014). Accordingly, the liver and the kidney exhibited huge vascular congestion. Vice versa, the normalized portal and caval pressure and aortal pressure as a cause-consequence are convincing evidence of the functioning "bypassing key" (i.e., the azygos vein). Consequently, BPC 157-treated rats exhibited no or minimal congestion in the gastrointestinal mucosa, with well-preserved intestinal villi and colonic crypts and no dilatation of the large bowel, as well as a maintained vascular supply and reduced vascular failure (Chan et al., 2014). In the liver and kidney, only mild congestion was observed at the highest intra-abdominal pressures.

Furthermore, high intra-abdominal pressures/increased intracranial pressures led to the severe presentation of brain lesions. Equally, with therapy, the reversed injury course (increased intra-abdominal pressure/reduced intracranial

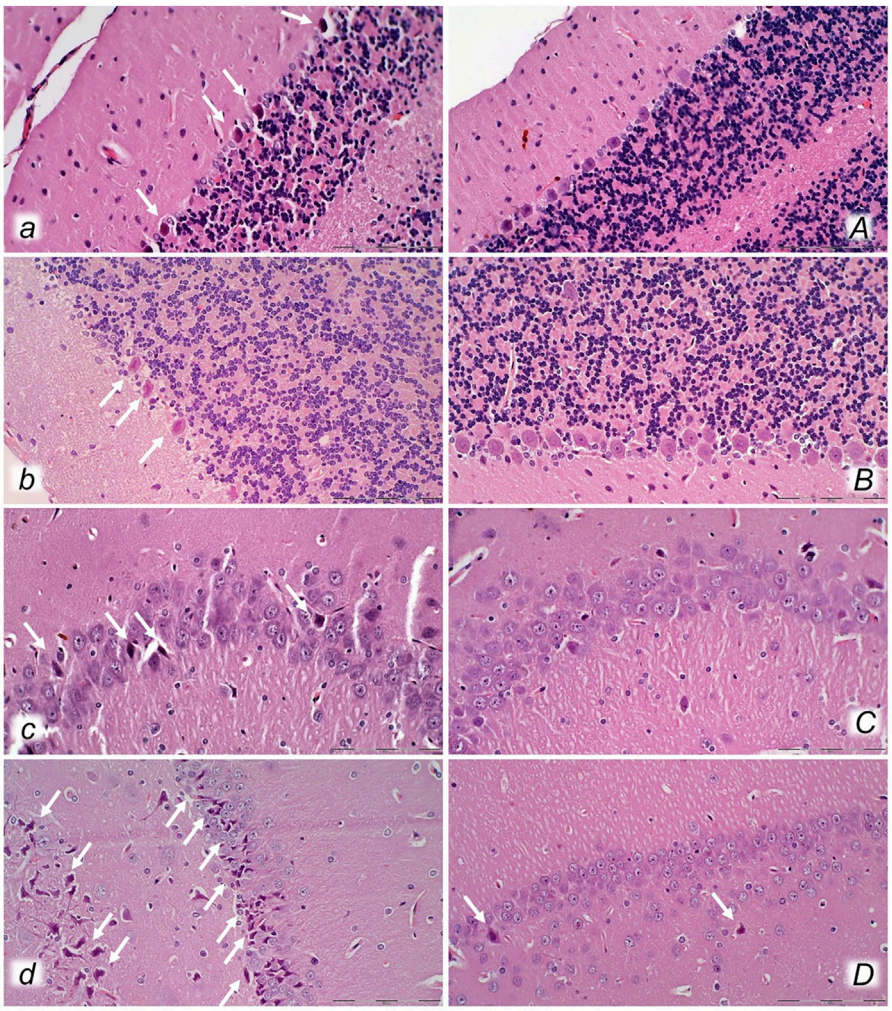

FIGURE 15 | Neuropathological changes of cerebellar cortex (*a, A*, *b, B*) and hippocampus (c, *C, d, D*) in rats with the increased intra-abdominal pressure at 25 mmHg for 60 min (*a, A, c, C*) or at 50 mmHg for 25 min (*b, B, d, D*), treated at 10 min increased intra-abdominal pressure time with saline (control, *a, b, c, d*) or BPC 157 (*A, B, C, D*). Control rats exhibited within cerebellar area karyopyknosis and degeneration of Purkinje cells (*a, b*). Marked and progressive karyopyknosis and degeneration of pyramidal cell of the hippocampus was observed in control rats (arrows) at 25 mmHg intraabdominal pressure (*c*) and even more at 50 mmHg intra-abdominal pressure (*d*). No change was found in the cerebellar and hippocampal area in BPC 157- treated rats at 25 mmHg intra-abdominal pressure (*A, B, C*) and only rare hippocampal karyopyknotic cells (arrows) at 50 mmHg intra-abdominal pressure (*D*) (HE; magnification ×400, scale bar 50 μm).

hypertension) led to reduced intracranial hypertension as the ultimate therapeutic outcome when the venous system was supported (i.e., activation of the azygos shunt). This was key in the brain as well, as pressures were not rapidly transmitted up through the venous system, and thereby brain presentation was preserved. The brain was preserved both grossly (absent brain swelling) and microscopically (consistent beneficial effect in all brain areas). Evidently, the beneficial effect of BPC 157 acted against the full range of brain lesions, in the order cerebellum cortex > hypothalamus/thalamus > cerebral cortex. The cerebellar cortex appeared to be the most affected, and the cerebral cortex was the least affected. The hippocampus, with increased lesion severity at higher intra-abdominal pressures, may be seen as a particular target. On the other hand, the vicious course induced by high intra-abdominal pressure can be simultaneously initiated and perpetuated from different sites (it should be noted that intracranial hypertension may essentially cause pulmonary edema and impair pulmonary circulation (Chen, 2009)).

Both BPC 157 regimens (μg and ng) had a similar therapeutic effect in all of the investigated protocols of abdominal compartment syndrome. Further cause-consequence evidence could be seen in BPC 157-treated rats with high intra-abdominal pressures, as treatment largely abrogated both arterial and venous thrombosis. This was seen before with vessel occlusion (Vukojevic et al., 2018; Gojkovic et al., 2020; Kolovrat et al., 2020; Gojkovic et al., 2021a; Knezevic et al., 2021a; Knezevic et al., 2021a; Knezevic et al., 2021b), alcohol and lithium intoxication (Gojkovic et al., 2021b; Strbe et al., 2021), and abdominal aorta anastomosis (Hrelec et al., 2009). The effect

occurred peripherally (i.e., the largest thrombosis initially (i.e., 25 mmHg) appeared just in the hepatic veins, resembling the presentation of Budd–Chiari syndrome (Gojkovic et al., 2020)), and centrally (superior sagittal sinus). Abrogated thrombosis, both peripherally and centrally (Vukojevic et al., 2018; Gojkovic et al., 2020; Kolovrat et al., 2020; Gojkovic et al., 2021a; Knezevic et al., 2021a; Knezevic et al., 2021a; Gojkovic et al., 2021b; Knezevic et al., 2021b), means that stasis was evidently avoided, or at least markedly reduced. Along with the "bypassing key" and rapidly activated collaterals, Virchow's triad was consistently reduced, both peripherally and centrally (Vukojevic et al., 2018; Gojkovic et al., 2020; Kolovrat et al., 2020; Gojkovic et al., 2021a; Knezevic et al., 2021a; Knezevic et al., 2021a; Gojkovic et al., 2021b; Knezevic et al., 2021b; Strbe et al., 2021). In particular, BPC 157-induced endothelial maintenance (Sikiric et al., 1994) and the "bypassing key" (Vukojevic et al., 2018; Gojkovic et al., 2020; Kolovrat et al., 2020; Gojkovic et al., 2021a; Knezevic et al., 2021a; Knezevic et al., 2021a; Gojkovic et al., 2021b; Knezevic et al., 2021b; Strbe et al., 2021) occur along with the previously noted BPC 157-NO system interactions. This can involve the release of NO on its own (Sikiric et al., 1997; Turkovic et al., 2004), as well as maintained NO system function against NOS blockade (L-NAME) or overfunction (L-arginine) (for review, see Sikiric et al., 2014). Furthermore, blood pressure maintenance (Sikiric et al., 1997), maintained thrombocyte function (Stupnisek et al., 2015; Konosic et al., 2019), and vasomotor tone occurred through BPC 157-specific activation of the Src-caveolin-1-eNOS pathway (Hsieh et al., 2020). Besides, the "bypassing key" also occurred with minor vessel occlusion, showing a therapeutic effect. The "bypassing pathway" may be the inferior anterior pancreaticoduodenal vein (with a reduction in duodenal congestion lesions) (Amic et al., 2018) and arcade vessels (with a reduction in left colic vein and artery occlusion-induced ischemic reperfusion colitis) (Duzel et al., 2017). An effect was also seen with parietal peritoneum removal (fewer adhesions) (Cesar et al., 2020); in cecum perforation (after perforation (Drmic et al., 2018), unlike empty vessels (not visible), blood vessels were filled with blood and were thereby clearly presented as blood vessels running toward the defect, with less bleeding and increased healing); in bile duct ligation-induced liver cirrhosis (prevention and reversal of portal hypertension) (Sever et al., 2019). Likewise, given during reperfusion after clamping the common carotid arteries, BPC 157 reduced stroke (i.e., both early and delayed hippocampal neural damage, achieving full functional recovery in the Morris water maze test, inclined beam-walking test, and lateral push test) (Vukojevic et al., 2020) or reduced L-NAME-induced retinal ischemia in rats (Zlatar et al., 2021).

Furthermore, the adequate activation of alternative pathways should occur along with the additional (direct) beneficial effects on affected targets. In addition to venous occlusion-induced lesions (Vukojevic et al., 2018; Gojkovic et al., 2020; Kolovrat et al., 2020), BPC 157 is known to reduce lesions in the entire gastrointestinal tract (Sikiric et al., 1994; Ilic et al., 2009; Sever et al., 2009; Ilic et al., 2010; Ilic et al., 2011a; Ilic et al., 2011b; Petrovic et al., 2011; Lojo et al., 2016; Drmic et al., 2017; Becejac et al., 2018). Likewise, BPC 157 may reduce lesions in the liver (Sikiric et al., 1993b; Ilic et al., 2009; Ilic et al., 2010; Ilic et al., 2011a; Ilic et al., 2011b; Lojo et al., 2016; Drmic et al., 2017), including liver cirrhosis, induced by bile duct ligation (Sever et al., 2019) or continuous alcohol consumption (Prkacin et al., 2001). Also, BPC 157 may prevent and reverse chronic heart failure induced by doxorubicin application (Lovric-Bencic et al., 2004). BPC 157 reduces various arrhythmias (i.e., potassium overdose-induced hyperkalemia (Barisic et al., 2013), digitalis (Balenovic et al., 2009), neuroleptics (i.e., prolonged QTc-intervals that may also be centrally related) (Strinic et al., 2017), bupivacaine (Zivanovic-Posilovic et al., 2016), lidocaine (Lozic et al., 2020), and succinylcholine (Stambolija et al., 2016)). Likewise, BPC 157 reduces lung congestion after vessel occlusion (Vukojevic et al., 2018; Gojkovic et al., 2020; Kolovrat et al., 2020; Gojkovic et al., 2021a; Knezevic et al., 2021a; Knezevic et al., 2021a; Gojkovic et al., 2021b; Knezevic et al., 2021b; Strbe et al., 2021), intratracheal alcohol instillation (Stancic-Rokotov et al., 2001a; Stancic-Rokotov et al., 2001b), and pulmonary hypertension syndrome in chickens (Grabarevic et al., 1997) and in monocrotaline-treated rats (Udovicic et al., 2021). As a recently reviewed subject (Vukojevic et al., 2022), BPC 157 has been shown to reduce brain lesions, trauma-induced brain injury (Tudor et al., 2010), compression-induced spinal cord injury (Perovic et al., 2019), and stroke (Vukojevic et al., 2020). In addition, BPC 157 reduces severe encephalopathies (NSAID overdose, Ilic et al., 2010; Ilic et al., 2011a; Ilic et al., 2011b; Lojo et al., 2016; Drmic et al., 2017), neurotoxin cuprizone-induced multiple sclerosis in a rat model (Klicek et al., 2013), and magnesium overdose (Medvidovic-Grubisic et al., 2017)). Importantly, BPC 157 also reduces the consequences of, i.e., gastrointestinal and/or liver lesions (Ilic et al., 2010; Ilic et al., 2011a; Ilic et al., 2011b; Lojo et al., 2016; Drmic et al., 2017) and severe muscle weakness (Klicek et al., 2013; Medvidovic-Grubisic et al., 2017)). Thus, these beneficial effects are interrelated and appear useful for the therapy of multiple vicious circles that may simultaneously appear in rats permanently maintained under severe intra-abdominal hypertension conditions. By themselves, all these disturbances, which were ameliorated/reduced, are quite severe. Considering the different causes of secondary abdominal compartment syndrome (Hunter and Damani, 2004; Hedenstierna and Larsson, 2012), these disturbances, each with a different set of causes, may also contribute to high intra-abdominal pressure, and thus when ameliorated/reduced, they may indicate the beneficial effect of BPC 157 therapy in cases of secondary high intra-abdominal pressure. There, due to its beneficial effect on damaged muscle and the recovery of its function (Staresinic et al., 2006; Novinscak et al., 2008; Mihovil et al., 2009; Pevec et al., 2010; Kang et al., 2018), it is possible that the BPC 157 therapeutic effect may also be related to improvements in abdominal wall compliance.

Finally, a summary would reveal a consistent demonstration of particular beneficial effects, i.e., the activation of collateral pathways related to the injurious occlusion (Vukojevic et al., 2018; Gojkovic et al., 2020; Kolovrat et al., 2020; Gojkovic et al., 2021a; Knezevic et al., 2021a; Knezevic et al., 2021a; Gojkovic et al., 2021b; Knezevic et al., 2021b; Strbe et al., 2021), with one or two

vessel ligations (Vukojevic et al., 2018; Gojkovic et al., 2020; Kolovrat et al., 2020; Gojkovic et al., 2021a; Knezevic et al., 2021a; Knezevic et al., 2021a; Knezevic et al., 2021b) or more (high intra-abdominal hypertension compressing all blood vessels), with either specific injury (vessel ligation) (Vukojevic et al., 2018; Gojkovic et al., 2020; Kolovrat et al., 2020; Gojkovic et al., 2021a; Knezevic et al., 2021a; Knezevic et al., 2021a; Knezevic et al., 2021b) or broad non-specific injuries (alcohol and lithium intoxication (Gojkovic et al., 2021b; Strbe et al., 2021) and intra-abdominal hypertension (present study)). These particular beneficial effects, i.e., the activation of collateral pathways, should occur along with the activated molecular pathways (Tkalčević et al., 2007; Chang et al., 2011, 2014; Huang et al., 2015; Hsieh et al., 2017; Kang et al., 2018; Vukojevic et al., 2018; Wang et al., 2019; Cesarec et al., 2013; Hsieh et al., 2020; Park et al., 2020; Vukojevic et al., 2020; Wu et al., 2020), illustrative of the complexity of the processes involved. Not only in theory but these results should also be combined with extensive studies on how BPC 157 exerts its specific effects. In one study, it affected *Egr*, *Nos*, *Srf*, *Vegfr*, *Akt1*, *Plcγ*, and *Kras* gene expression in the vessel that provides an alternative operating pathway (i.e., the left ovarian vein as the key for infrarenal occlusion-induced inferior vena cava syndrome in rats) (Vukojevic et al., 2018). In the hippocampus, BPC 157 strongly elevates *Egr1*, *Akt1*, *Kras*, *Src*, *Foxo*, *Srf*, *Vegfr2*, *Nos3,* and *Nos1* expression and decreases *Nos2* and *Nfkb* expression; these changes may indicate how BPC 157 exerts its effects (Vukojevic et al., 2020). Additionally, mitigated leaky gut syndrome suggests that BPC 157 is a stabilizer of cellular junctions by increasing tight junction protein ZO-1 expression and transepithelial resistance (Park et al., 2020). A reduction in the mRNA level of inflammatory mediators (iNOS, IL-6, IFN-γ, and TNF-α) and increased expression of HSP 70 and 90 and antioxidant proteins such as HO-1, NQO-1, glutathione reductase, glutathione peroxidase 2, and GST-pi were observed (Park et al., 2020). These findings clearly show that BPC 157 may successfully compete with the initial events in intra-abdominal hypertension (i.e., significant damage to the intestinal epithelium and dilation of intestinal tight junctions, increased mucosal barrier permeability, bacterial translocation, and sepsis (Gong et al., 2009)). Of note, the antioxidant effects of BPC 157 (Belosic Halle et al., 2017; Luetic et al., 2017; Sucic et al., 2019) occurred in both ischemic and reperfusion conditions in various tissues (i.e., colon, duodenum, cecum, liver, and veins) and plasma, in vessel occlusion studies in particular (Vukojevic et al., 2018; Kolovrat et al., 2020; Knezevic et al., 2021a; Knezevic et al., 2021a; Knezevic et al., 2021b).

Coming back to the mentioned general theoretic cytoprotection effects (Robert, 1979; Szabo et al., 1985; Sikiric et al., 2010; Sikiric et al., 2018), it should be noted that Robert's cytoprotection generally holds a defensive response against direct injuries. Possibly, as a final clue supporting cytoprotection theory, this upgraded defensive principle (i.e., preserved endothelial function promotes the organization of additional bypassing collaterals functioning to compensate against the ongoing injurious course; for review, see Sikiric et al., 2018) persists against the notion of continuous, direct injury (increased intra-abdominal hypertension) and shows that organs may adequately function despite continuously elevated intra-abdominal pressure.

Finally, calvariectomy and/or laparotomy, used in therapy to reduce abdominal compartment syndrome (Hunter and Damani, 2004; Hedenstierna and Larsson, 2012), and in the present study to assess intracranial (superior sagittal sinus), portal, inferior caval vein, and aortal pressure, and brain, organ, and vessel presentation, may not interfere with the worst circumstances created in the abdominal compartment syndrome. In fact, the evidence shows that superior sagittal sinus hypertension even increased slightly after laparotomy. Thereby, the evidenced severe superior sagittal sinus, portal, and caval hypertension and aortal hypotension occurred along with the rapid worsening that would appear along with decompression (Hsu et al., 2004). The reduction with BPC 157 is along with its previous reducing potential on severe superior sagittal sinus, portal, and caval hypertension and aortal hypotension (Vukojevic et al., 2018; Gojkovic et al., 2020; Kolovrat et al., 2020; Gojkovic et al., 2021a; Knezevic et al., 2021a; Knezevic et al., 2021a; Gojkovic et al., 2021b; Knezevic et al., 2021b; Strbe et al., 2021).

In conclusion, these findings related to BPC 157 therapy may be important in both shorter and more prolonged periods of abdominal compartment syndrome development and reduction. Of note, intra-abdominal hypertension is quite frequent in critically ill patients and the cause of multiorgan dysfunction (Hunter and Damani, 2004; Hedenstierna and Larsson, 2012). Also, we should acknowledge that animal models although quite different (Schachtrupp et al., 2007) (here, 25, 30, 40, and 50 mm Hg by intraperitoneal insufflation of ordinary air controlled and maintained by a manual manometer leads to invariable abdominal compartment syndrome), correlate fairly well with the circumstances in humans. Therefore, in principle, the application of pentadecapeptide BPC 157 therapy is effective in particular venous occlusion syndromes, as well as for recovery from all compressed blood vessels and the consequent syndrome (Vukojevic et al., 2018; Gojkovic et al., 2020; Kolovrat et al., 2020; Gojkovic et al., 2021a; Knezevic et al., 2021a; Knezevic et al., 2021a; Gojkovic et al., 2021b; Knezevic et al., 2021b; Strbe et al., 2021). Fully achieved reduction of severe lesions in the brain, heart, lungs, liver, kidneys, and gastrointestinal tract reduced thrombosis in both veins and arteries, peripherally and centrally, and fully abrogated intracranial (superior sagittal sinus), portal, and caval hypertension and aortal hypotension may be regarded as a proof of concept. This study provides evidence of reductions in all the consequences of intra-abdominal hypertension, even grade III and grade IV, which may not be concerned by the relative paucity of BPC 157 clinical data (Sikiric et al., 2018; Seiwerth et al., 2021; Vukojevic et al., 2022). BPC 157 has also been shown to be efficacious in ulcerative colitis (for review, see Sikiric et al., 2011; Sikiric et al., 2012; Sikiric et al., 2013; Sikiric et al., 2018; Sikiric et al., 2020b), in both the clinical setting (Veljaca et al., 2003; Ruenzi et al., 2005) and the experimental animal models (for review, see Sikiric et al., 2011; Sikiric et al., 2012; Sikiric et al., 2013; Sikiric et al., 2018; Sikiric et al., 2020b) and complications (for review, see Sikiric et al., 2020b). An important point regarding application in practice includes

various species (i.e., Tlak Gajger et al., 2018). However, the most important advantage is the very safe profile of BPC (the lethal dose (LD1) could be not achieved) (Seiwerth et al., 2018), emphasized in terms of its physiological role (assessed using *in situ* hybridization and immunostaining for BPC 157 in the human gastrointestinal mucosa, lung bronchial epithelium, the epidermal layer of the skin, and kidney glomeruli) (Seiwerth et al., 2018). This point was recently confirmed in a large study by Xu and collaborators (Xu et al., 2020). In this context, also for practical purposes, providing that the therapeutic effects speak for themselves, we provide a good background for further application of BPC 157 as a therapy.

DATA AVAILABILITY STATEMENT

The raw data supporting the conclusion of this article will be made available by the authors, without undue reservation.

ETHICS STATEMENT

The animal study was reviewed and approved the Ethics Committee of School of Medicine Zagreb.

AUTHOR CONTRIBUTIONS

MT and SG were responsible for the conceptualization. IK and SS were responsible for the methodology. IB, MK, and MS validated the results. ZM, GS, and HV conducted the formal analysis. LB, AS, and EL performed the investigation. IK, MM, and KS obtained the resources. AK, SS, and HZ contributed to the visualization. TK and IS administered the project. AB, SS, and PS wrote the original draft and reviewed and edited the work.

FUNDING

This work was supported by the University of Zagreb, Zagreb, Croatia (Grant BM 099).

SUPPLEMENTARY MATERIAL

The Supplementary Material for this article can be found online at: https://www.frontiersin.org/articles/10.3389/fphar.2021.718147/full#supplementary-material

REFERENCES

Amic, F., Drmic, D., Bilic, Z., Krezic, I., Zizek, H., Peklic, M., et al. (2018). Bypassing Major Venous Occlusion and Duodenal Lesions in Rats, and Therapy With the Stable Gastric Pentadecapeptide BPC 157, L-NAME and L-Arginine. *World J. Gastroenterol.* 24 (47), 5366–5378. doi:10.3748/wjg.v24.i47.5366

Balenovic, D., Bencic, M. L., Udovicic, M., Simonji, K., Hanzevacki, J. S., Barisic, I., et al. (2009). Inhibition of Methyldigoxin-Induced Arrhythmias by Pentadecapeptide BPC 157: A Relation With NO-System. *Regul. Pept.* 156 (1-3), 83–89. doi:10.1016/j.regpep.2009.05.008

Barisic, I., Balenovic, D., Klicek, R., Radic, B., Nikitovic, B., Drmic, D., et al. (2013). Mortal Hyperkalemia Disturbances in Rats Are NO-System Related. The Life Saving Effect of Pentadecapeptide BPC 157. *Regul. Pept.* 181, 50–66. doi:10.1016/j.regpep.2012.12.007

Becejac, T., Cesarec, V., Drmic, D., Hirsl, D., Madzarac, G., Djakovic, Z., et al. (2018). An Endogeous Defensive Concept, Renewed Cytoprotection/adaptive Cytoprotection: Intra(per)-Oral/Intragastric Strong Alcohol in Rat. Involvement of Pentadecapeptide BPC 157 and Nitric Oxide System. *J. Physiol. Pharmacol.* 69 (3), 429–440. doi:10.26402/jpp.2018.3.11

Belosic Halle, Z., Vlainic, J., Drmic, D., Strinic, D., Luetic, K., Sucic, M., et al. (2017). Class Side Effects: Decreased Pressure in the Lower Oesophageal and the Pyloric Sphincters After the Administration of Dopamine Antagonists, Neuroleptics, Anti-emetics, L-NAME, Pentadecapeptide BPC 157 and L-Arginine. *Inflammopharmacology*. 25, 511–522. doi:10.1007/s10787-017-0358-8

Bona, E., Hagberg, H., Løberg, E. M., Bågenholm, R., and Thoresen, M. (1998). Protective Effects of Moderate Hypothermia After Neonatal Hypoxia-Ischemia: Short- and Long-Term Outcome. *Pediatr. Res.* 43 (6), 738–745. doi:10.1203/00006450-199806000-00005

Cesar, L. B., Gojkovic, S., Krezic, I., Malekinusic, D., Zizek, H., Vuletic, L. B., et al. (2020). Bowel Adhesion and Therapy With the Stable Gastric Pentadecapeptide BPC 157, L-NAME and L-Arginine in Rats. *World J. Gastrointest. Pharmacol. Ther.* 11 (5), 93–109. doi:10.4292/wjgpt.v11.i5.93

Chan, C. W., Leung, Y. K., and Chan, K. W. (2014). Microscopic Anatomy of the Vasculature of the Human Intestinal Villus - a Study with Review. *Eur. J. Anat.* 18 (4), 291–301.

Chang, C. H., Tsai, W. C., Hsu, Y. H., and Pang, J. H. (2014). Pentadecapeptide BPC 157 Enhances the Growth Hormone Receptor Expression in Tendon Fibroblasts. *Molecules.* 19 (11), 19066–19077. doi:10.3390/molecules191119066

Chang, C. H., Tsai, W. C., Lin, M. S., Hsu, Y. H., and Pang, J. H. (2011). The Promoting Effect of Pentadecapeptide BPC 157 on Tendon Healing Involves Tendon Outgrowth, Cell Survival, and Cell Migration. *J. Appl. Physiol.* 110 (3), 774–780. doi:10.1152/japplphysiol.00945.2010

Chen, H. I. (2009). From Neurogenic Pulmonary Edema to Fat Embolism Syndrome: a Brief Review of Experimental and Clinical Investigations of Acute Lung Injury and Acute Respiratory Distress Syndrome. *Chin. J. Physiol.* 52 (5), 339–344. doi:10.4077/cjp.2009.amh036

Chen, M., Jiang, L., Li, Y., Bai, G., Zhao, J., Zhang, M., et al. (2017). Hydrogen Protects against Liver Injury during CO2 Pneumoperitoneum in Rats. *Oncotarget.* 9 (2), 2631–2645. doi:10.18632/oncotarget.23498

Chen, P., Tang, H., Zhang, Q., Xu, L., Zhou, W., Hu, X., et al. (2020). Basic Fibroblast Growth Factor (bFGF) Protects the Blood-Brain Barrier by Binding of FGFR1 and Activating the ERK Signaling Pathway after Intra-Abdominal Hypertension and Traumatic Brain Injury. *Med. Sci. Monit.* 26, e922009. doi:10.12659/MSM.922009

Cullen, D. J., Coyle, J. P., Teplick, R., and Long, M. C. (1989). Cardiovascular, Pulmonary, and Renal Effects of Massively Increased Intra-Abdominal Pressure in Critically Ill Patients. *Crit. Care Med.* 17 (2), 118–121. doi:10.1097/00003246-198902000-00002

Depauw, P. R. A. M., Groen, R. J. M., Van Loon, J., Peul, W. C., Malbrain, M. L. N. G., and De Waele, J. J. (2019). The Significance of Intra-Abdominal Pressure in Neurosurgery and Neurological Diseases: a Narrative Review and a Conceptual Proposal. *Acta Neurochir (Wien).* 161 (5), 855–864. doi:10.1007/s00701-019-03868-7

Drmic, D., Kolenc, D., Ilic, S., Bauk, L., Sever, M., Zenko Sever, A., et al. (2017). Celecoxib-Induced Gastrointestinal, Liver and Brain Lesions in Rats, Counteraction by BPC 157 or L-Arginine, Aggravation by L-NAME. *World J. Gastroenterol.* 23 (29), 5304–5312. doi:10.3748/wjg.v23.i29.5304

Drmic, D., Samara, M., Vidovic, T., Malekinusic, D., Antunovic, M., Vrdoljak, B., et al. (2018). Counteraction of Perforated Cecum Lesions in Rats: Effects of Pentadecapeptide BPC 157, L-NAME and L-Arginine. *World J. Gastroenterol.* 24 (48), 5462–5476. doi:10.3748/wjg.v24.i48.5462

Duzel, A., Vlainic, J., Antunovic, M., Malekinusic, D., Vrdoljak, B., Samara, M., et al. (2017). Stable Gastric Pentadecapeptide BPC 157 in the Treatment of Colitis and Ischemia and Reperfusion in Rats: New Insights. *World J. Gastroenterol.* 23 (48), 8465–8488. doi:10.3748/wjg.v23.i48.8465

Eustis, S., Elwell, M., and MacKenzie, W. (2017). *Boorman's Pathology of the Rat in Reference and Atlas*. 2nd Edition (Academic Press).

Gojkovic, S., Krezic, I., Vranes, H., Zizek, H., Drmic, D., Horvat Pavlov, K., et al. (2021a). BPC 157 Therapy and the Permanent Occlusion of the superior Sagittal Sinus in Rat: Vascular Recruitment. *Biomedicines*. 9 (7), 744. doi:10.3390/biomedicines9070744

Gojkovic, S., Krezic, I., Vranes, H., Zizek, H., Drmic, D., Batelja Vuletic, L., et al. (2021b). Robert's Intragastric Alcohol-Induced Gastric Lesion Model as an Escalated General Peripheral and Central Syndrome, Counteracted by the Stable Gastric Pentadecapeptide BPC 157. *Biomedicines*. 9, 1300. doi:10.3390/biomedicines9101300

Gojkovic, S., Krezic, I., Vrdoljak, B., Malekinusic, D., Barisic, I., Petrovic, A., et al. (2020). Pentadecapeptide BPC 157 Resolves Suprahepatic Occlusion of the Inferior Caval Vein, Budd-Chiari Syndrome Model in Rats. *World J. Gastrointest. Pathophysiol.* 11 (1), 1–19. doi:10.4291/wjgp.v11.i1.1

Gong, G., Wang, P., Ding, W., Zhao, Y., and Li, J. (2009). Microscopic and Ultrastructural Changes of the Intestine in Abdominal Compartment Syndrome. *J. Invest. Surg.* 22 (5), 362–367. doi:10.1080/08941930903214719

Grabarevic, Z., Tisljar, M., Artukovic, B., Bratulic, M., Dzaja, P., Seiwerth, S., et al. (1997). The Influence of BPC 157 on Nitric Oxide Agonist and Antagonist Induced Lesions in Broiler Chicks. *J. Physiol. Paris.* 91 (3-5), 139–149. doi:10.1016/s0928-4257(97)89478-8

Gwyer, D., Wragg, N. M., and Wilson, S. L. (2019). Gastric Pentadecapeptide Body Protection Compound BPC 157 and its Role in Accelerating Musculoskeletal Soft Tissue Healing. *Cell Tissue Res.* 377 (2), 153–159. doi:10.1007/s00441-019-03016-8

Hedenstierna, G., and Larsson, A. (2012). Influence of Abdominal Pressure on Respiratory and Abdominal Organ Function. *Curr. Opin. Crit. Care.* 18 (1), 80–85. doi:10.1097/MCC.0b013e32834e7c3a

Hrelec, M., Klicek, R., Brcic, L., Brcic, I., Cvjetko, I., Seiwerth, S., et al. (2009). Abdominal Aorta Anastomosis in Rats and Stable Gastric Pentadecapeptide BPC 157, Prophylaxis and Therapy. *J. Physiol. Pharmacol.* 60 (7), 161–165.

Hsieh, M. J., Lee, C. H., Chueh, H. Y., Chang, G. J., Huang, H. Y., Lin, Y., et al. (2020). Modulatory Effects of BPC 157 on Vasomotor Tone and the Activation of Src-Caveolin-1-Endothelial Nitric Oxide Synthase Pathway. *Sci. Rep.* 10 (1), 17078. doi:10.1038/s41598-020-74022-y

Hsieh, M. J., Liu, H. T., Wang, C. N., Huang, H. Y., Lin, Y., Ko, Y. S., et al. (2017). Therapeutic Potential of Pro-Angiogenic BPC157 Is Associated With VEGFR2 Activation and Up-Regulation. *J. Mol. Med. (Berl).* 95 (3), 323–333. doi:10.1007/s00109-016-1488-y

Hsu, Y. P., Chen, R. J., Fang, J. F., Lin, B. C., Huang, T. L., Cheng, M. L., et al. (2004). Increased Susceptibility to Oxidant Injury in Hepatocytes From Rats With Intra-Abdominal Hypertension. *J. Trauma.* 57 (3), 569–575. doi:10.1097/01.ta.0000087648.01543.9f

Huang, T., Zhang, K., Sun, L., Xue, X., Zhang, C., Shu, Z., et al. (2015). Body Protective Compound-157 Enhances Alkali-Burn Wound Healing *In Vivo* and Promotes Proliferation, Migration, and Angiogenesis *In Vitro*. *Drug Des. Devel Ther.* 9, 2485–2499. doi:10.2147/DDDT.S82030

Hunter, J. D., and Damani, Z. (2004). Intra-Abdominal Hypertension and the Abdominal Compartment Syndrome. *Anaesthesia.* 59 (9), 899–907. doi:10.1111/j.1365-2044.2004.03712.x

Ibrahim, M. Y., Abdul, A. B. H., Ibrahim, T. A. T., Abdelwahab, S. I., Elhassan, M. M., and Syam, M. M. (2010). Evaluation of Acute Toxicity and the Effect of Single Injected Doses of Zerumbone on the Kidney and Liver Functions in Sprague Dawley Rats. *Afr. J. Biotechnol.* 9, 442–445.

Ilic, S., Brcic, I., Mester, M., Filipovic, M., Sever, M., Klicek, R., et al. (2009). Over-dose Insulin and Stable Gastric Pentadecapeptide BPC 157. Attenuated Gastric Ulcers, Seizures, Brain Lesions, Hepatomegaly, Fatty Liver, Breakdown of Liver Glycogen, Profound Hypoglycemia and Calcification in Rats. *J. Physiol. Pharmacol.* 60 Suppl 7 (7), 107–114.

Ilic, S., Drmic, D., Zarkovic, K., Kolenc, D., Brcic, L., Radic, B., et al. (2011a). Ibuprofen Hepatic Encephalopathy, Hepatomegaly, Gastric Lesion and Gastric Pentadecapeptide BPC 157 in Rats. *Eur. J. Pharmacol.* 667 (1-3), 322–329. doi:10.1016/j.ejphar.2011.05.038s.2011.01.015

Ilic, S., Drmic, D., Franjic, S., Kolenc, D., Coric, M., Brcic, L., et al. (2011b). Pentadecapeptide BPC 157 and its Effects on a NSAID Toxicity Model: Diclofenac-Induced Gastrointestinal, Liver, and Encephalopathy Lesions. *Life Sci.* 88 (11-12), 535–542. doi:10.1016/j.lf10.1016/j.lfs.2011.01.015

Ilic, S., Drmic, D., Zarkovic, K., Kolenc, D., Coric, M., Brcic, L., et al. (2010). High Hepatotoxic Dose of Paracetamol Produces Generalized Convulsions and Brain Damage in Rats. A Counteraction With the Stable Gastric Pentadecapeptide BPC 157 (PL 14736). *J. Physiol. Pharmacol.* 61 (2), 241–250.

Kang, E. A., Han, Y. M., An, J. M., Park, Y. J., Sikiric, P., Kim, D. H., et al. (2018). BPC157 as Potential Agent Rescuing From Cancer Cachexia. *Curr. Pharm. Des.* 24 (18), 1947–1956. doi:10.2174/1381612824666180614082950

Klicek, R., Kolenc, D., Suran, J., Drmic, D., Brcic, L., Aralica, G., et al. (2013). Stable Gastric Pentadecapeptide BPC 157 Heals Cysteamine-Colitis and Colon-Colon-Anastomosis and Counteracts Cuprizone Brain Injuries and Motor Disability. *J. Physiol. Pharmacol.* 64 (5), 597–612.

Knezevic, M., Gojkovic, S., Krezic, I., Zizek, H., Vranes, H., Malekinusic, D., et al. (2021a). Complex Syndrome of the Complete Occlusion of the End of the Superior Mesenteric Vein, Opposed With the Stable Gastric Pentadecapeptide BPC 157 in Rats. *Biomedicines*. 9 (8), 1029. doi:10.3390/biomedicines9081029

Knezevic, M., Gojkovic, S., Krezic, I., Zizek, H., Malekinusic, D., Vrdoljak, B., et al. (2021b). Occluded superior Mesenteric Artery and Vein. Therapy With the Stable Gastric Pentadecapeptide BPC 157. *Biomedicines*. 9 (7), 792. doi:10.3390/biomedicines9070792

Kolovrat, M., Gojkovic, S., Krezic, I., Malekinusic, D., Vrdoljak, B., Kasnik Kovac, K., et al. (2020). Pentadecapeptide BPC 157 Resolves Pringle Maneuver in Rats, Both Ischemia and Reperfusion. *World J. Hepatol.* 12 (5), 184–206. doi:10.4254/wjh.v12.i5.184

Konosic, S., Petricevic, M., Ivancan, V., Konosic, L., Goluza, E., Krtalic, B., et al. (2019). Intragastric Application of Aspirin, Clopidogrel, Cilostazol, and BPC 157 in Rats: Platelet Aggregation and Blood Clot. *Oxid Med. Cell Longev.* 2019, 9084643. doi:10.1155/2019/9084643

Lojo, N., Rasic, Z., Zenko Sever, A., Kolenc, D., Vukusic, D., Drmic, D., et al. (2016). Effects of Diclofenac, L-NAME, L-Arginine, and Pentadecapeptide BPC 157 on Gastrointestinal, Liver, and Brain Lesions, Failed Anastomosis, and Intestinal Adaptation Deterioration in 24 hour-Short-Bowel Rats. *PLoS One.* 11 (9), e0162590. doi:10.1371/journal.pone.0162590

Lovric-Bencic, M., Sikiric, P., Hanzevacki, J. S., Seiwerth, S., Rogic, D., Kusec, V., et al. (2004). Doxorubicine-Congestive Heart Failure-Increased Big Endothelin-1 Plasma Concentration: Reversal by Amlodipine, Losartan, and Gastric Pentadecapeptide BPC157 in Rat and Mouse. *J. Pharmacol. Sci.* 95, 19–26. doi:10.1254/jphs.95.19

Lozic, M., Stambolija, V., Krezic, I., Dugandzic, A., Zivanovic-Posilovic, G., Gojkovic, S., et al. (2020). In Relation to NO-System, Stable Pentadecapeptide BPC 157 Counteracts Lidocaine-Induced Adverse Effects in Rats and Depolarisation *In Vitro*. *Emerg. Med. Int.* 2020, 6805354. doi:10.1155/2020/6805354

Luetic, K., Sucic, M., Vlainic, J., Halle, Z. B., Strinic, D., Vidovic, T., et al. (2017). Cyclophosphamide Induced Stomach and Duodenal Lesions as a NO-System Disturbance in Rats: L-NAME, L-Arginine, Stable Gastric Pentadecapeptide BPC 157. *Inflammopharmacology.* 25 (2), 255–264. doi:10.1007/s10787-017-0330-7

Malbrain, M. L., and Wilmer, A. (2007). The Polycompartment Syndrome: Towards an Understanding of the Interactions Between Different Compartments!. *Intensive Care Med.* 33 (11), 1869–1872. doi:10.1007/s00134-007-0843-4

Medvidovic-Grubisic, M., Stambolija, V., Kolenc, D., Katancic, J., Murselovic, T., Plestina-Borjan, I., et al. (2017). Hypermagnesemia Disturbances in Rats, NO-Related: Pentadecapeptide BPC 157 Abrogates, L-NAME and L-Arginine Worsen. *Inflammopharmacology.* 25 (4), 439–449. doi:10.1007/s10787-017-0323-6

Mihovil, I., Radic, B., Brcic, L., Brcic, I., Vukoja, I., Ilic, S., et al. (2009). Beneficial Effect of Pentadecapeptide BPC 157 on Denervated Muscle in Rats. *J. Physiol. Pharmacol.* 60 (2), 69.

Novinscak, T., Brcic, L., Staresinic, M., Jukic, I., Radic, B., Pevec, D., et al. (2008). Gastric Pentadecapeptide BPC 157 as an Effective Therapy for Muscle Crush Injury in the Rat. *Surg. Today.* 38 (8), 716–725. doi:10.1007/s00595-007-3706-2

Park, J. M., Lee, H. J., Sikiric, P., and Hahm, K. B. (2020). BPC 157 Rescued NSAID-Cytotoxicity via Stabilizing Intestinal Permeability and Enhancing Cytoprotection. *Curr. Pharm. Des.* 26 (25), 2971–2981. doi:10.2174/1381612826666200523180301

Perovic, D., Kolenc, D., Bilic, V., Somun, N., Drmic, D., Elabjer, E., et al. (2019). Stable Gastric Pentadecapeptide BPC 157 Can Improve the Healing Course of

Spinal Cord Injury and lead to Functional Recovery in Rats. *J. Orthop. Surg. Res.* 14 (1), 199. doi:10.1186/s13018-019-1242-6

Petrovic, I., Dobric, I., Drmic, D., Sever, M., Klicek, R., Radic, B., et al. (2011). BPC 157 Therapy to Detriment Sphincters Failure-Esophagitis-Pancreatitis in Rat and Acute Pancreatitis Patients Low Sphincters Pressure. *J. Physiol. Pharmacol.* 62 (5), 527–534.

Pevec, D., Novinscak, T., Brcic, L., Sipos, K., Jukic, I., Staresinic, M., et al. (2010). Impact of Pentadecapeptide BPC 157 on Muscle Healing Impaired by Systemic Corticosteroid Application. *Med. Sci. Monit.* 16 (3), BR81–88.

Prkacin, I., Separovic, J., Aralicia, G., Perovic, D., Gjurasin, M., Lovric-Bencic, M., et al. (2001). Portal Hypertension and Liver Lesions in Chronically Alcohol Drinking Rats Prevented and Reversed by Stable Gastric Pentadecapeptide BPC 157 (PL-10, PLD-116), and Propranolol, but Not Ranitidine. *J. Physiol. Paris.* 95 (1-6), 315–324. doi:10.1016/s0928-4257(01)00044-4

Robert, A., Nezamis, J. E., Lancaster, C., and Hanchar, A. J. (1979). Cytoprotection by Prostaglandins in Rats. Prevention of Gastric Necrosis Produced by Alcohol, HCl, NaOH, Hypertonic NaCl, and thermal Injury. *Gastroenterology.* 77, 433–443. doi:10.1016/0016-5085(79)90235-x

Ruenzi, M., Stolte, M., Veljaca, M., Oreskovic, K., and Peterson, J.Ulcerative Colitis Study Group (2005). A Multicenter, Randomized, Double Blind, Placebo Controlled Phase II Study of PL 14736 Enema in the Treatment of Mild-To-Moderate Ulcerative Colitis. *Gastroenterology.* 128, 584.

Scalea, T. M., Bochicchio, G. V., Habashi, N., McCunn, M., Shih, D., McQuillan, K., et al. (2007). Increased Intra-Abdominal, Intrathoracic, and Intracranial Pressure after Severe Brain Injury: Multiple Compartment Syndrome. *J. Trauma.* 62 (3), 647–656. doi:10.1097/TA.0b013e31802ee542

Schachtrupp, A., Wauters, J., and Wilmer, A. (2007). What Is the Best Animal Model for Acs? *Acta Clin. Belg.* 62 Suppl 1 (1), 225–232. doi:10.1179/acb.2007.62.s1.031

Seiwerth, S., Brcic, L., Vuletic, L. B., Kolenc, D., Aralica, G., Misic, M., et al. (2014). BPC 157 and Blood Vessels. *Curr. Pharm. Des.* 20 (7), 1121–1125. doi:10.2174/13816128113199990421

Seiwerth, S., Milavic, M., Vukojevic, J., Gojkovic, S., Krezic, I., Vuletic, L. B., et al. (2021). Stable Gastric Pentadecapeptide BPC 157 and Wound Healing. *Front. Pharmacol.* 12, 627533. doi:10.3389/fphar.2021.627533

Seiwerth, S., Rucman, R., Turkovic, B., Sever, M., Klicek, R., Radic, B., et al. (2018). BPC 157 and Standard Angiogenic Growth Factors. Gastrointestinal Tract Healing, Lessons From Tendon, Ligament, Muscle and Bone Healing. *Curr. Pharm. Des.* 24 (18), 1972–1989. doi:10.2174/1381612824666180712110447

Sever, A. Z., Sever, M., Vidovic, T., Lojo, N., Kolenc, D., Vuletic, L. B., et al. (2019). Stable Gastric Pentadecapeptide BPC 157 in the Therapy of the Rats With Bile Duct Ligation. *Eur. J. Pharmacol.* 847, 130–142. doi:10.1016/j.ejphar.2019.01.030

Sever, M., Klicek, R., Radic, B., Brcic, L., Zoricic, I., Drmic, D., et al. (2009). Gastric Pentadecapeptide BPC 157 and Short Bowel Syndrome in Rats. *Dig. Dis. Sci.* 54 (10), 2070–2083. doi:10.1007/s10620-008-0598-y

Sikiric, P., Hahm, K. B., Blagaic, A. B., Tvrdeic, A., Pavlov, K. H., Petrovic, A., et al. (2020a). Stable Gastric Pentadecapeptide BPC 157, Robert's Stomach Cytoprotection/Adaptive Cytoprotection/Organoprotection, and Selye's Stress Coping Response: Progress, Achievements, and the Future. *Gut Liver.* 14 (2), 153–167. doi:10.5009/gnl18490

Sikiric, P., Drmic, D., Sever, M., Klicek, R., Blagaic, A. B., Tvrdeic, A., et al. (2020b). Fistulas Healing. Stable Gastric Pentadecapeptide BPC 157 Therapy. *Curr. Pharm. Des.* 26 (25), 2991–3000. doi:10.2174/1381612826666200424180139

Sikirić, P., Petek, M., Rucman, R., Seiwerth, S., Grabarević, Z., Rotkvić, I., et al. (1993a). A New Gastric Juice Peptide, BPC. An Overview of the Stomach-Stress-Organoprotection Hypothesis and Beneficial Effects of BPC. *J. Physiol. Paris.* 87 (5), 313–327. doi:10.1016/0928-4257(93)90038-u

Sikiric, P., Seiwerth, S., Grabarevic, Z., Rucman, R., Petek, M., Rotkvic, I., et al. (1993b). Hepatoprotective Effect of BPC 157, a 15-Amino Acid Peptide, on Liver Lesions Induced by Either Restraint Stress or Bile Duct and Hepatic Artery Ligation or CCl4 Administration. A Comparative Study With Dopamine Agonists and Somatostatin. *Life Sci.* 53 (18), PL291–6. doi:10.1016/0024-3205(93)90589-u

Sikiric, P., Rucman, R., Turkovic, B., Sever, M., Klicek, R., Radic, B., et al. (2018). Novel Cytoprotective Mediator, Stable Gastric Pentadecapeptide BPC 157. Vascular Recruitment and Gastrointestinal Tract Healing. *Curr. Pharm. Des.* 24 (18), 1990–2001. doi:10.2174/1381612824666180608101119

Sikiric, P., Seiwerth, S., Brcic, L., Blagaic, A. B., Zoricic, I., Sever, M., et al. (2006). Stable Gastric Pentadecapeptide BPC 157 in Trials for Inflammatory Bowel Disease (PL-10, PLD-116, PL 14736, Pliva, Croatia). Full and Distended Stomach, and Vascular Response. *Inflammopharmacology.* 14 (5-6), 214–221. doi:10.1007/s10787-006-1531-7

Sikiric, P., Seiwerth, S., Brcic, L., Sever, M., Klicek, R., Radic, B., et al. (2010). Revised Robert's Cytoprotection and Adaptive Cytoprotection and Stable Gastric Pentadecapeptide BPC 157. Possible Significance and Implications for Novel Mediator. *Curr. Pharm. Des.* 16 (10), 1224–1234. doi:10.2174/138161210790945977

Sikiric, P., Seiwerth, S., Grabarevic, Z., Petek, M., Rucman, R., Turkovic, B., et al. (1994). The Beneficial Effect of BPC 157, a 15 Amino Acid Peptide BPC Fragment, on Gastric and Duodenal Lesions Induced by Restraint Stress, Cysteamine and 96% Ethanol in Rats. A Comparative Study With H2 Receptor Antagonists, Dopamine Promotors and Gut Peptides. *Life Sci.* 54 (5), PL63–8. doi:10.1016/0024-3205(94)00796-9

Sikiric, P., Seiwerth, S., Rucman, R., Drmic, D., Stupnisek, M., Kokot, A., et al. (2017). Stress in Gastrointestinal Tract and Stable Gastric Pentadecapeptide BPC 157. Finally, Do We Have a Solution? *Curr. Pharm. Des.* 23 (27), 4012–4028. doi:10.2174/1381612823666170220163219

Sikiric, P., Seiwerth, S., Rucman, R., Kolenc, D., Vuletic, L. B., Drmic, D., et al. (2016). Brain-gut Axis and Pentadecapeptide BPC 157: Theoretical and Practical Implications. *Curr. Neuropharmacol.* 14 (8), 857–865. doi:10.2174/1570159x13666160502153022

Sikiric, P., Seiwerth, S., Rucman, R., Turkovic, B., Rokotov, D. S., Brcic, L., et al. (2013). Toxicity by NSAIDs. Counteraction by Stable Gastric Pentadecapeptide BPC 157. *Curr. Pharm. Des.* 19 (1), 76–83. doi:10.2174/13816128130111

Sikiric, P., Seiwerth, S., Rucman, R., Turkovic, B., Rokotov, D. S., Brcic, L., et al. (2014). Stable Gastric Pentadecapeptide BPC 157-NO-System Relation. *Curr. Pharm. Des.* 20 (7), 1126–1135. doi:10.2174/13816128113190990411

Sikiric, P., Seiwerth, S., Rucman, R., Turkovic, B., Rokotov, D. S., Brcic, L., et al. (2012). Focus on Ulcerative Colitis: Stable Gastric Pentadecapeptide BPC 157. *Curr. Med. Chem.* 19 (1), 126–132. doi:10.2174/092986712803414015

Sikiric, P., Seiwerth, S., Rucman, R., Turkovic, B., Rokotov, D. S., Brcic, L., et al. (2011). Stable Gastric Pentadecapeptide BPC 157: Novel Therapy in Gastrointestinal Tract. *Curr. Pharm. Des.* 17 (16), 1612–1632. doi:10.2174/138161211796196954

Sikiric, P., Seiwerth, S., Grabarevic, Z., Rucman, R., Petek, M., Jagic, V., et al. (1997). The Influence of a Novel Pentadecapeptide, BPC 157, on N(G)-Nitro-L-Arginine Methylester and L-Arginine Effects on Stomach Mucosa Integrity and Blood Pressure. *Eur. J. Pharmacol.* 332 (1), 23–33. doi:10.1016/s0014-2999(97)01033-9

Stambolija, V., Stambolija, T. P., Holjevac, J. K., Murselovic, T., Radonic, J., Duzel, V., et al. (2016). BPC 157: The Counteraction of Succinylcholine, Hyperkalemia, and Arrhythmias. *Eur. J. Pharmacol.* 781, 83–91. doi:10.1016/j.ejphar.2016.04.004

Stancic-Rokotov, D., Sikiric, P., Seiwerth, S., Slobodnjak, Z., Aralica, J., Aralica, G., et al. (2001a). Ethanol Gastric Lesion Aggravated by Lung Injury in Rat. Therapy Effect of Antiulcer Agents. *J. Physiol. Paris.* 95 (1-6), 289–293. doi:10.1016/s0928-4257(01)00040-7

Stancic-Rokotov, D., Slobodnjak, Z., Aralica, J., Aralica, G., Perovic, D., Staresinic, M., et al. (2001b). Lung Lesions and Anti-Ulcer Agents Beneficial Effect: Anti-Ulcer Agents Pentadecapeptide BPC 157, Ranitidine, Omeprazole and Atropine Ameliorate Lung Lesion in Rats. *J. Physiol. Paris.* 95 (1-6), 303–308. doi:10.1016/s0928-4257(01)00042-0

Staresinic, M., Petrovic, I., Novinscak, T., Jukic, I., Pevec, D., Suknaic, S., et al. (2006). Effective Therapy of Transected Quadriceps Muscle in Rat: Gastric Pentadecapeptide BPC 157. *J. Orthop. Res.* 24 (5), 1109–1117. doi:10.1002/jor.20089

Strang, S. G., van der Hoven, B., Monkhorst, K., Ali, S., van Lieshout, E. M. M., van Waes, O. J. F., et al. (2020). Relation Between Intra-Abdominal Pressure and Early Intestinal Ischemia in Rats. *Trauma Surg. Acute Care Open.* 5 (1), e000595. doi:10.1136/tsaco-2020-000595

Strbe, S., Gojkovic, S., Krezic, I., Zizek, H., Vranes, H., Barisic, I., et al. (2021). Over-Dose Lithium Toxicity as an Occlusive-Like Syndrome in Rats and Gastric Pentadecapeptide BPC 157. *Biomedicines.* 9, 1506. doi:10.3390/biomedicines9111506

Strinic, D., Belosic Halle, Z., Luetic, K., Nedic, A., Petrovic, I., Sucic, M., et al. (2017). BPC 157 Counteracts QTc Prolongation Induced by Haloperidol,

Fluphenazine, Clozapine, Olanzapine, Quetiapine, Sulpiride, and Metoclopramide in Rats. *Life Sci.* 186, 66–79. doi:10.1016/j.lfs.2017.08.006

Stupnisek, M., Kokot, A., Drmic, D., Hrelec Patrlj, M., Zenko Sever, A., Kolenc, D., et al. (2015). Pentadecapeptide BPC 157 Reduces Bleeding and Thrombocytopenia After Amputation in Rats Treated With Heparin, Warfarin, L-NAME and L-Arginine. *PLoS One.* 10 (4), e0123454. doi:10.1371/journal.pone.0123454

Sucic, M., Luetic, K., Jandric, I., Drmic, D., Sever, A. Z., Vuletic, L. B., et al. (2019). Therapy of the Rat Hemorrhagic Cystitis Induced by Cyclophosphamide. Stable Gastric Pentadecapeptide BPC 157, L-Arginine, L-NAME. *Eur. J. Pharmacol.* 861, 172593. doi:10.1016/j.ejphar.2019.172593

Szabo, S., Trier, J. S., Brown, A., and Schnoor, J. (1985). Early Vascular Injury and Increased Vascular Permeability in Gastric Mucosal Injury Caused by Ethanol in the Rat. *Gastroenterology.* 88 (1-2), 228–236. doi:10.1016/s0016-5085(85)80176-1

Teshfam, M., Saeidi, J., and Zarei, A. (2010). Morphological and Enzymological Studies of the Small Intestine Villi of Rats Receiving Diets Containing Different Levels of Protein. *J. Appl. Anim. Res.* 37 (2), 207–211. doi:10.1080/09712119.2010.9707125

Tkalčević, V. I., Čužić, S., Brajša, K., Mildner, B., Bokulić, A., Šitum, K., et al. (2007). Enhancement by PL 14736 of Granulation and Collagen Organization in Healing Wounds and the Potential Role of Egr-1 Expression. *Eur. J. Pharmacol.* 570 (1-3), 212–221. doi:10.1016/j.ejphar.2007.05.072

Tlak Gajger, I., Ribarić, J., Smodiš Škerl, M., Vlainić, J., and Sikirić, P. (2018). Stable Gastric Pentadecapeptide BPC 157 in Honeybee (*Apis mellifera*) Therapy, to Control Nosema Ceranae Invasions in Apiary Conditions. *J. Vet. Pharmacol. Ther.* 41, 614–621. doi:10.1111/jvp.12509

Tudor, M., Jandric, I., Marovic, A., Gjurasin, M., Perovic, D., Radic, B., et al. (2010). Traumatic Brain Injury in Mice and Pentadecapeptide BPC 157 Effect. *Regul. Pept.* 160 (1-3), 26–32. doi:10.1016/j.regpep.2009.11.012

Turkovic, B., Sikiric, P., Seiwerth, S., Mise, S., Anic, T., Petek, M., et al. (2004). Stable Gastric Pentadecapeptide BPC 157 Studied for Inflammatory Bowel Disease (PLD-116, PL14736, Pliva) Induces Nitric Oxide Synthesis. *Gastroenterology.* 126, 287.

Udovicic, M., Sever, M., Kavur, L., Loncaric, K., Barisic, I., Balenovic, D., et al. (2021). Stable Gastric Pentadecapeptide BPC 157 Therapy for Monocrotaline-Induced Pulmonary Hypertension in Rats Leads to Prevention and Reversal. *Biomedicines.* 9 (7), 822. doi:10.3390/biomedicines9070822

Veljaca, M., Pavić-Sladoljev, D., Mildner, B., Brajsa, K., Krnic, Z., Bubenik, M., et al. (2003). Safety, Tolerability and Pharmacokinetics of PL 14736, a Novel Agent for Treatment of Ulcerative Colitis, in Healthy Male Volunteers. *Gut.* 51 (Suppl. III), A309.

Vukojevic, J., Milavić, M., Perović, D., Ilić, S., Čilić, A. Z., Đuran, N., et al. (2022). Pentadecapeptide BPC 157 and the central Nervous System. *Neural Regen. Res.* 17 (3), 482–487. doi:10.4103/1673-5374.320969

Vukojević, J., Siroglavić, M., Kašnik, K., Kralj, T., Stanćić, D., Kokot, A., et al. (2018). Rat Inferior Caval Vein (ICV) Ligature and Particular New Insights With the Stable Gastric Pentadecapeptide BPC 157. *Vasc. Pharmacol.* 106, 54–66. doi:10.1016/j.vph.2018.02.010

Vukojević, J., Vrdoljak, B., Malekinušić, D., Siroglavić, M., Milavić, M., Kolenc, D., et al. (2020). The Effect of Pentadecapeptide BPC 157 on Hippocampal Ischemia/Reperfusion Injuries in Rats. *Brain Behav.* 10 (8), e01726. doi:10.1002/brb3.1726

Wang, X. Y., Qu, M., Duan, R., Shi, D., Jin, L., Gao, J., et al. (2019). Cytoprotective Mechanism of the Novel Gastric Peptide BPC157 in Gastrointestinal Tract and Cultured Enteric Neurons and Glial Cells. *Neurosci. Bull.* 35 (1), 167–170. doi:10.1007/s12264-018-0269-8

Wu, H., Wei, M., Li, N., Lu, Q., Shrestha, S. M., Tan, J., et al. (2020). Clopidogrel-Induced Gastric Injury in Rats Is Attenuated by Stable Gastric Pentadecapeptide BPC 157. *Drug Des. Devel Ther.* 14, 5599–5610. doi:10.2147/DDDT.S284163

Xingwei, X., Xin, G., Peng, Z., Tao, F., Bowen, D., Xiaoming, K., et al. (2014). Low-Dose Ketamine Pretreatment Reduces Oxidative Damage and Inflammatory Response Following CO2 Pneumoperitoneum in Rats. *Clin. Invest. Med.* 37 (3), E124. doi:10.25011/cim.v37i3.21379

Xu, C., Sun, L., Ren, F., Huang, P., Tian, Z., Cui, J., et al. (2020). Preclinical Safety Evaluation of Body Protective Compound-157, a Potential Drug for Treating Various Wounds. *Regul. Toxicol. Pharmacol.* 114, 104665. doi:10.1016/j.yrtph.2020.104665

Youssef, A. M., Hamidian Jahromi, A., Vijay, C. G., Granger, D. N., and Alexander, J. S. (2012). Intra-Abdominal Hypertension Causes Reversible Blood-Brain Barrier Disruption. *J. Trauma Acute Care Surg.* 72 (1), 183–188. doi:10.1097/TA.0b013e31822a3254

Zivanovic-Posilovic, G., Balenovic, D., Barisic, I., Strinic, D., Stambolija, V., Udovicic, M., et al. (2016). Stable Gastric Pentadecapeptide BPC 157 and Bupivacaine. *Eur. J. Pharmacol.* 793, 56–65. doi:10.1016/j.ejphar.2016.10.035

Zlatar, M., Kokot, A., Vuletic, L. B., Masnec, S., Kralj, T., Perisa, M. M., et al. (2021). BPC 157 as a Therapy for Retinal Ischemia Induced by Retrobulbar Application of L-NAME in Rats. *Front. Pharmacol.* 12, 632295. doi:10.3389/fphar.2021.632295

Conflict of Interest: The authors declare that the research was conducted in the absence of any commercial or financial relationships that could be construed as a potential conflict of interest.

Publisher's Note: All claims expressed in this article are solely those of the authors and do not necessarily represent those of their affiliated organizations, or those of the publisher, the editors and the reviewers. Any product that may be evaluated in this article, or claim that may be made by its manufacturer, is not guaranteed or endorsed by the publisher.

frontiers in Pharmacology

CORRECTION
published: 21 January 2022
doi: 10.3389/fphar.2021.844785

Corrigendum: Stable Gastric Pentadecapeptide BPC 157 Therapy for Primary Abdominal Compartment Syndrome in Rats

Marijan Tepes[1,2,3,4], Slaven Gojkovic[4], Ivan Krezic[4], Helena Zizek[4], Hrvoje Vranes[4], Zrinko Madzar[5], Goran Santak[6], Lovorka Batelja[7], Marija Milavic[7], Suncana Sikiric[7], Ivica Kocman[4], Karol Simonji[8], Mariam Samara[4], Mario Knezevic[4], Ivan Barisic[4], Eva Lovric[7], Sanja Strbe[4], Antonio Kokot[9], Ivica Sjekavica[10], Toni Kolak[11], Anita Skrtic[7], Sven Seiwerth[7], Alenka Boban Blagaic[4] and Predrag Sikiric[4]**

[1]Department of Surgery, General Hospital Nasice, Nasice, Croatia, [2]Department of Clinical Medicine, Faculty of Dental Medicine and Health Osijek, Osijek, Croatia, [3]PhD Program Translational Research in Biomedicine—TRIBE, School of Medicine, University of Split, Split, Croatia, [4]Department of Pharmacology, School of Medicine, University of Zagreb, Zagreb, Croatia, [5]Clinical Department of Surgery, Sestre Milosrdnice University Hospital Center, Zagreb, Croatia, [6]Department of Surgery, Faculty of Medicine, University of Osijek, Osijek, Croatia, [7]Department of Pathology, School of Medicine, University of Zagreb, Zagreb, Croatia, [8]Internal Diseases Clinic, Faculty of Veterinary Medicine Zagreb, Zagreb, Croatia, [9]Department of Anatomy and Neuroscience, Faculty of Medicine, J.J. Strossmayer University of Osijek, Osijek, Croatia, [10]Department of Diagnostic and Interventional Radiology, University Hospital Centre, Zagreb, Croatia, [11]Department of Surgery, School of Medicine, University of Zagreb, Zagreb, Croatia*

Keywords: gastric pentadecapeptide BPC 157, primary abdominal compartment syndrome, rats, brain edema, lung edema

OPEN ACCESS

Approved by:
Frontiers Editorial Office, Frontiers Media SA, Switzerland

***Correspondence:**
Predrag Sikiric
sikiric@mef.hr

Specialty section:
This article was submitted to Translational Pharmacology, a section of the journal Frontiers in Pharmacology

Received: *29 December 2021*
Accepted: *29 December 2021*
Published: *21 January 2022*

Citation:
Tepes M, Gojkovic S, Krezic I, Zizek H, Vranes H, Madzar Z, Santak G, Batelja L, Milavic M, Sikiric S, Kocman I, Simonji K, Samara M, Knezevic M, Barisic I, Lovric E, Strbe S, Kokot A, Sjekavica I, Kolak T, Skrtic A, Seiwerth S, Blagaic AB and Sikiric P (2022) Corrigendum: Stable Gastric Pentadecapeptide BPC 157 Therapy for Primary Abdominal Compartment Syndrome in Rats. Front. Pharmacol. 12:844785. doi: 10.3389/fphar.2021.844785

A Corrigendum on

Stable Gastric Pentadecapeptide BPC 157 Therapy for Primary Abdominal Compartment Syndrome in Rats

by Tepes M, Gojkovic S, Krezic I, Zizek H, Vranes H, Madzar Z, Santak G, Batelja L, Milavic M, Sikiric S, Kocman I, Simonji K, Samara M, Knezevic M, Barisic I, Lovric E, Strbe S, Kokot A, Sjekavica I, Kolak T, Skrtic A, Seiwerth S, Boban Blagaic A and Sikiric P (2021). Front. Pharmacol. 12:718147. doi: 10.3389/fphar.2021.718147

In the published article, there was an error in **affiliations 2** and **3**. Instead of "[2]Department of Clinical Medicine, Faculty of Dental Medicine and Health Osijek, Zagreb, Croatia; [3]PhD Program Translational Research in Biomedicine—TRIBE, School of Medicine, University of Split, Zagreb, Croatia.," it should be "[2]Department of Clinical Medicine, Faculty of Dental Medicine and Health Osijek, Osijek, Croatia; [3]PhD Program Translational Research in Biomedicine—TRIBE, School of Medicine, University of Split, Split, Croatia."

The authors apologize for this error and state that this does not change the scientific conclusions of the article in any way. The original article has been updated.

frontiers | Frontiers in Pharmacology

ORIGINAL RESEARCH
published: 22 July 2022
doi: 10.3389/fphar.2022.692437

Effect of Acid Suppressants on Non–*Helicobacter pylori* Helicobacters Within Parietal Cells

Masahiko Nakamura[1], Futa Murasato[2], Anders Øverby[3], Yosuke Kodama[2], Hirofumi Michimae[4], Kazuki Sasaki[2], Bram Flahou[5], Freddy Haesebrouck[5], Somay Y. Murayama[6], Shinichi Takahashi[7], Masayuki Uchida[8], Hidekazu Suzuki[9] and Hidenori Matsui[1]*

[1]Ohmura Satoshi Memorial Institute, Kitasato University, Tokyo, Japan, [2]School of Pharmacy, Kitasato University, Tokyo, Japan, [3]Center of Education in Kongsvinger, Kongsvinger, Norway, [4]Department of Clinical Medicine (Biostatistics), School of Pharmacy, Kitasato University, Tokyo, Japan, [5]Department of Pathology, Bacteriology and Avian Diseases, Faculty of Veterinary Medicine, Ghent University, Merelbeke, Belgium, [6]Department of Fungal Infection, National Institute of Infectious Diseases, Tokyo, Japan, [7]Kyorin University School of Medicine, Mitaka, Japan, [8]Division of Research and Development, Meiji Dairies Corporation, Food Science Institute, Odawara, Japan, [9]Division of Gastroenterology and Hepatology, Department of Internal Medicine, Tokai University School of Medicine, Isehara, Japan

OPEN ACCESS

Edited by:
Duan Chen, Norwegian University of Science and Technology, Norway

Reviewed by:
Rinaldo Pellicano, Molinette Hospital, Italy
Mitsushige Sugimoto, Tokyo Medical University Hospital, Japan

***Correspondence:**
Masahiko Nakamura
mngast@mac.com

Specialty section:
This article was submitted to Gastrointestinal and Hepatic Pharmacology, a section of the journal Frontiers in Pharmacology

Received: *08 April 2021*
Accepted: *14 June 2022*
Published: *22 July 2022*

Citation:
Nakamura M, Murasato F, Øverby A, Kodama Y, Michimae H, Sasaki K, Flahou B, Haesebrouck F, Murayama SY, Takahashi S, Uchida M, Suzuki H and Matsui H (2022) Effect of Acid Suppressants on Non–Helicobacter pylori Helicobacters Within Parietal Cells. Front. Pharmacol. 13:692437. doi: 10.3389/fphar.2022.692437

We investigated the effect of increased pH induced by acid suppressants on the viability of non–*Helicobacter pylori* helicobacters (NHPHs) within parietal cell intracellular canaliculi and fundic glandular lumina by immunohistochemistry, electron microscopy, quantitative PCR, urea breath tests, and using a bilayer culture system. Three months before the experiment, mice were infected with the NHPH *H. suis* and then treated with famotidine (2 mg/kg body weight [BW], once daily), lansoprazole (30 mg/kg BW, once daily), or vonoprazan (20 mg/kg BW, once daily) for 3 days. Immunohistochemical studies using the TUNEL method, quantitative PCR analysis, and urea breath tests were performed. PCR analysis showed a decrease in the NHPH quantity after vonoprazan treatment. Urea breath tests revealed a significant decrease in the NHPH urease activity after vonoprazan, lansoprazole, and famotidine treatments for 3 days; however, 4 days after the treatment, urease activity reversed to the pretreatment level for each treatment group. Electron microscopy revealed an increase in the damaged NHPH after vonoprazan treatment. The TUNEL method revealed apoptotic NHPH within parietal cells after vonoprazan treatment. The bilayer culture results demonstrated that NHPH moved more quickly at a pH of 4.0 than at a pH of 3.0, 5.0, and 6.5, and electron microscopy revealed a change from the spiral form to the coccoid form under near-neutral pH conditions. We thus proposed that acid suppressants, especially vonoprazan, induce NHPH damage by altering pH.

Keywords: non-*Helicobacter pylori* helicobacter, *Helicobacter suis*, urea breath test, vonoprazan, TUNEL, bilayer culture, coccoid form

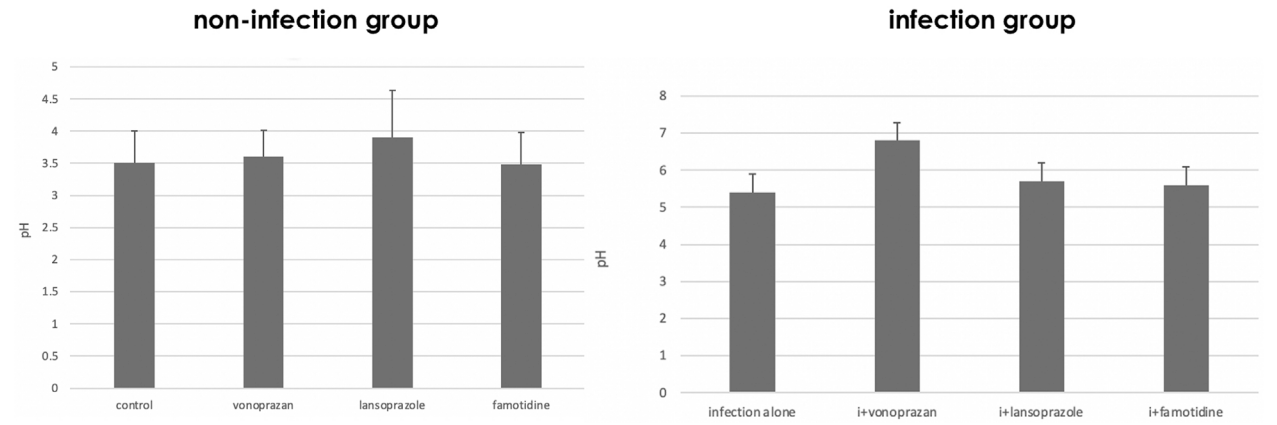

FIGURE 1 | Alteration of gastric pH by acid suppressants and NHPH infection. A significant interaction was found between infection and acid suppressants in the gastric mucosal pH ($F = 3.04$ and $p = 0.043$ by two-way ANOVA). In the infection group, vonoprazan treatment induced the highest increase in intragastric pH. i means infection in the left graph.

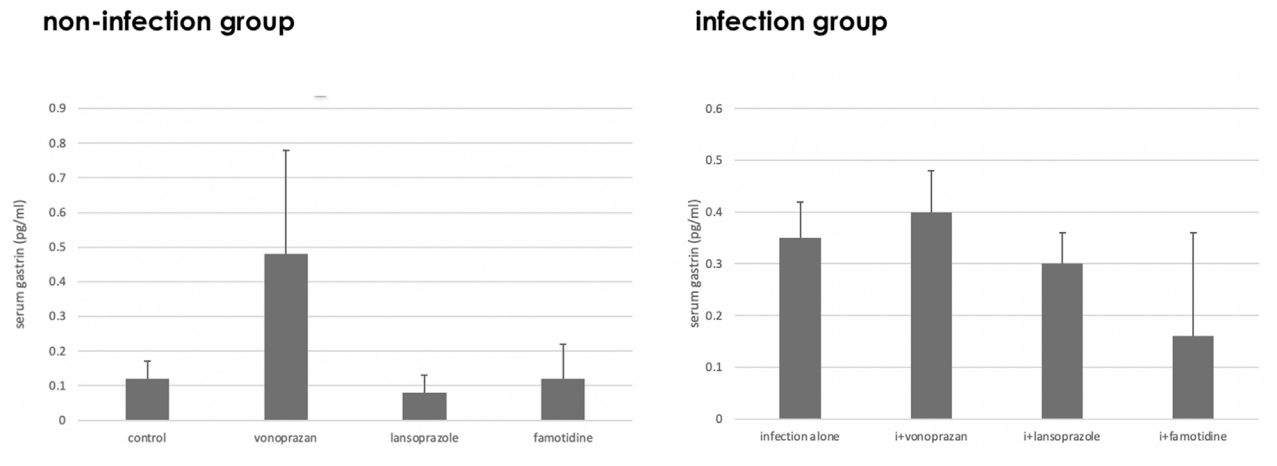

FIGURE 2 | Alteration of the serum gastrin level by acid suppressants and NHPH infection. A significant interaction was found between infection and acid suppressants in the serum gastrin level ($F = 5.61$; $p = 0.003$).

1 INTRODUCTION

Although the prevalence of non-*Helicobacter pylori* helicobacters (NHPHs) is relatively low, compared with *Helicobacter pylori* (Hp), this bacterium has also been reported to be related to the formation of the MALT lymphoma, nodular gastritis, and chronic gastritis, as well as gastric cancer (Heilmann and Borchard, 1991; Nakamura et al., 2020; Yasuda et al., 2022). In addition, the number of reports of NHPHs has been increasing lately, partly because of the worldwide application of the Hp eradication regimen.

The infection of helicobacters into the gastric parietal cells was first detected by Bizzozero (1893) and Salmon (1896) in the mammalian stomach, but the pathological significance of the *Helicobacter* invasion into the potent acidic lumen is not well understood. These *Helicobacter* species are now thought to belong to NHPHs since Hp resides in the mucus layer and in the upper part of the fundic glands in human and primate stomachs, whereas NHPH can inhabit the lower layers of the fundic glands where many parietal cells are located, in addition to the mucus layer in several kinds of mammals including dogs, cats, pigs, and humans (Flahou et al., 2010; Nakamura et al., 2020). The morphology of parietal cells is well known to be greatly altered based on the extent of acid secretion levels, which can be altered through the administration of acid stimulants and suppressants (Soll and Walsh, 1979; Inokuchi et al., 1992; Scott et al., 1994; Schubert, 2015).

The membrane-recycling theory, i.e., the massive membrane flow from an endosomal compartment of tubulovesicle membranes to the apical secretory surface during strong acid secretion within the parietal cell, was postulated in the 1980s to explain how the morphology of parietal cells changes in response to changes in acid secretion levels (Forte and Zhu, 2010; Helander and Sundell, 1984; Calhoun and Goldenring, 1996). It is, thus, of clinical interest

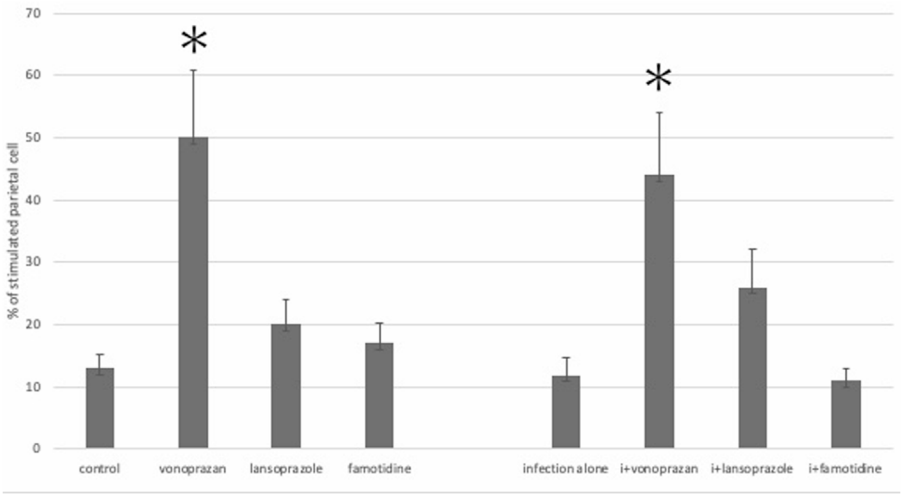

FIGURE 3 | Alteration of the parietal cell structure by acid suppressants and NHPH infection. No significant interaction was found between infection and acid suppressants in the percentage of the stimulated parietal cell ($F = 1.54$; $p = 0.224$). By the *post hoc* analysis, the vonoprazan-treated group showed a significant increase in the stimulated parietal cell in both non-infection and infection groups ($p < 0.05$).

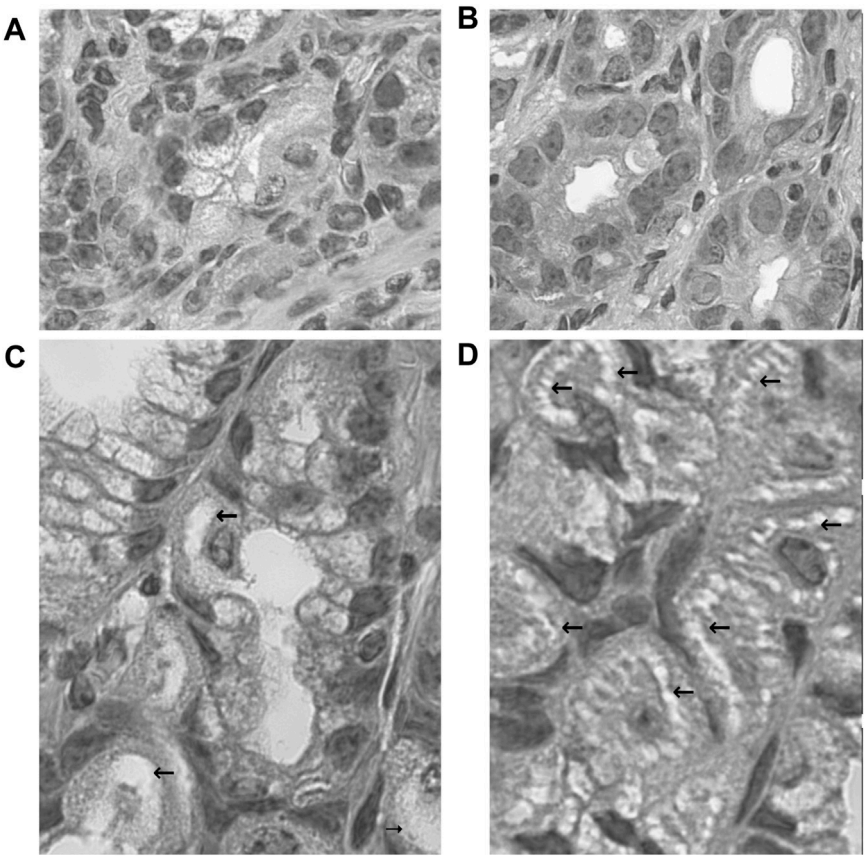

FIGURE 4 | Morphological changes of fundic glandular cells by acid suppressants under NHPH infection. HE stains **(A)** the control group fundic mucosa, X 400. **(B)** In famotidine-treated mice, no significant changes in the parietal cell were detected in the body portion of the fundic gland, X 400. **(C)** In the lansoprazole-treated mice, many parietal cells having very enlarged intracellular canaliculi (arrows) were seen, X 600. **(D)** In the vonoprazan-treated mice, most parietal cells had the enlarged intracellular canaliculi (arrows) surrounding the nucleus, X 600.

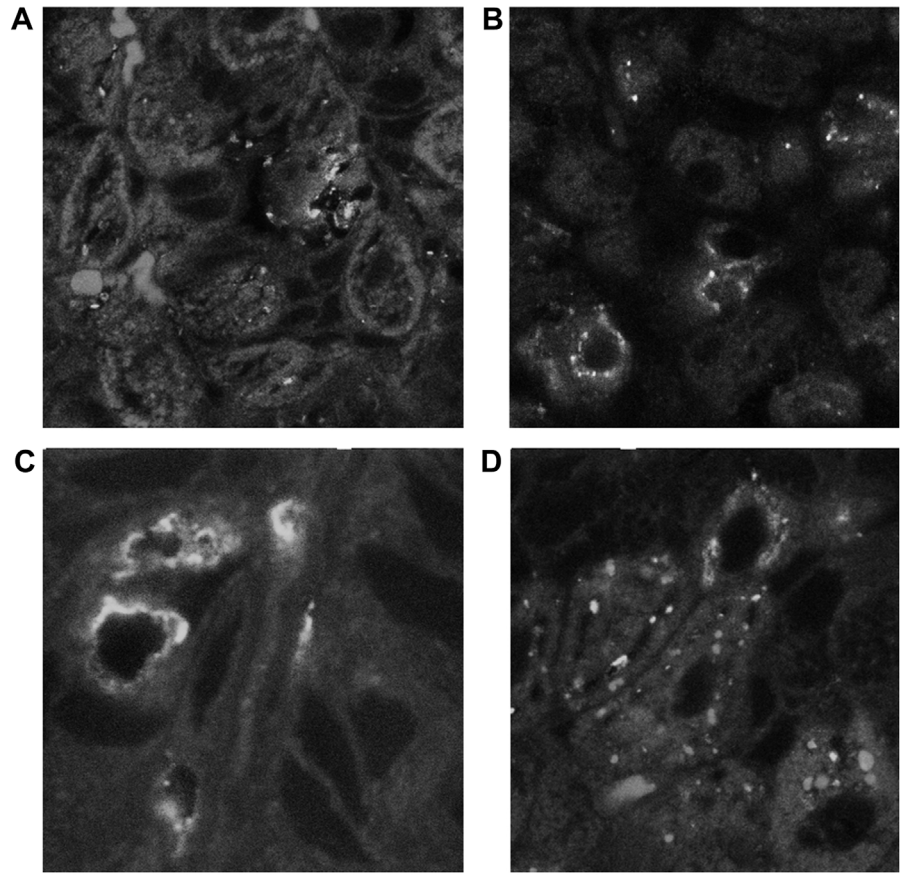

FIGURE 5 | Alteration of NHPH localization in the fundic gland in the infection group by acid suppressants by indirect fluorescent immunohistochemistry using an anti-HsvA antibody. **(A)** In the infection-alone group, linear-shaped NHPHs were mostly found within the intracellular canaliculi of the parietal cells and in the gastric glandular lumen, X 400. **(B)** In the famotidine-treated mice, many spiral-shaped NHPHs were seen in the intracellular canaliculi of the parietal cells and in the gastric glandular lumen, X 400. **(C)** In the lansoprazole-treated mice, many spiral-shaped NHPHs were seen in the enlarged intracellular canaliculus of the parietal cells and in the gastric glandular lumen, X 600. **(D)** In the vonoprazan-treated mice, the round-shaped NHPHs were mostly seen in the intracellular canaliculus of the parietal cells, X 400.

to understand the parietal cell morphology and NHPH viability during NHPH infection and acid suppression. We conducted this study to clarify the effects of the acid suppressants on NHPHs residing within parietal cells in mice with long-term NHPH infection. In this connection, we also investigated the influence of pH on the motility, survival, and morphology of NHPHs.

2 MATERIALS AND METHODS

2.1 *In Vivo* Study

2.1.1 Administration of Acid Suppressants

We obtained a urease-positive cynomolgus monkey stomach in 1993, and we perorally inoculated C3H mice with 0.1 ml of gastric mucosal and mucus homogenates. The bacteria were maintained *in vivo*, and this process was repeated every 12 months. Thereafter, 3 months before the present study, C57BL/6 mice were inoculated with gastric mucosal homogenates containing gastric mucosa and mucus from infected C57BL/6 mice (Nakamura et al., 2007).

We administered the following acid suppressants to these mice: famotidine (2 mg/kg body weight [BW], 1 × /day), lansoprazole (30 mg/kg BW, 1 × /day), and vonoprazan (20 mg/kg BW, 1 × /day), or physiological saline as a vehicle for 3 days through peroral intubation. Each group consisted of five mice. We determined the doses of agents following the references, mostly from animal experiments, because the dose for the animals cannot be calculated from the dose for humans, owing to the difference in the metabolism in animals. Famotidine dose was determined by Icatlo et. al (2000), which dealt with the *Helicobacter pylori* eradication in mice. The dose of lansoprazole was determined from the reports by Watanabe et al. (2004), where they used 3, 10, and 30 mg/kg BW once daily, and we selected 30 mg/kg BW. The dose of vonoprazan was determined from an animal study of the reports from the Pharmaceuticals and Medical Devices Agency of Japan (2004) and Sugano (2018).

2.1.2 Intragastric pH Estimation

After the 3-day treatment, anesthesia with 2% isoflurane was administered *via* inhalation, cardiac blood sampling was

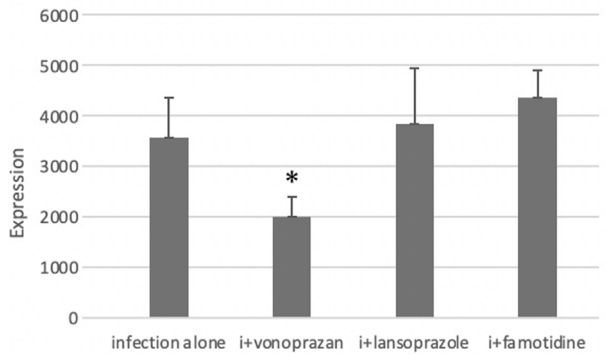

FIGURE 6 | Effect of acid suppressants on the NHPH number by PCR. PCR analysis showed significant difference between infection alone and administered agents (F = 5.33 and p = 0.008 by one-way ANOVA). *Post hoc* analyses (Bonferroni correction) revealed that the infection-alone group is significantly larger than the infection + vonoprazan group (*p = 0.008). Decrease in NHPH in the vonoprazan-treated mice, but significant interaction was found between infection and administered agents in NHPHs (F = 7.17; p = 0.008).

performed, and the stomachs were removed and opened along the greater curvature. Intragastric pH was estimated by attaching a test strip (Advantec BTB, 6.2–7.7, 1–11, Toyo Roshi Co., Tokyo) to the surface of the fundic mucosa.

2.1.3 Serum Gastrin Estimation

Blood samples from the mice were centrifuged at 11,000 X g for 5 min at 4°C. Serum gastrin I levels were estimated using an enzyme-linked immunosorbent assay kit specific to gastrin I (LS Bio, Seattle, WA, United States).

2.1.4 Observation of Gastric Parietal Cells *via* Light Microscopy

After the stomach tissues were fixed with a neutral-buffered 10% solution, they were embedded in paraffin, and 4-μm sections were prepared using a microtome. The sections were stained with hematoxylin and eosin for histological examination.

2.1.5 Immunohistochemical Examination and Electron Microscopy of *H. suis*

Immunohistochemical studies were performed using antibodies against the alpha subunits of H^+/K^+-ATPase (Smolka et al., 1982) and against the *H. suis* HsvA protein (Nakamura et al., 2020). Some tissues were fixed with Zamboni's fixative for a better immunohistochemical reaction (Stefanini et al., 1967) and embedded in paraffin. After deparaffinization with xylene, a graded ethanol series, and phosphate-buffered saline (PBS), immunohistochemical studies using monoclonal antibodies were performed by confocal laser microscopy (Leica TCS NT, Leica Microsystems GmbH, Wetzlar, Germany).

We used electron microscopy to examine the biopsied specimens which were first fixed with 4% formaldehyde and 1% glutaraldehyde solution for 12 h, postfixed with 1% osmium tetroxide and ruthenium red solution, and then embedded in Epon 812 epoxy resin. Ultrathin sections were then cut, counterstained with a 3% aqueous solution of uranyl acetate for 30 min, and observed using a JEOL EX-II electron microscope (Akishima, Japan) at an accelerating voltage of 80 kV.

2.1.6 TUNEL Method

Apoptosis was detected by terminal deoxynucleotidyl transferase (TdT)-mediated dUTP nick end labeling (TUNEL) using a TdT *in situ* detection kit that uses fluorescein for visualization (4812–30-K, R&D Systems; Minneapolis, MN, United States). After deparaffinization, sections were covered with a proteinase K solution, incubated for 15 min at 20°C, and washed three times with PBS for 5 min per wash. Then, the sections were immersed in a TdT labeling buffer for 5 min, allowed to react with a TdT labeling reaction mixture for 1 h at 37°C, washed once with phosphate-buffered saline (PBS) for 5 min, reacted with a TdT stop buffer, washed three times with PBS for 5 min per wash, and then left to react with a strep-fluorescein solution for 20 min at room temperature in the dark. Some sections were doubly stained with an anti-*H.-suis* antibody to clarify the relation to the TUNEL reaction and bacterial localization, embedded in PermaFluor (Thermo Scientific, Waltham, MA, United States), and observed by confocal laser microscopy.

2.1.7 Estimation of *H. suis* by Quantitative Polymerase Chain Reaction

Real-time or quantitative polymerase chain reaction (qPCR) was used to amplify 16S rRNA and urease genes from the gastric samples. These reactions incorporated universal eubacterial primers (TM16S-27F and TM16S-1492R) for the 16S rRNA gene and the primers U430F and U1735R or U430F and U2235R for the urease genes. The cycling conditions for the 16S rRNA gene were as follows: initial denaturation at 94°C for 1 min, followed by 35 cycles of 94°C for 45 s (denaturation), 55°C for 30 s (annealing), and 72°C for 2 min (extension), followed by an additional extension step at 72°C for 5 min. The cycling conditions for the urease genes were initial denaturation at 94°C for 3 min, followed by 35 cycles of 94°C for 10 s, 52°C for 30 s, and 72°C for1.5 min; and a final extension step at 72°C for 5 min.

The conditions for qPCR of the urease gene were the same as those listed previously, but with the following modifications: annealing at 42°C for 30 s and additional extension at 72°C for 2 min. Both strands were sequenced using the BigDye® Terminator v3.1 Cycle Sequencing Kit (Applied Biosystems, Carlsbad, CA, United States) on an ABI PRISM® 3100-Avant Genetic Analyzer (Applied Biosystems). Sequences were analyzed using NCBC BLAST.

qPCR was performed using a Bio-Rad iCycler iQ Detection System (Bio-Rad Laboratories, Inc., Hercules, CA, United States) with SYBR Green fluorophores (Bio-Rad Laboraties, Inc.). Reactions were performed in a total volume of 20 μL, which included 10 μL of 2× SYBR Green PCR Master Mix (Bio-Rad Laboraties, Inc.), 5 μL of each primer at a concentration of 5 μM, and 1 μL of the template DNA. A 112-bp fragment of the 16S rRNA gene was amplified using the primer pair HeilF (5′-AAG TCG AAC GAT GAA GCC TA-3′) and HeilR (5′-ATT TGG TAT TAA TCA CCA TTT C-3′). Data analysis was performed

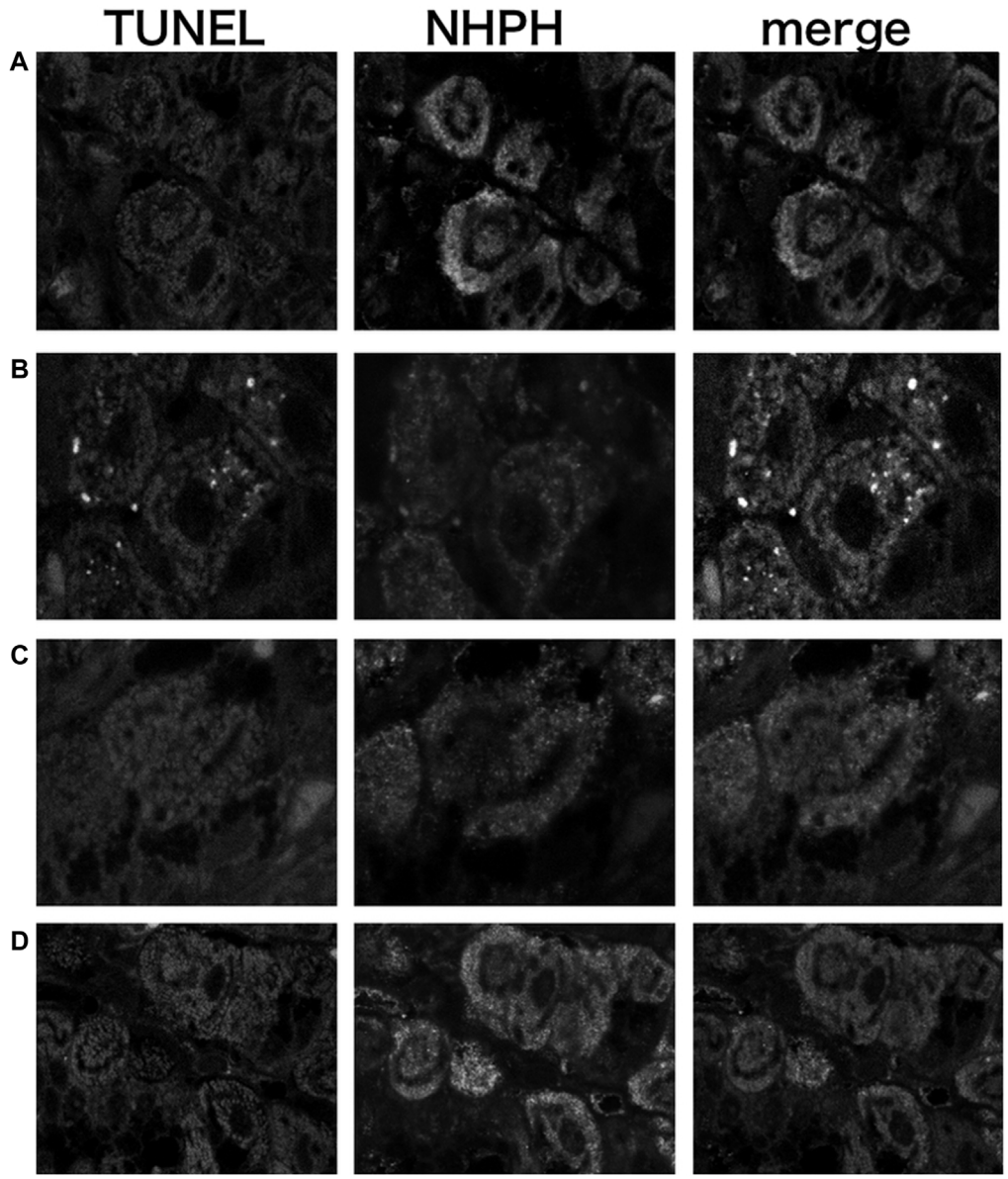

FIGURE 7 | Localization of apoptotic NHPHs in the infection group by acid suppressants by the TUNEL method X 200. **(A)** In the infection-alone group, no apoptosis was detected. **(B)** In the vonoprazan-treated group, apoptotic NHPHs were detected within the intracellular canaliculi of the parietal cells. **(C)** In the lansoprazole-treated group, many NHPHs were found, but no apoptotic reaction was recognized. **(D)** In the famotidine-treated group, NHPHs in the parietal cells were negative for the TUNEL reaction.

using an iCycler iQ real-time detection system (Bio-Rad Laboraties, Inc.) (Nakamura et al., 2020).

2.1.8 Estimation of the Urease Activity by Urea Breath Tests

After the administration of one of three acid suppressants or physiological saline as a vehicle for 3 days after the end of the treatments, 20 mice fasted for 8 h were perorally administered a solution of powder from a urea tablet and sterile water (4 mg/mouse) containing ^{13}C-urea. The mice were then housed in a desiccator, from which their expired air was collected in a breath-sampling bag using a tube and an aspiration pump (Uchida et al., 2005). $^{13}CO_2$ levels in the expired air were measured using an infrared spectrometer at appropriate intervals for 20 min. Thereafter, 4 days after the administration of acid suppressants, the same mice were used again for the estimation of the urease activity.

2.2 Culture Study

H. suis, *H. heilmannii*, and *H. felis* were kind gifts from Drs. B. Flahou and F. Haesebrouck. We cultured the bacteria *via* the bilayer culture method outlined by Flahou et al. (2010) and then

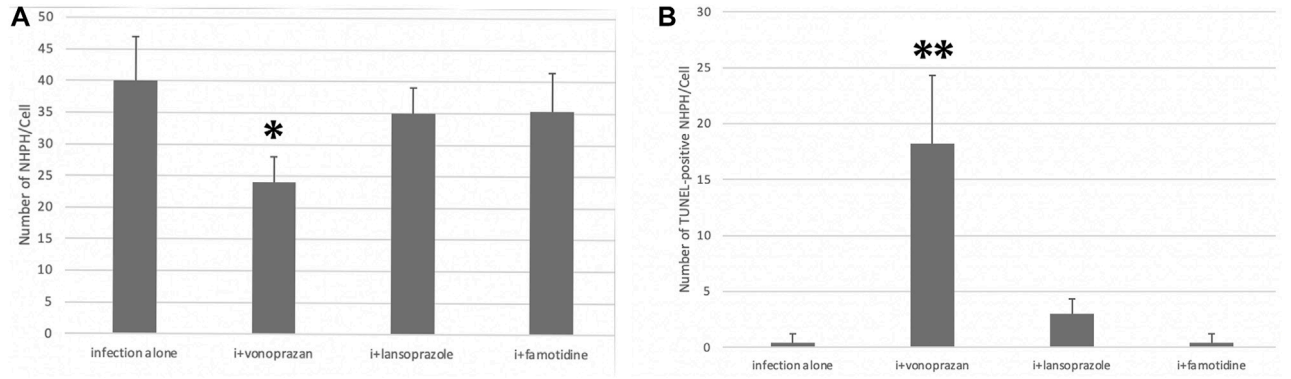

FIGURE 8 | Quantitative analysis of all NHPHs and apoptotic NHPHs by using acid suppressants by immunohistochemistry. **(A)** Significant difference was found between infection alone and administered agents in the NHPH number ($F = 6.14$; $p = 0.005$ by one-way ANOVA). *Post hoc* analyses (Bonferroni correction) revealed that the infection-alone group is significantly larger than the infection + vonoprazan group (*$p = 0.004$). **(B)** Significant difference was found between infection alone and administered agents in the TUNEL-positive NHPH number ($F = 28.1$; $p < 0.001$ by one-way ANOVA). *Post hoc* analyses (Bonferroni correction) revealed that the infection + vonoprazan group is significantly larger than the infection-alone group (**$p < 0.001$).

estimated the motility, urease activity, and morphological changes of the bacteria under different pH conditions of the culture medium by vital microscopy. We evaluated the urease activity of cultured NHPHs using 100 μL of the rapid urease test (RUT) solution per well of a microplate to which was added 1uL of cells collected after plate growth. Color change was determined after 15 min using a plate reader (ChroMate-6 Microplate reader, Microtec Co., LTD).

To estimate motility, we examined specimens *via* light microscopy. Glass slides were prepared with a loopful of growth from a nutrient agar subculture mixed with a drop of sterile distilled water on one end and another loopful of growth from the same subculture in a drop of peptone water on the other end. Both ends of the slides were covered with a cover glass and were examined under a light microscope with a ×40 objective.

Some specimens from each treatment group were observed by immunohistochemistry using an antibody against *Helicobacter* (Nakamura et al., 2007) and electron microscopy using the same method described earlier.

2.3 Statistics

All data are expressed as the mean ± standard deviation. Two-factor ANOVA was mostly used in this study. One-factor ANOVA and Bonferroni correction as a *post hoc* test were also used in some parts. The significance level was determined as less than 5%.

3 RESULTS

3.1 *In Vivo* Study

3.1.1 Effect of Acid Suppressants on the Gastric pH

In the NHPH infection group, administration of vonoprazan induced the highest increase in the intragastric pH both in the infected groups 3 days after the administration (**Figure 1**). A significant interaction was found between infection and acid suppressants in the gastric mucosal pH.

3.1.2 Effect of Acid Suppressants on the Serum Gastrin Concentration

As to the serum gastrin level, a significant interaction was found between infection and acid suppressants (**Figure 2**). The highest serum gastrin level was detected in the vonoprazan-treated mice both in non-infected and infected groups.

3.1.3 Effect of Acid Suppressants on Parietal Cell Morphology

Compared to the control group, vonoprazan-treated mice showed a significant increase in stimulated parietal cells, which are defined as having an enlarged intracellular canaliculus, whereas no significant differences were observed in the other treatment groups (**Figures 3**, **4**).

3.1.4 Effect of Acid Suppressants on the Localization and Shape of Non–*Helicobacter pylori* Helicobacters

Spiral-form NHPHs were observed in the intracellular canaliculi of the parietal cells of famotidine-treated, lansoprazole-treated, and control groups by fluorescent immunohistochemistry. In vonoprazan-treated mice, the shape of NHPHs was mostly altered from a spiral form to a round form (**Figure 5**).

3.1.5 Effect of Acid Suppressants on the Number of Non–*Helicobacter pylori* Helicobacters Shown by Polymerase Chain Reaction

PCR analysis showed a significant decrease in NHPHs in the infection and vonoprazan-treated mice, compared with the infection-alone group (**Figure 6**).

3.1.6 Vonoprazan Induced TUNEL-Detectable Apoptosis

The TUNEL method revealed that only the vonoprazan treatment induced the apoptosis of NHPHs within the parietal cells (**Figure 7**). The results of the quantitative analysis showed a significant decrease in NHPHs within the parietal cell in the

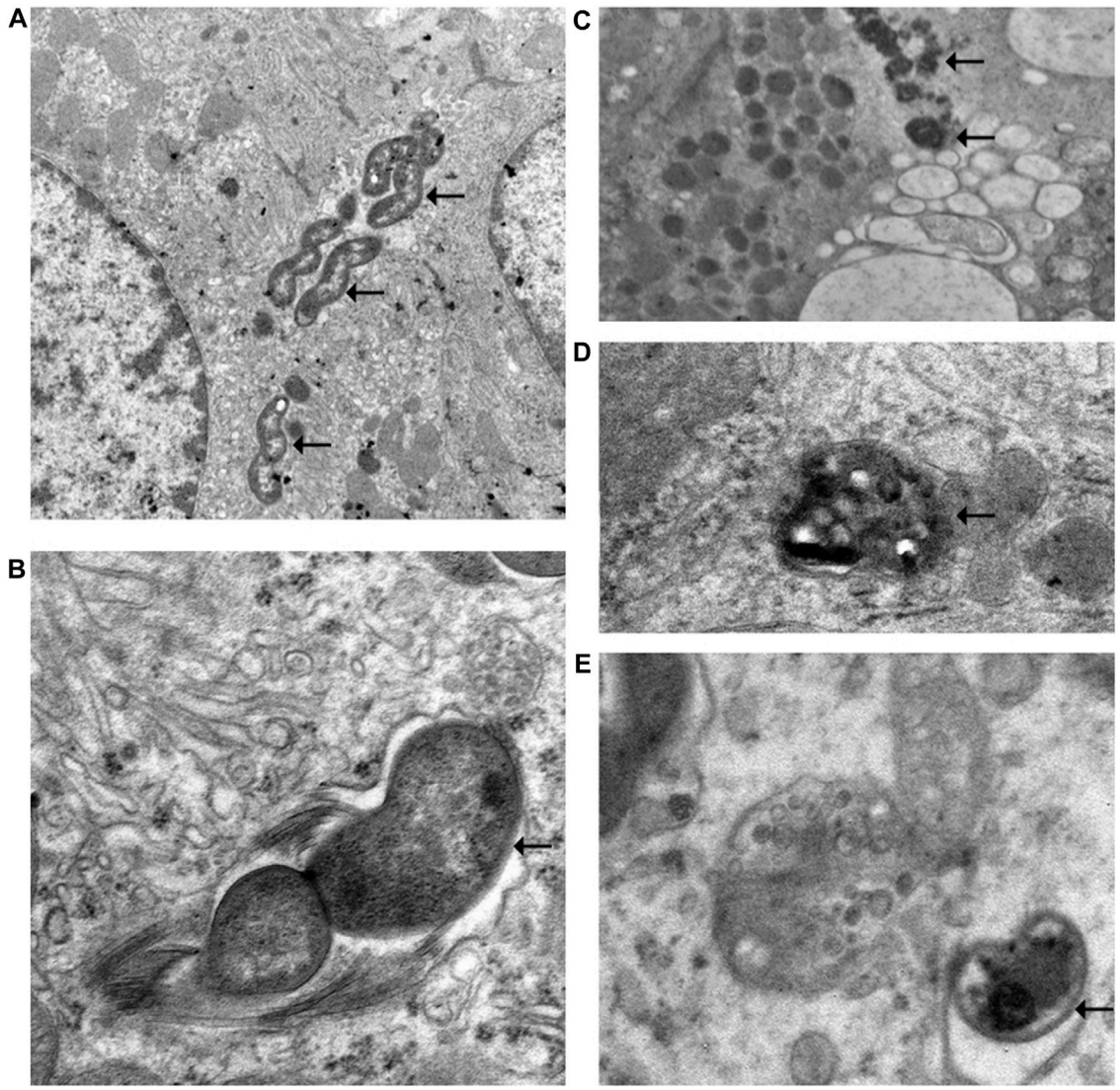

FIGURE 9 | Electron microscopic observation of NHPH in infection-alone and infection + vonoprazan-treated mouse gastric parietal cells. **(A)** In infection alone mouse, many NHPHs were seen within the intracellular canaliculus of the parietal cell in the gastric mucosa, X 8,000. **(B)** In a higher magnification, flagella were recognized adjacent to the NHPH cell body in the intracellular canaliculus, X 24,000. **(C)** In the infection + vonoprazan-treated mouse, the bacterial cell body became condensed and irregular (arrows) in the intracellular canaliculus of the parietal cell, X 8,000. **(D,E)** Many bacilli were found in the secondary lysosome in the infection + vonoprazan-treated group, X 8,000.

vonoprazan-treated group, compared with the infection-alone group. In addition, the TUNEL-positive apoptotic NHPHs within the parietal cells significantly increased in the vonoprazan-treated group (**Figure 8**).

3.1.7 Electron Microscopic Observation of Non–*Helicobacter pylori* Helicobacters Damaged by Vonoprazans

The electron microscopic cytochemical observations showed that the vonoprazan treatment of NHPH-infected mice induced condensation and deformity of the NHPHs within the intracellular canaliculi of the parietal cell (**Figure 9**). Many secondary lysosomes having NHPHs inside were found in the cytoplasm of the parietal cells in the infection and vonoprazan-treated mice.

3.1.8 Effects of the Acid Suppressants on the Urease Activity by the Urea Breath Test

The urea breath test revealed that vonoprazan, lansoprazole, and famotidine each significantly decreased the Cmax of $^{13}CO_2$ excretion compared to the untreated infection-alone group, signaling a decrease in the urease activity. Then, 4 days after the completion of the acid suppressant treatments, the urease activity showed no differences among infection-alone and all of the drug-treated groups (**Figure 10**). This means that the significant suppression of the urease activity took place by

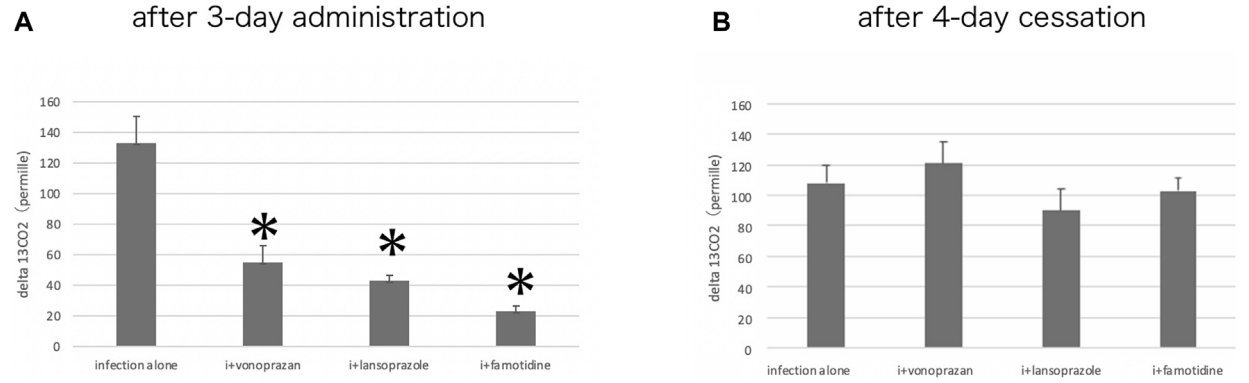

FIGURE 10 | Alteration of the urease activity by acid suppressants. **(A)** By the urea breath test, a significant interaction was found between infection alone and administered agents (F = 47.1; $p = 0.001$ by one-way ANOVA). *Post hoc* analyses (Bonferroni correction) revealed that the infection-alone group is significantly larger than the other three groups (*$p < 0.001$) after three-day administration. **(B)** Cessation of the administration for 4 days resulted in the recovery of the urease activity in all drug-administered groups.

3 days of administration of acid suppressants, and the urease activity of the bacteria could recover if no drugs were administered.

3.2 Culture Study

3.2.1 Effect of the Culture Medium pH on the Morphology of Non–*Helicobacter pylori* Helicobacters

Many NHPHs showed the spiral form when the culture pH was 3.0 (**Figure 11**). Ruthenium red *en bloc* staining during electron microscopy revealed that the coccoid form bacilli were observed in addition to the intact form at a pH of 5.0.

3.2.2 Effect of the Culture Medium pH on the Motility and Urease Activity of Non–*Helicobacter pylori* Helicobacters

The urease activity was the highest at a pH of 4.0, followed by that at a pH of 3.0 (**Figure 12**).

The motility of the bacteria was decreased at pH values > 5.0, compared to that at pH of 3.0 and 4.0 (**Figure 13**). These data coincided with the above-mentioned *in vivo* study that vonoprazan administration with a pH of more than 6 induced the damage of NHPHs.

4 DISCUSSION

As one of the most potent acid secreting cells in the human body, the parietal cells have fascinated many scientists for decades (Harms, 1910). The relationship between parietal cells and the formation of gastric ulcers has been investigated (Davenport, 1968). Schreiber et al. (2000) and Schreiber et al. (2007) used ultrafine double-barreled tip-sealed microelectrodes in their examinations of guinea pig stomachs and observed that the average glandular lumen pH was approximately 3.0 near the apical membrane of the intracellular canaliculus of the parietal cells and 4.6 at the crypt outlet, although Chu et al. (1999) reported that alkaline secretion protected the gastric mucosal surface by *in vivo* confocal imaging.

Regarding the alteration of parietal cells' morphology by the administration of acid suppressants, Stolte et al. (1992) demonstrated the pseudohypertrophy of parietal cells treated with omeprazole. They speculated that this phenomenon occurs due to hypergastrinemia since this change in morphology was not observed in post-antrectomy patients who had few gastrin-secreting cells. Karasawa et al. (1988) reported the vacuolation of parietal cells by omeprazole, and they postulated that the interaction of this structure was due to the direct acid-inhibiting effect of omeprazole. Inokuchi et al. (1992) reported parietal cell damage by omeprazole, and Scott et al. (1994) described the structural change of parietal cells to an enlarged intracanalicular space, following the administration of omeprazole, which is similar to the stimulated state of parietal cells. The secretory state is the opposite.

This study used lansoprazole (a proton pump inhibitor), vonoprazan, potassium competitive acid blockers (a new type of acid antisecretory agent), and famotidine, an H_2-receptor antagonist. Treatment with vonoprazan and lansoprazole induced a similar enlargement of intracellular canaliculi in parietal cells. Famotidine did not cause a significant change in the morphology of parietal cells, which is consistent with a report by Scott et al. (1994).

In our study, the serum gastrin level did not significantly alter 3 days after the drug administration. Larson et al. (1986) reported the induction of hypergastrinemia by omeprazole administration daily for 20 days in dogs, which suggests our study was performed in a too short a period to induce the changes in the serum gastrin level. This may also mean that the morphological changes of parietal cells occurred by other mechanisms than hypergastrinemia because these changes were observed without hypergastrinemia in this study.

During our histological observations, we were interested in the interaction of this enlarged intracellular canalicular lumen and the NHPHs preferentially inhabiting this lumen. As mentioned in the Introduction, the invasion of helicobacters into gastric parietal cells was first detected by Bizzozero (1893) and Salomon (1896); however, the pathological significance of the

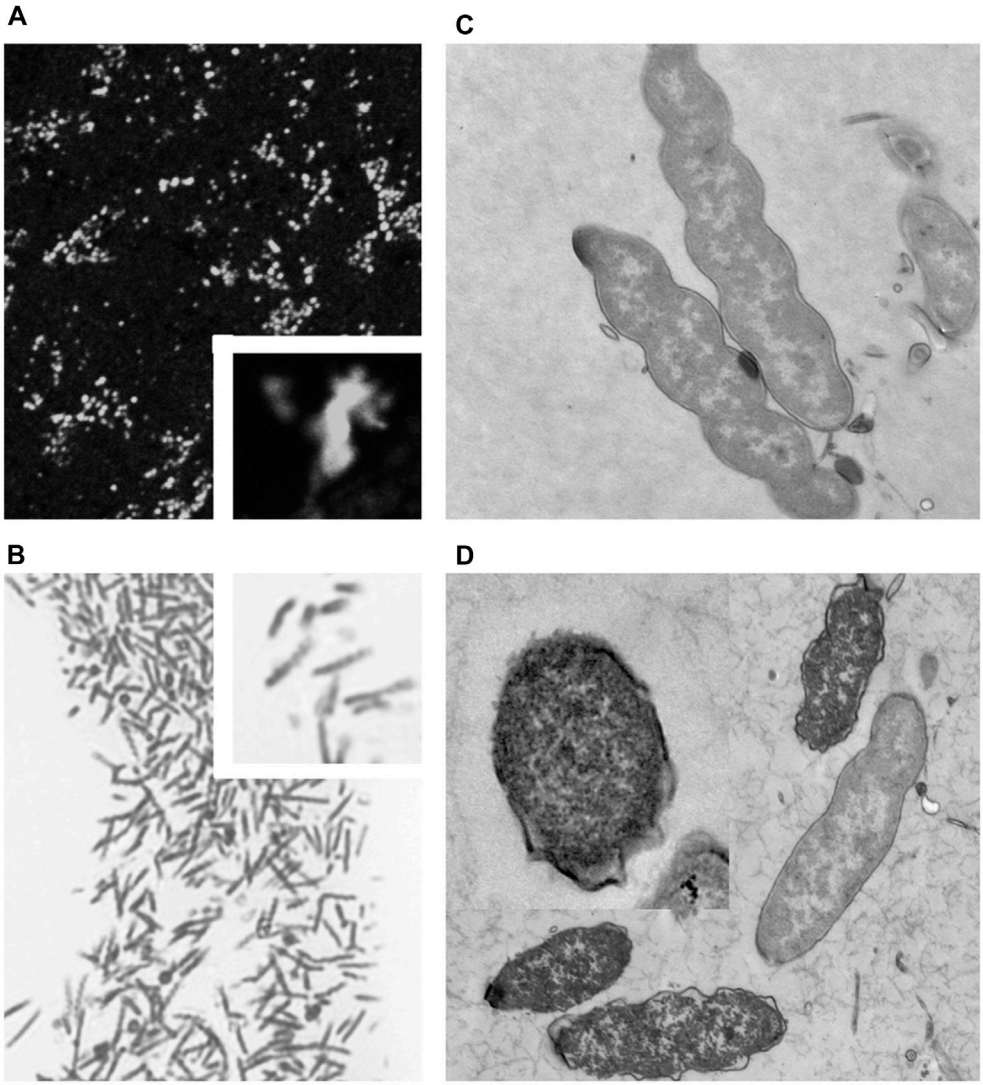

FIGURE 11 | Fluorescent, light, and electron microscopic observations of the cultured NHPH **(A)** By fluorescent immunohistochemical observation of the cultured NHPH using the HsvA antibody, many bacteria were observed in the incubation medium, X 400. Inset X 1800. **(B)** By light microscopic observation of the toluidine-blue stained Epon-embedded 2-μM section, many spiral bacilli were observed, X 600. Inset X 1800. **(C)** Electron microscopic observation of the cultured intact NHPH in pH 3. Intact bacilli were observed with flagella, X 15, 000. Ruthenium red *en bloc* staining. **(D)** Electron microscopic observation of the cultured NHPH in pH 6.5. Ruthenium red *en bloc* staining. The cytoplasm of some of the bacilli became condensed and homogeneous, and its plasma membrane became irregular, coinciding with the observation reported in the coccoid form, X 12,000, Inset x15, 000.

invasion into this potent acidic lumen is not well understood. In 2005, De Bock et al. reported the loss of gastric parietal cells and the abundance of bacteria by *H. felis* infection in Mongolian gerbils, demonstrating the deteriorating effect on acid secretion by NHPHs (De Bock et al., 2006). Liu et al. (2014) described the loss of parietal cells and the induction of gastric metaplasia in BALB/c mice infected with *Helicobacter heilmannii*. In humans, *Helicobacter heilmannii* infection has been reported to be rather mild and not strongly related to gastric atrophy and intestinal metaplasia (Heilmann and Borchard, 1991; Stolte, et al., 1997; Nakamura, et al., 2020).

As to the severity of gastric mucosal atrophy, we did not estimate the parietal cell density in this study; mild gastric atrophy with intestinal metaplasia was detected in our other study using *H. suis* infection (Rimbara et al., 2021). This could explain more effectiveness of acid suppressants in the infection group. The cytokines including IL-1beta could also play some role in the infection group to increase acid suppression (El-Omar, 2001).

Acid inhibition by lansoprazole is known to be slower than that of famotidine and vonoprazan, but 1 day after the treatment, intragastric pH is reported to increase from 2.11 to 3.57, and three-day treatment is thought to be enough to compare with other agents (Bell and Hunt, 1996).

In the present study, strong acid suppression was shown to be accompanied by a decrease in the NHPH urease activity

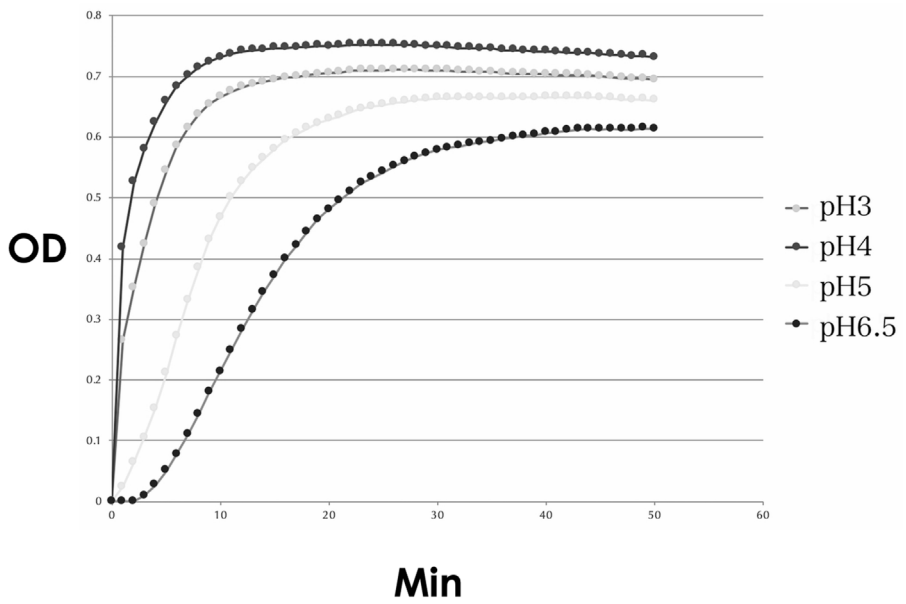

FIGURE 12 | Urease activity of the cultured NHPH. Urease activity was found to be strongest at pH 4, followed by pH 3, and became weak at pH 5 and 6.5. OD: optical density.

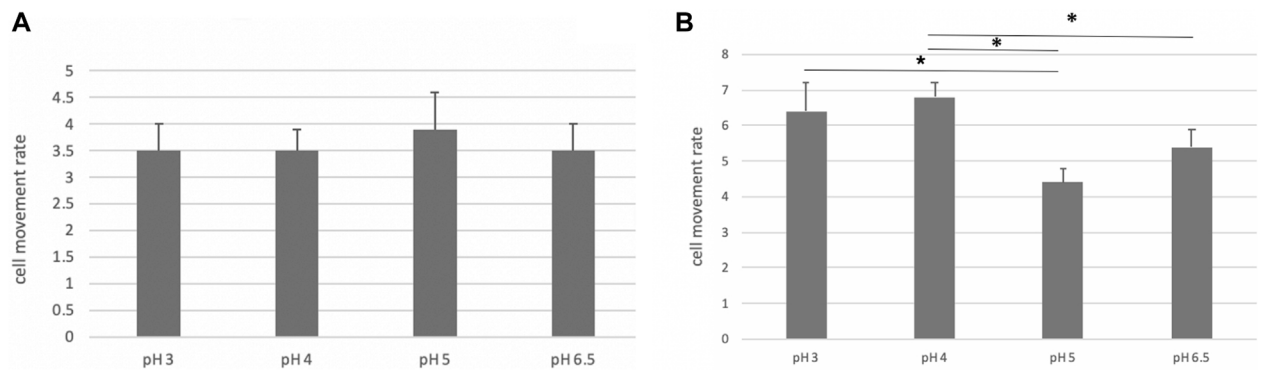

FIGURE 13 | Motility of the cultured NHPH. On day 2, no significant difference was found, as shown in **(A)**, while a significant decrease in motility was detected at pH 5 and 6.5 on day 3 **(B)** by *post hoc* analysis (*<0.05).

since significant differences were produced by treatments with vonoprazan, lansoprazole, or famotidine. This could be explained as an adaptation to the increase of the environmental pH where a strong urease activity is not necessary for the survival of the bacteria. However, the number of NHPH cells was slightly decreased in the vonoprazan-treated group, and about half of the NHPH cells in this group became apoptotic. The main difference between vonoprazan and the other two agents is the potency of acid suppression, which is thought to be closely related to the rate of apoptosis if vonoprazan does not have a direct effect. This hypothesis is supported by the results of our culture study: NHPHs adapted best to a pH of 3.0 or 4.0, and vonoprazan administration altered the gastric glandular surface pH by more than 6. To exclude the direct interaction of acid suppressants to NHPH, the PCR analysis of cultured NHPHs in different pH incubation media is thought to be quite helpful and should be tried in a future study. In addition, glycans and glycan-associated receptors were recently reported to have interacted with NHPH in the gastric mucosa. These factors could play some role in pH changes (Matos et al., 2021).

Lansoprazole was reported to have a direct suppressive effect on *H. pylori* other than acid suppression acting on the parietal cell (Iwahi et al., 1991) and could have some influence on NHPHs.

The relationship between apoptosis and coccoid formation has not been clarified in the case of *Helicobacter pylori,* although the alteration from the spiral form to the coccoid form has been

extensively investigated (Ogata et al., 1998, Azevedo et al., 2007). The coccoid formation was initially considered to be a viable but non-culturable form capable of surviving under unfavorable conditions. However, studies of *H. pylori* have suggested that coccoid formation represents a non-viable, degenerative form (Vijayakumari et al., 1995). In the present study, NHPHs affected by vonoprazan showed a structure similar to that of the coccoid form of *H. pylori*. Four-day cessations of the acid suppressant administration were shown to recover the urease activity, suggesting some of the damage of NHPHs by low pH could be reversible. PCR analysis may clarify this point, although the damaged NHPH other than viable NHPH could be also counted.

Escherichia coli has been reported to exhibit characteristic markers of apoptosis similar to those observed in multicellular organisms (Dwyer et al., 2012). Thus, we investigated the effect of anti-secretory agents on the NHPHs residing within the intracellular canaliculus of parietal cells, and the TUNEL method revealed apoptotic changes, following treatment with vonoprazan. We had speculated the apoptosis of the parietal cells having NHPH inside at first, but these changes could not be detected in our experiment.

Our present findings indicated a possible relationship between apoptotic NHPHs and TUNEL-positive bacteria. Further investigations are necessary to explore such a relationship.

DATA AVAILABILITY STATEMENT

The raw data supporting the conclusions of this article will be made available by the authors, without undue reservation.

ETHICS STATEMENT

The animal study was reviewed and approved by the Animal Ethics Committee of the Kitasato Institute for Life Sciences, Kitasato University.

AUTHOR CONTRIBUTIONS

All authors listed have made a substantial, direct, and intellectual contribution to the work and approved it for publication.

FUNDING

This work was supported by the grant from the Japanese Society of *Helicobacter* Research and by the JSPS KAKENHI grant nos. 22590690, 23790155, and 21590491.

REFERENCES

Azevedo, N.F., Almeida, C., Cerqueira, L., Dias, S., Keevil, C.W., and Vieira, M.J. (2007). Coccoid form of *Helicobacter pylori* as a morphological manifestation of cell adaptation to the environment. *Appl Environ Microbiol* 73, 3423–3427. Epub 2007 Mar 30. doi:10.1128/AEM.00047-07

Bell, NJ, and Hunt, RH (1996). Time to maximum effect of lansoprazole on gastric pH in normal male volunteers. *Aliment Pharmacol Ther* 10, 897–904. PMID: 8971286. doi:10.1046/j.1365-2036.1996.103242000.x

Bizzozero, G. (1893). Ueber die schlauchförmigen Drüsen des Magendarmkanals und die Beziehungen ihres Epithels zu dem Oberflächenepithel der Schleimhaut Dritte Mittheilung. *Archiv f. mikrosk. Anat.* 42, 82–152. doi:10.1007/bf02975307

Calhoun, BC, and Goldenring, JR (1996). Rab proteins in gastric parietal cells: evidence for the membrane recycling hypothesis. *Yale J Biol Med* 69, 1–8. PMID: 9041684; PMCID: PMC2588980.

Chu, S, Tanaka, S, Kaunitz, JD, and Montrose, MH (1999). Dynamic regulation of gastric surface pH by luminal pH. *J Clin Invest* 103, 605–12. doi:10.1172/JCI5217

Davenport, H. (1968). The mechanisms of acid secretion. *Gastroenterology* 54, 701–702. PMID, 4968244 PMID: 4968244. doi:10.1016/s0016-5085(68)80081-2

De Bock, M, Decostere, A, Hellemans, A, Haesebrouck, F, and Ducatelle, R (2006). *Helicobacter felis* and *Helicobacter bizzozeronii* induce gastric parietal cell loss in Mongolian gerbils. *Microbes Infect* 8, 503–10. Epub 2005 Oct 11. PMID: 16311055. doi:10.1016/j.micinf.2005.08.003

Dwyer, DJ, Camacho, DM, Kohanski, MA, Callura, JM, and Collins, JJ (2012). Antibiotic-induced bacterial cell death exhibits physiological and biochemical hallmarks of apoptosis. *Mol Cell* 46, 561–72. Epub 2012 May 24. PMID: 22633370; PMCID: PMC3710583. doi:10.1016/j.molcel.2012.04.027

El-Omar, EM (2001). The importance of interleukin 1beta in Helicobacter pylori associated disease. *Gut* 48, 743–7. PMID: 11358884; PMCID: PMC1728311. doi:10.1136/gut.48.6.743

Flahou, B, Haesebrouck, F, Pasmans, F, D'Herde, K, Driessen, A, Van Deun, K, Smet, A, Duchateau, L, Chiers, K, and Ducatelle, R (2010). *Helicobacter suis* causes severe gastric pathology in mouse and mongolian gerbil models of human gastric disease. *PLoS One* 5, e14083. doi:10.1371/journal.pone.0014083

Forte, JG, and Zhu, L (2010). Apical recycling of the gastric parietal cell H,K-ATPase. *Annu Rev Physiol* 72, 273–96. PMID: 20148676. doi:10.1146/annurev-physiol-021909-135744

Harms, W. (1910). Über den Ersatz der Haupt- und Belegzellen Magen der Maus. *Anatomische Hefte* 41, 392–398. doi:10.1007/bf02214362

Heilmann, KL, and Borchard, F (1991). Gastritis due to spiral shaped bacteria other than Helicobacter pylori: clinical, histological, and ultrastructural findings. *Gut* 32, 137–40. ; PMCID: PMC1378794. doi:10.1136/gut.32.2.137PMID: 1864530

Helander, H.F., and Sundell, G.W. (1984). Ultrastructure of inhibited parietal cells in the rat. *Gastroenterology* 87, 1064–1071. PMID: 6479531. doi:10.1016/s0016-5085(84)80066-9

Icatlo, FC, Jr, Kimura, N, Goshima, H, and Kodama, Y (2000). Enhanced reduction of Helicobacter pylori load in precolonized mice treated with combined famotidine and urease-binding polysaccharides. *Antimicrob Agents Chemother* 44, 2492–7. doi:10.1128/aac.44.9.2492-2497.2000

Inokuchi, H., Kawai, T., Hattori, T., and Kawai, K. (1992). Omeprazole causes parietal cell damage, DNA synthesis and cellular proliferation in rat oxyntic mucosa. *Eur J Gastroenterol Hepatol* 4, 207214.

Iwahi, T, Satoh, H, Nakao, M, Iwasaki, T, Yamazaki, T, Kubo, K, Tamura, T, and Imada, A (1991). Lansoprazole, a novel benzimidazole proton pump inhibitor, and its related compounds have selective activity against Helicobacter pylori. *Antimicrob Agents Chemother* 35, 490–6. PMID: 2039199; PMCID: PMC245037. doi:10.1128/AAC.35.3.490

Karasawa, H, Tani, N, and Miwa, T (1988). The effect of omeprazole on ultrastructural changes in gastric parietal cells. *Gastroenterol Jpn* 23, 1–8. PMID: 3350276. doi:10.1007/BF02918848

Larson, GM, Sullivan, HW, and Rayford, P (1986). Omeprazole-induced hypergastrinemia: role of gastric acidity. *J Surg Res* 40, 504–9. PMID: 3736035. doi:10.1016/0022-4804(86)90223-4

Liu, C, Smet, A, Blaecher, C, Flahou, B, Ducatelle, R, Linden, S, and Haesebrouck, F (2014). Gastric de novo Muc13 expression and spasmolytic polypeptide-expressing metaplasia during *Helicobacter heilmannii* infection. *Infect Immun* 82, 3227–39. Epub 2.014 May 27. PMID: 24866791; PMCID: PMC4136228. doi:10.1128/IAI.01867-14

Matos, R, Amorim, I, Magalhães, A, Haesebrouck, F, Gärtner, F, and Reis, CA (2021). Adhesion of *Helicobacter* species to the human gastric mucosa: a deep

look into glycans role. *Front Mol Biosci* 8, 656439. PMID: 34026832; PMCID: PMC8138122. doi:10.3389/fmolb.2021.656439

Nakamura, M, Murayama, SY, Serizawa, H, Sekiya, Y, Eguchi, M, Takahashi, S, Nishikawa, K, Takahashi, T, Matsumoto, T, Yamada, H, Hibi, T, Tsuchimoto, K, and Matsui, H (2007). "Candidatus Helicobacter heilmannii" from a cynomolgus monkey induces gastric mucosa-associated lymphoid tissue lymphomas in C57BL/6 mice. *Infect Immun* 75, 1214–22. doi:10.1128/IAI.01459-06

Nakamura, M, Øverby, A, Michimae, H, Matsui, H, Takahashi, S, Mabe, K, Shimoyama, T, Sasaki, M, Terao, S, Kamada, T, Yanaka, A, Iwamoto, J, Tanabe, S, Tari, A, Nasu, S, Suzuki, H, and Yamagata Murayama, S (2020). PCR analysis and specific immunohistochemistry revealing a high prevalence of non-Helicobacter pylori Helicobacters in Helicobacter pylori-negative gastric disease patients in Japan: High susceptibility to an Hp eradication regimen. *Helicobacter* 25, e12700. doi:10.1111/hel.12700

Ogata, M, Araki, K, and Ogata, T (1998). An electron microscopic study of *Helicobacter pylori* in the surface mucous gel layer. *Histol Histopathol* 13, 347–58. PMID: 9589892. doi:10.14670/HH-13.347

Pharmaceuticals and Medical Devices Agency of Japan (2014). Drug approval review for vonoprazan fumarate (in Japanese), the Pharmaceuticals and Medical Devices Agency of Japan, Available at: http://www/pmda/go.jp/ (accessed 25 August 2017).

Rimbara, E, Suzuki, M, Matsui, H, Nakamura, M, Morimoto, M, Sasakawa, C, Masuda, H, Nomura, S, Osaki, T, Nagata, N, Shibayama, K, and Tokunaga, K (2021). Isolation and characterization of *Helicobacter suis* from human stomach. *Proc Natl Acad Sci U S A* 118, e2026337118. PMID: 33753513; PMCID: PMC8020762. doi:10.1073/pnas.2026337118

Salomon, H. (1896). Ueber das spirillum des saugetiermagens und seinverhalten zu den belegzellen fur Bakteriologie and Parasitenkunde, Centralblatt fur Bakteriologie, Parasitenkunde V. *Infektionskrankheiten* XIX, 433–443.

Schreiber, S., Garten, D., Nguyen, T.H., Konradt, M., Bücker, R., and Scheid, P. (2007). *IN situ* measurement of pH in the secreting canaliculus of the gastric parietal cell and adjacent structures. *Cell Tissue Res* 329, 313–320. Epub 2007 May 16. PMID: 17505843. doi:10.1007/s00441-007-0427-1

Schreiber, S., Nguyen, T.H., Stüben, M., and Scheid, P. (2000). Demonstration of a pH gradient in the gastric gland of the acid-secreting guinea pig mucosa. *Am J Physiol Gastrointest Liver Physiol* 279, G597–G604. PMID: 10960360. doi:10.1152/ajpgi.2000.279.3.G597

Schubert, ML (2015). Functional anatomy and physiology of gastric secretion. *Curr Opin Gastroenterol* 31, 479–85. PMID: 26376477. doi:10.1097/MOG.0000000000000213

Scott, DR, Besancon, M, Sachs, G, and Helander, H (1994). Effects of antisecretory agents on parietal cell structure and H/K-ATPase levels in rabbit gastric mucosa *in Vivo*. *Dig Dis Sci* 39, 2118–26. doi:10.1007/BF02090359

Singhal, AV, and Sepulveda, AR (2005). *Helicobacter heilmannii* gastritis: a case study with review of literature. *Am J Surg Pathol* 29, 1537–9. PMID: 16 v; 224223. doi:10.1097/01.pas.0000169499.96658.6e

Smolka, A., Helander, H.F., and Sachs, G. (1982). A study of the proton translocating adenosine triphosphatase of the gastric mucosa using monoclonal antibodies. *Am J Physiol* 245, G589G596.

Soll, AH, and Walsh, JH (1979). Regulation of gastric acid secretion. *Annu Rev Physiol* 41, 35–53. PMID: 219762. doi:10.1146/annurev.ph.41.030179.000343

Stefanini, M, De Martino, C, and Zamboni, L (1967). Fixation of ejaculated spermatozoa for electron microscopy. *Nature* 216, 173–4. doi:10.1038/216173a0

Stolte, M, Bethke, B, Rühl, G, and Ritter, M (1992). Omeprazole-induced pseudohypertrophy of gastric parietal cells. *Z Gastroenterol* 30, 134–8. PMID: 1553828.

Stolte, M, Kroher, G, Meining, A, Morgner, A, Bayerdörffer, E, and Bethke, B (1997). A comparison of *Helicobacter pylori* and *H. heilmannii* gastritis. A matched control study involving 404 patients. *Scand J Gastroenterol* 32, 28–33. doi:10.3109/00365529709025059

Sugano, K (2018). Vonoprazan fumarate, a novel potassium-competitive acid blocker, in the management of gastroesophageal reflux disease: safety and clinical evidence to date. *Therap Adv Gastroenterol* 11, 1756283X17745776. doi:10.1177/1756283X17745776

Uchida, M, Endo, N, and Shimizu, K (2005). Simple and noninvasive breath test using 13C-acetic acid to evaluate gastric emptying in conscious rats and its validation by metoclopramide. *J. Pharmacol. Sci.* 98, 388–95. Epub 2005 Aug 5. PMID: 16082175. doi:10.1254/jphs.fp0050153

Vijayakumari, S, Khin, MM, Jiang, B, and Ho, B (1995). The pathogenic role of the coccoid form of Helicobacter pylori. *Helicobacter pyloriCytobios* 82, 251–60. PMID: 8565623.

Watanabe, K, Murakami, K, Sato, R, Kashimura, K, Miura, M, Ootsu, S, Miyajima, H, Nasu, M, Okimoto, T, Kodama, M, and Fujioka, T (2004). Effect of sucralfate on antibiotic therapy for *Helicobacter pylori* infection in mice. *Antimicrob Agents Chemother* 48, 4582–8. PMID: 15561829; PMCID: PMC529215. doi:10.1128/AAC.48.12.4582-4588.2004

Yasuda, T., Lee, H.S., Nam, S.Y., Katoh, H., Ishibashi, Y., Yamagata Murayama, S., et al. (2022). Non-*Helicobacter pylori* Helicobacter (NHPH) positive gastric cancer. *Sci Rep* 12, 4811. PMID: 35314746; PMCID: PMC8938428. doi:10.1038/s41598-022-08962-y

Conflict of Interest: The authors declare that the research was conducted in the absence of any commercial or financial relationships that could be construed as a potential conflict of interest.

Publisher's Note: All claims expressed in this article are solely those of the authors and do not necessarily represent those of their affiliated organizations, or those of the publisher, the editors, and the reviewers. Any product that may be evaluated in this article, or claim that may be made by its manufacturer, is not guaranteed or endorsed by the publisher.

Frontiers in Pharmacology

Explores the interactions between chemicals and living beings

The most cited journal in its field, which advances access to pharmacological discoveries to prevent and treat human disease.

Discover the latest Research Topics

See more →

Frontiers

Avenue du Tribunal-Fédéral 34
1005 Lausanne, Switzerland
frontiersin.org

Contact us

+41 (0)21 510 17 00
frontiersin.org/about/contact